Furthering the potential of apatite as a provenance indicator in sedimentary systems

Ph.D. Thesis

2019

Gary O'Sullivan

Trinity College Dublin
Coláiste na Tríonóide, Baile Átha Cliath
The University of Dublin

I declare that this thesis has not been submitted as an exercise for a degree at this or any other university and it is entirely my own work.

I agree to deposit this thesis in the University's open access institutional repository or allow the library to do so on my behalf, subject to Irish Copyright Legislation and Trinity College Library conditions of use and acknowledgement.

I consent to the examiner retaining a copy of the thesis beyond the examining period, should they so wish (EU GDPR May 2018).

Gary John O'Sullivan

Furthering the potential of apatite as a provenance indicator in sedimentary systems

Gary O'Sullivan

Summary

As a mineral that has only recently become possible to date routinely by the U-Pb method, apatite geochemistry (U-Pb isotopes and trace elements) has until now attracted less attention than longer-established detrital chronometers such as zircon. This has resulted in a mismatch between the potential of apatite as a detrital geochronometer and our understanding of what the geo- or thermo-chronological information that it contains means, and how its trace-element geochemistry relates to source lithology.

This thesis investigates U-Pb age data from apatite and other chronometers in detrital systems to provide insight into the different age-information that is recorded by apatite compared to other mineral chronometers, with apatite proving particularly effective at recording magma-poor orogenesis and recording more recent geological events in its source area than other chronometers.

This thesis also examines apatite trace-element compositions and their potential for use alongside U-Pb ages in detritus. While apatite trace-element compositions have previously been investigated in provenance studies (though never in combination with U-Pb ages), the choice of elemental ratios employed has led to poor separation on discrimination plots resulting in only generalised provenance determinations being possible. In this PhD a different approach has been taken, whereby a large database of apatite bedrock compositions was assembled and visualised using principal component analysis to create an empirical apatite discriminant diagram against which unknown detritus can be plotted. Using this methodology full separation of many lithological classes of apatite is possible (low- to medium-grade metamorphic, high-grade metamorphic, S-type granitoids, 'felsic' I-type granitoids, 'mafic' I-type granitoids and basic igneous rocks, alkaline igneous rocks, adakites, ultrabasic igneous rocks, and authigenic apatite).

Given that it is now possible to couple the U-Pb ages and source lithology of detrital apatite reliably using the methodology developed here, this opens the door to highly specific provenance determinations. The detrital case studies presented in this thesis demonstrate that novel insights can be gained from these data, including new information on the generation of sandstones, the history of denudation of the earth's surface, and the evolution of drainage networks and the tectonic forces that created them.

ACKNOWLEDGEMENTS

I am grateful to very many people who've been a part of my life over the past four years of my PhD and this can only be a non-exhaustive list of thanks.

I have been in the Trinity College Dublin Geology Department for eight years now, for the first half of those years as an undergraduate and for the second half as a PhD student. I have grown into being a scientist in my time at the Geology department, and the cast of characters there have been a big feature in my life In TCD. In no particular order I would like to thank Frank and Maura for all their help over the years. Mags and Sarah too have also provided a very friendly and thoughtful face to the department over my years here. I am also very grateful to the now emeritus academic staff such as John Graham and Ian Sanders who provided me with a solid understanding of Geology with which to pursue my PhD. Indeed I am thankful to all the academic staff and post-docs who taught me during my undergraduate degree. My peers in the Geology Department have also been a big part of my life during the PhD, and a special mention has to go out to two people in particular – Eoghan Corbett and Brendan Hoare, who have been close friends and great people to develop ideas with.

I would like to give particular thanks to Balz Kamber for giving me the opportunity to run the laser ablation lab and imparting his analytical wisdom, I have learned a lot over the last year that will be of great benefit to me in future. I must also give special mention to Cora McKenna, who has shepherded me through my time working in the lab. Cora is a very generous person and I very much value having gotten to know her over the last two years.

In my own research group the team of me, Chris and Isa have had some great discussions over the years and I would like to thank them for helping me develop my ideas so much. This leads me to my greatest single thank you, the man who hired the three of us, David Chew. David has been a fantastic supervisor. He is both extremely attentive and helpful while also leaving me plenty of space to discover new research interests and to grow as a scientist.

My friends outside of college have played a big part of my life too. Rob, Mark, Eibhlín, Darragh, Emer, Nils, Ella, Eoin, Sean, Nadia, Cecilia and Louis to name just a *few*, your friendship is forever appreciated.

To my partner Dónal who has had to put up with all of my panics and madness during my PhD, you have been my rock of stability through it all. I am beyond

grateful, as the completion of this thesis owes a great deal more than I can express to your support.

To my siblings, Aoife, Cormac and Daniel, you're the best brothers and sister. I'm glad to have grown up with you. To my dad, you're the one who got me interested in the natural world and geology in the first place on hikes through the Burren, so the beginning of this journey started with you. Lastly, my mother is the most selfless and caring person I know. She has been my biggest inspiration in life; from you I have learned everything. Getting to this point has largely been down to you, so *thank you*.

Table of Contents

CHAPTER 1: INTRODUCTION 1

1.1 THESIS CONTEXT 1

1.1.1 How did we get to this point? Early developments in sedimentary provenance methods 4

1.1.2 Towards modern provenance methods 5

1.2. LAYOUT OF THE THESIS 6

1.3 CO-AUTHOR STATEMENT 9

1.4 REFERENCES 11

CHAPTER 2: DETECTING MAGMA POOR OROGENS IN THE DETRITAL RECORD 18

2.1. INTRODUCTION 19

2.1.1 Heavy mineral provenance analysis and the U-Pb detrital zircon system 19

2.1.2 The advantages of apatite and rutile as heavy mineral provenance indicators 19

2.2. GEOLOGICAL BACKGROUND 20

2.2.1 Regional Geology 21

2.3. METHODS 22

2.4. RESULTS 25

2.4.1 Constraining the timing of Appalachian tectono-metamorphism 25

2.5. DISCUSSION AND CONCLUSIONS 29

2.6. REFERENCES CITED 30

2.7 SUPPORTING AND SUPPLEMENTARY INFORAMTION 34

CHAPTER 3: AN INTEGRATED APATITE GEOCHRONOLOGY AND GEOCHEMISTRY TOOL FOR SEDIMENTARY PROVENANCE ANALYSIS 74

3.1. INTRODUCTION 76

3.1.1 Why study the river Tarn? 78

3.1.2. Apatite: defining its use as a provenance indicator 78

3.2. DETAILED REGIONAL GEOLOGY & SAMPLING 83

3.2.1. The Variscan crystalline basement 83

3.2.2 Mesozoic to recent history 84

3.3. MATERIALS & METHODS 85

3.3.1 River sediment sampling 85

3.3.2 Single Grain LA-ICP-MS Analyses 88

3.4. RESULTS 90

3.5. DISCUSSION 100

3.5.1 Apatite trace-element and U-Pb systematics 100

3.5.2 Utilising apatite trace element compositions, is it possible to determine single-grain provenance without bedrock sampling? ... *104*
3.5.3 Apatite recycling and refractory apatite ... *104*
3.5.4 Implications for Massif Central tectonics ... *105*
3.5.5 Comparison of source-sample detrital rutile and apatite U-Pb ... *106*
3.6. CONCLUSIONS ... 107
3.6.1 Acknowledgements and Funding ... *107*
3.7. REFERENCES ... 108
3.8 SUPPORTING INFORMATION & SUPPLEMENTARY FIGURES ... 116

CHAPTER 4: THE TRACE ELEMENT COMPOSITION OF APATITE AND ITS APPLICATION TO DETRITAL PROVENANCE STUDIES ... 154

4.1. INTRODUCTION ... 156
4.1.1 Physical and chemical weathering properties of apatite ... *157*
4.1.2 Geochemistry of apatite ... *158*
4.1.3 Geochronology/thermochronology of apatite ... *169*
4.2 METHODOLOGY ... 171
4.2.1 Data Synthesis for Principal Component Analysis (PCA) Diagrams ... *171*
4.2.2 A recipe for an apatite PCA discriminant diagram ... *172*
4.3. RESULTS ... 176
4.3.1 Discrimination of bedrock samples on the PCA biplot ... *176*
4.3.2 PCA applied to case study 1 – Mesoproterozoic sediments from NW Scotland ... *178*
4.3.3 PCA applied to case study 2 – modern sediments, River Tarn, Central France ... *183*
4.3.4 PCA applied to case study 3 – Modern Sediments, French Broad River ... *185*
4.4. DISCUSSION ... 190
4.4.1 implication of the apatite discriminatory PCA, what information or insight does it provide, and how should it be used ... *190*
4.4.2 Stac Fada Discussion ... *190*
4.4.3 River Tarn Discussion ... *192*
4.4.4 French Broad River (FBR) Discussion ... *193*
4.5. CONCLUSIONS ... 195
4.5.1 Acknowledgements ... *195*
4.7 REFERENCES ... 195
4.8 SUPPORTING INFORMATION ... 207

CHAPTER 5: CONCLUSIONS AND FUTURE WORK ... 214

5.1 CONCLUSIONS ... 214
5.2 FUTURE WORK ... 219

5.3 REFERENCES 221

APPENDIX A: THE TRACE ELEMENT AND U-PB SYSTEMATICS OF METAMORPHIC APATITE 226

A.1. INTRODUCTION 228

A.1.1 Igneous apatite trace-element chemistry 228

A.1.2 Metamorphic apatite trace-element chemistry 229

A.1.3 U-Pb dating of apatite by LA-ICP-MS 230

A.1.4 Apatite as a provenance tool 231

A.2. SAMPLES – REGIONAL GEOLOGICAL SETTING 233

A.2.1 Ireland and Scotland 233

2.1.1 Grampian (ca. 470 Ma) regional metamorphism of Dalradian Supergroup samples 235

A.2.1.2 Grampian (ca. 470 Ma) regional metamorphism of Annagh Gneiss Complex samples 235

A.2.2 New Zealand Alps 236

A.2.3 Eastern Cordillera of Peru 236

A.2.4 Paros, Greek Cyclades 237

A.3. ANALYTICAL METHODS 237

A.4. RESULTS 240

A.4.1 Whole rock geochemistry 240

A.4.2 Apatite U-Pb ages and trace element chemistry 243

A.4.3 LA-Q-ICP-MS imaging of New Zealand metagreywackes and Caledonian metabasites 259

A.5. DISCUSSION 261

A.5.1 Paragenesis of metamorphic apatite 264

A.5.2 U-Pb systematics of metamorphic apatite 265

A.6. CONCLUSIONS 266

A.6.1. Acknowledgements 267

A.8. REFERENCES 268

APPENDIX B: ON THE TRACK OF A SCOTTISH IMPACT STRUCTURE: A DETRITAL ZIRCON AND APATITE PROVENANCE STUDY OF THE STAC FADA MEMBER AND THE WIDER STOER GROUP, NORTHWEST SCOTLAND 278

B.1. INTRODUCTION 280

B.1.1The Stac Fada Member 280

B.1.2. Locating the impact site 283

B.1.3. A new approach 288

B.2. MATERIALS AND METHODS 290
B.2.1. Samples *290*
B.2.2. Analytical Methods *290*
B.3. RESULTS 294
B.3.1. Shocked features in zircon *294*
B.3.2. Zircon U-Pb age data *294*
B.3.3. Apatite U-Pb age data *297*
B.4. DISCUSSION 300
B.4.1. Stratigraphic variation *300*
B.4.2. Provenance *304*
B.4.3. Comparison of apatite and zircon age distributions *307*
B.5. CONCLUSIONS 307
B.5.1 Acknowledgements *309*
B.7. REFERENCES CITED 309
APPENDIX C: TITLE PAGES OF OTHER CO-AUTHORED WORKS 321

Chapter 1
Introduction

1.1 THESIS CONTEXT

By determining the origin or provenance of detritus it is possible to reconstruct the history of the Earth's surface by identifying ancient sediment pathways and the tectonic forces that generated them. As sediment source areas are by definition non-extant sediments represent our only record of denuded landscapes. Provenance studies aim to make reconstructions of palaeogeograpy, palaeoflow, and palaeoclimate, and are also employed in basin analysis. Determining the origin of detritus is not a simple task, however, as due to sediment mixing and modification during the sedimentary cycle most detritus in clastic sediments provides little or no information that can be used to nail down its origin to specific locations, or even general localities (Weltje and Eynatten, 2004).

Amongst the minerals present in detritus, certain species are able to yield significantly more provenance-specific information than others, leading to the adoption of several key species for single-grain provenance determination. These include the accessory minerals zircon (e.g. Thomas, 2011), rutile (e.g. Luvizotto et al., 2009), titanite (e.g. McAteer et al., 2010), monazite (e.g. Hietpas et al. 2010), apatite (e.g. Carrapa et al., 2009), and rock-forming white mica (e.g. Stuart, 2002). The key aspects of detrital mineral species that encourage their widespread adoption as provenance indicators may include some or all of the following attributes: 1) their ability to be accurately, precisely, cheaply and rapidly dated, 2) their ubiquity in sediment that permits their widespread use, and 3) their ability to retain geochemical information that can reliably link them to specific source rocks.

In single-grain detrital provenance studies, i.e. those that focus on individual mineral species in sediments, the detrital zircon U-Pb method has the longest history of application and to the present day continues to be applied far more than all other detrital chronometers combined (e.g. Thomas, 2011). Its continued popularity stems from its

incorporation of significant U and insignificant Pb upon crystallization (common Pb or Pb_c), which permits accurate and precise dating, and its physical and chemical robustness during the sedimentary cycle, which ensures its survival in sediments (e.g. Morton and Hallsworth, 1999 and references therein). Countering these useful attributes, however, there are drawbacks to the detrital zircon U-Pb method that limit the possible provenance information that may be determined by relying solely on it. In broad terms, it is likely to over-represent the felsic plutonic record and severely under-represent the basic igneous record in detritus due to differences in fertility (e.g. Malusà et al., 2016); it is likely to under-represent the detrital record of low- to medium-grade metamorphism and magma poor orogenesis due to its retention of U-decay daughter products to very high temperatures (Cherniak, 2010) and limited growth in sub-anatectic conditions (Hay and Dempster, 2009); and its mechanical and chemical robustness during the sedimentary cycle may render zircon polycyclic in sediments and hence limit its provenance potential as the detrital zircon record may become biased towards ancient denuded orogens (Moecher and Samson, 2006). While zircon will almost certainly continue to be the most popular mineral for single-grain provenance studies, its drawbacks and limitations open opportunities to develop other mineral systems that can record information that zircon is insensitive to, and thus complement the detrital zircon record.

The past two decades have, therefore, seen an increasing amount of scientific investigation into the development of alternative detrital U-Pb geochronometers, with minerals such as titanite (e.g. McAteer et al., 2010), rutile (e.g. Zack et al., 2004), apatite (e.g. Carrapa et al., 2009), and monazite (e.g. Hietpas et al., 2010) all capable of providing useful provenance information in detritus from their U-Pb ages and in the case of rutile and titanite their associated geochemical compositions. The expansion in viable detrital U-Pb geochronometers has been made possible due to advances in instrumental precision and data reduction methods. Most of the mentioned phases contain significant Pb_c and much lower concentrations of U compared to zircon. The more widespread adoption of these techniques, for both *in-situ* and detrital samples, is thus associated with the development of suitable age standards and data reduction protocols that can take account of variable Pb_c in these primary age standards, and of suitable standardising materials themselves (e.g. Chew et al., 2014; Luvizotto et al., 2009; Thomson et al., 2012). As Pb_c-bearing mineral phases have only recently become widely employed as detrital U-Pb chronometers, consequentially it has become necessary to understand more fully how each of these mineral phases records the geological history of its source region

– to understand what their U-Pb ages mean in terms of their temperature history, to understand whether their trace-element compositions can be used to determine their source rock lithology, and to determine whether these minerals are likely to survive in the geological record so that these signals can ultimately be retrieved.

Rutile geochemistry is one example of a Pb_c-bearing mineral which has been the subject of detailed study as a provenance proxy over the past fifteen years. Routine laser-ablation inductively coupled plasma mass spectrometry (LA-ICP-MS) analysis of detrital rutile chemistry is now able to provide information about the temperature at which individual rutile crystals crystallised by employing the 'Zr-in-rutile thermometer' (e.g. Meinhold et al., 2008; Watson et al., 2006), and elemental ratios in detrital rutile are able to provide information about the composition of its source rock. These include Cr/Nb ratios, which can be used to determine whether the rutile source lithology was mafic or felsic (Zack et al., 2004; Triebold *et al.*, 2007; Meinhold *et al.*, 2008); Mg/Al ratios, which can be used to determine whether a rutile grain is sourced from crustal or mantle sources, and W contents, which are elevated in ore-derived rutile and thus useful for locating and fingerprinting ore-deposits (Meinhold, 2010 and references therein).

The focus of this PhD is the investigation of the detrital apatite provenance system with the specific aim of improving its provenance potential by providing a better understanding of how, where and when apatite is an advantageous mineral to use in provenance studies. These aims include characterising the U-Pb information that detrital apatite provides so as to better understand how the detrital apatite U-Pb system differs to those of other detrital chronometers such as zircon. Additionally, as unlike rutile there has been a lack of prior research into aspects of apatite geochemistry that have potential provenance applications, this PhD also focuses on improving methodologies of trace-element analysis in apatite and the application of apatite trace-element compositions in detritus. By integrating U-Pb and trace element information this PhD also expands the amount of provenance information that is possible to extract from sediments, so as to better understand the history of denudation of the Earth's surface.

The following two sections aim to present a concise history of the development of the field of detrital provenance, demonstrating the dependence of this thesis upon a century-and-a-half of previous scholarly work.

1.1.1 How did we get to this point? Early developments in sedimentary provenance methods

In detritus, the heavy minerals have been used since the nineteenth century to determine the source and origin of sediments. The heavy minerals are defined by their density, with a density of > 2.7 g/cm^2 qualifying a mineral as a heavy mineral (Dick, 1887), which excludes the less dense bulk (framework) components of most clastic sediment – quartz and feldspar. Despite accounting for about fifty common transparent and opaque minerals in detritus (Mange and Maurer, 1992), heavy minerals represent only a fraction of the typical clastic sediment budget and are thus accessory apart from within placer deposits.

Early developments in the history of heavy mineral analysis focussed on qualitative analysis of detrital assemblages, such as the presence or absence of minerals diagnostic of specific lithologies (e.g. Dick, 1887; Artini, 1891). Examples include the presence of spinel in sediment which strongly indicates a mantle-derived lithology is the sediment source, or the presence of galucophane which indicates that a blueschist-facies terrane is the sediment source as glaucophane is unique to that lithology (unless recycled). The goals of these studies also included the correlation of sedimentary units across wide areas (e.g. Dryden, 1931), and to identify characteristics of sandstones with unusually high modal abundances of the heavy minerals for the mining of the heavy minerals within them (e.g. Dick, 1887).

The early twentieth century saw a shift towards the adoption of quantitative methods of mineral analysis, beginning with Fleet (1926), who advocated for the first time the counting of large numbers of detrital heavy mineral grains to generate accurate percentages of the major heavy minerals present in a sand sample to determine its provenance. This work was refined further by Dryden (1931), who calculated the sample sizes required to capture different population-size components in a detrital heavy mineral sample.

As the field of bulk heavy mineral analysis matured during the twentieth century, it was recognised by researchers that provenance was not the only factor that controlled the bulk composition of a heavy mineral assemblage. Rubey (1933) recognised that heavy minerals behaved differently in water according to their density, while Pettijohn (1941) undertook the first published studies into the effects of source-rock weathering, transport processes, and diagenesis on the stability of detrital heavy minerals. Studies on the hydrodynamic behaviour and dissolution of the heavy minerals continue to the present day and this matter is discussed later in the text (next subsection).

1.1.2 Towards modern provenance methods

From the 1970s onwards methods of provenance analysis began to divide into two broad groups with different approaches to sediment characterisation. Firstly, those that attempted to characterise sediments by using as large a fraction of the sediment as possible to determine provenance and referred to here as broad-spectrum (BS) provenance methods. This is typically achieved using counting methods and focuses on the framework minerals (i.e. quartz and feldspar) and/or heavy minerals as a group, and is similar to the aforementioned methods as developed from the 1920s onward by Fleet (1926) and Rubey (1933). Secondly, there was a renewed interest concerning the analysis of single diagnostic mineral species within rocks, harking back to the original nineteenth century heavy mineral studies of diagnostic species (e.g. Dick, 1887), but incorporating statistical methods and employing trace element geochemical or U-Pb analysis of detrital heavy mineral species. These methods are known as single-grain (SG) provenance techniques.

In BS provenance studies, models of the major framework (i.e. non-heavy fraction) began to be used, using the method described by Dickinson and Suczek (1979). These studies aim to discern the tectonic setting under which a clastic rock was deposited based on the proportions of the major framework components (quartz, feldspar, and lithics or QFL), with for example quartzites associated with stable cratonic environments according to this scheme. Further developments in bulk sediment analysis continue to the present day with techniques such as those probing the textures acquired by grains during the sediment cycle (e.g. Andò et al., 2012), and ever-improving models of hydrodynamic behaviour (e.g. Resentini et al., 2013) and dissolution (Morton and Hallsworth, 1999 and references therein) of detritus contributing to greater understanding of detrital heavy mineral assemblages.

While bulk heavy mineral analysis has continued developing and can provide useful insight and provenance determinations (e.g. Andò et al., 2012), the methods employed and the underpinning philosophy would still be broadly recognisable to the researchers who developed statistical heavy mineral analysis in the 1930s. The major limiting factor of bulk heavy mineral analysis methods is the potential non-uniqueness of heavy mineral assemblages, i.e. even if there is a most probable model for how a detrital heavy mineral is generated, it is possible to generate a specific heavy mineral assemblage by nearly limitless combinations of initial inputs and weathering effects – limiting the

uniqueness of provenance determinations. In comparison, targeted SG geochonological and trace-element analysis of single heavy mineral species attempts to circumvent the problems of non-uniqueness by using age and trace element information that can be linked beyond reasonable doubt to specific sources. SG analysis methods began by analysis of different types of the mineral zircon (by colour, shape etc.) from bedrock specimens, by thermal ionization mass spectrometry (TIMS) (e.g. Lancelot et al., 1976), with these methods applied to detrital zircon samples by 1981 (Gaudette et al., 1981) to determine sources and to estimate maximum depositional ages based upon the youngest detrital zircon ages.

Developments in analytical methods have greatly assisted in the adoption of single-grain provenance techniques. Secondary ion mass spectrometry (SIMS) proved more suitable to studies of detrital provenance than TIMS due to the higher throughput of material possible with SIMS compared to TIMS (albeit at slightly reduced precision, Davis *et al.*, 2003), along with the essentially non-destructive nature of the technique and high spatial-resolution allowing the sampling of specific age-domains of minerals. Several important materials were made throughout the 1980s using detrital SIMS datasets, including the oldest known detrital grains on Earth (in fact the oldest known Earth material), the Jack Hills zircons (e.g. Compston and Pidgeon, 1986).

LA-ICP-MS was developed as a technique for geochronology and trace-element analysis from the late 1980s (with the first geological application by Gray, 1985). The LA-ICP-MS technique has been significantly refined since then, allowing for smaller ablation volumes, and increasing accuracy and precision. It is a more destructive technique than the detrital SIMS method, and generally permits less precise age dating. However, it is a very rapid and cost-effective procedure allowing the measurement of several grains for U-Pb isotopes per minute (e.g. Vermeesch et al., 2017), which makes it the ideal method for the measurement of detrital samples, as large detrital datasets are required to capture minor sediment sources (e.g. Andersen, 2005). Use of LA-ICP-MS is now routine for geochemical and geochronological analysis of detrital heavy mineral studies (e.g. Hietpas et al., 2010; Liu et al., 2014; Manzotti et al., 2014; Moecher et al., 2011), and it is the primary geochemical and geochronological analytical method employed in this PhD research.

1.2. LAYOUT OF THE THESIS

The three core chapters (2, 3 and 4) of this thesis consist of two published papers and one manuscript prepared for submission to a peer-reviewed journal. These chapters, having been prepared for individual publication, contain separate introductions and self-contained conclusions. Chapter 5 represents a synthesis of the findings of Chapters 2, 3 and 4 in which the principal outcomes and findings of the thesis are placed in a broader context with respect to the original aims. The publication statuses of each chapter at the time of submission of the thesis, as well as an author list, are provided at the beginning of each chapter.

Chapter 2 (O'Sullivan et al., 2016) is a comparative investigation of several detrital U-Pb chronometers, including apatite. The purpose of this study is to determine how the sensitivity of apatite to orogenic events differs from that of other commonly employed detrital chronometers. Previously published U-Pb age data for detrital monazite and zircon (Hietpas *et al.*, 2010; Moecher *et al.*, 2011) from the same sediment samples from the French Broad River in North Carolina, USA, are reanalysed here for detrital apatite and rutile U-Pb. The sample suite was provided by Prof. Scott Samson of Syracuse University. Hietpas et al. (2010) had already shown that detrital monazite was somewhat sensitive to the magma-poor Alleghanian orogen (c. 320 Ma), which was not detected at all by detrital zircon U-Pb. The addition of apatite and rutile U-Pb data makes the French Broad River one of the most comprehensively studied river systems for detrital U-Pb geochronology and permits detailed comparison of four mineral phases. In the analysed samples both rutile and apatite record systematically younger events than both zircon U-Pb and monazite U-Pb. Both zircon and monazite dominantly record voluminous magmatism during orogenesis at c. 460 Ma (Taconic) in the detrital samples, in comparison, detrital apatite and rutile mostly record regional metamorphic events at c. 370 Ma (Neo-Acadian) and 320 Ma (Alleghanian). The results of this study demonstrate that detrital apatite (and rutile) is capable of sensing and preserving a record of orogenic and tectonic events that the most commonly employed detrital chronometer (zircon) is insensitive to, and that greater insight into the source regions of sediments, especially regionally-metamorphosed hinterlands, can be provided by using 'alternative' detrital geochronometers such as apatite, monazite and rutile because of their lower U-Pb temperature sensitivity and/or lower temperatures of crystallization.

Having demonstrated at least one important setting in which detrital apatite is particularly sensitive to events which are difficult to sense with commonly used provenance methods, chapter 3 (O'Sullivan et al. 2018) builds on chapter 2 by, for the

first time, integrating a full comprehensive study of apatite trace-element compositions with apatite U-Pb ages in detrital samples. In this study I collected modern sediment samples from the river Tarn in the Massif Central of France, near Millau. The sampling location was chosen on the basis of the simple distribution of lithologies in the catchment of the river Tarn, making it a useful natural laboratory to investigate the link between lithology and the geochemistry of detrital grains. In the sampled detritus from the river Tarn there is successful separation of detritus according to bedrock composition. In this chapter a principal component analysis (PCA) on apatite trace-elements is used to match detrital grains to bedrocks with similar trace-element geochemistry. Using this method apatite from a catchment sourcing mostly metapelites matches the composition of metapelites from the published literature (Nutman, 2007; El Korh *et al.*, 2009; Henrichs *et al.*, 2018), the compositions of apatite from a catchment draining mostly felsic plutonic rocks matches the compositions of published felsic apatite (Sha and Chappell, 1999; Hsieh *et al.*, 2008; Chu *et al.*, 2009), and the compositions of apatite from a river draining basic igneous rocks contains a population of grains with compositions that match the composition of basic igneous bedrocks (Tang *et al.*, 2012; Chakhmouradian *et al.*, 2017). Additionally, all these categories of apatite are possible to separate in the downstream samples in which all these sediment sources have mixed – by both trace element composition *and* age. This study, by permitting the discrimination of detrital grains by two different complementary methods, increases the usefulness of apatite as a provenance proxy, as terranes of similar age but dominated by different lithologies may be discriminated, as can apatite of similar trace-element composition and different age.

The third, and final, main chapter of this thesis, chapter 4, concerns the refinement of trace-element fingerprinting of detrital apatite. The elemental ratios used on discriminant plots in earlier studies (e.g. Sr/Y, Belousova et al., 2002) had led to poor separation of lithology fields and hence only generalised provenance determinations being possible using apatite trace element compositions (e.g. Abdullin et al., 2016). However, the PCA-method of discrimination used in chapter 3 was very effective at discriminating the source-lithology of detrital apatite grains and so was further investigated.

Similar to chapter 3, a large database of apatite bedrock compositions was assembled and visualised using principal component analysis (PCA) and compared to unknown detritus. The PCA methodology was further developed in chapter 4. A distinction is made between ‘train’ data and ‘test’ data, i.e. between the bedrock samples

and unknown detritus. Only the train dataset is used for the calculation of the PCA, against which different test datasets can be plotted. As the train dataset always uses the same set of data points the scaling of the resulting PCA-diagram is always the same. Hence this unknown detritus can be plotted on this empirical apatite discriminant diagram and different test datasets can be directly compared.

In addition the bedrock database is much larger in chapter 4 compared to chapter 3 and encompasses almost all the common lithologies on the Earth's surface. Full separation of many lithological classes of apatite is achieved (low- to medium-grade metamorphic, high-grade metamorphic, S-type granitoids, felsic I-type granitoids, 'mafic' I-type granitoids and basic igneous rocks, alkaline igneous rocks, adakites, ultrabasic igneous rocks, and authigenic apatite).

Having developed an empirical apatite discriminant diagram, it is then applied to studies that collected both U-Pb and trace element information from detrital apatite, but that only utilised apatite U-Pb compositions for provenance determinations. These include the detrital dataset used in chapter 2 of this thesis (O'Sullivan et al., 2016), and a study of detrital apatite from a Mesoproterozoic Basin in NW Scotland. U-Pb age data from the latter study is currently under review at the time of submission of this thesis (Kenny et al., in review). The manuscript for that paper, for which I am second author, is included as an appendix to this PhD thesis to provide context for its use in chapter 4 (appendix B). The application of the discriminant PCA to these datasets permits the extraction of more provenance information than using U-Pb isotopes alone. For example it potentially permits the discrimination of detritus from specific terranes in the dataset of O'Sullivan et al. (2016).

1.3 CO-AUTHOR STATEMENT

As the first author on all three multi-author works forming chapters 2, 3 and 4, I undertook the bulk of the sample processing and analysis, and almost all figure drafting and writing. In addition I am a second author on one published paper (Henrichs et al., 2018) and one paper submitted for publication (Kenny et al, in review), and a co-author on two other published papers (Gaweda et al., 2018 and Chew et al., 2016). The papers on which I am a second author are included in Appendix A (Henrichs et al., 2018) and Appendix B (Kenny et al., in prep) . In addition I am a co-author on the following two papers:

i) Gawęda, A., Szopa, K., Chew, D., O'Sullivan, G.J., Burda, J., Klötzli, U., Golonka, J. (2018) Variscan post-collisional cooling and uplift of the Tatra Mountains crystalline block constrained by integrated LA ICP MS zircon, apatite and titanite U-Pb dating and Rare Earth Element analyses. Chemical Geology, 484, 191-209;

ii) Chew, D.M., Babechuk, M.G., Cogné, N., Mark, C., O'Sullivan, G.J., Henrichs, I.A., Doepke, D. and McKenna, C. (2016) (LA,Q)-ICPMS trace-element analyses of Durango and McClure Mountain apatite and implications for making natural LA-ICPMS mineral standards. Chemical Geology, 435, 35-48.

For Appendix A (Henrichs et al., 2018) I contributed data interpretation, analysis and editing of the manuscript, with the first author being another member of my PI's (Dr David Chew) research group in TCD, Isadora Henrichs. This study involved characterising the geochemical compositions of apatite from metamorphic bedrock samples. These low- to medium-grade metamorphic bedrock samples are similar to those found in the river Tarn catchment, and hence this study aided my interpretations in the Tarn River study (Chapter 3)

For appendix B (Kenny et al., in review), I contributed data-acquisition and reduction, interpretation of results, figure drafting, and manuscript editing, with the first author in this case being Gavin Kenny, a former PhD student in TCD now working at the Swedish Museum of Natural History.

The roles of each co-author to the manuscripts forming the basis of chapters 2, 3 and 4 of this thesis, of which I am the first author, are as follows:

David Chew, my PhD supervisor at Trinity College Dublin, has been the principal discussion partner for the interpretation of data presented in each paper presented in this thesis, assisted with the acquisition of samples in the field, and has contributed the most editorial support of the co-authors to each paper manuscript.

Scott Samson, Syracuse University, New York State, USA. He provided the mineral separates for the first paper (chapter 2). He also provided editorial comments for that first manuscript.

Andrew Morton, HM Research Associates, Pembrokeshire, UK, undertook heavy mineral analysis upon the samples in paper two (chapter 3) and also provided editorial comments for that paper.

Isadora Henrichs, Trinity College Dublin, was a discussion partner and provider of editorial comments for the second and third papers (chapters 3 and 4). She is the first author of the paper that constitutes Appendix A.

Chris Mark, Trinity College Dublin, was a very eager discussion partner and provided editorial comments for the second paper (chapter 3).

Gavin Kenny, Swedish Museum of Natural Sciences in Stockholm, formerly of Trinity College Dublin, was discussion partner and provided editorial comments for the third paper (chapter 4), which is based upon data that we collaborated on and collected together in Trinity College Dublin. The same data are used in a submitted paper first-authored by him, and that constitutes Appendix B of this thesis.

1.4 REFERENCES

Abdullin, F., Solé, J., Solari, L., Shchepetilnikova, V., Meneses-Rocha, J. J., Pavlinova, N. and Rodríguez-Trejo, A. (2016) 'Single-grain apatite geochemistry of Permian-Triassic granitoids and Mesozoic and Eocene sandstones from Chiapas, southeast Mexico: Implications for sediment provenance', International Geology Review, 58(9), pp. 1132–1157. doi: 10.1080/00206814.2016.1150212.

Andersen, T. (2005) 'Detrital zircons as tracers of sedimentary provenance: Limiting conditions from statistics and numerical simulation', Chemical Geology, 216, pp. 249–270. doi: 10.1016/j.chemgeo.2004.11.013.

Andò, S., Garzanti, E., Padoan, M. and Limonta, M. (2012) 'Corrosion of heavy minerals during weathering and diagenesis: A catalog for optical analysis', Sedimentary Geology, 280, pp. 165–178. doi: 10.1016/j.sedgeo.2012.03.023.

Artini, E., 1891. 'Intorno alla composizione delle sabbie del Ticino'. G. Mineralog. Cristallografia Petrologia, 2, pp.177-195

Belousova, E. A., Griffin, W. L., O'Reilly, S. Y. and Fisher, N. I. (2002) 'Apatite as an indicator mineral for mineral exploration: Trace-element compositions and their relationship to host rock type', Journal of Geochemical Exploration, 76(1), pp. 45–69. doi: 10.1016/S0375-6742(02)00204-2.

Carrapa, B., DeCelles, P. G., Reiners, P. W., Gehrels, G. E. and Sudo, M. (2009) 'Apatite triple dating and white mica^{40}Ar/^{39}Ar thermochronology of syntectonic detritus in the Central Andes: A multiphase tectonothermal history', Geology, 37(5), pp. 407–410. doi: 10.1130/G25698A.1.

Chakhmouradian, A. R., Reguir, E. P., Zaitsev, A. N., Couëslan, C., Xu, C., Kynický, J., Mumin, A. H. and Yang, P. (2017) 'Apatite in carbonatitic rocks: Compositional variation, zoning, element partitioning and petrogenetic significance', Lithos, 274–275, pp. 188–213. doi: 10.1016/j.lithos.2016.12.037.

Cherniak, D. J. (2010) 'Diffusion in Accessory Minerals: Zircon, Titanite, Apatite, Monazite and Xenotime', Reviews in Mineralogy and Geochemistry, 72(1), pp. 827–869. doi: 10.2138/rmg.2010.72.18.

Chew, D. M., Petrus, J. A., and Kamber, B. S. (2014) 'U-Pb LA-ICPMS dating using accessory mineral standards with variable common Pb', Chemical Geology, 363, pp. 185–199. doi: 10.1016/j.chemgeo.2013.11.006.

Chu, M.-F., Wang, K.-L., Griffin, W. L., Chung, S.-L., O'Reilly, S. Y., Pearson, N. J. and Iizuka, Y. (2009) 'Apatite Composition: Tracing Petrogenetic Processes in Transhimalayan Granitoids', Journal of Petrology, 50(10), pp. 1829–1855. doi: 10.1093/petrology/egp054.

Compston, W. and Pidgeon, R. T. (1986) 'Jack Hills, evidence of more very old detrital zircons in Western Australia', Nature, 321(6072), pp. 766–769. doi: 10.1038/321766a0.

Davis, D. W., Williams, I. S., Krogh, T. E., Ribbe, P. H. and Rosso, J. J. (2003) 'Historical development of zircon geochronology', Zircon, 53, pp. 145–181. doi: 10.2113/0530145.

Dick, A. B., (1887). 'On Zircons and Other Minerals Contained in Sand'. *Nature*, 36, p.91.

Dickinson, W. R. and Suczek, C. A. (1979) 'Plate Tectonics and Sandstone Compositions', The American Association of Petroleum Geologist Bulletin, pp. 2164–2182. doi: 0149-1423/79/B012-0003$03.00/0.

Dryden, A. L. J., (1931) 'Accuracy in percentage representation of heavy mineral frequencies'. Proceedings of the National Academy of Sciences, USA, 17(5), pp.233–238.

El Korh, A., Schmidt, S. T., Ulianov, A. and Potel, S. (2009) 'Trace Element Partitioning in HP-LT Metamorphic Assemblages during Subduction-related Metamorphism, Ile de Groix, France: a Detailed LA-ICPMS Study', Journal of Petrology, 50(6), pp. 1107–1148. doi: 10.1093/petrology/egp034.

Fleet, W. (1926). 'Petrological Notes on the Old Red Sandstone of the West Midlands'. Geological Magazine, 63(11), 505-516. doi:10.1017/S0016756800085484

Gaudette, H. E., Vitrac-Michard, A. and Allègre, C. J. (1981) 'North American Precambrian history recorded in a single sample: high-resolution UPb systematics of the Potsdam sandstone detrital zircons, New York State', Earth and Planetary Science Letters, 54(2), pp. 248–260. doi: 10.1016/0012-821X(81)90008-X.

Gray, A. L. (1985) 'Solid sample introduction by laser ablation for inductively coupled plasma source mass spectrometry', The Analyst, 110(May 1985), p. 551. doi: 10.1039/an9851000551.

Hay, D. C. and Dempster, T. J. (2009) 'Zircon behaviour during low-temperature metamorphism', Journal of Petrology, 50(4), pp. 571–589. doi: 10.1093/petrology/egp011.

Henrichs, I. A., O'Sullivan, G. J., Chew, D. M., Mark, C., Babechuk, M. G., McKenna, C. and Emo, R. (2018) 'The trace element and U-Pb systematics of metamorphic apatite', Chemical Geology, (February), 483, pp. 218-238. doi: 10.1016/j.chemgeo.2017.12.031.

Hietpas, J., Samson, S., Moecher, D. and Schmitt, A. K. (2010) 'Recovering tectonic events from the sedimentary record: Detrital monazite plays in high fidelity', Geology, 38(2), pp. 167–170. doi: 10.1130/G30265.1.

Hsieh, P. S., Chen, C. H., Yang, H. J. and Lee, C. Y. (2008) 'Petrogenesis of the Nanling Mountains granites from South China: Constraints from systematic apatite geochemistry and

whole-rock geochemical and Sr-Nd isotope compositions', Journal of Asian Earth Sciences, 33, pp. 428–451. doi: 10.1016/j.jseaes.2008.02.002.

Lancelot, J., Vitrac, A. and Allegre, C.J. (1976). 'Uranium and lead isotopic dating with grain-by-grain zircon analysis: a study of complex geological history with a single rock'. Earth and Planetary Science Letters, 29(2), pp.357-366.

Liu, C., Zhao, G. and Liu, F. (2014) 'Detrital zircon U–Pb, Hf isotopes, detrital rutile and whole-rock geochemistry of the Huade Group on the northern margin of the North China Craton: Implications on the breakup of the Columbia supercontinent', Precambrian Research, 254, pp. 290–305. doi: 10.1016/j.precamres.2014.09.011.

Luvizotto, G. L., Zack, T., Meyer, H. P., Ludwig, T., Triebold, S., Kronz, A., Munker, C., Stockli, D. F., Prowatke, S., Klemme, S., Jacob, D. E. and von Eynatten, H. (2009) 'Rutile crystals as potential trace element and isotope mineral standards for microanalysis', Chemical Geology, 261(3–4), pp. 346–369. doi: 10.1016/j.chemgeo.2008.04.012.

Malusà, M. G., Resentini, A. and Garzanti, E. (2016) 'Hydraulic sorting and mineral fertility bias in detrital geochronology', Gondwana Research, 31, pp. 1–19. doi: 10.1016/j.gr.2015.09.002.

Mange, M., and Maurer, H., 1992, Heavy minerals in colour: London, Chapman and Hall, 147 p.

Manzotti, P., Poujol, M. and Ballèvre, M. (2014) 'Detrital zircon geochronology in blueschist-facies meta-conglomerates from the Western Alps: implications for the late Carboniferous to early Permian palaeogeography', International Journal of Earth Sciences, pp. 703–731. doi: 10.1007/s00531-014-1104-8.

McAteer, C. A., Daly, J. S., Flowerdew, M. J., Connelly, J. N., Housh, T. B. and Whitehouse, M. J. (2010) 'Detrital zircon, detrital titanite and igneous clast U-Pb geochronology and basement-cover relationships of the Colonsay Group, SW Scotland: Laurentian provenance and correlation with the Neoproterozoic Dalradian Supergroup', Precambrian Research, 181(1–4), pp. 21–42. doi: 10.1016/j.precamres.2010.05.013.

Meinhold, G. (2010) 'Rutile and its applications in earth sciences', Earth-Science Reviews, 102 (1–2), pp. 1–28. doi: 10.1016/j.earscirev.2010.06.001.

Meinhold, G., Anders, B., Kostopoulos, D. and Reischmann, T. (2008) 'Rutile chemistry and thermometry as provenance indicator: An example from Chios Island, Greece', Sedimentary Geology, 203, pp. 98–111. doi: 10.1016/j.sedgeo.2007.11.004.

Moecher, D., Hietpas, J., Samson, S. and Chakraborty, S. (2011) 'Insights into southern Appalachian tectonics from ages of detrital monazite and zircon in modern alluvium', Geosphere, 7(2), pp. 494–512. doi: 10.1130/GES00615.1.

Moecher, D. P. and Samson, S. D. (2006) 'Differential zircon fertility of source terranes and natural bias in the detrital zircon record: Implications for sedimentary provenance analysis', Earth and Planetary Science Letters, 247, pp. 252–266. doi: 10.1016/j.epsl.2006.04.035.
Morton, A. C. and Hallsworth, C. R. (1999) 'Processes controlling the composition of heavy mineral assemblages in sandstones', Sedimentary Geology, 124, pp. 3–29. doi: 10.1016/S0037-0738(98)00118-3.

Nutman, A. P. (2007) 'Apatite recrystallisation during prograde metamorphism, Cooma, southeast Australia: implications for using an apatite – graphite association as a biotracer in ancient metasedimentary rocks', Australian Journal of Earth Sciences, 54, pp. 1023–1032. doi: 10.1080/08120090701488321.

O'Sullivan, G. J., Chew, D. M. and Samson, S. D. (2016) 'Detecting magma-poor orogens in the detrital record', Geology, pp. 1–4. doi: 10.1130/G38245.1.

O'Sullivan, G. J., Chew, D. M., Morton, A. C., Mark, C. and Henrichs, I. A. (2018) 'An Integrated Apatite Geochronology and Geochemistry Tool for Sedimentary Provenance Analysis', *Geochemistry, Geophysics, Geosystems*, pp. 1309–1326. doi: 10.1002/2017GC007343.

Pettijohn, F. J. (1941) 'Persistence of Heavy Minerals and Geologic Age'. The Journal of Geology, Vol. 49, No. 6, pp. 610-625

Piccoli, P. M. and Candela, P. A. (2002) 'Apatite in Igneous Systems', Reviews in Mineralogy and Geochemistry, 48, pp. 255–292. doi: 10.2138/rmg.2002.48.6.

Resentini, A., Malusà, M. G. and Garzanti, E. (2013) 'MinSORTING: An Excel® worksheet for modelling mineral grain-size distribution in sediments, with application to detrital geochronology and provenance studies', Computers and Geosciences, 59, pp. 90–97. doi: 10.1016/j.cageo.2013.05.015.

Rubey, W.W., (1933). ‘The size distribution of heavy minerals within a water-laid sandstone’. Journal of Sedimentary Research, 3(1), pp.3–29.

Sha, L.-K. and Chappell, B. W. (1999) ‘Apatite chemical composition, determined by electron microprobe and laser-ablation inductively coupled plasma mass spectrometry, as a probe into granite petrogenesis’, Geochimica et Cosmochimica Acta, 63(22), pp. 3861–3881. doi: 10.1016/S0016-7037(99)00210-0.

Spear, F. S. and Pyle, J. M. (2002) ‘Apatite, Monazite, and Xenotime in Metamorphic Rocks’, Reviews in Mineralogy and Geochemistry, 48, pp. 293–335. doi: 10.2138/rmg.2002.48.7.

Stuart, F.M., (2002) ‘The exhumation history of orogenic belts from Ar-40/Ar-39 ages of detrital micas’. *Mineralogical Magazine*, 66(February), pp.121–135. doi: 10.1180/0026461026610017

Tang, M., Wang, X. L., Xu, X. S., Zhu, C., Cheng, T. and Yu, Y. (2012) ‘Neoproterozoic subducted materials in the generation of Mesozoic Luzong volcanic rocks: Evidence from apatite geochemistry and Hf-Nd isotopic decoupling’, Gondwana Research, 21(1), pp. 266–280. doi: 10.1016/j.gr.2011.05.009.

Thomson, S. N., Gehrels, G. E., Ruiz, J. and Buchwaldt, R. (2012) ‘Routine low-damage apatite U-Pb dating using laser ablation-multicollector- ICPMS’, Geochemistry, Geophysics, Geosystems, 13(1), pp. 1–23. doi: 10.1029/2011GC003928.

Thomas, W. A. (2011) ‘Detrital zircon geochronology and sedimentary provenance’, *Lithosphere*, 3(4), pp. 304–308. doi: 10.1130/RF.L001.1.

Triebold, S., von Eynatten, H., Luvizotto, G. L. and Zack, T. (2007) ‘Deducing source rock lithology from detrital rutile geochemistry: An example from the Erzgebirge, Germany’, Chemical Geology, 244, pp. 421–436. doi: 10.1016/j.chemgeo.2007.06.033.

Vermeesch, P., Rittner, M., Petrou, E., Omma, J., Mattinson, C. and Garzanti, E. (2017) ‘High Throughput Petrochronology and Sedimentary Provenance Analysis by Automated Phase Mapping and LAICPMS’, Geochemistry, Geophysics, Geosystems, 18(11), pp. 4096–4109. doi: 10.1002/2017GC007109.

Watson, E. B., Wark, D. A. and Thomas, J. B. (2006) 'Crystallization thermometers for zircon and rutile', Contributions to Mineralogy and Petrology, 151, pp. 413–433. doi: 10.1007/s00410-006-0068-5.

Weltje, G. J. and von Eynatten, H. (2004) 'Quantitative provenance analysis of sediments: Review and outlook', Sedimentary Geology, 171(1–4), pp. 1–11. doi: 10.1016/j.sedgeo.2004.05.007.

Zack, T., von Eynatten, H. and Kronz, A. (2004) 'Rutile geochemistry and its potential use in quantitative provenance studies', Sedimentary Geology, 171(1–4), pp. 37–58. doi: 10.1016/j.sedgeo.2004.05.009.

Chapter 2

Detecting magma-poor orogens in the detrital record

Published in *Geology*, 2016, *44*(10), p. 871-874

The text of this chapter is slightly longer than the published version because it has not been subject to final copy editing by the journal. It also incorporates minor corrections suggested by the examiners.

Co-authors: David M. Chew, Scott D. Samson

ABSTRACT

The clastic record is commonly interrogated by analysis of detrital heavy mineral assemblages, with the bulk of modern detrital geochronological studies employing U-Pb dating of detrital zircon. However, the bias of zircon towards felsic igneous sources, and the limited ability of the U-Pb system in zircon to record low- to medium-grade metamorphic events, means that the U-Pb detrital zircon record is largely insensitive to magma-poor orogens. In this study, U-Pb ages were obtained by LA-ICPMS for apatite and rutile extracted from alluvium of the French Broad River (FBR) in the southern Appalachians. In contrast to previously published U-Pb zircon datasets from the FBR which yield essentially *no record* of the most-recent Appalachian metamorphic events (c. 320 Ma) associated with assembly of Pangaea, the U-Pb detrital rutile and especially the U-Pb apatite systems together provide a *complete* record of complex polyphase Appalachian orogenesis. Unexpectedly, the apatite and rutile U-Pb Appalachian age populations differ significantly, with probable low-temperature breakdown of rutile biasing the rutile dataset towards the most recent (Alleghanian) metamorphic event. These data demonstrate dependence of provenance information on mineral proxy choice, and emphasise the resolving power of multi-proxy provenance studies.

2.1. INTRODUCTION

2.1.1 Heavy mineral provenance analysis and the U-Pb detrital zircon system

Heavy mineral provenance analysis is one of the key techniques by which the complex dynamic development of ancient orogens can be understood, as clastic sediments often represent the key archive of fossil orogenic belts (e.g., Najman, 2006). Detrital zircon continues to be the primary phase employed in U-Pb heavy mineral provenance studies (e.g. Thomas, 2011), which is due to both the ubiquity of zircon in clastic sediments, and because it typically exhibits high U and low common Pb contents resulting in relatively precise age determinations. However, there are several factors that hinder the ability of the U-Pb detrital zircon system to detect key tectonomagmatic events. These include: 1) the refractory behaviour of zircon in sedimentary and magmatic systems meaning that it seldom represents first-cycle detritus (e.g. Meinhold et al., 2011); 2) an inherent lithological bias towards felsic igneous sources (e.g. Moecher and Samson, 2006); and 3) extremely high closure temperatures with respect to Pb (> c. 900 °C), combined with the limited growth of new zircon below upper-amphibolite/eclogite facies conditions (typically restricted to 1-2μm overgrowths that are unlikely to survive transport in detrital systems; e.g. Hay and Dempster, 2009). These characteristics render the detrital U-Pb zircon system insensitive to tectonic events in orogens that have experienced low- to medium-grade metamorphism, as evidenced by the virtual absence of Alpine metamorphic zircon in the pro- and retro-foreland basins of the European Alps (e.g. Malusà et al., 2016; Mark et al., 2016): to the detrital zircon U-Pb record, the Alpine orogen is effectively invisible.

2.1.2 The advantages of apatite and rutile as heavy mineral provenance indicators

Apatite and rutile have many advantages as provenance indicators in sedimentary systems. For example, apatite crystallizes in a wider range of igneous rock types than zircon (basic through to felsic rock compositions) as the major rock-forming minerals cannot incorporate significant P in their crystal structure (Piccoli and Candela, 2002), and unlike zircon, apatite crystallizes in metamorphic rocks of all grades and most protolith types (Spear and Pyle, 2002). Rutile crystallizes in a more restricted suite of lithologies (medium- to high-grade pelites, psammites and metabasites, especially during HPLT subduction metamorphism, and some felsic plutonic rocks). The ability of apatite and rutile to crystallize in medium- to high-grade metamorphic rocks in a range of protolith

types make these systems well suited to detecting medium-temperature metamorphic events in orogenic belts. The temperature sensitivity (i.e. the temperature at which Pb-isotopes may become mobile in the mineral lattice) of the U-Pb system in these phases is 375-550°C and 490-640°C respectively (e.g. Cochrane et al., 2014; Kooijman et al., 2010)

Apatite also more likely represents *first-cycle* detritus than zircon due to its chemical instability during prolonged periods of alluvial storage in humid climates or extensive tropical weathering at source (Morton and Hallsworth, 1999 and references therein). Apatite is, however, reasonably physically and chemically resilient during transport and diagenesis in temperate conditions. Coupled with work linking the trace-element composition of apatite to specific igneous source rock compositions (e.g. Belousova et al., 2002), recent advances in U-Pb dating of common Pb-bearing minerals (Thomson et al., 2012; Chew et al., 2014), and integration with the long-established apatite fission-track and (U-Th-Sm)/He methods, apatite has widespread application as a predominantly first-cycle, *triply-dateable* provenance proxy (e.g. Carappa et al., 2009; Zattin et al., 2012) with trace-element characteristics than can be linked back to the source rock protolith.

Rutile, the most common and stable TiO_2 polymorph, is hyperstable in sedimentary systems, helping define a zircon-tourmaline-rutile (ZTR) assemblage characteristic of the most evolved detrital heavy mineral assemblages. Rutile exhibits the unusual combination of chemical and physical stability at both surface and high-grade metamorphic conditions, but instability at greenschist-facies conditions (Zack et al., 2004; Luvizotto et al., 2009b). In comparison with apatite, rutile generally exhibits higher U contents (see supplementary data tables for this paper) and is therefore often more amenable to precise U-Pb dating. The trace-element geochemistry (in particular, Fe content and Cr/Nb ratio) of rutile can be linked to derivation from pelitic, metabasic or felsic-igneous protoliths (Zack et al., 2004; Meinhold et al., 2008; Triebold et al., 2012).

2.2. GEOLOGICAL BACKGROUND

The studies of Hietpas et al. (2010) and Moecher et al. (2011) on modern alluvium from the French Broad River (FBR) in the southern Appalachians have established that the U-Pb detrital monazite system preserved a more complete record of Appalachian orogenesis

than the U-Pb detrital zircon system. In particular, the detrital zircon record completely fails to record the culmination of Appalachian Orogenesis, responsible for the formation of the supercontinent Pangea (c. 320 Ma, the Alleghanian orogeny). Here, the same sample suites of Hietpas et al. (2010) and Moecher et al. (2011) were utilised to investigate the efficacy of the detrital apatite and rutile U-Pb systems for detecting orogenesis in magma-poor collisional mountain belts. The existing U-Pb detrital zircon and monazite datasets make an ideal framework with which to compare the U-Pb apatite and rutile data generated by this study. The addition of these data make the FBR one of the best characterised modern fluvial systems in terms of multi-method U-Pb accessory-mineral geochronology.

2.2.1 Regional Geology

The regional geology of the FBR catchment is complex, and the terrane-scale description below is only a brief synopsis of the polyphase orogenic events captured by the detrital heavy mineral U-Pb data (see Moecher et al. (2011) and references therein for a detailed discussion).

The study area comprises the c. 12,000km^2 catchment of the FBR in North Carolina and Tennessee. It is an orogen-perpendicular river system that samples detritus from polymetamorphic Laurentian terranes (Bream et al., 2004) of diverse metamorphic grades, lithological compositions and apparent ages (both in terms of protolith and the timing of orogenesis), which are separated by several major shear zones active throughout the Palaeozoic. Dominant lithologies in the catchment of the FBR include felsic and mafic orthogneisses, and metasedimentary schists and paragneisses. As the river flows northwest it bisects the Appalachian chain, sampling terranes that achieved progressively lower peak-metamorphic grade during the Paleozoic, ultimately flowing over the anchimetamorphic rocks of the Valley and Ridge province (Cambro-Ordovician sedimentary rocks which formed the Laurentian passive margin).

The crust in the FBR catchment has experienced four main orogenic episodes that are all detected in the U-Pb detrital apatite and rutile data. These include the c. 1 Ga Grenville Orogeny which is inferred to form much of the crystalline basement in the region, but represents only about 12% of the exposed crust in the watershed, and three Paleozoic orogens (the Taconic, the Acadian and the Alleghanian) that together define the Appalachian Mountains (Moecher and Samson, 2006).

The Taconic Orogeny (c. 470-440 Ma) formed from the collision of the Taconic Arc with the Laurentian margin, resulting in upper amphibolite-facies (and local granulite-facies) regional metamorphism with extensive anatexis, migmatisation and pluton emplacement (Hatcher, 2010). The Acadian Orogeny (c. 420-380 Ma) resulted from collision between Avalonia and associated terranes, and the post-Taconic Laurentian margin (Hatcher, 2010). Finally, the Alleghanian Orogeny (c. 320-290 Ma) formed as a result of the collision of Laurussia (post-Acadian Laurentia plus Baltica) with Gondwana, forming the supercontinent of Pangea (Hatcher, 2010).

With each successive Paleozoic collision, new terranes were accreted to the eastern margin of Laurentia, stepwise moving the metamorphic front to the east with each successive terrane accretion. As a result there is a decrease in the regional Paleozoic metamorphic grade from upper-amphibolite facies in the SE to sub-greenschist to the NW of the study area (Carpenter, 1970). It should be emphasized however that the regional metamorphic history is complex with pervasive overprinting and multiple retrogressive episodes (Massey and Moecher, 2005). The Acadian and Alleghanian orogenic episodes strongly deformed rocks in the region but were not characterized by *significant* plutonism, nor did they attain the peak metamorphic temperatures experienced by the Taconic orogen in the southern Appalachians, especially west of the Brevard Fault Zone (Dennis, 2007). Acadian and Alleghanian peak metamorphic conditions were sufficient to either neocrystallize monazite, or reset the U-Pb ages of older monazite, in the Western Inner Piedmont (Fig. 1). However, to the west in the Eastern Blue Ridge (Fig. 1), the lower Acadian and Alleghanian peak metamorphic temperatures resulted in minimal new monazite growth. Thus, the majority of monazite ages reflect Taconic orogenesis (Hietpas et al., 2010).

2.3. METHODS

Heavy-mineral separates collected by Hietpas et al. (2010) were re-processed using standard mineral-separation techniques to produce apatite- and rutile-mineral fractions. All grains were analyzed using a Photon Machines Analyte Exite ArF Excimer laser-ablation system coupled to a Thermo Scientific iCAP-Qc ICPMS at Trinity College Dublin. Recently developed matrix-matched standards (Madagascar apatite, Thomson et al., 2012; and McClure Mountain and Durango apatite; Schoene and Bowring, 2006; McDowell et al., 2005) were the primary and secondary apatite U-Pb age standards, respectively. Primary and secondary rutile U-Pb age standards were the R10, and R19

and RZ3 standards, respectively (Luvizotto et al., 2009b; Shi et al., 2012). Data reduction was undertaken using Iolite 3.1 using the VizualAge_UcomPbine Data Reduction Scheme (DRS) (Paton et al, 2011; Petrus and Kamber, 2012; Chew et al., 2014) which accounts for the presence of variable common Pb in the primary age standard and makes it possible to date those U-bearing phases that contain appreciable common-Pb. Common-Pb correction in the unknowns employed a starting estimate for the age of the unknown, calculating its corresponding $^{207}Pb/^{206}Pb$ initial ratio using the Stacey and Kramers (1975) terrestrial lead-evolution model and then adopting an iterative approach based on a ^{207}Pb-correction (Chew et al., 2011). A ^{207}Pb-correction means it is not possible to exclude U-Pb age data based upon discordance. All grains with ^{207}Pb-corrected age uncertainties either >25% or >100 Ma (2σ) were therefore excluded, similar to the procedure of Zattin et al. (2012) and Mark et al. (2016).

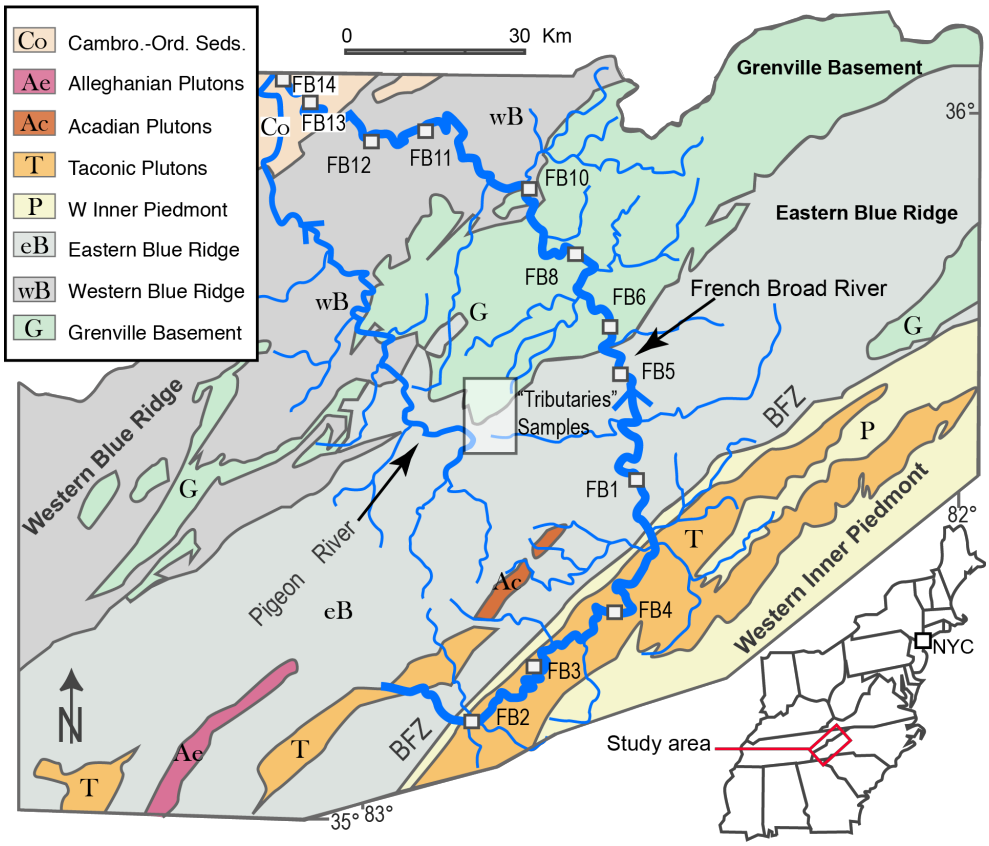

Figure 1. Geological map of the French Broad River catchment in western North Carolina with sample locations marked, modified from Moecher et al. (2011). BFZ = Brevard Fault Zone, Western Blue Ridge here defined = Great Smoky Group, Snowbird Group

2.4. RESULTS

The supplementary data tables for this publication (DR1 and DR2) can be found online at http://www.geosociety.org/pubs/ft2016.htm, or at the end of this chapter.

One disadvantage of U-Pb detrital rutile and apatite dating is the relatively high proportion of grains with low radiogenic (Pb*) to common (Pb_c) ratios. Because grains with low Pb^*/Pb_c are not uncommon in the dataset, particularly for the analysed detrital apatite, a high proportion of grains fail the age uncertainty rejection criteria, and are thus excluded from the data set. In this study 11% of the rutile ages and 42% of the apatite ages were rejected. While other provenance studies may yield detrital rutile and apatite with higher Pb^*/Pb_c, it is recommended that in detrital apatite U-Pb dating studies a large initial number of crystals be included per sample in case a significant proportion of analysed yield no useful age data (c.f. Zattin et al., 2012; Mark et al., 2016).

2.4.1 Constraining the timing of Appalachian tectono-metamorphism

2.4.2.1 – Western Inner Piedmont (FB2,3,4)

Despite containing large plutonic bodies of Taconic age the lack of almost any apatite or rutile yielding Taconic (c. 470-440 Ma) U-Pb ages (Fig. 2A) implies that the Western Inner Piedmont was heated above the apatite and rutile partial Pb retention zone during post-Taconic deformation. The very high abundance of Acadian and Alleghanian rutile and apatite fits well with the observation that most of the mid- to late-Paleozoic detrital monazite occurs in alluvial samples in the western Inner Piedmont (Hietpas et al., 2010; Moecher et al., 2011). The dearth of Alleghanian zircon in this region (Fig. 3; Hietpas et al., 2010) is consistent with a lack of widespread anatexis.

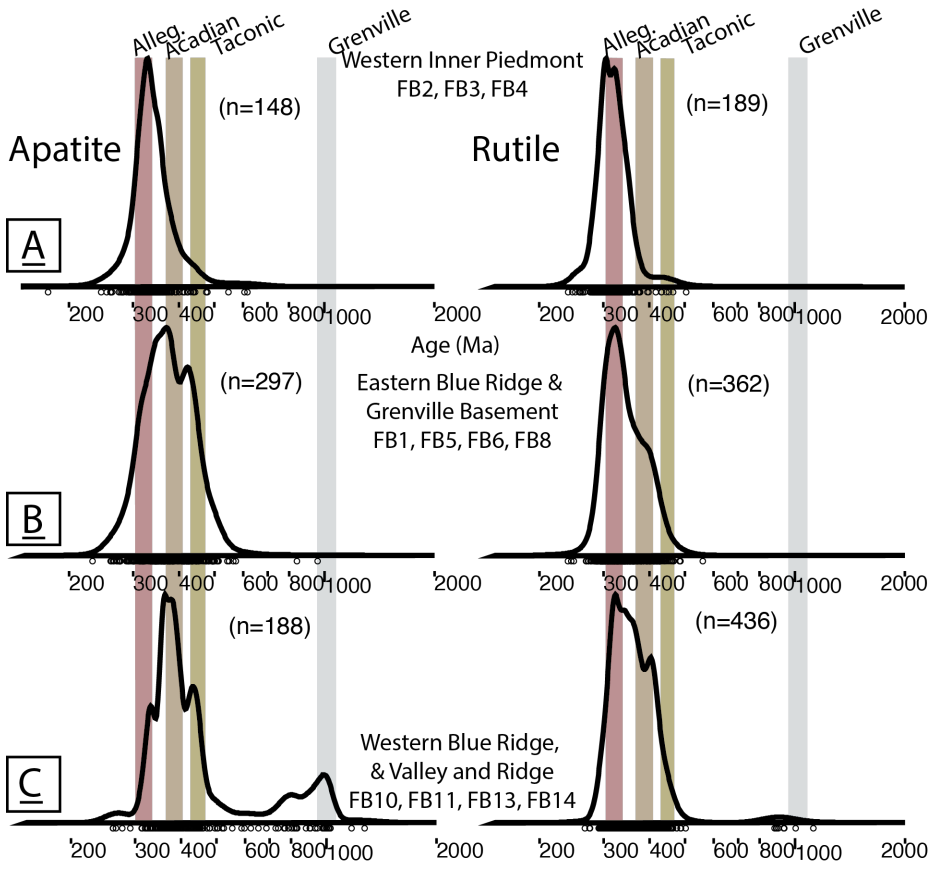

Figure 2. French Broad River detrital apatite and rutile U-Pb data with samples grouped according to geographical distribution and basement affinity. Horizontal scale (^{207}Pb-corrected age) is logarithmic. Coloured bars represent the duration of orogens as described in section 2.2.

2.4.2.2 – The Eastern Blue Ridge and Grenville Basement units (FB1,5,6,8)

An increasing proportion of Acadian *vs* Alleghanian apatite and rutile is encountered west of the Brevard Fault Zone (Fig. 2B). These data imply that during Alleghanian orogenesis temperatures were not high enough to reset Acadian (and older) apatite and rutile on a terrane-wide scale in the Eastern Blue Ridge and Grenville Basement units.

In this same region, Hietpas et al. (2010) documented homogenous Taconic monazite age populations in the westernmost East Blue Ridge "tributary" samples of the Canton Quadrangle. The limited amount of Taconic (c. 470-440 Ma) apatite and rutile (Fig. 2B) suggest that peak metamorphic temperatures during the Acadian Orogeny temperatures may have been high enough to recrystallize (or reset the U-Pb age of) Taconic and older rutile and to a lesser extent apatite, but too low to recrystallize monazite. This is supported by peak Acadian metamorphic assemblages, which range up to mid-amphibolite facies (Bream et al., 2004 and references therein).

2.4.2.3 – The Western Blue Ridge

In the Western Blue Ridge and the Valley and Ridge regions downstream of the internal portion of the orogenic belt, there is an appearance in the detrital dataset of pre-Phanerozoic apatite and rutile grains (Fig. 2C). Significant populations of Grenville-age apatite signify the capture of detritus from source regions that were not heated above the apatite U-Pb closure temperature (375-550°C) since the Grenville orogeny. Grenville apatite typically exhibits high ΣREE, high Th and low Sr contents, and a pronounced negative-Eu anomaly, which are all indicative of an unmetamorphosed felsic plutonic source (e.g. Belousova et al., 2002). The very low percentage of Grenville-age rutile in the dataset suggests that either there was minimal growth of rutile during the Grenville Orogeny, or that very low-grade metamorphic alteration of Grenville rutile occurred in the Western Blue Ridge and the Valley and Ridge during the Phanerozoic (see discussion). Phanerozoic-age apatite (in all samples) is depleted in Th and the LREE. This likely indicates growth synchronous with monazite or allanite during Appalachian metamorphism, and so the apatite trace-element data further confirm the greater significance of metamorphism versus plutonism during Appalachian orogenesis.

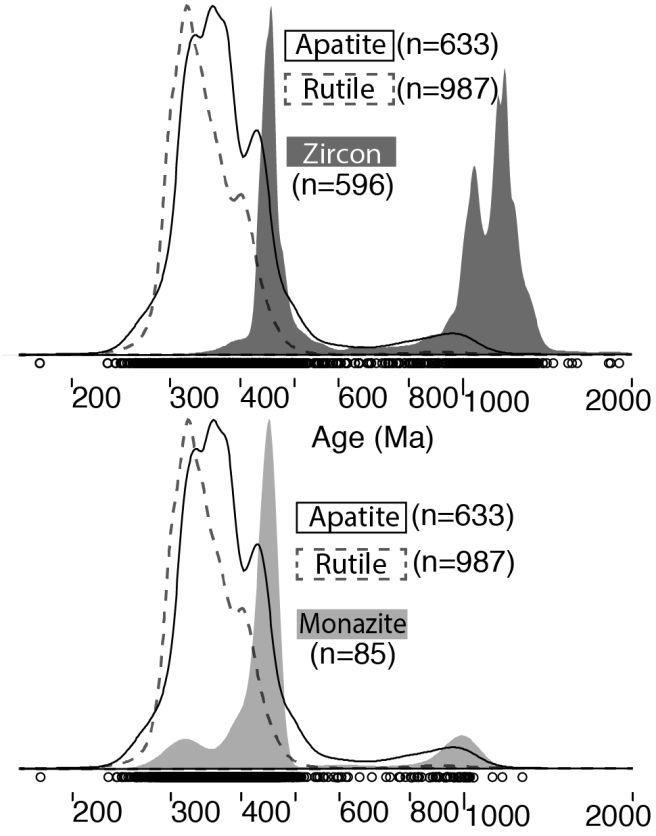

Figure 3. Kernel density estimate plots showing a comparison of detrital U-Pb apatite and rutile data with published detrital U-Pb zircon and monazite (Hietpas et al., 2010) data from the FBR. The U- Pb apatite system clearly records Grevillian orogenesis (c. 1 Ga) to a fuller extent than the U- Pb rutile system. A single U-Pb rim-age (318.4 ± 8.4 Ma) comprises the entire Alleghanian detrital zircon record (Hietpas et al., 2010).

2.5. DISCUSSION AND CONCLUSIONS

The major apatite and rutile U-Pb age peaks largely do not correspond to the main monazite and especially the zircon U-Pb age peaks, which are dominated by Grenville and Taconic zircon (Fig. 3). In contrast the U-Pb apatite and rutile age data more fully characterise the full duration of Appalachian orogenesis, particularly the Acadian and Alleghanian tectonic phases (Fig. 3). The insensitivity of the U-Pb detrital zircon system to magma-poor Acadian and Alleghanian orogenesis in the Southern Appalachians, a region central to the Paleozoic evolution of Laurentia, highlights the issue of the completeness of the detrital zircon record when investigating ancient orogenic systems; past orogenic episodes may be overlooked by narrowly focussing on the detrital zircon record.

In addition, this study highlights the divergence in behaviour between the apatite and rutile U-Pb systems, as the relative proportion of older apatite to rutile is greater in the detrital dataset (Fig. 3). Unexpectedly, the rutile dataset primarily records the youngest (Alleghanian) event, while the apatite dataset contains significantly more Acadian-, Taconic- and Grenville-age detritus despite the lower closure temperature (i.e. the temperature below which all radiogeneic Pb is retained in the crystalline lattice) of the U-Pb apatite system. This could be explained by rutile fertility differences between the various terranes, but it is also likely a result of low-temperature breakdown of rutile to other Ti-bearing phases during later low-grade metamorphic events (e.g. Triebold et al., 2012 and references therein). Crucially, low-grade alteration and breakdown of rutile results in the U-Pb rutile system being sensitive *only* to the most recent orogenic event in this segment of the Appalachian belt as rutile from older events is destroyed during each successive orogenic event.

Due to the different U-Pb temperature sensitivities, crystallization histories and fertility biases of different detrital chronometers, no single detrital phase can reliably capture the full scope of past geological events in complex, multiphase orogens such as the Appalachian or Alpine orogenic belts. Relying on a single detrital phase may misrepresent important geological events in certain tectonic settings, as demonstrated by the detrital zircon record of the FBR, which fails to detect the magma-poor Acadian and Alleghanian orogenic phases in this segment of the Appalachians. Therefore a *routine*

multi-mineral approach to accessory mineral chronometry is strongly recommended to more fully characterise the detrital record.

2.6. REFERENCES CITED

Belousova, E. A., Griffin, W. L., Reilly, S. Y., & Fisher, N. I. (2002). Apatite as an indicator mineral for mineral exploration: Trace-element compositions and their relationship to host rock type. Journal of Geochemical Exploration, 76, 45–69. doi:10.1016/S0375-6742(02)00204-2

Bream, B. R., Hatcher, R. D., Miller, C. F., & Fullagar, P. D. (2004). Detrital zircon ages and Nd isotopic data from the southern Appalachian crystallline core, Georgia, South Carolina, North Carolina, and Tennessee: New provenance constraints for part of the Laurentian margin. Geological Society of America Memoirs, 197, 459–475. doi:10.1130/0-8137-1197-5

Carpenter, R. H. (1970). Metamorphic history of the Blue Ridge province of Tennessee and North Carolina. Geological Society of America Bulletin, 81(3), 749-762.

Carrapa, B., DeCelles, P. G., Reiners, P. W., Gehrels, G. E., & Sudo, M. (2009). Apatite triple dating and white mica40Ar/39Ar thermochronology of syntectonic detritus in the Central Andes: A multiphase tectonothermal history. Geology, 37(5), 407–410. doi:10.1130/G25698A.1

Cochrane, R., Spikings, R. A., Chew, D., Wotzlaw, J. F., Chiaradia, M., Tyrrell, S., Schaltegger, U. & Van der Lelij, R. (2014). High temperature (>350°C) thermochronology and mechanisms of Pb loss in apatite. Geochimica et Cosmochimica Acta, 127, 39–56. doi:10.1016/j.gca.2013.11.028

Chew, D. M., Petrus, J. a., & Kamber, B. S. (2014). U-Pb LA-ICPMS dating using accessory mineral standards with variable common Pb. Chemical Geology, 363, 185–199. doi:10.1016/j.chemgeo.2013.11.006

Dennis, A. J. (2007). Cat Square basin, Catskill clastic wedge: Silurian-Devonian orogenic events in the central Appalachians and the crystalline southern Appalachians. Geological Society of America Special Papers, 433, 313-329.

Hay, D. C., & Dempster, T. J. (2009). Zircon behaviour during low-temperature metamorphism. Journal of Petrology, 50(4), 571–589. doi:10.1093/petrology/egp011

Hatcher Robert D., J., (2010). The Appalachian orogen: A brief summary, in: Tollo, R.P., Bartholomew, M.J., Hibbard, J.P., Karabinos, P.M. (Eds.), From Rodinia to Pangea: The Lithotectonic Record of the Appalachian Region. Geological Society of America.

Hietpas, J., Samson, S., Moecher, D., & Schmitt, A. K. (2010). Recovering tectonic events from the sedimentary record: Detrital monazite plays in high fidelity. *Geology*, *38*(2), 167–170. doi:10.1130/G30265.1

Kooijman, E., Mezger, K., & Berndt, J. (2010). Constraints on the U-Pb systematics of metamorphic rutile from in situ LA-ICP-MS analysis. Earth and Planetary Science Letters, 293(3-4), 321–330. doi:10.1016/j.epsl.2010.02.047

Luvizotto, G. L., Zack, T., Triebold, S., & Von Eynatten, H. (2009a). Rutile occurrence and trace element behavior in medium-grade metasedimentary rocks: Example from the Erzgebirge, Germany. Mineralogy and Petrology, 97(3-4), 233–249. doi:10.1007/s00710-009-0092-z

Luvizotto, G. L., Zack, T., Meyer, H. P., Ludwig, T., Triebold, S., Kronz, a., … von Eynatten, H. (2009b). Rutile crystals as potential trace element and isotope mineral standards for microanalysis. Chemical Geology, 261(3-4), 346–369. doi:10.1016/j.chemgeo.2008.04.012

Massey, M. A., & Moecher, D. P. (2005). Deformation and metamorphic history of the Western Blue Ridge-Eastern Blue Ridge terrane boundary, southern Appalachian Orogen. Tectonics, 24(5), 1–18. doi:10.1029/2004TC001643

Malusà, M. G., Anfinson, O. a., Dafov, L. N., & Stockli, D. F. (2016). Tracking Adria indentation beneath the Alps by detrital zircon U-Pb geochronology: Implications for the Oligocene–Miocene dynamics of the Adriatic microplate. Geology, 44(January), G37407.1. doi:10.1130/G37407.1

Mark, C., Cogné, N., and Chew, D. (2016) Tracking exhumation and drainage divide migration of the western Alps: a test of the apatite U-Pb thermochronometer as a detrital provenance tool. Geological Society of America Bulletin, 128 (9-10), p. 1439-1460, doi: 10.1130/B31351.1.

McDowell, F.W., McIntosh, W.C., and Farley, K. A., 2005, A precise 40Ar/39Ar reference age for the Durango apatite (U-Th)/He and fission-track dating standard: Chemical Geology, v. 214, p. 249–263, doi:10.1016/j.chemgeo.2004.10.002.

Meinhold, G., Anders, B., Kostopoulos, D., & Reischmann, T. (2008). Rutile chemistry and thermometry as provenance indicator: An example from Chios Island, Greece. Sedimentary Geology, 203, 98–111. doi:10.1016/j.sedgeo.2007.11.004

Meinhold, G., Morton, A. C., Fanning, C. M., Frei, D., Howard, J. P., Phillips, R. J., … Whitham, A. G. (2011). Evidence from detrital zircons for recycling of Mesoproterozoic and Neoproterozoic crust recorded in Paleozoic and Mesozoic sandstones of southern Libya. Earth and Planetary Science Letters, 312(1-2), 164–175. doi:10.1016/j.epsl.2011.09.056

Moecher, D., Hietpas, J., Samson, S., & Chakraborty, S. (2011). Insights into southern Appalachian tectonics from ages of detrital monazite and zircon in modern alluvium. *Geosphere*, *7*(2), 494–512. doi:10.1130/GES00615.1

Moecher, D. P., & Samson, S. D. (2006). Differential zircon fertility of source terranes and natural bias in the detrital zircon record: Implications for sedimentary provenance analysis. *Earth and Planetary Science Letters*, *247*, 252–266. doi:10.1016/j.epsl.2006.04.035

Najman, Y. (2006). The detrital record of orogenesis: A review of approaches and techniques used in the Himalayan sedimentary basins. Earth-Science Reviews, 74(1-2), 1–72. doi:10.1016/j.earscirev.2005.04.004

Paton, C., Hellstrom, J., Paul, B., Woodhead, J., and Hergt, J., 2011, Iolite: Freeware for the visualisation and processing of mass spectrometric data: Journal of Analytical Atomic Spectrometry, v. 26, p. 2508, doi: 10.1039/c1ja10172b.

Petrus, J. A., & Kamber, B. S. (2012). VizualAge: A Novel Approach to Laser Ablation ICP-MS U-Pb Geochronology Data Reduction. Geostandards and Geoanalytical Research, (1), 1–24. doi:10.1111/j.1751-908X.2012.00158.x

Piccoli, P. M., & Candela, P. A. (2002). Apatite in Igneous Systems. Reviews in Mineralogy and Geochemistry, 48, 255–292. doi:10.2138/rmg.2002.48.6

Schoene, B., Crowley, J. L., Condon, D. J., Schmitz, M. D., & Bowring, S. A. (2006). Reassessing the uranium decay constants for geochronology using ID-TIMS U-Pb data. Geochimica et Cosmochimica Acta, 70(2), 426–445. doi:10.1016/j.gca.2005.09.007

Shi, G., Li, X., Li, Q., Chen, Z., Deng, J., Liu, Y., Kang, Z., Pang, E., Xu, Y. & Jia, X. (2012). Ion Microprobe U-Pb age and Zr-in-Rutile thermometry of rutiles from the Daixian rutile deposit in the Hengshan Mountains, Shanxi Province, China. Economic Geology, 107, 525–535. doi:10.2113/econgeo.107.3.525

Spear, F. S., & Pyle, J. M. (2002). Apatite, Monazite, and Xenotime in Metamorphic Rocks. Reviews in Mineralogy and Geochemistry, 48, 293–335. doi:10.2138/rmg.2002.48.7

Stacey, J. T., & Kramers, J. (1975). Approximation of terrestrial lead isotope evolution by a two-stage model. Earth and Planetary Science Letters, 26(2), 207-221.

Thomas, W. A. (2011). Detrital-zircon geochronology and sedimentary provenance. Lithosphere, 3(4), 304–308. doi:10.1130/RF.L001.1

Thomson, S. N., Gehrels, G. E., Ruiz, J., & Buchwaldt, R. (2012). Routine low-damage apatite U-Pb dating using laser ablation-multicollector- ICPMS. Geochemistry, Geophysics, Geosystems, 13(1), 1–23. doi:10.1029/2011GC003928

Triebold, S., von Eynatten, H., & Zack, T. (2012). A recipe for the use of rutile in sedimentary provenance analysis. Sedimentary Geology, 282, 268–275. doi:10.1016/j.sedgeo.2012.09.008

Zack, T., von Eynatten, H., & Kronz, A. (2004). Rutile geochemistry and its potential use in quantitative provenance studies. Sedimentary Geology, 171(1-4), 37–58. doi:10.1016/j.sedgeo.2004.05.009

Zattin, M., Andreucci, B., Thomson, S. N., Reiners, P. W., & Talarico, F. M. (2012). New constraints on the provenance of the ANDRILL AND-2A succession (western Ross Sea, Antarctica) from apatite triple dating. Geochemistry, Geophysics, Geosystems, 13(10). doi:10.1029/2012GC004357

2.7 SUPPORTING AND SUPPLEMENTARY INFORAMTION

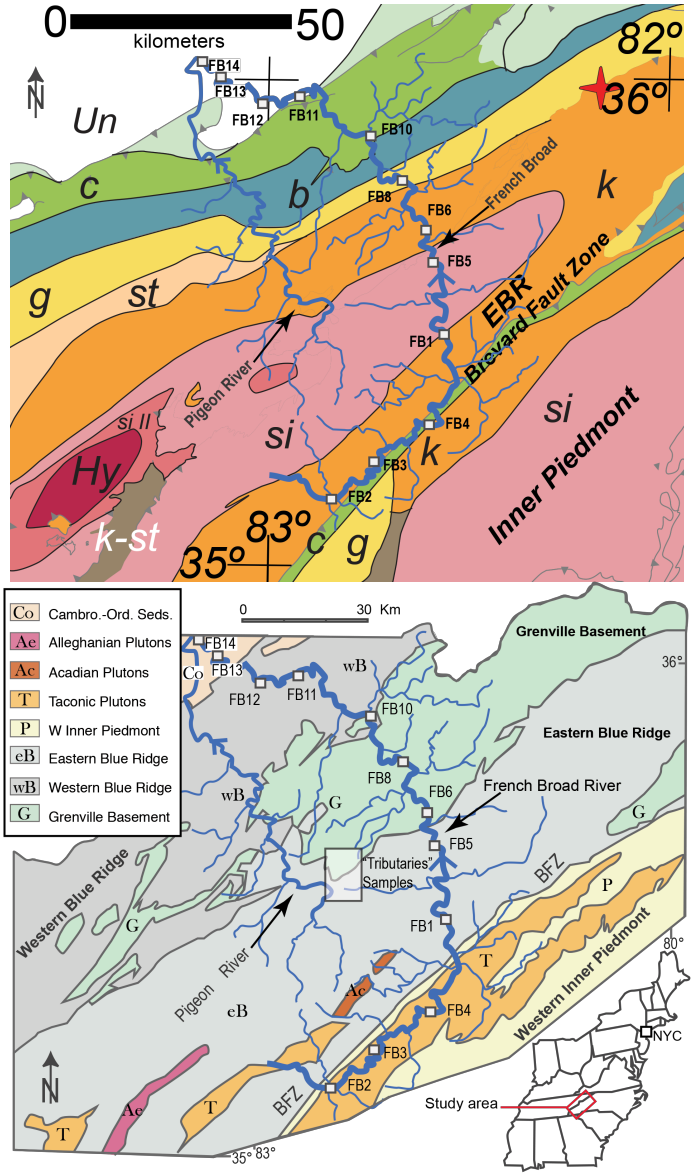

Figure S2.1. Metamorphic map of the study area modified from Merschat (2009). The geological map from the text is presented directly beneath for reference.

Key: Un = unmetamorphosed rocks; c = chlorite grade; b = biotite grade; g = garnet grade; st = staurolite grade; K = kyanite grade; K-st = kyanite-staurolite grade; si = silliminite grade; si II = silliminite 2 grade; Hy = hypersthene grade; red four-pointed star = eclogite facies rocks; EBR = Eastern Blue Ridge; BFZ = Brevard Fault Zone

Sample	Lat	Long
FB1	35.47938	82.5574
FB2	35.14553	82.8265
FB3	35.21752	82.72
FB4	35.29717	82.5809
FB5	35.62443	82.5985
FB6	35.6847	82.6172
FB8	35.79208	82.6695
FB10	35.89382	82.8226
FB11	35.91137	82.9893
FB13	35.9847	83.162
FB14	36.05	83.211

Table S2.1. Sample location coordiantes

Tables S.2.2 apatite U-Pb data tables

Apatite U-Pb and Trace element data - collected by LA-ICP-MS

	$^{207}Pb/^{235}U$	Prop2SE	$^{206}Pb/^{238}U$	Prop2SE	Rho	$^{238}U/^{206}Pb$	Prop2SE	$^{207}Pb/^{206}Pb$	Prop2SE	Rho	^{207}Pb corrected age	Prop2SE	$f^{206}Pb$
FB1ap_0	19.4	0.8	0.2152	0.0084	0.57	4.647	0.1814	0.653	0.016	0.47	344.9	31.3	0.74
FB1ap_1	60.7	2.5	0.56	0.022	0.24	1.786	0.0702	0.789	0.030	0.64	289.9	134.9	0.92
FB1ap_2	25.07	0.98	0.2657	0.0087	0.43	3.764	0.1232	0.685	0.017	0.31	361.2	38.9	0.78
FB1ap_3	41.62	1.4	0.4124	0.013	0.28	2.425	0.0764	0.735	0.015	0.60	408.3	53.6	0.84
FB1ap_4	23.05	0.81	0.2621	0.0079	0.39	3.815	0.1150	0.639	0.012	0.22	458.0	29.9	0.72
FB1ap_5	2250	230	18	1.7	0.94	0.056	0.0052	0.874	0.029	0.29	0.0	8668.5	1.00
FB1ap_6	80.7	2.9	0.745	0.026	0.56	1.342	0.0468	0.788	0.016	0.49	446.8	101.0	0.90
FB1ap_7	23.31	0.87	0.2467	0.0087	0.08	4.054	0.1429	0.692	0.021	0.43	318.0	43.4	0.80
FB1ap_8	24.18	0.91	0.2572	0.0088	0.39	3.888	0.1330	0.684	0.017	0.36	350.6	37.9	0.78
FB1ap_9	12.82	1.8	0.1599	0.018	0.78	6.254	0.7040	0.589	0.020	0.07	335.6	45.1	0.67
FB1ap_10	60	2.3	0.564	0.021	0.23	1.773	0.0660	0.773	0.024	0.65	387.8	109.0	0.89
FB1ap_11	13.24	0.53	0.1645	0.0056	0.39	6.079	0.2069	0.589	0.018	0.39	345.7	26.5	0.67
FB1ap_12	10.96	0.45	0.1454	0.0057	0.32	6.878	0.2696	0.552	0.018	0.55	347.6	24.8	0.62
FB1ap_13	25.4	1.3	0.2607	0.012	0.74	3.836	0.1766	0.708	0.019	0.11	301.8	43.0	0.82
FB1ap_14	32.15	1.2	0.3298	0.012	0.18	3.032	0.1103	0.711	0.021	0.58	384.6	57.2	0.81
FB1ap_15	15.86	0.65	0.1837	0.0065	0.52	5.444	0.1926	0.627	0.016	0.27	330.9	26.8	0.71
FB1ap_16	106.4	4.5	0.977	0.04	0.64	1.024	0.0419	0.795	0.020	0.45	608.3	155.6	0.90
FB1ap_17	3.31	0.12	0.0764	0.0026	0.35	13.089	0.4454	0.315	0.008	0.56	323.8	11.8	0.33
FB1ap_18	183.6	9.6	1.687	0.089	0.70	0.593	0.0313	0.798	0.020	0.04	1996.3	253.4	0.78
FB1ap_19	29.15	1.2	0.2995	0.012	0.33	3.339	0.1338	0.711	0.025	0.65	344.6	61.1	0.82
FB1ap_20	70.7	3.1	0.667	0.027	0.68	1.499	0.0607	0.771	0.019	0.27	504.1	103.7	0.88
FB1ap_21	24.24	0.92	0.2703	0.0095	0.53	3.700	0.1300	0.652	0.015	0.41	444.1	36.5	0.74
FB1ap_22	17.97	0.74	0.1966	0.0069	0.54	5.086	0.1785	0.669	0.018	0.29	286.6	30.8	0.77
FB1ap_23	40.59	1.5	0.416	0.014	0.51	2.404	0.0809	0.709	0.015	0.46	512.2	53.9	0.80
FB1ap_24	31.47	1.2	0.3305	0.013	0.43	3.026	0.1190	0.695	0.021	0.63	432.3	57.5	0.79
FB1ap_25	4.22	0.16	0.0832	0.0026	0.57	12.019	0.3756	0.368	0.008	0.05	318.2	11.1	0.39
FB1ap_26	7.88	0.32	0.1141	0.0042	0.47	8.764	0.3226	0.502	0.014	0.38	316.6	17.3	0.56
FB1ap_27	57.2	2.3	0.536	0.02	0.81	1.866	0.0696	0.769	0.015	-0.01	384.3	70.1	0.89
FB1ap_28	236	9	2.063	0.076	0.69	0.485	0.0179	0.828	0.016	0.44	1528.9	249.6	0.87
FB1ap_29	61.2	2.2	0.578	0.019	0.20	1.730	0.0569	0.770	0.019	0.55	419.0	90.5	0.88
FB1ap_30	6.23	0.22	0.1169	0.0038	0.46	8.554	0.2781	0.387	0.008	0.44	430.0	15.8	0.41
FB1ap_31	39.4	1.5	0.3931	0.015	0.40	2.544	0.0971	0.731	0.020	0.50	400.0	65.2	0.84
FB1ap_32	24.85	0.93	0.2626	0.0098	0.35	3.808	0.1421	0.690	0.019	0.62	345.2	42.5	0.79
FB1ap_33	40.6	1.6	0.401	0.015	0.19	2.494	0.0933	0.740	0.026	0.62	376.1	83.7	0.85
FB1ap_34	24.45	1.1	0.2508	0.011	0.41	3.987	0.1749	0.714	0.025	0.57	276.0	51.9	0.83
FB1ap_35	31.4	3.8	0.317	0.036	0.83	3.155	0.3582	0.722	0.016	0.22	336.6	56.8	0.83
FB1ap_36	8.17	0.3	0.1194	0.0038	0.49	8.375	0.2665	0.494	0.009	0.27	339.1	14.3	0.55
FB1ap_37	77.1	3	0.731	0.026	0.60	1.368	0.0487	0.763	0.016	0.31	641.5	96.7	0.86
FB1ap_38	53.1	2	0.515	0.019	0.24	1.942	0.0716	0.752	0.022	0.62	452.1	91.4	0.86
FB1ap_39	7.43	0.3	0.1121	0.0038	0.40	8.921	0.3024	0.480	0.013	0.34	330.6	16.2	0.53
FB1ap_40	23.84	0.96	0.2621	0.0092	0.42	3.815	0.1339	0.660	0.018	0.40	411.7	40.5	0.75
FB1ap_41	20.2	1.1	0.2192	0.01	0.82	4.562	0.2081	0.669	0.017	0.08	322.3	34.0	0.77
FB1ap_42	47	3.2	0.459	0.027	0.81	2.179	0.1282	0.742	0.026	0.05	434.8	96.8	0.85
FB1ap_43	33.97	1.3	0.3579	0.012	0.56	2.794	0.0937	0.689	0.015	0.35	492.6	46.8	0.78
FB1ap_44	28.67	1	0.2906	0.0092	0.26	3.441	0.1089	0.717	0.017	0.47	317.7	42.4	0.83
FB1ap_45	73	4.8	0.697	0.037	0.54	1.435	0.0762	0.754	0.026	0.03	666.0	140.9	0.84
FB1ap_46	17.7	12	0.209	0.097	0.94	4.785	2.2206	0.628	0.033	-0.33	377.8	180.3	0.71
FB1ap_48	2770	210	23.6	1.9	0.95	0.042	0.0034	0.860	0.021	0.12	0.0	7855.3	1.00
FB1ap_49	95.5	4.2	0.87	0.035	0.53	1.149	0.0462	0.806	0.026	0.38	370.4	181.1	0.93
FB1ap_50	28.97	1.1	0.2992	0.011	0.19	3.342	0.1229	0.706	0.021	0.60	357.4	52.2	0.81
FB1ap_51	60.8	3.9	0.572	0.032	0.43	1.748	0.0978	0.787	0.044	0.47	310.7	197.8	0.91
FB1ap_52	36.3	1.5	0.3541	0.013	0.39	2.824	0.1037	0.747	0.025	0.52	301.6	72.1	0.86
FB1ap_53	19.75	0.72	0.2232	0.0076	0.39	4.480	0.1526	0.639	0.014	0.52	384.9	29.0	0.72
FB1ap_54	285	16	2.46	0.13	0.88	0.407	0.0215	0.834	0.019	0.22	2376.9	371.1	0.82
FB1ap_55	34.09	1.3	0.3451	0.013	0.42	2.898	0.1092	0.720	0.019	0.55	377.4	55.1	0.83
FB1ap_56	206	7.9	1.828	0.072	0.62	0.547	0.0215	0.820	0.020	0.60	1399.7	266.1	0.87
FB1ap_57	37.3	1.6	0.3711	0.014	0.21	2.695	0.1017	0.734	0.028	0.54	363.4	83.1	0.84
FB1ap_58	23.75	0.9	0.2596	0.0091	0.42	3.852	0.1350	0.665	0.016	0.48	396.3	36.7	0.76
FB1ap_59	3.32	0.16	0.0723	0.0027	0.67	13.831	0.5165	0.333	0.010	-0.08	296.2	12.4	0.35
FB1ap_60	64	2.7	0.591	0.024	0.62	1.692	0.0687	0.787	0.022	0.41	325.0	106.9	0.91
FB1ap_61	10.95	0.44	0.1485	0.0053	0.54	6.734	0.2403	0.535	0.013	0.31	375.5	20.6	0.60
FB1ap_62	27.9	1.4	0.3	0.013	0.82	3.333	0.1444	0.673	0.014	0.13	444.5	39.7	0.76
FB1ap_63	51.6	2.2	0.501	0.019	0.44	1.996	0.0757	0.751	0.023	0.44	441.3	92.7	0.86
FB1ap_64	19.54	0.81	0.2126	0.0079	0.49	4.704	0.1748	0.669	0.019	0.43	311.8	34.9	0.77
FB1ap_65	21.43	0.87	0.2356	0.0087	0.23	4.244	0.1567	0.662	0.022	0.55	362.5	43.3	0.75
FB1ap_66	25.76	1	0.2702	0.0099	0.52	3.701	0.1356	0.693	0.017	0.47	349.3	39.9	0.79
FB1ap_67	11.11	0.45	0.1444	0.0054	0.47	6.925	0.2590	0.554	0.017	0.32	342.8	23.4	0.62
FB1ap_68	18.94	0.73	0.2138	0.0076	0.34	4.677	0.1663	0.649	0.019	0.42	349.7	35.0	0.74
FB1ap_69	7.88	0.29	0.1193	0.004	0.30	8.382	0.2810	0.480	0.012	0.51	352.2	16.5	0.53
FB1ap_70	13.26	0.53	0.1647	0.0054	0.51	6.072	0.1991	0.582	0.015	0.29	355.5	23.2	0.66
FB1ap_71	58.7	2.3	0.549	0.021	0.09	1.821	0.0697	0.782	0.027	0.66	322.7	119.3	0.91
FB1ap_72	34.82	1.3	0.342	0.012	0.43	2.924	0.1026	0.736	0.019	0.44	324.0	54.7	0.85
FB1ap_73	27.65	1.1	0.2902	0.01	0.42	3.446	0.1187	0.692	0.018	0.44	380.8	44.4	0.79
FB1ap_74	39.7	1.6	0.41	0.016	-0.07	2.439	0.0952	0.708	0.026	0.77	507.2	84.4	0.80
FB1ap_75	35.03	1.3	0.3503	0.012	0.37	2.855	0.0978	0.726	0.018	0.44	365.0	53.3	0.83
FB1ap_76	232	8.5	2.037	0.076	0.55	0.491	0.0183	0.829	0.019	0.58	1375.8	284.7	0.88
FB1ap_77	18.08	0.69	0.2051	0.0071	0.30	4.876	0.1688	0.641	0.018	0.49	348.1	32.2	0.73
FB1ap_78	71	2.7	0.663	0.024	0.41	1.508	0.0546	0.780	0.022	0.55	434.3	117.6	0.89
FB1ap_79	36.01	1.3	0.3555	0.012	0.31	2.813	0.0950	0.736	0.019	0.53	339.0	56.6	0.85
FB1ap_80	39.4	1.6	0.394	0.015	0.48	2.538	0.0966	0.722	0.019	0.46	433.7	62.4	0.82
FB1ap_81	29.74	1	0.307	0.011	0.09	3.257	0.1167	0.700	0.018	0.75	384.2	47.0	0.80
FB1ap_82	62.9	2.2	0.587	0.019	0.52	1.704	0.0551	0.781	0.015	0.33	359.7	76.6	0.90
FB1ap_83	5.81	0.24	0.0958	0.0031	0.44	10.438	0.3378	0.438	0.012	0.16	313.8	13.7	0.48
FB1ap_84	14.54	0.65	0.1751	0.0063	0.54	5.711	0.2055	0.603	0.017	0.19	349.1	27.1	0.68
FB1ap_86	207	10	1.82	0.078	0.73	0.549	0.0235	0.819	0.023	0.24	1432.5	298.3	0.86
FB1ap_87	54.5	2.1	0.54	0.021	0.62	1.852	0.0720	0.735	0.018	0.46	571.3	80.2	0.83

Tables S.2.2 apatite U-Pb data tables (continued)

	$^{207}Pb/^{235}U$	Prop2SE	$^{206}Pb/^{238}U$	Prop2SE	Rho	$^{238}U/^{206}Pb$	Prop2SE	$^{207}Pb/^{206}Pb$	Prop2SE	Rho	^{207}Pb corrected age	Prop2SE	$f^{206}Pb$
FB1ap_88	27.72	1	0.3016	0.01	0.66	3.316	0.1099	0.663	0.013	0.34	473.0	36.2	0.75
FB1ap_89	32.33	1.2	0.3258	0.012	0.24	3.069	0.1131	0.723	0.022	0.68	344.4	59.1	0.83
FB1ap_90	34.41	1.3	0.3475	0.012	0.65	2.878	0.0994	0.719	0.018	0.22	383.6	52.8	0.82
FB1ap_91	17.51	0.63	0.2123	0.0069	0.64	4.710	0.1531	0.599	0.013	0.36	434.8	26.7	0.67
FB1ap_92	13.58	0.52	0.1641	0.0057	0.24	6.094	0.2117	0.597	0.015	0.50	334.1	23.3	0.68
FB1ap_93	116	4.7	1.075	0.043	0.62	0.930	0.0372	0.785	0.020	0.45	883.9	165.1	0.86
FB1ap_94	3.61	0.14	0.0786	0.0028	0.49	12.723	0.4532	0.336	0.010	0.30	320.3	12.8	0.35
FB1ap_96	59.2	2.3	0.559	0.025	0.42	1.789	0.0800	0.770	0.028	0.65	400.5	124.3	0.89
FB1ap_97	9.89	0.43	0.1479	0.0055	0.28	6.761	0.2514	0.486	0.018	0.48	431.5	26.0	0.53
FB1ap_98	650	32	5.58	0.26	0.79	0.179	0.0084	0.845	0.022	0.30	-10198.8	5685.2	1.00
FB1ap_99	39.69	1.4	0.4126	0.014	0.47	2.424	0.0822	0.698	0.015	0.43	548.2	53.5	0.78
FB1ap_100	13.32	0.88	0.164	0.0081	0.61	6.098	0.3012	0.590	0.021	0.10	343.3	32.0	0.67
FB1ap_101	17.97	0.7	0.2037	0.0075	0.49	4.909	0.1808	0.642	0.016	0.48	343.9	29.6	0.73
FB1ap_102	121.3	4.2	1.106	0.039	0.68	0.904	0.0319	0.794	0.013	0.62	788.0	122.4	0.88
FB1ap_103	36.3	1.5	0.3646	0.013	0.67	2.743	0.0978	0.727	0.016	0.13	379.2	50.5	0.83
FB1ap_104	168.6	6.7	1.469	0.058	0.57	0.681	0.0269	0.835	0.022	0.50	193.2	271.2	0.98
FB1ap_105	392.3	15	3.415	0.13	0.67	0.293	0.0111	0.836	0.020	0.58	-29.5	606.8	1.00
FB2ap_0	87	3.3	0.808	0.029	0.46	1.238	0.0444	0.784	0.018	0.45	546.9	118.7	0.89
FB2ap_2	102.7	5	0.906	0.04	0.71	1.104	0.0487	0.824	0.023	0.14	169.9	175.0	0.97
FB2ap_3	9.4	0.46	0.1252	0.0055	0.53	7.987	0.3509	0.548	0.020	0.32	301.9	23.9	0.62
FB2ap_4	3.33	0.23	0.0731	0.0043	0.59	13.680	0.8047	0.334	0.017	0.15	298.9	19.9	0.35
FB2ap_5	40.7	1.7	0.408	0.016	0.51	2.481	0.0985	0.736	0.021	0.49	393.4	69.7	0.84
FB2ap_6	26.5	1.3	0.266	0.013	0.63	3.759	0.1837	0.723	0.023	0.43	273.6	51.4	0.84
FB2ap_7	2.606	0.11	0.0689	0.0027	0.38	14.514	0.5688	0.276	0.008	0.47	313.0	12.9	0.28
FB2ap_8	73	6.1	0.653	0.045	0.58	1.531	0.1055	0.821	0.053	0.16	118.5	279.7	0.97
FB2ap_9	7.01	0.3	0.1057	0.0038	0.34	9.461	0.3401	0.483	0.015	0.36	308.9	16.8	0.54
FB2ap_10	5.93	0.29	0.102	0.0038	0.60	9.804	0.3652	0.420	0.013	0.02	348.7	16.6	0.46
FB2ap_11	74.4	3.4	0.676	0.029	0.43	1.479	0.0635	0.804	0.029	0.42	261.7	158.6	0.94
FB2ap_12	361	21	3.23	0.16	0.72	0.310	0.0153	0.814	0.028	0.19	1419.0	675.6	0.92
FB2ap_13	195.6	10	1.691	0.076	0.62	0.591	0.0266	0.837	0.031	0.26	272.6	419.6	0.97
FB2ap_14	3.65	0.16	0.0797	0.0033	0.49	12.547	0.5195	0.337	0.011	0.35	324.0	14.9	0.35
FB2ap_15	112.8	6.5	1.002	0.055	0.83	0.998	0.0548	0.821	0.025	0.18	256.3	205.5	0.96
FB2ap_16	4.28	0.2	0.0831	0.0033	0.44	12.034	0.4779	0.375	0.013	0.38	313.1	15.0	0.40
FB2ap_17	73.5	6.8	0.669	0.053	0.88	1.495	0.1184	0.785	0.033	0.06	402.8	174.9	0.90
FB2ap_18	17.5	1.7	0.199	0.015	0.95	5.025	0.3788	0.627	0.023	-0.50	360.2	45.0	0.71
FB2ap_19	12.4	2.8	0.167	0.029	0.97	5.988	1.0398	0.523	0.042	-0.24	439.9	91.8	0.58
FB2ap_20	77	4.1	0.715	0.034	0.63	1.399	0.0665	0.779	0.029	0.27	493.3	161.8	0.89
FB2ap_21	58.6	4	0.553	0.033	0.79	1.808	0.1079	0.771	0.027	0.11	389.1	120.2	0.89
FB2ap_22	21.7	1.2	0.2384	0.011	0.76	4.195	0.1935	0.661	0.021	0.07	369.2	43.3	0.75
FB2ap_24	24.2	1.7	0.259	0.014	0.50	3.861	0.2087	0.702	0.045	1.00	313.1	92.4	0.81
FB2ap_25	29.6	1.3	0.2991	0.013	0.39	3.343	0.1453	0.722	0.026	0.37	315.0	63.6	0.83
FB2ap_26	63.2	3	0.583	0.026	0.46	1.715	0.0765	0.793	0.029	0.44	281.2	136.4	0.92
FB2ap_27	4.35	0.31	0.0834	0.0042	0.56	11.990	0.6038	0.376	0.020	0.09	313.6	20.3	0.40
FB2ap_28	14.03	0.73	0.1475	0.0072	0.09	6.780	0.3309	0.698	0.021	-0.01	175.3	27.1	0.81
FB2ap_29	29.8	1.6	0.301	0.014	0.42	3.322	0.1545	0.731	0.026	0.39	293.1	64.3	0.85
FB2ap_30	10.69	0.58	0.1369	0.0063	0.59	7.305	0.3362	0.569	0.023	0.25	307.8	28.6	0.64
FB2ap_31	7.24	0.38	0.1155	0.005	0.38	8.658	0.3748	0.453	0.018	0.28	365.4	22.5	0.50
FB2ap_32	36	1.7	0.351	0.014	0.52	2.849	0.1136	0.748	0.025	0.27	295.3	71.7	0.87
FB2ap_33	17.05	0.76	0.1965	0.0079	0.70	5.089	0.2046	0.630	0.015	0.15	350.5	28.0	0.72
FB2ap_34	51.8	2.5	0.491	0.023	0.52	2.037	0.0954	0.765	0.028	0.47	362.4	110.1	0.88
FB2ap_35	45.2	2.2	0.433	0.02	0.62	2.309	0.1067	0.763	0.025	0.31	317.7	88.3	0.88
FB2ap_36	23.96	1.2	0.2488	0.011	0.38	4.019	0.1777	0.697	0.025	0.44	310.2	51.5	0.80
FB2ap_37	170	6.7	1.511	0.063	0.44	0.662	0.0276	0.819	0.023	0.62	797.6	263.9	0.91
FB2ap_38	36.6	1.9	0.365	0.016	0.59	2.740	0.1201	0.732	0.025	0.33	363.0	74.2	0.84
FB2ap_39	76.6	2.9	0.705	0.027	0.52	1.418	0.0543	0.793	0.019	0.55	370.2	111.5	0.92
FB2ap_40	105.3	8.1	0.953	0.066	0.81	1.049	0.0727	0.805	0.035	0.13	450.1	259.1	0.92
FB2ap_41	54.5	3	0.518	0.025	0.39	1.931	0.0932	0.765	0.036	0.45	388.3	146.1	0.88
FB2ap_42	21.57	0.91	0.2356	0.0095	0.64	4.244	0.1711	0.666	0.017	0.33	354.5	35.7	0.76
FB2ap_43	15.11	0.83	0.1767	0.0082	0.41	5.659	0.2626	0.626	0.028	0.33	319.0	41.6	0.71
FB2ap_44	10.11	0.51	0.138	0.0056	0.65	7.246	0.2941	0.531	0.016	0.07	352.6	22.6	0.59
FB2ap_45	28.05	1.3	0.2823	0.011	0.47	3.542	0.1380	0.723	0.024	0.28	292.5	55.8	0.84
FB2ap_46	23.44	0.9	0.2474	0.0089	0.34	4.042	0.1454	0.688	0.017	0.57	327.5	36.7	0.79
FB2ap_47	1.929	0.085	0.0657	0.0025	0.55	15.221	0.5792	0.212	0.006	0.25	331.1	12.8	0.20
FB2ap_48	12.2	0.49	0.1478	0.006	0.36	6.766	0.2747	0.604	0.019	0.61	291.1	25.6	0.69
FB2ap_49	105.8	6	0.88	0.041	0.51	1.136	0.0529	0.869	0.035	0.26	-442.0	282.1	1.00
FB2ap_50	1.859	0.084	0.0634	0.0025	0.45	15.773	0.6220	0.214	0.008	0.27	318.8	13.0	0.20
FB2ap_51	11.7	0.58	0.1482	0.0065	0.28	6.748	0.2959	0.578	0.026	0.52	323.4	33.4	0.65
FB2ap_52	25.95	1.2	0.269	0.011	0.61	3.717	0.1520	0.702	0.021	0.26	326.6	47.6	0.81
FB2ap_53	37	1.8	0.364	0.017	0.43	2.747	0.1283	0.747	0.031	0.50	311.6	90.6	0.86
FB2ap_54	18.34	1.8	0.2119	0.017	0.59	4.719	0.3786	0.632	0.042	0.36	376.3	74.7	0.72
FB2ap_55	15.63	0.69	0.1716	0.0074	0.47	5.828	0.2513	0.665	0.023	0.51	253.7	33.7	0.77
FB2ap_56	3.12	0.14	0.0739	0.0029	0.62	13.532	0.5310	0.307	0.009	0.16	317.6	13.3	0.32
FB2ap_57	5.05	0.21	0.0907	0.0035	0.42	11.025	0.4255	0.402	0.011	0.38	322.7	14.7	0.43
FB2ap_58	132	8.2	1.155	0.063	0.59	0.866	0.0472	0.836	0.039	0.28	43.6	372.0	0.99
FB2ap_59	29.23	1.3	0.3005	0.013	0.44	3.328	0.1440	0.710	0.025	0.46	348.6	61.6	0.82
FB2ap_60	20.21	1	0.2228	0.0096	0.43	4.488	0.1934	0.656	0.025	0.34	352.4	46.5	0.75
FB2ap_61	24.9	1.5	0.262	0.013	0.46	3.817	0.1894	0.694	0.035	0.28	335.3	73.6	0.80
FB2ap_62	43.4	3.8	0.42	0.031	0.92	2.381	0.1757	0.741	0.024	-0.27	393.8	85.0	0.85
FB2ap_63	12.85	0.87	0.1656	0.01	0.63	6.039	0.3647	0.569	0.029	0.25	375.0	43.4	0.64
FB2ap_64	68.4	3.1	0.626	0.024	0.60	1.597	0.0612	0.795	0.022	0.15	296.9	113.7	0.92
FB2ap_65	8.81	0.4	0.1211	0.0048	0.55	8.258	0.3273	0.526	0.016	0.29	313.2	19.9	0.59
FB2ap_66	35.49	1.4	0.3298	0.013	0.29	3.032	0.1195	0.788	0.027	0.64	151.7	73.8	0.93
FB3ap_0	42.7	2.5	0.427	0.024	0.75	2.342	0.1316	0.732	0.026	0.32	437.9	90.1	0.84
FB3ap_1	72.6	3.4	0.642	0.029	0.18	1.558	0.0704	0.828	0.029	0.05	61.9	156.2	0.98
FB3ap_2	77	8.2	0.702	0.067	0.33	1.425	0.1360	0.773	0.036	0.08	527.2	197.9	0.88
FB3ap_3	98.8	3.5	0.897	0.032	0.78	1.115	0.0398	0.804	0.014	0.01	415.2	110.4	0.93

Tables S.2.2 apatite U-Pb data tables (continued)

	$^{207}Pb/^{235}U$	Prop2SE	$^{206}Pb/^{238}U$	Prop2SE	Rho	$^{238}U/^{206}Pb$	Prop2SE	$^{207}Pb/^{206}Pb$	Prop2SE	Rho	^{207}Pb corrected age	Prop2SE	$f^{206}Pb$
FB3ap_4	647	48	5.7	0.39	0.20	0.175	0.0120	0.843	0.026	-0.01	-6953.9	3994.9	1.00
FB3ap_5	19	2	0.216	0.018	0.67	4.630	0.3858	0.623	0.026	-0.09	400.2	54.6	0.70
FB3ap_6	23.52	0.99	0.2588	0.0099	-0.06	3.864	0.1478	0.658	0.026	0.54	410.4	54.7	0.75
FB3ap_7	18.09	0.75	0.2006	0.0082	0.53	4.985	0.2038	0.658	0.018	0.48	311.5	32.1	0.75
FB3ap_8	4.48	0.26	0.0866	0.0036	0.72	11.547	0.4800	0.371	0.013	-0.32	329.1	16.2	0.40
FB3ap_9	76.9	3.1	0.709	0.029	0.40	1.410	0.0577	0.789	0.022	0.57	406.2	126.5	0.91
FB3ap_10	4.023	0.15	0.084	0.0029	-0.03	11.905	0.4110	0.349	0.009	0.57	333.8	12.8	0.37
FB3ap_11	387	29	3.32	0.24	0.80	0.301	0.0218	0.856	0.027	0.02	-262.2	780.4	1.00
FB3ap_12	13.31	0.82	0.1702	0.0073	0.09	5.875	0.2520	0.583	0.028	-0.02	366.6	40.2	0.66
FB3ap_13	21.08	0.95	0.2323	0.0098	0.35	4.305	0.1816	0.665	0.023	0.51	351.1	44.9	0.76
FB3ap_14	82.3	3.6	0.764	0.032	0.51	1.309	0.0548	0.785	0.023	0.41	491.7	140.0	0.90
FB3ap_15	4.26	0.21	0.0857	0.0033	0.17	11.669	0.4493	0.362	0.012	-0.13	331.7	15.0	0.38
FB3ap_16	50.3	2.4	0.485	0.025	0.47	2.062	0.1063	0.740	0.025	-0.06	475.1	97.6	0.84
FB3ap_17	31.42	1.4	0.3158	0.013	0.81	3.167	0.1304	0.726	0.013	0.09	323.8	38.4	0.84
FB3ap_18	21.35	0.72	0.2229	0.0073	0.09	4.486	0.1469	0.696	0.011	0.02	276.9	24.1	0.80
FB3ap_19	150	6.7	1.395	0.08	0.48	0.717	0.0411	0.791	0.018	0.28	1384.8	195.3	0.83
FB3ap_20	1072	78	9.1	0.66	-0.02	0.110	0.0080	0.842	0.033	0.30	0.0	3219.0	1.00
FB3ap_21	21.9	2.5	0.2276	0.0097	0.22	4.394	0.1873	0.712	0.069	-0.03	251.9	123.5	0.82
FB3ap_22	57.6	2.5	0.547	0.023	0.64	1.828	0.0769	0.766	0.025	0.52	411.5	109.5	0.88
FB3ap_23	16.82	0.67	0.1814	0.0068	0.20	5.513	0.2066	0.671	0.019	0.62	260.0	30.0	0.77
FB3ap_24	10.33	0.45	0.127	0.005	0.42	7.874	0.3100	0.593	0.018	0.41	260.1	21.2	0.68
FB3ap_25	8.81	0.46	0.1208	0.0053	0.43	8.278	0.3632	0.528	0.018	0.32	310.5	22.0	0.59
FB3ap_26	28.25	1.1	0.291	0.012	-0.10	3.436	0.1417	0.704	0.026	0.39	351.5	61.6	0.81
FB3ap_27	11.3	1.3	0.1387	0.0048	-0.03	7.210	0.2495	0.591	0.057	0.08	287.2	62.3	0.67
FB3ap_28	208	10	1.854	0.089	0.84	0.539	0.0259	0.821	0.021	-0.17	1412.5	283.3	0.87
FB3ap_29	160	15	1.48	0.14	0.92	0.676	0.0639	0.785	0.029	0.03	1768.8	326.8	0.79
FB3ap_30	14.49	0.78	0.1743	0.0081	0.72	5.737	0.2666	0.604	0.018	0.10	346.0	29.8	0.68
FB3ap_31	30.8	1.8	0.324	0.015	-0.03	3.086	0.1429	0.692	0.020	0.01	431.2	55.2	0.79
FB3ap_32	16.98	0.7	0.1992	0.0076	0.36	5.020	0.1915	0.622	0.018	0.46	368.8	32.0	0.70
FB3ap_33	52.4	2.7	0.498	0.025	0.75	2.028	0.1029	0.769	0.022	0.27	344.6	89.6	0.89
FB3ap_34	2.352	0.11	0.0722	0.0025	0.40	13.850	0.4796	0.239	0.008	0.00	348.6	12.6	0.23
FB3ap_35	29.31	1.2	0.2803	0.01	0.00	3.568	0.1273	0.763	0.022	0.74	189.7	51.8	0.89
FB3ap_36	29.8	1.1	0.3126	0.011	0.21	3.199	0.1126	0.697	0.015	0.55	400.3	41.5	0.80
FB3ap_37	43.1	1.9	0.416	0.018	0.28	2.404	0.1040	0.758	0.023	0.66	322.3	78.7	0.88
FB3ap_38	20.74	0.9	0.2341	0.0094	0.63	4.272	0.1715	0.647	0.018	0.29	389.5	37.3	0.73
FB3ap_39	35.9	1.8	0.363	0.017	0.40	2.755	0.1290	0.713	0.022	0.52	423.2	66.3	0.81
FB3ap_40	23.2	0.91	0.2491	0.0098	0.02	4.014	0.1579	0.680	0.024	0.65	347.0	49.4	0.78
FB3ap_41	6.58	0.27	0.1125	0.007	0.24	8.889	0.5531	0.438	0.010	0.55	369.2	24.3	0.48
FB3ap_42	9.58	0.46	0.1321	0.0059	0.37	7.570	0.3381	0.528	0.016	-0.03	340.3	22.6	0.59
FB3ap_43	13.44	0.67	0.1638	0.007	0.47	6.105	0.2609	0.595	0.021	0.29	336.2	30.8	0.67
FB3ap_44	14.96	0.71	0.172	0.0089	0.29	5.814	0.3008	0.620	0.019	0.06	318.6	31.0	0.71
FB3ap_45	16.4	1.8	0.174	0.013	0.91	5.747	0.4294	0.648	0.025	0.00	282.1	40.5	0.74
FB3ap_46	18.54	1.1	0.212	0.011	0.70	4.717	0.2447	0.642	0.024	0.06	358.9	44.2	0.73
FB3ap_47	4.72	0.19	0.0876	0.0032	0.05	11.416	0.4170	0.394	0.013	0.54	317.1	14.6	0.42
FB3ap_48	3.268	0.14	0.0761	0.0027	0.29	13.141	0.4662	0.313	0.009	0.34	323.9	12.7	0.32
FB3ap_49	5.8	0.27	0.0952	0.0036	0.15	10.504	0.3972	0.443	0.010	0.31	308.0	14.0	0.49
FB3ap_50	141	8.1	1.289	0.057	0.26	0.776	0.0343	0.810	0.030	-0.03	729.7	289.0	0.91
FB3ap_51	4.64	0.39	0.0883	0.0043	0.01	11.325	0.5515	0.371	0.021	-0.04	335.5	21.6	0.39
FB3ap_52	69.7	2.6	0.656	0.023	0.72	1.524	0.0534	0.769	0.018	-0.02	506.5	97.1	0.88
FB3ap_53	37.6	1.8	0.369	0.016	0.03	2.710	0.1175	0.743	0.028	0.70	330.4	83.3	0.86
FB3ap_54	14.76	0.78	0.1799	0.0084	0.03	5.559	0.2595	0.601	0.021	0.50	362.1	34.3	0.68
FB3ap_55	18.7	1.3	0.2084	0.011	0.88	4.798	0.2533	0.651	0.035	0.09	336.7	59.5	0.74
FB3ap_56	21.16	1.2	0.2264	0.011	0.67	4.417	0.2146	0.676	0.023	0.13	320.3	44.4	0.77
FB3ap_57	14.81	0.72	0.1643	0.0063	0.18	6.086	0.2334	0.663	0.021	-0.06	245.0	29.7	0.76
FB3ap_59	10.94	0.8	0.1429	0.0088	0.86	6.998	0.4309	0.553	0.019	-0.16	340.2	29.9	0.62
FB3ap_60	6.14	0.23	0.0944	0.0033	-0.06	10.593	0.3703	0.477	0.012	0.71	279.9	13.5	0.53
FB3ap_61	75.9	3.5	0.706	0.031	0.18	1.416	0.0622	0.792	0.027	0.48	379.1	152.1	0.91
FB3ap_62	280	27	2.52	0.24	0.58	0.397	0.0378	0.809	0.027	0.21	1179.9	519.8	0.92
FB3ap_63	8.53	0.31	0.1183	0.0041	0.06	8.453	0.2930	0.526	0.013	0.37	305.8	16.5	0.59
FB3ap_64	60.1	2.8	0.564	0.025	0.63	1.773	0.0786	0.768	0.029	-0.07	417.0	129.2	0.88
FB3ap_65	16.45	0.96	0.1914	0.0094	0.71	5.225	0.2566	0.637	0.023	0.09	329.7	38.5	0.73
FB3ap_66	25.4	1.2	0.2655	0.011	0.52	3.766	0.1561	0.695	0.019	0.31	337.9	43.4	0.80
FB3ap_67	5.09	0.22	0.0911	0.0035	0.36	10.977	0.4217	0.404	0.014	0.53	322.7	15.9	0.44
FB3ap_68	8.71	0.32	0.12	0.0042	0.35	8.333	0.2917	0.531	0.014	0.50	305.5	17.4	0.60
FB3ap_69	6.44	0.26	0.1061	0.0039	-0.06	9.425	0.3464	0.444	0.014	0.64	342.8	17.2	0.49
FB3ap_70	47.7	2	0.464	0.02	0.38	2.155	0.0929	0.755	0.025	0.60	382.6	93.6	0.87
FB3ap_71	13.61	0.53	0.164	0.0063	-0.04	6.098	0.2342	0.601	0.020	0.59	328.6	29.1	0.68
FB3ap_72	15.63	0.93	0.1871	0.0087	0.18	5.345	0.2485	0.593	0.018	0.25	389.6	32.2	0.67
FB3ap_73	19.39	0.73	0.2111	0.0077	-0.05	4.737	0.1728	0.670	0.016	0.57	307.7	30.3	0.77
FB3ap_74	11.91	0.54	0.1507	0.0061	0.37	6.636	0.2686	0.587	0.022	0.46	318.0	29.3	0.66
FB3ap_75	45.4	1.9	0.522	0.073	0.08	1.916	0.2679	0.696	0.033	0.64	739.1	161.0	0.77
FB3ap_76	25.9	1.5	0.269	0.014	0.19	3.717	0.1935	0.694	0.026	0.42	345.2	58.2	0.80
FB3ap_77	6.66	0.29	0.1073	0.0042	0.24	9.320	0.3648	0.453	0.015	0.47	339.1	18.3	0.50
FB3ap_78	46.2	1.9	0.446	0.018	0.30	2.242	0.0905	0.754	0.023	0.59	368.4	83.6	0.87
FB3ap_79	39.4	1.8	0.4	0.018	0.81	2.500	0.1125	0.712	0.021	0.11	478.0	69.5	0.81
FB3ap_80	11.93	0.67	0.161	0.012	0.06	6.211	0.4629	0.555	0.020	0.43	382.3	37.8	0.62
FB3ap_81	28.59	1.1	0.2919	0.011	0.40	3.426	0.1291	0.712	0.019	0.52	332.2	47.1	0.82
FB3ap_82	11.97	0.44	0.1522	0.0054	-0.04	6.570	0.2331	0.573	0.013	0.50	338.6	20.3	0.65
FB3ap_83	11.15	0.42	0.1451	0.0054	0.14	6.892	0.2565	0.562	0.017	0.50	335.1	23.4	0.63
FB3ap_84	59.4	2.4	0.567	0.024	0.35	1.764	0.0747	0.764	0.023	0.07	443.4	105.0	0.87
FB3ap_85	18.95	0.86	0.2133	0.0088	0.41	4.688	0.1934	0.645	0.021	0.41	355.9	38.6	0.73
FB3ap_86	4.605	0.16	0.0916	0.003	0.25	10.917	0.3575	0.366	0.007	0.35	351.4	12.5	0.39
FB3ap_87	30.94	1.2	0.3129	0.012	0.10	3.196	0.1226	0.724	0.025	0.55	326.0	63.8	0.83
FB3ap_88	22.27	1.2	0.2392	0.0096	0.14	4.181	0.1678	0.669	0.030	0.18	354.3	57.9	0.76
FB3ap_89	35.8	1.7	0.366	0.017	0.50	2.732	0.1269	0.710	0.020	0.50	437.2	61.8	0.81
FB3ap_90	29.05	1	0.2987	0.01	0.67	3.348	0.1121	0.707	0.012	-0.05	354.1	33.8	0.81
FB3ap_91	609	35	5.35	0.3	0.08	0.187	0.0105	0.818	0.028	0.01	0.0	1113.6	0.74
FB3ap_92	32.98	1.2	0.3297	0.013	0.30	3.033	0.1196	0.731	0.018	0.49	325.4	50.8	0.84

Tables S.2.2 apatite U-Pb data tables (continued)

	$^{207}Pb/^{235}U$	Prop2SE	$^{206}Pb/^{238}U$	Prop2SE	Rho	$^{238}U/^{206}Pb$	Prop2SE	$^{207}Pb/^{206}Pb$	Prop2SE	Rho	^{207}Pb corrected age	Prop2SE	$f^{206}Pb$
FB3ap_93	382	24	3.31	0.19	0.79	0.302	0.0173	0.829	0.031	-0.03	473.3	817.1	0.98
FB3ap_94	22.97	0.87	0.2511	0.0092	0.11	3.982	0.1459	0.666	0.015	0.00	380.0	34.1	0.76
FB3ap_95	790	120	6.14	0.34	0.00	0.163	0.0090	0.930	0.120	0.03	-7808.1	19161.8	1.00
FB3ap_96	3.94	0.16	0.0797	0.0028	-0.12	12.547	0.4408	0.360	0.012	0.18	309.7	13.2	0.38
FB3ap_97	125.1	5.9	1.156	0.053	0.78	0.865	0.0397	0.791	0.028	0.01	915.1	237.8	0.87
FB3ap_98	312	15	2.665	0.12	0.77	0.375	0.0169	0.847	0.019	0.26	856.9	394.0	0.95
FB3ap_99	1740	210	14.6	1.3	0.98	0.068	0.0061	0.845	0.027	0.15	0.0	3751.2	1.00
FB3ap_100	72.2	2.9	0.683	0.03	0.49	1.464	0.0643	0.776	0.028	0.13	483.9	149.7	0.89
FB3ap_101	70.6	3.5	0.635	0.028	0.07	1.575	0.0694	0.800	0.035	0.65	267.4	177.5	0.93
FB3ap_102	5.91	0.24	0.099	0.0036	0.35	10.101	0.3673	0.437	0.015	-0.07	325.1	16.6	0.48
FB3ap_103	910	86	7.97	0.73	0.52	0.125	0.0115	0.838	0.032	0.05	-4710.2	4529.3	1.00
FB3ap_104	10.11	0.69	0.141	0.013	0.01	7.092	0.6539	0.540	0.020	0.28	350.3	38.8	0.60
FB3ap_105	9.7	0.39	0.1307	0.0047	-0.04	7.651	0.2751	0.533	0.015	0.34	331.3	19.8	0.60
FB3ap_106	7.48	0.3	0.1131	0.0044	0.52	8.842	0.3440	0.483	0.015	0.16	330.9	18.6	0.53
FB3ap_107	98.2	3.8	0.886	0.034	0.59	1.129	0.0433	0.807	0.017	0.45	370.6	127.8	0.93
FB3ap_108	4.05	0.17	0.0844	0.0029	0.43	11.848	0.4071	0.350	0.009	0.12	334.5	12.9	0.37
FB3ap_109	99.9	3.9	0.917	0.036	0.77	1.091	0.0428	0.789	0.015	0.14	615.1	115.8	0.89
FB3ap_110	72.2	2.8	0.684	0.025	0.08	1.462	0.0534	0.760	0.022	0.15	604.5	118.4	0.86
FB3ap_111	6.26	0.28	0.1051	0.0039	0.63	9.515	0.3531	0.432	0.011	0.09	349.5	15.9	0.47
FB4ap_1	35	1.7	0.345	0.0072	0.09	2.899	0.0620	0.735	0.023	0.13	330.4	64.3	0.85
FB4ap_2	18.6	1.4	0.2032	0.0094	0.83	4.921	0.2300	0.662	0.024	-0.06	309.0	41.4	0.76
FB4ap_3	38.1	1.8	0.369	0.01	-0.02	2.710	0.0760	0.754	0.020	0.87	292.7	61.4	0.87
FB4ap_4	78.7	3.7	0.721	0.016	0.81	1.387	0.0330	0.793	0.013	0.10	383.0	83.8	0.92
FB4ap_5	562	37	4.9	0.27	0.63	0.204	0.0110	0.849	0.030	0.38	-2203.3	1748.5	1.00
FB4ap_6	15.03	0.69	0.1759	0.0031	0.10	5.685	0.1000	0.621	0.014	0.57	324.7	21.4	0.71
FB4ap_7	41.5	3.1	0.4	0.023	0.71	2.500	0.1600	0.759	0.028	0.22	303.5	91.2	0.88
FB4ap_8	9.67	0.48	0.1214	0.0021	0.33	8.237	0.1400	0.579	0.016	0.32	262.1	16.6	0.66
FB4ap_9	9.62	0.45	0.1266	0.002	0.32	7.899	0.1400	0.551	0.012	0.47	302.4	13.7	0.62
FB4ap_10	14.88	0.77	0.1762	0.0043	0.53	5.675	0.1400	0.614	0.016	0.27	335.5	24.5	0.70
FB4ap_11	699	57	5.93	0.37	0.90	0.169	0.0110	0.852	0.031	0.23	-4345.8	3089.1	1.00
FB4ap_12	10.93	0.54	0.148	0.0027	0.26	6.757	0.1300	0.537	0.016	0.32	371.8	20.1	0.60
FB4ap_13	8.39	0.57	0.12	0.0046	0.68	8.333	0.3100	0.508	0.022	0.01	327.6	24.2	0.57
FB4ap_14	30.3	3.3	0.292	0.0086	0.07	3.425	0.1000	0.756	0.073	-0.03	217.4	168.2	0.88
FB4ap_15	4.26	0.25	0.083	0.0018	0.37	12.048	0.2700	0.370	0.012	0.33	316.0	10.4	0.39
FB4ap_16	13.73	0.75	0.1678	0.0046	0.35	5.959	0.1700	0.594	0.017	0.46	346.1	24.9	0.67
FB4ap_18	67	4.4	0.639	0.04	0.65	1.565	0.1000	0.776	0.043	0.52	439.8	212.0	0.89
FB4ap_19	20.66	0.92	0.2195	0.0033	0.09	4.556	0.0680	0.683	0.015	0.70	296.7	28.2	0.79
FB4ap_20	120.3	8.4	1.065	0.066	0.38	0.939	0.0750	0.813	0.023	0.16	427.5	197.7	0.94
FB4ap_21	11.91	0.61	0.1478	0.0033	0.25	6.766	0.1600	0.585	0.018	0.49	314.0	22.6	0.66
FB4ap_22	34	2.2	0.344	0.014	0.75	2.907	0.1200	0.718	0.023	0.19	382.2	64.8	0.82
FB4ap_23	52	3.1	0.483	0.015	0.22	2.070	0.0690	0.787	0.025	-0.07	248.0	99.0	0.92
FB4ap_24	71.3	3.9	0.662	0.025	0.62	1.511	0.0620	0.786	0.028	0.06	389.2	147.0	0.91
FB4ap_25	11.12	0.56	0.1472	0.0032	0.41	6.793	0.1500	0.546	0.013	0.44	359.1	17.5	0.61
FB4ap_26	10.81	0.6	0.1414	0.0047	0.82	7.072	0.2300	0.557	0.016	0.08	332.0	21.3	0.63
FB4ap_27	50.1	2.6	0.487	0.014	0.77	2.053	0.0600	0.752	0.020	0.31	420.9	79.5	0.86
FB4ap_28	354	30	3.01	0.21	0.51	0.332	0.0250	0.847	0.025	0.07	2206.1	563.8	0.86
FB4ap_29	13.87	0.68	0.1698	0.0036	0.40	5.889	0.1200	0.594	0.016	0.53	350.5	23.3	0.67
FB4ap_30	365	26	3.23	0.18	0.21	0.310	0.0190	0.838	0.028	0.37	-63.0	776.0	1.00
FB4ap_31	107.5	6.6	0.984	0.049	0.60	1.016	0.0440	0.816	0.021	0.51	320.4	171.1	0.95
FB4ap_32	18.23	0.87	0.1966	0.004	0.66	5.086	0.1000	0.673	0.012	0.29	280.0	21.6	0.77
FB4ap_33	95.7	5.2	0.889	0.028	0.64	1.125	0.0390	0.785	0.024	0.16	628.4	164.7	0.88
FB4ap_34	3.82	0.2	0.0883	0.0017	0.05	11.325	0.2200	0.314	0.009	0.01	374.4	9.3	0.32
FB4ap_35	15.13	0.71	0.1805	0.0048	0.31	5.540	0.1500	0.614	0.018	0.69	344.1	27.7	0.70
FB4ap_36	2620	430	22.4	3.1	0.98	0.045	0.0150	0.835	0.029	0.16	112.6	5454.6	1.00
FB4ap_37	730	64	6.46	0.48	0.88	0.155	0.0110	0.841	0.033	0.18	-7081.5	5653.8	1.00
FB4ap_38	30.5	1.7	0.3206	0.0096	0.64	3.119	0.0950	0.696	0.023	0.06	414.8	59.5	0.79
FB4ap_39	4.54	0.26	0.0871	0.0014	-0.07	11.481	0.1900	0.378	0.015	0.18	326.2	11.5	0.40
FB4ap_40	78.9	6.3	0.719	0.021	0.22	1.391	0.0580	0.826	0.052	-0.02	93.1	303.6	0.98
FB4ap_41	12.49	0.66	0.1602	0.0037	0.15	6.242	0.1400	0.569	0.021	0.51	362.3	27.8	0.64
FB4ap_42	8.72	0.44	0.1242	0.0027	0.15	8.052	0.1700	0.512	0.017	0.56	335.3	18.3	0.57
FB5ap_0	38.1	1.6	0.386	0.013	0.59	2.591	0.0880	0.718	0.026	0.23	437.3	79.7	0.82
FB5ap_1	758	42	6.59	0.34	0.72	0.152	0.0079	0.842	0.033	0.28	-11527.0	11671.6	1.00
FB5ap_2	16.79	0.63	0.1969	0.0065	0.55	5.079	0.1700	0.621	0.018	0.34	365.9	30.9	0.70
FB5ap_3	154.2	5.5	1.375	0.044	0.55	0.727	0.0230	0.820	0.027	0.45	582.9	285.5	0.93
FB5ap_4	15.5	0.46	0.1956	0.0043	0.49	5.112	0.1100	0.571	0.016	0.39	443.1	26.7	0.64
FB5ap_5	324	21	2.61	0.16	0.74	0.383	0.0250	0.891	0.040	0.42	0.0	1433.1	1.00
FB5ap_6	61.4	2.4	0.587	0.023	0.44	1.704	0.0620	0.767	0.030	0.43	446.3	137.8	0.88
FB5ap_7	2.95	0.11	0.0785	0.0023	0.58	12.739	0.3900	0.274	0.009	0.23	357.7	11.7	0.27
FB5ap_9	38.5	1.2	0.387	0.01	0.53	2.584	0.0710	0.725	0.020	0.34	413.9	63.1	0.83
FB5ap_10	10.1	0.42	0.1478	0.0043	0.46	6.766	0.1900	0.498	0.019	0.21	417.2	24.9	0.55
FB5ap_11	29.2	1	0.3109	0.0081	0.55	3.216	0.0890	0.680	0.022	0.26	443.9	55.0	0.77
FB5ap_12	30.2	1.1	0.3089	0.0081	0.49	3.237	0.0870	0.712	0.022	0.25	354.2	55.3	0.82
FB5ap_13	4.93	0.2	0.1008	0.0027	0.45	9.921	0.2600	0.356	0.013	0.18	394.9	14.6	0.37
FB5ap_14	36.1	1.5	0.375	0.012	0.54	2.667	0.0890	0.706	0.024	0.20	463.2	71.8	0.80
FB5ap_15	20.55	0.85	0.2179	0.0087	0.42	4.589	0.2000	0.696	0.032	0.55	270.2	56.4	0.80
FB5ap_16	59.3	2.6	0.562	0.02	0.59	1.779	0.0660	0.769	0.027	0.30	409.2	120.3	0.88
FB5ap_17	971	50	7.93	0.39	0.73	0.126	0.0067	0.891	0.033	0.37	0.0	2977.4	1.00
FB5ap_18	6.62	0.26	0.1199	0.0033	0.50	8.340	0.2300	0.401	0.014	0.17	428.3	17.5	0.43
FB5ap_19	20.03	0.65	0.2356	0.0057	0.63	4.244	0.1000	0.617	0.018	0.07	451.0	35.3	0.69
FB5ap_20	72.3	3.2	0.66	0.027	0.60	1.515	0.0680	0.803	0.031	0.36	260.1	164.7	0.94
FB5ap_21	25.6	1	0.2789	0.0084	0.38	3.586	0.1200	0.671	0.027	0.35	414.6	59.9	0.76
FB5ap_22	17.23	0.85	0.1993	0.0077	0.61	5.018	0.2000	0.626	0.024	0.26	362.4	40.1	0.71
FB5ap_23	11.97	0.53	0.1662	0.0051	0.42	6.017	0.1800	0.526	0.023	0.29	433.7	32.3	0.58
FB5ap_24	61.2	2	0.582	0.021	0.54	1.718	0.0610	0.776	0.026	0.57	386.3	120.8	0.89
FB5ap_25	35.3	1.6	0.364	0.015	0.69	2.747	0.1200	0.706	0.024	0.08	447.4	70.8	0.80
FB5ap_27	22.7	1	0.2436	0.0084	0.51	4.105	0.1400	0.674	0.026	0.21	351.1	51.4	0.77

Tables S.2.2 apatite U-Pb data tables (continued)

	$^{207}Pb/^{235}U$	Prop2SE	$^{206}Pb/^{238}U$	Prop2SE	Rho	$^{238}U/^{206}Pb$	Prop2SE	$^{207}Pb/^{206}Pb$	Prop2SE	Rho	^{207}Pb corrected age	Prop2SE	$f^{206}Pb$
FB5ap_28	29.89	0.94	0.3192	0.0093	0.55	3.133	0.0950	0.683	0.019	0.39	448.9	50.1	0.77
FB5ap_29	3.37	0.14	0.0885	0.0028	0.45	11.299	0.3500	0.278	0.011	0.29	400.1	14.5	0.28
FB5ap_30	27.4	1.2	0.281	0.01	0.46	3.559	0.1300	0.714	0.030	0.30	313.3	67.6	0.82
FB5ap_31	18.77	0.62	0.2198	0.0059	0.36	4.550	0.1300	0.616	0.020	0.44	420.5	36.4	0.69
FB5ap_32	402	22	3.43	0.16	0.72	0.292	0.0130	0.850	0.034	0.22	0.0	825.5	0.83
FB5ap_33	20.37	0.76	0.227	0.0074	0.63	4.405	0.1400	0.654	0.020	0.33	363.4	38.2	0.74
FB5ap_34	35.7	2.4	0.37	0.019	0.79	2.703	0.1400	0.699	0.027	0.02	479.1	80.8	0.79
FB5ap_35	43.8	1.8	0.412	0.015	0.65	2.427	0.0860	0.774	0.025	0.29	255.1	84.4	0.90
FB5ap_36	16.91	0.72	0.193	0.0067	0.41	5.181	0.1800	0.636	0.025	0.45	334.3	39.8	0.72
FB5ap_37	14.93	0.57	0.1879	0.0059	0.43	5.322	0.1700	0.580	0.022	0.40	411.2	34.7	0.65
FB5ap_38	66.6	2.2	0.631	0.021	0.54	1.585	0.0530	0.771	0.024	0.45	466.0	120.2	0.88
FB5ap_39	12.21	0.4	0.1617	0.0039	0.41	6.184	0.1500	0.549	0.017	0.30	391.9	23.8	0.61
FB5ap_40	5.31	0.21	0.0945	0.0029	0.44	10.582	0.3300	0.410	0.016	0.29	330.3	15.6	0.44
FB5ap_41	6.06	0.18	0.1141	0.003	0.54	8.764	0.2300	0.385	0.010	0.31	421.6	14.2	0.41
FB5ap_42	37.3	1.5	0.387	0.013	0.53	2.584	0.0890	0.697	0.023	0.37	511.8	71.1	0.79
FB5ap_43	43.6	1.9	0.394	0.015	0.55	2.538	0.0940	0.817	0.032	0.35	74.8	104.8	0.97
FB5ap_44	17.58	0.48	0.2106	0.0053	0.71	4.748	0.1200	0.611	0.014	0.24	410.4	26.3	0.69
FB5ap_45	164.9	6.3	1.508	0.061	0.62	0.663	0.0270	0.801	0.026	0.48	1375.2	275.2	0.84
FB5ap_46	14.72	0.6	0.1785	0.0058	0.57	5.602	0.1900	0.601	0.021	0.27	359.1	31.9	0.68
FB5ap_47	73.8	3	0.687	0.025	0.79	1.456	0.0570	0.782	0.022	0.25	442.0	121.7	0.90
FB5ap_48	11.85	0.49	0.1512	0.0049	0.40	6.614	0.2200	0.568	0.023	0.42	342.4	29.5	0.64
FB5ap_49	179	14	1.58	0.12	0.84	0.633	0.0530	0.827	0.034	0.14	600.8	407.3	0.94
FB5ap_50	57.7	2.3	0.547	0.019	0.52	1.828	0.0630	0.772	0.030	0.36	377.9	129.7	0.89
FB5ap_51	1440	220	12.1	1.8	0.97	0.083	0.0120	0.839	0.020	0.19	-340.3	2227.5	1.00
FB5ap_52	100.2	4.5	0.914	0.027	0.40	1.094	0.0300	0.799	0.035	0.21	491.0	245.3	0.91
FB5ap_53	62.3	2.7	0.585	0.022	0.50	1.709	0.0590	0.772	0.028	0.33	413.6	129.4	0.89
FB5ap_54	21.05	0.84	0.2213	0.0064	0.63	4.519	0.1300	0.687	0.021	0.08	291.8	38.7	0.79
FB5ap_55	28.7	1.1	0.2979	0.0088	0.71	3.357	0.0980	0.700	0.020	0.05	371.3	49.3	0.80
FB5ap_56	51.7	1.9	0.493	0.013	0.49	2.028	0.0550	0.769	0.026	0.17	344.6	102.8	0.89
FB5ap_57	102.9	3.6	0.937	0.03	0.58	1.067	0.0370	0.801	0.024	0.37	487.8	177.6	0.92
FB5ap_58	20.3	1.1	0.2254	0.009	0.74	4.437	0.1800	0.645	0.023	0.02	377.7	43.5	0.73
FB5ap_59	4.1	0.21	0.0896	0.0033	0.43	11.161	0.4300	0.335	0.016	0.35	365.6	17.3	0.35
FB5ap_60	24.13	0.77	0.2609	0.007	0.44	3.833	0.1100	0.677	0.017	0.39	371.8	37.6	0.77
FB5ap_61	17.85	0.56	0.2076	0.0047	0.57	4.817	0.1100	0.625	0.016	0.23	380.2	28.4	0.71
FB5ap_62	46.7	1.5	0.453	0.012	0.51	2.208	0.0590	0.751	0.022	0.33	388.7	80.6	0.86
FB5ap_63	32.4	2	0.332	0.018	0.81	3.012	0.1700	0.711	0.025	0.06	387.6	68.7	0.81
FB5ap_64	26.64	0.89	0.2983	0.0081	0.55	3.352	0.0920	0.646	0.017	0.33	510.2	42.5	0.72
FB5ap_65	60.7	2	0.582	0.015	0.47	1.718	0.0470	0.762	0.025	0.27	471.2	114.5	0.87
FB5ap_66	87	3.1	0.82	0.025	0.82	1.220	0.0380	0.770	0.016	0.10	696.9	106.8	0.86
FB5ap_67	96	6.2	0.875	0.062	0.67	1.143	0.0800	0.803	0.053	0.53	409.0	356.3	0.93
FB5ap_68	81.2	3.6	0.707	0.027	0.49	1.414	0.0550	0.833	0.032	0.39	28.1	189.8	0.99
FB5ap_69	17.84	0.63	0.2143	0.0061	0.57	4.666	0.1300	0.607	0.019	0.30	425.1	34.3	0.68
FB5ap_70	30.2	1.3	0.326	0.011	0.53	3.067	0.1100	0.670	0.027	0.39	496.5	69.5	0.75
FB5ap_71	32.4	1.1	0.346	0.01	0.54	2.890	0.0900	0.682	0.021	0.31	495.0	58.6	0.77
FB5ap_72	40	1.3	0.3997	0.0096	0.66	2.502	0.0630	0.724	0.018	0.17	433.8	59.3	0.83
FB5ap_73	574	17	5.12	0.15	0.80	0.195	0.0060	0.817	0.017	0.31	0.0	688.6	0.75
FB5ap_74	33	1.8	0.328	0.013	0.61	3.049	0.1300	0.731	0.031	0.19	323.5	81.3	0.84
FB5ap_75	10.07	0.51	0.1324	0.0045	0.54	7.553	0.2600	0.553	0.024	0.22	314.5	27.2	0.62
FB5ap_76	79.9	3.3	0.754	0.026	0.72	1.326	0.0490	0.770	0.022	0.22	612.3	130.0	0.87
FB5ap_77	16.14	0.49	0.192	0.0043	0.36	5.208	0.1200	0.609	0.018	0.40	375.2	28.9	0.69
FB5ap_78	42.9	1.3	0.412	0.01	0.47	2.427	0.0620	0.758	0.022	0.42	318.5	74.1	0.88
FB5ap_79	42.2	1.2	0.414	0.01	0.59	2.415	0.0610	0.741	0.018	0.30	387.0	61.9	0.85
FB5ap_80	20.75	0.66	0.2245	0.0064	0.53	4.454	0.1300	0.674	0.020	0.40	321.2	37.5	0.77
FB5ap_81	49.6	1.8	0.481	0.017	0.48	2.079	0.0760	0.756	0.028	0.52	395.6	106.8	0.87
FB5ap_82	160	8.6	1.436	0.069	0.80	0.696	0.0360	0.814	0.028	0.23	839.7	298.0	0.90
FB5ap_83	104.1	4.1	0.969	0.035	0.67	1.032	0.0370	0.784	0.025	0.35	742.6	183.4	0.87
FB5ap_84	24.88	0.77	0.2738	0.0073	0.29	3.652	0.1000	0.664	0.024	0.55	422.6	52.6	0.75
FB5ap_85	25.5	0.83	0.2708	0.0076	0.61	3.693	0.1000	0.681	0.017	0.29	378.2	39.1	0.78
FB5ap_86	523	32	4.59	0.28	0.88	0.218	0.0130	0.828	0.026	0.16	2428.8	1006.8	0.90
FB5ap_87	8.21	0.43	0.1183	0.0048	0.40	8.453	0.3700	0.498	0.023	0.45	332.3	25.1	0.55
FB5ap_88	78.1	2.7	0.719	0.02	0.33	1.391	0.0400	0.798	0.028	0.43	381.4	159.5	0.92
FB5ap_89	2.66	0.12	0.0833	0.0019	0.59	12.005	0.2800	0.229	0.008	0.00	408.1	10.4	0.22
FB5ap_90	38.3	1.1	0.39	0.01	0.64	2.564	0.0670	0.715	0.016	0.37	453.3	52.5	0.81
FB5ap_91	151.1	6	1.307	0.052	0.64	0.765	0.0310	0.840	0.030	0.47	-27.0	332.6	1.00
FB5ap_92	126.6	7.3	1.077	0.058	0.79	0.929	0.0640	0.857	0.032	0.09	-381.5	312.8	1.00
FB5ap_93	35.4	1.2	0.371	0.01	0.44	2.695	0.0760	0.696	0.023	0.33	490.5	67.7	0.79
FB5ap_94	39.6	1.4	0.397	0.011	0.49	2.519	0.0670	0.724	0.022	0.34	430.3	70.3	0.83
FB5ap_95	40.3	1.3	0.412	0.013	0.49	2.427	0.0780	0.712	0.024	0.57	495.1	78.4	0.81
FB5ap_96	45.6	2.7	0.45	0.022	0.82	2.222	0.1100	0.724	0.022	0.11	500.6	81.2	0.82
FB5ap_97	123.7	4.2	1.069	0.036	0.67	0.935	0.0320	0.844	0.024	0.39	-121.5	226.6	1.00
FB5ap_98	7.39	0.3	0.1184	0.0034	0.33	8.446	0.2400	0.450	0.018	0.33	377.5	19.8	0.49
FB5ap_99	98.4	4.1	0.91	0.03	0.85	1.099	0.0390	0.787	0.021	-0.04	630.5	150.0	0.89
FB5ap_100	55.2	2	0.531	0.015	0.54	1.883	0.0530	0.752	0.025	0.35	470.3	104.6	0.86
FB5ap_101	146.5	6.7	1.319	0.052	0.97	0.758	0.0300	0.800	0.014	-0.12	1010.3	150.9	0.87
FB5ap_103	34.3	1.2	0.346	0.011	0.42	2.890	0.0890	0.724	0.026	0.39	366.1	72.1	0.83
FB5ap_104	38.5	1.3	0.396	0.011	0.68	2.525	0.0730	0.706	0.018	0.18	493.8	58.6	0.80
FB5ap_105	254.5	7.9	2.201	0.071	0.59	0.454	0.0150	0.849	0.022	0.48	-258.5	436.7	1.00
FB5ap_106	17.64	0.66	0.2143	0.006	0.34	4.666	0.1300	0.601	0.023	0.40	435.6	40.2	0.67
FB5ap_107	14.34	0.7	0.1875	0.0072	0.69	5.333	0.2100	0.557	0.021	0.17	445.1	34.9	0.62
FB5ap_108	29.56	0.99	0.3165	0.0087	0.46	3.160	0.0870	0.681	0.022	0.31	450.1	56.1	0.77
FB5ap_109	105	2.5	0.908	0.022	0.48	1.101	0.0280	0.840	0.021	0.54	-44.5	168.8	1.00
FB5ap_110	173.2	8.2	1.434	0.07	0.57	0.697	0.0350	0.889	0.041	0.43	-2136.4	741.4	1.00
FB5ap_111	30.1	1.1	0.3263	0.0085	0.46	3.065	0.0830	0.671	0.021	0.28	494.2	55.0	0.76
FB5ap_112	1.671	0.056	0.0699	0.0017	0.39	14.306	0.3400	0.174	0.006	0.29	372.5	9.4	0.15
FB5ap_113	120.5	3.9	1.082	0.028	0.62	0.924	0.0240	0.809	0.021	0.22	509.7	181.5	0.92
FB5ap_114	21.41	0.93	0.241	0.01	0.75	4.149	0.1900	0.649	0.021	0.36	397.9	43.3	0.74
FB5ap_115	20.17	0.78	0.2406	0.0066	0.48	4.156	0.1200	0.615	0.023	0.32	465.2	44.7	0.69
FB5ap_116	30.63	0.72	0.3239	0.0068	0.52	3.087	0.0610	0.689	0.016	0.36	439.5	43.4	0.78

Tables S.2.2 apatite U-Pb data tables (continued)

	$^{207}Pb/^{235}U$	Prop2SE	$^{206}Pb/^{238}U$	Prop2SE	Rho	$^{238}U/^{206}Pb$	Prop2SE	$^{207}Pb/^{206}Pb$	Prop2SE	Rho	^{207}Pb corrected age	Prop2SE	$f^{206}Pb$
FB6ap_0	16.24	0.51	0.1999	0.0052	0.02	5.003	0.1300	0.589	0.025	0.17	424.2	40.2	0.66
FB6ap_1	25.54	0.68	0.2709	0.0067	-0.60	3.691	0.1000	0.688	0.018	1.00	362.0	40.8	0.79
FB6ap_2	39.2	1.4	0.379	0.012	-0.01	2.639	0.0840	0.749	0.027	0.11	319.9	82.3	0.87
FB6ap_3	55.7	2.1	0.539	0.015	0.19	1.855	0.0520	0.762	0.023	0.00	425.5	99.2	0.87
FB6ap_4	121	2.5	1.097	0.025	0.17	0.912	0.0190	0.799	0.015	0.52	693.3	135.2	0.90
FB6ap_5	25.95	0.69	0.2822	0.0068	0.59	3.544	0.0880	0.671	0.020	0.05	420.1	46.0	0.76
FB6ap_6	140.3	4.5	1.193	0.04	0.63	0.838	0.0290	0.863	0.029	0.14	-613.1	330.2	1.00
FB6ap_7	73.3	3.9	0.684	0.035	0.81	1.462	0.0770	0.785	0.027	0.12	416.0	146.9	0.90
FB6ap_8	624	37	5.26	0.34	0.84	0.190	0.0120	0.883	0.032	0.34	0.0	1720.7	1.00
FB6ap_9	95.9	3	0.806	0.024	0.31	1.241	0.0380	0.871	0.028	0.14	-406.3	208.6	1.00
FB6ap_10	1250	110	10.5	1.1	0.12	0.095	0.0100	0.923	0.047	0.40	0.0	4166.9	1.00
FB6ap_11	4.94	0.23	0.092	0.0023	0.72	10.870	0.2800	0.386	0.014	-0.06	338.9	13.2	0.41
FB6ap_12	204.7	7.7	1.763	0.074	0.45	0.567	0.0230	0.857	0.034	0.54	-930.4	593.8	1.00
FB6ap_13	29.61	0.63	0.3143	0.0059	0.40	3.182	0.0600	0.686	0.015	0.39	433.0	39.8	0.78
FB6ap_14	115.2	3.1	1.082	0.035	0.50	0.924	0.0300	0.781	0.023	0.58	956.1	184.2	0.85
FB6ap_15	121.6	3.1	1.099	0.03	0.68	0.910	0.0250	0.807	0.017	0.46	561.0	153.1	0.92
FB6ap_16	21.97	0.73	0.2291	0.0073	-0.39	4.365	0.1500	0.702	0.023	0.70	273.5	43.6	0.81
FB6ap_17	210.4	9.6	1.845	0.083	0.81	0.542	0.0240	0.833	0.025	0.27	688.0	352.5	0.94
FB6ap_18	39.57	0.9	0.3964	0.0068	0.59	2.523	0.0440	0.727	0.017	0.25	418.6	55.8	0.83
FB6ap_19	17.7	2.3	0.1834	0.0046	0.16	5.453	0.1400	0.673	0.025	-0.03	259.9	37.5	0.78
FB6ap_20	48.5	1.6	0.465	0.014	0.70	2.151	0.0640	0.765	0.015	0.11	338.1	60.8	0.88
FB6ap_21	131.8	6.4	1.193	0.056	0.60	0.838	0.0420	0.824	0.038	0.11	318.0	356.9	0.96
FB6ap_22	57.2	1.5	0.542	0.013	0.70	1.845	0.0500	0.772	0.018	0.26	373.3	81.3	0.89
FB6ap_23	11.58	0.23	0.1542	0.0026	0.00	6.485	0.1100	0.548	0.012	0.65	374.3	16.6	0.61
FB6ap_24	39.4	1.1	0.391	0.011	0.10	2.558	0.0760	0.735	0.021	0.54	383.0	67.0	0.84
FB6ap_25	96.9	3.2	0.83	0.027	0.38	1.205	0.0410	0.856	0.027	0.20	-235.6	200.6	1.00
FB6ap_26	29.99	0.83	0.3101	0.0071	0.56	3.225	0.0740	0.702	0.020	0.27	383.1	50.7	0.80
FB6ap_27	19.34	0.57	0.2221	0.0054	0.13	4.502	0.1100	0.638	0.019	0.57	384.7	35.0	0.72
FB6ap_28	24.42	0.44	0.2721	0.0039	0.26	3.675	0.0530	0.652	0.013	0.72	447.4	30.3	0.74
FB6ap_29	39.7	1	0.3951	0.0096	0.10	2.531	0.0610	0.735	0.023	0.21	387.8	73.1	0.84
FB6ap_30	53.9	1.5	0.525	0.012	0.27	1.905	0.0450	0.750	0.023	0.50	473.9	95.6	0.85
FB6ap_31	14.62	0.25	0.1932	0.0025	0.32	5.176	0.0670	0.550	0.010	0.41	470.1	17.4	0.61
FB6ap_32	4.04	0.1	0.0848	0.0013	0.26	11.792	0.1900	0.346	0.009	0.41	338.5	8.1	0.36
FB6ap_33	2.792	0.095	0.0781	0.0018	0.52	12.804	0.3100	0.258	0.007	0.18	365.4	9.3	0.25
FB6ap_34	16.64	0.31	0.196	0.004	0.24	5.102	0.0990	0.617	0.015	0.66	370.6	25.3	0.70
FB6ap_35	40.6	1.5	0.398	0.016	0.38	2.513	0.1000	0.747	0.022	0.59	346.7	72.1	0.86
FB6ap_36	1.73	0.045	0.0725	0.0011	0.12	13.793	0.2100	0.173	0.005	0.36	386.6	6.4	0.15
FB6ap_37	20.83	0.64	0.2225	0.0053	0.28	4.494	0.1100	0.679	0.022	0.44	308.7	40.1	0.78
FB6ap_38	21.15	0.53	0.2375	0.0056	0.36	4.211	0.1000	0.650	0.018	0.55	389.7	35.6	0.74
FB6ap_39	30.5	1.2	0.304	0.012	0.76	3.289	0.1300	0.728	0.019	0.35	304.6	49.1	0.84
FB6ap_40	57.3	1.8	0.554	0.016	-0.09	1.805	0.0530	0.755	0.019	0.74	480.4	85.7	0.86
FB6ap_41	25.69	0.84	0.2717	0.0071	0.27	3.681	0.0960	0.686	0.025	0.51	367.9	54.5	0.78
FB6ap_42	132.8	4.8	1.119	0.044	0.44	0.894	0.0350	0.870	0.034	0.52	-707.8	366.6	1.00
FB6ap_43	60.1	2.6	0.577	0.021	0.64	1.733	0.0650	0.756	0.027	0.33	501.2	121.8	0.86
FB6ap_44	10.95	0.99	0.1496	0.007	0.17	6.684	0.2800	0.519	0.031	-0.13	397.5	40.1	0.57
FB6ap_45	13.05	0.78	0.1712	0.0066	0.33	5.841	0.2200	0.552	0.023	0.03	411.7	34.3	0.61
FB6ap_46	4.68	0.15	0.0927	0.0018	0.27	10.787	0.2100	0.368	0.012	0.36	354.5	11.1	0.39
FB6ap_47	16.6	0.7	0.1959	0.0055	-0.01	5.105	0.1400	0.612	0.032	0.17	378.4	49.7	0.69
FB6ap_48	48.6	1.1	0.4716	0.0093	0.43	2.120	0.0420	0.750	0.018	0.40	413.4	70.0	0.86
FB6ap_49	41.84	0.92	0.405	0.0091	0.49	2.469	0.0540	0.750	0.016	0.54	342.6	55.3	0.87
FB6ap_50	19.59	0.43	0.2165	0.0052	0.22	4.619	0.1100	0.660	0.018	0.69	334.4	32.8	0.75
FB6ap_51	12.16	0.39	0.1556	0.0031	0.57	6.427	0.1300	0.570	0.015	0.12	350.2	20.2	0.64
FB6ap_52	233	11	1.923	0.086	0.49	0.520	0.0240	0.878	0.038	0.45	-3568.0	1187.3	1.00
FB6ap_53	125.1	5.2	1.071	0.043	0.22	0.934	0.0370	0.860	0.033	0.08	-439.2	323.5	1.00
FB6ap_54	5.8	0.18	0.1049	0.0026	0.33	9.533	0.2500	0.404	0.014	0.49	371.9	14.7	0.43
FB6ap_55	221.2	9.2	1.93	0.1	0.82	0.518	0.0250	0.852	0.030	-0.01	-632.9	545.0	1.00
FB6ap_56	2.092	0.063	0.0649	0.0012	0.10	15.408	0.2900	0.234	0.007	0.01	316.0	6.7	0.23
FB6ap_57	4.94	0.22	0.0888	0.0026	0.53	11.261	0.3200	0.402	0.016	0.43	315.9	14.5	0.43
FB6ap_58	13.83	0.3	0.1758	0.0034	0.28	5.688	0.1200	0.572	0.015	0.79	394.9	22.6	0.64
FB6ap_59	41.9	1.7	0.423	0.013	0.20	2.364	0.0720	0.721	0.031	0.48	476.0	101.7	0.82
FB6ap_60	25.05	0.92	0.2784	0.0083	0.36	3.592	0.1100	0.672	0.028	0.44	411.4	61.8	0.76
FB6ap_61	27.4	0.69	0.2816	0.0068	0.09	3.551	0.0880	0.712	0.021	0.09	319.0	48.6	0.82
FB6ap_62	565	23	4.9	0.19	0.34	0.204	0.0083	0.842	0.024	0.47	-3174.9	1697.1	1.00
FB6ap_63	46.5	1.6	0.422	0.012	0.28	2.370	0.0730	0.797	0.029	0.55	166.9	100.5	0.94
FB6ap_64	16.04	0.3	0.1899	0.0031	0.11	5.266	0.0850	0.615	0.013	-0.02	361.5	21.6	0.70
FB6ap_65	32.68	0.84	0.348	0.0072	0.40	2.874	0.0620	0.684	0.019	0.41	492.2	53.3	0.77
FB6ap_66	17.5	1.1	0.2032	0.0094	0.85	4.921	0.2500	0.628	0.021	0.02	366.6	37.8	0.71
FB6ap_67	777	46	6.29	0.33	0.49	0.159	0.0090	0.890	0.027	0.05	0.0	1877.7	1.00
FB6ap_68	13.02	0.37	0.1662	0.0041	0.26	6.017	0.1600	0.573	0.019	0.56	371.0	26.7	0.64
FB6ap_69	27.3	1.3	0.279	0.011	0.70	3.584	0.1700	0.710	0.025	0.16	320.6	57.1	0.82
FB6ap_70	20.49	0.43	0.2342	0.0045	0.10	4.270	0.0800	0.634	0.015	0.66	415.1	29.8	0.72
FB6ap_71	376	18	3.16	0.14	0.75	0.316	0.0140	0.865	0.028	0.35	-8360.4	3186.8	1.00
FB6ap_72	1109	77	9.03	0.66	0.92	0.111	0.0083	0.881	0.023	0.27	0.0	2687.4	1.00
FB6ap_74	20.8	0.54	0.2401	0.0056	0.30	4.165	0.1000	0.633	0.019	0.54	428.4	37.5	0.71
FB6ap_75	30.77	0.79	0.3323	0.0095	0.30	3.009	0.0920	0.682	0.021	0.59	472.8	56.4	0.77
FB6ap_76	16.14	0.65	0.1843	0.0056	0.34	5.426	0.1700	0.641	0.026	0.43	310.6	39.1	0.73
FB6ap_77	14.04	0.67	0.1631	0.0058	0.11	6.131	0.2200	0.628	0.028	0.58	290.5	37.6	0.72
FB6ap_78	13.56	0.6	0.1757	0.0053	0.68	5.692	0.1800	0.560	0.018	0.01	411.6	27.8	0.62
FB6ap_79	62.3	1.3	0.584	0.011	0.36	1.712	0.0320	0.778	0.018	0.51	375.8	87.4	0.90
FB6ap_80	7.49	0.19	0.118	0.0019	0.02	8.475	0.1400	0.463	0.014	0.53	364.1	14.4	0.51
FB6ap_81	480	22	4.03	0.18	0.82	0.248	0.0110	0.858	0.022	0.31	1608.0	648.6	0.93
FB6ap_82	16.22	0.38	0.2077	0.004	0.40	4.815	0.0940	0.564	0.012	0.42	483.7	22.4	0.62
FB6ap_83	148.5	7.3	1.27	0.069	0.19	0.787	0.0450	0.846	0.035	-0.02	-195.3	385.6	1.00
FB6ap_84	12.14	0.3	0.1496	0.0027	0.38	6.684	0.1200	0.590	0.015	0.46	311.9	19.3	0.67
FB6ap_85	23.11	0.37	0.2595	0.0046	0.23	3.854	0.0690	0.646	0.012	0.20	437.8	27.6	0.73
FB6ap_86	30.66	0.71	0.3083	0.0055	0.19	3.244	0.0580	0.725	0.019	0.53	317.8	48.5	0.84
FB6ap_87	37.73	0.81	0.3821	0.0079	0.01	2.617	0.0530	0.714	0.024	0.13	446.0	72.5	0.81

Tables S.2.2 apatite U-Pb data tables (continued)

	$^{207}Pb/^{235}U$	Prop2SE	$^{206}Pb/^{238}U$	Prop2SE	Rho	$^{238}U/^{206}Pb$	Prop2SE	$^{207}Pb/^{206}Pb$	Prop2SE	Rho	^{207}Pb corrected age	Prop2SE	$f^{206}Pb$
FB6ap_88	6.44	0.23	0.1043	0.0021	0.29	9.588	0.2000	0.450	0.016	0.32	332.0	14.8	0.49
FB6ap_89	50.8	1.4	0.486	0.011	0.70	2.058	0.0490	0.769	0.023	0.04	338.3	90.7	0.89
FB6ap_90	35.35	0.94	0.3624	0.0085	0.32	2.759	0.0650	0.712	0.019	0.25	425.7	56.3	0.81
FB6ap_91	34.4	0.68	0.3524	0.0072	0.23	2.838	0.0590	0.708	0.019	0.70	424.6	54.6	0.81
FB6ap_92	37.8	1.3	0.386	0.012	0.12	2.591	0.0850	0.709	0.032	0.37	468.8	95.8	0.80
FB6ap_93	8.11	0.33	0.1168	0.0038	0.67	8.562	0.2700	0.509	0.016	0.01	317.7	18.2	0.57
FB6ap_94	165.1	4.9	1.472	0.043	0.09	0.679	0.0200	0.823	0.028	0.66	608.6	314.7	0.93
FB6ap_95	31.37	0.78	0.3321	0.0076	0.12	3.011	0.0710	0.691	0.020	-0.01	446.4	53.7	0.78
FB6ap_96	3.926	0.094	0.0964	0.0013	0.33	10.373	0.1400	0.297	0.007	0.26	421.8	7.7	0.30
FB6ap_97	40.2	1.2	0.399	0.011	0.86	2.506	0.0740	0.731	0.011	0.17	407.2	41.3	0.84
FB6ap_98	26.96	0.74	0.2926	0.0064	0.62	3.418	0.0750	0.672	0.019	0.12	434.8	45.3	0.76
FB6ap_99	50.3	1.6	0.49	0.014	0.74	2.041	0.0600	0.746	0.017	0.12	452.9	69.4	0.85
FB6ap_100	96	2.8	0.867	0.023	0.28	1.153	0.0310	0.811	0.027	0.57	310.3	188.5	0.94
FB6ap_101	47.4	1.3	0.477	0.011	0.57	2.096	0.0460	0.723	0.018	0.33	542.3	69.4	0.82
FB6ap_102	47.3	1.2	0.46	0.012	0.74	2.174	0.0550	0.749	0.017	0.10	405.1	65.5	0.86
FB6ap_103	24.41	0.64	0.2587	0.0068	0.20	3.865	0.1100	0.682	0.021	0.64	357.3	44.6	0.78
FB6ap_104	26.26	0.97	0.2789	0.0091	0.53	3.586	0.1200	0.700	0.027	0.33	344.9	60.6	0.80
FB6ap_105	14.26	0.34	0.1801	0.0036	0.29	5.552	0.1100	0.577	0.015	0.52	397.7	23.2	0.65
FB6ap_106	13.51	0.33	0.1779	0.0037	0.11	5.621	0.1100	0.555	0.016	0.63	424.2	24.3	0.62
FB6ap_107	32.39	0.66	0.3476	0.0076	0.35	2.877	0.0630	0.682	0.017	0.61	497.7	48.5	0.77
FB6ap_108	452	17	3.93	0.16	0.86	0.254	0.0110	0.843	0.018	0.34	-758.2	712.2	1.00
FB6ap_109	56.9	5.4	0.521	0.027	0.72	1.919	0.1200	0.792	0.023	0.20	246.8	99.6	0.93
FB6ap_110	104.4	3.1	0.923	0.025	0.34	1.083	0.0290	0.818	0.025	0.54	256.4	189.0	0.96
FB6ap_111	47	1.6	0.457	0.013	0.34	2.188	0.0650	0.752	0.028	0.55	388.6	101.3	0.86
FB6ap_112	15.97	0.74	0.2111	0.0078	0.18	4.737	0.1700	0.559	0.030	0.57	500.5	51.3	0.62
FB6ap_113	39	1.5	0.391	0.015	0.49	2.558	0.1100	0.729	0.030	0.57	404.7	92.7	0.83
FB6ap_114	1049	51	8.53	0.39	0.89	0.117	0.0053	0.887	0.024	0.17	0.0	2431.5	1.00
FB6ap_116	16.05	0.38	0.1866	0.003	0.27	5.359	0.0890	0.628	0.016	0.38	334.9	25.1	0.71
FB6ap_117	135	18	1.066	0.058	0.23	0.938	0.0500	0.858	0.180	-0.04	-395.0	1684.7	1.06
FB6ap_118	4.235	0.075	0.0995	0.0013	0.17	10.050	0.1300	0.310	0.007	0.34	425.2	7.6	0.31
FB6ap_119	11.42	0.53	0.1543	0.0037	0.21	6.481	0.1700	0.542	0.020	0.00	382.0	25.9	0.60
FB8ap_0	131.2	6.5	1.09	0.05	0.80	0.917	0.0421	0.865	0.030	0.02	-561.6	309.2	1.00
FB8ap_1	47.1	2	0.463	0.018	0.67	2.160	0.0840	0.739	0.020	0.08	452.8	76.1	0.84
FB8ap_2	21.9	1.8	0.2294	0.011	0.25	4.359	0.2090	0.695	0.035	-0.03	287.7	64.8	0.80
FB8ap_3	43.7	1.8	0.403	0.019	0.52	2.481	0.1170	0.785	0.023	0.15	205.2	77.5	0.92
FB8ap_4	491	24	4.04	0.23	0.01	0.248	0.0141	0.885	0.024	-0.02	-1820.0	1077.0	1.00
FB8ap_5	48.7	2.5	0.439	0.024	0.49	2.278	0.1245	0.808	0.039	0.12	126.4	139.6	0.95
FB8ap_6	26.68	1.3	0.2898	0.011	0.40	3.451	0.1310	0.681	0.015	0.03	407.8	39.1	0.77
FB8ap_7	266	18	2.2	0.14	0.70	0.455	0.0289	0.889	0.042	-0.02	-11525.5	5972.6	1.00
FB8ap_8	468	43	3.55	0.24	0.34	0.282	0.0190	0.969	0.059	-0.09	-5520.3	3901.5	1.00
FB8ap_9	205.6	9.5	1.75	0.12	0.31	0.571	0.0392	0.872	0.030	-0.05	-2099.6	674.2	1.00
FB8ap_10	81.8	7.4	0.731	0.057	0.00	1.368	0.1067	0.830	0.068	-0.01	58.4	404.2	0.99
FB8ap_11	47.6	2.2	0.432	0.02	0.06	2.315	0.1072	0.817	0.033	0.56	84.1	118.1	0.97
FB8ap_12	43.1	3	0.432	0.036	0.01	2.315	0.1929	0.746	0.058	0.18	387.1	194.7	0.86
FB8ap_13	81.8	3.7	0.82	0.2	0.09	1.220	0.2974	0.829	0.030	0.59	84.4	205.9	0.98
FB8ap_14	8.21	0.47	0.1207	0.0054	0.27	8.285	0.3707	0.494	0.017	0.65	343.0	22.2	0.55
FB8ap_15	93.5	5.8	0.813	0.037	0.08	1.230	0.0560	0.845	0.042	0.12	-98.4	289.4	1.00
FB8ap_16	128	16	1.09	0.13	-0.01	0.917	0.1094	0.900	0.110	-0.01	-1408.7	1295.4	1.00
FB8ap_17	36.9	6.3	0.349	0.052	0.77	2.865	0.4269	0.666	0.041	-0.58	548.4	133.5	0.75
FB8ap_18	56.6	6.1	0.51	0.043	0.98	1.961	0.1653	0.799	0.049	0.00	202.5	199.8	0.94
FB8ap_19	29.6	1.6	0.29	0.015	0.22	3.448	0.1784	0.734	0.028	0.08	273.2	66.6	0.85
FB8ap_20	135.7	7.5	1.199	0.065	0.72	0.834	0.0452	0.834	0.027	0.32	99.4	270.8	0.99
FB8ap_21	278	21	2.33	0.19	0.85	0.429	0.0350	0.881	0.034	-0.04	-9628.1	3968.6	1.00
FB8ap_22	8.1	0.38	0.1235	0.0052	0.26	8.097	0.3409	0.483	0.021	0.37	361.9	25.2	0.53
FB8ap_23	48.6	2	0.447	0.018	0.53	2.237	0.0901	0.797	0.025	0.16	179.6	92.9	0.94
FB8ap_24	21.82	1.1	0.236	0.012	0.00	4.237	0.2155	0.676	0.034	0.10	335.1	65.0	0.77
FB8ap_25	17.4	1.1	0.196	0.01	0.35	5.102	0.2603	0.664	0.049	0.45	294.0	76.4	0.76
FB8ap_26	16.68	0.83	0.1879	0.0093	-0.03	5.322	0.2634	0.642	0.033	0.77	315.5	51.0	0.73
FB8ap_27	8.15	0.49	0.1197	0.0055	0.03	8.354	0.3839	0.487	0.019	-0.01	346.7	23.8	0.54
FB8ap_28	2150	260	17.7	2.7	0.21	0.056	0.0086	0.910	0.047	0.00	0.0	7090.7	1.00
FB8ap_29	10.26	0.46	0.146	0.014	0.14	6.849	0.6568	0.535	0.022	0.54	369.0	42.9	0.60
FB8ap_30	20.57	1	0.2152	0.01	0.14	4.647	0.2159	0.691	0.031	0.62	275.7	54.5	0.80
FB8ap_31	29.3	2.1	0.285	0.012	0.05	3.509	0.1477	0.750	0.047	0.02	226.9	106.6	0.87
FB8ap2_0	20.72	0.72	0.2214	0.0058	0.27	4.517	0.2000	0.676	0.029	0.59	312.7	51.4	0.78
FB8ap2_1	14.61	0.72	0.1735	0.0053	0.12	5.764	0.1700	0.616	0.033	0.07	327.2	45.8	0.70
FB8ap2_2	36.3	1.1	0.348	0.011	0.42	2.874	0.0900	0.749	0.023	0.56	289.1	65.7	0.87
FB8ap2_3	103.7	4.6	0.925	0.054	0.33	1.081	0.0480	0.838	0.023	0.45	-16.5	185.2	1.00
FB8ap2_4	6.66	0.19	0.1143	0.0022	0.11	8.749	0.1700	0.427	0.013	0.50	384.9	13.9	0.46
FB8ap2_5	8.13	0.15	0.1296	0.0019	0.20	7.716	0.1100	0.455	0.009	0.52	409.0	11.7	0.49
FB8ap2_6	473	37	3.77	0.28	0.90	0.265	0.0560	0.939	0.038	-0.08	-4153.1	2213.7	1.00
FB8ap2_7	256.5	9.5	2.188	0.068	0.60	0.457	0.0150	0.852	0.028	0.45	-646.0	577.4	1.00
FB8ap2_8	34.4	1.1	0.3345	0.0086	0.39	2.990	0.0790	0.751	0.023	0.44	269.9	63.2	0.87
FB8ap2_9	31.88	0.91	0.3155	0.0085	0.44	3.170	0.0870	0.734	0.020	0.49	300.8	52.5	0.85
FB8ap2_10	183	12	1.578	0.099	0.97	0.634	0.0360	0.856	0.015	0.05	-707.8	255.9	1.00
FB8ap2_11	37.59	0.81	0.3575	0.006	0.45	2.797	0.0460	0.759	0.016	0.40	265.2	49.3	0.88
FB8ap2_12	245	12	2.021	0.093	-0.08	0.495	0.0230	0.874	0.038	0.13	-3508.0	1227.3	1.00
FB8ap2_13	11.1	0.55	0.1394	0.0039	-0.04	7.174	0.2000	0.581	0.034	0.11	300.1	38.0	0.66
FB8ap2_14	295	16	2.44	0.13	0.61	0.410	0.0220	0.840	0.036	0.50	1402.5	607.0	0.90
FB8ap2_15	12.21	0.45	0.1565	0.0047	0.18	6.390	0.1800	0.570	0.024	0.53	352.3	31.3	0.64
FB8ap2_16	541	42	4.41	0.29	0.88	0.227	0.0150	0.875	0.033	0.00	-1557.5	1506.1	1.00
FB8ap2_17	10.31	0.31	0.136	0.0032	0.14	7.353	0.1700	0.556	0.021	0.60	320.0	23.9	0.63
FB8ap2_18	232.4	6.2	2.078	0.066	0.85	0.481	0.0950	0.807	0.021	-0.15	3598.6	1098.8	0.64
FB8ap2_19	33.9	1	0.327	0.0086	0.16	3.058	0.0800	0.747	0.028	0.58	274.8	73.8	0.87
FB8ap2_20	139.4	4	1.196	0.031	0.71	0.836	0.0210	0.862	0.021	0.20	-589.4	247.3	1.00
FB8ap2_21	57.4	2.1	0.539	0.022	-0.05	1.855	0.0690	0.777	0.033	0.63	342.8	140.7	0.90
FB8ap2_22	64.2	1.7	0.556	0.014	0.48	1.799	0.0450	0.847	0.022	0.49	-71.8	108.5	1.00

Tables S.2.2 apatite U-Pb data tables (continued)

	$^{207}Pb/^{235}U$	Prop2SE	$^{206}Pb/^{238}U$	Prop2SE	Rho	$^{238}U/^{206}Pb$	Prop2SE	$^{207}Pb/^{206}Pb$	Prop2SE	Rho	^{207}Pb corrected age	Prop2SE	$f^{206}Pb$
FB8ap2_23	32.87	0.86	0.3151	0.0077	0.20	3.174	0.0760	0.768	0.027	0.64	202.5	69.7	0.90
FB8ap2_24	51.9	2.1	0.456	0.016	0.57	2.193	0.0790	0.822	0.028	0.31	66.3	107.3	0.98
FB8ap2_25	69.7	2.6	0.667	0.024	0.63	1.499	0.0600	0.775	0.023	-0.11	474.9	122.3	0.89
FB8ap2_26	229	9.7	1.781	0.064	0.43	0.561	0.0210	0.905	0.038	0.44	-6876.9	2010.0	1.00
FB8ap2_27	14.74	0.33	0.164	0.0029	0.21	6.098	0.1000	0.651	0.017	0.48	260.9	23.6	0.75
FB8ap2_28	50.3	1.3	0.454	0.01	0.25	2.203	0.0500	0.793	0.021	0.58	201.6	80.2	0.93
FB8ap2_29	7.08	0.18	0.1138	0.0022	-0.06	8.787	0.1800	0.449	0.015	0.61	363.5	15.2	0.49
FB8ap2_30	19.21	0.7	0.2065	0.005	0.04	4.843	0.1200	0.730	0.110	-0.02	194.4	179.3	0.85
FB8ap2_31	125.8	3	1.056	0.036	0.12	0.947	0.0280	0.878	0.028	0.76	-805.0	295.5	1.00
FB8ap2_32	2610	230	20.5	1.8	0.93	0.049	0.0043	0.929	0.028	0.07	0.0	5079.5	1.00
FB8ap2_33	335	24	3.03	0.23	0.03	0.330	0.0260	0.842	0.040	0.49	0.0	856.1	0.78
FB8ap2_34	50.1	1.9	0.45	0.015	0.51	2.222	0.0730	0.794	0.029	0.44	194.8	106.7	0.93
FB8ap2_35	33.35	0.84	0.3189	0.0083	0.19	3.136	0.0780	0.762	0.022	0.70	223.1	58.4	0.89
FB8ap2_36	46.8	1.5	0.428	0.013	0.30	2.336	0.0730	0.791	0.030	0.44	195.6	104.7	0.93
FB8ap2_37	15.89	0.43	0.2017	0.0048	0.62	4.958	0.1200	0.573	0.014	0.26	454.4	25.2	0.64
FB8ap2_38	30.61	0.7	0.3072	0.006	0.41	3.255	0.0690	0.717	0.019	0.26	338.4	48.2	0.82
FB8ap2_39	52.7	1.7	0.475	0.015	0.11	2.105	0.0660	0.816	0.026	0.48	100.2	103.7	0.97
FB8ap2_40	291	15	2.42	0.19	0.25	0.413	0.0280	0.907	0.039	0.51	-1548.3	974.7	1.00
FB8ap2_41	321	12	2.53	0.12	0.25	0.395	0.0260	0.921	0.027	0.10	-1993.2	774.5	1.00
FB8ap2_42	10.94	0.46	0.1426	0.0043	-0.03	7.013	0.1900	0.557	0.029	0.08	334.9	33.8	0.63
FB8ap2_43	258.3	9.5	2.056	0.082	0.78	0.486	0.0220	0.912	0.026	-0.01	0.0	713.7	1.00
FB8ap2_44	556	64	4.48	0.47	0.30	0.223	0.0220	0.841	0.040	0.15	-685.3	1648.6	1.00
FB8ap2_45	158.3	7	1.327	0.062	0.56	0.754	0.0400	0.870	0.041	0.57	-1003.1	547.9	1.00
FB8ap2_46	42.2	1.1	0.3996	0.0087	0.23	2.503	0.0520	0.770	0.022	0.35	261.1	72.6	0.90
FB8ap2_47	99.2	3.7	0.829	0.031	0.60	1.206	0.0490	0.861	0.032	-0.03	-297.6	237.3	1.00
FB8ap2_48	322	22	2.536	0.098	0.03	0.394	0.0150	0.919	0.059	0.08	-1945.0	1599.6	1.00
FB8ap2_49	26.5	1.2	0.257	0.011	0.08	3.891	0.1700	0.729	0.033	0.04	249.7	68.5	0.85
FB8ap2_50	56.4	2.4	0.561	0.059	0.12	1.783	0.1000	0.807	0.035	0.74	181.6	160.1	0.95
FB8ap2_51	201	21	1.71	0.15	0.96	0.585	0.0410	0.821	0.015	0.37	1075.1	219.4	0.89
FB8ap2_52	2310	360	17.8	2.8	0.77	0.056	0.0075	0.919	0.044	-0.02	0.0	6782.0	1.00
FB8ap2_53	605	28	5.15	0.31	0.59	0.194	0.0130	0.902	0.031	0.00	0.0	1766.9	1.00
FB8ap2_54	7.34	0.26	0.1086	0.0029	0.40	9.208	0.2400	0.489	0.019	0.38	312.3	18.3	0.54
FB8ap2_55	32	2.2	0.303	0.016	0.30	3.300	0.1800	0.753	0.035	-0.01	235.1	85.6	0.88
FB8ap2_56	4540	600	36.9	4.6	0.97	0.027	0.0032	0.876	0.034	0.05	0.0	10656.4	1.00
FB8ap2_57	4.67	0.32	0.0887	0.0023	0.03	11.274	0.3000	0.394	0.034	0.38	321.1	24.7	0.42
FB8ap2_58	67.2	7.3	0.625	0.057	0.31	1.600	0.1400	0.736	0.031	-0.04	686.5	156.1	0.82
FB8ap2_59	40.7	2	0.395	0.018	-0.03	2.532	0.1100	0.746	0.033	0.07	347.3	103.5	0.86
FB8ap2_60	7.68	0.69	0.1213	0.0038	-0.06	8.244	0.2400	0.452	0.038	0.19	385.0	37.2	0.49
FB8ap2_61	18	0.77	0.2085	0.0067	0.41	4.796	0.1500	0.618	0.020	0.28	394.0	35.3	0.70
FB8ap2_62	10.94	0.53	0.1483	0.0037	0.02	6.743	0.2000	0.536	0.026	0.05	373.8	31.3	0.60
FB8ap2_63	69.4	6.2	0.59	0.034	-0.01	1.695	0.0930	0.818	0.072	0.13	121.8	341.2	0.97
FB8ap2_64	20.73	0.63	0.216	0.0049	0.23	4.630	0.1000	0.698	0.021	0.26	263.9	37.6	0.81
FB8ap2_65	75.5	6.1	0.658	0.039	0.00	1.520	0.1000	0.826	0.063	-0.04	80.4	336.2	0.98
FB8ap2_66	97	11	0.877	0.087	0.89	1.140	0.1100	0.764	0.013	-0.25	839.4	122.9	0.84
FB8ap2_67	21.4	3.5	0.213	0.012	0.00	4.695	0.2500	0.730	0.110	-0.02	201.1	185.0	0.85
FB8ap2_68	77.6	2.8	0.667	0.036	0.28	1.499	0.2200	0.818	0.047	0.82	146.5	252.8	0.97
FB8ap2_69	7.4	1.7	0.133	0.019	0.26	7.519	0.4900	0.500	0.130	0.02	372.3	141.9	0.55
FB8ap2_70	11.05	0.36	0.194	0.038	0.15	5.155	0.2700	0.491	0.038	0.88	562.6	120.6	0.53
FB8ap2_71	9.7	1.1	0.133	0.014	-0.04	7.519	0.5700	0.575	0.084	0.14	292.3	91.8	0.65
FB8ap2_72	5600	1300	45	11	1.00	0.022	0.0550	0.930	0.036	0.03	0.0	16006.5	1.00
FB8ap2_73	26	1.2	0.2537	0.0086	0.33	3.942	0.1400	0.759	0.030	-0.17	178.5	62.3	0.89
FB8ap2_74	34.3	3.1	0.348	0.024	0.15	2.874	0.1800	0.710	0.043	-0.03	412.3	118.1	0.81
FB8ap2_75	49.4	1.7	0.526	0.081	-0.02	1.901	0.1300	0.777	0.033	0.31	331.9	145.9	0.90
FB8ap2_76	25	3.7	0.238	0.022	0.01	4.202	0.3500	0.729	0.088	0.01	229.3	165.8	0.85
FB8ap2_77	135.8	4.8	1.182	0.07	0.52	0.846	0.0370	0.866	0.032	0.27	-681.3	364.8	1.00
FB8ap2_78	21.3	1.2	0.284	0.084	-0.02	3.521	0.2500	0.655	0.046	0.13	461.7	166.3	0.74
FB8ap2_79	90	4.7	0.76	0.034	-0.02	1.316	0.0450	0.857	0.047	0.20	-216.3	308.7	1.00
FB8ap2_80	57.3	1.9	0.531	0.021	0.40	1.883	0.0670	0.776	0.016	0.35	341.5	73.5	0.90
FB8ap2_81	55.1	2.1	0.488	0.021	0.11	2.049	0.1300	0.816	0.026	0.02	103.9	106.5	0.97
FB8ap2_82	32	0.99	0.327	0.052	-0.02	3.058	0.0810	0.778	0.025	0.54	181.0	73.3	0.91
FB8ap2_83	7.48	0.43	0.109	0.003	0.01	9.174	0.2500	0.492	0.034	-0.05	310.9	30.1	0.55
FB8ap2_84	48.9	1.6	0.466	0.011	0.00	2.146	0.0460	0.758	0.028	0.16	371.0	103.4	0.87
FB8ap2_85	10.52	0.36	0.1417	0.0046	0.23	7.057	0.1500	0.534	0.020	0.37	358.9	25.1	0.60
FB8ap3_0	54.1	1.3	0.518	0.015	0.40	1.931	0.0520	0.759	0.020	0.61	419.5	84.5	0.87
FB8ap3_1	247	11	2.05	0.089	0.76	0.488	0.0210	0.876	0.019	0.22	-4055.2	764.9	1.00
FB8ap3_2	347	17	2.79	0.12	0.76	0.358	0.0160	0.894	0.026	0.25	-1450.8	756.9	1.00
FB8ap3_3	104.2	4.8	0.881	0.038	0.71	1.135	0.0510	0.859	0.033	0.41	-300.7	259.6	1.00
FB8ap3_4	398	17	3.33	0.17	0.29	0.300	0.0140	0.874	0.029	0.35	0.0	1296.4	1.00
FB8ap3_5	31.46	0.73	0.3107	0.0098	0.38	3.219	0.1000	0.732	0.020	0.39	301.1	51.9	0.85
FB8ap3_6	8.42	0.34	0.125	0.0034	0.34	8.000	0.2200	0.491	0.016	-0.11	358.4	18.6	0.54
FB8ap3_7	37.5	1.3	0.353	0.011	0.75	2.833	0.0900	0.772	0.018	0.25	218.2	54.6	0.90
FB8ap3_8	4900	790	39.9	6.6	1.00	0.025	0.0041	0.906	0.031	0.23	0.0	11125.4	1.00
FB8ap3_9	54	2.2	0.48	0.018	0.73	2.083	0.0800	0.821	0.024	0.27	76.1	98.0	0.98
FB8ap3_10	459	18	3.69	0.15	0.85	0.271	0.0120	0.901	0.022	0.42	-14497.7	7697.1	1.00
FB8ap3_11	608	33	5.04	0.27	0.80	0.198	0.0092	0.883	0.029	0.18	0.0	1479.1	1.00
FB8ap3_12	52.5	1.7	0.493	0.014	0.67	2.028	0.0540	0.776	0.019	0.19	309.9	78.4	0.90
FB8ap3_13	48.6	1.5	0.443	0.013	0.54	2.257	0.0630	0.800	0.025	0.42	164.1	92.2	0.94
FB8ap3_14	84	2.6	0.746	0.025	0.33	1.340	0.0480	0.824	0.028	0.20	118.4	173.8	0.98
FB8ap3_15	17.72	0.51	0.2051	0.0045	0.46	4.876	0.1100	0.627	0.017	0.36	371.9	29.4	0.71
FB8ap3_16	36.32	0.78	0.3339	0.0067	0.57	2.995	0.0590	0.788	0.015	0.50	154.0	44.9	0.93
FB8ap3_17	1052	57	8.36	0.52	0.83	0.120	0.0067	0.926	0.030	0.33	-15733.4	23617.9	1.00
FB8ap3_18	9.95	0.3	0.1375	0.003	0.41	7.273	0.1500	0.527	0.015	0.35	355.7	18.3	0.59
FB8ap3_19	376	37	2.93	0.29	0.79	0.341	0.0300	0.957	0.033	-0.01	0.0	1276.8	1.00
FB8ap3_20	587	23	4.73	0.19	0.85	0.211	0.0087	0.904	0.020	0.28	0.0	1068.1	1.00
FB8ap3_21	55.9	1.9	0.489	0.013	0.39	2.045	0.0560	0.834	0.028	0.43	9.4	116.4	1.00
FB8ap3_22	34.03	0.6	0.3257	0.0056	0.11	3.070	0.0530	0.761	0.019	0.72	231.6	52.2	0.89
FB8ap3_23	6.05	0.14	0.103	0.0018	0.22	9.709	0.1700	0.428	0.011	0.47	345.7	11.0	0.47

Tables S.2.2 apatite U-Pb data tables (continued)

	$^{207}Pb/^{235}U$	Prop2SE	$^{206}Pb/^{238}U$	Prop2SE	Rho	$^{238}U/^{206}Pb$	Prop2SE	$^{207}Pb/^{206}Pb$	Prop2SE	Rho	^{207}Pb corrected age	Prop2SE	$f^{206}Pb$
FB8ap3_24	49.4	1.8	0.476	0.016	0.85	2.101	0.0710	0.753	0.014	0.09	404.3	58.8	0.86
FB8ap3_25	118.5	3.3	1.022	0.027	0.56	0.978	0.0240	0.841	0.020	0.36	-63.6	182.8	1.00
FB8ap3_26	308.3	9	2.521	0.074	0.70	0.397	0.0120	0.892	0.021	0.46	0.0	714.5	1.00
FB8ap3_27	1450	150	11.9	1.2	0.97	0.084	0.0080	0.878	0.028	0.09	0.0	4892.0	1.00
FB8ap3_28	526	23	4.56	0.23	0.90	0.219	0.0110	0.850	0.019	0.27	-2077.9	1070.0	1.00
FB8ap3_29	17.2	0.65	0.1937	0.0068	0.46	5.163	0.1800	0.648	0.026	0.52	316.2	41.4	0.74
FB8ap3_30	16.44	0.58	0.195	0.0056	0.38	5.128	0.1600	0.613	0.022	0.41	375.0	35.5	0.69
FB8ap3_31	204	12	1.737	0.091	0.83	0.576	0.0340	0.842	0.032	0.00	35.8	462.2	1.00
FB8ap3_32	51.5	1.7	0.467	0.014	0.64	2.141	0.0610	0.804	0.023	0.37	156.3	90.3	0.95
FB8ap3_33	2440	300	19.9	2.2	0.98	0.050	0.0059	0.885	0.030	0.01	0.0	5136.9	1.00
FB8ap3_34	13.21	0.61	0.1688	0.005	0.19	5.924	0.1800	0.568	0.027	0.45	383.9	37.1	0.64
FB8ap3_35	17.4	0.68	0.2062	0.0073	0.41	4.850	0.1900	0.611	0.024	0.50	401.3	41.1	0.69
FB8ap3_36	22.66	0.72	0.2354	0.0056	0.54	4.248	0.1000	0.693	0.018	0.26	300.0	35.7	0.80
FB8ap3_37	75	2.3	0.644	0.022	0.74	1.553	0.0570	0.848	0.032	0.32	-95.7	177.2	1.00
FB8ap3_38	20.71	0.57	0.2347	0.005	0.51	4.261	0.0920	0.639	0.016	0.34	406.3	31.7	0.72
FB8ap3_39	24.93	0.83	0.2732	0.0092	0.51	3.660	0.1300	0.665	0.023	0.53	419.2	51.3	0.75
FB8ap3_40	448	19	3.61	0.16	0.83	0.277	0.0130	0.905	0.022	0.34	-16087.7	9805.7	1.00
FB8ap3_41	18.7	1.1	0.208	0.012	0.64	4.808	0.2700	0.655	0.033	0.21	329.0	56.9	0.75
FB8ap3_42	63.7	1.5	0.555	0.014	0.05	1.802	0.0480	0.825	0.025	0.74	68.2	117.8	0.98
FB8ap3_43	2.45	0.16	0.0664	0.0016	0.83	15.060	0.3600	0.266	0.012	-0.67	306.9	9.6	0.27
FB8ap3_44	35	1	0.33	0.009	0.32	3.030	0.0810	0.771	0.026	0.54	204.6	70.5	0.90
FB8ap3_45	10.46	0.36	0.1306	0.0037	0.25	7.657	0.2200	0.585	0.022	0.51	276.2	24.3	0.66
FB8ap3_46	65.9	2.1	0.614	0.02	0.73	1.629	0.0540	0.783	0.021	0.35	369.6	105.6	0.90
FB8ap3_47	53.9	1.5	0.501	0.015	0.71	1.996	0.0560	0.781	0.016	0.47	291.0	69.5	0.91
FB8ap3_48	109.9	5.3	1.013	0.059	0.46	0.987	0.0580	0.806	0.032	-0.13	490.7	251.0	0.92
FB8ap3_49	32.9	1.5	0.324	0.013	0.77	3.086	0.1300	0.738	0.022	0.12	298.4	59.2	0.85
FB8ap3_50	56.2	1.6	0.53	0.015	0.56	1.887	0.0530	0.777	0.021	0.39	335.2	91.5	0.90
FB8ap3_51	47.5	2.5	0.427	0.019	0.36	2.342	0.1200	0.806	0.049	0.52	130.7	169.0	0.95
FB8ap3_52	329	17	2.79	0.14	0.76	0.358	0.0170	0.856	0.029	0.29	-1261.2	839.8	1.00
FB8ap3_53	69.2	2.1	0.59	0.015	0.56	1.695	0.0450	0.845	0.022	0.36	-63.7	114.9	1.00
FB8ap3_54	47.3	3	0.487	0.023	0.35	2.053	0.1000	0.710	0.040	0.04	615.6	147.3	0.79
FB8ap3_55	15.99	0.77	0.1796	0.0073	0.76	5.568	0.2400	0.643	0.020	0.26	299.3	31.5	0.74
FB8ap3_56	5.84	0.24	0.1059	0.0029	0.79	9.443	0.2600	0.402	0.011	-0.16	377.1	13.8	0.43
FB10ap_0	232.6	7.6	1.949	0.059	0.71	0.513	0.0155	0.869	0.020	0.25	-2450.8	545.7	1.00
FB10ap_1	16.89	1.3	0.1961	0.01	0.71	5.099	0.2600	0.625	0.018	0.15	357.8	33.7	0.71
FB10ap_2	162.9	4.9	1.395	0.041	0.67	0.717	0.0211	0.847	0.022	0.47	-245.8	279.5	1.00
FB10ap_4	115.5	2.2	1.044	0.018	0.69	0.958	0.0165	0.804	0.012	0.28	551.8	111.6	0.91
FB10ap_5	15.8	8.7	0.269	0.084	0.82	3.717	1.1608	0.426	0.021	-0.36	922.9	281.1	0.43
FB10ap_6	17.63	0.87	0.2013	0.0069	0.24	4.968	0.1703	0.646	0.036	0.31	332.8	57.6	0.74
FB10ap_7	2300	4500	13	51	0.99	0.077	3.3018	0.897	0.036	0.24	-21357.1	671166.3	1.00
FB10ap_8	9.12	0.27	0.199	0.0041	0.26	5.025	0.1035	0.333	0.010	0.12	816.2	21.7	0.32
FB10ap_9	22	2.2	0.252	0.019	0.83	3.968	0.2992	0.624	0.019	-0.25	470.3	51.2	0.70
FB10ap_10	406	20	3.52	0.18	0.84	0.284	0.0145	0.857	0.026	0.22	-189.6	788.9	1.00
FB10ap_11	42.9	2	0.475	0.019	0.69	2.105	0.0842	0.655	0.013	0.20	831.3	58.2	0.71
FB10ap_12	58.5	6.7	0.532	0.058	0.91	1.880	0.2049	0.794	0.024	0.20	242.5	108.1	0.93
FB10ap_13	34.5	1.1	0.359	0.0093	0.18	2.786	0.0722	0.704	0.026	0.52	446.7	73.6	0.80
FB10ap_14	49.3	2.3	0.472	0.024	0.76	2.119	0.1077	0.769	0.026	0.44	325.9	99.7	0.89
FB10ap_15	16.24	0.53	0.2666	0.0058	-0.01	3.751	0.0816	0.444	0.018	0.58	878.5	39.1	0.45
FB10ap_16	37.2	4.2	0.371	0.036	0.88	2.695	0.2616	0.727	0.016	0.04	387.0	61.7	0.83
FB10ap_17	31.02	0.54	0.3294	0.0057	0.36	3.036	0.0525	0.685	0.013	0.54	459.5	37.0	0.78
FB10ap_18	8.78	2.3	0.1662	0.017	0.85	6.017	0.6154	0.381	0.026	-0.44	620.8	69.5	0.39
FB10ap_19	85.7	2.5	0.772	0.022	0.57	1.295	0.0369	0.814	0.022	0.42	225.1	141.8	0.95
FB10ap_20	9.5	46	0.1349	0.32	0.84	7.413	17.5843	0.499	0.043	-0.27	378.9	883.6	0.55
FB10ap_21	560	40	4.4	0.3	0.93	0.227	0.0155	0.916	0.027	0.30	0.0	1419.6	1.00
FB10ap_22	4130	350	33.3	2.6	0.99	0.030	0.0023	0.871	0.013	-0.01	0.0	4268.2	1.00
FB10ap_23	1168	87	9.26	0.69	0.93	0.108	0.0080	0.920	0.030	0.23	-18552.3	40645.1	1.00
FB10ap_24	58	1.6	0.536	0.014	0.70	1.866	0.0487	0.788	0.016	0.33	278.9	74.4	0.92
FB10ap_26	267.4	8.7	2.242	0.077	0.65	0.446	0.0153	0.873	0.025	0.44	-4771.1	1155.8	1.00
FB10ap_27	269.6	6.5	2.26	0.052	0.70	0.442	0.0102	0.864	0.016	0.38	-2681.8	542.1	1.00
FB10ap_28	33.07	0.81	0.3347	0.0078	0.53	2.988	0.0696	0.723	0.017	0.45	355.3	47.9	0.83
FB10ap_29	1376	75	11.07	0.63	0.58	0.090	0.0051	0.890	0.022	0.38	-8418.8	7545.6	1.00
FB10ap_30	5.75	0.12	0.1975	0.0025	0.18	5.063	0.0641	0.212	0.005	0.44	980.8	14.0	0.17
FB10ap_31	17.86	0.93	0.2716	0.0084	0.74	3.682	0.1139	0.476	0.015	-0.23	829.8	38.9	0.49
FB10ap_32	470	29	3.73	0.19	0.85	0.268	0.0137	0.895	0.031	0.24	-11207.6	6199.2	1.00
FB10ap_33	90.2	2.7	0.791	0.022	0.66	1.264	0.0352	0.830	0.021	0.34	68.0	143.9	0.99
FB10ap_34	32.2	1.7	0.3297	0.015	0.69	3.033	0.1380	0.702	0.016	0.31	410.8	47.2	0.80
FB10ap_35	1560	130	13	1.1	0.94	0.077	0.0065	0.888	0.027	0.04	-11183.7	16353.5	1.00
FB10ap_36	71.4	2.7	0.641	0.023	0.80	1.560	0.0560	0.807	0.016	0.17	219.8	90.3	0.95
FB10ap_37	17.3	1.6	0.291	0.016	0.71	3.436	0.1889	0.420	0.021	-0.50	1014.0	68.6	0.41
FB10ap_38	37.1	2.1	0.364	0.02	0.85	2.747	0.1509	0.744	0.024	0.22	321.7	72.4	0.86
FB10ap_39	4.12	0.11	0.1005	0.0015	0.36	9.950	0.1485	0.298	0.007	0.10	438.5	8.6	0.30
FB10ap_40	62.5	2.6	0.584	0.019	0.58	1.712	0.0557	0.771	0.029	0.30	418.8	133.1	0.89
FB10ap_41	938	68	7.59	0.53	0.92	0.132	0.0092	0.901	0.028	0.20	-5947.4	4386.9	1.00
FB10ap_42	90.3	4.4	0.807	0.038	0.83	1.239	0.0583	0.816	0.019	0.34	221.5	131.0	0.96
FB10ap_43	29.19	0.87	0.3039	0.0075	-0.05	3.291	0.0812	0.703	0.027	0.66	371.8	65.2	0.80
FB10ap_44	724	25	5.82	0.21	0.85	0.172	0.0062	0.903	0.016	0.33	0.0	1153.7	1.00
FB10ap_45	5.18	0.18	0.1596	0.0025	0.70	6.266	0.0981	0.236	0.005	-0.30	767.3	13.1	0.21
FB10ap_46	52.4	1.6	0.496	0.017	0.72	2.016	0.0691	0.766	0.018	0.33	362.2	75.0	0.88
FB10ap_47	117.4	2.8	1.07	0.025	0.51	0.935	0.0218	0.792	0.020	0.49	769.2	164.8	0.88
FB10ap_48	16.2	0.34	0.201	0.0034	0.25	4.975	0.0842	0.586	0.013	0.43	431.6	22.7	0.66
FB10ap_49	429	14	3.59	0.12	0.76	0.279	0.0093	0.874	0.019	0.25	0.0	1001.4	1.00
FB10ap_50	23.2	2.2	0.255	0.018	0.54	3.922	0.2768	0.662	0.022	0.31	395.1	52.2	0.75
FB10ap_51	9.82	0.71	0.1446	0.0065	0.76	6.916	0.3109	0.488	0.017	-0.10	419.3	26.7	0.54
FB10ap_52	26.3	1.8	0.276	0.016	0.93	3.623	0.2100	0.675	0.014	-0.31	400.4	39.6	0.77
FB10ap_53	911	46	7.47	0.41	0.88	0.134	0.0073	0.900	0.025	0.27	-5656.6	3717.1	1.00
FB10ap_54	607	54	5.05	0.41	0.95	0.198	0.0161	0.872	0.025	0.05	-1658.5	1361.6	1.00
FB10ap_55	167.1	6.7	1.449	0.05	0.65	0.690	0.0238	0.841	0.027	0.21	-31.2	334.5	1.00

Tables S.2.2 apatite U-Pb data tables (continued)

	$^{207}Pb/^{235}U$	Prop2SE	$^{206}Pb/^{238}U$	Prop2SE	Rho	$^{238}U/^{206}Pb$	Prop2SE	$^{207}Pb/^{206}Pb$	Prop2SE	Rho	^{207}Pb corrected age	Prop2SE	$f^{206}Pb$
FB10ap_56	13.81	0.42	0.1764	0.0045	0.48	5.669	0.1446	0.567	0.016	0.37	403.4	24.8	0.63
FB10ap_57	14.06	1.4	0.2049	0.011	0.77	4.880	0.2620	0.497	0.017	-0.18	585.4	40.5	0.54
FB10ap_58	62.6	1.8	0.595	0.016	0.62	1.681	0.0452	0.768	0.021	0.45	448.3	100.7	0.88
FB10ap_59	-1700	4900	-14	39	0.98	-0.071	0.1990	0.925	0.036	0.13	0.0	28771.6	1.00
FB10ap_60	87.2	2.4	0.774	0.022	0.64	1.292	0.0367	0.818	0.021	0.52	186.4	137.6	0.96
FB10ap_61	15.14	0.43	0.2774	0.0047	0.53	3.605	0.0611	0.397	0.009	0.06	1012.9	25.0	0.39
FB10ap_62	8.39	0.43	0.1209	0.0039	0.70	8.271	0.2668	0.503	0.018	-0.09	334.9	20.3	0.56
FB10ap_63	391	23	3.04	0.18	0.85	0.329	0.0195	0.934	0.029	0.39	-43526.8	793839.1	1.00
FB10ap_64	110	3.4	0.953	0.029	0.46	1.049	0.0319	0.833	0.025	0.50	58.5	202.5	0.99
FB10ap_65	3.59	0.14	0.083	0.0018	0.73	12.048	0.2613	0.313	0.009	-0.22	352.9	9.5	0.32
FB10ap_67	86.2	3.8	0.76	0.035	0.56	1.316	0.0606	0.829	0.034	0.44	72.8	214.1	0.99
FB10ap_68	14.76	0.25	0.179	0.0031	0.12	5.587	0.0968	0.600	0.014	0.64	361.6	21.6	0.68
FB10ap_69	83.4	2.6	0.743	0.022	0.89	1.346	0.0399	0.815	0.012	0.25	202.0	84.9	0.96
FB10ap_70	2960	450	23.8	3.6	0.99	0.042	0.0064	0.896	0.018	0.09	0.0	4244.9	1.00
FB10ap_71	116.7	3.2	1.021	0.029	0.36	0.979	0.0278	0.838	0.027	0.61	-12.3	235.7	1.00
FB10ap_72	60.7	1.7	0.585	0.017	0.25	1.709	0.0497	0.757	0.021	0.67	504.6	98.2	0.86
FB10ap_73	150	330	1.24	2.6	0.99	0.806	1.6909	0.860	0.022	-0.18	-573.8	1273.1	1.00
FB10ap_74	13.04	0.35	0.169	0.003	0.39	5.917	0.1050	0.559	0.014	0.29	396.7	20.5	0.62
FB10ap_75	28.84	2.4	0.3053	0.022	0.60	3.275	0.2360	0.681	0.015	0.08	432.2	48.6	0.77
FB10ap_76	14.5	1.8	0.184	0.016	0.91	5.435	0.4726	0.552	0.027	-0.35	443.8	53.7	0.61
FB10ap_77	29.4	0.7	0.2976	0.0071	0.53	3.360	0.0802	0.716	0.017	0.55	329.0	42.8	0.82
FB10ap_78	30.46	2	0.3891	0.021	0.41	2.570	0.1387	0.570	0.018	0.38	932.3	70.3	0.60
FB10ap_79	73.7	2.1	0.67	0.022	0.23	1.493	0.0490	0.806	0.031	0.71	242.6	167.6	0.94
FB10ap_80	82.7	2.6	0.755	0.025	0.59	1.325	0.0439	0.801	0.024	0.50	338.4	146.9	0.93
FB10ap_81	2.676	0.084	0.2033	0.0029	0.52	4.919	0.0702	0.095	0.003	-0.08	1171.8	16.5	0.02
FB10ap_82	6.58	0.16	0.1181	0.0023	0.38	8.467	0.1649	0.406	0.010	0.41	417.2	12.4	0.43
FB10ap_83	2490	1100	19.5	9	0.76	0.051	0.0237	0.943	0.030	-0.02	0.0	9318.7	1.00
FB10ap_84	31.6	3.8	0.325	0.032	0.89	3.077	0.3030	0.708	0.019	0.03	386.9	62.5	0.81
FB10ap_85	397	20	3.18	0.22	0.85	0.314	0.0218	0.899	0.025	0.28	-1841.3	889.8	1.00
FB10ap_86	10	0.24	0.1491	0.0027	0.30	6.707	0.1215	0.488	0.012	0.39	432.7	16.4	0.53
FB10ap_87	14.79	0.67	0.1816	0.0085	-0.07	5.507	0.2577	0.597	0.022	0.71	371.6	35.8	0.67
FB10ap_88	2.93	2.7	0.082	0.025	0.47	12.195	3.7180	0.259	0.040	0.16	382.9	117.3	0.25
FB10ap_89	6.54	0.5	0.1076	0.0053	0.83	9.294	0.4578	0.440	0.012	-0.20	351.1	20.0	0.48
FB10ap_90	3.792	0.082	0.0965	0.0014	0.44	10.363	0.1503	0.284	0.006	0.26	431.5	7.5	0.28
FB10ap_91	11.01	2.7	0.1484	0.022	0.86	6.739	0.9990	0.535	0.033	-0.29	375.2	66.4	0.60
FB10ap_92	6.41	0.21	0.1199	0.0026	0.32	8.340	0.1809	0.389	0.013	0.33	439.4	15.3	0.41
FB10ap_93	233.5	8.6	1.931	0.083	0.68	0.518	0.0223	0.889	0.030	0.53	-5625.4	1412.1	1.00
FB10ap_94	4.05	0.12	0.0825	0.0017	0.39	12.121	0.2498	0.357	0.011	0.31	322.5	9.8	0.38
FB10ap_95	103.9	4.1	0.906	0.028	0.71	1.104	0.0341	0.824	0.019	0.14	169.9	148.3	0.97
FB10ap_96	524	29	4.36	0.21	0.73	0.229	0.0110	0.875	0.029	0.06	-1537.9	1316.3	1.00
FB10ap_97	1071	49	8.62	0.39	0.86	0.116	0.0052	0.907	0.023	0.28	-8809.4	6503.7	1.00
FB10ap_98	17.19	1	0.2825	0.0092	0.72	3.540	0.1153	0.445	0.016	-0.17	930.8	43.7	0.45
FB10ap_99	67.9	2.9	0.582	0.023	0.73	1.718	0.0679	0.852	0.026	0.34	-111.2	132.8	1.00
FB10ap_100	73.8	2.5	0.662	0.02	0.78	1.511	0.0456	0.810	0.019	0.16	207.4	107.5	0.95
FB10ap_101	34.8	1.1	0.407	0.01	0.19	2.457	0.0604	0.623	0.022	0.67	803.8	68.5	0.67
FB10ap_102	11.56	0.28	0.2506	0.0043	0.18	3.990	0.0685	0.336	0.009	0.44	1023.4	23.2	0.31
FB10ap_103	79.7	2.7	0.71	0.023	0.45	1.408	0.0456	0.822	0.029	0.52	126.5	170.6	0.97
FB10ap_105	5460	960	43.9	7.6	1.00	0.023	0.0039	0.913	0.028	0.05	0.0	11521.2	1.00
FB10ap_106	107.5	4.8	0.93	0.039	0.31	1.075	0.0451	0.851	0.044	0.55	-206.9	353.3	1.00
FB10ap_107	1356	83	11.2	0.72	0.93	0.089	0.0057	0.896	0.020	0.15	-10982.1	10565.7	1.00
FB10ap_108	47.9	1.2	0.47	0.01	0.34	2.128	0.0453	0.744	0.020	0.52	438.8	76.0	0.85
FB10ap_109	37.2	1.1	0.371	0.01	0.49	2.695	0.0727	0.729	0.022	0.49	380.3	66.2	0.84
FB10ap_110	17.49	0.57	0.2076	0.0057	0.33	4.817	0.1323	0.613	0.022	0.61	400.8	37.5	0.69
FB10ap_111	40	1.2	0.39	0.013	0.38	2.564	0.0855	0.744	0.022	0.58	349.3	70.2	0.86
FB10ap_112	34.6	1.7	0.352	0.017	0.44	2.841	0.1372	0.725	0.023	0.47	370.3	67.0	0.83
FB11ap_0	14.87	0.41	0.175	0.0037	0.12	5.714	0.1300	0.621	0.020	0.55	323.0	28.9	0.71
FB11ap_1	6900	1100	54.9	8.5	1.00	0.018	0.0032	0.919	0.024	0.09	0.0	12776.3	1.00
FB11ap_2	4.88	0.11	0.0982	0.0013	0.21	10.183	0.1400	0.360	0.009	0.37	381.4	8.5	0.38
FB11ap_3	7.18	0.21	0.1692	0.003	0.16	5.910	0.1000	0.307	0.009	0.40	725.7	17.1	0.30
FB11ap_4	28.3	0.53	0.2941	0.0053	0.48	3.400	0.0590	0.700	0.015	0.42	366.0	37.6	0.80
FB11ap_5	2.255	0.037	0.0718	0.00084	0.32	13.928	0.1700	0.228	0.004	0.43	352.8	4.7	0.22
FB11ap_6	3.31	0.2	0.0787	0.0021	0.71	12.706	0.3300	0.304	0.014	-0.34	340.2	12.4	0.31
FB11ap_7	8.81	0.86	0.1272	0.0085	0.86	7.862	0.5000	0.499	0.024	-0.39	356.8	33.4	0.55
FB11ap_8	19.1	0.6	0.2028	0.005	0.08	4.931	0.1200	0.690	0.026	0.59	260.3	42.9	0.80
FB11ap_9	29.8	1.2	0.2992	0.0082	0.44	3.342	0.0970	0.723	0.027	0.28	312.4	65.0	0.83
FB11ap_10	19.07	0.37	0.2186	0.0045	0.34	4.575	0.0960	0.636	0.015	0.61	381.8	28.1	0.72
FB11ap_11	1730	130	14.5	1.2	0.95	0.069	0.0060	0.886	0.022	0.19	-13825.8	23005.1	1.00
FB11ap_12	3.9	0.15	0.1085	0.0028	-0.06	9.217	0.2400	0.264	0.013	0.43	501.5	16.5	0.25
FB11ap_13	7.8	0.22	0.1221	0.0023	0.29	8.190	0.1600	0.463	0.013	0.35	377.0	14.5	0.51
FB11ap_14	8.59	0.19	0.1899	0.0026	0.42	5.266	0.0740	0.327	0.007	0.29	786.9	14.2	0.32
FB11ap_15	283.5	9.9	2.384	0.079	0.72	0.419	0.0140	0.868	0.023	0.28	-4239.3	1027.5	1.00
FB11ap_16	52.2	2	0.493	0.021	0.45	2.028	0.0870	0.784	0.033	0.58	269.9	130.3	0.91
FB11ap_17	326	23	2.87	0.2	0.85	0.348	0.0270	0.830	0.028	0.20	130.8	675.1	0.99
FB11ap_18	84.8	1.4	0.793	0.01	0.53	1.261	0.0170	0.777	0.012	0.39	596.7	83.2	0.88
FB11ap_19	41.4	1.4	0.377	0.012	0.52	2.653	0.0850	0.800	0.027	0.56	134.1	84.6	0.94
FB11ap_20	6.99	0.14	0.1248	0.0017	0.25	8.013	0.1100	0.405	0.009	0.40	441.7	10.5	0.43
FB11ap_21	206.4	8.3	1.723	0.069	0.63	0.580	0.0230	0.878	0.030	0.43	-2542.4	710.6	1.00
FB11ap_22	38.96	0.82	0.3892	0.0088	0.46	2.569	0.0560	0.730	0.016	0.50	398.9	52.6	0.84
FB11ap_23	319	13	2.62	0.11	0.70	0.382	0.0170	0.889	0.029	0.41	0.0	1018.3	1.57
FB11ap_24	14.41	0.62	0.1719	0.0083	0.03	5.817	0.2500	0.612	0.036	0.10	329.7	50.7	0.69
FB11ap_25	162.9	6.3	1.32	0.051	0.45	0.758	0.0300	0.908	0.033	0.54	-2610.0	615.5	1.00
FB11ap_26	78.7	2	0.694	0.022	0.44	1.441	0.0460	0.832	0.025	0.64	35.7	148.2	0.99
FB11ap_27	194.9	7.8	1.675	0.059	0.67	0.597	0.0210	0.848	0.025	0.25	-320.3	379.4	1.00
FB11ap_28	4230	680	34.5	5.8	0.99	0.029	0.0043	0.904	0.033	0.23	0.0	10120.6	1.00
FB11ap_29	588	25	4.82	0.2	0.76	0.207	0.0087	0.891	0.026	0.26	0.0	1293.3	1.00
FB11ap_30	44.7	1.7	0.427	0.013	0.77	2.342	0.0770	0.760	0.019	0.10	324.6	67.8	0.88
FB11ap_31	41.5	0.73	0.423	0.008	0.24	2.364	0.0460	0.710	0.016	0.61	518.7	55.7	0.80

Tables S.2.2 apatite U-Pb data tables (continued)

	$^{207}Pb/^{235}U$	Prop2SE	$^{206}Pb/^{238}U$	Prop2SE	Rho	$^{238}U/^{206}Pb$	Prop2SE	$^{207}Pb/^{206}Pb$	Prop2SE	Rho	^{207}Pb corrected age	Prop2SE	$f^{206}Pb$
FB11ap_32	138.6	3.5	1.152	0.03	0.50	0.868	0.0230	0.877	0.022	0.51	-932.2	266.3	1.00
FB11ap_33	12.51	0.38	0.171	0.0039	0.69	5.848	0.1400	0.536	0.014	0.14	433.1	21.5	0.59
FB11ap_34	102.8	3.7	0.888	0.029	0.62	1.133	0.0380	0.848	0.026	0.34	-150.3	202.6	1.00
FB11ap_35	15.7	0.62	0.1867	0.0049	0.58	5.356	0.1400	0.611	0.020	0.14	361.2	31.2	0.69
FB11ap_36	37.1	1.7	0.351	0.012	0.55	2.849	0.1000	0.765	0.031	0.28	239.8	87.9	0.89
FB11ap_37	395	13	3.21	0.11	0.79	0.312	0.0100	0.894	0.020	0.29	-1695.9	718.6	1.00
FB11ap_38	48.9	1.6	0.447	0.015	0.57	2.237	0.0760	0.787	0.023	0.58	224.6	85.4	0.92
FB11ap_39	50.4	3.7	0.463	0.031	0.75	2.160	0.1400	0.794	0.037	0.22	202.0	138.4	0.93
FB11ap_40	56.6	1.7	0.516	0.016	0.36	1.938	0.0610	0.811	0.030	0.60	139.8	127.6	0.96
FB11ap_41	7.91	0.56	0.1155	0.0052	0.91	8.658	0.3600	0.493	0.018	-0.42	328.8	22.0	0.55
FB11ap_42	84.2	2.3	0.736	0.018	0.47	1.359	0.0340	0.830	0.022	0.43	59.1	139.6	0.99
FB11ap_43	3.541	0.09	0.1551	0.0017	0.25	6.447	0.0690	0.167	0.004	0.16	824.1	9.8	0.12
FB11ap_44	54.2	1.5	0.488	0.014	0.23	2.070	0.0610	0.819	0.028	0.68	87.1	113.2	0.97
FB11ap_45	65.7	1.9	0.58	0.016	0.48	1.724	0.0490	0.830	0.027	0.52	39.4	132.7	0.99
FB11ap_46	92.8	4	0.804	0.031	0.52	1.244	0.0500	0.833	0.030	0.49	37.4	202.8	0.99
FB11ap_47	16.83	0.5	0.1906	0.0051	0.24	5.247	0.1300	0.643	0.023	0.58	318.8	36.0	0.73
FB11ap_48	88.6	3.8	0.753	0.029	0.67	1.328	0.0560	0.860	0.033	0.36	-245.0	219.6	1.00
FB11ap_49	2.704	0.083	0.0801	0.0014	0.04	12.484	0.2000	0.246	0.008	0.33	382.3	8.3	0.24
FB11ap_50	7.73	0.19	0.1234	0.0019	0.29	8.104	0.1300	0.456	0.012	0.35	387.9	13.3	0.50
FB11ap_51	35.08	0.89	0.3373	0.0078	0.06	2.965	0.0690	0.762	0.022	0.65	238.2	61.5	0.89
FB11ap_52	798	54	6.52	0.45	0.85	0.153	0.0120	0.900	0.035	0.23	-4610.7	3749.4	1.00
FB11ap_53	24.37	0.58	0.2643	0.0054	0.39	3.784	0.0760	0.668	0.017	0.51	397.5	37.4	0.76
FB11ap_54	4800	1000	38.1	7.8	1.00	0.026	0.0098	0.928	0.029	0.06	0.0	11078.9	1.00
FB11ap_55	39.2	1.1	0.388	0.0081	0.23	2.577	0.0530	0.736	0.023	0.47	375.9	71.7	0.85
FB11ap_56	4.12	0.15	0.1022	0.0015	0.27	9.785	0.1400	0.292	0.010	0.16	450.8	10.2	0.29
FB11ap_57	1230	100	10.3	1	0.93	0.097	0.0092	0.907	0.033	0.23	-14143.3	24891.7	1.00
FB11ap_58	68.9	1.6	0.605	0.013	0.56	1.653	0.0370	0.827	0.019	0.49	63.4	101.1	0.98
FB11ap_59	21.25	0.5	0.2341	0.0043	0.48	4.272	0.0800	0.660	0.015	0.32	363.9	29.9	0.75
FB11ap_60	8.56	0.22	0.1288	0.0024	0.71	7.764	0.1500	0.481	0.009	0.11	379.8	11.7	0.53
FB11ap_61	5	0.16	0.1947	0.0033	0.55	5.136	0.0870	0.186	0.005	-0.06	1002.3	17.8	0.14
FB11ap_62	5.13	0.26	0.0927	0.003	0.78	10.787	0.3500	0.401	0.013	-0.14	330.5	14.3	0.43
FB11ap_63	38.8	1.1	0.3649	0.0099	0.49	2.740	0.0750	0.775	0.020	0.46	216.6	61.6	0.91
FB11ap_64	4.11	0.13	0.0953	0.0017	0.52	10.493	0.1900	0.314	0.009	0.11	404.3	9.7	0.32
FB11ap_65	45.8	1.7	0.419	0.018	0.37	2.387	0.1000	0.800	0.039	0.69	152.9	132.5	0.94
FB11ap_66	7.08	0.2	0.1262	0.0022	0.56	7.924	0.1300	0.407	0.009	0.00	444.7	12.1	0.43
FB11ap_67	54.5	2.1	0.525	0.017	0.57	1.905	0.0650	0.753	0.022	0.37	458.3	92.7	0.86
FB11ap_68	20.4	0.39	0.2248	0.0028	0.56	4.448	0.0530	0.658	0.011	0.11	352.1	22.4	0.75
FB11ap_69	4.5	0.12	0.1876	0.0026	0.46	5.330	0.0700	0.174	0.004	0.08	982.7	14.3	0.12
FB11ap_70	9.31	0.27	0.1338	0.0034	0.38	7.474	0.1800	0.508	0.015	0.44	366.1	18.5	0.56
FB11ap_71	40.9	1.2	0.391	0.011	0.29	2.558	0.0720	0.768	0.027	0.62	261.7	85.6	0.89
FB11ap_72	66.9	1.9	0.592	0.018	0.36	1.689	0.0520	0.828	0.029	0.63	54.5	144.2	0.99
FB11ap_73	14.62	0.46	0.1821	0.0044	0.43	5.491	0.1200	0.584	0.017	0.31	392.0	26.5	0.66
FB11ap_74	8.8	0.39	0.137	0.0042	0.84	7.299	0.2300	0.465	0.011	-0.19	421.7	17.6	0.51
FB11ap_75	46	2.2	0.434	0.017	0.68	2.304	0.0960	0.772	0.028	0.19	280.6	98.3	0.90
FB11ap_76	24.1	1.1	0.261	0.011	0.77	3.831	0.1600	0.673	0.020	0.29	380.9	44.7	0.77
FB11ap_77	12.43	0.4	0.1595	0.0051	-0.11	6.270	0.2100	0.574	0.023	0.69	354.2	30.9	0.65
FB11ap_78	2.68	0.13	0.0707	0.0016	0.67	14.144	0.3200	0.271	0.010	-0.27	323.7	9.0	0.27
FB11ap_79	158.5	6.3	1.316	0.047	0.32	0.760	0.0280	0.882	0.028	-0.07	-1434.3	415.8	1.00
FB11ap_80	6.48	0.23	0.1106	0.0024	0.28	9.042	0.2000	0.424	0.015	0.32	374.9	15.3	0.46
FB11ap_81	12.67	0.66	0.1602	0.0073	0.67	6.242	0.3000	0.569	0.020	0.32	362.3	30.1	0.64
FB11ap_82	282	8.4	2.296	0.072	0.76	0.436	0.0130	0.900	0.020	0.36	0.0	627.8	1.00
FB11ap_83	2040	160	16.3	1.2	0.95	0.061	0.0052	0.917	0.031	0.29	0.0	4346.5	1.00
FB11ap_84	5.72	0.16	0.1017	0.002	0.70	9.833	0.2000	0.407	0.008	-0.06	357.7	10.0	0.44
FB11ap_85	36.48	0.92	0.3651	0.0076	0.17	2.739	0.0600	0.729	0.021	0.33	373.2	62.3	0.84
FB11ap_86	6.87	0.16	0.1265	0.0021	0.38	7.905	0.1400	0.395	0.010	0.37	457.6	12.4	0.42
FB11ap_87	18.86	0.92	0.2138	0.0068	0.64	4.677	0.1500	0.636	0.021	0.02	372.8	37.6	0.72
FB11ap_88	22.96	0.93	0.2533	0.0077	0.93	3.948	0.1200	0.666	0.023	-0.10	383.7	47.5	0.76
FB11ap_89	32.5	1	0.3333	0.0088	0.71	3.000	0.0820	0.709	0.016	0.11	395.3	45.4	0.81
FB11ap_90	2.567	0.081	0.082	0.0014	0.05	12.195	0.2200	0.229	0.008	0.49	401.7	8.5	0.22
FB11ap_91	65.1	3.1	0.586	0.023	0.71	1.706	0.0690	0.810	0.030	0.32	173.4	144.1	0.95
FB11ap_92	127.7	4.6	1.08	0.036	0.60	0.926	0.0330	0.859	0.028	0.46	-424.9	279.3	1.00
FB11ap_93	332.8	9.6	2.681	0.073	0.76	0.373	0.0110	0.904	0.020	0.32	-1654.5	597.5	1.00
FB11ap_94	4.11	0.15	0.1787	0.0031	0.30	5.596	0.0920	0.168	0.006	0.22	944.3	17.6	0.12
FB11ap_95	7.48	0.23	0.1151	0.0023	0.29	8.688	0.1800	0.468	0.014	0.42	350.5	14.7	0.51
FB11ap_96	13.9	0.42	0.1812	0.0051	0.27	5.519	0.1600	0.562	0.020	0.60	422.2	30.7	0.63
FB11ap_97	292	16	2.48	0.14	0.77	0.403	0.0240	0.877	0.034	0.45	-10373.6	4456.1	1.00
FB11ap_98	6.43	0.23	0.111	0.0025	0.62	9.009	0.1900	0.420	0.012	0.03	379.8	13.6	0.45
FB11ap_99	49.2	1.5	0.449	0.011	0.51	2.227	0.0600	0.795	0.023	0.42	189.7	86.2	0.93
FB11ap_100	45.7	1	0.4605	0.0094	0.64	2.172	0.0420	0.722	0.016	0.20	523.5	60.8	0.82
FB11ap_101	37.71	0.94	0.3769	0.0099	0.64	2.653	0.0710	0.729	0.016	0.46	387.4	51.3	0.84
FB11ap_102	8.89	0.39	0.2249	0.0044	0.75	4.446	0.0890	0.285	0.009	-0.39	999.2	23.6	0.25
FB11ap_103	12.34	0.42	0.2489	0.0049	0.38	4.018	0.0830	0.359	0.011	0.28	974.7	27.0	0.34
FB13ap_0	3.38	0.22	0.089	0.0015	-0.24	11.236	0.1900	0.276	0.015	0.33	403.8	12.2	0.27
FB13ap_1	9.14	0.5	0.1355	0.0026	0.20	7.380	0.1500	0.491	0.018	0.08	389.2	20.5	0.54
FB13ap_2	236	32	1.98	0.26	0.69	0.505	0.1300	0.885	0.035	-0.01	-5312.8	1854.8	1.00
FB13ap_3	45	2.1	0.452	0.011	0.58	2.212	0.0610	0.726	0.018	-0.08	494.8	66.4	0.82
FB13ap_4	29.5	1.6	0.304	0.012	0.59	3.289	0.1300	0.709	0.025	0.53	355.9	61.9	0.81
FB13ap_5	375	22	3.02	0.12	0.80	0.331	0.0270	0.903	0.027	-0.07	-1861.5	900.0	1.00
FB13ap_6	9.28	0.49	0.2324	0.0049	0.11	4.303	0.0910	0.290	0.010	0.24	1025.0	26.2	0.26
FB13ap_7	31.34	1.6	0.3207	0.0082	0.24	3.118	0.0790	0.712	0.022	0.66	369.7	57.3	0.82
FB13ap_8	6.6	0.36	0.1221	0.0032	0.02	8.190	0.1800	0.390	0.014	0.16	446.6	17.5	0.41
FB13ap_9	19.89	1.1	0.2354	0.0075	0.04	4.248	0.1400	0.629	0.030	0.45	427.2	56.0	0.71
FB13ap_10	17.02	0.86	0.1955	0.0049	0.09	5.115	0.1300	0.632	0.021	0.08	345.4	33.9	0.72
FB13ap_11	14.53	0.98	0.173	0.0066	0.00	5.780	0.2500	0.611	0.039	0.19	333.3	53.9	0.69
FB13ap_12	20.84	1.1	0.2236	0.0054	0.30	4.472	0.1100	0.678	0.023	0.47	312.2	41.9	0.78
FB13ap_13	157.4	12	1.398	0.087	0.57	0.715	0.0440	0.823	0.031	0.41	522.3	334.1	0.94
FB13ap_14	207.8	11	1.777	0.047	0.25	0.563	0.0150	0.854	0.023	0.47	-727.1	402.7	1.00

Tables S.2.2 apatite U-Pb data tables (continued)

	$^{207}Pb/^{235}U$	Prop2SE	$^{206}Pb/^{238}U$	Prop2SE	Rho	$^{238}U/^{206}Pb$	Prop2SE	$^{207}Pb/^{206}Pb$	Prop2SE	Rho	^{207}Pb corrected age	Prop2SE	$f^{206}Pb$
FB13ap_15	10.84	0.54	0.1468	0.0032	0.11	6.812	0.1500	0.537	0.017	0.60	368.7	21.4	0.60
FB13ap_16	23.44	1.3	0.2446	0.0083	0.72	4.088	0.1500	0.698	0.024	0.26	312.9	48.2	0.80
FB13ap_17	5.8	0.34	0.1027	0.0026	0.01	9.737	0.2600	0.408	0.020	0.11	360.8	18.3	0.44
FB13ap_18	208.9	11	1.913	0.093	0.13	0.523	0.0220	0.818	0.025	0.62	1761.5	335.2	0.84
FB13ap_19	100.9	5.5	0.909	0.032	0.67	1.100	0.0380	0.815	0.025	0.29	287.4	185.1	0.95
FB13ap_20	8.89	0.42	0.1234	0.0026	0.46	8.104	0.1600	0.524	0.012	0.44	321.3	14.0	0.59
FB13ap_21	86.4	4.3	0.8	0.038	0.17	1.250	0.0490	0.795	0.020	0.26	431.2	131.3	0.91
FB13ap_23	41.4	2	0.4156	0.0093	0.04	2.406	0.0560	0.725	0.019	0.63	450.7	64.2	0.83
FB13ap_24	50	2.5	0.457	0.015	-0.02	2.188	0.0700	0.803	0.030	0.12	156.7	112.6	0.95
FB13ap_25	54.7	2.9	0.527	0.019	0.82	1.898	0.0610	0.761	0.024	0.29	418.4	101.4	0.87
FB13ap_26	5.6	0.26	0.108	0.0017	0.25	9.259	0.1500	0.378	0.010	0.59	404.8	10.5	0.40
FB13ap_27	34.4	1.9	0.355	0.014	0.27	2.817	0.1100	0.719	0.032	0.65	393.2	89.7	0.82
FB13ap_28	6.37	0.34	0.106	0.0022	0.39	9.434	0.1900	0.439	0.014	0.12	346.7	13.8	0.48
FB13ap_29	40.56	1.9	0.3849	0.0077	0.49	2.598	0.0500	0.767	0.017	0.38	260.5	56.0	0.89
FB13ap_30	2.637	0.12	0.1597	0.0016	0.23	6.262	0.0610	0.120	0.002	0.34	900.9	9.1	0.06
FB13ap_31	111.9	6.5	0.959	0.043	0.63	1.043	0.0490	0.862	0.039	0.13	-395.6	336.8	1.00
FB13ap_32	4.44	0.23	0.1407	0.0023	0.12	7.107	0.1200	0.230	0.008	0.42	684.4	13.6	0.20
FB13ap_33	5.92	0.3	0.1116	0.002	0.18	8.961	0.1600	0.384	0.011	0.44	413.1	12.2	0.41
FB13ap_34	382	21	3.173	0.098	0.75	0.315	0.0100	0.881	0.022	0.22	-1267.6	721.4	1.00
FB13ap_35	29.69	1.4	0.2876	0.0066	0.14	3.477	0.0800	0.754	0.022	0.68	218.9	52.6	0.88
FB13ap_36	76.1	3.7	0.697	0.016	0.45	1.435	0.0330	0.792	0.019	0.39	371.9	109.6	0.91
FB13ap_37	9.55	0.47	0.1322	0.0033	0.08	7.564	0.1800	0.529	0.017	0.07	339.5	19.8	0.59
FB13ap_38	166.3	8.9	1.35	0.041	0.30	0.741	0.0220	0.890	0.030	0.46	-1875.0	494.1	1.00
FB13ap_39	76.7	3.8	0.672	0.017	0.25	1.488	0.0350	0.833	0.021	-0.01	25.3	123.3	0.99
FB13ap_40	196.2	12	1.653	0.07	0.66	0.605	0.0270	0.874	0.034	-0.04	-1954.9	683.4	1.00
FB13ap_41	3.257	0.16	0.1805	0.0023	0.26	5.540	0.0710	0.131	0.003	0.25	1000.3	13.0	0.07
FB13ap_42	37.45	1.8	0.3727	0.0079	0.59	2.683	0.0580	0.734	0.014	0.41	365.3	45.5	0.84
FB13ap_43	68.6	3.3	0.599	0.015	0.39	1.669	0.0430	0.836	0.024	0.56	-0.7	124.3	1.00
FB13ap_44	23.5	2	0.261	0.013	0.86	3.831	0.2100	0.641	0.025	-0.14	451.5	55.2	0.72
FB13ap_45	127.3	6.3	1.097	0.029	0.30	0.912	0.0240	0.843	0.025	0.70	-104.8	240.3	1.00
FB13ap_46	331	23	2.67	0.14	0.82	0.375	0.0200	0.899	0.032	0.12	-1513.4	884.2	1.00
FB13ap_47	26.4	1.6	0.288	0.012	0.40	3.472	0.1600	0.673	0.024	0.39	424.7	56.9	0.76
FB13ap_48	1730	140	13.73	0.89	1.00	0.073	0.0047	0.912	0.027	0.26	0.0	3216.5	1.00
FB13ap_49	52.8	3.2	0.513	0.021	0.70	1.949	0.0830	0.758	0.022	0.29	419.3	91.7	0.87
FB13ap_50	12.73	0.68	0.1625	0.0052	0.08	6.154	0.2100	0.579	0.026	0.68	354.5	34.9	0.65
FB13ap_51	6.26	0.34	0.1177	0.0026	0.57	8.496	0.1800	0.387	0.011	0.10	433.1	13.9	0.41
FB13ap_52	7.94	0.42	0.1386	0.0025	0.34	7.215	0.1300	0.417	0.011	0.23	478.5	14.7	0.44
FB13ap_53	76.8	4.1	0.662	0.021	0.21	1.511	0.0500	0.861	0.037	0.58	-210.4	213.6	1.00
FB13ap_54	15.37	0.99	0.1835	0.0068	0.29	5.450	0.2200	0.610	0.021	0.24	356.2	33.3	0.69
FB13ap_55	48.7	2.5	0.453	0.012	0.46	2.208	0.0590	0.781	0.024	0.45	255.6	89.2	0.91
FB13ap_56	128.9	9	1.116	0.059	0.79	0.896	0.0490	0.844	0.031	0.19	-126.9	298.9	1.00
FB13ap_57	7.59	0.39	0.1192	0.0024	0.30	8.389	0.1600	0.464	0.014	0.36	366.9	15.2	0.51
FB13ap_58	45.2	2.4	0.417	0.011	0.26	2.398	0.0630	0.789	0.027	0.49	197.6	92.4	0.93
FB13ap_59	4.34	0.21	0.0859	0.0013	0.51	11.641	0.1800	0.367	0.008	0.07	329.0	7.7	0.39
FB13ap_60	6.17	0.3	0.1025	0.0019	0.32	9.756	0.1800	0.441	0.012	0.44	333.5	11.7	0.48
FB13ap_61	1720	820	13.6	6.3	1.00	0.074	0.0750	0.888	0.027	0.11	-12729.3	28247.4	1.00
FB13ap_62	2.012	0.093	0.1291	0.0013	0.28	7.746	0.0780	0.113	0.002	0.24	738.5	7.5	0.06
FB13ap_63	26.9	1.6	0.2831	0.0096	0.49	3.532	0.1200	0.691	0.024	0.31	372.8	55.3	0.79
FB13ap_64	40.9	2	0.3839	0.0098	0.17	2.605	0.0680	0.777	0.027	0.64	222.9	84.6	0.91
FB13ap_65	26.6	1.6	0.337	0.01	0.09	2.967	0.0890	0.581	0.024	0.51	765.8	63.2	0.63
FB13ap_66	28.6	3.2	0.275	0.022	0.87	3.636	0.3700	0.726	0.037	-0.37	276.7	83.3	0.84
FB13ap_67	13.25	0.63	0.1693	0.0037	0.41	5.907	0.1300	0.570	0.014	0.41	382.4	21.1	0.64
FB13ap_68	63.8	3.1	0.559	0.013	0.42	1.789	0.0420	0.822	0.022	0.60	87.8	105.4	0.98
FB13ap_69	26.02	1.1	0.2778	0.0035	0.46	3.600	0.0450	0.680	0.009	0.40	390.9	24.8	0.77
FB13ap_70	207.8	11	1.691	0.051	0.72	0.591	0.0190	0.886	0.023	0.28	-3149.4	619.4	1.00
FB13ap_71	6.75	0.32	0.1106	0.0024	0.02	9.042	0.2000	0.446	0.013	0.51	355.8	13.8	0.49
FB13ap_72	163.4	11	1.367	0.068	0.78	0.732	0.0360	0.876	0.033	0.29	-1313.0	490.8	1.00
FB13ap_73	81.6	4	0.714	0.018	0.43	1.401	0.0350	0.834	0.022	0.52	19.5	136.6	1.00
FB13ap_74	49.4	2.7	0.447	0.013	0.68	2.237	0.0660	0.803	0.021	0.19	152.3	79.8	0.95
FB13ap_75	306	18	2.59	0.11	0.72	0.386	0.0170	0.864	0.028	0.35	-3863.0	1229.9	1.00
FB13ap_76	17.5	0.91	0.1983	0.0049	0.59	5.043	0.1300	0.643	0.018	0.30	332.5	30.1	0.73
FB13ap_77	348	22	3.08	0.2	0.13	0.325	0.0150	0.817	0.038	0.45	1142.8	867.1	0.94
FB13ap_78	32.7	2.3	0.329	0.017	-0.03	3.040	0.1700	0.738	0.030	0.44	303.7	79.9	0.85
FB13ap_79	9.67	0.49	0.1406	0.0028	-0.06	7.112	0.1400	0.501	0.014	0.63	393.0	17.6	0.55
FB13ap_80	8.16	0.52	0.1236	0.004	0.38	8.091	0.2700	0.483	0.022	0.25	362.2	24.1	0.53
FB13ap_81	41.8	2.2	0.401	0.013	0.43	2.494	0.0790	0.764	0.027	0.57	285.3	87.6	0.89
FB13ap_82	26.8	1.5	0.2843	0.0072	0.21	3.517	0.0910	0.686	0.028	0.38	386.9	63.0	0.78
FB13ap_83	20.03	1.2	0.2114	0.0066	0.36	4.730	0.1400	0.688	0.029	0.45	275.8	49.6	0.79
FB13ap_84	156.7	8.7	1.292	0.043	0.40	0.774	0.0290	0.886	0.036	0.36	-1526.2	523.1	1.00
FB13ap_85	304	16	2.484	0.074	0.33	0.403	0.0140	0.895	0.023	0.02	0.0	772.5	1.00
FB13ap_86	104.8	5.3	0.962	0.025	0.65	1.040	0.0290	0.794	0.016	0.14	604.4	126.6	0.90
FB13ap_87	206.8	12	1.683	0.062	0.27	0.594	0.0210	0.895	0.032	0.37	-4061.4	985.7	1.00
FB13ap_88	22.5	2.2	0.251	0.021	-0.02	3.984	0.1100	0.671	0.066	0.08	369.2	130.6	0.77
FB13ap_89	43.6	2.2	0.4	0.013	0.09	2.500	0.0900	0.789	0.028	0.27	187.6	91.9	0.93
FB13ap_90	125.8	11	1.17	0.15	0.01	0.855	0.3700	0.807	0.040	-0.03	641.2	356.5	0.91
FB13ap_91	159	13	1.281	0.035	0.09	0.781	0.0220	0.904	0.062	-0.04	-2228.5	1000.1	1.00
FB13ap_92	161	15	1.39	0.11	0.21	0.719	0.0590	0.851	0.031	0.26	-384.2	390.7	1.00
FB13ap_93	116.7	6.2	1.019	0.034	0.34	0.981	0.0340	0.837	0.033	0.59	4.5	282.4	1.00
FB13ap_94	624	40	5.04	0.24	0.24	0.198	0.0100	0.890	0.030	0.18	0.0	1554.0	1.00
FB13ap_95	10.8	0.57	0.1463	0.0031	-0.10	6.835	0.1500	0.544	0.016	0.04	359.2	20.3	0.61
FB13ap_96	21.99	1.2	0.2297	0.0081	-0.07	4.354	0.1600	0.694	0.035	0.45	290.1	64.2	0.80
FB13ap_97	10.36	0.58	0.1439	0.0049	0.03	6.949	0.2400	0.526	0.017	0.01	373.9	23.1	0.59
FB13ap_98	69.9	3.6	0.654	0.018	0.62	1.529	0.0420	0.778	0.020	0.36	440.3	106.3	0.89
FB13ap_99	3.031	0.16	0.0816	0.0014	0.04	12.255	0.2100	0.271	0.009	0.43	373.8	8.6	0.27
FB13ap_100	1660	210	12.9	1.3	0.53	0.078	0.0087	0.918	0.029	-0.04	0.0	3296.6	1.00
FB13ap_101	46.5	2.3	0.425	0.012	-0.02	2.353	0.0660	0.791	0.034	0.20	193.9	116.9	0.93
FB13ap_102	7.97	0.41	0.1211	0.0025	0.16	8.258	0.1700	0.479	0.016	0.64	358.5	17.0	0.53
FB13ap_103	21.42	1.1	0.2386	0.006	0.44	4.191	0.1100	0.652	0.018	0.45	387.6	35.9	0.74

Tables S.2.2 apatite U-Pb data tables (continued)

	$^{207}Pb/^{235}U$	Prop2SE	$^{206}Pb/^{238}U$	Prop2SE	Rho	$^{238}U/^{206}Pb$	Prop2SE	$^{207}Pb/^{206}Pb$	Prop2SE	Rho	^{207}Pb corrected age	Prop2SE	$f^{206}Pb$
FB13ap_104	257	15	2.101	0.081	0.80	0.476	0.0190	0.892	0.023	0.22	-10000.0	2587.3	1.00
FB13ap_105	25.39	1.3	0.3562	0.0079	0.00	2.807	0.0670	0.519	0.018	0.16	988.4	50.4	0.53
FB13ap_106	34.81	1.7	0.3566	0.0082	0.42	2.804	0.0580	0.709	0.018	0.52	427.3	52.9	0.81
FB13ap_107	29.58	1.4	0.3192	0.0066	0.58	3.133	0.0640	0.672	0.013	0.39	479.3	36.1	0.76
FB13ap_108	10.97	0.62	0.1557	0.0041	0.55	6.423	0.1600	0.514	0.019	0.30	420.3	25.5	0.57
FB13ap_109	5.49	0.33	0.0975	0.0029	0.12	10.256	0.3000	0.411	0.020	0.52	340.1	18.2	0.44
FB13ap_110	166.8	8.8	1.367	0.042	0.40	0.732	0.0240	0.887	0.026	0.61	-1794.7	433.2	1.00
FB13ap_111	79.3	3.7	0.683	0.014	0.56	1.464	0.0310	0.845	0.016	0.51	-77.6	102.4	1.00
FB13ap_112	22.42	1.3	0.2306	0.0068	0.70	4.337	0.1200	0.707	0.027	-0.06	265.5	50.6	0.82
FB13ap_113	18.46	0.88	0.2179	0.0048	0.07	4.589	0.1000	0.617	0.018	0.53	414.8	32.6	0.70
FB14ap_0	18.07	0.75	0.2022	0.0068	0.13	4.946	0.1663	0.648	0.031	0.59	331.1	50.4	0.74
FB14ap_1	142.6	6.5	1.202	0.052	0.72	0.832	0.0360	0.867	0.029	0.30	-731.8	341.3	1.00
FB14ap_2	118.4	2.3	1.024	0.02	0.45	0.977	0.0191	0.842	0.018	0.56	-81.0	168.3	1.00
FB14ap_3	192	2.8	1.659	0.022	0.78	0.603	0.0080	0.840	0.008	0.20	102.0	154.9	0.99
FB14ap_4	6.14	0.14	0.1882	0.0028	0.27	5.313	0.0791	0.237	0.006	0.34	901.6	15.4	0.20
FB14ap_5	804	61	6.54	0.53	0.92	0.153	0.0124	0.895	0.027	0.21	0.0	2225.8	1.00
FB14ap_6	49.1	1.8	0.442	0.014	0.19	2.262	0.0717	0.818	0.035	0.57	82.0	127.7	0.97
FB14ap_7	2.663	0.081	0.1604	0.0016	0.55	6.234	0.0622	0.122	0.004	-0.27	901.8	9.8	0.06
FB14ap_8	42.4	1.2	0.415	0.011	0.31	2.410	0.0639	0.748	0.024	0.54	360.8	80.2	0.86
FB14ap_9	8.1	0.25	0.2044	0.0042	0.26	4.892	0.1005	0.289	0.010	0.43	903.1	22.8	0.26
FB14ap_10	14.3	3.5	0.292	0.025	0.99	3.425	0.2932	0.298	0.028	-0.91	1271.7	118.1	0.25
FB14ap_11	13.27	0.33	0.2087	0.0036	0.58	4.792	0.0827	0.464	0.010	0.11	650.4	19.8	0.49
FB14ap_12	9.03	0.23	0.1336	0.0029	0.45	7.485	0.1625	0.492	0.012	0.41	382.5	15.4	0.54

S2.3 apatite trace-element data (element concs. calculated from isotopes)

	55Mn	±	86Sr	±	89Y	±	139La	±	140Ce	±	141Pr	±	146Nd	±	147Sm	±	153Eu	±	157Gd	±	159Tb	±	163Dy	±	165Ho	±	166Er	±	169Tm	±	172Yb	±	175Lu	±	232Th	±	238U	±
FBtap_0	617.7	9.6	167.5	2.6	1010	22	57.80	1.30	192.6	4	34.69	0.64	224.3	5.1	93.1	2.4	29.4	0.71	139.9	2.9	23.01	0.55	158.1	2.6	34.98	0.69	106.5	1.9	14.59	0.28	92.7	2	16.47	0.39	13.01	0.35	6.57	0.16
FBtap_1	310.8	6.1	353.2	5.3	610	14	2.17	0.15	8	0.41	1.43	0.12	10.72	0.84	6.11	0.36	1.95	0.13	16.7	0.66	4.34	0.14	55.4	1.2	20.62	0.39	95.1	1.5	17.62	0.42	127.9	2.5	19.21	0.45	0.703	0.036	3.571	0.085
FBtap_2	1426	23	122.3	2	2789	46	91.50	2.00	288.3	5.2	48.7	1	290.6	5.9	139.9	2.6	28.76	0.52	272.3	4.9	57.1	0.87	472.2	7.4	108.4	1.6	329.3	5.4	47.8	0.61	299.3	4.4	39.31	0.75	1.444	0.046	6.84	0.11
FBtap_3	316	4.5	373.8	5.7	726	11	9.05	0.24	64.7	1.3	16.75	0.4	137	2.3	71.3	1.3	6.7	0.18	116.7	1.8	20.42	0.28	146.3	2.2	31.89	0.43	90.8	1.4	11.73	0.23	65.1	1.2	8.72	0.16	0.848	0.05	5.267	0.081
FBtap_4	466.8	5.5	441	5.8	1189	23	18.64	0.44	83.4	1.4	17.76	0.34	135.7	2.5	71.3	1.6	10.06	0.2	132.9	2.3	24.09	0.42	190	2.7	46.69	0.58	165.1	1.8	28.53	0.46	209.4	3	32.57	0.57	1.205	0.048	12.88	0.21
FBtap_5	709	12	255.4	4.3	100.9	1.9	1.41	0.09	5.63	0.21	1.099	0.07	7.3	0.5	3.87	0.25	2.3	0.11	7.59	0.31	1.634	0.054	13.7	0.33	3.482	0.088	10.88	0.28	1.525	0.063	9.42	0.33	1.492	0.055	0.0092	0.0033	0.0537	0.0048
FBtap_6	374.8	6.4	364.2	5.9	815	17	2.53	0.13	15.29	0.41	4.86	0.17	51	1.6	36.88	0.86	3.21	0.12	90.3	1.7	17.45	0.3	144.1	1.9	33.65	0.43	106.2	1.6	16.4	0.28	112.4	2.1	15.44	0.32	0.271	0.015	3.296	0.066
FBtap_7	588.2	8.6	198.2	3.2	519.7	9.5	127.10	3.30	358.6	7.4	51.7	1.1	272	5.7	68.9	1.4	16.75	0.36	86.2	1.3	12.16	0.25	78.5	1.1	17.1	0.28	49.38	0.73	6.7	0.14	43.99	0.72	8.27	0.18	12.35	0.25	5.422	0.098
FBtap_8	651.2	9.6	159.9	2.8	979	19	5.43	0.21	21.57	0.55	4.42	0.16	34.01	0.87	23.39	0.73	6.44	0.17	63.3	1.2	14.81	0.28	136.3	2.1	35.87	0.48	135.5	1.8	26.03	0.4	193.4	3.3	29.74	0.59	0.212	0.013	8.31	0.21
FBtap_9	1089	27	159.9	5.2	790	40	49.60	2.80	166.4	9.6	26.3	1.6	148	10	56.7	3.8	14.5	0.98	88.8	5.8	15.9	1.1	122.6	7.9	27.9	1.8	84	6.1	11.92	0.9	75.2	5.3	12.17	0.83	8.5	1.2	10.79	0.63
FBtap_10	526.8	9.8	245	5.4	827	23	1.80	0.12	5.9	0.23	1.209	0.078	9.06	0.51	6.26	0.29	5.74	0.16	22.22	0.73	6.81	0.16	83.5	1.3	28.15	0.41	115.5	1.6	27.18	0.58	131.2	2.8	19.78	0.41	0.34	0.017	2.225	0.047
FBtap_11	884	15	129.4	2.7	2054	51	125.00	3.00	498	11	101.2	2.6	718	18	312.1	6.2	42.3	1.3	425.3	8.4	64.8	1.4	417.8	7.3	80.8	1.4	218.6	4.5	27.18	0.58	164.2	3.8	25.15	0.66	19.59	0.44	9.48	0.21
FBtap_12	704	12	223.5	4.8	1145	26	437.00	11.00	1007	24	157.9	3.9	823	19	213.5	4.7	41.43	0.93	255.8	4.6	34.91	0.59	226.5	3.4	46.56	0.54	128.9	1.6	16.62	0.29	103.9	1.9	17.44	0.37	22.05	0.4	10.61	0.19
FBtap_13	870	14	230.8	4	1372	37	10.50	0.35	39.4	1	7.21	0.27	47.9	1.4	25.87	0.61	6.19	0.18	59.3	1.5	14.8	0.35	156.5	3.6	49	1.1	204.2	4.6	37.3	0.81	271.2	6.8	41	1.1	1.352	0.069	8.18	0.34
FBtap_14	1072	16	139.2	2.9	822	16	45.00	1.10	147.8	3.2	28.55	0.7	194.6	4.6	101	2.1	16.32	0.37	160.2	3.5	23.39	0.43	146.3	1.9	28.66	0.55	69.8	1	8.09	0.15	50.49	0.96	8.07	0.21	1.414	0.04	5.44	0.11
FBtap_15	198.7	3.7	438.9	8.5	876	22	32.35	0.96	156.4	3.4	33.6	0.77	244.3	6.3	115.7	3	9.63	0.28	182.2	4.4	30.61	0.54	204.1	3.7	39.1	0.54	98.7	1.4	11.29	0.23	57.9	1.2	7.16	0.19	0.612	0.025	8.7	0.23
FBtap_16	1072	18	294.3	5.5	430.3	9.6	0.87	0.09	3.69	0.16	0.818	0.071	8.09	0.45	6.79	0.31	1.727	0.089	21.02	0.6	5.3	0.12	52.87	0.92	14.94	0.26	55.9	0.95	9.8	0.17	71.8	1.3	10.47	0.22	0.1229	0.0098	2.319	0.063
FBtap_17	813	14	160.7	3.2	3373	69	378.60	7.60	1271	29	272.2	5.3	1702	29	603	11	65.9	1.1	712	12	107	1.7	711	11	138.6	1.9	387	6.6	53.83	0.94	341.2	6.8	51.73	0.97	45.62	0.76	50.14	0.96
FBtap_18	384.2	6.3	238.1	5.2	120.9	4	1.48	0.13	2.45	0.14	0.601	0.061	2.88	0.57	1.98	0.16	0.684	0.057	5.95	0.34	1.473	0.064	15.3	0.51	4.55	0.17	16.7	0.6	2.955	0.094	19.09	0.79	3.16	0.11	0.21	0.017	1.017	0.033
FBtap_19	1475	31	90.5	2.7	2373	58	72.10	2.00	260.6	7	49.9	1.4	349	11	183.6	4.8	18.99	0.56	330.3	7.1	62.9	1.2	475.1	6.5	95.7	1.5	256.1	4.2	31.98	0.67	176.3	3.3	21.05	0.52	1.562	0.052	4.56	0.13
FBtap_20	283.7	3.7	420	7.8	422.7	8.3	1.76	0.12	6.96	0.25	1.441	0.076	11.99	0.5	8.13	0.34	9.93	0.26	22.71	0.54	5.11	0.11	50.51	0.86	14.46	0.24	52.37	0.74	8.23	0.16	55.76	0.99	8.69	0.17	0.261	0.016	2.349	0.046
FBtap_21	731	12	371.7	9.1	1373	40	28.85	0.82	102.1	2.9	20.05	0.53	138.5	3.3	69.2	2	10.76	0.25	135.2	3.2	25.9	0.55	212.8	3.2	53.41	0.69	183.7	2.4	30.54	0.54	210.4	3.6	28.01	0.51	1.347	0.054	12.46	0.28
FBtap_22	583.6	9.7	156.9	3	1245	31	15.95	0.45	66.3	1.5	15.15	0.39	120.1	2.5	86.7	1.9	14.17	0.34	180.5	2.6	37.4	0.57	275.2	4	53.12	0.74	137.4	2.1	17.3	0.3	96.1	1.5	11.19	0.22	1.099	0.032	14.02	0.25
FBtap_23	498	7.7	307.5	5.7	1153	25	32.04	0.93	104.7	2.3	19.06	0.51	126.7	2.9	60.2	1.5	10.72	0.32	115.4	2.5	23.52	0.44	192.4	2.6	44.62	0.57	138.8	1.8	20.42	0.27	125.8	1.8	16.59	0.34	0.414	0.022	6.62	0.13
FBtap_24	639	12	306.6	8.6	1247	33	45.60	1.10	164.1	4	29.6	0.87	192.1	4.8	90.1	2.7	20.31	0.47	164.8	3.7	31.67	0.69	238.6	4.4	49.93	0.68	136.7	2.1	16.97	0.29	96.1	1.5	11.73	0.2	0.614	0.029	4.84	0.12
FBtap_25	618.9	9.3	186.4	3.7	2853	57	36.46	0.94	128.3	2.5	24.79	0.65	167.1	3.7	92.7	1.9	20.21	0.46	215.6	4.2	48.34	0.93	437.8	6.3	114.6	1.4	379.1	5.5	53.6	0.81	328.5	4.7	48.36	0.92	29.12	0.5	45.89	0.85
FBtap_26	869	14	145.6	3.3	1610	48	110.10	3.20	398	12	73.5	2.1	475	16	196.8	5.7	47.1	1.5	279	7.9	42.3	1.1	284.1	7.8	59.5	1.6	165.5	4.7	21.89	0.6	145.8	4	25.45	0.75	29.46	0.88	15.15	0.4
FBtap_27	396.4	6.2	394.7	7.9	455.8	8.7	5.17	0.22	41	1	11.86	0.34	106.2	2.7	59.2	1.5	5.95	0.22	101.6	2.1	16.06	0.31	102.6	2	19.92	0.34	50.6	0.88	5.95	0.16	34.2	0.74	5.2	0.13	0.244	0.016	3.74	0.1
FBtap_28	783	12	537.1	9.8	664	12	0.39	0.05	2.49	0.12	0.801	0.062	7.68	0.43	8.28	0.34	1.868	0.086	25.76	0.63	7.19	0.13	75.5	1.3	22.37	0.35	86.9	1.4	15.32	0.31	108.1	2	15.62	0.31	0.0032	0.0015	1.503	0.033
FBtap_29	452.6	6.7	383.1	7.6	857	17	10.50	0.30	38.8	1	7.18	0.23	51.2	1.5	25.45	0.83	9.03	0.21	57.6	1.4	11.32	0.24	105.8	1.7	31.21	0.41	122.6	1.6	21.49	0.37	159.3	2.5	26.97	0.5	0.588	0.028	2.938	0.049
FBtap_30	1116	17	230.7	5	1565	36	172.20	3.80	649	13	117	2.5	690	15	281.5	5.4	26.84	0.6	362.6	5.9	65.7	1.1	425.8	5.3	71.2	1.1	172.5	2.8	21.56	0.37	121.8	2.5	14.71	0.28	0.648	0.025	54	1
FBtap_31	402.9	7.6	366.6	8.5	902	22	26.17	0.87	105.3	2.8	21.37	0.61	153.6	4.2	63.6	1.7	6.07	0.22	104.5	2.8	17.54	0.36	136.3	2.4	34.46	0.59	128.4	1.8	23.06	0.36	177.5	3.5	28.81	0.61	0.598	0.022	4.18	0.11
FBtap_32	739	10	67.7	1.5	519	10	40.80	1.10	136.6	2.6	28.45	0.66	204.2	4.8	88.8	2.1	11.39	0.32	111.9	2.1	14.8	0.28	87.6	1.4	17.02	0.24	44.78	0.74	5.19	0.12	31.02	0.76	5.08	0.13	2.426	0.068	5.78	0.11
FBtap_33	726	11	172	3.9	252.8	6	6.88	0.26	25.46	0.68	5.47	0.19	44.1	1.4	24.32	0.75	8	0.21	39.3	1.1	6.07	0.14	39.61	0.75	8.3	0.16	22.93	0.46	2.881	0.087	17.94	0.49	3.06	0.084	0.0781	0.008	3.044	0.063
FBtap_34	747	13	179.8	3.2	753	47	65.10	2.70	231	11	48.3	2.2	323	15	126.6	5.3	18.73	0.5	165	6.2	24.08	0.85	152.6	5.6	29.5	1.1	78.8	2.8	9.58	0.35	57.7	1.9	8.97	0.27	8.69	0.36	5.15	0.17
FBtap_35	406.1	6.4	312.7	6	1035	36	5.91	0.25	22.66	0.56	4.28	0.18	27.22	0.9	14.52	0.55	7.69	0.2	37.1	0.99	9.54	0.24	104.9	2.7	35.49	0.97	146.3	4.3	24.8	0.77	186.9	6	38.4	1.1	2.267	0.098	6.97	0.31
FBtap_36	885	13	132.6	2.6	2762	50	190.80	3.10	650	16	119.1	2.6	760	17	320.9	6.5	64.5	1.4	506.1	9.2	89.3	1.6	596.1	9.7	111.4	1.9	262.8	5.6	31.4	0.68	195.6	3.8	31.98	0.67	28.44	0.55	16.49	0.33
FBtap_37	310.2	4.5	217.7	4	992	21	4.61	0.17	15.67	0.4	3.06	0.12	20.67	0.81	12.74	0.53	8.25	0.2	35.54	0.89	10.19	0.19	115	1.9	35.95	0.54	138	2.3	22.72	0.43	155.7	3	21.57	0.36	0.256	0.016	2.911	0.06
FBtap_38	209	3.4	292.1	5.6	690	17	6.75	0.24	24.17	0.67	4.92	0.16	35.7	1.1	19.42	0.61	6.02	0.17	45.9	1.2	10.15	0.16	97.7	1.6	24.62	0.37	76.2	1.1	10.48	0.2	69	1.2	7.33	0.19	0.263	0.014	3.162	0.064
FBtap_39	645.2	8.4	157.2	3.3	1155	32	282.70	8.50	772	21	131.9	3.8	722	21	204.8	5.9	46.8	1.3	240.9	6.9	33.38	0.86	209.3	5.7	42.9	1.1	120.3	3	15.87	0.45	102.4	2.7	18.32	0.48	39.82	0.86	14.24	0.3
FBtap_40	213.3	4.3	302.4	6.5	824	18	64.60	1.80	206.3	5.1	40.7	1.1	269.6	7.3	116.8	3.2	21.23	0.61	188.3	4.2	31.09	0.66	191.1	3.2	30.43	0.54	60.8	1.1	5.85	0.13	25.87	0.5	2.769	0.094	0.966	0.037	10.61	0.27
FBtap_41	669	10	145.7	3.2	490	23	71.20	4.10	213	13	33.2	2	194	10	62.5	3	20.85	0.86	84.4	3.6	12.42	0.53	80.6	3.6	16.66	0.65	47	1.9	6.08	0.26	38.5	1.7	6.73	0.3	1.45	0.74	6.94	0.32
FBtap_42	1009	20	162.9	4.1	338	19	12.62	0.57	42.7	2.3	8.69	0.52	62.6	3.6	31.9	1.8	11.84	0.65	48.5	2.8	7.79	0.46	52.5	3.4	10.92	0.72	29.8	2	3.49	0.23	19.9	1.4	3.14	0.22	0.64	0.18	2.39	0.17
FBtap_43	403.3	5.8	225.2	4.4	837	20	7.14	0.26	28.81	0.84	5.81	0.2	45.1	1.6	21.85	0.76	5.95	0.18	50.2	1.3	10.15	0.22	94.4	1.6	28.61	0.49	109.7	1.7	18.36	0.29	133.2	2.3	22.75	0.31	1.337	0.039	5.488	0.093
FBtap_44	402.7	6.7	171.9	3.9	818	19	79.30	1.80	348.9	7.9	74.1	1.5	466.1	9.8	203	3.5	20.3	0.42	263.2	4.6	41	0.71	217.7	3	28.34	0.4	47.94	0.82	4.54	0.1	23.85	0.48	3.003	0.096	0.0276	0.0042	15.87	0.29
FBtap_45	794	17	275.2	7.7	128.8	3.9	74.60	5.60	214	15	33.2	2.2	171	10	37.7	1.8	9.4	0.38	34.8	1.1	4.08	0.12	22.65	0.67	4.39	0.11	11.7	0.32	1.424	0.06	9.01	0.29	1.577	0.065	3.94	0.36	1.835	0.082
FBtap_46	890	17	126.3	3.6	1400	160	137.00	19.00	481	67	87	12	523	70	187	24	37	4.2	248	30	37.6	4.4	247	30	51.5	6.1	147	18	19.8	2.3	126	15	22	2.6	30.7	3.6	7.81	0.84
FBtap_47	798	13	292.5	6.1	35.21	0.78	0.44	0.07	1.42	0.15	0.188	0.027	1.3	0.17	0.45	0.075	0.183	0.023	1.53	0.14	0.33	0.025	3.58	0.18	1.142	0.065	4.87	0.19	0.905	0.044	6.75	0.22	1.245	0.049	0.0358	0.0084	0.0871	0.0068
FBtap_48	1041	14	109.1	2.6	1767	40	34.92	0.98	113.8	2.4	20.01	0.46	118.5	2.9	54.9	1.4	10.97	0.3	108	2.3	24.31	0.45	223.6	4	58.6	1.1	206.8	3.7	32.34	0.52	210.9	3.4	29.85	0.55	0.918	0.039	1.575	0.037
FBtap_49	1141	14	109.1	2.6	1767	40	34.92	0.98	113.8	2.4	20.01	0.46	118.5	2.9	54.9	1.4	10.97	0.3	108	2.3	24.31	0.45	223.6	4	58.6	1.1	206.8	3.7	32.34	0.52	210.9	3.4	29.85	0.55	0.918	0.039	1.575	0.037
FBtap_50	674.9	9.1	179.9	3.2	164.8	3.3	8.07	0.28	29.46	0.92	6.25	0.25	44.7	1.1	19.67	0.68	7.32	0.21	28.74	0.76	3.968	0.092	24.68	0.6	5.26	0.12	14.79	0.31	1.883	0.061	12.08	0.34	2.122	0.063	0.0888	0.0077	4.063	0.078
FBtap_51	128	1.9	296.6	6	209.1	5	16.00	0.54	72.2	2	14.89	0.54	111.2	3.7	43.2	1.2	5.94	0.19	65.9	2	8.23	0.23	46.42	0.99	8.03	0.15	18.75	0.38	1.998	0.071	10.9	0.32	1.562	0.069	1.613	0.066	0.915	0.038
FBtap_52	1135	20	99.8	2.2	602	15	36.22	0.94	124	2.8	23.88	0.61	158.2	3.5	71.2	1.7	15.4	0.33	102.6	2.1	14.7	0.3	91.4	1.7	18.71	0.39	51.11	0.95	6.35	0.16	41.97	0.93	7.87	0.24	2.57	0.08	3.726	0.088
FBtap_53	314	6.1	310	6.5	907	23	16.40	0.55	71.7	1.9	15.29	0.47	117.2	2.8	63.2	1.6	8.02	0.21	124.3	2.9	22.99	0.45	165.5	2.7	34.49	0.55	93	1.7	11.8	0.24	67.8	1.3	8.59	0.18	1.041	0.038	9.78	0.22
FBtap_54	207	4.2	336.1	5.9	229.3	5.9	2.92	0.18	9.11	0.29	1.83	0.1	13.56	0.72	5.66	0.35	1.077	0.071	15.98	0.69	2.98	0.12	26.48	0.77	7.63	0.22	27.03	0.87	4.02	0.12	25.65	0.68	3.78	0.11	2.16	0.28	0.798	0.04
FBtap_55	1464	27	117.9	3.1	3024	75	140.10	3.30	447	11	72.9	2	408	11	183.4	4.1	20.6	1.077	292.4	5.7	62.6	1.2	507.9	7.8	108	1.8	327.1	5.6	48.31	0.95	308.2	6.7	39.57	0.8	2.009	0.06	4.84	0.11
FBtap_56	1515	33	243.6	6	900	21	24.52	0.62	81.9	1.5	14.42	0.32	90.2	2.4	43.5	1.1	9.73	0.28	90.2	1.7	19.94	0.4	168.1	2.8	35.5	0.53	160.3	2.4	25.16	0.47	138.6	2.8	20.13	0.44	0.138	0.013	1.204	0.032
FBtap_57	634.3	9.9	133.5	3	220.2	4.6	9.20	0.34	32.54	0.76	6.91	0.25	49.4	1.6	24.38	0.8	8.81	0.23	37.13	0.87	5.15	0.11	32.24	0.74	6.76	0.14	19.3	0.37	2.738	0.073	19.68	0.55	3.56	0.1	0.171	0.012	2.879	0.067
FBtap_58	551	11	314.8	7.2	1147	30	16.00	0.54	72.2	2	14.89	0.54	111.2	3.7	43.2	1.2	5.94	0.19	65.9	2	8.23	0.23	46.42	0.99	8.03	0.15	18.75	0.38	1.998	0.071	10.9	0.32	1.562	0.069	1.613	0.066	0.915	0.038
FBtap_59	521.9	9.5	236.4	5.6	1813	55	87.90	2.70	369	12	71	2.6	451	14	209.2	6.9	13.91	0.4	306.5	7.2	57.7	1.5	396.9	9.3	73.5	1.7	194.3	5	25.4	0.73	143.2	3.7	17.53	0.53	1.404	0.082	51.3	2.4
FBtap_60	424.8	6.6	391.9	7.9	837	21	3.34	0.16	12.66	0.31	2.57	0.12	19.67	0.77	12.75	0.53	4.96	0.16	34.9	1	8.6	0.2	92.9	1.9	30.05	0.5	118.9	2	20.78	0.36	149.2	2.6	21.02	0.39	0.401	0.024	1.916	0.06
FBtap_61	1392	25	300.8	5.9	954	26	45.70	1.20	192.2	4.7	38.1	0.97	254.5	6.8	52.3	1.4	8.62	0.23	95.5	2	18.92	0.38	147.5	2.4	32.05	0.47	82.2	1.3	8.84	0.19	40.03	0.75	3.818	0.096	0.508	0.02	9.22	0.24
FBtap_62	369.6	6.6	200.4	4.7	876	26	17.19	0.43	71.1	1.8	14.47	0.37	101.7	2.8	52.3	1.4	5.42	0.23	43.8	1.4	11.07	0.28	105.6	2.4	30.01	0.51	116.5	2.6	20.07	0.46	134.8	3.3	19.7	0.54	0.489	0.027	4.29	0.12
FBtap_63	613	13	268.4	7.7	861	24	27.61	0.82	102.9	2.8	20.9	0.62	150.4	3.9	78.6	2.1	19.97	0.51	168.3	3	34.49	0.65	275.4	3.9	59.93	0.8	173.2	2.2	24.38	0.46	146.2	2.6	18.52	0.37	0.465	0.027	8.41	0.17
FBtap_64	765	12	197.2	4.4	1426	34	27.61	0.82	102.9	2.8	20.9	0.62	150.4	3.9	78.6	2.1	19.97	0.51	168.3	3	34.49	0.65	275.4	3.9	59.93	0.8	173.2	2.2	24.38	0.46	146.2	2.6	18.52	0.37	0.465	0.027	8.41	0.17
FBtap_65	1082	16	104.9	2.5	1815	49	119.20	3.00	441	11	83.5	2.1	530	15	218.7	5.9	26.96	0.62	288.7	5.6	44.2	1	291.7	5.8	60.5	1	183.2	3.1	27.33	0.59	190.4	3.3	32.98	0.58	15.3	0.33	6.36	0.13
FBtap_66	331.2	4.9	341.7	6.6	930	23	10.40	0.43	48.7	1.2	11.03	0.32	83.5	2.1	50.8	1.2	9.15	0.3	112.5	2.2	21.49	0.38	166.9	3	37.59	0.6	106.5	1.8	13.91	0.25	78.2	1.3	10.28	0.21	0.502	0.025	8.76	0.16
FBtap_67	678	11	150.8	2.8	466	14	74.80	1.60	242.8	6	39.8	1.2	243.2	5.7	76.3	2.6	28.16	0.89	95	2.5	12.7	0.3	76.7	2.3	15.66	0.4	42.67	0.98	5.35	0.17	33.4	0.85	6.31	0.15	20.19	0.54	9.9	0.29

S2.3 apatite trace-element data (continued)

	55Mn	±	86Sr	±	89Y	±	139La	±	140Ce	±	141Pr	±	146Nd	±	147Sm	±	153Eu	±	157Gd	±	159Tb	±	163Dy	±	165Ho	±	166Er	±	169Tm	±	172Yb	±	175Lu	±	232Th	±	238U	±
FB1ap_68	313.5	5.3	296	6.3	1174	24	19.12	0.65	101.8	2.4	26.46	0.76	215.1	5.9	115.5	2.8	17.16	0.38	193.2	3.3	34.32	0.56	229.5	3.4	45.13	0.81	121.9	2.1	15.48	0.28	90.8	1.7	12.17	0.25	0.0596	0.0071	8.1	0.2
FB1ap_69	627	10	143.9	2.8	533	16	10.03	0.36	38	1.1	7.17	0.27	49.7	2	29.75	0.89	5.75	0.22	61.5	1.9	12.3	0.43	89.7	2.6	19.12	0.53	53.1	1.5	6.87	0.22	39.7	1.4	5.92	0.21	0.088	0.088	18.43	0.28
FB1ap_70	329.3	5.3	511.2	9.4	836	19	4.10	0.18	23.14	0.65	5.87	0.16	50.8	1.8	30.61	0.94	7.06	0.21	59.7	1.4	11.84	0.28	99.6	2	28.99	0.5	125.6	1.9	26.95	0.37	230.5	4.1	39.49	0.7	1.492	0.051	16.78	0.36
FB1ap_71	642.1	7.8	174.3	3.1	187.7	3.6	6.11	0.24	20.61	0.56	4.58	0.16	35.1	1	19.61	0.55	6.75	0.2	31.59	0.75	4.701	0.099	29.86	0.65	6.22	0.13	17.18	0.42	2.071	0.063	12.18	0.35	2.094	0.065	0.128	0.012	2.056	0.033
FB1ap_72	645.1	9.3	277.4	4.4	1537	30	24.26	0.58	87.3	1.8	16.96	0.46	112.6	2.3	67.1	1.3	11.77	0.27	140.1	2.3	31.94	0.48	273.1	4.4	61.41	0.92	193.2	2.7	25.1	0.45	149.2	2.6	18.56	0.36	1.139	0.044	5.13	0.11
FB1ap_73	1162	17	90.7	2	2289	44	42.13	0.90	137.5	2.5	24.74	0.49	159.1	3	97.4	2.1	28.37	0.88	215.6	3.6	44.28	0.81	350.4	7	79	1.6	233.3	3.8	30.49	0.6	181.3	2.9	29.17	0.51	2.084	0.052	4.515	0.085
FB1ap_74	341.1	6.5	415.9	7.7	917	26	34.70	1.00	122.8	2.7	21.98	0.61	140.9	3.4	57.9	1.6	7.06	0.24	101.5	2.4	18.66	0.4	144.6	2.5	34.2	0.64	101.8	2	13.47	0.28	80.8	1.6	11.27	0.26	1.729	0.067	4.51	0.12
FB1ap_75	1413	27	113.8	2.8	2401	48	66.90	1.60	205.2	5	35.28	0.87	209.1	6	100.3	2	16.23	0.49	195	4	43.53	0.84	360.6	6.4	82	1.3	253.7	4.1	37.63	0.62	236.1	4.2	31.26	0.72	0.545	0.031	6.21	0.12
FB1ap_76	408.5	5.8	639	11	572	10	10.94	0.33	38.21	0.76	6.76	0.19	42.3	1.4	21.71	0.74	9.95	0.22	43.1	1.1	8.56	0.18	71	1.4	19.05	0.35	71.1	1.2	12	0.23	87.7	1.7	13.96	0.31	0.0634	0.0078	0.936	0.022
FB1ap_77	1034	13	122.4	2.5	1175	26	84.50	1.50	295.7	5.5	52.74	0.84	286.7	4.8	123.1	1.7	20.48	0.36	162.1	2.3	33.71	0.49	235.9	3.7	44.65	0.73	127.3	1.9	18.88	0.26	125.8	1.7	16.7	0.25	1.783	0.041	11.08	0.16
FB1ap_78	143.8	2.8	144.9	3.3	480.1	9.4	2.58	0.14	10.91	0.31	2.44	0.13	22	1	13.38	0.53	3.136	0.091	34.93	0.93	7.24	0.17	64.4	1.2	15.7	0.28	44.48	0.85	5.09	0.11	24.12	0.58	2.545	0.081	0.152	0.011	3.053	0.075
FB1ap_79	1230	16	263.4	4.2	1776	41	16.48	0.48	57.4	1.5	10.33	0.25	69.4	2.2	38.18	0.94	11.19	0.28	88.7	1.8	22.07	0.4	224.9	4	64.13	0.99	237.5	3.9	38.88	0.68	256.8	4.7	35.2	0.78	0.489	0.024	6.94	0.14
FB1ap_80	253.8	4.6	171.5	4	674	15	7.45	0.28	44.8	1.1	12.24	0.35	107	2.6	70.5	2	8.85	0.23	123.9	3	23.48	0.36	155.5	2.4	26.62	0.41	57.03	0.98	5.73	0.15	26.7	0.52	2.915	0.081	0.142	0.012	3.76	0.071
FB1ap_81	497.7	7.5	523.4	8.7	1110	24	32.45	0.84	135.8	2.9	27.68	0.71	188.9	3.9	90.2	2.2	17.06	0.43	154.5	3.1	27.49	0.45	201	3.4	43.9	0.67	122.7	2.2	16.16	0.3	91.4	1.5	10.82	0.25	0.277	0.017	6.92	0.11
FB1ap_82	462.1	7	278.3	4.6	913	19	13.30	0.37	94.4	1.8	23.62	0.6	176.7	3.7	90.1	1.8	7.03	0.19	142.1	2.6	26.13	0.47	183.7	2.8	38.86	0.58	113.2	1.8	15.59	0.3	95.2	1.7	13.7	0.29	0.038	0.0057	4.861	0.094
FB1ap_83	562	8.5	151.5	3	839	19	66.10	1.50	246.6	5.1	50.8	1.2	343.3	7.7	140	3.2	42.96	0.8	204.5	3.7	28.35	0.54	156.6	2.4	28.91	0.48	73.1	1.2	9.16	0.14	54.4	1.1	9.24	0.18	8.82	0.19	19.06	0.3
FB1ap_84	734	13	220.2	5.1	1873	50	583.00	11.00	1803	39	336.1	7.5	1789	41	417.3	8	47.11	0.93	401.4	7.8	55.8	1.2	357.8	7.2	71.5	1.4	204.8	4.5	28.17	0.63	177.3	4	27.66	0.69	35.76	0.87	7.95	0.2
FB1ap_86	924	15	187.7	4.2	225.8	4.9	9.11	0.31	32	0.65	6.25	0.2	39.7	1.4	17.74	0.62	5.99	0.2	25.58	0.83	4.462	0.087	30.2	0.53	6.54	0.12	18.62	0.4	2.372	0.059	14.28	0.43	2.336	0.072	0.0072	0.0027	0.707	0.025
FB1ap_87	2565.5	4.1	346.9	6.6	544	11	11.67	0.35	44.9	1	8.13	0.26	52.8	1.9	24.7	0.75	7	0.2	49.9	1.2	9.43	0.24	73.8	1.6	18.2	0.35	56.9	1.2	7.98	0.17	51.9	1.3	8.13	0.19	3.9	0.16	3.124	0.067
FB1ap_88	1230	16	263.4	4.2	1776	41	16.48	0.48	57.4	1.5	10.33	0.25	69.4	2.2	38.18	0.94	11.19	0.28	88.7	1.8	22.07	0.4	224.9	4	64.13	0.99	237.5	3.9	38.88	0.68	256.8	4.7	35.2	0.78	0.489	0.024	6.94	0.14
FB1ap_89	765	13	115.5	3.2	212.8	4.3	12.45	0.43	41.7	1	8.61	0.25	62.3	1.7	29.79	0.92	7.5	0.22	44.12	0.88	5.41	0.13	32.53	0.66	6.57	0.14	18.48	0.47	2.326	0.068	13.79	0.43	2.31	0.072	0.167	0.015	3.839	0.078
FB1ap_90	426	6.4	441.4	7.9	959	20	12.39	0.39	42.06	0.93	8.24	0.26	58.9	2.2	29.67	0.89	6.48	0.23	66.2	1.5	13.92	0.27	126	2.3	34.02	0.67	106.7	2.3	13.67	0.3	67.5	1.5	7.15	0.17	0.245	0.015	6.09	0.12
FB1ap_91	794.9	9.7	466.1	7.6	1138	21	21.00	0.49	75.4	1.4	14.46	0.37	102.8	2.3	50.4	1.3	8.64	0.2	102.4	2	19.92	0.33	166.2	2.9	41.16	0.57	128.1	1.7	18.71	0.28	115.4	1.8	15.07	0.26	0.675	0.028	8.97	0.14
FB1ap_92	1181	20	129.2	2.6	355.4	5.6	20.58	0.58	76.5	1.8	14.41	0.43	88.7	2.4	30.29	0.91	7.75	0.21	40	1.1	5.95	0.13	40.71	0.68	9.49	0.16	30.64	0.61	4.67	0.11	32.17	0.85	5.85	0.15	3.841	0.085	10.6	0.18
FB1ap_93	329.4	5	409	7.1	896	21	8.02	0.29	50.4	1.1	13.56	0.39	111.3	2.3	62.8	1.4	10.7	0.25	116.6	2.3	22.62	0.36	168.2	2.4	35.71	0.69	94	1.3	11.33	0.26	61	1.2	7.58	0.16	0.0375	0.0067	1.779	0.038
FB1ap_94	856	16	161.2	3.4	768	22	208.30	5.50	570	16	78.6	2.2	377	13	101.3	2.9	49.3	1.5	116.4	3.4	16.97	0.38	110.7	2.9	23.87	0.7	74	2.1	11.26	0.33	79.4	2.3	15.49	0.55	44	1.2	33.65	0.96
FB1ap_95	1034	13	122.4	2.5	1175	26	84.50	1.50	295.7	5.5	52.74	0.84	286.7	4.8	123.1	1.7	20.48	0.36	162.1	2.3	33.71	0.49	235.9	3.7	44.65	0.73	127.3	1.9	18.88	0.26	125.8	1.7	16.7	0.25	1.783	0.041	11.08	0.16
FB1ap_96	357.4	5	157.1	3.7	196.3	3.9	0.70	0.07	3.38	0.16	0.793	0.064	7.86	0.55	4.97	0.3	2.86	0.13	13.81	0.56	2.814	0.084	24.07	0.62	6.69	0.17	23.2	0.56	3.66	0.11	27.53	0.73	5	0.14	0.124	0.011	1.862	0.041
FB1ap_97	586	11	233.2	5.4	1638	34	53.10	1.40	219.8	5.4	43.3	1.2	298.7	7.5	134.2	3.1	12.13	0.36	219.4	5.1	42.51	0.83	316	5.9	67.2	1.2	193.9	3.8	26.71	0.55	157	3.6	20.87	0.42	1.096	0.053	12.17	0.26
FB1ap_98	305.1	5.1	576.9	9.7	177	3.7	3.90	0.21	11.77	0.4	1.9	0.11	12.11	0.79	5.38	0.31	2.287	0.087	11.71	0.33	2.217	0.075	19.8	0.49	6	0.13	22.28	0.49	3.5	0.11	19.82	0.62	3.5	0.11	0.261	0.018	0.352	0.015
FB1ap_99	636.1	8.3	352.3	5.8	1026	21	18.38	0.47	64.8	1.3	11.31	0.33	77.7	2.3	29.85	0.89	5.41	0.16	59.5	1.8	11.73	0.22	112.7	1.9	35.53	0.62	148.6	2.6	27.18	0.51	192.6	3.3	29.11	0.5	1.058	0.033	6.45	0.14
FB1ap_100	689	12	175.8	3.7	1275	25	81.20	2.00	329	7.1	69	2	464	28	93.7	2	11.5	0.33	154.7	2.9	40.2	2.4	257	5	51.1	3.2	140.4	8.1	18.3	1.2	108.7	6.5	16.4	1	19.5	1.3	8.85	0.2
FB1ap_101	514.1	8.4	561	12	895	20	14.67	0.42	84.8	2	21.03	0.58	167.2	4.3	117.5	2.6	17.18	0.33	172.3	2.9	29.99	0.48	183.2	3.1	29.23	0.48	62.64	0.94	6.68	0.16	34.3	0.61	3.76	0.11	0.0608	0.0072	2.22	0.045
FB1ap_102	393	5.3	239.7	3.6	677	14	12.05	0.33	74.5	1.3	20.91	0.46	182.6	4.3	117.5	2.6	17.18	0.33	172.3	2.9	29.99	0.48	183.2	3.1	29.23	0.48	62.64	0.94	6.68	0.16	34.3	0.61	3.76	0.11	0.0608	0.0072	2.22	0.045
FB1ap_103	2353	4	344.2	6.1	566	13	33.93	0.84	127.1	3.5	22.16	0.73	152.1	4.3	69	1.5	13.2	0.36	127.8	3.1	22.51	0.4	135	2.3	18.34	0.31	29.74	0.62	2.402	0.087	9.07	0.32	0.86	0.04	2.182	0.06	6.03	0.14
FB1ap_104	374	6.8	189	4.2	634	11	3.45	0.16	11.31	0.33	1.95	0.11	12.44	0.7	6.86	0.3	4.07	0.12	17.11	0.58	5.1	0.13	63.3	1.2	21.35	0.33	80	1.1	12.09	0.21	74.6	1.4	11.99	0.25	0.385	0.02	1.214	0.029
FB1ap_105	797	11	324.3	5.8	548.6	8.3	1.09	0.10	3.28	0.16	0.782	0.062	5.47	0.36	5.42	0.084	1.564	0.084	19.04	0.65	5.45	0.15	57.4	1.3	18.17	0.32	73.7	1.2	13.96	0.25	105.4	2.3	16.73	0.39	0.0083	0.0029	0.748	0.018
FB2ap_0	890	13	231.9	5.1	959	25	15.62	0.46	59.3	1.1	11.11	0.39	75.7	1.9	45.3	1.4	9.42	0.24	104.4	2.5	22.56	0.43	184	3.1	38.99	0.54	109.9	1.7	15.61	0.35	109.1	2.1	14.89	0.23	0.0821	0.0089	4.826	0.099
FB2ap_2	835	25	369	15	1483	62	66.90	3.00	239	10	42.9	1.6	279	11	130.7	4.7	22.46	0.7	215.3	6.7	40.21	0.88	314.6	6	65.2	1.1	172.2	2.4	22.97	0.48	131.7	3.5	15.99	0.53	0.568	0.03	7.4	0.28
FB2ap_3	430	12	193.4	7.1	2260	110	89.50	4.70	354	18	65.2	3.7	384	18	138.1	6	27.1	1.1	206.1	7.9	40.3	1.3	347	10	85.3	2.8	273.7	8.9	42.2	1.5	282.1	9.9	45.6	1.6	33.1	1	15.82	0.54
FB2ap_4	940	42	206	12	3000	210	3.93	0.31	22.6	1.7	6.36	0.43	67.1	4.3	72.5	4.8	13.18	0.8	225	12	58	2.5	544	21	132.9	4.4	396	14	60.1	2.5	385	19	56.3	3.2	20.7	1.2	72.9	5.1
FB2ap_5	522.4	9.6	200.4	5.1	840	19	3.33	0.17	12.91	0.47	2.55	0.11	18.13	0.8	12.84	0.6	4.72	0.17	34.87	0.87	10.02	0.2	109.4	1.7	31.84	0.48	116.1	1.7	20.79	0.33	146.6	2.3	20.59	0.39	1.477	0.04	4.28	0.1
FB2ap_6	338.1	8.7	231.7	8.5	1372	56	6.87	0.31	33.3	1.3	8.71	0.36	73.5	2.7	49.3	1.5	16.61	0.49	103.1	2.4	22.82	0.57	205.8	3.3	52	0.9	169.8	2.5	26.76	0.49	184.9	4.2	31.32	0.83	3.15	0.11	4.66	0.17
FB2ap_7	478	10	194.1	5.4	2880	86	131.50	4.30	526	16	100.2	3	636	19	231.6	6.7	39.2	1	323.6	7.4	58.6	1.2	473.3	8.6	110.6	1.2	343.5	4.3	51.98	0.79	341.2	6.7	62.4	1.1	42.89	0.71	67.8	1.7
FB2ap_8	468	28	226	21	788	70	3.55	0.34	13.2	1.1	2.86	0.27	23.4	2.1	16.5	1.3	4.26	0.3	48.6	2.6	11.66	0.51	112.3	3.3	28.47	0.55	87.2	2.1	12.97	0.54	81.6	4.4	11.02	0.77	0.0391	0.0061	3.17	0.27
FB2ap_9	414.4	7.8	171.9	4.7	991	30	63.20	2.90	212.7	9	35.1	1.7	210.3	8.6	76.6	3.3	19.12	0.78	114.4	3.5	20.38	0.64	154.8	4.4	36.22	0.91	113	3	16.71	0.48	113	3.8	19.28	0.64	11.2	0.23	20.12	0.48
FB2ap_10	224.8	6	431	13	1587	52	3.80	0.19	12.48	0.4	2.3	0.11	16.1	0.79	8.39	0.4	2.65	0.11	18.61	0.53	3.701	0.095	29.51	0.62	6.48	0.14	15.9	0.36	1.69	0.053	7.74	0.29	0.969	0.041	0.73	0.029	23.07	0.62
FB2ap_11	708	16	205.3	7.2	832	26	6.09	0.27	22.58	0.81	4.49	0.2	31.8	1.3	21.98	0.78	4.19	0.18	50.9	1.4	12.97	0.31	118.9	2	28.75	0.42	88.6	1.8	12.36	0.24	72	2	8.86	0.25	0.101	0.02	2.827	0.08
FB2ap_12	153.6	3.7	218.3	6.6	696	24	7.77	0.30	25.58	0.97	5.28	0.21	38.2	1.5	21.4	0.86	5.63	0.21	69.6	1.9	15.88	0.33	129.4	2.8	26.46	0.48	57.3	1	5.19	0.13	20.53	0.67	2.021	0.074	0.0193	0.0038	0.578	0.028
FB2ap_13	1361	41	189.7	8.3	937	40	15.14	0.76	63.1	2.9	12.96	0.65	92.6	3.8	54.3	2.1	9.75	0.37	101.5	3.1	20.89	0.52	166.3	3.5	37.21	0.59	105.7	1.6	13.37	0.3	70.4	2.2	8.16	0.31	0.15	0.062	1.244	0.055
FB2ap_14	527	13	168.5	5.1	1620	60	71.40	2.30	265.1	7.9	44.6	1.5	271.2	8.8	96.9	3.2	17.49	0.6	144.3	4.8	27.33	0.82	220.9	7.6	56.3	1.6	184.9	5.3	28.62	0.79	187.6	5.7	30.53	0.94	65.6	2.1	45.9	1.3
FB2ap_15	214.7	5.4	685	23	202.5	8.3	5.67	0.27	29.2	1.1	7.37	0.31	62.1	2.3	30.1	1.1	10	0.32	41.8	1.3	6.12	0.16	36.95	0.97	6.56	0.15	15.39	0.4	1.681	0.06	8.48	0.35	1.103	0.049	0.101	0.01	1.739	0.072
FB2ap_16	618	17	193.9	6.8	2700	100	266.30	9.90	881	32	156.3	5.7	846	32	239.4	7.7	32.93	0.91	298.2	7.5	52.2	1.1	405.9	7.8	97.9	1.6	321	5.8	49.54	0.86	325	7.7	51.6	1.4	164.9	3.7	46.7	1.4
FB2ap_17	692	31	232	15	525	36	36.50	6.30	81	13	10.4	1.5	44.1	6	12.4	1.2	2.05	0.16	19	1.2	4.46	0.22	47.1	1.8	16.24	0.56	74	2.7	14.36	0.57	113.8	5.2	19.3	1	36	10	4.09	0.42
FB2ap_18	614	15	158.4	5.6	951	37	43.70	3.80	131	10	20.2	1.3	112.6	6.3	47	2.4	13.26	0.45	81.9	2.8	15.92	0.56	126.6	3.9	31.32	0.89	104.5	2.6	16.13	0.41	118.8	3	22.79	0.55	17.86	0.83	10.58	0.99
FB2ap_19	636	34	186	14	1399	88	7.10	1.20	42.6	3.8	10.3	1.3	98	10	94.9	8	9.25	0.84	239	16	54.9	3.5	338	20	53.6	4.4	114.5	8.3	12.2	1.2	63.6	5.8	7.47	0.69	0.0126	0.0077	22.5	5.3
FB2ap_20	517	16	242	10	1533	65	186.00	11.00	396	26	65.8	3.1	266	13	89.2	3.4	21.85	0.84	148	4.7	29.52	0.83	230.5	4.4	56.27	0.85	179.2	2.6	25.15	0.5	164.8	4.2	27.33	0.88	2.265	0.093	2.75	0.1
FB2ap_21	713	18	127.9	4.8	581	31	255.00	15.00	680	36	101.3	6.1	513	31	117.5	6.9	8.69	0.42	123	6.5	15.65	0.81	97.5	4.9	20.14	0.97	57.6	2.5	8.11	0.34	53.3	2.2	10.12	0.45	7.4	0.4	2.63	0.14
FB2ap_22	841	24	495	19	1136	47	30.20	1.30	100.9	3.9	17.94	0.69	116.7	4.6	59.8	2.3	15.51	0.57	113.8	3.4	21.38	0.54	167.2	3.7	38.42	0.75	118	2.2	17.22	0.34	108.5	2.7	14.19	0.46	5.62	0.36	7.89	0.42
FB2ap_24	858	27	305	14	1154	54	14.20	0.42	81	2	9.64	0.34	60.2	2.6	12.05	0.54	4.26	0.16	42.5	1.4	24.59	0.71	188.7	4.3	43.93	0.86	148.5	3.3	24.77	0.57	184.2	5.1	28.25	0.95	0.399	0.026	11.23	0.57
FB2ap_25	691	20	285	11	1118	46	8.98	0.43	36.9	1.5	7.7	0.34	56.2	2.3	36.9	1.4	10.84	0.34	79.4	2.2	17.78	0.4	159.4	3	41.41	0.61	150.9	2.2	25.72	0.65	184.5	4.8	27.65	0.78	0.17	0.013	7.98	0.29
FB2ap_26	929	28	223.2	9.4	940	35	8.13	0.39	31.4	1.4	5.6	0.24	36.4	1.5	18.94	0.93	4.78	0.25	41.1	1.3	9.6	0.28	90.4	2.1	31.13	0.61	130.7	2.5	26.14	0.66	204.6	5.1	32.25	0.98	0.754	0.03	4.4	0.18
FB2ap_27	536	22	168.8	9.3	1730	120	64.90	4.20	228	14	40	2.6	241	15	107.1	6	28.2	1.3	165.7	6.4	30.64	0.99	235.9	5.5	56.5	1.2	181.2	4.1	27.13	0.77	190.6	6.7	33	1.5	45.9	1.8	36.5	2.1
FB2ap_28	884	19	301.7	8.8	1259	42	263.00	21.00	110.4	5.4	76.3	5.9	343	19	117.5	5.4	22.49	0.89	168.4	5.1	30.55	0.7	225.6	4.2	50.43	0.89	166.8	2.8	27.42	0.44	199.9	4.1	29.04	0.71	0.605	0.036	21.78	0.75
FB2ap_29	1368	73	307	22	1700	130	55.00	5.00	191	14	34.7	1.9	240	18	127.3	7.7	27.7	1.4	217	11	42.4	1.3	324	11	68.4	1.8	190.5	4.7	26.61	0.86	153.3	6.3	18.4	1.1	0.814	0.088	11.98	0.88
FB2ap_30	628	21	274	14	1866	89	454.00	23.00	1028	51	147.5	7.3	636	27	169.5	6.6	36.1	1.4	208.9	6.7	36.58	0.96	275.8	5.2	62.9	1	190.2	3.2	29.3	0.68	202.3	5.8	33.4	1.3	125.9	4.3	22.18	0.96
FB2ap_31	474	14	273	10	1022	38	27.80	1.20	134.5	5.2	32.4	1.2	241.1	8.8	134.2	4.8	8.51	0.33	214.5	6.5	37.77	0.79	246.4	5.4	41.29	0.67	96.6	1.9	10.82	0.24	56.9	1.5	6.27	0.22	0.0683	0.0068	18.19	0.67

S2.3 apatite trace-element data (continued)

	55Mn	±	86Sr	±	89Y	±	139La	±	140Ce	±	141Pr	±	146Nd	±	147Sm	±	153Eu	±	157Gd	±	159Tb	±	163Dy	±	165Ho	±	166Er	±	169Tm	±	172Yb	±	175Lu	±	232Th	±	238U	±
FB2ap_32	1991	65	405	18	1981	97	87.20	3.60	292	13	49.6	1.8	276	11	129.8	5.2	22.94	0.76	193.6	5.7	38	0.88	303.8	5.9	68.6	1.1	223.2	3.8	36.25	0.84	246.7	7	31.4	1.2	1.307	0.051	13.19	0.52
FB2ap_33	1028	32	444	15	1358	62	47.30	2.00	150.2	4.3	25.3	1.2	136.3	6.8	57.2	2.5	15.58	0.61	85.6	2.9	17.27	0.44	159.2	4.1	44.5	1.4	168.9	5.7	28.48	0.76	200.1	6.4	26.49	0.99	2.96	0.14	12.83	0.75
FB2ap_34	815	23	292	11	1230	45	15.12	0.69	49.4	2	8.67	0.41	50.1	2.1	26	1.1	5.34	0.22	54	1.4	14.3	0.38	166.9	3.2	44.69	0.73	156.9	2.8	22.41	0.5	133.2	3.5	17.26	0.54	0.2	0.013	3.33	0.11
FB2ap_35	839	25	315	13	1449	60	66.90	3.10	215.6	8.3	39.4	1.5	228	9.9	117.7	4.5	16.77	0.65	194.5	5.3	36.27	0.87	267	4.3	65.78	0.8	259.6	4.6	21.05	0.5	124.7	3.5	15.13	0.64	1.29	0.16	4.36	0.16
FB2ap_36	489	11	225.4	8.3	2510	130	34.50	1.80	129.4	5.5	25.1	1.1	149.4	5.7	91.7	3.3	16.85	0.66	178.7	5.3	39.9	1.2	337.6	8.5	82.9	2	282.1	6.8	43	1.2	291	9.7	47.4	1.8	28.3	1.2	5.5	0.25
FB2ap_37	909	16	269.5	6.5	679	17	3.45	0.18	8.98	0.35	1.764	0.082	10.28	0.58	6.82	0.35	1.92	0.1	20.24	0.63	5.64	0.13	64.5	1.3	21.02	0.37	86.1	1.5	15.11	0.25	107.8	2	15.69	0.31	0.045	0.0052	1.222	0.033
FB2ap_38	572	17	370	16	616	27	71.30	3.10	225.7	9.8	33.2	1.5	166.6	6.6	65.9	2.5	10.36	0.39	90.8	2.6	15.31	0.38	104.7	2	19.52	0.3	50.57	0.97	6.49	0.15	37.1	1.1	4.63	0.16	1.277	0.065	4.48	0.17
FB2ap_39	921	17	263.8	5	972	18	5.50	0.25	19.77	0.5	3.69	0.19	22.59	0.76	13.91	0.55	4.51	0.15	33.49	0.95	8.48	0.17	92.8	1.5	29.61	0.41	128.4	2	23.92	0.4	179.1	3	25.57	0.41	0.0788	0.0084	3.257	0.069
FB2ap_40	611	18	277	11	1260	59	162.40	6.20	560	23	91.7	3.4	428	15	202.6	6.2	11.31	0.39	269.4	8	49.3	1.2	295.5	5.9	44.08	0.88	92.7	1.7	9.39	0.24	45.2	1.2	4.41	0.18	0.11	0.012	1.203	0.083
FB2ap_41	633	19	225	11	779	41	101.80	5.20	357	18	62.9	3.3	342	17	129.2	5.9	14.67	0.64	158	5.7	22.87	0.8	140.4	3.3	27.75	0.53	75.4	1.6	9.9	0.28	61.8	1.8	9.86	0.37	7.49	0.21	3.13	0.14
FB2ap_42	379	8.3	524	16	989	34	51.80	1.90	229.8	7.3	52.8	1.7	337	11	222.3	6.1	67	1.8	341.5	8	58	1.3	296.9	5.5	38.53	0.6	68.6	1.2	6.46	0.15	29.92	0.83	3.2	0.11	0.0075	0.0022	32.1	0.84
FB2ap_43	783	25	128.5	6	1397	73	119.70	5.60	442	22	82	4	471	21	194.3	7.9	47.4	1.8	258.6	7.8	37.9	0.93	239.5	3.7	48.96	0.78	137.2	2.3	17.42	0.37	110.7	3	19.54	0.7	14.42	0.51	9.1	0.38
FB2ap_44	721	16	360	10	1951	69	37.30	1.20	136.1	5.4	25.69	0.95	161.5	5.5	94.4	3.6	18.08	0.67	190.4	5.8	39.3	1.1	328.3	8.8	76.5	1.8	237.7	6.3	33.5	1	207.9	6.5	26.61	0.86	4.3	0.21	17.24	0.85
FB2ap_45	564	19	605	17	1465	39	45.30	1.50	140.5	4.2	23.06	0.6	131.6	4.1	57.9	1.4	22.2	0.61	85.9	2	13.54	0.31	90.7	2	18.68	0.36	53	1.1	7.25	0.15	43.4	1.1	5.62	0.17	6.05	0.16	6.35	0.19
FB2ap_46	1375	32	295.2	8.9	1416	39	78.90	2.10	323.7	9	60.9	1.7	370	10	260.1	6.5	45.5	1.1	423.8	9.1	77.5	1.4	425.5	7.5	61.19	0.89	129.5	2	14.94	0.36	79.1	1.9	8.67	0.26	2.106	0.066	29.46	0.61
FB2ap_47	825	20	136.4	4.3	1890	63	115.70	4.20	423	14	87.8	2.9	614	19	339.3	9.6	86.8	2.3	508	13	66.2	1.7	366.1	8.3	68.5	1.3	181.9	3.6	23.27	0.45	144.7	3.1	25.48	0.63	60.2	1.4	89.9	2.8
FB2ap_48	501	12	207.9	6.8	2379	82	244.30	8.50	718	26	118.7	4	807	27	202.1	5.9	34.95	0.93	271.8	7.2	48.3	1.1	366.1	7.5	85.7	1.7	269.6	5.1	40.89	0.95	272.6	6.5	43.8	1.3	41.7	1.1	11.63	0.33
FB2ap_49	324	12	1202	63	311	18	16.30	0.96	65.5	3.5	12.95	0.78	101.3	5.2	28.8	1.7	7.83	0.39	68.5	2.3	6.25	0.19	44.6	1.1	10.36	0.24	30.49	0.66	4.42	0.13	28.1	1.1	4.62	0.18	0.696	0.033	2.74	0.14
FB2ap_50	806	21	171.7	6.1	4060	160	103.50	3.60	367	12	65.5	2.3	525	18	178.3	5.9	44.5	1.3	289.1	7.9	60.1	1.4	508	12	135.2	2.8	490	11	83.1	2.1	612	18	105.8	3.7	77	2	103.5	3.5
FB2ap_51	500	12	323.3	8.2	110.9	3.5	0.04	0.02	0.217	0.037	0.053	0.018	0.78	0.12	0.91	0.037	0.316	0.023	3.35	0.23	1.011	0.049	11.37	0.36	3.86	0.13	16.4	0.46	3.06	0.1	23.33	0.75	3.63	0.13	1.31	0.054	6.64	0.18
FB2ap_52	600	17	578	23	581	24	47.00	2.00	151.7	5.9	26.1	1.2	198.3	7.5	62	2.2	13.37	0.29	91	1.8	19.54	0.38	54.1	1.2	7.74	0.2	46.4	1.5	6.3	0.2	8.5	0.24	6.66	0.23
FB2ap_53	494	17	173.8	7.8	475	22	4.01	0.24	15.48	0.79	3.1	0.18	26.9	1.7	12.37	0.5	3.98	0.2	27.8	1.1	6.36	0.22	57.8	1.3	15.15	0.35	51.9	1.3	8.26	0.26	56.9	1.7	9.59	0.35	0.134	0.013	4.03	0.16
FB2ap_54	289	10	208.6	7.2	901	29	51.70	2.00	218.3	7.8	44.5	2	383	13	144.8	4.8	21.89	0.81	230	6.8	43.7	1	249	5.8	32.99	0.67	54.1	1.3	4.54	0.15	19.33	0.73	1.9	0.11	0.218	0.017	15.66	0.6
FB2ap_55	385.9	7.8	232.5	6.1	992	51	31.70	2.70	126	9.4	25	1.8	222	16	63.6	4.2	11.61	0.64	97.5	5	18.48	0.87	150.9	7.1	38.3	1.9	128.8	6.8	19.2	1.1	124.9	7.1	19.1	1.1	4.94	0.22	9.33	0.39
FB2ap_56	459	11	161	4.9	1902	65	51.40	1.50	195.8	6	39.6	1.4	332	10	119.7	3.6	29.21	0.73	191.1	4	36.34	0.7	276.9	5.7	66.4	1.2	212.1	4.3	31.72	0.69	215.7	5.9	36.2	1.1	82.2	2.4	48.1	1.5
FB2ap_57	475	15	241.8	8	1974	75	125.00	4.80	434	15	70.8	2.5	534	18	150.2	4.2	27.69	0.82	218.8	5.8	40	0.95	299	5.8	69.2	1.3	216.4	4.3	32.44	0.81	219.2	5.3	35.8	1.1	51.3	1.3	34.03	0.93
FB2ap_58	1247	45	163.4	8.6	870	49	9.07	0.95	29.2	1.6	7.02	0.39	63.4	3.7	29.8	1.5	6.02	0.27	60.1	2.2	13.88	0.47	120.9	2.4	30.14	0.47	91.1	1.5	12.31	0.31	69.1	2.2	8.24	0.35	0.245	0.021	1.283	0.068
FB2ap_59	232.3	7	135.1	5.5	976	39	24.70	1.00	185.5	7.7	50.2	1.9	505	18	245.1	8.4	15.14	0.47	387.1	9.4	64.9	1.5	315.7	5.5	38.9	0.58	62.9	1.1	5.6	0.15	24.58	0.84	2.583	0.083	9E-05	2E-07	8.14	0.29
FB2ap_60	760	17	122.2	4.3	1084	38	274.00	10.00	824	26	148.9	5	1023	36	236.9	7.6	27.54	0.75	266.6	6.9	36.18	0.92	216.6	4.9	43.02	0.83	112.8	2.4	13.88	0.29	82.1	2.3	13.6	0.41	9.92	0.26	6.05	0.2
FB2ap_61	434	17	232	14	1241	73	16.11	0.97	93.5	5.3	23.5	1.4	225	12	117.5	6.5	14.16	0.7	208	8	41.6	1.2	275.5	6	48.76	0.79	115.7	2.7	13.26	0.4	70.3	2.5	8.52	0.38	0.0368	0.006	9.49	0.48
FB2ap_62	677	18	345	14	906	38	33.00	2.90	67.7	4.2	10.36	0.6	58.6	2.5	19.98	0.92	4.1	0.17	38.6	1.3	9.26	0.32	93.6	2.8	29.82	0.94	129	3.6	25.2	0.82	197.7	6.3	32	1.1	3.54	0.15	5.92	0.41
FB2ap_63	275	12	340	21	1045	72	27.50	1.70	119.4	8.1	26.7	1.9	229	15	111	6.2	9.79	0.5	184.8	7.5	33.6	1.2	215.1	5.2	39.25	0.76	93	1.9	10.59	0.3	55.5	2	6.59	0.32	0.214	0.027	15.82	0.98
FB2ap_64	964	21	262.5	8.7	1330	41	10.20	0.38	37.3	1.3	7.33	0.31	54.7	2	28.5	1	7.9	0.22	72.1	1.8	17.39	0.41	172.8	2.9	49.83	0.62	184.9	3.2	30.33	0.54	207.5	4.3	28.31	0.8	0.32	0.021	5.28	0.18
FB2ap_65	466	12	209.3	7.1	1271	49	75.10	7.90	264	25	43.4	3.5	214	11	89.4	3.1	29.2	1.1	140.7	4.5	24.95	0.68	183.2	4.2	44.88	0.97	144.8	3.1	20.84	0.43	144.3	3.5	24.53	0.73	63.7	2.6	16.92	0.6
FB2ap_66	562.8	9.8	218.9	5.4	528	20	25.10	1.40	97.4	5.2	17.05	0.93	94.6	5.2	33.7	1.8	6.38	0.26	51.4	2.3	8.27	0.35	63.8	2.3	17.05	0.63	61.8	2.1	10.15	0.39	73.4	2.5	12.73	0.45	17.39	0.4	4.12	0.12
FB3ap_0	863	8.2	121.1	1.8	403.9	9.1	13.96	0.39	52	1.2	9.52	0.31	59.3	1.8	26.93	0.79	4.59	0.16	40.2	1	7.43	0.23	54.7	1.3	12.59	0.3	38.81	0.96	5.64	0.13	37.7	1.1	6.45	0.18	0.902	0.044	3.21	0.14
FB3ap_1	635.8	5.1	142	2	300.1	3.5	4.72	0.18	17.71	0.45	3.71	0.14	27.18	0.97	15.43	0.47	6.79	0.18	30.24	0.68	5.53	0.12	41.23	0.63	9.64	0.14	28.7	0.39	3.649	0.09	21.28	0.51	3.215	0.081	0.0562	0.008	1.345	0.029
FB3ap_2	560.7	4.6	213	2.7	78.7	3.9	18.10	1.40	32.7	2.1	3.33	0.24	14.4	1.1	3.51	0.27	1.132	0.069	5.73	0.38	1.071	0.068	9.22	0.49	2.54	0.12	8.8	0.43	1.502	0.089	10.93	0.6	2.02	0.12	4.33	0.31	1.73	0.12
FB3ap_3	545.5	5	134.6	1.7	559.2	8.6	129.50	3.00	378.6	9.6	56.2	1.4	306.4	6	79.3	1.8	7.54	0.22	96	1.9	13.54	0.22	90.4	1.6	19.6	0.33	59.9	1.1	8.65	0.15	60.3	1.1	11.06	0.2	10.72	0.15	6.261	0.072
FB3ap_4	493.1	4.5	141.6	1.7	61.57	0.89	0.56	0.06	2.06	0.12	0.395	0.046	2.67	0.23	1.51	0.13	0.531	0.045	3.28	0.18	0.684	0.036	6.85	0.23	1.879	0.056	7.04	0.18	1.127	0.04	7.8	0.28	1.484	0.049	0.0079	0.0025	0.1913	0.0097
FB3ap_5	932	10	125.2	2.1	1310	120	63.30	5.70	228	22	43.4	4.1	278	26	128	13	28.8	2.5	185	18	28.1	2.9	195	19	42.3	4.2	134	13	19.7	2	140	14	25.6	2.6	16.4	1.9	8.74	0.77
FB3ap_6	392.9	5.3	380.4	5.2	1134	25	92.80	1.70	319.3	4.9	54.8	1.1	337.3	6.4	129.1	3.1	11.91	0.4	199.6	4	31.96	0.57	216.9	3.9	46.22	0.79	126.9	2.4	16.4	0.34	93.7	1.9	12.36	0.28	1.149	0.052	8.27	0.15
FB3ap_7	1154.4	7.6	112.9	1.6	2314	43	151.20	2.00	538.7	6.1	96.6	1.4	607.4	8	251.9	3.2	25.35	0.6	375.7	5.2	67.3	1	460.8	7.3	92.5	1.5	246.1	4.4	29.38	0.58	169.6	3.5	26.04	0.6	11.5	0.36	8.16	0.18
FB3ap_8	520.3	3.9	229.3	2.9	1366	50	42.50	1.40	156.9	5.2	27.73	0.98	175.5	6.5	91.7	3.6	27.6	1	176.1	6.5	33.4	1.2	254.7	9.4	57.2	2	165.6	6.4	21.26	0.86	118.8	5	15.92	0.67	7.64	0.54	43.9	2.5
FB3ap_9	942.2	7.2	137.2	2.2	345.1	4.5	7.20	0.23	22.23	0.52	3.86	0.14	22.46	0.81	11.7	0.44	6.28	0.19	23.25	0.62	4.9	0.11	40.08	0.71	9.83	0.19	34	0.66	5.74	0.13	44.82	0.83	8.19	0.15	0.0442	0.0054	1.977	0.037
FB3ap_10	369.3	3.2	209.2	2.7	1038	45	55.59	0.65	346.1	3.4	80.34	0.95	549.7	6.3	235.6	2.7	23.63	0.33	324.8	3.5	53.78	0.55	297.1	2.9	43	0.48	83.74	0.95	8.25	0.12	38.08	0.63	4.24	0.086	0.363	0.016	48.03	0.39
FB3ap_11	691.3	5.5	156.8	2.3	146.2	1.9	3.31	0.15	10.92	0.29	2.102	0.096	14.23	0.61	7.39	0.3	3.7	0.12	14.08	0.38	2.626	0.075	19.86	0.39	4.48	0.11	13.85	0.35	1.766	0.056	11.71	0.36	2.003	0.061	0.0033	0.0017	0.333	0.013
FB3ap_12	1097.1	9.9	108.5	2	1638	37	106.60	1.80	368.2	5.6	62.39	0.87	387.3	6.2	168.5	3.4	24.42	0.68	264.3	4.5	42.56	0.61	288.9	5.2	60.1	1.1	171	2.5	23.07	0.55	141.9	3.2	22.86	0.53	14.45	0.35	8.99	0.14
FB3ap_13	891.1	7.3	141.6	1.7	1557	27	248.20	6.40	808	21	137.2	3.6	813	17	263.9	5.9	42.27	0.67	320.8	5.9	45.31	0.77	283.6	5	57.16	0.98	168.9	2.6	21.14	0.41	137.4	2.4	23.68	0.36	16.39	0.4	5.66	0.11
FB3ap_14	905.9	6.2	142.6	1.7	529.6	5.4	17.30	0.52	48.72	0.65	8.84	0.22	52.4	1.4	27.09	0.51	7.67	0.17	48.3	0.9	9.3	0.14	72.7	1	17.01	0.24	52.93	0.68	7.56	0.14	50.49	0.92	8.18	0.15	0.859	0.032	2.167	0.04
FB3ap_15	698	5.9	156.8	1.8	1441	17	470.30	8.60	1002	15	133.2	2.9	616	13	166.7	3.4	53.71	0.77	211.8	3.5	33.27	0.49	223.4	2.7	48.96	0.55	149.4	1.6	21.48	0.26	151.6	1.7	28.72	0.34	61.78	0.8	27.17	0.6
FB3ap_16	856.6	6.3	166.2	2.3	267.3	3.1	14.00	0.31	48.26	0.76	9.23	0.22	62.2	1.4	27.93	0.73	12.69	0.44	41.89	0.79	5.93	0.12	37.04	0.66	7.9	0.14	22.1	0.41	2.921	0.081	18.95	0.44	3.57	0.086	0.0679	0.0094	2.432	0.052
FB3ap_17	254.3	2.3	368.5	3.5	1013	14	91.60	1.20	275.6	3.1	43.85	0.55	235.2	3.1	99.9	1.2	30.95	0.44	170.1	1.9	35.11	0.39	233.5	2.4	36.32	0.35	71.97	0.83	6.58	0.13	28.65	0.51	2.864	0.069	23.53	0.26	1.665	0.04	36.75	0.35
FB3ap_18	2675	20	326.1	3	1987	22	134.50	1.50	538.9	5.2	87.4	1.1	573.3	5	257.2	2.7	56.44	0.58	364.3	3.7	67.18	0.61	463.4	3.7	88.57	0.85	238.4	2.1	32.44	0.34	189.6	1.9	23.53	0.26	1.695	0.04	36.75	0.46
FB3ap_19	713.6	8.4	241.4	3.6	1076	14	10.73	0.47	37.3	0.93	6.78	0.21	46.6	1.2	34.6	0.81	7.26	0.19	87.6	1.3	21.77	0.28	195.3	2	46.38	0.59	142.9	1.7	21.28	0.28	142.3	1.8	19.68	0.26	0.199	0.023	2.562	0.046
FB3ap_20	745.6	5.1	190.7	2.5	162.5	2	0.70	0.06	2.99	0.15	0.676	0.062	5.67	0.38	4.72	0.26	1.934	0.08	10.51	0.37	2.319	0.074	19.21	0.39	4.66	0.11	14.95	0.27	2.114	0.065	13.56	0.31	2.25	0.065	0.0035	0.0016	0.1201	0.0069
FB3ap_21	635.4	5.4	152	2.5	729.8	8.8	337.40	6.00	851	13	115.4	2.1	566	11	128.9	2.1	22.44	0.46	139.2	2.2	18.47	0.29	118.2	1.5	25.51	0.34	76.8	1.3	10.6	0.17	69.2	1.2	12.55	0.22	17.12	0.33	4.92	0.11
FB3ap_22	1124.9	8.7	110	1.9	370.8	4.3	29.30	1.40	86.8	3.7	15.99	0.42	101.6	2.1	44.85	0.98	22.44	0.26	64.4	1.2	9.29	0.16	58.81	0.92	11.79	0.18	32.66	0.51	4.155	0.091	25.41	0.39	4.67	0.085	0.59	0.1	2.87	0.083
FB3ap_23	609.5	5.5	212.1	3	2660	32	134.00	1.90	487	4.9	88.4	1.1	532.7	6	184.6	2.3	31.6	0.49	263.1	3	48.8	0.56	390.4	4.3	94.59	0.94	317.4	2.8	47.65	0.53	320.8	3.2	52.72	0.47	14.67	0.27	8.25	0.21
FB3ap_24	408.9	3.8	192.2	2.6	1686	37	57.90	1.60	207.9	5.1	37.04	0.96	234	5.3	98.2	2.3	21.47	0.48	165.2	3.5	32.64	0.7	262.9	6	62.3	1.4	198.9	4.7	28.92	0.68	190.2	4.6	32.07	0.76	17.98	0.32	12.35	0.51
FB3ap_25	593.7	5.3	157.5	2.3	1120	18	99.50	5.00	288	14	43.9	1.9	238	10	71.3	2.1	20.56	0.36	107.3	1.9	18.4	0.29	138.7	2.4	33.91	0.47	115	1.7	17.38	0.26	120.6	1.7	22.6	0.38	26.1	1.2	14.12	0.54
FB3ap_26	927.3	5.3	145.8	2	771.1	8.4	5.97	0.19	22.28	0.5	4.57	0.15	31.74	0.83	17.59	0.59	4.13	0.13	40.49	0.84	9.41	0.16	91.8	1.3	26.1	0.35	97.8	1.3	15.89	0.22	105.9	1.4	15.32	0.24	0.935	0.032	7.2	0.1
FB3ap_27	508.5	5.5	371.6	4.1	240.8	3.5	149.80	3.90	246.3	6.1	24.57	0.69	107	2.9	19.44	0.68	5.32	0.16	23.64	0.67	3.798	0.098	30.47	0.51	8.04	0.13	28.7	0.55	4.69	0.11	33.3	0.64	5.61	0.11	42.97	0.68	22.59	0.36
FB3ap_28	564.4	5.6	154.4	2.1	127	1.8	1.40	0.18	5.02	0.26	0.912	0.082	5.93	0.38	3.15	0.23	1.093	0.07	6.56	0.3	1.535	0.054	14.6	0.4	4.323	0.09	17.09	0.36	2.899	0.088	21.21	0.51	3.626	0.082	0.133	0.019	0.79	0.023
FB3ap_29	632.5	5.7	190.6	2.7	61.2	2.8	10.20	1.30	23.9	2.2	3.42	0.31	18.7	1.5	5.19	0.39	1.38	0.1	7.01	0.38	1.098	0.068	7.91	0.42	2.02	0.1	6.89	0.36	1.027	0.059	7.11	0.36	1.345	0.066	2.08	0.28	0.81	0.14
FB3ap_30	646.6	3.9	148.6	2.1	987	15	699.00	7.50	1812	21	270.7	3.2	1271	13	270.9	3.4	19.41	0.33	261.3	3.4	33.94	0.46	201.6	2.8	38.56	0.52	103.9	1.3	13.16	0.22	79.7	1.2	11.5	0.18	23.98	0.5	10.15	0.42

S2.3 apatite trace-element data (continued)

	55Mn	±	86Sr	±	89Y	±	139La	±	140Ce	±	141Pr	±	146Nd	±	147Sm	±	153Eu	±	157Gd	±	159Tb	±	163Dy	±	165Ho	±	166Er	±	169Tm	±	172Yb	±	175Lu	±	232Th	±	238U	±
FB3ap_31	971.8	8.1	160.1	2	409.2	4.5	9.61	0.28	33.16	0.6	6.46	0.2	47.9	1.2	28.29	0.64	9.78	0.24	50.19	0.89	8.47	0.15	58.4	0.89	12.88	0.21	37.47	0.53	5.048	0.085	31.54	0.58	5.313	0.095	0.176	0.014	5.146	0.08
FB3ap_32	898.8	7.5	122.2	2	1667	25	185.00	2.80	760	10	149.8	2.1	929	12	336.9	4.5	38.09	0.55	392.4	4.4	54.8	0.67	335.8	4	64.43	0.79	174.9	2.1	22.27	0.33	133.3	1.7	21.24	0.31	18.65	0.32	8.07	0.18
FB3ap_33	828.4	6.4	77	24	1413	16	26.44	0.54	144.9	1.9	31.02	0.52	193.9	3.1	113.8	1.5	10.87	0.23	181.5	2.1	40.33	0.44	288.6	2.9	53.13	0.51	141.4	1.5	18.71	0.23	106.5	1.3	11.39	0.15	0.815	0.052	3.86	0.11
FB3ap_34	1407	13	137.8	2.6	770	12	142.30	2.00	517.1	8.3	94.3	1.4	560.8	9.2	182.5	3	22.51	0.33	206.9	2.9	30.66	0.39	179.1	2.3	32.25	0.48	74.3	1.1	7.22	0.14	30.51	0.66	3.604	0.098	1.269	0.099	48.12	0.99
FB3ap_35	485.4	5	215.8	2.6	1971	27	333.30	3.90	1137	14	193	2.4	1017	11	248.4	2.5	25.23	0.36	261.9	2.8	40.51	0.45	294.5	3.3	67.92	0.7	221.4	2.3	34.38	0.51	233.8	2.8	37.21	0.44	23.13	0.269	4.897	0.077
FB3ap_36	755.7	7.4	440.6	5	1294	20	35.09	0.62	141.5	1.8	28.74	0.53	204.1	3.3	97.5	1.5	15.61	0.23	175.1	2.7	31.37	0.42	228.3	2.9	48.94	0.65	156.3	2	25.72	0.4	178	2.3	24.84	0.36	0.326	0.021	10.27	0.18
FB3ap_37	1233.2	9.5	102.5	2	681.7	7.5	34.04	0.55	121.8	1.4	23.31	0.45	146.3	2.2	67.6	1.3	10.45	0.23	97.9	1.5	15.4	0.19	100.4	1.4	20.74	0.29	68.64	0.89	7.7	0.16	49.28	0.82	8.34	0.14	3.11	0.089	3.382	0.061
FB3ap_38	572	7.9	143.9	2.5	1021	18	310.50	5.50	919	13	143	2.3	756	13	184.6	3.1	16.46	0.39	207.6	3.3	29.68	0.53	192.3	2.6	40.33	0.71	115.9	2	16.04	0.3	101.8	1.8	16.39	0.26	21.98	0.41	9.64	0.17
FB3ap_39	860.3	6.5	158.8	2.8	337.3	9.4	8.84	0.20	28.54	0.67	5.73	0.2	43.1	1.2	25.54	0.87	9.19	0.3	43.5	1.2	7.29	0.22	51.1	1.5	11.1	0.3	31.7	1.1	4.17	0.14	25.99	0.94	4.25	0.14	1.19	0.11	3.407	0.098
FB3ap_40	880.2	6.7	143.2	2.2	417.8	5	20.50	0.44	76.4	1	15.17	0.32	101.4	2	43.96	0.9	11.14	0.21	63.68	0.96	9.85	0.15	64.41	0.97	13.56	0.24	37.3	0.55	4.62	0.11	28.92	0.57	5.151	0.095	0.222	0.016	5.541	0.071
FB3ap_41	599.9	5.9	170.1	2.6	909	17	111.50	2.40	280.5	4.9	37.77	0.77	193	4.1	53	1.3	23.49	0.55	87.2	1.9	15.57	0.3	122.5	2.3	31.11	0.49	102.2	1.7	14.97	0.26	102.4	1.7	19.25	0.37	120.1	2	43.36	0.57
FB3ap_42	894.2	7.3	159.6	2.2	1778	46	274.30	3.90	853	14	138	2.8	778	16	221.1	5.1	36.6	0.98	273.3	6.5	44	1.2	306.2	7.8	66.6	1.8	196.5	5.1	26.73	0.71	173.4	4.6	29.46	0.77	32.6	1.3	12.13	0.34
FB3ap_43	1043	21	76.9	1.5	2017	36	14.52	0.67	51.1	2.3	10.13	0.44	70.2	3.2	44.3	1.4	12.23	0.24	106.7	2.7	25.58	0.55	246.9	4.4	70.8	1.1	273.3	4.3	46.74	0.66	338	4.8	51.87	0.69	6.64	0.28	9.82	0.34
FB3ap_44	1219.9	8.6	99.1	1.7	2251	39	105.80	1.40	374.7	5.3	70.72	0.99	455.5	6.6	201	2.8	38.04	0.5	296	4.1	48.52	0.68	337.6	4.9	74.73	0.9	231.9	2.5	34.34	0.47	236.6	3	41.4	0.66	25.48	0.71	8.73	0.28
FB3ap_45	625.8	4.8	149.5	2.1	760	12	93.80	3.20	266	8.5	36.3	1.3	184.1	5.5	51.8	1.4	13.61	0.32	75.2	1.9	13.36	0.36	102.1	2	24.6	0.51	80.3	1.4	12.04	0.28	85.5	1.8	15.04	0.27	24.67	0.56	8.7	0.2
FB3ap_46	466.9	4.5	207.9	2.8	324.6	7.7	75.00	3.40	171.2	7.5	21.2	1	105.5	4.6	22.4	1.1	5.08	0.18	30.6	1.1	4.74	0.15	37.91	0.43	10.3	0.25	39.45	0.95	6.86	0.18	53.8	1.4	10.12	0.23	12.66	0.47	5.67	0.28
FB3ap_47	943.7	8.7	143.2	2.1	1501	20	276.90	3.70	885	13	144.3	1.8	766	10	216.6	2.7	32.65	0.45	282.1	2.9	37.91	0.43	295.2	3.2	54.51	0.76	164.8	1.9	19.37	0.35	153.8	2.2	25.31	0.35	75.8	1.2	28.39	0.44
FB3ap_48	1233.2	9.5	102.5	2	681.7	7.5	34.04	0.55	121.8	1.4	23.31	0.45	146.3	2.2	67.6	1.3	10.45	0.23	97.9	1.5	15.4	0.19	100.4	1.4	20.74	0.29	68.64	0.89	7.7	0.16	49.28	0.82	8.34	0.14	3.11	0.089	3.382	0.061
FB3ap_49	632.5	4.8	173.6	2	1562	19	91.80	1.10	351	4.3	27.87	0.74	418.2	4.2	174.1	2.3	27.87	0.35	265.7	3.1	44.67	0.46	317	3.1	67.8	0.64	192.7	1.9	24.37	0.27	140.8	1.8	19.84	0.29	6.19	0.11	39.11	0.37
FB3ap_50	593.4	4.4	157.2	2.1	106.1	1.2	1.79	0.11	6.43	0.21	1.328	0.093	9.84	0.46	5.2	0.3	2.97	0.11	10.71	0.38	1.882	0.06	14.72	0.29	3.466	0.074	10.86	0.28	1.407	0.047	9.47	0.26	1.746	0.065	0.0205	0.0043	3.072	0.046
FB3ap_51	946.7	7.5	101.7	1.6	2900	120	164.80	4.60	598	18	113.7	3.6	705	24	281	10	75.2	3.7	379	15	58.7	2.5	395	16	89.3	3.6	288	12	42.5	1.7	298	13	55.1	2.3	50.1	3.2	31.2	2
FB3ap_52	186.3	2.4	891.1	8.5	2196	47	18.86	0.40	69.7	1	13.26	0.29	92.2	2	48.1	1	10.36	0.25	102.1	1.2	20.14	0.27	153.3	1.9	32.08	0.45	82.52	0.82	9.89	0.15	53.56	0.84	6.16	0.13	0.243	0.016	5.388	0.083
FB3ap_53	853	10	56.8	1.7	2842	39	30.13	0.95	109.8	3.7	22.49	0.65	169.6	4.2	97.9	1.7	13.42	0.31	210	2.6	46.65	0.65	405.4	4.6	99.8	1.1	321.7	4	42.06	0.6	242.8	3.2	34.47	0.49	7.25	0.19	4.201	0.084
FB3ap_54	889	7.1	115.1	2	1315	48	370.60	6.10	1121	20	191.5	3.2	1047	21	295.6	6.2	29.21	0.7	319.1	7.8	44.31	0.91	272.7	6.7	51.6	1.3	136.1	3	16.96	0.44	100.2	2.5	15.97	0.38	20.28	0.45	7.99	0.34
FB3ap_55	1480	30	337.8	9.5	2196	47	112.50	3.60	376.2	6.4	69.1	2.8	413	10	225.1	3.4	16.36	0.44	335.2	9.1	61.2	2	408.6	3.9	77.5	1.9	209.4	5.1	28.2	1.1	168.3	3.2	19.23	0.51	4.85	0.22	12.04	0.35
FB3ap_56	1146	12	123.1	1.9	1849	26	26.72	0.45	87.7	1.4	15.84	0.33	98.5	2.1	50.53	0.8	10.37	0.21	107.5	1.6	25.04	0.34	234.3	2.9	61.49	0.66	215.3	2.6	33.73	0.41	225.5	2.9	31.85	0.44	1.089	0.076	7.25	0.26
FB3ap_57	430.3	3.6	212.5	2.9	1235	16	36.98	0.63	133.2	1.6	24.44	0.38	160	2.8	69.7	1.2	17.02	0.29	117.8	1.4	23.62	0.31	188.6	2.1	45.33	0.48	144.9	1.9	20.26	0.28	125.8	1.7	19.34	0.28	48.61	0.65	8.92	0.13
FB3ap_58	1027	32	137.8	2	1490	22	223.10	8.40	730	18	124.9	2.6	730	13	236.4	2.5	33.19	0.54	294	3.3	42.8	0.48	268.6	3.1	54.51	0.56	162.8	1.7	19.95	0.26	125	1.5	20.49	0.25	17.2	1.3	7.48	0.47
FB3ap_59	1038	10	123.3	2.1	2590	110	297.80	4.50	999	15	188.9	4	1157	27	428	14	48.8	1.9	557	21	89.1	3.6	581	23	111	4.7	285	12	32.4	1.4	166	7.3	22.6	1	30.6	2.1	11.75	0.77
FB3ap_60	543	4.6	196.4	2.7	3343	71	145.9	1.8	829	12	249.8	3.1	1157	12	249.8	3.1	40.24	0.56	343.9	4.2	62.46	0.77	491.4	5.3	118	1.4	388.9	4.3	59.66	0.81	400.9	4.5	63.66	0.82	40.28	0.69	27.38	0.39
FB3ap_61	1265.6	9.6	135.3	1.8	625.3	7	36.87	0.65	116.7	1.2	22.44	0.41	163.1	2.5	74.6	1.3	14.9	0.3	108.7	1.6	15.95	0.23	100.4	1.5	20.23	0.25	60.59	0.79	5.64	0.11	44.46	0.64	6.37	0.12	0.939	0.036	2.117	0.05
FB3ap_62	636.1	6.6	162.9	2.4	101.4	1.9	8.70	1.80	27	5	4.31	0.69	25.3	3.3	8.67	0.72	1.549	0.096	12.2	3.4	2.048	0.085	14.71	0.46	3.323	0.098	14.46	0.32	1.809	0.061	11.66	0.74	1.633	0.069	2.28	0.69	0.621	0.067
FB3ap_63	689	14	154.2	2	3937	47	112.50	1.60	439.2	5.6	76	1.1	443.8	5.2	193.5	2.9	32.5	0.55	522.2	3.4	68.75	0.73	560	5.8	135.7	1.5	440.7	4.7	61.78	0.66	390	5.1	63.04	0.69	66.22	0.71	28.58	0.29
FB3ap_64	5144.7	4.8	138.5	1.9	463.2	6.1	108.90	1.70	340.2	5	50.3	0.84	261.2	4.4	72.9	1.5	5.64	0.17	84.2	1.3	11.99	0.24	76.9	1.3	16.22	0.27	47.47	0.74	6.61	0.15	49.83	0.7	7.68	0.16	5.37	0.11	2.45	0.43
FB3ap_65	1027	32	137.8	2	1490	22	223.10	8.40	730	18	124.9	2.6	730	13	236.4	2.5	33.19	0.54	294	3.3	42.8	0.48	268.6	3.1	54.51	0.56	162.8	1.7	19.95	0.26	125	1.5	20.49	0.25	17.2	1.3	7.48	0.47
FB3ap_66	976	10	105.2	1.8	1898	31	25.30	0.56	84.6	1.2	15.05	0.34	93.5	1.6	46.7	1	10.85	0.23	100.2	1.7	24.23	0.38	232	3.4	61.97	0.91	221.8	3.2	35.93	0.6	246.7	4.2	34.69	0.57	3.02	0.09	5.91	0.15
FB3ap_67	722.8	7.9	132.6	2.1	1776	35	76.10	1.40	295.2	4.7	60.5	1.4	428.5	8.3	213.8	4.1	62	1.1	324.6	5.9	51.03	0.89	331.5	6.5	68	1.3	188.5	4	24.1	0.48	142.5	3.1	21.49	0.47	34	0.83	25.02	0.55
FB3ap_68	900.8	6.6	285.5	3.7	1001	14	4.92	0.22	18.8	0.39	3.73	0.16	24.86	0.85	14.77	0.54	4.1	0.14	33.5	0.7	9.06	0.14	100.8	1.2	33.78	0.4	156.3	1.6	32.87	0.38	279.4	2.9	45.65	0.56	1.667	0.047	25.97	0.4
FB3ap_69	924.7	6.8	148.4	2.5	1884	31	203.20	2.80	701.7	9.1	116.2	1.5	625.4	8.8	194	3	43.19	0.68	243.9	4.1	40.08	0.61	279.1	4.2	62.82	0.98	199.2	3.1	30.1	0.48	214.6	3.7	37.53	0.61	54.5	1	24.05	0.35
FB3ap_70	906.6	7.5	106.4	1.7	4983	5.1	15.17	0.34	50.53	0.78	9.25	0.22	60.4	1.4	32.8	0.69	8.55	0.19	56.7	0.97	10	0.16	69.38	0.94	15.42	0.2	45.51	0.69	5.93	0.13	36.92	0.46	6.28	0.11	0.184	0.015	3.082	0.051
FB3ap_71	1665	18	187.4	2.4	1894	27	92.70	1.10	283.6	3.3	44.49	0.67	246.1	3.7	109.9	1.3	12.51	0.28	179.7	1.9	37.34	0.42	292.3	3.2	64.4	0.68	183.7	1.7	24.27	0.29	137.3	1.5	16.54	0.21	1.766	0.059	12.86	0.2
FB3ap_72	750	13	145.6	4	1189	70	160.00	11.00	465	32	65.9	4.7	332	24	101.8	6.9	33.1	2.2	145.7	9.7	24.3	1.6	171	11	38.7	2.6	121	8	17.4	1.2	117.8	8.5	21.1	1.4	47.2	5.5	21.8	2.1
FB3ap_73	594.7	5.3	219.5	3	2364	26	40.26	0.60	143.1	1.8	26.23	0.4	170.6	2.3	81.8	1.1	16.69	0.31	159	1.9	35.23	0.41	323.6	2.7	88.61	0.82	321.9	2.9	51.28	0.53	335.1	3.1	45.77	0.44	1.276	0.037	11.56	0.11
FB3ap_74	968	13	367.1	4.9	812	16	18.86	0.40	69.7	1.2	9.63	0.31	53.8	2.2	22.99	0.62	7.85	0.25	42.8	1.1	10.26	0.21	95.9	1.8	24.37	0.46	86.7	1.4	14.18	0.27	92.7	1.6	12.1	0.27	1.612	0.067	11.68	0.15
FB3ap_75	953.1	7.8	114.4	1.9	1302	21	41.25	0.62	137.3	7.7	22.34	0.44	131.1	2.4	54.13	0.91	9.2	0.23	94.9	1.3	20.35	0.27	173.2	2.3	43.34	0.47	148.9	1.7	23.14	0.29	156.6	2	26.13	0.35	6.59	0.12	3.63	0.046
FB3ap_76	725	7.4	135.2	2.3	1689	56	114.40	3.60	394	11	70.6	1.9	444	13	171.2	5.2	30.65	0.95	250.5	7.7	42.1	1.3	292.9	8.1	63.6	1.9	184.4	6	24.45	0.84	149.7	4.9	23.74	0.73	28.5	2	8.85	0.2
FB3ap_77	694	8.4	191.5	2.2	1018	17	201.70	2.80	684.9	9.3	112.5	1.7	642	12	164.8	2.3	29.23	0.47	180.6	2.5	25.94	0.33	172.1	2.3	38.79	0.53	122.5	1.5	18.01	0.27	120.5	1.6	20.2	0.3	32.78	0.38	16.26	0.2
FB3ap_78	900.1	7.5	207.5	2.6	442.8	6	17.05	0.39	53.63	0.79	9.47	0.22	60.8	1.4	28.36	0.73	6.82	0.2	84	1.4	8.45	0.14	61.6	0.88	14.11	0.21	42.28	0.5	5.84	0.11	36.59	0.62	6.31	0.12	3.03	0.18	3.46	0.051
FB3ap_79	1347	10	92	12	841	12	42.68	0.74	128.7	1.7	20.79	0.42	111.4	2.3	51.3	1.1	9.54	0.2	84	1.4	15.28	0.23	108.6	1.4	24.91	0.35	78.3	0.89	11.54	0.17	79.1	1.2	14.46	0.18	2.238	0.073	3.969	0.062
FB3ap_80	637.4	5.3	130.2	2.3	161.3	2.3	10.20	0.74	33.96	0.61	5.57	0.17	35.4	1	15.46	0.58	5.59	0.17	24.58	0.68	3.589	0.081	23.63	0.42	5.04	0.11	14.46	0.32	1.809	0.061	11.66	0.39	2.1	0.068	0.77	0.033	13.24	0.21
FB3ap_81	825.4	6	144.2	2.1	557.7	5.6	17.44	0.38	58.08	0.64	10.95	0.26	73	1.5	39.49	0.78	10.75	0.22	67.7	1.2	11.56	0.15	80.3	1	17.56	0.23	51.05	0.67	7.17	0.14	47.64	0.74	8.04	0.13	0.1063	0.0091	4.502	0.043
FB3ap_82	1932	22	73.6	1.5	2005	23	167.10	2.00	590.9	6.5	98.18	0.97	493.7	6.7	206.3	2.4	24.1	0.36	266.4	2.7	57.5	0.51	418.3	3.7	79.3	0.81	228.6	1.9	35.13	0.37	236	2.4	30.66	0.31	2.228	0.056	23.54	0.2
FB3ap_83	1336	8.2	99.1	1.6	1002	15	18.32	0.42	59.7	1.3	10.88	0.31	65.9	1.9	39.99	0.89	11.64	0.24	87.2	1.4	19.18	0.23	150.1	1.7	33.11	0.32	95.4	1.2	12.44	0.18	78.5	1.1	12.72	0.18	0.164	0.012	2.362	0.041
FB3ap_84	1246	8.4	191.5	2.2	1018	17	201.70	2.80	684.9	9.3	112.5	1.7	642	12	164.8	2.3	29.23	0.47	180.6	2.5	25.94	0.33	172.1	2.3	38.79	0.53	122.5	1.5	18.01	0.27	120.5	1.6	20.2	0.3	32.78	0.38	16.26	0.2
FB3ap_85	822.4	6.3	258.1	2.9	812	14	115.50	2.00	367.1	6.7	63.7	1.5	384	7.4	122.4	2.8	22.78	0.4	150	2.8	22.14	0.42	140.9	2.6	28.69	0.47	78.3	1.3	9.83	0.2	61.3	1.2	10.25	0.19	15.79	0.31	8.29	0.11
FB3ap_86	828.7	6.4	401.8	3.6	2620	27	44.25	0.62	173.3	2	35.4	0.57	270.6	3.2	121.4	1.7	23.61	0.31	252.6	2.7	48.73	0.45	414.7	3.9	104.12	0.96	342.8	3.5	51.85	0.5	336.2	3.3	45.65	0.54	7.309	0.085	71.14	0.56
FB3ap_87	302.3	2.8	195.3	4	894	11	8.21	0.24	37.11	0.64	8	0.22	60.3	1.3	41.37	0.86	7.62	0.16	98.1	1.2	21.66	0.25	162.8	1.9	32.22	0.34	76.84	0.96	7.95	0.15	37.88	0.64	4.58	0.11	0.01	0.0034	5.623	0.074
FB3ap_88	637.7	5.7	197.4	2.5	648.3	7	12.08	0.32	40.12	0.59	7.01	0.19	42.6	1.1	20.63	0.51	4.13	0.13	39.5	0.82	8.65	0.16	75.14	0.87	19.11	0.23	65.27	0.84	9.93	0.19	65.9	1	10.9	0.17	0.328	0.017	6.834	0.092
FB3ap_89	434.3	4.4	295.9	3	893	12	47.00	2.50	222	13	45.1	1.6	294.9	7.3	171.7	3.6	16.72	0.34	302.5	4	65.09	0.79	283.1	3.4	32.18	0.36	45.53	0.78	3.57	0.093	14.37	0.37	1.363	0.049	0.04	0.01	9.13	0.29
FB3ap_90	1275.9	7.8	309.1	3.8	1331	17	45.64	0.74	216.6	2.2	47.4	0.49	341.2	4.2	165.7	2	34.82	0.43	268.6	2.3	46.78	0.466	316.9	3.1	59.31	0.5	167.5	1.4	18.22	0.25	101.7	1.3	11.73	0.19	0.58	0.029	14.02	0.17
FB3ap_91	527.3	4.5	302.5	3.5	2985.9	3	1.13	0.08	4.5	0.18	0.985	0.067	5.9	0.38	3.63	0.24	0.994	0.068	9.04	0.31	2.469	0.066	26.93	0.5	9.36	0.16	41.96	0.49	8.24	0.15	62.54	0.98	10.03	0.17	0.0189	0.0042	0.435	0.013
FB3ap_92	779	13	270.6	4.1	686.4	7.7	3.23	0.15	12.41	0.33	2.44	0.13	17.73	0.82	9.61	0.46	2.87	0.11	21.28	0.63	5.72	0.13	63.6	1	21.44	0.32	98.3	1.3	19.12	0.23	154.7	2.4	25.81	0.42	0.497	0.021	6.84	0.11
FB3ap_93	604.2	6.3	170.9	2.6	125.3	1.7	4.54	0.24	18	2.2	2.14	0.11	11.83	0.57	5.4	0.33	2.173	0.089	10.08	0.38	2.01	0.055	15.95	0.34	4.032	0.099	12.83	0.31	1.76	0.066	11.58	0.33	2.038	0.077	0.356	0.06	0.435	0.046
FB3ap_94	699.7	6.7	161.4	2.4	900	13	14.79	0.39	78.4	1.1	21.65	0.38	195.8	2.8	130.8	1.9	7.52	0.18	245.1	3.1	39.1	0.56	211.3	3.2	32.61	0.44	75.5	1	10.23	0.19	68.2	1	9.68	0.18	0.0371	0.0083	12.09	0.15
FB3ap_95	607.6	6.9	171.9	2.3	90.3	1.6	10.33	0.34	1.88	0.1	12.2	0.53	5.83	0.29	2.66	0.11	10.83	0.43	1.839	0.056	12.93	0.35	2.93	0.093	8.72	0.24	1.108	0.049	7.29	0.24	1.369	0.048	0.2	0.019	0.313	0.013
FB3ap_96	563.6	4.9	184.7	2.6	1901	22	267.80	5.10	935	18	161	2.7	917	13	269.6	3.7	71.55	0.8	324.2	3.3	70.77	0.64	215.7	2.2	30.94	0.37	210.1	2.3	35.3	0.37	67.36	0.58	27.14	0.22
FB3ap_97	839.1	6.9	121.4	1.7	400	4	5.32	0.27	16.57	0.74	3.3	0.18	22.2	1.2	14.99	0.57	6.76	0.2	30.69	0.94	5.45	0.14	50.61	0.76	12.14	0.17	37.53	0.54	6.17	0.14	32.75	0.5	6.44	0.11	0.0275	0.0061	0.983	0.02
FB3ap_98	564	4.7	184.9	2.7	512.2	5.1	3.07	0.15	12.07	0.33	2.586	0.096	22.27	0.74	16.41	0.58	3.08	0.11	43.42	0.86	9.21	0.14	76.36	0.94	18.08	0.24	53.09	0.68	6.74	0.14	36.83	0.85	5.39	0.1	0.0243	0.0049	0.977	0.031

S2.3 apatite trace-element data (continued)

	55Mn	±	86Sr	±	89Y	±	139La	±	140Ce	±	141Pr	±	146Nd	±	147Sm	±	153Eu	±	157Gd	±	159Tb	±	163Dy	±	165Ho	±	166Er	±	169Tm	±	172Yb	±	175Lu	±	232Th	±	238U	±
FB3ap_99	702.8	6.4	454.1	5	243.6	3.3	13.98	0.36	42.46	0.69	6.9	0.21	39.8	1.2	16.29	0.58	7.64	0.19	24.89	0.54	4.19	0.1	31.69	0.63	7.45	0.13	24.31	0.47	4.07	0.1	28.22	0.61	3.874	0.097	0.0027	0.0081		
FB3ap_100	643.7	5.1	181.8	2.5	160.8	2	4.64	0.15	16.87	0.4	3.85	0.15	28.96	0.9	15.27	0.46	5.76	0.15	25.35	0.7	3.84	0.1	24.9	0.52	5.35	0.12	14.93	0.32	1.887	0.066	11.7	0.36	1.907	0.062	0.0331	0.005	1.593	0.029
FB3ap_101	607.2	6.9	245.4	4.7	803	11	0.25	0.05	1.3	0.14	0.384	0.064	3.89	0.44	3.7	0.34	0.846	0.079	14.17	0.69	5.19	0.19	69.2	1.4	24.83	0.41	116	1.8	22.77	0.36	174.9	2.8	27.83	0.43	0.19	0.023	2.843	0.056
FB3ap_102	659.5	5.2	160	2.4	2417	35	463.90	7.40	1488	30	274.6	4.9	1561	28	431.1	7.7	47.18	0.64	465.4	8.6	69.6	1.1	451.4	7	93.4	1.2	273.8	3.5	36.4	0.5	233.5	3.8	38.71	0.51	76.3	1	23.23	0.33
FB3ap_103	525.4	4.2	167.6	2.1	46.11	0.8	3.57	0.23	10.89	0.46	1.127	0.094	4.43	0.38	1.42	0.16	0.837	0.066	2.65	0.21	0.532	0.032	4.95	0.18	1.424	0.049	5.51	0.19	0.906	0.046	6.59	0.24	1.26	0.04	0.157	0.028	0.154	0.012
FB3ap_104	689.6	5.6	150.2	2.1	1926	77	443.00	11.00	1363	33	247.4	5.2	1381	29	377.3	8.4	34.8	1.4	407	10	68.5	1.7	370	12	76	2.6	214	8.1	28	1.2	177.3	8.3	28	1.4	47.5	3.6	12.59	0.68
FB3ap_105	1047.9	7.7	208.5	2.5	1850	28	25.96	0.63	98.4	1.8	19.88	0.44	149	3.6	83.1	1.8	18.55	0.36	175.8	3.5	35.18	0.6	289	4.1	72.73	0.68	265.6	2.9	47.81	0.55	371.6	4.2	56.64	0.67	2.661	0.064	26.07	0.49
FB3ap_106	670.9	5.1	95.8	1.5	1190	18	311.20	4.60	852	13	120.8	2	603	11	145.3	2.7	16.32	0.32	164.2	2.6	25.48	0.33	183	2.5	43.33	0.55	143.9	1.9	22.31	0.31	163.3	2.3	29.78	0.45	32.65	0.54	17.37	0.27
FB3ap_107	1107	9.6	267	3.4	1366	18	10.09	0.27	34.22	0.52	6.37	0.17	42	1.2	21.78	0.66	7.23	0.17	51.03	0.84	13.83	0.22	163.8	1.9	48.75	0.68	198.4	2.1	33.93	0.42	234.6	2.9	33.48	0.39	0.437	0.022	2.668	0.054
FB3ap_108	855	13	175.3	2.6	2610	110	97.50	4.40	343	16	66.2	3	445	20	215.1	9.2	108.6	3.5	388	16	64	2.7	441	19	95.9	3.8	275	11	35	1.5	214.9	9.3	36.7	1.5	27.7	1.3	38.06	0.64
FB3ap_109	1414	13	234.8	2.7	694.2	8.2	7.04	0.26	26.64	0.5	5.33	0.16	40.1	1	21.36	0.66	4.98	0.15	50	1.1	10.39	0.18	92.7	1.2	24.78	0.35	86.5	1.1	13.72	0.21	93.6	1.4	13.58	0.21	0.411	0.018	3.03	0.067
FB3ap_110	1257.4	9.4	230.9	3.3	1054	18	4.96	0.21	18.76	0.4	3.79	0.14	26.01	0.88	15.45	0.42	4.47	0.12	39.24	0.77	10.13	0.17	109.5	1.2	35.48	0.39	150.6	1.8	27.35	0.31	203.3	2.5	30.34	0.32	0.099	0.01	4.205	0.069
FB3ap_111	1294	9.4	109	1.8	3520	110	230.70	7.40	815	22	154.4	5.4	947	32	397	14	54.17	0.89	540	17	86.1	2.8	574	19	122	4.1	361	11	51.4	1.6	363	11	61.8	1.7	68.7	2.1	27.63	0.5
FB4ap_1	976.2	8.7	145.5	2.5	436	5.3	18.14	0.38	63.58	0.87	12.42	0.25	85.9	1.8	46.21	0.99	13.74	0.23	74.8	1.3	11.6	0.22	71	1.3	14.67	0.26	38.92	0.69	4.99	0.13	31.77	0.71	5.45	0.13	0.284	0.014	5.51	0.12
FB4ap_2	648.1	7.2	116.9	2.2	2126	31	28.48	0.58	101.6	2	19.3	0.47	128.3	2.9	67.8	1.4	15.64	0.37	149.5	2.8	34.88	0.6	320	4.3	83.9	1.2	278.2	4	42	0.74	260.9	4.8	33.9	0.64	1.77	0.1	13.29	0.67
FB4ap_3	669	7.8	214.9	3.7	797	11	7.50	1.80	16.9	1.5	3.38	0.44	20.7	1.4	10.99	0.45	2.99	0.14	26.68	0.72	6.96	0.18	77.2	1.6	25.33	0.46	108.9	1.9	20.76	0.42	156.1	3	25.15	0.5	1.15	0.18	7.13	0.19
FB4ap_4	669.6	3.9	1078	17	12.46	0.30	44.87	0.76	9.62	0.27	77.9	1.5	51.5	1	11.25	0.25	118.3	1.8	24.35	0.37	193.4	3	44.67	0.73	134.9	2.3	19.51	0.29	125.3	2	17.69	0.35	0.146	0.012	6.43	0.17
FB4ap_5	636.4	5.8	178.1	2.5	78.5	1.2	1.16	0.08	3.55	0.16	0.639	0.047	4.52	0.33	2.37	0.18	1.533	0.067	5.07	0.25	1.066	0.065	9.4	0.29	2.604	0.068	9.42	0.29	1.484	0.047	10.77	0.34	2.157	0.065	0.005	0.0016	0.1784	0.0081
FB4ap_6	912.2	8.1	198	3.1	1287	40	22.16	0.44	91.1	1.5	18.29	0.39	133.1	2.3	77.5	1.5	12.55	0.27	147	2.3	29.05	0.44	224.9	3.5	52.61	0.84	180.3	3	30.41	0.54	213.4	3.7	30.81	0.59	0.605	0.028	13.32	0.28
FB4ap_7	689.7	8.4	251.2	4.3	758	16	7.13	0.41	23.79	0.67	5.09	0.2	32.3	1.3	18.23	0.68	2.85	0.14	37.2	1	9.75	0.24	91	2.1	25.05	0.58	98.2	2.1	14.78	0.38	96.9	2.5	14.28	0.32	6.58	0.36	5.15	0.15
FB4ap_8	643	24	256.7	3	1874	29	451.20	5.90	1118	17	155.3	2.1	740	11	166.2	2.8	22.67	0.42	196.8	3.2	33.5	0.52	266.6	3.9	67.15	0.97	228.9	3.1	37.12	0.61	257.6	4.4	42.13	0.7	84.5	1.5	17.71	0.36
FB4ap_9	625.5	7.2	255.8	4.1	1584	28	23.39	0.75	71.2	1.4	13.41	0.31	89.1	2.1	50.6	1.1	9.9	0.24	110.2	2.1	25.6	0.44	231	4.5	62.7	1.1	227.4	4.4	36.46	0.72	254.5	5.2	42.6	0.87	9.19	0.24	48.5	1.3
FB4ap_10	551	14	367.7	5.9	263.8	4.9	38.39	0.86	103.7	2	15.15	0.38	80.4	2.2	26.44	0.78	7.03	0.24	32.23	0.86	5.29	0.17	37.58	0.96	8.63	0.24	27.14	0.67	4.02	0.13	27.41	0.69	4.77	0.14	45.1	1.2	19.94	0.59
FB4ap_11	554.9	6.2	180.3	2.7	93.2	1.5	2.74	0.11	8.37	0.29	1.549	0.091	9.96	0.51	4.92	0.26	2.25	0.11	9.26	0.34	1.742	0.061	13.03	0.37	3.227	0.094	9.81	0.26	1.245	0.049	7.94	0.22	1.362	0.061	0.0056	0.002	0.1435	0.0082
FB4ap_12	172.3	2.2	389.4	6.4	458.9	7.7	78.00	3.50	249	12	44.3	2	282	13	124.7	5.3	16.52	0.63	214.6	7.5	34.8	0.8	158.8	2.1	14.75	0.35	17.34	0.63	1.227	0.071	4.67	0.26	0.442	0.034	1.519	0.07	14.94	0.33
FB4ap_13	595	12	214	4.6	720	36	869.00	62.00	1472	94	159.2	9.9	642	40	107.4	6.2	18.4	1.2	114.5	7.1	15.61	1.2	24.8	1.3	79.2	3.5	11.59	0.61	80.8	3.4	15.12	0.84	87.4	4.6	22.1	1.1
FB4ap_14	839	8.1	121	1.6	339.6	4.5	20.40	0.48	65.3	1.2	11.88	0.31	77.3	1.7	35.75	0.74	16.4	0.35	55.1	1.2	8.23	0.16	51.01	0.96	10.87	0.2	30.02	0.63	3.782	0.087	23.53	0.6	4.22	0.12	0.497	0.026	3.846	0.095
FB4ap_15	655.6	5.9	195.5	3.5	1118	23	313.50	5.10	965	15	171.4	2.5	966	14	249.5	3.9	33.25	0.59	264	4.3	36.21	0.6	224.8	4.3	45.58	0.89	128.7	2.8	16.57	0.41	103.8	2.6	16.1	0.41	34.5	1.6	28.3	1.2
FB4ap_16	1266	11	107.3	1.8	2319	45	164.10	4.40	579	15	101.9	2.4	608	17	260.2	6.4	22.75	0.46	365.7	8.4	62.6	1.5	432.5	9	91.2	1.9	268.3	5.6	37.64	0.84	239.8	5.1	38.06	0.86	26.3	0.81	8.92	0.26
FB4ap_18	581.8	7.5	192.4	4.7	127.2	6.2	40.60	3.10	86.9	7.1	10.23	0.94	48.2	3.7	12.1	1.1	2.98	0.17	15.4	1.4	2.36	0.19	17	1.1	4.13	0.25	13.53	0.88	1.9	0.13	13.55	0.72	2.69	0.18	5.3	0.37	2.25	0.14
FB4ap_19	1485	16	275.9	4.1	1499	22	38.24	0.73	138.6	2.3	26.82	0.51	185.3	3	102.8	1.7	27.95	0.51	204.4	3.3	41.74	0.71	320.9	4.8	67	1.1	182.3	3	24.5	0.47	144.5	2.8	17.95	0.33	0.55	0.027	15.98	0.36
FB4ap_20	678	6.6	237.4	3.9	381	12	3.21	0.15	12.44	0.39	1.69	0.089	10.59	0.62	5.64	0.34	1.565	0.078	13.91	0.54	3.37	0.11	36.1	1.2	11.93	0.36	54.4	1.6	11.36	0.35	93.9	3.1	16.13	0.49	0.382	0.024	1.88	0.14
FB4ap_21	804.6	8.8	137.4	2.5	1380	24	84.90	2.30	306.1	9.6	58.8	1.6	396	9.8	180.2	3.9	37.39	0.56	265.6	4.5	40.48	0.7	262.2	4.8	53.47	0.92	145.5	2.4	17.95	0.35	104.4	2.2	17.17	0.35	10.85	0.29	9.54	0.27
FB4ap_22	770	15	163.2	3.6	260	8.3	203.00	19.00	459	40	60.2	5.2	277	23	64	4.8	16.36	0.85	62.4	3.9	8.19	0.45	47.5	2	8.88	0.37	22.53	0.79	2.62	0.12	14.69	0.49	2.483	0.085	8.92	0.89	8.61	0.67
FB4ap_23	614.3	5.6	140.1	2.7	338.4	7.6	131.90	5.10	327	13	44.7	1.8	229.4	9.1	56.3	2.3	6.64	0.23	65.4	2.4	8.91	0.3	56.4	1.8	11.51	0.34	32.95	0.93	4.39	0.15	28.81	0.93	5.29	0.12	6.26	0.21	2.671	0.093
FB4ap_24	565.6	5.6	133.2	2.5	207.8	2.8	2.18	0.12	8.84	0.27	1.83	0.11	13.37	0.66	8.51	0.38	2.88	0.11	18.02	0.58	3.546	0.077	28.86	0.59	6.85	0.14	20.81	0.44	2.796	0.076	17.8	0.46	3.19	0.085	0.0854	0.0097	1.817	0.052
FB4ap_25	785	10	171.6	5.5	869	75	160.30	9.40	474	31	72.7	5.2	402	33	122	10	28.8	2	152	13	22.5	1.9	144	13	30.3	2.8	85.4	7.9	11.1	1.1	70.3	6.5	12.9	1.2	61.2	5.4	21.9	1.1
FB4ap_26	1084	12	117.7	2.3	1711	49	103.90	2.00	369.1	7.5	67.1	1.5	425	10	206.9	4.7	45.3	1.1	309.7	6.9	48.9	1.2	313.9	7.1	64.2	1.4	172.4	4.4	22.1	0.52	138.2	3.8	25	0.66	20.68	0.92	15.49	0.51
FB4ap_27	610.9	8	264.7	4.1	439.2	8.1	389.30	9.40	748	18	83.1	2	363.6	9.2	71.2	2.1	8.6	0.26	75.6	1.9	9.92	0.23	67.1	1.6	15.37	0.32	49.4	1.3	7.8	0.21	53.8	1.3	9.66	0.24	22.17	0.72	5.96	0.16
FB4ap_28	691.6	5.4	210.5	3.1	168.1	2.6	5.47	0.24	19.39	0.51	3.98	0.17	25.6	1	14.97	0.55	7.07	0.19	24.56	0.69	3.74	0.1	25.01	0.6	5.41	0.12	15.56	0.39	1.944	0.075	12.01	0.37	2.166	0.067	0.0353	0.0062	0.542	0.034
FB4ap_29	1127	11	152.9	2.8	1970	34	103.90	1.70	384.4	6.3	73.8	1.3	478.7	8.4	211	4.1	41.05	0.81	311.1	5.6	49.96	0.87	334.5	6	71.3	1.4	207.7	4.2	29.1	0.61	198.8	3.8	36.4	0.75	27.12	0.65	13.92	0.33
FB4ap_30	606.2	6.6	167.7	2.1	120.7	2.1	5.19	0.23	15.31	0.48	2.54	0.13	14.69	0.73	6.88	0.29	2.69	0.11	11.1	0.36	2.103	0.057	17	0.47	3.92	0.097	12.29	0.31	1.64	0.06	10.39	0.31	1.78	0.056	0.071	0.017	0.317	0.017
FB4ap_31	597.5	6.6	225.6	3	422.9	6	2.74	0.36	8.09	0.37	1.313	0.092	7.68	0.45	5	0.25	1.56	0.082	13.27	0.46	3.576	0.096	40.2	0.88	13.75	0.31	63.1	1.2	13.03	0.27	106.4	2.1	18.5	0.37	0.106	0.015	1.885	0.057
FB4ap_32	138	2.8	644.7	7.9	2901	57	55.20	1.40	228.2	4.7	48.7	1.2	356.5	7.8	226.6	5	54.1	1.5	439	10	89.3	2	672	14	133.7	2.9	350.7	8.1	45.6	1.1	256.7	6.3	31.15	0.74	20.96	0.62	34.73	0.94
FB4ap_33	414.7	4.2	468.8	5.8	848	12	623.70	7.70	1415	21	214.9	2.7	1063	15	241.7	3.4	41.64	0.61	229.7	3.7	29.82	0.45	177	2.9	32.84	0.51	83.5	1.3	10.39	0.18	58.5	1.1	7.91	0.18	3.301	0.078	1.64	0.052
FB4ap_34	554	5.9	200.7	3.9	2622	45	175.40	2.90	693	11	132.1	2.2	839	14	366.6	6	45.16	0.87	520.9	8.9	95.8	1.5	664	12	125.3	2.2	327.2	5.8	40.57	0.8	223	4.3	26.91	0.49	10.7	0.3	43.7	1.1
FB4ap_35	827	9.5	373.5	5.3	915	16	725.00	14.00	1828	41	265.4	4.9	1205	18	266.4	4.5	27.69	0.62	230.2	4.4	30.33	0.63	179.3	3.4	34.46	0.7	89.2	1.9	11.36	0.26	64.9	1.4	8.88	0.21	45.9	1.1	13.61	0.34
FB4ap_36	467.1	3.4	309.6	3.4	272	0.74	1.38	0.13	3.49	0.28	0.525	0.063	3.11	0.31	1.24	0.16	0.303	0.033	2.2	0.19	0.442	0.027	3.63	0.19	1.006	0.054	3.57	0.16	0.606	0.031	4.07	0.22	0.71	0.033	0.032	0.08	0.018	
FB4ap_37	207.5	2.3	211.5	3.5	54.9	1.1	0.73	0.06	2.63	0.16	0.479	0.047	2.91	0.25	1.93	0.18	0.513	0.04	4.5	0.22	0.901	0.045	6.83	0.27	1.747	0.064	7.19	0.19	1.629	0.065	15.09	0.45	2.822	0.078	0.0872	0.0089	0.163	0.011
FB4ap_38	929.5	9.4	117.3	1.9	1140	20	23.83	0.51	80.9	1.4	14.25	0.25	86.1	2	43.52	0.92	9.05	0.22	82.1	1.7	18.06	0.31	163.8	2.9	39.62	0.77	132.4	2.8	19.76	0.41	125	2.7	20.6	0.47	0.573	0.028	4.09	0.1
FB4ap_39	601	7.2	118.1	2.3	2216	35	85.60	1.70	338.3	5.1	64.9	1.2	416.4	6.4	198.6	3	39.74	0.67	310.8	5.2	61.22	0.99	453	6.7	97.7	1.2	283.5	4.4	40.27	0.67	243.3	4.2	32.95	0.65	8.12	0.22	38.86	0.69
FB4ap_40	367.8	3.7	226.4	3.7	859	13	4.20	0.12	11.6	2.2	2.3	0.34	14.2	1.2	11.63	0.5	1.059	0.073	37.07	0.91	10.88	0.22	109.9	1.9	29.43	0.5	94.4	1.7	12.56	0.24	71.4	1.4	9.72	0.23	0.0167	0.0044	2.49	0.12
FB4ap_41	925	11	116	2.1	2098	36	652.90	8.20	1921	32	338.4	5.3	1795	29	488	6.6	47.92	0.74	500.8	7.8	69.6	1	420	6.7	81.6	1.2	218	3.4	27.99	0.49	169.2	3.4	28.17	0.53	39.08	0.75	10.5	0.22
FB4ap_42	590.2	6.4	126.6	2.5	2735	39	885.00	15.00	2469	49	397	7.6	1992	35	498.1	8.5	36.51	0.57	514.3	8.8	77.3	1.3	608.1	7.9	106.3	1.9	307	4.9	43.26	0.86	273.5	5.2	45.44	0.88	64.3	1.3	17.3	0.39
FB5ap_0	1109	34	623	26	1323	63	44.30	2.80	152.6	8.1	27.2	1.5	185	10	85.3	4.3	14.93	0.7	145.6	5.7	26.69	0.93	205.2	4.7	51.08	0.93	182.3	3	31.71	0.76	235.5	6.2	34.9	1.1	0.418	0.028	8.41	0.35
FB5ap_1	155	4.5	337	16	160.8	7.9	0.94	0.08	3.36	0.2	0.73	0.059	5.36	0.38	3.48	0.26	1.15	0.075	9.78	0.43	2.308	0.089	21.56	0.48	5.44	0.15	25.46	0.48	3.44	0.1	29.43	0.64	1.77	0.05	0.0191	0.0049	0.212	0.011
FB5ap_2	701	23	425	19	1028	48	94.00	4.00	391	18	72.7	2.9	436	17	177.9	6.8	27.13	0.97	222.7	6.2	39.8	1	260.5	5	48.83	0.82	122.6	2.2	14.36	0.34	75.1	2.2	8.9	0.31	0.724	0.034	9.29	0.36
FB5ap_3	395.5	6.7	416.9	9.9	259.7	7.3	26.00	1.20	51.1	2	8.84	0.23	32.4	1.3	8.21	0.41	3	0.12	16.46	0.49	3.62	0.11	33.19	0.74	8.58	0.13	27.64	0.47	3.927	0.091	23.78	0.6	3.53	0.11	1.796	0.057	0.785	0.023
FB5ap_4	638	15	340.3	9	1123	34	66.00	2.20	240.9	8.1	43.8	1.5	273.2	9.1	121.6	3.5	13.36	0.42	191.3	4.5	34.28	0.77	235.9	4.6	47.76	0.77	129	2	16.49	0.31	94.1	2.1	12.36	0.32	1.351	0.037	14.21	0.37
FB5ap_5	315.8	7.8	433	15	48.9	1.8	1.06	0.09	4.56	0.21	0.948	0.067	7.92	0.49	3.16	0.21	0.619	0.039	5.53	0.31	0.812	0.037	6.42	0.23	1.657	0.057	5.53	0.17	0.883	0.039	6.4	0.29	1.159	0.046	0.0023	0.0012	0.215	0.012
FB5ap_6	264.7	7.6	333	13	285	11	13.96	0.66	45.6	1.8	7.88	0.31	47.4	2.2	19.18	0.85	11.57	0.36	35.8	1.2	6.21	0.17	45.37	0.99	10.22	0.2	29.48	0.73	3.6	0.11	19.79	0.66	3.03	0.1	0.82	0.032	2.46	0.088
FB5ap_7	983	26	165.7	6.2	1916	78	57.80	2.30	247.9	9.5	48.8	2	347	13	188.4	6.5	19.35	0.68	304	8.2	59.6	1.3	430.2	7.5	84	1.1	223.1	3.5	31.46	0.67	199	4.9	25.6	0.74	3.61	0.1	43.8	1.4
FB5ap_9	748	16	543	17	1143	40	56.10	2.30	188.8	7.9	34.2	1.4	223.6	8.2	96.7	3.6	13.28	0.45	174	5.1	30.79	0.87	225.4	5.4	47.46	0.84	134.6	2.6	19.37	0.43	129.7	2.9	17.31	0.42	0.784	0.028	7.12	0.22
FB5ap_10	517	17	278	14	1108	62	15.35	0.87	52	2.6	9.88	0.5	72.1	3.9	41.4	1.8	14.85	0.63	88.5	3	19.22	0.59	167.1	3.7	40.91	0.82	136.2	2.6	21.72	0.58	147.6	5.2	20.5	0.89	0.756	0.04	17.61	0.77
FB5ap_11	680	18	508	20	1484	61	44.20	1.90	155.9	6.4	28.5	1.2	193.1	7.4	89	3.2	17	0.53	171.6	4.9	32.25	0.78	252.4	5	57.93	0.75	175.2	3	25.21	0.65	161.6	4.1	22.3	0.64	0.668	0.03	7.35	0.25

S2.3 apatite trace-element data (continued)

	55Mn	±	86Sr	±	89Y	±	139La	±	140Ce	±	141Pr	±	146Nd	±	147Sm	±	153Eu	±	157Gd	±	159Tb	±	163Dy	±	165Ho	±	166Er	±	169Tm	±	172Yb	±	175Lu	±	232Th	±	238U	±
FBSap_12	467	12	377	14	756	26	4.64	0.27	30.4	1.1	8.94	0.37	82.1	2.9	52.4	1.6	7.72	0.24	102.7	2.6	17.03	0.35	119.5	1.9	27.41	0.4	88.1	1.5	13.52	0.27	86	2	11.34	0.34	0.199	0.014	6.3	0.21
FBSap_13	313.9	8.2	389	15	254	11	46.80	2.10	219.6	9.3	41.4	1.6	243.5	8.9	63.6	2.3	24.24	0.85	53.9	1.6	6.79	0.18	41.32	0.97	7.93	0.18	21.47	0.45	2.966	0.081	19.09	0.55	2.83	0.1	19.41	0.64	23.69	0.8
FBSap_14	714	21	454	20	1338	63	40.70	1.80	126.7	5.5	23.12	0.99	150.6	5.6	69.1	2.4	11.1	0.38	139.7	3.9	27.96	0.65	230.4	4.5	50.06	0.79	130.5	2.5	15.89	0.38	86.1	2.5	10.25	0.33	0.51	0.023	7.74	0.3
FBSap_15	459	12	433	15	132.8	5.7	6.26	0.30	32.5	1.3	7.01	0.32	53.3	2.3	21.91	0.92	5.54	0.23	27.15	0.96	3.465	0.096	21.38	0.58	4.365	0.097	12.13	0.29	1.591	0.066	10.31	0.39	1.753	0.066	0.122	0.012	3.39	0.12
FBSap_16	269.8	7.8	491	21	337	15	2.21	0.16	9.13	0.47	2.15	0.13	20.9	1.1	14.06	0.74	2.1	0.13	36.2	1.3	6.29	0.19	49.1	1.1	12.41	0.25	38.5	0.69	4.97	0.12	27.18	0.71	3.75	0.14	0.302	0.016	3.16	0.13
FBSap_17	147.9	5.3	804	37	34.5	1.9	26.50	1.30	53	2.2	5.65	0.26	25.6	1.3	4.37	0.3	1.468	0.089	4.92	0.3	0.635	0.036	4.33	0.19	1.026	0.041	3.73	0.15	0.569	0.025	4.15	0.23	0.788	0.044	0.437	0.021	0.208	0.011
FBSap_18	561	15	116	4.7	1577	65	21.05	0.93	80.7	3.4	15.8	0.68	125.3	4.8	87.2	3.3	31.4	1.1	227.2	6.7	46.3	1.3	340	7.3	63.8	1	155.1	2.9	19.14	0.47	108.5	3	13.38	0.44	6.27	0.25	20.21	0.79
FBSap_19	380.3	9.9	398	15	1198	46	86.80	5.50	263	11	117.9	4.3	263	11	117.4	4.6	68.2	2.3	217.6	5.5	41	1	281.9	5.2	43.64	0.63	70.4	1.3	5.5	0.14	19.95	0.71	1.665	0.069	1.39	0.24	11.26	0.37
FBSap_20	504	15	375	15	94.7	4.5	17.74	0.53	17.88	0.95	5.67	0.27	41.6	2	14.42	0.7	20.31	0.73	19.3	0.78	2.531	0.092	16.62	0.48	3.66	0.1	10.7	0.3	1.386	0.052	9.3	0.33	1.392	0.068	0.0345	0.0053	1.448	0.058
FBSap_21	871	32	490	19	1258	68	22.20	1.10	86.2	3.9	16.88	0.78	117.7	4.6	58.6	2.3	11.13	0.43	118.3	4.4	23.69	0.72	204.2	6.3	51.5	1.1	172.6	3.7	27.77	0.89	180.2	6.5	23.38	0.84	1.111	0.045	6.75	0.24
FBSap_22	945	26	195	8.4	750	31	230.00	10.00	562	26	74.8	3.2	384	16	94.3	3.9	24	0.73	113.8	3.6	16.44	0.43	112.4	2	25.23	0.42	75.1	1.3	10.37	0.26	66.9	1.8	11.62	0.35	14.57	0.42	5.94	0.23
FBSap_23	1121	34	259	10	1201	55	67.30	2.60	357	14	73.8	2.7	488	17	209.7	7.4	28.48	0.91	265.9	7.2	40.4	1	251.9	4.4	46.81	0.66	124.5	1.8	16.53	0.38	101.9	2.5	12.8	0.38	0.0081	0.0027	11.12	0.39
FBSap_24	173.8	4.7	264	10	625	27	4.93	0.27	15.48	0.72	3.24	0.19	23.5	1.3	14.32	0.75	4.08	0.17	45.3	1.6	11.67	0.3	106.8	2.3	24.14	0.47	67.4	1.1	9.07	0.19	52.1	1.2	6.25	0.21	1.597	0.088	2.217	0.07
FBSap_25	479	16	284	11	868	31	7.66	0.35	31.7	1.5	6.4	0.33	48.5	2.4	26.7	1.1	5.77	0.23	59.3	2.1	12.1	0.39	106.5	2.6	28.42	0.58	103.7	1.9	18.19	0.44	138.6	4.2	21.52	0.83	0.536	0.034	3.69	0.16
FBSap_27	153.5	4.8	453	20	434	20	30.8	1.5	8.11	0.36	3.4	0.16	43.6	1.8	6.12	0.25	89.1	2.6	13.76	0.32	84.1	1.6	15.52	0.27	38.08	0.92	4.31	0.12	20.78	0.6	2.36	0.1	0.271	0.015	5.43	0.22
FBSap_28	906	24	267	10	580	24	94.90	4.00	517	20	106	3.9	668	25	274.3	9.3	23.4	0.7	314.6	8.2	40.89	0.94	174.1	2.7	19.49	0.31	31.47	0.66	2.772	0.084	11.71	0.37	1.222	0.053	0.233	0.019	16.46	0.57
FBSap_29	524	14	165.5	7.1	222	10	18.50	0.84	68.4	2.9	13.15	0.61	85.1	3.5	41.5	1.5	12.38	0.46	57.9	2	9.34	0.23	51.3	1.3	7.27	0.16	14.41	0.4	1.478	0.051	6.45	0.27	0.646	0.028	1.363	0.036	24.46	0.78
FBSap_31	129.6	4.1	317	12	946	35	50.00	1.90	237.7	9.8	51.7	2.1	355	14	157.7	5.1	27.85	0.88	211.8	5.2	39.56	0.88	260.3	5	40.92	0.63	72.4	1.3	5.1	0.11	14.88	0.55	1.212	0.05	0.0892	0.0092	13.2	0.45
FBSap_32	264.2	7	365	14	563	25	1.11	0.09	4.53	0.25	1.016	0.073	9.02	0.54	7.26	0.38	4.68	0.04	24.05	0.75	5.94	0.16	61.8	1.2	19.2	0.3	74.7	1.4	14.42	0.44	145.2	3.7	26.85	0.83	0.452	0.021	0.3	0.016
FBSap_33	88.8	2.5	192.6	7.3	490	19	23.70	1.10	102.6	4.3	23	0.94	172.8	6.8	99.5	3.6	14.5	0.5	179.1	5.4	32.73	0.82	172.2	3.3	18.01	0.28	20.22	0.44	1.119	0.044	3.66	0.16	0.358	0.03	0.0333	0.0045	7.64	0.26
FBSap_34	749	30	407	23	434	20	11.08	0.76	87.7	4.5	24.8	1.3	201	10	81.1	4.1	15.26	0.62	89.6	3.4	12.82	0.47	78.1	2.1	14.77	0.38	39.3	1.2	5.07	0.2	29.3	1.2	4.08	0.2	0.0691	0.0099	7.86	0.51
FBSap_36	305.6	7.5	480	17	167.6	5.7	1.34	0.11	10.19	0.43	3.01	0.15	28.2	1.3	14.1	0.57	3.36	0.13	24.08	0.84	3.765	0.097	26.77	0.74	5.68	0.15	16.09	0.36	2.116	0.077	12.93	0.37	2.146	0.078	0.103	0.01	4.64	0.2
FBSap_37	478	14	184.6	8.3	882	37	44.00	2.20	176.6	7.4	36.1	1.6	268	12	141.5	5.5	13.64	0.49	227.8	6.4	40.7	1	235.9	5.2	35.16	0.68	70.3	1.5	7.66	0.21	42	1.3	5.3	0.218	0.013	7.74	0.29
FBSap_38	1676	35	99.5	2.9	5280	190	63.90	2.20	203.8	7.1	36.9	1.1	245	7.7	168	4.7	44.7	1.1	397.2	7.3	94.1	1.6	799	15	181.2	2.5	518.9	7	70.3	1.2	421	8.5	85.8	1.3	4.57	0.14	2.657	0.078
FBSap_39	565	14	181.9	5.4	1483	46	92.40	3.90	367	14	70.2	2.5	461	19	164	5.7	15.35	0.56	252.7	7.5	47.4	1.3	343.6	7.7	63.6	1.4	155.6	3.2	19.11	0.41	105.2	2.7	12.41	0.36	0.0437	0.0069	14.24	0.4
FBSap_40	787	25	169.2	7.2	1359	61	378.00	15.00	916	37	151.1	5.8	785	28	190.5	6.5	35	1.2	228.6	5.7	33.97	0.68	229.1	3.7	50.09	0.66	150	2.7	20.78	0.49	140.1	4.2	24.54	0.8	58.1	1.8	21.95	0.8
FBSap_41	1702	43	445	14	2438	92	45.40	1.70	176.7	6.8	35	1.3	269	10	118.7	4	22.21	0.78	225.4	6.2	44.9	1.1	387	7.5	95.2	1.5	308.9	5.3	49.01	0.91	316.8	7.2	43.2	1.1	3.56	0.1	46.2	1.5
FBSap_42	892	25	353	15	1522	74	94.50	4.50	396	17	75.9	3.5	475	21	210	9.2	15.97	0.61	294.5	9	53.4	1.5	369.3	7.5	66.51	0.91	164.3	2.4	19.22	0.41	103	2.6	12.51	0.38	0.171	0.014	6.53	0.27
FBSap_43	258.1	7.3	435	17	594	23	34.80	1.50	193.4	7.2	43.2	1.5	317	11	127.1	3.9	31.27	0.95	151.4	4.2	19.7	0.44	112.3	1.9	20.6	0.31	50.32	0.94	5.68	0.14	31.16	0.91	4.18	0.14	44.5	1.2	2.214	0.077
FBSap_44	763	22	416	9.8	1061	34	53.60	1.60	191	5.8	33.7	1.1	222.1	7.4	94.1	3	11.21	0.45	160.4	4.5	26.2	0.72	180.6	4.2	40.56	0.58	130.3	2.5	21.83	0.46	162.2	4.3	22.46	0.63	8.44	0.26	13.02	0.32
FBSap_45	384.3	9	399	15	203.2	9.1	4.10	0.27	16.97	0.74	3.65	0.19	28.7	1.1	16.02	0.75	1.687	0.096	30.4	1.1	4.92	0.14	33.82	0.75	7.28	0.14	20.11	0.4	2.434	0.076	13.39	0.49	2.067	0.069	0.203	0.015	1.44	0.059
FBSap_46	709	19	337	13	2024	87	348.00	14.00	1019	38	196.3	7.2	1139	39	404	13	82.7	2.5	457	11	71.3	1.5	446	6.8	86.7	1.4	241.2	4.4	32.45	0.8	198.4	4.7	26.85	0.83	0.62	0.032	14.41	0.54
FBSap_47	480	13	284	11	1253	53	352.00	20.00	568	28	98.3	5	411	20	110.1	4.4	16.07	0.72	158.1	4.8	30.89	0.95	240.5	6	54.2	1.2	156.8	2.9	20.71	0.49	112.2	3.1	13.47	0.4	3.29	0.11	12.06	0.44
FBSap_48	379	11	475	19	298	13	31.20	1.80	115.8	6.6	20.2	1.1	126.3	6.4	40.1	1.8	13.11	0.5	52.8	1.9	7.73	0.25	50.2	1.2	9.96	0.21	27.33	0.61	3.59	0.11	22.81	0.69	3.54	0.14	1.303	0.054	8.73	0.32
FBSap_49	262.4	7.7	509	21	161	10	3.92	0.23	24.2	1.4	6.56	0.4	58	3.5	29.6	1.8	3.99	0.23	45.1	2.4	5.77	0.3	31.8	1.8	5.57	0.29	12.56	0.73	1.312	0.092	6.41	0.36	0.899	0.065	0.0011	0.001	0.445	0.039
FBSap_50	330.3	8.8	425	18	878	36	6.21	0.27	23.8	1.1	4.95	0.26	40	2	27.1	1.2	3.41	0.14	73	2	15.08	0.38	131.5	2.5	31.72	0.57	92.1	1.7	11.19	0.29	56.9	1.6	6.82	0.21	0.101	0.01	2.71	0.11
FBSap_51	472	11	295.6	9.9	685	23	56.60	2.20	170.5	6.3	29.5	1.2	191.1	6.4	106.1	2.9	57.9	1.4	173.2	4	32.48	0.77	187.6	3.6	26.97	0.47	50.66	0.94	4.85	0.11	22.25	0.7	2.327	0.08	0.136	0.016	2.054	0.066
FBSap_52	631	17	436	15	969	41	3.56	0.26	13.03	0.73	2.49	0.16	17.1	1	9.34	0.52	4.13	0.17	23.77	0.89	6.44	0.2	81.5	1.8	30.93	0.49	140.1	2.3	23.65	0.44	154.3	3.3	22.78	0.57	1.64	0.3	1.761	0.069
FBSap_53	851	22	185	6.5	140.5	5.2	4.45	0.21	16.03	0.68	2.92	0.17	20.9	1.1	9.33	0.47	6.7	0.2	16.88	0.59	2.66	0.1	18.94	0.48	4.14	0.12	12.67	0.35	1.626	0.062	10.52	0.41	1.923	0.071	0.0642	0.0077	1.675	0.052
FBSap_54	2378	73	328	13	1732	73	128.40	5.40	459	19	79.6	2.7	492	18	221.9	7.5	46.8	1.4	327.8	9.2	60.9	1.4	413.1	7.7	75.2	0.99	192.8	2.3	25.06	0.59	145.4	3.3	17.58	0.44	1.61	0.059	24.14	0.85
FBSap_55	412	9.8	219.3	8.2	829	31	47.20	1.70	190.1	6.6	39.6	1.5	260.9	9.2	141.1	4.9	28.57	0.92	220.8	4.5	41.01	0.93	243.8	4.2	34.57	0.5	60.3	1	5.05	0.13	19.71	0.58	1.946	0.08	1.727	0.073	8.33	0.27
FBSap_56	646	18	438	17	824	32	3.24	0.21	13.25	0.56	3.13	0.18	26.3	1.3	17.59	0.87	4.72	0.22	47.6	1.4	11.25	0.31	106.7	2.3	28.65	0.54	94.1	1.7	13.09	0.32	73.8	1.9	9.42	0.31	0.0275	0.004	5.92	0.23
FBSap_57	203.4	4.7	302.1	9.8	590	20	7.10	0.32	29.57	0.95	6.81	0.25	54.9	2.3	32.6	1	4.42	0.16	84.9	2.1	18.36	0.37	133	2.5	21.01	0.36	36.85	0.68	3.033	0.075	11.99	0.33	1.168	0.047	0.17	0.012	1.856	0.057
FBSap_58	1067	26	296	10	1263	55	52.60	2.50	367	14	85.1	3.5	300	13	140.5	5.7	27.2	1.1	210.6	7.6	39.6	1.2	276.4	8	55.5	1.3	165.3	3.7	21.15	0.51	124.1	3.5	16.43	0.5	0.86	0.063	8.84	0.51
FBSap_59	292	10	420	20	246	12	9.90	0.66	31.7	1.5	6.53	0.34	52.7	2.7	29	1.4	8.08	0.35	45.3	1.5	6.27	0.22	39.6	1	8.27	0.2	23.78	0.66	3.22	0.1	20.57	0.69	3.39	0.14	1.06	0.062	17.86	0.78
FBSap_60	1306	30	279.1	9.9	1027	35	3.81	0.22	13.71	0.47	2.74	0.14	19.72	0.9	12.75	0.6	4.14	0.14	34.9	1.1	9.68	0.27	105.9	2.3	34.06	0.64	139.3	2.5	25.5	0.5	198.1	4.4	32.39	0.81	1.043	0.047	12.7	0.45
FBSap_61	310.2	6.6	248	6.3	837	22	45.30	1.20	208.6	4.9	47	1.2	325.8	8.5	175.9	4	26.56	0.61	265.6	5.6	60.09	0.83	280.3	4.3	32.96	0.49	41.79	0.72	2.626	0.069	9.86	0.31	0.979	0.044	0.0627	0.0079	12.16	0.25
FBSap_62	286.5	6.9	499	17	485	17	5.71	0.28	27.1	1.1	6.63	0.3	55.1	2.2	33.2	1.2	4.6	0.16	66.1	1.8	12.83	0.3	93.6	1.9	19.65	0.38	52.56	0.87	6.4	0.14	33.21	0.79	4.23	0.14	0.0872	0.0064	4.73	0.15
FBSap_63	294.4	7.5	325	12	72.7	2.8	55.80	2.10	180.4	6.2	32.1	1.1	197.2	6.8	45.7	1.6	9.27	0.3	38.6	1	3.406	0.099	15.98	0.42	2.604	0.068	5.97	0.17	0.706	0.032	4.17	0.2	0.674	0.028	1.518	0.048	5.07	0.15
FBSap_64	515.3	9.7	382	11	1055	34	77.50	2.40	286.8	8.4	53	1.7	321.5	8.7	139.7	4.3	14.16	0.39	209.7	5.5	36.29	0.7	240.7	4.6	45.72	0.75	113.5	2.2	13.47	0.32	72.7	1.8	8.93	0.24	0.645	0.026	6.83	0.19
FBSap_65	632	13	427	15	1158	46	22.20	0.86	86	3.8	17.21	0.72	125.8	5	56.7	2	7.27	0.26	106.2	3.5	19.94	0.51	164.2	3.1	44.1	0.82	162.7	2.7	28.66	0.59	209.9	4.7	31.19	0.83	0.662	0.025	2.787	0.094
FBSap_66	416.6	8.6	311	10	547	17	3.54	0.35	6.21	0.37	1.58	0.13	11.98	0.57	9.26	0.44	1.338	0.074	32.11	0.91	7.39	0.2	66.9	1.5	17.06	0.32	55	1	8.27	0.17	50.3	1.3	6.22	0.17	4	7.2	3.95	0.11
FBSap_67	515	22	266	15	40.6	3.3	39.00	2.80	92	4.8	11.52	0.8	54.8	4.1	12.4	1.1	6.53	0.46	13.3	1.1	1.47	0.14	7.81	0.64	1.57	0.11	3.72	0.23	0.387	0.061	1.79	0.25	0.406	0.052	1.17	0.14	2.18	0.12
FBSap_68	537	15	331	13	186.9	8.5	4.46	0.29	12.31	0.68	2.26	0.13	15.77	0.8	9.06	0.5	3.76	0.18	23.84	0.87	4.34	0.14	33.3	0.8	8.07	0.16	22.54	0.51	2.609	0.088	15.32	0.54	2.561	0.093	0.0188	0.0035	1.497	0.055
FBSap_69	298.6	7.7	440	15	431	14	74.20	2.60	368	12	79.1	2.6	561	16	196.5	5.4	22.02	0.56	193.1	4.2	21.26	0.44	105.7	1.8	16.9	0.29	36.17	0.72	3.71	0.11	18.05	0.49	2.325	0.084	1.308	0.04	11.37	0.31
FBSap_70	163.1	3.9	319	15	91.2	3.7	16.15	0.73	72.2	2.5	13.75	0.65	87.5	3.7	26.5	1.1	6.93	0.23	28.4	1	3.482	0.094	18.07	0.54	2.838	0.091	5.66	0.22	0.573	0.028	2.66	0.14	0.29	0.024	0.934	0.039	3.61	0.14
FBSap_71	931	25	405	15	1298	50	97.20	3.60	351	13	64.7	2.2	400	14	175.5	5.4	24.22	0.74	258.5	6.4	46.5	1.1	306.7	5.3	56.3	0.86	144.7	2.4	20.06	0.45	128.7	3.4	16.95	0.47	0.517	0.022	9.02	0.31
FBSap_72	215.5	4.7	265.8	8.9	689	23	9.79	0.42	32	1.2	6.06	0.26	44.9	1.9	25.48	0.95	8.66	0.29	61.2	1.7	13.12	0.25	107.2	2	21.61	0.27	51.79	0.87	5.76	0.13	29.01	0.68	3.38	0.13	0.304	0.017	7.39	0.22
FBSap_73	562.3	8.8	586	13	689	18	5.05	0.22	16.36	0.56	2.94	0.12	20.37	0.76	9.53	0.4	1.498	0.071	23.56	0.68	5.84	0.14	65.3	1.1	21.43	0.35	83.8	1.4	13.18	0.24	78.3	1.6	9.85	0.25	0.46	0.019	0.623	0.033
FBSap_74	159.1	5.6	372	18	270	13	30.10	1.80	138.5	8	30.7	1.5	232	12	117.6	5.3	17.38	0.87	177.9	7	24.44	0.8	99.4	3.2	9.07	0.26	30.6	0.39	3.07	0.045	2.51	0.19	0.213	0.027	0.143	0.016	6.6	0.33
FBSap_75	854	27	122.2	5.1	1722	82	84.90	4.40	310	16	55.3	2.7	345	17	141	4.5	36.6	1.2	219.9	6.5	37.9	1	274.3	6.9	60.9	1.6	181.7	4.8	25.71	0.93	168.7	6.8	30.1	1.2	24.6	0.96	9.93	0.44
FBSap_76	473.8	9.9	339.1	9.6	844	27	11.20	0.37	42.7	1.4	8.47	0.29	61.2	1.9	31.63	0.95	7.06	0.19	68.7	1.7	14.89	0.39	132.9	3.4	31.99	0.64	91.6	1.9	11.34	0.29	60.4	1.6	7.32	0.2	0.977	0.051	2.81	0.13
FBSap_77	636	12	212.4	5.3	981	26	45.80	1.30	186	5.7	35.42	0.84	231.8	6.4	117	2.7	21.59	0.47	174.6	3.6	33.35	0.55	234.3	4.1	45.78	0.83	127.3	2.4	20.06	0.45	128.7	3.4	16.95	0.47	0.517	0.022	9.02	0.31
FBSap_78	135.2	3	145.9	3.7	439	11	4.02	0.19	19.41	0.64	5.29	0.24	48.6	2.1	38.8	1.4	3.86	0.16	83.6	2.4	16.25	0.42	104.6	2	16.81	0.29	34.8	0.71	3.439	0.092	15.18	0.52	1.753	0.067	0.0024	0.0013	4.41	0.11
FBSap_79	502.1	9.8	337	7.8	978	29	17.43	0.65	73.4	2.5	15.7	0.52	119.8	3.8	59.3	1.9	9.66	0.3	112.4	2.9	21.12	0.5	162	2.7	36.93	0.59	112.2	1.8	16.8	0.29	110.9	2.2	15.55	0.35	1.006	0.046	7.13	0.19

S2.3 apatite trace-element data (continued)

	55Mn	±	86Sr	±	89Y	±	139La	±	140Ce	±	141Pr	±	146Nd	±	147Sm	±	153Eu	±	157Gd	±	159Tb	±	163Dy	±	165Ho	±	166Er	±	169Tm	±	172Yb	±	175Lu	±	232Th	±	238U	±
FB5ap_80	804	15	232.3	5.3	992	26	351.10	7.40	926	23	159.7	4	867	20	234.9	5.5	32.75	0.75	250.9	5	32.97	0.72	205	4.1	40.9	0.64	111.5	1.9	14.7	0.28	88.9	1.8	14	0.33	18.15	0.33	5.37	0.12
FB5ap_81	370	7.6	301.4	8.1	725	23	5.34	0.25	20.07	0.81	3.78	0.14	24.6	1.2	10.16	0.48	1.406	0.086	20.25	0.64	4.79	0.14	60.2	1.4	23.67	0.37	108	2.5	20.88	0.52	156.7	3.4	24.69	0.6	0.997	0.034	2.625	0.084
FB5ap_82	1191	29	114.9	4	1801	68	20.00	0.85	61.4	2.2	10.46	0.41	65	2.5	33.6	1.2	10.6	0.35	77.9	2.3	19.2	0.48	194	4	55.5	1.1	203.8	3.7	33.87	0.76	227.2	6.2	32.75	0.9	0.733	0.035	0.825	0.037
FB5ap_83	311.7	9.4	425	17	305	13	3.22	0.23	12.95	0.59	2.61	0.15	18.12	0.97	11.62	0.62	4.23	0.2	27	1	5.32	0.17	43.3	1	10.54	0.25	31.61	0.76	4.03	0.14	23.41	0.74	3.26	0.13	1.562	0.05	3.47	0.13
FB5ap_84	722	14	160.7	4.3	1040	30	6.85	0.27	22.09	0.74	3.72	0.18	24.7	1.2	13.87	0.6	6.11	0.21	42.4	1	11.99	0.32	128.2	2.5	35.34	0.67	123.5	2.2	19.22	0.42	120.6	2.7	16.21	0.39	0.469	0.024	4.69	0.14
FB5ap_85	135.6	2.9	271.1	8.1	171.4	5.3	17.19	0.50	63.6	2	12.82	0.42	95.2	3.1	54.1	1.6	10.51	0.24	109.7	2.3	17.26	0.38	70.7	1.4	6.31	0.15	6.16	0.21	0.276	0.02	0.62	0.067	0.0434	0.0071	0.278	0.013	7.39	0.2
FB5ap_86	424	8.8	320.5	9.9	127.7	4.5	21.75	0.85	59.9	2.1	9.63	0.36	58.9	2.2	18.63	0.78	5.07	0.19	23.77	0.91	3.54	0.12	22.75	0.73	4.56	0.14	12.09	0.31	1.488	0.065	8.59	0.31	1.233	0.049	0.131	0.014	0.191	0.012
FB5ap_87	280.7	8.1	90.3	3.7	1416	57	76.00	3.10	372	16	76.8	2.9	513	21	243.1	8.3	20.29	0.69	333.9	9	59.1	1.3	374	7.4	62.5	1.1	135	2	13.6	0.28	61.8	1.4	6.72	0.19	0.536	0.025	6.56	0.25
FB5ap_88	338.8	8.2	345	12	728	25	20.92	0.86	107.7	4.1	25.57	0.93	193.7	6	112.7	3.6	15.94	0.48	173.3	4.5	32.82	0.67	202.2	3.6	30.96	0.54	63	1.1	7.01	0.17	37.25	0.8	4.41	0.15	0.186	0.014	4.19	0.12
FB5ap_89	383.2	9.3	465	14	566	26	87.00	3.30	367	14	71	2.7	450	16	136.2	4.5	28.7	1	133.4	4.2	17.45	0.56	102.3	3.2	19.55	0.61	62	1.7	6.97	0.28	42.6	1.7	6.36	0.27	6.61	0.33	46.5	2.1
FB5ap_90	179.5	3.5	503	13	903	25	53.00	1.50	175.4	4.9	31.23	0.83	186.4	4.3	80.8	2.1	28.63	0.67	131.3	2.7	25.97	0.55	183.1	3.2	33.85	0.58	78.4	1.5	8.5	0.21	39.7	1	4.42	0.14	0.322	0.016	6.73	0.19
FB5ap_91	175.5	4.3	235.1	7.3	233	7.8	1.18	0.09	4.78	0.25	0.997	0.062	8.03	0.52	5.02	0.27	1.108	0.065	17.09	0.49	4.09	0.13	36.93	0.85	7.75	0.19	16.39	0.47	1.448	0.052	5.59	0.28	0.546	0.035	0.115	0.011	0.874	0.031
FB5ap_92	347	10	576	22	482	22	5.74	0.53	26.7	2.3	5.7	0.48	41.7	2.8	23.8	1.2	6.4	0.3	48.5	1.6	9.73	0.29	78.1	2.1	18.95	0.48	57.5	1.4	7.59	0.23	42.1	1.6	5.59	0.22	0.0171	0.0075	1.39	0.12
FB5ap_93	561	13	443	14	956	32	44.10	1.80	148.9	6.1	26.5	1.1	171	7.6	72.4	2.3	10.2	0.35	124.6	3.4	21.96	0.55	159.6	3.3	35.56	0.66	111.8	1.7	18.56	0.38	141.6	3.3	24.13	0.56	0.515	0.025	5.53	0.17
FB5ap_94	275.7	5.8	232.5	7	811	24	36.80	1.20	145.5	4.5	27.25	0.87	183.2	5.1	93.4	3	14.33	0.42	156.5	3.8	28.39	0.55	186.9	3.4	33.62	0.57	81.8	1.5	9.4	0.17	50.2	1.2	5.78	0.17	0.354	0.022	5.19	0.14
FB5ap_95	592	15	493	17	927	34	20.59	0.96	72.3	3	13.08	0.53	86.6	3.5	39.4	1.4	6.46	0.22	76.1	2.4	14.24	0.38	117.2	2.1	31.67	0.54	117.7	2.1	20.69	0.4	154.9	3.7	23.93	0.63	1.133	0.044	4.44	0.14
FB5ap_96	215.3	4.9	284.6	8.8	748	27	2.27	0.14	14.73	0.78	4.36	0.27	43.3	2.6	28.8	1.6	2.79	0.17	68.5	3.3	13.5	0.58	112.2	4.3	26.79	0.87	75.6	2	9.01	0.27	44.2	1.6	4.94	0.22	0.637	0.034	3.38	0.21
FB5ap_97	468	10	1086	30	311.6	8.9	131.70	4.50	566	18	111.6	3.3	716	23	195.1	6.2	40.5	1.2	165.7	4.3	16.93	0.36	75.2	1.5	10.69	0.2	21.63	0.52	2.478	0.077	13.55	0.4	1.936	0.075	2.665	0.057	2.028	0.056
FB5ap_98	568	14	215.6	7.1	741	29	101.71	0.45	47	1.9	10.51	0.43	90.8	3.7	67.2	2.5	17.68	0.55	130.7	3.9	21.63	0.59	141	3.4	27.2	0.61	66.7	1.5	7.6	0.19	40.3	1.3	5.78	0.2	0.592	0.028	17.98	0.66
FB5ap_99	682	15	548	18	835	29	53.00	1.50	175.4	4.9	31.23	0.83	186.4	4.3	80.8	2.1	28.63	0.57	131.3	2.7	25.97	0.55	183.1	3.2	33.85	0.58	78.4	1.5	8.5	0.21	39.7	1	4.42	0.14	0.322	0.016	6.73	0.19
FB5ap_100	462	11	398	13	986	26	54.70	1.80	192.4	6.6	34.8	1.2	229.3	6.1	89	2.7	8.2	0.28	138.1	3.3	22.04	0.62	159.3	3.1	37.84	0.62	126.6	1.9	20.27	0.43	137.6	2.8	20.15	0.54	0.819	0.028	3.68	0.12
FB5ap_101	472.8	7.9	938	16	677	12	25.96	0.86	139.7	2.7	34.24	0.7	243.6	4.4	147.7	2.6	59.09	0.88	207.6	3.2	36.17	0.51	197.7	2.4	26.88	0.32	47.69	0.81	4.15	0.1	16.43	0.4	1.488	0.055	0.82	0.67	3.265	0.067
FB5ap_102	297.2	5.1	461.6	7.7	288.3	5.4	4.32	0.19	17.63	0.47	3.99	0.15	29.39	0.92	16.67	0.55	5.69	0.14	31.98	0.73	6.01	0.15	45.2	1	10.02	0.17	26.79	0.49	3.308	0.091	18.68	0.43	2.764	0.073	0.151	0.011	1.863	0.043
FB5ap_103	499.5	9.2	321.5	8.7	840	19	1.04	0.10	8.94	0.37	2.93	0.15	31.5	1.2	25.5	1	2.39	0.12	57.9	1.5	12.29	0.3	109.3	2.3	29.63	0.5	105	1.8	16.64	0.34	106.5	1.9	15.77	0.39	0.0034	0.0015	2.741	0.067
FB5ap_104	785	17	323.1	9.5	1259	46	24.50	0.87	62.8	1.9	9.34	0.3	53.8	1.7	24.14	0.76	4.41	0.14	55.9	1.3	12.7	0.29	138.4	2.8	45.04	0.73	175.7	3	29.42	0.54	189.2	3.8	25.69	0.51	0.466	0.021	7.17	0.23
FB5ap_105	394.1	7.5	224.7	5.2	447	12	2.85	0.14	10.35	0.34	1.893	0.098	14.17	0.77	9.64	0.34	2.79	0.14	26.8	0.9	6.34	0.15	58.1	1.3	15.42	0.31	52.7	1	7.94	0.17	47.8	1.1	6.67	0.17	0.169	0.011	0.883	0.029
FB5ap_106	1916	39	126.9	4.2	1575	49	131.80	4.10	529	14	91.3	3	518	17	230	7	41.6	1.3	306.7	8.5	59.5	1.4	403.6	9.1	72.7	1.3	181.8	3.1	21.83	0.47	115.1	2.1	13.56	0.28	0.524	0.027	8.25	0.2
FB5ap_107	256.3	6.1	268.3	9	1608	54	72.20	3.20	286	12	56.1	2.3	386	18	178	7.7	11.2	0.49	281.8	9.4	60.2	1.4	352.3	9.5	70.1	1.9	180.2	4.1	20.55	0.56	100.6	2.9	11.88	0.36	2.12	0.12	11.15	0.62
FB5ap_108	818	20	416	15	1441	54	41.40	1.70	151.8	6.1	29.2	1.2	196.3	8.5	92.2	3.6	14.11	0.5	171.2	5.3	33.37	0.85	265.7	4.9	60.19	0.95	175.9	2.7	25.6	0.45	161.7	3.8	20.81	0.51	0.768	0.027	10.29	0.3
FB5ap_109	297.2	5.1	461.6	7.7	288.3	5.4	4.32	0.19	17.63	0.47	3.99	0.15	29.39	0.92	16.67	0.55	5.69	0.14	31.98	0.73	6.01	0.15	45.2	1	10.02	0.17	26.79	0.49	3.308	0.091	18.68	0.43	2.764	0.073	0.151	0.011	1.863	0.043
FB5ap_110	336	7.6	420	15	264	10	3.07	0.21	13.76	0.65	3.23	0.17	25.9	1.2	15.97	0.69	6.6	0.27	32.1	1.2	5.51	0.15	38.31	0.81	8.43	0.21	24.12	0.55	3.317	0.082	20.9	0.68	3.41	0.11	0.0047	0.0019	0.686	0.033
FB5ap_111	956	21	484	16	1190	44	52.40	2.10	187.6	6.7	33.1	1.2	217.1	8.4	77.7	2.6	9.02	0.3	125	3.5	20.55	0.51	162.4	3.1	44.76	0.74	176.3	2.9	33.42	0.63	261.6	5.7	41.8	1.2	0.644	0.027	7.91	0.25
FB5ap_112	844	20	205.3	6.1	3990	160	20.65	0.92	92.3	3.6	16.72	0.66	119.2	5.1	67.9	2.4	20.72	0.73	166.5	5.6	43.4	1.1	468	12	146.4	3.6	597	13	107	2.5	787	23	121.3	4	10.9	0.3	115.1	3.6
FB5ap_113	604	12	392	12	655	20	3.07	0.16	9.52	0.34	1.79	0.1	12.15	0.68	7.13	0.35	1.611	0.076	19.26	0.67	4.88	0.14	57	1.2	20.44	0.37	93.9	1.6	18.2	0.36	140	2.9	22.51	0.52	0.535	0.023	2.087	0.056
FB5ap_114	210	4.4	236.9	4.1	951	24	4.77	0.22	16.41	0.52	3.29	0.15	24.41	0.92	19.7	0.75	9.85	0.25	95.4	2.2	25.63	0.48	213.5	3.7	41.18	0.74	98.9	1.8	10.92	0.23	62	1.1	5.79	0.15	0.406	0.021	3.718	0.064
FB5ap_115	544	13	322	11	1299	52	31.10	1.20	107.3	3.7	19.2	0.73	127.7	4.7	59.4	2	11.06	0.37	121.3	3.2	24.8	0.56	209.2	4.5	50.97	0.87	157.5	2.8	21.37	0.45	122.9	2.9	16.37	0.44	1.211	0.044	6.56	0.23
FB5ap_116	1032	18	447.5	9.7	1484	39	61.90	1.90	193.1	5.2	34	1.1	221.2	6.2	98.9	2.6	16.33	0.39	182.7	4.2	34.61	0.69	272.3	5.4	61.4	0.87	185.6	3	27.69	0.51	176.9	3.1	23.99	0.44	0.862	0.04	11.4	0.26
FB6ap_0	239.8	2.1	492.1	6.1	137.7	2.1	21.05	0.40	74.3	1	11.85	0.29	68.1	1.6	19.41	0.53	5.18	0.15	24.3	0.59	3.366	0.082	21.84	0.56	4.6	0.12	12.64	0.31	1.75	0.06	10.94	0.36	1.904	0.058	0.542	0.023	6.18	0.13
FB6ap_1	81.8	1.2	283.4	4.1	588.5	8.9	18.30	0.41	81.4	1.5	18.13	0.37	143.3	3	82.2	1.8	9.47	0.24	162.6	2.7	28.22	0.5	161.2	2.8	21.84	0.36	34.36	0.6	2.283	0.073	7.37	0.24	0.646	0.038	0.126	0.046	8.03	0.18
FB6ap_2	557.9	7.8	235	3.8	636	13	155.80	4.60	411	14	58.7	1.9	309	12	87.1	3	23.32	0.46	112.8	3.5	16.26	0.44	105.2	2.3	22.81	0.5	65	1.4	8.65	0.2	54.4	1.2	9.76	0.21	8.52	0.24	3.41	0.11
FB6ap_3	191.7	2.1	316.5	3.5	868	10	16.73	0.38	81	1.1	17.83	0.37	135.1	2.5	69.1	1.4	6.88	0.16	120.1	1.9	21.49	0.34	156.1	2.5	33.8	0.49	94.8	1.5	11.88	0.2	65.8	1.2	9.06	0.2	0.344	0.015	2.792	0.068
FB6ap_4	397.1	3.8	591.9	6.4	776	12	9.26	0.27	48.19	0.95	11.79	0.31	97.8	2.4	66.9	1.4	9.49	0.22	126.1	1.8	25.08	0.36	170.6	2.4	30.45	0.45	73.9	1.1	8.76	0.15	48.98	0.85	5.91	0.13	0.655	0.029	3.805	0.068
FB6ap_5	699.1	8.2	539.8	6.2	1514	19	52.80	1.20	212.2	4.7	41.87	0.85	287.9	6.2	149.5	2.8	16.46	0.28	248.8	3.4	45.31	0.67	319.3	4.5	64.43	0.88	178.2	2.6	23.57	0.39	142	2.3	18.35	0.34	0.099	0.01	6.49	0.14
FB6ap_6	235.2	2.4	334.8	4.9	58.1	1.2	22.98	0.77	83.1	2.7	13.06	0.44	68.3	2.3	16.92	0.6	3.48	0.14	14.78	0.42	1.628	0.056	9.28	0.25	1.818	0.07	5.03	0.17	0.615	0.03	3.82	0.19	0.562	0.034	0.384	0.019	0.906	0.026
FB6ap_7	236.4	2.7	405.1	5.5	585	18	7.30	0.29	30.9	0.74	6.43	0.23	46.7	1.7	24.9	0.83	7.9	0.21	51.6	1.9	9.84	0.35	80.4	2.7	20.32	0.63	64.1	2	8.64	0.28	51	1.6	7.62	0.22	0.21	0.015	1.996	0.091
FB6ap_8	293.4	3.4	492.8	6.5	131.8	2.1	8.20	0.25	27.18	0.52	5.03	0.17	33.04	0.99	11.72	0.38	2.93	0.11	18.48	0.59	2.828	0.081	19.39	0.48	4.49	0.12	13.67	0.35	1.948	0.068	12.89	0.35	2.325	0.073	0.0226	0.0042	0.1716	0.0094
FB6ap_9	498.8	5	221	3.4	1692	28	112.70	1.70	530.9	7.2	105.9	1.4	671.2	8	278	3.7	55.44	0.89	368.4	4.8	62.79	0.89	429.7	7	83	1.3	214.3	3.3	25.21	0.49	129.1	2.2	14.56	0.3	0.132	0.011	1.588	0.043
FB6ap_10	107.2	1.6	231.4	4.6	37.53	0.92	1.78	0.11	10.73	0.42	2.53	0.12	18.72	0.8	5.06	0.29	2.3	0.11	6.18	0.28	0.783	0.042	5.28	0.24	1.195	0.063	3.73	0.16	0.65	0.034	3.41	0.19	0.545	0.042	0.0049	0.0021	0.0577	0.005
FB6ap_11	613.7	6.7	209.3	2.8	1730	27	27.80	0.55	112.7	2	22.33	0.49	154.1	3.3	83.9	1.5	19.81	0.34	168.7	3.1	36.37	0.6	304.4	5	71.2	1.3	208.1	3.5	28.94	0.49	178.9	3.2	22.24	0.46	4.73	0.22	21.88	0.7
FB6ap_12	239.5	2.8	373.5	4.7	89.9	1.3	19.14	0.73	59.1	1.8	8.89	0.32	47	1.8	11.78	0.42	4.84	0.16	13.63	0.4	1.761	0.057	12.06	0.32	2.724	0.082	8.48	0.25	1.323	0.049	9.5	0.25	1.93	0.066	0.332	0.019	0.589	0.02
FB6ap_13	470	5	459.6	5.7	894	17	15.49	0.29	84.2	1.3	19.97	0.44	166.2	3.1	82.6	1.5	11.02	0.23	140.5	2.4	24.1	0.4	168.7	2.9	35.8	0.59	109.1	1.7	16.99	0.32	118.5	1.9	18.21	0.38	0.432	0.023	8.61	0.19
FB6ap_14	409.9	3.8	420.9	4.8	913	16	7.49	0.24	28.29	0.65	5.37	0.17	38.5	1.1	18.42	0.54	5.61	0.16	39.9	1	8.79	0.18	95.4	1.6	32.42	0.47	138.9	2.3	24.25	0.43	169.5	3	25.78	0.45	0.186	0.013	1.734	0.053
FB6ap_15	474.8	5	232.5	2.9	895	13	1.79	0.10	7.77	0.21	1.825	0.084	14.76	0.64	12.94	0.34	3.66	0.12	39.65	0.73	11.13	0.17	113.8	1.6	31.11	0.47	110	1.7	16.86	0.3	105.7	1.6	15.14	0.25	0.117	0.011	2.41	0.066
FB6ap_16	278.1	2.5	557.2	6.1	237.3	2.4	8.02	0.25	39.34	0.67	10.02	0.21	96	1.7	59.3	1.1	16.53	0.32	90.5	1.3	11.07	0.2	58.93	0.99	10.31	0.19	24.05	0.49	2.517	0.072	13.36	0.33	2.047	0.062	0.0547	0.0059	4.201	0.066
FB6ap_17	293.3	3.1	544.2	6.1	84.8	1.9	23.16	0.83	43.22	0.83	5.54	0.19	29.63	0.96	9.59	0.33	2.42	0.12	13.31	0.46	1.966	0.067	13.09	0.35	2.811	0.089	8.2	0.3	1.012	0.047	6.77	0.27	1.14	0.058	0.393	0.023	0.737	0.024
FB6ap_18	260	3.2	456.7	6.3	754	11	1.79	0.11	10.28	0.38	3.03	0.11	32.86	0.87	19.7	0.29	3.23	0.12	34.7	1.4	2.91	0.12	29.39	0.87	5.94	0.14	28.71	0.59	4.03	0.1	28.73	0.59	4.03	0.1	0.186	0.012	6.92	0.13
FB6ap_19	403.8	3.5	474.7	6.6	1157	21	17.98	0.45	71.6	1.2	16.02	0.41	140.7	3.1	85.7	1.8	24.99	0.46	171.6	2.5	29.69	0.37	214	2.8	44.38	0.56	126	1.6	16.69	0.25	100.3	1.5	14.33	0.25	0.822	0.033	7.25	0.13
FB6ap_20	532.5	6	277.6	4.8	1125	23	56.00	1.00	229	3.3	48.13	0.73	343.2	6	156.2	2.6	18.23	0.32	222.7	3.5	38.49	0.62	263	4.2	51.27	0.83	137	2.7	17.07	0.36	97.9	2.1	12.21	0.27	0.499	0.028	8.62	0.39
FB6ap_21	336.7	3.3	671.3	7.9	159.4	2.3	1.30	0.19	5.03	0.25	0.948	0.074	7.51	0.46	4.79	0.29	0.836	0.06	12.64	0.4	2.953	0.07	24.73	0.5	5.5	0.11	15.62	0.35	1.955	0.063	10.22	0.34	1.306	0.046	0.386	0.022	0.601	0.023
FB6ap_22	210.5	3.1	182.2	2.8	608	9.1	20.26	0.66	51.6	2.4	45.3	1.5	377.4	5.5	143.7	2	93	1.1	213.6	2.4	38.58	0.5	313.5	3.7	80.9	0.88	303.5	2.9	55.34	0.64	432.8	5.4	72.41	0.74	9.19	0.16	6.439	0.092
FB6ap_23	361.7	4.1	283.7	3.9	1363	17	90.20	1.10	405.6	4.5	82.2	1.1	503.6	5.8	237	2.9	26.07	0.4	346.7	3.7	68.06	0.77	425.6	4.7	61.03	0.76	98.8	1.2	11.44	0.16	60.03	0.96	6.96	0.13	0.0336	0.005	4.091	0.067
FB6ap_24	754	5.6	381.6	4.7	1039	16	52.28	0.85	259.6	2.7	52.96	0.67	362	4.8	193.8	2.5	16.93	0.28	289.1	3.1	48.31	0.55	287.3	2.7	46.74	0.52	103.4	1.3	11.44	0.16	60.03	0.96	6.96	0.13	0.0336	0.005	4.091	0.067
FB6ap_25	300.4	2.9	449.7	5.1	176.5	1.9	32.94	0.75	97.3	1.9	14.91	0.34	89.2	2	24.33	0.68	5.49	0.15	32.5	0.7	4.221	0.092	27.34	0.5	5.9	0.11	17.06	0.35	2.354	0.067	14.99	0.42	2.562	0.073	0.246	0.014	1.431	0.032
FB6ap_26	203.7	1.9	190.6	2.8	884	13	7.77	0.24	40.19	0.51	10.61	0.22	100.8	1.8	73.9	1.3	9.38	0.19	145.4	1.8	29.81	0.37	207.6	2.2	36.86	0.44	86.8	1.1	9.84	0.17	51.5	0.74	6.21	0.12	0.303	0.016	5.268	0.075
FB6ap_27	440.3	5.1	218.6	2.9	2239	32	112.60	1.50	387.5	5.2	63.54	0.95	377.4	5.5	143.7	2	93	1.1	213.6	2.4	38.58	0.5	313.5	3.7	80.9	0.88	303.5	2.9	55.34	0.64	432.8	5.4	72.41	0.74	9.19	0.16	6.439	0.092
FB6ap_28	811.6	6.9	561.1	5.4	1391	17	139.80	1.60	482.3	4.7	86.3	1.1	518.9	6.4	217.2	2.9	29.28	0.39	313.4	3.4	55.64	0.62	368	3.6	57.97	0.52	114.8	1.4	11.12	0.16	54.57	0.96	6.35	0.13	0.471	0.019	12.54	0.12
FB6ap_29	325.5	3.1	275.3	3.4	1053	13	18.87	0.39	104.1	1.2	25.1	0.38	184.9	3	105	1.2	9.69	0.19	183.8	2.1	36.74	0.36	248	2.8	43.3	0.49	96.1	1.2	10.15	0.16	48.06	0.69	5.27	0.1	0.0376	0.0054	3.641	0.052

S2.3 apatite trace-element data (continued)

	55Mn	±	86Sr	±	89Y	±	139La	±	140Ce	±	141Pr	±	146Nd	±	147Sm	±	153Eu	±	157Gd	±	159Tb	±	163Dy	±	165Ho	±	166Er	±	169Tm	±	172Yb	±	175Lu	±	232Th	±	238U	±
FBsap_30	493.8	3.9	380.8	4	1298	17	38.63	0.62	138.6	1.4	27.84	0.41	176.1	2.6	80.7	1.2	10.53	0.2	137.2	1.5	28.5	0.33	235	2.4	54.26	0.47	155.1	1.8	19.15	0.25	99	1.2	11.35	0.19	0.221	0.035	4.048	0.053
FBsap_31	190.2	1.8	437.8	4.4	380.1	3.8	133.70	1.40	462.1	4.6	85.2	1.2	498.3	5.5	229	2.9	43.1	0.57	322.2	3.3	43.08	0.39	145.2	1.4	12.38	0.2	15.44	0.31	1.001	0.042	3.1	0.15	0.255	0.021	0.457	0.024	29.65	0.23
FBsap_32	358.9	3.3	226.4	2.6	636.4	7.6	29.99	0.56	144	2	34.43	0.55	273.4	4.6	126.1	1.6	16.67	0.31	177.9	2.3	25.86	0.34	160.9	1.9	27.03	0.34	65.11	0.82	7.46	0.16	40.78	0.76	5.91	0.11	29.19	0.42	39.49	0.47
FBsap_33	168.3	3.9	267.3	3.2	1013	17	12.25	0.36	50.9	1.2	11.71	0.36	106.8	2.6	98.5	2.1	30.63	0.89	257	5.1	45.33	0.85	247	4.7	38.9	0.76	83.3	1.6	8.81	0.2	41.27	0.89	4.69	0.13	3.92	0.12	92.3	1.6
FBsap_34	1476	13	419.1	4	1234	17	86.67	0.98	371.2	4.3	72.37	0.89	445.3	6.3	205	2.3	15.61	0.24	271.5	3	47.49	0.61	282.9	3.2	49.15	0.44	117.9	1.3	14.3	0.2	77.3	1	8.98	0.17	0.0904	0.009	14.61	0.16
FBsap_35	484.7	5	427.1	6.6	387.3	7.8	9.17	0.48	26.65	0.67	5.51	0.23	37.1	1.7	20.53	0.7	8.2	0.33	52.9	1.6	9.86	0.3	70.4	1.6	14.69	0.33	40.8	1	5.05	0.14	29	1	4.24	0.13	0.37	0.027	3.7	0.11
FBsap_36	307.7	3.7	255.2	3.3	2775	53	16.74	0.42	71.1	1.6	14.37	0.38	107.3	2.9	57.5	1.4	14.95	0.45	136.4	2.8	31.73	0.66	317.6	5.2	97	1.9	405	7.2	76.6	1.5	594	11	92.3	1.7	29.15	0.8	184.3	4.5
FBsap_37	194.5	2.4	215.4	3.2	964	14	7.15	0.21	44.66	0.67	11.2	0.27	92.8	1.9	55.7	1.1	4.63	0.13	118.1	1.6	23.29	0.34	174.3	2.2	38	0.4	102.3	1.2	12	0.2	59.5	0.98	7.31	0.15	0.239	0.024	5.69	0.09
FBsap_38	787.7	7.3	203	3	1470	19	28.53	0.56	180.5	2	45.09	0.54	340.1	4.3	208.6	2.9	13.1	0.21	345.9	4.5	66.28	0.75	416.3	4.4	66.64	0.79	135	1.7	12.86	0.2	54.77	0.78	6.06	0.12	0.0225	0.0044	8.06	0.11
FBsap_39	331.3	3.8	399.2	5.2	190.3	4.8	22.22	0.69	171.8	3.8	41	1	275.8	6.8	77.6	2.2	16.37	0.42	79.6	1.5	19.06	0.36	170.3	2.9	41.33	0.74	128.2	2.1	17.59	0.36	106.1	1.9	14.18	0.26	0.0313	0.007	4.96	0.12
FBsap_40	356.2	4.1	347.6	6.4	1038	24	1.84	0.10	8.68	0.28	2.35	0.14	24.6	1	24.76	0.82	4.78	0.22	79.6	1.5	19.06	0.36	170.3	2.9	41.33	0.74	128.2	2.1	17.59	0.36	106.1	1.9	14.18	0.26	0.0313	0.007	4.96	0.12
FBsap_41	311.2	3.4	514.2	5.7	1156.6	1.9	35.16	0.70	109.7	1.5	16.53	0.27	84.6	1.9	18.58	0.71	7.06	0.17	20.95	0.52	2.709	0.086	17.42	0.49	3.72	0.1	11.05	0.25	1.547	0.06	10.52	0.33	1.834	0.06	1.587	0.046	5.591	0.086
FBsap_42	338.7	7.4	575	12	76.5	1.7	27.62	0.74	56.1	1.5	7.49	0.29	37.5	1.4	10.36	0.53	3.13	0.12	12.58	0.5	1.814	0.078	12	0.36	2.462	0.092	7.25	0.26	0.99	0.063	6.3	0.27	1.082	0.061	0.21	0.017	0.96	0.031
FBsap_43	175.1	1.8	184.1	2.8	249.5	3	0.90	0.06	3.23	0.17	0.647	0.053	5.6	0.39	3.56	0.24	1.32	0.077	9.7	0.36	2.35	0.072	25.09	0.59	8.43	0.17	37.81	0.64	6.81	0.14	48.59	0.98	7.79	0.2	0.0138	0.0037	2.78	0.12
FBsap_44	499.5	4.5	268.6	3.8	1256	36	5.89	0.24	22.04	0.72	4.63	0.2	36.7	1.4	21.79	0.9	3.04	0.14	51.2	1.8	11.44	0.39	126.6	4.1	45.6	1.3	209.5	6	41.3	1.3	322.9	9.8	51.5	1.5	2.23	0.17	19	1.3
FBsap_45	223.9	2.5	422.6	4.5	737	20	28.93	0.88	114.8	3.5	21.64	0.71	147.6	4.7	64.2	2.2	7.42	0.22	110.1	3.2	18.27	0.57	129.6	3.3	28.16	0.84	76	2.2	9.4	0.32	61.3	1.8	6.78	0.26	2.46	0.12	9.43	0.48
FBsap_46	161.3	1.8	395.5	4.3	237.1	3.4	30.45	0.69	162.8	2.5	40.17	0.75	365.7	6.5	178.5	2.9	11.99	0.3	208.7	3.6	20.82	0.35	70.5	1.2	9.46	0.19	25.96	0.74	3.75	0.098	20.24	0.57	2.848	0.085	0.142	0.013	7.49	0.13
FBsap_47	333.7	3.3	639.8	6.7	336.6	5.1	8.59	0.32	60.1	1.1	23.24	0.48	223.1	3.8	103	1.8	14.29	0.4	102.5	1.9	12.68	0.27	70.5	1.5	12.9	0.26	31.95	0.74	3.75	0.098	20.24	0.57	2.848	0.085	0.142	0.013	7.49	0.13
FBsap_48	575.3	6	450.2	6.1	1075	16	5.65	0.22	37.59	0.74	10.66	0.27	89.3	1.9	72.8	1.4	9.06	0.2	155.3	2.5	34.4	0.6	246.5	4	44.45	0.67	103.4	1.9	11.33	0.22	54.4	1.2	5.86	0.15	0.0114	0.0031	5.14	0.12
FBsap_49	397.5	3.9	475.8	4.5	1194	16	27.53	0.49	108.4	1.7	21.02	0.4	147	2.9	74.2	1.4	13.28	0.26	145.9	2.3	27.98	0.4	218.2	2.8	48.5	0.66	135.1	2.2	17.65	0.29	101.2	1.8	12.98	0.23	0.292	0.018	5.47	0.13
FBsap_50	568.9	5.3	216.6	3.3	1057	16	66.40	1.30	256.9	3.7	47.64	0.72	302.1	4.5	141.7	2.3	38.06	0.61	207.6	3.3	37.64	0.56	248.8	3.9	46.86	0.63	114.4	1.9	12.86	0.28	63.8	1.2	7.33	0.15	1.525	0.048	10.28	0.25
FBsap_51	395.8	4.1	361.5	5.4	1231	26	32.62	0.59	128.6	2.1	23.23	0.42	147.2	3.1	93.2	2.1	20.93	0.61	168.5	2.6	31.59	0.52	229.3	2.6	42.05	0.94	176.1	3.8	31.46	0.67	231.7	5.2	34.29	0.83	2.457	0.097	22.59	0.72
FBsap_52	160.1	2.1	546.9	6.7	111.5	1.5	17.97	0.53	53.38	0.97	9.92	0.24	66.4	1.3	21.01	0.85	2.97	0.12	15.16	0.41	3.046	0.081	20.37	0.44	4.15	0.11	10.76	0.26	1.317	0.051	7.44	0.28	1.111	0.049	0.256	0.017	0.488	0.019
FBsap_53	215.2	2.5	403.8	4.3	112.3	1.3	3.59	0.16	14.33	0.34	2.89	0.12	21.00	0.85	9.58	0.4	2.97	0.12	15.16	0.41	2.403	0.063	16.32	0.37	3.664	0.086	10.69	0.28	1.354	0.045	8.22	0.26	1.444	0.056	0.0786	0.0098	0.783	0.022
FBsap_54	311.6	3.6	465	4.9	427.1	4.3	12.87	0.36	53.68	0.93	11.23	0.26	90.9	2.1	43.8	1	10.89	0.24	66.2	1.2	10.11	0.18	68.14	0.91	14.22	0.26	40.49	0.69	5.44	0.1	33.69	0.64	5.27	0.1	1.521	0.047	12.5	0.2
FBsap_55	401.8	4.2	518.3	6.6	238.9	3.9	23.90	0.63	83.6	1.3	14.64	0.32	93	2.1	30.75	0.71	7.22	0.2	40.35	0.85	5.8	0.13	38.34	0.92	8.5	0.17	24.44	0.48	3.309	0.099	21.11	0.63	3.493	0.093	0.208	0.015	0.668	0.027
FBsap_56	734.4	5.4	148.9	2.3	2720	38	326.60	4.40	112.8	1.6	16.3	0.3	37.1	1.7	20.53	0.7	8.2	0.33	52.9	1.6	9.86	0.3	70.4	1.6	14.69	0.33	40.8	1	5.05	0.14	29	1	4.24	0.13	0.37	0.027	3.7	0.11
FBsap_57	151.2	2	998	11	321.1	4.6	5.70	0.43	87.4	1.3	39.54	0.61	388.8	4.8	149.6	1.9	20.93	0.39	133.4	1.8	15.3	0.24	77.1	1.2	12.68	0.21	28.88	0.54	3.146	0.065	15.85	0.39	1.964	0.069	7.09	0.13	20.22	0.29
FBsap_58	295.8	3	335.6	3.9	689.3	9.9	36.08	0.65	158.4	2.4	32.62	0.47	232.7	3.3	100.2	1.7	22.65	0.5	142.8	1.7	20.54	0.26	131.1	1.9	24.76	0.38	63.85	0.87	7.67	0.15	39.78	0.77	5.12	0.1	0.476	0.023	11.71	0.19
FBsap_59	239.8	2.6	113.5	2	948	15	3.63	0.14	14.37	0.26	3.44	0.12	32.9	1	17.77	0.62	5.5	0.14	40.4	0.78	8.82	0.17	82	1.2	25.03	0.38	73.4	1.1	19.3	0.33	150.1	2.3	25.85	0.37	3.069	0.08	5.57	0.13
FBsap_60	303.6	3.5	320.9	4.3	765	12	6.89	0.23	25.89	0.54	4.93	0.17	34	1	17.77	0.69	5.55	0.15	107.7	1.5	17.97	0.28	121.9	1.6	25.62	0.38	68.9	1	9.25	0.15	61.8	1.1	9.52	0.19	0.257	0.017	5.59	0.1
FBsap_61	323	3.7	344.2	4.5	647.2	8.5	7.59	0.23	46.43	0.66	12.08	0.24	107.3	1.9	58.87	0.99	5.56	0.15	107.7	1.5	17.97	0.28	121.9	1.6	25.62	0.38	68.9	1	9.25	0.15	61.8	1.1	9.52	0.19	0.257	0.017	5.59	0.1
FBsap_62	281.5	3.1	392	4.9	481.9	6.6	5.29	0.20	19.04	0.43	3.71	0.14	25.69	0.82	15.13	0.35	10.61	0.24	40.2	0.81	8.39	0.13	69.27	0.97	17.4	0.28	51.75	0.8	6.35	0.11	34.07	0.7	4.834	0.095	0.198	0.013	0.346	0.013
FBsap_63	195.8	3.1	439.8	6.6	257.1	4.4	2.68	0.10	171.8	3.8	41	1	275.8	6.8	77.6	2.2	16.37	0.42	79.6	1.5	19.06	0.36	170.3	2.9	41.33	0.74	128.2	2.1	17.59	0.36	106.1	1.9	14.18	0.26	0.0313	0.007	4.96	0.12
FBsap_64	99.8	1.4	337.7	5.4	548	7.4	18.73	0.43	112.9	1.7	30.29	0.44	240.9	3.2	159.4	2.2	36.47	0.58	280.7	3.4	47.16	0.63	209.8	2.5	18.95	0.32	20.45	0.41	1.111	0.045	3.64	0.16	0.337	0.026	0.217	0.017	20.74	0.38
FBsap_65	332	3.7	403.3	4.6	934	17	53.40	0.87	193.4	3	34.94	0.59	230.8	3.6	94.2	1.5	11.06	0.27	151.9	2	24.52	0.32	168.9	2.3	36.42	0.49	101.5	1.4	13.41	0.22	79.9	1.4	10.94	0.2	1.019	0.033	5.72	0.1
FBsap_66	797.6	8.6	227	3.7	1006	21	65.00	1.10	270.7	4.3	49.32	0.97	316.4	6.1	160.4	2.9	27.27	0.62	183	3.3	33.16	0.69	230.2	4.3	46.24	0.95	130.2	2.8	18.3	0.39	110.2	2.1	13.51	0.32	0.583	0.05	9.57	0.57
FBsap_67	334.2	3.2	620.5	7.8	85.9	1.3	22.26	0.47	68.5	1.1	9.91	0.24	52.6	1.2	12	0.44	4.83	0.14	14.78	0.44	1.964	0.062	12.78	0.32	2.719	0.059	8.04	0.23	1.092	0.043	7.62	0.23	1.223	0.046	0.124	0.012	0.23	0.012
FBsap_68	303.9	2.8	970	10	231.9	3.1	10.89	0.30	125.9	2.1	43.09	0.65	340	4.7	103	1.4	16.44	0.31	84.8	1.3	9.48	0.17	49.23	0.78	8.61	0.17	20.84	0.4	2.336	0.063	13.5	0.34	1.887	0.063	0.14	0.01	8.26	0.13
FBsap_69	738.6	6.5	134.5	2	334	26	29.90	3.20	101	10	18.8	1.8	118	11	45.2	3.6	12.47	0.73	56.8	4.2	8.01	0.64	50.3	4.2	10.69	0.84	30.4	2.5	3.75	0.29	23.4	2	3.96	0.34	2.4	0.61	4.2	0.2
FBsap_70	573.9	4.9	365.1	4.1	1674	25	32.62	0.59	128.6	1.4	23.23	0.42	147.2	3.1	93.2	2.1	20.93	0.61	168.5	2.6	31.59	0.52	229.3	2.6	42.05	0.94	176.1	3.8	31.46	0.67	231.7	5.2	34.29	0.83	2.457	0.097	22.59	0.72
FBsap_71	255.5	2.9	446.7	3.9	84.8	1.4	8.63	0.28	16.52	0.35	3.71	0.15	20.92	0.73	7.5	0.35	1.886	0.086	10.79	0.37	1.727	0.064	12.27	0.32	2.775	0.084	8.64	0.25	1.24	0.044	8.12	0.23	1.363	0.055	0.0579	0.0081	0.399	0.012
FBsap_72	232.2	2.4	727	5.7	87.18	0.53	41.14	0.98	110.3	2.3	13.86	0.39	64.8	1.7	8.95	0.39	2.045	0.097	7	0.33	0.658	0.034	3.34	0.15	0.631	0.033	1.68	0.095	0.206	0.021	1.34	0.1	0.238	0.019	0.087	0.01	0.1467	0.0092
FBsap_74	826.3	7	451.9	3.8	1517	20	70.30	1.00	257.3	2.9	45.62	0.67	301.2	5	128.9	1.9	17.01	0.27	183.5	2.2	31.71	0.36	244.2	2.2	60.81	0.61	225.9	2.5	40.79	0.47	307.1	3.6	45.45	0.57	2.3	0.2	9.08	0.11
FBsap_75	410.1	4.4	381.3	5.1	1176	15	13.32	0.33	51.06	0.91	9.65	0.25	66.1	1.9	33.88	0.92	7.77	0.22	72.5	1.4	15.11	0.25	141.9	1.9	43.96	0.56	172.4	2.1	29.69	0.36	214.7	2.7	33.66	0.48	1.425	0.043	5.223	0.079
FBsap_76	202	2.4	501.1	7.2	272.6	4.6	0.46	0.06	4.76	0.21	2.18	0.12	32.1	1.2	35.9	0.94	4.85	0.15	64.4	1.3	9.36	0.2	54.31	0.94	9.94	0.18	23.89	0.41	2.68	0.079	14.3	0.46	1.923	0.063	0.0542	0.0093	4.808	0.083
FBsap_77	325.6	3.3	566.2	7	267.1	8.7	33.80	2.10	128.7	7	22.3	1	134.7	6.3	42.1	1.7	19.69	0.72	53.6	2	7.22	0.28	44.1	1.5	9.16	0.36	23.76	0.81	2.88	0.11	17.14	0.67	2.98	0.11	1.881	0.084	5.33	0.19
FBsap_78	448.7	5.3	340.4	5.5	890	23	141.80	3.50	454.4	9.5	74.5	1.6	417.4	8.3	135.1	3.3	35.57	0.89	182.7	4.3	26.7	0.58	167.3	3.7	33.22	0.79	86.4	2.1	9.98	0.26	55.2	1.4	8.03	0.24	6.52	0.27	15.29	0.37
FBsap_79	480.7	3.8	252.3	2.9	1015	19	12.55	0.34	53.12	0.65	12.01	0.25	98.1	2	66.4	1.2	11.9	0.22	136.1	1.5	28.81	0.38	212.8	2.2	42.07	0.61	106.3	1.2	13.04	0.18	71.9	1.1	8.98	0.16	0.19	0.015	4.666	0.061
FBsap_80	669.8	6.4	415.2	6	1529	23	6.85	0.24	29.57	0.71	6.25	0.2	52.5	1.5	29.17	0.78	5.5	0.18	70.9	1.5	14.9	0.24	162.4	2.4	56.75	0.79	242.6	2.6	44.21	0.55	326.8	3.8	46.45	0.5	2.431	0.052	21.69	0.3
FBsap_81	382.2	4.9	523.8	5.5	107.3	1.4	81.30	1.40	241.5	3.7	36.06	0.58	179.4	3.1	35.55	0.81	8.74	0.21	30.56	0.72	3.334	0.085	17.83	0.43	3.494	0.082	9.23	0.24	1.124	0.051	7.29	0.25	1.155	0.05	1.065	0.084	0.508	0.015
FBsap_82	221.8	2.2	387.9	5.5	596.5	8.7	95.10	1.50	370.2	4.7	72.2	1	447.1	6.6	217.9	3.5	41.38	0.95	329.9	5	56.32	0.68	245.2	2.8	17.79	0.31	12.06	0.31	0.508	0.037	1.37	0.12	0.083	0.016	0.469	0.029	29.79	0.39
FBsap_83	247.6	2.7	506.2	4.4	102.1	1.2	6.66	0.18	25.44	0.41	4.71	0.16	29.94	0.93	9.78	0.41	3.23	0.12	12.87	0.39	1.88	0.064	13.43	0.35	3.212	0.073	10.84	0.25	1.601	0.049	11.56	0.35	2.206	0.07	0.232	0.014	0.574	0.02
FBsap_84	784.8	7.4	290	4	475.5	6.1	1.10	0.08	4.13	0.17	0.763	0.06	5.81	0.39	4.86	0.24	1.668	0.094	14.77	0.48	4.015	0.084	45.18	0.77	15.47	0.23	71.2	0.86	14.47	0.21	121.1	1.9	20.52	0.33	0.854	0.033	18.97	0.33
FBsap_85	1129.3	9.5	546.8	5.6	1912	29	256.80	3.30	819.9	9	134.7	1.6	739.6	7.1	292.3	3.8	35.57	0.49	375.9	4.2	68.22	0.68	455.4	4.8	87.74	0.99	213.8	2.4	23.62	0.32	109.8	1.3	11.7	0.17	1.682	0.046	18.26	0.23
FBsap_86	229.1	2.4	504.3	5.6	262.3	3.2	13.17	0.37	77.2	1.3	18.56	0.38	140.3	2	51.8	1	10.62	0.22	58.33	0.99	7.8	0.15	45.65	0.65	8.8	0.17	23.94	0.45	3.097	0.076	18.59	0.49	2.693	0.062	0.599	0.032	5.837	0.082
FBsap_87	683.2	5.9	352.1	3.9	1169	17	34.80	0.86	138.2	2.5	26.9	0.59	185.8	3.2	84.1	1.7	10.62	0.25	138.7	2.2	24.64	0.45	185.7	2.3	44.4	0.57	152.4	2	26.5	0.31	175.7	2.1	25.82	0.3	0.293	0.016	6.78	0.11
FBsap_88	237.9	2.6	388.4	5	944	16	6.83	0.28	41.95	0.9	11.51	0.31	97.4	2.2	67	1.4	22.22	0.42	121.4	1.8	21.98	0.34	155.4	2.3	33.66	0.52	97.7	1.3	13.23	0.23	80.9	1	11.89	0.21	1.795	0.072	12.71	0.22
FBsap_89	329.8	3.8	535.8	6	1175	17	20.06	0.45	84.4	1.3	17.28	0.37	126.3	2.4	62.5	1.3	10.26	0.22	122.9	1.9	23.29	0.32	186	2.4	43.84	0.53	119	1.6	13.75	0.21	65	0.95	7.11	0.17	0.193	0.013	4.127	0.072
FBsap_90	362.3	4.1	505.8	5.9	763	11	8.94	0.29	35.16	0.65	6.89	0.18	48.4	1.3	26.45	0.83	9.91	0.21	57.1	1.2	11.51	0.2	97.4	1.7	25.55	0.43	84.5	1.2	12.44	0.25	80.3	1.2	12.14	0.23	1.6	0.044	6.81	0.14
FBsap_91	494.4	6.2	442.2	5	1315	24	78.80	1.50	305.3	5	59.63	0.93	386.9	6	180.5	2.4	24.06	0.4	276.2	3.4	49.01	0.67	320.8	4	55.31	0.73	115.8	1.9	10.83	0.19	46.99	0.74	4.8	0.094	0.295	0.017	6.96	0.11
FBsap_92	199.3	2.2	201.2	3	681.6	8.6	0.55	0.06	2.68	0.1	0.721	0.062	6.88	0.36	11.22	0.35	3.48	0.12	50.6	1.1	12.83	0.19	104	1.3	21.46	0.34	53.77	0.81	5.74	0.12	27.26	0.54	2.904	0.079	0.0062	0.0025	1.838	0.045
FBsap_93	958.1	9.7	125.5	2.6	2048	47	140.10	2.30	545.8	9	102	1.7	630	10	256.9	4.7	18.96	0.49	358.3	6.5	60.9	1.2	403.9	8.1	83.4	1.8	232.4	5.3	32.37	0.78	200	5	27.64	0.64	12.2	0.62	18.27	0.71
FBsap_94	406.3	4.2	367.4	5	1142	19	97.30	1.40	188.2	3	19.83	0.32	85.1	1.8	17.06	0.5	4.54	0.12	17.81	0.47	2.546	0.064	16.42	0.39	3.6	0.11	10.86	0.23	1.481	0.06	9.92	0.32	1.898	0.062	1.102	0.037	1.006	0.023
FBsap_95	386.4	4.4	281.5	4	1023	17	74.69	0.74	149.6	2.2	28.63	0.56	189.2	3	84.9	1.6	25.57	0.44	133	1.9	24.95	0.4	189	2.7	40.72	0.51	115.6	1.5	16.18	0.21	96	1.2	12.72	0.19	0.801	0.029	4.611	0.07
FBsap_96	825.3	7.6	492.2	4	1142	19	152.20	1.80	528.2	6.1	90.8	1.2	542.3	6.9	194.6	2.8	33.01	0.53	229.8	3.1	36.33	0.51	235.4	3.5	46.54	0.66	131.1	1.8	17.88	0.26	109.1	1.5	14.47	0.22	19.88	0.38	59.37	0.94
FBsap_97	501.4	4.4	360.5	4.6	1075	18	48.30	1.40	192.2	3	38.67	0.69	259.2	4.6	124.8	2	24.86	0.49	190	3.4	33.62	0.48	228.7	3.8	45.5	0.82	127.5	2.3	18.43	0.36	123.1	2.3	17.29	0.31	0.641	0.057	12.72	0.5

S2.3 apatite trace-element data (continued)

	55Mn	±	86Sr	±	89Y	±	139La	±	140Ce	±	141Pr	±	146Nd	±	147Sm	±	153Eu	±	157Gd	±	159Tb	±	163Dy	±	165Ho	±	166Er	±	169Tm	±	172Yb	±	175Lu	±	232Th	±	238U	±
FB6ap_98	592.8	5.6	171.6	2.4	899	15	24.80	0.47	91	1.5	15.67	0.33	103.9	2.3	35.96	0.81	7.5	0.16	61.5	1	11.38	0.22	98.4	1.5	27.72	0.44	110.8	1.6	20.95	0.35	157	2.1	23.42	0.35	0.943	0.033	6.243	0.092
FB6ap_99	719.1	6.7	398.3	4.9	1164	17	27.28	0.59	101.2	2.1	19.13	0.47	123.8	3.3	58	1.3	6.96	0.21	99.1	2.1	18.94	0.34	165	2.1	42.03	0.55	171.5	1.9	34.45	0.38	287.5	3.2	46.96	0.5	0.35	0.019	4.77	0.12
FB6ap_100	233.8	2.7	332.8	4.7	25.86	0.54	87.20	1.10	137.7	1.8	13.57	0.31	55.3	1.3	8.91	0.35	2.262	0.095	8.78	0.31	0.939	0.038	4.98	0.2	0.979	0.037	2.5	0.12	0.3	0.024	1.74	0.12	0.336	0.024	0.763	0.026	1.773	0.035
FB6ap_101	377	4.2	378.2	4.7	1013	18	43.12	0.72	154.1	2.1	28.93	0.59	193.9	3.3	96	1.6	13.07	0.25	154.7	2.3	28.93	0.41	199.4	2.5	40.73	0.59	107.4	1.2	13.32	0.21	74.5	1.2	9.73	0.17	0.498	0.023	4.002	0.073
FB6ap_102	261.7	2.7	329.4	4	637	9	9.40	0.33	63.7	1.1	15.76	0.41	120.1	2.5	74.9	1.4	5.88	0.17	123.1	1.9	23.97	0.31	152.2	2.1	26.18	0.34	62.65	0.79	5.37	0.11	25.97	0.49	3.082	0.083	0	0	6.44	0.12
FB6ap_103	366	3.4	541.7	4.4	153.8	2.2	20.31	0.42	84.1	1.4	16.61	0.31	111.1	2.2	34.07	0.8	6.24	0.15	36.8	0.88	4.205	0.094	23.83	0.51	4.78	0.1	13.85	0.34	1.918	0.071	13.66	0.36	2.462	0.068	0.851	0.029	6.026	0.085
FB6ap_104	1081.3	9	169.1	2.5	875	21	20.16	0.60	80.6	2.3	17.43	0.55	129	4.1	69.9	2	17.49	0.46	115.8	3.1	19.45	0.52	132.7	3.5	28.84	0.8	82.4	2.2	10.99	0.31	68.5	1.8	11.21	0.33	5.12	0.24	4.96	0.17
FB6ap_105	592.3	5.6	419.6	3.5	1106	16	42.49	0.61	167.9	2.1	32.43	0.55	222	3.3	101.2	1.4	14.37	0.31	163.9	2	29.19	0.38	213.1	2.8	46.89	0.53	136.4	1.1	19.11	0.25	124.5	1.4	17.7	0.22	0.919	0.034	13.41	0.13
FB6ap_106	443.5	4.4	528.4	5.5	300	4.1	18.70	0.46	71.9	1.4	13.4	0.33	90.8	1.9	35.11	0.92	8.45	0.19	50.3	1.1	7.51	0.14	50	0.76	10.31	0.18	28.46	0.49	3.7	0.089	22.09	0.48	3.457	0.078	1.526	0.047	10.36	0.12
FB6ap_107	781.7	6.6	457.7	3.9	1239	18	113.70	1.40	400.8	4.6	70.07	0.78	432.2	5.6	172.5	2	20.63	0.37	243	2.4	39.39	0.42	259.7	2.6	51.82	0.62	137.2	1.2	17.42	0.24	106	1.1	14.1	0.17	0.603	0.024	5.194	0.052
FB6ap_108	430.7	4.6	435.3	4.1	526.1	6.5	1.07	0.09	3.59	0.17	0.701	0.057	6.38	0.39	6.94	0.34	0.458	0.041	29.31	0.66	6.77	0.14	64.91	0.82	18.89	0.25	67.02	0.82	10.45	0.13	71.4	0.92	11.76	0.18	0.887	0.04	0.56	0.019
FB6ap_109	304.8	8.7	296.6	7.6	800	43	1.31	0.18	5.11	0.58	1.43	0.27	18.2	2.3	19.2	1.6	3.22	0.4	62.3	3.1	12.95	0.52	110.4	3.9	31.2	1.5	100.8	5.2	16.92	0.99	107.9	4.2	16.85	0.84	4.71	0.22	3.2	0.25
FB6ap_110	435.1	2.8	575.1	5	63.9	1.1	15.94	0.34	52.59	0.92	8.76	0.24	52.8	1.3	13.73	0.47	3.64	0.14	15.61	0.51	1.737	0.061	10.08	0.28	2.052	0.07	5.81	0.15	0.749	0.035	4.7	0.2	0.881	0.035	0.165	0.013	1.257	0.024
FB6ap_111	796	10	240.8	3.3	1023	20	4.05	0.21	15.54	0.35	3.02	0.15	20.33	0.92	12.18	0.55	3.93	0.15	34.26	0.83	9.44	0.18	103.7	1.8	34.67	0.47	150	2.1	30.09	0.48	242.4	3.6	40.25	0.58	0.096	0.01	2.26	0.048
FB6ap_112	330.6	3.5	150	1.8	87.1	1.2	8.46	0.23	40.63	0.61	7.89	0.24	46.3	1.2	15.02	0.52	3.93	0.12	17.99	0.57	2.72	0.072	15.06	0.37	2.593	0.068	5.33	0.19	0.538	0.037	2.62	0.16	0.276	0.022	0.267	0.017	2.452	0.038
FB6ap_113	217.7	2.3	264.4	3.4	182.5	3.3	2.77	0.15	13.47	0.36	3.34	0.16	27.33	0.97	16.12	0.55	3.74	0.14	25.49	0.72	4.27	0.11	29.5	0.61	6.59	0.14	20.63	0.45	3.137	0.087	22.03	0.59	3.97	0.097	0.3	0.019	2.36	0.075
FB6ap_114	331.7	3	553.3	5.3	23.24	0.49	41.85	0.69	76.21	0.8	8.23	0.2	37.5	1.1	7.14	0.36	1.936	0.092	6.63	0.29	0.796	0.027	4.11	0.2	0.836	0.039	2.08	0.11	0.261	0.022	1.7	0.11	0.287	0.023	0.295	0.019	0.1859	0.0077
FB6ap_115	355.7	4.8	568	12	492.70	7.90	1303	21	190.6	2.9	911	14	208.4	3	20.85	0.34	5.35	0.13	24.18	0.35	3.52	0.2	18.34	0.2	3.78	0.16	9.82	0.37	1.117	0.086	6.18	0.34	1.015	0.089	0.116	0.019	31.53	0.56
FB6ap_116	638	7.6	496.5	6.2	1.14	0.08	9.25	0.28	3.46	0.13	45	1.4	42.19	0.8	12.7	0.28	4.69	0.13	25.3	1.7	15.46	0.21	99.8	1.6	18.87	0.25	45.09	0.83	4.95	0.11	25.97	0.54	3.567	0.082	0.84	0.03	3.28	0.45
FB6ap_117	497.3	7.2	749	14	100	2.1	7.25	0.24	28.09	0.7	5.43	0.43	39.5	2	17.75	0.83	4.69	0.28	26.3	0.95	3.52	0.2	19.4	1.2	3.78	0.15	9.82	0.37	1.117	0.086	6.18	0.34	1.015	0.089	0.116	0.019	1.171	0.042
FB6ap_118	327.2	3.4	426	4.2	428.4	5.1	117.20	1.40	393.4	4.8	65.57	0.85	380.2	4.1	126.3	1.8	27.7	0.38	141.2	1.9	18.34	0.2	99.4	1.2	16.75	0.23	36.46	0.52	3.616	0.085	16.61	0.35	1.936	0.069	4.096	0.076	56.05	0.48
FB6ap_119	447	4.1	871.9	8.1	640	16	123.10	3.40	421	11	71.7	2	418	11	135.8	3.6	37.17	0.92	148.5	4	19.31	0.53	111.3	2.9	21.53	0.56	57.7	1.4	7.71	0.22	46.6	1.4	7.3	0.19	2.149	0.093	13.45	0.41
FB8ap_0	206.3	6.9	1047.5	8.8	206.9	2.2	9.80	0.28	61.54	0.9	17.96	0.34	146.4	2.5	61.9	1.3	19.49	0.34	70	1.1	8.44	0.15	44.89	0.66	7.42	0.13	16.99	0.41	1.902	0.064	10.1	0.32	1.353	0.054	0.0314	0.0053	2.4	1.7
FB8ap_1	795.8	7	309.1	3.3	835	10	16.78	0.38	93.9	1.4	23.07	0.42	188.4	3.2	132.2	1.7	11.44	0.23	242.7	3.5	44.74	0.53	266.6	3.2	35.01	0.43	63.86	0.97	5.98	0.11	25.43	0.62	2.435	0.072	0.0823	0.0093	5.28	0.15
FB8ap_2	194.2	2.6	638	7.6	496.5	6.2	1.14	0.08	9.25	0.28	3.46	0.13	45	1.4	42.19	0.8	12.7	0.28	95.3	1.7	15.46	0.21	99.8	1.6	18.87	0.25	45.09	0.83	4.95	0.11	25.97	0.54	3.567	0.082	0.84	0.03	3.28	0.45
FB8ap_3	225.2	2.5	417.6	4.8	885	13	49.30	1.20	291.2	6.1	75.6	1.6	596	11	239.1	4.1	45.99	0.87	255.3	3.8	33.55	0.65	193.3	2.9	35.29	0.56	88.4	1.3	10.56	0.22	58.29	0.96	7.94	0.15	4.03	0.12	3.393	0.063
FB8ap_4	334.1	2.8	1497	11	211.5	2.5	5.37	0.21	42.01	0.61	14.09	0.26	139.9	2	61.9	1	15.11	0.26	69.8	1.1	8.22	0.11	43.52	0.62	7.43	0.14	17.54	0.35	1.941	0.065	10.59	0.3	1.52	0.06	0.0503	0.0061	0.421	0.014
FB8ap_5	286	2.8	596.4	6.2	519.6	7	33.10	3.80	97.6	9.6	16	1.3	104.6	6.2	51.2	1.5	20.63	0.43	92.2	1.7	15.22	0.27	99.1	1.5	19.27	0.27	50.77	0.82	6.33	0.12	37.41	0.7	5.71	0.09	0.949	0.094	1.795	0.054
FB8ap_6	448.4	3.9	432.6	5	1528	20	127.50	9.00	453	23	73.1	2.8	382	12	144.2	3.1	40.76	0.69	196.5	2.9	41.41	0.57	319.3	3.3	64.82	0.67	173.5	1.8	21.42	0.27	111	1.3	12.78	0.18	0.532	0.036	12.55	0.26
FB8ap_7	491.1	4	729.7	6.8	138.3	2.4	2.01	0.12	7.85	0.25	1.583	0.093	11.83	0.6	6.36	0.33	1.642	0.087	15.34	0.61	3.069	0.075	23.7	0.55	5.82	0.14	17.21	0.36	2.156	0.068	12.4	0.3	2.006	0.062	0.01	0.0029	0.221	0.01
FB8ap_8	645.5	5.7	268.4	3.5	372	16	2.27	0.15	6.83	0.4	1.27	0.1	10.35	0.75	6.48	0.46	3.26	0.24	18.9	1.1	4.43	0.25	44	2.1	13.07	0.59	50.3	1.9	8.8	0.34	64.6	2.2	11.38	0.35	0.139	0.013	0.326	0.02
FB8ap_9	299.2	2.5	388.3	4.5	213.1	2.8	7.54	0.24	20.1	0.39	3.41	0.14	17.74	0.72	5.89	0.29	3.57	0.11	10.45	0.38	2.407	0.079	23.97	0.36	6.86	0.13	23.74	0.38	3.444	0.092	21.14	0.43	3.22	0.079	0.9	0.1	0.642	0.019
FB8ap_10	309.6	3.4	214.5	3	944	14	3.90	1.20	13.81	0.32	2.86	0.12	20.65	0.76	12.11	0.41	4.27	0.14	43.88	0.94	12.18	0.23	125.9	2.2	34.97	0.68	125.4	2	19.88	0.34	128.7	2.2	17.57	0.36	0.16	0.015	1.9	0.62
FB8ap_11	315	3.7	1190	14	489.6	5.9	17.93	0.39	132.4	1.9	39.07	0.74	327.3	4.6	131.4	2.2	31.79	0.54	140	2.3	17.82	0.26	100.7	1.7	17.8	0.33	43.49	0.82	5.14	0.13	27.31	0.61	3.536	0.085	0.083	0.0092	2.323	0.056
FB8ap_12	194.5	2.9	183.2	4.9	131.6	2.3	0.88	0.12	4.54	0.29	1.23	0.1	11.34	0.64	7.91	0.38	1.84	0.095	16.79	0.52	3.029	0.098	20.63	0.48	4.19	0.11	10.69	0.31	1.22	0.058	6.37	0.25	0.874	0.042	0.024	0.024	1.096	0.035
FB8ap_13	319.8	3.5	917	12	462.4	6.7	21.78	0.45	185.5	2.5	52.14	0.84	403.2	6.1	148.6	2.2	33.84	0.52	147.6	2.5	18.08	0.32	100.3	1.4	17.01	0.31	41.27	0.75	4.96	0.13	26.62	0.61	3.564	0.087	0.037	0.0064	1.493	0.043
FB8ap_14	283.5	3.8	417	5.5	66.5	2.3	14.83	0.56	50.9	1.4	8.76	0.37	55.1	2.3	14.11	0.61	4.69	0.23	18.39	0.74	2.119	0.098	12.27	0.51	2.55	0.11	6.84	0.29	0.867	0.054	5.54	0.29	1.007	0.053	0.76	0.048	21.72	0.99
FB8ap_15	330.3	3.4	547.5	6.8	46.77	0.87	15.18	0.38	33.48	0.73	4.42	0.14	23.54	0.81	6.11	0.28	2.206	0.096	7.96	0.33	1.033	0.039	6.57	0.2	1.425	0.061	4.34	0.17	0.593	0.033	4.01	0.15	0.733	0.036	0.257	0.017	1.704	0.049
FB8ap_16	245.5	3.1	900	12	585.6	8.6	46.87	0.86	284.3	4.3	70.2	1.1	515.3	7.9	180.5	2.8	37.5	0.66	176.7	2.9	22.02	0.36	123.4	2.1	20.87	0.38	50.7	1.1	5.96	0.13	32.94	0.73	4.14	0.1	0.0637	0.0068	1.21	0.25
FB8ap_17	249.5	2.9	778.9	9.6	185	18	19.10	1.80	74.8	7	14.8	1.5	97.3	5.2	75.2	1.1	462.5	6.6	110.8	1.7	23.11	0.4	87.7	1.7	9.02	0.19	41.63	0.86	6.2	0.13	12.78	0.31	1.169	0.051	5.44	0.038	0.0165	0.0036	1.95	0.22
FB8ap_18	241.7	3.1	1694	22	167.2	2.7	81.60	1.20	382.5	5.2	75.2	1.1	462.5	6.6	110.8	1.7	23.11	0.4	87.7	1.7	9.02	0.19	41.63	0.86	6.2	0.13	12.78	0.31	1.169	0.051	5.44	0.038	0.0165	0.0036	1.95	0.22
FB8ap_19	597.9	7.2	382.3	4.4	1020	31	26.18	0.98	109.5	4.2	22.21	0.95	166.1	6	92.1	3.5	25.2	1	162.1	6.3	27.44	0.94	190	6.8	40.5	1.5	117.5	4.1	16.56	0.53	108.9	3.4	17.02	0.57	7.9	0.33	6.43	0.21
FB8ap_20	250.8	3.2	3781	45	35.2	2	3.58	0.28	13.8	1.1	2.7	0.2	18.5	1.3	5.87	0.49	1.231	0.094	7.04	0.48	0.931	0.07	5.77	0.37	1.159	0.082	3.41	0.22	0.438	0.034	2.81	0.21	0.426	0.032	0.816	0.09	1.025	0.051
FB8ap_21	343.5	4	1269	15	133.9	2.5	6.37	0.31	26.08	0.72	6.9	0.19	66	1.8	38.05	0.92	10.06	0.25	47.9	1.1	5.48	0.13	29.02	0.79	4.97	0.11	11.25	0.32	1.221	0.051	6.3	0.28	0.946	0.044	0.0444	0.0077	0.541	0.081
FB8ap_22	245.6	2.6	530.5	6.7	992	18	40.16	0.70	272.1	3.7	69.93	0.85	541.8	7.8	234.2	3.2	22.57	0.43	276	4	36.41	0.64	206.1	2.9	37	0.63	89.8	1.5	10.59	0.2	57	1.1	7.52	0.16	0.537	0.028	9.68	0.22
FB8ap_23	348.2	3.7	321.2	4.3	724.7	9.3	4.69	0.21	16.65	0.81	3.52	0.15	25.1	1.2	15.15	0.64	5.51	0.19	40.2	1.1	9.17	0.2	89	1.4	24.89	0.36	92.5	1.3	14.83	0.22	102.4	1.6	16.93	0.3	9.34	0.14	2.858	0.056
FB8ap_24	276	3.3	493.7	6.7	192.5	2.7	6.34	0.24	9.8	0.37	2.37	0.11	12.54	0.6	4.88	0.29	1.333	0.069	9.81	0.41	2.21	0.069	22.07	0.49	6.53	0.14	26.09	0.54	4.72	0.11	35.09	0.77	6.18	0.15	2.477	0.073	3.777	0.07
FB8ap_25	88.1	1.3	501.9	7.8	996	22	80.00	6.60	194	16	28.7	2	167.3	8.4	86.9	2.2	24.01	0.58	172.9	3.3	31.27	0.6	219.8	3.8	41.48	0.82	98.5	1.9	10.22	0.25	49.2	1.4	5.61	0.15	2.27	0.14	3.223	0.081
FB8ap_26	310	6.2	279.2	4.4	787	13	11.07	0.35	88.2	1.4	27.71	0.54	247.4	4.4	120.4	2	28.75	0.49	169.7	2.6	24.75	0.38	195.3	2.2	29.54	0.45	73.9	1.3	8.65	0.15	44.3	1	5.81	0.13	0.0434	0.0068	3.728	0.076
FB8ap_27	210	2.3	422.4	5.2	175.2	2.3	26.95	0.48	102.7	1.3	17.36	0.34	99.2	1.8	27.67	0.74	7.61	0.18	30.9	0.75	4.754	0.092	30.59	0.62	6.1	0.13	16.48	0.36	2.101	0.066	12.36	0.35	1.717	0.065	16.13	0.31	17.67	0.85
FB8ap_28	709.2	7.5	840	10	6.19	0.25	3.21	0.16	8.22	0.25	1.314	0.076	6.12	0.37	1.36	0.15	0.241	0.026	1.44	0.12	0.188	0.016	1.065	0.082	0.199	0.016	0.533	0.05	0.0723	0.0095	0.466	0.068	0.084	0.01	0.159	0.012	0.111	0.074
FB8ap_29	163.4	1.8	274.3	3.2	2272	34	16.58	0.37	118.4	1.8	37.44	0.57	383.7	4.9	254.8	3.2	21.53	0.37	464.9	6.1	72.5	1.1	466.9	6.2	85.1	1.2	194.9	3	19.11	0.33	81.4	1.5	8.84	0.18	1.102	0.04	6.76	0.14
FB8ap_30	450	5	476.5	6.7	597	12	9.94	0.34	48.6	1.5	10.86	0.36	85.2	2.2	51.4	1.4	7.96	0.24	90.5	2.1	14.88	0.36	89	2.4	21.03	0.46	61.2	1.4	8.66	0.23	55.4	1.2	8.58	0.19	2.78	0.11	4.59	0.13
FB8ap_31	356.7	3.5	268.8	3.4	318.9	4	7.74	0.22	57.97	0.86	16.64	0.34	132.2	1.9	55.6	1.1	16.32	0.28	66.35	0.95	9.18	0.16	55.3	0.84	11	0.2	29.69	0.44	3.715	0.082	22.89	0.52	3.535	0.094	0.474	0.028	4.474	0.09
FB8ap2_0	319.6	2.6	469	4.8	207.6	2.4	95.45	0.99	355.3	2.7	64.78	0.92	419.3	4.8	114.5	1.6	12.01	0.26	101.2	1.2	9.83	0.16	46.48	0.61	7.83	0.15	18.46	0.35	2.219	0.077	13.09	0.28	1.933	0.054	0.232	0.017	4.91	0.21
FB8ap2_1	149.4	2.7	559.5	8.7	252.1	4.8	2.17	0.15	16.58	0.38	5.82	0.19	64	1.7	47.6	1.2	18.65	0.28	79.2	1.4	10.66	0.23	61.4	1.2	9.61	0.18	17.35	0.36	1.6	0.066	6.51	0.33	0.671	0.044	0.188	0.016	4.533	0.086
FB8ap2_2	240.5	1.8	1764	14	376.6	6.9	32.52	0.84	196.8	4.5	47.9	1.1	342.7	7.7	116.2	2.1	16.68	0.31	104.9	2.3	12.8	0.29	71.2	1.4	12.87	0.27	33.65	0.69	4.61	0.12	28.23	0.55	4.33	0.11	1.47	0.049	2.792	0.069
FB8ap2_3	413.2	3.2	661.4	7	189.9	3.5	20.66	0.48	78.2	1.7	15.33	0.44	102.7	2.7	32.94	0.66	8.17	0.21	39.66	0.97	4.98	0.12	28.97	0.67	6.16	0.16	17.05	0.4	2.204	0.072	14.42	0.39	2.569	0.078	1.838	0.074	1.853	0.055
FB8ap2_4	319.4	2.7	475.1	4.8	725.2	8.9	5.98	0.19	24.55	0.4	5.6	0.14	42.3	1.1	24.72	0.65	5.86	0.18	56.3	0.79	10.68	0.15	89	1.1	24.1	0.36	84.79	0.91	13.82	0.18	99.85	0.96	18.16	0.21	18.7	0.2	14.3	0.16
FB8ap2_5	198.2	1.6	772.5	6	512.7	4.8	194.80	2.10	660.6	6.6	110.8	1	688.4	5.5	152.1	1.7	33.73	0.37	138.6	1.5	16.79	0.22	93.6	1	17.55	0.19	44.97	0.54	5.785	0.092	34.83	0.52	5.3	0.1	12.96	0.15	24.4	0.19
FB8ap2_6	315.2	2.6	580.9	5.1	369	18	5.61	0.50	24.3	2	5.52	0.45	41.1	3.1	21.44	1.5	3.53	0.27	40.1	2.3	7.38	0.42	55.2	3.3	13.2	0.63	40.7	1.9	5.17	0.23	31.3	1.6	4.59	0.2	0.527	0.039	0.266	0.066
FB8ap2_7	341.1	2.8	1335	12	265	3.5	8.79	0.27	68	1.1	22.61	0.43	202.6	2.4	87.4	1.4	11.53	0.19	59.7	1	9.82	0.17	59.7	1	8.88	0.17	21.43	0.37	2.322	0.076	12.33	0.31	1.625	0.059	0.0334	0.0075	0.663	0.022
FB8ap2_8	229.8	1.7	693.4	4.4	121.1	1.1	1.72	0.09	8.45	0.18	2.059	0.086	18.03	0.6	9.09	0.28	3.66	0.11	16.12	0.44	2.356	0.063	16.74	0.35	4.006	0.088	12.17	0.26	1.861	0.049	13.11	0.3	2.244	0.066	1.371	0.041	2.999	0.054
FB8ap2_9	307	2	362.8	3.6	673.7	8.7	4.93	0.16	16.47	0.37	3.72	0.14	26.34	0.85	16.68	0.5	3.82	0.12	39.19	0.88	9.7	0.2	88.7	1.4	22.71	0.4	73.7	1.3	10.64	0.2	64.06	0.99	9.17	0.15	2.173	0.06	4.128	0.073
FB8ap2_10	462.4	4.6	841.8	8.1	231.9	7.7	36.90	1.90	138.4	8.8	27.7	1.5	168.4	9.1	44.6	2.1	10.74	0.46	45.6	2	5.66	0.23	35.6	1.4	7.56	0.27	22.3	0.74	3.12	0.11	20.81	0.75	3.65	0.12	2.32	0.13	1.215	0.063
FB8ap2_11	493.6	3.7	238	2.2	1540	17	7.72	0.20	46.36	0.61	12.99	0.28	131.4	2.1	106.4	1.5	13.87	0.2	216.7	2.2	38.84	0.39	275.4	2.4	58.47	0.52	165	1.5	22.34	0.21	133.9	1.3	18.84	0.21	0.075	0.0078	5.123	0.052

S2.3 apatite trace-element data (continued)

	55Mn	±	86Sr	±	89Y	±	139La	±	140Ce	±	141Pr	±	146Nd	±	147Sm	±	153Eu	±	157Gd	±	159Tb	±	163Dy	±	165Ho	±	166Er	±	169Tm	±	172Yb	±	175Lu	±	232Th	±	238U	±
FB8sap2_12	375.1	2.9	381.1	3.6	100.5	1.2	18.14	0.38	73.44	0.99	14.2	0.29	94.6	1.5	24.59	0.61	3.74	0.13	30.18	0.68	3.37	0.087	18.98	0.42	3.816	0.092	9.44	0.25	1.118	0.046	6.4	0.23	1.091	0.049	0.0068	0.0023	0.458	0.017
FB8sap2_13	167.6	1.4	459.9	3.8	325.5	3.4	20.70	2.40	44.8	4.1	7.96	0.55	47.6	2	26.83	0.59	11.11	0.23	55.45	0.77	9.08	0.11	59.88	0.8	12.03	0.15	31.35	0.45	3.833	0.077	21.02	0.4	3.06	0.068	0.934	0.041	3.833	0.062
FB8sap2_14	298	3.1	450.2	5.2	68.26	0.94	9.14	0.26	49.28	0.94	11.92	0.24	90	1.7	25.02	0.76	7.57	0.21	27.19	0.62	2.963	0.077	14.19	0.36	2.491	0.087	6.06	0.23	0.701	0.034	4.25	0.22	0.73	0.035	0.0087	0.0034	0.323	0.015
FB8sap2_15	291.2	2.4	321.7	3.3	128.3	1.5	3.30	0.15	17.25	0.42	4.56	0.15	42.9	1.1	23.14	0.44	4.09	0.11	32.3	0.72	3.818	0.09	21.1	0.45	4.23	0.11	12.17	0.28	1.9	0.057	13.53	0.37	2.672	0.057	0.281	0.019	4.957	0.089
FB8sap2_16	309.2	2.7	566	6.8	48.82	0.83	13.00	2.30	40.1	4.7	6.46	0.53	38.8	2.2	12.38	0.68	2.46	0.11	15.66	0.56	1.801	0.071	10.04	0.31	1.757	0.075	4.08	0.14	0.488	0.036	2.56	0.17	0.431	0.035	0.071	0.029	0.288	0.022
FB8sap2_17	264.3	2.2	364.5	2.7	490.8	4.3	24.47	0.36	120.9	1.2	28.16	0.39	220	3.1	98.1	1.1	18.39	0.24	129.7	1.3	17.57	0.2	98.2	0.79	17.71	0.18	43.72	0.44	5.118	0.086	28.29	0.48	4.197	0.079	0.152	0.011	6.747	0.065
FB8sap2_18	283	2.6	174.7	2.1	632.7	5.7	2.30	0.12	10.78	0.27	2.93	0.12	29.72	0.71	27.53	0.63	6.31	0.16	74.8	1	16.31	0.2	125	1.3	25.06	0.27	63.06	0.68	7.58	0.1	43.08	0.65	5.652	0.097	0.016	0.0036	1.19	0.22
FB8sap2_19	147.2	1.4	499.8	4.8	515.9	4.5	69.49	0.84	267.7	2.5	48.58	0.55	294.1	3.5	85.8	1	21.6	0.31	102.6	1.4	13.77	0.19	85.6	0.79	17.98	0.2	49.98	0.5	6.61	0.11	41.41	0.57	7.01	0.1	3.17	0.059	2.338	0.031
FB8sap2_20	395.7	2.6	415.7	2.6	905	14	9.80	0.36	51.2	1.6	11.5	0.35	87.3	2.5	52.7	1.4	7.42	0.19	111.3	2.2	20.59	0.36	162.4	2.5	33.81	0.53	92.7	1.4	11.13	0.19	59.8	1.1	8.25	0.14	0.134	0.013	1.367	0.024
FB8sap2_21	418.8	3.1	541.1	3.8	90	1.1	9.20	1.20	10.6	2.2	1.89	0.24	6.91	0.78	1.58	0.15	0.208	0.025	3.56	0.19	0.825	0.034	8.98	0.21	2.977	0.06	12.25	0.24	2.197	0.062	16.56	0.3	3.03	0.069	5.08	0.29	1.064	0.025
FB8sap2_22	372	3.1	1019.5	7.6	377.2	3.2	11.25	0.21	101.84	0.96	32.83	0.44	279.9	3.4	107.7	1.2	26.79	0.35	111.5	1.1	13.96	0.17	77.32	0.72	13.39	0.18	32.63	0.37	2.763	0.087	21.41	0.35	2.79	0.074	0.184	0.013	1.859	0.03
FB8sap2_23	400.3	3.7	792.1	7.6	1138	14	11.52	0.27	54.21	0.85	11.32	0.24	84.1	1.6	49.42	0.81	7.6	0.15	110.5	1.6	22.63	0.22	182.9	2.2	43.03	0.48	124.9	1.5	16.31	0.24	88.62	0.98	12.27	0.2	32.15	0.54	3.054	0.044
FB8sap2_24	241	2.4	375.1	3.4	77.2	1	19.98	0.40	50.09	0.72	11.08	0.24	74.7	1.4	25.57	0.58	6.696	0.099	33.12	0.66	3.707	0.08	19.58	0.42	3.339	0.076	6.69	0.14	0.607	0.029	2.16	0.12	0.261	0.021	0.148	0.012	2.003	0.062
FB8sap2_25	501.3	4	364.1	3.2	910	11	3.42	0.29	10.37	0.37	1.937	0.096	12.83	0.73	6.91	0.28	2.598	0.09	20.32	0.51	5.351	0.087	68.95	0.74	28.75	0.37	147.9	1.8	29.49	2.9	40.26	0.51	0.563	0.022	2.06	0.041
FB8sap2_26	307.3	2.5	278.6	3.1	460.8	5	3.26	0.14	1.8	0.11	0.866	0.07	5.71	0.36	5.41	0.28	0.781	0.048	24.23	0.54	5.87	0.1	56.65	0.79	15.41	0.19	48.92	0.68	6.78	0.12	39.93	0.64	5.77	0.1	0.0069	0.0028	0.408	0.012
FB8sap2_27	759.7	5.1	401	3	990	12	4.44	0.16	15.68	0.33	4.9	0.12	49.9	1.1	60.61	0.86	8.2	0.16	167.3	1.7	29.37	0.27	196.8	2.1	39.69	0.43	99.8	1	11.51	0.15	60.27	0.79	8.08	0.12	0.42	0.019	10.98	0.14
FB8sap2_28	87	1.2	986.8	8.5	494.1	5.1	52.99	0.67	349	3.5	90.27	0.86	658.1	6.4	214	2.4	44.41	0.47	200.5	2.1	22.82	0.23	113.3	1.4	17.48	0.19	37.93	0.49	4.217	0.075	23.2	0.45	3.008	0.075	0.0931	0.0096	2.505	0.046
FB8sap2_29	237.2	2	514.3	4.5	428.5	4.9	12.26	0.37	42.17	0.96	7.72	0.2	54.3	1.1	26.52	0.7	7.84	0.17	52.55	0.79	8.91	0.13	64.99	0.78	15.19	0.14	45.35	0.62	6.582	0.094	42.79	0.61	7.01	0.11	41.13	0.49	12.38	0.12
FB8sap2_30	348.3	2.3	368.8	3	537	5.2	2.99	0.11	14.68	0.33	3.69	0.14	34.76	0.81	23.08	0.6	7.73	0.15	47.38	0.84	8.41	0.11	64.57	0.72	16.89	0.17	59.06	0.61	9.52	0.11	69.69	0.83	13.35	0.19	0.0945	0.0085	5.222	0.069
FB8sap2_31	1303	10	267.9	2.6	52.37	2.6	0.64	279.1	2.4	62.1	0.63	419	4.9	117.7	1.5	24.67	0.31	104.7	1.3	11.56	0.18	58.91	0.74	9.71	0.15	21.55	0.37	2.138	0.061	10.18	0.31	1.233	0.035	0.0368	0.0058	1.404	0.026
FB8sap2_32	219.1	2.1	411	4.2	168.1	2.1	1.61	0.10	5.97	0.17	1.13	0.061	8.01	0.43	3.81	0.19	0.965	0.05	9.73	0.33	2.006	0.064	17.59	0.36	4.84	0.11	15.45	0.26	2.108	0.06	13.04	0.31	2.388	0.067	0.0083	0.0025	0.0673	0.0047
FB8sap2_33	85.7	2	318.5	3.6	68.28	0.96	6.90	0.33	22.94	0.76	3.8	0.11	22.03	0.87	8.07	0.35	2.588	0.091	12.3	0.35	1.813	0.05	12.34	0.3	2.254	0.058	5.23	0.18	0.463	0.027	3.26	0.18	0.223	0.018	1.69	0.15	0.189	0.011
FB8sap2_34	352.4	2.9	622.4	5.3	266.5	7.1	3.06	0.20	13.02	0.51	3.09	0.16	26.8	1	17.11	0.67	4.53	0.21	34	1	5.5	0.17	38.24	0.99	8.62	0.23	24.98	0.73	3.38	0.1	20.96	0.65	3.51	0.11	5.15	0.21	2.471	0.083
FB8sap2_36	281	1.5	1414	13	318.9	3.3	58.54	0.86	437.5	4.7	108.7	1.1	728.6	8.6	173.1	1.9	47.81	0.61	131.4	1.4	14.19	0.2	70.54	0.81	11.4	0.19	24.98	0.69	2.881	0.07	15.37	0.3	2.125	0.054	0.803	0.026	5.318	0.08
FB8sap2_37	264.9	2.7	423.2	4.3	1340	17	42.54	0.60	168.9	2	32.78	0.45	223.1	2.7	106.8	1.4	18.16	0.3	187.3	2.2	34.26	0.36	252.9	3.3	54.87	0.69	152	2.1	19.49	0.35	116.8	1.9	15.65	0.27	1.49	0.041	10.82	0.21
FB8sap2_38	165.3	1.5	717	12	515.3	5.4	4.71	0.15	45.38	0.71	15.84	0.35	163.1	2.6	84.3	1.3	14.52	0.26	118.5	1.6	15.83	0.24	95.9	1.3	18.81	0.25	49.75	0.69	6.25	0.12	36.55	0.6	5.341	0.099	0.538	0.024	1.686	0.038
FB8sap2_39	230.9	2.4	1043	10	637.2	9.1	48.20	1.00	132.7	2	22.48	0.39	116.4	1.9	30.77	0.53	9.58	0.21	32.61	0.57	4.66	0.11	28.14	0.67	5.21	0.13	12.56	0.34	1.511	0.065	8.69	0.3	1.063	0.04	4.773	0.095	9.59	0.18
FB8sap2_40	328.3	3.1	641.4	7.2	54	2	0.72	0.09	2.97	0.4	0.554	0.057	6.83	0.45	2.15	0.22	0.687	0.072	4.45	0.32	0.861	0.063	6.83	0.35	1.733	0.079	6.05	0.28	0.912	0.043	6.47	0.27	1.077	0.05	0.288	0.037	0.354	0.02
FB8sap2_41	554.8	5.3	581.4	5.8	248	2.5	3.64	0.13	16.91	0.32	4.12	0.13	36.45	0.79	26.43	0.55	9.13	0.18	48.69	0.85	7.38	0.11	46.44	0.71	8.88	0.15	22.46	0.42	2.669	0.065	15.07	0.38	2.07	0.064	0.0119	0.0037	0.541	0.034
FB8sap2_42	313.5	2.5	651.1	5.6	225.2	2.5	1.24	0.08	8.82	0.21	2.98	0.1	32.99	0.79	23.86	0.58	9.81	0.2	42.31	0.67	6.26	0.1	40.93	0.68	8.45	0.14	22.47	0.48	2.83	0.068	16.69	0.35	2.568	0.059	0.347	0.018	0.858	0.17
FB8sap2_43	289.4	3	410	5.5	116.4	2	41.90	4.50	111	16	1.2	87.1	5.3	25.9	0.94	14.43	0.23	30.05	0.79	3.54	0.097	19.94	0.48	3.798	0.098	9.58	0.25	1.021	0.037	6.44	0.19	1.031	0.039	0.387	0.092	0.624	0.022
FB8sap2_44	210.6	3.3	440.3	5.5	72.2	1.3	7.95	0.34	29.13	0.68	4.94	0.16	29.34	0.96	8.08	0.38	2.48	0.1	11.06	0.42	1.451	0.053	9.99	0.32	2.39	0.07	7.43	0.18	1.021	0.051	7.34	0.29	1.385	0.057	0.193	0.016	0.442	0.02
FB8sap2_45	172.8	1.8	834.8	7.8	510.2	4.8	2.83	0.12	33.16	0.64	13.68	0.35	149.2	2.6	101.8	1.7	16.5	0.31	156	2.2	21.41	0.28	119	1.7	19.53	0.3	41.87	0.73	4.18	0.082	19.65	0.5	2.342	0.056	0.0081	0.0033	0.455	0.014
FB8sap2_46	267.7	2.2	1017.5	9.4	302.7	3	54.89	0.67	288	3.1	61.96	0.68	415.6	4.3	122.5	1.6	24.46	0.32	118.1	1.5	13.25	0.2	68.7	1	11.17	0.2	24.15	0.38	2.408	0.056	11.42	0.27	1.411	0.045	0.1339	0.0097	4.435	0.069
FB8sap2_47	461.3	4	1098	10	56.5	1.5	10.07	0.40	38.4	1.4	7.29	0.28	48.6	2	13.88	0.47	2.96	0.15	15.88	0.56	1.814	0.07	9.8	0.4	1.997	0.075	4.98	0.19	0.839	0.04	3.82	0.14	0.342	0.022	0.522	0.018
FB8sap2_48	182.8	2.4	871	17	482.1	7	31.69	0.63	223.6	3.3	62.03	0.98	471.2	6.5	161.9	2.4	41.66	0.58	154	2.2	18.72	0.26	103	1.5	17.61	0.33	42.08	0.79	5.01	0.1	27.34	0.62	3.61	0.1	0.222	0.015	3.864	0.091
FB8sap2_49	63.2	1.1	346.5	4.3	675	7.5	88.30	1.20	486.2	5.4	102.5	1.2	642.7	6.9	203.9	2.6	21.39	0.55	282.1	3.3	24.53	0.33	134	1.4	22.8	0.33	52.66	0.7	5.5	0.11	24.93	0.52	2.776	0.086	0.295	0.018	1.053	0.026
FB8sap2_50	341	4.2	363.4	4.4	843	13	19.24	0.39	147.3	1.9	43.79	0.87	328.7	4.3	193.1	2.4	30.9	0.62	282.1	3.3	52.82	0.77	305.7	3.5	41.68	0.57	115.1	1.6	14.89	0.24	94.3	1.4	12.37	0.25	0.378	0.029	0.0075	3.378	0.081
FB8sap2_51	225.4	2.6	728.9	7.8	8.7	0.26	0.17	0.16	0.207	0.03	0.043	0.013	0.248	0.072	0.118	0.041	0.033	0.0096	0.257	0.045	0.06	0.01	0.94	0.1	0.283	0.021	1.239	0.08	0.282	0.022	2.41	0.13	0.558	0.026	0.024	0.01	0.046	0.022
FB8sap2_52	170.3	1.9	550	5.5	54.67	0.74	7.40	0.24	19.17	0.34	2.772	0.079	17.02	0.67	4.4	0.2	0.855	0.044	6.26	0.24	0.901	0.043	7.32	0.16	1.811	0.053	5.85	0.16	0.76	0.033	4.73	0.2	0.735	0.028	0.372	0.017	0.1863	0.0096
FB8sap2_53	251.5	2.6	451.6	5	1033	14	48.10	0.58	314.5	3.6	80.06	0.9	617.5	7.1	262.4	2.4	16.34	0.2	297.5	3.4	39.2	0.5	228.1	2.6	40.9	0.52	100.8	1.3	11.88	0.19	64.9	1.2	8.28	0.17	18.69	0.3	11.6	0.22
FB8sap2_54	233.8	2.6	661.7	5.9	310	14	5.47	0.38	20.3	1.3	4.19	0.29	29	2.2	14.28	0.93	2.91	0.2	26.3	1.5	4.99	0.25	40.4	2.2	9.94	0.53	33.6	1.5	5.18	0.24	37.8	1.6	6.21	0.22	3.812	0.076	3.75	0.22
FB8sap2_55	379	12	398.4	4.6	63	1	2.34	0.13	8.37	0.28	1.576	0.076	10.61	0.6	4.85	0.26	0.93	0.062	7.84	0.29	1.388	0.051	9.93	0.3	2.16	0.075	5.83	0.21	0.686	0.037	4.12	0.2	0.535	0.031	0.0038	0.0019	0.0314	0.0036
FB8sap2_56	213.1	5.5	603	19	508	11	25.10	1.80	60.5	3.7	8.85	0.6	58.6	3.8	38.4	1.6	19.54	0.94	85.7	3.8	13.73	0.61	90.8	3.1	19.14	0.55	84	2.1	9.52	0.19	48.4	2.4	7.63	0.37	1.813	0.089	17.87	0.56
FB8sap2_57	316	2.4	377.1	4.2	914	12	15.80	2.50	52.1	1.7	10.72	0.31	76.1	1.9	50.11	0.9	8.34	0.2	128.4	1.8	25.87	0.33	188.8	2.6	34.88	0.5	84	1.5	9.52	0.19	68.4	1	5.49	0.15	0.621	0.053	3.064	0.081
FB8sap2_58	116.4	1.3	354.3	3.5	69.8	1.1	203.60	2.50	595.5	5.9	79.14	0.87	370.6	4.6	62.57	0.97	6.77	0.15	47.52	0.69	4.269	0.082	18.23	0.28	2.581	0.075	5.35	0.15	0.53	0.027	2.58	0.13	0.332	0.022	0.273	0.018	1.59	0.046
FB8sap2_59	296.6	3.6	195.8	2.6	171.7	3.2	48.20	1.00	132.7	2	22.48	0.39	116.4	1.9	30.77	0.53	9.58	0.21	32.61	0.57	4.66	0.11	28.14	0.67	5.21	0.13	12.56	0.34	1.511	0.065	8.69	0.3	1.063	0.04	4.773	0.095	9.59	0.18
FB8sap2_60	152	2.2	224	2.5	753	11	22.92	0.42	133	2.1	35.27	0.55	291.2	4.4	188.4	2.6	22.14	0.36	311.9	4	52.86	0.54	269.2	3.8	30.73	0.41	41.19	0.59	2.529	0.06	8.05	0.26	0.66	0.03	0.099	0.056	10.17	0.24
FB8sap2_61	130.4	2.7	236.9	3.2	349.4	4.2	99.00	1.80	598.7	8.9	124.3	1.9	752.8	9.6	221	2.8	37.32	0.46	200.3	2.7	20.93	0.3	93.7	1.4	11.98	0.22	21.52	0.44	2.037	0.053	9.03	0.28	1.016	0.037	5.01	0.15	13.16	0.32
FB8sap2_62	281.9	5.8	823	12	212.2	4.2	12.72	0.56	62.2	1.3	16.31	0.38	140.2	2.9	69.2	1.8	15.73	0.33	74.7	1.5	8.65	0.21	44.9	1.2	7.36	0.22	17.47	0.51	1.94	0.11	9.73	0.41	1.267	0.05	0.496	0.028	1.914	0.068
FB8sap2_63	263.4	2.3	1614	15	476.1	4.8	283.70	2.80	1083	14	201.9	2.1	1073.3	9.8	228.3	2.7	53.92	0.56	173.8	2.1	19.66	0.23	104.2	1.3	17.37	0.23	42.03	0.62	5.045	0.098	28.67	0.62	3.843	0.08	12.1	0.2	11.19	0.19
FB8sap2_64	292.5	2.2	337.8	3.6	161	2.1	2.37	0.12	11.21	0.21	2.669	0.089	21.79	0.61	11.54	0.4	1.967	0.073	21.69	0.53	3.499	0.083	24.78	0.42	5.62	0.11	16.22	0.31	2.148	0.05	13.36	0.28	2.278	0.059	0.0365	0.0056	0.983	0.052
FB8sap2_65	167.8	4.3	460	18	731	12	97.30	6.50	222.2	5.5	53.6	1.3	339.1	5.3	199.8	2.5	28.43	0.47	337	3.7	56.36	0.61	272.8	3.2	28.78	0.35	35.95	0.62	2.454	0.064	10.98	0.34	1.218	0.039	0.08	0.01	13.02	0.21
FB8sap2_66	383.6	3.8	626.3	6.8	930	12	36.40	1.40	149.3	5.7	28.4	1	186.1	7.6	65.5	2.3	19	0.74	80.2	2.8	10.48	0.36	62.8	2.2	12.75	0.43	36.8	1.3	5.01	0.2	32.5	1.1	5.75	0.2	8.03	0.36	4.54	0.19
FB8sap2_67	285.7	2.3	514.5	6	121.9	2	3.16	0.13	9.26	0.2	1.537	0.071	10.11	0.48	4.45	0.23	1.602	0.065	11.4	0.39	2.22	0.062	17.97	0.44	4.25	0.1	12.34	0.28	1.703	0.054	10.26	0.25	1.561	0.053	0.0927	0.009	1.24	0.35
FB8sap2_68	324.5	5.6	775	14	781	15	26.51	0.93	106.8	3.9	21.56	0.73	149.5	5.2	68.3	2.1	16.42	0.54	115.8	2.7	18.57	0.47	134.9	3	30.08	0.61	90.3	1.8	13.6	0.33	88.7	1.9	14.18	0.34	7.29	0.2	22.08	0.62
FB8sap2_69	607.7	6.8	346.8	5.6	1385	23	75.40	1.40	270.6	4.7	49.62	0.78	309.8	7.8	141.6	2.3	14.39	0.33	224.4	4.2	40.33	0.69	276.3	4.3	57.39	0.84	162.5	2.8	22.7	0.45	142.5	3	19.06	0.45	0.985	0.056	21.01	0.36
FB8sap2_70	335.8	4.4	767.7	7.5	376.5	4.3	24.20	4.90	83	12	14.7	1.3	93.1	4.8	43	1.1	8.71	0.24	65.2	1.2	9.68	0.16	62.8	1	12.76	0.24	35.5	0.62	4.53	0.12	26.66	0.46	4.17	4	29.6	11.41	0.35
FB8sap2_71	418.3	3.6	564.3	4.9	150.3	2	107.60	1.60	363.3	4.6	57.74	0.84	311.5	3.9	65.2	1.2	10.96	0.21	59.21	0.95	20.98	0.3	81.3	1.2	10.65	0.16	63.28	0.9	12.8	0.21	102.5	1.4	14.35	0.22	1.071	0.044	0.08	0.11	0.1
FB8sap2_72	602.4	8.5	420.1	5.8	767	18	10.58	0.53	46.3	1.3	10.81	0.32	96.1	2.9	66.3	1.6	23.96	0.66	136.3	2.4	21.61	0.43	146.7	3.3	30.82	0.7	81.5	2	9.78	0.24	53.8	1.5	7.74	0.22	1.849	0.072	9.72	0.27
FB8sap2_73	343.9	3.9	773.5	8.2	368.2	4	24.05	0.47	87.3	1.2	20.27	0.4	146	2.2	59.21	0.95	20.98	0.3	81.3	1.2	10.65	0.16	63.28	0.9	12.8	0.21	34.95	0.6	4.71	0.11	28.35	0.6	4.21	0.11	0.662	0.029	3.73	0.19
FB8sap2_74	149.7	1.9	1222	12	183.3	2.3	27.62	0.42	168.3	2.3	46.34	0.74	329.5	5.6	94.1	1.4	22.81	0.36	81.7	1.2	8.94	0.13	43.82	0.78	6.96	0.13	14.81	0.3	1.496	0.044	7.28	0.23	0.936	0.039	0.108	0.011	2.008	0.049
FB8sap2_75	141.6	3	589	12	141.6	3	24.44	0.67	129.8	3.1	30.86	0.74	243.7	6.5	113.3	2.7	26.93	0.75	160	2.7	20.72	0.5	125.4	2.4	22.49	0.55	52.8	1.4	5.87	0.22	32.8	1.3	4.58	0.16	2.57	0.12	2.9	0.13
FB8sap2_76	518	5.1	218	3	673	11	2.34	0.10	10.4	0.28	2	0.1	13.54	0.56	7.22	0.29	1.71	0.072	23.82	0.84	6.704	0.29	75.8	1.1	23.47	0.34	82.1	1	11.32	0.12	63.13	0.82	7.81	0.14	0.14	0.013	0.916	0.023
FB8sap2_77	209.4	2.2	828	8.1	538.9	6.8	69.71	0.91	375.8	4.2	84.5	1.1	574.3	7.8	170.2	2.4	30.45	0.4	161.7	2.4	19.78	0.29	110.6	1.6	19.53	0.29	47.38	0.75	5.7	0.12	30.84	0.61	3.863	0.081	0.491	0.019	2.426	0.07
FB8sap2_78	813.1	9.2	321.6	4.7	957	22	4.18	0.20	26.38	0.53	7.57	0.24	84.6	2.7	73	2	27	0.42	159.4	3	26.61	0.58	184.5	3.6	39.76	0.81	118	2.4	16.31	0.38	104.1	2.3	16.21	0.39	0.629	0.034	2.887	0.082

S2.3 apatite trace-element data (continued)

	55Mn	±	86Sr	±	89Y	±	139La	±	140Ce	±	141Pr	±	146Nd	±	147Sm	±	153Eu	±	157Gd	±	159Tb	±	163Dy	±	165Ho	±	166Er	±	169Tm	±	172Yb	±	175Lu	±	232Th	±	238U	±
FB8ap2_79	464	5.4	286	17	780	11	10.28	0.29	41.42	0.63	8.89	0.22	66.8	1.3	35.42	0.79	6.28	0.15	76.1	1.5	14.27	0.23	116.5	1.5	29.48	0.41	102	1.8	17.05	0.31	121.1	2.8	18.5	0.46	0.394	0.018	5.16	0.17
FB8ap2_80	289.3	3.3	336.3	3.2	201.6	2.6	15.86	0.41	71.89	0.94	16.17	0.29	118.9	2.1	50.06	0.9	14.12	0.22	63.51	0.98	7.83	0.11	41.87	0.54	7.31	0.11	17.08	0.31	1.991	0.069	10.74	0.26	1.505	0.055	1.089	0.037	3.9	0.2
FB8ap2_81	334.8	3	1124.2	7.6	664.5	6.2	24.70	0.43	236.5	3.1	71.42	0.78	669.9	6.2	203	2.2	49.26	0.56	188.1	2.1	23.16	0.27	123.5	1.7	20.12	0.28	46.43	0.78	5.342	0.094	27.13	0.47	3.413	0.066	0.45	0.021	4.896	0.08
FB8ap2_82	335.9	3.7	281.9	3.7	260.6	3.6	5.13	0.28	17.47	0.49	3.74	0.13	29.14	0.43	14.58	0.43	3.28	0.11	26.94	0.69	4.686	0.096	35.75	0.62	8.67	0.16	28.56	0.53	4.276	0.098	28.76	0.61	5.1	0.1	0.304	0.02	12.35	0.22
FB8ap2_83	343.3	3.4	766	12	516.7	6.2	1.61	0.10	8.12	0.23	2.29	0.14	22.55	0.72	15.69	0.55	2.98	0.11	40.4	0.78	7.73	0.13	67	1.1	18.79	0.25	68.88	0.96	10.59	0.15	68.5	1	11.76	0.19	0.196	0.015	4.597	0.082
FB8ap2_84	360.1	3.3	393.3	5	843	14	37.83	0.72	151.8	2	30.18	0.62	196.3	3.7	95.1	1.6	11.67	0.22	158.6	2.6	24.87	0.36	158.7	2.4	31.75	0.47	86.2	1.1	10.59	0.21	62.9	1.2	9.47	0.13	10.17	0.17	12.63	0.18
FB8ap2_85	390.4	3.1	317.7	2.9	608.6	6.1	2.93	0.12	16.02	0.3	4.12	0.12	39.24	0.9	27.51	0.55	3.75	0.12	64.7	1.1	11.64	0.15	87.1	1.1	21.65	0.28	71.51	0.96	11.47	0.16	74.67	0.87	11.22	0.18	0.341	0.021	3.522	0.068
FB8ap3_0	529.4	5.8	276.8	4.3	1017	14	65.50	1.30	247.4	4.1	46.2	0.89	305.5	5.8	127.3	1.8	18.15	0.37	185.4	2.6	32.55	0.38	217.1	2.2	40.79	0.37	104.9	1.3	12.73	0.21	70.2	0.96	8.44	0.17	0.796	0.056	4.961	0.08
FB8ap3_1	456.1	5.8	404.6	5.4	484	15	24.10	1.10	93.9	4.3	23.4	1.2	200	10	91.9	4.7	17.18	0.96	122.8	5.1	16.07	0.66	93.4	3.4	17.43	0.55	44.6	1.3	5.22	0.16	29	0.85	4.38	0.13	0.463	0.03	1.115	0.05
FB8ap3_2	213.4	2.6	680.6	8.8	57.03	0.9	12.84	0.34	45.9	0.81	8.82	0.23	53.5	1.4	16.63	0.45	3.92	0.13	17.83	0.48	2.134	0.071	11.05	0.29	1.94	0.069	4.68	0.22	0.518	0.036	2.96	0.16	0.422	0.027	0.084	0.012	0.394	0.015
FB8ap3_3	370.1	3.7	647.5	8.9	304.9	5.2	8.62	0.35	25.07	0.7	5.25	0.16	30.9	1.2	13.47	0.57	3.37	0.13	24.64	0.78	4.735	0.099	38.54	0.86	10	0.22	34.94	0.69	5.77	0.13	41.46	0.79	6.13	0.15	3.74	0.1	0.985	0.031
FB8ap3_4	497.3	4.7	671.8	6.5	52.82	0.77	28.24	0.46	89	1.5	16.66	0.33	97.9	1.8	23.22	0.59	6.14	0.17	20.59	0.52	1.988	0.059	9.86	0.29	1.848	0.056	4.37	0.14	0.563	0.031	3.28	0.18	0.603	0.033	0.251	0.016	0.361	0.013
FB8ap3_5	339	3.1	362.5	3.8	1777	29	54.50	4.70	197	10	35.8	1.3	230	5.3	107.1	2.9	25.98	0.68	194.5	4	37.38	0.8	280.5	4.6	61.95	0.94	185.6	2.7	25.76	0.36	167.3	2.3	26.44	0.34	1.91	0.12	5.52	0.1
FB8ap3_6	209.6	2.8	622	9.6	392.5	8.5	4.54	0.22	34	1.2	12.84	0.48	148.5	4.2	97.9	2.6	24.47	0.65	118.9	2.8	14.73	0.38	78.8	1.5	13.05	0.29	31.65	0.79	3.815	0.097	26.5	0.53	2.75	0.1	0.111	0.014	13.13	0.41
FB8ap3_7	500.5	7.4	429.9	7.3	1049	23	6.42	0.21	47.87	0.98	17.01	0.46	185.4	4	136.3	2.9	13.3	0.38	223.5	4.8	33.31	0.64	205.9	3.9	38.14	0.72	91	1.7	9.71	0.22	46.5	1	5.55	0.18	0.0197	0.0048	7.11	0.23
FB8ap3_8	364.2	4.7	349.2	6.5	82.1	1.7	8.31	0.31	25.07	0.68	4.5	0.15	27.07	0.86	10.06	0.39	1.648	0.073	14.31	0.44	2.028	0.065	12.54	0.31	2.679	0.071	7.3	0.21	0.931	0.043	5.04	0.16	0.808	0.039	0.234	0.0048	0.0296	0.0035
FB8ap3_9	304	5.4	631	11	142.3	3.5	6.36	0.27	24.62	0.76	5.4	0.2	38.4	1.2	17.32	0.64	5.78	0.17	24.99	0.65	3.461	0.08	21.86	0.51	4.75	0.11	13.83	0.36	1.8	0.067	11.54	0.36	2.122	0.084	0.166	0.017	3.67	0.12
FB8ap3_11	141.4	2.7	613.1	8.8	315.8	5.2	1.80	0.09	8.25	0.3	2.282	0.092	25.67	0.88	24.06	0.88	6.69	0.21	55.3	1.2	8.66	0.17	56.45	1.2	11.32	0.16	28.75	0.42	3.44	0.084	19.01	0.43	2.712	0.084	0.0485	0.0073	0.432	0.017
FB8ap3_12	288.5	3.6	1915	19	182.9	4.7	48.29	0.83	168.4	2.2	30.56	0.51	189.8	3	56.5	1.2	13.79	0.32	59.7	1.2	7.25	0.16	39.27	0.84	7	0.17	16.62	0.49	1.744	0.063	8.88	0.34	1.248	0.064	0.257	0.023	3.006	0.089
FB8ap3_13	284.6	4.1	820	16	238.9	4.3	13.87	0.35	70.4	1.5	18.62	0.43	160.7	4.3	76.9	1.8	17.72	0.47	83.5	1.8	9.79	0.22	60.6	1.2	8.32	0.16	18.58	0.4	2.102	0.067	15.47	0.31	1.417	0.05	0.252	0.021	2.608	0.063
FB8ap3_14	456.8	8.7	500.5	7.7	910	23	4.92	0.20	19.49	0.74	3.58	0.18	23.45	0.95	6.75	0.39	1.23	0.072	8.92	0.43	1.124	0.052	7.42	0.27	1.596	0.053	4.36	0.14	0.525	0.031	3.39	0.17	0.623	0.03	0.029	0.0018	0.0543	0.0059
FB8ap3_15	282	4.2	1288	26	283.7	6.5	182.50	4.20	686	14	125.4	2.4	702	14	157.7	2.7	36.84	0.67	122.6	2.2	13.08	0.23	63.51	0.98	9.97	0.17	21.65	0.41	2.424	0.065	13.18	0.33	1.69	0.05	10.64	0.33	8.69	0.16
FB8ap3_16	497.1	6.4	420.6	7.2	664	11	7.99	0.19	39.61	0.78	9.53	0.22	84	1.8	57.5	1.1	19.68	0.36	113.9	2.1	17.7	0.32	117.4	1.6	25.33	0.33	65.56	0.82	7.82	0.17	41.7	0.82	5.521	0.103	1.354	0.051	7.26	0.14
FB8ap3_17	352.4	6.7	483.9	8.9	36.07	0.95	4.55	0.35	11.85	0.78	1.82	0.14	9.11	0.55	3.06	0.21	0.605	0.042	4.67	0.27	0.729	0.036	5.34	0.22	1.187	0.052	3.61	0.15	0.53	0.033	3.25	0.18	0.521	0.033	2.2	0.1042	11.71	0.21
FB8ap3_18	481.9	7.4	274.2	4.1	827	24	62.90	5.10	227	13	41	1.8	248.5	9.8	108	4.1	43.5	1.4	159.3	5.4	25	0.78	157.3	4.6	30.81	0.78	78.6	2	9.25	0.25	51.2	1.4	7.34	0.2	62	1.5	11.71	0.21
FB8ap3_19	410.6	4.3	631	6.6	53.1	1.3	0.40	0.05	1.8	0.11	0.355	0.034	2.63	0.26	1.54	0.15	0.212	0.033	3.74	0.22	0.713	0.034	6.21	0.3	1.738	0.06	6.02	0.22	0.924	0.043	6.65	0.26	1.168	0.047	0.952	0.062	0.292	0.021
FB8ap3_20	459.1	4.1	561	6.8	463	7.2	6.44	0.28	34.94	0.9	9.2	0.26	84.3	1.9	48.8	1.2	10.63	0.27	82.6	1.5	11.86	0.19	75.7	1.3	15.47	0.22	40.46	0.65	4.76	0.1	27.72	0.61	4.487	0.096	0.0333	0.0067	0.398	0.016
FB8ap3_21	279.4	3.2	595.1	8.2	664	10	15.19	0.35	65.9	1	13.96	0.36	99.9	2.1	48.2	1.2	9.11	0.25	82.8	1.7	14	0.22	102.7	1.9	23.24	0.34	69.2	1.1	9.22	0.16	54.7	1.1	8.52	0.17	1.073	0.046	1.903	0.039
FB8ap3_22	423.1	3.9	1128.9	9.6	762.5	9.3	207.30	2.60	963	10	191.7	2	1123	10	286	3.2	63.43	0.6	233.1	2.7	29.12	0.35	160.6	1.6	28.27	0.36	70.37	0.92	8.9	0.13	50.49	0.81	6.85	0.12	6.185	0.093	8.154	0.09
FB8ap3_23	609.7	4.6	175.4	2.3	1540	18	54.35	0.64	211.5	2.2	37.61	0.62	227.8	3.1	126.3	1.7	26.47	0.39	226.3	2.4	49.07	0.57	347.5	2.8	64.06	0.84	165.5	1.6	21.5	0.25	131.1	1.5	16.44	0.2	1.419	0.038	28.76	0.32
FB8ap3_24	446	5.3	293.7	4	848	18	2.42	0.11	10.96	0.37	2.57	0.099	22.86	0.96	13.71	0.58	3.247	0.099	39.51	0.98	8.91	0.17	92.1	1.3	28.79	0.54	112.6	2.4	18.75	0.48	126.4	3.2	17.66	0.47	0.266	0.028	7.19	0.21
FB8ap3_25	309.8	2.8	927.4	9.1	356.9	4.3	42.79	0.61	242.7	3.2	57.52	0.83	401.8	5.5	127.2	2	28.56	0.44	117.6	1.8	14.19	0.23	75.9	1.1	13.13	0.17	31.6	0.43	3.595	0.088	18.74	0.42	2.447	0.069	0.1087	0.0098	1.498	0.032
FB8ap3_26	426.9	4.2	1423	12	174.9	2.3	47.18	0.95	210.9	4.2	44.06	0.91	294.1	5.7	81.5	1.5	19.61	0.39	72.7	1.3	7.74	0.15	38.8	0.61	6.37	0.12	14.66	0.33	1.636	0.053	9	0.34	1.296	0.049	0.0734	0.0088	0.859	0.021
FB8ap3_27	248	4.8	694	12	7.42	0.36	1.03	0.13	2.41	0.25	0.278	0.038	1.81	0.24	0.65	0.1	0.187	0.025	1.07	0.12	0.153	0.019	1.047	0.098	0.234	0.023	0.776	0.059	0.122	0.016	0.82	0.1	0.152	0.017	0.077	0.012	0.0947	0.008
FB8ap3_28	408.1	7.5	1504	33	226.5	5.1	12.99	0.39	89.9	2	26.78	0.66	231.3	5.4	85.1	2	16.55	0.4	89.3	1.9	10.06	0.23	51.35	0.83	8.27	0.14	17.54	0.34	1.901	0.071	9.64	0.31	1.336	0.052	0.0468	0.009	0.553	0.021
FB8ap3_29	335.3	4	447	6.7	233.4	8.8	92.50	1.80	336.6	5.8	61.6	1.1	392.5	7.4	106.4	2.3	11.9	0.35	98.9	2.4	10.02	0.31	49	1.8	8.43	0.32	20.6	0.81	2.48	0.11	15.04	0.7	2.22	0.11	0.245	0.017	4.72	0.12
FB8ap3_30	163.2	1.8	560.6	5	238.5	2.6	1.65	0.08	12.15	0.25	4.41	0.14	49.8	1.1	38.76	0.65	15.68	0.28	67.6	1	10.03	0.15	55.88	0.83	8.94	0.16	16.54	0.34	1.517	0.061	5.93	0.2	0.528	0.028	0.172	0.011	4.072	0.083
FB8ap3_32	545	17	246.9	5.5	1525	42	5.45	0.28	29.7	1	7.69	0.29	79.5	2.9	69.5	2	10.44	0.29	168	3.9	31.98	0.79	238.6	4.6	51.92	0.93	150	3.1	20.47	0.48	125.1	3.3	16.87	0.44	0.127	0.02	3.71	0.11
FB8ap3_33	366.5	5.9	389.9	8.3	45.8	1.2	4.92	0.20	19.49	0.74	3.58	0.18	23.45	0.95	6.75	0.39	1.23	0.072	8.92	0.43	1.124	0.052	7.42	0.27	1.596	0.053	4.36	0.14	0.525	0.031	3.39	0.17	0.623	0.03	0.029	0.0018	0.0543	0.0059
FB8ap3_34	188.2	3.6	441.2	9.2	242.6	5.5	80.00	25.00	181	56	23.9	7.1	108	29	28.3	4.7	7.62	0.63	43.9	3	6.64	0.28	43.3	1.2	8.81	0.18	23.78	0.54	2.799	0.066	16.5	0.48	2.439	0.073	2.32	0.56	3.39	0.18
FB8ap3_35	122.2	4.1	344	13	310	15	80.60	3.60	448	20	99.3	4.7	638	28	211	8.5	36	1.4	203	7.7	21.94	0.76	94.7	3.1	11.09	0.44	17.24	0.65	1.287	0.061	4.82	0.28	0.465	0.037	0.4	0.03	4.42	0.21
FB8ap3_36	552.3	4.5	692.6	5.1	1234	19	52.41	0.72	332	3.4	90.6	1.2	756	10	316.8	3.7	44.84	0.73	361.2	4.8	45.54	0.5	245.1	3.2	41.48	0.57	98.8	1.5	11.83	0.19	67.8	1.1	9.44	0.18	1.351	0.044	8.59	0.13
FB8ap3_37	401.7	4.6	719.1	9.4	469.6	8.2	15.89	0.54	104.6	2.1	32.34	0.72	281.1	6.6	118	2.3	18.47	0.43	135.3	2.4	17.74	0.34	100.4	1.8	17.58	0.27	40.8	0.59	4.606	0.087	23.53	0.49	3.187	0.082	0.081	0.0084	1.262	0.031
FB8ap3_38	723.3	9.5	411.8	8	2187	49	24.65	0.64	93.4	2.1	18.19	0.45	126.4	2.9	64.7	1.4	12.97	0.31	129.1	2.3	26.67	0.45	245	3.4	72.88	0.97	301.2	4.1	57.1	1	451.2	8.5	70.9	1.4	1.504	0.051	10.77	0.24
FB8ap3_39	137	2	372.3	5.7	280.4	4.4	82.70	2.00	444.7	8.5	96.3	1.9	630	14	204.9	4.3	34.32	0.74	195.5	3.8	21.27	0.39	89.1	1.8	10.75	0.22	16.73	0.41	1.213	0.056	4.87	0.22	0.462	0.032	5	9.1	3.637	0.088
FB8ap3_40	446.2	4.9	1159	15	141.1	2.2	18.27	0.42	89.7	1.7	20.9	0.4	160.1	3.2	53.3	1.2	13.62	0.29	54.6	1.1	6.03	0.13	31.51	0.56	5.45	0.12	12.86	0.27	1.447	0.05	7.5	0.26	1.13	0.039	0.0728	0.0083	0.409	0.016
FB8ap3_41	145.1	2.8	659	14	91.8	6.1	16.10	1.30	70.1	5.5	14.4	1.2	97.1	7.8	34.5	2.7	9.58	0.83	36.1	2.4	3.71	0.24	18.8	1.3	3.1	0.21	7.5	0.67	0.88	0.077	4.84	0.39	0.814	0.071	1.3	0.12	5.81	0.39
FB8ap3_42	568.7	6.4	449.4	4.9	1329	21	11.99	0.33	69.3	1.6	18.24	0.52	168.6	4	114.9	2.8	29.16	0.55	206.3	4.1	34.62	0.68	232.8	3.9	48.74	0.76	134.7	2	17.12	0.28	105.4	1.8	15.64	0.33	1.287	0.06	3.923	0.087
FB8ap3_43	208.6	2.8	188.4	3.3	1489	56	52.50	1.90	292.2	9.8	65.2	2.1	454	19	254.2	9.2	41.1	1.3	382	13	7.12	2.9	435	19	65	2.5	121.4	4.7	10.1	0.51	36.3	1.8	3.21	0.2	3.05	0.24	72.7	5
FB8ap3_44	515.8	4.9	308	4.3	823	14	2.66	0.13	17.95	0.56	4.92	0.16	47.2	1.3	38.92	0.99	2.379	0.098	93.2	2.1	17.62	0.33	130.3	2.2	29.21	0.48	81.1	1.2	10.22	0.19	59	1.1	7.67	0.18	4.062	0.084	3.277	0.063
FB8ap3_45	365	6	501.1	9.8	239.7	5.8	5.13	0.18	26.96	0.7	6.72	0.21	59.3	1.7	26.29	0.78	9.79	0.27	43.2	1.2	6.18	0.14	39.59	0.88	8.67	0.21	23.71	0.51	3.061	0.097	19.58	0.52	3.54	0.11	1.601	0.078	7.06	0.19
FB8ap3_46	425.8	5.9	376	7.5	183.2	4.9	5.76	0.24	18.84	0.5	3.76	0.17	27.2	0.94	12.45	0.56	4.73	0.17	23.69	0.77	3.93	0.12	27.3	0.64	6.45	0.18	19.71	0.58	2.808	0.095	19.32	0.59	3.72	0.11	0.118	0.012	2.538	0.08
FB8ap3_47	294.4	4.8	252.9	4.9	862	17	1.30	0.08	6.26	0.25	1.421	0.082	11.74	0.58	10.67	0.41	2.42	0.1	35.09	0.93	10.45	0.21	105.6	1.3	28.24	0.36	89.2	1.3	12.94	0.22	79.3	1.4	10.8	0.24	0.044	0.0063	8.19	0.22
FB8ap3_48	262	3.3	406.1	4.1	295.2	3.9	13.37	0.49	47.23	0.87	8.53	0.32	57.7	1.9	27.39	0.95	5.74	0.24	45.5	1.2	7.29	0.15	49.7	1.1	10.45	0.21	28.9	0.52	3.821	0.079	23.54	0.69	3.6	0.11	0.308	0.028	1.053	0.036
FB8ap3_49	460	6	1234	16	109.5	4.2	7.20	0.28	28.85	0.84	6.07	0.21	45.9	1.6	19.05	0.75	6.84	0.23	27.5	1	3.55	0.12	20.42	0.75	3.99	0.14	10.59	0.45	1.262	0.066	7.6	0.34	1.231	0.065	0.22	0.017	4.1	0.16
FB8ap3_50	338.6	6.1	856	20	357.1	9.4	38.90	1.40	159.9	4.5	33.85	0.9	239.9	6	87.7	2.3	27.61	0.61	99.9	2.2	12.59	0.26	70.7	1.3	12.75	0.25	30.26	0.56	3.543	0.098	19.73	0.53	2.701	0.083	0.462	0.024	3.641	0.096
FB8ap3_51	218.7	4.1	734	25	129.8	4.4	3.14	0.19	16.49	0.6	5.42	0.2	50.7	2.1	27	1.2	8.38	0.3	37.3	1.1	4.88	0.15	27.53	0.68	4.83	0.14	10.71	0.32	1.163	0.067	6.25	0.29	0.824	0.046	0.0612	0.0093	1.56	0.073
FB8ap3_52	382.5	7.2	339	6.5	88.8	2	15.83	0.45	47.9	1.5	8.08	0.27	47.7	1.5	11.73	0.45	4.25	0.13	14.96	0.46	1.836	0.063	12.08	0.36	2.89	0.083	8.5	0.27	1.189	0.045	7.96	0.26	1.861	0.059	0.0424	0.0073	0.327	0.015
FB8ap3_53	304	4.4	876	12	510	12	17.84	0.35	162.1	2.6	48.44	0.93	403.1	7.4	162.8	2.7	35.62	0.63	155.4	3	19.58	0.41	105.5	2.1	18.72	0.39	44.26	0.91	5.16	0.13	29.01	0.78	3.7	0.12	0.0476	0.0086	1.56	0.043
FB8ap3_54	202.8	3.2	181.5	4.4	128.9	3.3	2.75	0.18	8.5	0.41	1.662	0.099	12.21	0.68	7.34	0.35	1.608	0.095	15.94	0.52	2.808	0.082	19.53	0.45	4.07	0.1	9.69	0.32	1.189	0.049	6.38	0.26	0.861	0.05	0.0082	0.0028	0.855	0.033
FB8ap3_55	681.2	6.7	153.1	2.4	1253	64	190.70	9.90	629	35	105	6.4	591	36	173	11	24.7	1.3	202	12	29.7	1.7	193	11	42.1	2.2	120.8	6.1	16.15	0.84	104.3	5.1	17.92	0.85	25.2	1	7.07	0.31
FB8ap3_56	239.6	3.8	503.9	9.9	585	14	23.20	0.51	93	2.2	19.15	0.5	133.1	3.3	62.1	1.4	17.66	0.48	96.6	2.5	15.52	0.37	98.1	2.2	20.7	0.44	56.6	1.3	7.5	0.2	47.2	1.3	7.55	0.24	21.85	0.75	20.12	0.62
FB10ap_0	198.4	2.1	1115	16	215.5	3.5	2.43	0.13	21.09	0.4	7.7	0.19	83.5	1.6	46	1	16.48	0.3	63.1	1	7.97	0.13	45.35	0.76	8.29	0.13	19.75	0.3	2.225	0.059	11.66	0.31	1.621	0.064	0.0439	0.0067	0.965	0.026

S2.3 apatite trace-element data (continued)

	55Mn	±	86Sr	±	89Y	±	139La	±	140Ce	±	141Pr	±	146Nd	±	147Sm	±	153Eu	±	157Gd	±	159Tb	±	163Dy	±	165Ho	±	166Er	±	169Tm	±	172Yb	±	175Lu	±	232Th	±	238U	±
FB10ap_1	237	4.4	211.6	6.5	1573	86	39.30	3.80	151	15	30.2	2.8	205	19	98.7	8.5	23.1	1.7	168	13	30.4	2.3	227	15	53	3	159.6	7	22.9	0.86	146.6	5	23.25	0.66	82	41	7.29	0.43
FB10ap_2	389.4	7.7	647	11	82.4	2.5	21.73	0.69	70.2	2.5	11.6	0.42	67.6	2.3	15.61	0.6	4.49	0.17	18.72	0.71	2.205	0.081	12.85	0.46	2.683	0.086	7.38	0.26	1.035	0.052	6.47	0.3	1.215	0.05	0.121	0.014	0.922	0.026
FB10ap_4	558.6	6.9	1962	32	1450	28	85.80	1.70	351.1	6.7	68.3	1.5	463.4	8.5	187	3.3	28.29	0.58	264.4	3.5	43.82	0.63	290.4	3.6	57.58	0.6	149.6	1.7	20.04	0.32	111.1	1.6	13.46	0.23	3.493	0.069	10.95	0.22
FB10ap_5	622.5	6	326.2	5.6	292	4.9	766.00	19.00	1405	32	163.7	3.6	583	13	80.8	1.8	15.35	0.33	66.7	1.4	7.44	0.15	43.42	0.71	9.23	0.16	25.55	0.46	3.563	0.092	21.82	0.52	3.87	0.11	26.4	1.2	17.33	0.47
FB10ap_6	274	3.4	74	1.5	868	19	3.87	0.14	16.69	0.41	3.46	0.13	26.76	0.93	20.76	0.67	12.65	0.28	66	1.5	14.86	0.28	129	2.2	32.88	0.58	97.6	1.8	12.55	0.29	68.3	1.5	10.44	0.19	0.0989	0.0093	2.531	0.065
FB10ap_7	263.8	3.8	416.7	9.5	14.9	0.48	0.47	0.05	1.38	0.086	0.275	0.036	1.93	0.22	0.84	0.11	0.828	0.058	1.6	0.13	0.254	0.022	2.19	0.12	0.629	0.035	2	0.1	0.309	0.021	2.44	0.13	0.472	0.029	0.0017	0.0012	0.0217	0.0029
FB10ap_8	234	2.8	357.5	4.9	1187	20	1390.00	23.00	3601	52	528.4	6.6	2431	34	468.1	6.9	27.21	0.4	377.5	5.4	46.22	0.54	261.1	3.2	46.54	0.6	111.8	1.3	13.52	0.23	68.5	1.2	8.42	0.16	29.28	0.51	7.66	0.13
FB10ap_9	380.9	5.8	321.5	5.8	1579	47	25.38	0.68	98.1	2.8	20.17	0.68	156.5	4.5	75.6	2.3	14.59	0.44	144.8	4	27	0.66	228	5.7	61.1	1.4	198.6	5	29.39	0.78	177.6	4.6	24.98	0.72	1.175	0.066	6.55	0.39
FB10ap_10	243.8	2.3	447.7	5.6	31.27	0.57	9.22	0.21	32.2	0.67	5.78	0.16	37.2	1	9.68	0.46	2.76	0.1	10.7	0.35	1.07	0.04	5.38	0.21	1.071	0.044	2.83	0.12	0.326	0.021	2.22	0.13	0.412	0.0048	0.344	0.015
FB10ap_11	991	16	556	11	1543	42	139.60	4.70	505	12	89.7	1.9	533	11	208.5	3.8	24.37	0.43	248.4	4.4	43.09	0.69	300.5	3.9	58.64	0.82	154.8	2.6	21.5	0.46	124.4	2.6	14.5	0.36	2.43	0.28	10.14	0.24
FB10ap_12	390.5	4.9	545.8	7.7	448	9	95.90	6.90	345	28	60.3	4.6	352	28	89.8	6.5	19.6	1.5	93.3	6.8	11.66	0.84	70.7	5	15	1	43.4	3	6.4	0.43	42.2	3	7.44	0.53	6.93	0.65	2.11	0.13
FB10ap_13	281.9	3.1	197.2	3.4	140.7	2.6	3.06	0.12	12.09	0.33	2.37	0.1	16.04	0.57	8.37	0.31	2.126	0.096	15.45	0.44	2.825	0.072	20.41	0.4	4.55	0.11	12.78	0.24	1.816	0.06	11.44	0.33	1.96	0.057	0.836	0.03	3.1	0.068
FB10ap_14	413	46	582	8.4	134.6	2	6.57	0.72	19.4	1.3	3.28	0.13	20.84	0.86	10.01	0.45	4.7	0.15	19.13	0.6	3.306	0.08	22.82	0.45	4.841	0.091	12.81	0.23	1.646	0.054	9.39	0.34	1.396	0.058	0.45	0.11	1.503	0.062
FB10ap_15	438.9	4.7	69	1.2	1872	30	81.90	1.20	409.9	5.8	94.2	1.5	704.6	9.5	304.5	4.4	29.21	0.45	429.3	5.6	66.72	0.86	420.5	4.6	76.81	0.83	174.3	2.3	19.63	0.27	97.2	1.4	11.89	0.26	3.495	0.088	4.347	0.057
FB10ap_16	686.8	8.6	224.6	4.5	1127	36	11.27	0.42	41.4	1.5	8.49	0.34	72.5	3.3	45.9	1.9	9.49	0.35	111.8	4.4	25.52	0.96	203.1	7.4	44	1.5	125.1	4.2	17.95	0.64	111.1	4.3	15.34	0.56	1.3	0.11	5.73	0.53
FB10ap_17	161.8	1.8	260.4	4.2	1086	17	12.89	0.41	57.9	1.4	12.71	0.38	97.9	2.7	55.8	1.5	11.57	0.25	132	2.2	27.44	0.44	206.6	2.7	40.46	0.41	90.22	0.97	9.08	0.17	39.1	0.72	4.36	0.1	0.246	0.023	9.22	0.17
FB10ap_18	441.5	7.5	611	17	646	21	1629.00	60.00	3020	110	337	12	1288	43	179.5	5.7	38.7	1.2	143.4	4	16.39	0.43	95.9	1.7	20.02	0.36	58.1	1.1	8.3	0.2	54.5	1.3	9.23	0.26	140.3	3.9	24.87	0.82
FB10ap_19	350.9	4.3	484.9	6.3	411.7	6.4	49.57	0.80	158.8	2.5	26.71	0.52	165.8	3.1	53.1	1.4	30.02	0.62	92.8	1.7	13.46	0.24	83.7	1.3	16.2	0.25	40.24	0.73	4.69	0.11	23.94	0.62	2.916	0.081	0.953	0.035	1.58	0.04
FB10ap_20	320.1	4.8	529.9	7.5	690	100	6.09	0.94	25.4	3.9	5.57	0.87	43.1	6.7	24.8	3.8	5.57	0.88	60.5	7.6	10.2	1.5	89	13	23.3	3.4	87	13	14.4	2.1	101	15	15.9	2.3	5.38	0.82	6.34	0.97
FB10ap_21	371.4	3.8	348.3	4.5	69.4	1.7	0.70	0.06	2.5	0.12	0.442	0.041	2.81	0.24	1.25	0.14	0.503	0.045	2.51	0.19	0.678	0.034	6.73	0.23	1.99	0.079	9.06	0.27	1.951	0.063	18.15	0.69	3.59	0.11	0.0193	0.0039	0.267	0.017
FB10ap_22	410.9	4.3	388.4	9	292	12	0.75	0.08	1.65	0.11	0.373	0.036	5.24	0.44	6.01	0.43	2.25	0.11	28.1	1.5	5.76	0.29	48	2.3	11.5	0.49	32.5	1.4	4.01	0.17	24.23	0.92	3.81	0.12	0.0033	0.0016	0.1051	0.0076
FB10ap_23	346.4	3.4	193.4	2.9	25.69	0.6	0.09	0.02	0.363	0.044	0.076	0.017	0.529	0.098	0.31	0.056	0.1	0.018	0.808	0.092	0.182	0.018	2.12	0.13	0.823	0.038	4.44	0.13	0.978	0.038	8.76	0.26	1.664	0.064	0.0051	0.0019	0.1093	0.0077
FB10ap_24	495.5	6.3	383.8	4.9	710	14	10.07	0.28	34.52	0.9	5.99	0.19	38.7	1.4	19.06	0.73	7.03	0.18	40.3	1.1	8.27	0.2	75	1.7	22.56	0.48	103.1	1.8	20.34	0.4	167.4	3.4	29.65	0.53	0.412	0.022	4.47	0.12
FB10ap_26	197.1	2.6	617.9	6.6	84.4	1.1	30.08	0.45	127	1.9	22.28	0.37	130.9	2.3	31.48	0.75	6.16	0.14	32.78	0.62	3.488	0.084	17.78	0.38	2.961	0.071	6.86	0.14	0.709	0.032	3.54	0.17	0.517	0.031	0.169	0.01	0.612	0.018
FB10ap_27	508.8	5	935	11	1124	16	239.50	3.10	689.2	8.3	111.3	1.4	660.7	9.3	213	2.5	63.56	0.86	269.1	3.5	41.87	0.54	253.4	3.4	43	0.51	107.8	1.4	13.93	0.23	79.3	1.4	9.67	0.16	3.395	0.074	1.254	0.025
FB10ap_28	207	4.4	246.9	6	1005	29	11.63	0.43	40.1	1.4	7.98	0.27	58.5	2.2	28.3	1	7	0.23	68.3	1.9	14.94	0.35	136	3.2	34.56	0.68	109.2	2.4	14.47	0.32	77.4	2.1	9.22	0.25	0.99	0.04	7.68	0.21
FB10ap_31	556.2	5.5	193.4	2.9	1990	29	9.40	1.60	163	4.9	27.43	0.88	161.3	4.4	45.6	1.1	9.56	0.24	50.3	1.1	6.32	0.13	38.13	0.67	7.26	0.13	20	0.43	2.527	0.066	15.21	0.33	2.462	0.067	11	17	0.274	0.015
FB10ap_32	476.8	8.3	534.4	7.8	213.4	3.8	47.20	1.60	163	4.9	27.43	0.88	161.3	4.4	45.6	1.1	9.56	0.24	50.3	1.1	6.32	0.13	38.13	0.67	7.26	0.13	20	0.43	2.527	0.066	15.21	0.33	2.462	0.067	11	17	0.274	0.015
FB10ap_33	318.5	3.2	504.4	7	78.1	1.6	4.57	0.17	17.78	0.39	3.47	0.11	25.61	0.86	11.47	0.42	4.33	0.13	17.53	0.58	2.299	0.069	14.09	0.43	2.83	0.08	7.94	0.24	1.082	0.042	7.1	0.25	1.216	0.045	0.064	0.0072	1.788	0.041
FB10ap_34	233	2.4	284.2	3.7	1079	14	8.66	0.23	34.18	0.63	6.5	0.19	50.3	1.1	30.17	0.55	10.92	0.2	82.3	1.4	21.01	0.27	188.9	2	39.26	0.36	95.5	1	11.06	0.18	56.89	0.94	6.57	0.13	0.53	0.03	6.51	0.27
FB10ap_35	374.5	3	778	10	21.98	0.6	7.15	0.26	34.76	0.96	6.53	0.2	42.8	1.4	9.26	0.35	1.896	0.096	8.35	0.38	0.812	0.04	3.9	0.18	0.727	0.037	1.817	0.089	0.207	0.017	1.127	0.082	0.179	0.017	0.047	0.008	0.0918	0.0075
FB10ap_36	285.1	3.6	391.9	4.4	107	3.6	32.10	0.92	104.6	2.8	17.37	0.55	109.8	4	36.7	1.3	6.71	0.27	45.7	1.4	5.06	0.17	25.03	0.89	4.05	0.14	8.66	0.35	0.814	0.041	3.41	0.15	0.446	0.029	0.206	0.017	3.51	0.13
FB10ap_37	230.6	3.4	290	13	1027	74	427.00	23.00	1266	74	205	13	985	63	209	14	21.3	1.5	206	14	28.2	2	172	12	33.5	2.4	91.3	6.8	11.78	0.91	71.4	5.6	10.64	0.87	26.2	5.9	16.6	3.2
FB10ap_38	369	6.5	469.4	6.6	369	15	86.50	5.10	262	15	39.9	2.2	218	11	60.6	3.1	22.41	0.84	69.2	3.3	8.91	0.41	56.7	2.5	12.31	0.51	34.4	1.3	4.17	0.17	22.81	0.76	3.35	0.12	3.07	0.22	2.07	0.11
FB10ap_39	347.1	4.4	366.7	5.2	1598	23	76.00	1.20	272.9	3.6	48.91	0.73	302.2	4.2	129.4	2.2	23.28	0.4	189.9	2.4	33.55	0.49	244.6	3.6	54.99	0.64	174.3	2.3	26.86	0.44	174.6	2.7	25.24	0.38	36.54	0.52	40.81	0.81
FB10ap_40	106.1	1.6	749	10	192.7	3.2	2.65	0.16	14.04	0.33	4	0.12	40.6	1.1	25.46	0.65	8.16	0.21	42.92	0.89	6.13	0.11	35.6	0.65	6.56	0.12	15.87	0.34	1.861	0.061	10.29	0.27	1.412	0.06	0.0368	0.0024	0.922	0.023
FB10ap_41	266.6	3.7	1451	16	300.8	6.5	28.70	1.20	134.3	5	30.5	1.1	223.8	6.8	77.9	2.2	21.78	0.6	88.1	2.1	10.72	0.3	58.2	1.5	10.61	0.26	25.36	0.65	3.031	0.099	16.51	0.53	2.304	0.082	0.262	0.028	2.38	0.12
FB10ap_42	314.8	3.6	601.1	5.9	664.9	8.2	34.89	0.57	161.3	2.1	37.65	0.62	302.8	5.1	169.3	2.5	45.39	0.63	227.5	3.1	31.71	0.45	161.7	1.7	24.45	0.31	47.55	0.64	4.52	0.11	19.15	0.45	2.042	0.054	0.417	0.023	3.812	0.064
FB10ap_43	149.4	1.9	231.7	2.4	453.8	5.7	8.40	0.23	29.92	0.59	5.61	0.16	37.9	1	14.91	0.52	5.5	0.14	22.1	0.45	3.241	0.079	20.82	0.48	4.571	0.094	12.51	0.3	1.61	0.069	9.5	0.29	1.497	0.069	0.0715	0.009	0.381	0.014
FB10ap_44	231.7	2.4	453.8	5.7	137.7	2.1	8.40	0.23	29.92	0.59	5.61	0.16	37.9	1	14.91	0.52	5.5	0.14	22.1	0.45	3.241	0.079	20.82	0.48	4.571	0.094	12.51	0.3	1.61	0.069	9.5	0.29	1.497	0.069	0.0715	0.009	0.381	0.014
FB10ap_45	480.1	6.2	247.1	5.9	2959	78	576.00	11.00	2123	46	396.1	9	2110	51	524	12	48.3	1.5	524	13	75.7	1.9	482	12	101.6	2.7	285.1	7.6	40.3	1.1	242.4	7.2	33.1	1	65.5	3.2	82	3.8
FB10ap_46	330.2	4.1	1454	12	115.2	2.1	30.89	0.53	148.3	2.1	33.26	0.51	240.1	3.8	80	1.6	21.86	0.38	70.1	1	6.77	0.12	28.32	0.63	4.038	0.088	7.53	0.24	0.75	0.034	3.62	0.16	0.492	0.028	0.117	0.011	3.296	0.098
FB10ap_47	197.4	3.2	203.6	2.5	903	11	1.84	0.12	18.55	0.8	5.62	0.29	71.7	2.6	41	1.2	0.786	0.067	101.8	2.1	20.73	0.39	153.5	2.1	33.17	0.37	86.47	0.8	11.63	0.16	69.79	0.95	9.48	0.2	0.51	0.023	1.954	0.045
FB10ap_48	304.4	3	419.6	4.2	248.9	3.3	1.75	0.09	6.28	0.2	1.301	0.075	9.79	0.49	5.41	0.29	1.981	0.095	14.12	0.38	3.233	0.086	31.41	0.53	9.36	0.14	31.34	0.51	4.399	0.098	25.32	0.44	3.391	0.076	0.0201	0.0043	0.553	0.017
FB10ap_50	151.8	1.6	615.2	6.4	491	23	55.70	2.50	215.7	9.7	40.6	1.8	278	12	131.8	5.8	30.2	1.4	188	8.3	27.1	1.2	135.3	6	19.17	0.86	32.8	1.5	2.299	0.14	11.51	0.62	1.26	0.087	2.78	0.2	4.32	0.27
FB10ap_51	393	5.3	169.9	2.5	1592	48	287.80	7.60	1024	30	219.3	5.8	1425	38	487	14	51.5	1.3	448	13	53.9	1.7	288.6	8.9	55.2	1.5	139.8	4.3	18.08	0.61	100.2	3.2	14.54	0.48	197	16	14.3	0.87
FB10ap_52	794.9	0.93	453	4.7	449.7	8.1	106.00	10.00	431	37	86.8	7	549	37	275	12	49.1	1.8	409	13	65.2	1.6	237.7	4.8	17.32	0.36	15.04	0.38	0.753	0.036	1.93	0.14	0.132	0.017	0.365	0.035	13.95	0.84
FB10ap_53	247.9	3.1	397.5	4.6	144.3	2.3	5.46	0.19	18.12	0.39	3.48	0.12	23.01	0.83	10.98	0.38	4.13	0.13	21.3	0.47	3.967	0.088	27.57	0.46	5.74	0.12	12.77	0.31	1.277	0.044	5.62	0.21	0.762	0.033	0.0096	0.0031	0.222	0.011
FB10ap_54	248.5	2.6	356.1	4.2	187.7	7.5	1.99	0.13	8.46	0.38	1.67	0.11	11.84	0.69	7.32	0.38	2.56	0.14	16.37	0.75	3.21	0.15	25.3	1.1	5.65	0.3	20.45	0.94	2.74	0.14	15.03	0.73	2.43	0.12	0.0191	0.0044	0.206	0.016
FB10ap_55	268.9	3.2	305.6	3.8	867	11	5.94	0.18	19.92	0.42	4.12	0.14	35.32	0.88	23.18	0.63	2.931	0.097	56.3	1	12.43	0.17	112.5	1.2	30.97	0.3	104.8	1	16.73	0.22	108.6	1.8	15.48	0.24	0.108	0.009	0.666	0.019
FB10ap_56	361.8	3.8	580.9	5.4	1354	19	147.70	9.10	411	22	59.1	2.6	321	11	105.5	2.1	18.53	0.39	146.9	2.2	26.87	0.34	192.9	2.2	44.11	0.47	130.8	1.4	19.78	0.25	124	1.7	19.37	0.3	42.4	1	7.62	0.18
FB10ap_57	251.5	3.4	637	13	1876	49	696.00	28.00	2144	80	357	12	1816	55	446	12	39.74	0.94	418	10	58	1.4	341.2	7.3	66.8	1.5	176.1	4.3	24.19	0.61	142.1	3.5	18.6	0.51	8.37	0.86	39.3	2.3
FB10ap_58	689.7	6.9	299.2	3.3	643	11	3.08	0.21	7.02	0.3	1.416	0.084	9.27	0.54	5.18	0.3	2.494	0.086	16.51	0.55	4.51	0.11	54.6	1.1	20.26	0.43	87	1.8	15.51	0.38	109.6	2.6	16.67	0.38	0.238	0.034	2.68	0.1
FB10ap_59	241.7	2.8	349.4	4.6	182.3	2.2	0.38	0.05	1.697	0.087	0.418	0.038	3.41	0.27	2.47	0.18	0.4	0.034	8.66	0.33	2.087	0.057	20.64	0.38	6.06	0.11	19.63	0.36	2.682	0.074	16	0.39	2.325	0.064	0.0033	0.0017	0.0206	0.0033
FB10ap_60	368.4	4.6	357.9	4.9	520	14	12.78	0.40	42.4	1.1	7.22	0.26	42.4	1.4	17.56	0.66	11.48	0.36	32.78	0.99	7.03	0.19	63	1.7	16.78	0.36	59.9	1.5	8.25	0.22	60.7	1.4	7.1	0.24	0.366	0.024	2.29	0.063
FB10ap_61	736.9	9.8	172.8	2.7	428.2	7.9	404.30	6.30	848	13	111.2	2	504.6	8.2	108.4	2.1	8.96	0.23	98.4	1.8	12.75	0.25	74.8	1.3	13.96	0.25	38.47	0.69	4.94	0.12	30.04	0.73	4.18	0.11	14.57	0.64	12.96	0.38
FB10ap_62	230.4	2.7	934	10	1097	28	4.72	0.17	28.22	0.72	9.15	0.24	98.1	2.3	84.3	1.7	23.33	0.51	169.8	3.2	28.15	0.66	192.5	4.2	39.81	0.88	110.2	2.7	13.59	0.33	79.8	2.2	11.14	0.31	1.26	0.11	12.84	0.61
FB10ap_63	367.7	4.8	611.4	9	83.3	2.3	0.34	0.05	1.75	0.11	0.468	0.037	3.5	0.28	2.21	0.19	0.601	0.044	4.95	0.25	1	0.047	9.23	0.37	2.661	0.093	11.32	0.34	2.166	0.078	18.67	0.56	3.79	0.12	2.6	0.17	0.274	0.015
FB10ap_64	412	5.3	825	12	606	12	39.00	1.00	151.9	3.9	27.72	0.81	163.3	4.5	60.7	1.9	16.02	0.49	76.1	2.1	12.66	0.33	87.4	1.9	17.76	0.36	51.8	1	7.14	0.15	46.5	1.2	7.09	0.19	11.28	0.21	1.608	0.033
FB10ap_65	574.2	7	269.1	4.3	795	35	364.00	15.00	849	25	111.2	2.7	495	11	104.4	1.7	22.79	0.54	111.9	3	18.03	0.7	121.4	5.6	21.04	0.99	50.2	2.4	5.69	0.28	28.7	1.3	3.17	0.15	220.4	7.5	38.9	1.3
FB10ap_67	215.8	2.3	520.1	6.5	170	2.3	1.42	0.11	4.4	0.18	1.239	0.065	10.76	0.56	8.82	0.33	4.47	0.13	22.64	0.56	4.175	0.089	28.94	0.5	6.06	0.11	19.53	0.36	2.682	0.074	16	0.39	2.325	0.064	0.0033	0.0017	0.0206	0.0033
FB10ap_68	422	3.7	342.9	3.8	427.7	5.8	10.04	0.26	62.81	0.91	17.51	0.33	148.7	2.6	78	1.2	19.85	0.34	104.7	1.6	15.32	0.22	85.6	0.59	361.5	3.5	71.06	0.78	185.9	2.1	24.32	0.36	14.32	0.87	1.569	0.053	0.023	0.004
FB10ap_69	649.7	7.4	234.3	3.1	1889	26	106.30	2.00	377.8	7	64.6	1.3	391.7	6.6	168.1	2.9	14.59	0.31	265	3.5	49.95	0.59	361.5	3.5	71.06	0.78	185.9	2.1	24.32	0.36	146.8	2.8	18.95	0.37	1.627	0.071	7.84	0.23
FB10ap_70	362.3	4.2	1192	11	22	1.8	20.70	1.90	65.4	5.6	10	0.87	52.2	4.3	8.75	0.7	1.9	0.18	7.72	0.66	0.705	0.062	3.76	0.36	0.743	0.067	1.91	0.18	0.243	0.025	1.6	0.16	0.303	0.03	0.078	0.012	0.123	0.016

S2.3 apatite trace-element data (continued)

	55Mn	±	85Sr	±	89Y	±	139La	±	140Ce	±	141Pr	±	146Nd	±	147Sm	±	153Eu	±	157Gd	±	159Tb	±	163Dy	±	165Ho	±	166Er	±	169Tm	±	172Yb	±	175Lu	±	232Th	±	238U	±
FB10ap_71	214.4	2	801.5	8.2	136.5	1.8	6.89	0.18	35.08	0.61	8.4	0.22	64.6	1.6	25.45	0.59	9.79	0.2	31.84	0.71	4.075	0.091	24.28	0.49	4.72	0.11	12.42	0.26	1.567	0.047	9.08	0.24	1.414	0.046	0.038	0.006	1.094	0.02
FB10ap_72	262.3	4.1	79.9	1.8	507.2	9.5	3.98	0.28	7.99	0.38	1.89	0.11	16.48	0.7	21.33	0.65	6.13	0.18	79.8	1.5	16.51	0.24	107.4	1.6	17.32	0.32	35.33	0.73	3.636	0.093	16.61	0.48	1.799	0.051	0.086	0.011	2.183	0.053
FB10ap_73	425.2	4.3	439.6	5	69	17	0.79	0.19	3.28	0.77	0.61	0.15	3.88	0.92	1.98	0.48	0.53	0.13	3.97	0.96	0.96	0.23	9	2.1	2.54	0.61	8.7	2.1	1.27	0.3	8.5	2.1	1.32	0.33	0.05	0.02	0.55	0.19
FB10ap_74	267.8	3.4	513.2	5.7	1655	23	13.91	0.32	60.3	1.1	13.31	0.28	98.4	2.1	68.3	1.3	9.4	0.21	144.5	2.2	30.98	0.42	248.2	3.1	57.87	0.6	182.2	2.2	27.04	0.45	171.3	2.7	27.19	0.36	15.1	0.28	10.17	0.17
FB10ap_75	269.7	4.6	744.8	9.6	485	12	20.34	0.84	155.7	6	44.9	1.6	361	11	140.3	4.3	36.1	1.1	159.3	4	19.87	0.49	106.6	2.5	17.89	0.42	40.2	1	4.29	0.14	21.06	0.56	2.689	0.087	1.202	0.088	10.09	0.36
FB10ap_76	360.8	4.2	557.8	7.2	130	8.8	31.70	2.60	111.5	8.7	19.1	1.5	111.7	8.7	35.1	2.7	8.38	0.65	35.8	2.7	4.33	0.32	22.9	1.7	4.05	0.28	9.91	0.75	1.217	0.091	7.03	0.48	0.874	0.071	2.68	0.34	8.97	0.79
FB10ap_77	502.6	5.1	498.7	4.7	388.7	5.7	2.85	0.12	21.76	0.53	8.11	0.23	89.8	2.1	58.8	1.4	11.29	0.29	89.5	1.5	12.89	0.2	14.89	0.2	39.38	0.64	4.723	0.098	26.22	0.55	3.526	0.082	0.1013	0.0099	4.965	0.071
FB10ap_78	870.8	9.1	370.2	5.2	995	15	319.00	16.00	907	37	154.1	5.6	815	22	238.6	4.2	12.97	0.25	240	2.9	32.23	0.37	186.7	2	35.04	0.35	89.14	0.87	11.16	0.18	61.64	0.98	8.03	0.16	18.08	0.33	4.697	0.082
FB10ap_79	643.5	7	344.8	3.1	2401	28	8.65	0.27	30.54	0.65	5.82	0.18	40.3	1.1	23.24	0.58	17.45	0.32	73.7	1.2	21.75	0.32	250.1	2.6	81.37	0.67	327.5	3.3	55.87	0.67	386.9	4.7	56.07	0.75	1.281	0.039	1.214	0.029
FB10ap_80	442.5	4.1	290.1	3.3	427.4	5.1	4.76	0.15	19.93	0.4	5.11	0.16	48.6	1.3	38.59	0.82	7.49	0.17	77.4	1.2	12.86	0.2	84.6	1	17.52	0.27	46.47	0.63	5.68	0.13	33.13	0.67	4.76	0.097	0.0926	0.0087	1.087	0.029
FB10ap_81	515.4	7.8	193.5	2.4	2400	120	2143.00	81.00	5310	210	685	23	3080	110	595	26	66.5	3.3	541	24	72	3.2	434	20	86.7	3.9	234	11	30.3	1.5	188.3	9.9	29.4	1.7	164	16	65	6.1
FB10ap_82	621.3	7.7	165.8	2.9	2889	47	35.96	0.66	128.6	2.1	23.45	0.47	164.5	3.4	96.9	1.9	22.5	0.45	243.3	3.8	55.27	0.69	465.5	4.9	108.2	1.1	314.8	2.8	44.77	0.65	284.2	4	36.47	0.56	6.53	0.13	23.62	0.43
FB10ap_83	326.1	3.3	295.9	4.8	344.5	2.3	0.27	0.03	0.823	0.08	0.162	0.024	1.13	0.17	0.517	0.086	0.105	0.019	1.1	0.12	0.265	0.028	2.78	0.21	1.01	0.074	5.58	0.38	1.307	0.078	12.73	0.89	2.47	0.16	0.0028	0.0015	0.0468	0.0072
FB10ap_84	344.3	4.8	211.5	3.2	266	16	7.77	0.51	30.8	1.9	6.24	0.4	42.7	2.6	18.4	1.1	4.76	0.29	32.9	2	5.47	0.33	38.5	2.2	8.86	0.55	25.5	1.5	3.18	0.2	18.4	1.1	2.9	0.18	0.08	0.013	4.98	0.41
FB10ap_85	453.6	5.2	284.5	4.8	107.8	3.3	2.68	0.06	12.68	0.17	2.68	0.06	18.8	1.4	11.29	0.29	89.5	1.5	12.89	0.2	14.89	0.2	38.04	0.64	4.723	0.098	26.22	0.55	3.526	0.082	0.1013	0.0099	4.965	0.071				
FB10ap_86	460	7.6	373.7	8.7	170.9	4.5	8.32	0.28	61	1.7	18.27	0.5	148.9	3.9	56.3	1.6	9.85	0.23	53.8	1.2	6.29	0.16	33.21	0.62	5.92	0.12	14.76	0.34	1.921	0.06	11.6	0.32	1.783	0.068	0.149	0.012	16.04	0.36
FB10ap_87	198.6	2.2	189.8	3.3	443.1	8.3	1.71	0.08	6.91	0.22	1.442	0.071	11.21	0.56	8.09	0.32	5.69	0.19	28.63	0.59	7.94	0.16	69.39	0.97	15.5	0.2	40.17	0.63	5.165	0.093	29.98	0.64	3.83	0.11	0.125	0.013	5.7	0.23
FB10ap_88	258.3	3.7	346.6	6.1	1750	190	76.10	7.00	336	35	68	7.3	450	49	218	25	21.5	2.3	340	38	60.8	7	387	44	72.3	8	172	19	20.2	2.1	108	11	13.4	1.4	6.1	1.1	37.5	6.6
FB10ap_89	226.8	3.3	229.1	7.2	1147	33	8.94	0.97	27.4	2.1	4.82	0.28	37.4	1.8	28.1	1	8.03	0.25	69.2	1.7	16.88	0.32	160.5	2.3	39.54	0.46	121.8	1.6	16.12	0.27	86.7	1.5	11.59	0.26	44.1	1.3	51.4	1.8
FB10ap_90	402	5.1	260.5	4.4	562	12	28.99	0.77	105.4	2.2	19.14	0.53	122.2	3.1	57.8	1.6	14.58	0.33	89.2	2	14.6	0.23	95	1.2	20.35	0.28	55.82	0.96	7.54	0.17	43.66	0.86	6.67	0.14	4.97	0.12	60.3	1.2
FB10ap_91	219	14	264.9	4.1	552.9	8.3	7.38	0.28	26.52	0.67	5.62	0.19	40.2	1.7	23.29	0.87	6	0.42	104	1.8	11.81	0.22	64.61	0.96	11.94	0.16	30.42	0.35	3.823	0.084	23.05	0.47	3.403	0.092	2.96	0.12	8.25	0.19
FB10ap_92	318.5	4	344.5	5.7	736	14	14.39	0.35	91.4	1.8	26.96	0.47	229.8	4	110.4	2.1	29.22	0.45	146.7	2.3	21.77	0.29	133.1	1.6	27.35	0.36	71.86	0.98	9.17	0.16	55.2	1.2	8.23	0.19	0.145	0.012	14.54	0.28
FB10ap_93	630	26	683	17	421	11	3170.00	230.00	6480	600	657	38	2420	140	289	12	16.47	0.6	185	5.4	19.55	0.4	94.7	1.8	16.47	0.35	38.73	0.79	4.66	0.13	26.46	0.62	3.74	0.11	33	2.3	0.67	0.041
FB10ap_94	341.8	5.9	180.5	3.5	286.3	7.5	11.73	0.65	47	2.1	8.8	0.36	61	2.3	23.94	0.81	8.09	0.29	43.8	1.1	7.04	0.17	47.9	1.1	11.13	0.24	30.6	0.58	4.01	0.12	23.51	0.57	4.19	0.11	1.036	0.036	24.99	0.57
FB10ap_95	419.3	4.4	267.2	4.6	440.5	8	0.51	0.06	2.33	0.12	0.566	0.043	6.35	0.35	7	0.31	4.5	0.14	27.68	0.68	6.4	0.12	58.33	0.9	16.07	0.23	50.58	0.6	7.09	0.13	40.96	0.79	5.86	0.14	0.094	0.01	2.234	0.073
FB10ap_96	420	5.5	543.4	8.8	203.2	3.6	8.04	0.22	25.02	0.57	4.15	0.17	26.43	0.82	10.31	0.38	4.01	0.11	19.26	0.57	3.48	0.078	28.88	0.55	7.65	0.14	24.81	0.43	3.565	0.093	21.29	0.55	3.322	0.095	0.0531	0.007	0.23	0.011
FB10ap_97	474.7	5.8	1089	16	78	1.5	72.20	1.40	225	3.6	34.41	0.54	175.2	3.5	33.46	0.85	7.39	0.19	27.14	0.66	2.79	0.074	14.56	0.37	2.728	0.069	6.68	0.2	0.884	0.036	5.15	0.21	0.888	0.043	0.108	0.01	0.237	0.01
FB10ap_98	376.9	4.4	607.2	9	347.8	6.2	399.20	6.30	1084	20	163.5	2.4	747	11	131.2	2.2	22.95	0.42	104	1.8	11.81	0.22	64.61	0.96	11.94	0.16	30.42	0.35	3.823	0.084	23.05	0.47	3.403	0.092	2.96	0.12	8.25	0.19
FB10ap_99	473.9	5.9	426.9	4.7	639.3	7.2	278.00	4.50	1114	18	198.6	3.1	1065	14	248.2	3.4	32.4	0.5	209.3	2.4	25.11	0.27	136.5	1.7	23.69	0.31	60.3	0.66	6.92	0.12	39.09	0.79	5.38	0.12	0.84	0.032	1.293	0.025
FB10ap_100	424.4	6.1	404.3	5.4	219.4	4.9	5.38	0.21	30.44	0.67	9.22	0.27	88.8	2.9	47.8	1.4	14.82	0.4	64.8	1.5	8.61	0.19	48.1	1	8.02	0.2	18.08	0.44	1.815	0.067	8.69	0.3	0.981	0.046	0.082	0.01	2.448	0.077
FB10ap_101	369.1	3.7	467.4	5.7	851	16	472.10	7.10	1482	24	242.3	3.7	1166	16	223.1	3.4	15.05	0.32	188.7	2.7	24.97	0.4	148.2	2.1	27.24	0.4	76.5	1	9.94	0.16	63	1.2	8.65	0.18	3.49	0.074	2.364	0.045
FB10ap_102	633.8	5.8	1833	2.7	1015	18	165.40	2.50	608	8.8	107.6	1.5	623.8	9.8	180.7	2.7	20.99	0.41	195.9	2.6	26.74	0.37	163.8	1.8	33.06	0.29	95.2	1	12.11	0.15	75.9	1.2	12.35	0.19	10.85	0.5	8.79	0.11
FB10ap_103	475.3	3.6	396.1	3.6	167	1.9	2.51	0.13	11.12	0.31	2.51	0.1	21.15	0.75	11	0.39	1.376	0.066	20.07	0.49	3.29	0.081	24.86	0.46	5.712	0.099	19.25	0.33	2.754	0.066	18.56	0.43	2.939	0.078	0.151	0.013	1.31	0.031
FB10ap_105	446.8	3.5	381	3.9	6.1	0.19	0.01	0.01	0.034	0.012	0.0072	0.005	0.072	0.035	0.041	0.021	0.0307	0.0086	0.101	0.034	0.0428	0.009	0.504	0.056	0.183	0.015	0.897	0.058	0.196	0.017	1.71	0.13	0.337	0.018	0.0028	0.0014	0.0309	0.0037
FB10ap_106	104.5	1.3	794.6	9.2	90.8	1.3	9.80	0.26	44.06	0.77	9.88	0.23	69.7	1.4	21.36	0.53	7.43	0.18	24.42	0.54	2.862	0.074	15.85	0.38	2.877	0.061	7.46	0.18	0.887	0.031	5.21	0.21	0.869	0.042	0.0641	0.0063	0.539	0.018
FB10ap_107	395.5	3.3	482.3	5.4	24.7	1.1	0.37	0.04	1.447	0.098	0.255	0.029	1.98	0.21	0.949	0.097	0.255	0.029	1.82	0.16	0.39	0.03	3.09	0.17	0.737	0.046	2.84	0.17	0.45	0.038	3.7	0.26	0.703	0.048	0.0335	0.008	0.1242	0.0073
FB10ap_108	226.8	4.5	910.9	9.9	119.7	1.8	14.72	0.33	58.19	0.91	12.32	0.25	92.7	1.8	36.09	0.75	9.51	0.17	42.95	0.79	5.021	0.094	26.68	0.47	4.271	0.079	9.59	0.2	1.004	0.044	4.95	0.18	0.657	0.031	0.289	0.018	2.85	0.043
FB10ap_109	378.4	5.1	362.5	6.1	399	7.4	23.60	0.48	76.6	1.4	12.64	0.34	76.4	1.6	29.21	0.7	6.53	0.17	45.79	0.95	7.91	0.16	56.86	0.83	12.95	0.21	40.74	0.65	5.51	0.11	33.66	0.71	4.77	0.12	1.235	0.079	3.799	0.093
FB10ap_110	644.9	6.9	453.4	6.7	404.3	6.9	444.60	8.20	1362	25	204.1	3.4	937	16	177.4	3	14.74	0.27	139.8	2.2	15.93	0.24	83.75	0.84	14.39	0.2	35.04	0.48	3.91	0.082	20.73	0.43	2.717	0.077	19.33	0.31	3.265	0.064
FB10ap_111	443.3	5.9	465.8	8.5	232.2	3.9	12.05	0.34	62.1	1.1	14.56	0.36	108.2	2.4	43.16	0.94	13.78	0.25	47.01	0.99	5.69	0.12	39.89	0.66	7.65	0.1	21.34	0.38	2.783	0.065	17.5	0.35	2.62	0.076	0.059	0.0087	2.699	0.065
FB10ap_112	336.6	3	480.3	4	265.6	7.7	18.59	0.65	59.3	1.7	9.61	0.34	55.6	1.7	18.91	0.66	7.74	0.28	27.6	1	4.48	0.14	35	1.2	9.06	0.33	30.05	0.94	4.06	0.16	24.07	0.85	3.68	0.14	0.232	0.019	3.1	0.11
FB11ap_0	368.9	3.5	272.4	3.2	974	17	13.50	0.26	110.6	1.9	34.32	0.6	321.3	3.6	179.5	2.6	45.06	0.66	260.2	3.6	36.6	0.5	207.1	2.9	36.59	0.68	88.6	1.6	10.06	0.19	53.5	1.1	6.89	0.15	0.309	0.018	8.23	0.14
FB11ap_1	422.6	4.2	661.7	7.7	53.2	1	0.51	0.05	2.25	0.14	0.547	0.041	4.76	0.29	2.96	0.18	0.901	0.064	6.53	0.28	1.038	0.038	6.86	0.24	1.603	0.055	4.87	0.17	0.645	0.032	4.18	0.18	0.813	0.041	0.0035	0.0019	0.0266	0.0033
FB11ap_2	337.4	3.8	2830	30	699.8	9.5	68.30	1.00	388.5	4.9	89.8	1.5	636.5	8.2	214.7	3.2	61.42	0.87	219.1	2.3	27.07	0.28	142.7	2	24.62	0.33	57.79	0.83	6.81	0.13	38	0.69	5.44	0.11	7.28	0.11	30.97	0.37
FB11ap_3	394.4	5.1	889.9	9.4	501.4	6.5	468.30	9.30	1376	29	219.4	4.1	1072	19	214.1	3.4	43.48	0.74	199.9	2.8	26.8	0.41	153.4	2.2	27.96	0.43	68.43	0.98	8.12	0.15	45.63	0.98	6.09	0.12	5.4	0.2	9.36	0.14
FB11ap_4	581.2	5.8	798.3	9.3	778	14	66.10	1.60	282.8	5	60.2	1	430.1	7.3	167.6	2.6	48.18	0.74	167.4	2.3	19.8	0.26	106.8	1.3	18.86	0.25	45.37	0.63	5.68	0.12	45.63	0.98	6.09	0.12	5.4	0.2	9.36	0.14
FB11ap_5	416.7	3.9	1738	2.5	2135	28	93.10	1.60	485.5	6.6	106.1	1.4	729	10	383.5	4.8	28.79	0.4	596.5	5.3	108.3	1.2	614.3	6.5	84	0.95	143.8	1.4	11.62	0.18	45.64	0.71	4.363	0.083	3.48	0.068	115.8	1.4
FB11ap_6	2168	39	101.7	2.9	1070	32	563.00	26.00	1325	59	230	12	1308	63	375	16	38.8	1.3	331	10	37.7	1.4	198.8	5.6	35.75	0.84	91.7	2.2	11	0.31	63.4	1.5	10.16	0.3	269	11	60.8	3.3
FB11ap_7	1234	23	302.1	9.2	1365	51	404.00	13.00	1268	59	214.9	6.8	1107	43	387	15	28.7	1.1	417	15	65.7	2.6	388	16	63	2.2	140.5	5.8	15.35	0.58	74.1	3.2	8.02	0.35	1.27	0.16	19	1.6
FB11ap_8	412.7	4.1	275.3	3.7	482.1	8.9	25.32	0.60	164.4	3.5	38.11	0.88	274.6	5.7	102.1	1.9	13.64	0.29	125.5	2.1	16.89	0.27	100.4	1.4	18.85	0.26	47.34	0.75	5.57	0.1	33.03	0.59	4.99	0.11	0.425	0.025	4.042	0.075
FB11ap_9	713.9	6.4	368.8	4.8	396	10	2.29	0.12	10.27	0.39	2.09	0.12	15.14	0.77	9.17	0.38	3.38	0.13	21.95	0.71	5.27	0.17	48.6	1.3	13.4	0.34	48.4	1.3	7.46	0.2	53.8	1.5	10.02	0.24	4.038	0.086	2.763	0.057
FB11ap_10	267.8	2.6	260.7	3.1	768	10	16.98	0.37	123.1	1.6	34.74	0.49	287.9	4.1	185.3	2.7	17.26	0.26	280.6	3.3	43.31	0.5	223.9	1.9	32.11	0.27	66.22	0.75	6.89	0.12	37.62	0.59	4.72	0.1	0.118	0.015	9.42	0.12
FB11ap_11	623.1	8	184.9	3.5	48.8	1.4	5.08	0.25	11.38	0.56	1.41	0.1	7.22	0.43	2.01	0.16	1.01	0.066	3.22	0.23	0.613	0.036	5.16	0.2	1.504	0.048	5.62	0.2	0.863	0.037	6.53	0.27	1.228	0.045	0.793	0.049	0.319	0.018
FB11ap_12	562.3	6.9	368.3	5	1225	24	207.70	5.50	1019	21	207.5	4	1149	22	331.9	5.6	43.23	0.78	299.1	4.9	41.55	0.63	246.3	3.9	45.06	0.74	118.8	1.7	15.24	0.31	87.3	1.6	11.6	0.25	3.98	0.25	12.15	0.31
FB11ap_13	852.8	8.5	93.4	1.7	37	2.4	7.37	0.20	28.6	0.51	5.87	0.17	42.4	1.1	16.32	0.53	4.33	0.14	22.52	0.61	2.77	0.072	15.4	0.41	3.123	0.077	8.29	0.21	1.016	0.044	6.11	0.24	1.089	0.048	0.0177	0.0046	0.106	0.0078
FB11ap_14	456.7	4.7	693.2	9.7	666	11	837.00	12.00	3228	49	439.4	5.9	1944	30	347.6	4.9	55.12	0.75	241.9	3.2	27.15	0.38	140.2	1.7	23.52	0.29	57.65	0.7	6.85	0.12	38.08	0.65	5.2	0.11	6.81	0.12	19	1.6
FB11ap_15	778.1	5.9	688.2	7.6	122.8	2	46.46	0.81	150.6	2.5	23.88	0.44	132.9	2.8	30.66	0.77	9.22	0.2	32.06	0.71	3.542	0.098	20.68	0.42	4.223	0.098	11.77	0.29	1.432	0.052	8.87	0.3	1.524	0.058	0.117	0.01	0.694	0.022
FB11ap_16	405.7	6.9	494.1	6.9	126.3	3.3	7.29	0.24	25.23	0.48	5.03	0.16	33.4	1	12.56	0.4	3.56	0.12	17.1	0.54	2.71	0.079	18.15	0.56	3.98	0.11	12.06	0.39	1.739	0.07	10.57	0.45	1.805	0.071	0.346	0.022	1.312	0.042
FB11ap_17	623.1	8	184.9	3.5	48.8	1.4	5.08	0.25	11.38	0.56	1.41	0.1	7.22	0.43	2.01	0.16	1.01	0.066	3.22	0.23	0.613	0.036	5.16	0.2	1.504	0.048	5.62	0.2	0.863	0.037	6.53	0.27	1.228	0.045	0.793	0.049	0.319	0.018
FB11ap_18	681.1	7	668	12	419	10	44.10	1.10	196.2	3.9	26.59	0.74	153.9	4.5	72.5	2.1	46.8	1.6	123	2.9	21.88	0.48	119.4	2.3	16.33	0.44	29.61	0.62	4.4	0.1	22.22	0.4	2.826	0.084	0.0274	0.0057	2.587	0.068
FB11ap_19	89.46	0.89	848	11	485.4	8.4	10.79	0.27	98.4	1.4	36.6	0.69	346.1	6	152.6	2.4	37.02	0.54	168.5	2.3	20.62	0.35	107.1	1.4	18.01	0.3	40.88	0.62	4.4	0.1	22.22	0.4	2.826	0.084	0.0274	0.0057	2.587	0.068
FB11ap_20	527.8	5.6	815.1	7.9	2521	44	115.20	1.90	412.3	7.2	73.9	1.3	464.1	7.8	207.2	3.3	40.39	0.7	323.2	4.1	58.84	0.68	425.3	4.9	91.9	1.1	271.5	3.3	38.72	0.6	241.6	4.4	31.92	0.67	3.286	0.083	48.99	0.85
FB11ap_21	151.3	1.4	1639	18	18.29	0.41	7.61	0.22	29.98	0.71	5.79	0.19	37.8	1.1	9.47	0.4	2.506	0.097	8.05	0.33	0.682	0.035	3.2	0.14	0.607	0.03	1.567	0.076	0.168	0.017	1.061	0.083	0.188	0.017	0.0604	0.0078	0.518	0.016
FB11ap_22	237.6	2.5	794.8	10	315.9	4.6	44.56	0.76	212.3	3	47.28	0.74	327.3	5.1	112	1.6	32.32	0.51	119.3	1.6	14.26	0.23	73.6	1.1	11.4	0.16	23.17	0.37	2.23	0.063	10.02	0.28	1.151	0.05	0.655	0.024	5.664	0.083
FB11ap_23	215.5	1.9	628.9	8.1	90.8	1.5	6.27	0.04	2.4	0.11	0.874	0.055	10.12	0.62	6.18	0.27	1.314	0.067	12.22	0.41	1.834	0.061	13.1	0.36	3.16	0.073	9.74	0.24	1.385	0.046	8.96	0.24	1.384	0.046	0.025	0.0042	0.342	0.014
FB11ap_24	167.4	2.7	547.8	9.2	449.6	8.4	7.38	0.18	59.3	1.5	18.65	0.47	174.4	3.4	92.4	2	28.8	0.48	126	2.2	17.25	0.31	96.6	1.6	16.76	0.3	39.27	0.66	4.21	0.12	21.84	0.58	2.72	0.1	1.809	0.062	5.27	0.11

S2.3 apatite trace-element data (continued)

	55Mn	±	86Sr	±	89Y	±	139La	±	140Ce	±	141Pr	±	146Nd	±	147Sm	±	153Eu	±	157Gd	±	159Tb	±	163Dy	±	165Ho	±	166Er	±	169Tm	±	172Yb	±	175Lu	±	232Th	±	238U	±
FB11ap_25	177.3	1.9	882.2	9.5	124.5	1.7	0.73	0.06	9.39	0.23	4.32	0.13	56.8	1.2	36.43	0.67	9.13	0.2	53.49	0.81	5.7	0.11	28.16	0.46	4.479	0.093	9.38	0.21	0.961	0.037	4.75	0.17	0.714	0.037	0.0034	0.0018	0.582	0.018
FB11ap_26	373.2	4.3	538.6	6.9	6.81	0.21	5.70	0.20	22.65	0.41	4.18	0.13	25.65	0.82	6.96	0.3	1.854	0.082	6.07	0.24	0.44	0.028	1.532	0.09	0.218	0.019	0.485	0.051	0.068	0.011	0.384	0.065	0.075	0.011	1.302	0.039	1.639	0.036
FB11ap_27	370.3	3.6	419.9	5.4	213	3	5.21	0.16	16.52	0.33	3.031	0.095	19.4	0.66	9.68	0.3	2.81	0.11	17.94	0.46	3.501	0.079	28.75	0.5	7.39	0.13	24.4	0.36	3.42	0.078	19.78	0.45	3.053	0.077	0.0052	0.0023	0.607	0.018
FB11ap_28	286.8	2.5	1203	11	227.8	3.2	1.32	0.08	3.88	0.17	1.092	0.061	12.01	0.51	10.48	0.4	2.74	0.11	27.38	0.59	4.85	0.1	35.33	0.62	8.15	0.14	23.65	0.4	3.146	0.07	19.3	0.36	3.025	0.074	0.0029	0.0017	0.0359	0.0043
FB11ap_29	102.7	1.2	840	12	20.22	0.42	46.95	0.85	133.8	2.1	19.03	0.39	98	2	18.43	0.51	4.8	0.13	16.39	0.47	1.419	0.051	5.57	0.19	0.705	0.033	1.07	0.065	0.081	0.011	0.303	0.04	0.0299	0.0059	0.11	0.01	0.339	0.013
FB11ap_30	1266	16	78.6	1.4	1229	23	54.90	1.10	176	2.6	33.52	0.6	224.3	4.4	113.2	2.1	16.09	0.3	179.9	3.2	30.44	0.38	191.5	2.3	39.83	0.58	100.7	1.6	10.17	0.18	47.01	0.95	6.71	0.17	2.75	0.12	3.6	0.11
FB11ap_31	663	5.7	436.3	6	1030	18	113.90	2.10	387.5	7.2	66.2	1.3	396.8	7.5	142.4	2.5	9.68	0.18	198.6	3.2	30.44	0.38	191.5	2.3	37.9	0.43	101.3	1.1	13.87	0.19	94.8	1.2	14.81	0.22	0.812	0.027	4.842	0.072
FB11ap_32	168	2.4	1007	12	291.7	4	2.56	0.11	30.57	0.53	13.32	0.24	152.7	2.4	78.4	1.2	18.1	0.3	95	1.1	11.52	0.18	60.99	0.74	10.32	0.14	24.04	0.36	2.756	0.069	14.59	0.32	2.043	0.062	0.0273	0.0046	1.079	0.023
FB11ap_33	299.9	2.5	813.7	8.2	992	13	10.84	0.34	37.15	0.88	7.6	0.18	61.9	1.3	52.96	0.74	11.33	0.24	125	1.5	24.49	0.29	178.5	1.9	38.73	0.44	107.1	1.3	13.43	0.17	72.9	1.1	10.09	0.17	2.963	0.082	9.16	0.13
FB11ap_34	550.1	7.6	1053	17	553	13	463.00	11.00	1023	26	126.1	2.9	501	12	104.6	2.9	11.99	0.31	102.1	2.1	14.86	0.31	93.4	1.7	18.76	0.39	60.4	1.3	5.87	0.2	32.17	0.84	4.57	0.17	15	0.48	2.027	0.04
FB11ap_35	371.5	3.4	130.6	2.5	1446	20	16.56	0.51	63.3	1.3	12.51	0.32	91.4	2.1	50.6	1.4	13.79	0.32	114.2	2.1	24.68	0.41	210.8	2.9	50.03	0.71	148.1	2.1	19.16	0.31	110	1.8	14.54	0.28	18	5.76	0.13
FB11ap_36	227.6	2.1	666.7	8.9	263.4	6.8	10.90	1.10	40.1	3.9	7.68	0.71	52.1	4.2	21.4	4.1	7.03	1.4	32.5	1.5	4.98	0.18	34.9	1.1	8.54	0.2	28.23	0.63	4.23	0.11	29.41	0.67	5.69	0.13	0.731	0.047	2.031	0.09
FB11ap_37	497.1	4.8	613.9	7.8	224.4	4.3	10.92	0.25	51.03	0.99	12.78	0.3	107.8	1.9	49.6	1.1	11.47	0.26	64.2	1.3	8.21	0.18	47.18	0.84	8.92	0.18	22.39	0.48	2.684	0.067	13.82	0.36	2.083	0.066	0.0721	0.0078	0.559	0.017
FB11ap_38	315.5	2.8	546.5	5.6	517.5	9.9	7.30	0.26	30.75	0.71	6.03	0.19	41.6	1.3	19.7	0.67	4.32	0.14	37.34	0.9	7.76	0.17	66.1	1.3	17.55	0.32	62.7	1.2	10.1	0.2	71.8	1.4	11.69	0.23	1.393	0.056	2.092	0.044
FB11ap_39	309.5	3.1	294.1	4	354	16	18.70	1.10	67.4	4	12.13	0.72	76.9	4	28.6	1.7	8.26	0.45	42.9	2.1	6.61	0.34	47.9	2.4	11.32	0.45	37.4	1.5	5.69	0.26	40.3	1.8	8.17	0.32	0.528	0.039	1.91	0.12
FB11ap_40	203.9	2.2	330.9	4.6	466.4	8.1	105.00	1.90	367.8	6.2	56.69	0.97	289.7	5.6	67.8	1.4	13.48	0.28	74.3	1.5	10.45	0.17	68.7	1.2	15.44	0.25	46.65	0.74	6.79	0.14	44.68	0.8	8	0.17	0.713	0.026	1.541	0.046
FB11ap_41	868	9.8	123	2.2	2526	73	162.50	4.80	607	17	119.9	2.9	813	23	353	10	38.4	1	471	13	72.5	2	461	14	91.9	2.7	248.4	7.6	30.1	0.89	168.2	4.8	25.79	0.79	19.03	0.58	17.69	0.98
FB11ap_42	64.21	0.84	1265	13	263.9	3.5	45.73	0.76	337.4	4.1	96	1.4	746.5	9.9	259.7	3.3	48.2	0.61	226.8	2.4	22.09	0.28	86.6	1.1	10.18	0.13	15.08	0.28	1.066	0.049	3.6	0.15	0.364	0.025	0.0192	0.0039	1.922	0.036
FB11ap_43	724.3	7.7	365.3	4.9	1121	17	623.30	9.30	1901	26	297.5	4.2	1422	17	305.8	3.4	19.83	0.34	245.8	3.3	32.92	0.44	196.8	2.3	37.71	0.47	107.8	1.2	15.55	0.21	98.3	1.5	13.87	0.23	19.61	0.31	40.28	0.63
FB11ap_44	534.3	5.4	410.9	5.8	304.2	5	2.18	0.17	9.93	0.33	2.51	0.11	22.76	0.82	14.69	0.47	4.05	0.13	31.62	0.66	5.444	0.086	42.09	0.78	11	0.18	39.39	0.69	6.49	0.13	50.08	0.95	9.26	0.18	4.74	0.12	2.04	0.044
FB11ap_45	240	3.1	1275	20	139.3	2.9	35.62	0.84	211.2	5	47.3	1.2	299.2	6.4	75.7	1.9	19.29	0.42	57.9	1.3	6.16	0.13	31.07	0.69	5.1	0.13	11.74	0.33	1.305	0.056	6.62	0.25	0.942	0.048	0.098	0.015	2.071	0.05
FB11ap_46	369.7	3.4	418.7	5.1	135.6	3.4	4.42	0.20	16.39	0.54	3.44	0.15	29.9	1.1	21.3	0.78	8.28	0.28	43.8	1.4	5.71	0.17	30.98	0.85	5.44	0.16	12.48	0.38	1.282	0.053	6.79	0.25	1.063	0.044	0.0091	0.0027	1.007	0.035
FB11ap_47	718.7	6.9	605.9	6.8	478.1	7.9	13.00	0.33	62.9	1.3	15.06	0.3	125.5	2.1	75.4	1.6	25.97	0.45	104.1	1.9	14.71	0.25	86.3	1.2	16.55	0.26	45.07	0.79	5.98	0.13	37.14	0.77	5.66	0.13	1.55	0.043	5.99	0.12
FB11ap_48	419	11	454.7	6.6	624	15	16.74	0.49	67.1	1.7	13.11	0.43	87.8	2.7	42.3	1.4	13.17	0.41	73.7	2.1	13.03	0.39	94.5	2.1	21.77	0.43	64.8	1.6	8.46	0.22	49.7	1.5	7.86	0.22	1.601	0.058	1.239	0.041
FB11ap_49	106.8	1.4	316.6	4.1	877	20	365.20	6.40	1540	27	287.5	5.5	1518	24	330.2	5.7	81.7	1.3	251.1	4	29.35	0.41	157.3	2.3	29.09	0.38	76.2	1	9.79	0.16	65.63	0.95	7.77	0.16	5.79	0.14	21.12	0.39
FB11ap_50	374.7	3.7	1998	24	532.2	8	40.25	0.60	252.2	3	59.97	0.78	426.2	6.1	155.5	2.6	37.16	0.48	156.1	2.2	19.44	0.24	107.5	1.1	18.63	0.24	47.55	0.58	6.06	0.12	34.55	0.52	4.726	0.094	1.438	0.044	24.22	0.31
FB11ap_51	336.8	4.1	706.3	9.7	41.38	0.83	2.77	0.11	9.03	0.33	1.5	0.06	14.78	0.34	8.54	0.19	4.06	0.11	23.59	0.54	2.347	0.07	10.17	0.26	1.497	0.047	3.25	0.13	0.363	0.025	1.86	0.11	0.292	0.023	0.392	0.019	4.183	0.081
FB11ap_52	535.6	5.4	433.5	5.2	14.25	0.34	1.52	0.08	5.81	0.17	1.13	0.062	7.25	0.43	2.89	0.18	1.071	0.046	3.66	0.19	0.436	0.029	2.54	0.11	0.47	0.026	1.356	0.082	0.161	0.013	0.852	0.063	0.181	0.015	0.061	0.012	0.1188	0.0076
FB11ap_53	568.6	7	916	14	279.1	4.2	63.20	1.10	216.1	4.9	39.24	0.71	250	5.8	78.2	1.8	20.78	0.5	79.6	1.8	9.26	0.17	60.4	1	9.36	0.16	25.3	0.49	3.398	0.065	22.18	0.44	3.78	0.1	0.856	0.032	6.41	0.12
FB11ap_54	252.4	4.1	452.2	6.8	121.7	7.5	7.80	0.55	116.1	4.4	20.38	1.2	103.5	2.5	73	1.7	4.95	0.13	157.5	2.4	28.09	0.43	180.1	3.1	29.2	0.44	55.73	0.89	4.79	0.11	18.84	0.47	1.958	0.084	0.175	0.016	4.009	0.076
FB11ap_55	115.2	1.6	298.7	5.1	796	17	6.40	0.18	38.25	0.86	10.88	0.32	103.5	2.5	79.2	1.7	4.95	0.13	157.5	2.4	42.1	1.2	287	8.2	61.6	1.7	182	5.4	26.11	0.73	164.9	4.8	24.93	0.66	3.89	0.19	41.5	1.4
FB11ap_56	289.9	4.6	83.6	1.7	1819	49	48.90	1.70	206.4	7	45.1	1.5	329	11	171.4	5.9	19.2	0.54	4.16	0.16	25.45	0.65	3.327	0.089	20.01	0.46	3.9	0.1	10.25	0.29	12.59	0.26	1.069	0.041	0.0109	0.0032	0.0708	0.0059
FB11ap_57	238	2.2	874	11	108	1.8	8.44	0.27	34.74	0.7	7.1	0.23	49	1.4	19.2	0.54	4.16	0.16	25.45	0.65	3.227	0.089	20.01	0.46	3.9	0.1	10.25	0.29	12.59	0.26	1.069	0.041	0.0109	0.0032	0.0708	0.0059
FB11ap_58	492.8	4.6	453.7	6.3	980	16	43.01	0.88	189.6	3.8	39.95	0.77	288.5	5.9	137.8	2.5	36.28	0.57	191.2	2.9	28.26	0.42	179.8	2.6	35.69	0.49	97.6	1.4	16.78	0.31	58.3	0.98	9.35	0.2	68.9	1.5	13.13	0.3
FB11ap_59	442.2	4.5	223.1	3	925	14	53.55	0.74	228.2	2.6	42.7	0.58	259.6	3.4	110.2	1.5	19.09	0.32	117	1.6	21.26	0.24	170.7	1.8	39.38	0.43	126.8	1.3	19.7	0.28	127.8	1.5	16.47	0.24	0.675	0.031	9.88	0.22
FB11ap_60	554.9	4.7	623.4	6.7	2277	40	105.40	1.80	457.1	7.2	92.8	1.6	626	11	277.7	4.6	25.63	0.47	400.4	5.4	69.6	1	464	5.9	88.64	0.99	233.2	3.5	30.62	0.5	185	3	24.57	0.43	3.82	0.13	31.8	0.7
FB11ap_61	588.6	5.1	447.9	4.9	939	19	1795.00	32.00	4222	70	537.8	8	2242	40	389.7	6.3	33.59	0.53	286.4	4.4	33.99	0.57	182.5	2.9	32.29	0.49	81.9	1.5	10.06	0.2	57.3	1.1	7.85	0.17	58.3	2	28.27	0.73
FB11ap_62	779.5	9.1	257.1	5.1	1864	54	7.80	0.30	30.58	0.78	6.49	0.3	46.7	1.8	28.74	0.94	7.58	0.27	71	1.9	17.84	0.54	183.5	4.6	59.2	1.4	266.9	7.7	54.5	1.7	421	13	65.4	2.3	3.3	0.23	61.7	2.6
FB11ap_63	338.5	3.8	217.4	2.7	905	14	14.51	0.58	80	3.2	21.85	0.85	190.2	6.3	101.6	2.2	32.94	0.68	162.9	3.2	24.26	0.41	153.5	2.3	31.27	0.44	84.7	1.1	10.71	0.18	64.1	1.1	10.17	0.2	1.616	0.067	5.45	0.13
FB11ap_64	302.8	3.6	286.5	3.2	347.2	8.6	27.10	1.00	114.6	4.3	24.43	0.91	168.4	6	63.7	2.3	16.78	0.61	76.2	2.1	9.86	0.28	57.9	1.7	11.86	0.36	33.47	0.99	4.37	0.15	27.96	0.84	4.82	0.15	5.68	0.19	30	1
FB11ap_65	254.8	4.5	437	11	189.1	4.9	1.17	0.14	8.03	0.28	2.66	0.17	28.1	1.3	17.15	0.89	6.32	0.24	27	1.1	4.52	0.15	31.64	0.73	7.2	0.21	20.81	0.74	2.56	0.14	14.19	0.54	0.774	0.086	0.015	2.988	0.077
FB11ap_66	327	3.8	358.9	5.1	1883	46	158.40	3.10	663	11	127.8	2.4	845	15	293.7	5.2	22.96	0.56	369.7	6.3	53	1	333.6	5.9	65.8	1.3	179.5	3.7	23.28	0.54	139.5	3.2	20.76	0.51	1.507	0.054	30.25	0.74
FB11ap_67	290.3	2.9	370	5.9	201.8	5.9	1.51	0.09	7.14	0.26	1.705	0.088	14.24	0.7	8.02	0.34	2.73	0.12	14.79	0.49	2.698	0.089	23.97	0.75	6.37	0.2	24.65	0.73	4.45	0.15	32.7	1.1	4.57	0.15	0.434	0.023	2.383	0.065
FB11ap_68	1700	23	362.6	5.3	1413	24	103.40	1.70	424.6	7	78.8	1.5	478	8.5	222.9	3.5	51.8	0.79	330.4	4.5	58.83	0.66	353	4.3	55.56	0.61	124.8	1.5	15.7	0.25	89.9	1.6	10.99	0.21	2.689	0.063	36.15	0.7
FB11ap_69	626.7	6.6	483.5	5.9	1267	21	2501.00	41.00	6142	96	738	13	3159	42	634.8	7.4	41.61	0.59	390.7	4.9	46.35	0.54	252.5	3	44.65	0.45	112.4	1.5	129.6	3.5	33.3	0.3	85.9	1.5	10.79	0.2	2.485	0.056	8.51	0.16
FB11ap_70	340.9	4	391.9	5.6	1353	27	28.10	1.30	114	3.9	22.63	0.81	159.5	5.3	88.1	2.2	22.21	0.64	162.5	3.3	28.83	0.6	209.7	4.1	47.51	0.83	140.6	2.1	18.75	0.39	115.4	2.2	18.01	0.37	18.15	0.5	12.32	0.21
FB11ap_71	122.6	1.6	1110	13	242.9	3.7	8.10	0.23	39.91	0.73	10.78	0.19	97.9	2	46.5	1	15.5	0.32	60.21	0.94	7.73	0.14	43.89	0.67	8.35	0.18	21.37	0.43	2.54	0.083	14.58	0.43	2.161	0.07	0.1096	0.0099	2.312	0.04
FB11ap_72	311.2	4	711	13	484.4	9.5	3.48	0.16	17.15	0.58	4.12	0.19	34.3	1.2	21.29	0.68	4.29	0.13	45.9	1.1	8.32	0.18	65.3	1.4	16.78	0.31	58.3	0.98	9.35	0.2	68.9	1.5	13.13	0.3	5.23	0.13	1.374	0.038
FB11ap_73	658.2	7.9	199.2	3.7	1245	22	71.40	1.60	316.3	4.4	67.2	1.2	427.8	6.7	197.2	3.5	26.4	0.47	231.3	3.4	41.99	0.53	279.4	3.9	54.19	0.75	149.8	2.2	20.87	0.4	133.7	2.3	17.84	0.38	0.0496	0.0088	8.35	0.18
FB11ap_74	350.9	4.1	261.1	4.6	1241	37	18.96	0.96	63.6	3.6	12.94	0.73	92.3	5.6	46.8	2.7	11.82	0.56	85.9	2.3	16.13	0.68	146.1	5.2	39.9	1.2	144.5	3.1	23.82	0.46	159.8	2.5	23.05	0.42	1.772	0.077	41	1.9
FB11ap_75	254.4	3.6	675.4	8.9	123.9	3.5	34.60	1.30	120.9	4.5	20.38	0.81	117.5	4.4	32.2	1.1	11.48	0.39	36.4	1.2	4.33	0.14	23.49	0.83	4.6	0.17	11.65	0.38	1.368	0.076	7.79	0.31	1.389	0.071	1.194	0.051	2.049	0.081
FB11ap_76	293	3.5	469.6	7.3	1285	23	7.25	0.27	27.65	0.48	5.05	0.18	34.3	1.3	20.06	0.67	3.03	0.14	64.6	1.5	17.47	0.31	171.5	2.3	44.32	0.5	129.6	1.6	15.33	0.3	85.9	1.5	10.79	0.2	2.485	0.056	8.51	0.16
FB11ap_77	300.1	3.9	487	11	270.2	6.7	40.90	2.60	143.2	8.7	25.7	1.5	159.2	8.6	62.8	2.4	25.9	1.2	81.5	2.1	9.23	0.22	49.9	1.2	9.74	0.21	23.93	0.55	2.65	0.084	14.92	0.39	2.696	0.085	4.32	0.31	6.58	0.23
FB11ap_78	774.3	6.6	263.8	3.9	679	12	580.00	14.00	883	21	87.9	2	366.5	8	67.6	1.6	19.03	0.43	79.5	1.5	12.24	0.22	91.7	1.6	22.29	0.37	72.8	1.2	10.72	0.19	74.4	1.4	13.42	0.25	133.7	6.1	54.5	3
FB11ap_79	431.6	4.7	452.9	5.7	147.3	3.9	2.91	0.14	10.85	0.4	2.22	0.1	15.3	0.73	7.32	0.4	2.61	0.1	13.84	0.56	2.55	0.1	20.54	0.65	5.25	0.16	17.09	0.47	2.304	0.077	15.33	0.46	2.785	0.064	0.0272	0.0066	1.142	0.04
FB11ap_80	378.3	4.3	300.2	4.8	368	7.3	1.67	0.16	9.38	0.76	2.54	0.2	22.6	1.8	12.27	0.77	2.7	0.14	26.7	1	5.24	0.17	45.9	1	12.83	0.26	46.54	0.86	7.47	0.16	47.49	0.91	6.47	0.13	1.996	0.049	11.26	0.21
FB11ap_81	929	13	103.8	3.4	1319	30	140.30	4.00	524	14	92	2.3	536	14	175.9	3.7	15.54	0.5	222.8	4.5	35.92	0.77	235.7	4.2	47.73	0.76	135	2.3	18.06	0.41	113.7	2.4	17.93	0.52	16.41	0.59	11.37	0.47
FB11ap_82	502.2	4.8	1188	14	379.6	4.8	118.50	2.20	474.8	8	85.6	1.2	508.1	7.9	120.9	1.9	28.28	0.44	110	1.3	12.03	0.18	66.17	0.77	12.53	0.17	33.23	0.53	4.261	0.085	26.52	0.49	4.49	0.11	2.08	0.051	1.028	0.03
FB11ap_83	494.7	5.5	1491	18	130.5	1.8	2.46	0.10	9.07	0.29	1.914	0.083	15.17	0.64	8.49	0.36	3.34	0.13	19.59	0.61	3.326	0.072	22.4	0.45	4.566	0.098	11.96	0.25	1.473	0.046	10.39	0.3	1.191	0.046	0.0079	0.003	0.0733	0.00053
FB11ap_84	599	11	240.4	5.9	2158	51	42.40	1.00	218	5.3	47.8	1.3	345	8.5	181.5	5.7	213.5	2.7	20.81	0.31	80.38	0.96	534.9	4.6	91.19	0.63	197.6	2	20.26	0.28	92.6	1.4	10.84	0.19	0.0419	0.0065	4.498	0.075
FB11ap_85	645.1	6.3	227.4	2.8	2457	42	29.63	0.55	178.2	2.8	43.67	0.67	325.5	5.7	383.3	5.8	20.81	0.31	87	1.3	13.68	0.22	102.8	1.3	24.59	0.23	83.7	1.2	15.58	0.23	12.6	0.2	28.22	0.34				
FB11ap_86	300	2.5	366.7	3.3	812.3	9.1	403.80	5.10	928	14	108.9	1.4	461	6.1	80.3	1.4	12.05	0.27	87	1.3	13.68	0.22	102.8	1.3	24.59	0.23	83.7	1.2	15.58	0.23	12.6	0.2	28.22	0.34				
FB11ap_87	264	2.7	521.2	7.4	316	10	29.60	1.10	111.3	3.9	19.82	0.81	122.7	4.9	44	1.7	9.01	0.33	61.2	2.2	8.77	0.31	55.3	1.8	11.09	0.36	29.5	0.94	3.46	0.14	19.37	0.63	2.96	0.11	1.076	0.052	7.63	0.29
FB11ap_88	755.2	7.4	205.8	3.1	601	23	127.00	5.10	362	15	52.8	2.1	278	11	76	2.8	19.68	0.77	98.6	4.2	14.66	0.51	98.5	3.9	20.85	0.86	59	2.3	7.86	0.32	46.2	1.8	8.03	0.32	14.05	0.48	5.98	0.21
FB11ap_89	101.4	1.2	264.8	3.6	979	18	22.68	0.52	97.5	1.7	21.33	0.43	156	3	80.9	1.5	13.22	0.32	144.2	2.1	27.5	0.36	188.5	2.1	35.43	0.39	82.1	1	8.32	0.14	36.14	0.67	3.734	0.096	0.257	0.017	8.62	0.28
FB11ap_90	172.6	2.4	417.9	5.3	922	17	10.78	0.32	47.05	0.9	10.16	0.26	80	1.9	51.6	1.1	15.1	0.32	105.6	1.7	19.07	0.31	141	1.8	32.1	0.44	98.6	1.2	14.43	0.25	96.9	1.6	15.63	0.29	7.95	0.16	22.66	0.37
FB11ap_91	401.1	3.8	600.8	9.8	75	2.6	9.35	0.47	29.9	1.3	5.26	0.26	33.5	1.7	9.46	0.56	3.44	0.17	11.74	0.53	1.492	0.074	9.84	0.43	2.488	0.078	8.61	0.27	1.489	0.068	12.72	0.43	2.96	0.089	0.322	0.023	1.538	0.068

S2.3 apatite trace-element data (continued)

	55Mn	±	86Sr	±	89Y	±	139La	±	140Ce	±	141Pr	±	146Nd	±	147Sm	±	153Eu	±	157Gd	±	159Tb	±	163Dy	±	165Ho	±	166Er	±	169Tm	±	172Yb	±	175Lu	±	232Th	±	238U	±
FB11ap_92	282.1	3.1	968	13	378.2	6	2.97	0.17	13.34	0.46	3.36	0.15	29.6	1.2	18.53	0.56	6.48	0.18	38.89	0.83	7.02	0.15	55.59	0.8	13.1	0.18	39.77	0.58	5.52	0.11	33.53	0.67	4.97	0.1	0.101	0.01	1.197	0.031
FB11ap_93	423.2	5.5	758	12	100.7	2	300.00	33.00	562	58	59.8	6	242	21	44.5	2.2	10.13	0.34	46	1.3	4.74	0.12	23.11	0.53	3.918	0.078	8.91	0.21	1.027	0.039	5.2	0.2	0.77	0.038	2.58	0.3	0.786	0.024
FB11ap_94	557.4	6.2	360.7	6	1098	23	2606.00	48.00	5890	110	710	12	2935	49	486.3	8.6	39.82	0.72	361.9	5.4	41.89	0.62	221.9	3	37.83	0.48	88.9	1.1	10.31	0.17	57.9	1.1	7.77	0.14	79.9	1.5	19.31	0.37
FB11ap_95	414.9	4.7	607	11	866	21	28.88	0.70	154.7	3.4	39.77	0.9	313.8	6.7	146.1	2.7	45.55	0.79	177.3	2.6	25.02	0.34	151.1	2.2	29.07	0.35	77.4	0.98	10.42	0.17	64.3	1.2	9.87	0.18	5.81	0.14	10.52	0.2
FB11ap_96	236.6	2.4	1207	19	439.7	7.7	45.10	1.00	198	3.7	37.58	0.81	234.4	5	80.8	1.6	19.49	0.39	93.5	1.8	12.25	0.22	73.1	1.2	14.63	0.21	39.69	0.55	6.119	0.092	32.04	0.63	5.35	0.094	21.62	0.4	8.66	0.16
FB11ap_97	402	5.3	480.7	7.6	151.3	2.7	5.89	0.24	16.44	0.46	3.24	0.13	19.83	0.76	7.89	0.37	3.53	0.11	13.43	0.5	2.293	0.063	18.56	0.46	4.97	0.12	17.32	0.38	2.61	0.077	17.21	0.46	3.253	0.085	0.099	0.013	0.336	0.017
FB11ap_98	375.4	6.5	104	1.9	4112	80	111.70	4.30	485	17	99.5	3.3	723	22	300.4	8.6	35.13	0.8	471.6	9.9	86.1	1.7	642	12	147.6	2.3	449.3	6.1	63.71	0.83	391.2	5.5	51.94	0.78	8.99	0.22	20.46	0.51
FB11ap_99	399.8	4.4	866	13	276.2	6.1	8.25	0.30	43	1.2	11.08	0.33	91.9	2.3	42.1	1.2	11.8	0.33	52.7	1.3	7.28	0.17	46.02	0.89	9.57	0.21	28.2	0.51	4.01	0.11	24.83	0.49	4.06	0.11	0.214	0.014	2.731	0.065
FB11ap_100	706.6	8.8	401.3	5.6	1680	29	56.60	1.00	224.5	3.7	43.9	0.86	303.8	5.7	143.2	2.4	13.54	0.28	229.6	3.2	39.25	0.47	275.8	2.9	58.02	0.68	162	1.8	21.44	0.29	124	1.8	16.39	0.26	0.184	0.014	6.35	0.12
FB11ap_101	356.6	4.2	454.7	8.2	433	6.9	66.80	1.20	220.1	4.3	40.21	0.79	242.9	5	84	1.5	13.17	0.25	100.3	1.6	14.1	0.2	85.1	1.4	16.27	0.24	41.67	0.68	4.915	0.099	27.47	0.64	3.787	0.096	0.489	0.025	4.822	0.097
FB11ap_102	714.4	7.2	409.3	6.4	832	20	2220.00	270.00	5070	450	587	35	2320	110	361	11	33.29	0.73	260.9	4.5	29.12	0.44	158.7	2.1	27.75	0.44	70.5	1.1	9.1	0.18	52.3	1.1	7.36	0.16	62.6	1.7	19.88	0.47
FB11ap_103	447.9	4.6	404.7	6.6	771	16	1281.00	24.00	3352	58	448.2	7.1	1894	32	318.3	4.8	27.74	0.47	232.5	3.3	27.71	0.44	151.6	2.3	26.69	0.41	68.28	0.95	8.45	0.16	48.33	0.9	6.43	0.12	13.02	0.3	8.12	0.18
FB13ap_0	238.9	2.8	343.8	4.8	490.4	8.9	56.00	1.50	247.4	6.3	49.6	1.2	327.8	7.4	104.5	2.4	26.79	0.64	110.4	2.6	13.54	0.33	79.1	1.5	15.74	0.33	44.77	0.93	6.09	0.13	39.81	0.89	6.73	0.16	20.25	0.53	31.61	0.66
FB13ap_1	337.8	3.5	488.7	5.7	673.2	9.1	68.40	1.00	269	3.8	53.38	0.77	369.4	5.4	133.3	2	42.9	0.54	146.8	1.9	19.95	0.29	120.6	1.7	23.44	0.38	64.7	1.1	8.84	0.17	58.3	1.1	8.94	0.18	8.72	0.16	17.11	0.33
FB13ap_2	441.3	4.2	601.2	6.9	319	31	10.50	1.90	44.3	8.2	7.4	1.1	51	6.8	24.3	3.1	7.49	0.97	42.6	4.7	7.3	0.8	52.7	5.4	11.9	1.2	34.3	3.3	4.5	0.46	27.5	2.7	4.06	0.41	8.4	1.4	0.76	0.16
FB13ap_3	215.4	2.2	196.7	2.5	939	14	16.24	0.38	88.7	1.3	21.16	0.41	164.7	2.4	96.5	1.6	12.73	0.25	132.1	1.9	26.85	0.4	204.5	3.1	41.38	0.63	110.4	1.7	13.73	0.23	74.9	1.4	8.49	0.18	0.331	0.019	5.1	0.11
FB13ap_4	386.1	5.1	238.8	4.3	786	19	26.00	1.30	96.3	3.6	19.1	0.62	134.5	3.9	70.4	1.8	16.96	0.43	119.9	3.1	20.13	0.51	139.5	3.2	28.44	0.79	84.7	2.1	11.21	0.27	67.6	1.6	10.67	0.29	1.638	0.078	6.65	0.17
FB13ap_5	337	3.6	1035	13	110.3	1.8	1.26	0.09	5.06	0.17	1.099	0.066	9.09	0.5	5.72	0.26	2.58	0.11	14.11	0.44	2.426	0.064	17.91	0.4	3.89	0.1	11.39	0.3	1.448	0.048	8.86	0.24	1.224	0.047	0.0345	0.0062	0.493	0.037
FB13ap_6	369.5	3.9	418.3	5.7	812	14	841.00	15.00	2469	35	370.4	5.1	1663	24	310.5	4.3	35.96	0.56	240.6	3.2	29.91	0.49	166.4	2.9	29.5	0.51	75.9	1.4	9.63	0.22	55.6	1	7.4	0.13	4.98	0.1	12.93	0.27
FB13ap_7	216.8	2.2	267	3.8	686.7	9.2	12.88	0.25	52.33	0.84	10.25	0.22	78.5	1.7	39.53	0.82	3.2	0.11	88.5	1.5	16.88	0.28	120.2	2.1	24.62	0.43	63.6	1.1	7.91	0.17	47.2	1	6.36	0.13	0.726	0.03	5.53	0.11
FB13ap_8	424	5	277.7	3.5	744	15	133.80	2.00	528.5	7.5	93.7	1.5	522.1	9	165.7	2.7	40.56	0.77	159.8	3.1	21.86	0.42	130.8	2.5	25.01	0.49	69.5	1.4	9.66	0.23	63.5	1.5	10.21	0.22	3.618	0.086	19.57	0.5
FB13ap_9	314	3.8	1119	15	640	12	54.44	0.91	286.9	3.7	66.8	1.1	470.9	7.2	166.8	2.8	32.5	0.52	169.3	3.1	22.43	0.43	128.7	2.4	23.56	0.48	61.2	1.1	8	0.2	47.6	1.2	6.47	0.16	0.174	0.013	5.53	0.15
FB13ap_10	290.1	3.2	396.9	5.6	623.1	8.5	32.19	0.68	132.1	2.2	25.08	0.53	169.8	3	61.2	1.1	13.5	0.27	88.8	1.7	14.07	0.28	96.4	1.9	21.95	0.39	69.1	1.2	10.04	0.21	69.3	1.4	12.46	0.23	1.12	0.039	8.4	0.23
FB13ap_11	216.2	2.9	257.4	4.1	809	14	120.40	2.10	686	10	145.8	2.4	912	14	270.1	4.8	22.43	0.49	265.9	4.2	31.73	0.6	171.8	2.8	30.14	0.65	72	1.3	8.13	0.18	43.84	0.95	5.52	0.15	2.89	0.1	3.157	0.082
FB13ap_12	132	1.7	622.5	8.7	196.2	3	43.41	0.74	298	4.5	68.81	0.99	459.2	7	137.9	2.1	25.47	0.46	112.9	1.6	11.02	0.21	48.66	0.98	6.93	0.16	12.81	0.27	1.067	0.048	11.92	0.34	2.011	0.073	0.1067	0.009	1.409	0.028
FB13ap_13	366.1	4.3	384.2	6	63.1	2.2	23.70	0.61	77.4	2.1	12.01	0.37	64.9	2	15.28	0.61	4.4	0.17	15.2	0.59	1.94	0.08	10.9	0.48	2.172	0.091	5.95	0.27	0.762	0.042	4.96	0.27	0.465	0.052	0.36	0.029	1.031	0.059
FB13ap_14	230.5	2.7	276.8	4	686.7	10	49.60	0.73	126.9	2.2	15.46	0.33	74.1	1.7	14.22	0.47	4.06	0.15	13.88	0.44	1.488	0.068	8.06	0.28	1.434	0.062	3.56	0.14	0.383	0.021	2.12	0.11	0.32	0.025	0.307	0.016	1.019	0.026
FB13ap_15	221.6	2.7	864	12	395.5	6.8	15.12	0.36	102.2	1.8	30.88	0.57	286	5.2	125.9	2.1	30.31	0.58	124.5	2.3	14.8	0.27	80.4	1.6	13.8	0.29	34.22	0.76	4.21	0.12	24.81	0.63	3.59	0.1	0.55	0.028	12.94	0.27
FB13ap_16	500.5	5.6	361.9	5.3	531	16	2.12	0.15	5.77	0.31	1.19	0.11	7.3	0.41	3.97	0.25	1.454	0.071	11.89	0.53	3.31	0.13	43.2	1.4	15.79	0.51	69	2	13.21	0.38	101.9	2.9	14.71	0.41	0.301	0.023	4.87	0.15
FB13ap_17	250.2	2.8	1901	29	269.7	5	10.49	0.39	66.9	1.4	19.25	0.4	157.5	2.7	66	1.2	19.21	0.38	74.1	1.5	8.92	0.19	49.32	0.94	9.2	0.19	23.78	0.49	2.962	0.089	18.45	0.53	2.875	0.083	11.86	0.21	10.65	0.2
FB13ap_18	724.2	8.5	121.1	2.3	219.2	3.8	13.12	0.29	44.75	0.83	8.69	0.2	58.2	1.6	26.97	0.71	12.17	0.25	37.07	0.85	5.52	0.11	33.78	0.78	7.1	0.14	19.4	0.26	2.226	0.064	12.55	0.35	2.066	0.059	0.0336	0.0058	0.727	0.026
FB13ap_19	319.5	4.2	793	12	65.7	1.5	2.71	0.14	4.44	0.21	0.951	0.079	4.94	0.46	2.74	0.18	0.797	0.064	6.04	0.35	1.231	0.058	10.16	0.37	2.581	0.085	7.58	0.26	0.949	0.051	5.65	0.32	0.989	0.054	0.55	0.027	1.528	0.057
FB13ap_20	1808	23	67.4	1.4	2144	35	191.40	2.50	668.7	9.5	106.7	1.4	486	6.3	197.3	3.1	19.37	0.37	256.3	4.3	58.55	0.91	423.6	5.9	78.8	1.3	217.3	3.7	30.17	0.44	181	3.4	21.3	0.44	2.604	0.064	27.39	0.58
FB13ap_21	510.7	6.5	104	1.9	4112	80	111.70	4.30	485	17	99.5	3.3	723	22	300.4	8.6	35.13	0.8	471.6	9.9	86.1	1.7	642	12	147.6	2.3	449.3	6.1	63.71	0.83	391.2	5.5	51.94	0.78	8.99	0.22	20.46	0.51
FB13ap_22	473.1	3.8	436.5	5.4	494.8	9.5	5.09	0.18	18.45	0.37	3.31	0.13	21.77	0.95	10.48	0.35	3.62	0.11	22.57	0.6	5.14	0.13	48.9	1.1	15.55	0.28	69.4	1.3	13.08	0.26	106.9	2.2	21.35	0.39	0.549	0.025	3.844	0.089
FB13ap_23	871.7	6.7	716.2	7.9	755	12	37.85	0.69	148.8	2.3	30.92	0.55	222.1	4.3	110.4	1.9	31.78	0.55	145.7	2.3	21.7	0.32	136.3	2.3	26.99	0.49	75.7	1.2	10.34	0.17	67.7	1.3	10.36	0.2	0.483	0.024	2.385	0.056
FB13ap_24	391.9	5.1	380.4	7.3	645	13	4.82	0.26	17.85	0.52	3.36	0.16	23.3	0.98	12	0.56	2.51	0.12	28.36	0.89	6.19	0.17	62.4	1.2	20.34	0.47	89.7	2.1	17.35	0.36	138.6	3.4	22.92	0.5	3.306	0.084	3.492	0.092
FB13ap_25	491.4	4.2	222.3	2.3	2150	27	11.05	0.25	45.76	0.82	9.03	0.23	63.9	1.4	40.54	0.79	12.54	0.27	100.6	1.4	25.97	0.3	262.9	3	78.66	0.7	312.7	3.2	54.18	0.54	399.2	4.8	63.9	0.72	1.854	0.048	27.01	0.35
FB13ap_26	534.3	7.2	331.4	3.9	171.7	3.7	41.50	1.00	144.1	3	26.58	0.6	178.9	4.3	54.4	1.3	18.94	0.36	60.5	1.4	6.88	0.16	36.7	0.84	6.77	0.17	16.96	0.45	2.084	0.068	11.92	0.34	2.011	0.073	0.1067	0.009	1.409	0.028
FB13ap_27	199.5	1.7	617.5	5.5	696.6	9.3	18.06	0.60	94.2	1.7	24.76	0.65	209.7	3.8	106	1.5	36.36	0.57	144	2	20.52	0.36	125.9	1.8	24.97	0.45	67.21	0.99	8.84	0.14	54.6	1	8.52	0.18	1.921	0.07	15.04	0.27
FB13ap_28	199.5	1.7	617.5	5.5	696.6	9.3	18.06	0.60	94.2	1.7	24.76	0.65	209.7	3.8	106	1.5	36.36	0.57	144	2	20.52	0.36	125.9	1.8	24.97	0.45	67.21	0.99	8.84	0.14	54.6	1	8.52	0.18	1.921	0.07	15.04	0.27
FB13ap_29	207.8	3.3	1088	10	164.1	2.7	274.80	7.90	763	20	100	2.3	469.6	9.3	79.4	1.7	21.81	0.34	63.4	1.4	6.92	0.14	35.86	0.62	5.86	0.12	12.76	0.3	1.321	0.054	6.75	0.27	0.793	0.035	9.97	0.49	5.4	0.14
FB13ap_30	749.9	6.8	430	5.2	2159	28	1941.00	27.00	5602	69	773	11	3560	54	715.4	8.8	78.18	0.96	558.4	6.4	75.47	0.95	449.9	5.5	83.25	0.91	228.2	3.3	31.59	0.43	196.8	2.9	27.37	0.43	128.7	1.8	92.6	1.5
FB13ap_31	313.4	2.1	382.6	4.1	180.3	2.7	7.73	0.28	34.44	0.9	7.13	0.22	50.5	1.2	21.46	0.68	3.67	0.14	31.85	0.84	4.93	0.11	32.38	0.62	6.79	0.15	18.08	0.42	2.193	0.069	12.23	0.33	1.938	0.061	2.371	0.085	0.569	0.026
FB13ap_32	624.1	6.3	443.9	4	1089	20	183.70	2.60	817	9.4	163.1	2.2	1018	13	339.8	4	25.94	0.41	346.2	4.4	46.69	0.61	261.4	3.4	45.14	0.66	107	1.5	11.6	0.24	58.6	1.1	7.2	0.17	3.969	0.084	20.72	0.33
FB13ap_33	343.5	3.2	122.8	1.9	653.3	9.5	11.93	0.29	44.56	0.77	9.27	0.26	79.3	1.6	67.8	1.2	12.67	0.25	179.7	2.6	28.51	0.34	149.1	2	22.21	0.33	45.85	0.7	4.47	0.12	19.82	0.49	2.219	0.069	1.288	0.091	21.69	0.31
FB13ap_34	349.8	3.9	448.5	5.2	30.22	0.72	28.48	0.68	65.8	1.6	8.39	0.26	38.6	1	7.3	0.28	3.66	0.12	7.36	0.31	0.854	0.048	4.99	0.19	1.006	0.042	2.95	0.13	0.395	0.024	2.53	0.13	0.461	0.022	0.472	0.018	0.583	0.018
FB13ap_35	433.3	3.3	1037.3	8.8	209.7	2.4	44.60	0.64	188	2.1	38.37	0.58	262.1	3.4	76.8	1.2	19.18	0.28	72.7	1.1	8.33	0.13	43.12	0.57	7.46	0.15	17.93	0.37	2.146	0.069	12.14	0.34	1.72	0.054	0.839	0.033	5.823	0.085
FB13ap_36	130.8	1.8	247.1	3	840	11	7.50	0.27	33.5	0.57	7.59	0.18	61	1.4	39.98	0.76	6.04	0.14	96.8	1.4	19.13	0.26	140.2	1.7	28.56	0.36	71.5	1	7.56	0.17	34.7	0.63	3.639	0.085	0.322	0.051	2.288	0.049
FB13ap_37	373.3	4.1	306.7	4.2	348.5	5	1.65	0.08	8.74	0.21	2.627	0.098	30.18	0.97	24.88	0.63	15.67	0.28	48.41	0.97	7.6	0.15	52.08	0.8	11.19	0.22	33.84	0.65	5.01	0.1	36.51	0.75	6.31	0.13	0.164	0.012	13.24	0.26
FB13ap_38	549.3	6.3	375.6	4.2	762	11	9.79	0.29	37.43	0.86	7.92	0.24	62.2	1.9	41.9	1.1	6.22	0.17	93.7	1.9	16.71	0.24	119.3	1.9	25.04	0.35	69.6	1	8.94	0.15	62.79	0.95	7.45	0.14	0.379	0.02	0.937	0.034
FB13ap_39	81.7	1	960	11	417.5	5.6	89.10	1.10	534.5	7.4	128.2	1.7	881	12	253.6	2.7	48.74	0.7	223.3	3.3	24.58	0.34	113.1	1.8	15.71	0.28	28.65	0.52	2.462	0.068	9.76	0.31	1.02	0.04	0.315	0.018	2.699	0.065
FB13ap_40	245.3	3	1642	19	228.8	3.3	20.80	0.50	131.5	2.4	35.23	0.62	282.6	5.2	96.7	1.8	22.17	0.38	92.5	1.5	10.29	0.19	50.22	0.84	8.2	0.16	17.93	0.4	1.921	0.065	9.73	0.29	1.315	0.045	0.0182	0.0038	0.549	0.022
FB13ap_41	477.8	4.6	448	5.4	1411	20	2029.00	27.00	5333	61	699.3	9.9	3210	40	605.8	6.9	58.52	0.88	471.3	5.8	57.73	0.72	323.2	5.1	56.72	0.88	144.2	2.3	17.89	0.28	102.5	1.6	13.47	0.26	62	1.2	71.5	1.4
FB13ap_42	320.7	3.8	265	3.7	458	5.9	4.67	0.19	22.84	0.37	5.4	0.14	45	1.1	24.71	0.65	4.05	0.14	48.09	0.93	8.44	0.16	64.6	1	16.9	0.29	60.5	1	9.49	0.16	64.9	1.2	11.56	0.19	0.444	0.021	6.12	0.13
FB13ap_43	241.6	2.6	1050	11	395.2	5.4	26.17	0.45	173.8	2.3	45.2	0.64	343.8	4.4	120.5	1.5	28.79	0.4	118.7	2	14.67	0.24	81.2	1.2	14.24	0.25	34.73	0.59	4.054	0.082	22.71	0.53	3.029	0.078	0.0507	0.0064	2.365	0.061
FB13ap_44	305.8	3.7	561.6	7.9	55.7	2.8	29.50	1.20	83.9	3.6	12.47	0.61	71.5	3.7	17.5	1	5.3	0.34	19.3	3	2.14	0.13	11.67	0.69	2.26	0.14	5.5	0.32	0.642	0.053	3.71	0.26	0.637	0.043	0.191	0.022	6.39	0.44
FB13ap_45	108.3	1.8	1447	14	330.2	4.4	194.40	2.50	764	11	149.2	1.8	929	11	227.4	3	45.73	0.6	194.2	3.1	19.34	0.3	87	1.2	12.3	0.23	23.54	0.35	2.15	0.065	9.64	0.32	1.096	0.044	0.14	0.012	1.479	0.034
FB13ap_46	351	3.4	1225	12	78.2	1.4	1.69	0.11	4.37	0.19	1.262	0.085	11.63	0.54	8.5	0.38	3.36	0.12	16.62	0.45	2.366	0.07	14.44	0.37	2.875	0.077	7.49	0.22	0.855	0.039	4.8	0.19	0.708	0.03	0.0248	0.0043	0.37	0.016
FB13ap_47	311.7	3.2	367.1	4.8	185.1	7	48.80	1.20	157.4	3.9	24.72	0.7	151.2	4.2	40.9	1.5	6.34	0.2	49.3	1.7	6.11	0.26	34.7	1.2	6.73	0.29	17.59	0.4	1.524	0.12	14.32	0.63	2.24	0.12	0.739	0.04	3.55	0.15
FB13ap_48	291.1	3.2	553.2	5.9	42.08	0.74	1.16	0.07	4.94	0.16	0.993	0.061	7.35	0.4	3.35	0.19	1.365	0.07	5.72	0.25	0.909	0.04	6.37	0.22	1.515	0.061	4.67	0.17	0.579	0.028	3.75	0.17	0.629	0.03	0.0083	0.0025	0.0907	0.0049
FB13ap_49	730.4	7.4	142.5	2.4	264.7	3.9	7.17	0.25	25.66	0.51	5.5	0.16	42.9	1.2	24.63	0.58	7.33	0.17	41.58	0.76	6.29	0.13	40.44	0.78	8.45	0.16	23.31	0.49	2.921	0.087	17.51	0.42	2.766	0.072	0.247	0.017	2.254	0.08
FB13ap_50	171.7	1.7	510.7	5.9	660.6	9.4	1.01	0.08	4.53	0.18	1.927	0.095	25.48	0.88	31.06	0.69	10.35	0.24	109.8	1.7	24.1	0.35	188.7	2.8	31.07	0.46	88.7	1.6	12.73	0.87	7.5	0.14	0.725	0.029	5.65	0.12
FB13ap_51	420	4.1	508.8	5.3	1812	24	203.90	5.60	1052	23	228.8	4	1338	20	388.3	4	56.18	0.73	381.7	4.8	55.81	0.69	356.5	4.3	72.56	0.96	207.3	2.7	28.99	0.41	187.7	2.8	28.86	0.45	33.93	0.7	22.05	0.42
FB13ap_52	379.6	2.9	269.3	2.8	1028	25	52.90	1.30	246.4	6.8	55.6	1.6	415	11	167.7	4.9	10.42	0.27	210.5	5.2	31.66	0.84	205.9	5.2	39.76	0.98	103.8	2.8	12.22	0.33	62.5	1.7	7.48	0.25	1.8	0.081	16.33	0.6
FB13ap_53	565.1	4.9	243.7	3.1	460.8	5.4	7.74	0.21	64.23	0.99	17.73	0.37	146.7	2.6	65.9	1.1	12.47	0.22	93.9	1.3	13.3	0.2	80.2	1.2	15.27	0.21	37.48	0.59	4.13	0.1	21.36	0.5	2.882	0.075	0.0658	0.008	1.288	0.031
FB13ap_54	432.9	3.8	303.6	3.4	564	17	283.00	12.00	627	26	72.9	2.8	320	13	93.3	3.2	12.55	0.48	109.8	3.8	16.08	0.54	98.2	3.1	18.9	0.62	51.5	1.7	6.96	0.25	44.6	1.5	7.15	0.23	18.78	0.93	9.68	0.5

S2.3 apatite trace-element data (continued)

	55Mn	±	86Sr	±	89Y	±	139La	±	140Ce	±	141Pr	±	146Nd	±	147Sm	±	153Eu	±	157Gd	±	159Tb	±	163Dy	±	165Ho	±	166Er	±	169Tm	±	172Yb	±	175Lu	±	232Th	±	238U	±
FB13ap_55	238.8	2.4	592	6.1	104.1	1.9	2.24	0.13	4.97	0.2	1.462	0.092	12.69	0.71	9.43	0.44	3.06	0.11	18.05	0.61	2.565	0.068	16.2	0.39	3.448	0.088	9.67	0.28	1.323	0.051	8.54	0.3	1.451	0.053	6.46	0.17	2.238	0.056
FB13ap_56	433.4	4.3	279	3.8	164.8	4.8	1.84	0.15	6.21	0.42	1.13	0.1	8.07	0.6	4.01	0.25	2.275	0.086	8.07	0.41	1.719	0.076	16.37	0.58	4.85	0.18	19.2	0.66	3.23	0.13	24.41	0.87	4.75	0.15	0.0225	0.0047	1.069	0.056
FB13ap_57	456.2	3.7	701.4	6.3	269.7	2.8	102.80	1.60	392.1	4.7	67.43	0.91	389.9	5.6	95.4	1.5	31.04	0.4	80.8	1.1	9.28	0.16	51.32	0.74	9.45	0.16	24.91	0.4	3.219	0.082	19.84	0.5	3.022	0.07	5.2	0.11	12.6	0.2
FB13ap_58	486.6	3.9	146.4	2.2	786	10	22.42	0.47	102.3	1.4	24.11	0.39	197.9	3	106.6	1.6	27.15	0.38	178.9	2.3	26.65	0.32	161	1.9	29.28	0.38	68.6	1	7.72	0.13	43.92	0.69	6.42	0.12	0.325	0.018	2.911	0.05
FB13ap_59	286.1	2.5	180.9	2.2	1181	16	71.50	1.10	302	3.9	58.91	0.82	360	4.7	200.7	2.6	29.58	0.42	297.8	3.5	58.99	0.66	364.4	4.5	56.45	0.76	112.2	1.2	11.48	0.18	59.51	0.82	6.57	0.11	0.997	0.052	37.3	1
FB13ap_60	750	5.6	277.2	3.3	1834	26	44.85	0.87	167.6	2.5	32.17	0.55	224.1	3.9	115.5	2	22.2	0.39	209.2	3.2	41.94	0.57	342.3	4.5	78.8	1	240	3.6	35.41	0.52	224.1	3.3	27.67	0.43	5.87	0.17	25.02	0.54
FB13ap_61	276.9	2.5	739.1	5.6	123	19	3.66	0.20	8.22	0.82	1.86	0.2	12.6	1.6	6.9	1.1	1.69	0.28	14.2	2.2	2.42	0.37	18	2.8	4.16	0.66	12.6	1.9	1.87	0.29	12.4	1.8	2.09	0.31	1.73	0.32	4.08	0.54
FB13ap_62	494.3	4	961.6	8.4	915	13	724.00	12.00	2344	33	407.9	5.3	2062	21	450.8	4.1	132.7	1.4	319.5	3	36	0.39	186.6	2.2	32.31	0.38	82.5	1.1	11.05	0.16	70.6	1	10.37	0.16	23.9	0.56	123.6	1.2
FB13ap_63	621.8	6.2	155.1	1.7	1395	26	13.50	0.48	52.8	1.7	11.5	0.36	92.2	2.6	58.2	1.6	9.24	0.17	130.8	2.5	27.61	0.49	230.9	4.1	53.16	0.73	165.1	2.5	23.86	0.41	143.9	2.5	18.74	0.37	1.14	0.1	3.37	0.15
FB13ap_64	349.6	2.9	351.5	4.2	1619	26	133.70	3.00	498	11	98.3	1.9	661	12	269.2	3.8	50.05	0.75	369.2	5.3	62.98	0.71	327.5	4.3	64.59	0.85	169.7	2.5	20.37	0.34	118.3	2	18.46	0.31	22.93	0.34	3.391	0.058
FB13ap_65	424.9	3.2	352.3	4.2	914	14	1065.00	15.00	3301	43	509.8	7.3	2378	30	440.3	6.4	42.16	0.75	323.3	5.2	36.87	0.6	196.5	3.7	34.64	0.6	84.1	1.6	9.98	0.22	65	1.2	7.28	0.2	5.26	0.11	2.652	0.055
FB13ap_66	510.5	7.1	514.5	5.8	1212	25	17.40	1.50	53.7	2.7	9.52	0.37	62.5	2.2	28.15	0.84	9.97	0.24	60.4	1.5	15.03	0.32	164.7	3.2	48.65	0.94	175.3	3.6	26.78	0.58	172	3.2	23.2	0.51	123	38	4.08	0.54
FB13ap_67	685.6	7	349.7	4.8	1493	39	67.20	1.20	287.4	4.9	57.5	1.1	397	7.3	182.5	2.7	19.6	0.36	281.6	4.7	51.93	0.76	351.8	8	65.1	1.5	164.4	4.4	21.17	0.52	126.9	3.2	16.11	0.41	0.294	0.025	13.99	0.33
FB13ap_68	243.9	2.6	988	10	407.8	5.5	12.36	0.41	61.3	1.1	15.57	0.34	128.6	2.7	61.3	1.1	23.15	0.39	88.1	1.5	12.79	0.24	77.1	1.2	14.82	0.24	38.35	0.69	4.674	0.096	26.93	0.65	3.785	0.091	0.556	0.025	2.962	0.064
FB13ap_69	384	4	629.8	7	924	15	49.25	0.77	205.4	2.7	41.73	0.65	265.4	3.9	139.6	1.8	41.53	0.53	216.1	2.9	42.38	0.52	258.3	3.2	38.25	0.43	67.9	1.2	5.53	0.12	21.63	0.57	2.099	0.065	0.262	0.017	20.71	0.39
FB13ap_70	486.4	4.7	643	7.1	814	11	20.98	0.37	127	1.8	37.24	0.67	359.8	5.5	191.7	2.5	41.44	0.55	232.2	3.3	30.16	0.43	169.2	2.5	30.35	0.5	74.2	1.2	8.57	0.2	46.17	0.82	6.18	0.13	0.0852	0.0091	1.082	0.03
FB13ap_71	326.8	3.1	454.9	5	1269	18	66.40	2.40	256	5.6	50.73	0.83	368.2	5.1	187.5	2.2	40	0.5	277.5	3	42.28	0.56	263.3	3.4	50.66	0.74	133.8	2.1	16.98	0.28	100.4	1.6	13.99	0.24	19.54	0.37	14.62	0.27
FB13ap_72	294.3	2.4	565.7	6.2	205.4	2.6	12.09	0.80	30.2	2.4	3.53	0.31	15.3	1.1	4.56	0.28	0.468	0.038	11.17	0.33	2.274	0.064	21.66	0.43	5.73	0.14	27.26	0.58	4.828	0.098	38.59	0.77	7.8	0.17	4.63	0.21	0.453	0.017
FB13ap_73	362.7	3.8	816.2	9.2	712.1	9.7	39.09	0.82	168	3	37.03	0.66	276.6	5.1	120.6	2.1	42.42	0.76	159.5	2.1	22.42	0.34	136.2	2.4	25.91	0.41	66.8	1.2	8.26	0.17	48.79	0.97	6.97	0.14	1.923	0.061	2.123	0.047
FB13ap_74	312.9	3.9	1083	13	931	16	8.07	0.27	69.2	1.2	27.28	0.55	297.9	5.7	187.8	3.1	29.38	0.51	247.7	3	35.21	0.54	205.5	2.7	38.11	0.58	91.8	1.5	10.63	0.24	76.1	1.7	7.21	0.17	0.369	0.022	5.17	0.12
FB13ap_75	441.9	4.3	455.1	5.2	38.3	0.75	3.76	0.14	12.13	0.32	2.066	0.088	13.67	0.57	5.21	0.24	1.284	0.066	8.41	0.29	1.194	0.046	7.11	0.24	1.506	0.055	4.01	0.15	0.477	0.025	2.74	0.15	0.445	0.027	0.0626	0.008	0.383	0.014
FB13ap_76	368.7	4.5	415.5	6.1	1000	25	22.62	0.71	91	2.9	17.53	0.67	125.8	4.7	61.7	2.3	13.66	0.4	123.2	3.9	23.03	0.77	174.9	5.4	38.8	1	110.4	2.8	14.06	0.37	81.1	2.1	10.81	0.29	1.687	0.054	12.13	0.37
FB13ap_77	218.9	2.6	533.5	7.9	135.5	1.8	28.79	0.72	45.64	0.96	6.8	0.21	25.5	0.88	7.23	0.34	1.659	0.089	12.3	0.56	2.333	0.07	18.19	0.46	4.73	0.11	15.88	0.37	2.268	0.071	14.47	0.37	2.344	0.08	1.26	0.049	6.896	0.023
FB13ap_78	553.2	6.9	176.8	3	171.5	4.8	35.80	1.30	75.1	2	8.5	0.26	39.8	1.1	10.6	0.43	3.38	0.14	15.88	0.56	2.83	0.1	21.54	0.67	5.48	0.19	17.79	0.57	2.59	0.11	18.22	0.77	3.34	0.13	7.91	0.42	3.25	0.17
FB13ap_79	577.9	6.1	328.9	4.3	1614	32	17.53	0.49	69.5	1.1	11.17	0.29	76.9	2	39.66	0.86	8.09	0.21	92.9	1.7	20.31	0.35	203.2	3.2	61.48	0.99	237.9	3.8	41.98	0.78	305.3	5.9	45.4	0.99	6.33	0.24	29.66	0.73
FB13ap_80	243.5	2.4	435.7	5.1	264.7	5	12.49	0.33	81	1.5	19.47	0.42	146.2	2.8	51.2	1.1	14.4	0.31	56.2	1.1	7.42	0.15	45.92	0.92	8.99	0.22	24.18	0.57	3.143	0.096	19.09	0.51	2.596	0.075	0.918	0.045	5.13	0.12
FB13ap_81	493	4.9	1301	12	250.5	4.2	5.39	0.20	20.9	2	5.92	0.31	61.8	1.8	45.36	0.92	12.57	0.26	70.4	1.2	9.32	0.15	52.58	0.97	9.21	0.19	22.11	0.51	2.473	0.075	12.98	0.35	1.733	0.053	0.315	0.053	3.602	0.083
FB13ap_82	279.4	4	1653	23	249.4	4.6	81.40	1.80	290.2	7.4	51.6	1.4	309.7	7.5	84.1	2	20.56	0.44	79.3	1.6	8.49	0.18	44.3	1.2	7.91	0.19	22.10	0.51	2.56	0.1	16.24	0.49	2.609	0.079	0.5	0.2	5.42	0.15
FB13ap_83	196.4	2.1	436.3	4.7	66.68	0.95	30.07	0.55	101.3	1.4	17.56	0.33	109.5	1.9	27.22	0.5	5.34	0.11	28.67	0.63	2.949	0.069	14.77	0.32	2.76	0.08	5.69	0.14	0.783	0.037	4.95	0.14	0.849	0.036	0.0949	0.009	4.109	0.071
FB13ap_84	317.3	2.9	549.5	5.9	198	3.4	4.97	0.16	19.77	0.45	4.18	0.13	32.4	0.97	17.15	0.39	3.43	0.11	30.13	0.63	4.92	0.12	33.21	0.77	7.13	0.17	19.66	0.47	2.392	0.079	13.08	0.4	1.931	0.062	0.0777	0.0076	0.791	0.024
FB13ap_85	380.8	4.5	1230	15	74.2	1.1	55.90	1.10	186.3	3.6	30.24	0.56	168.4	3.3	34.74	0.76	6.75	0.18	29.99	0.63	2.933	0.077	15.03	0.46	2.753	0.07	6.63	0.21	0.734	0.034	4.3	0.18	0.71	0.036	0.33	0.016	0.824	0.027
FB13ap_86	474	6.2	328.3	4.6	754	12	1.20	0.09	9.12	0.22	2.68	0.13	24.53	0.81	15.96	0.54	1.665	0.074	40.02	0.77	9.57	0.17	89	1.4	24.21	0.38	83.8	1.3	13.54	0.21	92.2	1.7	13.72	0.23	0.324	0.0045	2.671	0.069
FB13ap_87	182.6	2.3	917	11	366.8	4.9	0.46	0.06	5.2	0.21	2.6	0.14	40	1.1	42.96	0.85	13.41	0.26	86.9	1.6	12.72	0.22	75.4	1.2	13.25	0.21	31.23	0.5	3.398	0.092	16.87	0.36	2.221	0.067	0.0067	0.0027	0.601	0.018
FB13ap_88	393.6	3.5	477	5.3	756	12	23.95	0.55	95.7	1.4	20.24	0.36	162.5	3.1	96.3	1.5	39.68	0.59	169.5	3.1	25.27	0.43	155.3	2.3	28.57	0.47	70.9	1.3	8.4	0.17	49	1	7.07	0.16	0.309	0.018	6.49	0.14
FB13ap_89	341.6	3.6	383.7	5	372.5	4.8	9.26	0.26	45.56	0.81	11.42	0.31	100.8	2.1	53.3	1.1	16.88	0.29	81.4	1.3	11.56	0.21	69.4	1	13.42	0.19	34.97	0.53	4.217	0.082	23.88	0.5	3.485	0.085	0.0514	0.0063	2.991	0.057
FB13ap_90	225.4	2.4	302.9	3.5	320.9	6.3	4.00	1.10	11.76	0.38	2.16	0.1	15.08	0.52	8.73	0.35	2.47	0.1	21.55	0.69	4.41	0.12	38.4	1	10.31	0.22	36.29	0.79	5.61	0.14	37.89	0.91	6.01	0.14	0.773	0.08	1.53	0.52
FB13ap_91	489.4	4.2	401	4.7	1022	15	69.69	0.78	260.1	2.3	48.48	0.68	325	3.4	151.9	1.7	31.82	0.34	220.6	2.1	34.24	0.39	211.4	2	40.76	0.45	103.3	1.2	11.81	0.17	63.43	0.86	9.04	0.16	17.23	0.21	1.14	0.024
FB13ap_92	411.7	4.1	515.8	6	111.9	4.8	8.74	0.51	29.6	1.6	5.2	0.33	32.5	1.9	12.23	0.79	2.73	0.16	18.8	1	2.8	0.14	18.48	0.86	4.11	0.19	11.65	0.48	1.561	0.079	9.71	0.43	1.726	0.084	0.725	0.054	0.98	0.27
FB13ap_93	175.1	2.1	260.4	3.8	944	14	11.16	0.33	67.7	1	20.83	0.4	199.1	3.6	142.7	2.1	15.79	0.32	223.3	2.9	34.8	0.38	207.2	2.7	36.56	0.42	87.9	1.2	10.14	0.18	53.3	0.79	6.36	0.13	0.0064	0.0021	0.694	0.016
FB13ap_94	142.1	1.9	864.2	9	224.4	2.8	1.79	0.12	14.4	0.38	5.57	0.15	68.2	1.5	40.9	0.73	8.46	0.17	58.3	1	7.81	0.13	44.23	0.81	7.91	0.14	19.03	0.39	2.146	0.07	11.74	0.3	1.663	0.048	0.0341	0.0058	0.273	0.012
FB13ap_95	390.9	3.7	165.3	2.3	1176	18	42.16	0.55	179.4	2.3	35.06	0.58	233.6	3.7	117.7	2	17.17	0.32	203.7	3	40.98	0.56	289	3.8	51.27	0.8	108.7	1.7	10.94	0.21	50.69	0.84	5.55	0.13	1.756	0.047	13.23	0.26
FB13ap_96	367.9	2.8	280.2	3.3	860	9.3	8.14	0.27	36.4	0.71	7.96	0.2	63.9	1.4	40.81	0.73	6.84	0.17	86.8	1.2	15.82	0.21	120.7	1.3	28.42	0.3	94.2	1	13.99	0.21	92.9	1.1	16.12	0.22	1.764	0.069	4.168	0.087
FB13ap_97	376.6	3.6	382.1	4	1059	17	15.57	0.35	129.5	1.8	37.78	0.6	312.9	4.9	166.5	1.8	9.6	0.2	243.3	3.1	46.01	0.55	287.7	3.5	45.84	0.64	96.3	1.5	9.34	0.16	40.34	0.6	4.19	0.11	0.0396	0.0067	13.22	0.28
FB13ap_98	439.8	2.8	410.6	4	1068	15	5.62	0.24	42.54	0.87	12.42	0.32	111.7	2.5	73.9	1.2	3.42	0.11	137.8	1.8	27.03	0.36	206.3	2.3	44.62	0.53	121.6	1.5	14.78	0.23	79.4	1.2	9.78	0.16	0.104	0.01	3.213	0.066
FB13ap_99	456.9	3.8	1064.4	9.6	524	6	89.10	1.20	381.7	4	71.76	0.94	414.2	6.3	113.4	1.6	31.62	0.47	104.5	1.4	14.06	0.19	84.9	1.3	17.37	0.21	50.26	0.67	5.48	0.14	49.07	0.65	8.18	0.15	21.92	0.2	39.84	0.29
FB13ap_100	575.9	5.9	962.3	9.2	20.26	0.94	0.33	0.08	1.4	0.16	0.345	0.045	2.75	0.3	1.38	0.16	0.434	0.04	2.83	0.2	0.413	0.033	3.17	0.22	0.707	0.054	2.21	0.14	0.266	0.023	1.74	0.13	0.302	0.024	0.0148	0.004	0.125	0.011
FB13ap_101	134.9	1.4	705.2	6.5	275.2	2.6	12.08	0.33	85.87	0.96	25.16	0.39	219.6	3.4	91.1	1.3	23.99	0.35	104.6	1.5	12.81	0.16	65.58	0.89	10.25	0.17	20.24	0.31	1.905	0.065	8.3	0.25	0.932	0.034	0.423	0.025	3.662	0.054
FB13ap_102	189.7	1.4	1022.7	7.2	329.9	3.3	183.10	1.80	724.6	7.1	119.4	1.4	625.3	6.2	127.6	1.4	26.64	0.31	99.5	1.3	11.42	0.19	62.52	0.64	11.52	0.16	29.97	0.54	3.853	0.084	23.67	0.48	3.501	0.084	0.1	0.1	10.66	0.1
FB13ap_103	305.4	2.2	357.5	3.7	159.6	1.8	25.46	0.49	96.2	1.2	18.45	0.3	128.6	2.3	38.16	0.84	8.83	0.18	45.35	0.92	5.194	0.081	28.13	0.52	5.8	0.13	14.9	0.28	1.946	0.054	13.27	0.36	2.482	0.077	0.444	0.02	5.438	0.068
FB13ap_104	430.8	3.3	624.1	6.6	243.2	5.2	3.71	0.18	11.4	0.32	2.75	0.12	21.76	0.91	14.92	0.52	4.25	0.18	34	1.1	5.64	0.17	39.6	1	8.91	0.22	25.44	0.65	3.282	0.082	20.33	0.49	3.193	0.072	0.601	0.036	0.806	0.03
FB13ap_105	441.7	3.5	371.4	3.5	845	11	849.10	9.80	2192	24	332.3	3.3	1540	17	294.8	3.1	25.52	0.39	231.6	2.8	29.25	0.35	166.7	2.2	30.17	0.37	76.09	0.95	8.95	0.14	46.38	0.76	5.89	0.11	6.73	0.13	4.366	0.076
FB13ap_106	161.2	1.9	253.4	3.1	703.2	6.5	6.09	0.20	24.1	0.45	4.59	0.15	32.7	1.1	17.17	0.6	4.26	0.12	40.01	0.84	9.11	0.15	86.4	1.1	23.54	0.3	78.85	0.83	11.53	0.16	67.37	0.89	8.92	0.16	0.31	0.017	6.493	0.088
FB13ap_107	429.7	3.2	364.5	3.8	1408	16	80.80	1.10	275.4	2.7	47.5	0.72	302	4.1	119.5	1.8	12.99	0.21	190.8	2.2	33.88	0.42	260.3	2.5	55.91	0.54	153.8	1.8	22.18	0.28	129.4	1.6	17.35	0.24	1.373	0.038	6.71	0.1
FB13ap_108	432.3	3.8	455.3	5.1	471.2	5.7	47.35	0.84	192	2.9	35.44	0.58	216.4	3.1	61.9	1	12.77	0.23	69.1	1.1	10.39	0.14	73.04	0.93	16.2	0.24	47.83	0.59	6.44	0.12	39.61	0.63	5.88	0.11	0.723	0.029	10.07	0.11
FB13ap_109	132.2	1.6	415.2	4.5	689.3	7.5	12.28	0.24	79.6	1.1	21.05	0.38	178.3	2.8	91.8	1.5	37.7	0.49	144.4	1.7	21.04	0.27	129.5	1.6	25.16	0.34	61.42	0.81	6.98	0.12	37.54	0.64	5.23	0.1	2.492	0.05	7.85	0.11
FB13ap_110	408.8	3.1	869.2	8.2	204.6	1.9	2.11	0.20	6.16	0.29	1.52	0.1	11.96	0.66	6.73	0.32	1.813	0.089	17.46	0.48	3.546	0.085	28.62	0.51	7.12	0.14	21.03	0.39	2.741	0.069	15.58	0.36	2.362	0.069	0.115	0.018	1.003	0.025
FB13ap_111	458.8	3.7	666.8	6.7	500.5	7.5	14.52	0.33	67.5	1.4	16.01	0.4	128.2	2.8	63.6	1.5	19.43	0.39	98.6	1.6	14.72	0.24	92.5	1.3	18.11	0.29	46.91	0.8	5.86	0.13	34.44	0.73	5.11	0.12	1.721	0.044	4.674	0.081
FB13ap_112	349.2	3.2	739.1	6.8	923	14	52.90	5.60	116.7	8.7	25.6	1.3	192.7	4.4	98.5	1.7	18.01	0.3	156.9	2.4	25.8	0.35	172.2	2.3	34.78	0.57	92.9	1.3	11.6	0.24	62.4	1.2	8.13	0.18	2.95	0.24	4.8	0.1
FB13ap_113	357.6	3.4	372	3.4	1026	16	60.80	1.00	226.8	3.3	44.62	0.66	296.4	4.5	130.5	2	20.07	0.37	222.2	3.1	41.11	0.57	271.8	3.6	44.1	0.6	88.1	1.2	8.41	0.16	37.76	0.82	4.12	0.11	1.267	0.068	13.82	0.22
FB14ap_0	319.4	5.1	487.8	5.3	919	15	802.00	17.00	2243	35	375.5	4.9	1790	20	352.1	3.4	32.7	0.69	288.7	3.5	34.08	0.46	181.6	2.2	32.02	0.45	81	1.2	10.03	0.21	60.6	1.3	9	0.24	2.276	0.055	2.808	0.041
FB14ap_1	220.4	3.3	786	11	325.4	5.6	2.38	0.11	10.74	0.33	2.83	0.11	28.6	1.1	20.44	0.51	2.82	0.09	27.55	0.98	7.37	0.15	51.83	0.96	11.41	0.2	33.15	0.57	4.48	0.11	27.55	0.61	4.09	0.11	0.0276	0.0057	0.871	0.036
FB14ap_2	390.8	5	657	11	792	12	406.00	18.00	1058	37	165.7	5.5	890	26	212	5.5	40.67	0.86	215.8	4.6	26.27	0.46	149	2.3	28.75	0.4	74.48	0.74	9.71	0.18	57.5	1	9.26	0.22	10.24	0.37	2.605	0.05
FB14ap_3	1618	22	1607	68	1592	35	1547.00	26.00	4530	66	648.6	9.9	3155	40	618.2	8.9	33.17	0.88	502.9	7.3	61.53	0.99	346.6	6.1	61.3	1.1	147.4	2.8	18.64	0.45	102.3	2.4	13.55	0.36	63.7	0.97	12.08	0.22
FB14ap_4	501.9	5.2	94.9	1.5	1895	34	438.40	6.90	1720	27	345.6	5.2	2045	32	815	12	10.04	0.21	893	13	114.7	1.3	524.9	6.4	66.92	0.86	112.2	1.4	9.95	0.19	41.93	0.76	4.38	0.1	2.04	0.053	21.48	0.41
FB14ap_5	253.5	2.7	1060	13	151.4	3	3.56	0.22	14.16	0.48	3.54	0.16	31.1	1.3	17.21	0.63	2.75	0.11	30.46	0.82	3.95	0.1	24.91	0.57	5.21	0.13	18.11	0.29	4.784	0.068	11.04	0.34	2.001	0.054	0.083	0.0097	0.1255	0.0084
FB14ap_6	149	1.8	676	11	233.1	4.4	0.82	0.07	5.21	0.21	1.806	0.09	22.02	0.76	16.89	0.56	3.73	0.14	33.77	0.82	5.35	0.12	37.1	0.63	8.11	0.15	23.45	0.43	3.091	0.076	18.43	0.43	2.632	0.074	0.026	0.0053	1.514	0.041

S2.3 apatite trace-element data (continued)

	55Mn	±	86Sr	±	89Y	±	139La	±	140Ce	±	141Pr	±	146Nd	±	147Sm	±	153Eu	±	157Gd	±	159Tb	±	163Dy	±	165Ho	±	166Er	±	169Tm	±	172Yb	±	175Lu	±	232Th	±	238U	±
FB14ap_7	452	9.5	382.8	5.6	3832	68	1889.00	46.00	6150	140	866	20	4023	79	866	15	59.6	1.2	722	13	101.2	1.6	616.9	8.9	122.9	1.6	357.1	5.1	60.04	0.68	318.2	4.5	45.12	0.73	209.9	7.3	203.8	5.5
FB14ap_8	473.2	4.5	289.8	4.6	116.5	1.7	11.75	0.31	46	0.89	8.93	0.24	63.7	1.5	23.51	0.61	4.49	0.13	31.23	0.73	3.89	0.085	22.08	0.43	4.261	0.087	10.86	0.25	1.15	0.043	6.2	0.24	1.006	0.048	0.137	0.012	2.742	0.042
FB14ap_9	1750	22	518.3	7.5	2118	42	577.90	9.50	2057	36	373.9	6	1943	31	469.7	7.8	66.2	1	394.2	5.1	58.81	0.8	363.4	4.1	71.25	0.81	199.2	2.2	26.89	0.42	161.1	2.7	21.35	0.33	1.425	0.062	13.16	0.27
FB14ap_10	1480	18	571.6	7.7	2305	33	101.80	1.70	353.1	7.7	63	1.1	452.2	7.4	225	3.7	14.96	0.24	341.8	4.1	53.29	0.59	352.3	3.8	75.48	0.63	232.1	2.5	36.01	0.44	254.9	3	39.35	0.59	9.97	0.19	28.06	0.55
FB14ap_11	2067	5.9	380.4	6.8	2116	55	1017.00	30.00	3330	120	540	16	2803	84	661	18	15.62	0.36	592	15	79.6	1.6	441.4	7.6	81.5	1.4	206	3.1	24.42	0.41	131.8	2.1	16.8	0.32	15.42	0.48	17.11	0.32
FB14ap_12	351.2	4.5	1116	19	743	15	6.79	0.24	27.15	0.8	5.63	0.19	43.9	1.6	26.17	0.99	8.68	0.28	57.8	1.6	11.69	0.21	93.5	1.6	24.78	0.3	87.4	1.1	14.33	0.25	97.7	1.6	14.99	0.29	10.95	0.19	22.17	0.38

S2.4 Rutile U-Pb data tables

Rutile U-Pb data - collected by LA-ICP-MS - All spots 60µm

	Approx U PPM	Prop2SE	207Pb/235U	Prop2SE	206Pb/238U	Prop2SE	Rho	238U/206Pb	Prop2SE	207Pb/206Pb	Prop2SE	Rho	207Pb corrected age	Prop2SE	f206Pb
FB1ru_0	0.262	0.021	6.2	2.1	0.103	0.02	0.05	9.7087	5.8	0.46	0.25	0.42	319.7	207.5	0.51
FB1ru_1	5.5	0.18	0.58	0.14	0.0546	0.0031	0.04	18.3150	1.1	0.08	0.019	0.22	331.5	20.2	0.03
FB1ru_2	7.15	0.19	0.561	0.08	0.049	0.0023	0.07	20.4082	1	0.086	0.014	0.23	295.7	14.7	0.04
FB1ru_3	9.76	0.26	3.54	0.46	0.0739	0.0046	0.74	13.5318	0.87	0.333	0.033	-0.33	302.8	26.5	0.35
FB1ru_4	19.91	0.47	0.361	0.037	0.0506	0.0015	0.20	19.7628	0.58	0.0534	0.0056	0.19	318.0	9.5	0.00
FB1ru_5	1.714	0.062	0.49	0.2	0.0545	0.0051	-0.06	18.3486	2.2	0.065	0.034	0.02	337.2	34.1	0.01
FB1ru_6	0.172	0.016	56.6	9.8	0.566	0.091	0.56	1.7668	0.34	0.76	0.1	0.08	465.5	432.0	0.87
FB1ru_7	0.168	0.014	3.6	2.5	0.046	0.02	0.30	21.7391	4.7	0.1	0.26	0.26	272.8	149.4	0.06
FB1ru_8	6.03	0.23	0.324	0.084	0.0484	0.0025	0.23	20.6612	1.2	0.049	0.013	0.07	306.0	16.3	0.00
FB1ru_9	16.1	0.53	0.367	0.045	0.0478	0.0018	0.05	20.9205	0.84	0.06	0.0071	0.21	298.2	11.4	0.01
FB1ru_10	2.04	0.12	23.7	3.3	0.262	0.031	0.92	3.8168	0.48	0.656	0.042	0.10	420.3	97.3	0.74
FB1ru_11	19	0.36	1.47	0.14	0.0721	0.0022	0.38	13.8696	0.41	0.148	0.013	-0.05	398.5	13.9	0.12
FB1ru_13	0.674	0.043	1.4	0.67	0.061	0.011	0.03	16.3934	14	0.25	0.21	0.40	269.7	111.7	0.25
FB1ru_14	6.48	0.17	2.11	0.3	0.0655	0.0037	0.56	15.2672	0.91	0.234	0.027	0.05	319.0	22.4	0.23
FB1ru_15	13.83	0.47	0.35	0.038	0.0469	0.0021	0.04	21.3220	1.1	0.0577	0.0073	0.44	293.5	13.2	0.01
FB1ru_16	2.403	0.086	0.74	0.2	0.0527	0.0046	0.08	18.9753	2	0.099	0.029	0.57	312.4	29.3	0.06
FB1ru_17	0.416	0.031	2.7	1.3	0.064	0.012	0.18	15.6250	6.5	0.23	0.3	0.41	313.8	156.9	0.22
FB1ru_18	5.06	0.14	0.509	0.099	0.048	0.0028	0.07	20.8333	1.3	0.084	0.017	0.28	290.5	17.9	0.04
FB1ru_19	0.541	0.032	0.72	0.79	0.046	0.01	0.29	21.7391	9.6	0.11	0.23	0.34	269.2	100.5	0.07
FB1ru_20	0.993	0.046	0.73	0.46	0.0563	0.0087	0.08	17.7620	7.6	0.099	0.098	0.14	333.5	68.1	0.06
FB1ru_21	9.43	0.27	0.374	0.071	0.0521	0.0025	0.03	19.1939	0.97	0.054	0.011	0.20	327.0	16.1	0.00
FB1ru_22	1.391	0.063	12.5	2	0.17	0.019	0.80	5.8824	1.1	0.557	0.065	0.44	401.8	95.0	0.62
FB1ru_23	64.5	3.1	0.626	0.074	0.0566	0.0034	0.23	17.6678	1.2	0.0799	0.0068	0.22	343.5	20.7	0.03
FB1ru_24	1.253	0.055	0.72	0.35	0.0567	0.0061	0.09	17.6367	3.1	0.117	0.071	0.78	327.9	46.5	0.08
FB1ru_26	2.42	0.078	9.26	0.98	0.128	0.01	0.43	7.8125	0.67	0.553	0.057	0.19	303.7	61.2	0.62
FB1ru_27	3.318	0.093	22.2	1.3	0.246	0.015	0.62	4.0650	0.25	0.668	0.034	0.44	367.4	68.6	0.76
FB1ru_28	7.59	0.23	0.71	0.12	0.0683	0.0039	-0.05	14.6413	0.88	0.082	0.016	0.32	412.1	24.5	0.03
FB1ru_29	2.87	0.11	0.34	0.15	0.0522	0.0042	-0.08	19.1571	1.7	0.056	0.027	0.40	326.0	28.0	0.01
FB1ru_30	0.826	0.045	0.45	0.39	0.0598	0.0096	-0.18	16.7224	10	0.11	0.11	0.05	348.8	75.5	0.07
FB1ru_31	0.51	0.025	3.3	1.3	0.084	0.012	-0.11	11.9048	3.8	0.44	0.21	0.51	273.5	142.3	0.48
FB1ru_32	6.16	0.19	0.4	0.1	0.052	0.0026	0.25	19.2308	0.91	0.054	0.014	-0.07	326.4	17.0	0.00
FB1ru_33	1.145	0.05	3.19	0.67	0.0772	0.0091	0.17	12.9534	1.8	0.333	0.062	0.03	316.3	61.1	0.35
FB1ru_34	9.42	0.34	1.38	0.18	0.0602	0.0038	0.36	12.4688	0.64	0.135	0.018	0.25	450.4	23.6	0.10
FB1ru_35	1.616	0.056	0.49	0.24	0.0528	0.0055	0.04	18.9394	2.7	0.062	0.04	0.45	319.9	36.6	0.04
FB1ru_36	2.99	0.12	0.74	0.2	0.0583	0.0044	-0.01	17.1527	1.5	0.103	0.03	0.45	343.3	28.8	0.06
FB1ru_37	5.32	0.19	0.411	0.089	0.0515	0.0034	0.00	19.4175	1.3	0.061	0.015	0.11	320.5	21.7	0.01
FB1ru_39	42.9	1.3	0.699	0.043	0.0683	0.0019	0.25	14.6413	0.43	0.0734	0.0044	0.16	416.6	11.6	0.02
FB1ru_40	7.65	0.25	0.609	0.096	0.0537	0.0027	0.11	18.6220	0.96	0.086	0.014	0.14	323.7	17.0	0.04
FB1ru_41	0.768	0.043	0.66	0.73	0.069	0.014	0.00	14.4928	5.3	0.04	0.1	0.30	438.2	101.4	0.00
FB1ru_42	3.79	0.12	2.59	0.37	0.0648	0.0045	0.29	15.4321	1.3	0.291	0.041	0.39	286.9	28.5	0.30
FB1ru_44	3.39	0.11	0.8	0.17	0.051	0.0041	0.09	19.6078	1.8	0.117	0.028	0.18	295.4	25.9	0.08
FB1ru_45	30	1.2	0.364	0.041	0.049	0.0016	0.15	20.4082	0.77	0.0569	0.006	0.15	306.7	10.1	0.01
FB1ru_46	23.9	0.71	0.343	0.037	0.0465	0.0021	0.06	21.5054	0.93	0.0554	0.0068	0.37	291.8	13.2	0.00
FB1ru_48	0.72	0.034	0.7	0.5	0.0502	0.0078	-0.04	19.9203	9.8	0.13	0.14	0.23	285.7	69.9	0.10
FB1ru_49	9.91	0.36	1.2	0.15	0.0567	0.0024	0.16	17.6367	0.99	0.157	0.016	0.05	310.4	15.2	0.13
FB1ru_50	6.93	0.19	0.75	0.12	0.0607	0.0032	0.13	16.4745	0.92	0.096	0.016	0.21	360.5	20.1	0.05
FB1ru_51	7.22	0.24	0.486	0.09	0.0532	0.0033	0.01	18.7970	1.3	0.071	0.014	0.37	326.8	20.8	0.02
FB1ru_52	1.417	0.065	0.54	0.26	0.0568	0.0056	-0.02	17.6678	2.5	0.064	0.044	0.41	341.7	36.3	0.04
FB1ru_53	5.18	0.23	13.62	0.95	0.1664	0.0093	0.64	6.0096	0.34	0.605	0.032	0.22	328.2	45.4	0.69
FB1ru_54	0.15	0.015	4.9	4	0.162	0.045	0.13	6.1728	3.6	0.39	0.24	0.37	593.9	327.4	0.40
FB1ru_55	1.303	0.06	12	1.2	0.147	0.013	0.26	6.8027	0.6	0.635	0.061	0.66	252.0	95.6	0.73
FB1ru_56	4.39	0.15	0.75	0.15	0.0598	0.0039	0.00	16.7224	1.2	0.096	0.019	0.27	355.3	24.4	0.05
FB1ru_57	1.326	0.063	6.8	2	0.107	0.02	0.92	9.3458	2.4	0.52	0.11	0.55	281.1	105.0	0.58
FB1ru_58	4.14	0.14	0.42	0.11	0.0481	0.0037	0.10	20.7900	1.7	0.074	0.02	0.20	294.8	23.6	0.03
FB1ru_59	6.84	0.21	1.96	0.23	0.0645	0.0036	0.21	15.5039	0.89	0.229	0.026	0.16	316.7	21.7	0.22
FB1ru_61	1.496	0.052	4.02	0.73	0.0707	0.0062	0.44	14.1443	2.9	0.51	0.1	0.90	190.2	59.9	0.58
FB1ru_62	21.04	0.72	0.364	0.052	0.052	0.0019	0.03	19.2308	0.69	0.054	0.0073	0.10	326.4	12.1	0.00
FB1ru_63	1.419	0.07	11.1	1.2	0.147	0.013	0.46	6.8027	0.78	0.579	0.064	0.44	319.4	77.8	0.65
FB1ru_64	22.34	0.83	0.525	0.06	0.0524	0.0021	0.12	19.0840	0.82	0.0737	0.0089	0.23	320.9	13.2	0.03
FB1ru_65	2.463	0.076	0.74	0.23	0.0495	0.0044	0.21	20.2020	3.1	0.114	0.037	0.76	267.9	28.9	0.08
FB1ru_66	0.658	0.045	39	4.5	0.386	0.039	0.67	2.5907	0.33	0.756	0.067	0.31	301.6	203.2	0.88
FB1ru_67	1.07	0.052	15.4	2	0.176	0.021	0.69	5.6818	2.1	0.609	0.096	0.78	342.3	138.4	0.69
FB1ru_68	6.96	0.19	1.92	0.25	0.0759	0.0041	0.33	13.1752	0.76	0.186	0.024	-0.08	397.2	25.2	0.16
FB1ru_69	1.729	0.059	0.42	0.22	0.0545	0.0059	-0.16	18.3486	2.8	0.053	0.036	0.11	342.2	39.4	0.00
FB1ru_70	10.5	0.28	0.94	0.17	0.0562	0.0026	0.39	17.7936	0.92	0.114	0.019	-0.07	326.4	18.0	0.06
FB1ru_71	0.453	0.03	1.21	0.66	0.065	0.013	0.07	15.3846	9	0.14	0.2	0.16	363.8	122.3	0.11
FB1ru_72	0.727	0.036	23.6	3.4	0.24	0.031	0.80	4.1667	0.65	0.79	0.11	0.60	100.8	212.5	0.93
FB1ru_73	0.572	0.035	3.35	0.96	0.075	0.011	0.23	13.3333	5.5	0.45	0.15	0.69	236.0	94.5	0.50
FB1ru_74	1.402	0.062	0.56	0.27	0.0567	0.0073	0.35	17.6367	5	0.062	0.051	0.61	351.9	49.7	0.01
FB1ru_75	0.0736	0.0067	368	60	3.35	0.52	0.89	0.2985	0.066	0.92	0.1	0.43	-34833.7	712374.8	1.00
FB1ru_76	1.76	0.11	8.1	0.65	0.0978	0.0093	0.45	10.2249	1.6	0.684	0.069	0.60	125.4	70.6	0.80
FB1ru_77	41.9	1.1	0.43	0.036	0.0576	0.0015	0.06	17.3611	0.44	0.0534	0.0045	0.21	361.2	9.5	0.00
FB1ru_78	3.46	0.14	0.91	0.17	0.0626	0.0047	0.10	15.9744	1.3	0.117	0.024	0.19	361.6	29.0	0.09
FB1ru_79	5.36	0.14	0.45	0.098	0.0548	0.0031	0.15	18.2482	1.1	0.061	0.013	0.10	340.7	19.7	0.01
FB1ru_80	36.1	1.2	0.379	0.038	0.0472	0.0015	0.12	21.1864	0.65	0.0587	0.0057	0.09	295.0	9.5	0.01
FB1ru_81	2.653	0.085	0.9	0.24	0.0462	0.0044	-0.03	21.6450	3.1	0.163	0.053	0.67	244.1	29.9	0.16
FB1ru_82	0.902	0.042	1.05	0.43	0.0568	0.0062	0.07	17.6056	5	0.18	0.12	0.41	300.8	67.8	0.16
FB1ru_83	0.465	0.03	2.46	0.9	0.065	0.017	-0.12	11.7647	7.6	0.18	0.2	0.49	448.1	155.1	0.15
FB1ru_85	0.711	0.037	1.29	0.61	0.0514	0.0078	-0.01	19.4553	10	0.13	0.17	0.56	292.5	80.5	0.10
FB1ru_86	0.297	0.024	6.1	2.2	0.126	0.023	-0.03	7.8125	4.6	0.26	0.42	0.63	594.6	407.9	0.25
FB1ru_87	6.38	0.19	0.436	0.09	0.0545	0.0028	0.20	18.3486	1.1	0.059	0.013	0.06	339.7	18.0	0.01
FB1ru_88	12.11	0.28	0.591	0.075	0.0695	0.0032	0.27	14.3885	0.68	0.0647	0.0065	0.19	428.3	19.8	0.01
FB1ru_89	6.75	0.22	0.526	0.092	0.0745	0.0035	-0.04	13.4228	0.63	0.0539	0.0092	0.29	464.5	22.0	0.00
FB1ru_90	5.48	0.18	0.6	0.11	0.0622	0.0036	-0.03	16.0772	0.96	0.073	0.014	0.35	390.2	23.8	0.02
FB1ru_91	1.73	0.063	0.69	0.22	0.0527	0.0052	0.00	18.9753	3.2	0.11	0.045	0.29	307.9	35.1	0.07
FB1ru_92	0.836	0.061	69	11	0.626	0.096	0.88	1.5924	0.36	0.801	0.065	0.22	256.0	322.6	0.94
FB1ru_93	10.2	1.5	121.3	5.3	1.073	0.044	0.88	0.9320	0.037	0.824	0.017	0.19	245.2	158.2	0.96
FB1ru_94	3.124	0.09	1.52	0.27	0.0591	0.004	0.26	16.9205	1.4	0.193	0.036	0.26	306.9	26.2	0.17
FB1ru_95	4.34	0.33	1.54	0.21	0.0767	0.0052	0.09	13.0378	0.98	0.157	0.025	0.33	418.3	31.4	0.13
FB1ru_96	2.6	0.14	0.73	0.21	0.0469	0.0037	0.02	21.3220	2.1	0.105	0.035	0.19	276.3	25.0	0.07
FB1ru_97	21.75	0.6	0.572	0.056	0.0704	0.0021	0.20	14.2045	0.46	0.0589	0.0055	0.11	436.8	13.1	0.00
FB1ru_98	2.56	0.1	0.44	0.13	0.0498	0.0045	0.13	20.0803	3.6	0.067	0.024	-0.59	307.8	28.9	0.02
FB1ru_99	3.71	0.12	0.63	0.14	0.0503	0.0039	-0.13	19.8807	2	0.101	0.025	0.47	297.6	24.7	0.06
FB1ru_100	21.93	0.71	0.363	0.04	0.0506	0.0017	0.03	19.7628	0.66	0.0553	0.006	0.36	317.2	10.6	0.00
FB1ru_101	6.42	0.25	0.595	0.096	0.0584	0.0036	0.13	17.1233	1.1	0.076	0.012	0.15	355.1	22.2	0.03
FB1ru_102	0.526	0.037	2.01	0.89	0.064	0.012	0.07	15.6250	6	0.27	0.19	0.19	293.9	108.6	0.27
FB1ru_103	16.6	0.44	0.436	0.049	0.0493	0.0021	-0.14	20.2840	0.61	0.0677	0.0061	0.37	304.5	13.1	0.02
FB1ru_104	44.2	1	0.596	0.036	0.0749	0.002	0.45	13.3511	0.35	0.0567	0.0034	0.14	464.3	12.3	0.00
FB1ru_105	0.231	0.02	1.9	1.4	0.066	0.019	-0.32	15.1515	6.4	0.05	0.23	0.24	414.5	164.0	0.00
FB1ru_107	3.97	0.14	0.49	0.13	0.0514	0.0035	0.17	19.4553	1.5	0.074	0.021	0.01	314.7	22.7	0.03
FB1ru_108	2.252	0.077	5.62	0.55	0.0956	0.0059	-0.07	10.4603	0.8	0.459	0.055	0.53	297.2	44.6	0.51
FB1ru_109	4.64	0.16	0.368	0.083	0.0526	0.0031	0.16	19.0114	1.3	0.054	0.012	0.04	330.1	19.7	0.00
FB2rut_0	0.11	0.011	70	16	0.57	0.12	1.00	1.7544	1.9	0.65	0.68	0.72	1062.9	2648.6	0.69
FB2rut_1	2.289	0.093	0.62	0.18	0.057	0.0061	-0.02	17.5439	3.7	0.109	0.041	-0.32	333.2	39.4	0.07
FB2rut_2	56.2	1.4	0.718	0.038	0.0531	0.0016	0.10	18.8324	0.58	0.097	0.0055	0.32	315.6	9.6	0.06
FB2rut_3	4.18	0.13	14.5	1.9	0.168	0.017	0.88	5.9524	0.66	0.595	0.041	-0.33	345.2	63.4	0.67
FB2rut_4	7.5	0.18	0.477	0.097	0.0471	0.0024	0.09	21.2314	1.1	0.076	0.016	0.16	288.0	15.6	0.03
FB2rut_5	8.67	0.24	0.462	0.079	0.0468	0.0029	0.17	20.4918	1.3	0.074	0.013	0.38	299.0	18.2	0.03
FB2rut_6	11.62	0.3	0.471	0.076	0.0499	0.0023	0.04	20.0401	1.1	0.066	0.011	0.22	308.8	14.6	0.02
FB2rut_7	5.12	0.16	0.41	0.11	0.0469	0.0031	0.08	20.4499	1.4	0.061	0.016	0.15	304.6	20.0	0.01
FB2rut_8	2.417	0.086	0.71	0.18	0.0512	0.0049	-0.04	19.5313	3.7	0.119	0.036	-0.67	295.7	31.3	0.06
FB2rut_9	1.625	0.067	11.41	0.92	0.146	0.012	0.33	6.8493	0.6	0.594	0.054	0.57	299.4	65.9	0.67
FB2rut_10	79.7	2.3	0.364	0.023	0.048	0.0012	0.22	20.8333	0.54	0.055	0.0035	0.20	301.3	7.5	0.00
FB2rut_11	11.82	0.36	0.447	0.07	0.0473	0.002	0.09	21.1416	0.9	0.067	0.011	0.25	292.5	12.8	0.02
FB2rut_12	2.684	0.087	7.3	1.3	0.112	0.011	0.63	8.9286	1	0.44	0.048	0.05	365.7	54.2	0.48
FB2rut_13	9.16	0.21	0.364	0.061	0.0501	0.0026	0.11	19.9601	1.2	0.056	0.0096	0.09	313.9	17.7	0.00
FB2rut_14	1.437	0.067	3.19	0.56	0.0784	0.0064	0.07	12.7551	1.9	0.375	0.072	0.60	295.4	53.7	0.40
FB2rut_15	19.62	0.43	0.409	0.049	0.0464	0.002	-0.06	21.5517	0.89	0.065	0.0084	0.45	267.8	12.6	0.02
FB2rut_16	1.772	0.057	0.84	0.24	0.0551	0.0054	0.27	18.1488	2.4	0.112	0.038	0.18	320.9	34.9	0.07
FB2rut_17	1.64	0.064	6.6	1.6	0.097	0.014	0.85	10.3093	1.9	0.458	0.07	0.40	302.4	67.9	0.50
FB2rut_18	1.214	0.048	0.68	0.29	0.0486	0.0066	-0.02	20.4918	3.9	0.168	0.09	0.68	263.4	49.0	0.15
FB2rut_19	6.06	0.2	0.99	0.22	0.0545	0.0044	0.27	18.3486	1.6	0.134	0.028	-0.05	308.2	27.2	0.10
FB2rut_20	5.17	0.13	0.9	0.17	0.0527	0.0033	0.15	18.9753	1.4	0.125	0.026	0.16	301.6	21.4	0.09
FB2rut_21	2.65	0.12	2.73	0.63	0.0725	0.0066	0.82	13.7931	1.7	0.271	0.048	0.54	332.1	40.0	0.27
FB2rut_22	3.63	0.23	0.62	0.51	0.059	0.01	-0.11	16.9492	3.7	0.069	0.062	0.23	353.7	69.6	0.04
FB2rut_23	2.65	0.18	7.6	1.4	0.11	0.015	0.38	9.0909	1.6	0.528	0.096	0.16	282.1	90.3	0.59
FB2rut_24	1.156	0.05	167	11	1.46	0.1	0.86	0.6849	0.049	0.843	0.03	0.37	-102.6	376.3	1.00
FB2rut_25	1.036	0.045	9.9	2.4	0.139	0.025	0.85	7.1942	2.7	0.57	0.11	0.65	311.6	130.3	0.64
FB2rut_26	1.444	0.055	6.24	0.83	0.124	0.011	0.35	8.0645	0.89	0.522	0.057	0.70	324.9	61.5	0.58
FB2rut_27	1.474	0.058	0.31	0.22	0.0479	0.0058	0.14	20.8768	5	0.083	0.069	0.57	290.3	43.1	0.04
FB2rut_28	12.77	0.57	0.408	0.057	0.0507	0.0024	0.19	19.7239	1	0.0595	0.0064	0.21	316.2	15.1	0.01
FB2rut_29	4.04	0.15	2.11	0.35	0.0672	0.0056	0.57	14.8810	1.5	0.236	0.033	-0.08	326.2	31.7	0.23
FB2rut_30	2.506	0.087	3.32	0.64	0.0797	0.0063	0.56	12.5471	1.8	0.305	0.055	0.38	343.9	48.7	0.31
FB2rut_31	6.27	0.22	0.351	0.083	0.0499	0.0035	0.03	20.0401	1.5	0.054	0.013	0.22	313.4	22.2	0.00

S2.4 Rutile U-Pb data tables (continued)

	Approx U PPM	Prop2SE	207Pb/235U	Prop2SE	206Pb/238U	Prop2SE	Rho	238U/206Pb	Prop2SE	207Pb/206Pb	Prop2SE	Rho	207Pb corrected age	Prop2SE	f206Pb
FB2rut_32	1.351	0.048	2.55	0.65	0.067	0.0094	0.46	14.9254	4.3	0.35	0.095	-0.18	265.6	61.7	0.37
FB2rut_33	2.46	0.18	3.22	0.71	0.0717	0.0067	0.64	13.9470	2.7	0.335	0.07	0.38	292.6	52.3	0.35
FB2rut_34	5.66	0.16	2.46	0.59	0.0705	0.0066	0.65	14.1844	1.4	0.227	0.036	-0.30	347.0	37.4	0.22
FB2rut_35	3.62	0.1	0.71	0.21	0.0587	0.0058	-0.21	17.0358	2.1	0.106	0.039	0.56	343.4	37.7	0.07
FB2rut_36	63.6	1.8	0.4	0.028	0.0479	0.0014	0.38	20.8768	0.72	0.0602	0.0038	0.11	298.7	8.7	0.01
FB2rut_37	3.58	0.12	0.61	0.16	0.0526	0.004	0.14	19.0114	1.9	0.121	0.031	0.14	302.9	26.0	0.09
FB2rut_38	3.41	0.1	0.37	0.12	0.0446	0.0036	0.13	22.4215	2.5	0.07	0.024	0.98	275.0	23.4	0.02
FB2rut_39	7.07	0.26	0.68	0.14	0.0525	0.0037	0.20	19.0476	1.7	0.129	0.02	0.27	299.1	22.3	0.10
FB2rut_40	3.04	0.1	0.46	0.16	0.0527	0.0043	-0.10	18.9753	1.9	0.067	0.023	0.19	325.4	27.7	0.02
FB2rut_41	2.411	0.089	4.01	0.57	0.081	0.0075	0.42	12.3457	1.4	0.364	0.052	0.47	299.5	42.5	0.41
FB2rut_42	0.966	0.051	11.4	2.8	0.136	0.023	0.84	7.3529	3.1	0.57	0.12	0.88	304.6	135.9	0.64
FB2rut_43	3.55	0.1	0.92	0.19	0.0541	0.005	0.26	18.4843	2.1	0.133	0.029	0.23	306.4	30.4	0.10
FB2rut_44	0.869	0.049	2.35	0.59	0.069	0.01	-0.24	14.4928	13	0.37	0.12	0.87	262.6	74.6	0.40
FB2rut_45	15.26	0.36	0.357	0.054	0.0481	0.0021	0.05	20.7900	0.96	0.0536	0.0079	0.22	302.4	13.3	0.00
FB2rut_46	3.7	0.2	4.05	0.98	0.088	0.013	0.92	11.3636	1.4	0.347	0.05	-0.22	350.9	61.1	0.36
FB2rut_46	1.918	0.061	0.93	0.27	0.056	0.0053	0.21	17.2414	2	0.106	0.036	0.34	340.3	34.5	0.07
FB2rut_49	6.43	0.21	3.17	0.48	0.0742	0.0048	0.42	13.4771	0.94	0.311	0.047	-0.02	316.8	33.6	0.32
FB2rut_50	0.526	0.031	3.52	0.98	0.074	0.011	0.08	13.5135	11	0.16	0.36	0.54	402.1	210.4	0.13
FB2rut_51	1.679	0.065	1.36	0.36	0.0578	0.007	0.16	17.3010	4	0.211	0.072	0.83	292.2	47.5	0.20
FB2rut_52	3.93	0.11	0.79	0.19	0.0601	0.0047	0.16	16.6389	1.6	0.086	0.024	-0.10	361.6	29.9	0.04
FB2rut_53	1.805	0.061	6.5	1.1	0.0963	0.0097	0.47	10.3842	1.5	0.484	0.071	0.57	260.3	60.0	0.54
FB2rut_54	3.11	0.17	0.8	0.18	0.0577	0.0045	0.26	17.3310	1.7	0.106	0.025	0.26	337.6	28.2	0.07
FB2rut_55	0.129	0.016	357	67	2.9	0.54	1.00	0.3448	0.12	0.919	0.081	0.55	-9703.4	10322.7	1.00
FB2rut_56	3.93	0.15	0.48	0.11	0.0503	0.0038	-0.06	19.8807	1.8	0.072	0.018	0.17	306.9	24.0	0.02
FB2rut_57	34	1	0.51	0.046	0.0479	0.0016	0.18	20.8768	0.65	0.0781	0.007	0.11	292.1	10.0	0.03
FB2rut_58	1.65	0.1	0.3	0.22	0.0543	0.0065	0.02	18.4162	5.2	0.054	0.04	-0.54	340.6	43.4	0.00
FB2rut_59	4.58	0.12	0.59	0.12	0.0614	0.0043	0.06	16.2866	1.3	0.07	0.016	0.18	376.8	27.0	0.02
FB2rut_60	4.7	0.12	0.46	0.11	0.0474	0.0035	0.14	21.0970	1.9	0.076	0.019	0.26	269.8	22.2	0.03
FB2rut_61	2.477	0.097	2.04	0.34	0.0649	0.0054	-0.14	15.4083	1.9	0.26	0.059	0.64	292.9	38.2	0.26
FB2rut_62	26.69	0.91	1.55	0.2	0.0582	0.0029	0.69	17.1821	0.89	0.191	0.013	-0.33	303.2	16.7	0.17
FB2rut_63	5.4	0.17	3.75	0.53	0.0773	0.0051	0.33	12.9366	0.95	0.353	0.048	0.14	304.6	34.9	0.37
FB2rut_64	5.6	0.22	0.93	0.18	0.0501	0.0038	0.34	19.9601	1.7	0.141	0.028	0.13	260.9	23.7	0.11
FB2rut_65	2.353	0.087	0.77	0.2	0.0534	0.0047	0.27	18.7266	3.3	0.116	0.032	-0.55	309.5	29.9	0.09
FB2rut_67	1.461	0.062	5.73	0.83	0.103	0.011	0.46	9.7087	1.1	0.455	0.074	0.35	323.8	67.9	0.50
FB2rut_68	1.436	0.059	12.5	1.1	0.153	0.014	0.36	6.5359	0.8	0.652	0.075	0.64	241.3	92.5	0.75
FB2rut_69	10.69	0.29	0.327	0.064	0.0472	0.0024	-0.04	21.1864	1.1	0.0501	0.0096	0.31	298.1	15.3	0.00
FB2rut_70	2.887	0.098	0.44	0.15	0.0492	0.0047	0.06	20.3252	2.9	0.065	0.025	-0.03	304.9	30.2	0.02
FB2rut_71	1.973	0.069	0.91	0.27	0.0516	0.0057	0.35	19.3798	3.9	0.15	0.052	0.66	265.6	37.4	0.12
FB2rut_72	3.21	0.13	0.65	0.16	0.0516	0.0048	0.04	19.3798	2.1	0.097	0.024	0.34	306.6	29.7	0.06
FB2rut_74	5.65	0.23	0.382	0.074	0.0456	0.0031	0.14	21.9341	2	0.062	0.012	0.42	285.2	19.5	0.01
FB2rut_75	2.06	0.092	1.41	0.32	0.0573	0.0062	0.07	17.4520	4	0.194	0.1	0.96	297.2	54.5	0.16
FB2rut_76	1.525	0.063	0.6	0.25	0.0513	0.0061	0.08	19.4932	4.6	0.118	0.058	-0.22	296.7	41.7	0.06
FB2rut_77	7.96	0.29	0.72	0.11	0.0539	0.0029	0.13	18.5529	1	0.097	0.015	0.00	320.3	18.1	0.05
FB2rut_78	3.51	0.14	0.75	0.16	0.0488	0.0036	0.11	20.4918	2.1	0.115	0.027	0.72	283.5	23.0	0.08
FB2rut_79	2.988	0.091	0.68	0.18	0.0537	0.005	0.15	18.6220	2.5	0.092	0.029	0.29	321.2	31.8	0.05
FB2rut_80	6.11	0.21	0.54	0.11	0.0469	0.003	0.12	21.3220	1.5	0.09	0.018	0.27	281.7	18.9	0.05
FB2rut_81	0.825	0.04	1.24	0.47	0.052	0.0078	0.35	19.2308	20	0.252	0.098	0.44	246.4	54.0	0.25
FB2rut_82	4.12	0.14	0.54	0.17	0.0431	0.0047	0.06	23.2019	3.9	0.093	0.032	0.45	256.2	29.8	0.05
FB2rut_83	7.98	0.21	0.82	0.13	0.0514	0.0026	0.07	19.4553	1.1	0.118	0.02	0.17	297.3	16.8	0.08
FB2rut_84	4.1	0.13	3.25	0.63	0.0758	0.0068	0.78	13.1926	1.3	0.335	0.049	-0.03	309.4	39.6	0.35
FB2rut_85	9.62	0.39	0.651	0.083	0.0496	0.0031	0.29	20.1613	1.4	0.101	0.013	0.20	293.5	18.8	0.06
FB3ru_0	2.611	0.038	0.51	0.1	0.0525	0.0028	-0.02	19.0476	1.1	0.07	0.015	0.43	323.0	18.0	0.02
FB3ru_1	3.221	0.054	1.77	0.18	0.0632	0.0032	0.14	15.8228	0.89	0.213	0.025	-0.13	316.2	20.0	0.20
FB3ru_2	6.392	0.1	1.29	0.14	0.0602	0.0024	-0.09	16.6113	0.69	0.156	0.018	0.32	328.8	15.4	0.13
FB3ru_3	0.0996	0.0079	150	16	1.31	0.14	0.86	0.7634	0.093	0.896	0.075	0.01	-1577.0	1100.2	1.00
FB3ru_4	2.909	0.096	7.73	0.47	0.1173	0.0056	-0.06	8.5251	0.46	0.497	0.033	0.10	330.3	33.8	0.55
FB3ru_5	34.1	1.3	1.313	0.08	0.0508	0.0012	-0.07	19.7628	0.47	0.195	0.014	0.37	262.4	8.3	0.18
FB3ru_6	1.347	0.043	2.81	0.42	0.0802	0.0072	0.10	12.4688	1.3	0.261	0.053	0.28	360.9	45.5	0.28
FB3ru_7	0.729	0.024	42.3	3.3	0.424	0.034	0.67	2.3585	0.2	0.771	0.054	0.43	276.7	160.7	0.90
FB3ru_8	9.53	0.33	0.684	0.072	0.0818	0.0024	0.07	12.2249	0.38	0.0611	0.0065	0.26	504.6	15.0	0.00
FB3ru_9	3.41	0.14	0.69	0.13	0.0713	0.0036	-0.17	14.0252	0.73	0.077	0.016	0.41	432.6	23.1	0.03
FB3ru_10	0.676	0.024	14	2.7	0.17	0.023	0.19	5.8824	1.9	0.57	0.11	-0.10	384.0	151.3	0.64
FB3ru_11	5.55	0.12	0.51	0.068	0.0544	0.0023	0.14	18.3824	0.86	0.0694	0.0099	0.19	334.8	14.5	0.02
FB3ru_12	24.65	0.36	0.709	0.04	0.0684	0.0014	-0.01	14.6199	0.29	0.0754	0.0041	0.07	416.1	8.6	0.03
FB3ru_14	3.451	0.098	4.52	0.34	0.0871	0.0044	0.34	11.4811	0.64	0.392	0.033	0.42	316.6	27.3	0.42
FB3ru_15	10.36	0.19	0.478	0.052	0.0547	0.0017	-0.06	18.2815	0.62	0.065	0.0074	0.31	338.4	10.8	0.01
FB3ru_16	0.325	0.016	3.54	0.65	0.098	0.015	-0.01	10.2041	2.6	0.45	0.14	0.66	311.7	115.8	0.49
FB3ru_17	3.044	0.083	5.34	0.42	0.0936	0.0054	0.61	10.6838	0.63	0.445	0.035	0.11	301.3	30.7	0.49
FB3ru_19	0.679	0.019	0.65	0.26	0.0538	0.0068	0.00	18.5874	3.5	0.23	0.19	0.51	264.1	86.0	0.22
FB3ru_20	0.933	0.024	6.28	0.9	0.125	0.01	0.38	8.0000	0.68	0.513	0.067	0.72	336.5	69.7	0.57
FB3ru_21	2.4	0.14	0.65	0.14	0.0528	0.0039	0.15	18.9394	1.7	0.091	0.021	-0.06	316.3	24.5	0.05
FB3ru_22	0.686	0.019	0.79	0.25	0.0532	0.0058	-0.20	18.7970	3.7	0.177	0.066	0.98	283.2	40.8	0.16
FB3ru_23	1.131	0.042	0.7	0.17	0.0559	0.0048	0.05	17.8891	1.9	0.095	0.027	0.60	332.8	30.4	0.05
FB3ru_24	0.62	0.02	16.7	2	0.167	0.018	0.60	5.3476	0.58	0.655	0.076	0.34	293.6	113.8	0.75
FB3ru_25	0.365	0.016	10.8	1.8	0.133	0.015	0.44	7.5188	1.5	0.77	0.23	0.95	75.8	246.5	0.91
FB3ru_26	4.098	0.058	0.557	0.089	0.0574	0.0026	0.17	17.4216	0.76	0.072	0.012	0.17	351.8	16.5	0.02
FB3ru_27	4.76	0.13	0.84	0.1	0.0579	0.0029	-0.08	17.2712	1	0.11	0.014	0.10	337.9	17.8	0.07
FB3ru_28	0.907	0.026	0.77	0.21	0.0545	0.0055	0.06	18.3486	3.6	0.107	0.032	-0.34	319.6	34.5	0.07
FB3ru_29	10.96	0.12	0.46	0.057	0.0501	0.0016	-0.03	19.9601	0.61	0.0712	0.0068	0.31	306.0	10.3	0.02
FB3ru_30	10.29	0.3	1.44	0.23	0.064	0.0028	0.04	15.6250	0.69	0.157	0.023	0.17	349.9	18.8	0.13
FB3ru_31	10.32	0.17	0.441	0.049	0.0542	0.0015	0.13	18.4502	0.54	0.0589	0.0067	0.17	337.9	9.6	0.01
FB3ru_32	4.267	0.068	0.482	0.082	0.0549	0.0027	-0.07	18.2149	0.95	0.065	0.011	0.11	339.6	17.1	0.01
FB3ru_33	1.399	0.027	0.6	0.16	0.0504	0.0044	0.02	19.8413	2.7	0.08	0.023	0.33	306.4	27.8	0.03
FB3ru_34	0.779	0.028	42.5	3	0.433	0.03	0.71	2.3095	0.17	0.732	0.044	0.34	445.4	148.5	0.83
FB3ru_35	1.016	0.061	5.68	0.58	0.1001	0.0077	0.16	9.9900	0.96	0.469	0.063	0.63	303.4	54.0	0.52
FB3ru_36	5.737	0.083	0.376	0.07	0.0452	0.002	-0.02	22.1239	1.1	0.064	0.014	0.03	280.8	13.2	0.02
FB3ru_38	3.26	0.12	3.85	0.43	0.0868	0.0053	0.26	11.5207	0.94	0.308	0.032	0.06	372.4	30.8	0.31
FB3ru_39	1.95	0.058	0.49	0.12	0.0573	0.0044	-0.07	17.4520	1.6	0.07	0.018	0.33	352.0	27.7	0.02
FB3ru_40	0.333	0.015	256	19	2.31	0.17	0.66	0.4329	0.033	0.811	0.036	0.27	453.9	667.2	0.97
FB3ru_41	1.797	0.042	0.5	0.13	0.0526	0.0036	-0.09	19.0114	1.6	0.075	0.021	0.46	321.6	24.4	0.03
FB3ru_43	0.9	0.026	3.8	1.2	0.074	0.01	0.62	13.5135	2.4	0.329	0.077	0.30	305.5	59.9	0.34
FB3ru_44	1.772	0.044	0.55	0.13	0.0519	0.0042	-0.07	19.2678	1.7	0.079	0.019	0.30	315.8	26.3	0.03
FB3ru_45	1.368	0.049	15.3	2.3	0.175	0.018	0.58	5.7143	0.59	0.622	0.068	0.16	321.6	62.5	0.71
FB3ru_46	28.14	0.68	1.55	0.13	0.0592	0.0016	0.59	16.8919	0.47	0.188	0.014	-0.38	309.7	10.5	0.17
FB3ru_47	11.03	0.2	4.58	0.63	0.0823	0.0058	0.91	12.1507	0.9	0.371	0.031	-0.67	312.7	29.4	0.40
FB3ru_48	28.75	0.57	0.451	0.034	0.0544	0.0011	0.25	18.3824	0.37	0.0604	0.0046	0.05	336.5	7.0	0.01
FB3ru_49	1.805	0.048	0.54	0.13	0.054	0.0042	0.16	18.5185	1.6	0.083	0.023	0.31	326.7	26.8	0.04
FB3ru_50	5.46	0.13	0.53	0.16	0.0547	0.0024	-0.03	18.2815	0.84	0.074	0.02	0.01	334.6	16.7	0.03
FB3ru_51	0.994	0.027	0.65	0.2	0.0546	0.0055	0.13	18.3150	2	0.097	0.037	0.41	324.4	35.7	0.05
FB3ru_53	0.0869	0.007	380	47	3.32	0.36	0.89	0.3012	0.038	0.863	0.053	0.22	-6338.6	4376.3	1.00
FB3ru_54	7.06	0.23	5.86	0.46	0.0972	0.0051	0.16	10.2881	0.56	0.44	0.025	0.11	316.8	25.1	0.48
FB3ru_55	2.145	0.09	1.96	0.23	0.0676	0.0048	0.03	14.7929	1.1	0.232	0.03	0.46	330.2	27.9	0.22
FB3ru_56	1.448	0.036	0.71	0.19	0.0504	0.0048	0.18	19.8413	4.3	0.103	0.031	-0.35	297.4	30.4	0.06
FB3ru_57	3.72	0.074	0.56	0.13	0.0497	0.0034	-0.01	20.1207	1.9	0.092	0.03	-0.03	297.6	23.1	0.05
FB3ru_58	0.533	0.034	563	6	0.516	0.053	0.89	1.9380	0.2	0.835	0.064	0.36	4.5	271.6	1.00
FB3ru_59	6.62	0.24	0.856	0.069	0.0561	0.0023	0.05	17.8253	0.8	0.11	0.011	0.36	327.5	14.0	0.07
FB3ru_60	0.1266	0.0081	34.1	7	0.306	0.049	0.28	3.2680	3.3	0.48	0.76	0.63	931.2	1621.6	0.49
FB3ru_61	4.133	0.066	0.477	0.087	0.0512	0.0028	0.01	19.5313	1.2	0.075	0.015	0.34	313.1	17.9	0.03
FB3ru_62	36.58	0.28	0.373	0.024	0.0506	0.0011	-0.08	19.7628	0.46	0.0535	0.0037	0.34	317.9	7.0	0.00
FB3ru_63	7.74	0.11	0.61	0.14	0.0515	0.0021	0.31	19.4175	0.83	0.08	0.012	0.00	313.0	13.4	0.03
FB3ru_64	0.969	0.024	0.6	0.2	0.0508	0.0057	-0.08	19.6850	4.4	0.136	0.06	0.84	286.7	39.5	0.10
FB3ru_65	0.703	0.033	0.68	0.26	0.0608	0.0074	0.01	16.4474	3.3	0.167	0.076	0.48	327.9	53.0	0.14
FB3ru_66	0.268	0.012	4.4	1.1	0.104	0.017	0.51	9.6154	25	0.43	0.11	0.47	347.4	104.0	0.47
FB3ru_67	4.19	0.17	1.96	0.28	0.063	0.0034	0.27	15.8730	0.84	0.222	0.03	0.14	312.6	22.1	0.21
FB3ru_68	37.04	0.31	0.425	0.029	0.0561	0.0011	0.00	17.2117	0.33	0.0532	0.0036	0.12	364.3	7.0	0.00
FB3ru_69	5.456	0.077	0.815	0.093	0.0534	0.003	0.09	18.7266	1.4	0.116	0.014	0.24	309.5	18.1	0.08
FB3ru_70	6.1	0.21	1.05	0.1	0.0615	0.0022	0.01	16.2602	0.6	0.127	0.013	0.32	350.6	13.6	0.09
FB3ru_71	60.2	2.5	0.514	0.035	0.069	0.0034	0.32	14.4928	0.73	0.0541	0.0036	-0.13	430.8	20.8	0.10
FB3ru_72	0.913	0.025	0.8	0.24	0.0542	0.0064	-0.13	18.4502	4.4	0.36	0.28	0.95	210.5	121.7	0.39
FB3ru_73	10.9	0.17	2.54	0.2	0.0735	0.0027	0.62	13.6054	0.52	0.251	0.016	-0.09	348.0	15.5	0.25
FB3ru_74	4.05	0.1	0.433	0.081	0.0603	0.003	-0.06	16.5837	0.93	0.053	0.01	0.34	376.0	19.0	0.00
FB3ru_75	1.292	0.035	0.38	0.14	0.053	0.0045	-0.03	18.8679	1.9	0.066	0.025	0.42	327.7	29.2	0.02
FB3ru_76	7.71	0.11	0.426	0.055	0.0522	0.0022	0.06	19.1571	0.87	0.0581	0.0072	0.23	326.0	13.8	0.01
FB3ru_77	4.155	0.076	0.453	0.076	0.0536	0.0026	0.00	18.6567	0.96	0.063	0.011	0.32	332.5	16.5	0.01
FB3ru_78	1.676	0.035	0.54	0.14	0.0552	0.0035	0.09	18.1159	1.3	0.075	0.021	0.15	337.2	22.8	0.03
FB3ru_79	3.693	0.063	2.96	0.75	0.0722	0.0048	0.12	13.8504	1.1	0.274	0.032	-0.04	329.0	27.9	0.27
FB3ru_80	43.16	0.54	0.61	0.029	0.0751	0.0011	0.06	13.3156	0.2	0.0595	0.0029	0.25	465.0	6.9	0.00
FB3ru_81	2.507	0.053	0.52	0.11	0.0537	0.0037	0.11	18.6220	1.4	0.079	0.017	-0.06	326.5	23.2	0.03
FB3ru_82	1.18	0.035	11.79	0.86	0.146	0.01	0.49	6.8493	0.55	0.627	0.054	0.42	259.9	64.2	0.72
FB3ru_83	3.416	0.052	5.12	0.34	0.0857	0.0038	0.16	11.6686	0.56	0.443	0.033	0.51	277.0	25.2	0.49
FB3ru_84	1.691	0.04	1.03	0.37	0.0567	0.0058	0.89	17.6367	1.8	0.133	0.036	-0.24	320.9	35.9	0.10
FB3ru_86	2.412	0.046	0.47	0.12	0.0508	0.0032	0.02	19.6850	1.4	0.064	0.027	0.09	307.2	21.8	0.04
FB3ru_87	17.4	0.21	0.436	0.042	0.0574	0.0016	0.20	17.4216	0.49	0.0556	0.0052	-0.11	359.0	10.1	0.00
FB3ru_88	4.979	0.096	0.522	0.079	0.0485	0.0024	0.06	20.6186	1.1	0.082	0.013	0.25	294.2	15.2	0.04
FB3ru_89	1.532	0.041	0.57	0.15	0.0513	0.0042	0.03	19.4932	1.9	0.086	0.026	0.12	309.4	27.0	0.04
FB3ru_90	1.005	0.032	0.76	0.22	0.0586	0.0057	0.28	17.0648	2.1	0.094	0.031	0.45	349.1	36.2	0.05

S2.4 Rutile U-Pb data tables (continued)

	Approx U PPM	Prop2SE	207Pb/235U	Prop2SE	206Pb/238U	Prop2SE	Rho	238U/206Pb	Prop2SE	207Pb/206Pb	Prop2SE	Rho	207Pb corrected age	Prop2SE	f206Pb
FB3ru_92	3.21	0.11	0.99	0.35	0.0564	0.0043	-0.08	17.1233	1.5	0.133	0.052	0.09	330.4	33.4	0.10
FB3ru_93	2.654	0.047	0.54	0.12	0.0501	0.003	-0.09	19.5601	1.4	0.08	0.017	0.64	304.6	19.1	0.03
FB3ru_94	6.47	0.12	0.512	0.07	0.0548	0.0024	-0.14	18.2482	0.9	0.0715	0.0089	0.34	336.3	15.1	0.02
FB3ru_95	7.42	0.39	2.02	0.45	0.0739	0.005	0.78	13.5501	0.88	0.165	0.026	-0.51	398.2	30.8	0.14
FB3ru_97	6.116	0.085	0.402	0.056	0.052	0.0022	-0.06	19.2306	0.87	0.0579	0.0083	0.31	324.6	13.9	0.01
FB3ru_98	16.53	0.16	0.415	0.039	0.0522	0.0015	-0.03	19.1571	0.55	0.0598	0.0062	0.29	325.3	9.5	0.01
FB3ru_100	22.88	0.21	0.379	0.03	0.048	0.0011	-0.08	20.8333	0.48	0.0582	0.005	0.40	300.1	7.0	0.01
FB3ru_101	1.245	0.031	0.7	0.21	0.0528	0.0051	-0.06	18.9394	2.4	0.122	0.039	0.60	303.6	33.0	0.09
FB3ru_102	2.049	0.041	0.53	0.12	0.0469	0.004	0.02	21.3675	2	0.088	0.022	0.18	281.9	25.1	0.04
FB3ru_103	0.918	0.024	0.56	0.22	0.0544	0.0058	0.17	18.3624	3	0.136	0.06	-0.08	306.8	40.9	0.10
FB3ru_105	0.649	0.021	4.31	0.67	0.0791	0.0085	0.24	12.6422	2.1	0.52	0.11	0.84	206.7	71.9	0.59
FB3ru_106	2.293	0.076	0.58	0.12	0.0528	0.0036	0.19	18.9394	1.5	0.082	0.018	0.27	319.9	22.7	0.04
FB3ru_107	4.16	0.15	4.04	0.57	0.0887	0.0052	0.78	11.2740	0.73	0.317	0.033	-0.26	374.3	31.1	0.33
FB3ru_108	0.207	0.025	211	23	1.91	0.21	0.62	0.5236	0.11	0.824	0.06	0.56	1361.9	781.0	0.67
FB3ru_109	1.019	0.042	13.4	1.1	0.148	0.011	0.19	6.7568	0.69	0.711	0.074	0.18	159.7	69.0	0.83
FB3ru_110	13.8	1.5	0.362	0.044	0.0446	0.0015	-0.06	22.4215	0.79	0.0596	0.0077	0.25	278.6	9.6	0.01
FB3ru_111	2.363	0.074	5.35	0.47	0.0946	0.0057	0.32	10.5708	0.67	0.424	0.037	0.13	320.2	33.1	0.46
FB3ru_113	14.32	0.43	0.459	0.048	0.0575	0.0021	0.04	17.3913	0.69	0.0577	0.0061	-0.01	358.7	13.2	0.00
FB3ru_114	1.376	0.058	0.75	0.18	0.058	0.0048	0.05	17.2414	1.9	0.095	0.025	0.24	345.2	30.2	0.05
FB3ru_115	5.503	0.071	0.37	0.063	0.0499	0.0023	0.07	20.0401	0.94	0.054	0.0098	0.11	313.4	14.7	0.00
FB3ru_116	1.499	0.05	0.71	0.21	0.056	0.0049	0.26	17.8571	1.8	0.097	0.031	0.18	332.6	31.6	0.05
FB3ru_117	0.618	0.019	1.15	0.39	0.0522	0.0063	-0.04	19.1571	9.1	0.27	0.087	-0.02	239.9	45.6	0.27
FB3ru_118	2.013	0.043	6.01	0.51	0.1	0.006	-0.02	10.0000	0.67	0.47	0.051	0.08	302.3	43.4	0.52
FB4_0	3.447	0.074	0.449	0.084	0.0491	0.0026	0.36	20.3666	1.2	0.066	0.011	-0.07	303.9	16.4	0.02
FB4_1	3.176	0.069	0.51	0.1	0.0518	0.0023	0.48	19.3050	0.88	0.074	0.015	-0.12	317.2	15.1	0.03
FB4_2	1.536	0.056	1	0.2	0.0569	0.0042	0.14	17.5747	1.3	0.136	0.026	0.33	320.7	26.3	0.10
FB4_3	3.65	0.24	0.73	0.096	0.054	0.0025	0.57	18.5185	0.96	0.104	0.014	0.02	317.9	15.6	0.06
FB4_4	3.564	0.085	0.456	0.076	0.0562	0.0031	0.10	17.7936	1.1	0.06	0.01	0.40	349.7	19.4	0.01
FB4_5	7.65	0.36	2.01	0.24	0.0677	0.0027	0.74	14.7710	0.62	0.215	0.019	-0.31	339.6	16.6	0.20
FB4_6	8.55	0.48	0.563	0.078	0.0592	0.0026	0.29	16.8919	0.76	0.0676	0.0085	0.08	364.6	16.2	0.02
FB4_7	0.984	0.023	0.98	0.28	0.0613	0.0061	0.01	16.3132	2.3	0.13	0.047	0.32	348.0	40.6	0.10
FB4_8	3.319	0.087	0.7	0.19	0.0601	0.0042	0.30	16.6389	1.2	0.083	0.02	0.08	363.0	26.6	0.04
FB4_9	0.1409	0.0074	15	5.7	0.173	0.042	0.89	5.7803	4	0.21	0.25	0.47	863.6	365.0	0.17
FB4_10	2.83	0.1	2.47	0.23	0.0733	0.0032	-0.01	13.6426	0.61	0.25	0.025	0.44	347.7	20.5	0.24
FB4_11	4.5	0.2	0.88	0.1	0.0744	0.0036	0.21	13.4409	0.73	0.088	0.011	0.10	444.8	23.1	0.04
FB4_13	0.789	0.026	1.42	0.35	0.065	0.0061	0.32	15.3846	2.6	0.202	0.057	0.81	332.7	41.9	0.19
FB4_14	0.0538	0.0049	37	11	0.46	0.17	0.28	2.1739	1.6	0.57	0.31	0.62	1125.7	1042.7	0.59
FB4_15	0.651	0.02	1.33	0.45	0.0625	0.0079	0.55	16.0000	2.6	0.169	0.067	0.12	326.4	51.8	0.17
FB4_16	2.068	0.053	6.6	1.5	0.136	0.014	0.91	7.3529	0.86	0.433	0.044	-0.16	452.6	64.2	0.47
FB4_17	0.585	0.016	0.56	0.27	0.0595	0.0074	0.02	17.0940	7.1	0.066	0.074	0.44	361.1	55.8	0.02
FB4_18	2.614	0.047	5.54	0.39	0.0965	0.0045	0.43	10.3627	0.53	0.43	0.031	0.21	322.2	27.5	0.47
FB4_19	0.986	0.026	0.73	0.23	0.0446	0.0045	0.31	22.4215	5.4	0.14	0.065	0.80	250.7	33.7	0.11
FB4_21	2.917	0.056	2.75	0.31	0.066	0.0041	0.66	15.1515	0.98	0.316	0.033	-0.01	279.2	24.1	0.33
FB4_22	1.07	0.17	27.1	3.6	0.278	0.027	0.54	3.5971	0.4	0.708	0.094	0.17	324.2	203.9	0.81
FB4_23	1.432	0.044	4.6	1.2	0.083	0.012	0.83	12.0482	3.7	0.321	0.073	0.01	347.8	67.8	0.33
FB4_24	11.15	0.19	0.89	0.13	0.05	0.0022	0.71	20.0000	0.85	0.125	0.016	-0.40	286.6	13.9	0.09
FB4_26	6.198	0.084	0.58	0.097	0.0433	0.0022	0.13	23.0947	1.3	0.1	0.018	0.31	257.0	14.2	0.06
FB4_27	6.02	0.11	0.49	0.1	0.0475	0.0024	0.09	21.0526	1.2	0.075	0.016	0.26	290.8	15.6	0.03
FB4_28	20.27	0.29	1.63	0.14	0.0571	0.0018	0.45	17.5131	0.56	0.203	0.015	-0.07	292.2	11.3	0.19
FB4_29	9.67	0.92	3.25	0.4	0.0869	0.0069	0.44	11.5207	1	0.274	0.028	0.16	395.2	36.0	0.27
FB4_30	1.747	0.045	16.9	5.8	0.205	0.059	0.96	4.8780	1.4	0.515	0.06	0.03	557.1	161.0	0.56
FB4_31	2.71	0.15	1.71	0.55	0.0668	0.0068	0.71	15.0150	2.8	0.179	0.06	0.59	352.7	55.1	0.16
FB5ru_0	7.8	0.31	0.88	0.14	0.0734	0.0047	0.45	13.6240	0.93	0.083	0.012	-0.06	441.7	28.5	0.03
FB5ru_1	4.58	0.14	1.08	0.18	0.0579	0.0037	0.09	17.2712	1.4	0.146	0.026	0.38	321.8	23.3	0.12
FB5ru_3	4.98	0.16	0.75	0.14	0.0637	0.0041	0.48	15.6986	1.1	0.092	0.017	-0.11	360.0	25.4	0.05
FB5ru_4	8.14	0.3	0.61	0.1	0.0651	0.0035	0.37	15.3610	1.1	0.066	0.011	-0.02	401.1	21.8	0.01
FB5ru_5	1.562	0.066	0.79	0.26	0.0599	0.0061	0.22	16.6945	3.8	0.136	0.055	0.99	337.4	42.2	0.10
FB5ru_7	3.28	0.14	1.1	0.21	0.0688	0.0049	0.04	14.5349	1.4	0.129	0.028	0.38	390.5	31.0	0.09
FB5ru_8	5.53	0.19	0.434	0.077	0.0487	0.003	0.05	20.5339	1.4	0.07	0.013	0.34	299.9	18.9	0.02
FB5ru_9	1.471	0.051	10.4	1.2	0.144	0.01	0.45	6.9444	0.67	0.546	0.062	0.28	351.1	72.7	0.61
FB5ru_10	5.37	0.17	0.51	0.1	0.049	0.0024	0.26	20.4082	0.96	0.074	0.015	0.06	300.3	15.6	0.03
FB5ru_11	1.52	0.054	3.59	0.51	0.077	0.0066	-0.02	12.9870	2.8	0.45	0.11	1.00	244.4	69.3	0.50
FB5ru_12	7.95	0.16	0.618	0.093	0.0644	0.0025	0.19	15.5280	0.69	0.073	0.01	0.06	393.4	15.8	0.02
FB5ru_13	4.62	0.14	0.67	0.13	0.065	0.0035	0.37	15.3846	0.94	0.077	0.015	-0.09	395.0	22.1	0.03
FB5ru_14	10.67	0.31	0.446	0.063	0.0577	0.0022	0.17	17.3310	0.7	0.0564	0.0064	0.14	359.6	14.0	0.01
FB5ru_15	14.56	0.29	0.564	0.07	0.05	0.0023	0.36	20.0000	0.93	0.0655	0.0092	0.02	301.9	14.1	0.04
FB5ru_16	29.03	0.91	0.525	0.043	0.0628	0.0019	0.36	15.9236	0.49	0.0602	0.0046	0.05	389.9	11.8	0.01
FB5ru_17	9.27	0.22	0.53	0.076	0.0597	0.0022	0.07	16.7504	0.63	0.069	0.011	0.36	367.0	14.2	0.02
FB5ru_18	4.74	0.14	1.67	0.24	0.0604	0.0042	0.38	16.5563	1.2	0.233	0.031	0.15	294.9	24.9	0.23
FB5ru_19	3.94	0.11	2.22	0.26	0.0674	0.0045	0.43	14.8368	0.93	0.242	0.031	0.08	324.0	26.7	0.24
FB5ru_20	4.16	0.15	1.8	0.31	0.0854	0.0055	0.69	11.7096	0.86	0.155	0.024	-0.20	466.3	33.2	0.12
FB5ru_21	12.83	0.29	14.48	0.61	0.1855	0.006	0.66	5.3908	0.17	0.569	0.016	-0.03	422.2	27.2	0.64
FB5ru_22	0.969	0.045	12.5	2	0.174	0.022	0.60	5.7471	0.88	0.589	0.078	0.35	366.6	113.4	0.66
FB5ru_23	0.51	0.029	16.1	4	0.181	0.035	0.74	5.5249	9.8	0.56	0.18	0.73	424.6	259.1	0.62
FB5ru_24	39.8	1.1	0.361	0.031	0.047	0.0017	0.26	21.2766	0.79	0.0566	0.0047	0.00	294.5	10.6	0.01
FB5ru_25	7.9	0.23	0.66	0.11	0.0617	0.0034	0.44	16.2075	0.99	0.084	0.014	0.25	372.0	21.2	0.04
FB5ru_26	5.62	0.18	0.59	0.116	0.0652	0.005	0.13	15.3374	1.2	0.083	0.025	0.28	393.2	32.1	0.04
FB5ru_27	17.81	0.63	0.36	0.063	0.0493	0.0027	0.30	20.2840	1.3	0.057	0.01	0.04	306.5	17.1	0.01
FB5ru_28	1.544	0.07	1.06	0.43	0.0579	0.0098	-0.01	17.2712	16	0.08	0.21	0.58	351.2	109.9	0.03
FB5ru_29	9.74	0.36	0.68	0.14	0.0636	0.0037	0.11	15.7233	1.1	0.081	0.017	0.21	384.7	23.5	0.03
FB5ru_30	8.95	0.38	0.74	0.21	0.0513	0.0042	0.81	19.4932	1.9	0.101	0.024	-0.14	303.4	26.3	0.06
FB5ru_31	10.11	0.36	0.56	0.13	0.0621	0.0037	0.24	16.1031	1	0.067	0.015	0.09	382.4	23.5	0.02
FB5ru_32	2.111	0.088	0.45	0.31	0.0598	0.0076	-0.06	16.7224	3.8	0.094	0.063	0.57	356.2	53.0	0.05
FB5ru_33	12.64	0.45	0.88	0.15	0.0503	0.0032	0.80	19.8807	1.4	0.129	0.021	0.03	286.7	19.8	0.10
FB5ru_34	6.93	0.23	6.57	0.6	0.1058	0.0071	0.46	9.4518	0.64	0.46	0.042	0.24	326.5	40.6	0.51
FB5ru_35	9.92	0.3	0.75	0.15	0.0583	0.0039	0.11	17.1527	1.2	0.092	0.018	0.13	348.3	24.3	0.05
FB5ru_36	63.7	1.7	3.48	0.47	0.0851	0.0049	0.83	11.7509	0.76	0.278	0.027	-0.55	384.9	28.0	0.28
FB5ru_37	13.46	0.27	2.82	0.4	0.0797	0.0047	0.37	12.5471	0.77	0.259	0.034	0.11	372.3	29.9	0.25
FB5ru_38	22.9	0.61	0.606	0.063	0.06	0.0027	0.09	16.6667	0.74	0.077	0.01	0.11	365.1	16.8	0.03
FB5ru_39	7.92	0.34	0.67	0.13	0.0521	0.0042	0.16	19.1939	1.8	0.127	0.03	0.31	297.6	26.6	0.09
FB5ru_40	9.15	0.36	0.59	0.15	0.0571	0.0032	0.29	17.5131	1.1	0.071	0.018	0.18	350.4	20.6	0.02
FB5ru_41	38.5	1.1	1.36	0.12	0.0601	0.002	0.26	16.6389	0.58	0.165	0.014	0.12	325.1	12.5	0.14
FB5ru_42	14.16	0.51	0.563	0.08	0.0559	0.0029	-0.02	17.8891	0.96	0.072	0.01	0.35	342.7	18.0	0.02
FB5ru_43	4.07	0.15	0.57	0.2	0.0508	0.0048	0.06	19.6850	2.8	0.084	0.034	0.60	307.2	31.5	0.04
FB5ru_44	2.72	0.14	1.04	0.32	0.0487	0.0056	-0.10	20.5339	4.9	0.207	0.067	0.33	248.0	36.0	0.19
FB5ru_45	42.6	1.2	0.404	0.031	0.0524	0.0015	0.08	19.0840	0.56	0.0572	0.0045	0.18	327.6	9.4	0.01
FB5ru_46	16.1	0.37	0.612	0.067	0.0639	0.0022	0.11	15.6495	0.59	0.0695	0.0075	0.18	392.1	13.7	0.02
FB5ru_47	6.3	0.25	0.413	0.079	0.0515	0.0029	0.17	19.4175	1.2	0.061	0.012	0.23	320.5	18.4	0.01
FB5ru_48	4.19	0.14	1.68	0.34	0.0741	0.0046	0.18	13.4953	0.94	0.179	0.034	0.17	391.9	30.6	0.15
FB5ru_49	1.027	0.054	50.6	4.4	0.498	0.041	0.77	2.0080	0.19	0.746	0.046	0.45	462.3	178.1	0.85
FB5ru_50	0.881	0.043	1.48	0.52	0.0588	0.0086	0.04	17.0068	20	0.04	0.36	0.59	374.6	180.6	0.00
FB5ru_51	9.4	0.3	0.561	0.071	0.0604	0.0031	0.09	16.5563	0.86	0.0705	0.0094	0.11	370.5	19.2	0.02
FB5ru_52	12.13	0.34	0.568	0.063	0.0493	0.0022	-0.13	20.2840	0.97	0.056	0.01	0.38	306.9	14.1	0.00
FB5ru_53	3.9	0.12	0.63	0.13	0.0668	0.0044	0.16	14.9701	1	0.071	0.015	0.15	406.8	27.5	0.02
FB5ru_54	3.3	0.12	0.68	0.15	0.054	0.0038	0.09	18.5185	1.5	0.103	0.022	0.23	318.4	23.9	0.06
FB5ru_55	1.684	0.069	2.17	0.44	0.0668	0.0076	0.18	14.9701	4.8	0.26	0.065	0.89	301.4	47.6	0.26
FB5ru_56	4.17	0.17	0.55	0.14	0.0518	0.0034	0.18	19.3050	1.7	0.074	0.019	0.09	317.2	21.9	0.03
FB5ru_57	5.78	0.19	0.71	0.13	0.0558	0.0037	0.11	17.9211	1.4	0.093	0.016	0.36	333.1	22.8	0.05
FB5ru_58	3.65	0.17	13	1	0.16	0.0095	0.67	6.2500	0.41	0.599	0.04	0.18	322.8	53.2	0.68
FB5ru_59	9.01	0.27	1.75	0.21	0.0691	0.0037	0.48	14.4718	0.81	0.187	0.021	0.07	361.5	22.0	0.17
FB5ru_60	70.9	2.1	0.521	0.029	0.0674	0.0015	0.00	14.8368	0.33	0.0565	0.0034	0.35	419.8	9.3	0.00
FB5ru_61	5.06	0.13	6.6	0.81	0.115	0.017	0.32	8.6957	1.3	0.45	0.067	0.68	366.5	79.4	0.49
FB5ru_63	24.09	0.54	0.525	0.045	0.0638	0.0021	-0.15	15.6740	0.52	0.062	0.0062	0.52	395.1	13.1	0.01
FB5ru_64	5.34	0.2	0.65	0.14	0.0526	0.0033	0.37	19.0114	1.5	0.092	0.02	-0.04	314.7	21.1	0.05
FB5ru_65	0.754	0.044	1.61	0.7	0.075	0.011	0.17	13.3333	23	0.1	0.2	0.27	226.0	122.0	0.52
FB5ru_66	27.43	0.7	0.444	0.046	0.0552	0.0017	0.21	18.2306	0.65	0.0649	0.0073	0.03	322.0	10.8	0.01
FB5ru_67	6.51	0.17	4	0.49	0.089	0.0052	0.49	11.2360	0.73	0.321	0.032	-0.03	372.8	30.5	0.33
FB5ru_68	5.27	0.17	1.62	0.3	0.058	0.0039	0.59	17.2414	1.4	0.208	0.037	0.06	294.5	25.6	0.19
FB5ru_69	5.63	0.23	0.65	0.12	0.0507	0.0034	0.75	19.7239	1.6	0.098	0.02	-0.14	301.1	21.4	0.06
FB5ru_70	9.09	0.27	0.7	0.13	0.0601	0.0027	0.28	16.6389	0.78	0.087	0.016	-0.12	361.1	17.6	0.04
FB5ru_71	3.82	0.14	0.75	0.17	0.0557	0.0037	0.34	17.9533	1.5	0.102	0.023	0.47	326.7	23.6	0.06
FB5ru_72	3.27	0.12	0.4	0.12	0.0504	0.0036	0.08	19.8413	2	0.061	0.02	0.05	313.8	23.4	0.01
FB5ru_73	0.531	0.031	1.76	0.62	0.078	0.012	0.56	12.8205	30	0.41	0.17	0.23	272.3	111.0	0.45
FB5ru_74	10.58	0.35	0.516	0.078	0.0639	0.0034	0.38	15.6495	0.89	0.0616	0.0092	0.10	395.9	21.1	0.01
FB5ru_75	5.12	0.2	0.66	0.13	0.0643	0.0041	0.43	15.5521	1.1	0.09	0.019	0.31	384.5	25.8	0.04
FB5ru_76	2.804	0.097	1.06	0.26	0.0584	0.0054	0.42	17.1233	2	0.126	0.03	0.14	333.6	33.2	0.09
FB5ru_77	17.7	0.63	0.879	0.095	0.0515	0.002	0.54	19.4175	0.79	0.129	0.015	-0.07	293.4	12.7	0.10
FB5ru_78	0.963	0.04	1.72	0.66	0.0606	0.0092	0.91	16.5017	15	0.26	0.12	0.70	293.1	70.5	0.26
FB5ru_80	4.99	0.14	0.62	0.13	0.0568	0.0041	0.32	17.0068	1.3	0.077	0.015	0.05	356.0	25.4	0.03
FB5ru_81	10.43	0.36	0.585	0.091	0.0641	0.0027	0.26	15.6006	0.69	0.067	0.01	-0.07	394.5	17.0	0.02
FB5ru_82	5.02	0.17	0.91	0.15	0.0689	0.0037	0.60	14.5138	0.81	0.1	0.018	0.09	406.3	23.4	0.06
FB5ru_83	2.375	0.083	57.7	4.3	0.558	0.039	0.93	1.7921	0.16	0.75	0.028	0.15	513.1	125.2	0.85
FB5ru_84	4.14	0.13	0.85	0.16	0.0636	0.0045	0.33	15.7233	1.5	0.095	0.018	0.10	377.9	27.7	0.05
FB5ru_85	3.315	0.087	7.69	0.68	0.1161	0.0078	0.56	8.6133	0.64	0.499	0.041	0.23	325.0	42.7	0.55
FB5ru_86	3.97	0.19	0.64	0.17	0.0525	0.0043	-0.15	19.0476	1.7	0.098	0.029	0.52	311.7	27.7	0.06

S2.4 Rutile U-Pb data tables (continued)

	Approx U PPM	Prop2SE	207Pb/235U	Prop2SE	206Pb/238U	Prop2SE	Rho	238U/206Pb	Prop2SE	207Pb/206Pb	Prop2SE	Rho	207Pb corrected age	Prop2SE	f206Pb
FB5ru_87	9.36	0.28	4.07	0.31	0.0865	0.0043	0.21	11.5607	0.57	0.352	0.028	0.33	341.5	25.1	0.37
FB5ru_88	1.582	0.061	0.69	0.28	0.0549	0.0062	0.10	18.2149	4.2	0.215	0.097	0.67	275.9	51.5	0.20
FB6ru_0	2.769	0.045	1.56	0.31	0.0633	0.0041	0.07	15.7978	1.1	0.179	0.034	-0.04	395.4	27.0	0.16
FB6ru_1	5.67	0.12	1.75	0.15	0.0719	0.0029	0.41	13.9082	0.58	0.179	0.015	0.08	380.4	17.2	0.15
FB6ru_2	2.899	0.054	0.67	0.13	0.0516	0.003	0.50	19.3798	1.3	0.099	0.019	-0.01	306.0	19.1	0.06
FB6ru_3	3.592	0.095	0.72	0.16	0.0712	0.0031	0.10	14.0449	0.65	0.074	0.016	-0.09	433.6	20.4	0.02
FB6ru_4	6.516	0.076	0.519	0.064	0.0585	0.0022	0.42	17.0991	0.74	0.069	0.012	-0.06	347.6	14.3	0.02
FB6ru_5	9.9	0.11	0.427	0.046	0.0503	0.0016	0.51	19.8807	0.65	0.064	0.0072	-0.15	312.0	10.2	0.01
FB6ru_6	1.771	0.057	1.15	0.28	0.0653	0.0059	0.19	15.3139	1.6	0.143	0.033	0.36	363.9	36.3	0.11
FB6ru_7	1.929	0.087	4.2	3.9	0.106	0.065	1.00	9.4340	1.5	0.211	0.036	-0.16	532.3	319.9	0.19
FB6ru_8	4.121	0.057	0.67	0.12	0.052	0.0026	0.52	19.2308	0.91	0.094	0.016	0.02	310.3	16.6	0.05
FB6ru_9	21.15	0.6	0.562	0.043	0.0716	0.0018	0.18	13.9665	0.37	0.0573	0.0047	0.12	445.0	11.2	0.00
FB6ru_10	21.69	0.19	0.528	0.036	0.0659	0.0015	0.06	15.1745	0.33	0.058	0.004	0.20	409.9	9.4	0.00
FB6ru_11	5.901	0.068	0.673	0.09	0.0701	0.0022	0.14	14.2653	0.46	0.074	0.01	0.20	427.0	14.2	0.02
FB6ru_12	0.336	0.014	1.04	0.53	0.065	0.012	0.71	15.3846	11	0.31	0.2	0.53	278.1	112.8	0.32
FB6ru_13	11.05	0.2	0.467	0.056	0.0558	0.0014	-0.02	17.9211	0.47	0.0641	0.0076	0.16	345.5	9.1	0.01
FB6ru_14	1.684	0.052	1	0.36	0.0635	0.0048	-0.04	15.7480	1.4	0.114	0.033	0.03	368.1	31.7	0.07
FB6ru_15	14.53	0.17	0.505	0.048	0.0562	0.0014	0.16	17.7936	0.46	0.0662	0.0064	0.10	347.0	8.9	0.02
FB6ru_16	2.811	0.053	2.07	0.4	0.0684	0.0042	0.68	14.6092	1	0.219	0.03	0.01	331.1	25.7	0.21
FB6ru_17	2.03	0.058	0.82	0.15	0.0556	0.004	0.46	17.9856	1.6	0.117	0.023	0.06	321.7	24.8	0.09
FB6ru_18	2.237	0.044	1.09	0.17	0.0569	0.0038	0.24	17.6056	1.7	0.158	0.026	0.31	310.5	23.4	0.13
FB6ru_19	2.069	0.041	0.81	0.16	0.0717	0.0044	0.56	13.9470	0.92	0.093	0.02	-0.10	426.3	27.8	0.05
FB6ru_20	1.434	0.055	10.72	0.72	0.1407	0.0092	0.64	7.1073	0.51	0.585	0.044	0.46	298.4	51.9	0.66
FB6ru_21	2.992	0.053	0.68	0.14	0.059	0.0034	0.49	16.9492	0.98	0.09	0.019	-0.05	353.3	21.8	0.05
FB6ru_22	0.0672	0.0063	31.3	9.9	0.33	0.11	0.44	3.0303	5.4	0.29	0.59	0.55	1457.0	1344.5	0.23
FB6ru_23	1.904	0.034	1.76	0.26	0.0656	0.0039	0.07	15.2439	1.1	0.202	0.033	0.54	335.8	25.7	0.18
FB6ru_24	1.862	0.077	19.7	1.6	0.216	0.013	0.70	4.6296	0.3	0.662	0.043	0.23	293.4	74.8	0.78
FB6ru_25	3.378	0.053	0.49	0.11	0.0519	0.0031	0.38	19.2678	1.3	0.073	0.017	0.10	318.2	19.9	0.03
FB6ru_26	1.415	0.032	0.69	0.2	0.0646	0.0054	0.27	15.4799	1.6	0.112	0.026	0.09	375.4	33.4	0.07
FB6ru_27	9.08	0.31	0.699	0.06	0.0702	0.0026	0.22	14.2450	0.55	0.0735	0.0063	0.07	427.9	16.1	0.02
FB6ru_28	5.574	0.064	1.01	0.15	0.0541	0.0024	0.34	18.4843	0.85	0.132	0.017	0.01	306.8	15.2	0.10
FB6ru_29	37.8	1.1	0.46	0.031	0.0571	0.0016	-0.03	17.5131	0.48	0.0567	0.0043	0.38	355.8	10.0	0.01
FB6ru_30	1.766	0.079	0.66	0.18	0.0601	0.0045	0.39	16.6389	1.6	0.09	0.025	0.07	359.8	28.9	0.05
FB6ru_31	4.7	0.18	0.68	0.13	0.0695	0.0031	0.33	14.3885	0.7	0.069	0.013	-0.06	426.1	19.8	0.02
FB6ru_32	10.19	0.37	0.69	0.074	0.0788	0.0025	-0.13	12.6904	0.41	0.063	0.0068	0.25	485.4	15.6	0.01
FB6ru_33	1.245	0.031	19	1.9	0.205	0.016	0.80	4.8780	0.43	0.667	0.043	0.28	303.3	72.7	0.77
FB6ru_34	7.89	0.12	6.59	0.3	0.1133	0.0035	0.20	8.8261	0.29	0.429	0.022	0.47	379.7	22.5	0.46
FB6ru_35	0.337	0.014	2.35	0.83	0.07	0.014	0.15	14.2857	20	0.09	0.27	0.44	418.0	164.8	0.04
FB6ru_36	11.69	0.3	0.52	0.058	0.0646	0.0019	0.04	15.4799	0.49	0.0585	0.0066	0.25	401.7	12.0	0.00
FB6ru_37	5.549	0.077	0.491	0.07	0.0555	0.0024	0.00	18.0180	0.65	0.0651	0.0095	0.26	343.2	15.1	0.01
FB6ru_38	3.1	0.063	0.63	0.13	0.0564	0.003	-0.09	17.7305	1.1	0.108	0.017	0.39	330.1	18.6	0.07
FB6ru_39	2.758	0.059	2.4	0.27	0.0732	0.0044	0.32	13.6612	0.88	0.243	0.027	0.24	351.2	25.7	0.24
FB6ru_41	2.61	0.11	1.33	0.38	0.0616	0.0046	0.04	16.2338	1.3	0.138	0.024	0.10	345.9	27.8	0.11
FB6ru_42	2.137	0.062	12.1	1.6	0.1433	0.0099	0.35	6.9784	0.51	0.607	0.052	-0.05	278.4	61.2	0.69
FB6ru_43	32.53	0.32	0.495	0.029	0.0619	0.0013	0.07	16.1551	0.32	0.0585	0.0036	0.25	386.2	8.1	0.01
FB6ru_44	2.795	0.044	1.69	0.19	0.0626	0.0028	0.16	15.9744	0.89	0.21	0.027	0.48	316.7	19.1	0.20
FB6ru_45	1.817	0.033	0.89	0.62	0.05	0.0039	-0.07	20.0000	1.8	0.115	0.069	0.07	290.4	34.8	0.08
FB6ru_46	1.544	0.041	0.69	0.19	0.0519	0.0044	0.22	19.2678	2.2	0.111	0.033	0.62	302.9	28.6	0.07
FB6ru_47	2.067	0.039	2.55	0.26	0.0644	0.0041	0.16	15.5280	1.1	0.318	0.038	0.45	271.5	25.6	0.33
FB6ru_48	18.69	0.16	0.502	0.042	0.0632	0.0014	-0.09	15.8228	0.35	0.0583	0.0051	0.33	393.3	8.9	0.00
FB6ru_49	2.58	0.053	0.107	0.035	0.0476	0.0027	0.24	21.0084	1.4	0.057	0.016	-0.06	298.1	17.7	0.01
FB6ru_50	5.69	0.11	0.98	0.13	0.0573	0.0024	0.50	17.4520	0.74	0.126	0.016	-0.07	327.4	15.2	0.09
FB6ru_51	10.96	0.41	0.509	0.067	0.0584	0.0024	0.27	17.1233	0.72	0.0637	0.0079	-0.01	361.5	15.0	0.01
FB6ru_52	2.975	0.06	0.531	0.096	0.0532	0.0029	0.14	18.7970	1.1	0.075	0.014	0.12	325.2	18.4	0.03
FB6ru_53	3.346	0.048	0.413	0.09	0.0497	0.0027	0.02	20.5339	1.2	0.064	0.014	0.27	302.2	17.3	0.01
FB6ru_54	9.25	0.36	2.25	0.18	0.088	0.0025	0.05	11.3636	0.31	0.188	0.016	0.26	458.3	16.6	0.16
FB6ru_55	3.565	0.05	1.67	0.22	0.0588	0.0033	0.76	17.0068	1.1	0.217	0.026	0.03	294.4	20.7	0.21
FB6ru_56	9.4	0.15	0.423	0.048	0.0542	0.0016	0.21	18.4502	0.55	0.0575	0.007	0.02	338.5	10.3	0.01
FB6ru_57	3.944	0.087	0.72	0.12	0.0602	0.0026	0.07	16.6113	0.85	0.09	0.015	0.35	360.4	16.8	0.04
FB6ru_58	0.673	0.027	0.67	0.23	0.0567	0.0074	0.01	17.6367	2.9	0.101	0.04	0.13	334.9	46.4	0.06
FB6ru_59	4.311	0.097	1.05	0.57	0.0582	0.0036	-0.01	17.1821	1.3	0.15	0.11	0.00	321.7	53.0	0.12
FB6ru_60	0.49	0.024	4	1.6	0.087	0.011	0.14	11.4943	2.7	0.22	0.21	0.12	432.0	147.9	0.20
FB6ru_61	2.796	0.09	1.76	0.28	0.0653	0.0037	0.21	15.3139	0.78	0.201	0.034	0.42	334.8	25.3	0.18
FB6ru_62	1.42	0.05	0.75	0.23	0.0551	0.0048	0.33	18.1488	1.8	0.113	0.038	0.03	320.5	31.9	0.07
FB6ru_63	5.065	0.079	1.14	0.11	0.0583	0.0022	0.20	17.1527	0.69	0.145	0.015	0.25	324.5	13.6	0.11
FB6ru_64	0.937	0.038	0.9	0.35	0.058	0.0063	0.64	17.2414	2.9	0.145	0.058	0.28	322.8	43.1	0.11
FB6ru_65	1.077	0.027	0.93	0.4	0.0534	0.0053	0.29	18.7266	2.6	0.123	0.045	-0.08	306.6	35.2	0.09
FB6ru_66	14.66	0.41	0.618	0.057	0.0735	0.002	0.31	13.6054	0.38	0.0617	0.0053	0.02	454.7	12.5	0.01
FB6ru_67	4.187	0.057	0.67	0.1	0.07	0.0027	0.32	14.2857	0.58	0.0692	0.0098	-0.10	429.0	17.0	0.02
FB6ru_68	5.361	0.066	1.17	0.2	0.0941	0.0094	0.13	10.6270	1	0.088	0.013	-0.02	559.9	55.3	0.04
FB6ru_69	5.232	0.063	0.58	0.14	0.052	0.0029	0.70	19.2308	1.1	0.076	0.015	-0.13	317.6	18.4	0.03
FB6ru_70	2.517	0.038	0.5	0.28	0.0488	0.0035	0.67	20.4918	1.6	0.114	0.031	0.17	283.9	23.3	0.08
FB6ru_71	1.487	0.032	3.27	0.56	0.0768	0.0058	0.16	13.0208	1.1	0.338	0.064	0.11	311.6	44.5	0.36
FB6ru_72	8.01	0.24	6.92	0.56	0.1152	0.0052	0.84	8.6806	0.39	0.431	0.021	-0.05	384.4	25.3	0.47
FB6ru_73	0.337	0.013	6.2	1.4	0.093	0.017	-0.01	10.7527	2.6	0.34	0.33	0.31	375.9	243.4	0.35
FB6ru_74	3.927	0.05	0.499	0.098	0.0486	0.0023	-0.02	20.5761	1.1	0.075	0.015	0.04	297.5	15.0	0.03
FB6ru_75	2.604	0.05	0.8	0.18	0.0542	0.0031	0.15	18.4502	1.3	0.118	0.025	-0.08	313.2	20.5	0.06
FB6ru_76	3.31	0.1	0.68	0.16	0.0552	0.0032	0.29	18.1159	1.1	0.086	0.018	0.02	332.6	20.4	0.04
FB6ru_77	1.58	0.027	1.24	0.37	0.082	0.042	-0.04	12.1951	1.9	0.15	0.04	0.18	451.1	227.6	0.12
FB6ru_78	2.281	0.061	0.7	0.18	0.0568	0.0038	0.15	17.5747	1.4	0.093	0.024	0.11	338.6	24.6	0.05
FB6ru_79	1.504	0.068	0.66	0.21	0.0611	0.0063	0.58	16.3666	1.6	0.097	0.03	0.11	362.4	39.3	0.05
FB6ru_80	4.161	0.061	0.76	0.15	0.0687	0.0032	0.53	14.5560	0.67	0.079	0.015	-0.20	416.1	20.5	0.03
FB6ru_81	3.242	0.054	0.36	0.24	0.049	0.0031	0.11	20.4082	1.4	0.08	0.023	-0.06	298.0	20.5	0.03
FB6ru_82	1.317	0.032	1	0.54	0.06	0.0072	0.92	16.6667	1.9	0.136	0.052	0.04	338.0	46.5	0.10
FB6ru_83	7.725	0.096	0.203	0.078	0.046	0.0019	0.15	21.7391	0.91	0.066	0.012	-0.02	285.0	12.4	0.02
FB6ru_84	3.95	0.066	0.392	0.076	0.0477	0.0027	0.23	20.9644	1.3	0.065	0.014	0.15	295.7	17.3	0.02
FB6ru_85	1.509	0.048	0.65	0.33	0.0551	0.0047	0.84	18.1488	2	0.138	0.045	0.96	309.9	32.3	0.11
FB6ru_86	2.553	0.043	0.86	0.24	0.0564	0.0037	0.02	17.7305	1.2	0.111	0.024	-0.02	328.8	23.6	0.07
FB6ru_87	8.31	0.12	15.7	3.4	0.185	0.03	0.86	5.4054	0.87	0.527	0.037	-0.64	483.2	92.4	0.58
FB6ru_88	1.378	0.058	3.72	0.89	0.073	0.0076	0.21	13.6986	1.8	0.326	0.053	0.00	303.1	43.1	0.34
FB6ru_89	9.44	0.11	0.415	0.051	0.0504	0.0016	0.30	19.8413	0.62	0.0599	0.0073	0.03	314.2	10.2	0.01
FB6ru_90	2.709	0.066	0.64	0.15	0.0668	0.0042	-0.04	14.9701	0.9	0.071	0.015	0.05	409.8	26.3	0.02
FB6ru_91	2.039	0.033	0.61	0.13	0.0534	0.004	0.45	18.7266	1.8	0.102	0.023	0.03	315.3	25.1	0.06
FB6ru_92	6.828	0.064	1.78	0.17	0.0657	0.0026	0.43	15.2207	0.61	0.197	0.018	0.03	338.8	16.0	0.16
FB6ru_93	20.37	0.2	0.553	0.043	0.0628	0.0013	0.00	15.9236	0.32	0.0644	0.0053	0.26	367.9	8.3	0.01
FB6ru_94	0.536	0.023	1.25	0.48	0.0622	0.0087	0.46	16.0772	3.7	0.209	0.081	0.47	315.2	58.2	0.19
FB6ru_95	7.446	0.092	0.539	0.063	0.0677	0.0021	0.05	14.7710	0.46	0.0599	0.0074	0.15	419.9	13.3	0.01
FB6ru_96	4.642	0.062	4.96	0.5	0.0853	0.0046	0.20	11.7233	0.74	0.41	0.036	0.07	398.0	29.7	0.45
FB6ru_97	3.62	0.055	0.8	0.19	0.0577	0.0042	0.50	17.3310	1.5	0.102	0.02	-0.11	340.3	25.9	0.06
FB6ru_98	9.09	0.1	0.527	0.061	0.0612	0.0018	0.10	16.3399	0.5	0.0644	0.0078	0.10	378.2	11.5	0.01
FB6ru_99	1.733	0.043	7.75	0.81	0.1169	0.0066	0.62	8.5543	0.73	0.496	0.041	0.24	330.1	44.1	0.55
FB6ru_100	2.534	0.042	0.62	0.12	0.062	0.0031	0.30	16.1290	0.78	0.072	0.014	-0.03	379.5	19.6	0.02
FB6ru_101	9.36	0.11	1.036	0.087	0.057	0.0019	0.00	17.5439	0.58	0.134	0.012	0.41	322.2	11.8	0.10
FB6ru_102	6.032	0.067	0.446	0.07	0.0499	0.0018	0.24	20.0401	0.74	0.065	0.01	0.13	309.2	11.6	0.02
FB6ru_103	7.005	0.095	0.517	0.069	0.0522	0.0018	0.23	19.1571	0.6	0.0723	0.0098	0.05	320.3	11.6	0.02
FB6ru_104	6.72	0.19	0.616	0.09	0.0578	0.0022	0.09	17.3010	0.75	0.106	0.012	0.30	339.1	13.8	0.07
FB6ru_105	1.298	0.037	2.9	0.43	0.0741	0.0058	0.50	13.4953	1.5	0.332	0.055	0.86	304.2	39.3	0.35
FB6ru_106	3.033	0.054	1.4	0.35	0.0599	0.0046	0.84	16.6945	1.3	0.184	0.034	-0.19	315.2	26.5	0.16
FB6ru_107	0.862	0.024	1.42	0.43	0.0654	0.006	0.73	15.2905	1.8	0.202	0.06	0.61	334.8	42.7	0.16
FB6ru_108	7.334	0.09	0.55	0.095	0.0577	0.0025	0.76	17.3310	0.82	0.071	0.011	-0.25	354.0	15.6	0.02
FB6ru_109	2.3	0.065	0.77	0.17	0.067	0.0039	0.61	14.9254	0.96	0.084	0.018	-0.03	403.4	24.8	0.04
FB6ru_110	0.69	0.025	10.9	1.9	0.143	0.018	0.93	6.9930	0.84	0.567	0.069	0.34	301.1	85.1	0.67
FB6ru_111	4	0.063	0.65	0.13	0.0661	0.0033	0.62	15.1286	0.78	0.069	0.012	-0.21	405.6	20.8	0.02
FB8ru_0	9.56	0.15	0.494	0.044	0.0645	0.0017	0.01	15.5039	0.43	0.0554	0.005	0.31	402.6	10.7	0.00
FB8ru_1	39.59	0.52	0.423	0.024	0.0549	0.0013	0.23	18.2149	0.4	0.0554	0.0029	0.17	343.7	8.1	0.00
FB8ru_2	6.66	0.22	0.498	0.067	0.0606	0.0027	0.18	16.5017	0.74	0.0609	0.0063	0.19	376.2	16.9	0.01
FB8ru_3	2.5	0.06	0.8	0.15	0.0636	0.0036	0.10	15.7233	0.89	0.097	0.025	0.35	377.0	24.2	0.05
FB8ru_4	5.181	0.082	0.444	0.072	0.0523	0.0022	0.02	19.1205	0.84	0.0604	0.0095	0.22	325.6	14.0	0.01
FB8ru_5	5.39	0.084	0.491	0.058	0.0562	0.0021	0.01	17.7936	0.69	0.0651	0.0078	0.22	347.5	13.2	0.01
FB8ru_6	1.293	0.057	14.2	1.5	0.178	0.014	0.72	5.6180	0.46	0.592	0.05	-0.07	371.1	74.1	0.67
FB8ru_7	10.43	0.15	0.445	0.038	0.0539	0.0016	0.07	18.5529	0.53	0.0605	0.0054	0.26	335.4	10.0	0.01
FB8ru_8	2.377	0.047	1.22	0.17	0.066	0.0035	0.15	15.1515	0.8	0.14	0.02	0.26	369.3	21.7	0.11
FB8ru_9	0.722	0.039	4.49	0.67	0.0989	0.0061	0.43	10.1112	1.1	0.321	0.058	-0.10	414.2	54.7	0.33
FB8ru_10	21.76	0.4	0.529	0.034	0.0669	0.0016	0.02	14.9477	0.35	0.0573	0.0037	0.35	416.4	9.9	0.00
FB8ru_11	2.507	0.058	0.71	0.12	0.0572	0.0033	0.26	17.4825	1.1	0.092	0.015	0.07	341.8	20.5	0.05
FB8ru_12	5.371	0.097	0.452	0.058	0.063	0.0025	0.06	15.8730	0.62	0.0549	0.0074	0.22	393.7	15.7	0.00
FB8ru_13	5.92	0.21	0.559	0.074	0.065	0.0029	0.12	15.3846	0.65	0.0635	0.0063	0.18	401.7	16.1	0.01
FB8ru_14	3.59	0.14	0.456	0.045	0.055	0.0017	0.04	18.1818	0.58	0.0602	0.006	0.26	342.3	10.7	0.01
FB8ru_15	0.2505	0.0088	2.54	0.81	0.069	0.0097	0.07	14.7059	4.7	0.31	0.15	0.67	290.9	88.9	0.32
FB8ru_16	10.3	0.16	0.596	0.046	0.0712	0.002	0.20	14.0449	0.41	0.0619	0.005	0.12	440.1	12.4	0.01
FB8ru_17	3.296	0.084	3.26	0.26	0.0784	0.0042	0.36	12.7551	0.71	0.308	0.025	0.29	336.5	23.3	0.32
FB8ru_18	7.14	0.15	2.91	0.34	0.0727	0.0033	0.80	13.7552	0.67	0.275	0.024	-0.57	330.7	20.0	0.26
FB8ru_19	11.9	0.16	0.401	0.035	0.048	0.0013	0.11	20.8333	0.58	0.0616	0.0056	0.23	298.8	8.2	0.01
FB8ru_20	4.57	0.13	0.455	0.075	0.0501	0.003	-0.09	19.9601	1.2	0.069	0.012	0.21	308.8	18.8	0.02
FB8ru_21	14.66	0.17	0.396	0.033	0.0535	0.0014	0.13	16.6916	0.52	0.054	0.0045	0.17	335.6	8.8	0.00

S2.4 Rutile U-Pb data tables (continued)

	Approx U PPM	Prop2SE	207Pb/235U	Prop2SE	206Pb/238U	Prop2SE	Rho	238U/206Pb	Prop2SE	207Pb/206Pb	Prop2SE	Rho	207Pb corrected age	Prop2SE	f206Pb
FB8ru_22	13.93	0.43	0.598	0.062	0.0666	0.002	0.19	15.0150	0.4	0.0648	0.0069	0.20	410.7	12.6	0.01
FB8ru_23	2.767	0.05	2.19	0.22	0.0649	0.0029	0.38	15.4083	0.8	0.242	0.022	0.19	312.1	17.6	0.24
FB8ru_24	12.36	0.18	0.379	0.037	0.0501	0.0015	0.43	19.9601	0.65	0.0547	0.0049	0.04	314.4	9.5	0.00
FB8ru_25	23.56	0.31	0.373	0.025	0.0483	0.0012	0.09	20.7039	0.51	0.0572	0.004	0.26	302.3	7.5	0.01
FB8ru_26	4.193	0.079	0.432	0.074	0.0495	0.0019	0.31	20.2020	0.89	0.065	0.012	-0.09	306.7	12.5	0.02
FB8ru_27	3.66	0.13	0.62	0.14	0.0507	0.003	0.26	19.7239	1.2	0.09	0.02	0.05	304.3	19.4	0.05
FB8ru_28	2.9	0.15	0.51	0.13	0.0619	0.0039	-0.02	16.1551	1.2	0.057	0.018	0.22	386.9	25.3	0.00
FB8ru_29	5.35	0.18	0.548	0.097	0.0514	0.0027	0.13	19.4553	0.95	0.08	0.015	0.06	312.4	17.2	0.03
FB8ru_30	1.581	0.061	0.45	0.13	0.0439	0.0032	0.13	22.7790	1.8	0.077	0.023	0.08	268.4	20.8	0.03
FB8ru_31	3.2	0.16	3.37	0.39	0.0821	0.0046	0.37	12.1803	0.7	0.293	0.03	0.15	361.6	27.5	0.30
FB8ru_32	3.41	0.1	0.378	0.068	0.0474	0.0024	0.16	21.0970	1.2	0.061	0.012	0.09	295.4	15.4	0.01
FB8ru_33	1.16	0.03	0.53	0.17	0.0485	0.0042	-0.05	20.6186	2.5	0.098	0.035	0.10	286.2	27.9	0.06
FB8ru_34	5.39	0.19	0.409	0.069	0.0542	0.0034	0.17	18.4502	1.2	0.054	0.0088	0.11	340.0	21.3	0.00
FB8ru_35	4.66	0.19	2.36	0.27	0.071	0.0042	0.03	14.0645	0.95	0.249	0.035	0.43	337.4	27.4	0.24
FB8ru_36	1.803	0.039	0.62	0.14	0.0537	0.0036	0.11	18.6220	1.4	0.08	0.019	0.11	326.1	22.9	0.03
FB8ru_37	2.471	0.045	0.53	0.1	0.054	0.003	0.18	18.5185	1.1	0.077	0.015	0.09	329.2	19.0	0.03
FB8ru_38	10.99	0.26	0.636	0.059	0.0614	0.002	0.26	16.2866	0.57	0.073	0.0061	0.08	375.4	12.3	0.02
FB8ru_39	9.01	0.18	0.569	0.055	0.0476	0.0019	0.16	21.0084	0.92	0.0679	0.0086	0.26	286.7	11.7	0.04
FB8ru_40	1.749	0.045	2.66	0.38	0.0777	0.0059	0.49	12.8700	1	0.267	0.049	0.11	358.2	39.5	0.26
FB8ru_41	10.47	0.38	1.19	0.13	0.0701	0.0026	0.02	14.2653	0.52	0.125	0.014	0.32	399.9	16.4	0.09
FB8ru_42	1.657	0.06	0.7	0.14	0.0557	0.0042	0.10	17.9533	1.5	0.091	0.021	0.28	333.4	26.3	0.05
FB8ru_43	3.916	0.067	0.474	0.07	0.0571	0.0029	-0.16	17.5131	0.95	0.0643	0.0099	0.36	353.3	18.2	0.01
FB8ru_44	19.69	0.6	0.499	0.04	0.0643	0.0019	-0.02	15.5521	0.47	0.0571	0.005	0.32	400.6	11.9	0.00
FB8ru_45	5.88	0.11	0.482	0.066	0.0557	0.0021	-0.06	17.9533	0.71	0.0656	0.0097	0.36	344.3	13.4	0.02
FB8ru_46	11.88	0.26	0.522	0.043	0.0737	0.0027	0.02	13.5685	0.52	0.0523	0.0049	0.46	460.5	16.7	0.00
FB8ru_47	3.58	0.15	0.83	0.13	0.0676	0.0043	0.18	14.7929	1	0.086	0.014	0.28	405.9	26.3	0.04
FB8ru_48	7.54	0.12	0.424	0.053	0.0574	0.0021	0.09	17.4216	0.61	0.0543	0.0072	0.18	359.5	13.3	0.00
FB8ru_49	8.5	0.17	0.53	0.056	0.0555	0.0018	0.09	18.0180	0.55	0.0691	0.0073	0.26	341.5	11.3	0.02
FB8ru_50	7.63	0.11	0.755	0.065	0.0662	0.002	0.23	15.1057	0.44	0.0627	0.0091	-0.04	399.3	12.7	0.03
FB8ru_51	2.29	0.038	0.357	0.084	0.0517	0.003	0.10	19.3424	1.2	0.052	0.013	0.19	325.3	19.3	0.00
FB8ru_52	4.53	0.13	0.464	0.072	0.0584	0.003	0.06	17.1233	0.84	0.06	0.01	0.28	363.2	18.9	0.01
FB8ru_53	6.09	0.12	0.734	0.069	0.0575	0.0024	0.01	17.3813	0.67	0.094	0.0092	0.50	342.7	14.6	0.05
FB8ru_54	7.97	0.11	0.546	0.064	0.0686	0.0025	0.26	14.5773	0.54	0.0577	0.0068	0.08	426.5	15.6	0.00
FB8ru_55	6.54	0.13	0.758	0.077	0.0556	0.0021	0.17	17.9211	0.73	0.101	0.011	0.25	329.7	13.1	0.06
FB8ru_56	11.34	0.59	0.61	0.11	0.0622	0.0031	0.47	16.0772	0.94	0.098	0.014	0.15	369.3	19.2	0.05
FB8ru_57	6.54	0.19	6.25	0.53	0.1047	0.0059	0.65	9.5511	0.59	0.434	0.03	-0.01	346.5	31.0	0.47
FB8ru_58	1.616	0.034	0.39	0.11	0.0444	0.0033	-0.14	22.5225	1.9	0.074	0.03	0.40	272.4	22.5	0.03
FB8ru_59	0.426	0.019	8.8	1.3	0.129	0.014	0.52	7.7519	1.1	0.563	0.095	0.68	295.8	100.0	0.64
FB8ru_60	1.036	0.032	0.88	0.26	0.0551	0.0051	0.19	18.1488	2	0.136	0.052	0.98	310.7	35.9	0.10
FB8ru_61	0.778	0.047	2.68	0.69	0.0709	0.0075	0.49	14.1044	1.8	0.256	0.049	-0.24	333.1	43.8	0.25
FB8ru_62	3.87	0.19	0.43	0.1	0.0573	0.0029	0.05	17.4520	0.93	0.055	0.013	0.10	358.6	18.7	0.00
FB8ru_63	4.23	0.13	0.542	0.076	0.0684	0.0032	0.09	14.6199	0.69	0.0595	0.0082	0.17	424.4	19.9	0.01
FB8ru_64	3.007	0.094	0.398	0.095	0.0496	0.0031	-0.04	20.1613	1.5	0.063	0.016	0.20	309.1	19.9	0.01
FB8ru_65	5.48	0.14	0.491	0.06	0.0606	0.0022	-0.09	16.4474	0.61	0.0607	0.0077	0.37	377.5	13.9	0.01
FB8ru_66	7.27	0.13	0.483	0.055	0.0647	0.0022	0.06	15.4560	0.53	0.0555	0.0065	0.26	403.8	13.8	0.00
FB8ru_67	21.82	0.47	0.505	0.036	0.0677	0.0017	0.36	14.7710	0.4	0.0535	0.0035	0.00	423.2	10.6	0.00
FB8ru_68	6.31	0.11	0.519	0.072	0.0631	0.0021	0.13	15.8479	0.56	0.0607	0.0084	0.22	391.5	13.4	0.01
FB8ru_69	1.138	0.051	0.68	0.19	0.0608	0.0047	0.10	16.4474	1.7	0.078	0.023	0.15	369.5	30.0	0.03
FB8ru_70	10.47	0.15	0.475	0.051	0.0609	0.0019	0.02	16.4204	0.52	0.0577	0.0064	0.24	379.5	12.0	0.00
FB8ru_71	7.94	0.14	0.469	0.053	0.0658	0.0024	0.05	15.1976	0.57	0.0533	0.0061	0.34	411.6	15.0	0.00
FB8ru_72	5.114	0.067	0.456	0.069	0.0537	0.0019	0.09	18.6220	0.67	0.0609	0.0093	0.21	334.0	12.2	0.01
FB8ru_73	3.3	0.1	0.425	0.084	0.0597	0.0032	0.03	16.7504	0.97	0.052	0.011	0.17	374.7	20.4	0.00
FB8ru_74	3.911	0.078	0.452	0.077	0.0568	0.0025	0.06	17.6056	0.82	0.059	0.011	0.14	353.8	16.0	0.01
FB8ru_75	3.792	0.071	2.08	0.25	0.065	0.0032	0.36	15.3846	0.87	0.233	0.026	-0.07	317.1	20.2	0.22
FB8ru_76	16.75	0.45	0.496	0.036	0.0441	0.0012	0.20	22.6757	0.66	0.0618	0.0059	-0.06	267.9	7.5	0.04
FB8ru_77	3.43	0.11	0.5	0.1	0.0523	0.0032	0.10	19.1205	1.3	0.071	0.016	0.37	321.4	20.4	0.02
FB8ru_78	26.4	0.43	0.36	0.023	0.0469	0.0011	0.22	21.3220	0.48	0.056	0.0036	0.12	294.1	6.9	0.00
FB8ru_79	4.026	0.095	0.781	0.063	0.0467	0.0023	0.20	20.5339	0.96	0.12	0.013	0.31	281.1	14.0	0.06
FB8ru_80	2.077	0.053	0.446	0.093	0.0507	0.0035	0.06	19.7239	1.4	0.07	0.016	0.54	312.1	22.1	0.02
FB8ru_81	4.88	0.11	0.401	0.058	0.0481	0.0018	-0.06	20.7900	0.84	0.0613	0.0094	0.40	299.5	11.6	0.01
FB8ru_82	9.95	0.18	0.458	0.046	0.0471	0.0014	0.38	21.2314	0.69	0.0722	0.0075	0.03	289.4	8.9	0.03
FB8ru_83	1.516	0.031	0.44	0.11	0.0457	0.0037	0.11	21.8818	2.2	0.068	0.019	0.10	282.4	23.5	0.02
FB8ru_84	3.474	0.074	0.523	0.06	0.0572	0.0033	0.43	17.4825	1.1	0.0661	0.0095	0.07	353.1	20.5	0.02
FB8ru_85	1.991	0.044	0.79	0.12	0.0577	0.0034	0.10	17.3310	1.2	0.105	0.016	0.30	339.0	20.9	0.06
FB8ru_86	4.06	0.11	1.53	0.19	0.0568	0.0029	0.40	17.0068	0.88	0.187	0.02	-0.03	308.1	17.5	0.17
FB8ru_87	5.895	0.078	1.78	0.16	0.0581	0.0024	0.42	17.2117	0.74	0.223	0.02	-0.07	286.2	14.6	0.21
FB8ru_88	5.14	0.13	0.591	0.079	0.0595	0.0026	0.25	16.8067	0.83	0.0728	0.011	0.05	364.1	16.4	0.02
FB8ru_89	1.022	0.025	6.13	0.59	0.0921	0.0072	0.39	10.8578	1.2	0.523	0.054	0.59	239.1	43.2	0.59
FB8ru_90	12.39	0.42	0.387	0.041	0.0511	0.002	0.06	19.5795	0.6	0.0562	0.0064	0.22	319.9	12.6	0.00
FB8ru_91	4.51	0.12	0.547	0.09	0.0534	0.0026	0.21	18.7266	1	0.078	0.013	0.07	325.2	16.5	0.03
FB8ru_92	4.992	0.096	1.3	0.16	0.0659	0.0023	0.14	15.1745	0.55	0.137	0.016	0.07	370.2	15.0	0.10
FB8ru_93	2.594	0.063	1.48	0.23	0.0598	0.0034	0.31	16.7224	1	0.177	0.031	0.02	316.0	22.8	0.15
FB8ru_94	7.79	0.14	0.575	0.067	0.0522	0.0019	0.19	19.1571	0.7	0.0801	0.0092	0.22	317.1	12.0	0.03
FB8ru_95	9.36	0.36	0.93	0.12	0.0695	0.0026	0.07	14.3885	0.53	0.096	0.012	0.25	411.9	16.4	0.05
FB8ru_96	16.24	0.59	0.476	0.037	0.0569	0.0017	0.11	17.5747	0.52	0.062	0.0049	0.23	353.1	10.6	0.01
FB8ru_97	16.25	0.7	0.845	0.065	0.0592	0.0022	0.31	16.8919	0.63	0.1037	0.0075	0.11	348.2	13.2	0.06
FB8ru_98	4.94	0.15	1.74	0.2	0.0668	0.0028	0.51	14.9701	0.68	0.188	0.02	-0.22	349.1	17.7	0.17
FB8ru_99	3.268	0.072	0.354	0.077	0.049	0.0024	0.23	20.4082	1.1	0.051	0.011	0.01	309.0	15.5	0.00
FB8ru_100	3.68	0.1	0.683	0.075	0.0629	0.003	0.03	15.8983	0.75	0.0611	0.014	0.29	380.5	19.0	0.03
FB8ru_101	10.6	0.14	0.451	0.046	0.053	0.0018	-0.06	18.8679	0.67	0.064	0.0072	0.41	329.5	11.4	0.01
FB8ru_102	50.2	1.9	0.564	0.026	0.0695	0.0017	0.26	14.3885	0.34	0.0597	0.0027	0.26	430.9	10.4	0.01
FB8ru_103	6.25	0.12	0.377	0.051	0.0492	0.0024	0.00	20.3252	1.1	0.0582	0.0085	0.27	307.5	15.1	0.01
FB8ru_104	3.75	0.13	4.78	0.37	0.0974	0.0053	0.29	10.2669	0.6	0.368	0.03	0.52	372.5	30.0	0.39
FB8ru_105	3.279	0.053	0.498	0.097	0.048	0.0024	-0.11	20.8333	1.1	0.077	0.017	0.29	293.1	15.8	0.03
FB8ru_106	0.815	0.034	1.02	0.24	0.0614	0.0063	-0.02	16.2866	5	0.167	0.066	0.93	331.1	45.7	0.14
FB8ru_107	4.179	0.059	1.3	0.2	0.0705	0.0031	0.59	14.1844	0.58	0.13	0.016	-0.24	399.5	19.2	0.09
FB8ru_108	1.915	0.045	1.13	0.19	0.0606	0.0041	0.07	16.5017	1.3	0.142	0.026	0.28	336.5	25.6	0.11
FB10_0	7.9	0.13	0.55	0.093	0.0701	0.0032	0.95	14.2653	0.39	0.0565	0.008	-0.06	436.3	20.0	0.00
FB10_1	2.9	0.047	0.63	0.13	0.0595	0.008	0.14	16.8067	0.91	0.077	0.017	0.13	362.2	48.5	0.03
FB10_2	17.79	0.33	0.507	0.037	0.0657	0.0011	-0.16	15.2207	0.26	0.0564	0.0043	0.18	409.5	7.1	0.00
FB10_3	18.1	0.3	0.502	0.032	0.0636	0.0012	0.01	15.7233	0.3	0.0578	0.0039	0.11	396.0	7.6	0.00
FB10_4	7.51	0.11	0.346	0.065	0.0496	0.0015	0.13	20.0603	0.61	0.0496	0.0093	0.05	314.6	10.0	0.00
FB10_5	12.26	0.21	0.536	0.046	0.0661	0.0013	-0.06	15.1286	0.31	0.0594	0.0054	0.21	410.4	8.4	0.01
FB10_6	6.63	0.13	0.717	0.084	0.0565	0.0019	0.06	17.6991	0.63	0.094	0.011	0.21	336.8	12.1	0.05
FB10_7	2.857	0.043	0.51	0.11	0.0524	0.0022	0.00	19.0840	0.66	0.073	0.015	0.23	321.2	14.6	0.03
FB10_8	3.143	0.043	0.57	0.13	0.0676	0.0024	0.16	14.7929	0.58	0.061	0.014	0.06	418.7	16.2	0.01
FB10_9	4.03	0.091	1.4	1.7	0.0554	0.0018	-0.06	18.0505	0.62	0.17	0.2	0.06	297.8	86.2	0.15
FB10_10	8.246	0.066	0.41	0.053	0.0533	0.0015	0.09	18.7617	0.54	0.0576	0.0076	0.10	332.9	9.7	0.01
FB10_11	3.303	0.069	0.5	0.11	0.0496	0.0021	-0.06	20.1613	0.91	0.078	0.017	0.22	302.3	14.2	0.03
FB10_12	5.19	0.11	0.378	0.066	0.0525	0.0017	0.06	19.0476	0.63	0.0529	0.0089	-0.09	329.9	11.2	0.00
FB10_13	4.915	0.069	0.531	0.077	0.0497	0.0019	0.76	20.1207	0.84	0.079	0.012	-0.28	302.6	12.3	0.03
FB10_14	14.23	0.26	0.535	0.037	0.0677	0.0013	0.09	14.7710	0.28	0.0576	0.004	0.19	421.1	8.2	0.00
FB10_15	3.27	0.1	1.19	0.23	0.0604	0.0032	0.19	16.5563	0.86	0.142	0.026	0.14	337.4	21.3	0.11
FB10_16	8.02	0.12	0.364	0.058	0.0507	0.0013	0.04	19.7239	0.54	0.0523	0.0086	-0.03	319.0	8.7	0.00
FB10_17	6.02	0.11	0.561	0.073	0.0692	0.002	0.06	14.4509	0.44	0.0612	0.0076	0.12	428.3	12.8	0.01
FB10_18	10.83	0.19	0.535	0.045	0.0675	0.0011	0.03	14.8148	0.24	0.058	0.0049	0.19	419.7	7.2	0.00
FB10_19	6.17	0.22	1.03	0.12	0.0592	0.0017	0.16	16.8919	0.53	0.128	0.015	0.15	337.2	11.7	0.09
FB10_20	7.76	0.17	1.03	0.11	0.0656	0.0021	0.37	15.2439	0.44	0.113	0.011	0.00	380.6	13.2	0.07
FB10_21	2.874	0.052	0.41	0.12	0.0528	0.0023	0.01	18.9394	0.62	0.059	0.017	0.10	329.3	15.7	0.01
FB10_22	10.44	0.16	0.403	0.047	0.0534	0.0014	0.13	18.7266	0.45	0.0552	0.0066	0.08	334.5	9.0	0.00
FB10_23	7.2	0.11	0.348	0.055	0.0494	0.0014	-0.10	20.2429	0.58	0.0526	0.0084	0.33	310.8	9.2	0.00
FB10_24	7.69	0.14	0.466	0.055	0.062	0.0014	-0.03	16.1290	0.37	0.0552	0.0067	0.20	387.4	9.1	0.00
FB10_25	15.95	0.35	0.459	0.036	0.0589	0.0016	0.12	16.9779	0.44	0.056	0.0044	0.11	369.0	10.0	0.00
FB10_26	13.16	0.2	0.486	0.036	0.0626	0.0013	-0.13	15.9744	0.35	0.0572	0.0048	0.42	390.1	8.3	0.00
FB10_27	7.5	0.16	0.336	0.053	0.0475	0.0013	0.00	21.0526	0.61	0.052	0.0087	0.25	299.3	8.7	0.00
FB10_28	24.54	0.47	0.663	0.026	0.0769	0.001	0.07	13.0039	0.17	0.0627	0.0027	0.25	474.1	6.2	0.01
FB10_29	34.83	0.44	0.474	0.019	0.05928	0.00096	0.10	16.8691	0.27	0.0578	0.0024	0.28	369.5	6.0	0.00
FB10_30	7.66	0.16	0.458	0.058	0.0572	0.0015	-0.12	17.4825	0.5	0.0577	0.0074	0.33	356.8	9.8	0.01
FB10_31	7.22	0.14	0.471	0.057	0.0595	0.0015	0.03	16.8067	0.42	0.058	0.0072	0.17	370.8	9.7	0.00
FB10_32	12.72	0.18	0.388	0.036	0.048	0.001	-0.11	20.8333	0.47	0.0594	0.0058	0.32	299.6	6.5	0.01
FB10_33	4.52	0.11	0.662	0.09	0.0569	0.0021	0.13	17.6056	0.7	0.084	0.012	0.22	342.9	13.5	0.04
FB10_34	10.41	0.18	0.474	0.045	0.0647	0.0015	-0.09	15.4560	0.36	0.0538	0.0054	0.29	404.6	9.6	0.00
FB10_35	6.53	0.17	0.473	0.061	0.0606	0.0018	0.00	16.5017	0.52	0.0577	0.0078	0.28	377.7	11.6	0.00
FB10_36	4.35	0.12	0.602	0.079	0.0586	0.0027	0.17	17.0648	0.78	0.076	0.01	0.20	357.2	16.8	0.03
FB10_37	32.85	0.69	0.526	0.026	0.0674	0.0012	0.24	14.8368	0.26	0.0567	0.0028	0.17	419.7	7.5	0.00
FB10_38	13.53	0.23	0.356	0.035	0.04839	0.00093	0.05	20.6654	0.39	0.0539	0.0054	0.17	304.1	6.1	0.00
FB10_39	6.7	0.13	0.393	0.053	0.0483	0.0013	0.06	20.7039	0.57	0.0594	0.0079	0.11	301.5	8.5	0.01
FB10_40	8.52	0.17	0.751	0.066	0.066	0.0014	-0.04	15.1515	0.32	0.0631	0.0076	0.26	397.9	9.1	0.04
FB10_41	16.46	0.36	0.484	0.032	0.06373	0.00098	-0.06	15.6912	0.23	0.0559	0.0039	0.24	397.7	6.3	0.00
FB10_42	16.96	0.33	0.439	0.026	0.0572	0.0011	0.11	17.4825	0.35	0.0562	0.0037	0.00	357.5	6.9	0.00
FB10_43	9.29	0.15	0.441	0.049	0.0561	0.0014	-0.06	17.8253	0.47	0.0589	0.0071	0.28	349.6	9.1	0.01
FB10_44	7.313	0.091	0.476	0.05	0.0642	0.0015	0.07	15.5763	0.39	0.0538	0.006	0.24	401.6	9.7	0.00
FB10_45	3.012	0.067	0.38	0.1	0.0544	0.0023	-0.13	18.3824	0.8	0.051	0.014	0.25	342.4	15.4	0.00
FB10_46	9.02	0.18	0.499	0.043	0.0637	0.0015	-0.05	15.6986	0.36	0.0563	0.0048	0.28	397.3	9.5	0.00
FB10_47	23.06	0.45	1.465	0.042	0.1484	0.0025	0.14	6.7385	0.11	0.0718	0.0022	0.43	888.8	14.6	0.00
FB10_48	12.52	0.24	0.402	0.036	0.0534	0.0012	-0.10	18.7266	0.42	0.0545	0.0051	0.33	334.8	7.7	0.00

S2.4 Rutile U-Pb data tables (continued)

	Approx U PPM	Prop2SE	207Pb/235U	Prop2SE	206Pb/238U	Prop2SE	Rho	238U/206Pb	Prop2SE	207Pb/206Pb	Prop2SE	Rho	207Pb corrected age	Prop2SE	f206Pb
FB10_49	7.2	0.1	0.572	0.055	0.057	0.0014	-0.09	17.5439	0.44	0.074	0.0074	0.36	348.5	9.0	0.03
FB10_50	7.51	0.12	1.098	0.092	0.0624	0.0017	-0.01	16.0256	0.45	0.128	0.011	0.02	355.2	10.9	0.09
FB10_51	13.95	0.21	0.369	0.036	0.0502	0.001	0.01	19.9203	0.41	0.0535	0.0054	0.11	315.4	6.5	0.00
FB10_52	12.8	0.25	0.454	0.034	0.05569	0.00096	0.03	17.9565	0.32	0.0592	0.0045	0.20	346.9	6.2	0.01
FB10_53	25.61	0.53	0.505	0.025	0.0647	0.0011	-0.09	15.4560	0.26	0.0568	0.0029	0.33	403.2	6.9	0.00
FB10_54	5.72	0.15	0.526	0.066	0.0515	0.0017	-0.12	19.4175	0.61	0.077	0.01	0.37	314.2	11.0	0.03
FB10_55	3.648	0.081	1.63	0.13	0.0606	0.0023	0.04	16.5017	0.61	0.201	0.017	0.37	310.9	14.1	0.18
FB10_56	8.24	0.15	0.473	0.053	0.0627	0.0018	0.07	15.9490	0.41	0.0563	0.0067	-0.07	391.2	11.5	0.00
FB10_57	4.62	0.12	1.38	0.24	0.0693	0.003	0.58	14.4300	0.64	0.141	0.021	-0.30	387.0	19.8	0.11
FB10_58	0.89	0.025	0.64	0.36	0.0494	0.004	-0.03	20.2429	2	0.107	0.057	0.22	290.1	31.8	0.07
FB10_59	5.4	0.13	0.556	0.097	0.0538	0.0018	0.11	18.5874	0.65	0.075	0.013	-0.04	328.8	12.1	0.03
FB10_60	9.12	0.16	0.414	0.042	0.0536	0.0015	-0.02	18.6567	0.52	0.0564	0.0059	0.23	335.3	9.5	0.00
FB10_61	12.93	0.22	0.504	0.044	0.0636	0.0013	-0.04	15.7233	0.33	0.0581	0.0052	0.17	395.8	8.3	0.00
FB10_62	5.097	0.062	0.419	0.075	0.052	0.0017	-0.01	19.2306	0.62	0.059	0.012	-0.01	324.4	11.5	0.01
FB10_63	26.96	0.54	0.411	0.024	0.05194	0.00065	0.12	19.2530	0.32	0.0562	0.0034	0.28	325.1	5.4	0.00
FB10_64	6.58	0.12	0.527	0.065	0.0611	0.0018	-0.02	16.3666	0.49	0.0627	0.0079	0.24	378.4	11.5	0.01
FB10_65	3.649	0.046	0.46	0.1	0.05	0.0019	-0.07	20.0000	0.78	0.071	0.017	0.35	307.5	13.2	0.02
FB10_66	30.9	0.65	0.425	0.032	0.05454	0.00097	0.17	18.3352	0.33	0.056	0.0042	0.11	341.2	6.2	0.00
FB10_67	10.49	0.1	0.473	0.05	0.0622	0.0013	-0.11	16.0772	0.31	0.0557	0.006	0.29	388.4	8.5	0.00
FB10_68	2.896	0.079	0.71	0.12	0.0631	0.003	0.07	15.8479	0.72	0.084	0.015	0.22	380.3	19.2	0.04
FB10_69	2.783	0.08	0.58	0.15	0.0653	0.0028	0.10	15.3139	0.71	0.061	0.016	0.05	404.8	16.8	0.01
FB10_70	9.65	0.19	0.361	0.046	0.047	0.0012	0.34	21.2766	0.56	0.0556	0.0071	-0.14	294.8	7.9	0.00
FB10_71	7.72	0.13	0.416	0.056	0.0483	0.0013	-0.01	20.7039	0.56	0.0636	0.0089	0.21	299.9	8.6	0.01
FB10_72	7.97	0.12	0.725	0.071	0.0655	0.0016	0.15	15.2672	0.38	0.0808	0.008	0.16	396.1	10.3	0.03
FB10_73	3.004	0.062	2.57	0.28	0.0784	0.0036	0.33	12.7551	0.69	0.24	0.026	0.14	377.7	23.6	0.23
FB10_74	3.278	0.079	0.481	0.096	0.0625	0.0025	0.17	16.0000	0.66	0.055	0.012	0.06	390.6	16.4	0.00
FB10_75	2.896	0.066	7.04	0.73	0.1265	0.0066	0.69	7.9051	0.44	0.397	0.03	-0.19	455.9	37.0	0.42
FB10_76	8.92	0.17	0.461	0.047	0.0616	0.0015	-0.02	16.2338	0.4	0.0541	0.0054	0.24	385.5	9.6	0.00
FB10_77	9.14	0.17	0.504	0.046	0.0646	0.0014	0.02	15.4799	0.33	0.0574	0.0055	0.01	402.3	9.0	0.00
FB10_78	28.86	0.64	1.462	0.044	0.1502	0.002	0.14	6.6578	0.092	0.0707	0.0022	0.32	900.4	11.8	0.00
FB10_79	5.04	0.11	0.54	0.18	0.0608	0.0027	0.22	16.4474	0.71	0.063	0.021	0.07	376.4	19.1	0.01
FB10_81	2.115	0.039	0.39	0.16	0.0475	0.0024	-0.05	21.0526	1.3	0.06	0.025	0.20	296.3	17.4	0.01
FB10_82	13.23	0.34	0.453	0.041	0.0596	0.0016	0.19	16.7785	0.44	0.055	0.0049	0.05	372.8	10.1	0.00
FB10_83	2.421	0.099	3.4	0.41	0.0652	0.0048	0.60	11.7371	0.63	0.285	0.026	-0.14	380.7	27.9	0.29
FB10_84	11.57	0.17	0.388	0.041	0.0505	0.0013	-0.01	19.8020	0.52	0.0557	0.0059	0.25	316.4	8.3	0.00
FB10_85	16.27	0.46	0.368	0.036	0.0504	0.0014	0.11	19.8413	0.51	0.0532	0.0052	0.11	316.8	8.9	0.00
FB10_86	9.12	0.26	0.651	0.061	0.0769	0.0024	0.06	13.0208	0.39	0.062	0.0059	0.24	473.9	14.9	0.01
FB10_87	7.83	0.15	0.472	0.053	0.0618	0.0015	0.25	16.1812	0.41	0.0552	0.0062	-0.06	386.2	9.7	0.00
FB10_88	41.43	0.86	0.524	0.022	0.0658	0.0012	0.19	15.1976	0.28	0.0575	0.0026	0.33	409.5	7.4	0.00
FB10_89	16.81	0.34	0.475	0.037	0.0601	0.0014	0.20	16.6389	0.4	0.0575	0.0044	0.05	374.7	8.6	0.00
FB10_90	1.515	0.052	1.07	0.79	0.0548	0.0039	-0.01	18.2482	1.2	0.16	0.14	0.00	298.9	61.7	0.13
FB10_91	3.445	0.062	0.49	0.13	0.0593	0.0023	0.15	16.8634	0.7	0.06	0.016	-0.10	368.7	15.8	0.01
FB10_92	4.095	0.099	0.458	0.096	0.0554	0.0021	0.12	18.0505	0.68	0.06	0.013	0.12	344.8	14.0	0.01
FB10_93	7.3	0.22	0.501	0.063	0.0657	0.0022	-0.11	15.2207	0.45	0.0552	0.0069	0.14	410.1	13.9	0.00
FB10_94	4.73	0.11	0.316	0.073	0.0546	0.002	0.00	18.3150	0.66	0.043	0.01	0.22	347.0	13.2	0.00
FB10_95	7.28	0.29	0.38	0.13	0.0547	0.0042	0.38	18.2815	1.4	0.05	0.015	-0.09	344.7	26.8	0.00
FB10_96	7	0.13	0.509	0.057	0.063	0.0016	0.15	15.8730	0.4	0.0589	0.0068	-0.04	391.8	10.3	0.01
FB10_97	9.33	0.2	0.451	0.049	0.0561	0.0017	0.26	17.2117	0.5	0.0561	0.0059	-0.23	363.1	10.8	0.00
FB10_98	13.93	0.23	0.306	0.03	0.0492	0.0012	-0.12	20.3252	0.49	0.0456	0.0048	0.29	312.2	7.7	0.00
FB10_99	16.38	0.54	0.35	0.031	0.0503	0.0012	0.13	19.8607	0.47	0.0514	0.0049	0.11	316.9	7.7	0.00
FB10_100	1.367	0.035	0.53	0.31	0.0516	0.0034	-0.10	19.3798	1.3	0.072	0.041	0.49	316.7	26.2	0.02
FB10_101	5.7	0.11	0.43	0.07	0.0628	0.002	-0.04	15.9236	0.53	0.0506	0.0083	0.23	394.4	12.9	0.00
FB10_102	12.16	0.24	0.498	0.04	0.0648	0.0015	0.10	15.4321	0.36	0.0559	0.0043	-0.09	404.2	9.4	0.00
FB10_103	16.45	0.32	0.493	0.046	0.0641	0.0019	0.19	15.6006	0.46	0.0558	0.0054	0.06	400.0	11.9	0.00
FB10_104	11.72	0.14	0.363	0.043	0.0501	0.0014	0.06	19.9601	0.56	0.0541	0.0068	0.06	314.6	9.0	0.00
FB10_105	5.58	0.1	0.4	0.077	0.0537	0.0016	-0.02	18.6220	0.56	0.054	0.01	0.04	336.9	10.7	0.00
FB10_106	5.387	0.079	0.489	0.079	0.0645	0.0022	0.20	15.5039	0.53	0.0552	0.0086	-0.03	402.7	14.1	0.00
FB10_107	10.8	0.19	0.503	0.052	0.0651	0.0015	-0.23	15.3610	0.37	0.0567	0.0063	0.37	405.7	9.7	0.00
FB10_109	3.397	0.054	0.44	0.1	0.0605	0.0024	0.04	16.5289	0.66	0.054	0.012	0.12	378.7	15.8	0.00
FB10_110	4.201	0.076	0.447	0.099	0.05	0.0019	-0.02	20.0000	0.72	0.068	0.015	0.05	306.6	12.9	0.02
FB10_111	2.232	0.044	0.69	0.43	0.0519	0.0028	0.08	19.2678	1.2	0.078	0.03	0.03	316.2	20.6	0.03
FB10_112	3.839	0.092	0.56	0.097	0.0578	0.002	0.16	17.3010	0.61	0.07	0.012	0.03	355.1	13.2	0.02
FB10_113	1.756	0.053	17.5	1	0.202	0.012	0.70	4.9505	0.29	0.648	0.032	0.37	330.7	54.2	0.74
FB10_114	8.5	0.12	0.568	0.061	0.0529	0.0013	-0.13	18.9036	0.43	0.0783	0.0085	0.22	322.0	8.5	0.03
FB10_115	5.98	0.098	0.474	0.085	0.0572	0.0017	0.05	17.4825	0.55	0.061	0.012	0.18	355.4	11.6	0.01
FB10_116	10.34	0.2	0.799	0.067	0.054	0.0015	-0.03	18.5185	0.52	0.1061	0.0085	0.04	316.2	9.5	0.07
FB10_117	35.4	0.84	0.525	0.025	0.0676	0.0013	0.15	14.7929	0.27	0.0563	0.0027	0.19	421.1	8.1	0.00
FB10_118	12.31	0.21	0.561	0.041	0.0656	0.0015	-0.01	15.2439	0.32	0.0627	0.0048	0.37	405.7	9.4	0.01
FB10_119	4.011	0.069	0.434	0.099	0.05	0.002	0.06	20.0000	0.84	0.064	0.015	-0.05	310.2	13.5	0.01
FB10_120	12.34	0.24	0.449	0.043	0.0529	0.0014	-0.03	18.9036	0.54	0.0627	0.0063	0.20	328.4	8.9	0.01
FB10_121	3.03	0.056	5.55	0.35	0.0931	0.0036	0.46	10.7411	0.4	0.43	0.024	0.21	310.7	21.1	0.47
FB11ru_0	2.495	0.075	0.54	0.17	0.0714	0.0043	-0.09	14.0056	0.92	0.058	0.019	0.44	443.4	26.1	0.00
FB11ru_1	5.64	0.22	0.485	0.06	0.0562	0.0018	0.09	17.7936	0.56	0.0627	0.008	0.14	348.5	11.5	0.01
FB11ru_2	15.16	0.64	0.654	0.049	0.0625	0.0017	-0.16	16.0000	0.43	0.0776	0.0063	0.43	379.8	10.6	0.03
FB11ru_3	1.382	0.068	0.38	0.17	0.0709	0.0047	0.05	14.1243	0.95	0.04	0.02	0.09	449.3	31.1	0.00
FB11ru_4	3.85	0.25	0.454	0.077	0.0518	0.0023	0.05	19.3050	0.99	0.067	0.012	0.26	320.0	14.8	0.02
FB11ru_5	4.49	0.1	0.438	0.061	0.0538	0.0018	-0.11	18.5874	0.65	0.0593	0.0091	0.36	335.0	11.7	0.01
FB11ru_6	0.278	0.011	1.08	0.7	0.0523	0.0061	-0.18	19.1205	10	0.21	0.29	0.36	265.0	124.7	0.20
FB11ru_7	2.126	0.075	0.75	0.14	0.0548	0.0029	0.02	18.2482	0.95	0.102	0.02	0.28	323.4	18.8	0.06
FB11ru_8	7.28	0.22	0.65	0.1	0.0673	0.0036	0.12	14.8588	0.81	0.071	0.011	0.29	411.8	22.3	0.02
FB11ru_9	7.5	0.19	0.477	0.05	0.0528	0.0017	0.02	18.9394	0.63	0.0668	0.0075	0.34	326.1	10.8	0.02
FB11ru_10	0.942	0.025	0.76	0.21	0.0685	0.005	0.20	14.5985	1.4	0.085	0.026	0.08	411.8	32.4	0.04
FB11ru_11	15.29	0.34	0.491	0.035	0.0651	0.0012	0.08	15.3610	0.28	0.0549	0.0039	0.22	406.5	7.6	0.00
FB11ru_12	19.8	0.47	0.516	0.033	0.0673	0.0012	-0.02	14.8588	0.28	0.0561	0.0037	0.25	419.4	7.6	0.00
FB11ru_13	3.4	0.16	0.67	0.14	0.0722	0.0045	0.09	13.8504	0.96	0.072	0.016	0.24	440.7	26.3	0.02
FB11ru_14	16.95	0.4	0.458	0.051	0.0572	0.0018	-0.26	17.4825	0.53	0.0588	0.0068	0.47	356.3	11.4	0.01
FB11ru_15	0.895	0.035	0.57	0.19	0.0651	0.0059	0.11	15.3610	3.2	0.08	0.029	0.98	394.1	37.9	0.03
FB11ru_16	4.495	0.077	0.441	0.073	0.0542	0.002	0.20	18.4502	0.75	0.062	0.011	0.01	336.6	13.0	0.01
FB11ru_17	2.02	0.052	0.34	0.11	0.0504	0.0028	0.20	19.8413	1.3	0.045	0.015	-0.04	320.0	18.4	0.00
FB11ru_18	11.12	0.32	1.15	0.22	0.0648	0.0024	0.62	15.4083	0.59	0.133	0.024	0.23	395.7	17.9	0.10
FB11ru_19	17.91	0.34	0.472	0.037	0.0592	0.0012	0.14	16.8919	0.35	0.0574	0.0064	0.09	369.2	7.6	0.00
FB11ru_20	17.2	0.39	0.76	0.15	0.0643	0.002	0.06	15.5521	0.47	0.088	0.017	0.02	395.5	14.4	0.04
FB11ru_21	30.71	0.61	0.458	0.026	0.0569	0.001	0.45	17.5747	0.31	0.059	0.0034	0.02	354.4	6.3	0.01
FB11ru_22	0.461	0.014	11.4	3	0.141	0.023	-0.02	7.0922	2	0.541	0.065	0.00	349.2	107.7	0.61
FB11ru_23	21.23	0.27	0.371	0.025	0.0486	0.001	-0.10	20.5761	0.44	0.0562	0.0041	0.36	304.5	6.4	0.00
FB11ru_24	9.09	0.24	0.482	0.047	0.0579	0.0016	0.03	17.2712	0.45	0.0613	0.0063	0.20	359.5	10.2	0.01
FB11ru_25	24.36	0.82	0.52	0.042	0.0648	0.0025	0.28	15.4321	0.62	0.0587	0.0045	0.22	402.8	15.4	0.00
FB11ru_26	2.475	0.054	0.67	0.1	0.0533	0.0023	-0.07	18.7617	0.85	0.091	0.014	0.28	319.2	14.7	0.05
FB11ru_27	3.75	0.11	0.74	0.21	0.0724	0.0049	0.14	13.8122	0.87	0.079	0.024	0.25	438.0	31.9	0.03
FB11ru_28	13.06	0.27	0.722	0.053	0.0671	0.0015	0.06	14.9031	0.34	0.0787	0.0058	0.13	406.7	9.4	0.03
FB11ru_29	2.478	0.047	0.42	0.13	0.0511	0.0026	0.02	19.5695	1	0.068	0.021	0.16	315.3	17.6	0.02
FB11ru_30	7.64	0.16	3.15	0.38	0.0937	0.0053	0.58	11.9474	0.7	0.271	0.029	-0.18	383.1	30.2	0.27
FB11ru_31	2.511	0.062	1.22	0.21	0.0666	0.0034	0.15	15.0150	0.96	0.135	0.021	0.20	375.1	27.1	0.10
FB11ru_32	1.824	0.062	4.56	0.42	0.088	0.005	0.21	11.3636	0.67	0.369	0.035	-0.03	322.0	29.9	0.42
FB11ru_33	1.774	0.067	2.87	0.54	0.0776	0.0079	0.62	12.6535	1.4	0.258	0.046	0.31	364.0	45.5	0.25
FB11ru_34	7.67	0.14	0.83	0.072	0.0571	0.0017	0.39	17.5131	0.49	0.106	0.0096	-0.09	334.2	10.7	0.07
FB11ru_35	8.07	0.19	3.25	0.32	0.0923	0.0038	0.76	10.8342	0.51	0.246	0.02	-0.57	439.8	22.6	0.24
FB11ru_36	3.875	0.091	0.446	0.07	0.0494	0.0019	0.02	20.2429	0.8	0.066	0.011	0.30	305.7	12.3	0.02
FB11ru_37	4.77	0.16	0.681	0.083	0.0669	0.0028	0.32	14.9477	0.7	0.0775	0.0093	0.01	406.1	17.3	0.03
FB11ru_38	7.18	0.16	0.37	0.043	0.0522	0.0017	-0.03	19.1571	0.59	0.0516	0.0063	0.34	328.6	10.8	0.00
FB11ru_39	4.87	0.17	0.63	0.11	0.0564	0.0026	-0.07	17.7305	0.92	0.08	0.014	0.43	342.3	16.7	0.03
FB11ru_40	0.487	0.017	2.09	0.73	0.075	0.011	0.63	13.3333	3.4	0.246	0.086	-0.87	358.0	71.4	0.24
FB11ru_41	0.509	0.015	0.44	0.29	0.048	0.0056	-0.06	20.6333	4.6	0.129	0.075	-1.00	273.7	42.1	0.10
FB11ru_42	3.07	0.12	0.437	0.085	0.0505	0.002	-0.02	19.8020	0.66	0.061	0.012	0.22	314.4	13.1	0.01
FB11ru_43	4.602	0.074	0.474	0.074	0.0581	0.002	0.06	17.2117	0.59	0.061	0.01	0.12	360.9	13.0	0.01
FB11ru_44	0.85	0.031	1.65	1.6	1.48	0.14	0.97	0.6711	0.12	0.885	0.024	0.19	1211.4	258.3	0.86
FB11ru_45	7.666	0.09	0.544	0.051	0.0678	0.0018	0.08	14.7493	0.37	0.06	0.006	0.17	420.5	11.4	0.01
FB11ru_46	12.16	0.15	0.843	0.052	0.062	0.0014	0.40	16.1290	0.4	0.0997	0.006	-0.06	366.4	8.6	0.06
FB11ru_47	1.087	0.036	3.08	0.53	0.0729	0.0051	0.15	13.7174	1	0.303	0.052	0.53	315.8	36.4	0.31
FB11ru_48	4.858	0.071	0.316	0.052	0.0509	0.0015	-0.06	19.6464	0.62	0.0448	0.0073	0.23	323.2	9.8	0.00
FB11ru_49	1.73	0.031	0.46	0.22	0.0476	0.004	-0.05	21.0084	1.7	0.076	0.039	0.45	291.1	28.1	0.03
FB11ru_50	7.24	0.12	0.518	0.056	0.062	0.0017	-0.15	16.1290	0.42	0.0621	0.0071	0.34	384.1	10.9	0.01
FB11ru_51	0.316	0.011	-0.17	0.45	0.0549	0.0062	0.16	18.2149	17	0.061	0.098	-0.41	341.3	64.9	0.01
FB11ru_52	1.047	0.022	0.36	0.18	0.0547	0.0042	0.19	18.2815	1.8	0.038	0.027	-0.28	349.7	28.7	0.00
FB11ru_53	1.543	0.031	0.47	0.18	0.054	0.0037	0.52	18.5185	1.4	0.067	0.025	0.06	333.3	24.7	0.02
FB11ru_54	12.18	0.14	0.369	0.036	0.0472	0.0011	-0.15	21.1864	0.49	0.057	0.0056	0.40	295.6	7.1	0.01
FB11ru_55	8.55	0.26	5.59	0.61	0.1068	0.0062	0.80	9.3809	0.52	0.374	0.027	-0.43	402.8	31.8	0.40
FB11ru_56	3.691	0.069	0.486	0.084	0.0548	0.0029	0.12	18.2482	0.96	0.066	0.012	0.19	338.6	18.3	0.02
FB11ru_57	2.205	0.052	0.65	0.17	0.0533	0.0031	0.48	18.7617	1.4	0.094	0.023	-0.02	318.0	20.5	0.05
FB11ru_58	0.981	0.045	0.93	0.39	0.0656	0.0063	0.27	15.2439	1.4	0.112	0.053	0.06	361.1	44.6	0.07
FB11ru_59	11.48	0.28	0.506	0.04	0.0585	0.0013	0.10	17.0940	0.41	0.0632	0.0049	0.19	362.3	8.2	0.01
FB11ru_60	4.912	0.091	0.7	0.13	0.0538	0.002	0.35	18.5874	0.72	0.093	0.015	-0.10	321.3	13.3	0.05
FB11ru_61	6.34	0.12	0.572	0.074	0.0602	0.0019	0.12	16.6113	0.52	0.0689	0.0065	0.05	369.6	12.1	0.02
FB11ru_62	8.17	0.27	1.014	0.088	0.0574	0.0018	0.23	17.4216	0.58	0.126	0.01	0.14	328.0	11.0	0.09
FB11ru_63	1.713	0.031	2.25	0.3	0.0666	0.0041	0.04	15.0150	1.1	0.246	0.038	0.04	316.2	27.4	0.24
FB11ru_64	14.46	0.23	0.361	0.033	0.0466	0.0011	0.13	21.4592	0.53	0.0608	0.0059	0.17	290.5	7.1	0.01

S2.4 Rutile U-Pb data tables (continued)

	Approx U PPM	Prop2SE	207Pb/235U	Prop2SE	206Pb/238U	Prop2SE	Rho	238U/206Pb	Prop2SE	207Pb/206Pb	Prop2SE	Rho	207Pb corrected age	Prop2SE	f206Pb
FB11ru_65	5.27	0.099	2.19	0.15	0.0729	0.0024	0.23	13.7174	0.44	0.221	0.015	0.26	362.1	14.4	0.21
FB11ru_66	5.42	0.16	0.409	0.062	0.049	0.0016	0.06	20.4082	0.74	0.061	0.0094	-0.04	305.2	11.6	0.01
FB11ru_67	1.698	0.098	0.44	0.11	0.0552	0.0032	-0.12	18.1159	1.2	0.061	0.016	0.37	343.2	20.7	0.01
FB11ru_68	2.422	0.073	0.5	0.12	0.0566	0.0043	0.01	17.6678	1.3	0.07	0.018	0.40	347.6	27.1	0.02
FB11ru_69	5.09	0.21	0.617	0.097	0.0676	0.0027	0.16	14.7929	0.55	0.065	0.011	0.15	416.7	17.3	0.01
FB11ru_70	2.505	0.063	1.62	0.16	0.0579	0.0031	0.08	17.2712	1	0.21	0.023	0.39	293.1	18.6	0.20
FB11ru_71	2.451	0.05	1.75	0.22	0.0565	0.0034	0.31	17.6991	1.1	0.236	0.031	0.33	274.6	21.2	0.23
FB11ru_72	6.6	1.3	3.15	0.26	0.0946	0.004	0.12	10.5708	0.47	0.245	0.023	0.32	451.4	24.9	0.23
FB11ru_73	7.71	0.13	0.398	0.037	0.0504	0.0015	0.15	19.8413	0.62	0.058	0.0055	0.10	314.9	9.5	0.01
FB11ru_74	1.852	0.037	0.67	0.13	0.0535	0.0042	0.48	18.6916	1.8	0.094	0.018	0.03	319.2	25.8	0.05
FB11ru_75	19.15	0.2	0.966	0.048	0.0556	0.0012	0.19	17.9211	0.35	0.1262	0.0063	0.08	318.6	7.3	0.09
FB11ru_76	4.89	0.15	3.5	0.38	0.0792	0.0037	0.75	12.6263	0.64	0.309	0.025	-0.45	339.3	21.6	0.32
FB11ru_77	1.808	0.036	0.7	0.15	0.06	0.0036	0.05	16.6667	1	0.093	0.024	0.10	357.6	23.6	0.05
FB11ru_78	3.81	0.11	0.445	0.073	0.0483	0.0016	-0.15	20.7039	0.79	0.07	0.012	0.38	297.5	11.6	0.02
FB11ru_79	2.062	0.058	3.06	0.26	0.0725	0.0045	0.10	13.7931	0.94	0.306	0.032	0.45	299.9	25.7	0.34
FB11ru_80	13.28	0.14	0.397	0.033	0.0501	0.0011	-0.02	19.9601	0.42	0.0574	0.0052	0.21	313.3	7.1	0.01
FB11ru_81	6.79	0.11	1.024	0.075	0.0563	0.0016	0.24	17.7620	0.54	0.1323	0.0097	0.12	319.0	9.9	0.10
FB11ru_82	4.924	0.057	0.498	0.065	0.0492	0.0017	0.09	20.3252	0.73	0.076	0.011	0.11	300.7	11.1	0.03
FB11ru_83	5.93	0.21	0.504	0.072	0.066	0.0025	0.21	15.1515	0.58	0.0557	0.0082	0.02	411.7	15.8	0.00
FB11ru_84	0.1397	0.0093	2.9	1.9	0.068	0.019	0.39	14.7059	7.4	0.36	0.28	0.19	264.2	165.0	0.38
FB11ru_85	32.25	0.61	1.406	0.081	0.0679	0.0017	0.00	14.7275	0.36	0.1501	0.0075	0.00	374.5	10.0	0.12
FB11ru_86	5.37	0.21	1.64	0.15	0.0805	0.005	0.43	12.4224	0.83	0.152	0.013	0.35	441.6	28.0	0.12
FB11ru_87	3.24	0.11	4.62	0.77	0.0914	0.0054	0.80	10.9409	0.65	0.344	0.045	-0.55	366.6	38.0	0.36
FB11ru_88	1.327	0.031	0.75	0.15	0.057	0.0041	-0.04	17.5439	1.5	0.104	0.022	0.30	335.4	25.6	0.06
FB11ru_89	3.584	0.043	0.54	0.11	0.048	0.0018	0.49	20.8333	0.8	0.08	0.015	-0.29	292.0	12.1	0.03
FB11ru_90	3.413	0.047	0.516	0.074	0.0503	0.0022	0.30	19.8807	0.86	0.074	0.01	0.02	306.1	13.8	0.03
FB11ru_91	2.609	0.06	0.508	0.068	0.053	0.0029	0.07	18.8679	1.2	0.073	0.014	0.28	324.6	18.4	0.02
FB11ru_92	6.53	0.08	0.417	0.051	0.0497	0.0016	0.20	20.1207	0.7	0.0627	0.0079	0.09	309.8	10.2	0.01
FB11ru_93	3.96	0.16	2.2	0.91	0.1104	0.0065	0.70	9.0580	0.53	0.139	0.051	-0.49	403.5	48.7	0.41
FB11ru_94	7.58	0.12	0.509	0.057	0.0501	0.0014	0.11	19.9601	0.57	0.0744	0.0066	0.11	306.7	9.1	0.03
FB11ru_95	10.72	0.35	0.756	0.077	0.0682	0.0016	-0.10	14.6628	0.33	0.0812	0.0064	0.29	411.9	10.4	0.03
FB11ru_96	4.16	0.16	0.78	0.15	0.0578	0.0029	0.51	17.3010	1	0.1	0.019	-0.26	341.6	18.9	0.06
FB11ru_97	1.18	0.022	1.28	0.34	0.0557	0.0042	0.39	17.9533	1.5	0.162	0.056	-0.11	294.2	32.6	0.16
FB11ru_98	3.269	0.053	0.291	0.066	0.0471	0.0016	-0.05	21.2314	0.88	0.045	0.011	0.26	299.3	12.0	0.00
FB11ru_99	2.799	0.063	0.425	0.062	0.0483	0.0025	0.01	20.7039	1.1	0.07	0.015	0.16	297.5	16.2	0.02
FB11ru_10(	2.467	0.043	0.51	0.11	0.0549	0.0024	-0.01	18.2149	0.82	0.069	0.015	0.01	338.0	15.8	0.02
FB11ru_10'	3.59	0.05	0.565	0.091	0.0516	0.0022	0.23	19.3798	0.86	0.08	0.012	0.02	313.6	14.0	0.03
FB11ru_10:	14.67	0.23	0.637	0.054	0.0626	0.0016	0.22	15.9744	0.41	0.0744	0.0065	0.06	381.9	10.1	0.02
FB11ru_10;	1.194	0.033	0.26	0.13	0.0505	0.0034	-0.13	19.8020	1.7	0.056	0.026	0.61	316.3	23.3	0.00
FB11ru_10<	7.76	0.18	1.39	0.15	0.0644	0.0022	0.40	15.5260	0.53	0.155	0.017	-0.18	353.0	14.5	0.13
FB11ru_10=	12.67	0.25	0.38	0.038	0.0507	0.0013	0.05	19.7239	0.5	0.0544	0.0058	0.23	318.2	8.3	0.00
FB11ru_10>	0.292	0.019	0.96	0.53	0.16	0.21	0.20	6.2500	4.9	0.09	0.11	0.25	935.7	1191.6	0.02
FB11ru_10?	4.833	0.094	0.567	0.079	0.0655	0.0031	-0.04	15.2672	0.74	0.065	0.0092	0.35	404.0	19.3	0.01
FB11ru_10@	5.563	0.094	1.23	0.18	0.056	0.0025	0.78	17.8571	0.84	0.166	0.022	-0.51	302.7	16.4	0.14
FB11ru_10A	0.924	0.024	10.5	1.1	0.139	0.012	0.53	7.1942	0.79	0.58	0.059	0.34	300.3	68.6	0.66
FB11ru_11C	8.53	0.19	0.474	0.044	0.0617	0.0018	0.05	16.2075	0.49	0.0568	0.0056	0.23	384.8	11.3	0.00
FB11ru_111	1.63	0.045	0.66	0.14	0.062	0.0038	-0.04	16.1290	1	0.086	0.019	0.31	372.8	24.2	0.04
FB11ru_11E	3.707	0.099	0.479	0.071	0.0624	0.0034	0.05	16.0256	0.95	0.0598	0.0098	0.30	387.7	21.2	0.01
FB11ru_11G	1.091	0.034	0.71	0.25	0.0539	0.0062	-0.26	18.5529	2.6	0.112	0.039	0.59	314.0	39.1	0.07
FB11ru_11I	8.01	0.26	0.466	0.073	0.0645	0.0027	0.13	15.5039	0.66	0.051	0.0078	0.20	404.8	17.1	0.00
FB11ru_11K	11.6	0.23	0.432	0.041	0.0574	0.0016	0.04	17.4216	0.5	0.0543	0.0051	0.22	359.5	10.1	0.00
FB11ru_11M	1.653	0.062	0.56	0.15	0.0604	0.0055	0.01	16.5563	1.7	0.072	0.022	0.62	369.8	34.6	0.02
FB11ru_11O	7.47	0.22	0.6	0.077	0.0651	0.0026	0.17	15.3610	0.64	0.0679	0.009	0.21	400.1	16.3	0.02
FB11ru_11Q	3.84	0.16	0.77	0.16	0.07	0.0034	0.10	14.2857	0.73	0.082	0.018	0.06	422.2	22.2	0.03
FB13_0	2.277	0.05	0.45	0.12	0.0508	0.0034	0.21	19.6850	1.6	0.069	0.02	0.06	313.1	22.1	0.02
FB13_1	3.68	0.11	0.58	0.1	0.063	0.0031	0.33	15.8730	0.76	0.07	0.013	0.02	396.4	19.7	0.02
FB13_2	5.05	0.11	0.436	0.084	0.0488	0.0023	-0.02	20.4918	0.96	0.069	0.014	0.16	300.9	14.9	0.02
FB13_3	1.571	0.05	0.43	0.15	0.0522	0.0039	0.12	19.1571	1.5	0.068	0.023	-0.01	322.0	25.4	0.02
FB13_4	1.066	0.052	0.99	0.26	0.0549	0.0051	0.03	18.2149	2.9	0.142	0.04	0.43	307.1	32.8	0.11
FB13_5	16.48	0.25	1.589	0.075	0.149	0.0032	0.37	6.7114	0.16	0.0767	0.0034	0.33	887.2	18.7	0.01
FB13_6	6.28	0.15	0.397	0.048	0.0515	0.0019	-0.13	19.4175	0.73	0.0568	0.0073	0.39	322.2	12.1	0.00
FB13_7	6.15	0.12	0.561	0.072	0.0666	0.0025	0.15	15.0150	0.53	0.062	0.008	0.09	412.2	15.7	0.01
FB13_8	9.63	0.56	5.53	0.44	0.1141	0.0048	0.48	8.7642	0.37	0.345	0.022	-0.17	456.8	26.6	0.36
FB13_9	6.33	0.12	0.656	0.097	0.0494	0.002	0.31	20.2429	0.9	0.096	0.014	-0.06	293.5	12.9	0.06
FB13_10	1.248	0.032	0.85	0.31	0.0619	0.0052	0.46	16.1551	1.6	0.108	0.036	0.38	361.9	34.4	0.07
FB13_11	2.464	0.066	0.47	0.12	0.0646	0.0042	0.07	15.4799	1.1	0.056	0.016	0.13	402.9	26.9	0.00
FB13_12	7.97	0.26	1.71	0.2	0.0716	0.005	0.38	13.9665	1.1	0.175	0.021	0.27	381.0	28.5	0.15
FB13_13	1.943	0.076	42.4	3.1	0.434	0.029	0.78	2.3041	0.16	0.694	0.033	0.19	597.9	114.1	0.78
FB13_14	2.115	0.041	1.58	0.35	0.0652	0.0048	0.49	15.3374	1.4	0.166	0.034	-0.12	351.9	30.6	0.14
FB13_15	12.89	0.26	0.569	0.046	0.0644	0.0021	0.09	15.5280	0.52	0.065	0.0055	0.27	397.3	13.0	0.01
FB13_16	14.27	0.51	16.8	2.1	0.217	0.022	0.93	4.6083	0.46	0.567	0.029	-0.39	501.3	68.9	0.63
FB13_17	6.81	0.13	0.471	0.072	0.053	0.0025	0.28	18.8679	0.94	0.065	0.01	0.01	328.1	15.8	0.01
FB13_18	9.47	0.18	0.414	0.048	0.0569	0.002	-0.08	17.5747	0.64	0.0559	0.0071	0.35	355.8	12.7	0.00
FB13_19	7.66	0.15	0.496	0.052	0.0599	0.0017	0.00	16.6945	0.54	0.0598	0.0063	0.20	372.4	10.8	0.01
FB13_20	4.528	0.095	0.517	0.08	0.0618	0.0036	0.23	16.1812	0.98	0.066	0.012	0.20	381.1	22.5	0.01
FB13_21	14.45	0.23	0.72	0.11	0.0542	0.002	0.12	18.4502	0.71	0.093	0.012	-0.10	323.7	12.6	0.05
FB13_22	5.39	0.29	0.596	0.084	0.0734	0.003	0.14	13.6240	0.5	0.0562	0.0081	0.14	455.5	18.6	0.00
FB13_23	3.63	0.12	10.7	1.6	0.14	0.015	0.85	7.1429	0.79	0.523	0.044	-0.22	366.6	61.1	0.58
FB13_24	6.66	0.14	0.499	0.064	0.0638	0.002	-0.08	15.6740	0.55	0.0591	0.0083	0.34	396.5	12.8	0.01
FB13_25	10.45	0.39	0.41	0.059	0.0567	0.0024	0.08	17.6367	0.78	0.0531	0.0077	0.16	355.8	15.2	0.00
FB13_26	3.608	0.074	0.501	0.094	0.0574	0.003	0.13	17.4216	0.95	0.063	0.012	0.16	355.7	19.0	0.01
FB13_27	3.883	0.069	0.361	0.083	0.0516	0.0026	0.09	19.3798	1.1	0.057	0.014	0.24	322.7	16.9	0.01
FB13_28	0.843	0.036	69	30	0.57	0.23	0.98	1.7544	2.7	0.37	0.11	-0.65	2284.5	1026.5	0.25
FB13_29	8.45	0.18	0.413	0.054	0.0577	0.0023	-0.05	17.3310	0.74	0.0519	0.007	0.29	362.4	14.5	0.00
FB13_30	8.34	0.12	0.606	0.068	0.0569	0.0019	0.04	17.6056	0.61	0.0797	0.0094	0.29	344.8	12.1	0.03
FB13_31	31.9	1.3	0.68	0.042	0.0711	0.0018	0.45	14.0647	0.34	0.0701	0.004	-0.02	435.1	11.0	0.02
FB13_32	10.94	0.35	1.3	0.11	0.0718	0.0027	0.23	13.9276	0.5	0.134	0.011	0.34	404.5	16.1	0.10
FB13_33	1.131	0.043	0.66	0.24	0.0602	0.0052	0.14	16.6113	1.7	0.082	0.03	0.16	364.0	33.8	0.03
FB13_34	1.512	0.051	10.51	0.95	0.147	0.01	0.40	6.8027	0.61	0.54	0.048	0.47	395.7	59.4	0.60
FB13_35	0.544	0.018	3.5	0.73	0.0876	0.0089	0.07	11.4155	2	0.336	0.08	0.51	356.8	66.7	0.35
FB13_36	8.5	1.4	3.5	0.42	0.105	0.0058	0.47	9.5238	0.56	0.261	0.03	0.16	467.8	35.4	0.25
FB13_37	7.21	0.17	0.583	0.076	0.0606	0.0027	0.24	16.5017	0.77	0.074	0.01	0.03	370.1	16.8	0.02
FB13_38	6.27	0.24	0.491	0.068	0.059	0.0026	0.11	16.9492	0.61	0.0637	0.0094	0.20	365.2	17.5	0.01
FB13_39	2.75	0.13	0.58	0.15	0.0554	0.004	-0.06	18.0505	1.4	0.076	0.02	0.28	338.0	25.5	0.03
FB13_40	5.293	0.065	1.03	0.13	0.0535	0.0035	0.10	18.6916	1.5	0.142	0.02	0.48	299.3	21.0	0.11
FB13_41	1.179	0.036	0.77	0.28	0.0546	0.0058	0.45	18.3150	2.9	0.126	0.048	0.17	311.3	38.3	0.09
FB13_42	30.54	0.65	0.48	0.025	0.0609	0.0017	0.17	16.4204	0.44	0.0573	0.0032	0.34	379.7	10.5	0.00
FB13_43	4.07	0.16	1.36	0.18	0.0726	0.0035	-0.05	13.7741	0.76	0.14	0.02	0.30	405.7	22.1	0.11
FB13_44	13.55	0.2	0.542	0.042	0.0671	0.0021	-0.01	14.9031	0.49	0.06	0.0053	0.33	416.2	13.1	0.01
FB13_45	4.1	0.14	3.23	0.3	0.0939	0.0047	0.26	10.6496	0.55	0.255	0.025	0.24	440.9	28.0	0.25
FB13_46	9.04	0.19	3.19	0.22	0.0793	0.0033	0.57	12.6103	0.54	0.295	0.017	0.09	348.3	17.7	0.30
FB13_47	6.98	0.27	0.514	0.068	0.0565	0.0027	-0.04	17.6991	0.87	0.0682	0.0096	0.41	347.6	16.9	0.02
FB13_48	5.66	0.13	0.624	0.076	0.0523	0.0027	0.25	19.1205	1	0.088	0.011	0.16	314.5	16.6	0.04
FB13_49	1.66	0.061	1.06	0.24	0.0666	0.0006	-0.02	15.0150	1.5	0.13	0.03	0.36	377.7	34.7	0.09
FB13_50	2.91	0.1	0.51	0.13	0.0539	0.0031	0.23	18.5529	1.1	0.068	0.017	0.12	332.3	20.1	0.02
FB13_51	3.18	0.076	0.58	0.13	0.0531	0.0032	0.40	18.8324	1.3	0.076	0.016	-0.10	324.2	20.3	0.03
FB13_52	1.015	0.027	6.99	0.97	0.1091	0.0069	0.48	9.1659	0.95	0.465	0.062	0.48	317.2	58.1	0.54
FB13_53	4.504	0.087	3.17	0.27	0.0774	0.0035	0.29	12.9199	0.62	0.303	0.026	0.19	335.2	21.5	0.31
FB13_54	15.79	0.25	1.08	0.067	0.0625	0.0019	0.16	16.0000	0.52	0.1277	0.0084	0.19	355.9	11.4	0.09
FB13_55	1.013	0.029	1.2	0.28	0.0603	0.0062	0.04	16.5837	2.4	0.178	0.043	0.31	320.1	38.1	0.16
FB13_56	10.21	0.23	0.665	0.059	0.0582	0.0025	0.34	17.1821	0.64	0.0829	0.007	0.07	351.7	15.2	0.04
FB13_57	10.42	0.25	0.44	0.046	0.051	0.0017	0.17	19.6078	0.7	0.0641	0.0065	0.16	316.2	10.7	0.01
FB13_58	2.063	0.047	1.45	0.19	0.1563	0.007	0.05	6.3980	0.32	0.072	0.01	0.26	934.3	41.8	0.00
FB13_59	6.03	0.26	0.423	0.069	0.0581	0.0027	0.03	17.2117	0.61	0.0548	0.0087	0.31	363.6	17.2	0.00
FB13_60	17.49	0.24	0.512	0.038	0.0665	0.0017	0.00	15.0376	0.41	0.056	0.0043	0.31	414.6	10.6	0.00
FB13_61	4.172	0.096	1.07	0.11	0.0546	0.0031	-0.05	15.4799	0.77	0.122	0.013	0.39	370.5	18.6	0.08
FB13_62	7.59	0.13	1.96	0.1	0.1567	0.0046	-0.02	6.3816	0.16	0.0773	0.0049	0.30	930.8	28.0	0.01
FB13_63	2.955	0.056	1.45	0.18	0.0676	0.0041	0.37	14.7929	0.96	0.156	0.019	0.11	369.8	24.1	0.13
FB13_64	1.212	0.033	0.42	0.2	0.0523	0.0043	0.14	19.1205	2	0.07	0.033	0.36	321.6	29.2	0.02
FB13_65	8.85	0.18	0.344	0.038	0.0485	0.0015	0.14	20.6186	0.66	0.0544	0.0066	0.31	304.6	9.6	0.00
FB13_66	1.41	0.15	64	18	0.57	0.11	0.61	1.7544	0.35	0.79	0.14	-0.31	290.9	620.9	0.92
FB13_67	1.858	0.034	16.9	5.7	0.2	0.051	0.98	5.0000	1.7	0.322	0.064	-0.67	935.7	225.1	0.31
FB13_68	0.963	0.043	3.13	0.6	0.086	0.019	0.37	11.6279	2.7	0.307	0.092	0.42	369.6	100.4	0.31
FB13_69	1.621	0.059	6.11	0.57	0.1086	0.0072	0.28	9.2081	0.67	0.426	0.044	0.38	366.4	43.7	0.46
FB13_70	11	0.21	1.411	0.093	0.1463	0.003	0.28	6.8353	0.14	0.0707	0.0044	0.01	877.8	18.0	0.00
FB13_71	21.9	1	0.479	0.039	0.059	0.002	0.28	16.9492	0.59	0.0577	0.0044	0.16	367.9	12.4	0.00
FB13_72	1.023	0.06	53.9	3.1	0.504	0.029	0.70	1.9841	0.12	0.798	0.037	0.28	204.6	150.4	0.94
FB13_73	13.7	0.49	0.659	0.055	0.0788	0.0024	0.25	12.6904	0.38	0.0611	0.005	0.10	486.5	14.8	0.01
FB13_74	4.426	0.093	1.15	0.15	0.0526	0.0025	0.36	19.1744	0.7	0.156	0.017	0.01	352.4	16.1	0.10
FB13_75	43.08	0.54	0.393	0.024	0.0529	0.0012	0.08	18.9394	0.42	0.0542	0.0034	0.24	331.2	7.5	0.00
FB13_76	6.88	0.14	1.46	0.12	0.082	0.0029	0.17	12.1951	0.47	0.131	0.011	0.27	462.9	17.4	0.09
FB13_77	7.2	0.23	2.1	0.25	0.0683	0.0029	0.24	14.6413	0.64	0.22	0.022	-0.09	340.0	18.3	0.21
FB13_78	2.46	0.049	8.4	1.1	0.126	0.013	0.87	7.9365	0.99	0.487	0.042	0.00	365.3	55.0	0.54
FB13_79	2.051	0.041	1.32	0.26	0.0608	0.0047	0.44	16.4474	1.3	0.168	0.031	0.05	327.4	28.8	0.14
FB13_80	2.87	0.14	0.64	0.16	0.0582	0.0041	0.06	17.1821	1.4	0.078	0.02	0.16	353.9	26.1	0.03
FB13_82	6.22	0.11	1.009	0.099	0.0595	0.0021	0.26	16.8067	0.66	0.123	0.012	0.06	341.2	13.1	0.09

S2.4 Rutile U-Pb data tables (continued)

	Approx U PPM	Prop2SE	207Pb/235U	Prop2SE	206Pb/238U	Prop2SE	Rho	238U/206Pb	Prop2SE	207Pb/206Pb	Prop2SE	Rho	207Pb corrected age	Prop2SE	f206Pb
FB13_83	10.55	0.18	2.43	0.14	0.1627	0.0042	0.31	6.1463	0.17	0.1079	0.0058	0.13	930.7	24.1	0.05
FB13_84	17.34	0.25	0.462	0.036	0.0586	0.0015	0.23	17.0648	0.46	0.0567	0.0052	0.11	365.0	9.5	0.01
FB13_85	4.55	0.15	0.64	0.1	0.0651	0.0033	0.02	15.3610	0.65	0.075	0.013	0.26	396.6	20.7	0.03
FB13_86	0.293	0.016	51.1	4.3	0.475	0.035	0.45	2.1053	0.19	0.822	0.073	0.35	70.0	261.2	0.98
FB13_87	2.021	0.043	4.76	0.63	0.0919	0.0062	0.56	10.8814	0.71	0.38	0.043	0.11	342.8	36.0	0.41
FB13_88	2.98	0.12	0.65	0.11	0.0667	0.004	0.01	14.9925	1.1	0.077	0.014	0.34	405.2	24.9	0.03
FB13_89	1.253	0.037	1.24	0.28	0.0627	0.0052	0.30	15.9490	1.7	0.146	0.04	0.05	348.2	34.3	0.11
FB13_90	1.66	0.095	2.26	0.42	0.085	0.0066	0.25	11.7647	1	0.208	0.04	0.34	430.0	41.6	0.19
FB13_91	7.17	0.1	2.73	0.37	0.0784	0.0036	0.77	12.7551	0.66	0.244	0.028	-0.49	375.3	23.8	0.24
FB13_92	2.68	0.071	4.43	0.6	0.0916	0.006	0.64	10.9170	0.85	0.342	0.037	-0.01	368.8	35.2	0.36
FB13_93	2.81	0.11	0.6	0.12	0.0582	0.003	0.06	17.1821	0.98	0.082	0.018	0.19	352.1	19.6	0.04
FB13_94	41.6	2.1	1.934	0.091	0.1898	0.0058	0.60	5.2687	0.19	0.0754	0.0029	0.18	1122.3	33.2	0.00
FB13_95	16.9	0.32	2.65	0.12	0.176	0.0042	0.57	5.6818	0.13	0.1085	0.0041	-0.13	1003.6	23.6	0.04
FB13_96	4.6	0.13	3.38	0.39	0.0833	0.0052	0.77	12.0048	0.74	0.304	0.027	-0.24	360.0	28.0	0.31
FB14_0	7.41	0.12	0.476	0.075	0.0555	0.0019	-0.14	18.0180	0.62	0.065	0.011	0.39	343.3	12.5	0.01
FB14_1	5.414	0.094	0.49	0.12	0.0528	0.0025	-0.05	18.9394	0.98	0.07	0.018	0.32	324.8	16.8	0.02
FB14_2	8.69	0.17	1.56	0.11	0.1494	0.0033	0.07	6.6934	0.15	0.0754	0.0052	0.41	890.9	19.6	0.01
FB14_3	2.192	0.066	0.62	0.2	0.0664	0.0035	0.13	15.0602	0.67	0.075	0.023	-0.04	404.4	23.9	0.02
FB14_4	8.67	0.14	0.427	0.057	0.0542	0.0016	0.06	18.4502	0.57	0.0579	0.008	0.16	338.3	10.4	0.01
FB14_5	5.17	0.13	0.54	0.1	0.0676	0.0026	0.16	14.7929	0.59	0.058	0.011	0.03	420.3	16.8	0.00
FB14_6	15.94	0.28	0.974	0.084	0.0604	0.0017	0.12	16.5563	0.45	0.1156	0.0093	0.20	349.7	10.6	0.08
FB14_7	5.066	0.081	0.402	0.081	0.0541	0.0018	0.06	18.4843	0.63	0.054	0.011	0.07	339.3	12.0	0.00
FB14_8	3.248	0.067	0.48	0.13	0.0511	0.0026	0.06	19.5695	1.1	0.071	0.021	0.19	314.1	17.8	0.02
FB14_9	5.396	0.096	0.446	0.076	0.0554	0.0018	0.05	18.0505	0.62	0.059	0.01	0.03	345.2	11.8	0.01
FB14_10	7.55	0.23	0.531	0.073	0.0707	0.0026	0.05	14.1443	0.52	0.0577	0.0065	0.23	439.3	16.5	0.00
FB14_11	9.59	0.12	0.383	0.049	0.0519	0.0014	0.03	19.2678	0.55	0.0556	0.0073	0.17	325.1	9.1	0.00
FB14_12	11.53	0.21	0.407	0.047	0.0548	0.0016	-0.19	18.2482	0.59	0.0556	0.0067	0.41	342.9	10.2	0.00
FB14_13	10.12	0.26	0.536	0.052	0.0653	0.0022	0.14	15.3139	0.55	0.0609	0.0061	0.25	404.8	13.7	0.01
FB14_14	12.04	0.23	0.507	0.049	0.0671	0.0019	0.06	14.9031	0.42	0.0555	0.0055	0.24	418.5	11.9	0.00
FB14_15	2.34	0.31	0.98	0.23	0.0555	0.0038	0.06	18.0180	1.8	0.135	0.041	-0.01	313.4	27.5	0.10
FB14_16	10.59	0.18	0.464	0.054	0.0522	0.0015	-0.11	19.1571	0.57	0.0658	0.008	0.29	322.9	9.7	0.02
FB14_17	0.803	0.019	2.33	0.59	0.0652	0.0051	-0.02	15.3374	1.6	0.26	0.067	0.01	294.2	49.4	0.28
FB14_18	12.91	0.26	0.466	0.055	0.0569	0.0014	0.13	17.5747	0.44	0.0596	0.0068	-0.09	354.2	9.1	0.01
FB14_19	9.22	0.2	0.435	0.066	0.0638	0.0016	0.04	15.6740	0.43	0.0502	0.0076	0.10	400.9	10.5	0.00
FB14_20	5.25	0.11	0.52	0.084	0.0525	0.0019	-0.03	19.0476	0.69	0.072	0.012	0.19	322.2	12.5	0.02
FB14_21	14.12	0.16	0.394	0.033	0.0509	0.0011	0.12	19.6464	0.45	0.0564	0.0048	0.14	318.6	7.0	0.00
FB14_22	11.16	0.24	0.547	0.058	0.0676	0.0018	0.13	14.7929	0.4	0.0599	0.0064	-0.10	419.3	11.4	0.01
FB14_23	4.076	0.064	0.452	0.095	0.0535	0.0023	0.08	18.6916	0.82	0.061	0.013	0.25	332.8	15.1	0.01
FB14_24	7.76	0.2	0.596	0.06	0.0683	0.002	0.06	14.6413	0.44	0.0654	0.007	0.25	420.7	12.6	0.01
FB14_25	5.2	0.12	0.97	0.14	0.0527	0.0021	0.26	18.9753	0.71	0.133	0.019	-0.07	296.6	14.1	0.10
FB14_26	1.566	0.051	1.34	0.29	0.0592	0.0035	-0.03	16.8919	1.1	0.184	0.041	0.07	311.6	26.1	0.16
FB14_27	5.42	0.14	0.503	0.063	0.0531	0.0022	0.04	18.8324	0.77	0.069	0.011	0.18	327.0	14.1	0.02
FB14_28	5.31	0.12	0.486	0.061	0.054	0.0021	0.19	18.5185	0.75	0.064	0.011	0.27	334.6	13.6	0.01
FB14_29	12.69	0.34	0.6	0.045	0.0722	0.0018	0.17	13.8504	0.35	0.0608	0.0046	0.21	446.7	11.2	0.01
FB14_30	7.05	0.14	0.429	0.064	0.055	0.0018	-0.01	18.1818	0.61	0.0562	0.0063	0.23	344.0	11.6	0.00
FB14_31	11.06	0.16	0.399	0.044	0.0513	0.0013	-0.04	19.4932	0.47	0.0573	0.0066	0.31	320.7	8.4	0.01
FB14_32	0.616	0.026	1.2	0.97	0.0614	0.0058	-0.04	16.2866	2.1	0.14	0.13	0.13	343.9	69.0	0.11
FB14_33	11.7	0.2	0.468	0.047	0.0524	0.0013	0.07	19.0840	0.5	0.0655	0.0068	0.06	324.2	8.4	0.02
FB14_34	64	1.9	0.538	0.023	0.0717	0.0016	0.28	13.9470	0.33	0.0545	0.0021	0.41	447.1	9.8	0.00
FB14_35	5.71	0.13	0.343	0.077	0.0572	0.0019	-0.06	17.4825	0.65	0.047	0.011	0.14	361.5	12.7	0.00
FB14_36	41.79	0.92	0.505	0.025	0.0628	0.0011	-0.14	15.9236	0.28	0.0585	0.003	0.22	390.7	6.9	0.00
FB14_37	5.96	0.12	0.76	0.13	0.0549	0.0022	0.18	18.2149	0.75	0.104	0.016	-0.04	323.2	14.8	0.06
FB14_38	7.13	0.19	0.395	0.071	0.0537	0.0016	-0.09	18.6220	0.65	0.0547	0.0089	0.23	336.6	11.8	0.00
FB14_39	30.09	0.58	0.528	0.024	0.067	0.0014	0.07	14.9254	0.32	0.0577	0.0029	0.35	416.8	8.7	0.00
FB14_40	16.57	0.35	0.485	0.039	0.0659	0.0014	0.15	15.1745	0.32	0.0538	0.0045	0.07	412.0	8.9	0.00
FB14_41	4.18	0.095	0.39	0.1	0.0485	0.0022	0.18	20.6186	1	0.062	0.018	-0.09	301.7	15.1	0.01
FB14_42	7.71	0.22	0.465	0.06	0.0599	0.0015	0.19	16.6945	0.44	0.0565	0.0072	0.01	373.9	9.8	0.00
FB14_43	5.78	0.14	2.56	0.25	0.0773	0.0031	0.25	12.9366	0.48	0.242	0.023	0.09	371.3	20.0	0.23
FB14_45	15.76	0.33	0.492	0.048	0.0649	0.0013	-0.09	15.4083	0.31	0.0554	0.0057	0.19	405.1	8.4	0.00
FB14_46	15.52	0.38	0.595	0.042	0.0739	0.0014	0.00	13.5318	0.27	0.0589	0.0043	0.30	458.1	8.8	0.00
FB14_47	37.59	0.73	0.536	0.028	0.0702	0.0011	0.09	14.2450	0.23	0.0554	0.0029	-0.05	437.5	6.9	0.00
FB14_48	14.98	0.34	0.51	0.041	0.0639	0.0017	0.12	15.6495	0.4	0.0576	0.0044	0.17	397.9	10.6	0.00
FB14_49	6.48	0.13	0.555	0.061	0.067	0.0023	-0.03	14.9254	0.52	0.0618	0.0094	0.03	414.7	14.7	0.01
FB14_50	5.01	0.15	1.41	0.13	0.0761	0.0026	0.05	13.1406	0.45	0.136	0.013	0.40	427.2	16.1	0.10
FB14_51	34.94	0.73	0.548	0.029	0.0693	0.0011	0.04	14.4300	0.23	0.0574	0.0029	0.15	430.9	6.9	0.00
FB14_52	4.45	0.13	0.579	0.097	0.0582	0.0021	-0.01	17.1821	0.66	0.077	0.013	0.32	354.4	13.8	0.03
FB14_53	27.51	0.65	0.419	0.032	0.055	0.0012	-0.06	18.1818	0.39	0.0553	0.0043	0.15	344.3	7.6	0.00
FB14_54	15.38	0.26	0.526	0.048	0.064	0.0017	0.20	15.6250	0.42	0.0603	0.0054	-0.09	397.2	10.7	0.01
FB14_55	3.23	0.1	0.38	0.12	0.0557	0.0027	0.07	17.9533	0.98	0.051	0.016	-0.03	350.5	18.0	0.00
FB14_56	4.186	0.089	0.51	0.11	0.0733	0.0032	0.13	13.6426	0.6	0.055	0.013	0.03	456.6	20.8	0.00
FB14_57	4.38	0.1	0.44	0.11	0.0573	0.0023	0.12	17.4520	0.76	0.054	0.014	0.06	359.1	15.4	0.00
FB14_58	4.546	0.067	0.266	0.068	0.0524	0.0021	-0.11	19.0840	0.76	0.04	0.013	0.24	334.5	14.2	0.00
FB14_59	13.74	0.27	0.435	0.044	0.0547	0.0014	-0.07	18.2815	0.45	0.0587	0.0062	0.33	341.1	9.0	0.01
FB14_60	6.21	0.18	1.71	0.13	0.0714	0.0021	0.06	14.0056	0.41	0.176	0.014	0.26	379.4	13.4	0.15
FB14_61	209.4	5.7	0.532	0.014	0.0695	0.0012	0.49	14.5965	0.26	0.0564	0.0013	0.18	426.6	7.4	0.00
FB14_62	2.904	0.052	0.57	0.14	0.0719	0.0028	0.13	13.9082	0.52	0.057	0.014	0.02	447.0	18.7	0.00
FB14_63	21.12	0.3	0.524	0.041	0.0565	0.0012	-0.24	17.6991	0.39	0.0661	0.0054	0.47	348.9	7.7	0.02
FB14_64	6.78	0.11	0.438	0.073	0.0521	0.0017	-0.04	19.1939	0.65	0.0569	0.0095	0.26	325.8	11.1	0.00
FB14_65	5.155	0.085	0.377	0.076	0.0501	0.0019	0.01	19.9601	0.82	0.059	0.012	0.65	312.7	12.6	0.01
FB14_66	16.39	0.29	0.789	0.05	0.0714	0.0016	0.17	14.0056	0.32	0.0807	0.0053	0.16	431.2	9.9	0.03
FB14_67	4.31	0.12	0.56	0.1	0.072	0.0029	0.05	13.8689	0.56	0.056	0.01	0.18	448.1	18.5	0.00
FB14_68	15.41	0.24	0.38	0.036	0.0547	0.0016	0.05	18.2815	0.55	0.0521	0.0053	0.26	343.8	10.1	0.00
FB14_69	4.46	0.12	0.52	0.089	0.074	0.0027	-0.15	13.5135	0.52	0.054	0.0093	0.22	461.4	17.3	0.00
FB14_70	3.956	0.061	0.45	0.11	0.0668	0.0023	-0.03	14.9701	0.51	0.05	0.012	0.16	419.4	15.4	0.00
FB14_71	19.25	0.28	0.54	0.13	0.0655	0.0013	-0.13	15.2672	0.32	0.059	0.011	0.24	407.0	9.6	0.01
FB14_72	5.61	0.18	0.414	0.078	0.0599	0.0021	0.00	16.6945	0.6	0.054	0.011	0.25	375.1	13.9	0.00
FB14_73	1.487	0.044	0.23	0.25	0.0511	0.0035	-0.08	19.5695	1.7	0.038	0.04	0.04	327.1	27.1	0.00
FB14_74	10.21	0.19	0.604	0.07	0.0693	0.0017	-0.05	14.4300	0.38	0.0644	0.0061	0.37	427.3	11.1	0.01
FB14_75	5.71	0.12	0.383	0.077	0.0568	0.002	-0.12	17.6056	0.65	0.052	0.011	0.28	356.8	13.2	0.00
FB14_76	17.64	0.43	0.415	0.037	0.0537	0.0014	0.16	18.6220	0.46	0.0564	0.005	0.11	335.9	8.9	0.00
FB14_77	4.293	0.078	0.374	0.093	0.0517	0.0022	-0.14	19.3424	0.79	0.052	0.014	0.34	325.3	14.7	0.00
FB14_78	125.7	1.8	0.501	0.015	0.0665	0.0011	0.35	15.0376	0.25	0.0548	0.0016	0.22	415.2	6.8	0.00
FB14_79	4.45	0.11	0.61	0.12	0.0599	0.0031	0.22	16.6945	0.84	0.073	0.015	-0.09	368.4	19.9	0.02
FB14_80	1.089	0.027	0.66	0.3	0.0569	0.0043	0.04	17.5747	1.7	0.084	0.047	0.68	343.5	32.7	0.04
FB14_81	9.8	0.24	0.421	0.056	0.0602	0.0017	0.36	16.6113	0.5	0.0496	0.0064	-0.01	378.9	10.9	0.00
FB14_82	28.01	0.46	0.535	0.038	0.0681	0.0015	0.11	14.6843	0.33	0.0572	0.0042	0.10	423.7	9.4	0.00
FB14_83	5.749	0.096	0.368	0.071	0.0539	0.0021	-0.10	18.5529	0.79	0.053	0.011	0.43	338.5	13.7	0.00
FB14_84	62	1.4	0.482	0.016	0.0638	0.001	0.36	15.6740	0.25	0.0549	0.0017	0.13	396.6	6.2	0.00
FB14_85	13.38	0.19	0.376	0.045	0.0528	0.0014	0.05	18.9394	0.51	0.0517	0.0063	0.09	332.2	9.0	0.00
FB14_86	6.552	0.095	0.463	0.064	0.0553	0.0016	0.00	18.0832	0.55	0.0635	0.0093	0.20	342.7	10.5	0.01
FB14_87	6.49	0.13	0.549	0.063	0.067	0.0019	-0.03	14.9254	0.44	0.0603	0.0074	0.27	415.4	12.1	0.01
FB14_88	4.42	0.11	0.498	0.09	0.0529	0.0021	-0.01	18.9036	0.77	0.069	0.013	0.22	325.8	13.8	0.02
FB14_89	5.39	0.1	0.691	0.094	0.0622	0.002	0.16	16.0772	0.57	0.079	0.011	0.12	377.4	13.0	0.03
FB14_90	2.197	0.049	0.42	0.2	0.0579	0.0039	-0.12	17.2712	1.3	0.051	0.026	0.14	364.1	26.7	0.00
FB14_91	4.705	0.075	0.411	0.085	0.0522	0.002	0.14	19.1571	0.75	0.057	0.012	-0.05	326.4	13.2	0.01
FB14_92	3.783	0.06	3.56	0.3	0.0799	0.0034	0.27	12.5156	0.58	0.336	0.03	0.27	325.5	23.0	0.35
FB14_93	15.5	0.27	0.673	0.063	0.0632	0.0019	0.25	15.8228	0.49	0.079	0.0077	0.08	383.3	11.9	0.03
FB14_94	6.24	0.15	0.99	0.15	0.075	0.0029	0.59	13.3333	0.52	0.095	0.013	-0.34	444.4	18.4	0.05
FB14_95	8.77	0.15	0.358	0.056	0.0468	0.0013	-0.12	21.3675	0.66	0.057	0.0093	0.31	293.1	8.7	0.01
FB14_96	7.54	0.11	0.395	0.066	0.0546	0.0016	0.06	18.3150	0.55	0.0527	0.0092	0.07	343.0	10.6	0.00
FB14_97	3.758	0.051	0.38	0.12	0.0534	0.0024	0.04	18.7266	0.79	0.052	0.016	0.26	335.8	16.2	0.00
FB14_98	2.944	0.048	0.69	0.18	0.0605	0.0032	0.19	16.5289	0.88	0.091	0.026	0.11	361.7	22.3	0.05
FB14_99	15.65	0.12	0.864	0.054	0.0613	0.0014	-0.06	16.3132	0.37	0.1034	0.0071	0.35	360.5	8.8	0.06
FB14_100	6.42	0.12	0.36	0.086	0.0566	0.0022	0.09	17.6678	0.67	0.046	0.012	0.08	358.2	14.6	0.00
FB14_101	11.08	0.15	0.487	0.053	0.0617	0.0016	-0.08	16.2075	0.5	0.0586	0.0064	0.36	384.0	11.4	0.01
FB14_102	7.88	0.25	0.79	0.11	0.0593	0.0027	0.03	16.8634	0.88	0.099	0.014	0.00	351.0	16.9	0.06
FB14_103	5.658	0.058	1.84	0.15	0.0643	0.0023	0.22	15.5521	0.56	0.211	0.018	0.21	324.7	14.5	0.20
FB14_104	3.413	0.064	0.61	0.15	0.0634	0.0026	-0.03	15.7729	0.68	0.073	0.018	0.21	367.4	17.8	0.02
FB14_105	6.26	0.094	0.614	0.089	0.0569	0.002	0.10	17.5747	0.64	0.077	0.011	0.20	346.6	12.9	0.03
FB14_106	24.7	0.25	0.469	0.027	0.0565	0.0011	0.12	17.0940	0.3	0.0562	0.0035	0.20	364.6	6.9	0.01
FB14_107	3.437	0.062	0.41	0.11	0.0516	0.0023	0.22	19.3050	0.96	0.057	0.017	0.08	323.9	15.7	0.01
FB14_108	1.569	0.033	0.31	0.27	0.0523	0.0032	-0.11	19.1205	1.3	0.05	0.04	0.10	329.8	25.5	0.00
FB14_109	12.52	0.28	0.644	0.08	0.0555	0.0024	0.20	18.0180	0.75	0.0846	0.0098	0.09	334.9	14.8	0.04
FB14_110	3.453	0.065	1.31	0.15	0.0676	0.0035	-0.04	14.7929	0.77	0.148	0.018	0.31	374.0	21.2	0.12
FB14_111	0.598	0.025	2.69	0.74	0.0656	0.006	-0.14	15.2439	2	0.338	0.099	0.49	266.2	55.9	0.36
FB14_112	2.228	0.045	0.57	0.21	0.0579	0.0042	-0.07	17.2712	1.8	0.085	0.031	0.24	349.0	28.4	0.04

Chapter 3

An Integrated Apatite Geochronology and Geochemistry Tool for Sedimentary Provenance Analysis

Published in 'Geochemistry, Geophysics, Geosystems', April 2018 *19*(4) p. 1309–1326

The text of this chapter differs from the published version because it incorporates minor corrections suggested by the examiners.

Co-authors: David M. Chew, Andrew C. Morton, Chris Mark, Isadora A. Henrichs

ABSTRACT

Sediment provenance studies utilizing detrital geochronology are often limited by source-rock non-uniqueness with respect to mineral age. Thus, the development of integrated techniques which permit identification of source rock age and lithology are highly desirable. In this case study from the southern Massif Central, France, we target modern-river sediment from the river Tarn to assess the utility of combined U-Pb and multiple trace-element geochemical analysis of detrital apatite as a provenance tool. The study area was chosen because the sediment source areas chiefly comprise a relatively simple mix of medium- to low-grade Variscan metasediments and late Variscan granitoids, which should yield detrital apatite readily distinguishable by age, trace-element chemistry, or both. Based on comparison with previously published apatite trace-element data from metasedimentary rocks and granitoids, pelitic apatite in the river Tarn detritus is primarily distinguished by high Sr/Mn, light rare-earth element depletion (LREE) and low actinide contents, whereas granitic apatite is characterised by much lower Sr/Mn, and high LREE and actinide abundances. These source rock determinations are highly consistent with apatite trace-element data from Tarn tributaries that drain either predominantly metapelitic or granitoid catchments. U-Pb analysis of detrital rutile was also undertaken on those catchments for comparative

purposes. As pelitic and granitic apatite can be readily distinguished, samples that have experienced downstream sediment mixing can then be comprehensively characterised. Using this method we identify a source lithology for nearly every analysed apatite grain in the river sediment, even though 59% of the analysed grains do not yield reliable U-Pb ages.

3.1. INTRODUCTION

Isotopic age and trace-element information from detrital minerals permits their use as tracers of source-rock lithology, age and metamorphic grade (e.g., Morton and Chenery, 2009). This enables the evolution of source-area exhumation and the transport pathways of the resulting sediments to be tracked through time when applied to consecutive sedimentary strata (e.g., Mark et al., 2016). The utility of different detrital phases as tracers of source rock provenance depends on a variety of critical factors. These include both the ability to link the geochemical composition to the original source rock, whether by means of trace- or major-element geochemistry, and also their ability to host sufficient radioisotope contents (e.g. U, K or Th) to permit geochronology.

Detrital heavy minerals vary greatly in their ability to preserve an unambiguous geochemical "fingerprint" or age-signature of their source-rock. Hence, most single-phase provenance studies choose from a very limited range of mineral-isotope systems, for example the widely-used U-Pb zircon method (cf. Thomas, 2011; Gehrels, 2012). However, advances in analytical methods and data reduction have expanded the range of provenance information available from less commonly-used detrital U-Pb mineral geochronometers (such as monazite, rutile, apatite, and titanite), and have thus prompted greater adoption of these phases for novel provenance applications (e.g., Carrapa et al., 2009; Hietpas et al., 2010; McAteer et al., 2010; Meinhold et al., 2008). Here, we employ the detrital apatite U-Pb thermochronometer. While detrital apatite fission-track is a well-known and well-established field of sediment tracking (e.g., Carter, 1999), apatite U-Pb analysis is still an under-utilised, though proven (e.g. Carrapa et al., 2009; Zattin et al., 2012; Mark et al., 2016; O'Sullivan et al., 2016) provenance tool. We investigate the efficacy of pairing the expanding field of detrital apatite trace-element analysis (e.g., Abdullin et al., 2016) with recent improvements to the apatite U-Pb method (Chew et al., 2011; Thomson et al., 2012). In this study combined geochronology-geochemistry in apatite is able to detect all known major Phanerozoic geological events to have occurred within this catchment area, whether extensional, collisional, or intraplate. We also provide rutile U-Pb data from each of the two major "source-proximal" river samples, thereby providing a multi-proxy detrital database for two upstream tributaries of the Tarn catchment.

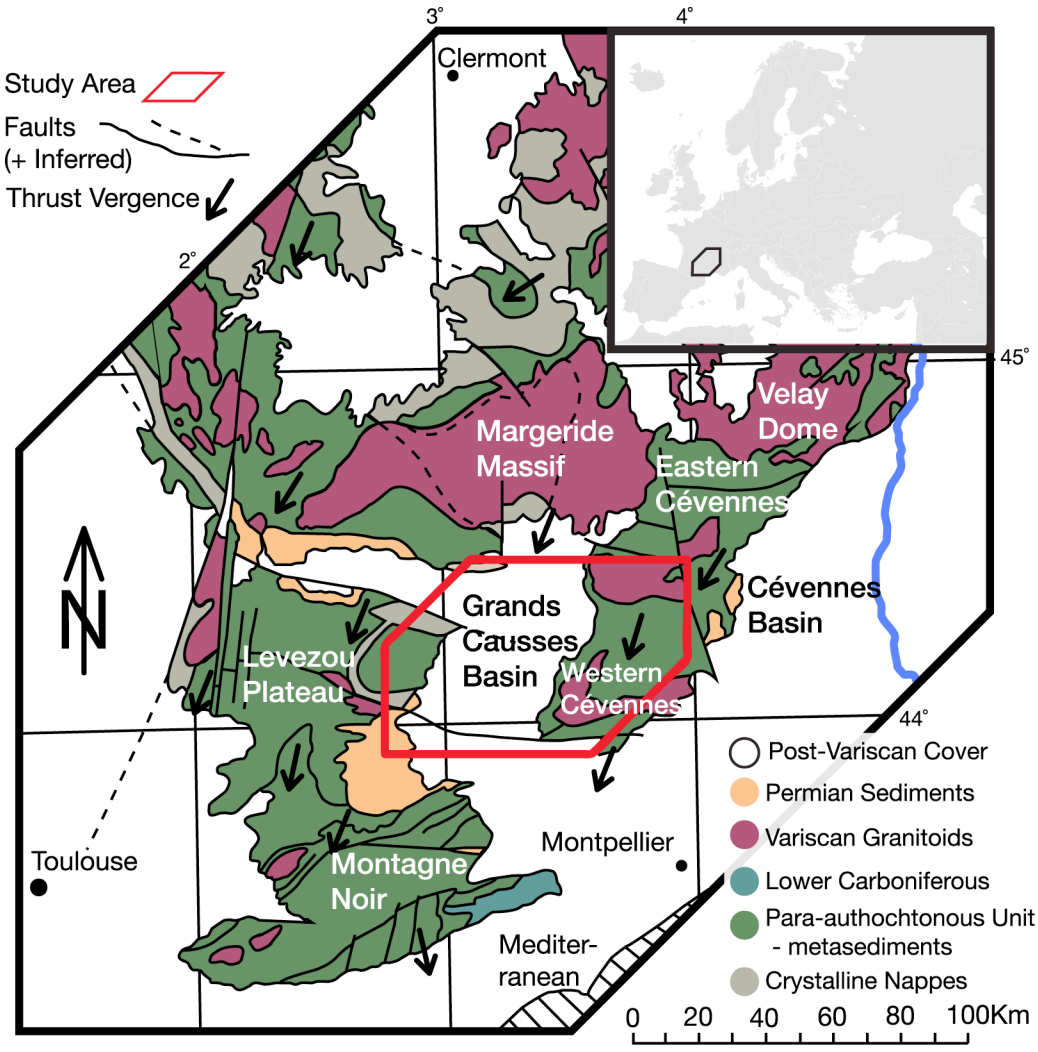

Figure 1. Regional geological map of the Massif Central. The river Tarn (not shown) flows east-to-west across the study area (red box is an inset displayed in Figure 2). Adapted from Matte (1986).

3.1.1 Why study the river Tarn?

The river Tarn is a major tributary of the Garonne in southwest France that rises in the Cévennes Mountains, a southern sub-range of the Massif Central (Figure 1, catchment shown in Figure 2). The river Tarn provides a geologically and hydrologically well-constrained study area (Figure 2) in which to investigate the suitability of detrital apatite trace-element analysis for use as a provenance proxy. The river Tarn source area in the Cévennes Mountains consists of a relatively simple two-component system; unmetamorphosed late-Variscan granitoids, and peak-Variscan greenschist- to amphibolite-facies metapelites (Brichau et al., 2008). These lithologies are sufficiently distinct in both protolith and age to potentially distinguish apatite using trace-element composition and/or U-Pb age in the downstream detritus.

Heavy mineral-rich detritus shed from the river Tarn source areas flows for c. 100 km through minor Permian-Triassic siliciclastics and Jurassic carbonate rocks of the Grands Causses basin. Our heavy mineral analysis (supplementary table S3.1) shows that this carbonate succession contains minimal silicate or heavy mineral detritus and hence will not contribute a significant heavy mineral flux to the river-load (section 3.4.1.3). This means that the bulk of the heavy mineral load can only have been derived from the well-identified river Tarn source areas. A detailed description of the regional geology is given in section 3.2.

3.1.2. Apatite: defining its use as a provenance indicator

Due to the inability of the major rock-forming minerals to incorporate significant P, apatite is a near-ubiquitous accessory mineral in crystalline rocks (Piccoli & Candela, 2002). Apatite may crystallise in metamorphic rocks of all grades and most compositions, and intrusive and extrusive rocks from felsic through basic compositions. In contrast, apatite is usually absent in chemically-precipitated sediments, and depleted ultramafic rocks (Spear & Pyle, 2002). This ubiquity is in contrast to some other commonly employed detrital geochronometers such as monazite, titanite and rutile, which have more restricted parageneses (e.g., Kohn et al. 2015), and are thus tracers of specific lithologies or tectonic regimes.

Due to its instability under weathering at source and during alluvial storage, apatite more likely represents first-cycle detritus than chemically-resistant minerals such as zircon, rutile or tourmaline (e.g., Morton and Hallsworth, 1999 and references therein).

Although it is unstable during intense weathering, apatite is often highly persistent during diagenesis and anchimetamorphism (due to destabilisation and liberation of organic- and adsorbed-P, Ruttenberg & Berner, 1992), often acquiring overgrowths (e.g. Vermeesch et al., 2009). Though in some cases diagenesis may also promote dissolution/recrystallization (e.g. Bouch et al., 2002), the stability of apatite during diagenesis is often comparable to that of zircon and tourmaline, meaning that the first-cycle sedimentary apatite signal is more likely to be preserved once apatite has been buried beyond the reach of low-pH meteoric water sources (Morton, 1986; Morton & Hallsworth, 1999 and references within; see discussion).

Physical weathering is often erroneously identified as a factor in the destruction of heavy mineral species in fluvial transport settings, leading to the so-called "maturity myth" (Garzanti, 2017) that postulates that sediments evolve towards more physically "mature" compositions with increasing transport distance or time. This is despite abrasion having been repeatedly demonstrated to be of almost no importance in the reduction of heavy mineral species diversity in fluvial settings (e.g. Morton & Smale, 1991; Russell, 1937; van Andel, 1950).

Thus, as abrasion can largely be discarded as a mechanism for destroying minerals in subaqueous detritus, the absence of apatite in any given sediment can be mainly attributed to either the source fertility or dissolution: whether at source; during intermediate storage/upon recycling; or during diagenetic reactions that favour the leaching of P. The survival of apatite in sediment is thus likely highly dependent on temperature, rainfall and pH of soils, and the residence time therein.

3.1.2.1 U-Pb dating of detrital apatite by LA-ICPMS

Due to advances in LA-ICP-MS data reduction and matrix-matched standards, it is now possible to accurately, precisely and rapidly date apatite grains containing appreciable common-Pb by U-Pb geochronology (e.g. Chew et al. 2014; Thomson et al. 2012). This has led to a number of provenance studies employing the apatite U-Pb system in recent years (e.g. Carrapa et al., 2009; Mark et al., 2016; O'Sullivan et al., 2016; Zattin et al., 2012).

Due to its intermediate U-Pb closure temperature (c. 375-550°C; Cochrane et al., 2014), apatite is sensitive to the temperatures of medium-grade regional metamorphic events, and hence records lower-temperature events in metamorphosed terranes than the U-Pb zircon system.

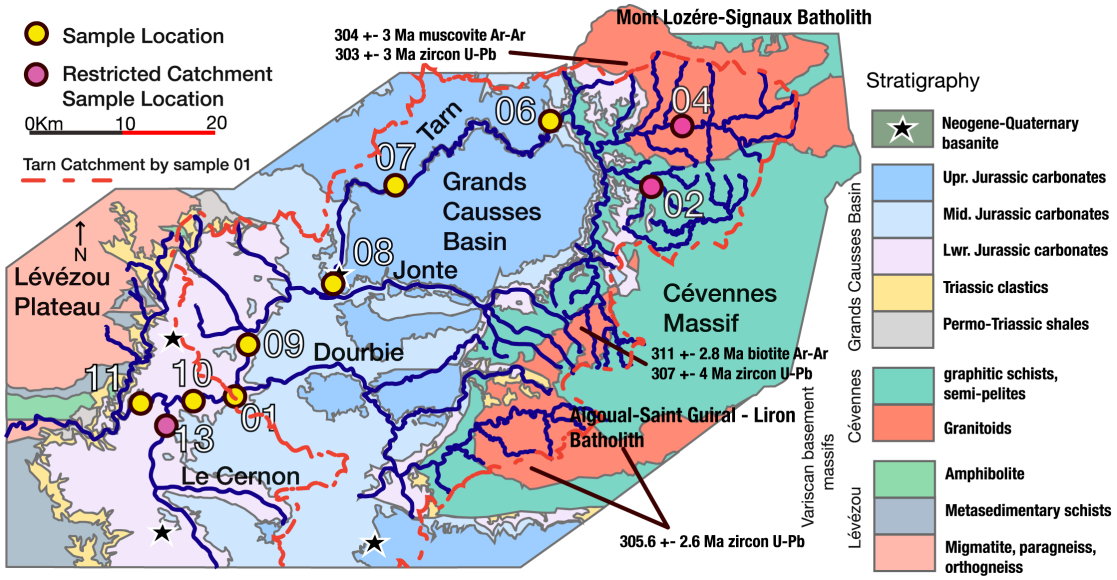

Figure 2. Geological map of the river Tarn catchment; Cévennes Massif and Grands Causses Basin. Numbered sample locations marked. Massif ages from Brichau et al., 2008 and references therein.

Examples of source regions in which the detrital U-Pb apatite system exhibits greater sensitivity to orogenic events than the detrital zircon U-Pb record include the Alpine orogeny, wherein detrital zircon from modern rivers and both the pro- and retro-foreland basins fails to record Alpine metamorphism (Krippner & Bahlburg, 2013; Malusà et al., 2016) but detrital apatite does (Mark et al., 2016), and the Southern Appalachians of the USA, where detrital zircon in both modern rivers and the Appalachian foreland basins fails to record the Alleghanian Orogeny, whilst detrital monazite, rutile and apatite do (e.g. Hietpas et al. 2010; O'Sullivan et al., 2016).

One potential limitation of the apatite U-Pb method (especially in detritus where only single grain-ages may be used) is that for low U, very young, or high common Pb grains, apatite often yields low ratios of radiogenic Pb (Pb*) to common Pb (Pb_c). Due to the high levels of common-Pb typically incorporated by apatite, a common-Pb correction is virtually always required during U-Pb dating. Therefore, unless a ^{204}Pb-based common correction is undertaken (^{204}Pb not measured in this study), apatite U-Pb analyses cannot be screened using traditional measures of discordance. Instead, most studies filter apatite U-Pb age data using relative age uncertainty thresholds (e.g., Mark et al., 2016; O'Sullivan et al., 2016; Zattin et al., 2012). Because the percentage of grains with low Pb^*/Pb_c in some datasets (e.g. young metamorphic terranes) can often be quite high, a high percentage of detrital apatite grains may therefore not pass age-uncertainty screening criteria for the U-Pb dataset, and are thus rejected. The primary sources of low-U and/or high Pb_c detrital apatite encountered in this study are low- and medium-grade metapelites, lithologies that seemingly represent a challenge for dating by the apatite U-Pb geochronometer (see results and discussion).

As low- and medium-grade metapelites dominate much of the sediment source areas (Figure 2), this study presents a near worst-case scenario in terms of the proportion of non-dateable grains (c. 60%) compared to previously published detrital apatite U-Pb datasets (cf. Mark et al., 2016; O'Sullivan et al., 2016; Zattin et al., 2012). Additionally, apatite can sometimes be too small for geochronological analysis (e.g. in very fine-grained lithologies or interstitial apatite in magmatic rocks); using the LA-Q-ICP-MS apatite U-Pb method employed in this study, for example, a grain size of at least c. 40 μm is required to acquire sufficient counts of U and Pb isotopes for precise dating.

3.1.2.2 Trace-elements in apatite and their use for detrital provenance

In addition to its increasing adoption as a U-Pb chronometer, apatite trace-element geochemistry has also attracted attention in recent years. Research to date has focused primarily on the trace-element composition of apatite from igneous rocks (e.g. Belousova et al., 2001; Hsieh et al., 2008; O'Reilly and Griffin, 2000; Sha & Chappell, 1999; Tang et al., 2012). Consequently, apatite from igneous lithologies (e.g. "S-type" and "I-type" granitoid-derived apatite, basic apatite, and mantle-derived apatite) can be readily distinguished from one another geochemically (e.g. Hsieh et al., 2008). Using LA-ICPMS, useful lithological information can be obtained by the abundances of the REE, the topology of chondrite-normalised REE+Y data; U/Th and Sr/Mn ratios; and the presence and magnitude of Eu and Ce anomalies, amongst others (e.g. Belousova et al., 2001; Hsieh et al., 2008; Sha & Chappell, 1999).

The available data on metamorphic apatite compositions (Bingen et al., 1996; El Korh et al., 2009; Abdullin et al., 2016; Henrichs et al., 2018) suggests that apatite from these rock types is extremely heterogeneous in terms of its trace element geochemistry, and readily distinguishable from igneous apatite. Metamorphic apatite differs from igneous apatite in several ways – it contains lower overall REE-contents, often contains higher Sr-contents, and often presents positive or mildly negative Eu-anomalies in comparison to the large negative Eu/Eu* ratios present in non-ultramafic igneous apatite (Henrichs et al., 2018; El Korh et al., 2009). Whilst high-grade metamorphic and anatectic apatite can be distinguished from lower-grade metamorphic apatite (e.g. Henrichs et al., 2018), detrital metamorphic apatite cannot yet be used to determine the protolith composition of its source (i.e. whether it is basic igneous or pelitic). No element ratios or elemental abundances have yet been found that systematically link metamorphic apatite to its protolith composition, probably due to the similar paragenesis of apatite in metabasites and metapelites, as they likely both grow simultaneously with REE- and actinide rich-epidote (Henrichs et al., 2018).

Although few studies have used apatite trace elements as a provenance tool, those that have successfully distinguished igneous lithologies and metamorphic rocks based on trace-element analysis (Abdullin et al., 2016; Morton & Yaxley, 2007). It should be noted these studies do not combine apatite trace-element analysis with U-Pb dating as in this study.

3.2. DETAILED REGIONAL GEOLOGY & SAMPLING

3.2.1. The Variscan crystalline basement

The Cévennes massif is composed of metasedimentary rocks, chiefly pelites, originally derived from the Rheic margin of Gondwana (Faure et al., 2009). The sediments were metamorphosed during the Variscan orogeny, which has long been recognized as representing the final collision of Laurussia and Gondwana and which formed the supercontinent of Pangaea (e.g. Matte, 1986). The Variscan orogeny in this region is comprised of a series of events ranging from the early Devonian to the early Permian (c. 410-290 Ma), with "hard" collision characterized by southward-propagating ductile shearing (Talbot et al., 2005) occurring at c. 360-350 Ma in the northern part of the Massif Central. In the south, including in the Cévennes, deformation occurred later, at around 330 Ma (Faure et al., 2009). Structurally, the Cévennes massif is considered to be part of the para-autochthonous domain of the Massif Central (e.g. Matte, 1986).

The metasedimentary rocks of the Cévennes are composed of graphitic mica-schists, semi-pelites and minor quartzites that experienced greenschist- to amphibolite-facies peak regional metamorphism at c. 330 Ma (Faure et al., 2009). The protoliths were organic-rich shales and detrital sediments (Faure et al., 2009 and references therein). The metasediments were subsequently intruded by late Carboniferous plutons of monzogranitic-granodioritic composition, during the post-orogenic extensional collapse of the Variscan orogen (Brichau et al., 2008; Chauvet et al., 2012). There are two main batholiths in the Cévennes: the Mont-Lozere and Signaux batholith in the north of the Cévennes (including the source of the river Tarn) and the Aigoual-Saint Guiral-Liron batholith in the south (Figure 2). The country rock underwent local contact metamorphism during batholith emplacement (Faure et al., 2001).

Recent U-Pb zircon and monazite, and $^{40}Ar/^{39}Ar$ muscovite and biotite geochronology studies (e.g. Brichau et al., 2008 and references therein), imply that the Cévennes plutons were emplaced near-synchronously at c. 308-303 Ma. The Cévennes granitoids are broadly contemporaneous with widespread examples of granitoid and migmatite emplacement in the southern Massif Central, which were associated with the onset of Late Variscan orogenic collapse and mantle-underplating (Barbey et al., 2015). Batholiths and migmatite domes of similar age occur in nearby massifs, including the Margeride Complex to the NW; the Rocles pluton and Velay dome to the N; and the

Montagne Noir to the SW of the Cévennes (Brichau et al., 2008 and references therein)(Figure 1).

3.2.2 Mesozoic to recent history

The Grands Causses basin, through which the river Tarn and its tributaries flow after leaving the Cévennes Massif, is a north-south trending, east-dipping half-graben. It formed in the Permian during a second stage of post-Variscan orogenic collapse. The basin fill records a broadly transgressive sequence (e.g. Harazim et al. 2013) that is attributed to subsidence associated with regional post-Variscan extension. The basal basin fill comprises thin, marginal deposits of Permo-Triassic fluvial sandstone and conglomerate channel deposits. These units are overlain by several hundred metres of Jurassic platform carbonates that comprise the vast bulk of the basin fill (e.g. Charlier et al., 2015).

The termination of Mesozoic carbonate deposition in the Cévennes and Grands Causses region is attributed to Cretaceous surface uplift, as evidenced by fossilized Cretaceous karst landscape features on top of the present-day Millau/Grands Causses carbonate plateaus (Séranne et al., 2002). This Cretaceous karst landscape also attests to relatively minor post-Cretaceous denudation of the Grands Causses carbonate plateau. However, the Grands Causses carbonate plateau was locally incised by major surface drainage systems (i.e. the palaeo-Tarn and its tributaries), particularly during the mid-Miocene (e.g. Séranne et al., 2002). These fluvial drainage systems, primarily the river Tarn and its major tributaries, have incised steep-sided gorges (up to 400-500m deep) separated by the expansive flat dry karst plateaus of the Grands Causses. Surface drainage is minimal and extremely confined (e.g. Séranne et al., 2002), while the Grands Causses carbonates likely contribute negligible material to the heavy mineral load of the river Tarn, thus making the area very attractive as a site to study well-defined source areas for detrital heavy mineral provenance analysis.

Lastly, minor Miocene basanitic volcanic pipes, maars and flows locally intrude the Grands Causses carbonates, notably at Eglazines at the bottom of the Gorges du Tarn (sample GOS11/14-08, figure 2). However, none of these exposures is volumetrically significant, and over the whole study area comprise an erupted volume of no more than 2km^3 (Dautria et al., 2010). Ultimately, they represent an insignificant amount of the total exposure in the river Tarn catchment. These juvenile mantle-derived igneous rocks, probably derived from a putative mantle anomaly that dynamically supports the Massif

Central (Dautria et al., 2010 and references therein), are, however, unexpectedly (due to the small volume of erupted material) recorded in the detrital apatite dataset and heavy mineral assemblages (see section 3.5.1).

3.3. MATERIALS & METHODS

3.3.1 River sediment sampling

Eleven detrital samples were collected (Figure 2). The samples were taken from emergent and submerged point-bars and braid-bars along the river Tarn and its tributaries. Samples (c. 2 kg) of raw <1000 μm sand from the river Tarn were first sieved to <250 μm. 200g of the <250 μm fraction was retained from each sample for heavy mineral analysis (HMA, performed upon the 63-125 μm fraction), and the remainder was subsequently processed using standard magnetic and heavy liquid mineral-separation techniques. Apatite from all 11 detrital samples was analysed for trace elements and U-Pb isotopes by LA-ICP-MS.

3.3.1.1 Sampling Strategy

The purpose of the sampling strategy was not to obtain 'pure' single-lithology derived sediment samples to then track downstream. A hypothesis tested in this paper is that the available literature on apatite trace element compositions should make it possible to assign lithology to individual grains without reverting to exact bedrock-matching of grains. This is preferable to direct bedrock matching, as when applying this method to fossil sedimentary systems, the source-rock is necessarily non-extant.

Samples GOS 11/14-02 and -04 come from tributaries or headwaters of the river Tarn whose catchments are almost entirely comprised of metamorphic (11/14-02) and granitic igneous (11/14-04) rocks, respectively. Rutile from these two samples has also been analysed by LA-ICP-MS. In the text below, the sample prefix (GOS 11/14-), which is common to all samples, is omitted.

Sample 13 was taken from a minor tributary of the river Tarn that is sourced from and flows almost exclusively over Jurassic Grands Causses carbonate, with the exception of a minor Cenozoic basanite intrusion in the catchment. This sample is used to test whether the Grands Causses basin contributes significant heavy mineral detritus to the river Tarn's sediment load (Table 1).

The other seven detrital samples were taken from locations downstream of the sediment source areas, after mixing of the three major source components: granitoids,

metamorphic schists, and carbonates (and minor basic extrusives) has occurred. These samples are used to verify whether we can pull apart the different apatite sources in these "mixed" samples, which represent a more typical analogue of fossil clastic sediment than the restricted-catchment detritus captured in samples 2, 4, and 13.

No.	An	At	Ap	Br	Ca	Cp	Cr	Ct	Ep	Gt	Mo	Ol	Op	Ru	Ti	St	To	Zr
2	0	31	18	R	1	1	0	4.5	R	31	R	0	R	1	R	0	11	2.5
4	1	5.5	30	R	29	1.5	0	0.5	2.5	8.5	0.5	0	0	0.5	0.5	0	9.5	12
6	0	16	14	R	7	1.5	0	16	0	27	R	0	R	0.5	R	R	12	7
7	1.5	20	15	R	5	1.5	0	10	2	22	1	0	0	0.5	0	1	11	10
8	R	12	15	R	6	2	0	14	2.5	20	1	0	R	0.5	0	0	17	11
9	R	15	18	R	9	2	0	13	1.5	17	2	0	R	1	R	0	16	6.5
1	1.5	8.5	19	0.5	11	2	0	5.5	1.5	29	2.5	0	0	2	0	0	7	11
10	0	9	16	1	11	2.5	0	8.5	1.5	16	1	0	1.5	2.5	1	0	19	10
13	0	1.5	4.5	0.5	17	45	0.5	0.5	3	7	0.5	1	7	2	0.5	0	6.5	4
11	R	12	14	R	6.5	9.5	0	8	0.5	19	2	0	2	0.5	0.5	0.5	10	16

Table 1. River Tarn heavy mineral abundance data (63 – 125μm fraction - note that the single grain apatite and rutile U-Pb and trace-element analyses were carried out upon a sediment fraction that contained grains up to 250 μm); all totals add to 100%. R = trace. Samples 6 – 11 are listed in order downstream. Samples 2, 4, and 13 are source-tributary samples of Cévennes pelites, Cévennes granitoids, and Grands Causses carbonates respectively. The mineral load of sample 13 mostly reflects input from a small basanite pipe in its carbonate-dominated catchment, illustrating the paucity of clastic detritus in the Grands Causses carbonates. The data acquisition methodology, and information about the proportions of other detrital components, is provided in a supplementary file.

An = Andalusite; At = Anatase; Ap = Apatite; Br = Brookite; Ca = Calcic Amphibole; Cp = Clinopyroxene; Cr = Chrome Spinel; Ct = Chloritoid; Ep = Epidote; Gt = Garnet; Mo = Monazite; Ol = Olivine; Op = Orthopyroxene; Ru = Rutile; St = Staurolite; Ti = Titanite; To = Tourmaline; Zr = Zircon.

3.3.2 Single Grain LA-ICP-MS Analyses

Apatite and rutile were processed by heavy liquid separation into different density classes, such that the 'apatite fraction' contained all heavy minerals of density 2.9-3.29 g/cm^3 and the 'rutile fraction' contained all minerals with density greater than 3.29 g/cm^3. Aliquots of these multi-mineral fractions were mounted in resin, ground to expose grain interiors, and polished. Prior to LA-ICP-MS analysis, a Zeiss AxioImager Z1m microscope equipped with an Autoscan automated stage was used to systematically identify the spatial positions of apatite and rutile grains amongst the other heavy mineral detritus, with the aim of reducing operator grain-size bias during grain selection. All U-Pb data were acquired using a Photon Machines Analyte Exite 193 nm ArF Excimer laser-ablation system with a Helex 2-volume ablation cell, coupled to a Thermo Scientific iCAP Qc at Trinity College Dublin. 0.65 l/min He carrier gas was split evenly between the large outer sample chamber and the small inner volume (the 'cup') where ablation occurs. A small volume of N_2 (ca. 6 ml/min) to enhance signal sensitivity and reduce oxide formation and 0.7 l/min Ar nebulizer gas was then introduced to the sample-gas mixture via an in-house smoothing device. ^{202}Hg, ^{204,206,207,208}Pb, ^{232}Th and ^{238}U were acquired for all U-Pb analyses. The ^{43}Ca and ^{48}Ti abundances were utilised for internal standardisation of element concentrations for apatite and rutile, respectively. All apatite and rutile analyses were acquired using 60μm laser spot, a 5 Hz laser repetition rate and a fluence of 3.9 J/cm^2.

For both apatite and rutile, conventional standard-sample bracketing utilising matrix-matched natural apatite and rutile standards, corrects for downhole isotopic fractionation, elemental mass bias, and intra-session analytical drift. For apatite analyses, the Madagascar natural mineral standard (Thomson et al. 2012; weighted average ID-TIMS concordia age of this crystal of 473.5 ± 0.7 Ma for an in-house aliquot) is used as the sole primary reference material; and the McClure Mountain apatite (weighted mean ^{207}Pb/^{235}U age of 523.51 ± 2.09 Ma, Schoene & Bowring 2006: this study, Tera-Wasserburg (TW) lower-intercept age of 517.5 ± 4.8 Ma; MSWD = 4.2; n = 90) and Durango apatite (31.44 ± 0.18 Ma, McDowell et al. 2005: this study, TW lower-intercept age of 31.59 ± 0.36 Ma; MSWD = 1.15; n = 172) are used as secondary standards and processed as unknowns, both to verify the accuracy of the method in each session and to approximate the behaviour of the unknowns. For rutile analyses, R10 rutile (U–Pb TIMS age of c. 1090 Ma, Luvizotto et al. 2009a) is used as the primary standard while R19b

rutile (weighted mean TIMS $^{206}Pb/^{238}U$ age of 489.5 ± 0.9 Ma, Zack et al. 2011: this study, 493.5 ± 2.8 Ma; MSWD = 2.4; n = 25) is used as the secondary standard.

The raw isotope data were reduced using the "VizualAge_UcomPbine" data reduction scheme of Chew et al. (2014) which can account for the presence of variable common-Pb in the primary age standards, within the freeware IOLITE package of Paton et al. (2011). Common Pb in the apatite and rutile primary and secondary standards was corrected for using a ^{207}Pb-based correction method using an initial $^{207}Pb/^{206}Pb$ ratio derived from the terrestrial Pb isotope evolution model of Stacey and Kramers (1975). Variable common-Pb content in the unknowns was also corrected for using an offline ^{207}Pb-based correction. This correction employed an initial starting estimate for the common-Pb composition derived from the Stacey and Kramers (1975) model to generate an initial estimate for the age of each rutile, followed by an iterative calculation (Chew et al., 2011). The Stacey and Kramers (1975) Pb-evolution model is used as the starting guess for the Pb-composition of the unknowns as it is not possible to analyse common-Pb bearing minerals in detritus which are unequivocally co-genetic (apart from composite clasts in micro-conglomerates). Additionally, the pairing of point-sourced Pb-isotope data with diffusively-sourced detritus would introduce sampling bias. A detailed explanation of the method used to date these grains is given by Chew et al., (2011; 2014).

Using a ^{207}Pb-correction means it is not possible to exclude U-Pb age data based on discordance. Therefore, for unknown grains yielding Mesozoic or older ages, ^{207}Pb-corrected age uncertainties either >25% or >100 Ma at the 2σ level were thus excluded from single-grain age-plots (though not from Tera Wasserburg). This approach is ultimately arbitrary, but is similar to previously published approaches used in Zattin et al. (2012), Mark et al. (2016) and O'Sullivan et al. (2016). This method is unsatisfactory for very young grains, however, as a given fixed age uncertainty as a percentage of the total age approaches infinity as the age of grains approaches 0 Ma. Therefore, a cutoff of +/-20 Ma was applied as the maximum allowable age uncertainty for grains with Cenozoic ^{207}Pb-corrected ages. The median U-content of grains that passed the inclusion criteria (of any age) was 17.6 ppm, whilst for excluded grains it was 0.4 ppm. For clarity, in the data repository apatite and rutile U-Pb data are presented in separate tables of grains that failed these criteria, and grains that passed these inclusion criteria. Comparison of filtered and unfiltered U-Pb age data is presented on kernel density plot (KDP) in a supplementary file, though the results are not very different as the vast majority of metamorphic grains have f_{206} values of 1 or close to 1 (i.e. the proportion of Pb_c is close

to, or is 100%), and thus cannot be meaningfully plotted on a histogram, KDP, or probability density plot (PDP). KDP and PDP were made using 'density plotter' (Vermeesch, 2004).

3.4. RESULTS

All apatite unknowns from this study has been plotted with apatite from bedrock samples of diverse composition from the literature on a principal component analysis (PCA) biplot (figure 3), using the 'Provenance' package for 'R' (Vermeesch et al., 2016). Rutile has only been analysed in the Cévennes source samples (02 and 04) to provide an alternative medium-temperature thermometer to compare with the apatite U-Pb age-distributions.

3.4.1.1 Metamorphic source sample – GOS 11/14-02

Apatite is abundant in sample -02, comprising 18% of the heavy mineral load in the 63-125 um fraction (Table 1). In this sample the vast majority of analysed apatite is compositionally similar to *in-situ* metamorphic apatite analyses from the literature (e.g. Henrichs et al., 2018; El Korh et al., 2009) on a PCA biplot (figure 3a. Two broad metamorphic apatite populations can be distinguished in this sample on a spidergram (populations metamorphic 1 and metamorphic 2 on figure 4). No grains with metamorphic compositions yield reliable single-grain ages in this sample, as the U-contents of these grains vary between 0-3 ppm and the proportion of Pb_c is high. Imprecise U-Pb age information may be extracted from the metamorphic population when plotted on Tera Wasserburg concordia (e.g. figure 5a).

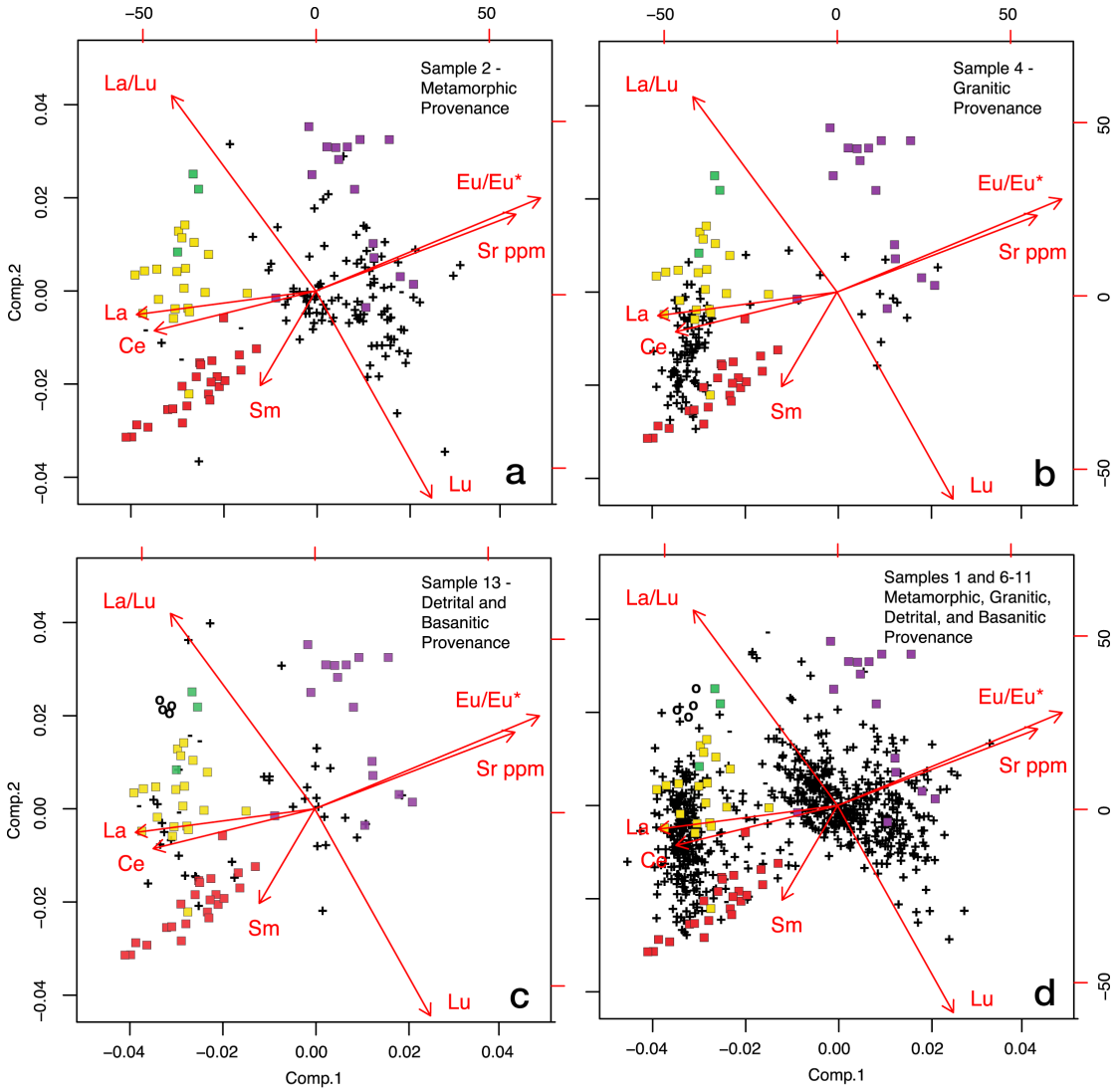
Sample 2 - Metamorphic Provenance
Sample 4 - Granitic Provenance
Sample 13 - Detrital and Basanitic Provenance
Samples 1 and 6-11 Metamorphic, Granitic, Detrital, and Basanitic Provenance
La/Lu
Eu/Eu*
Sr ppm
La
Ce
Sm
Lu
a
b
c
d
Comp.1
Comp.2
S-type/high ASI granitoids (Belousova et al., 2001; Chu et al., 2009; Hsieh et al., 2008; Sha & Chappel, 1999)
I-type/low ASI granitoids (Belousova et al., 2001; Chu et al., 2009; Hsieh et al., 2008; Sha & Chappel, 1999)
Basic Igneous rocks (Belousova et al., 2001; Tang et al., 2012)
Metamorphic rocks (El Korh et al., 2009; Henrichs et al., 2018)
+ Detrital apatite from the river Tarn
- Detrital apatite from the river Tarn with refractory ages (> 400 Ma)
o Detrital apatite from the river Tarn with Miocene ages

Figure 3: PCA biplot of multi-element data from Tarn samples compared to published bedrock apatite data from the literature (Belousova et al., 2001; Henrichs et al., 2018; Hsieh et al., 2008; El Korh et al, 2009; Sha and Chapell, 1999; Tang et al., 2012). The vectors on the PCA biplot were chosen according to known ratios in apatite. High Sr-contents, flat or positive Eu-anomalies, and low REE-contents are characteristic features of metamorphic apatite (e.g. Broska et al., 2004; Henrichs et al., 2018) - metamorphic apatite is hence "pulled" towards the Sr and Eu/Eu* vectors on a PCA biplot, and "repelled" by the REE-vectors. Basic apatite is typically LREE-enriched and HREE-deficient, as apatite reflects the whole-rock LREE budget due to the lack of other LREE-hosts in basic igneous melts (e.g. Tang et al., 2012) and is hence "pulled" towards the La/Lu vector. S-type granite apatite typically displays flat REE-patterns (e.g. Sha and Chapell, 1999), probably due to the high ASI-indices in these lithologies permitting the growth of LREE-bearing primary monazite (e.g. Hsieh et al., 2008), along with very negative Eu-anomalies and very low Sr-contents (e.g. Hsieh et al., 2008) – these features "push" S-type apatite away from the La/Lu, Sr and Eu/Eu* vectors, and towards the Sm (MREE) and Lu (HREE) vectors. Other categories display intermediate characteristics.

Of 110 analysed grains, only four (or 3.6%), which yield trace-element compositions characteristic of granitoid apatite from the literature (figure 3), pass the U-Pb inclusion criteria. All of these grains yield ages that are older than 380 Ma, much older than Variscan orogenesis at 330 Ma (Faure et al., 2009), or of the Cévennes plutons (c. 305 Ma; e.g. Brichau et al., 2008), which are the major source of the detritus present in sample 04.

Detrital rutile in sample 02 provides more useful age information than apatite, though the proportion of rutile detritus is far lower (table 1), which means that only 77 grains could be found for analysis. The proportion of rutile grains passing the inclusion criteria is quite low at 22/77 total grains (29%), as like apatite, the rutile U-content is low in this sample with a median of 1 ppm. Dateable rutile mostly records peak-Variscan metamorphism in this sample (figure 6), with some older refractory ages.

3.4.1.2 Igneous source sample – GOS 11/14-04

Apatite is very abundant in this sample, comprising 29% of the total heavy mineral load in the 63-125 um fraction (Table 1). In sample 04 the bulk of grains have trace-element compositions that overlap with *in-situ* granitoid analyses from the literature, plotting intermediate between I- and S-type granite end-member compositions (figure 3b). The trace-element composition of the Variscan-age granitic apatite grains implies derivation from a melt that has experienced moderate crustal contamination (e.g. slightly HREE deficient, Mn ppm > Sr ppm, Hsieh et al., 2008), and matches closely with granitoids from the Fuzhou-Zhangzhou Complex (FZC) in southeastern China of monzogranitic composition (figure 4A: Zudi pluton; Hsieh et al., 2008). This is in agreement with the documented monzogranitic to granodioritic composition of the Cévennes batholiths (e.g. Brichau et al., 2008; Sabourdy, 1975). However, as the Cévennes plutons are almost identical in age and composition to one another (Brichau et al., 2008), it cannot be determined from which pluton individual apatite grains were derived.

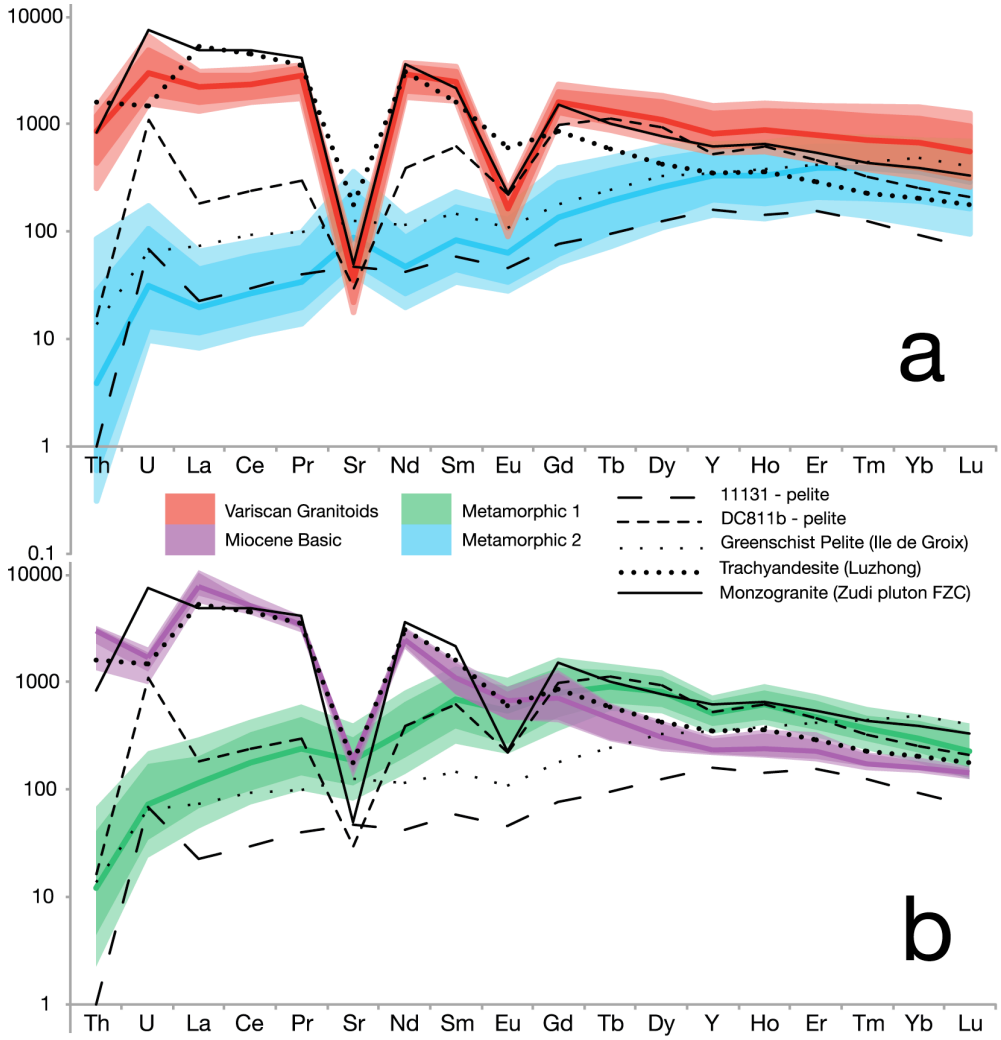

Figure 4. Chondrite (CI) normalised trace element plots of apatite populations from the river Tarn detritus (all samples combined). Shading corresponds to the median (line), 30th - 70th percentiles (dark), and 10th – 90th percentiles of the data (light). 11/13/1 and DC811b = Dalradian amphibolite facies pelites (Henrichs et al., 2018); Ile de Groix = greenschist-facies micaschist (El Korh et al., 2009); Zudi pluton, FZC = monzogranite pluton from the Fuzhou complex in southeastern China (Hsish et al., 2008); Luzhong volcanics = trachyandesitic apatite from the Luzhong basin, southern China (Tang et al. 2012). Miocene basic = detrital grains with broadly Neogene ages; Variscan granitoids = grains with ages corresponding to Cévennes plutons; Metamorphic 1 = mostly undateable grains derived from the Cévennes metapelites, with higher middle-REE contents; Metamorphic 2 = mostly undateable grains derived from the Cévennes metapelites with low middle-REE contents. A figure is provided in the supplementary files demonstrating the difference between these two metamorphic detrital populations (figure S3.1).

102 of 117 apatite grains (87%) in this sample passed the age inclusion criteria. As the bulk of the grains in this sample are near-identical in terms of age and trace-element composition they are plotted on Tera-Wasserburg concordia in figure 5d, yielding an age of 304.3 ± 4 Ma, and on a KDP in figure 7, with a single age peak at 306 ± 1.9 Ma, which agrees with *in-situ* bedrock ages of c. 305 Ma for the Cévennes granitoids based on $^{40}Ar/^{39}Ar$ white mica and biotite, and U-Pb zircon and monazite geochronology (e.g. Brichau, 2008). Several grains of metamorphic-affinity are present in this sample (figure 3); compositionally these are indistinguishable from metamorphic grains present in sample -02 and again provide no useful U-Pb age information.

Rutile in this sample is, in common with apatite, more amenable to dating than sample 02, and 65 of 80 (81%) grains passed the age inclusion criteria. Again, in common with detritus in sample 02, rutile is scarce in this sample at 1% of the sediment load, and only 80 grains were found for analysis. Rutile in this sample is far less refractory than in sample 02 with only 2 or 3 grains predating Variscan orogenesis, and there are grains that overlap in age with Cévennes pluton emplacement at 305 Ma, which again is a difference from sample 02. However, the paucity of dateable detrital rutile in sample 02 means that definitive conclusions should not be drawn if comparing the relative distribution of rutile U-Pb age peaks in samples 02 and 04 as the U-Pb age data in sample 02 is based upon few analyses.

3.4.1.3 Carbonate source sample – GOS 11/14-13

Apatite is exceptionally scarce in this sample which is dominated by carbonate and opaque minerals (supplementary table S1). Heavy minerals comprise only 1% of the non-framework sediment load, mostly pyroxene (table 1), reflecting the presence of a small basanitic pipe in the catchment (figure 2). Only 4.5% of the much-reduced heavy mineral budget is apatite, as a result only 45 grains were found for LA-ICP-MS analysis in a sample several kilograms in weight. These results demonstrate a paucity, though not *complete* absence, of heavy mineral detritus in the Grands Causses carbonates. Still, there is *significantly* less heavy mineral detritus compared to the basement-sampling streams in the Cévennes Mountains.

The 45 analysed grains are heterogeneous by age and composition. There are 15 grains that have trace-element characteristics and ages that match the Cévennes granitoid grains in sample -04 (figure 7b), and there are 19 grains that have trace-element profiles that match the metamorphic grains in sample -02 (figure 3b), and again provide no useful

age data. There are four grains that present Miocene-recent ages and have trace-element profiles that are similar to apatite from *in-situ* bedrock analyses of basic rocks from the literature (e.g. Tang et al., 2012; Hsieh et al., 2008; O'Reilly and Griffin, 2000) on PCA (figure 3c). They exhibit LREE-enrichment, minor negative Eu-anomalies, moderate U-contents (c. 13.5 ppm vs c. 24 ppm of Variscan granitic grains), and high Sr contents (c.1100 ppm vs c. 210 ppm for Variscan granitic grains). These are likely derived from the same source as the pyroxene detected by heavy mineral analysis in this sample (table 1). Lastly, there are several apatite grains (seven) with ages and/or compositions that do not match the ages or compositions of the local basement.

3.4.1.4 Downstream mixed samples: -06; -07; -08; -09; -01; -10; -11

Apatite is abundant in the detritus downstream of the main clastic sediment sources, comprising between 14% and 19% of the heavy mineral load (63-125 um) in any given sample (Table 1). On a PCA biplot these samples show mixed populations of grains of mostly granitic and metamorphic composition (figure 3d). The downstream samples are essentially indistinguishable from one-another, whether by age or trace element composition, and the dateable igneous grains almost all cluster around the age of pluton emplacement (305 Ma, figure 7c, 7d). Also present within these seven samples are four more basic grains with Miocene-recent ages – identical in all respects to the four Miocene basic grains in the carbonate source sample.

In these downstream samples there are grains present that date peak-Variscan collisional orogenesis and metamorphism at c. 330 Ma (the age of the Cévennes metapelites), unlike the metamorphic source sample (-02). Of this population, a tiny proportion (7/960 of the total analysed apatite grains in this study) is comprised of grains with metamorphic apatite trace-element compositions that match the composition of the pelite grains from the metamorphic source sample (e.g. low Y+REE content, low Th:U ratios, high Sr:Mn ratios), but that contain U in higher concentrations which makes dating possible. These grains are treated as a single population on Tera-Wasserburg concordia in figure 5b, yielding a lower intercept age of 333 ± 13 Ma). However, the majority of grains with peak-Variscan metamorphic ages yield igneous trace element profiles similar to the "Tarn granitoids" (figure 4A), despite recording a Barrovian metamorphic event with no associated plutonic activity (figure 5c, 5d). Lastly, there are older grains that vary greatly in terms of both their age (c. 360 – 1500 Ma) and their trace element compositions. These grains range from both typical S- and I-type granitoid compositions,

through to grains with basic igneous trace element signatures, and include grains of unambiguous metamorphic origin. This variation in composition and age (they are older than any local basement lithologies) implies a recycled origin for these grains.

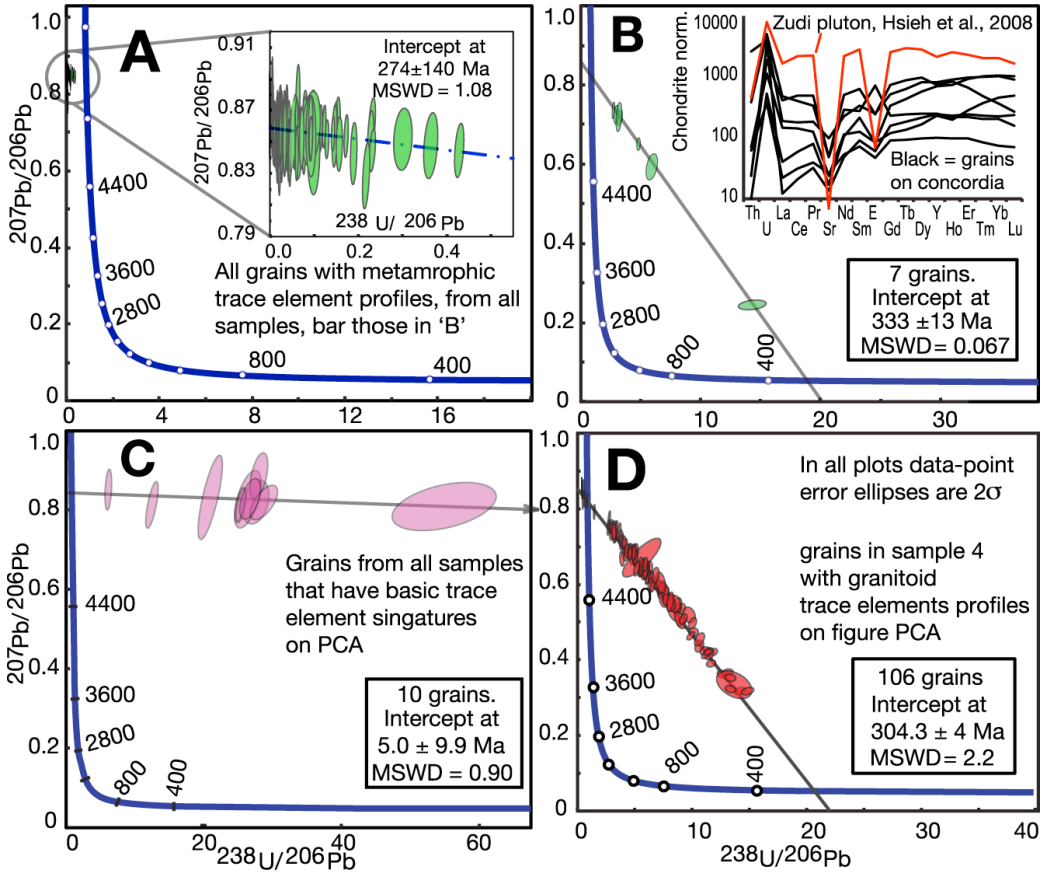

Figure 5: Tera Wasserburg concordias of river Tarn detrital apatite. A) Grains with metamorphic trace element profiles from the metamorphic source sample 02 which failed the inclusion criteria described in section 3.3.2.1 (cf figure 4, "metamorphic 1 + 2"); The Tera Wasserburg concordia lower-intercept age is highly imprecise but consistent with a Variscan origin. B) Metamorphic grains from several samples that passed the "inclusion criteria", the upper intercept is anchored to a $^{207}Pb/^{206}Pb$ ratio of 0.856 which is the median Pb-composition of Cévennes metamorphic grains with $f_{206} = 1$ in metamorphic source sample 02. C) Basic igneous grains from several samples (cf figure 4 – "Miocene basics"), implicating Miocene-recent intraplate volcanism (e.g. Dautria et al., 2010). D) Granitic grains from granitic source sample 04 (cf figure 4, Variscan granitoids), the lower intercept at c. 304 Ma is defined by grains with igneous trace element profiles, and clearly defines an age in agreement with previous *in situ* bedrock zircon and white mica ages from the Cévennes granitoids (e.g. Brichau et al., 2008 and references therein). Note the changes of scale on the x-axis.

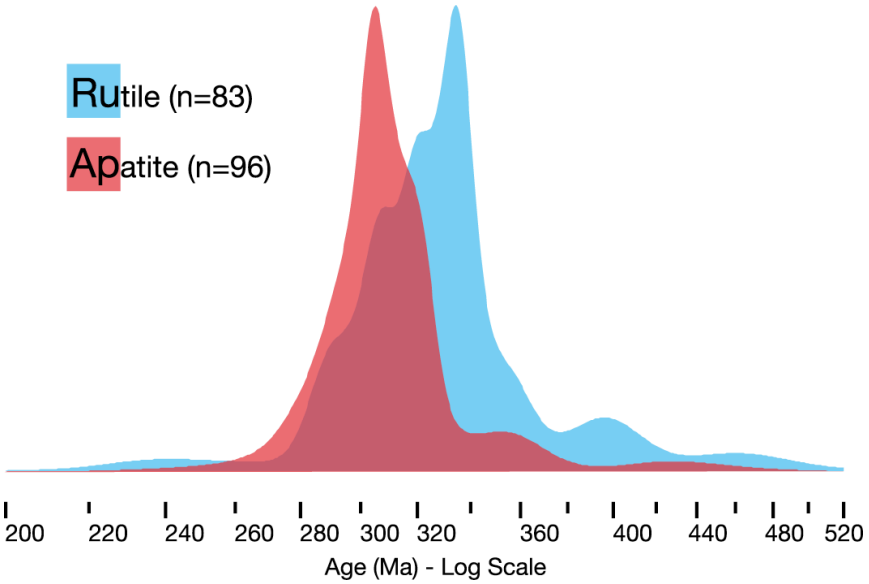

Figure 6: Comparison of detrital apatite and rutile from samples 02 and 04 (the only samples from which detrital rutile was analysed). The rutile mostly records collisional regional metamorphism at c. 335 Ma, in these samples apatite mostly records extension-related plutonism at c. 305 Ma.

3.5. DISCUSSION

3.5.1 Apatite trace-element and U-Pb systematics

The results of this study demonstrate the utility of integrated apatite geochronology and geochemistry in provenance analysis. It is readily possible to distinguish apatite from felsic-igneous, basic-igneous and metapelitic sources based on their trace-element compositions (e.g. the metamorphic, basic, and felsic populations; Figure 3), their U-Pb ages (e.g. the late Variscan granitoid grains and the Miocene basic grains; Figure 5, Figure 7), or both, depending on the source-rock lithology and its amenability to U-Pb dating. The trace-element and U-Pb age data can be collected simultaneously by LA-ICPMS during the same analytical session using a rapid (and hence cost-effective, at c. 25-30 s per grain) analytical protocol. The range of source-rock information that can be gathered using the combination of apatite trace-element and U-Pb analysis is wide due to the near-ubiquity of apatite in crystalline source-lithologies. Consequently, there is an opportunity to deploy this tool to assess both the age and source-lithology of apatite grains in fossil detritus.

However, some drawbacks on the applicability of the apatite detrital chronometer are highlighted by this study. The first is that the detrital apatite U-Pb method is not as precise as some other detrital chronometers, in particular the zircon U-Pb system. This means that the detrital apatite U-Pb method as employed in this study will generally be useful for higher-order conclusions only. Whilst this is a drawback, it must be remembered that the range of lithologies and thermal conditions in which apatite regularly *crystallises*, including low-grade metamorphic rocks and basic-ultrabasic rocks, still probably exceeds that for any other mineral used for detrital chronometry – imprecise age determinations are more useful than no age determinations, and often first-order information is sufficient to discriminate between distinct sediment sources.

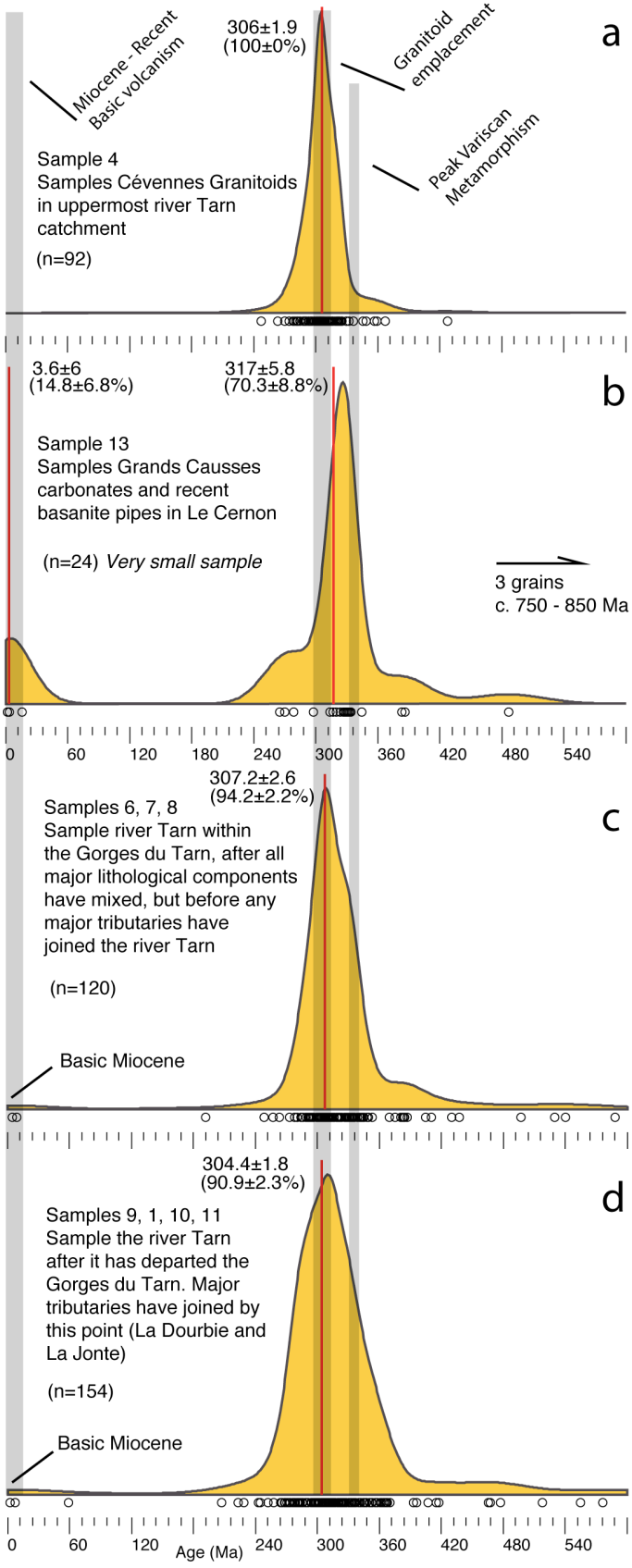
a
306±1.9
(100±0%)
Miocene - Recent
Basic volcanism
Granitoid
emplacement
Peak Variscan
Metamorphism
Sample 4
Samples Cévennes Granitoids
in uppermost river Tarn
catchment
(n=92)
b
3.6±6
(14.8±6.8%)
317±5.8
(70.3±8.8%)
Sample 13
Samples Grands Causses
carbonates and recent
basanite pipes in Le Cernon
(n=24) Very small sample
3 grains
c. 750 - 850 Ma
0
60
120
180
240
300
360
420
480
540
c
307.2±2.6
(94.2±2.2%)
Samples 6, 7, 8
Sample river Tarn within
the Gorges du Tarn, after all
major lithological components
have mixed, but before any
major tributaries have
joined the river Tarn
(n=120)
Basic Miocene
d
304.4±1.8
(90.9±2.3%)
Samples 9, 1, 10, 11
Sample the river Tarn
after it has departed the
Gorges du Tarn. Major
tributaries have joined by
this point (La Dourbie and
La Jonte)
(n=154)
Basic Miocene
0
60
120
240
300
360
420
480
540
Age (Ma)

Figure 7: ^{207}Pb corrected U-Pb age kernel density plots of Tarn detrital samples, which fulfilled the inclusion criteria laid out in section 3.3.3.1. Sample 2 cannot be plotted as only four single-grain ages passed the inclusion criteria. Sample 4 (5a) is the granitic source sample, and sample 13 (5b) is from the carbonate source sample. 305 Ma igneous activity is the dominant signal in the Tarn detritus (e.g. 5c, 5d). The plots were constructed using DensityPlotter (Vermeesch, 2012)

A second issue, however, is that this study demonstrates how certain lithologies are highly challenging to date using the detrital apatite U-Pb method. It should be noted that methods that permit the dating of low-U, high Pb_c phases in bedrock samples, such as fitting a Tera-Wasserburg concordia intercept through multiple datapoints or anchoring the Pb_c-composition by analyzing cogenetic Pb-bearing phases, are not typically possible in detrital samples. Hence neocrystalline apatite in the Cévennes greenschist-to-amphibolite-facies metapelites is not possible to date by the apatite U-Pb method, whereas the Cévennes granitoids may be readily
dated. The amenability of these two source populations to LA-ICPMS U-Pb dating is clearly linked to the substantial difference in U contents between these two discrete basement sources (c. 0-3 ppm U in the apatite derived from the metapelites versus an average of 24 ppm U in the granitic apatite detritus), and not to differences in mineral fertility between the sources.

Though apatite from igneous rocks typically contains sufficient U for U-Pb age determinations (typically 10-80 ppm, e.g. Belousova, 2001; Nutman, 2007; Hsieh et al., 2008; Tang et al., 2015; this study), with exceptions (cf. Lianjing pluton, 1.3 ppm U average, Hsieh et al., 2008), apatite from metamorphic rocks is often U-deficient and Pb_c-enriched (e.g. Henrichs et al., 2018). However, it should be noted that this is likely a problem that chiefly affects low- to medium-grade metamorphic terranes dominated by pelitic and basic protoliths. In contrast apatite detritus derived from medium-to-high grade metamorphic terranes with diverse protolith types is amenable to U-Pb dating (e.g. the Appalachians, O'Sullivan et al., 2016; the western Alps pro-foreland; Mark et al, 2016), while apatite crystallized from pelitic metamorphic complexes that have experienced anatexis also yields high U contents (e.g. Nutman, 2007; Henrichs et al., 2018).

3.5.1.1 Basic apatite

It is interesting that basic apatite grains can be detected in this study given the very limited areal extent of basic sources in the study area (figures 3, 4, 5, 7). These grains are identified based on both their age and trace-element composition, and are almost certainly derived from inextensive mantle-derived basanitic pipes, which locally crop out in the Grand Causses basin and are identified elsewhere across the Massif Central (e.g. Dautria et al., 2010). That this lithology with minimal exposure is picked-up by the apatite U-Pb and trace-element systems using standard sample sizes (c. 85-200 grains e.g.

Vermeesch, 2004) is highly encouraging, as there are few common detrital chronometers which are as fertile as apatite in basic rocks (e.g. Spear & Pyle, 2002). The apatite U-Pb and trace-element method may therefore be useful as a detector of basic magmatism in sediment sources.

3.5.2 Utilising apatite trace element compositions, is it possible to determine single-grain provenance without bedrock sampling?

As discussed in section 3.1.2.2 and displayed on a PCA biplot in figure 3, the literature available on apatite compositions covers all the most commonly found lithologies in the crust, with 59 separate bedrock samples displayed in figure 3. The PCA biplot and spidergrams presented in this paper shows that apatite compositions provide very clear separation of different detrital apatite populations (e.g. figure 3, figure 4). Importantly, the vectors on the PCA biplots provide separation that is both logically- and geologically-consistent (explanation on figure 3) and are thus not an abuse of statistical provenance methods (cf Vermeesch et al., 2016). The addition of age-information also makes these plots even more meaningful. It permits identification of multi-cyclic (recycled) grains (i.e. those grains older than the oldest bedrock known in the region), and sub-populations of grains derived from similar lithologies but with vastly different age (e.g. the difference between Miocene and Eo-Variscan basic apatite grains), to further deconvolute the provenance signal.

3.5.3 Apatite recycling and refractory apatite

To what extent detrital apatite can be recycled during successive weathering and transportation cycles is not quantified by this study. Apatite is very unstable during transport-limited weathering at source, so the potential for extensive apatite recycling is likely more limited than that of minerals that are chemically unreactive during Earth-surface or near Earth-surface sedimentary processes (e.g. the zircon-tourmaline-rutile [ZTR] mineral suite; Morton and Hallsworth, 1999, and references therein). However, there are indications from the U-Pb age data (e.g. figures 5, 7) that a small amount of recycled/refractory apatite is present in the detrital samples as there are grains present in the dataset that are older than the local basement source rocks.

Unequivocally refractory and recycled grains yield pre-Variscan (330 Ma) U-Pb ages and exhibit diverse trace element profiles. As refractory grains are found topographically and hydrographically above any Permian sedimentary units (figure 2,

sample 2), the grains are likely sourced from the Cévennes metapelites, and thus represent detrital apatite hosted within these units.

Refractory apatite is a small proportion of the total analysed; there are only 25 out of 915 analysed grains with ages >400 Ma in the trunk river Tarn samples. It has previously been demonstrated that detrital apatite cannot easily survive in metapelites above upper-greenschist facies conditions (e.g. Nutman, 2007; Henrichs et al., 2018). This study therefore shows that in low- to medium-grade metapelites, apatite is predominantly neocrystalline and hence will record information on the lithological composition of its host rock, though clearly some refractory grains can survive.

Another low-abundance population in the dataset, with igneous trace element profiles but recording peak-metamorphic ages (c. 330 Ma), is found in the downstream samples only (i.e. 6-11). These may represent either peak-broadening around the 305 Ma igneous peak (figure 7), or perhaps detritus reworked into the Cévennes pelites. In the latter case, such grains would likely represent detrital apatite which has experienced upper-greenschist facies metamorphism - a relatively restricted temperature window where the apatite was cold enough to have escaped pervasive metamorphic recrystallization and thus preserve its earlier protolith trace-element signature, yet sufficiently hot enough to have been age-reset by volume diffusion of Pb.

3.5.4 Implications for Massif Central tectonics

Due to the configuration of the lithologies in its catchment, the river Tarn is a useful testbed drainage area in which to test the combined apatite trace element/U-Pb method. That the regional geology is already well understood and well constrained by geochronology is key in this proof-of-concept study for demonstrating the veracity of our results. Consequently, the aim of this detrital study was not to unearth cryptic orogenic events or previously undocumented deformation phases, nor was any evidence of such activity found in the detrital U-Pb dataset. Our results are in accordance with previous studies of the regional geology.

The major age-peak in the source-proximal detrital apatite U-Pb dataset at c. 305 Ma (figure 5d, 6, 7) overlaps with the 303-308 Ma age for the Cévennes plutons determined by Brichau et al. (2008) using bedrock zircon U-Pb and biotite ^{40}Ar-^{39}Ar dating. That the apatite U-Pb, biotite $^{40}Ar/^{39}Ar$ and zircon U-Pb ages are coeval indicates that cooling of the Cévennes batholiths was swift (~ 1 - 2 Ma). This implies either rapid

post-emplacement exhumation and/or shallow (likely < 5 km) pluton emplacement depths, in agreement with earlier studies (e.g. Najoui et al., 2000; Brichau et al., 2008).

3.5.5 Comparison of source-sample detrital rutile and apatite U-Pb

Detrital rutile from the source-proximal samples dominantly records regional metamorphism at 330 Ma, and to a lesser extent pluton emplacement at c. 305 Ma. This is in marked contrast with the detrital apatite U-Pb data, which is weighted towards the c. 305 Ma pluton emplacement due to the low U-contents of neocrystalline or recrystallized metapelitic apatite observed in the source area metapelites and are therefore complimentary (figure 6).

There are also several detrital rutile grains present in the igneous source sample (04) with Mesozoic ages, corresponding approximately to the age of magmatism in NE Iberia and southernmost France (e.g. Ubide et al., 2014), and the Eo-Alpine orogen as reported from the western Alps (Carrapa et al., 2004). The origin of these anomalously-young grains on a topographically-isolated, tectonically-quiescent Variscan massif is unknown, but because they correspond to mineral cooling and crystallisation ages reported from nearby orogenic and magmatic belts, and the modal proportion of rutile in these samples is very low and therefore more easily overwhelmed by exotic sources (0.5 – 1.0 % of the HM load in samples 02 and 04; Table 1), a windblown origin cannot be excluded for these grains.

The disparity in age information obtained from apatite and rutile, two medium-temperature chronometers, is not due to apatite infertility in the Cévennes pelites. The results of our trace element analysis show that a majority of apatite grains in the river Tarn are metamorphic, and the HMA shows that 18% of the heavy minerals in the 63-125 um fraction in sample 02 are apatite (table 1). Instead, this disparity is a consequence of i) the failure of the apatite U-Pb system to reliably date metamorphic grains in this source region due to low U and/or high Pb_c/Pb^* contents, and ii) probable rutile infertility in the Cévennes plutons as rutile is not a common phase in granitoids. Because of these differences, the detrital rutile and apatite U-Pb records of the Variscan in the Cévennes source-samples differ and are therefore complimentary (figure 6), together providing a more complete view of Variscan orogenesis in this area than either does alone. Due to the low U-contents of pelitic apatite, rutile may prove a more useful recorder of orogenesis in low- to medium-grade metasedimentary terranes. By contrast, due to the scarcity of rutile in igneous lithologies, apatite is likely to be a much more useful recorder of basic or

felsic magmatism, whether recording primary igneous activity or thermal resetting of those lithologies due to metamorphic overprinting. It is thus recommended that where possible rutile be analysed alongside apatite, as it typically yields complementary provenance information in metamorphic belts (cf. O'Sullivan et al., 2016).

3.6. CONCLUSIONS

This study demonstrates the effectiveness of combined geochronology and geochemical analysis of detrital apatite, as this integrated approach is successful in determining the source rock composition, or age (or both) of almost every individual grain analysed. While integrated apatite geochronology and multiple trace-element geochemistry has yet to be applied in detail to provenance studies of clastic sedimentary rocks in the geological record, the results of this modern detrital case study clearly demonstrate that detrital apatite derived from the Massif Central reliably retains high-resolution source-rock provenance information. This includes information from almost all basement lithologies, whether sedimentary, metamorphic, plutonic or extrusive. The results also demonstrate that apatite has been generated during every tectonic regime that the source region has experienced, be it collisional (Variscan peak metamorphism), extensional (late Variscan extensional collapse and plutonism) or intraplate (plume-related Miocene basaltic volcanism), making apatite a versatile recorder of lithology; and in time, the ever increasing body of published apatite trace element compositions will permit even more specific apatite provenance determination.

3.6.1 Acknowledgements and Funding

This material is based upon works supported by Science Foundation Ireland under Grant Number 12/IP/1663. We would also like to thank Cora McKenna for her assistance during LA-ICP-MS data acquisition.

Supporting Information

While also included at the end of this chapter, the U-Pb and trace element data, sample locations and heavy mineral analysis methods may also be found at: https://doi.org/10.1594/PANGAEA.883191

3.7. REFERENCES

Abdullin, F., Solé, J., Solari, L., Shchepetilnikova, V., Meneses-Rocha, J.J., Pavlinova, N., Rodríguez-Trejo, A., 2016. Single-grain apatite geochemistry of Permian–Triassic granitoids and Mesozoic and Eocene sandstones from Chiapas, southeast Mexico: implications for sediment provenance. Int. Geol. Rev. 58, 1132–1157. doi:10.1080/00206814.2016.1150212

Barbey, P., Villaros, A., Marignac, C., Montel, J.-M., 2015. Multiphase melting , magma emplacement and P-T-time path in late-collisional context : the Velay example (Massif Central , France) 93–115.

Belousova, E. A., Walters, S., Griffin, W.L., O'Reilly, S.Y., 2001. Trace-element signatures of apatites in granitoids from the Mt Isa Inlier, Northwestern Queensland. Aust. J. Earth Sci. 48, 603–619. doi:10.1046/j.1440-0952.2001.00879.x

Bingen, B., Demaiffe, D., Hertogen, J., 1996. Redistribution of rare earth elements, thorium, and uranium over accessory minerals in the course of amphibolite to granulite facies metamorphism: The role of apatite and monazite in orthogneisses from southwestern Norway. Geochim. Cosmochim. Acta 60, 1341–1354. doi:10.1016/0016-7037(96)00006-3

Brichau, S., Respaut, J.P., Monié, P., 2008. New age constraints on emplacement of the Cévenol granitoids, South French Massif Central. Int. J. Earth Sci. 97, 725–738. doi:10.1007/s00531-007-0187-x

Carrapa, B., Wijbrans, J. and Bertotti, G., 2004. Detecting provenance variations and cooling patterns within the western Alpine orogen through 40Ar/39Ar geochronology on detrital sediments: The Tertiary Piedmont Basin, northwest Italy. Geological Society of America Special Papers, 378, pp.67-103. Doi: 10.1002/2013TC003511

Carrapa, B., DeCelles, P.G., Reiners, P.W., Gehrels, G.E., Sudo, M., 2009. Apatite triple dating and white mica $^{40}Ar/^{39}Ar$ thermochronology of syntectonic detritus in the Central Andes: A multiphase tectonothermal history. Geology 37, 407–410. doi:10.1130/G25698A.1

Carter, A., 1999. Present status and future avenues of source region discrimination and characterization using fission track analysis: Sedimentary Geology, v. 124, p. 31–45, doi:

10.1016/S0037-0738(98)00119-5.

Charlier, J.B., Moussa, R., Bailly-Comte, V., Danneville, L., Desprats, J.F., Ladouche, B., Marchandise, A., 2015. Use of a flood-routing model to assess lateral flows in a karstic stream: implications to the hydrogeological functioning of the Grands Causses area (Tarn River, Southern France). Environ. Earth Sci. 74, 7605–7616. doi:10.1007/s12665-015-4704-0

Chauvet, A., Volland-Tuduri, N., Lerouge, C., Bouchot, V., Monié, P., Charonnat, X., Faure, M., 2012. Geochronological and geochemical characterization of magmatic-hydrothermal events within the Southern Variscan external domain (Cévennes area, France). Int. J. Earth Sci. 101, 69–86. doi:10.1007/s00531-011-0639-1

Chew, D.M., Petrus, J. A., Kamber, B.S., 2014. U-Pb LA-ICPMS dating using accessory mineral standards with variable common Pb. Chem. Geol. 363, 185–199. doi:10.1016/j.chemgeo.2013.11.006

Chew, D.M., Sylvester, P.J., Tubrett, M.N., 2011. U-Pb and Th-Pb dating of apatite by LA-ICPMS. Chem. Geol. 280, 200–216. doi:10.1016/j.chemgeo.2010.11.010

Cochrane, R., Spikings, R. A., Chew, D., Wotzlaw, J.F., Chiaradia, M., Tyrrell, S., Schaltegger, U., Van der Lelij, R., 2014. High temperature (>350°C) thermochronology and mechanisms of Pb loss in apatite. Geochim. Cosmochim. Acta 127, 39–56. doi:10.1016/j.gca.2013.11.028

Dautria, J.M., Liotard, J.M., Bosch, D., Alard, O., 2010. 160 Ma of sporadic basaltic activity on the Languedoc volcanic line (Southern France): A peculiar case of lithosphere-asthenosphere interplay. Lithos 120, 202–222. doi:10.1016/j.lithos.2010.04.009

El Korh, A., Schmidt, S.T., Ulianov, A., Potel, S., 2009. Trace Element Partitioning in HP-LT Metamorphic Assemblages during Subduction-related Metamorphism, Ile de Groix, France: a Detailed LA-ICPMS Study. J. Petrol. 50, 1107–1148. doi:10.1093/petrology/egp034

Faure, M., Lardeaux, J.M., Ledru, P., 2009. A review of the pre-Permian geology of the Variscan French Massif Central. Comptes Rendus - Geosci. 341, 202–213. doi:10.1016/j.crte.2008.12.001

Faure, M., Charronat, X., Chauvet, A., Chen, Y., Talbot, J-Y., Martelet, G., Courrioux, G., Monié, P., Milesi, J-P. 2001. Tectonic evolution of the Cévennes para-autochthonous domain of the Hercynian French Massif Central and its bearing on ore deposits formation. Bulletin de la Société Géologique de France 172, pp. 687-696.

Garzanti, E., 2017. The maturity myth in sedimentology and provenance analysis. Journal of Sedimentary Research, 2017, v. 87, 353–365. doi: 10.2110/jsr.2017.17

Gehrels, G 2012. Detrital Zircon U-Pb Geochronology: Current Methods and New Opportunities. in Tectonics of Sedimentary Basins: Recent Advances. John Wiley and Sons, pp. 45-62. DOI: 10.1002/9781444347166.ch2

Harazim, D., Van De Schootbrugge, B., Sorichter, K., Fiebig, J., Weug, A., Suan, G., Oschmann, W., 2013. Spatial variability of watermass conditions within the European Epicontinental Seaway during the Early Jurassic (Pliensbachian-Toarcian). Sedimentology 60, 359–390. doi:10.1111/j.1365-3091.2012.01344.x

Henrichs, I.A., O'Sullivan, G., Chew, D.M., Mark, C., Babechuk, M.G., McKenna, C., Emo, R., 2018. The trace element and U-Pb systematics of metamorphic apatite. Chemical Geology, 483, pp. 218-238. doi:10.1016/j.chemgeo.2017.12.031

Hietpas, J., Samson, S., Moecher, D., Schmitt, A.K., 2010. Recovering tectonic events from the sedimentary record: Detrital monazite plays in high fidelity. Geology 38, 167–170. doi:10.1130/G30265.1

Hsieh, P.S., Chen, C.H., Yang, H.J., Lee, C.Y., 2008. Petrogenesis of the Nanling Mountains granites from South China: Constraints from systematic apatite geochemistry and whole-rock geochemical and Sr-Nd isotope compositions. J. Asian Earth Sci. 33, 428–451. doi:10.1016/j.jseaes.2008.02.002

Kohn, M.J., Corrie, S.L., Markley, C., 2015. The fall and rise of metamorphic zircon. Am. Mineral. 100, 897–908. doi:10.2138/am-2015-5064

Krippner, A., Bahlburg, H., 2013. Provenance of Pleistocene Rhine River Middle Terrace sands between the Swiss-German border and Cologne based on U-Pb detrital zircon ages. Int. J. Earth Sci. 102, 917–932. doi:10.1007/s00531-012-0842-8

Luvizotto, G.L., Zack, T., Meyer, H.P., Ludwig, T., Triebold, S., Kronz, A., Münker, C., Stockli, D.F., Prowatke, S., Klemme, S., Jacob, D.E., von Eynatten, H., 2009. Rutile crystals as potential trace element and isotope mineral standards for microanalysis. Chem. Geol. 261, 346–369. doi:10.1016/j.chemgeo.2008.04.012

Luvizotto, G.L., Zack, T., Triebold, S., Von Eynatten, H., 2009. Rutile occurrence and trace element behavior in medium-grade metasedimentary rocks: Example from the Erzgebirge, Germany. Mineral. Petrol. 97, 233–249. doi:10.1007/s00710-009-0092-z

Malusà, M.G., Anfinson, O. A., Dafov, L.N., Stockli, D.F., 2016. Tracking Adria indentation beneath the Alps by detrital zircon U-Pb geochronology: Implications for the Oligocene–Miocene dynamics of the Adriatic microplate. Geology 44, G37407.1. doi:10.1130/G37407.1

Mark, C., Cogné, N., Chew, D., 2016. Tracking exhumation and drainage divide migration of the western Alps: a test of the apatite U-Pb thermochronometer as a detrital provenance tool. GSA Bull. 1–22. doi:10.1130/B31351.1

Matte, P., 1986. Tectonics and plate tectonics model for the Variscan belt of Europe. Tectonophysics 126. doi:10.1016/0040-1951(86)90237-4

McAteer, C.A., Daly, J.S., Flowerdew, M.J., Connelly, J.N., Housh, T.B., Whitehouse, M.J., 2010. Detrital zircon, detrital titanite and igneous clast U-Pb geochronology and basement-cover relationships of the Colonsay Group, SW Scotland: Laurentian provenance and correlation with the Neoproterozoic Dalradian Supergroup. Precambrian Res. 181, 21–42. doi:10.1016/j.precamres.2010.05.013

McDowell, F.W., McIntosh, W.C., Farley, K. A., 2005. A precise 40Ar-39Ar reference age for the Durango apatite (U-Th)/He and fission-track dating standard. Chem. Geol. 214, 249–263. doi:10.1016/j.chemgeo.2004.10.002

Meinhold, G., Anders, B., Kostopoulos, D., Reischmann, T., 2008. Rutile chemistry and thermometry as provenance indicator: An example from Chios Island, Greece. Sediment. Geol. 203, 98–111. doi:10.1016/j.sedgeo.2007.11.004

Morton, A., C., 1986. Dissolution of apatite in North Sea Jurassic sandstones: implications for the generation of secondary porosity. Clay Minerals (1986) 21, 711-733

Morton, A., Chenery, S., 2009. Detrital Rutile Geochemistry and Thermometry as Guides to Provenance of Jurassic-Paleocene Sandstones of the Norwegian Sea. J. Sediment. Res. 79, 540–553. doi:10.2110/jsr.2009.054

Morton, A.C., Smale, D., 1991. The effects of transport and weathering on heavy minerals from the Cascade River, New Zealand. Sediment. Geol. 68, 117–123

Morton, A.C, Yaxley, G., 2007. Detrital apatite geochemistry and its application in Provenance Studies. GSA special papers 2007;420; 319–344. doi:10.1130/2006.2420(19).

Morton. A.C., Hallsworth, C., 1999. Processes controlling the composition of heavy mineral assemblages in sandstones. Sediment. Geol. 124, 3-29. doi:10.1016/S0037-0738(98)00118-3

Najoui, K., 1996. Conditions et âges de mise en place des granïtoides de la zone externe Sud de Massif Central français: étude pétro- structurale et géochronologique Ar–Ar des roches et de leurs auréoles de contact. Implications géotectoniques. Thèse Univ Montp II, pp 1–247

Nutman, A. P., 2007. Apatite recrystallisation during prograde metamorphism, Cooma, southeast Australia: implications for using an apatite – graphite association as a biotracer in ancient metasedimentary rocks. Aust. J. Earth Sci. 54, 1023–1032. doi:10.1080/08120090701488321

O'Sullivan, G.J., Chew, D.M. and Samson, S.D., 2016. Detecting magma-poor orogens in the detrital record. *Geology*, *44*(10), pp.871-874. doi:10.1130/G38245.1

O'Reilly, S.Y., Griffin, W.L., 2000. Apatite in the mantle: Implications for metasomatic processes and high heat production in Phanerozoic mantle. Lithos 53, 217–232. doi:10.1016/S0024-4937(00)00026-8

Paton, C., Hellstrom, J., Paul, B., Woodhead, J., Hergt, J., 2011. Iolite: Freeware for the visualisation and processing of mass spectrometric data. J. Anal. At. Spectrom. 26, 2508. doi:10.1039/c1ja10172b

Piccoli, P.M., Candela, P. A., 2002. Apatite in Igneous Systems. Rev. Mineral. Geochemistry 48, 255–292. doi:10.2138/rmg.2002.48.6

Russell, R.D., 1937. Mineral composition of Mississippi river sands. Bull. Geol. Soc. Am., 48: 1308-1348

Sabourdy, G., 1975. Apport de la géochimie à la connaissance de la pétrogenèse des granitoÏdes des Cévennes méridionales. PhD thesis, 278 pp., Univ. de Clermont-Ferrand, Clermont-Ferrand, France.

Schoene, B., Bowring, S.A., 2006. U-Pb systematics of the McClure Mountain syenite: Thermochronological constraints on the age of the 40Ar/39Ar standard MMhb. Contrib. to Mineral. Petrol. 151, 615–630. doi:10.1007/s00410-006-0077-4

Séranne M., Camus H., Lucazeau F., Barbarand J., Quinif Y. (2002). Surrection et érosion polyphasées de la bordure cévenole. Un exemple de morphogenèse lente. Bull. Soc. géol. Fr., 173 (2), 97-112.

Sha, L.-K., Chappell, B.W., 1999. Apatite chemical composition, determined by electron microprobe and laser-ablation inductively coupled plasma mass spectrometry, as a probe into granite petrogenesis. Geochim. Cosmochim. Acta 63, 3861–3881. doi:10.1016/S0016-7037(99)00210-0

Spear, F.S., Pyle, J.M., 2002. Apatite, Monazite, and Xenotime in Metamorphic Rocks. Rev. Mineral. Geochemistry 48, 293–335. doi:10.2138/rmg.2002.48.7

Stacey, J.S., Kramers, J.D., 1975. Approximation of terrestrial lead isotope evolution by a two-stage model. Earth Planet. Sci. Lett. 26, 207–221. doi:10.1016/0012-821X(75)90088-6

Talbot, J.Y., Faure, M., Chen, Y., Martelet, G., 2005. Pull-apart emplacement of the Margeride granitic complex (French Massif Central). Implications for the late evolution of the Variscan orogen. J. Struct. Geol. 27, 1610–1629. doi:10.1016/j.jsg.2005.05.008

Tang, M., Wang, X.L., Xu, X.S., Zhu, C., Cheng, T., Yu, Y., 2012. Neoproterozoic subducted materials in the generation of Mesozoic Luzong volcanic rocks: Evidence from apatite geochemistry and Hf-Nd isotopic decoupling. Gondwana Res. 21, 266–280. doi:10.1016/j.gr.2011.05.009

Thomas, W. A., 2011. Detrital-zircon geochronology and sedimentary provenance. Lithosphere 3, 304–308. doi:10.1130/RF.L001.1

Thomson, S.N., Gehrels, G.E., Ruiz, J., Buchwaldt, R., 2012. Routine low-damage apatite U-Pb dating using laser ablation-multicollector- ICPMS. Geochemistry, Geophys. Geosystems 13, 1–23. doi:10.1029/2011GC003928

Ubide, T., Wijbrans, J.R., Gale, C., Arranz, E., Lago, M. and Larrea, P., 2014. Age of the Cretaceous alkaline magmatism in northeast Iberia: implications for the Alpine cycle in the Pyrenees. Tectonics, 33(7), pp.1444-1460. doi:10.1002/2013TC003511

Van Andel, T.H., 1950. Provenance, Transport and Deposition of Rhine Sediments. Veenman en Zonen, Wagenin- gen, 129 pp.

Vermeesch, P., 2004. How many grains are needed for a provenance study? Earth Planet. Sci. Lett. 224, 441–451. doi:10.1016/j.epsl.2004.05.037

Vermeesch, P., 2012. On the visualisation of detrital age distributions. Chemical Geology, v.312-313, 190-194, doi: 10.1016/j.chemgeo.2012.04.021

Vermeesch, P., 2013. Multi-sample comparison of detrital age distributions. Chem. Geol. 341, 140–146. doi:10.1016/j.chemgeo.2013.01.010

Vermeesch, P., Resentini, A. and Garzanti, E., 2016. An R package for statistical provenance analysis. Sedimentary Geology, doi:10.1016/j.sedgeo.2016.01.009.

Zack, T., Stockli, D.F., Luvizotto, G.L., Barth, M.G., Belousova, E., Wolfe, M.R., Hinton, R.W., 2011. In situ U-Pb rutile dating by LA-ICP-MS: ^{208}Pb correction and prospects for geological applications. Contrib. to Mineral. Petrol. 162, 515–530. doi:10.1007/s00410-011-0609-4

Zattin, M., Andreucci, B., Thomson, S.N., Reiners, P.W., Talarico, F.M., 2012. New constraints on the provenance of the ANDRILL AND-2A succession (western Ross Sea, Antarctica) from apatite triple dating. Geochemistry, Geophys., Geosystems 13. doi:10.1029/2012GC004357

3.8 SUPPORTING INFORMATION & SUPPLEMENTARY FIGURES

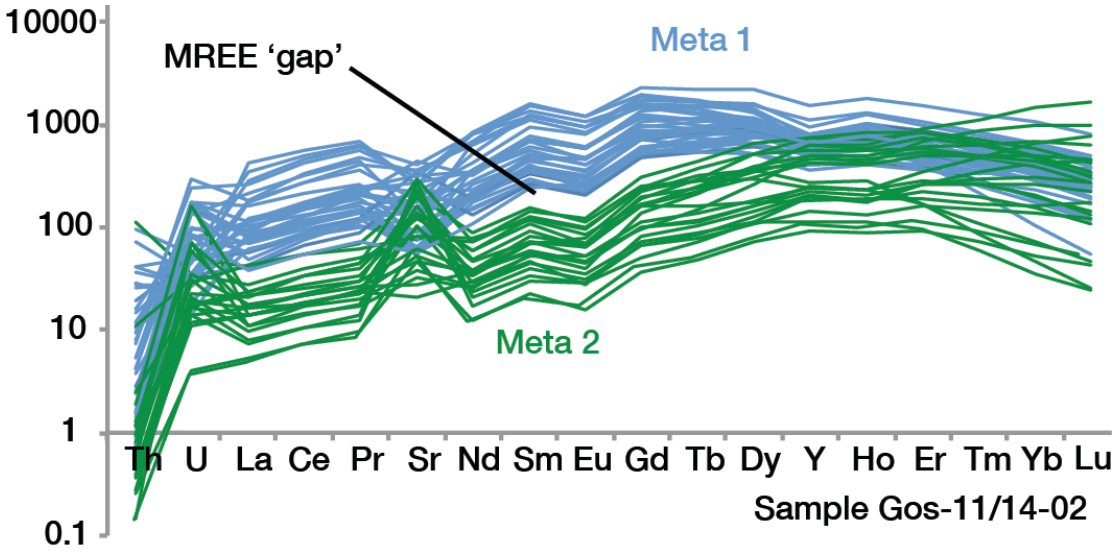

Figure S3.1. The two primary metamorphic detrital populations are discriminated on the basis of the much lower light- and mid-rare earth (LREE and MREE) contents in population "Meta 2". This manifests as the "MREE-gap" in the diagram above. The detailed paragenesis of these sub-populations is beyond the scope of this detrital study.

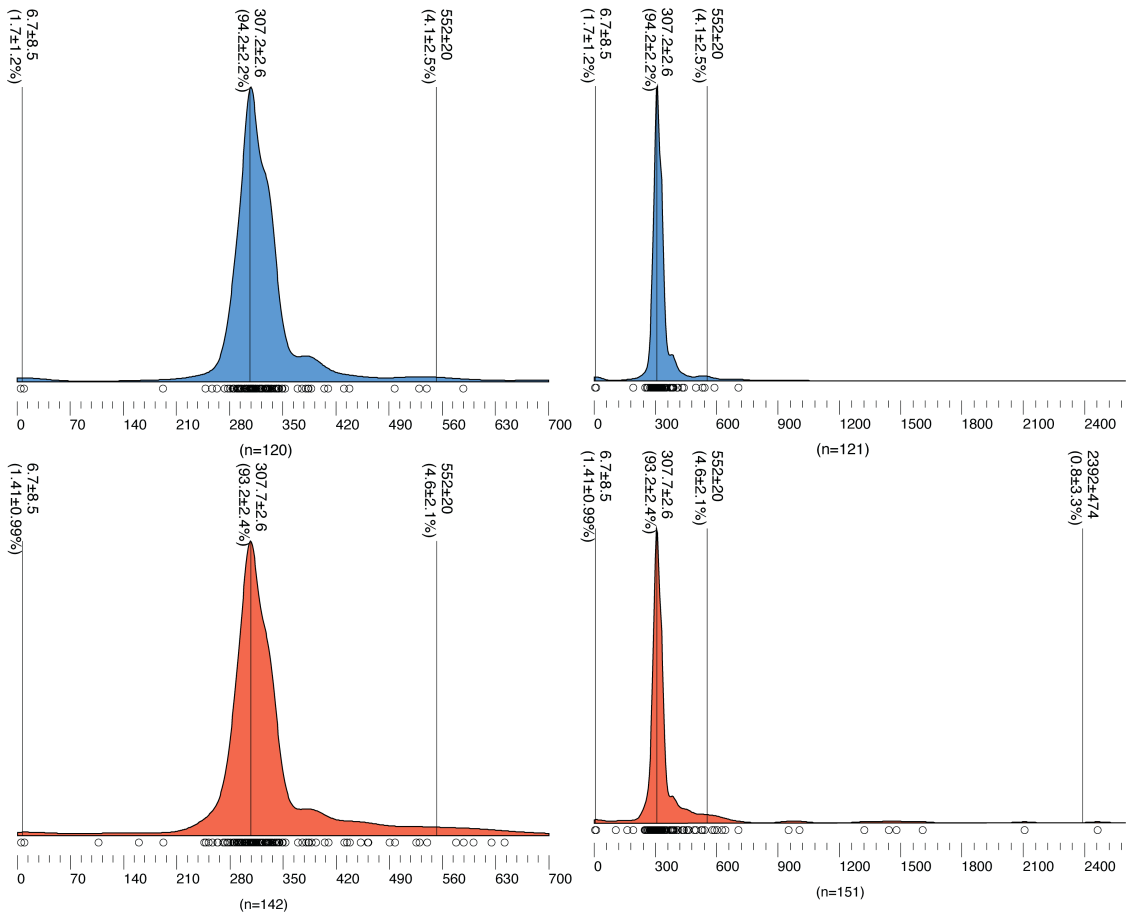

Figure S3.2. Comparison of filtered (blue) and unfiltered (red) age data from samples 6, 7 and 8 (Gorges du Tarn), scale on x-axis in Ma. The filtered data has less scatter, with most grain showing apprarent Proterozoic ages being rejected due to high uncertainty on their central age (more than 25 percent). The filter causes no change to the location or magnitude of the age peaks. Figure generated using Density Plotter (Vermeesch, 2012).

Sample	Provenace	OP	CB	BY	PH	MC	HM
2	Meta.	38	5	0	0	33	24
4	Granitic	24	0	0	0	29	47
6	Mixed	45	6	2	0	26	21
7	Mixed	51	9	1	0	14	25
8	Mixed	39	29	0	0	8	24
9	Mixed	51	21	0	1	12	15
1	Mixed	29	38	3	1	12	17
10	Mixed	34	26	5	4	5	26
13	Carbonate	23	74	0	2	0	1
11	Mixed	34	39	0	0	17	10

Table S3.1. OP = opaque minerals; CB = carbonate; BY = barite; PH = biogenic phosphate; MC = mica and chlorite; HM = translucent heavy minerals. Meta. = metamorphic. 63-125um fraction
Table is in same format as table 1 in the main text, lain out in hydrographic order, and methods are the same, described in text S1. Carbonate content increases as the Tarn samples ever more of the Grands Causses basin fill downstream. In sample 13 heavy minerals are only 1% of the total, demonstrating the paucity of detrital material in the Grands Causses sediments.

Sample (in hydrographic order)	River sampled	Nearest Settlement	UTM coordinates	Additional Comments
GOS11/14-02	La Mimente	Saint Julien d'Aparaon	31T 0552945 4905690	"Metamorphic tributary"
GOS11/14-04	Upper Tarn	Between Cocurés and le Pont-de-Monvert	31T 0553508 4912207	"Granitic tributary"
GOS11/14-06	Tarn, below confluence with la Mimente	Quézac	31T 0541519 4913661	source mixing sample
GOS11/14-07	Tarn	Sainte-Enimie	31T 0525670 4905357	
GOS11/14-08	Tarn	Upstream of Le Rozier	31T 0517841 4896512	
GOS11/14-09	Tarn, below confluence with la Jonte	Between Cabrassas and Paulhe	31T 0508097 4887787	
GOS11/14-01	Tarn, below confluence with la Dourbie	Millau	31T 0506930 4882366	
GOS11/14-10	Tarn	Comprégnac	31T 0499364 4881259	
GOS11/14-13	Le Cernon	Saint-Georges-de-Luzençon	31T 0498866 4880811	"Carbonate tributary"
GOS11/14-11	Tarn	Candas	31T 0494219 4879610	Sourcing Triassic s'stone

Table S3.2. Sample locations and other sampling information

Text S3.1.

Heavy Mineral Analysis (HMA) methods

1. Sample preparation

The samples were cleaned using detergent and a Soniprep ultrasonic probe to remove and disperse any clay that might have been adhering to grain surfaces, washed through a 63 μm sieve and resubjected to ultrasonic treatment until no more clay passed into suspension, and wet sieved through the 125 and 63 μm sieves. The resulting >125 μm and 63-125 μm fractions were dried in an oven at 80°C and the 63–125 μm fraction was placed in bromoform with a measured specific gravity of 2.8. Heavy minerals were allowed to separate under gravity, with frequent stirring to ensure complete separation. The heavy mineral separate was mounted under Canada Balsam for optical study using a polarising microscope, with a split being retained for additional work where recovery allowed.

2. Conventional analysis and ratio determination

Heavy mineral proportions were estimated by counting 200 non-opaque detrital grains using the ribbon method described by Galehouse (1971). Identification
was made on the basis of optical properties, as described for grain mounts by Mange and Maurer (1992). A qualitative assessment was also made of other components, such as carbonate, opaques and mica. Provenance-sensitive mineral ratios (Morton and Hallsworth, 1994) were also determined using the ribbon counting method on the basis of a 100+ grain count per mineral pair (where grain availability allowed). Conventional heavy mineral and provenance-sensitive ratio data are given in Tables x and y.

References

Galehouse, J.S., 1971. Point-counting. In: Carver R.E. (ed.), Procedures in Sedimentary Petrology. Wiley-Interscience, New York, 385-407.

Mange, M.A., Maurer, H.F.W., 1992. Heavy minerals in colour. Chapman and Hall, London.

Morton, A.C., Hallsworth, C., 1994. Identifying provenance-specific features of detrital heavy mineral assemblages in sandstones. Sediment. Geol. 90, 241–256. doi:10.1016/0037-0738(94)90041-8

Supporting Information Tables S3.3: Rutile U-Pb data

Integration	$^{207}Pb/^{235}U$	Prop2SE	$^{206}Pb/^{238}U$	Prop2SE	Rho	$^{238}U/^{206}Pb$	Prop2SE	$^{207}Pb/^{206}Pb$	Prop2SE	Rho	^{207}Pb corrected age	Prop2SE	$f^{206}Pb$	Approx U ppm
Tarn04_32	0.68	0.1	0.056	0.002	0.59	17.79	0.63	0.090	0.013	-0.30	336.8	12.5	0.05	17.2
Tarn04_33	0.969	0.05	0.020	0.001	0.65	49.09	2.30	0.348	0.013	0.41	81.1	4.4	0.38	120
Tarn04_34	0.323	0.10	0.051	0.003	0.10	19.53	1.10	0.045	0.014	0.23	325.0	18.9	0.00	3.66
Tarn04_35	23.58	0.44	0.245	0.004	0.77	4.08	0.08	0.702	0.01	0.36	294.9	23.2	0.81	31.2
Tarn04_37	2.91	0.24	0.072	0.003	0.62	13.93	0.59	0.287	0.018	-0.17	320.0	16.6	0.29	9.06
Tarn04_38	15.14	0.54	0.180	0.007	0.34	5.56	0.23	0.611	0.028	0.48	347.5	41.5	0.69	7.15
Tarn04_39	5.79	0.47	0.099	0.006	0.43	10.10	0.62	0.428	0.036	0.33	332.1	33.2	0.47	6.16
Tarn04_40	14.2	1.3	0.171	0.011	0.69	5.85	0.40	0.605	0.039	-0.01	337.7	56.0	0.69	1.76
Tarn04_41	0.819	0.09	0.056	0.002	0.72	17.83	0.76	0.108	0.012	-0.23	328.4	14.8	0.07	7.25
Tarn04_42	6.21	0.56	0.102	0.005	0.47	9.85	0.51	0.444	0.034	0.04	327.8	31.6	0.49	3.86
Tarn04_43	12.13	0.71	0.157	0.006	0.20	6.36	0.25	0.569	0.039	0.34	355.2	49.4	0.64	3.91
Tarn04_44	5.09	0.43	0.094	0.004	0.01	10.66	0.48	0.394	0.026	0.35	339.6	23.9	0.42	11.2
Tarn04_48	8.54	0.54	0.123	0.006	0.43	8.16	0.40	0.514	0.033	0.30	328.7	35.4	0.57	3.65
Tarn04_49	2.16	0.28	0.055	0.004	0.17	18.21	1.50	0.307	0.043	0.36	236.3	24.8	0.32	2.97
Tarn04_50	2.32	0.26	0.067	0.003	0.30	14.97	0.69	0.248	0.025	0.13	318.1	19.4	0.24	7.05
Tarn04_51	0.79	0.13	0.057	0.002	0.01	17.64	0.71	0.104	0.017	0.21	333.6	14.7	0.06	5.9
Tarn04_53	3.6	0.29	0.079	0.003	0.15	12.61	0.51	0.340	0.031	0.27	320.5	22.9	0.36	5.24
Tarn04_55	0.552	0.06	0.050	0.002	0.08	19.84	0.72	0.080	0.009	0.21	306.2	10.8	0.03	10.8
Tarn04_56	1.19	0.16	0.058	0.003	0.38	17.15	0.72	0.152	0.020	-0.03	321.3	16.3	0.12	7.27
Tarn04_57	0.76	0.13	0.056	0.003	0.01	17.86	0.94	0.110	0.021	0.47	327.0	18.0	0.07	3.63
Tarn04_58	3.13	0.11	0.077	0.002	0.39	12.94	0.31	0.296	0.01	0.25	339.0	9.6	0.30	25.9
Tarn04_59	3.03	0.22	0.079	0.003	0.51	12.71	0.41	0.276	0.018	-0.06	357.3	15.9	0.28	16.2
Tarn04_60	1.1	0.21	0.053	0.004	0.01	18.83	1.90	0.164	0.035	0.39	288.0	27.6	0.14	1.93
Tarn04_62	8.25	0.33	0.119	0.004	0.23	8.44	0.27	0.508	0.025	0.45	323.4	25.3	0.57	8.76
Tarn04_63	3.03	0.43	0.074	0.005	0.39	13.51	1.10	0.312	0.047	0.27	315.3	33.8	0.32	2.77
Tarn04_64	1.59	0.12	0.025	0.002	0.74	40.16	2.40	0.458	0.024	0.04	77.0	7.2	0.52	48.5
Tarn04_65	6.25	0.46	0.095	0.006	0.42	10.48	0.69	0.494	0.035	0.36	270.0	30.8	0.55	3.09
Tarn04_66	3.09	0.12	0.048	0.002	0.51	20.92	0.76	0.477	0.016	0.46	140.8	8.0	0.54	40
Tarn04_67	1.36	0.12	0.056	0.002	0.03	17.73	0.56	0.178	0.016	0.33	299.6	11.3	0.16	14.2

Integration	$^{207}Pb/^{235}U$	Prop2SE	$^{206}Pb/^{238}U$	Prop2SE	Rho	$^{238}U/^{206}Pb$	Prop2SE	$^{207}Pb/^{206}Pb$	Prop2SE	Rho	^{207}Pb corrected age	Prop2SE	$f^{206}Pb$	Approx U ppm
Passed inclusion criteria														
Tarn04_0	0.87	0.36	0.052	0.007	0.16	19.34	3.10	0.142	0.072	0.14	289.4	46.0	0.11	0.77
Tarn04_1	1.42	0.22	0.062	0.004	0.55	16.08	0.96	0.164	0.021	-0.13	336.8	23.1	0.14	8.5
Tarn04_4	6.89	0.44	0.109	0.005	0.04	9.19	0.43	0.472	0.035	0.53	327.6	33.2	0.52	4.46
Tarn04_5	0.756	0.06	0.054	0.002	0.63	18.42	0.63	0.102	0.008	-0.29	320.5	10.5	0.06	16.2
Tarn04_6	0.344	0.02	0.046	0.002	0.36	21.79	0.84	0.056	0.003	0.30	287.8	11.8	0.01	175
Tarn04_7	6.49	0.46	0.108	0.004	0.76	9.28	0.41	0.435	0.023	-0.03	356.0	24.0	0.47	11.8
Tarn04_9	1.2	0.12	0.060	0.002	0.33	16.58	0.47	0.141	0.012	-0.09	337.3	10.9	0.11	21.0
Tarn04_10	1.172	0.09	0.019	0.001	0.81	54.05	4.60	0.466	0.028	0.24	55.9	5.8	0.53	52.6
Tarn04_11	5.28	0.37	0.092	0.005	0.34	10.83	0.54	0.424	0.034	0.39	312.4	28.8	0.46	5.61
Tarn04_12	1.244	0.06	0.059	0.001	0.21	17.06	0.37	0.157	0.008	0.24	320.9	7.9	0.13	84.1
Tarn04_13	1.036	0.08	0.054	0.001	0.49	18.66	0.43	0.139	0.01	-0.18	301.1	7.8	0.11	50.4
Tarn04_14	0.557	0.08	0.051	0.002	0.07	19.80	0.86	0.079	0.011	0.34	307.4	13.3	0.03	9.1
Tarn04_15	0.91	0.12	0.054	0.002	0.03	18.55	0.74	0.125	0.017	0.17	308.6	13.8	0.09	4.75
Tarn04_16	0.859	0.10	0.054	0.002	0.18	18.48	0.71	0.114	0.013	0.12	314.4	12.7	0.08	7.7
Tarn04_17	2.1	0.27	0.077	0.004	0.01	13.05	0.62	0.202	0.027	0.35	391.5	23.6	0.18	7.66
Tarn04_18	5.2	0.48	0.090	0.005	0.45	11.15	0.69	0.422	0.035	0.16	304.9	30.2	0.46	6.97
Tarn04_19	6.67	0.47	0.100	0.005	0.37	9.96	0.54	0.486	0.033	0.33	290.8	30.0	0.54	13.8
Tarn04_20	1.38	0.11	0.062	0.002	0.27	16.16	0.49	0.162	0.013	0.11	336.2	12.4	0.14	25.7
Tarn04_22	3.4	0.53	0.077	0.008	0.05	13.05	1.70	0.342	0.062	0.60	308.4	47.7	0.36	0.82
Tarn04_23	0.61	0.13	0.053	0.003	0.07	18.83	1.30	0.094	0.022	0.29	316.8	21.4	0.05	4.25
Tarn04_24	7.88	0.75	0.116	0.007	0.39	8.59	0.63	0.491	0.044	0.53	333.3	44.4	0.54	2.03
Tarn04_25	0.817	0.09	0.043	0.002	0.76	23.31	1.20	0.138	0.014	-0.43	241.9	12.1	0.11	40
Tarn04_26	0.76	0.12	0.050	0.003	0.06	20.12	1.00	0.109	0.018	0.35	291.0	16.5	0.07	5.57
Tarn04_27	2.7	0.77	0.071	0.006	0.09	14.14	1.20	0.307	0.093	0.01	304.1	55.9	0.32	1.24
Tarn04_28	0.84	0.11	0.054	0.002	0.42	18.42	0.68	0.114	0.015	-0.03	315.5	12.6	0.08	6.66
Tarn04_29	6.35	0.32	0.104	0.004	0.45	9.66	0.37	0.444	0.02	0.44	334.3	20.4	0.49	6.23
Tarn04_30	0.321	0.02	0.045	0.001	0.20	22.03	0.62	0.053	0.003	0.16	286.0	8.2	0.00	459
Tarn04_31	0.78	0.12	0.067	0.003	0.01	15.02	0.67	0.087	0.013	0.19	399.5	18.3	0.04	10.5

Supporting Information Tables S3.3: Rutile U-Pb data (continued)

Integration	$^{207}Pb/^{235}U$	Prop2SE	$^{206}Pb/^{238}U$	Prop2SE	Rho	$^{238}U/^{206}Pb$	Prop2SE	$^{207}Pb/^{206}Pb$	Prop2SE	Rho	^{207}Pb corrected age	Prop2SE	$f^{206}Pb$	Approx U ppm
Tarn02ru_9	610	65	5.200	0.540	0.98	0.19	0.03	0.848	0.018	0.14	-	-	-	4.18
Tarn02ru_11	73.1	9.2	0.750	0.110	0.84	1.33	0.22	0.816	0.086	0.63	195.7	510.6	0.96	0.17
Tarn02ru_12	263	17	2.260	0.150	0.91	0.44	0.03	0.849	0.019	0.33	-	-	-	1.39
Tarn02ru_14	29	3.5	0.320	0.039	0.61	3.13	0.52	0.710	0.061	0.29	374.4	156.3	0.81	0.63
Tarn02ru_15	44.4	9.5	0.314	0.061	0.31	3.18	1.30	0.880	0.340	0.59	-	-	-	0.08
Tarn02ru_17	62.2	6.6	0.548	0.060	0.86	1.82	0.24	0.822	0.042	0.29	85.3	188.6	0.98	1.64
Tarn02ru_18	207	25	1.800	0.200	0.92	0.56	0.08	0.831	0.043	0.11	732.4	571.4	0.93	0.17
Tarn02ru_19	17.4	3.1	0.403	0.029	0.84	2.48	0.18	0.298	0.038	-0.62	1765.4	157.2	0.22	4.3
Tarn02ru_21	10.9	2.1	0.157	0.025	0.30	6.37	1.50	0.570	0.120	0.59	353.5	154.6	0.64	0.40
Tarn02ru_22	15.9	1.7	0.195	0.025	0.88	5.13	0.73	-	-	-	-	-	-	0.67
Tarn02ru_23	32	2.8	0.325	0.023	0.93	3.08	0.21	-	-	-	-	-	-	3.82
Tarn02ru_25	19.5	2.2	0.211	0.016	0.30	4.74	0.47	0.733	0.092	0.39	193.5	154.1	0.86	0.38
Tarn02ru_26	34.9	1.6	0.345	0.016	0.57	2.90	0.15	0.743	0.032	0.53	305.2	88.5	0.86	2.02
Tarn02ru_27	57.3	1.8	0.546	0.020	0.57	1.83	0.07	0.775	0.026	0.48	360.0	113.9	0.89	2.36
Tarn02ru_28	322	35	2.610	0.230	0.83	0.38	0.03	0.861	0.037	0.14	-	-	-	1.06
Tarn02ru_29	950	250	7.700	2.000	0.97	0.13	0.04	0.894	0.065	0.14	-	-	-	0.05
Tarn02ru_30	8.2	2.3	0.139	0.028	0.95	7.19	1.90	-	-	-	-	-	-	1.01
Tarn02ru_31	67.8	8.2	0.639	0.070	0.45	1.56	0.22	0.860	0.11	0.87	-	-	-	0.14
Tarn02ru_33	1.35	0.64	0.057	0.008	0.03	17.70	5.80	0.420	0.33	0.18	192.5	149.2	0.46	0.38
Tarn02ru_36	60	12	0.537	0.082	0.10	1.86	0.28	0.950	0.30	0.04	-	-	-	0.12
Tarn02ru_38	32.1	7.7	0.306	0.057	0.74	3.27	1.60	0.810	0.12	0.45	75.4	296.6	0.96	0.47
Tarn02ru_40	19.1	1.2	0.212	0.013	0.38	4.72	0.29	0.680	0.047	0.58	291.1	79.8	0.78	1.31
Tarn02ru_41	48.5	8.2	0.448	0.068	0.07	2.23	0.57	0.960	0.280	0.68	-	-	-	0.06
Tarn02ru_42	68.3	3.9	0.631	0.029	0.78	1.58	0.07	0.786	0.027	0.00	363.3	136.4	0.91	1.32
Tarn02ru_44	35.1	8.4	0.326	0.062	0.20	3.07	0.69	0.780	0.130	0.86	174.2	337.2	0.92	0.09
Tarn02ru_46	263	15	2.310	0.150	0.85	0.43	0.02	0.835	0.026	0.26	1632.5	426.8	0.88	1.02
Tarn02ru_48	250	30	2.110	0.240	0.95	0.47	0.06	0.838	0.027	-0.14	789.0	433.8	0.94	0.56
Tarn02ru_49	60.8	5.7	0.585	0.048	0.63	1.71	0.15	0.760	0.038	0.19	486.6	173.8	0.87	1.31
Tarn02ru_50	96.8	9.5	0.836	0.087	0.54	1.20	0.13	0.865	0.048	0.55	-	-	-	0.74

Integration	$^{207}Pb/^{235}U$	Prop2SE	$^{206}Pb/^{238}U$	Prop2SE	Rho	$^{238}U/^{206}Pb$	Prop2SE	$^{207}Pb/^{206}Pb$	Prop2SE	Rho	^{207}Pb corrected age	Prop2SE	$f^{206}Pb$	Approx U ppm
Tarn02ru_10	2.22	0.63	0.069	0.008	0.11	14.47	1.90	0.223	0.052	0.53	342.3	47.3	0.21	2.25
Tarn02ru_13	1.78	0.67	0.068	0.009	0.01	14.79	2.50	0.130	0.12	0.69	383.3	80.9	0.09	0.7
Tarn02ru_16	21.5	1.8	0.240	0.019	0.60	4.17	0.34	0.650	0.034	0.32	394.1	70.1	0.74	2.11
Tarn02ru_20	2.65	0.41	0.072	0.005	0.09	13.99	1.10	0.274	0.029	0.21	325.9	27.5	0.27	3.94
Tarn02ru_24	4.52	0.39	0.087	0.003	0.18	11.53	0.48	0.385	0.032	-0.11	319.9	24.8	0.41	3.41
Tarn02ru_32	9.6	1.8	0.130	0.015	0.86	7.69	1.40	0.493	0.061	-0.43	371.0	73.8	0.54	1.90
Tarn02ru_34	1.045	0.09	0.081	0.003	0.09	12.39	0.46	0.094	0.007	0.35	478.0	16.7	0.05	17.1
Tarn02ru_35	0.35	0.26	0.048	0.006	0.01	20.75	4.30	0.063	0.054	0.77	299.5	41.3	0.01	1.35
Tarn02ru_37	2.48	0.55	0.077	0.008	0.36	12.94	1.40	0.265	0.063	0.48	357.5	52.7	0.26	1.66
Tarn02ru_39	9.7	1	0.151	0.013	0.29	6.62	0.58	0.513	0.05	0.51	408.5	67.0	0.57	2.43
Tarn02ru_43	11	1	0.143	0.011	0.68	6.99	0.53	0.556	0.04	-0.08	337.0	51.1	0.62	7.99
Tarn02ru_45	7.92	0.44	0.128	0.005	0.41	7.83	0.28	0.452	0.02	0.43	405.6	24.8	0.49	16.0
Tarn02ru_47	0.362	0.06	0.049	0.002	0.20	20.49	0.92	0.054	0.009	0.05	306.5	14.0	0.00	11.7
Tarn02ru_52	0.3	0.17	0.050	0.004	0.01	19.92	2.10	0.044	0.03	0.10	319.1	27.6	0.00	1.43
Tarn02ru_56	0.423	0.07	0.056	0.002	0.01	17.83	0.68	0.056	0.01	0.41	350.8	13.6	0.00	6.67
Tarn02ru_57	4.54	0.57	0.089	0.007	0.19	11.29	1.10	0.376	0.042	0.41	333.2	39.6	0.40	1.29
Tarn02ru_59	20.2	1.7	0.236	0.015	0.96	4.24	0.30	0.614	0.021	-0.45	457.6	48.0	0.69	6.95
Tarn02ru_63	5.03	0.39	0.094	0.005	0.23	10.62	0.53	0.390	0.019	0.44	344.0	21.4	0.42	14.5
Tarn02ru_66	19.37	0.6	0.213	0.006	0.66	4.69	0.15	0.657	0.017	0.42	334.3	31.3	0.75	7.86
Tarn02ru_72	5.18	0.61	0.103	0.010	0.09	9.71	1.00	0.374	0.045	0.39	389.2	50.7	0.40	2.25
Failed inclusion criteria														
Tarn02ru_0	6.19	0.66	0.108	0.010	0.54	9.26	0.87	0.462	0.057	0.36	333.7	109.2	0.51	1.67
Tarn02ru_1	40.7	3.3	0.398	0.027	0.79	2.51	0.19	0.736	0.034	0.23	387.6	343.7	0.84	1.06
Tarn02ru_3	6.9	1.4	0.105	0.018	0.36	9.52	1.90	0.500	0.086	0.89	292.6	85.7	0.56	0.72
Tarn02ru_4	3.4	2.2	0.068	0.025	0.24	14.71	4.20	-	-	-	-	-	-	0.09
Tarn02ru_5	17	4.3	0.223	0.041	0.54	4.48	1.60	0.600	0.063	0.35	456.3	134.1	0.67	0.36
Tarn02ru_6	53.8	6.6	0.491	0.044	0.52	2.04	0.20	0.810	0.069	0.41	136.0	271.8	0.96	0.64
Tarn02ru_8	38.7	5.7	0.324	0.042	0.55	3.09	0.44	0.860	0.10	0.01	-	-	-	0.41

Supporting Information Tables S3.3: Rutile U-Pb data (continued)

Integration	$^{207}Pb/^{235}U$	Prop2SE	$^{206}Pb/^{238}U$	Prop2SE	Rho	$^{238}U/^{206}Pb$	Prop2SE	$^{207}Pb/^{206}Pb$	Prop2SE	Rho	^{207}Pb corrected age	Prop2SE	$f^{206}Pb$	Approx U ppm
Tarn04_68	1.77	0.3	0.062	0.005	0.10	16.21	1.40	0.214	0.038	0.22	310.3	29.9	0.20	1.66
Tarn04_69	20.7	1.1	0.230	0.009	0.35	4.36	0.18	0.656	0.017	0.41	364.1	34.9	0.75	8.47
Tarn04_70	8.15	0.41	0.119	0.004	0.59	8.39	0.30	0.499	0.022	0.19	333.9	23.8	0.55	5.97
Tarn04_71	2.69	0.26	0.073	0.004	0.23	13.64	0.64	0.274	0.028	0.26	334.0	22.6	0.27	4.14
Tarn04_73	0.441	0.05	0.049	0.002	0.13	20.33	0.69	0.064	0.007	0.16	305.1	10.8	0.01	9.45
Tarn04_75	0.901	0.10	0.054	0.003	0.01	18.62	1.10	0.126	0.016	0.47	307.1	17.1	0.09	5.89
Tarn04_76	3.73	0.42	0.082	0.005	0.79	12.18	0.74	0.338	0.027	-0.32	333.1	27.2	0.35	11.9
Tarn04_79	8.5	1.4	0.124	0.013	0.58	8.06	0.85	0.503	0.05	0.06	343.7	59.5	0.56	1.36
Failed inclusion criteria														
Tarn04_2	409	15	3.480	0.110	0.85	0.29	0.01	0.847	0.015	0.28	-	-	-	0.95
Tarn04_3	17.4	1.7	0.183	0.017	0.59	5.46	0.52	0.697	0.063	0.48	222.2	93.1	0.81	3.21
Tarn04_8	166	13	1.570	0.120	0.96	0.64	0.05	0.787	0.03	0.24	1994.1	343.7	0.77	0.59
Tarn04_21	173.1	8.3	1.520	0.071	0.94	0.66	0.04	0.825	0.014	0.00	599.8	182.8	0.94	2.57
Tarn04_36	580	740	5.900	6.000	0.95	0.17	0.02	0.903	0.064	0.20	-	-	-	0.02
Tarn04_45	67	2.3	0.613	0.020	0.58	1.63	0.05	0.800	0.024	0.36	254.1	121.0	0.93	4.33
Tarn04_46	19.3	1	0.187	0.009	0.13	5.36	0.29	0.801	0.058	0.56	58.0	88.3	0.95	1.07
Tarn04_47	13	2.3	0.157	0.022	0.15	6.37	1.90	0.790	0.25	0.80	63.1	317.0	0.94	0.22
Tarn04_52	28.3	2.4	0.286	0.026	0.63	3.50	0.39	0.752	0.043	0.41	222.7	99.8	0.88	1.01
Tarn04_54	158	11	1.389	0.094	0.92	0.72	0.07	0.835	0.025	0.25	149.1	289.7	0.98	0.90
Tarn04_61	32	4.3	0.318	0.043	0.58	3.14	0.66	0.860	0.12	0.90	-	-	-	0.33
Tarn04_72	950	160	8.500	1.500	0.98	0.12	0.02	0.839	0.042	0.11	-	-	-	0.06
Tarn04_74	-	-	-	-	-	-	-	0.583	0.094	-	-	-	-	0.09
Tarn04_77	261	19	2.270	0.160	0.92	0.44	0.04	0.841	0.011	-0.02	812.9	229.9	0.94	4.64
Tarn04_78	8.78	0.33	0.093	0.004	0.01	10.73	0.40	0.697	0.038	0.76	109.2	29.1	0.82	4.81
Passed inclusion criteria														
Tarn02ru_2	7.3	1.8	0.120	0.019	0.98	8.33	1.50	0.374	0.041	-0.77	453.7	79.5	0.39	10.1
Tarn02ru_7	3.12	0.44	0.077	0.006	0.12	12.95	1.10	0.301	0.045	0.16	335.5	36.7	0.31	1.79

Integration	$^{207}Pb/^{235}U$	Prop2SE	$^{206}Pb/^{238}U$	Prop2SE	Rho	$^{238}U/^{206}Pb$	Prop2SE	$^{207}Pb/^{206}Pb$	Prop2SE	Rho	^{207}Pb corrected age	Prop2SE	$f^{206}Pb$	Approx U ppm
Tarn02ru_51	192	65	1.760	0.590	0.99	0.57	0.49	0.787	0.035	-0.30	2797.0	1204.8	0.69	1.78
Tarn02ru_53	9.2	1.4	0.128	0.014	0.72	7.81	0.95	0.518	0.092	-0.05	339.7	97.6	0.58	1.84
Tarn02ru_54	123.9	6.2	1.102	0.047	0.83	0.91	0.04	0.811	0.022	0.08	494.8	193.7	0.93	1.23
Tarn02ru_55	468	36	3.830	0.280	0.74	0.26	0.02	0.879	0.047	0.22	-	-	-	0.15
Tarn02ru_58	173	18	1.410	0.130	0.85	0.71	0.08	0.895	0.035	0.20	-	-	-	0.40
Tarn02ru_60	273	31	2.400	0.300	0.77	0.42	0.06	0.846	0.072	0.63	412.5	1310.21	0.97	0.19
Tarn02ru_61	154	48	1.300	0.410	0.98	0.77	0.15	0.856	0.061	0.18	-	-	-	0.55
Tarn02ru_62	600	67	4.900	0.500	0.97	0.20	0.03	0.864	0.016	-0.08	-	-	-	0.52
Tarn02ru_64	0.71	0.63	0.059	0.009	0.01	16.98	7.50	0.110	0.190	0.23	343.7	99.2	0.07	0.38
Tarn02ru_65	170	11	1.530	0.100	0.71	0.65	0.04	0.824	0.040	0.35	649.0	456.0	0.93	0.21
Tarn02ru_67	710	100	6.280	0.980	0.38	0.16	0.02	0.863	0.043	0.08	-	-	-	0.12
Tarn02ru_68	600	68	5.080	0.580	0.90	0.20	0.02	0.867	0.041	0.02	-	-	-	0.29
Tarn02ru_69	93	30	1.130	0.390	0.86	0.88	0.29	0.660	0.038	0.30	2749.6	1131.3	0.53	0.11
Tarn02ru_70	206	16	1.880	0.150	0.90	0.53	0.05	0.812	0.037	0.32	2004.5	484.31	0.81	0.36
Tarn02ru_71	58.2	7.2	0.511	0.074	0.38	1.96	0.33	0.880	0.071	0.44	-	-	-	0.42
Tarn02ru_73	102.5	9.1	0.963	0.082	0.86	1.04	0.11	0.784	0.038	0.28	734.5	274.5	0.87	0.52
Tarn02ru_74	65	18	0.600	0.150	0.45	1.67	0.88	1.020	0.073	0.34	-	-	-	0.10
Tarn02ru_75	247	17	2.100	0.140	0.85	0.48	0.03	0.858	0.020	0.19	-	-	-	0.74
Tarn02ru_76	38.6	3.4	0.377	0.029	0.49	2.65	0.23	0.761	0.044	0.46	275.4	132.3	0.88	0.66

Supporting Information Tables S3.4: Apatite U-Pb data

Integration	$^{207}Pb/^{235}U$	Prop2SE	$^{206}Pb/^{238}U$	Prop2SE	Rho	$^{238}U/^{206}Pb$	Prop2SE	$^{207}Pb/^{206}Pb$	Prop2SE	Rho	^{207}Pb corrected age	Prop2SE	$f^{206}Pb$	^{238}U
All apatite and rutile spots are 60um														
All UPb errors are propogated errors at the 2SE level														
For each sample grains which have passed or failed the inclusion criteria are listed separately; the inclusion criteria are as follows:														
1. For all grains with ages >65 Ma, an error of < ±25% and an absolute error of <100 Ma is required to be included in the U-Pb dataset														
2. For all grains with ages <65 Ma, an absolute error of < ±20 Ma is required to be included in the U-Pb dataset														
Many grains that failed the inclusion criteria have near-zero U-concentrations, resulting in extreme 207/235 and 206/238 ratios, negative values are removed														
f206Pb is not reported for grains with f206Pb=1; for these grains ages are not reported.														
Passed inclusion criteria														
Tarn1Aap_5	13.86	0.32	0.158	0.003	0.25	6.321	0.140	0.635	0.017	0.60	272.2	22.9	0.73	13.8
Tarn1Aap_6	16	0.47	0.182	0.004	0.51	5.504	0.130	0.634	0.016	0.37	316.5	25.1	0.72	18.0
Tarn1Aap_9	14.42	0.61	0.168	0.005	0.83	5.938	0.170	0.622	0.017	-0.19	308.8	25.1	0.71	28.6
Tarn1Aap_10	23.5	0.82	0.251	0.007	0.60	3.984	0.120	0.682	0.019	0.28	345.6	39.9	0.78	10.2
Tarn1Aap_12	20.93	0.85	0.222	0.008	0.78	4.507	0.170	0.685	0.017	0.12	296.4	33.0	0.79	23.7
Tarn1Aap_20	9.63	0.25	0.152	0.003	0.44	6.575	0.140	0.458	0.011	0.40	477.4	16.7	0.49	27.5
Tarn1Aap_23	6.26	0.16	0.097	0.002	0.52	10.309	0.190	0.468	0.010	0.22	294.7	9.8	0.52	55.3
Tarn1Aap_25	20.39	0.89	0.224	0.008	0.74	4.472	0.170	0.672	0.024	0.18	323.6	44.5	0.77	11.0
Tarn1Aap_26	20.97	0.52	0.222	0.005	0.45	4.500	0.097	0.681	0.017	0.44	304.4	32.0	0.78	13.5
Tarn1Aap_28	13.16	0.34	0.153	0.003	0.42	6.519	0.120	0.620	0.014	0.27	282.5	18.8	0.71	28.4
Tarn1Aap_37	13.06	0.35	0.156	0.003	0.59	6.402	0.130	0.605	0.013	0.18	307.1	18.0	0.69	20.1
Tarn1Aap_39	22.2	1.1	0.228	0.010	0.84	4.380	0.190	0.706	0.019	-0.02	264.6	37.6	0.82	15.3
Tarn1Aap_40	25.79	0.63	0.260	0.005	0.24	3.840	0.076	0.719	0.021	0.59	276.3	45.1	0.83	10.4
Tarn1Aap_41	43.5	1.1	0.422	0.011	0.69	2.370	0.063	0.751	0.017	0.31	356.2	60.6	0.87	7.9
Failed inclusion criteria														
Tarn1Aap_0	2150	190	18.00	1.60	0.99	0.056	0.005	0.862	0.013	0.19	-	-	-	0.4
Tarn1Aap_1	7150	770	59.80	6.40	0.97	0.017	0.002	0.866	0.019	0.10	-	-	-	0.1
Tarn1Aap_2	2570	300	21.90	2.80	0.99	0.046	0.006	0.856	0.021	0.53	-	-	-	0.1
Tarn1Aap_3	1302	46	11.08	0.40	0.89	0.090	0.003	0.853	0.016	0.31	-	-	-	0.6

Integration	$^{207}Pb/^{235}U$	Prop2SE	$^{206}Pb/^{238}U$	Prop2SE	Rho	$^{238}U/^{206}Pb$	Prop2SE	$^{207}Pb/^{206}Pb$	Prop2SE	Rho	^{207}Pb corrected age	Prop2SE	$f^{206}Pb$	^{238}U
Tarn1Aap_4	11800	1200	100.40	9.60	0.99	0.010	0.001	0.859	0.017	0.08	-	-	-	0.1
Tarn1Aap_7	-	-	-	-	-	0.024	0.005	0.873	0.032	0.00	-	-	-	0.0
Tarn1Aap_8	330	11	2.83	0.10	0.88	0.353	0.012	0.844	0.013	0.16	2172.5	303.7	0.86	2.4
Tarn1Aap_11	196.8	7	1.72	0.07	0.72	0.582	0.023	0.834	0.023	0.45	453.5	315.3	0.96	2.2
Tarn1Aap_13	1147	47	9.75	0.39	0.91	0.103	0.004	0.855	0.014	0.13	-	-	-	1.3
Tarn1Aap_14	3020	280	25.80	2.20	0.95	0.039	0.004	0.861	0.027	-0.13	-	-	-	0.1
Tarn1Aap_15	2730	190	23.10	1.50	0.95	0.043	0.003	0.868	0.022	-0.12	-	-	-	0.2
Tarn1Aap_16	21.7	1.5	0.18	0.01	0.52	5.556	0.340	0.854	0.043	0.37	-	-	-	7.1
Tarn1Aap_17	3750	180	31.90	1.40	0.96	0.031	0.002	0.852	0.012	-0.09	-	-	-	0.3
Tarn1Aap_18	2077	77	17.54	0.60	0.93	0.057	0.002	0.852	0.011	0.18	-	-	-	0.8
Tarn1Aap_19	44.7	2.1	0.41	0.02	0.07	2.433	0.100	0.798	0.038	0.30	157.4	126.7	0.94	1.4
Tarn1Aap_21	1329	74	11.29	0.66	0.92	0.089	0.005	0.861	0.024	0.24	-	-	-	0.2
Tarn1Aap_22	1401	65	11.87	0.50	0.87	0.084	0.004	0.851	0.019	0.17	-	-	-	0.5
Tarn1Aap_24	80	2.3	0.73	0.02	0.64	1.372	0.031	0.798	0.017	0.15	346.4	105.1	0.92	10.0
Tarn1Aap_27	3940	250	34.40	2.30	0.95	0.029	0.002	0.834	0.015	0.38	-	-	0.96	0.3
Tarn1Aap_29	2770	230	23.90	1.90	0.96	0.042	0.003	0.846	0.023	-0.04	-	-	-	0.1
Tarn1Aap_30	7390	650	62.30	5.30	0.98	0.016	0.001	0.855	0.015	-0.18	-	-	-	0.1
Tarn1Aap_31	14100	1500	115.00	11.00	0.98	0.009	0.001	0.861	0.022	0.06	-	-	-	0.1
Tarn1Aap_32	1021	50	9.08	0.52	0.72	0.110	0.006	0.836	0.031	0.19	-	-	-	0.6
Tarn1Aap_33	4110	700	33.90	5.50	0.97	0.029	0.007	0.873	0.029	-0.12	-	-	-	0.2
Tarn1Aap_34	843	22	7.20	0.19	0.82	0.139	0.004	0.851	0.013	0.35	-	-	-	1.5
Tarn1Aap_35	2680	160	22.10	1.20	0.93	0.045	0.003	0.870	0.018	0.10	-	-	-	0.2
Tarn1Aap_36	2720	200	21.90	1.40	0.88	0.046	0.003	0.876	0.021	-0.02	-	-	-	0.2
Tarn1Aap_38	17300	3600	146.00	30.00	1.00	0.007	0.002	0.850	0.020	0.10	-	-	-	0.0
Tarn1Aap_42	445	11	3.77	0.10	0.79	0.265	0.008	0.856	0.015	0.46	1825.7	442.2	0.91	0.1
Tarn1Aap_43	8330	660	68.60	4.90	0.98	0.015	0.001	0.864	0.015	0.14	-	-	-	2.2
Tarn1Aap_44	3390	170	28.50	1.30	0.96	0.035	0.002	0.865	0.014	0.08	-	-	-	0.2
Tarn1Aap_45	652	20	5.53	0.17	0.88	0.181	0.006	0.857	0.015	0.11	-	-	-	1.0

Supporting Information Tables S3.4: Apatite U-Pb data (continued)

Integration	$^{207}Pb/^{235}U$	Prop2SE	$^{206}Pb/^{238}U$	Prop2SE	Rho	$^{238}U/^{206}Pb$	Prop2SE	$^{207}Pb/^{206}Pb$	Prop2SE	Rho	^{207}Pb corrected age	Prop2SE	$f^{206}Pb$	^{238}U
Passed inclusion criteria														
Tarn1Bap_1	44.27	0.96	0.421	0.008	0.58	2.378	0.045	0.752	0.013	0.39	350.7	48.7	0.87	14.3
Tarn1Bap_3	32.44	0.75	0.321	0.006	0.43	3.114	0.059	0.720	0.014	0.33	347.3	39.1	0.83	14.1
Tarn1Bap_6	22.51	0.53	0.267	0.006	0.25	3.750	0.088	0.599	0.018	0.46	555.0	39.1	0.66	11.3
Tarn1Bap_8	12.22	0.37	0.157	0.004	0.19	6.365	0.150	0.559	0.011	0.06	367.7	17.2	0.63	42.4
Tarn1Bap_9	21.87	0.58	0.231	0.005	0.37	4.323	0.100	0.674	0.017	0.46	331.8	33.3	0.77	11.8
Tarn1Bap_10	17.86	0.65	0.246	0.007	0.72	4.068	0.120	0.519	0.014	-0.11	665.7	31.9	0.56	10.7
Tarn1Bap_11	5.48	0.25	0.093	0.003	0.57	10.787	0.330	0.419	0.014	0.18	317.4	14.0	0.46	22.1
Tarn1Bap_14	17.07	0.55	0.191	0.005	0.56	5.249	0.130	0.645	0.018	0.31	315.4	29.2	0.74	13.4
Tarn1Bap_16	7.85	0.18	0.111	0.002	0.41	9.042	0.160	0.508	0.011	0.39	301.4	11.6	0.57	32.0
Tarn1Bap_18	11.5	0.23	0.142	0.002	0.45	7.032	0.120	0.579	0.011	0.51	308.6	14.5	0.66	20.1
Tarn1Bap_22	15.94	0.44	0.182	0.004	0.34	5.510	0.100	0.630	0.018	0.29	322.2	27.3	0.72	9.7
Tarn1Bap_23	13.19	0.38	0.158	0.004	0.46	6.321	0.140	0.602	0.017	0.40	315.1	23.0	0.68	11.5
Tarn1Bap_24	12.22	0.67	0.149	0.005	0.85	6.711	0.230	0.578	0.015	-0.16	325.2	21.5	0.65	24.8
Tarn1Bap_25	22.69	0.44	0.238	0.005	0.43	4.209	0.086	0.681	0.016	0.70	327.5	32.3	0.78	12.5
Tarn1Bap_26	33.13	0.89	0.329	0.007	0.67	3.043	0.063	0.720	0.013	0.25	356.6	37.9	0.83	17.0
Tarn1Bap_29	28.16	0.58	0.289	0.004	0.48	3.457	0.051	0.698	0.014	0.16	364.3	34.8	0.80	13.9
Tarn1Bap_32	25.89	0.67	0.264	0.007	0.63	3.786	0.099	0.706	0.016	0.36	310.8	36.5	0.81	14.3
Tarn1Bap_35	18.02	0.61	0.201	0.005	0.66	4.970	0.120	0.638	0.014	0.31	346.1	25.2	0.73	19.5
Tarn1Bap_40	18.76	0.54	0.206	0.005	0.75	4.864	0.120	0.652	0.013	0.17	330.1	24.1	0.74	36.9
Tarn1Bap_48	26.9	1.6	0.285	0.013	0.91	3.509	0.170	0.684	0.022	-0.17	392.9	52.8	0.78	16.3
Tarn1Bap_50	34.24	0.83	0.342	0.008	0.50	2.926	0.074	0.722	0.018	0.63	367.1	51.3	0.83	8.1
Failed inclusion criteria														
Tarn1Bap_0	1383	93	11.70	0.77	0.91	0.085	0.006	0.843	0.019	0.16	-	-	-	0.3
Tarn1Bap_2	571	20	4.82	0.17	0.77	0.207	0.007	0.849	0.021	0.39	-	-	-	0.5
Tarn1Bap_4	2330	100	19.63	0.79	0.94	0.051	0.002	0.844	0.013	0.18	-	-	-	0.5
Tarn1Bap_5	68.8	1.9	0.63	0.02	0.22	1.582	0.039	0.782	0.022	0.44	391.8	112.4	0.90	3.5
Tarn1Bap_7	106.5	3.4	0.94	0.03	0.70	1.059	0.033	0.807	0.019	0.40	415.9	147.8	0.93	4.1
Tarn1Bap_12	3670	290	31.60	2.70	0.98	0.032	0.003	0.840	0.024	0.39	-	-	-	0.1

Integration	$^{207}Pb/^{235}U$	Prop2SE	$^{206}Pb/^{238}U$	Prop2SE	Rho	$^{238}U/^{206}Pb$	Prop2SE	$^{207}Pb/^{206}Pb$	Prop2SE	Rho	^{207}Pb corrected age	Prop2SE	$f^{206}Pb$	^{238}U
Tarn1Bap_13	1040	52	8.72	0.36	0.77	0.115	0.005	0.855	0.026	0.18	-	-	-	0.7
Tarn1Bap_15	151.6	5.6	1.34	0.05	0.78	0.749	0.029	0.815	0.020	0.18	669.4	210.3	0.92	4.6
Tarn1Bap_17	590	140	4.80	1.10	0.98	0.208	0.400	0.850	0.029	-0.25	-	-	-	2.0
Tarn1Bap_19	2890	550	23.80	4.80	0.99	0.042	0.015	0.861	0.027	0.04	-	-	-	0.2
Tarn1Bap_20	1063	39	8.95	0.33	0.89	0.112	0.004	0.851	0.016	0.32	-	-	-	0.5
Tarn1Bap_21	1710	150	14.50	1.30	0.98	0.069	0.007	0.846	0.014	0.02	-	-	-	0.5
Tarn1Bap_27	-	-	-	-	-	0.000	0.001	0.829	0.018	0.12	-	-	0.99	0.0
Tarn1Bap_28	1352	99	11.47	0.89	0.96	0.087	0.008	0.851	0.016	0.25	-	-	-	0.2
Tarn1Bap_30	2590	220	22.60	1.80	0.95	0.044	0.004	0.821	0.019	0.21	-	-	-	0.1
Tarn1Bap_31	464	77	3.95	0.65	0.97	0.253	0.055	0.834	0.020	-0.06	-	-	-	2.2
Tarn1Bap_33	1348	52	11.33	0.45	0.92	0.088	0.004	0.851	0.014	0.22	-	-	-	0.6
Tarn1Bap_34	956	42	8.25	0.35	0.37	0.121	0.006	0.827	0.014	0.44	564.7	1039.6	0.99	0.5
Tarn1Bap_36	2070	140	17.20	1.10	0.94	0.058	0.004	0.843	0.018	0.04	-	-	-	0.2
Tarn1Bap_37	1114	38	9.46	0.28	0.80	0.106	0.003	0.838	0.017	0.26	-	-	-	0.8
Tarn1Bap_38	440	16	3.82	0.11	0.80	0.262	0.008	0.823	0.016	0.11	2541.7	558.2	0.87	1.7
Tarn1Bap_39	2240	170	19.00	1.30	0.94	0.053	0.004	0.846	0.023	0.11	-	-	-	0.1
Tarn1Bap_41	1766	77	14.97	0.61	0.92	0.067	0.003	0.845	0.012	0.14	-	-	-	0.4
Tarn1Bap_42	1326	53	11.35	0.45	0.90	0.088	0.004	0.838	0.014	0.24	-	-	-	0.4
Tarn1Bap_43	13100	1700	112.00	15.00	0.99	0.009	0.001	0.842	0.021	0.26	-	-	-	0.1
Tarn1Bap_44	621	22	5.52	0.17	0.83	0.181	0.006	0.808	0.016	0.28	1184.1	745.1	0.96	1.0
Tarn1Bap_45	314.7	7.8	2.76	0.06	0.57	0.363	0.008	0.822	0.017	0.33	302.0	412.6	0.98	1.7
Tarn1Bap_46	1334	72	11.78	0.71	0.87	0.085	0.005	0.827	0.022	0.36	-	-	0.92	0.3
Tarn1Bap_47	1950	200	16.90	1.70	0.99	0.059	0.007	0.822	0.015	0.12	-	-	0.83	0.3
Tarn1Bap_49	681	24	5.85	0.20	0.86	0.171	0.006	0.832	0.015	0.37	2154.9	764.1	0.93	0.7
Tarn1Bap_51	3270	450	28.60	3.90	0.99	0.035	0.005	0.805	0.017	0.16	-	-	0.96	0.2
Tarn1Bap_52	2080	110	17.67	0.85	0.92	0.057	0.003	0.831	0.016	0.17	-	-	-	0.4
Tarn1Bap_53	1960	130	16.83	0.89	0.67	0.059	0.003	0.841	0.037	0.12	-	-	-	0.5
Tarn1Bap_54	5510	460	47.70	4.30	0.95	0.021	0.002	0.823	0.025	0.38	-	-	0.98	0.1

Supporting Information Tables S3.4: Apatite U-Pb data (continued)

Integration	$^{207}Pb/^{235}U$	Prop2SE	$^{206}Pb/^{238}U$	Prop2SE	Rho	$^{238}U/^{206}Pb$	Prop2SE	$^{207}Pb/^{206}Pb$	Prop2SE	Rho	^{207}Pb corrected age	Prop2SE	$f^{206}Pb$	^{238}U
Passed inclusion criteria														
Tam02ap_24	23.9	2.3	0.257	0.020	0.92	3.891	0.310	0.651	0.027	-0.46	422.4	62.8	0.74	7.2
Tam02ap_31	44.26	0.79	0.424	0.007	0.55	2.361	0.040	0.753	0.012	0.50	349.8	46.1	0.87	10.6
Tam02ap_75	31.7	1	0.320	0.009	0.71	3.123	0.092	0.714	0.016	0.29	363.3	44.0	0.82	9.5
Tam02ap_92	44.8	1.1	0.440	0.009	0.51	2.271	0.041	0.732	0.015	0.40	454.5	55.8	0.83	7.0
Failed inclusion criteria														
Tam02ap_0	1145	29	9.62	0.24	0.88	0.104	0.003	0.861	0.011	0.32	-	-	-	1.3
Tam02ap_1	2900	180	24.80	1.50	0.97	0.040	0.003	0.850	0.015	0.11	-	-	-	0.1
Tam02ap_2	1037	33	8.73	0.27	0.89	0.115	0.004	0.859	0.012	0.25	-	-	-	0.7
Tam02ap_3	7100	570	60.50	4.90	0.98	0.017	0.001	0.862	0.014	0.06	-	-	-	0.1
Tam02ap_4	3830	230	32.70	2.00	0.96	0.031	0.002	0.854	0.016	0.31	-	-	-	0.1
Tam02ap_5	2770	170	23.10	1.40	0.96	0.043	0.003	0.858	0.015	0.10	-	-	-	0.2
Tam02ap_6	32400	5400	267.00	43.00	1.00	0.004	0.001	0.872	0.015	-0.02	-	-	-	0.0
Tam02ap_7	3070	150	25.80	1.30	0.93	0.039	0.002	0.868	0.015	0.11	-	-	-	0.2
Tam02ap_8	6710	440	56.60	3.60	0.98	0.018	0.001	0.856	0.013	-0.08	-	-	-	0.1
Tam02ap_9	5080	260	42.70	2.20	0.97	0.023	0.001	0.862	0.013	0.21	-	-	-	0.2
Tam02ap_10	1307	39	10.98	0.34	0.91	0.091	0.003	0.862	0.011	0.26	-	-	-	0.7
Tam02ap_11	908	24	7.74	0.21	0.88	0.129	0.004	0.852	0.010	0.18	-	-	-	1.3
Tam02ap_12	1512	81	12.53	0.64	0.94	0.080	0.004	0.867	0.013	0.16	-	-	-	0.2
Tam02ap_13	987	79	9.10	0.64	0.95	0.110	0.009	0.782	0.026	-0.14	-	-	-	0.1
Tam02ap_14	775	27	6.54	0.22	0.86	0.153	0.005	0.859	0.016	0.33	-	-	-	0.5
Tam02ap_15	1434	49	11.99	0.39	0.91	0.083	0.003	0.859	0.012	0.27	-	-	-	0.6
Tam02ap_16	2082	78	17.39	0.63	0.93	0.058	0.002	0.867	0.011	0.14	-	-	-	0.4
Tam02ap_17	6290	470	51.30	3.20	0.98	0.019	0.001	0.863	0.015	0.17	-	-	-	0.1
Tam02ap_18	4740	330	40.70	3.00	0.96	0.025	0.002	0.856	0.018	0.12	-	-	-	0.1
Tam02ap_19	2320	100	19.75	0.96	0.93	0.051	0.002	0.854	0.016	0.35	-	-	-	0.2
Tam02ap_20	41400	7000	347.00	58.00	1.00	0.003	0.000	0.859	0.010	-0.07	-	-	-	0.0
Tam02ap_21	803	17	6.73	0.15	0.76	0.149	0.003	0.862	0.011	0.35	-	-	-	1.1
Tam02ap_22	2337	76	19.80	0.66	0.94	0.051	0.002	0.853	0.011	0.25	-	-	-	0.5

Integration	$^{207}Pb/^{235}U$	Prop2SE	$^{206}Pb/^{238}U$	Prop2SE	Rho	$^{238}U/^{206}Pb$	Prop2SE	$^{207}Pb/^{206}Pb$	Prop2SE	Rho	^{207}Pb corrected age	Prop2SE	$f^{206}Pb$	^{238}U
Tam02ap_23	1494	81	12.65	0.71	0.95	0.079	0.004	0.853	0.015	0.21	-	-	-	0.3
Tam02ap_25	516	12	4.34	0.11	0.81	0.230	0.007	0.861	0.014	0.46	-	-	-	1.2
Tam02ap_26	1381	48	11.64	0.42	0.90	0.086	0.003	0.855	0.013	0.23	-	-	-	0.6
Tam02ap_27	6040	410	50.80	3.50	0.99	0.020	0.001	0.860	0.013	0.11	-	-	-	0.1
Tam02ap_28	6720	630	56.50	5.30	0.99	0.018	0.001	0.862	0.014	-0.07	-	-	-	0.1
Tam02ap_29	1531	51	12.86	0.44	0.90	0.078	0.003	0.862	0.014	0.32	-	-	-	0.4
Tam02ap_30	1985	72	16.67	0.60	0.94	0.060	0.002	0.861	0.010	0.06	-	-	-	0.5
Tam02ap_32	802	26	6.84	0.22	0.83	0.146	0.005	0.854	0.016	0.23	-	-	-	0.5
Tam02ap_33	4490	330	37.10	2.60	0.97	0.027	0.002	0.863	0.016	0.02	-	-	-	0.1
Tam02ap_34	17300	3300	144.00	27.00	1.00	0.007	0.001	0.864	0.016	0.06	-	-	-	0.0
Tam02ap_35	4170	370	35.20	3.10	0.99	0.028	0.002	0.856	0.016	-0.08	-	-	-	0.1
Tam02ap_36	20000	3400	162.00	27.00	1.00	0.006	0.001	0.857	0.013	0.08	-	-	-	0.0
Tam02ap_37	520	14	4.39	0.11	0.79	0.228	0.006	0.853	0.014	0.31	-	-	-	1.2
Tam02ap_38	1460	41	12.19	0.31	0.82	0.082	0.002	0.861	0.014	0.15	-	-	-	0.6
Tam02ap_39	325	12	2.76	0.09	0.84	0.363	0.013	0.848	0.017	0.31	896.7	369.8	0.95	1.0
Tam02ap_40	-	-	-	-	-	0.000	0.000	0.873	0.018	0.03	-	-	-	0.0
Tam02ap_41	10040	990	84.90	8.00	0.99	0.012	0.001	0.853	0.015	0.11	-	-	-	0.1
Tam02ap_42	4690	370	38.20	2.70	0.90	0.026	0.002	0.861	0.016	-0.05	-	-	-	0.1
Tam02ap_43	1517	67	12.89	0.54	0.91	0.078	0.003	0.847	0.014	0.18	-	-	-	0.5
Tam02ap_44	1230	120	10.14	0.86	0.93	0.099	0.012	0.850	0.027	-0.02	-	-	-	0.2
Tam02ap_45	831	19	7.00	0.15	0.86	0.143	0.003	0.855	0.009	0.30	-	-	-	1.8
Tam02ap_46	6010	450	50.00	3.60	0.98	0.020	0.002	0.858	0.012	0.28	-	-	-	0.1
Tam02ap_47	686	16	5.80	0.13	0.83	0.172	0.004	0.854	0.011	0.35	-	-	-	2.2
Tam02ap_48	1890	110	15.79	0.95	0.94	0.063	0.004	0.871	0.023	0.30	-	-	-	0.1
Tam02ap_49	2040	190	17.20	1.50	0.97	0.058	0.007	0.856	0.019	0.07	-	-	-	0.3
Tam02ap_50	6570	450	57.30	4.10	0.96	0.017	0.001	0.844	0.016	0.12	-	-	-	0.1
Tam02ap_51	5710	650	46.80	4.90	0.99	0.021	0.003	0.851	0.014	-0.17	-	-	-	0.2
Tam02ap_52	1501	97	12.59	0.77	0.97	0.079	0.005	0.860	0.015	0.06	-	-	-	0.5
Tam02ap_53	3620	140	30.20	1.20	0.94	0.033	0.001	0.868	0.012	0.23	-	-	-	0.4

Supporting Information Tables S3.4: Apatite U-Pb data (continued)

Integration	$^{207}Pb/^{235}U$	Prop2SE	$^{206}Pb/^{238}U$	Prop2SE	Rho	$^{238}U/^{206}Pb$	Prop2SE	$^{207}Pb/^{206}Pb$	Prop2SE	Rho	^{207}Pb corrected age	Prop2SE	$f^{206}Pb$	^{238}U
Tam02ap_54	1383	27	11.88	0.27	0.83	0.084	0.002	0.848	0.010	0.19	-	-	-	1.0
Tam02ap_55	3430	160	29.00	1.40	0.95	0.034	0.002	0.858	0.011	0.25	-	-	-	0.2
Tam02ap_56	2290	140	19.40	1.20	0.97	0.052	0.003	0.853	0.015	0.21	-	-	-	0.2
Tam02ap_57	494	11	4.30	0.10	0.80	0.233	0.005	0.834	0.012	0.25	457.5	483.7	0.98	1.3
Tam02ap_58	968	25	8.14	0.21	0.87	0.123	0.003	0.860	0.011	0.38	-	-	-	1.2
Tam02ap_59	7820	690	66.20	5.70	0.99	0.015	0.001	0.850	0.015	-0.06	-	-	-	0.1
Tam02ap_60	503	11	4.32	0.11	0.83	0.231	0.006	0.845	0.011	0.47	-	-	-	1.3
Tam02ap_61	12800	1500	110.00	13.00	0.98	0.009	0.002	0.854	0.015	-0.07	-	-	-	0.1
Tam02ap_62	16200	2600	136.00	22.00	1.00	0.007	0.001	0.868	0.016	0.14	-	-	-	0.0
Tam02ap_63	3910	290	33.00	2.40	0.99	0.030	0.003	0.853	0.017	0.11	-	-	-	0.1
Tam02ap_64	2100	130	17.70	1.10	0.96	0.056	0.004	0.852	0.015	0.01	-	-	-	0.2
Tam02ap_65	1260	130	10.70	1.10	0.98	0.093	0.017	0.859	0.019	0.25	-	-	-	0.4
Tam02ap_66	1975	90	16.42	0.72	0.95	0.061	0.003	0.862	0.013	0.11	-	-	-	0.4
Tam02ap_67	2530	110	21.52	0.88	0.95	0.046	0.002	0.849	0.013	0.07	-	-	-	0.2
Tam02ap_68	1287	33	10.90	0.26	0.89	0.092	0.002	0.852	0.010	0.16	-	-	-	1.0
Tam02ap_69	5060	490	42.40	4.30	0.99	0.024	0.002	0.869	0.014	0.34	-	-	-	0.1
Tam02ap_70	2150	120	18.25	0.97	0.95	0.055	0.003	0.851	0.014	0.06	-	-	-	0.2
Tam02ap_71	19600	3000	162.00	25.00	0.99	0.006	0.001	0.877	0.022	0.10	-	-	-	0.0
Tam02ap_72	6860	450	57.20	3.80	0.97	0.017	0.001	0.862	0.017	0.29	-	-	-	0.1
Tam02ap_73	2660	350	23.70	3.10	1.00	0.042	0.004	0.812	0.023	0.13	-	-	0.97	0.1
Tam02ap_74	272.5	5.4	2.34	0.05	0.67	0.427	0.009	0.845	0.014	0.40	446.3	286.7	0.97	2.5
Tam02ap_76	6950	640	58.80	5.30	0.98	0.017	0.002	0.856	0.018	-0.04	-	-	-	0.1
Tam02ap_77	-	-	-	-	-	0.000	0.000	0.872	0.015	-0.05	-	-	-	0.0
Tam02ap_78	2680	170	23.00	1.40	0.96	0.043	0.003	0.845	0.016	0.10	-	-	-	0.2
Tam02ap_79	4460	230	38.70	2.40	0.97	0.026	0.002	0.856	0.013	0.18	-	-	-	0.2
Tam02ap_80	1300	120	10.75	0.91	0.96	0.093	0.009	0.854	0.021	-0.02	-	-	-	0.3
Tam02ap_81	5090	300	42.40	2.40	0.95	0.024	0.002	0.867	0.015	0.02	-	-	-	0.1
Tam02ap_82	4330	250	37.10	2.10	0.96	0.027	0.002	0.842	0.014	0.12	-	-	-	0.2
Tam02ap_83	749	30	6.37	0.23	0.91	0.157	0.006	0.849	0.014	0.16	-	-	-	0.7

Integration	$^{207}Pb/^{235}U$	Prop2SE	$^{206}Pb/^{238}U$	Prop2SE	Rho	$^{238}U/^{206}Pb$	Prop2SE	$^{207}Pb/^{206}Pb$	Prop2SE	Rho	^{207}Pb corrected age	Prop2SE	$f^{206}Pb$	^{238}U
Tam02ap_84	1820	66	15.39	0.54	0.92	0.065	0.002	0.852	0.013	0.20	-	-	-	0.3
Tam02ap_85	620	21	5.28	0.17	0.85	0.189	0.006	0.843	0.016	0.24	-	-	-	1.1
Tam02ap_86	10400	1300	86.00	10.00	1.00	0.012	0.002	0.859	0.014	-0.03	-	-	-	0.0
Tam02ap_87	1290	61	10.83	0.49	0.93	0.092	0.004	0.859	0.017	0.14	-	-	-	0.4
Tam02ap_88	3340	190	27.80	1.60	0.97	0.036	0.002	0.868	0.011	0.19	-	-	-	0.2
Tam02ap_89	6110	310	51.70	2.70	0.97	0.019	0.001	0.855	0.015	0.07	-	-	-	0.1
Tam02ap_90	5220	430	45.30	3.80	0.99	0.022	0.002	0.835	0.015	0.16	-	-	-	0.1
Tam02ap_91	1760	140	15.20	1.20	0.96	0.066	0.006	0.844	0.014	0.27	-	-	-	0.7
Tam02ap_93	4860	360	40.60	2.90	0.97	0.025	0.002	0.855	0.017	0.28	-	-	-	0.1
Tam02ap_94	2389	97	20.58	0.98	0.92	0.049	0.002	0.850	0.017	0.44	-	-	-	0.3
Tam02ap_95	393	27	3.33	0.22	0.96	0.300	0.017	0.852	0.016	0.16	1852.7	422.1	0.90	1.8
Tam02ap_96	3020	140	25.70	1.10	0.91	0.039	0.002	0.859	0.017	-0.03	-	-	-	0.3
Tam02ap_97	523	14	4.60	0.15	0.78	0.217	0.007	0.829	0.017	0.45	-	-	-	0.7
Tam02ap_98	2170	100	18.36	0.76	0.95	0.054	0.002	0.852	0.014	-0.22	-	-	-	0.3
Tam02ap_99	-	-	-	-	-	0.000	0.000	0.855	0.014	0.06	-	-	-	0.0
Tam02ap_100	1908	79	16.33	0.65	0.93	0.061	0.003	0.843	0.014	0.18	-	-	-	0.3
Tam02ap_101	2520	110	21.80	1.00	0.91	0.046	0.002	0.843	0.017	0.22	-	-	-	0.2
Tam02ap_102	1271	41	10.76	0.34	0.91	0.093	0.003	0.853	0.011	0.20	-	-	-	1.0
Tam02ap_103	1623	84	13.82	0.75	0.95	0.072	0.004	0.853	0.016	0.17	-	-	-	0.3
Tam02ap_104	3450	280	29.30	2.40	0.95	0.034	0.003	0.853	0.020	0.15	-	-	-	0.2
Tam02ap_105	2320	140	19.30	1.20	0.95	0.052	0.003	0.856	0.018	0.42	-	-	-	0.1
Tam02ap_106	2810	270	24.90	2.30	0.99	0.040	0.003	0.815	0.018	0.08	-	-	0.97	0.1
Tam02ap_107	14100	1900	122.00	17.00	0.99	0.008	0.002	0.845	0.021	0.29	-	-	-	0.0
Tam02ap_108	1970	130	17.20	1.10	0.94	0.058	0.004	0.822	0.017	0.05	-	-	0.83	0.2
Tam02ap_109	1224	32	10.35	0.25	0.81	0.097	0.002	0.853	0.012	0.20	-	-	-	0.8
Passed inclusion criteria														
Tam04ap_2	3.065	0.088	0.072	0.002	0.32	13.947	0.408	0.315	0.008	0.32	303.8	10.0	0.33	43.1
Tam04ap_3	5.69	0.18	0.097	0.003	0.32	10.363	0.311	0.435	0.013	0.31	318.4	13.8	0.48	25.0

Supporting Information Tables S3.4: Apatite U-Pb data (continued)

Integration	$^{207}Pb/^{235}U$	Prop2SE	$^{206}Pb/^{238}U$	Prop2SE	Rho	$^{238}U/^{206}Pb$	Prop2SE	$^{207}Pb/^{206}Pb$	Prop2SE	Rho	^{207}Pb corrected age	Prop2SE	$f^{206}Pb$	^{238}U
Tam04ap_4	16.77	0.74	0.189	0.008	0.83	5.294	0.224	0.652	0.016	-0.08	301.6	28.1	0.75	14.9
Tam04ap_5	43.32	0.81	0.412	0.013	0.47	2.427	0.077	0.776	0.016	0.56	247.1	57.6	0.91	5.8
Tam04ap_6	24.4	1.5	0.262	0.015	0.93	3.817	0.219	0.680	0.014	-0.12	366.8	37.3	0.78	13.3
Tam04ap_7	6.55	0.21	0.101	0.003	0.79	9.862	0.331	0.473	0.009	0.04	304.5	12.7	0.52	42.5
Tam04ap_8	28.8	1.7	0.289	0.015	0.89	3.460	0.180	0.722	0.019	-0.16	303.0	47.9	0.83	9.7
Tam04ap_9	10.71	0.29	0.137	0.004	0.55	7.310	0.224	0.569	0.013	0.34	307.6	17.6	0.64	23.0
Tam04ap_10	19.49	0.42	0.212	0.007	0.34	4.719	0.158	0.674	0.018	0.65	301.8	32.9	0.77	10.5
Tam04ap_11	27.84	0.65	0.285	0.009	0.42	3.512	0.110	0.713	0.017	0.58	320.5	41.5	0.82	10.0
Tam04ap_12	4.01	0.15	0.081	0.003	0.75	12.422	0.386	0.360	0.008	-0.22	313.0	11.1	0.38	74.6
Tam04ap_13	11.55	0.33	0.141	0.005	0.65	7.072	0.230	0.593	0.013	0.11	290.7	18.1	0.67	25.5
Tam04ap_14	16.2	0.34	0.185	0.006	0.46	5.417	0.167	0.639	0.015	0.50	314.2	25.0	0.73	16.9
Tam04ap_16	14.63	0.28	0.170	0.005	0.38	5.872	0.186	0.620	0.014	0.51	315.3	22.3	0.71	17.0
Tam04ap_17	3.913	0.093	0.078	0.002	0.55	12.853	0.397	0.364	0.008	0.23	300.0	10.6	0.39	55.3
Tam04ap_18	11.63	0.33	0.142	0.005	0.53	7.032	0.232	0.591	0.013	0.38	294.8	18.3	0.67	17.6
Tam04ap_19	14.6	0.28	0.172	0.005	0.08	5.831	0.177	0.617	0.014	0.67	321.8	22.3	0.70	16.6
Tam04ap_20	3.49	0.72	0.074	0.007	0.73	13.441	1.265	0.332	0.030	-0.41	305.4	33.2	0.35	49.1
Tam04ap_21	5.14	0.16	0.089	0.003	0.36	11.211	0.339	0.415	0.013	0.20	308.2	13.1	0.45	18.1
Tam04ap_22	8.77	0.2	0.118	0.004	0.51	8.453	0.272	0.534	0.012	0.32	298.2	15.2	0.60	23.7
Tam04ap_23	12.54	0.56	0.150	0.006	0.88	6.680	0.268	0.601	0.012	-0.36	298.7	19.4	0.68	26.9
Tam04ap_24	25.23	0.98	0.258	0.009	0.77	3.876	0.141	0.701	0.017	0.11	314.0	38.2	0.81	10.9
Tam04ap_25	7.78	0.47	0.106	0.005	0.85	9.461	0.439	0.518	0.017	-0.22	279.3	19.3	0.58	20.6
Tam04ap_26	9.88	0.25	0.126	0.004	0.39	7.918	0.232	0.556	0.012	0.38	296.5	15.4	0.63	22.3
Tam04ap_27	5.45	0.13	0.092	0.003	0.57	10.858	0.342	0.422	0.009	0.19	313.2	12.0	0.46	62.4
Tam04ap_28	21.44	0.49	0.222	0.007	0.54	4.509	0.136	0.689	0.014	0.31	288.7	28.1	0.79	12.9
Tam04ap_29	14.24	0.34	0.163	0.005	0.47	6.131	0.184	0.617	0.013	0.33	305.3	20.2	0.70	17.6
Tam04ap_30	40.6	2.3	0.387	0.019	0.87	2.584	0.127	0.741	0.019	-0.12	356.9	62.7	0.85	7.6
Tam04ap_31	35.6	1.7	0.341	0.015	0.80	2.933	0.129	0.740	0.023	0.13	310.4	64.9	0.86	4.5
Tam04ap_32	12.88	0.32	0.153	0.005	0.64	6.553	0.210	0.605	0.014	0.04	299.8	20.3	0.69	18.7
Tam04ap_33	23.14	0.63	0.238	0.008	0.69	4.196	0.139	0.690	0.014	0.35	310.2	30.3	0.79	12.8

Integration	$^{207}Pb/^{235}U$	Prop2SE	$^{206}Pb/^{238}U$	Prop2SE	Rho	$^{238}U/^{206}Pb$	Prop2SE	$^{207}Pb/^{206}Pb$	Prop2SE	Rho	^{207}Pb corrected age	Prop2SE	$f^{206}Pb$	^{238}U
Tam04ap_35	43.7	1.1	0.429	0.013	0.41	2.332	0.071	0.752	0.017	0.46	359.2	61.8	0.87	6.3
Tam04ap_36	16.47	0.46	0.192	0.006	0.71	5.198	0.167	0.634	0.012	0.25	336.3	22.6	0.72	17.5
Tam04ap_37	25.79	0.89	0.269	0.010	0.79	3.717	0.137	0.711	0.014	0.20	305.4	34.3	0.82	9.5
Tam04ap_38	7.64	0.17	0.114	0.004	0.53	8.780	0.277	0.501	0.011	0.41	316.9	14.4	0.56	33.7
Tam04ap_39	6.5	0.12	0.104	0.003	0.27	9.615	0.277	0.462	0.009	0.61	320.8	12.0	0.51	52.3
Tam04ap_40	13.29	0.4	0.165	0.005	0.30	6.079	0.181	0.599	0.015	0.20	332.3	22.5	0.68	18.8
Tam04ap_41	16.79	0.58	0.191	0.008	0.43	5.244	0.220	0.645	0.018	0.68	315.8	30.9	0.74	16.0
Tam04ap_42	12.83	0.3	0.160	0.005	0.33	6.250	0.180	0.597	0.014	0.45	325.4	20.8	0.68	22.0
Tam04ap_44	34.1	1.4	0.347	0.014	0.80	2.882	0.116	0.731	0.017	0.10	345.3	51.0	0.84	7.7
Tam04ap_45	8.67	0.52	0.123	0.006	0.91	8.137	0.404	0.521	0.016	-0.51	322.9	22.4	0.58	35.9
Tam04ap_46	25.81	0.98	0.282	0.012	0.86	3.544	0.151	0.668	0.016	-0.22	427.3	40.9	0.76	8.9
Tam04ap_47	10.66	0.66	0.138	0.007	0.72	7.257	0.369	0.571	0.026	-0.08	307.7	32.2	0.65	7.3
Tam04ap_48	5.092	0.098	0.091	0.003	0.16	10.989	0.338	0.414	0.010	0.64	315.1	12.1	0.45	47.6
Tam04ap_49	5.11	0.09	0.090	0.002	0.49	11.161	0.299	0.420	0.007	0.27	306.3	9.7	0.46	52.9
Tam04ap_50	10.64	0.27	0.135	0.004	0.50	7.396	0.224	0.577	0.013	0.37	295.1	17.2	0.65	28.2
Tam04ap_51	23.61	0.9	0.250	0.010	0.79	3.997	0.158	0.689	0.015	0.16	329.4	34.1	0.79	11.4
Tam04ap_52	9.65	0.56	0.122	0.006	0.64	8.210	0.391	0.548	0.018	-0.06	293.5	22.4	0.62	18.9
Tam04ap_53	15.94	0.33	0.175	0.005	0.24	5.705	0.169	0.635	0.015	0.57	303.3	23.7	0.73	19.9
Tam04ap_54	20.5	0.55	0.209	0.007	0.61	4.789	0.158	0.687	0.017	0.22	274.0	31.0	0.79	12.3
Tam04ap_55	35.06	0.82	0.327	0.010	0.53	3.055	0.093	0.751	0.015	0.42	263.1	43.4	0.87	10.5
Tam04ap_57	12.21	0.22	0.144	0.004	0.32	6.944	0.203	0.589	0.012	0.61	301.0	17.1	0.67	22.8
Tam04ap_58	7.28	0.16	0.102	0.003	0.33	9.766	0.286	0.496	0.012	0.40	288.5	13.2	0.55	33.2
Tam04ap_59	3.083	0.072	0.068	0.002	0.42	14.620	0.449	0.315	0.008	0.39	290.0	9.9	0.33	53.7
Tam04ap_60	20.19	0.45	0.210	0.006	0.19	4.755	0.136	0.669	0.017	0.49	308.2	30.8	0.77	10.6
Tam04ap_62	15.82	0.37	0.175	0.006	0.15	5.724	0.187	0.636	0.018	0.62	300.8	27.5	0.73	6.5
Tam04ap_65	37.3	2.5	0.355	0.023	0.93	2.817	0.183	0.741	0.017	-0.15	322.2	54.6	0.86	10.0
Tam04ap_66	12.2	0.73	0.144	0.007	0.81	6.959	0.344	0.604	0.023	-0.34	282.7	29.8	0.69	22.6
Tam04ap_67	9.8	0.37	0.127	0.005	0.79	7.880	0.298	0.545	0.014	-0.03	309.2	18.6	0.61	37.8
Tam04ap_68	13.36	0.46	0.154	0.006	0.63	6.515	0.238	0.624	0.017	0.28	277.7	23.7	0.71	11.2

Supporting Information Tables S3.4: Apatite U-Pb data (continued)

Integration	$^{207}Pb/^{235}U$	Prop2SE	$^{206}Pb/^{238}U$	Prop2SE	Rho	$^{238}U/^{206}Pb$	Prop2SE	$^{207}Pb/^{206}Pb$	Prop2SE	Rho	^{207}Pb corrected age	Prop2SE	$f^{206}Pb$	^{238}U
Tam04ap_69	21.64	0.55	0.236	0.008	0.43	4.232	0.141	0.688	0.017	0.39	311.4	34.9	0.79	10.7
Tam04ap_70	5.78	0.18	0.096	0.003	0.38	10.384	0.356	0.453	0.014	0.49	304.0	15.0	0.50	23.1
Tam04ap_71	21.2	0.55	0.234	0.008	0.68	4.270	0.146	0.682	0.014	0.16	320.4	30.0	0.78	16.8
Tam04ap_73	7.78	0.48	0.116	0.005	0.84	8.658	0.375	0.504	0.018	-0.50	318.7	21.4	0.56	33.6
Tam04ap_74	3.227	0.09	0.076	0.002	0.64	13.123	0.379	0.321	0.008	-0.18	319.6	10.3	0.33	88.1
Tam04ap_75	9.87	0.25	0.135	0.004	0.65	7.435	0.238	0.559	0.012	0.07	313.1	16.8	0.63	29.4
Tam04ap_76	17.08	0.47	0.206	0.009	0.70	4.850	0.202	0.642	0.016	0.52	348.4	30.7	0.73	20.7
Tam04ap_77	15.85	0.25	0.189	0.006	0.11	5.285	0.154	0.638	0.014	0.68	324.1	24.2	0.73	16.8
Tam04ap_79	15.13	0.52	0.182	0.006	0.70	5.510	0.194	0.629	0.014	0.31	323.7	24.1	0.72	11.6
Tam04ap_80	29.41	0.72	0.302	0.010	0.45	3.309	0.109	0.740	0.019	0.57	270.0	48.6	0.86	9.1
Tam04ap_81	9.13	0.31	0.128	0.004	0.22	7.800	0.243	0.553	0.021	0.40	304.2	23.4	0.62	23.3
Tam04ap_82	38.39	0.93	0.385	0.012	0.61	2.598	0.081	0.754	0.015	0.32	307.8	50.7	0.87	7.6
Tam04ap_83	3.59	0.1	0.076	0.002	0.71	13.089	0.394	0.351	0.008	-0.19	302.5	10.3	0.37	78.9
Tam04ap_84	4.59	0.11	0.088	0.003	0.55	11.403	0.325	0.389	0.008	0.24	321.1	10.6	0.42	44.3
Tam04ap_86	7.71	0.2	0.112	0.003	0.54	8.961	0.273	0.507	0.011	0.42	305.1	13.8	0.57	37.8
Tam04ap_87	15.35	0.34	0.178	0.005	0.25	5.634	0.171	0.633	0.015	0.51	310.3	24.1	0.72	9.9
Tam04ap_88	16.75	0.42	0.179	0.005	0.44	5.602	0.163	0.653	0.015	0.29	282.4	24.0	0.75	19.0
Tam04ap_89	21.34	0.61	0.218	0.007	0.60	4.591	0.148	0.683	0.016	0.30	294.2	30.7	0.79	16.1
Tam04ap_91	21.28	0.77	0.220	0.010	0.85	4.554	0.201	0.688	0.016	0.31	287.5	32.1	0.79	12.7
Tam04ap_92	16.78	0.45	0.184	0.006	0.37	5.447	0.166	0.646	0.017	0.45	301.7	27.3	0.74	14.4
Tam04ap_93	21.3	0.88	0.225	0.009	0.75	4.446	0.184	0.674	0.018	0.31	321.8	35.7	0.77	7.1
Tam04ap_94	15.03	0.6	0.168	0.006	0.69	5.970	0.214	0.641	0.017	0.14	280.7	25.5	0.73	16.0
Tam04ap_95	8.92	0.3	0.118	0.004	0.49	8.460	0.279	0.543	0.017	0.28	289.4	18.8	0.61	20.4
Tam04ap_96	15.89	0.46	0.179	0.006	0.53	5.590	0.172	0.644	0.015	0.20	296.5	24.2	0.74	17.5
Tam04ap_97	9.81	0.25	0.129	0.004	0.33	7.770	0.248	0.555	0.015	0.47	303.4	18.5	0.63	23.4
Tam04ap_98	10.13	0.59	0.131	0.006	0.86	7.616	0.360	0.558	0.015	-0.12	306.5	21.5	0.63	22.8
Tam04ap_99	4.95	0.1	0.086	0.002	0.50	11.574	0.322	0.419	0.008	0.25	295.7	10.0	0.46	53.9
Tam04ap_101	8.2	0.22	0.114	0.004	0.61	8.811	0.272	0.535	0.011	0.16	284.9	13.7	0.60	35.4
Tam04ap_102	36.97	0.82	0.364	0.012	0.34	2.746	0.090	0.747	0.019	0.57	311.8	58.1	0.86	6.4

Integration	$^{207}Pb/^{235}U$	Prop2SE	$^{206}Pb/^{238}U$	Prop2SE	Rho	$^{238}U/^{206}Pb$	Prop2SE	$^{207}Pb/^{206}Pb$	Prop2SE	Rho	^{207}Pb corrected age	Prop2SE	$f^{206}Pb$	^{238}U
Tam04ap_103	15.18	0.59	0.176	0.007	0.71	5.685	0.220	0.643	0.017	0.21	292.7	27.1	0.74	12.0
Tam04ap_104	20.61	0.72	0.226	0.009	0.80	4.433	0.171	0.673	0.012	0.18	324.8	26.8	0.77	13.0
Tam04ap_106	11.23	0.52	0.143	0.005	0.53	7.008	0.265	0.582	0.016	0.20	306.3	21.9	0.66	20.9
Failed inclusion criteria														
Tam04ap_0	17.06	3.4	0.19	0.05	0.08	5.291	1.372	0.671	0.042	0.81	271.6	93.4	0.77	2.2
Tam04ap_1	489	96	4.23	0.84	0.99	0.236	0.047	0.828	0.018	0.01	1962.0	721.2	0.92	1.4
Tam04ap_15	690	23	5.88	0.27	0.85	0.170	0.008	0.860	0.016	0.36	-	-	-	0.6
Tam04ap_34	3080	120	25.50	1.20	0.95	0.039	0.002	0.865	0.010	0.20	-	-	-	0.4
Tam04ap_43	5780	610	50.00	5.00	1.00	0.020	0.002	0.856	0.016	0.09	-	-	-	0.1
Tam04ap_56	1742	74	14.13	0.62	0.93	0.071	0.003	0.855	0.013	0.14	-	-	-	0.4
Tam04ap_61	2890	160	23.80	1.50	0.95	0.042	0.003	0.850	0.016	0.27	-	-	-	0.1
Tam04ap_63	253.3	5.6	2.16	0.07	0.73	0.462	0.015	0.822	0.015	0.42	2429.0	262.5	0.79	1.8
Tam04ap_64	20600	3800	167.00	32.00	0.99	0.006	0.001	0.864	0.016	0.14	-	-	-	0.0
Tam04ap_72	1190	350	11.00	3.20	0.99	0.091	0.026	0.824	0.019	0.33	-	-	0.90	1.0
Tam04ap_78	8300	680	72.80	5.70	0.97	0.014	0.001	0.848	0.016	-0.03	-	-	-	0.1
Tam04ap_85	24900	4600	210.00	38.00	1.00	0.005	0.001	0.868	0.014	0.08	-	-	-	0.0
Tam04ap_90	8490	940	69.20	7.60	0.99	0.014	0.002	0.860	0.013	-0.02	-	-	-	0.1
Tam04ap_100	2210	140	19.30	1.40	0.95	0.052	0.004	0.854	0.017	0.01	-	-	-	0.2
Tam04ap_105	97.5	3.3	0.91	0.04	0.85	1.104	0.051	0.793	0.016	0.35	555.2	121.9	0.90	4.4
Passed inclusion criteria														
Tam06ap_2	17.05	0.68	0.190	0.012	0.70	5.258	0.332	0.648	0.020	0.44	310.1	36.3	0.74	13.8
Tam06ap_4	6.01	0.18	0.096	0.005	0.46	10.395	0.573	0.449	0.013	0.46	306.7	19.5	0.49	77.0
Tam06ap_6	5.51	0.29	0.090	0.005	0.82	11.173	0.662	0.440	0.014	-0.28	291.5	19.8	0.48	51.3
Tam06ap_9	12.64	0.5	0.151	0.009	0.71	6.618	0.381	0.599	0.017	0.16	304.1	27.1	0.68	22.5
Tam06ap_10	5.56	0.25	0.099	0.006	0.49	10.101	0.582	0.406	0.017	0.19	349.3	23.8	0.44	35.1
Tam06ap_11	28.06	0.76	0.283	0.015	0.57	3.534	0.187	0.716	0.016	0.24	310.8	41.5	0.83	13.8
Tam06ap_13	7.99	0.17	0.113	0.006	0.41	8.842	0.477	0.514	0.012	0.50	302.9	19.7	0.57	30.0
Tam06ap_16	13.07	0.48	0.155	0.009	0.39	6.456	0.375	0.614	0.023	0.45	293.0	33.1	0.70	13.7

Supporting Information Tables S3.4: Apatite U-Pb data (continued)

Integration	$^{207}Pb/^{235}U$	Prop2SE	$^{206}Pb/^{238}U$	Prop2SE	Rho	$^{238}U/^{206}Pb$	Prop2SE	$^{207}Pb/^{206}Pb$	Prop2SE	Rho	^{207}Pb corrected age	Prop2SE	$f^{206}Pb$	^{238}U
Tarn06ap_17	24.36	0.58	0.257	0.014	0.30	3.897	0.213	0.689	0.018	0.49	338.7	42.0	0.79	11.4
Tarn06ap_22	11.49	0.36	0.145	0.008	0.64	6.920	0.398	0.581	0.016	0.31	311.5	25.8	0.66	36.2
Tarn06ap_23	16	1.2	0.184	0.014	0.94	5.435	0.414	0.621	0.021	-0.51	340.6	40.0	0.71	20.2
Tarn06ap_24	10.48	0.35	0.136	0.008	0.62	7.369	0.418	0.563	0.017	0.29	311.6	25.5	0.64	20.6
Tarn06ap_25	30.01	0.79	0.303	0.017	0.62	3.303	0.185	0.718	0.016	0.41	330.2	44.6	0.83	29.4
Tarn06ap_28	13.57	0.37	0.160	0.009	0.44	6.238	0.342	0.615	0.017	0.43	302.4	27.7	0.70	21.0
Tarn06ap_31	17.73	0.65	0.201	0.012	0.58	4.968	0.296	0.639	0.020	0.30	344.6	38.1	0.73	20.9
Tarn06ap_36	7.6	0.19	0.110	0.006	0.49	9.058	0.476	0.500	0.013	0.26	307.9	19.8	0.56	31.0
Tarn06ap_38	13.02	0.39	0.157	0.009	0.60	6.365	0.353	0.604	0.018	0.31	310.3	28.5	0.69	23.7
Tarn06ap_39	18.57	0.63	0.207	0.012	0.56	4.838	0.281	0.650	0.018	0.19	335.5	35.8	0.74	18.8
Tarn06ap_42	10.86	0.46	0.136	0.008	0.55	7.358	0.433	0.580	0.021	0.15	293.4	28.5	0.66	34.4
Tarn06ap_49	6.73	0.43	0.102	0.006	0.87	9.833	0.609	0.469	0.016	-0.38	308.3	22.9	0.52	47.4
Tarn06ap_50	10.71	0.49	0.139	0.008	0.81	7.184	0.413	0.554	0.018	-0.22	330.0	27.4	0.62	34.2
Tarn06ap_52	18.54	0.62	0.206	0.012	0.73	4.866	0.284	0.654	0.017	0.08	326.5	34.3	0.75	19.6
Tarn06ap_55	15.29	0.6	0.178	0.010	0.59	5.615	0.315	0.622	0.021	0.18	327.6	35.0	0.71	22.9
Tarn06ap_58	13.02	0.7	0.159	0.012	0.74	6.289	0.475	0.589	0.021	0.29	333.7	36.3	0.67	27.3
Tarn06ap_63	18.37	0.83	0.203	0.013	0.74	4.933	0.316	0.660	0.021	0.07	311.6	39.6	0.76	20.2
Tarn06ap_67	5.51	0.16	0.092	0.005	0.51	10.870	0.614	0.433	0.012	0.42	304.8	19.2	0.47	70.3
Tarn06ap_69	7.39	0.23	0.109	0.006	0.48	9.141	0.501	0.490	0.015	0.28	313.8	21.5	0.54	31.6
Tarn06ap_70	10.89	0.32	0.142	0.008	0.35	7.052	0.393	0.555	0.017	0.53	335.3	26.7	0.62	25.2
Tarn06ap_71	33.5	1.1	0.332	0.018	0.61	3.010	0.163	0.726	0.019	0.28	343.2	54.9	0.84	14.0
Tarn06ap_78	19.04	0.46	0.206	0.011	0.19	4.852	0.259	0.664	0.016	0.64	310.2	31.9	0.76	16.1
Tarn06ap_80	37	1.2	0.352	0.019	0.71	2.841	0.153	0.748	0.018	0.11	296.3	55.3	0.87	9.8
Tarn06ap_81	24.51	0.69	0.253	0.013	0.54	3.951	0.203	0.685	0.017	0.24	342.3	39.5	0.78	14.5
Tarn06ap_82	26.51	0.85	0.271	0.015	0.50	3.695	0.205	0.700	0.022	0.44	333.4	51.2	0.80	8.1
Tarn06ap_84	40.6	1.4	0.395	0.023	0.63	2.532	0.147	0.737	0.020	0.26	380.4	67.6	0.85	12.1
Tarn06ap_85	37.2	1.3	0.373	0.022	0.51	2.681	0.158	0.715	0.023	0.28	430.1	72.1	0.82	10.0
Tarn06ap_88	36.6	1.1	0.352	0.020	0.43	2.839	0.161	0.745	0.024	0.41	306.2	70.4	0.86	8.4
Tarn06ap_90	27.59	0.8	0.279	0.015	0.45	3.579	0.192	0.704	0.020	0.41	335.8	48.7	0.81	9.7

Integration	$^{207}Pb/^{235}U$	Prop2SE	$^{206}Pb/^{238}U$	Prop2SE	Rho	$^{238}U/^{206}Pb$	Prop2SE	$^{207}Pb/^{206}Pb$	Prop2SE	Rho	^{207}Pb corrected age	Prop2SE	$f^{206}Pb$	^{238}U
Tarn06ap_91	4.57	0.18	0.083	0.005	0.53	11.990	0.704	0.390	0.014	0.34	304.4	19.9	0.42	30.3
Tarn06ap_92	8.72	0.31	0.121	0.007	0.68	8.292	0.474	0.516	0.013	0.25	321.5	22.2	0.58	47.8
Failed inclusion criteria														
Tarn06ap_0	1320	64	10.96	0.75	0.84	0.091	0.006	0.866	0.024	0.30	-	-	-	0.4
Tarn06ap_1	10320	670	86.30	6.70	0.98	0.012	0.001	0.858	0.018	0.02	-	-	-	0.1
Tarn06ap_3	3410	190	29.00	2.20	0.91	0.034	0.003	0.864	0.022	0.26	-	-	-	0.2
Tarn06ap_5	1108	91	9.39	0.92	0.89	0.106	0.010	0.846	0.022	0.23	-	-	-	0.9
Tarn06ap_7	-	-	-	-	-	0.004	0.001	0.861	0.029	0.02	-	-	-	0.0
Tarn06ap_8	55	1.7	0.51	0.03	0.74	1.972	0.117	0.787	0.021	-0.06	264.2	89.7	0.92	4.9
Tarn06ap_12	64.9	2.4	0.61	0.04	0.68	1.650	0.098	0.772	0.022	0.21	434.1	109.4	0.89	3.8
Tarn06ap_14	566	35	4.81	0.39	0.97	0.208	0.017	0.851	0.012	0.07	-	-	-	2.1
Tarn06ap_15	1681	52	14.47	0.87	0.85	0.069	0.004	0.842	0.015	0.45	-	-	-	0.8
Tarn06ap_18	965	68	8.24	0.68	0.90	0.121	0.010	0.847	0.024	-0.02	-	-	-	0.8
Tarn06ap_19	4330	230	36.30	2.60	0.87	0.028	0.002	0.868	0.024	0.26	-	-	-	0.2
Tarn06ap_20	1212	72	10.36	0.78	0.90	0.097	0.007	0.855	0.023	0.00	-	-	-	0.6
Tarn06ap_21	4040	260	34.20	3.00	0.93	0.029	0.003	0.865	0.024	0.36	-	-	-	0.1
Tarn06ap_26	1337	78	11.50	0.84	0.93	0.087	0.006	0.841	0.022	0.14	-	-	-	0.3
Tarn06ap_27	1880	160	16.20	1.60	0.98	0.062	0.006	0.840	0.018	0.00	-	-	-	0.3
Tarn06ap_29	314	10	2.68	0.15	0.63	0.373	0.021	0.851	0.023	0.34	-	-	-	1.9
Tarn06ap_30	4410	450	36.30	3.80	0.95	0.028	0.003	0.863	0.026	0.09	-	-	-	0.1
Tarn06ap_32	3580	320	29.50	3.00	0.95	0.034	0.003	0.867	0.029	0.09	-	-	-	0.1
Tarn06ap_33	1510	270	12.80	2.40	1.00	0.078	0.015	0.845	0.012	-0.18	-	-	-	1.6
Tarn06ap_34	1860	93	16.01	1.10	0.91	0.062	0.004	0.844	0.016	0.17	-	-	-	0.3
Tarn06ap_35	149.3	4.9	1.32	0.08	0.58	0.755	0.044	0.818	0.021	0.36	577.7	221.7	0.93	3.9
Tarn06ap_37	651	23	5.52	0.32	0.78	0.181	0.011	0.848	0.019	0.22	-	-	-	1.5
Tarn06ap_40	5640	430	46.80	4.20	0.93	0.021	0.002	0.871	0.024	0.16	-	-	-	0.2
Tarn06ap_41	24100	3700	205.00	33.00	0.99	0.005	0.001	0.852	0.022	0.24	-	-	-	0.0
Tarn06ap_43	4680	280	39.60	2.80	0.93	0.025	0.002	0.847	0.024	0.18	-	-	-	0.2
Tarn06ap_44	6860	480	57.60	4.70	0.93	0.017	0.001	0.864	0.026	-0.10	-	-	-	0.1

Supporting Information Tables S3.4: Apatite U-Pb data (continued)

Integration	$^{207}Pb/^{235}U$	Prop2SE	$^{206}Pb/^{238}U$	Prop2SE	Rho	$^{238}U/^{206}Pb$	Prop2SE	$^{207}Pb/^{206}Pb$	Prop2SE	Rho	^{207}Pb corrected age	Prop2SE	$f^{206}Pb$	^{238}U
Tam06ap_45	3210	410	26.40	3.20	0.97	0.038	0.005	0.841	0.017	-0.08	-	-	-	0.5
Tam06ap_46	19700	3300	167.00	29.00	1.00	0.006	0.001	0.861	0.020	0.13	-	-	-	0.0
Tam06ap_47	5710	490	48.30	4.60	0.99	0.021	0.002	0.837	0.012	0.12	-	-	-	0.4
Tam06ap_48	1856	88	15.41	0.96	0.81	0.065	0.004	0.861	0.023	0.08	-	-	-	0.5
Tam06ap_51	790	54	6.70	0.55	0.84	0.149	0.012	0.854	0.034	0.18	-	-	-	1.1
Tam06ap_53	1048	41	8.92	0.56	0.77	0.112	0.007	0.852	0.024	0.32	-	-	-	1.2
Tam06ap_54	2940	180	24.70	1.80	0.77	0.040	0.003	0.863	0.035	0.11	-	-	-	0.3
Tam06ap_56	5730	520	48.30	5.40	0.95	0.021	0.002	0.871	0.034	0.25	-	-	-	0.1
Tam06ap_57	1880	570	15.80	4.70	0.98	0.063	0.019	0.849	0.035	-0.13	-	-	-	1.9
Tam06ap_59	1080	36	9.32	0.56	0.87	0.107	0.006	0.836	0.016	0.12	-	-	-	0.5
Tam06ap_60	1471	80	12.57	0.89	0.88	0.080	0.006	0.845	0.021	0.16	-	-	-	0.4
Tam06ap_61	1774	79	15.08	0.98	0.81	0.066	0.004	0.858	0.025	0.23	-	-	-	0.6
Tam06ap_62	801	33	6.85	0.42	0.58	0.146	0.009	0.840	0.029	0.27	-	-	-	1.4
Tam06ap_64	3310	200	28.80	2.20	0.97	0.035	0.003	0.828	0.017	0.16	-	-	0.85	0.1
Tam06ap_65	2990	170	25.40	1.80	0.95	0.039	0.003	0.836	0.016	0.09	-	-	-	0.2
Tam06ap_66	4020	280	33.70	2.80	0.96	0.030	0.002	0.852	0.016	0.12	-	-	-	0.1
Tam06ap_68	252	32	2.25	0.32	0.95	0.444	0.063	0.835	0.025	0.08	1440.1	440.6	0.89	2.3
Tam06ap_72	793	27	6.86	0.41	0.72	0.146	0.009	0.834	0.021	0.36	1478.8	1128.0	0.96	1.5
Tam06ap_73	8700	1500	74.00	14.00	1.00	0.014	0.003	0.855	0.029	0.24	-	-	-	0.1
Tam06ap_74	2050	150	16.80	1.30	0.93	0.060	0.005	0.848	0.024	0.08	-	-	-	0.2
Tam06ap_75	130.5	5.3	1.17	0.07	0.62	0.856	0.054	0.809	0.029	0.42	600.4	260.2	0.92	2.2
Tam06ap_76	313	22	2.73	0.25	0.94	0.366	0.034	0.822	0.017	0.21	299.0	409.3	0.98	1.9
Tam06ap_77	257.1	9	2.24	0.13	0.42	0.447	0.026	0.833	0.030	0.49	1607.0	465.6	0.87	1.7
Tam06ap_79	81.1	3.2	0.74	0.05	0.41	1.350	0.086	0.787	0.033	0.53	451.8	191.0	0.90	1.1
Tam06ap_83	1216	50	10.21	0.63	0.80	0.098	0.006	0.852	0.020	0.30	-	-	-	0.8
Tam06ap_86	1660	110	13.78	1.10	0.90	0.073	0.006	0.860	0.029	0.22	-	-	-	0.3
Tam06ap_87	1842	88	15.49	1.10	0.87	0.065	0.005	0.851	0.021	0.22	-	-	-	0.3
Tam06ap_89	1603	98	13.43	0.99	0.85	0.074	0.005	0.853	0.027	0.11	-	-	-	0.3
Tam06ap_93	88.9	4.8	0.82	0.05	0.69	1.225	0.081	0.777	0.034	0.25	624.2	211.5	0.88	3.7

Integration	$^{207}Pb/^{235}U$	Prop2SE	$^{206}Pb/^{238}U$	Prop2SE	Rho	$^{238}U/^{206}Pb$	Prop2SE	$^{207}Pb/^{206}Pb$	Prop2SE	Rho	^{207}Pb corrected age	Prop2SE	$f^{206}Pb$	^{238}U
Tam06ap_94	1450	120	12.20	1.20	0.95	0.082	0.008	0.849	0.027	0.16	-	-	-	0.3
Tam06ap_95	3590	250	30.20	2.70	0.97	0.033	0.003	0.854	0.014	0.23	-	-	-	0.2
Tam06ap_96	593	17	5.04	0.28	0.74	0.198	0.011	0.843	0.017	0.22	-	-	-	1.3
Passed inclusion criteria														
Tam07ap_0	59.8	2	0.593	0.041	0.87	1.686	0.117	0.725	0.016	0.37	704.1	88.5	0.81	6.8
Tam07ap_2	15.91	0.35	0.180	0.011	0.60	5.552	0.339	0.633	0.012	0.42	315.1	26.6	0.72	23.1
Tam07ap_4	16.61	0.42	0.186	0.012	0.37	5.385	0.348	0.642	0.017	0.46	311.6	32.7	0.73	17.9
Tam07ap_7	25.54	0.72	0.270	0.017	0.46	3.702	0.233	0.678	0.019	0.45	384.0	47.7	0.77	19.1
Tam07ap_8	7.2	0.17	0.107	0.007	0.41	9.320	0.565	0.480	0.011	0.26	316.2	21.3	0.53	42.4
Tam07ap_9	3.99	0.14	0.036	0.002	0.17	28.169	1.904	0.819	0.038	0.66	4.9	11.3	0.98	14.0
Tam07ap_10	16.87	0.4	0.189	0.012	0.38	5.280	0.335	0.640	0.017	0.56	321.3	33.1	0.73	15.5
Tam07ap_11	9.63	0.24	0.126	0.008	0.53	7.924	0.483	0.548	0.013	0.25	304.4	22.8	0.62	30.0
Tam07ap_12	6.92	0.23	0.137	0.009	0.52	7.315	0.455	0.362	0.010	0.11	529.7	33.9	0.37	28.4
Tam07ap_14	14.81	0.75	0.172	0.012	0.54	5.811	0.405	0.620	0.027	0.14	318.8	42.7	0.71	24.8
Tam07ap_15	13.02	0.57	0.151	0.010	0.53	6.609	0.437	0.615	0.018	0.11	284.7	29.0	0.70	23.2
Tam07ap_16	7.35	0.24	0.107	0.007	0.60	9.320	0.599	0.492	0.013	0.22	305.9	22.5	0.55	33.8
Tam07ap_21	8.25	0.22	0.112	0.007	0.45	8.961	0.562	0.535	0.016	0.38	280.0	22.6	0.60	31.0
Tam07ap_23	21.55	0.57	0.226	0.014	0.51	4.433	0.275	0.685	0.017	0.35	301.8	36.8	0.79	14.8
Tam07ap_24	19.3	0.48	0.208	0.013	0.40	4.817	0.302	0.667	0.017	0.42	307.4	34.8	0.76	14.5
Tam07ap_25	32.5	1	0.317	0.020	0.71	3.153	0.199	0.735	0.017	0.23	299.8	49.0	0.85	10.3
Tam07ap_28	3.81	0.10	0.081	0.005	0.12	12.376	0.751	0.338	0.010	0.49	327.6	20.5	0.35	66.6
Tam07ap_29	6.43	0.21	0.097	0.006	0.45	10.267	0.664	0.474	0.015	0.37	291.3	22.0	0.53	38.9
Tam07ap_30	28.6	1.5	0.278	0.021	0.78	3.597	0.272	0.739	0.025	0.23	248.0	59.4	0.86	12.2
Tam07ap_33	21.18	0.41	0.222	0.014	0.39	4.515	0.285	0.687	0.015	0.55	292.1	33.6	0.79	17.6
Tam07ap_34	4.02	0.18	0.077	0.005	0.61	13.004	0.846	0.372	0.013	-0.06	291.5	20.3	0.40	51.1
Tam07ap_35	22.41	0.7	0.234	0.015	0.61	4.270	0.273	0.687	0.017	0.23	310.4	38.4	0.79	14.7
Tam07ap_36	41.1	1	0.398	0.025	0.53	2.515	0.158	0.737	0.017	0.41	383.4	60.8	0.85	6.9
Tam07ap_37	11.83	0.28	0.143	0.009	0.57	6.974	0.433	0.589	0.013	0.40	299.7	24.2	0.67	24.2

Supporting Information Tables S3.4: Apatite U-Pb data (continued)

Integration	$^{207}Pb/^{235}U$	Prop2SE	$^{206}Pb/^{238}U$	Prop2SE	Rho	$^{238}U/^{206}Pb$	Prop2SE	$^{207}Pb/^{206}Pb$	Prop2SE	Rho	^{207}Pb corrected age	Prop2SE	$f^{206}Pb$	^{238}U
Tarn07ap_40	27.43	0.71	0.278	0.017	0.48	3.597	0.220	0.705	0.018	0.40	331.5	45.8	0.81	12.3
Tarn07ap_41	40.7	1.1	0.383	0.024	0.65	2.610	0.164	0.757	0.016	0.26	295.3	55.4	0.88	11.7
Tarn07ap_43	9.48	0.86	0.107	0.009	0.90	9.337	0.758	0.623	0.029	-0.48	191.9	29.4	0.72	54.0
Tarn07ap_46	13.36	0.42	0.161	0.010	0.55	6.223	0.387	0.596	0.017	0.29	328.2	29.9	0.67	19.9
Tarn07ap_47	46.2	1.1	0.444	0.028	0.36	2.252	0.142	0.745	0.021	0.60	404.6	79.0	0.85	5.3
Tarn07ap_49	7.47	0.24	0.113	0.007	0.40	8.865	0.582	0.477	0.015	0.32	335.3	25.5	0.53	31.8
Tarn07ap_50	54.8	3.3	0.498	0.037	0.96	2.008	0.149	0.775	0.018	-0.19	319.0	78.6	0.90	9.5
Tarn07ap_51	18.87	0.47	0.205	0.013	0.49	4.873	0.309	0.658	0.017	0.49	319.1	34.9	0.75	16.1
Tarn07ap_53	4.95	0.17	0.090	0.006	0.37	11.062	0.722	0.389	0.013	0.36	330.8	23.2	0.42	23.9
Tarn07ap_56	5.84	0.21	0.093	0.006	0.66	10.707	0.688	0.447	0.012	0.12	299.2	21.0	0.49	50.4
Tarn07ap_58	21.1	1	0.227	0.016	0.84	4.403	0.310	0.669	0.021	0.19	334.9	44.8	0.77	10.0
Tarn07ap_59	36.5	1.4	0.358	0.025	0.56	2.793	0.195	0.734	0.022	0.33	348.3	67.9	0.84	7.3
Tarn07ap_61	10.56	0.55	0.134	0.009	0.75	7.468	0.508	0.559	0.019	-0.02	311.7	29.2	0.63	40.3
Tarn07ap_66	43	1.1	0.411	0.025	0.47	2.434	0.148	0.751	0.018	0.35	344.7	64.7	0.87	14.0
Tarn07ap_70	13.9	0.42	0.196	0.012	0.59	5.112	0.314	0.509	0.013	0.28	539.8	38.1	0.55	16.4
Tarn07ap_72	21.11	0.49	0.234	0.015	0.29	4.277	0.274	0.648	0.016	0.41	387.0	39.1	0.74	12.3
Tarn07ap_82	16.04	0.43	0.184	0.012	0.56	5.435	0.354	0.628	0.015	0.30	329.9	31.2	0.71	21.9
Tarn07ap_83	4.17	0.17	0.038	0.003	0.00	26.455	1.820	0.807	0.041	0.72	9.0	12.9	0.96	13.8
Tarn07ap_85	2.41	0.1	0.070	0.005	0.31	14.306	0.941	0.248	0.010	0.31	332.7	22.2	0.24	25.8
Tarn07ap_86	8.7	0.29	0.117	0.008	0.53	8.525	0.545	0.536	0.017	0.22	293.7	24.5	0.60	38.2
Tarn07ap_93	25.91	0.77	0.259	0.017	0.60	3.860	0.253	0.715	0.018	0.39	283.9	42.9	0.83	10.7
Tarn07ap_96	7.82	0.2	0.110	0.007	0.45	9.083	0.561	0.507	0.012	0.40	300.9	21.4	0.57	31.2
Tarn07ap_97	11.15	0.25	0.142	0.009	0.33	7.067	0.435	0.569	0.015	0.54	318.5	26.0	0.64	34.5
Tarn07ap_98	13.22	0.51	0.150	0.010	0.68	6.684	0.447	0.635	0.018	0.30	256.7	27.9	0.73	27.1
Tarn07ap_100	17.17	0.46	0.192	0.012	0.49	5.200	0.325	0.642	0.017	0.49	323.4	33.4	0.73	22.0
Tarn07ap_101	16.76	0.54	0.190	0.012	0.59	5.258	0.332	0.628	0.017	0.26	341.7	33.8	0.71	28.5
Tarn07ap_102	3.274	0.085	0.116	0.007	0.45	8.628	0.529	0.203	0.005	0.27	587.9	35.4	0.18	50.4
Tarn07ap_103	6.82	0.15	0.101	0.006	0.24	9.940	0.623	0.487	0.012	0.66	290.5	20.5	0.54	41.7
Tarn07ap_107	26.31	0.78	0.269	0.018	0.68	3.716	0.249	0.701	0.017	0.44	329.0	43.7	0.81	16.2

Integration	$^{207}Pb/^{235}U$	Prop2SE	$^{206}Pb/^{238}U$	Prop2SE	Rho	$^{238}U/^{206}Pb$	Prop2SE	$^{207}Pb/^{206}Pb$	Prop2SE	Rho	^{207}Pb corrected age	Prop2SE	$f^{206}Pb$	^{238}U
Failed inclusion criteria														
Tarn07ap_1	990	33	8.43	0.56	0.86	0.119	0.008	0.835	0.014	0.36	1003.9	1019.7	0.98	0.7
Tarn07ap_3	1277	56	10.73	0.83	0.92	0.093	0.007	0.864	0.017	0.42	-	-	-	0.3
Tarn07ap_5	907	80	7.75	0.79	0.97	0.129	0.013	0.832	0.015	-0.11	-	-	0.90	0.8
Tarn07ap_6	1329	56	11.25	0.82	0.92	0.089	0.006	0.856	0.016	0.05	-	-	-	0.4
Tarn07ap_13	4590	530	38.90	5.00	0.98	0.026	0.003	0.851	0.028	0.21	-	-	-	0.1
Tarn07ap_17	464	29	3.98	0.32	0.93	0.251	0.020	0.834	0.022	-0.08	160.1	748.8	0.99	0.8
Tarn07ap_18	2750	170	23.50	2.00	0.94	0.043	0.004	0.837	0.018	0.19	-	-	-	0.2
Tarn07ap_19	56	4.4	0.51	0.05	0.93	1.965	0.185	0.786	0.023	-0.06	270.9	99.3	0.92	7.1
Tarn07ap_20	339	12	2.88	0.21	0.85	0.347	0.025	0.848	0.018	0.38	1320.5	398.5	0.92	1.6
Tarn07ap_22	33.5	2.2	0.35	0.03	0.47	2.833	0.233	0.676	0.041	0.32	525.0	116.7	0.76	1.2
Tarn07ap_26	992	53	8.53	0.69	0.88	0.117	0.009	0.832	0.020	0.26	-	-	0.88	0.3
Tarn07ap_27	1152	43	9.61	0.66	0.83	0.104	0.007	0.860	0.020	0.23	-	-	-	0.5
Tarn07ap_31	2210	120	18.25	1.40	0.95	0.055	0.004	0.858	0.014	0.11	-	-	-	0.3
Tarn07ap_32	2690	180	22.60	2.00	0.97	0.044	0.004	0.850	0.017	0.16	-	-	-	0.2
Tarn07ap_38	3490	270	28.30	2.60	0.93	0.035	0.003	0.859	0.022	0.23	-	-	-	0.1
Tarn07ap_39	719	57	6.18	0.62	0.97	0.162	0.016	0.847	0.016	0.01	-	-	-	1.2
Tarn07ap_42	960	100	8.31	1.00	0.95	0.120	0.014	0.844	0.023	0.34	-	-	-	0.2
Tarn07ap_44	303	31	2.56	0.29	0.97	0.391	0.044	0.845	0.021	0.05	951.7	418.3	0.94	2.4
Tarn07ap_45	1192	63	9.89	0.72	0.84	0.101	0.007	0.853	0.021	0.03	-	-	-	0.3
Tarn07ap_48	343.2	9	2.89	0.18	0.71	0.346	0.022	0.851	0.016	0.30	489.9	390.0	0.97	2.3
Tarn07ap_52	532	33	4.37	0.35	0.86	0.229	0.018	0.863	0.025	0.06	-	-	-	3.1
Tarn07ap_54	9370	950	75.60	7.80	0.95	0.013	0.001	0.863	0.030	0.08	-	-	-	0.1
Tarn07ap_55	480	30	4.17	0.35	0.79	0.240	0.020	0.816	0.033	0.40	-	-	0.81	0.3
Tarn07ap_57	1755	83	14.78	1.10	0.87	0.068	0.005	0.843	0.020	0.11	-	-	-	0.5
Tarn07ap_60	-	-	-	-	-	0.000	0.000	0.845	0.036	0.07	-	-	-	0.0
Tarn07ap_62	1322	56	11.03	0.78	0.89	0.091	0.006	0.858	0.017	0.17	-	-	-	0.4
Tarn07ap_63	6220	500	52.20	5.30	0.98	0.019	0.002	0.853	0.016	0.40	-	-	-	0.2
Tarn07ap_64	2500	230	20.70	2.10	0.93	0.048	0.005	0.860	0.027	-0.05	-	-	-	0.2

Supporting Information Tables S3.4: Apatite U-Pb data (continued)

Integration	$^{207}Pb/^{235}U$	Prop2SE	$^{206}Pb/^{238}U$	Prop2SE	Rho	$^{238}U/^{206}Pb$	Prop2SE	$^{207}Pb/^{206}Pb$	Prop2SE	Rho	^{207}Pb corrected age	Prop2SE	$f^{206}Pb$	^{238}U
Tam07ap_65	2210	110	18.41	1.40	0.91	0.054	0.004	0.858	0.017	0.04	-	-	-	0.2
Tam07ap_67	1975	90	16.51	1.20	0.93	0.061	0.004	0.858	0.015	0.31	-	-	-	0.4
Tam07ap_68	775	44	6.52	0.51	0.95	0.153	0.012	0.849	0.014	-0.01	-	-	-	1.5
Tam07ap_69	2150	150	18.30	1.60	0.92	0.055	0.005	0.851	0.020	0.15	-	-	-	0.2
Tam07ap_71	1890	140	15.80	1.50	0.94	0.063	0.006	0.851	0.021	0.21	-	-	-	0.2
Tam07ap_73	4900	1100	39.80	8.80	1.00	0.025	0.006	0.867	0.025	0.06	-	-	-	0.1
Tam07ap_74	3240	370	26.30	3.20	0.98	0.038	0.005	0.865	0.019	0.06	-	-	-	0.2
Tam07ap_75	1023	38	8.62	0.58	0.86	0.116	0.008	0.844	0.017	0.12	-	-	-	0.6
Tam07ap_76	2490	210	21.20	2.10	0.97	0.047	0.005	0.835	0.017	-0.03	106.6	3241.9	1.00	0.2
Tam07ap_77	35.4	2.4	0.34	0.03	0.86	2.959	0.254	0.750	0.025	0.02	276.3	72.3	0.87	6.9
Tam07ap_78	2270	130	19.30	1.60	0.91	0.052	0.004	0.839	0.018	0.15	-	-	-	0.2
Tam07ap_79	721	28	6.09	0.41	0.81	0.164	0.011	0.848	0.019	0.16	-	-	-	1.1
Tam07ap_80	1770	69	14.80	1.00	0.90	0.068	0.005	0.850	0.014	0.18	-	-	-	0.5
Tam07ap_81	330.2	8.5	2.81	0.18	0.88	0.355	0.023	0.839	0.013	-0.08	-	-	0.80	1.7
Tam07ap_84	4290	200	35.80	2.70	0.91	0.028	0.002	0.863	0.019	0.20	-	-	-	0.2
Tam07ap_87	2530	180	21.60	2.10	0.92	0.046	0.005	0.862	0.020	0.29	-	-	-	0.1
Tam07ap_88	1260	450	10.40	3.70	0.99	0.096	0.034	0.858	0.021	-0.06	-	-	-	1.6
Tam07ap_89	2290	150	19.50	1.70	0.95	0.051	0.004	0.846	0.019	-0.05	-	-	-	0.2
Tam07ap_90	1600	100	13.68	1.30	0.96	0.073	0.007	0.841	0.023	0.28	-	-	-	0.4
Tam07ap_91	2530	160	21.20	1.80	0.93	0.047	0.004	0.855	0.020	0.03	-	-	-	0.2
Tam07ap_92	880	30	7.34	0.48	0.79	0.136	0.009	0.854	0.019	0.20	-	-	-	1.1
Tam07ap_94	20200	2900	175.00	28.00	0.99	0.006	0.001	0.849	0.012	0.17	-	-	-	0.8
Tam07ap_95	4800	400	41.30	4.40	0.96	0.024	0.003	0.852	0.021	0.15	-	-	-	0.1
Tam07ap_99	638	32	5.46	0.43	0.96	0.183	0.014	0.837	0.012	0.25	-	-	-	2.6
Tam07ap_104	163	6.2	1.40	0.09	0.63	0.713	0.047	0.832	0.024	0.14	251.8	277.3	0.97	3.1
Tam07ap_105	340.3	9.2	2.86	0.19	0.65	0.350	0.023	0.856	0.020	0.48	-	-	-	1.9
Tam07ap_106	1040	51	8.73	0.65	0.90	0.115	0.009	0.844	0.019	0.15	-	-	-	0.4

Passed inclusion criteria

Integration	$^{207}Pb/^{235}U$	Prop2SE	$^{206}Pb/^{238}U$	Prop2SE	Rho	$^{238}U/^{206}Pb$	Prop2SE	$^{207}Pb/^{206}Pb$	Prop2SE	Rho	^{207}Pb corrected age	Prop2SE	$f^{206}Pb$	^{238}U
Tam08ap_1	22.69	0.98	0.250	0.009	0.09	4.000	0.140	0.651	0.025	0.28	409.9	51.0	0.74	7.8
Tam08ap_6	15.7	1.5	0.172	0.013	0.85	5.814	0.450	0.652	0.032	-0.04	273.0	48.1	0.75	33.1
Tam08ap_8	18.33	0.99	0.199	0.007	0.95	5.018	0.200	0.654	0.016	-0.01	316.0	28.9	0.75	17.6
Tam08ap_10	11.33	0.3	0.145	0.003	0.28	6.920	0.140	0.568	0.017	0.45	326.7	20.7	0.64	16.2
Tam08ap_14	11.42	0.33	0.139	0.003	0.20	7.210	0.180	0.594	0.021	0.54	283.8	24.3	0.68	12.8
Tam08ap_17	35.03	0.96	0.357	0.008	0.56	2.801	0.069	0.706	0.017	0.38	437.4	50.4	0.80	12.7
Tam08ap_18	36.88	0.81	0.355	0.008	0.44	2.814	0.063	0.749	0.018	0.58	296.4	53.9	0.87	13.7
Tam08ap_22	16.23	0.67	0.183	0.007	0.54	5.464	0.200	0.642	0.025	0.40	306.8	38.1	0.73	15.3
Tam08ap_32	23.15	0.77	0.245	0.007	0.03	4.087	0.120	0.674	0.023	0.27	352.8	45.8	0.77	12.7
Tam08ap_33	6.86	0.16	0.101	0.002	0.17	9.950	0.210	0.495	0.014	0.58	283.8	12.8	0.55	33.7
Tam08ap_34	8.85	0.37	0.118	0.005	0.32	8.503	0.410	0.545	0.026	0.67	286.0	27.2	0.61	13.1
Tam08ap_40	9.8	0.25	0.122	0.003	0.36	8.177	0.190	0.580	0.015	0.51	263.1	16.4	0.66	19.2
Tam08ap_45	24.41	0.74	0.251	0.007	0.44	3.982	0.110	0.702	0.021	0.54	302.5	43.7	0.81	11.3
Tam08ap_46	10.78	0.28	0.139	0.003	0.41	7.205	0.170	0.560	0.015	0.40	322.3	18.6	0.63	24.4
Tam08ap_47	40.5	1.2	0.397	0.011	0.17	2.519	0.068	0.739	0.028	0.59	375.3	88.2	0.85	5.4
Tam08ap_50	12.64	0.36	0.153	0.003	0.41	6.549	0.130	0.590	0.015	0.34	318.7	19.8	0.67	19.2
Tam08ap_55	18.65	0.53	0.206	0.005	0.47	4.845	0.130	0.651	0.020	0.39	333.2	34.3	0.74	17.1
Tam08ap_62	9.37	0.39	0.127	0.003	0.37	7.886	0.220	0.531	0.022	0.25	323.2	23.5	0.59	14.3
Tam08ap_66	11.27	0.27	0.137	0.003	0.09	7.278	0.140	0.590	0.018	0.56	285.6	20.9	0.67	22.0
Tam08ap_69	3.12	0.14	0.068	0.002	0.65	14.815	0.450	0.331	0.011	-0.04	277.6	10.4	0.35	66.9
Tam08ap_70	30.39	0.91	0.325	0.009	0.26	3.080	0.081	0.669	0.023	0.54	497.0	59.3	0.75	12.3
Tam08ap_75	37.6	1.5	0.358	0.014	0.64	2.793	0.110	0.748	0.024	0.47	302.2	70.4	0.87	3.7
Tam08ap_76	16.04	0.69	0.177	0.006	0.37	5.650	0.200	0.647	0.028	0.38	288.8	40.7	0.74	13.7
Tam08ap_80	18.43	0.52	0.201	0.006	0.38	4.985	0.150	0.657	0.022	0.52	313.1	36.5	0.75	7.7
Tam08ap_82	10.3	1	0.131	0.010	0.94	7.634	0.820	0.544	0.025	-0.59	320.6	35.3	0.61	25.1
Tam08ap_83	45.4	1.1	0.435	0.010	0.61	2.299	0.056	0.751	0.017	0.48	369.7	62.1	0.86	9.6
Tam08ap_85	15.99	0.33	0.180	0.003	0.23	5.571	0.110	0.638	0.015	0.58	306.5	23.2	0.73	20.2
Tam08ap_92	36	1.2	0.357	0.010	0.22	2.803	0.079	0.723	0.027	0.50	382.7	76.6	0.83	5.2
Tam08ap_94	7.94	0.38	0.112	0.004	0.62	8.897	0.310	0.505	0.019	0.26	309.1	19.9	0.56	18.7

Supporting Information Tables S3.4: Apatite U-Pb data (continued)

Integration	$^{207}Pb/^{235}U$	Prop2SE	$^{206}Pb/^{238}U$	Prop2SE	Rho	$^{238}U/^{206}Pb$	Prop2SE	$^{207}Pb/^{206}Pb$	Prop2SE	Rho	^{207}Pb corrected age	Prop2SE	$f^{206}Pb$	^{238}U
Failed inclusion criteria														
Tam08ap_0	2840	180	23.60	1.50	0.98	0.042	0.003	0.868	0.013	0.05	-	-	-	0.3
Tam08ap_2	968	48	8.05	0.36	0.93	0.124	0.006	0.862	0.015	-0.05	-	-	-	0.9
Tam08ap_3	1120	96	9.55	0.80	0.95	0.105	0.009	0.844	0.026	0.06	-	-	-	0.4
Tam08ap_4	467	28	4.01	0.25	0.83	0.249	0.016	0.840	0.030	0.39	-	-	-	0.7
Tam08ap_5	950	58	8.12	0.50	0.87	0.123	0.008	0.846	0.029	0.22	-	-	-	0.4
Tam08ap_7	729	59	6.34	0.51	0.97	0.158	0.012	0.827	0.019	-0.05	-	-	0.84	0.8
Tam08ap_9	-	-	-	-	-	0.000	0.001	0.863	0.023	0.04	-	-	-	0.0
Tam08ap_11	834	28	6.93	0.21	0.88	0.144	0.005	0.856	0.014	0.34	-	-	-	1.3
Tam08ap_12	1201	51	10.00	0.41	0.93	0.100	0.004	0.864	0.014	0.18	-	-	-	0.9
Tam08ap_13	6150	560	50.90	4.50	0.98	0.020	0.002	0.868	0.016	0.06	-	-	-	0.1
Tam08ap_15	896	30	7.62	0.26	0.95	0.131	0.004	0.846	0.009	0.14	-	-	-	1.6
Tam08ap_16	372	11	3.22	0.09	0.89	0.311	0.009	0.834	0.012	0.06	-	-	-	3.1
Tam08ap_19	375	15	3.26	0.12	0.85	0.307	0.011	0.829	0.021	0.05	462.0	566.7	0.98	1.1
Tam08ap_20	2170	190	18.20	1.60	0.98	0.055	0.005	0.859	0.019	-0.01	-	-	-	0.2
Tam08ap_21	8200	1100	69.00	9.20	0.99	0.014	0.002	0.853	0.014	0.12	-	-	-	0.1
Tam08ap_23	202.4	7.2	1.73	0.06	0.80	0.579	0.020	0.850	0.017	0.41	-	-	-	2.5
Tam08ap_24	-	-	-	-	-	0.000	0.005	0.861	0.025	-0.03	-	-	-	0.1
Tam08ap_25	1700	140	14.20	1.20	0.93	0.070	0.006	0.854	0.024	0.18	-	-	-	0.2
Tam08ap_26	528	26	4.35	0.20	0.81	0.230	0.010	0.874	0.025	0.24	-	-	-	0.8
Tam08ap_27	558	28	4.64	0.21	0.91	0.216	0.009	0.858	0.018	0.12	-	-	-	0.9
Tam08ap_28	116.6	4.5	1.07	0.04	0.81	0.936	0.037	0.800	0.023	0.25	641.4	190.9	0.90	3.0
Tam08ap_29	1590	78	13.36	0.65	0.92	0.075	0.004	0.856	0.018	0.18	-	-	-	0.4
Tam08ap_30	978	53	8.40	0.46	0.92	0.119	0.007	0.837	0.020	0.30	-	-	-	0.5
Tam08ap_31	2850	370	24.30	3.20	0.99	0.041	0.009	0.852	0.024	0.12	-	-	-	0.2
Tam08ap_35	316	11	2.70	0.10	0.72	0.371	0.013	0.840	0.020	0.36	2463.6	420.3	0.83	1.0
Tam08ap_36	1760	150	14.70	1.20	0.95	0.068	0.006	0.862	0.027	0.14	-	-	-	0.2
Tam08ap_37	815	38	6.81	0.36	0.90	0.147	0.008	0.867	0.022	0.41	-	-	0.83	0.5
Tam08ap_38	8200	1300	68.00	11.00	1.00	0.015	0.008	0.849	0.022	-0.12	-	-	-	0.1

Integration	$^{207}Pb/^{235}U$	Prop2SE	$^{206}Pb/^{238}U$	Prop2SE	Rho	$^{238}U/^{206}Pb$	Prop2SE	$^{207}Pb/^{206}Pb$	Prop2SE	Rho	^{207}Pb corrected age	Prop2SE	$f^{206}Pb$	^{238}U
Tam08ap_39	84.6	2.1	0.77	0.02	0.66	1.299	0.028	0.789	0.016	0.30	461.1	103.4	0.90	6.8
Tam08ap_41	2130	230	17.70	2.00	0.96	0.056	0.007	0.881	0.027	0.25	-	-	-	0.2
Tam08ap_42	1740	160	14.20	1.20	0.96	0.070	0.007	0.881	0.024	0.12	-	-	-	0.2
Tam08ap_43	503	17	4.21	0.15	0.77	0.238	0.009	0.860	0.020	0.35	290.3	697.0	0.99	1.0
Tam08ap_44	1144	98	9.57	0.81	0.96	0.104	0.010	0.849	0.019	0.16	-	-	-	0.3
Tam08ap_48	2490	220	21.40	1.90	0.98	0.047	0.004	0.849	0.018	-0.02	-	-	-	0.2
Tam08ap_49	3000	330	24.40	2.30	0.98	0.041	0.004	0.860	0.023	0.04	-	-	-	0.1
Tam08ap_51	1800	230	15.00	1.90	0.96	0.067	0.009	0.878	0.033	0.41	-	-	-	0.2
Tam08ap_52	44	1.6	0.41	0.01	0.47	2.415	0.067	0.766	0.025	0.29	288.6	84.1	0.89	4.9
Tam08ap_53	1020	120	9.00	1.10	0.94	0.111	0.014	0.845	0.031	0.10	-	-	-	0.3
Tam08ap_54	7120	730	58.00	5.80	0.99	0.017	0.002	0.879	0.015	0.09	-	-	-	0.1
Tam08ap_56	7000	1300	59.00	11.00	0.91	0.017	0.004	0.817	0.022	-0.05	-	-	0.98	0.1
Tam08ap_57	74.6	2	0.66	0.02	0.62	1.511	0.041	0.805	0.019	0.42	246.0	106.7	0.94	8.2
Tam08ap_58	9400	1200	79.00	11.00	1.00	0.013	0.002	0.871	0.022	0.32	-	-	-	0.1
Tam08ap_59	2370	280	19.20	2.20	0.97	0.052	0.006	0.881	0.024	0.13	-	-	-	0.2
Tam08ap_60	-	-	-	-	-	0.000	0.002	0.864	0.033	0.00	-	-	-	0.0
Tam08ap_61	1830	140	15.00	1.10	0.94	0.067	0.005	0.865	0.022	-0.07	-	-	-	0.3
Tam08ap_63	1058	71	9.03	0.62	0.98	0.111	0.009	0.837	0.018	0.25	-	-	-	0.5
Tam08ap_64	730	49	5.97	0.37	0.93	0.168	0.010	0.875	0.022	0.08	-	-	-	0.4
Tam08ap_65	36.5	1.8	0.35	0.02	0.64	2.857	0.120	0.746	0.033	0.34	300.8	92.3	0.86	10.5
Tam08ap_67	1331	68	11.02	0.59	0.94	0.091	0.005	0.868	0.017	0.37	-	-	-	0.4
Tam08ap_68	2290	210	18.60	1.70	0.96	0.054	0.005	0.875	0.024	0.21	-	-	-	0.1
Tam08ap_71	747	45	6.17	0.38	0.91	0.162	0.010	0.866	0.026	0.34	2105.4	1214.1	0.94	0.6
Tam08ap_72	9300	2300	77.00	20.00	0.99	0.013	0.003	0.860	0.026	-0.05	-	-	-	0.1
Tam08ap_73	592	23	4.86	0.20	0.81	0.206	0.009	0.869	0.021	0.43	-	-	-	1.1
Tam08ap_74	5.54	0.42	0.05	0.00	0.00	20.576	1.500	0.837	0.088	0.75	-	-	-	9.2
Tam08ap_77	1103	50	9.27	0.46	0.93	0.108	0.005	0.864	0.018	0.18	-	-	-	0.6
Tam08ap_78	76	10	0.68	0.09	0.17	1.462	0.200	0.788	0.025	0.12	392.8	145.3	0.91	7.4
Tam08ap_79	9700	1600	79.00	12.00	1.00	0.013	0.002	0.871	0.022	-0.09	-	-	-	0.1

Supporting Information Tables S3.4: Apatite U-Pb data (continued)

Integration	$^{207}Pb/^{235}U$	Prop2SE	$^{206}Pb/^{238}U$	Prop2SE	Rho	$^{238}U/^{206}Pb$	Prop2SE	$^{207}Pb/^{206}Pb$	Prop2SE	Rho	^{207}Pb corrected age	Prop2SE	$f^{206}Pb$	^{238}U
Tam08ap_81	2010	170	16.40	1.30	0.96	0.061	0.005	0.875	0.022	0.16	-	-	-	0.2
Tam08ap_84	1210	180	9.80	1.30	0.98	0.102	0.016	0.854	0.022	0.07	-	-	-	0.3
Tam08ap_86	9600	1600	79.00	13.00	1.00	0.013	0.003	0.865	0.019	0.23	-	-	-	0.1
Tam08ap_87	421	16	3.55	0.14	0.80	0.282	0.011	0.849	0.021	0.40	-	-	-	1.1
Tam08ap_88	574	23	4.78	0.20	0.80	0.209	0.009	0.864	0.023	0.27	-	-	-	0.5
Tam08ap_89	1380	87	11.53	0.74	0.94	0.087	0.006	0.861	0.018	0.14	-	-	-	0.4
Tam08ap_90	3970	750	33.20	6.60	1.00	0.030	0.006	0.869	0.032	0.36	-	-	-	0.1
Tam08ap_91	761	23	6.34	0.19	0.91	0.158	0.005	0.857	0.011	0.25	-	-	-	1.5
Tam08ap_93	364	15	3.00	0.11	0.76	0.333	0.012	0.855	0.022	0.21	-	-	-	1.6
Tam08ap_95	741	28	6.28	0.24	0.82	0.159	0.006	0.848	0.018	0.30	-	-	-	0.8
Tam08ap_96	1520	120	12.45	0.96	0.99	0.080	0.007	0.866	0.019	0.00	-	-	-	0.3
Tam08ap_97	179	11	1.48	0.09	0.90	0.674	0.040	0.862	0.025	0.29	-	-	-	2.3
Passed inclusion criteria														
Tam09ap_0	12.56	0.39	0.149	0.004	0.67	6.725	0.190	0.610	0.016	0.37	285.7	21.2	0.70	25.6
Tam09ap_1	36.15	0.71	0.358	0.009	0.54	2.796	0.067	0.731	0.015	0.63	357.8	46.3	0.84	11.1
Tam09ap_2	4.11	0.16	0.084	0.003	0.44	11.848	0.400	0.352	0.014	0.35	333.2	14.6	0.37	57.1
Tam09ap_4	6.79	0.15	0.102	0.002	0.26	9.843	0.170	0.482	0.012	0.47	297.5	11.2	0.54	39.2
Tam09ap_5	9.71	0.26	0.129	0.003	0.37	7.758	0.150	0.543	0.014	0.37	316.3	16.0	0.61	41.3
Tam09ap_6	18.37	0.48	0.196	0.005	0.33	5.092	0.120	0.677	0.020	0.56	273.1	32.8	0.78	9.1
Tam09ap_8	37.1	1.2	0.360	0.011	0.67	2.778	0.089	0.737	0.017	0.42	340.7	52.1	0.85	8.3
Tam09ap_9	10.49	0.28	0.135	0.004	0.37	7.424	0.210	0.562	0.016	0.56	310.3	19.5	0.63	26.5
Tam09ap_10	10.9	0.23	0.134	0.003	0.35	7.474	0.140	0.588	0.015	0.41	280.0	17.4	0.67	26.0
Tam09ap_13	19.34	0.5	0.233	0.005	0.01	4.301	0.091	0.600	0.013	0.82	477.1	26.5	0.67	21.7
Tam09ap_14	35.7	1	0.343	0.009	0.70	2.914	0.079	0.747	0.015	0.30	290.8	45.1	0.87	8.8
Tam09ap_20	19.46	0.45	0.389	0.006	0.00	2.572	0.041	0.364	0.010	0.78	1526.6	35.4	0.31	13.6
Tam09ap_22	3.3	0.12	0.074	0.002	0.24	13.569	0.300	0.326	0.012	0.35	306.0	9.6	0.34	20.6
Tam09ap_23	12.94	0.31	0.152	0.003	0.31	6.566	0.130	0.618	0.016	0.50	282.9	21.0	0.71	13.0
Tam09ap_24	19.89	0.83	0.210	0.007	0.48	4.766	0.170	0.691	0.027	0.39	268.2	46.3	0.80	7.7

Integration	$^{207}Pb/^{235}U$	Prop2SE	$^{206}Pb/^{238}U$	Prop2SE	Rho	$^{238}U/^{206}Pb$	Prop2SE	$^{207}Pb/^{206}Pb$	Prop2SE	Rho	^{207}Pb corrected age	Prop2SE	$f^{206}Pb$	^{238}U
Tam09ap_35	12.32	0.56	0.116	0.005	0.11	8.606	0.420	0.777	0.049	0.69	58.7	46.6	0.92	3.3
Tam09ap_36	18.64	0.43	0.206	0.005	0.49	4.866	0.100	0.661	0.015	0.49	314.5	26.7	0.76	11.2
Tam09ap_37	16.92	0.33	0.191	0.003	0.25	5.227	0.098	0.643	0.015	0.58	320.0	24.6	0.73	11.8
Tam09ap_38	21.83	0.5	0.235	0.004	0.26	4.250	0.075	0.672	0.017	0.53	342.1	33.5	0.77	9.3
Tam09ap_40	49.2	1.7	0.474	0.014	0.88	2.110	0.065	0.752	0.013	-0.02	406.8	55.1	0.86	11.7
Tam09ap_41	27.7	0.69	0.282	0.007	0.41	3.542	0.098	0.717	0.021	0.62	307.5	48.9	0.83	7.7
Tam09ap_44	25.01	0.76	0.255	0.007	0.06	3.925	0.100	0.713	0.016	0.04	283.1	35.3	0.82	15.8
Tam09ap_49	10.92	0.26	0.137	0.003	0.32	7.289	0.140	0.582	0.015	0.36	294.1	17.9	0.66	21.0
Tam09ap_50	5.11	0.11	0.087	0.002	0.16	11.455	0.200	0.426	0.011	0.56	294.0	9.3	0.47	38.1
Tam09ap_52	9.53	0.29	0.124	0.003	0.34	8.065	0.160	0.558	0.017	0.32	289.0	18.1	0.63	21.5
Tam09ap_56	19.51	0.94	0.206	0.008	0.61	4.857	0.210	0.675	0.025	0.25	290.8	42.8	0.78	8.0
Tam09ap_58	28.35	0.82	0.290	0.009	0.47	3.448	0.110	0.703	0.022	0.52	352.7	52.2	0.81	6.7
Tam09ap_60	4.47	0.16	0.040	0.001	0.13	24.938	0.680	0.814	0.035	0.56	7.2	11.7	0.97	15.5
Tam09ap_61	38.9	1.6	0.416	0.013	0.27	2.404	0.077	0.676	0.028	0.52	635.0	89.3	0.75	2.3
Tam09ap_62	11.7	0.29	0.144	0.004	0.56	6.944	0.170	0.590	0.013	0.52	299.8	17.4	0.67	27.6
Tam09ap_63	14.15	0.52	0.168	0.005	0.70	5.970	0.170	0.607	0.016	0.26	327.7	23.8	0.69	21.4
Tam09ap_64	39.1	2.6	0.377	0.023	0.96	2.653	0.150	0.750	0.019	-0.06	314.3	62.2	0.87	8.6
Tam09ap_66	31.66	0.78	0.312	0.006	0.53	3.210	0.059	0.739	0.017	0.40	282.4	45.0	0.86	8.7
Tam09ap_68	6.65	0.18	0.101	0.002	0.24	9.911	0.210	0.479	0.014	0.46	297.9	13.0	0.53	44.8
Tam09ap_69	39.8	1	0.389	0.007	0.39	2.570	0.048	0.738	0.017	0.34	370.0	55.4	0.85	5.9
Tam09ap_76	12.55	0.3	0.155	0.003	0.78	6.439	0.150	0.586	0.010	0.25	329.9	15.4	0.66	58.2
Tam09ap_79	32.98	0.79	0.322	0.007	0.45	3.108	0.065	0.744	0.017	0.42	278.4	46.6	0.86	10.3
Tam09ap_80	24.47	0.52	0.258	0.006	0.57	3.879	0.085	0.687	0.013	0.52	344.9	30.0	0.79	12.1
Tam09ap_81	56.8	1.4	0.537	0.012	0.60	1.862	0.042	0.767	0.016	0.34	396.1	72.8	0.88	5.3
Tam09ap_85	20.31	0.89	0.215	0.009	0.55	4.651	0.200	0.687	0.029	0.43	282.8	50.8	0.79	9.0
Tam09ap_87	12.39	0.27	0.153	0.003	0.40	6.532	0.130	0.586	0.013	0.46	324.5	17.8	0.66	20.1
Tam09ap_88	42.8	1.2	0.407	0.012	0.71	2.457	0.073	0.761	0.016	0.42	302.2	56.3	0.88	13.1
Tam09ap_92	31.36	0.75	0.314	0.008	0.62	3.184	0.080	0.722	0.015	0.47	333.1	40.9	0.83	8.5
Tam09ap_94	17.02	0.36	0.211	0.004	0.51	4.730	0.087	0.580	0.011	0.38	465.5	21.3	0.65	21.9

Supporting Information Tables S3.4: Apatite U-Pb data (continued)

Integration	$^{207}Pb/^{235}U$	Prop2SE	$^{206}Pb/^{238}U$	Prop2SE	Rho	$^{238}U/^{206}Pb$	Prop2SE	$^{207}Pb/^{206}Pb$	Prop2SE	Rho	^{207}Pb corrected age	Prop2SE	$f^{206}Pb$	^{238}U
Tam09ap_96	2.884	0.077	0.067	0.001	0.40	14.837	0.240	0.308	0.008	0.24	289.6	6.3	0.32	49.0
Tam09ap_98	3.8	0.14	0.073	0.002	0.51	13.755	0.380	0.376	0.013	0.22	273.3	10.6	0.40	74.8
Tam09ap_99	8.85	0.21	0.122	0.003	0.23	8.190	0.200	0.521	0.015	0.61	320.7	16.8	0.58	24.0
Failed inclusion criteria														
Tam09ap_3	3140	300	26.10	2.60	0.97	0.038	0.004	0.869	0.021	-0.04	-	-	-	0.2
Tam09ap_7	45.3	1.7	0.42	0.02	0.50	2.370	0.084	0.778	0.028	0.42	246.3	96.0	0.91	8.5
Tam09ap_11	1221	45	10.37	0.35	0.89	0.096	0.003	0.848	0.014	0.10	-	-	-	0.7
Tam09ap_12	9940	990	80.90	7.70	0.99	0.012	0.001	0.880	0.020	0.03	-	-	-	0.0
Tam09ap_15	343.7	9.6	2.94	0.07	0.72	0.341	0.008	0.847	0.017	0.31	1839.7	372.8	0.89	1.4
Tam09ap_16	560	34	4.78	0.27	0.96	0.209	0.012	0.839	0.015	0.00	-	-	-	1.3
Tam09ap_17	2207	95	18.33	0.79	0.93	0.055	0.002	0.871	0.016	0.18	-	-	-	0.3
Tam09ap_18	3590	230	30.30	1.90	0.96	0.033	0.002	0.856	0.016	0.04	-	-	-	0.1
Tam09ap_19	2335	98	19.33	0.78	0.89	0.052	0.002	0.875	0.018	0.19	-	-	-	0.4
Tam09ap_21	439	20	3.76	0.17	0.87	0.266	0.012	0.847	0.018	0.22	-	-	-	1.5
Tam09ap_25	6450	630	53.60	5.10	0.98	0.019	0.002	0.875	0.016	0.04	-	-	-	0.1
Tam09ap_26	1582	82	13.55	0.74	0.97	0.074	0.004	0.850	0.015	0.21	-	-	-	0.3
Tam09ap_27	639	24	5.41	0.21	1.00	0.185	0.006	0.861	0.016	0.04	-	-	-	1.0
Tam09ap_28	579	11	4.97	0.09	0.41	0.201	0.004	0.846	0.012	0.22	-	-	-	1.7
Tam09ap_29	70.6	2.1	0.64	0.02	0.60	1.563	0.050	0.813	0.021	0.41	174.9	114.0	0.96	3.8
Tam09ap_30	1820	230	15.50	2.10	0.97	0.065	0.009	0.860	0.025	0.19	-	-	-	0.2
Tam09ap_31	1493	70	12.42	0.52	0.93	0.081	0.004	0.865	0.014	0.12	-	-	-	0.3
Tam09ap_32	830	19	7.13	0.15	0.90	0.140	0.003	0.845	0.009	0.15	-	-	-	1.5
Tam09ap_33	720	34	6.05	0.21	0.15	0.165	0.006	0.873	0.023	0.00	-	-	-	0.6
Tam09ap_34	3360	360	28.60	3.00	0.99	0.035	0.004	0.854	0.018	-0.01	-	-	-	0.1
Tam09ap_39	1238	60	10.58	0.52	0.94	0.095	0.005	0.853	0.016	0.20	-	-	-	0.4
Tam09ap_42	282.1	7.1	2.45	0.06	0.72	0.408	0.011	0.837	0.016	0.34	1885.8	293.2	0.86	1.6
Tam09ap_43	751	23	6.39	0.19	0.85	0.156	0.005	0.858	0.014	0.14	-	-	-	0.8
Tam09ap_45	-	-	-	-	-	-0.001	0.001	0.870	0.018	0.20	-	-	-	0.0
Tam09ap_46	915	30	7.81	0.27	0.90	0.128	0.005	0.851	0.014	0.29	-	-	-	0.8

Integration	$^{207}Pb/^{235}U$	Prop2SE	$^{206}Pb/^{238}U$	Prop2SE	Rho	$^{238}U/^{206}Pb$	Prop2SE	$^{207}Pb/^{206}Pb$	Prop2SE	Rho	^{207}Pb corrected age	Prop2SE	$f^{206}Pb$	^{238}U
Tam09ap_47	609	12	5.25	0.11	0.74	0.190	0.004	0.843	0.013	0.40	-	-	-	2.5
Tam09ap_48	1020	110	8.72	0.94	0.98	0.115	0.021	0.846	0.016	0.02	-	-	-	0.8
Tam09ap_51	483	13	4.12	0.11	0.78	0.243	0.007	0.850	0.015	0.38	-	-	-	1.7
Tam09ap_53	3050	210	25.70	1.80	0.96	0.039	0.003	0.862	0.017	0.23	-	-	-	0.1
Tam09ap_54	358.9	6.9	3.06	0.08	0.72	0.327	0.008	0.857	0.014	0.53	-	-	-	1.4
Tam09ap_55	4840	800	40.80	7.00	1.00	0.025	0.004	0.860	0.027	0.06	-	-	-	0.0
Tam09ap_57	2199	93	18.60	0.80	0.93	0.054	0.003	0.857	0.015	0.08	-	-	-	0.3
Tam09ap_59	1893	78	16.35	0.68	0.92	0.061	0.003	0.840	0.015	0.16	-	-	-	0.3
Tam09ap_65	1631	63	13.86	0.53	0.89	0.072	0.003	0.852	0.015	0.19	-	-	-	0.5
Tam09ap_67	1237	53	10.66	0.46	0.87	0.094	0.004	0.842	0.019	0.23	-	-	-	0.4
Tam09ap_70	1437	58	12.26	0.48	0.85	0.082	0.003	0.850	0.019	0.29	-	-	-	0.5
Tam09ap_71	1330	130	11.00	1.10	0.95	0.091	0.011	0.872	0.022	0.07	-	-	-	0.4
Tam09ap_72	2600	400	21.90	3.30	0.98	0.046	0.042	0.855	0.018	-0.02	-	-	-	0.4
Tam09ap_73	23100	3800	195.00	32.00	1.00	0.005	0.001	0.857	0.017	0.01	-	-	-	0.0
Tam09ap_74	1220	65	10.45	0.54	0.93	0.096	0.005	0.842	0.016	0.01	-	-	-	0.3
Tam09ap_75	2118	99	17.87	0.83	0.91	0.056	0.003	0.848	0.018	0.30	-	-	-	0.2
Tam09ap_77	882	35	7.42	0.28	0.78	0.135	0.005	0.863	0.018	0.37	-	-	-	1.1
Tam09ap_78	578	27	4.88	0.21	0.87	0.205	0.009	0.857	0.020	-0.01	-	-	-	1.0
Tam09ap_82	1471	77	12.87	0.73	0.87	0.078	0.005	0.834	0.021	0.31	168.7	2333.3	1.00	0.2
Tam09ap_83	-	-	-	-	-	0.000	0.001	0.869	0.024	0.04	-	-	-	0.0
Tam09ap_84	450	14	3.88	0.10	0.77	0.258	0.007	0.832	0.016	0.16	339.1	546.9	0.99	1.1
Tam09ap_86	5680	480	48.30	4.30	0.99	0.021	0.002	0.857	0.017	0.23	-	-	-	0.1
Tam09ap_89	88.8	5.4	0.78	0.04	0.88	1.279	0.076	0.820	0.024	0.17	169.5	157.1	0.97	2.6
Tam09ap_90	1081	68	9.04	0.55	0.92	0.111	0.007	0.862	0.022	0.11	-	-	-	0.3
Tam09ap_91	5940	620	49.30	4.80	0.99	0.020	0.002	0.863	0.017	-0.09	-	-	-	0.1
Tam09ap_93	2410	170	20.60	1.30	0.91	0.049	0.003	0.850	0.023	0.09	-	-	-	0.1
Tam09ap_95	7790	820	65.70	6.80	0.99	0.015	0.002	0.848	0.018	0.00	-	-	-	0.1
Tam09ap_97	9750	970	83.60	8.40	0.99	0.012	0.001	0.839	0.018	0.02	-	-	-	0.1
Tam09ap_100	1345	72	11.39	0.63	0.93	0.088	0.005	0.856	0.016	0.19	-	-	-	0.3

Supporting Information Tables S3.4: Apatite U-Pb data (continued)

Integration	$^{207}Pb/^{235}U$	Prop2SE	$^{206}Pb/^{238}U$	Prop2SE	Rho	$^{238}U/^{206}Pb$	Prop2SE	$^{207}Pb/^{206}Pb$	Prop2SE	Rho	^{207}Pb corrected age	Prop2SE	$f^{206}Pb$	^{238}U
Passed inclusion criteria														
Tam10ap_0	14.4	1.2	0.167	0.010	0.96	6.002	0.380	0.578	0.022	-0.73	365.2	35.4	0.65	29.7
Tam10ap_7	8.22	0.25	0.117	0.003	0.44	8.540	0.210	0.489	0.015	0.49	337.2	16.3	0.54	23.5
Tam10ap_8	14.77	0.37	0.159	0.005	0.58	6.274	0.170	0.642	0.015	0.51	265.1	21.5	0.74	19.7
Tam10ap_12	2.65	0.22	0.068	0.002	0.48	14.684	0.510	0.268	0.018	-0.07	313.6	14.1	0.27	132.0
Tam10ap_13	32.56	0.89	0.310	0.007	0.53	3.227	0.076	0.733	0.021	0.32	297.4	53.6	0.85	9.4
Tam10ap_14	8.21	0.32	0.116	0.003	0.83	8.636	0.220	0.497	0.011	-0.30	326.0	13.5	0.55	64.2
Tam10ap_18	6.59	0.21	0.097	0.002	0.39	10.267	0.260	0.501	0.016	0.43	270.3	14.2	0.56	22.7
Tam10ap_26	79.6	2.5	0.742	0.020	0.82	1.348	0.036	0.791	0.015	0.23	417.8	95.7	0.91	5.1
Tam10ap_30	10.76	0.24	0.137	0.003	0.34	7.305	0.150	0.578	0.012	0.60	297.8	15.3	0.65	25.7
Tam10ap_33	29.19	0.84	0.317	0.009	0.69	3.155	0.086	0.675	0.014	0.33	467.4	38.9	0.76	8.1
Tam10ap_36	5.39	0.23	0.091	0.003	0.77	10.989	0.320	0.438	0.012	-0.12	297.9	12.5	0.48	44.5
Tam10ap_39	9.93	0.35	0.129	0.005	0.36	7.752	0.270	0.577	0.024	0.52	281.1	26.6	0.65	10.4
Tam10ap_40	33.4	1.7	0.333	0.016	0.79	3.003	0.140	0.752	0.022	0.24	265.4	61.4	0.87	10.5
Tam10ap_41	24.88	0.71	0.258	0.006	0.35	3.879	0.097	0.716	0.019	0.52	280.0	41.1	0.83	9.8
Tam10ap_50	7.08	0.52	0.106	0.006	0.73	9.479	0.530	0.514	0.022	0.38	282.2	23.6	0.58	105.5
Tam10ap_53	4.26	0.21	0.078	0.003	0.83	12.755	0.450	0.402	0.013	-0.16	278.7	12.8	0.44	45.5
Tam10ap_55	39.8	1.2	0.401	0.011	0.56	2.494	0.068	0.744	0.020	0.36	361.1	66.0	0.86	5.4
Tam10ap_56	16.74	0.36	0.185	0.003	0.43	5.397	0.093	0.686	0.014	0.37	242.5	22.8	0.79	13.5
Tam10ap_57	29.1	1	0.297	0.008	0.59	3.370	0.091	0.728	0.021	0.32	296.3	51.5	0.84	7.5
Tam10ap_59	12.13	0.29	0.157	0.003	0.53	6.382	0.120	0.580	0.013	0.25	340.1	18.2	0.65	32.4
Tam10ap_60	7.66	0.21	0.112	0.002	0.34	8.929	0.180	0.504	0.014	0.43	308.9	14.1	0.56	23.1
Tam10ap_61	24.15	0.73	0.256	0.007	0.70	3.903	0.100	0.697	0.016	0.21	320.4	35.3	0.80	10.3
Tam10ap_64	11.83	0.54	0.149	0.005	0.73	6.729	0.230	0.581	0.018	-0.03	320.6	23.7	0.66	17.5
Tam10ap_66	16.9	0.44	0.180	0.005	0.31	5.556	0.150	0.694	0.018	0.57	222.9	27.8	0.80	11.8
Tam10ap_67	26.97	0.66	0.280	0.007	0.43	3.569	0.089	0.715	0.019	0.58	309.9	44.4	0.82	8.4
Tam10ap_76	6.8	0.15	0.100	0.002	0.32	10.020	0.240	0.487	0.013	0.65	288.2	12.7	0.54	47.4
Tam10ap_77	24.11	0.6	0.245	0.007	0.06	4.088	0.120	0.719	0.027	0.70	257.8	53.7	0.83	9.8

Integration	$^{207}Pb/^{235}U$	Prop2SE	$^{206}Pb/^{238}U$	Prop2SE	Rho	$^{238}U/^{206}Pb$	Prop2SE	$^{207}Pb/^{206}Pb$	Prop2SE	Rho	^{207}Pb corrected age	Prop2SE	$f^{206}Pb$	^{238}U
Tam10ap_78	29.15	0.81	0.290	0.007	0.43	3.449	0.081	0.742	0.021	0.44	252.3	50.6	0.86	8.7
Tam10ap_80	3.74	0.27	0.078	0.002	0.79	12.821	0.420	0.345	0.018	-0.53	312.2	14.2	0.36	160.0
Tam10ap_82	29.2	1.6	0.290	0.012	0.94	3.448	0.130	0.724	0.020	-0.23	299.0	49.1	0.84	0.7
Tam10ap_83	17.58	0.5	0.191	0.004	0.36	5.244	0.099	0.669	0.019	0.43	277.4	30.2	0.77	9.8
Tam10ap_84	17.29	0.5	0.185	0.005	0.30	5.411	0.130	0.684	0.021	0.55	244.9	32.3	0.79	15.2
Tam10ap_85	17.54	0.38	0.190	0.004	0.25	5.255	0.120	0.674	0.017	0.64	268.8	27.6	0.78	9.6
Tam10ap_86	18.09	0.33	0.196	0.004	0.07	5.092	0.100	0.671	0.018	0.69	283.0	29.7	0.77	14.7
Tam10ap_91	14.84	0.5	0.168	0.007	0.59	5.963	0.240	0.638	0.024	0.41	285.3	34.0	0.73	0.2
Tam10ap_93	22.21	0.79	0.233	0.006	0.59	4.284	0.120	0.699	0.019	0.19	285.2	37.3	0.81	0.4
Tam10ap_94	7.76	0.33	0.140	0.004	0.67	7.128	0.210	0.386	0.011	0.07	518.0	18.2	0.40	11.6
Failed inclusion criteria														
Tam10ap_1	3480	610	28.10	4.80	0.99	0.036	0.007	0.841	0.030	0.17	-	-	-	0.1
Tam10ap_2	1072	56	8.37	0.40	0.95	0.119	0.006	0.860	0.015	-0.13	-	-	-	0.9
Tam10ap_3	943	34	7.62	0.28	0.87	0.131	0.005	0.853	0.018	0.20	-	-	-	1.3
Tam10ap_4	77.4	2.7	0.64	0.02	0.62	1.555	0.051	0.821	0.028	0.38	115.7	149.9	0.97	3.2
Tam10ap_5	8000	1300	64.00	10.00	0.99	0.016	0.003	0.850	0.020	-0.07	-	-	-	0.1
Tam10ap_6	970	55	7.94	0.49	0.94	0.126	0.008	0.854	0.017	0.31	-	-	-	0.5
Tam10ap_9	951	41	7.65	0.32	0.96	0.131	0.005	0.859	0.011	0.14	-	-	-	2.1
Tam10ap_10	5490	930	45.30	7.60	0.99	0.022	0.003	0.841	0.020	0.05	-	-	-	0.1
Tam10ap_11	1004	76	8.07	0.57	0.95	0.124	0.008	0.875	0.021	-0.01	-	-	-	0.4
Tam10ap_15	1526	82	12.72	0.70	0.97	0.079	0.004	0.858	0.014	0.25	-	-	-	0.5
Tam10ap_16	1470	120	12.30	1.00	0.96	0.081	0.007	0.867	0.020	0.26	-	-	-	0.3
Tam10ap_17	2140	540	18.40	4.90	1.00	0.054	0.026	0.842	0.021	-0.54	-	-	-	1.5
Tam10ap_19	1317	84	11.26	0.80	0.89	0.089	0.006	0.854	0.015	0.21	-	-	-	0.5
Tam10ap_20	1219	60	10.23	0.48	0.95	0.098	0.005	0.863	0.014	-0.01	-	-	-	0.6
Tam10ap_21	780	65	6.84	0.59	0.98	0.146	0.012	0.851	0.012	-0.06	-	-	-	0.9
Tam10ap_22	14500	2500	121.00	21.00	1.00	0.008	0.002	0.867	0.013	0.10	-	-	-	0.1
Tam10ap_23	299	13	2.59	0.12	0.83	0.386	0.018	0.842	0.022	0.31	1590.3	410.1	0.89	1.1
Tam10ap_24	4680	570	40.40	4.90	0.99	0.025	0.004	0.855	0.017	0.09	-	-	-	0.1

Supporting Information Tables S3.4: Apatite U-Pb data (continued)

Integration	$^{207}Pb/^{235}U$	Prop2SE	$^{206}Pb/^{238}U$	Prop2SE	Rho	$^{238}U/^{206}Pb$	Prop2SE	$^{207}Pb/^{206}Pb$	Prop2SE	Rho	^{207}Pb corrected age	Prop2SE	$f^{206}Pb$	^{238}U
Tam10ap_25	9800	1600	82.00	14.00	1.00	0.012	0.002	0.867	0.020	0.08	-	-	-	0.1
Tam10ap_27	993	53	8.55	0.49	0.97	0.117	0.007	0.847	0.013	0.33	-	-	-	0.7
Tam10ap_28	2660	490	22.50	4.00	1.00	0.044	0.006	0.870	0.023	0.16	-	-	-	0.2
Tam10ap_29	1880	130	15.90	1.20	0.98	0.063	0.005	0.863	0.014	0.11	-	-	-	0.3
Tam10ap_31	1450	150	12.50	1.30	0.99	0.080	0.007	0.865	0.023	0.01	-	-	-	0.3
Tam10ap_32	4070	680	34.10	5.30	0.98	0.029	0.005	0.872	0.026	0.06	-	-	-	0.1
Tam10ap_34	77.1	1.6	0.69	0.01	0.66	1.447	0.030	0.830	0.015	0.43	52.7	95.7	0.99	9.2
Tam10ap_35	1359	51	11.67	0.47	0.92	0.086	0.003	0.860	0.012	0.22	-	-	-	0.8
Tam10ap_37	516	38	4.52	0.33	0.97	0.221	0.016	0.854	0.018	0.03	-	-	-	1.1
Tam10ap_38	1600	190	14.00	1.70	0.99	0.071	0.009	0.845	0.020	0.25	-	-	-	0.3
Tam10ap_42	2330	720	20.10	4.90	0.98	0.050	0.011	0.821	0.049	-0.37	0.0	9436.7	0.79	0.1
Tam10ap_43	206	33	1.86	0.29	0.95	0.538	0.080	0.862	0.040	0.17	-	-	-	1.2
Tam10ap_44	1320	110	11.08	0.86	0.96	0.090	0.007	0.897	0.017	0.00	-	-	-	0.4
Tam10ap_45	724	78	6.27	0.68	0.99	0.159	0.025	0.873	0.013	0.05	-	-	-	1.4
Tam10ap_46	907	51	7.62	0.38	0.91	0.131	0.007	0.869	0.020	0.06	-	-	-	0.5
Tam10ap_47	70.2	2.4	0.67	0.02	0.77	1.493	0.033	0.789	0.018	-0.10	373.5	100.7	0.91	8.5
Tam10ap_48	1413	55	12.20	0.49	0.91	0.082	0.003	0.865	0.013	0.14	-	-	-	0.8
Tam10ap_49	3360	380	29.20	3.40	0.98	0.034	0.004	0.880	0.020	0.26	-	-	-	0.1
Tam10ap_51	27.9	1.5	0.29	0.01	0.36	3.497	0.150	0.717	0.038	0.43	312.0	86.2	0.83	7.7
Tam10ap_52	4.21	0.21	0.04	0.00	0.10	27.624	1.100	0.884	0.053	0.54	-	-	-	11.2
Tam10ap_54	366	10	3.20	0.10	0.79	0.313	0.010	0.858	0.016	0.52	-	-	-	1.4
Tam10ap_58	-	-	-	-	-	0.000	0.004	0.875	0.040	0.14	-	-	-	0.0
Tam10ap_62	342	14	2.94	0.13	0.89	0.340	0.015	0.871	0.019	0.37	-	-	-	1.5
Tam10ap_63	212.2	9.2	1.86	0.08	0.85	0.537	0.023	0.863	0.023	0.19	-	-	-	1.3
Tam10ap_65	1049	82	8.94	0.69	0.99	0.112	0.011	0.866	0.011	-0.05	-	-	-	1.8
Tam10ap_68	-	-	-	-	-	0.086	0.015	0.873	0.045	0.19	-	-	-	0.1
Tam10ap_69	39.8	1.3	0.37	0.01	0.37	2.717	0.086	0.774	0.025	0.60	222.3	75.7	0.90	4.2
Tam10ap_70	234	8.9	2.03	0.09	0.72	0.494	0.021	0.874	0.027	0.52	-	-	-	1.0
Tam10ap_71	3980	740	32.90	5.70	1.00	0.030	0.005	0.873	0.026	-0.01	-	-	-	0.1

Integration	$^{207}Pb/^{235}U$	Prop2SE	$^{206}Pb/^{238}U$	Prop2SE	Rho	$^{238}U/^{206}Pb$	Prop2SE	$^{207}Pb/^{206}Pb$	Prop2SE	Rho	^{207}Pb corrected age	Prop2SE	$f^{206}Pb$	^{238}U
Tam10ap_72	372	14	3.17	0.11	0.87	0.315	0.011	0.858	0.018	0.13	-	-	-	1.2
Tam10ap_73	1294	81	10.78	0.70	0.95	0.093	0.006	0.887	0.019	0.24	-	-	-	0.4
Tam10ap_74	882	35	7.59	0.32	0.90	0.132	0.005	0.850	0.014	0.42	-	-	-	1.0
Tam10ap_75	1087	43	9.09	0.37	0.88	0.110	0.004	0.875	0.017	0.29	-	-	-	1.1
Tam10ap_79	886	54	7.25	0.44	0.90	0.138	0.008	0.886	0.026	0.26	-	-	-	0.4
Tam10ap_81	1158	46	9.50	0.36	0.92	0.105	0.004	0.878	0.017	0.34	-	-	-	59.5
Tam10ap_87	4060	540	33.10	4.10	1.00	0.030	0.004	0.871	0.025	0.26	-	-	-	17.2
Tam10ap_88	6400	1000	53.10	8.50	0.99	0.019	0.004	0.881	0.025	0.11	-	-	-	0.1
Tam10ap_89	2050	140	16.80	1.10	0.97	0.060	0.004	0.867	0.016	0.13	-	-	-	0.1
Tam10ap_90	2970	340	25.10	2.70	0.98	0.040	0.004	0.867	0.018	-0.15	-	-	-	0.3
Tam10ap_92	1355	87	10.94	0.72	0.94	0.091	0.006	0.891	0.017	0.14	-	-	-	16.3
Passed inclusion criteria														
Tam11ap_4	25.4	1.3	0.248	0.013	0.45	4.039	0.212	0.697	0.022	0.32	308.6	46.8	0.80	18.4
Tam11ap_10	10.76	0.59	0.140	0.007	0.85	7.168	0.365	0.526	0.015	-0.16	362.1	24.7	0.59	46.1
Tam11ap_11	8.94	0.35	0.116	0.004	0.80	8.628	0.313	0.529	0.013	0.02	296.7	16.4	0.59	25.4
Tam11ap_15	18.15	0.36	0.202	0.008	0.56	4.953	0.184	0.654	0.014	0.65	320.4	26.6	0.75	20.0
Tam11ap_16	35.84	1.2	0.354	0.015	0.71	2.823	0.120	0.733	0.014	0.30	347.2	45.1	0.84	14.4
Tam11ap_17	8.93	0.58	0.162	0.009	0.65	6.161	0.357	0.405	0.022	0.05	576.5	42.1	0.42	32.0
Tam11ap_20	22.4	0.89	0.243	0.011	0.87	4.115	0.186	0.673	0.014	0.02	352.2	32.8	0.77	22.4
Tam11ap_21	17.53	0.42	0.197	0.007	0.47	5.079	0.181	0.645	0.015	0.34	326.7	27.2	0.74	23.4
Tam11ap_22	10.42	0.3	0.123	0.005	0.64	8.157	0.313	0.615	0.015	0.32	228.7	17.8	0.71	19.5
Tam11ap_26	17.25	1.8	0.190	0.016	0.51	5.260	0.443	0.658	0.018	0.34	294.1	37.2	0.75	20.0
Tam11ap_27	23.04	0.74	0.239	0.010	0.66	4.181	0.166	0.690	0.018	0.33	311.5	37.5	0.79	15.2
Tam11ap_31	9.07	0.67	0.126	0.007	0.80	7.962	0.456	0.507	0.025	-0.12	344.2	31.3	0.56	38.5
Tam11ap_34	12.94	0.58	0.156	0.008	0.68	6.402	0.307	0.595	0.020	0.18	319.9	29.2	0.67	27.6
Tam11ap_36	19.53	0.69	0.211	0.009	0.52	4.742	0.191	0.675	0.021	0.25	298.4	37.8	0.78	16.7
Tam11ap_39	19.99	0.73	0.220	0.009	0.70	4.541	0.192	0.663	0.017	0.16	335.0	33.8	0.76	22.9
Tam11ap_40	19.17	0.96	0.208	0.011	0.46	4.801	0.254	0.680	0.033	0.29	285.6	56.3	0.78	13.7

Supporting Information Tables S3.4: Apatite U-Pb data (continued)

Integration	$^{207}Pb/^{235}U$	Prop2SE	$^{206}Pb/^{238}U$	Prop2SE	Rho	$^{238}U/^{206}Pb$	Prop2SE	$^{207}Pb/^{206}Pb$	Prop2SE	Rho	^{207}Pb corrected age	Prop2SE	$f^{206}Pb$	^{238}U
Tam11ap_46	44.6	2.1	0.432	0.024	0.72	2.315	0.129	0.751	0.018	0.24	366.6	67.3	0.86	11.5
Tam11ap_56	8.95	0.44	0.122	0.007	0.65	8.217	0.479	0.524	0.016	-0.06	316.7	24.0	0.59	41.1
Tam11ap_58	5.68	0.55	0.094	0.006	0.71	10.661	0.636	0.434	0.016	-0.03	310.1	21.8	0.47	46.8
Tam11ap_62	10.99	0.58	0.141	0.008	0.86	7.077	0.376	0.557	0.018	-0.09	331.8	26.8	0.63	36.3
Tam11ap_64	18.34	0.71	0.186	0.009	0.86	5.379	0.272	0.709	0.013	0.28	206.9	23.9	0.82	18.1
Tam11ap_66	10.87	0.28	0.141	0.005	0.55	7.082	0.256	0.553	0.014	0.32	336.1	20.2	0.62	27.0
Tam11ap_67	9.07	0.35	0.124	0.006	0.46	8.091	0.360	0.531	0.020	0.41	314.9	24.0	0.60	16.2
Tam11ap_72	41.7	1.6	0.415	0.018	0.57	2.410	0.105	0.734	0.024	0.23	415.3	80.7	0.84	8.1
Tam11ap_73	1.303	0.045	0.061	0.002	0.53	16.313	0.612	0.156	0.005	0.16	335.9	12.6	0.13	278.0
Tam11ap_74	10.11	0.6	0.130	0.005	0.31	7.680	0.313	0.555	0.023	0.11	307.0	26.7	0.63	25.9
Tam11ap_75	12.28	0.31	0.151	0.006	0.28	6.631	0.242	0.598	0.015	0.51	304.7	21.7	0.68	28.9
Tam11ap_76	31.2	1.9	0.313	0.016	0.79	3.195	0.163	0.724	0.027	-0.10	326.1	69.2	0.83	9.6
Tam11ap_78	10.35	0.27	0.138	0.006	0.47	7.257	0.290	0.550	0.016	0.41	331.0	22.1	0.62	25.5
Tam11ap_79	10.58	1.8	0.139	0.017	0.85	7.220	0.886	0.550	0.020	-0.28	332.8	45.8	0.62	33.2
Tam11ap_80	24.4	1.2	0.258	0.013	0.84	3.876	0.195	0.691	0.016	0.05	336.3	38.2	0.79	31.1
Tam11ap_81	12.1	0.26	0.149	0.006	0.43	6.707	0.247	0.592	0.014	0.53	308.4	20.7	0.67	33.2
Tam11ap_83	4.2	0.12	0.085	0.003	0.71	11.792	0.403	0.358	0.009	0.02	330.6	12.6	0.38	83.3
Tam11ap_87	40.56	0.94	0.388	0.015	0.64	2.577	0.100	0.743	0.014	0.59	350.7	48.8	0.86	12.9
Tam11ap_88	17.62	0.37	0.191	0.007	0.56	5.233	0.178	0.649	0.012	0.31	310.1	22.5	0.74	20.2
Tam11ap_89	14.21	0.46	0.366	0.015	0.50	2.732	0.112	0.272	0.008	0.30	1662.5	69.1	0.20	23.5
Tam11ap_90	9.15	0.18	0.120	0.004	0.24	8.326	0.277	0.541	0.013	0.51	296.1	16.2	0.61	27.5
Tam11ap_94	9.96	0.76	0.126	0.007	0.81	7.937	0.460	0.551	0.021	-0.30	300.9	27.2	0.62	25.0
Tam11ap_96	4.45	0.21	0.038	0.002	0.28	26.455	1.260	0.829	0.043	0.50	2.1	13.5	0.99	12.5
Failed inclusion criteria														
Tam11ap_0	701	38	5.65	0.31	0.81	0.177	0.010	0.849	0.028	0.06	-	-	-	0.9
Tam11ap_1	785	60	6.34	0.48	0.91	0.158	0.012	0.855	0.026	0.11	-	-	-	0.8
Tam11ap_2	194.3	9.3	1.58	0.07	0.62	0.633	0.029	0.843	0.032	0.11	-	-	-	2.2
Tam11ap_3	76.7	4.4	0.66	0.05	0.87	1.515	0.112	0.790	0.021	0.25	357.9	116.1	0.91	4.4
Tam11ap_5	3140	290	26.70	3.20	0.97	0.037	0.004	0.839	0.022	0.48	-	-	-	0.2

Integration	$^{207}Pb/^{235}U$	Prop2SE	$^{206}Pb/^{238}U$	Prop2SE	Rho	$^{238}U/^{206}Pb$	Prop2SE	$^{207}Pb/^{206}Pb$	Prop2SE	Rho	^{207}Pb corrected age	Prop2SE	$f^{206}Pb$	^{238}U
Tam11ap_6	984	48	8.22	0.53	0.86	0.122	0.008	0.845	0.021	0.39	-	-	-	0.5
Tam11ap_7	570	20	4.61	0.19	0.70	0.217	0.009	0.853	0.021	0.16	-	-	-	0.7
Tam11ap_8	20400	2800	165.00	24.00	1.00	0.006	0.001	0.858	0.015	0.18	-	-	-	0.0
Tam11ap_9	3250	230	26.50	1.80	0.93	0.038	0.003	0.852	0.029	0.11	-	-	-	0.2
Tam11ap_12	2500	130	20.70	1.20	0.89	0.048	0.003	0.846	0.018	0.17	-	-	-	0.3
Tam11ap_13	693	77	5.79	0.66	0.93	0.173	0.020	0.846	0.025	0.14	-	-	-	1.4
Tam11ap_14	1056	41	8.63	0.38	0.79	0.116	0.005	0.863	0.022	0.08	-	-	-	0.7
Tam11ap_18	1810	130	14.92	1.00	0.95	0.067	0.004	0.870	0.020	0.15	-	-	-	0.5
Tam11ap_19	1405	46	11.89	0.51	0.81	0.084	0.004	0.857	0.017	0.26	-	-	-	0.6
Tam11ap_23	132.2	13	1.15	0.11	0.94	0.871	0.083	0.843	0.022	0.23	-	-	-	4.5
Tam11ap_24	114.7	4.1	1.02	0.04	0.60	0.981	0.041	0.816	0.027	0.41	344.0	220.5	0.95	2.5
Tam11ap_25	2030	87	17.29	0.79	0.87	0.058	0.003	0.840	0.017	0.02	-	-	-	0.5
Tam11ap_28	5410	980	44.90	8.40	0.99	0.022	0.004	0.875	0.034	0.07	-	-	-	0.2
Tam11ap_29	1800	110	15.10	1.10	0.91	0.066	0.005	0.866	0.025	0.36	-	-	-	0.2
Tam11ap_30	3070	270	24.70	2.00	0.95	0.040	0.003	0.880	0.027	0.11	-	-	-	0.1
Tam11ap_32	309	49	2.76	0.29	0.80	0.362	0.038	0.757	0.029	-0.14	1671.5	654.7	0.89	22.3
Tam11ap_33	703	22	5.98	0.25	0.74	0.167	0.007	0.848	0.020	0.25	-	-	-	1.2
Tam11ap_35	1280	53	10.76	0.52	0.82	0.093	0.004	0.859	0.022	0.26	-	-	-	0.4
Tam11ap_37	602	28	5.18	0.27	0.90	0.193	0.010	0.848	0.024	0.24	-	-	-	2.3
Tam11ap_38	9400	1700	81.00	16.00	1.00	0.012	0.002	0.865	0.028	0.17	-	-	-	0.1
Tam11ap_41	1407	72	11.83	0.65	0.72	0.085	0.005	0.875	0.031	0.16	-	-	-	0.4
Tam11ap_42	1694	98	14.13	0.83	0.92	0.071	0.004	0.869	0.021	0.15	-	-	-	0.2
Tam11ap_43	1850	130	15.43	0.99	0.82	0.065	0.004	0.864	0.036	0.07	-	-	-	0.2
Tam11ap_44	660	120	5.59	0.94	0.98	0.179	0.030	0.841	0.032	-0.21	-	-	-	1.1
Tam11ap_45	1630	200	14.00	1.70	0.98	0.071	0.009	0.850	0.022	-0.07	-	-	-	0.7
Tam11ap_47	1780	140	15.40	1.40	0.44	0.065	0.006	0.857	0.056	0.29	-	-	-	0.3
Tam11ap_48	1193	66	10.20	0.59	0.53	0.098	0.006	0.858	0.042	0.26	-	-	-	1.1
Tam11ap_49	7420	740	61.80	5.80	0.94	0.016	0.002	0.866	0.033	0.08	-	-	-	0.1
Tam11ap_50	798	78	6.86	0.72	0.95	0.146	0.015	0.858	0.030	0.17	-	-	-	0.6

Supporting Information Tables S3.4: Apatite U-Pb data (continued)

Integration	$^{207}Pb/^{235}U$	Prop2SE	$^{206}Pb/^{238}U$	Prop2SE	Rho	$^{238}U/^{206}Pb$	Prop2SE	$^{207}Pb/^{206}Pb$	Prop2SE	Rho	^{207}Pb corrected age	Prop2SE	$f^{206}Pb$	^{238}U
Tam11ap_6	984	48	8.22	0.53	0.86	0.122	0.008	0.845	0.021	0.39	-	-	-	0.5
Tam11ap_7	570	20	4.61	0.19	0.70	0.217	0.009	0.853	0.021	0.16	-	-	-	0.7
Tam11ap_8	20400	2800	165.00	24.00	1.00	0.006	0.001	0.858	0.015	0.18	-	-	-	0.0
Tam11ap_9	3250	230	26.50	1.80	0.93	0.038	0.003	0.852	0.029	0.11	-	-	-	0.2
Tam11ap_12	2500	130	20.70	1.20	0.89	0.048	0.003	0.846	0.018	0.17	-	-	-	0.3
Tam11ap_13	693	77	5.79	0.66	0.93	0.173	0.020	0.846	0.025	0.14	-	-	-	1.4
Tam11ap_14	1056	41	8.63	0.38	0.79	0.116	0.005	0.863	0.022	0.08	-	-	-	0.7
Tam11ap_18	1810	130	14.92	1.00	0.95	0.067	0.004	0.870	0.020	0.15	-	-	-	0.5
Tam11ap_19	1405	46	11.89	0.51	0.81	0.084	0.004	0.857	0.017	0.26	-	-	-	0.6
Tam11ap_23	132.2	13	1.15	0.11	0.94	0.871	0.083	0.843	0.022	0.23	-	-	-	4.5
Tam11ap_24	114.7	4.1	1.02	0.04	0.60	0.981	0.041	0.816	0.027	0.41	344.0	220.5	0.95	2.5
Tam11ap_25	2030	87	17.29	0.79	0.87	0.058	0.003	0.840	0.017	0.02	-	-	-	0.5
Tam11ap_28	5410	980	44.90	8.40	0.99	0.022	0.004	0.875	0.034	0.07	-	-	-	0.2
Tam11ap_29	1800	110	15.10	1.10	0.91	0.066	0.005	0.866	0.025	0.36	-	-	-	0.2
Tam11ap_30	3070	270	24.70	2.00	0.95	0.040	0.003	0.880	0.027	0.11	-	-	-	0.1
Tam11ap_32	309	49	2.76	0.29	0.80	0.362	0.038	0.757	0.029	-0.14	1671.5	654.7	0.89	22.3
Tam11ap_33	703	22	5.98	0.25	0.74	0.167	0.007	0.848	0.020	0.25	-	-	-	1.2
Tam11ap_35	1280	53	10.76	0.52	0.82	0.093	0.004	0.859	0.022	0.26	-	-	-	0.4
Tam11ap_37	602	28	5.18	0.27	0.90	0.193	0.010	0.848	0.024	0.24	-	-	-	2.3
Tam11ap_38	9400	1700	81.00	16.00	1.00	0.012	0.002	0.865	0.028	0.17	-	-	-	0.1
Tam11ap_41	1407	72	11.83	0.65	0.72	0.085	0.005	0.875	0.031	0.16	-	-	-	0.4
Tam11ap_42	1694	98	14.13	0.83	0.92	0.071	0.004	0.869	0.021	0.15	-	-	-	0.2
Tam11ap_43	1850	130	15.43	0.99	0.82	0.065	0.004	0.864	0.036	0.07	-	-	-	0.2
Tam11ap_44	660	120	5.59	0.94	0.98	0.179	0.030	0.841	0.032	-0.21	-	-	-	1.1
Tam11ap_45	1630	200	14.00	1.70	0.98	0.071	0.009	0.850	0.022	-0.07	-	-	-	0.7
Tam11ap_47	1780	140	15.40	1.40	0.44	0.065	0.006	0.857	0.056	0.29	-	-	-	0.3
Tam11ap_48	1193	66	10.20	0.59	0.53	0.098	0.006	0.858	0.042	0.26	-	-	-	1.1
Tam11ap_49	7420	740	61.80	5.80	0.94	0.016	0.002	0.866	0.033	0.08	-	-	-	0.1
Tam11ap_50	798	78	6.86	0.72	0.95	0.146	0.015	0.858	0.030	0.17	-	-	-	0.6

Integration	$^{207}Pb/^{235}U$	Prop2SE	$^{206}Pb/^{238}U$	Prop2SE	Rho	$^{238}U/^{206}Pb$	Prop2SE	$^{207}Pb/^{206}Pb$	Prop2SE	Rho	^{207}Pb corrected age	Prop2SE	$f^{206}Pb$	^{238}U
Tam11ap_51	1827	68	15.39	0.74	0.89	0.065	0.003	0.850	0.018	0.19	-	-	-	0.6
Tam11ap_52	191	10	1.66	0.09	0.90	0.602	0.034	0.830	0.020	0.05	578.3	266.1	0.94	4.2
Tam11ap_53	1850	140	15.00	1.10	0.68	0.067	0.005	0.876	0.048	0.19	-	-	-	0.3
Tam11ap_54	496	38	4.23	0.33	0.87	0.236	0.018	0.819	0.023	0.07	-	-	0.83	1.0
Tam11ap_55	9500	1200	79.10	10.00	0.99	0.013	0.002	0.857	0.021	0.21	-	-	-	0.1
Tam11ap_57	1616	98	13.29	0.77	0.83	0.075	0.004	0.865	0.029	-0.01	-	-	-	0.5
Tam11ap_59	2340	200	19.60	1.80	0.87	0.051	0.005	0.864	0.030	0.09	-	-	-	0.1
Tam11ap_60	424	22	3.56	0.21	0.86	0.281	0.017	0.855	0.024	0.29	1350.5	622.0	0.93	1.0
Tam11ap_61	1770	250	15.30	2.20	0.32	0.065	0.009	0.844	0.013	-0.08	-	-	-	0.7
Tam11ap_63	1891	69	15.79	0.70	0.87	0.063	0.003	0.849	0.015	0.20	-	-	-	0.6
Tam11ap_65	470	19	3.98	0.19	0.58	0.251	0.012	0.852	0.029	0.35	-	-	-	1.1
Tam11ap_68	1920	100	15.92	0.86	0.67	0.063	0.003	0.852	0.024	0.11	-	-	-	0.4
Tam11ap_69	517	27	4.54	0.25	0.60	0.220	0.012	0.851	0.039	0.30	-	-	-	0.6
Tam11ap_70	3610	260	30.80	2.50	0.92	0.032	0.003	0.866	0.026	0.03	-	-	-	0.1
Tam11ap_71	1163	48	10.03	0.48	0.88	0.100	0.005	0.848	0.018	0.18	-	-	-	0.5
Tam11ap_77	424	12	3.77	0.17	0.15	0.265	0.012	0.830	0.019	0.71	497.6	600.4	0.98	2.6
Tam11ap_82	214.5	6.1	1.87	0.08	0.47	0.535	0.023	0.843	0.025	0.57	58.1	394.3	1.00	2.0
Tam11ap_84	4760	770	41.20	6.80	0.99	0.024	0.004	0.833	0.020	-0.08	-	-	0.93	0.1
Tam11ap_85	-	-	-	-	-	-0.001	0.000	0.885	0.077	-0.17	-	-	-	0.0
Tam11ap_86	1810	130	15.10	1.20	0.95	0.066	0.005	0.837	0.020	0.21	-	-	-	0.2
Tam11ap_91	7370	840	59.30	6.30	0.82	0.017	0.002	0.876	0.049	0.15	-	-	-	0.1
Tam11ap_92	2260	190	18.70	1.70	0.96	0.053	0.005	0.854	0.017	0.17	-	-	-	0.4
Tam11ap_93	1385	62	11.32	0.57	0.91	0.088	0.004	0.863	0.016	0.14	-	-	-	0.3
Tam11ap_95	725	33	6.02	0.28	0.51	0.166	0.008	0.851	0.032	0.22	-	-	-	0.5
Passed inclusion criteria														
Tam13ap_4	4.14	0.2	0.037	0.002	0.07	27.248	1.633	0.824	0.045	0.26	3.5	13.7	0.98	14.1
Tam13ap_5	7.57	0.21	0.114	0.006	0.62	8.795	0.464	0.487	0.011	0.16	329.0	20.0	0.54	33.7
Tam13ap_6	3.82	0.45	0.173	0.011	0.16	5.797	0.370	0.157	0.017	0.20	925.9	60.6	0.10	9.6

Supporting Information Tables S3.4: Apatite U-Pb data (continued)

Integration	$^{207}Pb/^{235}U$	Prop2SE	$^{206}Pb/^{238}U$	Prop2SE	Rho	$^{238}U/^{206}Pb$	Prop2SE	$^{207}Pb/^{206}Pb$	Prop2SE	Rho	^{207}Pb corrected age	Prop2SE	$f^{206}Pb$	^{238}U
Tam13ap_7	7.72	0.5	0.123	0.008	0.26	8.163	0.546	0.458	0.029	0.43	383.1	37.2	0.50	3.3
Tam13ap_9	2.37	0.13	0.060	0.003	0.40	16.611	0.938	0.284	0.014	0.23	269.9	16.4	0.29	21.3
Tam13ap_10	7.78	0.31	0.114	0.006	0.37	8.741	0.489	0.488	0.020	0.37	330.2	25.6	0.54	9.3
Tam13ap_13	13.75	0.67	0.155	0.010	0.56	6.435	0.414	0.626	0.026	0.30	278.7	36.7	0.72	7.8
Tam13ap_14	4.76	0.11	0.087	0.005	0.48	11.534	0.599	0.390	0.008	0.28	316.5	17.3	0.42	67.2
Tam13ap_16	2.08	0.19	0.018	0.002	0.45	54.945	6.340	0.812	0.050	0.41	3.5	7.5	0.97	30.8
Tam13ap_18	2.542	0.06	0.071	0.004	0.58	14.184	0.744	0.256	0.006	0.18	331.4	17.4	0.25	117.3
Tam13ap_19	3.54	0.12	0.159	0.009	0.20	6.289	0.336	0.158	0.005	0.39	854.5	44.6	0.11	20.7
Tam13ap_21	4.4	0.24	0.172	0.010	0.18	5.821	0.339	0.183	0.011	0.39	890.7	51.8	0.14	5.3
Tam13ap_22	36.06	0.82	0.351	0.019	0.18	2.847	0.154	0.738	0.019	0.43	327.8	57.7	0.85	10.6
Tam13ap_23	13.72	0.62	0.168	0.011	0.47	5.963	0.391	0.595	0.027	0.40	344.6	41.9	0.67	4.0
Tam13ap_24	2.51	0.18	0.094	0.005	0.52	10.672	0.581	0.190	0.012	-0.20	486.2	27.2	0.16	36.7
Tam13ap_25	20.51	0.86	0.226	0.013	0.95	4.425	0.255	0.641	0.010	-0.42	386.3	29.8	0.73	41.9
Tam13ap_29	4.34	0.22	0.038	0.002	0.00	26.316	1.593	0.844	0.051	0.57	1.8	15.5	0.99	12.3
Tam13ap_30	8.55	0.19	0.121	0.006	0.21	8.264	0.430	0.515	0.012	0.48	323.6	20.5	0.57	23.0
Tam13ap_31	30.8	1.4	0.309	0.019	0.30	3.236	0.199	0.720	0.030	0.34	332.4	75.9	0.83	2.8
Tam13ap_33	16.06	0.42	0.186	0.010	0.24	5.379	0.289	0.637	0.020	0.60	319.7	34.4	0.73	6.8
Tam13ap_37	22.29	0.56	0.238	0.013	0.57	4.207	0.230	0.688	0.016	0.21	313.4	36.0	0.79	11.9
Tam13ap_39	18.53	0.34	0.209	0.011	0.23	4.789	0.252	0.653	0.014	0.51	333.9	30.1	0.75	15.4
Tam13ap_40	9.18	0.42	0.083	0.005	0.00	12.019	0.737	0.813	0.049	0.68	16.0	33.7	0.97	5.6
Tam13ap_41	5.53	0.16	0.092	0.005	0.04	10.929	0.585	0.441	0.012	0.22	297.4	18.1	0.48	34.6
Tam13ap_42	20.11	0.37	0.221	0.012	0.21	4.533	0.247	0.668	0.015	0.70	326.4	32.8	0.76	15.8
Tam13ap_43	8.83	0.19	0.123	0.007	0.03	8.150	0.432	0.527	0.014	0.62	316.5	21.7	0.59	31.9
Tam13ap_44	32.83	0.98	0.320	0.017	0.54	3.125	0.166	0.748	0.018	0.20	265.1	50.4	0.87	8.2
Failed inclusion criteria														
Tam13ap_0	2240	310	19.40	3.30	0.88	0.052	0.009	0.860	0.041	0.07	-	-	-	0.1
Tam13ap_1	1376	56	11.75	0.73	0.90	0.085	0.005	0.858	0.015	0.30	-	-	-	0.7
Tam13ap_2	227.8	5.6	1.95	0.11	0.73	0.513	0.029	0.842	0.011	0.36	206.7	210.9	0.98	6.4
Tam13ap_3	832	73	7.03	0.65	0.23	0.142	0.013	0.826	0.047	0.15	-	-	0.78	1.0

Integration	$^{207}Pb/^{235}U$	Prop2SE	$^{206}Pb/^{238}U$	Prop2SE	Rho	$^{238}U/^{206}Pb$	Prop2SE	$^{207}Pb/^{206}Pb$	Prop2SE	Rho	^{207}Pb corrected age	Prop2SE	$f^{206}Pb$	^{238}U
Tam13ap_8	1500	150	12.80	1.50	0.98	0.078	0.009	0.846	0.017	-0.07	-	-	-	0.3
Tam13ap_11	1132	50	9.43	0.65	0.82	0.106	0.007	0.861	0.019	0.40	-	-	-	0.3
Tam13ap_12	11.8	2	0.15	0.02	0.48	6.536	0.726	0.564	0.089	0.45	351.6	111.3	0.63	0.4
Tam13ap_15	760	28	6.36	0.38	0.90	0.157	0.009	0.847	0.016	0.12	-	-	-	1.2
Tam13ap_17	128.6	3.1	1.11	0.06	0.65	0.903	0.048	0.816	0.015	0.37	410.5	144.5	0.94	4.6
Tam13ap_20	3890	200	30.30	2.00	0.97	0.033	0.002	0.907	0.009	-0.08	-	-	-	0.6
Tam13ap_26	1091	39	9.10	0.53	0.88	0.110	0.006	0.860	0.016	0.03	-	-	-	0.8
Tam13ap_27	526	98	4.46	0.87	0.99	0.224	0.044	0.856	0.021	0.16	-	-	-	1.4
Tam13ap_28	1710	120	15.10	1.30	0.65	0.066	0.006	0.841	0.018	0.12	-	-	-	0.3
Tam13ap_32	1082	73	9.37	0.81	0.76	0.107	0.009	0.859	0.023	-0.08	-	-	-	0.3
Tam13ap_34	38	5.9	0.37	0.06	0.97	2.725	0.416	0.743	0.025	-0.20	328.3	88.5	0.86	8.4
Tam13ap_35	505	19	4.55	0.27	0.88	0.220	0.013	0.810	0.013	0.15	-	-	-	1.4
Tam13ap_36	55.2	9	0.50	0.05	0.41	1.984	0.205	0.817	0.092	0.16	103.1	372.9	0.97	0.1
Tam13ap_38	1710	150	14.60	1.50	0.98	0.068	0.007	0.862	0.019	0.11	-	-	-	0.2
Tam13ap_45	97.8	3.7	0.85	0.05	0.06	1.175	0.068	0.837	0.028	0.09	-	-	-	1.3

Supporting Information Tables S3.5: Apatite trace-element data (element concs.)

All values are ppm , except where indicated
For all analyses the spot size is 60 μm
For trace elements errors are interal analytical errors only, given at 2SE
For U-Pb analyses errors are propogated, given at 2SE
LOD = limits of detection

	55Mn	±	86Sr	±	89Y	±	90Zr	±	139La	±	140Ce	±	141Pr	±	146Nd	±	147Sm	±	153Eu	±	157Gd	±	159Tb	±	163Dy	±	165Ho	±	166Er	±	169Tm	±	172Yb	±	175Lu	±	182W	±	232Th	±	238U	±
Tarn1Aap_0	461.6	5.8	3609	67	666	12	0.52	0.2	11.56	0.94	36.1	1.5	8.2	0.37	62.4	2.8	36.6	1.3	12.94	0.45	76.4	2.5	13.28	0.38	92.8	1.9	21.66	0.55	76.2	1.7	14.35	0.36	101.8	2.2	18.39	0.37	0.515	0.072	0.795	0.082	0.38	0.02
Tarn1Aap_1	324	5.1	554	10	278.1	6.7	0.228	0.077	3.97	0.24	11.27	0.42	2.29	0.13	16.24	0.99	7.99	0.46	2.28	0.15	17.74	0.74	3.6	0.13	29.6	0.96	8.33	0.26	28.35	0.74	3.96	0.11	20.92	0.56	2.919	0.084	0.457	0.074	0.94	0.32	0.075	0.007
Tarn1Aap_2	759	12	932	15	653	14	0.5	0.2	8.28	0.3	26.98	0.81	5.15	0.19	35.1	1.7	20.38	0.99	5.88	0.25	51.8	1.5	10.85	0.28	92.9	2.4	22.07	0.51	65.7	1.7	9.4	0.29	57.2	1.7	9.51	0.28	0.222	0.061	0.934	0.047	0.131	0.016
Tarn1Aap_3	1014	23	936	16	545	12	0.185	0.055	9.8	0.33	42.5	1.1	9.43	0.3	81.6	2	53.7	1.4	15.03	0.27	97	1.7	15.74	0.31	104	2	19.36	0.38	52.4	1	7.42	0.19	41.9	0.94	6.24	0.17	0.33	0.058	0.412	0.026	0.569	0.022
Tarn1Aap_4	283	4.9	350.9	7.7	276.6	6	0.031	0.015	2.71	0.15	9.67	0.41	1.801	0.094	12.03	0.71	6.07	0.32	1.797	0.092	13.63	0.51	3.187	0.096	30.39	0.65	8.25	0.18	25.73	0.63	3.27	0.11	14.98	0.52	1.882	0.068	0.254	0.037	0.026	0.006	0.058	0.005
Tarn1Aap_5	1469	23	897	13	1207	23	0.488	0.06	174.9	7.7	542	18	86.7	2.7	482	13	175.6	3.5	6.79	0.2	243.4	4.3	39.92	0.61	260.2	4.7	51.64	0.93	136.1	2.2	17.54	0.32	95.2	1.7	14.51	0.32	0.322	0.052	5.19	0.16	13.78	0.23
Tarn1Aap_6	3467	62	132.3	3.3	2073	56	0.436	0.073	701	19	1916	52	351.1	9.1	1759	46	531	12	6.64	0.21	483.9	9.5	73	1.3	445	7.8	80.2	1.5	206.6	3.3	27.2	0.52	150.2	3.4	20.43	0.47	0.163	0.034	18.24	0.63	18	0.48
Tarn1Aap_7	764	13	255.1	5.5	1076	25	0.015	0.01	280.4	6.8	758	17	121.5	2.8	640	16	252.6	5.7	89.6	1.9	253.2	4.9	39.26	0.63	223.1	3.1	37.87	0.48	89.8	1.4	10.95	0.23	59.8	1.2	8.4	0.18	0.062	0.02	0.443	0.024	0.029	0.005
Tarn1Aap_8	999	15	606	11	531	9.9	0.031	0.017	15.06	0.36	47.8	1.1	7.82	0.22	47.6	1.3	25.73	0.75	7.22	0.19	67.8	1.4	14.69	0.33	101.7	1.8	19.43	0.27	52.83	0.91	7.29	0.17	41.9	1.1	5.72	0.15	0.079	0.024	0.954	0.047	2.352	0.082
Tarn1Aap_9	852	13	239.9	7.4	2015	68	2.93	0.2	458	13	1330	36	267	7.5	1512	36	499	12	8.37	0.27	457	11	66.6	1.3	410.9	8.4	74.9	1.6	205.1	4.5	29.51	0.77	176.9	4.9	25.39	0.67	0.152	0.037	33.26	0.73	28.57	0.78
Tarn1Aap_10	424.9	7.3	292.8	6.2	1008	26	0.345	0.06	218.6	5.8	699	17	109.1	2.9	596	14	191.3	4.7	4.35	0.16	222.3	5.3	33.54	0.65	210.3	3.9	40.87	0.69	109.3	1.7	14.66	0.27	87.4	1.6	12.48	0.27	5.73	0.23	5.88	0.16	10.2	0.3
Tarn1Aap_11	1587	35	3390	83	665	14	0.246	0.075	27.16	0.87	95.5	2.4	16.99	0.53	117	4	52.9	1.3	13.03	0.45	96	2.3	16.09	0.37	115.8	2.2	24.37	0.49	73.4	1.5	11.09	0.23	70.9	1.7	9.85	0.31	2.67	0.71	2.2	0.1	2.195	0.07
Tarn1Aap_12	825	14	383.6	9	970	28	0.647	0.086	556	15	1346	36	232.8	6.1	1164	28	306.5	7.2	12.04	0.34	265.2	5.7	35.79	0.54	203	3.3	35.7	0.42	87.7	1.4	10.69	0.24	57.6	1.3	7.18	0.19	0.2	0.045	20.68	0.5	23.71	0.6
Tarn1Aap_13	119.6	1.9	735	14	758	32	0.04	0.016	38.29	0.91	145.6	3.4	29.31	0.69	210.3	4.5	118.3	2.5	37.17	0.83	205.7	5	32.74	0.92	195.6	7.6	32.6	1.4	71.9	3.6	8.33	0.53	44	3.3	4.96	0.45	0.161	0.033	0.097	0.012	1.308	0.066
Tarn1Aap_14	159.4	2.8	4400	110	692	22	0.028	0.013	20.29	0.7	85.2	2.4	19.66	0.63	162.7	4.8	102.6	2.8	25.93	0.62	211.3	4.3	34.63	0.74	197.6	4	29.68	0.6	57.8	1.2	5.83	0.17	25.89	0.79	2.527	0.091	0.158	0.033	0.268	0.02	0.093	0.008
Tarn1Aap_15	662	16	1488	66	500	22	0.053	0.024	10.91	0.59	40.4	1.8	8.25	0.39	62.3	3	33.5	1.4	6.99	0.32	58.5	1.6	9.31	0.26	62.5	1.5	15.92	0.33	65.9	1.1	14.31	0.41	128.7	4	18.86	0.62	0.163	0.039	0.317	0.02	0.158	0.012
Tarn1Aap_16	1197	18	1025	30	498	13	13.49	0.38	1507	45	3013	84	377.7	9.4	1491	35	237.4	5.7	46.2	1	171	3.3	20.14	0.37	107.6	2	18.27	0.42	44.24	0.9	5.31	0.15	31.55	0.88	3.475	0.099	0.084	0.023	37.74	0.86	7.13	0.2
Tarn1Aap_17	412	6.8	585	12	683	14	LOD	LOD	3.1	0.14	10.63	0.3	1.9	0.1	12.76	0.66	6.93	0.37	2.53	0.11	15.81	0.54	3.97	0.11	47.69	0.98	19.39	0.38	94.2	1.6	17.9	0.33	127.9	2.3	13.6	0.26	0.088	0.028	0.217	0.017	0.303	0.012
Tarn1Aap_18	575.5	8.4	577	11	1202	26	0.013	0.009	14.33	0.39	49.2	1.1	9.45	0.29	66.8	1.9	41.4	1	12.21	0.32	116.7	2.3	27.52	0.45	245.4	3.5	54.76	0.73	138.4	2.1	15.67	0.28	82.9	1.6	7.64	0.18	0.087	0.027	0.036	0.015	0.794	0.028
Tarn1Aap_19	351.1	6	455	10	1016	20	7.81	0.28	299.8	7.4	874	21	136.8	3.6	743	16	186.9	4.4	33.06	0.59	203.5	3.8	28.58	0.49	184.9	3.2	38.09	0.59	103.7	1.8	13.82	0.26	86.4	1.7	9.64	0.24	0.445	0.064	6.9	0.14	1.384	0.042
Tarn1Aap_20	550.4	9	549	13	492	11	0.598	0.064	21.92	0.58	86.3	2	14.9	0.44	90.3	2.5	39	1.1	46.3	0.91	55.9	1.3	9.48	0.18	70.6	1.1	16.26	0.25	51.78	0.83	8.53	0.2	65.9	1.4	8.92	0.19	0.885	0.069	9.69	0.22	27.45	0.6
Tarn1Aap_21	197.4	3	3257	34	1048	21	0.06	0.019	60.6	1.4	274	6.1	54.9	1.1	365.6	7.7	181.9	3.2	50.81	0.87	279.1	4.5	50.7	1	309.1	5.3	49.13	0.86	103	2.2	10.81	0.28	52.6	1.3	4.48	0.15	0.058	0.022	0.569	0.025	0.224	0.011
Tarn1Aap_22	286.1	4.4	4267	66	1181	27	0.075	0.028	63.5	1.5	294.2	6.6	59	1.2	392.9	8.3	219.8	4.2	70.9	1.3	355.8	6.2	64.3	1.1	371.8	5.5	58.13	0.78	128.8	1.6	15.21	0.3	86.8	1.4	8.59	0.22	0.07	0.026	0.312	0.02	0.512	0.02
Tarn1Aap_23	925	13	288.1	6	1414	35	0.512	0.061	628	16	1726	38	313.7	7.3	1710	40	486.8	9.7	12.07	0.33	405.6	6.7	56	1	322	4.7	58.06	0.82	148	1.9	19.78	0.3	128	2	14.28	0.3	0.097	0.03	53.9	1.1	55.3	1.2
Tarn1Aap_24	358.1	6.2	1482	38	991	28	15.98	0.58	448	13	971	25	126.3	4.2	563	16	110.8	2.9	18.05	0.5	114.3	2.7	18.3	0.34	139.5	2.5	33.57	0.68	116.8	1.7	20.73	0.53	164	3.6	20.55	0.44	0.151	0.04	35.28	0.89	9.99	0.25
Tarn1Aap_25	311.7	6.3	875	22	347.3	9.2	6.28	0.28	606	17	1260	42	191.5	5.3	910	28	170	5.3	23.06	0.65	131.4	3.7	14.58	0.41	78.5	1.9	13.67	0.37	31.96	0.84	3.73	0.16	22.5	1	2.82	0.11	0.37	0.084	24.46	0.63	11.04	0.28
Tarn1Aap_26	907	15	884	20	791	20	10.85	0.53	689	18	1635	45	272.6	6.5	1358	38	309.6	7.8	22.54	0.58	229.4	4.8	28.59	0.58	156.4	3	26.93	0.51	65.5	1.4	8.38	0.2	50.7	1.3	5.72	0.17	0.177	0.044	39.12	0.82	13.48	0.34
Tarn1Aap_27	151.3	3	1037	24	339.5	9.4	0.285	0.064	17.3	1.9	41.7	4	7.97	0.63	75.9	4.2	118.9	4.3	33.01	0.83	173.6	4.5	19.11	0.42	90.9	1.7	14.1	0.3	33.44	0.73	4.07	0.13	23.59	0.68	2.48	0.11	0.593	0.087	1.66	0.061	0.286	0.02
Tarn1Aap_28	1138	16	316.2	7	1276	31	0.219	0.046	574	14	1552	38	282.5	6.7	1489	34	419.1	8.2	10.33	0.29	347.9	6.6	47.67	0.8	275.8	4.3	50.08	0.76	129.9	2	18.83	0.37	126.7	2.3	15.61	0.39	0.129	0.032	29.01	0.58	28.36	0.58
Tarn1Aap_29	704.8	8.5	99.4	1.8	462.6	7.3	LOD	LOD	1.113	0.091	3.64	0.18	0.621	0.052	4.27	0.4	2.55	0.21	1.064	0.062	8.56	0.34	2.306	0.075	29.09	0.65	13.01	0.23	85.5	1.4	23.78	0.4	246.2	3.8	44.73	0.75	1.02	0.091	0.026	0.005	0.076	0.006
Tarn1Aap_30	377.4	6.4	1991	39	837	41	0.032	0.016	22.63	0.55	103.8	2.3	24.31	0.67	208.2	5.6	134.5	3.3	41.1	1	270.7	7.7	41.3	1.3	241	10	37.7	1.9	77.1	4.9	8.26	0.59	42.1	3.6	4.24	0.39	0.269	0.037	0.291	0.019	0.095	0.008
Tarn1Aap_31	335.5	6.2	401	12	257.6	8.1	LOD	LOD	2.26	0.15	7.38	0.28	1.396	0.087	9.18	0.61	4.82	0.32	1.399	0.087	11.91	0.54	2.8	0.086	27.7	0.59	8.26	0.2	28.17	0.7	3.47	0.1	13.74	0.44	1.381	0.069	0.185	0.041	0.014	0.005	0.055	0.006
Tarn1Aap_32	580	11	830	18	753	14	0.119	0.042	13.8	1.3	28.4	1.5	5.92	0.43	32.4	1.6	15.86	0.62	4.83	0.21	41.9	1.6	10.14	0.29	98.9	1.8	26.51	0.44	80.5	1.4	11.68	0.29	68.6	1.6	10.52	0.29	0.534	0.094	2.25	0.49	0.567	0.03
Tarn1Aap_33	533	14	421	16	456	19	0.199	0.071	5.16	0.7	16.1	1.6	2.54	0.19	17.5	1.3	9.68	0.42	2.91	0.16	25.24	0.9	5.61	0.2	55.4	1.4	15.04	0.34	51.2	1.1	7.53	0.22	45.7	1.1	6.98	0.29	0.23	0.053	0.87	0.2	0.232	0.041
Tarn1Aap_34	544	7.9	608	10	917	16	0.013	0.009	24.1	0.57	85.2	1.7	16.41	0.43	119.3	2.7	90.9	1.9	27.66	0.6	218.2	3.5	38.62	0.79	231.3	3.9	37.7	0.52	86.4	1.5	10.47	0.23	53.61	0.97	6.48	0.15	0.053	0.02	0.047	0.008	1.501	0.037
Tarn1Aap_35	269.5	4.1	2750	56	1023	25	0.009	0.008	3.88	0.17	13.37	0.37	2.6	0.12	18.5	0.75	10.53	0.42	4.29	0.13	33.22	0.84	9.98	0.23	117.1	1.7	37.19	0.58	122.5	2.1	15.35	0.36	69.7	1.3	6.82	0.17	0.201	0.035	0.072	0.012	0.221	0.012
Tarn1Aap_36	314.3	5.3	3066	76	807	21	0.041	0.015	3.23	0.18	14.65	0.48	3.56	0.14	33	1.3	28.01	0.94	8.21	0.26	91.1	1.9	21.07	0.44	164.8	3.1	31.7	0.64	71.6	1.3	7.92	0.18	37.38	0.91	4.02	0.13	0.92	0.093	0.112	0.01	0.173	0.012
Tarn1Aap_37	924	17	416	11	783	22	0.193	0.035	507	14	1237	32	217.2	5.3	1116	25	281.7	6.8	9.74	0.24	229.7	5	28.87	0.55	161.1	3.2	27.98	0.44	68.4	1	8.4	0.18	44.4	1.1	5.91	0.18	0.801	0.098	13.44	0.3	20.09	0.46
Tarn1Aap_38	262.6	3.7	377.7	7.3	57.6	1.4	0.162	0.041	0.712	0.081	1.7	0.15	0.349	0.04	2.11	0.24	1.17	0.13	0.232	0.031	2.7	0.17	0.545	0.033	5.63	0.21	1.783	0.07	7.36	0.26	1.426	0.059	11.17	0.35	2.09	0.078	0.106	0.033	0.07	0.01	0.037	0.006
Tarn1Aap_39	1078	18	222.1	6.9	1386	57	1.94	0.13	528	17	1368	44	252.5	7.6	1352	42	387	12	11.14	0.32	344.3	9.5	49.3	1.3	291	7.3	52.3	1.2	135.3	3.8	18.63	0.61	111.5	3.7	15.42	0.65	0.128	0.033	36.7	1.4	15.26	0.76
Tarn1Aap_40	1114	12	327.9	5.2	1010	21	6.44	0.24	560	11	1354	23	240.3	4.2	1240	22	320.6	5.7	11.9	0.3	277.2	3.9	37.48	0.48	218.8	3.2	38.67	0.49	95.9	1.4	12.18	0.27	68.9	1.2	9.21	0.2	0.073	0.025	24.22	0.41	10.42	0.17
Tarn1Aap_41	1387	15	208	3	1874	39	6.86	0.26	502.7	9.8	1279	24	242.9	4.5	1330	23	426.9	7	8.61	0.21	413.9	5.8	63.27	0.91	394.5	6.1	74.1	1.1	195	2.7	26.5	0.37	160.9	2.6	21.23	0.38	0.084	0.024	30.92	0.46	7.85	0.17
Tarn1Aap_42	86.5	1.6	3231	47	1299	26	0.025	0.014	93.7	6.7	366	20	69.9	3.4	448	18	245.2	6.8	72.6	1.7	383.7	8.5	67.6	1.4	391.9	7.1	61.87	0.89	138.1	1.9	16.14	0.27	90.1	1.7	10.38	0.23	0.151	0.033	0.521	0.032	2.245	0.065
Tarn1Aap_43	363.4	5.3	409.1	6.9	434.5	9.3	LOD	LOD	2.67	0.13	9.06	0.36	1.69	0.11	12.37	0.55	6.46	0.31	1.963	0.092	15.99	0.52	3.796	0.095	40.77	0.82	13.66	0.27	54.86	0.91	9.77	0.19	71.7	1.3	9.9	0.23	0.057	0.023	3.02	0.16	0.112	0.008
Tarn1Aap_44	163.9	2.9	9510	170	991	20	LOD	LOD	41	1	201.6	4.1	46.2	1.1	323.2	7.3	196.3	4	61.3	1.1	310.8	5.2	54.16	0.88	308.2	4.1	45.67	0.61	98.7	1.3	10.94	0.18	59.5	1.2	6.47	0.14	0.065	0.025	0.13	0.012	0.23	0.013
Tarn1Aap_45	721	8.9	485.1	8.8	559	11	0.01	0.008	6.88	0.24	22.89	0.51	4.25	0.16	29.1	1.1	14.57	0.54	3.4	0.14	34.57	0.87	7.63	0.19	68.3	1.2	18.34	0.3	64.8	1.1	11.11	0.21	85.5	1.8	12.42	0.24	0.074	0.023	0.125	0.017	1.018	0.033
Tarn1Bap_0	340.4	4.9	1293	26	563	12	2.88	0.59	33.6	1.1	138.3	3.3	29.2	0.66	217.4	5.7	129.2	3.1	36.57	0.69	193.4	3.9	31.36	0.63	167.1	3.6	24.51	0.59	52.4	1.4	6.05	0.2	31.3	1.1	3.34	0.15	0.117	0.037	2.33	0.19	0.33	0.023
Tarn1Bap_1	639.1	7.7	830	12	2627	48	1.037	0.089	366.5	6.2	1077	24	188.4	3.5	1032	19	374.8	6.2	4.37	0.16	493	9.7	84.8	1.3	565	8.4	112.4	1.8	300.3	4.9	38.19	0.67	220.8	3.9	28.2	0.61	0.224	0.043	8.03	0.15	14.31	0.26
Tarn1Bap_2	248.4	3.8	6173	86	1140	25	0.023	0.012	10.45	0.28	38.39	0.83	7.44	0.28	52.7	1.6	31.25	0.98	9.57	0.25	77.5	1.8	18	0.37	165.4	2.7	42.89	0.71	126.9	2.1	14.27	0.32	62.7	1.2	5.45	0.15	0.197	0.041	0.098	0.01	0.508	0.019
Tarn1Bap_3	917	12	236	4.5	1558	27	2.26	0.15	435	6.5	1282	23	242.7	4.2	1359	25	417	7.4	8.56	0.24	378	5.5	53.54	0.88	320.1	4.5	58.89	0.85	161.1	2.3	22.97	0.4	150.7	2.8	19.91	0.39	0.154	0.043	29.74	0.53	14.11	0.24
Tarn1Bap_4	792	11	501.4	8.4	838	14	3.36	0.3	20.14	0.66	49.8	1.2	9.01	0.32	55.4	1.6	27.6	1	9.64	0.29	61.1	1.6	13.33	0.26	118.3	1.9	29.82	0.49	93.9	1.4	12.83	0.28	74.3	1.4	8.8	0.18	0.129	0.032	4.83	0.21	0.51	0.024
Tarn1Bap_5	977	17	3003	50	1313	27	0.034	0.015	15.38	0.47	37.88	0.96	5.22	0.19	30.3	1.2	18.02	0.58	2.49	0.11	49.4	1.2	14.52	0.25	155	2.3	46.41	0.65	170.4	2.5	25.7	0.43	161.9	3.2	24.83	0.5	1.44	0.12	0.364	0.021	3.495	0.074
Tarn1Bap_6	473.4	8.3	450.3	9.4	221.3	6.1	0.67	0.11	104.8	2.2	179.9	3.4	19.29	0.46	90.9	3.2	29.1	1.2	8.8	0.26	39.7	1.7	5.81	0.18	37.7	1.1	7.74	0.24	22.71	0.62	3.31	0.15	21.78	0.67	3.05	0.1	0.099	0.027	23.2	2.7	11.26	0.35
Tarn1Bap_7	995	13	252.3	6.5	1771	39	7.32	0.28	446.7	9	1347	31	244.6	5.5	1328	27	415.4	9.5	14.02	0.31	368.6	7.2	55.76	0.93	345.3	5.7	63.94	0.76	177.6	2.1	26.06	0.42	168.6	2.9	21.87	0.45	0.321	0.055	18.79	0.4	4.11	0.11
Tarn1Bap_8	917	10	248.2	5.1	2106	38	2.66	0.15	604	11	1752	30	342.9	5.4	1865	33	570.6	9	9.42	0.24	510.4	7.7	73	1.1	438.1	6.3	82	1.2	228	3.4	33.09	0.52	211.7	3.2	28.03	0.5	0.162	0.043	41.41	0.75	42.4	0.89
Tarn1Bap_9	1063	18	430.5	9.5	1076	23	4.91	0.21	572	13	1410	33	242	5.8	1237	30	321.5	7.4	13.43	0.34	277.3	5.8	37.83	0.67	222.1	3.4	39.55	0.5	104.4	1.4	13.98	0.31	82.5	2.1	10.32	0.28	0.174	0.047	23.06	0.48	11.83	0.29
Tarn1Bap_10	391.3	5.2	1110	28	514	12	0.095	0.026	50.4	1.6	159.5	5.3	25.9	1	155.1	5.7	58.1	1.9	12.62	0.31	85.9	2.2	13.33	0.24	88.7	2.1	17.66	0.46	49.4	1.1	7.14	0.2	47.4	1.1	6.45	0.17	1	0.1	2.79	0.23	10.71	0.47
Tarn1Bap_11	1445	29	168.1	4.4	1524	39	1.02	0.11	593	14	1644	38	298.3	7.5	1568	36	433	11	8.23	0.25	379.6	7.7	54.7	1.1	321.4	4.6	59.96	0.83	159.4	2.7	22.12	0.51	136.1	2.8	17.26	0.38	0.103	0.033	25.8	0.58	22.09	0.72
Tarn1Bap_12	466.5	8.1	152	4.2	295.8	8.4	4E-07	7E-09	2.54	0.14	8.19	0.34	1.51	0.13	10.69	0.67	5.47	0.36	2.18	0.11	14.19	0.56	2.908	0.089	27.83	0.6	9.47	0.19	43.98	0.91	8.71	0.21	72.7	1.7	12.23	0.3	0.162	0.042	0.326	0.021	0.091	0.007
Tarn1Bap_13	44.1	1.6	1183	46	623	25	0.013	0.01	55.2	4.4	254	18	47.4	3.1	276	15	127.5	5.3	33	1.1	161.7	5.3	28.84	0.77	172.3	3.5	27.48	0.49	58.2	1.4	5.96	0.17	28.08	0.89	2.72	0.11	0.053	0.022	0.113	0.014	0.718	0.035
Tarn1Bap_14	1501	28	320.1	8.3	1216	29	2.87	0.23	557	15	1421	37	251.9	7.5	1274	31	343.1	8	11.03	0.34	294.3	5.7	41.37	0.74	249.9	3.9	45.23	0.78	121.4	2.1	16.95	0.32	107.2	2.7	14.05	0.34	0.046	0.022	25.58	0.57	13.36	0.34
Tarn1Bap_15	554	12	1829	70	928	35	0.165	0.037	62.4	3.2	224	11	38.8	1.9	231	10	93	4.1	4.48	0.18	144.2	5.6	24.58	0.86	177.6	5.8	37.2	1	104.5	2.7	14.21	0.39	91.9	3.2	12.89	0.46	0.819	0.096	3.56	0.42	4.63	0.2
Tarn1Bap_16	1008	14	354.5	6.5	1111	24	0.562	0.074	606	11	1545	28	266.6	4.9	1339	28	345.3	6.9	13.65	0.33	296.8	6.3	40.62	0.82	235.6	5	41.34	0.77	105.6	2.2	13.6	0.3	79.4	1.8	9.76	0.22	0.308	0.047	25.89	0.47	32.03	0.57
Tarn1Bap_17	282.6	5.8	326.4	7.8	129	22	0.61	0.22	1.97	0.2	6.37	0.56	1.25	0.17	10.1	1.5	6.2	1.3	1.8	0.47	13.1	3.2	2.38	0.57	17.2	3.9	4.46	0.86	16	2.4	2.66	0.31	20.3	2.2	3.13	0.29	2.55	0.2	10.1	3.6	2.03	0.8
Tarn1Bap_18	870	11	449.8	7.7	978	22	2.38	0.13	852	17	1992	36	312.3	5	1488	28	335.8	5.7	16.37	0.33	272.9	4.4	35.38	0.52	198.7	3.4	35.44	0.55	89.9	1.3	11.47	0.23	64.5	1.3	7.91	0.18	0.074	0.022	31.9	0.51	20.11	0.23
Tarn1Bap_19	371.4	6.7	752	16	1038	32	1.31	0.58	3.64	0.5	13.8	1.4	2.43	0.19	21.5	1.4	16.73	0.86	3.72	0.2	53.9	1.9	12.13	0.33	117.3	2.6	34.5	0.85	118.9	2.7	16.22	0.46	89.4	1.6	10.27	0.34	0.12	0.041	0.38	0.2	0.172	0.043
Tarn1Bap_20	420.1	6.4	2415	36	994	21	0.021	0.012	72.8	1.6	263.8	4.5	46.1	1	285.2	5.7	134.6	3	35.11	0.64	173.2	3.3	34.57	0.59	248.7	4.1	42.74	0.67	99.1	1.2	10.93	0.2	52.17	0.95	5.43	0.12	0.044	0.019	0.257	0.018	0.453	0.016
Tarn1Bap_21	681	11	414.7	6.5	426.4	6.7	0.78	0.39	10.16	0.55	36.4	1.4	6.24	0.26	37.8	1.7	17.62	0.82	4.22	0.14	32.63	0.91	6.53	0.16	57.3	1.2	14.26	0.28	46.93	0.84	7	0.16	42.1	1	5.74	0.14	0.332	0.052	6.23	0.51	0.525	0.05
Tarn1Bap_22	1268	16	203.2	3.3	1223	18	3.42	0.19	600.1	8.7	1555	25	265	4.4	1328	24	347.7	6.3	7.98	0.24	295.3	5.5	41.53	0.6	247.2	3.6	44.84	0.62	119.7	1.9	16.67	0.29	104.9	1.8	13.18	0.28	0.172	0.038	22.99	0.37	9.71	0.15
Tarn1Bap_23	1371	18	366.4	5.1	994	21	5.44	0.42	558	11	1390	25	237.5	3.9	1198	25	310.7	5.3	12.19	0.29	268.1	4.6	36.17	0.58	206.2	3.4	36.44	0.61	93.5	1.4	11.8	0.24	68.7	1.4	8.23	0.19	0.122	0.033	23.89	0.45	11.48	0.26
Tarn1Bap_24	1042	14	436.5	7.7	1015	19	1.97	0.13	682	13	1711	30	297.8	6	1515	27	382.7	6.5	12.93	0.34	316.9	5.6	40.61	0.7	224.9	3.4	39.07	0.7	97.2	1.6	11.88	0.21	63.3	1.3	7.66	0.2	0.154	0.035	35.27	0.73	24.81	0.48
Tarn1Bap_25	1145	14	849	12	799	12	11.32	0.39	758	13	1803	32	303	6	1456	25	322.4	5.5	21.8	0.42	242	3.8	28.96	0.56	155.5	2.4	26.47	0.36	64.1	1.1	8.09	0.2	45	0.68	5.48	0.12	0.06	0.022	38.44	0.61	12.5	0.2

Supporting Information Tables S3.5: Apatite trace-element data (continued)

	55Mn	±	86Sr	±	89Y	±	90Zr	±	139La	±	140Ce	±	141Pr	±	146Nd	±	147Sm	±	153Eu	±
Tarn1Bap_26	389.2	5.5	1379	24	2328	61	0.787	0.081	86.2	2.5	336.7	9.8	62.2	1.5	404.7	9.6	190.8	4.6	8.4	0.27
Tarn1Bap_27	614.6	8.2	242.8	4	81.1	1.8	LOD	LOD	1.51	0.18	1.48	0.11	0.491	0.055	2.47	0.27	0.89	0.12	0.334	0.041
Tarn1Bap_28	278.7	5.2	4250	61	1164	83	0.045	0.018	15.89	0.38	64.2	1.4	13.84	0.33	111.9	2.8	83.1	2.7	28.32	0.95
Tarn1Bap_29	1104	15	267.1	4.8	1127	21	9.72	0.56	541.6	8.9	1451	24	264.6	4.2	1385	28	377.9	6.6	9.08	0.25
Tarn1Bap_30	431.3	6.3	80.9	1.7	215.5	5	0.014	0.01	3.01	0.16	5.74	0.24	1.073	0.072	6.67	0.4	3.33	0.24	1.74	0.1
Tarn1Bap_31	412.3	7.7	3071	91	828	28	3.34	0.66	15.5	1.1	51.2	2.5	9.21	0.38	63.2	2.4	32.26	0.88	9.06	0.34
Tarn1Bap_32	1236	13	275.6	6.3	1265	27	8.39	0.35	536	10	1424	25	263.5	4.6	1397	23	393.9	7.2	10.2	0.3
Tarn1Bap_33	657.7	8.4	2651	43	455	11	0.86	0.28	19.74	0.77	69.5	2	11.59	0.4	67.6	2.2	27.6	1	2.35	0.11
Tarn1Bap_34	2140	42	1040	19	640	15	0.033	0.015	2.5	0.14	18.2	0.55	7.48	0.23	100.9	2.2	192.8	3.9	87.8	1.5
Tarn1Bap_35	1661	24	221	4	1945	42	2.05	0.13	484	11	1402	30	261.5	4.7	1421	27	436.8	7.6	10.63	0.29
Tarn1Bap_36	611.6	9.3	3542	65	957	24	0.61	0.27	20.51	0.73	78.9	2.1	16.18	0.53	123.7	3.7	78.6	2.3	24.73	0.69
Tarn1Bap_37	206.2	3.1	1485	33	994	25	0.02	0.011	43.3	1.2	202.5	4.2	41.6	1.1	284.1	8.5	161.2	3.6	50.2	1.1
Tarn1Bap_38	417.2	6.5	703	15	701	17	0.02	0.012	16.19	0.52	69.6	1.9	15.61	0.42	127.5	3.7	86.6	2.4	19.25	0.49
Tarn1Bap_39	506.2	9.5	2532	48	747	40	0.019	0.011	38.4	1.1	166.1	4.3	30.25	0.83	201.5	4.9	117.8	3.2	36.3	1.1
Tarn1Bap_40	3755	72	348.8	6.6	386.7	8.6	0.046	0.02	114.1	2.4	246.8	5.8	31.11	0.83	130.8	3	40.5	1.2	40.5	1.2
Tarn1Bap_41	527.3	6.3	2222	28	255.3	4.1	LOD	LOD	3.94	0.19	14.06	0.39	2.8	0.13	20.22	0.74	11.97	0.46	3.34	0.11
Tarn1Bap_42	397.9	5.4	356.5	4.9	782	15	0.019	0.011	2.02	0.11	6.37	0.23	1.164	0.066	8.06	0.47	6.74	0.33	2.94	0.12
Tarn1Bap_43	360.3	5.4	397.5	9.8	205.7	5.8	LOD	LOD	1.86	0.12	6.27	0.27	1.092	0.095	7.7	0.46	4	0.26	1.199	0.076
Tarn1Bap_44	237.5	4	1865	38	434	10	0.046	0.025	9.82	0.33	34.36	0.98	6.39	0.23	44.5	1.6	29.68	0.84	6.3	0.18
Tarn1Bap_45	346	5.2	832	17	1048	24	12.96	0.47	165.6	5.4	460	16	68.2	2.3	374	12	95.4	2.7	17.35	0.45
Tarn1Bap_46	549.1	8.5	1177	23	897	22	0.025	0.014	27.59	0.96	145.7	4.1	32.94	0.94	235.5	6	137.1	3.6	44.9	1.1
Tarn1Bap_47	270.1	3.5	2048	29	611	11	0.029	0.013	20.1	2.3	170	16	56	4.2	507	31	388	16	114.2	3.8
Tarn1Bap_48	1247	22	295.4	9.1	1260	43	5.23	0.35	639	17	1620	50	286.2	8.3	1453	41	388	10	10.79	0.37
Tarn1Bap_49	759.9	9.2	538	9.9	636	11	0.011	0.009	17.48	0.49	54.4	1.2	9.22	0.25	63.7	1.8	37.4	1	9.49	0.23
Tarn1Bap_50	738	11	216.7	3.3	1225	22	5.93	0.24	332.4	5.7	995	23	181.8	3.6	993	17	299.8	6.1	7.78	0.23
Tarn1Bap_51	474.8	7.7	1203	23	921	21	0.03	0.014	25.7	9.3	36	11	4.12	0.87	20.8	2.6	10.71	0.55	3.64	0.15
Tarn1Bap_52	682	13	1868	44	612	13	0.37	0.13	11.48	0.44	35.62	0.78	7.03	0.22	43	1.7	22.31	0.98	6.96	0.26
Tarn1Bap_53	596	23	807	42	777	47	0.078	0.031	7.06	0.53	23.1	1.5	4.05	0.27	24.9	1.7	12.98	0.84	3.92	0.24
Tarn1Bap_54	276.3	6.5	742	28	373	15	LOD	LOD	3.36	0.23	12.18	0.46	2.15	0.15	14.5	1.1	7.59	0.54	2.1	0.15
Tarn02ap_0	616.9	7	647.6	7.7	1253	21	0.011	0.009	26.98	0.58	91.7	1.6	17.41	0.44	117.8	2.8	64.5	1.3	20.36	0.44
Tarn02ap_1	245.1	7.7	1416	19	287.5	4.3	LOD	LOD	3.95	0.21	13.61	0.33	2.83	0.11	21.78	0.97	13.49	0.46	3.57	0.14
Tarn02ap_2	406.3	7.6	543.8	8.1	1096	40	LOD	LOD	24.24	0.57	82.6	1.6	15.22	0.39	100.8	2.1	51.7	1.3	14.29	0.29
Tarn02ap_3	234.5	3.3	275.3	4.2	174.8	2.8	LOD	LOD	3.25	0.16	10.61	0.28	1.883	0.095	12.1	0.59	6.62	0.27	2.006	0.093
Tarn02ap_4	335	4.2	1012	14	733	12	0.016	0.012	5.68	0.22	20.32	0.46	3.73	0.11	27.32	0.9	15.87	0.52	3.88	0.14
Tarn02ap_5	222.1	3.1	2128	28	1163	21	LOD	LOD	4.99	0.19	20.74	0.52	4.13	0.14	33.5	1.2	21.07	0.64	6.97	0.18
Tarn02ap_6	243.7	3	470.8	6.7	186.8	2.9	LOD	LOD	1.2	0.087	4.72	0.19	0.835	0.066	5.91	0.33	3.26	0.2	1.04	0.066
Tarn02ap_7	761.8	9	585.4	8.4	661	16	LOD	LOD	10.27	0.33	33.15	0.84	5.69	0.22	35.4	1.2	17.46	0.61	4.72	0.15
Tarn02ap_8	216.7	2.7	940	14	374.8	5.8	LOD	LOD	5.17	0.19	17.17	0.41	3.08	0.12	21.2	0.9	10.61	0.42	2.92	0.14
Tarn02ap_9	290.2	3.6	766	11	309.8	4.5	LOD	LOD	2.35	0.12	8.69	0.24	1.623	0.083	10.84	0.52	5.85	0.31	1.757	0.077
Tarn02ap_10	596.9	7.4	398.2	5.5	999	17	LOD	LOD	16.48	0.35	60.03	0.95	11.43	0.24	78.9	1.7	43.7	1	12.32	0.33
Tarn02ap_11	632.8	7.9	538	7.4	1163	22	LOD	LOD	38.63	0.87	132.1	2.4	24.52	0.48	163.1	2.4	89.1	1.7	27.03	0.48
Tarn02ap_12	193.3	2.8	725	11	1153	21	0.38	0.11	2.59	0.14	10.56	0.34	2.29	0.1	17.5	0.77	11.9	0.45	4	0.12
Tarn02ap_13	366.9	4.6	1011	14	320.1	5.7	LOD	LOD	3.32	0.15	11.46	0.31	2.07	0.11	13.42	0.59	6.91	0.33	1.585	0.092
Tarn02ap_14	592.6	7.1	238.4	3.7	985	15	LOD	LOD	2.63	0.13	8.99	0.24	1.608	0.077	11.76	0.58	7.99	0.37	2.242	0.098
Tarn02ap_15	457.2	6.4	406.9	6.1	1020	15	LOD	LOD	8.93	0.26	33.12	0.71	6.67	0.21	48.9	1.4	35.86	0.93	15.32	0.28
Tarn02ap_16	681.7	8.2	154	2.3	789	11	LOD	LOD	3.9	0.19	11.06	0.35	2.19	0.1	13.86	0.54	7.65	0.32	2.98	0.12
Tarn02ap_17	394.8	5	334	5.3	348.7	6.1	0.062	0.025	3.89	0.19	13.24	0.39	2.47	0.13	16.61	0.73	8.62	0.52	2.62	0.11
Tarn02ap_18	331.4	4.1	1195	17	987	19	LOD	LOD	3.26	0.16	11.39	0.29	2.22	0.11	16.3	0.67	10.78	0.43	3.68	0.14
Tarn02ap_19	507.9	5.3	1939	25	814	13	LOD	LOD	100.6	2	341.2	5.3	62.6	1.1	375.7	6.7	181.5	3	53.68	0.94
Tarn02ap_20	275.5	3.9	339.5	4.3	146.4	2.5	LOD	LOD	1.285	0.097	4.47	0.17	0.905	0.072	5.6	0.49	3.35	0.21	0.88	0.059
Tarn02ap_21	781.5	8.4	539.8	6.8	1278	24	LOD	LOD	19.16	0.47	68.2	1	13.33	0.29	89.1	1.8	50.2	1	15.05	0.28
Tarn02ap_22	370	4.1	963	12	1135	19	LOD	LOD	17.39	0.44	64.3	1	13.37	0.29	96.8	2.2	72.8	1.5	25.78	0.45
Tarn02ap_23	468.8	8.2	198.6	3.5	390	6.7	LOD	LOD	4.25	0.17	13.55	0.36	2.47	0.11	16.7	0.8	8.33	0.41	2.48	0.12
Tarn02ap_24	431	5.9	1144	57	1110	100	0.364	0.081	110	18	364	58	59.7	9.2	339	51	126	18	5.75	0.32
Tarn02ap_25	670.6	7.7	454.2	6.7	781	12	0.014	0.011	5.14	0.21	15.76	0.39	2.77	0.14	17.44	0.74	10.38	0.43	3.94	0.14
Tarn02ap_26	359.1	4.8	1273	17	927	13	0.012	0.01	26.26	0.64	98	1.6	20.08	0.45	151.2	3.3	105.3	2	32.95	0.48
Tarn02ap_27	375	4.6	1717	22	317	11	LOD	LOD	1.9	0.1	6.48	0.23	1.151	0.091	7.67	0.57	4.37	0.3	1.627	0.085
Tarn02ap_28	509.7	6.3	1997	30	224.1	3.6	LOD	LOD	1.773	0.093	6.42	0.24	1.298	0.085	9.59	0.55	5.07	0.28	1.623	0.087
Tarn02ap_29	424.6	5	1920	22	888	12	LOD	LOD	81	1.5	311.5	4.4	59.15	0.98	384.1	5.7	205.2	3.1	60.63	0.9
Tarn02ap_30	856	11	900	20	876	13	LOD	LOD	5.5	0.48	20.5	1.8	4.18	0.35	27	2	18.4	1.2	5.45	0.41
Tarn02ap_31	418.9	5	656.2	8.7	2104	31	0.665	0.086	296	5	915	16	157.2	2.5	871	13	317.6	5.1	4.15	0.14
Tarn02ap_32	424.7	4.8	532	7.5	897	14	LOD	LOD	1.88	0.11	7.95	0.24	1.922	0.098	14.83	0.62	12.08	0.42	3.91	0.14
Tarn02ap_33	351.5	4.7	3101	41	466.3	7.7	LOD	LOD	4.49	0.15	16.75	0.36	3.24	0.12	23.63	0.76	13.62	0.49	3.96	0.15
Tarn02ap_34	195.8	2.7	356.7	5.9	143.5	6	LOD	LOD	1.496	0.096	5.31	0.19	0.929	0.067	6.64	0.47	3.51	0.29	1.062	0.07
Tarn02ap_35	330.1	4	631	12	717	13	LOD	LOD	2.03	0.13	7.39	0.24	1.471	0.091	10.79	0.61	6.93	0.43	2.37	0.11
Tarn02ap_36	410.4	4.8	291.7	4.4	187.5	3.6	LOD	LOD	2.04	0.12	6.65	0.23	1.126	0.065	7.6	0.5	3.69	0.23	1.102	0.065
Tarn02ap_37	1172	11	430.4	6.5	1048	17	LOD	LOD	18.37	0.48	63.9	1.1	12.92	0.26	90.3	2.1	51.4	1	14.67	0.28
Tarn02ap_38	581.2	6.1	540.3	7.7	1124	22	LOD	LOD	13.36	0.38	49.34	0.85	9.82	0.26	70.4	1.7	40.72	0.94	12.62	0.25
Tarn02ap_39	383.7	4.5	2919	69	296.3	5.6	0.127	0.032	2.61	0.14	11.15	0.29	2.23	0.13	16.68	0.68	10.29	0.51	2.43	0.11
Tarn02ap_40	235.5	4.1	459	10	41.79	0.93	LOD	LOD	0.161	0.028	0.573	0.057	0.125	0.025	0.85	0.15	0.423	0.082	0.134	0.022
Tarn02ap_41	318.8	4.3	460	6	237.6	3.5	LOD	LOD	2.03	0.11	6.54	0.24	1.173	0.069	7.86	0.41	4.06	0.23	1.298	0.077
Tarn02ap_42	513.7	6.6	231.7	3.9	222.5	3.3	LOD	LOD	1.95	0.11	6.82	0.21	1.224	0.082	8.6	0.49	4.33	0.25	1.344	0.066
Tarn02ap_43	505.3	6.8	1101	20	936	17	LOD	LOD	5.82	0.25	21.23	0.73	4.13	0.18	30.1	1.1	19.72	0.69	6.89	0.22
Tarn02ap_44	261.6	4.5	1629	28	867	34	0.104	0.036	19.25	0.51	67.2	1.3	13.19	0.37	105.6	2.4	68.3	1.6	27.02	0.56
Tarn02ap_45	622.1	7.7	598.6	8.2	255.7	3.7	LOD	LOD	34.58	0.71	131.1	2	25.48	0.47	174.9	3.3	97.9	1.7	28.32	0.53
Tarn02ap_46	281.9	4.9	382.8	5.9	356	10	LOD	LOD	1.53	0.11	5.44	0.24	0.979	0.058	7.11	0.39	3.74	0.26	1.083	0.072
Tarn02ap_47	280.2	3.8	1340	18	1238	23	LOD	LOD	44.07	0.84	165.7	2.5	33.95	0.57	239.4	4.3	184.6	2.8	53.18	0.81
Tarn02ap_48	245.4	8.7	896	14	791	32	0.013	0.01	14.51	0.46	49.3	1.4	9.29	0.3	69.4	1.9	39.7	1.1	13.75	0.29
Tarn02ap_49	431	6.4	562.5	9.4	648	17	2.21	0.43	6.53	0.35	24.1	1.1	4.77	0.26	33.4	1.9	18.71	0.95	5.67	0.24
Tarn02ap_50	452	6.3	572.4	9.7	240.6	3.3	LOD	LOD	1.876	0.088	6.62	0.21	1.172	0.091	8.48	0.51	4.26	0.27	1.304	0.058
Tarn02ap_51	500.7	6.8	326.8	5.4	328.8	5.8	0.049	0.027	4.75	0.26	14.82	0.58	2.81	0.15	16.73	0.97	8.78	0.38	2.46	0.15

	157Gd	±	159Tb	±	163Dy	±	165Ho	±	166Er	±	169Tm	±	172Yb	±	175Lu	±	182W	±	232Th	±	238U	±
Tarn1Bap_26	321.7	7.2	60.2	1.1	449.5	9.7	97	1.9	271.3	6.2	34.96	0.93	196	5.7	22.76	0.73	0.144	0.03	6.38	0.15	17	0.44
Tarn1Bap_27	2.06	0.14	0.604	0.034	6.96	0.31	2.713	0.069	15.7	0.35	4.15	0.11	46.6	1	11.28	0.28	1.36	0.11	0.052	0.008	0.016	0.003
Tarn1Bap_28	233	11	46.4	2.7	302	21	48.5	3.7	101.4	9.1	11	1.1	54.5	5.9	5.65	0.67	0.32	0.053	0.367	0.023	0.245	0.019
Tarn1Bap_29	309.9	5.3	42.2	0.71	240.1	3.9	42.19	0.72	109.2	1.9	14.4	0.28	86.3	1.7	10.73	0.23	0.068	0.025	28.33	0.52	13.86	0.23
Tarn1Bap_30	11.8	0.46	3.1	0.084	31.04	0.77	8.22	0.15	22.37	0.47	2.477	0.077	15.77	0.41	2.767	0.084	0.184	0.038	0.052	0.008	0.103	0.008
Tarn1Bap_31	65.2	1.6	12.7	0.3	105.4	3	27.24	0.89	98.8	3.6	16.4	0.66	112.5	4.2	14.84	0.65	0.299	0.057	5.59	0.7	2.18	0.31
Tarn1Bap_32	339	5.1	46.2	0.67	269	4.4	47.92	0.75	125.8	2	16.76	0.41	100.7	2.2	12.83	0.35	0.86	0.11	38.33	0.77	14.27	0.23
Tarn1Bap_33	44.7	1.2	8.72	0.24	67.8	1.4	15.68	0.29	49	1.2	6.99	0.16	45.4	1	6.31	0.16	0.067	0.022	0.316	0.02	0.591	0.026
Tarn1Bap_34	513	9	64.6	1	257.7	4	30.87	0.48	59.2	1.1	6.47	0.14	35.71	0.86	4.52	0.12	0.155	0.04	2.09	0.1	0.466	0.021
Tarn1Bap_35	402.4	7.7	61.2	1	380.7	4.9	70.7	1.1	200.6	2.8	29.37	0.53	192.1	3.2	24.86	0.42	0.178	0.036	29.22	0.96	19.5	0.64
Tarn1Bap_36	193.1	5.8	34.72	0.89	225.2	4.5	39.6	0.81	94.1	1.6	11.15	0.23	61.7	1.5	7.65	0.21	0.151	0.044	0.517	0.032	0.246	0.014
Tarn1Bap_37	271.6	5.6	49.23	0.85	290.9	4.5	45.55	0.66	104	1.8	12.08	0.22	64.8	1.5	7.27	0.2	0.03	0.017	0.158	0.014	0.775	0.023
Tarn1Bap_38	164.9	3.4	27.41	0.54	169.8	2.3	28.42	0.39	65.8	1.1	7.97	0.18	43.99	0.84	5.22	0.13	0.049	0.017	0.283	0.05	1.675	0.053
Tarn1Bap_39	178.1	4.8	30.3	1	185.2	7.2	30.1	1.3	65.7	3.3	7.08	0.44	33.1	2.4	3.29	0.26	0.035	0.016	0.055	0.008	0.143	0.01
Tarn1Bap_40	45.4	1.2	8.72	0.2	61	1.5	11.97	0.27	35.09	0.71	5.04	0.16	32.38	0.9	3.91	0.14	0.96	0.11	11.1	0.33	36.93	0.71
Tarn1Bap_41	26.57	0.75	4.54	0.11	33.2	0.73	8.09	0.16	25.86	0.52	4.174	0.099	31.39	0.65	5.05	0.12	0.283	0.049	0.052	0.008	0.371	0.015
Tarn1Bap_42	31.36	0.79	9.11	0.17	98.4	1.7	27.36	0.46	87.5	1.4	12.06	0.21	66.6	1.1	7.58	0.17	0.167	0.042	0.026	0.005	0.387	0.016
Tarn1Bap_43	9.86	0.43	2.201	0.082	22.22	0.62	6.56	0.19	21.26	0.48	2.543	0.082	10.92	0.42	1.049	0.056	0.068	0.022	0.007	0.003	0.053	0.006
Tarn1Bap_44	79.5	1.8	17.42	0.31	118.7	2.1	16.82	0.33	25.13	0.61	1.555	0.063	4.79	0.21	0.393	0.027	0.165	0.038	0.081	0.01	1.044	0.036
Tarn1Bap_45	106.2	2.4	16.26	0.29	125.1	2.2	33.69	0.73	144.3	2.7	29.68	0.58	240.3	5.2	34.99	0.85	0.175	0.037	6.79	0.38	1.675	0.043
Tarn1Bap_46	247.2	4.7	43.11	0.78	248.7	4.2	38.83	0.67	83.7	1.5	9.24	0.25	46.38	0.98	5.27	0.16	0.213	0.045	0.3	0.034	0.25	0.014
Tarn1Bap_47	443	13	50	1.2	212	4.3	27.09	0.52	52.6	1	5.45	0.15	26.1	0.66	2.583	0.096	0.069	0.02	0.84	0.14	0.271	0.027
Tarn1Bap_48	326.9	7.9	43.9	1	254.3	4.6	45.46	0.76	120	2.2	16.34	0.37	106.3	2.6	13.69	0.34	0.158	0.04	23.7	0.54	16.33	0.51
Tarn1Bap_49	90.4	2.1	17.16	0.36	122.1	2.1	24.28	0.43	70	1.3	10.42	0.24	75.2	1.8	12.53	0.28	0.234	0.047	0.102	0.013	0.701	0.03
Tarn1Bap_50	267.9	4.7	39.3	0.65	241.1	4.2	44.16	0.78	120.5	2.1	17.12	0.34	108	1.6	14.02	0.29	0.178	0.033	15.67	0.35	8.08	0.17
Tarn1Bap_51	32.6	1.1	8.76	0.19	104.2	1.9	30.42	0.56	91.4	1.5	11.4	0.27	59.7	1.4	6.72	0.17	0.089	0.028	2.77	0.93	0.248	0.038
Tarn1Bap_52	47.8	1.3	9.95	0.25	85.9	1.9	20.43	0.45	62.7	1.4	8.72	0.22	50.6	1.3	6.25	0.2	1.26	0.23	0.376	0.028	0.399	0.019
Tarn1Bap_53	31	1.5	7.33	0.29	76.3	2.1	23.42	0.43	95.5	2	16.84	0.48	121	5.4	16.38	0.82	0.156	0.037	0.346	0.042	0.466	0.03
Tarn1Bap_54	18.29	0.78	4.11	0.19	40.5	1.6	11.49	0.35	38.5	1.3	5.25	0.25	27.3	1.2	3.06	0.15	0.202	0.053	LOD	LOD	0.147	0.013
Tarn02ap_0	153.8	2.4	33.69	0.42	275.6	3.6	56.7	0.56	140.2	1.7	16.84	0.24	85.7	1.2	9.48	0.15			0.07	0.007	1.322	0.032
Tarn02ap_1	31.75	0.85	5.81	0.12	43.71	0.71	10.5	0.19	30.79	0.59	4.081	0.095	26.24	0.72	4.36	0.13			0.072	0.01	0.141	0.008
Tarn02ap_2	104.6	2.2	22.94	0.49	195.6	5.1	44.5	1.5	122.6	4.6	15.2	0.62	80.5	3.4	8.37	0.41			0.032	0.006	0.708	0.044
Tarn02ap_3	14.71	0.53	3.185	0.081	27.73	0.67	6.25	0.12	15.4	0.34	1.442	0.048	5.64	0.21	0.6	0.033			0.038	0.007	0.088	0.006
Tarn02ap_4	39.11	0.9	8.81	0.14	84.8	1.1	24.76	0.35	87.8	1.2	12.04	0.2	62.6	1.1	6.71	0.13			0.028	0.005	0.13	0.008
Tarn02ap_5	62.3	1.2	15.64	0.23	162.1	1.8	45.43	0.52	137.1	2	16.64	0.3	81.7	1.4	8.71	0.15			0.013	0.004	0.169	0.01
Tarn02ap_6	8.76	0.37	1.97	0.074	20.3	0.43	6.01	0.14	20.54	0.32	2.545	0.076	12.61	0.43	1.455	0.061			0.004	0.002	0.029	0.004
Tarn02ap_7	33.52	0.98	7.99	0.21	75.5	1.7	22.09	0.5	78.9	1.7	12.1	0.25	78.8	1.5	11.23	0.23			0.018	0.004	0.214	0.012
Tarn02ap_8	22.58	0.66	5.02	0.12	45.21	0.77	12.5	0.17	44.86	0.72	6.48	0.14	33	0.75	3.22	0.1			0.011	0.003	0.126	0.009
Tarn02ap_9	13.42	0.45	3.09	0.088	31.31	0.57	9.83	0.17	42.7	0.58	8.44	0.16	67.2	1.1	10.82	0.19			0.008	0.003	0.158	0.009
Tarn02ap_10	98.5	1.8	22.47	0.32	187.6	2.3	36.15	0.44	69	1.2	5.23	0.11	16.94	0.42	1.341	0.045			0.023	0.004	0.731	0.022
Tarn02ap_11	190.1	2.7	37.96	0.56	280.2	3.4	52.13	0.6	124.1	1.8	14.29	0.26	73.2	1.2	8.07	0.19			0.07	0.008	1.282	0.032
Tarn02ap_12	37.97	0.8	10.74	0.18	125.7	1.6	39.75	0.5	133.9	1.6	17.69	0.25	94.3	1.4	10.3	0.2			0.321	0.054	0.228	0.011
Tarn02ap_13	16.16	0.55	3.71	0.1	35.81	0.8	9.86	0.2	35.11	0.79	4.88	0.12	25.19	0.72	2.71	0.1			0.011	0.003	0.12	0.008
Tarn02ap_14	27.66	0.64	7.81	0.13	93.6	1.2	34.35	0.44	148.5	1.9	27.91	0.38	234.2	3.2	41.29	0.66			0.004	0.002	0.538	0.017
Tarn02ap_15	117	1.8	28.04	0.4	221.4	2.5	42.15	0.59	102.6	1.3	12.29	0.18	67	1.1	7.68	0.14			0.028	0.006	0.6	0.018
Tarn02ap_16	18.94	0.52	5.38	0.11	64.92	0.83	23.06	0.31	108.5	1.5	21.25	0.31	160.9	2.1	24.6	0.38			0.027	0.005	0.433	0.015
Tarn02ap_17	19.65	0.68	4.149	0.098	39.43	0.82	11.16	0.19	41.12	0.66	6.37	0.13	41.39	0.92	5.58	0.15			0.037	0.007	0.104	0.007
Tarn02ap_18	32.47	0.79	8	0.17	91.4	1.7	31.69	0.61	119.9	2.1	15.67	0.32	76.2	1.7	7.64	0.19			0.01	0.004	0.08	0.005
Tarn02ap_19	288.8	4	45.05	0.59	249.5	3.5	37.06	0.54	73.4	1.2	7.05	0.14	30.56	0.61	3.058	0.093			1.198	0.043	0.201	0.009
Tarn02ap_20	7.34	0.34	1.777	0.059	17.55	0.46	4.781	0.092	14.67	0.31	1.784	0.061	8.3	0.28	1.039	0.041			0.007	0.003	0.03	0.004
Tarn02ap_21	118.2	1.6	28.03	0.39	247.6	3	53.62	0.73	141.8	1.7	17.69	0.32	95.2	1.4	10.44	0.19			0.034	0.006	1.12	0.024
Tarn02ap_22	214.2	2.7	41.98	0.61	280	4	48.66	0.63	111.3	1.6	11.87	0.21	57.8	1.1	6.35	0.14			0.044	0.006	0.493	0.017
Tarn02ap_23	19.6	0.65	4.16	0.093	40.28	0.73	12.67	0.24	56.09	0.95	11.64	0.22	105.2	2.2	19.44	0.48			0.018	0.005	0.26	0.014
Tarn02ap_24	179	23	30.6	3.7	208	24	43	4.6	119	12	15.9	1.4	96.8	8	13.5	1.1			6.82	0.38	7.24	0.78
Tarn02ap_25	32.84	0.83	9.12	0.2	94.9	1.6	27.28	0.49	96.5	1.6	15.93	0.31	109.6	2	15.73	0.3			0.055	0.008	1.204	0.034
Tarn02ap_26	238.2	3.5	39.41	0.45	236.2	3.6	38.88	0.55	86.7	1.1	10.22	0.18	54.72	0.94	6.56	0.15			0.343	0.021	0.57	0.021
Tarn02ap_27	10.08	0.44	2.59	0.11	28.3	1.1	9.67	0.36	41.3	1.5	7.42	0.21	49.31	0.99	6.75	0.13			0.024	0.005	0.133	0.009
Tarn02ap_28	13.49	0.48	2.893	0.083	26.31	0.57	7.24	0.12	25.45	0.46	3.668	0.086	22.08	0.46	3.013	0.077			0.008	0.003	0.104	0.008
Tarn02ap_29	320.9	3.8	50.88	0.63	277.7	3.4	40.34	0.51	84	1.2	9.13	0.15	47.27	0.82	5.42	0.11			2.774	0.061	0.407	0.014
Tarn02ap_30	48.6	2.2	13.41	0.48	125.3	2.6	30.62	0.36	91.9	1.4	12.37	0.23	69.8	1.8	7.97	0.22			0.033	0.006	0.509	0.018
Tarn02ap_31	423.4	5.5	70.15	0.93	452.1	5	87.13	0.95	223.2	2.8	26.23	0.35	139	1.9	18.81	0.34			5.285	0.093	10.61	0.16
Tarn02ap_32	45.93	0.88	12.45	0.22	120.6	1.6	31.58	0.38	99.1	1.2	13.98	0.17	83.1	1.1	9.98	0.16			0.015	0.004	0.464	0.015
Tarn02ap_33	33.12	0.73	6.68	0.12	60.09	0.83	15.6	0.25	48.9	0.73	5.83	0.11	26.94	0.53	2.75	0.077			0.01	0.003	0.111	0.008
Tarn02ap_34	7.94	0.46	1.8	0.081	17.52	0.63	4.6	0.2	15.28	0.79	2.11	0.12	11.42	0.65	1.072	0.066			0.002	0.001	0.038	0.005
Tarn02ap_35	22.71	0.77	5.97	0.15	68	1.3	22.49	0.42	80.3	1.6	10.15	0.18	51.01	0.94	5.91	0.15			0.011	0.003	0.087	0.006
Tarn02ap_36	7.96	0.33	1.83	0.07	18.13	0.41	5.71	0.12	27.74	0.5	6.17	0.15	52.04	0.99	7.87	0.19			0.003	0.002	0.04	0.005
Tarn02ap_37	119.2	1.8	25.11	0.31	198.6	2.8	41.66	0.52	113.4	1.3	15.28	0.25	90.2	1.5	11.07	0.22			0.121	0.013	1.244	0.03
Tarn02ap_38	96.3	1.7	21.48	0.27	186.1	2.6	43.96	0.59	122.5	1.4	14.63	0.22	74.6	1.1	8.12	0.16			0.041	0.007	0.625	0.016
Tarn02ap_39	23.43	0.7	4.77	0.13	38.74	0.81	9.61	0.21	31.24	0.6	4.52	0.14	29.39	0.74	4.82	0.11			0.041	0.006	1.007	0.035
Tarn02ap_40	1.14	0.1	0.295	0.024	3.24	0.16	1.201	0.057	5.94	0.18	1.244	0.049	10.45	0.36	1.91	0.067			0.03	0.008	0.007	0.002
Tarn02ap_41	9.27	0.39	2.251	0.073	23.03	0.43	6.99	0.12	27.74	0.43	4.423	0.097	23.08	0.49	2.559	0.071			0.003	0.002	0.055	0.005
Tarn02ap_42	8.87	0.36	1.947	0.062	19.02	0.37	6.57	0.13	33.76	0.44	7.84	0.12	67.6	1.1	10.63	0.17			0.003	0.002	0.095	0.007
Tarn02ap_43	56.7	1.3	14.33	0.24	138.9	2	33.57	0.42	94.8	1.7	12.12	0.25	68.9	1.7	8.47	0.23			0.045	0.006	0.486	0.03
Tarn02ap_44	176.9	4.3	31.64	0.89	205.1	6.1	34.7	1.3	77.2	3.8	8.59	0.58	47.8	3.9	5.65	0.48			0.795	0.044	0.196	0.021
Tarn02ap_45	170	2.4	25.73	0.38	113.3	1.3	10.52	0.19	12.53	0.33	0.821	0.039	2.84	0.15	0.289	0.025			0.042	0.008	1.763	0.034
Tarn02ap_46	10.22	0.42	2.416	0.072	27.75	0.6	10.41	0.27	53.6	1.2	11.44	0.3	93.8	2	14.46	0.29			0.002	0.001	0.135	0.009
Tarn02ap_47	380.1	4.3	60.6	0.68	344.8	4.2	55.21	0.57	126.5	1.6	14.29	0.21	70.5	1.1	7.37	0.16			0.211	0.015	2.193	0.041
Tarn02ap_48	108.6	1.9	21.65	0.46	161.9	3.7	31.42	0.96	67	2.7	6.31	0.38	27.9	1.9	2.88	0.21			0.83	0.11	0.139	0.008
Tarn02ap_49	46.2	1.6	10.35	0.29	94.4	2.5	22.92	0.58	61.5	1.4	6.91	0.19	32.14	0.83	3.51	0.12			3.3	0.61	0.256	0.026
Tarn02ap_50	10.91	0.4	2.42	0.065	24.22	0.48	7.52	0.13	31.75	0.53	6.33	0.14	55.01	0.97	10.02	0.2			0.007	0.003	0.074	0.006
Tarn02ap_51	18.93	0.98	4.3	0.16	39.9	1	10.66	0.2	38.62	0.59	6.55	0.14	46.9	1	7.02	0.14			0.298	0.037	0.152	0.019

Supporting Information Tables S3.5: Apatite trace-element data (continued)

	55Mn	±	86Sr	±	89Y	±	90Zr	±	139La	±	140Ce	±	141Pr	±	146Nd	±	147Sm	±	153Eu	±	157Gd	±	159Tb	±	163Dy	±	165Ho	±	166Er	±	169Tm	±	172Yb	±	175Lu	±	182W	±	232Th	±	238U	±
Tarn02ap_52	632.6	8.5	524.9	8.6	2390	150	LOD	LOD	6.2	0.24	21.84	0.52	4.47	0.17	32.6	1.2	23.78	0.78	8.22	0.33	89.2	3.2	28.2	1.2	342	17	96.6	5.1	297	18	40.1	2.7	223	17	24.9	1.9			0.063	0.01	0.454	0.029
Tarn02ap_53	314	4.4	1509	18	378.9	6.5	LOD	LOD	9.81	0.26	33.97	0.6	6.39	0.19	41.3	1.1	22.78	0.7	6.38	0.18	49.5	1.1	10.2	0.21	72.5	1.3	12.61	0.23	27.14	0.45	2.714	0.098	11.85	0.34	1.167	0.046			0.022	0.005	0.373	0.014
Tarn02ap_54	259.1	3.7	903	13	1499	24	LOD	LOD	50.34	0.87	200.3	3.3	41.29	0.85	299	5	176.8	2.9	53.96	0.82	350.6	5	60.48	0.73	388.1	4.8	68.1	1	160.8	2.2	19	0.32	100.7	1.6	11.38	0.23			0.121	0.012	0.976	0.024
Tarn02ap_55	564	5.7	998	17	360.1	6.8	0.019	0.012	4.33	0.22	10.71	0.26	2.23	0.12	12.63	0.73	6	0.33	1.699	0.081	12.47	0.49	2.896	0.081	29.98	0.61	10.68	0.21	53.9	0.9	11.92	0.21	105.5	1.6	17.24	0.3			1.205	0.055	0.235	0.011
Tarn02ap_56	705.2	8.4	1795	24	802	13	0.055	0.021	9.66	0.26	40.84	0.91	8.18	0.24	59.7	1.5	39.15	0.87	11.65	0.23	94.9	1.6	19.76	0.33	150	2.2	30.58	0.43	81.1	1.1	10.36	0.2	59.6	1	7.37	0.15			0.082	0.009	0.249	0.013
Tarn02ap_57	283.7	3.1	376.8	5.4	431.6	6.9	LOD	LOD	3.28	0.16	11.36	0.31	2.074	0.084	15.32	0.69	10.17	0.41	4.44	0.15	44	1	11.46	0.2	89.2	1.4	15.22	0.23	26.97	0.51	2.11	0.06	7.62	0.27	0.623	0.032			0.014	0.004	1.262	0.031
Tarn02ap_58	693.2	8.5	558.6	8	935	14	LOD	LOD	20.69	0.47	70.2	1.4	13.45	0.31	90.5	2	50.5	1	15.63	0.38	114.5	1.9	24.11	0.34	187.1	2.9	37.04	0.51	91.7	1.3	10.53	0.21	55.9	0.9	6.28	0.15			0.046	0.008	1.186	0.03
Tarn02ap_59	321.3	4.5	1595	29	391	17	LOD	LOD	1.463	0.082	5.09	0.27	1.006	0.07	6.66	0.44	4.21	0.31	1.56	0.1	10.87	0.53	3.01	0.14	33.4	1.5	11.6	0.47	49.7	2.1	8.19	0.3	51.8	1.8	6.78	0.24			0.004	0.002	0.088	0.007
Tarn02ap_60	407.8	5.3	985	13	1022	16	LOD	LOD	19.09	0.41	77.9	1.5	16.41	0.39	128.4	3	77.3	1.5	23.41	0.44	167	2.4	29.67	0.5	200.3	3.1	38.04	0.52	98.4	1.4	12.75	0.19	72.78	0.95	8.55	0.17			0.155	0.013	1.322	0.034
Tarn02ap_61	1632	24	1000	15	180.6	3.1	LOD	LOD	2.22	0.13	7.24	0.27	1.456	0.095	9.34	0.56	5.28	0.31	1.674	0.09	12.23	0.51	2.998	0.082	26.45	0.69	5.84	0.14	12.75	0.4	1.107	0.053	3.74	0.2	0.329	0.029			LOD	LOD	0.071	0.012
Tarn02ap_62	347.4	3.9	358.5	5	269.3	4.9	LOD	LOD	1.688	0.096	5.83	0.21	1.07	0.073	7.42	0.41	4.4	0.29	1.293	0.064	11.05	0.45	2.627	0.086	26.53	0.55	8.49	0.17	35.75	0.62	6.84	0.13	50.2	1	6.87	0.15			0.006	0.002	0.039	0.004
Tarn02ap_63	580.9	7	2340	29	570.6	9.6	LOD	LOD	20.75	0.55	101.4	1.8	22.32	0.42	161.9	2.7	84.4	1.6	22.94	0.44	141.7	2.5	22.52	0.35	128	1.6	22.11	0.32	57	0.84	8.31	0.16	60.02	0.79	9.34	0.17			0.345	0.02	0.103	0.007
Tarn02ap_64	477	10	1374	35	642	20	LOD	LOD	10.37	0.31	46.1	1	10.31	0.34	84.7	2.3	60.4	2.4	13.71	0.5	111.5	2.4	19.31	0.36	127.1	2.9	24.02	0.64	64.4	2	8.41	0.25	48.1	1.6	5.84	0.23			0.022	0.005	0.213	0.012
Tarn02ap_65	446.5	5.9	2483	35	1025	31	0.061	0.031	13.44	0.38	54.4	1.1	11.15	0.29	86.2	2.1	55	1.6	17.62	0.4	143.1	3	28.65	0.72	215.6	5.5	41.1	1.1	98.1	3.3	11.56	0.48	60.3	2.5	7.15	0.34			0.557	0.038	0.363	0.052
Tarn02ap_66	1079	11	1084	14	1030	19	LOD	LOD	13.9	0.41	54.17	0.98	10.87	0.32	82.7	1.8	54.3	1	16.98	0.3	146.9	2	31.59	0.4	240.1	2.9	45.25	0.66	103.8	1.3	11.04	0.19	50.91	0.85	4.91	0.1			0.027	0.005	0.396	0.015
Tarn02ap_67	762	11	667	10	694	10	LOD	LOD	3.31	0.17	12.53	0.28	2.57	0.12	19.58	0.66	14.38	0.52	4.11	0.13	53.3	1	13.56	0.22	115.1	1.5	25.35	0.35	75.7	1.1	11.52	0.21	82.5	1.3	11.97	0.23			0.029	0.005	0.219	0.01
Tarn02ap_68	662.2	7.1	457.6	6.6	1206	21	LOD	LOD	20.4	0.47	72.3	1.3	13.78	0.32	97.8	2.2	57	1.3	18.19	0.36	143	2.4	32.35	0.42	260.5	3.2	52.58	0.72	130.8	1.4	15.15	0.23	76	1.2	8.34	0.16			0.026	0.006	1.047	0.028
Tarn02ap_69	347.4	5.6	1517	27	186.6	3	LOD	LOD	2.01	0.13	7.32	0.29	1.452	0.086	11.49	0.56	6.71	0.31	1.603	0.08	15.66	0.51	3.084	0.095	24.82	0.58	6.15	0.13	19.03	0.42	2.504	0.077	15.1	0.43	2.359	0.075			0.037	0.007	0.126	0.01
Tarn02ap_70	357.2	4.5	1018	15	774	13	LOD	LOD	28.86	0.56	97.8	2	20.94	0.46	166.3	3.4	102.6	1.9	33.85	0.59	230.6	3.4	34.95	0.55	200.7	3.1	32.04	0.45	72.03	0.94	8.47	0.15	48.47	0.8	6.22	0.14			0.748	0.036	0.215	0.01
Tarn02ap_71	200.2	3.5	454.3	7.2	139.1	2.5	LOD	LOD	0.446	0.051	1.718	0.097	0.302	0.035	2.3	0.23	1.44	0.17	0.463	0.034	3.95	0.24	1.053	0.047	13.09	0.38	4.4	0.11	17.67	0.41	2.856	0.077	15.94	0.54	1.48	0.049			LOD	LOD	0.023	0.003
Tarn02ap_72	688	10	1233	26	281.2	6.5	0.062	0.038	3.44	0.17	12.32	0.41	2.37	0.13	15.7	0.91	9.59	0.58	2.18	0.13	21.06	0.81	4.96	0.16	41.3	1.1	9.9	0.23	31.78	0.75	5.08	0.15	33.9	1.1	4.44	0.15			0.043	0.009	0.121	0.008
Tarn02ap_73	206.1	3.2	863	13	447.8	8.3	LOD	LOD	2.26	0.15	8.74	0.28	1.76	0.094	11.95	0.63	7.52	0.43	1.9	0.1	17.84	0.52	4.31	0.11	43.43	0.89	13.52	0.26	55.68	0.81	9.91	0.2	65.8	1	7.65	0.18			0.004	0.002	0.082	0.007
Tarn02ap_74	294.4	4.1	515.1	7.6	970	14	LOD	LOD	5.25	0.22	17.34	0.46	3.26	0.13	22.39	0.89	15.69	0.54	6.12	0.17	56.7	1.2	15.7	0.24	154.7	1.9	36.75	0.46	103.7	1.5	13.19	0.21	71.7	1.1	8.14	0.2			0.025	0.006	2.505	0.049
Tarn02ap_75	828.1	9.2	267.7	4.4	1274	23	0.437	0.061	624.9	9.7	1633	21	270	3.8	1395	21	363	4.7	6.66	0.2	372.5	4.5	50.43	0.58	297.2	3.1	54.92	0.58	136.7	1.8	16.12	0.28	92.2	1.3	12.33	0.21			205	36	9.53	0.3
Tarn02ap_76	359.9	5.5	400.5	5.6	726	11	LOD	LOD	4.1	0.19	15.73	0.42	3.19	0.14	23.04	0.79	13.32	0.39	3.92	0.12	32	0.77	7.36	0.13	74.1	1.1	22.62	0.31	87.8	1.1	12.87	0.24	70	1.2	7.46	0.16			0.009	0.003	0.078	0.007
Tarn02ap_77	524.5	7	132.3	2.5	14.3	0.35	LOD	LOD	LOD	LOD	LOD	LOD	LOD	LOD	LOD	LOD	0.014	0.014	0	2E-07	0.201	0.043	0.077	0.013	1.24	0.11	0.546	0.033	2.75	0.094	0.569	0.036	4.54	0.2	0.975	0.045			LOD	LOD	0.001	0.001
Tarn02ap_78	400.4	5.2	420.8	6.1	783.7	9.8	0.02	0.012	5.68	0.34	13.94	0.38	3.03	0.16	18.58	0.79	10.58	0.41	3.16	0.1	29.22	0.68	7.52	0.15	86.5	1.3	26.69	0.4	93.5	1.5	12.78	0.2	69.4	1.3	8.32	0.19			0.514	0.038	0.185	0.012
Tarn02ap_79	400.2	5.3	1134	14	405.8	5.8	LOD	LOD	3.02	0.15	11.17	0.34	2.237	0.091	15.15	0.69	8.89	0.37	2.441	0.099	22.69	0.64	5.09	0.12	49.11	0.82	13.49	0.2	42.38	0.7	4.88	0.12	19.5	0.49	1.559	0.051			0.015	0.004	0.151	0.009
Tarn02ap_80	405.5	7.1	1601	23	1270	130	0.015	0.013	27.79	0.73	108.1	2.2	23.3	0.65	191	5.1	138.8	3.7	45.6	1.8	320	16	55.1	3.9	339	28	54.6	5.2	120	14	13.2	1.8	67	11	7.3	1.3			2.1	2	0.253	0.02
Tarn02ap_81	232.3	3.5	479.4	7.4	420.3	6.7	LOD	LOD	4.94	0.18	16.24	0.36	2.86	0.11	18.27	0.68	9.63	0.43	2.73	0.11	20.95	0.66	4.59	0.11	42.92	0.67	13.19	0.19	56.76	0.76	10.19	0.17	70.2	1.1	9.37	0.18			0.012	0.004	0.146	0.009
Tarn02ap_82	622.9	8.8	234.8	4.7	318	8.5	LOD	LOD	2.73	0.16	8.53	0.33	1.477	0.098	9.74	0.66	5.13	0.32	1.468	0.086	11.31	0.58	2.683	0.084	27.88	0.79	9.12	0.27	40.5	1	8.16	0.2	71.9	1.1	12.74	0.22			0.009	0.002	0.201	0.014
Tarn02ap_83	607.8	6.6	3158	43	1754	28	LOD	LOD	22.35	0.51	89.9	1.4	19.36	0.41	149.1	3	105.9	1.9	32.87	0.57	268.8	3.7	53.45	0.6	379.8	4.8	71.73	0.87	174.2	2.2	20.42	0.33	107.3	1.2	12.29	0.23			0.464	0.023	0.722	0.027
Tarn02ap_84	406.7	5.4	1163	18	730	14	LOD	LOD	9.73	0.33	82.9	1.5	25.06	0.53	205	4.2	130.2	2.6	37.34	0.6	218.3	3.1	34.6	0.58	190.8	3.1	30.08	0.43	67.8	1.1	7.85	0.15	42.77	0.92	5.04	0.12			0.319	0.021	0.301	0.012
Tarn02ap_85	606.5	9.1	1028	30	632	17	0.032	0.018	11.69	0.43	50.2	1.3	11.24	0.37	90.4	2.8	69.4	1.7	19.23	0.61	165	3.2	27.21	0.59	162.1	3.7	26.36	0.66	59.4	1.7	6.85	0.22	36.7	1.1	4.13	0.16			0.231	0.025	1.076	0.047
Tarn02ap_86	357.2	7	559.6	8.5	166.9	7.1	LOD	LOD	1.58	0.11	5.89	0.28	1.155	0.079	9.11	0.55	4.99	0.35	1.519	0.091	12.35	0.62	2.6	0.11	21.58	0.84	5.43	0.23	16.2	0.77	1.895	0.085	10.44	0.58	1.648	0.082			0.007	0.003	0.048	0.005
Tarn02ap_87	997	12	1971	46	840	18	0.011	0.009	23	1	99.4	3.4	21.72	0.76	160.1	4.9	100.4	2.6	26.05	0.72	193.3	3.7	32.97	0.62	197.9	3.5	34.04	0.63	85.9	1.5	11.92	0.27	79.9	1.5	11.13	0.26			1.184	0.083	0.367	0.017
Tarn02ap_88	620.7	7.7	2078	51	336.7	7	LOD	LOD	3.17	0.14	12.03	0.36	2.41	0.11	16.88	0.75	10.14	0.5	2.68	0.12	23.68	0.66	5.15	0.12	45.3	1	11.26	0.21	36.93	0.68	5.53	0.12	36.38	0.78	5.12	0.15			0.014	0.004	0.213	0.011
Tarn02ap_89	446.2	5.4	312.9	5.3	348.7	6.4	LOD	LOD	5.16	0.19	15.93	0.46	2.7	0.12	17.37	0.74	10.01	0.37	2.48	0.1	22.61	0.53	5.24	0.12	45.49	0.83	11.39	0.2	34.16	0.6	3.971	0.095	18.27	0.48	1.801	0.068			0.009	0.003	0.136	0.008
Tarn02ap_90	660.6	7.1	310.6	4.6	460.1	7.6	LOD	LOD	3.14	0.15	10.02	0.28	1.98	0.1	14.31	0.64	7.13	0.33	2.349	0.091	17.4	0.54	3.65	0.11	38.32	0.8	13.54	0.22	62.7	1	12.47	0.23	101.2	1.7	16.88	0.26			0.011	0.003	0.113	0.009
Tarn02ap_91	362	8.8	5126	78	280.1	5	0.048	0.023	5.47	0.33	19.61	0.55	4.71	0.2	38	1.1	22.27	0.63	5	0.17	45.9	1.1	6.44	0.14	41.64	0.74	9.46	0.2	30.14	0.54	4.16	0.11	27.48	0.65	4.98	0.11			0.268	0.052	0.681	0.03
Tarn02ap_92	947	11	359.9	6.1	1528	25	0.781	0.07	450.2	7	1268	22	223.1	4	1183	20	356.5	6.1	5.51	0.15	394.8	5.2	58.01	0.79	356.2	4.4	67.68	0.97	169.5	2	20.08	0.28	110.2	1.7	14.28	0.23			9.68	0.16	6.96	0.11
Tarn02ap_93	372.6	5.7	1700	40	223.3	5.2	2E-07	9E-09	1.72	0.11	6.33	0.22	1.301	0.084	9.46	0.43	5.77	0.32	1.528	0.072	13.95	0.52	2.937	0.089	25.09	0.58	6.9	0.16	25.42	0.65	4.34	0.17	31.4	1.4	5.05	0.21			0.007	0.003	0.094	0.007
Tarn02ap_94	299.1	4.3	2498	37	1062	22	0.057	0.022	43.6	1	202	3.6	44.99	0.77	316.3	5.8	224.3	3.5	68.2	1.1	385.9	5.5	59.7	0.8	324.6	3.2	48.7	0.65	104.9	1.5	11.98	0.23	60.9	1.4	6.47	0.14			0.303	0.017	0.261	0.012
Tarn02ap_95	496.1	6.9	2268	34	2390	160	4E-07	1E-08	62.1	2.2	259.9	6.6	53.1	1.4	389.8	8.7	234.2	5.9	68.9	2.1	453	18	80.3	3.8	541	30	99.7	6.2	250	17	31.3	2.3	171	13	19.8	1.6			0.272	0.018	1.822	0.091
Tarn02ap_96	390.3	8.4	2057	41	903	23	5E-07	1E-08	4.31	0.21	15.44	0.57	3.04	0.15	20.1	1.1	11.02	0.59	3.52	0.16	27.82	0.95	6.97	0.16	78.3	1.6	26.42	0.52	121.7	2.4	24.07	0.46	186.1	3.2	26.68	0.6			0.018	0.004	0.276	0.014
Tarn02ap_97	531.6	7	188.1	3.2	590	10	5E-07	1E-08	10.85	0.29	35.58	0.72	6.46	0.25	42.1	1.2	20.32	0.66	5.25	0.17	41.17	0.82	8.96	0.2	78.6	1.1	19.57	0.27	60.2	1.1	7.43	0.16	37.89	0.74	4.59	0.11			0.144	0.012	0.725	0.022
Tarn02ap_98	401.7	5.3	2552	35	280.2	4.3	5E-07	1E-08	4.23	0.16	15.78	0.41	3.2	0.12	24.53	0.87	13.95	0.52	3.33	0.12	31.05	0.69	5.46	0.12	40.15	0.59	9.36	0.21	27.64	0.51	3.697	0.087	23.69	0.5	3.785	0.098			0.02	0.004	0.256	0.012
Tarn02ap_99	254.4	3.4	489.3	6.7	34.88	0.81	LOD	LOD	0.235	0.042	0.813	0.075	0.172	0.027	1.1	0.2	0.597	0.088	0.165	0.026	1.22	0.12	0.307	0.024	3.05	0.16	1.012	0.05	4.9	0.17	1.175	0.048	12.43	0.37	2.615	0.074			LOD	LOD	0.005	0.001
Tarn02ap_100	122.2	2.1	3003	39	997	19	6E-07	2E-08	66.9	1.3	283.1	4.3	56.9	0.96	375.8	6.1	229.1	3.9	69.1	1.1	384.2	5.1	63.55	0.79	332.5	4.8	46.13	0.55	93.3	1.3	9.79	0.19	46.48	0.9	4.67	0.1			0.427	0.022	0.328	0.014
Tarn02ap_101	657.4	8.8	1143	18	1021	20	0.049	0.021	17.79	0.47	79.1	1.4	19.1	0.43	165.6	4.1	116.8	2.1	34.88	0.56	250.7	3.5	40.63	0.48	253.1	3.7	43.55	0.6	96.3	1.2	10.92	0.14	55	1.1	6.19	0.12			0.109	0.013	0.238	0.011
Tarn02ap_102	857	12	586.2	8.2	1075	20	0.008	0.008	15.4	0.33	50.61	0.88	9.49	0.26	63.4	1.6	35.41	0.77	11.22	0.25	87.5	1.5	20.26	0.28	184.7	2.4	42.5	0.55	112.5	1.4	12.92	0.19	61.4	1.1	6.31	0.13			0.075	0.008	0.951	0.029
Tarn02ap_103	579.6	7.3	156.4	2.8	968	20	LOD	LOD	0.989	0.081	3.05	0.16	0.557	0.049	4.35	0.33	3.41	0.2	1.591	0.082	11	0.37	3.78	0.11	59.18	0.94	33.46	0.41	220.9	2.7	49.65	0.57	428.1	5.8	78.9	1.3			LOD	LOD	0.276	0.014
Tarn02ap_104	423.7	9.2	489	11	887	24	0.055	0.04	1.84	0.16	6.84	0.33	1.35	0.1	8.1	0.75	4.97	0.41	1.625	0.095	13.92	0.59	3.97	0.14	54	1.7	25.37	0.71	140.4	3.8	24.24	0.65	137.1	3.9	14.71	0.41			0.673	0.039	0.155	0.012
Tarn02ap_105	408.2	4.8	146	2.3	219.7	3.5	8E-07	3E-08	1.164	0.095	3.93	0.16	0.724	0.06	5.7	0.39	3.05	0.21	0.771	0.051	7.52	0.36	1.886	0.068	20.24	0.43	6.91	0.16	28.34	0.52	4.63	0.11	29.6	0.72	3.565	0.095			0.009	0.003	0.129	0.007
Tarn02ap_106	605	6.3	1013	14	209.8	3.5	LOD	LOD	2.68	0.15	9.66	0.32	1.78	0.11	11.58	0.44	6.79	0.32	1.623	0.089	15.45	0.49	3.557	0.076	30.72	0.64	7.2	0.14	22.62	0.42	3.387	0.084	22.88	0.54	3.005	0.083			0.007	0.003	0.071	0.005
Tarn02ap_107	410.7	5.8	293.5	5.1	90.1	1.9	1E-06	2E-08	3.53	0.16	11.24	0.3	2.2	0.11	14.47	0.65	6.26	0.31	1.861	0.084	7.96	0.33	1.182	0.047	9.35	0.27	2.781	0.082	11.55	0.28	2.139	0.06	15.04	0.33	2.653	0.074			0.304	0.028	0.018	0.003
Tarn02ap_108	639.2	8.6	2613	38	1006	18	0.021	0.012	41.44	0.86	167.7	3.1	37.38	0.75	288.8	5.4	161.8	2.5	47.75	0.85	306.5	4	47.7	0.59	284.4	3.1	44.89	0.57	98.4	1.5	10.94	0.18	59.8	1.1	7.32	0.13			1.05	0.06	0.202	0.013
Tarn02ap_109	1054	13	423.4	7	839	15	LOD	LOD	10.89	0.37	36.16	0.9	6.67	0.23	41.08	0.98	24.19	0.68	7.26	0.2	58.5	1.1	14.57	0.24	134.6	2	30.73	0.48	81.7	1.4	9.65	0.19	51.48	0.99	5.72	0.14			0.022	0.005	0.847	0.024
Tarn04ap_0	207	17	383	15	589	49	0.015	0.013	43.9	3.8	152	14	29.3	2.8	176	16	76.6	6.8	14.36	0.55	92.2	7.4	14.8	1.2	97.2	7.4	18.7	1.6	50.7	4.2	7.56	0.63	51.2	4.4	6.99	0.64			1.48	0.12	2.18	0.2
Tarn04ap_1	400.5	8.4	582.3	9.7	764	16	1.38	0.7	20.71	0.74	76.2	2.1	16.06	0.54	116.3	4.4	79.1	2.3	26.88	0.62	196	4.7	36.1	0.71	218.6	4.8	33.75	0.78	67.1	1.7	7.46	0.26	35.4	1.2	3.64	0.12			0.284	0.035	1.4	0.4
Tarn04ap_2	1343	20	150.2	2.6	2215	36	0.406	0.06	590.7	9.6	1754	26	311.6	5	1660	26	492.2	7	5.65	0.18	454	5.5	67.69	0.98	431	5.8	81.2	1.3	220.4	3.6	33.67	0.62	216.9	3.4	28.23	0.48			36.68	0.76	43.13	0.86
Tarn04ap_3	929	14	117.7	2.3	1902	39	0.327	0.061	432.3	8.5	1434	26	272.6	4.2	1501	24	452.9	7.1	4.86	0.17	421.4	6.4	61.14	0.94	381.4	6.8	72.3	1.3	189.1	3.7	28.5	0.56	177.7	3.9	23.31	0.53			16.14	0.8	25	1.4
Tarn04ap_4	977.8	9.6	606.5	7.6	592.8	9.7	0.146	0.031	709	12	1755	31	271.7	4.8	1270	21	265.6	5	14.4	0.31	203.1	3.3	23.46	0.38	123.1	2	20.39	0.35	50.18	0.95	6.79	0.16	42.5	1	5.25	0.15			15.85	0.29	14.88	0.25
Tarn04ap_5	1185	16	283.1	8.3	784	21	0.221	0.092	248	4.5	770	12	124	1.9	653.1	9.7	184.7	3.5	5.13	0.18	163.5	2.9	22.87	0.44	139.5	2.8	25.38	0.56	64.6	1.7	9.26	0.29	57.1	2.1	7.12	0.25			2.726	0.073	5.818	0.098
Tarn04ap_6	1104	11	174.5	4.1	1844	36	5.81	0.26	494	11	1488	28	267.4	4.1	1440	20	428.3	6.1	9.37	0.28	395	5.5	57.51	0.87	357.1	5.4	65.7	1.2	172.3	3.3	25.58	0.65	167.3	4	21.49	0.58			29.47	0.65	13.28	0.76
Tarn04ap_7	3904	47	188	2.8	4137	73	2.31	0.13	643	12	1912	31	337.3	6.2	1738	27	643.9	8.6	10.31	0.26	715	10	122.8	1.6	826	10	159.8	2.2	432.3	6.1	64.6	1	411.9	6.6	54.8	1.1			51.22	0.92	42.5	1.2
Tarn04ap_8	1148	11	228.4	5.9	1458	53	6.71	0.25	414.3	6.2	1198	17	223.1	3.6	1193	21	350.3	7.9	9.66	0.25	318.6	8.9	45.3	1.3	279.6	8.3	51.3	1.7	133.3	4.6	19.57	0.75	124.6	5.2	15.7	0.67			26	1.1	9.69	0.55
Tarn04ap_9	1083	14	197.6	3.9	1449	26	0.516	0.071	461.7	8.1	1375	26	247.2	3.9	1311	23	374.6	5.6	7.21	0.21	338	4.9	47.98	0.65	295.5	4.6	53.84	0.78	136.5	2.2	19.51	0.39	117.9	2	14.41	0.32			22.83	0.41	23.03	0.43
Tarn04ap_10	1420	20	558.8	8.8	983	18	5.05	0.26	604.7	8.7	1556	25	250.3	3.6	1225	18	300	5	15.41	0.34	253.1	4.1	33.3	0.48	196.4	2.8	34.84	0.52	84.9	1.1	11.12	0.2	61.8	1	7.41	0.17			27.62	0.39	10.54	0.19
Tarn04ap_11	1029	13	227.2	5.9	1511	37	7.62	0.29	414.1	8.5	1211	23	222	3.4	1197	19	362.8	6	9.4	0.25	327.4	6	47.33	0.95	294	6.4	53.6	1.2	140.6	3.8	20.77	0.6	132.5	4.2	16.4	0.53			33.3	0.49	10.04	0.18
Tarn04ap_12	7519	84	180.8	3.6	1425	28	0.477	0.078	309.2	6.9	995	22	173.7	3.5	885	17	306.2	4.8	13.9	0.3	306.6	4.8	50.15	0.74	309.1	4.1	53.69	0.78	135.9	1.8	19.93	0.33	123.1	2.2	14.74	0.28			8.94	0.15	74.6	3.3
Tarn04ap_13	2265	29	148.9	3.2	2185	42	0.224	0.045	415.3	8.4	1264	23	226.7	4.5	1190	22	418.3	6.4	4.98	0.17	432.4	6.4	67.71	0.98	440.6	5.7	83.1	1.2	221	3.5	30.87	0.52	186.7	3.2	23.42	0.43			9.6	0.43	25.48	0.77
Tarn04ap_14	1898	27	212	4	1990	38	3.26	0.19	591	11	1652	32	287.6	5.3	1476	23	437	6.5	6.06	0.22	407.4	7.9	61.27	0.87	392.8	6.4	72.7	1.2	194.9	2.9	29.07	0.47	183.2	3.6	23.05	0.51			21.4	0.42	16.91	0.29
Tarn04ap_15	773.5	9.3	881	12	640	10	LOD	LOD	5.34	0.2	24.72	0.81	5.75	0.21	53.3	1.7	43.5	1	11.48	0.28	102.6	2	17.11	0.3	115.1	1.5	23.69	0.32	67.6	1.1	10.65	0.22	71.8	1.3	10.6	0.18			0.252	0.019	0.621	0.021
Tarn04ap_16	912	14	373.3	8.9	744	13	0.192	0.039	316.3	7.8	871	19	134.9	2.8	692	13	179.5	2.7	6.27	0.23	155.8	2.6	21.21	0.34	126.5	1.7	23.23	0.41	59.2	1.1	8.48	0.19	51.8	1.2	6.53	0.17			4.538	0.093	16.99	0.41
Tarn04ap_17	1148	16	191	3.7	2833	48	0.559	0.061	793	18	2356	50	417.9	7.7	2141	38	633.4	9.8	6.12	0.16	571.7	9.6	85.7	1.5	546	8.1	102.7	1.5	286.8	4.6	46.18	0.76	323.9	4.6	43.44	0.74			49.3	1.2	55.3	1.2
Tarn04ap_18	905	34	257	11	1529	48	1.13	0.1	537	17	1522	50	265.6	8.9	1370	41	385	11	21.9	2.4	344.3	9.5	48.4	1.4	300.9	8.3	55.8	1.6	147.5	4.2	21.47	0.61	134.5	4.4	17.28	0.51			39.66	0.99	17.58	0.54
Tarn04ap_19	1017	12	388.8	6.2	1078	22	2.63	0.15	590.6	9.6	1544	24	259.6	4.1	1317	18	344.5	4.2	13.15	0.27	306.1	4.1	41.09	0.64	238.2	2.7	42.23	0.52	102.6	1.4	12.79	0.22	71.1	1.4	8.37	0.18			27.71	0.37	16.58	0.23
Tarn04ap_20	1233	28	145.1	3.3	3700	160	0.166	0.045	346	32	1370	100	307	21	1870	100	712	32	9.02	0.25	727	31	115.2	4.6	739	30	142.8	5.7	393	15	59.4	2.4	387	14	51.6	1.9			24.3	2.3	49.1	4.3
Tarn04ap_21	1306	12	269.3	4	1217	23	0.665	0.083	646.7	9.4	1723	29	281.4	4.1	1405	23	354.4	5.2	10.21	0.23	300.3	4.2	41.72	0.66	251.8	3.5	45.49	0.71	118.8	1.9	16.28	0.32	100.2	1.9	12.65	0.26			19.52	0.31	18.11	0.28
Tarn04ap_22	1460	16	338.9	6.7	1182	22	0.866	0.084	672	12	1759	32	291.7	4.8	1465	22	376.3	6.2	12.62	0.4	321	4.9	43.09	0.66	253.3	3.3	44.69	0.53	112.7	1.4	14.48	0.24	85.7	1.6	10.65	0.19			34.3	0.94	23.67	0.48

Supporting Information Tables S3.5: Apatite trace-element data (continued)

	55Mn	±	86Sr	±	89Y	±	90Zr	±	139La	±	140Ce	±	141Pr	±	146Nd	±	147Sm	±	153Eu	±	157Gd	±	159Tb	±	163Dy	±	165Ho	±	166Er	±	169Tm	±	172Yb	±	175Lu	±	182W	±	232Th	±	238U	±
Tarn04ap_23	4401	58	161.5	3.3	3516	71	2.88	0.19	438.1	8	1338	24	243.6	4.5	1298	24	483.7	7.5	6.99	0.19	536.1	7.6	96.6	1.5	677	8.7	133.9	1.4	384.7	5	58.57	0.83	375.7	5.5	50	0.75			39.94	0.57	26.9	1
Tarn04ap_24	935	12	322	10	1168	38	5.21	0.25	497	9	1358	25	233.6	4.3	1213	26	321.2	8.2	12.55	0.29	275.6	9	38.4	1.4	228.6	8.7	40.7	1.5	105.7	4.1	14.36	0.58	86.1	3.8	10.61	0.49			27.7	1.2	10.92	0.41
Tarn04ap_25	932	13	445.6	7.9	1122	22	0.251	0.082	670	16	1701	49	271.6	7.4	1312	37	338.2	8.9	8.63	0.32	296.8	8.2	41.5	1	245.2	6.1	43.9	1.1	109.2	3.1	13.28	0.42	70.6	2	8.27	0.27			11.7	0.66	20.6	1
Tarn04ap_26	1059	11	330.6	5.8	953	19	0.275	0.049	526.5	9.2	1364	23	223.2	4.1	1142	23	292.3	5.6	10.35	0.29	255.2	4.1	33.67	0.61	193.7	2.9	34.69	0.58	87.4	1.7	10.93	0.3	61.3	1.5	7.67	0.22			16.48	0.42	22.25	0.49
Tarn04ap_27	6378	79	118.1	2.7	2038	28	0.183	0.041	338.9	5.8	952	17	149.4	2.4	686	13	246.4	3.6	5.38	0.21	267	3.4	53.36	0.79	372.6	4.2	70.25	0.89	211.1	2.5	33.68	0.45	228.8	3.3	30.01	0.54			2.912	0.065	62.4	1
Tarn04ap_28	1412	15	142.1	2.5	2112	36	7.46	0.3	429.2	9.7	1353	27	256.9	4.3	1429	23	461.7	7.4	5.73	0.24	434.3	6.7	66.15	0.84	415.9	4.7	78	1.1	214	2.7	29.97	0.42	187.4	2.6	24.05	0.37			41.64	0.82	12.92	0.22
Tarn04ap_29	1120	14	193	3.3	1804	36	3.17	0.26	335	9.6	1051	28	202.4	4.4	1160	23	396.3	6.4	7.97	0.2	393	5.7	58.67	0.8	361.6	5.3	67.63	0.87	184.5	2.7	25.85	0.43	163.6	2.6	21.6	0.43			30.3	1.1	17.55	0.31
Tarn04ap_30	2450	35	158.1	3.8	1886	46	4.74	0.32	377.9	6.7	1139	20	217.3	4.1	1166	17	379.4	7.3	6.89	0.22	364	6.6	56.2	1.1	356.9	6.6	67	1.5	190.6	4.5	29.04	0.74	194.3	4.5	26.58	0.69			19.37	0.48	7.62	0.42
Tarn04ap_31	1284	16	328	11	1099	22	6.03	0.39	516	10	1377	25	232.8	4.6	1189	19	308.1	4.5	10.18	0.34	264.5	4.1	37.08	0.5	221.5	2.8	40.37	0.58	107.4	1.7	14.38	0.33	88.8	1.5	11.18	0.24			12.78	0.23	4.505	0.082
Tarn04ap_32	1128	13	256.1	8.6	1168	24	0.064	0.021	250.5	6.5	784	15	131.4	2.3	719	12	234.5	3.9	4.93	0.19	231	3.8	35.14	0.57	216.2	2.9	39.97	0.63	112.1	2	16.46	0.3	107.4	2.3	14.3	0.32			5.98	0.14	18.7	0.5
Tarn04ap_33	1134	14	219.1	7.7	1498	44	2.66	0.16	416.5	9.1	1194	24	214.8	3.6	1164	19	350.3	6.4	9.11	0.27	320.4	7.1	47.5	1.2	292.9	8	53.3	1.7	147.6	5.1	20.99	0.78	133.3	5.6	17.82	0.83			27.55	0.64	12.84	0.3
Tarn04ap_34	603	7.8	476.6	7.4	1031	22	LOD	LOD	8.16	0.23	27.63	0.61	5.33	0.16	37.7	1	20.52	0.5	6.82	0.16	54.2	1.1	12.86	0.21	134.6	1.6	38.22	0.49	121.4	1.6	14.88	0.22	73.6	1.1	7.83	0.15			0.013	0.003	0.354	0.013
Tarn04ap_35	1396	16	684	11	1198	23	6.87	0.33	496.2	8.4	1302	28	219.4	4.4	1087	19	282.6	5	14	0.35	237.1	3.6	35.06	0.51	217.2	3.2	40.43	0.53	114.5	1.8	16.71	0.29	108.9	2	14.46	0.24			16.88	0.28	6.31	0.13
Tarn04ap_36	881	14	361	12	1240	37	2.4	0.15	659	16	1723	35	290.6	5.6	1435	25	336.2	6.8	14.59	0.36	271.1	6.1	38.37	0.98	233.3	6.6	43.9	1.2	129.3	4.2	19.89	0.68	137.6	4.6	19.37	0.61			33.96	0.81	17.51	0.38
Tarn04ap_37	1177	15	224.8	5.4	2356	57	7.43	0.34	328.4	7.1	1038	22	201.3	3.8	1201	19	428.7	8.5	8.55	0.21	431.3	8.6	68.2	1.2	439.4	8.5	83.5	1.7	243	4.5	36.06	0.73	239.1	5.4	32.43	0.71			30.6	1.1	9.53	0.23
Tarn04ap_38	986	12	296.7	7.2	1250	25	1.39	0.2	561	21	1522	52	263.3	8	1355	38	366	8.8	13.06	0.55	322.7	6.9	45.24	0.79	261.8	4.6	47.53	0.9	121.3	2.2	15.75	0.32	91.6	2.2	11.23	0.25			29.6	1.9	33.71	0.74
Tarn04ap_39	1109	12	325.4	6.7	1376	37	0.67	0.084	451.6	8	1270	26	225.4	4.1	1212	25	356.6	8.3	10.53	0.26	327.5	7.1	47.66	0.97	290.1	6.4	53.2	1.3	139.1	3.4	18.3	0.49	109	2.7	13.82	0.37			24.53	0.72	52.3	1.3
Tarn04ap_40	1347	16	255.3	4.1	2276	42	0.12	0.036	479.1	7.8	1369	25	254.8	3.8	1408	23	463.6	6.6	8.85	0.24	451.8	5.6	69.9	1.1	448.7	6.1	84.4	1.2	239.6	3.3	35.47	0.62	233.6	3.5	31.33	0.43			11.62	0.26	18.81	0.41
Tarn04ap_41	3607	90	160	5.4	1626	43	0.64	0.38	388	10	1109	37	203.4	5.4	1080	22	334.6	8.8	4.97	0.25	309.3	9.4	48.6	1.6	309.5	7.1	57.8	2	164.4	5.4	24.26	0.7	159.6	4.4	21.5	1			7.67	0.4	16	0.58
Tarn04ap_42	888	12	321	7.5	1277	27	1.9	0.15	653	12	1740	29	294.5	4.8	1516	19	393	6.7	15.47	0.3	333.6	6	45.62	0.99	267.3	6.2	47.5	1.1	123.6	3	15.95	0.45	94	2.6	11.84	0.35			32.69	0.59	21.99	0.39
Tarn04ap_43	1766	95	1097	23	183.3	3.6	LOD	LOD	3.89	0.3	13.2	1.1	2.21	0.19	11.64	0.9	5.91	0.44	1.54	0.11	11.48	0.47	2.65	0.11	22.87	0.76	5.88	0.16	20.58	0.47	3.253	0.085	21.39	0.54	3.12	0.1			0.29	0.11	0.101	0.01
Tarn04ap_44	1159	15	245.2	5.7	1468	29	8.88	0.28	383.9	8.9	1120	21	210.8	3.6	1157	18	365.9	5.3	11.3	0.31	335.2	5.8	49.39	0.88	299.7	5.5	54.1	1.1	143.9	3	20.07	0.5	123.3	3.5	15.58	0.47			26.77	0.72	7.72	0.3
Tarn04ap_45	1898	23	153.9	4	2755	85	3.81	0.3	497	11	1568	37	300.4	7.5	1646	42	538	14	5.13	0.17	517	15	82.8	2.4	533	17	100.6	3	288.1	8.9	42.2	1.4	269.1	9.3	35.4	1.3			40.8	2	35.9	2.4
Tarn04ap_46	1486	20	194.4	5.3	1134	18	0.023	0.013	233.3	4.7	771	15	136.1	2.8	761	12	243	4.4	3.88	0.16	228	4.4	34.13	0.66	215.6	3.9	39.92	0.79	110.4	2.4	16.08	0.38	101.5	2.1	13.5	0.28			2.66	0.11	8.89	0.42
Tarn04ap_47	1720	160	676	30	961	57	0.009	0.009	115	6.2	434	18	77.9	2.5	452	13	190.6	5.5	13	0.55	208.4	8.1	32	1.9	192	13	32.4	2.4	81.1	6.3	10.5	0.85	62	5.4	7.5	0.66			2.831	0.063	7.28	0.71
Tarn04ap_48	1099	13	155	3.8	2720	94	3.01	0.31	504	13	1649	30	329.7	5.8	1859	32	609.4	9.9	10.57	0.28	583.6	8.5	88.4	1.4	550.4	8.3	102.7	1.6	284.3	4.7	40.57	0.64	258.1	4.8	34.16	0.53			51.8	2.7	47.55	0.75
Tarn04ap_49	1216	14	345.2	5.8	1308	23	0.101	0.031	331.7	5.8	957	16	153.7	2.7	776	13	251.5	4.1	12.09	0.25	266.8	4.2	43.62	0.64	282.1	3.5	53.6	0.76	142.4	2.1	17.92	0.31	97.4	1.4	11.94	0.22			2.813	0.067	52.88	0.8
Tarn04ap_50	1968	25	182.3	3.6	1679	26	0.441	0.06	570.1	8.8	1595	27	274.7	5.1	1407	27	402.5	6.6	7.86	0.24	357.1	5.6	52.92	0.8	330	5.2	60.02	0.8	162.4	2.3	23.58	0.39	151.1	2.6	19.78	0.37			18.72	0.34	28.17	0.53
Tarn04ap_51	990	11	249	5.7	1541	39	6.47	0.23	427.2	8.6	1215	19	222.8	3.8	1205	20	360	6.9	10.28	0.22	324.1	6.7	48.1	1.2	296.2	7.4	54	1.4	146.7	4.3	21.39	0.62	133.9	4.1	17.31	0.57			30.76	0.93	11.41	0.37
Tarn04ap_52	1275	19	155.1	4.5	1939	46	3.92	0.19	379.3	9.1	1184	24	231.5	4.1	1329	21	435.5	7.9	6.84	0.22	422.4	9	63.1	1.2	399.7	9.1	74.2	1.5	198.1	4.2	28.57	0.7	174.5	4.3	22.24	0.53			34.46	0.8	18.92	0.86
Tarn04ap_53	2908	46	106.9	2.4	1873	35	4.69	0.35	418	9	1306	24	238.8	4	1278	21	406.5	6	6.21	0.17	392.2	6	60.14	0.88	383.4	4.6	70.57	0.85	188.6	2.2	26.29	0.48	162.4	2.5	21.16	0.39			30.48	0.55	19.92	0.38
Tarn04ap_54	946	13	219.8	5.6	944	17	0.08	0.025	188.7	4.1	621	9.9	107.2	1.8	595	11	190.1	3.1	4.2	0.14	182.9	3.3	26.64	0.48	165	3	30.98	0.61	83.8	1.9	11.86	0.27	75.9	1.4	10.04	0.25			2.757	0.089	12.28	0.26
Tarn04ap_55	1276	16	166.8	5.2	1830	41	3.61	0.19	396	11	1155	25	211.9	4.2	1166	20	380.6	7	6.54	0.2	358.6	6.1	55.1	1.1	347.2	8	65.1	1.5	177	4.5	25.89	0.64	166.6	4.7	21.66	0.67			20.82	0.37	10.49	0.22
Tarn04ap_56	1395	52	796	11	403.3	7.5	LOD	LOD	7.85	0.33	24.76	0.87	4.3	0.2	25.5	1.1	13.85	0.56	2.44	0.1	28.42	0.91	6.45	0.15	55.25	0.82	13	0.22	38.03	0.77	4.88	0.13	24.97	0.69	2.604	0.088			0.061	0.007	0.387	0.016
Tarn04ap_57	1183	12	280.4	6	1308	29	1.08	0.1	509.4	8	1411	23	245.5	3.7	1277	17	353.2	5.7	11.51	0.26	309.8	5.6	42.72	0.71	255.3	4.5	46.12	0.9	120.5	2.7	16.81	0.4	101.6	2.5	12.67	0.38			25.45	0.39	22.81	0.34
Tarn04ap_58	1177	14	333.8	7	994	20	0.353	0.069	509	10	1297	26	218.7	3.9	1110	21	293.8	5.5	10.67	0.28	252.9	4.3	33.96	0.51	198	2.8	34.9	0.5	86.8	1.1	11.14	0.22	62.7	1.3	7.61	0.16			22.65	0.84	33.16	0.63
Tarn04ap_59	2395	30	102	2.3	2827	83	0.243	0.047	470	12	1474	40	272.3	7.4	1481	43	502	15	4.12	0.13	505	12	82.3	2.1	538	14	104.6	2.9	296.7	8	46	1.4	307	11	42	1.4			25.1	1	53.67	0.91
Tarn04ap_60	1152	14	446.1	7.5	872	13	0.188	0.04	409.6	6.5	1074	19	177.9	2.5	898	14	226.2	3.7	9.45	0.23	191.2	3.1	26.56	0.42	159.6	2.3	28.95	0.41	75.8	1	10.79	0.18	64.6	1	8.39	0.2			9.32	0.18	10.55	0.16
Tarn04ap_61	538	7	1023	13	521.3	8.9	LOD	LOD	6.1	0.19	20.82	0.47	3.9	0.15	25.56	0.85	12.61	0.48	4.01	0.15	29.47	0.78	6.27	0.14	57.28	0.99	16.81	0.37	60.3	1.1	8.55	0.17	48.7	1.2	6.15	0.12			0.022	0.005	0.12	0.007
Tarn04ap_62	1219	20	373	12	1192	22	6.53	0.27	637	13	1616	30	265.9	4.9	1296	25	325.5	6.2	11.25	0.53	276.3	5.1	39.04	0.64	234.8	4	42.82	0.59	114.6	2	16.36	0.28	101.5	1.9	13.18	0.26			17.77	0.28	6.49	0.11
Tarn04ap_63	3634	49	276.5	5.2	1095	20	LOD	LOD	243.9	4.5	588.5	9.6	81.9	1.5	391.3	7.2	155.6	2.9	110.3	1.7	231.8	3.7	45.13	0.67	287.6	4.3	47.7	0.65	104.6	1.5	11.21	0.19	50.25	0.97	5.29	0.14			2.655	0.063	1.833	0.037
Tarn04ap_64	820	12	76.3	1.5	323.3	9.1	0.018	0.012	2.09	0.13	4.84	0.2	0.719	0.058	3.72	0.33	1.64	0.17	1.121	0.069	4.86	0.29	1.495	0.062	21.46	0.65	10.08	0.26	48.3	1.2	8.11	0.25	55.6	1.8	8.26	0.35			0.065	0.009	0.033	0.005
Tarn04ap_65	1053	16	221.4	5.6	1689	35	6.18	0.49	492	17	1407	48	255	7.3	1396	42	408.3	9.2	11.11	0.47	374.1	6.9	55.1	1	332.1	5.3	60.42	0.89	162.3	3.7	23.32	0.43	143	2.7	18.46	0.35			26.71	0.97	10.04	0.6
Tarn04ap_66	1157	14	213	4.6	1283	46	0.158	0.073	385	14	1070	36	192.6	6.6	1051	31	311.4	8.2	7.05	0.27	288.7	7.7	41.8	1.3	258	7.2	47.4	1.4	123.9	3.4	17.63	0.53	111	3.5	14.61	0.52			24.8	4.9	22.6	1.7
Tarn04ap_67	2596	52	160.8	3.2	3150	71	1.76	0.16	413	14	1284	36	238.2	6.3	1295	32	494	11	6.14	0.21	538	12	93.1	2.1	617	12	119.7	2.7	336.6	7.3	49.5	1.1	319.3	8.1	41.05	0.94			32.7	1.1	37.8	1.5
Tarn04ap_68	1355	17	237.4	6.1	1361	26	5.37	0.3	539.4	7.5	1433	25	248.3	3.4	1296	20	356.3	5.4	9.04	0.3	315.4	4.9	44.62	0.62	268.2	4.4	49.47	0.85	132.3	2.8	18.35	0.42	112.2	2.3	14.5	0.36			26.71	0.45	11.17	0.26
Tarn04ap_69	1514	19	179.2	4.2	1239	21	0.106	0.026	374.7	6.2	1050	19	182.5	3	951	14	281.5	4.6	3.72	0.16	259.1	4.4	38.94	0.68	239.2	3.5	44.78	0.79	122.2	2.2	17.82	0.31	114.9	2.1	15.46	0.33			9.36	0.18	10.67	0.17
Tarn04ap_70	1254	19	128.8	3.2	1421	26	0.085	0.027	758	12	1937	35	314.7	5	1528	26	395.3	7.1	5.06	0.16	338.8	5.1	48.21	0.71	289.2	4.2	53.14	0.86	142.5	1.9	19.62	0.3	122.9	2	15.88	0.3			9.91	0.33	23.12	0.49
Tarn04ap_71	1325	13	184.5	5.8	1750	32	2.34	0.21	445	14	1325	39	243.6	5.7	1361	35	418.2	8.7	9.79	0.42	388.9	7.2	57.9	1.1	350.5	5.3	64.05	0.98	169.4	2.8	23.36	0.41	138.3	2.6	17.18	0.31			37	1.9	16.76	0.56
Tarn04ap_72	556.8	6.6	159.9	2.8	484	38	0.015	0.012	5.81	0.23	20.08	0.65	3.7	0.19	23.2	1.2	12.83	0.63	4.13	0.23	26.4	1.5	5.74	0.46	53.1	4.5	15.5	1.1	62.6	4.5	11.62	0.77	100.5	6.4	18.8	1.2			0.82	0.17	1	0.24
Tarn04ap_73	1368	17	186.2	4.7	1479	63	0.374	0.068	554	19	1540	59	261	9.8	1329	45	372	16	5.37	0.2	334	14	48.8	2.2	291	14	54.2	2.6	147.8	7.4	20.6	1	127.4	6.8	16.82	0.87			19.2	1.9	33.6	1.8
Tarn04ap_74	1538	20	168.9	4.2	2277	43	1.44	0.13	605	11	1746	29	309.6	5.2	1650	29	502.8	7.5	8.46	0.24	464	6.6	71	1.1	438.1	5.6	82.2	1.3	230.6	3.6	34.73	0.59	232.3	3.9	31.65	0.63			51	1.1	88.1	2.8
Tarn04ap_75	6258	73	150.5	3	1888	38	0.037	0.018	219.2	5.2	733	16	123.7	2.7	662	13	273.2	5.1	5.06	0.15	309.8	5.2	56.2	0.93	368.5	6	70.5	1.3	199.3	3.6	29.08	0.56	188.2	3.8	24.62	0.59			3.04	0.25	29.35	0.94
Tarn04ap_76	1186	20	540	12	747	16	0.133	0.052	592	12	1493	32	244.5	4.7	1243	25	330.2	6.1	13.85	0.43	262.7	6.4	30.07	0.59	145.2	2.9	22.52	0.53	56.6	1.2	8.03	0.24	51.6	1.3	6.84	0.21			11.16	0.24	20.67	0.4
Tarn04ap_77	1221	18	202.9	3.9	2007	37	2.7	0.19	360	10	1088	25	206.3	4.9	1166	26	400.2	8.5	7.12	0.25	396.1	7.5	61.5	1.2	387.5	5.5	73	1.1	203.4	3.2	29.62	0.53	189.3	3.2	25.52	0.45			21.77	0.47	16.79	0.3
Tarn04ap_78	434	5.3	327.4	5.4	371.6	8.9	LOD	LOD	2.49	0.12	8.27	0.33	1.535	0.075	10.42	0.45	5.56	0.31	1.806	0.098	14.2	0.57	3.51	0.11	35.53	0.86	11.39	0.32	47.6	1.3	7.49	0.19	43.4	1.1	4.87	0.14			0.015	0.004	0.066	0.005
Tarn04ap_79	1504	15	125.6	2.5	1684	26	2.83	0.18	566.8	9.6	1551	28	267.9	3.9	1389	22	396.8	5.7	3.76	0.12	361.5	4.4	54.42	0.76	329.8	3.8	60.67	0.75	169.9	2.3	24.03	0.36	151	2.4	19.85	0.32			15.82	0.25	11.57	0.27
Tarn04ap_80	1139	16	150.5	3.4	1627	31	4.48	0.22	450.5	9.4	1335	23	247.3	4	1337	21	395.9	5.5	5.71	0.21	353.1	5.4	53.29	0.73	320.7	3.9	58.57	0.96	161.1	2.5	22.37	0.39	139.7	2.5	17.91	0.36			17.24	0.33	9.14	0.16
Tarn04ap_81	1234	16	384.2	8.5	1103	35	1.16	0.22	350.4	8.8	991	37	173.5	6.5	892	27	261.4	9.4	6.09	0.21	243.6	9.5	36	1.4	218.8	7.9	40.4	1.5	108.8	4.1	14.69	0.54	90.5	3.8	11.99	0.45			8.87	0.79	23.34	0.48
Tarn04ap_82	1750	23	582	11	1282	20	3.11	0.17	537	8.1	1403	26	235.3	3.3	1190	19	319.2	4.8	14.63	0.4	270.5	5.1	40.27	0.84	236.7	3.9	42.53	0.86	115.6	2.1	16.23	0.35	101	2.1	13.17	0.28			18.19	0.38	7.56	0.17
Tarn04ap_83	3305	44	176.4	3.5	2991	65	0.22	0.043	529.9	9.9	1757	36	332.2	7.1	1750	35	576	11	8.54	0.26	554.9	9.8	91.6	1.7	590	11	111.2	2	318.9	5.4	47.41	0.92	304.7	6.4	40.25	0.9			39	1.8	78.9	2.5
Tarn04ap_84	1314	18	159.2	4.2	2086	34	2.07	0.18	595	19	1730	50	316.3	7.8	1695	36	506.3	7.9	9.62	0.44	457.4	6.8	68.11	0.95	404.1	5.6	75.7	1.3	207.5	3.8	28.83	0.54	182.8	3.3	23.87	0.46			44.9	1.8	44.34	0.89
Tarn04ap_85	159.4	3	275.2	8.4	111.1	4	LOD	LOD	0.338	0.046	1.1	0.11	0.2	0.03	1.67	0.22	1.13	0.13	0.27	0.036	3.67	0.28	0.913	0.058	10.8	0.49	3.42	0.15	13.04	0.38	1.794	0.073	10.76	0.31	1.702	0.062			0.004	0.002	0.031	0.004
Tarn04ap_86	2837	41	155	3.1	3068	56	0.24	0.046	547	11	1729	31	313.1	5.2	1649	30	552.6	9	6.41	0.18	541.4	6.8	92.3	1.4	596.3	9.1	113.8	1.5	324.3	4.7	47.95	0.88	322.1	5.4	43.52	0.79			23.07	0.4	37.75	0.72
Tarn04ap_87	1132	17	265	5.8	1194	23	0.153	0.034	316.6	5.6	980	18	177.1	2.8	949	17	279.2	5.3	5.13	0.18	257.6	3.6	37.6	0.58	226.9	2.8	42.67	0.62	119.2	1.8	16.65	0.3	104.3	1.8	13.94	0.24			8.76	0.17	9.9	0.16
Tarn04ap_88	1544	22	169.5	3.9	2241	45	1.63	0.12	623	11	1746	35	297.7	5.1	1523	23	459.3	6.4	6.01	0.22	426.6	7.1	68.3	1.2	435.1	7.4	81.4	1.4	228.3	4.6	32.07	0.65	197.8	4.2	25.44	0.53			27.3	0.49	18.98	0.39
Tarn04ap_89	3206	44	216.7	6.5	2086	54	4.41	0.2	570	13	1572	35	282.2	4.8	1519	28	460.6	8.3	10.96	0.33	423.4	8.7	64.9	1.4	397.8	8.9	72.7	1.7	205.9	5.7	29.97	0.91	195.2	5.6	26.35	0.86			41.26	0.94	16.05	0.37
Tarn04ap_90	280	4.3	417.7	7.2	319.3	5.5	LOD	LOD	2.8	0.21	8.93	0.43	1.64	0.097	9.99	0.63	5.23	0.37	1.67	0.098	12.39	0.44	3.186	0.074	32.79	0.72	10.26	0.19	40.91	0.7	6.83	0.16	43.12	0.94	5.9	0.16			0.106	0.022	0.094	0.013
Tarn04ap_91	2004	26	195.9	3.7	1633	25	9.97	0.53	460.9	7.8	1334	24	243.3	4.3	1322	23	390.9	6	9.87	0.24	344.5	4.6	51.18	0.66	307.7	3.5	55.53	0.77	150.9	2.5	20.93	0.33	131.5	2	17.24	0.33			45.42	0.94	12.68	0.23
Tarn04ap_92	1990	24	156.2	2.9	1757	32	1.82	0.15	552.2	8.6	1513	27	262.8	4.2	1358	22	395	6.3	5.11	0.15	358.6	6.2	54.46	0.98	338.3	4.8	63.6	0.74	178.3	2.6	26.21	0.41	169.4	2.9	22.41	0.42			20.66	0.31	14.37	0.23
Tarn04ap_93	1782	24	107.3	2.8	2092	43	6.64	0.45	455	10	1345	26	246.4	4.3	1322	24	420.4	7.4	4.87	0.2	392	6.8	61.5	1	387.8	6.6	73	1.4	210	3.7	31.56	0.64	212.9	4.6	29.02	0.62			25.5	1.7	7.07	0.25
Tarn04ap_94	2600	37	235.3	6.5	1803	55	6.73	0.3	692	13	1857	35	312.1	5.2	1582	30	434.4	7.3	11.71	0.29	390.1	8.1	58.4	1.4	356.5	8.3	65.8	1.7	180.2	5.4	25.68	0.87	162.8	5.6	21.38	0.76			38.89	0.95	16.02	0.41
Tarn04ap_95	2666	37	106.6	2	2223	38	3.02	0.19	724	12	1974	35	340.7	5.2	1710	27	502.1	7.4	4.47	0.16	460.1	6.5	71.5	1	438	6.4	81.3	1.2	226.8	3.1	32.43	0.59	205.4	3.3	27.59	0.43			30.73	0.51	20.41	0.66
Tarn04ap_96	2550	30	211.6	5	1575	31	1.47	0.12	409	7.9	1182	23	216.1	4	1178	23	360	6.3	8.37	0.21	326.3	5.7	48.96	0.81	297.4	5.2	55.2	1.2	152.2	3.4	21.82	0.52	140.4	3.3	18.79	0.47			21.43	0.33	17.5	0.28
Tarn04ap_97	3279	44	171.1	3.3	1943	58	0.673	0.086	741	12	2262	37	408.7	7.6	2125	38	540	12	14.03	0.4	444	11	63.8	1.7	390	11	71.1	2.1	204.1	6	32.4	1	230.3	7.3	33	0.94			30.3	1.5	23.39	0.63
Tarn04ap_98	1435	20	121.5	2.4	2289	41	3.95	0.28	503	12	1553	32	292.6	5.1	1600	25	501.2	7.4	5.62	0.2	464.1	6	71.13	0.86	442.6	5.1	82.6	1.1	233	3.6	33.82	0.46	220.1	3.7	29.96	0.5			31.91	0.54	22.75	0.96
Tarn04ap_99	1185	14	331.6	6	1073	20	0.076	0.026	407.8	6.7	1089	21	181.8	3.5	910	15	262.6	5	8.43	0.2	258.8	4.1	38.35	0.58	231	3.3	41.89	0.62	106.8	1.4	13.01	0.23	72	1.2	9.15	0.2			6.79	0.19	53.91	0.98
Tarn04ap_100	245.7	5	1420	22	503.4	9	LOD	LOD	43.89	0.89	238.5	4.8	51.8	1.1	348	7.6	166.9	3.3	56.1	1	238.7	4.5	33.56	0.57	166.7	2.9	22.87	0.42	44.33	0.72	4.6	0.11	22.55	0.55	2.888	0.071			3.63	0.18	0.212	0.017
Tarn04ap_101	1296	16	121.2	2.3	2469	88	1.013	0.098	480.3	7.5	1530	24	295	3.9	1643	22	536.9	8.3	6.65	0.2	498.4	7.1	77.2	1.1	480.8	7.7	89.9	1.4	253.1	4	36.9	0.53	235.7	4.1	31.22	0.61			38.33	0.57	35.42	0.74
Tarn04ap_102	910	13	384.9	7.9	993	15	0.02	0.013	267.7	4.9	828	15	135.3	1.9	728	11	214	2.7	6.37	0.19	193.5	3.3	28.1	0.46	172.4	2.7	31.8	0.47	86.6	1.4	11.99	0.21	74.9	1.4	10.1	0.24			3.257	0.079	6.41	0.1
Tarn04ap_103	1310	17	212.7	3.5	1870	54	0.212	0.041	431.6	7	1246	25	228.9	3.7	1275	19	421.6	7.8	10.66	0.28	417	9.6	61	1.3	370.7	8.9	68.3	1.8	183.3	4.6	25.07	0.72	154.3	4.4	20.41	0.52			17.57	0.66	12.02	0.38
Tarn04ap_104	1053	16	278.5	7.3	1198	30	2.13	0.18	399	10	1104	24	196.4	3.4	1045	19	293.5	4.4	9.77	0.26	259.8	4.6	37.62	0.71	226.8	4.3	41.83	0.99	112.1	3.4	15.79	0.55	95.7	3.7	12.4	0.53			14.45	0.56	12.96	0.45

Supporting Information Tables S3.5: Apatite trace-element data (continued)

	55Mn	±	86Sr	±	89Y	±	90Zr	±	139La	±	140Ce	±	141Pr	±	146Nd	±	147Sm	±	153Eu	±
Tarn04ap_105	1099	12	243.9	3.6	1468	21	4.48	0.26	470.6	5.8	1309	21	234.3	3.7	1224	21	349.9	5.1	11.47	0.29
Tarn04ap_106	1304	21	262.6	5.9	1069	25	3.29	0.3	470.9	9.9	1294	27	225.1	4.8	1158	28	322.3	7.9	10.6	0.36
Tarn06ap_0	444	9.7	2290	77	491	15	0.01	0.009	16.97	0.61	87.9	2.9	19.3	0.67	132	4.1	73.1	2.1	21.47	0.69
Tarn06ap_1	477	10	596	16	655	19	LOD	LOD	4.31	0.19	15.8	0.53	3.07	0.14	20	1	11.18	0.54	3.3	0.16
Tarn06ap_2	1308	26	243.6	7.8	1510	40	6.22	0.44	541	14	1417	38	262.5	6.6	1329	30	372.3	8	9.53	0.39
Tarn06ap_3	658	23	642	25	658	29	0.012	0.009	8.85	0.42	29	1.1	5.03	0.21	32.4	1.5	15.41	0.64	4.3	0.21
Tarn06ap_4	15930	400	117.7	4.2	2144	65	11.2	1.8	315	10	991	33	159.1	4.8	806	27	291.4	8.1	8.59	0.46
Tarn06ap_5	337.5	6.6	1595	31	1183	30	0.86	0.12	26.25	0.86	99.6	2.4	20.4	0.56	145.8	3.6	92.1	2.5	30.58	0.61
Tarn06ap_6	6030	130	254.8	8.5	1907	63	0.172	0.037	244.7	6.6	883	25	151	4.3	811	24	308.6	8.5	10.6	0.32
Tarn06ap_7	230.8	6.5	254.1	9.8	192.4	6.9	0.181	0.046	1.52	0.19	3.54	0.21	0.648	0.06	4.33	0.36	2.02	0.22	0.546	0.056
Tarn06ap_8	1386	20	214.1	5.2	1734	45	8.9	0.71	385.3	8.3	1173	26	223.4	5.4	1226	25	385.5	8.5	7.9	0.24
Tarn06ap_9	1245	21	314.1	8.1	1073	22	3.09	0.27	736	18	1745	40	296	7	1481	33	365.1	7.1	13.87	0.37
Tarn06ap_10	1216	20	153.8	4.1	1504	35	1	0.29	740	18	1874	44	330.3	8.2	1653	49	435	11	7.67	0.24
Tarn06ap_11	1350	26	121.3	3.6	1977	63	5.1	0.26	297.4	8.2	1065	28	211.2	5.8	1239	33	419	10	6.43	0.24
Tarn06ap_12	391.2	6	281.5	5.6	600	23	0.317	0.053	258	11	750	29	110	4.4	585	24	147.5	5.3	2.95	0.16
Tarn06ap_13	1471	25	173.1	3.8	1425	33	0.423	0.059	545	11	1542	33	291.6	5.5	1523	33	427.5	8.9	7.9	0.25
Tarn06ap_14	706	13	383.2	8.6	49	1.6	0.64	0.17	34	2.4	70.8	5.1	8.09	0.61	34.6	2.6	7.05	0.56	1.68	0.13
Tarn06ap_15	1063	16	906	20	617	13	0.025	0.013	28.16	0.7	125.6	3.5	30.83	0.94	270.1	7.6	199	5.1	50.4	1
Tarn06ap_16	1392	39	84.7	3.8	2290	100	4.96	0.41	605	26	1690	72	312	13	1610	63	477	18	3.31	0.16
Tarn06ap_17	627	12	342	12	1464	38	0.171	0.037	335	8.4	991	26	166.8	3.9	878	21	283.5	6.9	4.62	0.18
Tarn06ap_18	403	12	474	17	525	18	0.139	0.08	10.38	0.44	35.8	1.2	7.17	0.3	55.2	2.1	33.9	1.4	10.72	0.36
Tarn06ap_19	585	16	1838	66	558	21	LOD	LOD	2.89	0.18	10.3	0.43	1.98	0.13	13.44	0.83	6.86	0.41	2.17	0.11
Tarn06ap_20	480.3	9.7	2564	78	854	31	0.085	0.026	19.41	0.73	118.3	3.9	26.79	0.96	197.3	6.6	132.2	3.8	48.2	1.3
Tarn06ap_21	1289	19	2160	57	795	20	LOD	LOD	11.35	0.39	46.9	1.4	10.87	0.37	100.7	2.9	72.6	1.9	18.2	0.46
Tarn06ap_22	5530	100	113.7	4	1146	34	0.312	0.057	316	13	974	33	153.4	5.3	784	27	233.7	6.8	6.78	0.28
Tarn06ap_23	394	7.9	280	8	1989	69	3.27	0.78	92.5	3.4	390	14	76.2	2.4	498	15	237.5	6.4	13.27	0.42
Tarn06ap_24	1685	28	279.5	7.9	944	29	0.146	0.065	445	13	1148	28	191.8	5.2	963	27	254.7	6	5.01	0.2
Tarn06ap_25	627	15	713	23	1297	39	0.69	0.19	45	3.6	109.5	6.5	16.91	0.86	103.4	4.4	49.9	1.8	13.88	0.47
Tarn06ap_26	577	13	491	19	432	17	0.267	0.088	14.04	0.66	37.8	1.6	7.63	0.36	45.8	2	26.9	1.3	5.97	0.28
Tarn06ap_27	448.7	8	707	18	835	23	0.079	0.038	9.02	0.7	29.2	1.8	5.12	0.37	31.4	2.1	14.86	0.66	3.38	0.13
Tarn06ap_28	1061	16	450	11	877	20	1.72	0.13	615	17	1520	38	267.6	6.9	1349	37	330.9	7.9	11.85	0.34
Tarn06ap_29	604	13	556	18	678	21	0.035	0.014	35.1	1.4	107.8	3.9	17.57	0.54	103	3.7	47.8	1.6	10.6	0.34
Tarn06ap_30	476.4	9.8	550	22	636	30	0.083	0.028	27.1	4.8	56.8	9.3	7.4	1	34.3	4	11.7	1.1	3.13	0.21
Tarn06ap_31	1268	27	980	33	692	30	1.73	0.16	992	34	2295	87	355	14	1606	56	310	11	17.82	0.66
Tarn06ap_32	395.1	8.5	563	18	209.2	7.2	0.019	0.012	6.87	0.66	25.6	2.5	4.96	0.47	36.1	3.6	14.6	1.2	4.35	0.27
Tarn06ap_33	809	15	1046	20	920	150	0.64	0.12	100	14	279	27	47.5	3.1	291	14	149.2	6.2	44.1	2.5
Tarn06ap_34	735	12	1826	28	729	13	LOD	LOD	32.47	0.81	141	2.9	31.2	0.77	229.8	5	124.3	2.8	32.79	0.75
Tarn06ap_35	637	13	285.7	8	253.3	7.8	0.009	0.008	21.14	0.75	69.7	2.4	12.64	0.46	83.5	3	41.4	1.3	9.39	0.29
Tarn06ap_36	1381	19	268	5.1	1475	32	0.899	0.087	602	11	1612	31	289.1	5.3	1495	27	412.4	6.4	11.23	0.26
Tarn06ap_37	825	15	1312	33	1011	33	0.2	0.17	85.6	2.6	321.4	8.6	60.9	2	380	10	198.5	5.6	61.3	1.7
Tarn06ap_38	1024	22	224.3	7	1294	46	0.876	0.088	476	15	1285	41	237.9	6.9	1284	39	360	10	10.46	0.36
Tarn06ap_39	1123	24	256.8	8.3	1307	42	3.55	0.21	421	14	1170	38	219.4	7.6	1174	38	334	11	9.16	0.33
Tarn06ap_40	413	10	360	12	909	33	0.063	0.038	3.86	0.26	12.74	0.45	2.32	0.14	15.38	0.94	8.29	0.46	2.52	0.15
Tarn06ap_41	368.5	9.7	1467	57	468	21	0.106	0.056	32.1	1.4	125.7	4.7	24.4	1	150.7	5.4	64.5	2.8	20.19	0.77
Tarn06ap_42	1047	26	358	15	1236	57	4.2	0.28	810	33	2104	86	368	15	1866	73	480	17	13.01	0.5
Tarn06ap_43	318.1	6.7	547	22	534	22	0.03	0.017	2.56	0.17	8.94	0.45	1.74	0.12	12.07	0.75	6.4	0.36	1.99	0.12
Tarn06ap_44	426	10	329	13	1057	41	0.009	0.009	1.89	0.15	6.53	0.35	1.276	0.089	8.21	0.61	4.89	0.32	1.739	0.097
Tarn06ap_45	469	37	352	12	1178	34	0.27	0.16	12.3	4.6	18.2	4.3	3.55	0.93	15.5	2.5	7.7	1.4	2.41	0.24
Tarn06ap_46	378.9	8.1	345.1	8.8	175.5	5.4	LOD	LOD	1.65	0.13	5.49	0.28	1	0.088	6.23	0.46	3.74	0.28	1.119	0.073
Tarn06ap_47	599	9.9	1083	23	752	18	7.1	1.4	77.1	5	148	7.7	25.6	1.2	156.6	6.8	68.6	2.4	18.24	0.67
Tarn06ap_48	673	17	522	16	755	23	LOD	LOD	13.26	0.46	45	1.3	8.78	0.37	60	2.2	32.5	1.2	10.03	0.39
Tarn06ap_49	652	13	563	18	1128	40	1.8	0.17	942	31	2198	80	374	13	1793	53	421	12	15.82	0.51
Tarn06ap_50	3118	52	127.2	3.9	2495	77	1.34	0.12	847	25	2311	72	416	12	2107	51	637	15	8.14	0.28
Tarn06ap_51	400	12	1001	51	720	43	3.2	1.1	33.6	3.8	118.6	8.6	20.7	1.2	155.9	9	117.7	6.1	25	1.2
Tarn06ap_52	1208	25	311.2	8.1	1208	37	2.56	0.18	693	17	1786	44	313.9	7.5	1618	38	430	10	10.52	0.34
Tarn06ap_53	496	11	877	28	958	35	LOD	LOD	16.62	0.67	57.5	2.1	11.62	0.52	79.3	3	53.3	1.9	17.59	0.55
Tarn06ap_54	157.1	4.3	1461	80	872	47	LOD	LOD	29.1	1.6	136.3	7	30.9	1.7	234	12	149.2	7.3	49.7	2.2
Tarn06ap_55	976	21	150.2	7	1523	76	0.186	0.039	221	11	819	39	152.7	7.1	884	42	305	12	4.23	0.2
Tarn06ap_56	288	7.1	229	11	59.1	3.1	0.172	0.045	1.97	0.19	4.46	0.36	0.75	0.07	3.89	0.37	1.72	0.21	0.743	0.068
Tarn06ap_57	213.2	7	1684	95	455	26	0.51	0.15	14.2	2.2	53.1	7.5	9.7	1	60.9	5.2	28	1.6	9.23	0.51
Tarn06ap_58	1032	26	380	21	1349	72	10.68	0.68	775	42	1990	110	357	19	1843	88	489	24	17.05	0.95
Tarn06ap_59	555.1	9	1030	25	954	22	0.047	0.022	36	1.8	153.8	5.8	35.3	1.2	274.9	8.3	166.9	4.2	48.4	1.1
Tarn06ap_60	539	14	992	33	802	29	LOD	LOD	17.8	0.78	92.3	3.2	22.66	0.89	192.8	7.7	124.7	4.3	38.1	1.4
Tarn06ap_61	770	18	1004	38	765	32	LOD	LOD	19.33	0.81	65.2	2.5	12.46	0.57	88.4	3.6	54.7	2	16.14	0.49
Tarn06ap_62	520	14	851	38	1097	51	0.033	0.018	28.9	1.4	113.9	5.4	23.7	1.2	169.3	7.3	110.3	4.6	36.4	1.5
Tarn06ap_63	1823	42	123.3	5.5	2630	110	2.2	0.16	279	11	1041	29	208.4	7.8	1222	48	495	17	3.93	0.21
Tarn06ap_64	596	12	2953	76	674	22	0.049	0.022	63.4	1.8	259.7	7.2	49.6	1.5	330.7	8.7	149.2	3.6	48.9	1.2
Tarn06ap_65	304.5	4.8	1644	28	615	15	0.017	0.011	33.3	3.1	140	11	28.7	1.8	200.5	8.4	115.3	3.9	34.3	1.1
Tarn06ap_66	1480	23	1050	18	310.1	6.4	0.018	0.011	3.76	0.17	11.9	0.35	2.18	0.11	15.39	0.84	8.41	0.45	2.37	0.094
Tarn06ap_67	1217	32	488	12	1263	40	1.69	0.12	638	16	1548	38	263.2	7.1	1252	31	332.6	9.1	13.28	0.4
Tarn06ap_68	352.5	8.9	474	20	366	16	0.116	0.036	22.6	3.5	59.4	8.9	8.8	1.2	45.7	6.3	14.2	1.4	1.72	0.12
Tarn06ap_69	1312	27	230.7	8	1675	64	0.464	0.09	748	29	1836	66	329	12	1622	53	455	15	5.87	0.22
Tarn06ap_70	941	19	441	13	934	33	0.281	0.055	639	22	1577	50	277.4	9.6	1408	47	354	12	11.4	0.36
Tarn06ap_71	2013	50	352	13	1163	40	0.13	0.033	98.1	3.4	303.9	9.6	45.6	1.6	230.3	7.1	93.7	3.2	13.56	0.49
Tarn06ap_72	537	12	983	32	982	35	0.109	0.035	36.1	1.4	125.1	4.6	24.31	0.83	170.8	6.1	104.5	3.7	33.5	1.1
Tarn06ap_73	200.7	4.8	303	11	397	13	0.014	0.01	2.97	0.16	10.43	0.47	1.96	0.11	13.88	0.77	7.52	0.47	2.46	0.13
Tarn06ap_74	515	11	2150	64	859	29	0.53	0.19	90.1	3.1	359	13	67.2	2.3	437	15	194.2	6	61.9	1.8
Tarn06ap_75	2684	87	188.1	9.8	589	25	0.047	0.019	12.9	0.67	58.5	2.6	13.91	0.65	112.3	5.5	72.5	3.3	12.65	0.51
Tarn06ap_76	574	13	606	13	815	22	9.1	1.4	22.4	1	67.1	2.2	13.3	0.47	98	3.1	62.3	1.8	21.19	0.79
Tarn06ap_77	621	17	1424	50	493	18	0.013	0.01	5.78	0.32	20.52	0.96	4.14	0.2	30.6	1.4	18.25	0.87	4.7	0.2
Tarn06ap_78	882	14	177.1	4.6	1136	30	1.13	0.12	286.9	8.3	975	22	167.9	4.8	919	26	279.9	7.5	5.84	0.23

	157Gd	±	159Tb	±	163Dy	±	165Ho	±	166Er	±	169Tm	±	172Yb	±	175Lu	±	182W	±	232Th	±	238U	±
Tarn04ap_105	303.9	3.6	44.46	0.62	269.8	3.2	48.81	0.57	133.8	1.6	19.38	0.3	125.4	2	15.97	0.24			12.51	0.22	4.398	0.081
Tarn04ap_106	283.3	6.6	38.5	0.85	226.4	4.8	39.8	0.88	99.6	2.1	12.41	0.26	68.7	2	8.34	0.25			44.2	1.1	20.9	0.76
Tarn06ap_0	118.7	2.8	19.64	0.31	118.4	2.4	19.8	0.39	50.13	0.97	6.9	0.21	44.6	1.3	7.38	0.25	0.029	0.015	0.186	0.016	0.411	0.019
Tarn06ap_1	25.92	0.75	6.23	0.16	63	1.4	19.6	0.33	80	1.5	13.93	0.41	92.4	2.2	12.83	0.34	0.178	0.037	0.008	0.003	0.095	0.007
Tarn06ap_2	334.6	7.2	49.5	1	305.7	5.7	56.7	1	155.1	2.9	22.2	0.54	134.2	3	17.97	0.45	0.54	0.24	20.5	0.54	13.8	0.53
Tarn06ap_3	34	1.2	7.81	0.25	76.9	2.3	21.81	0.81	72.9	2.7	9.4	0.33	43.9	1.6	4.82	0.18	0.141	0.035	0.138	0.014	0.232	0.013
Tarn06ap_4	342.5	9.2	62.9	1.3	428.8	8.2	80.1	1.7	231.7	5	34.3	1	204.3	5.9	25.2	0.71	0.147	0.059	8.11	0.47	77	2.1
Tarn06ap_5	227.1	4.6	44.88	0.87	303.2	5.3	51.33	0.81	117.3	1.7	13.49	0.28	65.5	1.5	7.22	0.18	0.2	0.056	0.271	0.024	0.863	0.032
Tarn06ap_6	342.9	8.5	60.1	1.5	389.1	6.7	71.3	1.5	199.9	3.7	28.86	0.6	172.2	4.3	21.42	0.67	0.57	0.11	14.16	0.48	51.3	2
Tarn06ap_7	5.47	0.33	1.35	0.06	15.75	0.49	5.69	0.14	28.08	0.76	5.86	0.2	43.6	1.4	7.21	0.26	1.29	0.1	0.134	0.02	0.025	0.004
Tarn06ap_8	361.9	6.4	55.5	1	347.8	6.4	64.4	1.1	178.9	2.6	25.56	0.47	160.7	2.8	21.71	0.5	0.148	0.037	17.49	0.42	4.89	0.13
Tarn06ap_9	315.1	6.9	42.12	0.85	243.1	4.3	42.57	0.8	106.6	2.1	13.68	0.32	75.2	2.2	9.42	0.29	0.234	0.048	80	12	22.54	0.91
Tarn06ap_10	368.2	8.6	52.77	0.99	316.2	5.5	57.6	1	156.2	3.3	21.64	0.49	133.8	3.8	17.24	0.47	0.208	0.048	32.56	0.68	35.12	0.83
Tarn06ap_11	399	8.7	61.6	1.1	388.1	6.7	72.7	1.4	205.4	3	30.65	0.52	196.5	4.2	26.38	0.6	0.104	0.034	28.73	0.68	13.81	0.37
Tarn06ap_12	153.7	5.5	19.42	0.66	116.1	3.7	22.54	0.68	62.5	1.9	8.47	0.27	49	1.5	6.19	0.21	1.27	0.1	4.4	0.18	3.82	0.14
Tarn06ap_13	377.3	7.3	53.19	0.98	321.2	5.3	56.54	0.87	152.6	2.2	22.26	0.37	144	2.8	19.58	0.41	0.096	0.03	20.06	0.37	30.04	0.54
Tarn06ap_14	6.65	0.54	0.999	0.067	7.03	0.41	1.605	0.079	5.66	0.23	0.994	0.052	7.34	0.32	1.199	0.058	0.18	0.044	8.94	0.59	2.08	0.11
Tarn06ap_15	251.7	4.8	32.97	0.69	167.3	3	25.37	0.43	57.3	1.1	6.88	0.18	38.21	0.92	4.5	0.13	0.047	0.018	1.004	0.044	0.814	0.031
Tarn06ap_16	449	12	69.2	1.4	434.1	7.8	82.8	1.3	237.6	4.2	36.07	0.86	243.6	7.7	33	1.2	0.194	0.037	19.66	0.68	13.65	0.56
Tarn06ap_17	339.3	7.6	52.6	1.1	338.1	6.6	66.6	1.2	173.9	3.3	21.58	0.45	120.6	3	15.07	0.35	1.68	0.15	7.3	0.18	11.44	0.25
Tarn06ap_18	94.5	2.4	16.78	0.43	112.1	2.3	21.47	0.37	57.3	1.2	8.02	0.25	53.4	1.7	8.07	0.25	0.474	0.071	0.24	0.14	0.824	0.074
Tarn06ap_19	16.4	0.61	3.71	0.12	41	1	15.65	0.31	83.1	1.6	16.72	0.44	124.9	3.4	18.22	0.6	0.16	0.039	0.029	0.006	0.198	0.011
Tarn06ap_20	226	5.3	39.57	0.86	229.3	3.7	34.93	0.6	75.7	1.2	8.62	0.23	42.7	1.2	4.6	0.14	0.145	0.032	0.202	0.018	0.613	0.035
Tarn06ap_21	179	4	29.34	0.67	184.3	3.5	31.91	0.63	73.3	1.4	8.66	0.19	50.1	1.3	6.22	0.18	0.159	0.038	0.427	0.03	0.12	0.008
Tarn06ap_22	220.8	6	34.14	0.76	214.2	4.1	40.9	0.75	118	1.9	18.16	0.35	128.4	3.2	18.4	0.52	0.137	0.036	3.92	0.27	36.2	1.5
Tarn06ap_23	389.3	8.4	69.1	1.5	460.1	7.3	89.4	1.3	222.1	3.6	24.86	0.43	119.9	2.5	14.08	0.31	0.229	0.068	29.4	1.1	20.2	2.6
Tarn06ap_24	219.4	4.5	29.99	0.49	174	2.6	31.69	0.45	85.2	1.5	11.42	0.26	68.7	1.7	8.85	0.25	0.208	0.042	9.1	0.33	20.56	0.68
Tarn06ap_25	103.4	2.6	22.64	0.54	200.1	3.7	49.09	0.82	157.5	2.4	24.93	0.53	166.2	4.3	22.12	0.73	2.86	0.22	76.1	2.3	29.37	0.96
Tarn06ap_26	66.8	1.9	13.33	0.36	87.2	1.6	16.04	0.34	43.08	0.88	5.77	0.14	33.21	0.97	4.13	0.15	0.201	0.048	2.658	0.089	0.336	0.023
Tarn06ap_27	34.4	1.5	7.81	0.27	80	2	26.05	0.66	100.5	2.2	15.48	0.32	89.8	2	10.38	0.25	0.246	0.039	0.303	0.024	0.325	0.024
Tarn06ap_28	265.1	5.6	33.69	0.65	184	3.6	31.76	0.58	79.4	1.8	9.56	0.27	52.2	1.3	6.42	0.18	0.177	0.045	25.7	0.68	21.02	0.55
Tarn06ap_29	95.9	2.5	18.41	0.41	134.2	2.5	25.93	0.55	66.4	1.4	8.51	0.18	49.2	1.3	5.79	0.18	0.073	0.025	0.84	0.074	1.878	0.069
Tarn06ap_30	24.5	1.1	5.62	0.19	59.7	2.2	19.15	0.72	69.5	2.7	9.11	0.39	41.9	1.7	4.04	0.16	0.184	0.046	1.22	0.2	0.131	0.012
Tarn06ap_31	224.6	6.8	26.9	0.73	145.7	3.2	24.91	0.47	61	1.3	7.11	0.2	38.2	1.2	4.79	0.17	0.457	0.07	37.2	1.3	20.91	0.78
Tarn06ap_32	21.6	1.1	3.58	0.13	27.12	0.79	6.7	0.18	19.84	0.48	2.526	0.086	14.05	0.46	1.758	0.068	0.164	0.033	0.26	0.025	0.106	0.009
Tarn06ap_33	268	19	47.7	5.5	275	40	42.3	6.9	98	18	11.3	2.4	56	13	6.6	1.5	0.115	0.034	0.518	0.088	1.56	0.35
Tarn06ap_34	219.3	4	34.38	0.62	196.2	3	31.3	0.49	67.6	1.1	7.71	0.17	41.03	0.91	4.75	0.14	0.075	0.025	0.314	0.022	0.256	0.012
Tarn06ap_35	93	2.6	16.51	0.44	87	2	9.42	0.25	11.29	0.33	0.699	0.045	2.22	0.16	0.222	0.023	0.303	0.067	0.142	0.013	3.92	0.14
Tarn06ap_36	365.7	5.3	52.82	0.91	321.5	4.7	57.6	0.95	158	3	21.63	0.39	137.1	2.8	17.47	0.32	0.097	0.03	28.18	0.4	30.96	0.37
Tarn06ap_37	323.7	7.5	55.6	1.3	317.3	7	48.86	0.93	106.8	2.1	11.77	0.28	62.6	1.5	7.28	0.22	0.059	0.023	1.89	0.089	1.506	0.052
Tarn06ap_38	319.6	8.7	45.32	0.99	271.6	6	48.59	0.99	128.2	2.5	16.9	0.35	101.8	2.6	13.02	0.36	0.061	0.024	26.1	0.64	23.65	0.7
Tarn06ap_39	301.1	8.9	44.1	1.1	268.1	5.5	49.4	0.79	135.3	2.2	19.4	0.44	124.5	2.8	16.27	0.44	0.077	0.025	27.28	0.85	18.81	0.6
Tarn06ap_40	21.19	0.84	5.81	0.19	73.9	1.8	30.09	0.65	132.1	2.9	19.07	0.51	102.3	3.4	10.35	0.39	0.505	0.076	0.024	0.006	0.167	0.012
Tarn06ap_41	108.3	3.6	22.44	0.61	140.2	3.2	21.14	0.43	45.2	1.1	5.08	0.18	27.86	0.86	3.47	0.15	0.043	0.021	0.425	0.029	0.047	0.006
Tarn06ap_42	387	11	49.8	1.3	284	6.9	49.16	0.88	122.7	2.8	15.55	0.44	88.6	2.7	10.83	0.41	0.123	0.03	68.6	2.5	34.4	1.4
Tarn06ap_43	13.62	0.52	3.24	0.1	35.74	0.88	14.79	0.31	83.4	1.6	16.47	0.4	108	2.9	13.33	0.41	0.229	0.048	0.01	0.003	0.176	0.011
Tarn06ap_44	19.41	0.7	6.32	0.17	81.1	1.6	33.27	0.62	163.9	2.6	28.44	0.53	182.1	4.8	21.98	0.58	0.22	0.045	0.004	0.002	0.118	0.01
Tarn06ap_45	23.6	1.3	6.94	0.17	93.1	1.9	38.77	0.73	192.2	3.8	34.54	0.8	231.1	5.2	28.56	0.79	0.69	0.22	0.082	0.03	0.475	0.099
Tarn06ap_46	8.28	0.4	1.918	0.083	19.38	0.57	5.75	0.15	20.05	0.48	2.617	0.098	12.72	0.56	1.381	0.063	0.149	0.035	0.035	0.006	0.05	0.006
Tarn06ap_47	136.9	3.9	22.79	0.56	153.1	4.2	29.33	0.69	77.8	1.8	11.42	0.29	84.2	1.8	13.13	0.34	0.4	0.054	19.1	2.3	0.437	0.029
Tarn06ap_48	76.3	2.5	16.23	0.42	134.9	2.7	29.12	0.51	76.7	1.6	9.27	0.23	49.8	1.6	5.46	0.18	0.046	0.019	0.033	0.006	0.536	0.025
Tarn06ap_49	331.1	8.9	41.97	0.97	234.3	5.1	41.9	1	104	2.3	12.86	0.34	69.3	2	8.55	0.28	2.6	0.18	58.5	2.2	47.4	1.8
Tarn06ap_50	598	13	87.9	1.8	542	9.1	97.6	1.4	261.2	3.4	35.8	0.56	214	4.2	26.83	0.61	0.755	0.095	33.49	0.69	34.2	1
Tarn06ap_51	193	7.4	29.2	1	170.4	5.2	28.24	0.63	68.3	2.3	8.49	0.34	48.5	2.3	5.72	0.29	0.78	0.15	15.1	2.5	1.125	0.082
Tarn06ap_52	345.1	8.2	46.2	1.2	263.7	6.7	46.9	1	116.8	2.9	15.23	0.4	86.3	2.7	10.49	0.33	0.23	0.054	25.12	0.74	19.56	0.56
Tarn06ap_53	140.4	3.4	29.26	0.61	211	4.2	37.94	0.7	95.4	1.8	12.09	0.29	70.9	1.8	8.53	0.28	0.135	0.045	0.35	0.026	1.247	0.051
Tarn06ap_54	252.3	8.6	42.2	1.2	250.3	5.4	39.39	0.74	85.7	1.9	9.74	0.32	48.4	1.9	5.08	0.21	0.04	0.018	0.021	0.005	0.338	0.022
Tarn06ap_55	281.9	9.1	44.5	1.2	282.5	5.5	54.16	0.88	153.7	2.4	23.54	0.52	156.6	4.6	20.8	0.77	0.152	0.04	9	0.4	22.9	1
Tarn06ap_56	3.86	0.26	0.887	0.054	7.33	0.33	1.745	0.064	4.72	0.19	0.558	0.039	2.77	0.17	0.354	0.031	0.183	0.041	0.056	0.009	0.064	0.006
Tarn06ap_57	53.4	2.1	9.16	0.27	63.4	1.8	14.37	0.39	49	1.7	8.41	0.32	58.3	2.6	8.9	0.46	0.114	0.034	9	1.8	1.86	0.54
Tarn06ap_58	401	16	52.5	1.9	295.2	9.7	51.7	1.1	131	3.2	16.53	0.55	91.4	3.9	10.9	0.58	1.24	0.2	61.9	3.8	27.3	1.6
Tarn06ap_59	294.3	6.7	45.47	0.97	259.2	4.6	40.58	0.7	86.5	1.5	9.52	0.22	47.4	1.2	5.24	0.14	0.039	0.02	0.284	0.026	0.548	0.02
Tarn06ap_60	226.7	6.8	36.45	0.97	212.2	4.6	33.13	0.6	72.4	1.4	8.18	0.18	40	1.1	4.44	0.12	0.075	0.025	0.087	0.01	0.402	0.022
Tarn06ap_61	132.4	4.2	25.29	0.67	181.3	4.3	33.42	0.66	73.2	1.4	7.63	0.22	31.73	0.93	3.18	0.13	0.23	0.05	0.056	0.008	0.638	0.03
Tarn06ap_62	244.7	8.5	44.5	1.4	285.1	6.5	49.7	1.1	119.5	2.7	14.53	0.4	78.2	2.6	9.91	0.36	0.075	0.027	0.183	0.016	1.4	0.07
Tarn06ap_63	509	14	82.7	2	525.1	9.5	99.4	1.4	287.4	4.8	43.5	1	271.5	7.3	37.4	1.2	0.29	0.054	14.08	0.51	20.18	0.83
Tarn06ap_64	231.5	5.4	29.88	0.64	145.4	2.6	23.52	0.43	67	1.3	12.03	0.26	95.8	2.1	15.53	0.34	0.116	0.041	6.33	0.23	0.133	0.007
Tarn06ap_65	187.8	5.7	29.82	0.66	165.4	3.6	26.16	0.55	55.8	1.2	6.09	0.14	27.59	0.67	2.936	0.09	0.071	0.024	0.104	0.012	0.198	0.01
Tarn06ap_66	18.86	0.51	3.92	0.11	35.86	0.89	10.27	0.23	39.84	0.86	6.97	0.14	50.5	1	8.11	0.25	0.169	0.039	0.071	0.009	0.146	0.01
Tarn06ap_67	311.4	8.6	47	1.2	296.6	7.2	56.3	1.2	144	3.4	18.19	0.5	96.3	2.9	12.45	0.44	0.475	0.073	14.41	0.43	70.3	2.1
Tarn06ap_68	21.7	1.1	4.52	0.19	40.1	1.1	11.36	0.26	42.29	0.92	7.07	0.22	47.3	1.4	7.64	0.29	0.247	0.052	0.6	0.066	2.3	0.24
Tarn06ap_69	398.4	9.7	58.6	1.3	356.3	7.2	65.3	1.1	175.5	2.7	25.37	0.45	156.4	4.1	20.58	0.55	0.075	0.029	17.8	0.47	31.6	1.1
Tarn06ap_70	282.9	7.7	35.83	0.76	198.4	3.5	34.51	0.61	84.4	1.6	10.08	0.26	54	1.5	6.67	0.22	0.125	0.034	23.13	0.66	25.2	0.79
Tarn06ap_71	146	3.5	31.77	0.67	240.1	4.7	45.27	0.72	106.3	1.9	11.99	0.27	58.7	1.9	6.6	0.23	0.132	0.036	0.698	0.033	13.95	0.47
Tarn06ap_72	232.5	5.4	41.23	0.92	254.9	5.7	42.56	0.82	98.2	1.9	11.55	0.31	61.6	1.9	7.53	0.25	0.127	0.037	0.31	0.02	1.455	0.052
Tarn06ap_73	17.48	0.67	3.78	0.12	37.48	0.92	12.33	0.31	56.4	1.3	9.74	0.28	52.2	1.5	6.02	0.21	0.325	0.048	0.026	0.007	0.055	0.006
Tarn06ap_74	280.6	7.1	42.2	1.1	228.4	4.8	36.38	0.61	81	1.2	10.02	0.26	59.5	1.4	8.4	0.24	0.202	0.039	5.01	0.15	0.212	0.016
Tarn06ap_75	130.5	5	21.77	0.56	133	3.2	23.76	0.56	57.3	1.4	7	0.26	36.7	1.5	4.42	0.2	0.514	0.071	1.98	0.11	2.18	0.1
Tarn06ap_76	142.6	4	25.69	0.73	178.6	5.2	34.44	0.9	87.8	2.2	11.76	0.35	65.3	2.3	8.28	0.26	0.249	0.055	0.921	0.099	1.88	0.16
Tarn06ap_77	39.4	1.3	8.4	0.29	73.9	1.9	16.96	0.32	47.22	0.91	5.63	0.17	26.49	0.82	2.48	0.1	0.808	0.079	2.163	0.088	1.725	0.066
Tarn06ap_78	244.1	6.5	35.06	0.83	218.8	5.1	40	1	107.1	2.7	14.84	0.36	91.9	2.8	11.91	0.32	0.149	0.039	13.54	0.67	16.06	0.58

Supporting Information Tables S3.5: Apatite trace-element data (continued)

	55Mn	±	86Sr	±	89Y	±	90Zr	±	139La	±	140Ce	±	141Pr	±	146Nd	±	147Sm	±	153Eu	±	157Gd	±	159Tb	±	163Dy	±	165Ho	±	166Er	±	169Tm	±	172Yb	±	175Lu	±	182W	±	232Th	±	238U	±
Tarn06ap_79	14.1	1.4	478	11	289.8	7.4	6.42	0.3	233.7	5.8	555	14	78.1	2	410	10	99.1	2.7	20.01	0.53	102.5	2.8	12.41	0.31	69	1.2	12.03	0.28	27.68	0.65	2.85	0.1	14.2	0.53	1.667	0.069	3.91	0.21	4.01	0.12	1.119	0.035
Tarn06ap_80	1684	31	140.4	4.1	2082	58	5.39	0.28	573	17	1530	42	283.7	8.4	1488	40	451	12	6.83	0.25	410.9	8.2	64.5	1.3	403.6	6.8	76.6	1.1	217.3	3.4	32	0.71	213.8	4.8	27.43	0.69	0.209	0.045	14.58	0.37	9.83	0.3
Tarn06ap_81	1070	21	540	12	732	17	3.84	0.22	798	21	1824	47	304.2	7.2	1458	30	312.9	7	12.44	0.41	231.2	5.3	28.27	0.65	151.5	3.1	26.12	0.65	64.9	1.5	8.05	0.23	44.9	1.1	5.44	0.18	0.367	0.07	28.46	0.62	14.47	0.25
Tarn06ap_82	968	15	442	10	814	18	8.14	0.35	745	19	1730	43	292.9	7.5	1447	33	327.6	6.8	10.19	0.28	254.8	5.1	31.1	0.56	169.6	2.9	29.48	0.46	72.1	1.1	8.72	0.22	48.2	1.2	5.73	0.17	0.295	0.056	27.01	0.6	8.14	0.21
Tarn06ap_83	255.9	4.5	2178	64	1104	35	0.01	0.009	35.9	1.2	134.9	4.3	28.09	0.88	213.5	6.8	174.6	5.2	59.9	1.5	347.9	8.3	52.9	1	298.9	5.3	49.4	0.72	112.4	2.2	12.71	0.34	65.8	1.7	6.83	0.22	0.037	0.018	0.155	0.013	0.812	0.033
Tarn06ap_84	3098	61	89.1	3	1932	55	0.127	0.03	335	11	1090	28	188.5	6	1003	30	363	11	4.34	0.17	378	11	61.7	1.4	396.5	8.1	74.9	1.3	205.9	4.5	29.71	0.63	192.4	4.4	23.57	0.62	0.289	0.05	3.18	0.1	12.11	0.33
Tarn06ap_85	818	16	231.2	8.1	3890	140	0.198	0.051	294	11	994	35	174.4	6.2	1085	38	499	15	33.94	0.99	685	18	108	2.6	669	13	125.6	2.2	330	6.5	43.73	0.95	276.3	6.4	36.77	0.98	0.138	0.041	76.7	2.2	9.97	0.36
Tarn06ap_86	315.1	7.2	967	34	630	23	LOD	LOD	9.55	0.38	33.6	1.3	6.55	0.3	45.3	1.7	29.6	1.1	7.49	0.25	75.6	2.1	15.99	0.34	121.4	2.4	23.44	0.45	54.9	1.2	5.85	0.17	29.87	0.84	3.01	0.11	0.104	0.027	1.87	0.27	0.345	0.023
Tarn06ap_87	376.2	7.1	2844	73	1074	33	0.039	0.017	8.33	0.31	33.7	1.1	6.87	0.27	54.2	1.8	36.8	1.3	13.2	0.41	115.9	2.5	29.28	0.56	243.2	4.1	47.63	0.74	105.5	1.8	10.73	0.25	48.3	1.2	3.88	0.12	0.075	0.022	0.061	0.009	0.314	0.015
Tarn06ap_88	1132	21	454	15	1218	34	10.12	0.5	666	21	1660	51	294.2	9.1	1476	42	373	11	19.15	0.58	306.5	7.6	42.53	0.84	249.7	4.8	43.85	0.78	117	2.5	15.88	0.4	102.4	2.9	12.59	0.41	0.155	0.033	40.1	1.2	8.36	0.25
Tarn06ap_89	259.3	5.8	1063	35	517	16	0.01	0.009	27	1.2	105.8	4	20.75	0.85	139.9	5.1	74.9	2.3	22.85	0.71	125.4	3.7	21.83	0.52	127	2.5	20.83	0.38	51.58	0.98	7.19	0.17	54.5	1.6	8.33	0.2	0.041	0.018	0.936	0.036	0.286	0.016
Tarn06ap_90	1188	21	397	10	981	24	4.06	0.36	519	13	1324	39	223.1	5.2	1124	29	285.9	7	12.35	0.36	242.1	5	32.93	0.61	191.2	3	33.32	0.59	85.9	1.6	11.08	0.29	63.8	1.5	7.52	0.17	0.158	0.04	18.75	0.7	9.7	0.26
Tarn06ap_91	1197	26	500	19	670	21	0.085	0.023	457	16	1110	32	179.2	5.4	877	28	213.7	6.1	7.91	0.32	165.8	3.8	22.05	0.45	122.7	2.4	21.82	0.47	57.5	1.2	7.92	0.21	53.3	1.6	6.64	0.19	0.086	0.027	7.53	0.23	30.3	1.1
Tarn06ap_92	5130	100	107.7	3.2	2575	86	3.03	0.21	530	17	1538	45	282.3	8.6	1443	43	479	13	5.84	0.2	461	10	76.7	1.4	508.6	9.8	96.6	1.5	279.6	4.9	42.06	0.79	290	6.1	37.43	0.89	0.178	0.039	31.97	0.78	47.8	1.8
Tarn06ap_93	313.9	6.5	3010	110	334	16	0.74	0.12	94.1	3.4	398	14	70	2.4	354	12	62.8	1.9	16.36	0.49	51	1.6	7.05	0.24	50.3	1.5	11.47	0.34	32.91	0.77	4.49	0.15	28.6	1.2	3.68	0.17	0.347	0.066	7.17	0.31	3.72	0.16
Tarn06ap_94	687	17	931	33	626	24	0.24	0.15	74.2	3.1	191.1	8	29.6	1.3	174.8	6.3	73	2.4	18.48	0.71	94.3	2.5	15.96	0.36	117.6	2.4	23.51	0.52	59.7	1.4	7.56	0.2	45.5	1.4	5.2	0.2	0.162	0.041	1.249	0.053	0.349	0.03
Tarn06ap_95	538	8.5	325.7	6.4	517	12	1.09	0.26	3.62	0.16	12.91	0.51	2.53	0.13	16.41	0.84	9.15	0.52	2.7	0.11	25.09	0.83	6.2	0.17	59.1	1.1	16.6	0.26	62.6	1.3	10.41	0.2	74.1	1.6	9.59	0.22	0.093	0.029	0.02	0.005	0.211	0.013
Tarn06ap_96	276	3.9	665	12	734	14	0.017	0.011	27.68	0.8	108	2.4	21.78	0.58	159.3	3.7	85.7	2	27.32	0.55	152.5	2.5	24.95	0.4	161.4	2.6	30.2	0.43	71	1	7.94	0.18	41.8	1	4.25	0.13	0.06	0.026	0.333	0.032	1.256	0.035
Tarn07ap_0	1385	17	462.1	7.1	1035	18	9.25	0.41	659	12	1559	23	263	3.6	1275	20	320.1	5.4	15.92	0.35	267.9	4.2	36.43	0.47	204.6	3.2	35.77	0.47	90.2	1.4	11.25	0.22	62.7	1.4	7.61	0.16	0.23	0.046	23.98	0.41	6.81	0.12
Tarn07ap_1	442.5	6.2	2000	24	1119	27	0.019	0.012	75.7	1.3	276.6	4.5	54.35	0.88	380.8	5.9	197.1	3.2	56.9	1.1	337.9	4.7	52.36	0.81	312.1	3.8	51.44	0.72	113.6	1.8	12.72	0.26	65	1.3	7.41	0.2	0.049	0.019	0.603	0.03	0.657	0.019
Tarn07ap_2	780	11	519.1	6.9	866	13	0.506	0.067	642.4	9.5	1577	24	276.1	4.6	1349	24	331.5	5.9	12.15	0.34	268	4.8	33.95	0.55	184.9	3.3	32	0.47	77.9	1.2	9.39	0.19	50.5	1.1	6.13	0.15	0.111	0.031	31.72	0.66	23.11	0.38
Tarn07ap_3	296.6	4.1	1403	16	700	10	0.016	0.011	93.4	1.6	326.4	4.7	59.2	1.1	368.3	6.2	190.9	3.6	40.47	0.7	208	2.8	29.65	0.53	186.7	2.6	30.78	0.43	66	1.1	6.71	0.18	31.87	0.73	3.7	0.11	0.031	0.016	0.688	0.038	0.333	0.015
Tarn07ap_4	1012	14	353.6	6.5	1024	24	1.6	0.12	597	13	1510	34	265.7	6	1338	30	345.2	6.8	10.35	0.31	287.2	5.6	37.13	0.72	203.8	3.8	35.68	0.64	89.2	1.6	11.42	0.22	62.9	1.3	7.88	0.19	0.067	0.025	33.26	0.75	17.87	0.42
Tarn07ap_5	472.2	6.3	1452	20	648	11	1.47	0.28	12.64	0.43	50.9	1.2	10.08	0.3	72.6	2.1	43.2	1.2	13.49	0.41	91.4	2	16.79	0.32	119.5	2	24.38	0.43	65	1.1	8.48	0.17	46.4	1	5.79	0.17	0.173	0.044	5.53	0.32	0.846	0.078
Tarn07ap_6	552.7	7.2	1390	17	318.9	5.1	LOD	LOD	5.99	0.21	23.63	0.66	4.34	0.16	29.3	1	15	0.44	3.12	0.12	29.35	0.74	5.37	0.14	42.79	0.78	10.41	0.2	33.38	0.62	5.09	0.13	32.61	0.83	4.34	0.13	0.282	0.054	0.261	0.022	0.353	0.015
Tarn07ap_7	1079	21	296.9	6.2	1285	41	3.12	0.25	559	14	1450	44	261.1	6.7	1314	31	359.4	9.8	12.41	0.38	315.7	7.9	45.2	1	271.5	6.2	49.16	0.98	130.3	2.9	18.02	0.43	110.7	3.2	14.56	0.36	0.286	0.095	28.27	0.52	19.09	0.31
Tarn07ap_8	968	12	507.7	7.7	640	11	0.062	0.021	474	9.3	1140	25	187.9	4	929	20	220.6	4.6	7.72	0.23	185.9	3.9	23.21	0.41	130.2	2.3	23.45	0.45	59.1	1.3	7.73	0.19	42.8	1	5.54	0.16	0.301	0.052	4.59	0.14	42.4	1.1
Tarn07ap_9	1148	15	1517	20	367.9	6.4	8.25	0.33	1847	35	3054	55	316.9	4.7	1061	19	146.5	2.8	36.67	0.71	106.8	2	12.48	0.23	69.5	1.2	12.75	0.24	32.5	0.49	4.23	0.11	25.5	0.6	3.488	0.098	0.065	0.022	94.1	1.5	14.03	0.21
Tarn07ap_10	2682	49	236.6	4.9	1022	21	4.69	0.19	1165	22	2980	54	464.9	8.3	2125	37	432.4	7.5	15.29	0.34	320.8	5.4	40.02	0.65	221.5	3.7	39.01	0.63	96.2	1.7	12.46	0.25	71	1.3	9.03	0.2	0.082	0.025	38.64	0.64	15.54	0.25
Tarn07ap_11	914.5	9.8	450.6	7.1	571	9.3	0.407	0.056	376	6.4	1028	22	160.4	2.8	819	14	203.9	3.6	7.4	0.17	172.9	2.9	21.52	0.34	118.5	2.2	20.46	0.3	49.36	0.9	6.13	0.15	33.56	0.68	4.17	0.11	0.33	0.056	10.83	0.19	30.02	0.46
Tarn07ap_12	507.6	7.7	247.3	4.8	476.3	8.1	0.052	0.018	261.9	5.2	788	17	113.6	2.2	580	12	133.5	2.8	36.15	0.76	128.3	2.3	15.96	0.31	87.6	1.6	16.24	0.27	42.95	0.83	6.43	0.18	46.04	0.98	7.23	0.2	1.94	0.12	0.535	0.022	28.36	0.48
Tarn07ap_13	419	9.1	1686	64	480	20	0.22	0.14	3.38	0.21	18.3	0.86	4.03	0.25	29.7	1.9	15.92	0.89	4.56	0.24	28.2	1.2	5.09	0.17	43.9	1.2	14.25	0.28	60.3	1.1	10.21	0.25	67.2	1.8	9.33	0.28	0.067	0.024	0.144	0.015	0.071	0.008
Tarn07ap_14	1017	32	179	10	1561	86	1.77	0.18	489	27	1481	82	279	15	1456	71	428	20	6.88	0.33	378	14	54.9	1.5	330.8	6.3	60.7	0.88	161.3	2.8	22.5	0.56	140.4	4.4	18.22	0.73	0.222	0.046	27.7	1.3	24.8	1.3
Tarn07ap_15	925	11	454.6	8.8	606	17	0.556	0.072	507	13	1205	36	187.6	5.7	887	26	207.9	6.4	10.4	0.35	175.5	5.4	22.53	0.6	125.3	3.9	21.79	0.65	53.5	1.7	6.41	0.22	35.1	1.3	4.26	0.19	0.105	0.031	20.1	1	23.21	0.95
Tarn07ap_16	1396	21	341.4	8	1436	45	0.855	0.067	738	18	1886	48	330.9	7.3	1669	43	460	10	12.89	0.27	413.1	6.9	57.88	0.92	336.8	6.8	59.9	1.1	148.7	2.5	19.16	0.42	106.8	2.3	13.3	0.34	0.075	0.022	37	1.1	33.77	0.96
Tarn07ap_17	675	26	524	38	510	17	0.62	0.57	15	2	49.1	6.3	12	1.6	85	11	46.9	5.1	13.7	1.7	83.6	6.2	14.8	0.72	98.8	2.7	19.3	0.39	53.6	1.4	7.48	0.22	46.6	1.5	6.45	0.27	2.91	0.26	3.58	0.93	0.819	0.045
Tarn07ap_18	296.1	4.4	1079	23	593	12	0.065	0.028	35.6	0.82	196.4	5.1	50.1	1.3	384	10	219.4	5.3	65.8	1.5	280.9	5.5	36.58	0.56	184.7	3.3	26.39	0.48	51.6	1	5.26	0.16	25.27	0.81	2.641	0.093	0.055	0.02	1.731	0.076	0.187	0.011
Tarn07ap_19	1145	25	788	29	1329	50	34.4	7	105.9	6.1	347	17	54.9	2.9	292	15	86.8	3.1	13.96	0.44	121.9	4	23.76	0.77	207.4	5.5	53.3	1.5	186.8	6	31.3	1.1	209.6	7.8	28.8	1.2	0.625	0.088	22.7	2.2	7.09	0.58
Tarn07ap_20	358.5	8.6	942	19	65	1.9	0.242	0.041	22.4	1.2	48.8	2.3	5.81	0.34	24	1.5	5.71	0.47	1.031	0.081	5.97	0.36	1.046	0.065	8.14	0.39	2.089	0.084	7.84	0.3	1.402	0.055	11.1	0.46	1.774	0.078	0.904	0.093	4.76	0.21	1.582	0.073
Tarn07ap_21	1537	27	225.5	6.4	1518	44	0.491	0.067	588	15	1588	38	287.7	7.3	1475	39	414.9	9.4	10.28	0.29	361.5	8.8	52.1	1.1	316.5	6	57.9	1	155.3	2.5	22.44	0.54	144.9	3.5	18.6	0.46	0.079	0.023	28.85	0.67	30.96	0.81
Tarn07ap_22	372.5	6.9	402	10	929	25	8.01	0.35	368	13	992	27	159.3	4.8	808	23	199.1	5	36.64	0.95	210.9	5	28.84	0.6	178.6	3.9	34.26	0.82	86.8	1.8	10.49	0.25	57.5	1.6	7.24	0.2	0.337	0.056	6.19	0.17	1.194	0.047
Tarn07ap_23	970	18	318.4	7.3	1041	23	6.92	0.71	550	14	1460	38	268.6	7.1	1378	29	368.9	8	10.31	0.32	307.5	5.6	40.64	0.87	229.9	4	40.48	0.65	103.6	2	13.05	0.28	74.9	1.7	9.28	0.22	0.132	0.031	31.49	0.68	14.77	0.38
Tarn07ap_24	971	18	527	14	884	19	4.19	0.19	821	21	1934	48	322.9	8.5	1548	36	352.7	7.6	12.56	0.38	270	4.8	33.77	0.66	184.5	3.1	31.85	0.53	77.5	1.3	9.52	0.21	52.2	1.2	6.38	0.17	0.093	0.026	33.47	0.69	14.46	0.32
Tarn07ap_25	905	16	504	11	671	19	0.084	0.023	450	10	1136	29	187.3	4.7	890	22	218.9	5.3	10.56	0.25	182	4.2	23.69	0.5	131.3	2	23.14	0.39	59.2	1.1	7.9	0.17	49.8	1.4	6.57	0.15	1.18	0.11	6.11	0.16	10.33	0.26
Tarn07ap_26	190.9	4.5	541	14	1090	28	0.054	0.034	4.84	0.2	18.44	0.54	4.07	0.19	31.8	1.4	23.91	0.91	8.26	0.28	75.9	1.5	18.34	0.38	169	2.7	40.34	0.73	112.4	2.1	14.33	0.31	76.7	1.6	8.85	0.23	0.085	0.03	0.215	0.016	0.309	0.017
Tarn07ap_27	635	11	557	13	1175	30	0.022	0.012	19.2	0.46	68.8	1.8	12.84	0.39	88.1	2.4	46.8	1.3	14.14	0.42	112.9	2.4	26.09	0.62	227.9	5.4	52.8	1.2	149.7	3.5	18.41	0.47	95.5	2.9	9.51	0.27	0.148	0.033	0.177	0.015	0.51	0.018
Tarn07ap_28	4291	78	147.4	4.2	1601	44	0.112	0.024	161.9	4.2	595	16	100.5	2.6	557	14	241.3	5.7	9.09	0.26	324.2	6.6	59.4	1.1	397.8	6.4	73	1.1	190.7	3.2	26	0.49	166	3.8	21.6	0.47	0.327	0.057	0.567	0.03	66.6	1.5
Tarn07ap_29	964	19	185	5.9	2165	61	0.204	0.038	360	11	1039	32	171.5	5.2	884	25	327.9	9	8.79	0.26	446	10	82.2	1.8	543.6	8.8	97.4	1.7	223.1	4.1	24.25	0.54	115.5	2.9	12.66	0.3	0.125	0.033	3.84	0.19	38.9	1.4
Tarn07ap_30	1449	32	300	10	1162	46	14.9	1.3	754	32	1951	71	340	13	1652	59	435	15	9.35	0.39	348	12	46.6	1.3	259.5	6.6	45.8	1.3	113.3	2.7	15.1	0.48	87.4	2.8	10.79	0.48	0.83	0.16	34.7	1.2	12.21	0.45
Tarn07ap_31	418.6	7	1909	52	698	14	0.061	0.028	27.87	0.81	106.3	2.8	21.45	0.58	153.4	4	90.7	2.2	26.39	0.67	162.9	3.4	26.13	0.51	165	2.5	29.05	0.44	69.7	1.1	8.53	0.19	48.6	1	6.09	0.18	0.084	0.025	0.204	0.016	0.275	0.015
Tarn07ap_32	500	10	1463	47	863	29	0.182	0.048	4.06	0.2	13.48	0.49	2.81	0.15	18.55	0.79	12.14	0.59	4.41	0.17	39	1.3	10.09	0.27	103.6	2.2	29.32	0.52	98.2	1.7	15.57	0.32	107.4	2.5	14.99	0.34	0.162	0.034	0.269	0.03	0.213	0.013
Tarn07ap_33	2629	56	291.1	7.2	1275	38	4.84	0.24	639	17	1709	43	302	7.5	1477	36	403.8	9.5	8.9	0.27	336.7	7.3	47.27	0.93	272.8	4.3	49.09	0.69	126.4	1.8	16.96	0.29	101.5	1.9	12.84	0.33	0.088	0.026	28.25	0.61	17.62	0.39
Tarn07ap_34	868	16	410.9	9.9	765	20	0.361	0.05	532	14	1342	35	231.2	5.2	1142	26	285	6.7	9.55	0.29	234.1	5.4	28.98	0.65	159.5	2.9	27.57	0.46	67	1.3	8.27	0.22	46.7	1.1	5.8	0.17	1.77	0.13	18.54	0.76	51.1	2.9
Tarn07ap_35	1092	22	221.4	7.2	1738	51	4.4	0.28	436	13	1267	35	249.3	7.1	1365	33	418.1	9	9.84	0.31	376.5	6.5	57	1.1	348.6	5.8	65.1	1.1	177.3	3	26.23	0.54	167.8	3.5	22.35	0.58	0.192	0.036	23.17	0.57	14.68	0.48
Tarn07ap_36	289.6	5.2	287.8	7.7	950	30	0.433	0.063	149.3	4.4	486	14	78.9	2.2	444	12	150.9	3.9	4.13	0.15	187.6	4.8	27.99	0.57	185	4	38.33	0.65	107.2	1.9	14.26	0.29	83.4	2.3	10.01	0.28	2.49	0.16	6.21	0.16	6.91	0.17
Tarn07ap_37	1095	19	295.3	6.8	1081	26	0.498	0.065	514	13	1366	33	246.4	5.7	1259	32	335.8	7.4	11.77	0.38	292.3	6.3	40.12	0.78	235.9	4.3	42.05	0.71	107.1	2	13.8	0.26	79.2	2	9.44	0.26	0.09	0.028	23.9	0.54	24.18	0.45
Tarn07ap_38	312.8	5.3	468	11	513	12	LOD	LOD	5.2	0.26	16.95	0.55	3.15	0.18	21.24	0.96	12.29	0.65	4.34	0.18	29.2	1	5.97	0.2	57.2	1.3	16.83	0.32	55.4	1	6.89	0.18	36.19	0.91	4.34	0.14	0.195	0.037	0.33	0.052	0.093	0.007
Tarn07ap_39	533	10	1343	34	360	11	0.65	0.18	11.55	0.47	56.1	1.6	13.07	0.37	107.9	3	80	2.1	22.27	0.6	143.9	3.2	22.29	0.5	114.5	2.2	15.71	0.36	30.67	0.66	2.977	0.099	13.97	0.48	1.567	0.06	1.21	0.12	0.309	0.047	1.185	0.072
Tarn07ap_40	1047	18	307.7	8	1080	27	4.34	0.26	563	13	1499	33	267.7	6.5	1360	31	365.8	8.8	9.68	0.28	306.8	6.3	40.75	0.96	231	3.4	40.78	0.73	102.1	1.7	13.18	0.26	76.3	1.8	9.13	0.21	0.074	0.024	25.15	0.62	12.33	0.31
Tarn07ap_41	1001	16	248.9	5.4	1497	30	5.16	0.25	605	15	1618	38	295.4	6.1	1507	32	430.5	8.4	14.33	0.41	374.4	6.7	53.4	0.81	317.9	4.8	57.78	0.64	150.7	2.5	20.68	0.36	124.4	2.5	15.34	0.32	0.379	0.057	25.43	0.55	11.67	0.29
Tarn07ap_42	159.9	2.9	4389	90	651	19	LOD	LOD	86.1	7.6	511	29	114.5	5.4	765	34	334	12	84.7	2.2	376.3	9.1	49.1	1	223.2	4.7	28.82	0.75	52.6	1.5	5.14	0.2	22	1	2.15	0.12	0.066	0.022	11.09	0.44	0.245	0.028
Tarn07ap_43	389.4	9.1	399	12	395	14	4080	410	3.03	0.23	11.34	0.46	2.13	0.16	14.94	0.93	10.05	0.58	3.76	0.22	24.94	0.88	5.61	0.25	49.5	1.8	13.45	0.43	43.2	1.6	6.01	0.25	38.1	2	5.62	0.38	0.487	0.078	66	7.7	54	5.6
Tarn07ap_44	694	11	790	15	784	15	1.96	0.27	17.87	0.47	63.2	1.2	12.19	0.34	86.9	2	51.2	1	17.32	0.42	115.8	2.6	21.56	0.42	152.4	2.7	30.08	0.5	85.3	1.4	12.73	0.28	88.6	1.7	13.07	0.31	0.73	0.12	3.67	0.35	2.44	0.2
Tarn07ap_45	344.8	6.8	642	12	615	12	0.185	0.045	6.88	0.25	22.42	0.57	4.18	0.16	28.8	1.1	16.14	0.54	4.6	0.17	44.45	0.88	10.58	0.21	96.1	1.8	23.24	0.3	63.9	1.2	7.25	0.16	34.34	0.78	3.615	0.086	2.64	0.34	0.24	0.035	0.303	0.014
Tarn07ap_46	1378	25	281.1	7.9	1394	39	1.89	0.15	675	18	1719	50	304.4	8.3	1498	39	415	13	10.66	0.41	369	11	52.6	1.5	305.3	7.8	55.6	1.2	143.4	3	19.47	0.47	116.6	2.7	14.45	0.41	0.123	0.031	29.3	1.4	19.87	0.69
Tarn07ap_47	476	11	292.6	6.9	1079	29	0.322	0.065	154.9	4.4	510	15	81.7	2.2	446	12	142	4.3	4.16	0.15	177.1	4.6	27.41	0.69	188.3	4.4	43	0.81	145.5	2.9	25.01	0.51	189.7	4.3	27.46	0.76	0.371	0.056	5.04	0.14	5.33	0.14
Tarn07ap_48	280.7	5	708	16	1063	29	0.019	0.011	10.82	0.37	37.37	0.92	6.79	0.25	43.1	1.5	26.51	0.72	10.75	0.32	86.6	2.3	22.94	0.49	204.1	3.2	45.76	0.63	122.7	2	15.11	0.31	78.6	1.9	9.11	0.24	0.18	0.035	0.042	0.007	2.254	0.055
Tarn07ap_49	1277	24	161.1	5.7	1841	70	0.341	0.048	494	19	1406	55	265	9.8	1379	51	411	15	8.45	0.33	378	12	58.2	1.9	359.2	9.9	67.7	1.7	190.9	4.8	28.36	0.73	185.2	5.1	24.66	0.83	0.356	0.055	22.32	0.75	31.8	1.2
Tarn07ap_50	580	12	502	11	1428	59	0.662	0.065	155	10	500	32	80	4.9	457	28	166.8	9.5	4.68	0.21	242	12	40.5	1.9	279	11	59.5	2.2	177.5	5.6	26.82	0.8	198.7	5.4	32.17	0.97	0.206	0.042	5.16	0.25	9.45	0.45
Tarn07ap_51	982	19	129.9	4	1713	51	4.82	0.28	464	13	1393	39	270.3	7.3	1427	36	424	10	6.18	0.19	388.9	8.6	57.1	1.2	352	6.6	64.8	1	175.6	3.1	25.07	0.61	156.5	3.3	20.57	0.52	0.22	0.041	27.38	0.57	16.09	0.37
Tarn07ap_52	1562	38	587	28	446	24	0.027	0.014	26.5	1.6	75.3	4.6	11.56	0.67	63.8	3.3	33	1.5	16.63	0.82	70.3	2.4	13	0.38	89.8	2	17.41	0.36	46.32	0.88	6.29	0.17	39.6	1.3	5.21	0.21	0.213	0.045	0.726	0.047	3.11	0.2
Tarn07ap_53	1688	37	80.3	2.8	1828	65	0.065	0.02	127.3	5	444	16	74.9	2.5	417	13	205	6.4	3.82	0.18	289.9	8.2	58.1	1.5	394.3	9.3	71.3	1.4	187.5	4.7	25.49	0.66	155.6	4.3	19.22	0.55	0.786	0.089	2.237	0.091	23.87	0.79
Tarn07ap_54	559	14	2270	120	643	29	LOD	LOD	37	2	122.6	7	28.4	1.6	207	12	87.7	4.5	24.4	1.2	136	5.4	19.7	0.63	120.5	3.1	23.72	0.45	67.3	1.5	10	0.28	72.6	2.1	10.39	0.35	0.082	0.026	0.173	0.017	0.074	0.006
Tarn07ap_55	807	17	1839	50	494	16	0.065	0.022	24.02	0.95	56	1.9	8.53	0.31	51.2	1.9	30.6	1	5.44	0.18	70.2	1.9	10.52	0.24	69.7	1.7	16.78	0.33	53.5	1.1	8.72	0.21	61.3	1.6	8.66	0.25	3.45	0.23	0.892	0.057	0.297	0.016
Tarn07ap_56	1198	27	283.5	8.9	950	32	0.381	0.065	442	15	1119	29	184.8	6.3	912	27	253	7.8	5.57	0.24	238.6	6.4	34.85	0.8	196.2	3.1	31.78	0.56	74.5	1.2	9.57	0.24	59.3	1.4	7.6	0.26	0.188	0.045	12.58	0.52	50.4	1.7
Tarn07ap_57	603.2	9.9	1418	27	965	21	0.266	0.057	17.69	0.56	57.9	1.5	11.05	0.37	79.5	2.4	43.6	1.5	14.2	0.43	109.3	2.6	23.68	0.46	188	3.1	38.03	0.7	93	2	10.82	0.34	58.1	1.9	6.63	0.22	0.144	0.038	2.99	0.11	0.462	0.019
Tarn07ap_58	1197	27	403.3	9.5	1223	33	6.27	0.29	673	19	1721	49	300.1	8	1509	40	405	9.9	15.82	0.47	350.9	8.1	48.8	1.1	280.5	4.8	49.29	0.71	122.5	1.7	15.45	0.3	87.1	2	10.32	0.22	0.28	0.066	30.01	0.83	10.03	0.26
Tarn07ap_59	1037	19	1041	29	546	17	0.32	0.15	524	16	1208	36	196.1	5.5	952	25	223.7	5.9	10.11	0.28	193.1	4.2	23.41	0.46	127.8	1.8	21.88	0.35	50.54	0.87	5.63	0.13	28.71	0.84	3.47	0.11	0.517	0.068	5.1	0.16	7.34	0.25
Tarn07ap_60	392.8	6.8	268.3	6.6	67.1	1.8	LOD	LOD	0.518	0.077	1.72	0.16	0.285	0.048	1.79	0.27	0.96	0.15	0.306	0.046	2.26	0.21	0.569	0.048	6.29	0.3	2.152	0.077	9.49	0.29	1.928	0.08	14.94	0.56	2.705	0.084	1.68	0.13	0.037	0.008	0.014	0.003
Tarn07ap_61	1371	40	170	9.5	2730	130	2.04	0.16	556	30	1679	84	335	16	1865	84	622	27	8.54	0.41	573	21	84.7	2.4	526	12	97.2	2.4	277.5	7	42.7	1.2	294	10	39.5	1.5	0.184	0.04	66.3	2.8	40.3	1.9
Tarn07ap_62	554	8.9	2011	41	893	20	0.013	0.009	46.1	1.2	190.6	4.6	36.82	0.91	239.6	5.9	126.2	2.5	39.93	0.93	215.4	4.2	35.88	0.68	213.4	3.7	35.66	0.55	88.6	1.5	11.93	0.24	77.3	1.7	11.19	0.27	0.151	0.034	0.388	0.021	0.446	0.02

Supporting Information Tables S3.5: Apatite trace-element data (continued)

	55Mn	±	86Sr	±	89Y	±	90Zr	±	139La	±	140Ce	±	141Pr	±	146Nd	±	147Sm	±	153Eu	±	157Gd	±	159Tb	±	163Dy	±	165Ho	±	166Er	±	169Tm	±	172Yb	±	175Lu	±	182W	±	232Th	±	238U	±
Tarn07ap_63	539.2	7.5	445.7	9.5	484.9	9.8	LOD	LOD	1.92	0.11	6.78	0.21	1.25	0.084	8.47	0.54	4.66	0.31	1.407	0.076	10.05	0.41	2.499	0.08	30.51	0.66	12.98	0.25	72	1.1	14.96	0.34	107.6	2	13.31	0.27	0.08	0.025	0.008	0.003	0.153	0.008
Tarn07ap_64	589	13	781	22	1084	32	1.45	0.8	4.63	0.28	16.1	0.64	2.96	0.22	19.61	0.94	10.54	0.61	3.25	0.16	30.3	1.2	8.59	0.23	105.2	1.7	35.73	0.53	129.9	2.5	18.87	0.49	110.6	3.2	13.44	0.34	0.182	0.054	0.113	0.016	0.186	0.014
Tarn07ap_65	401.6	8.1	1347	35	1048	26	LOD	LOD	23.99	0.6	225.6	4.9	66.6	1.7	526	14	322.3	7.7	108.1	2.6	456.5	9.5	62.6	1.1	306.8	4	44.84	0.61	93.1	1.8	9.85	0.21	45.4	1.2	4.5	0.13	0.046	0.021	0.784	0.037	0.226	0.011
Tarn07ap_66	1142	23	307.4	9.4	1503	45	1.87	0.52	115.8	3	418	10	71.5	2	399	11	197.4	5	6.06	0.2	326	6.7	59.3	1.2	362.6	6.4	60.94	0.86	134.2	2.2	14.26	0.32	65.7	1.2	6.79	0.19	0.302	0.054	12.2	0.32	14.04	0.4
Tarn07ap_67	249.3	3.7	2005	28	1059	20	0.015	0.01	2.44	0.16	11.39	0.32	2.66	0.12	26.96	0.88	25.15	0.67	4.79	0.16	81.1	1.5	17.64	0.32	151.2	2.3	37.47	0.56	120.8	1.7	18.32	0.32	110.7	1.8	12.95	0.26	0.054	0.023	0.015	0.005	0.36	0.017
Tarn07ap_68	422.9	7.4	1653	30	1091	42	0.258	0.042	53.4	1.7	206.3	5.8	41.8	1.1	298.5	7.9	170.2	4.6	50.9	1.5	321.6	9.2	52	1.8	307	12	49.6	2.2	113.4	5.9	13.23	0.75	71.2	4.5	7.98	0.54	0.538	0.074	0.169	0.018	1.451	0.09
Tarn07ap_69	648	13	1008	22	541	15	1.01	0.37	20.66	0.78	79.8	1.9	17.64	0.55	147.3	4.2	88.9	2.2	28.64	0.69	178.1	3.6	25.13	0.44	136.8	2.1	22.22	0.39	54.43	0.89	7.45	0.2	51	1.3	7.74	0.24	0.43	0.19	0.405	0.035	0.237	0.017
Tarn07ap_70	1788	36	881	28	1090	29	0.168	0.039	161.8	4.5	785	20	168.9	4.9	1006	29	248.1	6.4	28.35	0.72	208.3	4.7	28.73	0.6	184.7	3.3	39.11	0.61	125.3	2.5	20.18	0.42	138.1	3.1	19.35	0.45	0.515	0.061	2.813	0.084	16.4	0.43
Tarn07ap_71	378.6	7.5	824	18	631	19	0.059	0.023	5.07	0.21	19.05	0.63	4.24	0.19	33.6	1.2	27.48	0.79	8.45	0.27	94.5	1.8	20.32	0.4	143.1	3.6	25.59	0.72	60.1	1.7	6.96	0.25	37.1	1.6	4.42	0.2	0.582	0.08	0.256	0.018	0.15	0.01
Tarn07ap_72	693	10	275.1	6.2	1673	40	0.635	0.059	405	10	1124	28	204	5	1094	27	359.7	7.7	5.45	0.18	421.9	7	62.8	1	392.4	5.4	75.89	0.93	193	2.7	23.35	0.35	129.5	2.3	16.36	0.36	0.648	0.072	10.04	0.22	12.28	0.26
Tarn07ap_73	288.8	5.1	246.2	5.6	125.6	6.4	LOD	LOD	1.009	0.082	3.3	0.15	0.569	0.054	3.62	0.34	2.48	0.38	0.95	0.16	6.3	1.1	1.36	0.16	12.46	0.98	3.81	0.21	15.4	0.65	2.8	0.12	19.25	0.76	2.637	0.095	2.06	0.19	0.033	0.009	0.063	0.01
Tarn07ap_74	475.5	7	841	16	278	11	LOD	LOD	7.29	0.45	45.1	2.2	16.56	0.67	211.1	7.4	317.5	8.6	93	2.6	421	13	36.5	1	124.9	4	13.71	0.44	22.56	0.85	2.07	0.1	10.42	0.6	1.177	0.053	0.051	0.019	0.73	0.12	0.197	0.03
Tarn07ap_75	671.2	7.7	1633	21	1161	28	0.032	0.014	9.96	0.35	25.42	0.53	4.63	0.17	27.36	0.95	13.43	0.52	5.42	0.18	34.06	0.85	9.43	0.17	115.8	1.9	41.11	0.6	166.1	2.5	26.1	0.46	144.4	2.4	15.31	0.29	0.196	0.044	0.368	0.025	0.616	0.022
Tarn07ap_76	466.6	5.6	599.2	8.4	1220	24	0.45	0.3	2.56	0.13	9.55	0.3	1.93	0.11	12.02	0.7	7.08	0.36	2.34	0.11	21.44	0.56	6.68	0.13	92.9	1.3	38.75	0.55	163.9	2.2	23.87	0.34	123	2.1	12.45	0.26	0.151	0.034	0.013	0.005	0.175	0.012
Tarn07ap_77	1221	19	282.4	6.6	822	19	0.4	0.065	354.5	8.2	1040	26	154.3	3.8	752	19	194.6	4.2	5.3	0.17	167.7	3.3	23.89	0.38	142.4	2	26.29	0.38	71.1	1	10.19	0.23	66.1	1.3	8.79	0.24	0.14	0.039	2.81	0.15	6.88	0.57
Tarn07ap_78	166.6	2.9	865	16	447.1	8.4	0.111	0.036	26.03	0.62	108.7	2.4	21.29	0.57	135.8	3.1	83.9	1.8	24.54	0.54	141.5	2.5	23.21	0.33	126.3	1.7	18.77	0.27	41.05	0.67	4.45	0.13	21.93	0.47	2.357	0.076	0.086	0.029	0.185	0.03	0.238	0.012
Tarn07ap_79	701	15	1694	37	741	17	0.31	0.13	17.18	0.63	58.9	1.5	11.59	0.33	80.6	2.3	47.9	1.3	13.87	0.29	105.4	2	19.95	0.37	145.7	1.9	28.69	0.44	77.2	1.1	10.59	0.21	66.9	1.6	8.9	0.21	0.135	0.03	1.98	0.22	1.089	0.043
Tarn07ap_80	837	11	536.8	9.7	665	14	0.25	0.062	22.6	1	54.4	2	7.36	0.24	40.6	1.3	17	0.61	5.13	0.15	36.56	0.84	8.28	0.18	80.1	1.2	21.89	0.31	75.5	1.2	11.68	0.23	77.6	1.4	10.82	0.25	0.534	0.081	3.21	0.3	0.459	0.018
Tarn07ap_81	655	10	3077	48	869	17	0.47	0.15	7.14	0.3	24.99	0.57	4.98	0.2	34.2	1	20.22	0.6	5.17	0.16	49.1	1.2	10.92	0.23	97.2	1.9	26.59	0.52	94.7	1.7	14.69	0.34	97.2	1.9	14.11	0.33	0.07	0.023	0.192	0.014	1.661	0.048
Tarn07ap_82	1151	22	304.7	8.6	1176	33	1.35	0.11	551	16	1445	43	262.8	6.8	1373	36	378	8.9	9.17	0.27	319	6.3	43.48	0.78	251.6	3.8	44.46	0.72	116.2	2	15.88	0.31	94.9	2.3	12.04	0.3	0.095	0.026	29.86	0.76	21.87	0.56
Tarn07ap_83	1125	22	1041	30	354	11	6.1	0.3	2234	72	3247	91	310.5	9.4	976	27	120.1	3.3	24.94	0.66	88.5	2	10.37	0.28	59.5	1.2	11.48	0.21	31.22	0.65	4.24	0.13	25.88	0.75	3.85	0.13	0.102	0.029	93.5	2.3	13.76	0.39
Tarn07ap_84	659	11	1374	41	406	11	LOD	LOD	3.73	0.2	13	0.43	2.48	0.11	16.25	0.77	10.18	0.48	2.79	0.11	23.9	0.81	5.53	0.15	51.14	0.94	13.4	0.22	46.23	0.71	7.93	0.17	55.9	1.1	7.36	0.21	0.468	0.066	0.019	0.006	0.188	0.01
Tarn07ap_85	303.1	6	99.2	2.9	383	11	0.117	0.03	2.88	0.14	12.89	0.44	2.97	0.15	21.82	0.92	13.31	0.55	3.4	0.14	31.49	0.93	6.64	0.17	53.1	1.2	12.61	0.28	38.57	0.94	5.7	0.15	36.6	1.1	5.83	0.17	16.76	0.57	0.687	0.031	25.78	0.69
Tarn07ap_86	1150	28	382	14	1148	37	1.46	0.12	885	30	2265	82	386	14	1972	68	510	17	11.06	0.43	418	12	51	1.2	276	4.7	47.5	0.8	113.6	1.7	13.11	0.28	67.9	1.8	7.97	0.26	0.325	0.048	56	1.4	38.2	1.1
Tarn07ap_87	467.4	6.9	443.1	7.4	311.2	6.7	0.283	0.067	3.42	0.18	10.76	0.31	1.95	0.12	12.67	0.55	6.15	0.34	2.107	0.096	12.35	0.46	2.635	0.078	26.65	0.65	9.15	0.2	39.38	0.76	7.22	0.15	50.3	1	7.01	0.13	0.372	0.066	1	0.1	0.143	0.01
Tarn07ap_88	186.6	3.9	479	14	161	18	0.98	0.45	4.04	0.71	14.4	2.6	2.6	0.46	15.1	2.8	7.4	1.4	1.38	0.21	12.7	1.9	2.6	0.39	23.1	3.2	5.46	0.67	16.9	1.8	2.26	0.21	12.3	1.2	1.41	0.12	1.3	0.15	13.3	2.8	1.58	0.29
Tarn07ap_89	531.4	7.8	1904	34	1044	25	0.009	0.008	4.5	0.2	17.09	0.49	3.63	0.15	27.3	1.1	18.48	0.57	5.77	0.2	57.6	1.3	14.75	0.33	151.9	2.6	41.23	0.74	119.7	1.9	15.35	0.32	82.5	1.7	9.25	0.21	0.079	0.024	0.067	0.009	0.167	0.009
Tarn07ap_90	463	14	375.3	9.9	378.3	8.9	0.27	0.13	10.18	0.37	32.99	0.99	5.7	0.28	33.9	1.8	16.85	0.74	4.43	0.2	34.1	1.2	7.57	0.22	64.7	1.6	13.61	0.35	32.82	0.99	3.51	0.14	14.97	0.65	1.251	0.066	0.321	0.056	0.174	0.027	0.353	0.023
Tarn07ap_91	344.8	6	524	10	942	18	0.007	0.007	9.82	0.31	36.7	1	7.31	0.22	52.3	1.7	29.8	1	9.14	0.28	73.5	1.7	15.35	0.38	128.7	2.2	32.61	0.51	114.1	1.9	16.87	0.34	93.9	1.7	9.65	0.21	0.287	0.047	0.163	0.013	0.181	0.011
Tarn07ap_92	1797	34	902	23	668	16	0.314	0.071	33.6	1.2	127.3	3.9	24.19	0.85	158.9	4.8	93.1	2.7	20.65	0.63	177.9	4.1	30.46	0.73	178.7	3.8	28.33	0.58	62.4	1.2	7.27	0.19	38.3	0.81	4.64	0.17	0.238	0.048	0.755	0.045	1.148	0.038
Tarn07ap_93	1685	35	169.9	5.4	2589	85	4.9	0.5	581	19	1567	57	285	10	1456	61	437	15	7.61	0.32	415	11	68.5	1.4	457.8	7.1	90.7	1.3	269.9	4.4	43.53	0.95	306.1	8.7	40.9	1.3	0.178	0.042	27.65	0.84	10.68	0.35
Tarn07ap_94	1131	21	1125	26	726	54	0.065	0.021	16.45	0.95	58.5	1.5	22.21	0.62	260.2	6.4	330.2	8.9	60.5	2.3	400	16	48	2.4	225	15	32.1	2.6	69.5	6.8	7.96	0.85	41.8	5.1	4.82	0.64	0.279	0.05	1.31	0.27	0.84	0.11
Tarn07ap_95	465.2	9.2	3738	81	659	14	LOD	LOD	4.89	0.25	70	1.9	28.16	0.71	266.3	6.6	226.6	5.9	71.8	1.8	331.8	6.6	43.8	1	207.7	3.9	28.36	0.54	56.2	1.2	5.64	0.15	25.79	0.74	2.533	0.098	0.047	0.02	1.476	0.05	0.101	0.008
Tarn07ap_96	974	16	367.9	7.1	969	24	0.276	0.044	540	11	1367	30	239.8	5.6	1198	30	304.1	7.6	12.53	0.38	266.5	6.5	36.23	0.73	205.6	3.9	36.57	0.61	92.5	1.5	11.83	0.26	66.7	1.4	8.26	0.22	0.08	0.024	19.81	0.64	31.16	0.8
Tarn07ap_97	1452	25	270.2	6.3	1342	36	0.369	0.051	720	18	1856	50	330.7	7.9	1683	42	440	11	10.53	0.27	373.6	7.5	50.65	0.91	293.9	4.8	52.98	0.7	138.6	1.9	19.51	0.29	121.8	2.4	15.89	0.38	0.214	0.041	34.97	0.72	34.49	0.76
Tarn07ap_98	981	15	781	15	811	16	15.2	1.2	906	20	2127	44	338.2	6.9	1589	37	332.6	7.3	21.82	0.65	249.7	5.3	30.25	0.57	164	3.1	28.04	0.62	68.5	1.3	8.5	0.21	46.6	1.2	5.57	0.15	1.98	0.26	49	1.3	27.1	1.1
Tarn07ap_99	1072	21	553	11	1129	22	1.68	0.3	101.4	2.6	320.9	8.4	52.8	1.4	287.7	7.6	105.2	2.6	12.47	0.31	152.2	3.5	28.53	0.54	213.1	3.6	43.22	0.75	110.3	1.8	14.26	0.36	81.2	1.6	9.97	0.2	0.486	0.079	1.289	0.058	2.636	0.08
Tarn07ap_100	1314	21	223.9	7.1	1542	50	0.91	0.12	573	17	1498	43	266	7.5	1358	37	388	11	7.42	0.25	348.7	9.2	52	1.1	313.6	6.3	58.5	1.2	159.5	3.4	22.73	0.61	143.4	3.4	18.49	0.6	0.312	0.058	15.53	0.4	21.95	0.63
Tarn07ap_101	1002	19	225	6.8	1703	55	4.41	0.41	497	15	1414	47	277.9	8.5	1530	50	471	13	8.78	0.34	425	10	60.1	1.5	351.3	7.6	65.9	1.5	176.8	4	25.05	0.63	155.4	4.1	20.18	0.58	0.284	0.055	41.3	1.1	28.52	0.9
Tarn07ap_102	788	15	410	16	952	26	1.27	0.37	695	16	1914	49	313.7	7.9	1433	32	288.7	6.7	28.46	0.62	240.7	5.5	29.58	0.6	169.8	3.4	32.27	0.62	88.7	1.9	12.43	0.32	79.9	1.9	12.29	0.33	0.141	0.034	42.2	1.1	50.4	1.1
Tarn07ap_103	4515	80	188.6	4.8	353.1	8.4	0.105	0.028	231.8	5.5	512	11	58.9	1.6	216.2	6.7	54.6	1.5	8.04	0.24	47.7	1.2	9.18	0.23	59.2	1.3	10.04	0.22	28.63	0.68	4.89	0.12	37.6	1.1	4.95	0.15	0.131	0.031	9.57	0.26	41.71	0.91
Tarn07ap_104	622	13	1507	38	664	20	4.2	1.3	40.7	1.7	149.5	6.2	26.9	1.1	159.8	7	62.8	2.7	3.28	0.15	94.8	3.5	15.73	0.45	110.1	3.2	23.92	0.61	70.3	1.7	10.15	0.27	63.7	1.7	8.2	0.24	0.412	0.065	2.78	0.21	3.08	0.13
Tarn07ap_105	2051	41	1731	41	703	16	0.059	0.021	25.4	0.73	67.2	1.8	11.02	0.4	70.4	2.5	38.9	1.2	11.91	0.33	102.8	2.5	20.17	0.48	141.7	3.5	27.24	0.58	71.6	1.7	10.26	0.3	69.5	2	9.51	0.29	0.067	0.023	0.906	0.05	1.872	0.047
Tarn07ap_106	608	11	750	14	910	23	LOD	LOD	17.03	0.49	58.9	1.5	11.24	0.29	81.8	2.6	45.7	1.3	13.6	0.41	116.4	2.7	22.75	0.53	177.3	3	36.51	0.71	82.7	1.4	8.22	0.18	36.08	0.84	3.7	0.11	0.165	0.034	0.268	0.016	0.377	0.016
Tarn07ap_107	1131	23	259.5	9.2	1355	50	6.39	0.33	543	19	1466	51	272	10	1450	55	406	14	8.8	0.33	362	10	49.2	1.2	286	8.4	52.6	1.3	135.7	3.5	18.54	0.53	111.1	2.8	14.15	0.43	4.63	0.36	32.01	0.91	16.21	0.48
Tarn08ap_0	454.6	8.9	4526	62	868	18	1E-05	2E-07	40.3	2.4	213.9	7.9	47.9	1.8	350	10	194.9	5	59.6	1.3	156.5	3.3	51.2	1	272	5.2	39	0.72	109.5	2.1	8.54	0.22	42.8	1	4.34	0.2			0.222	0.032	0.311	0.019
Tarn08ap_1	727	15	298	12	1381	30	1.61	0.72	314	11	1008	26	161.8	3.6	881	24	266	7.1	4.65	0.37	230.3	5.4	51	1.2	279.6	7.6	52.9	1.4	197.7	4.2	16.41	0.44	93.2	2.8	11.57	0.43			7.64	0.33	7.82	0.18
Tarn08ap_2	617	14	779	15	1597	32	1E-05	2E-07	23	1.5	85.7	3.4	16.7	0.92	115.1	6.1	69.6	3	22.85	0.68	80.8	2.3	37.12	0.82	311.1	6.4	65.2	1.4	232.6	4.7	21.96	0.55	122.3	2.5	13.6	0.39			0.155	0.032	0.895	0.038
Tarn08ap_3	593	15	1582	30	843	15	1E-05	2E-07	26.6	2.2	116.3	3.7	26.5	1.3	205	10	125.9	4.8	42.3	1	111.5	3.1	38.13	0.87	221.9	4.8	36.03	0.84	107.2	3.1	8.8	0.31	46.6	1.3	5.19	0.26			0.151	0.034	0.362	0.029
Tarn08ap_4	524	12	3609	57	462	14	1E-05	1E-07	9.2	1.2	40.2	2.4	8.57	0.72	65.8	5.1	37	1.8	8.76	0.37	36.7	1.4	11.52	0.41	74	2	15.85	0.59	57.2	1.3	4.68	0.21	24.1	1	3.41	0.24			0.397	0.051	0.681	0.032
Tarn08ap_5	1028	24	1359	35	750	18	1E-05	2E-07	31.3	2.2	148.3	5.3	31.8	1.7	237	11	134.3	3.8	38.7	1.2	110.5	3.3	38.4	1.2	224.4	5.5	33.39	0.92	104.2	3.3	8.32	0.37	45.8	1.9	5.03	0.27			0.534	0.062	0.448	0.028
Tarn08ap_6	1278	42	312	16	681	20	19.3	3.9	302	17	875	41	142.2	7.7	743	26	183	8.4	6.62	0.54	151.7	6.5	28.6	1.4	127.1	5.3	23.1	1.1	92.8	4.3	8.27	0.41	50.8	2.7	6.2	0.48			9.55	0.85	33.09	0.91
Tarn08ap_7	2584	45	274.6	8.8	308.1	7.4	0.38	0.25	7.06	0.89	22.8	1.6	3.81	0.47	26.9	3.1	15.7	1.3	7.39	0.37	17	1.1	7.26	0.34	52.7	1.8	10.83	0.31	43.7	1.5	5	0.2	34.5	1.2	4.97	0.24			0.247	0.035	0.756	0.039
Tarn08ap_8	1351	19	478	9.8	899	16	1.31	0.38	535	13	1643	33	253.7	5.9	1271	24	321	6.1	12.48	0.45	272.8	4.6	45.77	0.89	189.8	3.7	32.51	0.55	128.5	2.4	9.78	0.23	54.5	1.4	6.42	0.26			23.18	0.5	17.58	0.22
Tarn08ap_9	465	12	1019	20	89.7	3.6	0.28	0.2	0.76	0.26	2.78	0.48	0.68	0.14	3.3	0.85	1.41	0.31	0.497	0.098	1.9	0.27	0.877	0.094	8.82	0.53	2.64	0.17	14.68	0.9	2.08	0.12	18.39	0.74	2.95	0.15			0.031	0.01	0.01	0.004
Tarn08ap_10	1766	28	248.7	7	1461	32	3.41	0.67	602	14	1748	37	266.1	6.2	1306	32	333.9	7.7	9.72	0.34	294.6	5.2	55.9	1.1	269.8	5.5	48.92	0.95	194.7	3.9	18.58	0.47	116.5	2.7	14.8	0.39			29.69	0.65	16.15	0.32
Tarn08ap_11	358.4	9.6	731	13	1040	20	1E-05	2E-07	35	1.8	141.2	4.6	27.8	1.1	193.5	6.6	120.1	2.8	39.5	1.1	126.7	3.2	45.71	0.99	268.5	4.4	44.76	0.85	134.6	2.6	11.68	0.31	61.9	1.9	6.61	0.24			0.071	0.018	1.306	0.046
Tarn08ap_12	763	17	827	16	1018	20	9E-06	2E-07	40.7	2.3	152.8	4.5	29.9	1.1	196.2	7.5	101.5	3.2	33.02	0.79	102.7	2.6	38.12	0.77	236.7	4.2	41.57	0.77	129.8	2.5	11.41	0.35	58.5	1.4	6.46	0.24			0.057	0.016	0.854	0.038
Tarn08ap_13	537	13	6300	110	1043	21	1E-05	1E-07	38.8	2.3	172	5.4	40.1	1.5	301.5	8.6	173	4.5	56.3	1.3	163.3	3.7	53.7	1.2	287.9	5.5	45.1	1	119.3	2.3	8.96	0.26	43.3	1.2	4.3	0.18			0.122	0.026	0.128	0.011
Tarn08ap_14	1673	29	389.3	8.9	1285	25	3.36	0.61	724	15	2144	41	315.4	6.7	1534	31	352.9	7.6	14.9	0.5	312.1	6.8	53.3	1	234.4	4.3	41.89	0.77	158	2.5	15.07	0.41	93.2	2	11.83	0.32			31.85	0.58	12.77	0.2
Tarn08ap_15	912	16	1072	19	1387	33	9E-06	1E-07	29.3	1.6	117	3.3	23.4	1.1	162.2	5.7	101.9	3.3	35.38	0.88	125.8	2.7	54.7	1.3	352.2	6.8	59.3	1.4	168.7	3.7	16.91	0.5	90.6	2.4	10.35	0.39			0.585	0.061	1.584	0.053
Tarn08ap_16	3450	55	571	14	121.5	4.6	9E-06	1E-07	46.5	2.5	158.7	5.3	27.9	1.5	162.5	6.8	73.7	3	22.35	0.62	56.3	1.9	12.17	0.45	40.7	1.5	4.67	0.23	10.19	0.52	0.477	0.056	2.81	0.26	0.329	0.053			0.21	0.035	3.13	0.12
Tarn08ap_17	830	17	607	14	3441	73	1.65	0.66	491	13	1574	36	246	6.1	1272	30	429	9.8	8.21	0.42	391.2	7.7	108.7	2	662	14	125.5	2.2	371.4	7.2	36.9	1	192.5	5.1	21.55	0.63			7.19	0.25	12.66	0.27
Tarn08ap_18	118.8	7.3	393.8	8.8	2557	49	0.74	0.32	214.8	6.8	776	16	128.1	3.9	697	18	277.8	6.5	9.44	0.39	259.4	5.5	78.2	1.7	513.3	9.9	99.6	1.9	219.5	4.8	28.54	0.72	141.4	3.1	17.2	0.54			21.32	0.71	13.7	0.37
Tarn08ap_19	379.1	9.9	1492	25	368.3	9.3	5E-06	1E-07	3.9	0.66	12.8	1	2.65	0.32	15.7	1.4	9.94	0.93	2.33	0.17	12.25	0.74	5.44	0.23	47.5	1.4	12.59	0.39	33.6	0.96	5.45	0.23	32.2	1.2	5.19	0.2			0.303	0.039	1.095	0.043
Tarn08ap_20	327.7	8.2	2439	37	1755	38	5E-06	8E-08	22.1	1.5	88.7	3.4	19.3	0.84	150.1	6	108.2	3.6	31.29	0.8	118.9	3.4	47.7	1.1	338.2	5.8	60.5	1.2	119.4	2.7	14.86	0.41	68.7	1.7	7.65	0.26			0.728	0.063	0.224	0.017
Tarn08ap_21	313.6	8.3	494	10	290	7.5	4E-06	6E-08	3.64	0.58	12.7	1.1	2.07	0.27	14	1.4	7.86	0.86	2.65	0.22	9.7	0.7	4.23	0.21	37.6	1.2	9.75	0.33	24.04	0.72	3.24	0.15	11.57	0.65	1.011	0.089			0.114	0.022	0.088	0.009
Tarn08ap_22	1279	26	398	11	1027	24	1.7	0.54	553	11	1704	32	266.6	6	1325	35	359.1	8.2	11.49	0.49	289	5.4	48.5	1.1	219.4	4.3	38.62	0.93	91.8	2	11.48	0.37	65.6	1.8	7.63	0.22			30.7	0.8	15.3	0.29
Tarn08ap_23	466	13	1265	23	656	16	1.87	0.57	12.6	1.3	35.8	2	7.4	0.6	49.6	2.8	28.5	1.4	8.17	0.41	30.2	1.3	9.99	0.39	76.1	2.2	20.02	0.53	72	1.8	16.96	0.45	146.6	2.8	23.44	0.55			7.51	0.29	2.489	0.096
Tarn08ap_24	362	11	1118	23	743	23	0.64	0.38	41.4	2.6	169.1	6.5	41.6	1.8	322	12	181.4	6.1	53.9	1.5	154.6	4.9	45.3	1.2	238.2	7.1	35.18	0.96	60.2	1.4	6.76	0.29	33.2	1.4	3.22	0.19			0.128	0.031	0.064	0.012
Tarn08ap_25	1500	26	2043	34	715	16	3E-06	6E-08	3.89	0.56	15.4	1.2	3.2	0.32	21.6	2	14.58	0.99	4.84	0.3	19.41	0.91	9.59	0.32	94.5	2.1	24.73	0.63	71.3	1.5	13.96	0.36	107.3	2.5	17.36	0.38			0.176	0.031	0.248	0.016
Tarn08ap_26	1270	26	379	10	647	17	3E-06	5E-08	23.5	1.7	71.2	3.3	11.24	0.71	60.8	3.5	34	1.9	6.8	0.33	37	1.6	13.09	0.42	106.2	2.7	23.32	0.6	62.3	1.7	10.27	0.33	59.2	1.7	7.17	0.26			0.213	0.036	0.76	0.035
Tarn08ap_27	933	17	322.5	7.8	583	13	0.14	0.13	15.6	1.5	42.6	2	6.22	0.54	24.1	2	10.78	0.79	4.24	0.25	11.88	0.72	4.87	0.22	48.2	1.4	16.73	0.46	70.2	1.7	14.69	0.38	86	2	10.19	0.35			0.313	0.044	0.916	0.044
Tarn08ap_28	385	12	220.2	7.3	287.4	8.3	2E-06	3E-08	10.54	0.96	31.6	1.8	6.52	0.48	37.4	3.1	19.4	1.4	4.98	0.32	21.7	1.2	7.39	0.31	52.9	1.6	10.05	0.31	19.97	0.79	2.18	0.13	7.51	0.46	0.845	0.085			0.221	0.047	2.967	0.079
Tarn08ap_29	778	16	1704	25	718	16	2E-06	4E-08	80.8	3.4	307.1	8.5	57.3	1.7	376	11	178	4.5	50.6	1.1	162	3.7	43.04	0.83	225.6	4	33.35	0.67	61.5	1.6	6.49	0.24	31.7	1	3.15	0.16			0.681	0.059	0.393	0.021
Tarn08ap_30	580	13	2348	40	967	23	2E-06	2E-08	68	3.6	272.4	8	53.2	2	313	10	171.6	4.5	55.2	1.3	151.5	3.7	47.4	1	272	6.6	42.2	1	84.7	1.9	10.01	0.3	52.4	1.5	5.84	0.28			0.555	0.061	0.543	0.031
Tarn08ap_31	777	23	636	14	772	18	1.8	1.3	4.52	0.74	18	1.3	3.58	0.39	23.6	2.8	13.4	1.1	4.43	0.26	20.2	1	8.02	0.26	90.9	2.1	26.28	0.63	78.5	2	10.95	0.35	55.9	1.2	6.36	0.27			0.436	0.056	0.185	0.032
Tarn08ap_32	1944	36	488	15	1803	46	1.75	0.62	643	15	1965	54	299.3	8.3	1359	37	374.3	7.9	14.81	0.75	322.5	7.3	58.3	1.5	300.9	6.1	57.8	1.2	161.6	4	25.24	0.59	172.7	3.1	23.61	0.62			26.25	0.6	12.72	0.28
Tarn08ap_33	1336	20	377.3	7.4	892	18	1E-06	1E-08	403.6	8.9	1256	26	186.9	4.4	832	18	255.8	5.6	7.79	0.33	218.7	3.7	41.85	0.9	193.8	4	32.74	0.66	81.3	1.6	9.53	0.28	51.4	1.1	6.23	0.22			3.96	0.15	33.67	0.47
Tarn08ap_34	1427	31	97.9	4.2	2102	46	0.63	0.37	241.8	7.1	942	25	176.5	4.6	968	23	364.9	8.6	3.21	0.28	260.6	5.9	64.3	1.4	368.9	8.4	70.8	1.4	196.5	3.6	31.37	0.82	204.8	4.6	27.62	0.81			9.11	0.45	13.08	0.24
Tarn08ap_35	240.3	9.1	269.4	8	361	10	LOD	LOD	12.4	1.1	45.7	2	8.95	0.5	62.9	3.8	58	2.3	7.2	0.32	45.5	1.5	13.8	0.44	78.9	1.9	15.19	0.43	42.3	1.2	6.1	0.2	41.9	1.2	5.97	0.25			0.801	0.087	1.008	0.033

Supporting Information Tables S3.5: Apatite trace-element data (continued)

	55Mn	±	86Sr	±	89Y	±	90Zr	±	139La	±	140Ce	±	141Pr	±	146Nd	±	147Sm	±	153Eu	±
Tarn08ap_36	418	14	841	18	1829	32	LOD	LOD	5.03	0.63	21.6	1.6	3.89	0.41	26.4	2.3	21.6	1.3	7.43	0.42
Tarn08ap_37	507	13	3382	50	418	11	LOD	LOD	6.74	0.89	26.2	1.4	5.07	0.41	37.3	2.4	20.8	1.3	6.25	0.33
Tarn08ap_38	380	11	492	13	162.3	6	LOD	LOD	3.04	0.65	8.08	0.83	1.68	0.25	9.4	1.3	5.44	0.69	1.94	0.18
Tarn08ap_39	1269	23	1046	18	704	16	1.19	0.41	36.1	2.1	134	4.6	21.7	1	124.7	5.6	49.2	2.1	13.13	0.52
Tarn08ap_40	3176	41	207	6.1	982	19	0.3	0.21	348.5	8.3	1205	20	191.5	4.8	870	18	252.9	6	7.99	0.35
Tarn08ap_41	927	21	1057	25	963	28	0.86	0.54	9.3	1.3	38.7	2.2	7.29	0.55	52.6	4.2	31.6	1.9	11.36	0.52
Tarn08ap_42	579	12	1980	29	690	13	LOD	LOD	32.8	2	190.8	5.8	41.9	1.5	265.8	8.8	149.4	4.7	49	1.1
Tarn08ap_43	443.9	9.9	901	18	659	15	0.37	0.22	8.73	0.83	47.4	2.1	10.5	0.68	82.1	4.1	52.2	1.7	17.49	0.62
Tarn08ap_44	688	11	1592	28	772	14	LOD	LOD	10.8	2.5	25.4	1.8	5.95	0.94	30.7	4.2	13	1.1	3.87	0.25
Tarn08ap_45	1480	20	364.2	9.5	1149	30	3.83	0.79	635	17	1986	49	306.4	7.5	1433	29	374.9	8.6	11.32	0.44
Tarn08ap_46	16050	240	136.9	4.9	1107	23	LOD	LOD	269.8	6.5	782	16	110.2	2.8	465	11	156.3	4.1	16.74	0.61
Tarn08ap_47	1590	27	449	10	1452	32	7.4	1.2	620	15	1970	46	298.6	7.3	1399	35	373.5	9.1	17.29	0.63
Tarn08ap_48	685	14	400.7	8.9	387.8	8	LOD	LOD	113	38	35.7	4	26.1	7.3	95	24	25.1	4.4	5.37	0.62
Tarn08ap_49	600	12	642	12	798	19	LOD	LOD	3.89	0.66	15.5	1.1	4.41	0.45	39.3	3	33.9	1.5	9.84	0.49
Tarn08ap_50	1207	21	500	11	861	20	1.25	0.39	648	16	2032	41	289.7	6.8	1344	29	337.9	7.9	12.45	0.47
Tarn08ap_51	458	10	1399	32	890	23	0.4	0.29	4.74	0.88	21	1.5	4.56	0.49	36.4	3.6	25.2	2.1	9.41	0.46
Tarn08ap_52	710	18	322.7	7.5	916	29	0.17	0.15	209.2	8.3	697	23	106.3	3.8	549	19	174	6.5	2.9	0.23
Tarn08ap_53	570	11	3018	49	816	20	LOD	LOD	48.6	2.6	366	13	92.8	3.6	621	16	299.8	7.5	88.4	1.9
Tarn08ap_54	246.7	8.4	1326	24	476	14	LOD	LOD	2.76	0.56	10.61	0.99	1.9	0.27	12.4	1.6	7.02	0.9	2.27	0.21
Tarn08ap_55	1154	42	440	13	538	17	LOD	LOD	396	12	1205	34	178.6	5	833	23	203.9	6.9	7.4	0.4
Tarn08ap_56	1035	26	2332	57	333	12	LOD	LOD	3.37	0.68	9.7	1.3	2.07	0.38	10.9	1.9	5.74	0.92	2.11	0.27
Tarn08ap_57	942	19	551	13	1756	50	3.3	1.1	215.5	8.3	742	23	120.3	3.9	625	18	231.7	7	5.59	0.37
Tarn08ap_58	450	11	2281	38	158.7	6.1	LOD	LOD	1.88	0.48	6.88	0.72	1.4	0.22	9.1	1.5	5.1	0.72	1.68	0.18
Tarn08ap_59	798	13	1081	19	516	11	LOD	LOD	14	1.2	80.6	3	22.4	1.2	159.4	6	91.8	3.2	25.52	0.76
Tarn08ap_60	312	11	442	13	61.2	3.2	LOD	LOD	0.27	0.17	1.68	0.35	0.31	0.11	2.13	0.7	1.27	0.34	0.292	0.07
Tarn08ap_61	486	14	1426	31	568	16	LOD	LOD	36.8	2.4	148.7	4.7	28.6	1.3	195.3	8.9	108.7	3.7	32.9	1.1
Tarn08ap_62	2243	30	957	15	632	14	1.44	0.43	1792	35	4226	91	527	10	2196	35	382.6	7.3	26.56	0.73
Tarn08ap_63	484	12	673	18	756	19	LOD	LOD	10.7	1.2	29.6	2.2	4.5	0.38	23.6	2	11.9	1.1	3.35	0.27
Tarn08ap_64	1299	21	167.9	5.2	623	13	LOD	LOD	1.03	0.28	7.4	0.67	2	0.24	19.9	2	20.9	1.4	1.84	0.15
Tarn08ap_65	1117	29	108	11	1844	56	0.5	0.42	224.1	9.9	794	21	149.1	5.5	847	30	308	11	3.31	0.3
Tarn08ap_66	5030	71	130.1	5.3	3234	52	0.9	0.41	350.6	8	1325	25	226.3	4.2	1171	31	481.9	9.4	4.36	0.27
Tarn08ap_67	460.1	9.9	3853	61	222.8	6.8	LOD	LOD	4.06	0.64	15.3	1	2.94	0.28	21.5	2.4	10.64	0.86	2.63	0.2
Tarn08ap_68	508.5	9.8	700	16	823	22	LOD	LOD	3.83	0.58	15.2	1	2.89	0.27	20.8	2	13.7	1.1	4.05	0.26
Tarn08ap_69	1191	16	213.1	5.5	1143	22	0.52	0.23	371.5	7.9	1188	24	187.1	3.7	943	23	274.1	5.8	6.02	0.28
Tarn08ap_70	1215	31	370	13	1101	29	0.78	0.44	509	13	1619	41	245.3	8.4	1128	30	294	10	8.74	0.48
Tarn08ap_71	328	10	1619	31	541	15	LOD	LOD	29.7	2.3	114.8	4.5	23.1	1.1	150.3	6.9	79.6	2.7	23.24	0.78
Tarn08ap_72	501	23	2514	65	219.8	8.9	LOD	LOD	3.5	0.89	11.7	1.5	2.14	0.44	13.2	2.4	9.2	1.2	2.55	0.31
Tarn08ap_73	101.1	8.8	701	16	595	16	LOD	LOD	49.9	3.2	210.9	4.8	37.9	1.9	229	10	120.9	4.1	33.7	1.1
Tarn08ap_74	1289	20	1640	40	363.2	9.6	8.5	1.7	1831	47	3344	72	316.6	7.2	1128	35	164.3	6.5	38.2	1.3
Tarn08ap_75	1217	21	337.7	8.3	1534	31	4.8	0.75	570	15	1784	42	276.7	6.5	1314	30	341.9	8.1	11.49	0.51
Tarn08ap_76	1008	21	527	15	621	21	LOD	LOD	493	15	1496	48	209.7	6.1	1018	29	248.9	9.4	9.31	0.53
Tarn08ap_77	537	12	1576	26	1073	26	LOD	LOD	15.7	1.2	70.5	2.5	14.12	0.75	104.7	4.4	74.4	2.7	27.1	0.8
Tarn08ap_78	1066	27	423	14	881	24	4.4	0.91	597	16	1688	42	246.7	7.1	1233	39	301.2	9	12.86	0.63
Tarn08ap_79	334	10	82.1	4.6	92.4	3.8	LOD	LOD	0.6	0.26	2.74	0.48	0.51	0.14	4.25	0.83	1.98	0.48	0.63	0.11
Tarn08ap_80	1042	18	234	5.1	1101	24	0.26	0.19	398.6	9.4	1244	27	193.2	4	990	21	264.1	5.6	4.33	0.27
Tarn08ap_81	638	14	640	16	484	12	LOD	LOD	5.72	0.75	20.1	1.4	3.76	0.38	24.6	2.1	12.9	1.1	3.85	0.28
Tarn08ap_82	829	13	469.9	9.7	586	12	0.35	0.21	438.9	9.2	1279	25	180.6	3.8	892	17	215.7	4.7	7.53	0.38
Tarn08ap_83	897	16	614	12	1965	37	0.51	0.26	283	11	971	29	147.8	3.9	802	23	270.2	7.5	4.96	0.3
Tarn08ap_84	1299	23	1968	31	555	28	4.8	1.1	38.6	6.2	250	31	58.6	6.4	413	34	198	10	53.8	2.1
Tarn08ap_85	1397	20	227.5	5.2	2107	37	1.17	0.45	701	16	2253	42	335.9	7.2	1674	29	459	10	9.97	0.41
Tarn08ap_86	480	13	322.3	7.6	219.7	6.5	LOD	LOD	2.58	0.45	8.28	0.9	1.36	0.19	9.5	1.2	4.86	0.71	1.35	0.16
Tarn08ap_87	475	11	3394	41	551	14	LOD	LOD	7.66	0.82	37.9	1.9	8.07	0.55	62.3	3.6	35.3	2.1	8.4	0.38
Tarn08ap_88	1226	19	825	18	663	14	LOD	LOD	13.1	1.2	81.9	2.8	19.39	0.86	149	6.1	90.7	3.3	24.02	0.75
Tarn08ap_89	445.3	9.9	828	16	510	10	LOD	LOD	28.2	3.1	87.9	6.2	15.8	1	107.4	5.6	57.2	2.7	18.94	0.58
Tarn08ap_90	436	12	1035	22	663	17	LOD	LOD	2.49	0.49	11.8	1	2.11	0.26	14.1	1.5	8.34	0.81	2.58	0.26
Tarn08ap_91	424.9	9.7	1514	28	598	12	LOD	LOD	9.63	0.89	48.7	2.5	11.28	0.68	84.7	4	64.2	2.3	13.97	0.52
Tarn08ap_92	333.7	9.4	317.7	9.8	950	21	7.4	1.7	396	10	1168	24	175.1	4	929	21	249.6	7.5	5.73	0.33
Tarn08ap_93	379	11	1746	35	233.5	8.3	LOD	LOD	39.7	3	86.3	5.1	10.3	1.1	36.6	3.9	8.9	1.1	2.28	0.29
Tarn08ap_94	1210	22	134.3	5.5	1794	36	4.2	1	613	17	2072	50	317.7	8.7	1545	35	429	11	4.12	0.31
Tarn08ap_95	285.3	7.9	4578	60	1107	20	LOD	LOD	76.9	2.9	309.3	6.7	60.9	1.8	397	11	181	3.7	50.6	1.1
Tarn08ap_96	205.6	6.6	2987	48	757	18	LOD	LOD	5.54	0.82	21.5	1.3	4.53	0.45	32.7	2.5	22.9	1.4	9.05	0.43
Tarn08ap_97	313.4	8.2	1204	22	261.6	7.8	0.36	0.22	5.09	0.8	20	1.7	3.58	0.45	23	2.7	9.6	1	1.73	0.17
Tarn09ap_0	1041	19	881	15	1067	18	5	0.45	1666	61	3980	120	596	18	2669	70	525	13	15.07	0.48
Tarn09ap_1	385.9	7.9	332.1	6.3	1424	28	0.575	0.064	363.2	6.9	1030	23	182.7	4	1024	22	320.4	6.7	6.69	0.21
Tarn09ap_2	2328	71	263	11	1571	65	1.25	0.26	122.2	5.2	521	22	95.8	4.1	594	23	285	11	27.3	1
Tarn09ap_3	413.5	4.6	3275	51	750	15	0.102	0.032	30.61	0.74	216	4	53.1	1.3	404.1	8.8	237	4.9	70.6	1.5
Tarn09ap_4	884	11	172.7	3.2	2335	53	2.14	0.12	627	11	1712	35	328.6	5.8	1767	33	559	10	9.89	0.26
Tarn09ap_5	1001	15	357.1	8.1	1453	31	2.39	0.16	937	25	2579	57	454	10	2278	52	595	12	16.13	0.41
Tarn09ap_6	1144	16	225.4	3.8	958	22	0.053	0.022	381.7	7.9	998	24	170.7	3.5	854	15	234.7	4.6	3.63	0.15
Tarn09ap_7	1693	30	183.5	6.2	1024	39	0.63	0.1	103.4	4.2	371	13	66.6	2.4	361	12	134.8	4.6	7.47	0.27
Tarn09ap_8	1816	23	171.9	3.4	358.8	8.1	0.065	0.021	35	1.2	86.6	2.6	11.55	0.39	52.3	1.7	18.44	0.68	4.7	0.17
Tarn09ap_9	862	13	317.2	6.7	1112	26	2.67	0.13	526	10	1345	26	238.6	4.3	1204	24	323.9	5.8	11.19	0.31
Tarn09ap_10	844.1	9.5	435.7	6.7	1017	21	2.4	0.16	709	12	1780	28	307.8	5.5	1550	25	391.9	6.3	13.25	0.29
Tarn09ap_11	920	11	522.3	9.3	873	18	0.064	0.023	29.03	0.68	99	2.3	16.39	0.45	95.4	2.9	43.5	1.1	9.97	0.32
Tarn09ap_12	372.7	4.1	3464	47	302.9	4.6	0.029	0.013	4.72	0.18	18.25	0.37	4.14	0.16	35.4	1.3	20.69	0.56	5.72	0.13
Tarn09ap_13	494.2	9.4	519	18	454	14	0.6	0.11	581	18	910	23	91.6	3.1	374	11	67.8	2.1	7.84	0.31
Tarn09ap_14	787.9	8.7	415.1	5.1	930	18	10.54	0.56	665	13	1646	32	284.3	5.5	1447	29	355.7	6.5	12.15	0.29
Tarn09ap_15	284.2	3.9	672.3	8.8	729	12	0.092	0.027	19.62	0.65	87.8	2.2	18.94	0.44	155.4	3.7	120.3	2.5	32.61	0.56
Tarn09ap_16	299	7.2	1468	38	809	22	0.79	0.15	10.6	1.8	25	3.3	4.07	0.41	30	1.9	23.7	1.1	5.65	0.25
Tarn09ap_17	384.2	4.9	2310	33	228.5	4.1	LOD	LOD	2.16	0.12	8.38	0.25	1.734	0.08	12.65	0.64	7.4	0.31	2.504	0.098
Tarn09ap_18	487.3	6.2	85.7	1.8	316.8	7	0.013	0.008	1.267	0.084	4.42	0.18	0.84	0.067	5.98	0.38	3.47	0.22	1.144	0.066

	157Gd	±	159Tb	±	163Dy	±	165Ho	±	166Er	±	169Tm	±	172Yb	±	175Lu	±	182W	±	232Th	±	238U	±
Tarn08ap_36	35.4	1.5	21.48	0.57	242.9	4.8	64.3	1.4	183.7	3.9	19.74	0.64	84.8	1.9	8.59	0.36			0.03	0.014	0.217	0.017
Tarn08ap_37	22.44	0.96	8.1	0.32	56.8	1.7	13.35	0.42	43.6	1.2	5.69	0.21	34.1	1	4.48	0.17			0.116	0.022	0.543	0.025
Tarn08ap_38	9.68	0.68	2.36	0.21	18.09	0.96	5.09	0.25	18.33	0.86	2.06	0.14	10.52	0.56	1.46	0.11			0.204	0.045	0.077	0.027
Tarn08ap_39	57.2	1.9	20.28	0.5	138.3	2.6	27.33	0.65	81.6	1.6	10.55	0.3	67.3	1.6	8.88	0.28			32.98	0.74	6.75	0.15
Tarn08ap_40	212.9	4.6	41.3	0.93	190.7	3.6	31.87	0.74	101.9	2.3	12.19	0.36	76.8	1.7	9.75	0.39			5.01	0.17	19.24	0.3
Tarn08ap_41	42.9	1.7	20.78	0.74	174.9	4.6	38.5	1.2	110.1	3.5	13.14	0.36	76	2.4	10	0.39			3.27	0.2	0.216	0.021
Tarn08ap_42	143.7	3.5	43.46	0.95	211.6	4.1	30.72	0.67	76.1	2.1	8.25	0.28	45	1.3	5.36	0.22			1.117	0.075	0.218	0.02
Tarn08ap_43	63.5	1.8	24.94	0.61	159.8	3.1	27.56	0.58	70.6	1.7	7.22	0.25	38.3	1.2	4.43	0.22			0.58	0.081	1.048	0.033
Tarn08ap_44	18.3	1.2	8.41	0.27	80.6	1.7	25.39	0.63	101.3	2.3	15.14	0.37	99.2	2.1	15.08	0.41			0.178	0.062	0.322	0.027
Tarn08ap_45	312.6	5.5	51.8	1.1	228.7	4.8	39.52	0.85	125.2	3	13.47	0.4	79.8	1.9	9.71	0.33			22	0.4	11.27	0.21
Tarn08ap_46	133.9	3.4	32.38	0.78	191	4	32.33	0.71	101.1	2.5	14.16	0.33	95.2	2.1	12.13	0.36			2.435	0.092	24.35	0.41
Tarn08ap_47	307.8	6.3	54.9	1.3	261.1	5.3	46.8	1.1	148.3	3.3	18.02	0.43	110.7	2.5	14.43	0.46			33.41	0.76	5.38	0.11
Tarn08ap_48	28.7	5.4	6.38	0.43	47.2	1.6	13.03	0.35	50.3	1.4	6.4	0.22	30	1.1	2.9	0.15			0.64	0.1	0.249	0.023
Tarn08ap_49	53.8	1.9	23.46	0.61	167.6	3.3	31.37	0.61	82.5	1.6	9.66	0.29	51.6	1.5	5.92	0.24			0.041	0.013	0.137	0.012
Tarn08ap_50	294.7	6.3	44.9	1.1	190.6	4.4	31.59	0.73	96.3	2.6	9.48	0.3	51.7	1.6	6.19	0.21			31.54	0.79	19.2	0.45
Tarn08ap_51	37.4	1.8	18.03	0.52	165.4	4.6	34.5	1	90.1	3.4	10.07	0.44	49.9	1.9	5.74	0.3			0.179	0.037	0.207	0.024
Tarn08ap_52	156.1	5.1	33.5	1.1	195.3	6.8	36.6	1.2	86.9	2.7	11.31	0.4	62.4	1.6	7.91	0.33			4.34	0.18	4.9	0.14
Tarn08ap_53	234.6	5.3	56	1.2	268.4	5.6	36.11	0.85	68.6	1.6	8.05	0.28	40.8	1.4	4.52	0.22			3.98	0.15	0.278	0.028
Tarn08ap_54	10.72	0.68	4.33	0.22	47.7	1.9	15.43	0.4	54.4	1.4	10.7	0.29	62.1	1.6	7.38	0.27			0.015	0.008	0.132	0.012
Tarn08ap_55	183.5	5	25.44	0.83	116.4	3.1	20.04	0.58	48.1	1.5	5.88	0.21	31.4	1.3	3.84	0.2			9.36	0.58	17.09	0.86
Tarn08ap_56	6.72	0.76	2.63	0.2	28.5	1.2	8.99	0.35	39.5	1.7	9.54	0.36	57	2.1	5.73	0.36			0.059	0.021	0.108	0.016
Tarn08ap_57	219.7	4.7	53.9	1.5	350.7	9.1	68.3	1.9	143.7	4.3	18.88	0.68	94.7	3.9	10.82	0.6			4.49	0.24	8.23	0.26
Tarn08ap_58	6.6	0.51	2.18	0.13	19.63	0.82	5.32	0.28	15.27	0.67	2.99	0.16	20.93	0.94	3.08	0.18			0.025	0.01	0.063	0.008
Tarn08ap_59	82.5	2.3	24.12	0.64	139.8	3	22.73	0.56	47	1.4	7.28	0.28	44.5	1.4	6.27	0.26			0.332	0.047	0.17	0.015
Tarn08ap_60	1.42	0.29	0.656	0.086	6.53	0.59	2.01	0.15	6.43	0.43	1.342	0.096	8.82	0.54	1.47	0.1			0.185	0.034	0.01	0.004
Tarn08ap_61	102.2	3.1	28.97	0.73	162.8	4.1	24.3	0.69	46.4	1.3	6.32	0.24	38.3	1.3	4.99	0.27			0.139	0.027	0.286	0.022
Tarn08ap_62	427.9	7.5	42.68	0.73	150.7	2.6	24.62	0.58	64.9	1.4	6.54	0.22	33	1.2	4.17	0.19			35.17	0.71	14.32	0.27
Tarn08ap_63	17	1	5.46	0.24	63.2	2.1	22.24	0.49	89.1	1.9	19.98	0.52	129.4	3.1	15	0.51			8.47	0.76	0.463	0.036
Tarn08ap_64	37	1.4	14.82	0.42	122.7	2.8	26.24	0.74	60.8	1.6	10.52	0.3	72.6	1.9	11.23	0.31			0.027	0.012	0.387	0.02
Tarn08ap_65	225.3	6.2	49.8	1.5	315.5	8	60.7	1.7	151.1	4.5	26.88	0.92	176.8	4.9	23.6	0.98			9.36	0.52	10.49	0.34
Tarn08ap_66	376	7.1	96.4	1.5	626	10	115.2	1.8	269.6	4	43.56	0.76	264.3	4.6	33.38	0.69			22.43	0.43	21.95	0.32
Tarn08ap_67	11.37	0.8	3.51	0.19	28.2	1	6.99	0.23	19.97	0.68	4.03	0.19	29.2	1	4.39	0.2			0.054	0.017	0.415	0.021
Tarn08ap_68	20.8	1.1	10.18	0.32	111.3	2.5	29.31	0.61	73.4	1.7	10.89	0.28	58.4	1.5	6.91	0.23			0.052	0.023	0.138	0.013
Tarn08ap_69	221	4.4	39.89	0.76	216.3	4.3	39.32	0.74	99.8	2.1	14.29	0.42	85	1.8	11.24	0.32			23.61	0.95	66.9	3.2
Tarn08ap_70	254.1	7.9	41	1.2	206.6	5.9	36.8	1.3	94.6	2.4	13.65	0.46	85.2	1.9	11.28	0.46			16.54	0.67	12.33	0.27
Tarn08ap_71	78.4	3.3	22.12	0.61	131.6	3.6	22.03	0.55	51	1.6	7.84	0.31	54.3	2	8	0.28			0.399	0.062	0.627	0.033
Tarn08ap_72	11.9	1.2	4.65	0.3	33.3	2.2	7.82	0.39	24	1.3	2.47	0.19	13.4	1.1	1.65	0.13			0.439	0.078	0.107	0.018
Tarn08ap_73	112.8	3.9	33.67	0.91	179.6	3.7	27.08	0.73	72.8	1.9	6.48	0.3	32.5	1.3	3.55	0.17			0.222	0.033	1.107	0.038
Tarn08ap_74	242.2	6.1	23.03	0.75	76.4	2.4	13.24	0.46	55	2	4.26	0.28	24.6	1.2	3.2	0.23			74.1	1.5	9.18	0.24
Tarn08ap_75	290.4	6.7	56	1.2	275.2	5.6	50.9	1.2	172.4	3.8	20.89	0.51	134.3	3.1	17.07	0.47			10.49	0.34	3.68	0.12
Tarn08ap_76	215.1	6.8	33.3	1.3	140.7	4.1	22.74	0.78	71.5	2.4	6.65	0.36	38.4	1.9	4.61	0.31			17.82	0.69	13.69	0.37
Tarn08ap_77	104.8	2.8	41.42	0.99	261.7	5.1	45.2	1.1	114.6	2.4	14.38	0.41	91.7	2.2	13.17	0.39			0.181	0.029	0.554	0.027
Tarn08ap_78	267.7	7	41.9	1.1	205.1	5.5	35.4	1.1	90.7	2.7	10.5	0.55	55.7	1.8	6.32	0.33			25.19	0.62	7.43	0.19
Tarn08ap_79	3.13	0.39	1.35	0.13	12.12	0.74	3.59	0.19	11.48	0.6	1.58	0.13	8.18	0.55	0.757	0.089			0.049	0.02	0.073	0.01
Tarn08ap_80	214.1	4.2	39.63	0.92	213.2	3.5	38.35	0.77	103.8	2.2	14.15	0.36	84.5	2.2	10.85	0.32			10.47	0.28	7.74	0.13
Tarn08ap_81	17.32	0.94	6.45	0.3	60.6	1.7	16.08	0.49	53.8	1.6	8.47	0.32	51.8	1.5	6.89	0.31			0.174	0.034	0.194	0.014
Tarn08ap_82	198.6	4.2	30.77	0.61	149.2	2.6	24.21	0.5	56.6	1.3	5.64	0.2	29.07	0.88	3.26	0.14			16.1	2.2	25.1	3.7
Tarn08ap_83	253.6	7.4	60.8	1.3	390.8	7.7	75.1	1.7	189.6	3.5	22.76	0.57	117.6	2.7	13.7	0.37			5.05	0.16	9.63	0.23
Tarn08ap_84	150.5	7	37.9	1.3	202	7.8	27.1	1.3	52.9	2.8	4.9	0.37	22.6	1.8	2.09	0.17			1.46	0.15	0.314	0.037
Tarn08ap_85	385.5	7.5	68.3	1.1	392.4	6.2	71.5	1.4	201	3.6	28.98	0.49	194	3.9	24.79	0.5			25.2	0.5	20.22	0.32
Tarn08ap_86	8.78	0.75	2.49	0.19	26.5	1.2	7.53	0.28	27.76	0.96	5.07	0.22	35.3	1.3	4.69	0.21			0.236	0.06	0.073	0.01
Tarn08ap_87	35.6	1.4	10.38	0.35	76.6	2	18.09	0.48	54.4	1.4	8.46	0.3	57.7	1.4	8.17	0.26			0.321	0.046	1.106	0.039
Tarn08ap_88	89.9	2.7	27.38	0.57	176.4	3.7	29.47	0.67	68.5	1.7	8.96	0.33	50.1	1.5	6.46	0.23			0.378	0.05	0.537	0.025
Tarn08ap_89	65.6	2.1	18.86	0.54	124.9	2.7	21.91	0.56	55.1	1.5	7.98	0.28	54.4	1.5	7.92	0.27			0.175	0.035	0.425	0.032
Tarn08ap_90	11.18	0.8	5.4	0.24	62.3	1.9	20.8	0.59	90.1	2.2	15.68	0.45	91.3	2.2	10.74	0.39			0.019	0.01	0.106	0.015
Tarn08ap_91	74.4	2.4	24.84	0.64	166.3	3.6	26.09	0.57	56.5	1.4	6.97	0.26	38.2	1.3	4.32	0.23			0.029	0.011	1.45	0.048
Tarn08ap_92	219.6	4.2	37.22	0.86	209.2	4	38.34	0.78	102.9	2	11.87	0.33	66.2	1.8	7.95	0.3			10.48	0.28	5.19	0.12
Tarn08ap_93	11.65	0.86	2.71	0.26	26.9	1.4	7.81	0.35	29	1.2	4.69	0.32	28.7	1.7	3.24	0.23			10.3	0.43	1.579	0.059
Tarn08ap_94	362.1	8.8	61.6	1.6	342.2	7.5	62.5	1.4	181.1	3.5	24.5	0.66	156	3.6	19.99	0.5			35.16	0.87	18.72	0.61
Tarn08ap_95	171.1	3.5	42.84	0.82	272.6	4.9	45.93	0.9	110.2	2.5	12.62	0.33	68	1.6	7.29	0.27			0.452	0.046	0.759	0.026
Tarn08ap_96	39.6	1.5	18.11	0.48	167.5	3.8	28.52	0.74	54.2	1.3	4.83	0.19	18.57	0.73	1.36	0.12			0.059	0.016	0.257	0.015
Tarn08ap_97	11.9	1.1	3.94	0.27	36	1.8	8.98	0.37	27.6	1.2	3.58	0.16	19.08	0.7	2.36	0.12			1.996	0.092	2.28	0.12
Tarn09ap_0	401.7	9.4	47.71	0.93	257.6	4	43.9	0.64	103.6	2	12.22	0.28	64	1.5	7.85	0.26	0.93	0.1	78.8	5.1	25.56	0.69
Tarn09ap_1	371.2	7.8	54.35	0.99	337.5	5.2	64.5	1	161.7	2.6	19.12	0.48	100.8	2.5	12.29	0.35	1.4	0.12	8.56	0.22	11.11	0.21
Tarn09ap_2	439	12	80.3	2.2	467.4	9.4	65.3	1.1	121.9	2.4	13.11	0.42	71.1	2.4	8.56	0.33	0.214	0.047	2.41	0.12	57.1	2.2
Tarn09ap_3	334.5	6.1	43.57	0.86	214.4	4.4	31.53	0.57	70.7	1.3	9.33	0.23	61.9	1.2	9.07	0.24	0.246	0.07	6.28	0.18	0.167	0.013
Tarn09ap_4	516.4	9.9	78.4	1.4	484.7	8.5	88.9	1.6	240.2	4.1	35.78	0.71	230.7	4.9	29.28	0.62	0.093	0.027	43.8	1	39.18	0.77
Tarn09ap_5	498	7.9	64.6	1.3	354.8	7.6	61.3	1.3	149.6	2.8	18.63	0.43	102.7	2.6	12.4	0.34	0.599	0.093	57.3	1.4	41.3	1
Tarn09ap_6	204.3	3.6	30.07	0.71	184	3.3	33.95	0.67	93.3	2.1	13.89	0.31	86.4	1.9	11.42	0.3	0.036	0.018	4.06	0.16	9.08	0.23
Tarn09ap_7	179.4	5.2	34.11	0.74	238.1	4.2	42.91	0.74	93	1.5	9.97	0.23	41.7	1	3.81	0.14	0.373	0.067	0.575	0.036	8.53	0.3
Tarn09ap_8	23.85	0.74	4.89	0.15	40.5	1	10.94	0.25	45.01	0.89	9.14	0.22	74.3	1.5	12.01	0.25	0.268	0.045	2.037	0.061	8.34	0.24
Tarn09ap_9	276	4.6	38.73	0.68	229.4	3.6	42.21	0.77	108.8	1.9	15.8	0.32	97.2	2.1	12.67	0.32	0.126	0.034	32.76	0.59	26.46	0.59
Tarn09ap_10	321.1	4.9	41.36	0.66	230.5	3.3	40.24	0.67	96	1.5	12.09	0.21	66.5	1.2	8.1	0.17	0.24	0.045	31.31	0.59	25.96	0.42
Tarn09ap_11	72.1	1.6	15.57	0.28	127.5	1.9	30.88	0.52	95.2	1.7	14.8	0.3	93.5	1.7	12.14	0.26	0.292	0.055	0.178	0.016	0.672	0.024
Tarn09ap_12	49.3	1.2	7.4	0.15	51.5	0.86	11.01	0.16	31.65	0.5	5.313	0.098	38.89	0.81	5.62	0.13	0.332	0.047	0.095	0.011	0.041	0.004
Tarn09ap_13	67.9	2	8.74	0.19	62.3	1.4	14.89	0.34	46.7	1.7	7.1	0.26	41.5	1.5	5.16	0.19	0.269	0.055	30.49	0.73	21.69	0.45
Tarn09ap_14	285.9	5.4	37.15	0.58	205.6	3.4	35.42	0.51	85.8	1.2	10.82	0.19	59.64	0.95	7.15	0.14	0.743	0.08	30.59	0.6	8.81	0.21
Tarn09ap_15	228.1	3.8	35.39	0.52	197.7	2.8	30.83	0.39	73	1.1	8.4	0.17	44.31	0.8	5.21	0.14	0.117	0.031	0.154	0.016	1.368	0.035
Tarn09ap_16	69.2	1.7	17.13	0.39	137.9	3.3	28.73	0.76	80.7	1.6	10.19	0.3	56.9	1.5	6.65	0.24	0.74	0.1	0.79	0.13	1.293	0.064
Tarn09ap_17	18.46	0.55	3.64	0.1	28.75	0.62	6.98	0.13	23.35	0.46	3.003	0.081	18.5	0.46	3.32	0.097	0.128	0.031	0.013	0.004	0.262	0.011
Tarn09ap_18	8.34	0.39	2.097	0.073	23.41	0.59	9.42	0.2	54.4	1	12.5	0.24	125.3	2.5	26.65	0.4	1.039	0.091	0.006	0.003	0.13	0.008

Supporting Information Tables S3.5: Apatite trace-element data (continued)

Supporting Information Tables S3.5: Apatite trace-element data (continued)

	55Mn	±	86Sr	±	89Y	±	90Zr	±	139La	±	140Ce	±	141Pr	±	146Nd	±	147Sm	±	153Eu	±	157Gd	±	159Tb	±	163Dy	±	165Ho	±	166Er	±	169Tm	±	172Yb	±	175Lu	±	182W	±	232Th	±	238U	±
Tarn10ap_0	4116	94	197	10	2329	73	2.16	0.89	1281	52	3790	120	590	21	2618	92	756	22	14.75	0.78	673	16	173.5	4.3	499	14	86.6	2.6	305.8	7.4	26.13	0.81	167.4	4.7	20.05	0.68			71.7	2.2	29.72	0.82
Tarn10ap_1	741	18	1329	32	492	16	6E-05	2E-06	7.5	1.2	38.2	2.7	10.36	0.94	78.1	6.6	60.1	3.6	16.82	0.84	41.4	1.8	25.32	0.99	141.1	4.4	22.14	0.76	45.3	1.6	4.91	0.3	28.7	1.1	3.51	0.23			0.101	0.033	0.105	0.018
Tarn10ap_2	605	15	587	15	840	26	5E-05	1E-06	14.2	1.5	50	3.3	10.52	0.81	59.1	4	35.7	1.9	10.66	0.45	28.2	1.1	20.98	0.62	160.7	4.2	32.91	0.81	83.3	2	10.51	0.3	55.1	1.8	6.65	0.3			LOD	LOD	0.919	0.055
Tarn10ap_3	229.8	6.8	1406	22	681	19	5E-05	9E-07	44.5	3.2	187.7	7.7	36.5	1.8	209	10	107.9	4.6	33.7	1.2	70	2	35.95	0.88	187.9	4.6	30.39	0.83	71.7	2.1	7.74	0.28	41.5	1.3	5.05	0.26			0.136	0.036	1.307	0.055
Tarn10ap_4	377.3	8.5	597	13	650	16	0.18	0.18	136.8	6.7	465	18	75	3.3	376	15	113.4	4.6	3.06	0.21	90.9	2.7	28.72	0.79	133.1	3.8	27.1	0.79	80.6	2.5	8.92	0.31	47.2	1.8	6.26	0.27			3.13	0.15	3.23	0.11
Tarn10ap_5	300.4	9.1	549	13	777	23	LOD	LOD	LOD	LOD	7	1.1	1.24	0.32	8.5	1.6	5.06	0.73	1.67	0.19	4.29	0.4	4.1	0.24	52.8	2	22.36	0.67	114.5	3.1	23.04	0.58	144.8	3.9	17.43	0.53			LOD	LOD	0.063	0.012
Tarn10ap_6	437	11	3228	51	330	12	4E-05	8E-07	3.89	0.84	17.2	1.6	3.2	0.45	22.3	2.7	13.1	1.1	3.17	0.24	10.26	0.61	6.3	0.29	45.4	1.8	11.15	0.4	33.1	1.3	4.52	0.22	26	1	4.17	0.21			0.036	0.017	0.492	0.03
Tarn10ap_7	901	15	572	13	614	16	0.21	0.19	415	12	1080	28	146.1	4.8	620	22	142.2	3.8	7.81	0.42	140.4	2.7	34.21	0.92	126.5	3.5	24.01	0.56	75.4	2.1	7.17	0.26	39.6	1.4	5.21	0.22			4.04	0.22	23.54	0.7
Tarn10ap_8	1036	17	365.5	9.8	1799	48	1.24	0.5	859	24	2607	69	402	11	1850	46	470	11	8.48	0.42	385.4	7.7	95.4	2	338.8	7.9	60.8	1.3	213.7	5.1	24.11	0.72	157.9	3.9	21.7	0.7			33.05	0.93	19.67	0.55
Tarn10ap_9	440	10	2985	51	1424	30	1.76	0.64	46.8	3.4	181.2	7	36	1.7	225	10	144.3	4.2	47.2	1	100.8	3.3	59.7	1.9	355.9	7.8	59.9	1.5	144.3	3.4	16.63	0.52	92.8	2.5	10.78	0.43			0.492	0.069	2.126	0.091
Tarn10ap_10	492	11	531	11	459	13	LOD	LOD	3.43	0.75	12.1	1.3	1.97	0.31	12.4	1.6	7.41	0.82	2.2	0.18	5.61	0.42	4.23	0.22	45.1	1.5	15.05	0.45	66.7	2	11.87	0.29	70.5	1.7	9.86	0.32			0.02	0.013	0.121	0.024
Tarn10ap_11	463.4	9.8	2130	41	1078	28	LOD	LOD	16.7	1.7	59.4	2.9	12.06	0.87	80.1	3.9	52	2.4	18.61	0.67	49	1.7	36.69	0.97	276.2	6.2	47.9	1.1	104.1	2.4	10.61	0.33	49.7	1.4	5.56	0.26			0.087	0.022	0.376	0.027
Tarn10ap_12	8720	200	112.4	7.1	1920	81	5.7	2.6	900	120	2300	250	314	32	1270	120	385	18	8.79	0.8	308	22	86	4.9	367	12	63.2	2.8	198.1	7.3	25.6	1	157	3.6	19.5	1			306	55	132	14
Tarn10ap_13	1123	21	357	9.8	1406	33	2.13	0.66	735	21	2215	61	313.9	8.1	1483	45	379.8	8.8	7.69	0.4	310	6.1	72.5	1.4	257.3	5.4	46.4	1.1	162.2	3.5	17.87	0.51	110.6	2.6	14.86	0.5			20.88	0.59	9.43	0.24
Tarn10ap_14	3123	50	65.1	3.1	2794	55	0.3	0.23	423	11	1461	41	225.2	5.3	1101	28	361.7	7.2	3.75	0.25	261.3	5.4	86.8	1.8	476	9.6	95.3	2	302	6.7	42.94	0.98	271.3	5.3	37.09	0.87			10.51	0.34	64.2	1.5
Tarn10ap_15	1125	19	758	16	522	13	8E-06	1E-07	21.5	2	86.8	3.6	16.8	1	104	5.8	57.5	2.7	16.76	0.68	42.9	1.9	21.33	0.63	130.4	3.3	21.86	0.6	52.1	1.6	5.86	0.27	29.6	1.1	3.56	0.19			0.157	0.037	0.489	0.027
Tarn10ap_16	801	18	1179	24	530	16	LOD	LOD	37.6	2.7	148.4	6.6	26.2	1.6	159.3	7.1	82.4	3.5	23.8	0.77	57.1	2.1	25.51	0.87	133.6	3.7	21.74	0.71	56.7	1.7	6.95	0.34	43.2	1.6	5.78	0.31			1.36	0.13	0.3	0.023
Tarn10ap_17	139.8	6.4	1849	30	662	19	1.76	0.95	36	3.7	192	13	39.4	2.1	261	14	146.9	5.2	45.6	1.6	85.6	2.8	38.21	0.78	205.4	5.4	29.92	0.75	67.3	1.9	7.08	0.24	37.6	1.1	4.1	0.25			0.138	0.059	1.46	0.83
Tarn10ap_18	1312	36	248	13	1429	45	0.63	0.55	671	20	2088	54	306	13	1402	51	352	11	8.08	0.56	294.1	9.6	64.2	1.7	263.4	8.3	48	1.5	163.1	4.2	19.22	0.94	118.9	4.1	15.81	0.67			23.01	0.83	22.66	0.69
Tarn10ap_19	378	10	3413	50	387	11	0.43	0.25	6.8	1.1	21.7	1.5	3.74	0.5	21.9	2.2	12.6	1.1	4.7	0.35	10.09	0.6	5.64	0.28	44.9	1.4	11.91	0.39	39.3	1.1	5.52	0.2	31.05	0.97	4.72	0.25			1.249	0.099	0.491	0.033
Tarn10ap_20	460	10	1630	35	613	17	LOD	LOD	42.5	2.6	186.8	7.1	35.5	1.4	213.1	8.2	112.3	4.1	35.2	1.2	76.1	2.2	35.2	0.94	188.2	4.4	27.54	0.74	61.5	1.8	6.33	0.24	35.2	1.2	4.03	0.2			0.125	0.036	0.638	0.035
Tarn10ap_21	977	21	1470	25	741	18	18.4	4.6	19.5	1.8	76.7	3.8	15.15	0.97	107.2	6.5	67.5	3.1	19.34	0.66	52.7	1.7	27.15	0.78	172.8	4.3	30.31	0.77	79.1	2.1	10.44	0.27	63.6	1.9	8.15	0.23			1.99	0.14	0.86	0.11
Tarn10ap_22	511	11	697	18	775	22	LOD	LOD	4.97	0.94	18.9	1.6	3.1	0.37	23.6	2.2	11.8	1.1	4.11	0.34	12.91	0.79	9.41	0.46	104.5	3.5	28.7	1.1	93.3	3.2	12.5	0.38	72.3	2.4	9.81	0.38			0.017	0.012	0.08	0.012
Tarn10ap_23	895	17	767	17	378	11	4.2	1.2	6.3	1.2	18.8	2.4	3.09	0.46	17.8	2.3	10.65	0.9	3.17	0.27	10.88	0.59	5	0.29	41.4	1.9	11.69	0.4	48.6	1.5	9.58	0.42	66.5	1.7	10.04	0.39			3.57	0.25	1.083	0.055
Tarn10ap_24	604	16	607	16	893	26	LOD	LOD	2.74	0.68	14.2	1.5	2.98	0.45	17	2.7	9.66	0.93	3.42	0.27	10.24	0.82	7.31	0.33	77.8	2.6	27.88	0.71	120.9	3.1	20.03	0.59	109.4	3	11.18	0.46			0.048	0.028	0.105	0.015
Tarn10ap_25	408	11	1190	25	347	11	LOD	LOD	2.87	0.65	12.2	1.3	2.15	0.36	14.6	2	8.2	1.1	1.99	0.23	6.23	0.59	3.53	0.24	33.3	1.5	10.52	0.33	45.2	1.2	8.14	0.34	46.4	1.4	5.36	0.28			0.024	0.017	0.071	0.011
Tarn10ap_26	626	16	1094	23	1266	31	6	2	141.5	6.2	484	14	74.4	2.6	419	14	147.2	5.7	6.09	0.38	115.1	3.9	39.9	1.2	237.7	6.6	47	1.1	130.5	3.4	14.65	0.42	75.2	2.3	9.08	0.37			5.51	0.28	5.13	0.18
Tarn10ap_27	1114	22	826	19	738	22	0.57	0.4	11.6	1.4	65.8	3.7	18.2	1.1	186.7	9.3	180.7	8.3	43.9	1.6	70.8	3.1	28.66	0.91	162	4	28.94	0.73	73.5	1.7	9.05	0.35	49.7	1.6	5.74	0.22			4.92	0.29	0.687	0.042
Tarn10ap_28	370	9.2	1531	27	663	17	LOD	LOD	28.6	2.7	109.1	5.1	22.6	1.3	156.1	6.6	93.2	3.4	30.71	0.9	74.8	2.1	30.55	0.91	184.1	4.2	28.65	0.66	63.6	1.9	6.31	0.24	31.1	1	3.68	0.21			0.462	0.053	0.174	0.018
Tarn10ap_29	393	11	2017	37	703	16	0.22	0.19	18.1	1.3	74.7	2.7	14.45	0.83	111.9	4.7	83.1	2.7	25.18	0.78	66.9	1.8	32.32	0.84	195.6	3.9	30.69	0.63	68.7	1.8	7.62	0.25	40.9	1.2	4.77	0.25			0.574	0.066	0.341	0.029
Tarn10ap_30	1466	23	287	9	1391	27	3.76	0.88	365	13	1259	26	195	4.9	1046	25	338	7.2	7.7	0.37	245.9	4	63.9	1.1	284	4.9	46.88	0.92	140.1	2.6	17.49	0.41	112.4	2.8	15.37	0.53			7.56	0.31	25.67	0.55
Tarn10ap_31	776	16	3742	67	161.3	6.8	LOD	LOD	4.14	0.84	13.7	1.4	2.37	0.39	16.9	1.8	7.86	0.93	2.62	0.21	6.63	0.62	2.91	0.2	21.6	1.2	5.16	0.24	17.28	0.72	2.38	0.16	15.22	0.66	2.22	0.2			0.084	0.028	0.259	0.023
Tarn10ap_32	452	12	844	21	836	18	LOD	LOD	3.95	0.76	18.6	1.7	4	0.45	29.7	2.8	18.5	1.6	6.51	0.45	19.59	0.86	12.36	0.48	119.5	3.1	30	0.87	86	2.5	9.82	0.43	42	1.5	4.33	0.24			0.048	0.017	0.073	0.011
Tarn10ap_33	479	19	479	11	1509	34	LOD	LOD	170.1	6	556	12	80.7	2.6	417	12	122	4.1	5.44	0.3	108.1	3	34.3	0.69	228.7	4.9	52.8	1.2	176.1	3.9	25.8	0.68	148.3	3.4	20.38	0.58			2.81	0.16	8.06	0.21
Tarn10ap_34	485	12	280	8.9	1347	35	2.9	1.1	259.1	8.4	886	26	133.1	4.6	722	22	224.7	6.4	4.52	0.3	174.9	4.3	48	1.1	252.3	5.8	52.09	0.94	170.2	3.7	24.32	0.63	155	3.5	20.25	0.54			9.5	0.3	9.24	0.23
Tarn10ap_35	790	14	721	15	866	19	LOD	LOD	25.2	2	99.2	4.6	18.8	1.4	134.7	6.4	95.6	4	37.2	1	86.5	2.5	42.1	1.2	252.5	5.9	38.21	0.84	89.4	2.1	9.45	0.31	50.6	1.5	5.7	0.24			0.077	0.027	0.79	0.037
Tarn10ap_36	570	15	237.7	8.3	576	19	0.25	0.25	32.2	2.5	123.1	4.2	20.4	1.5	114.6	6.9	48.8	2.6	1.84	0.18	39.4	1.4	16.45	0.64	108.2	3.7	21.43	0.57	64	2.2	8.87	0.37	60.2	1.8	9.52	0.33			2.7	0.15	44.5	1.9
Tarn10ap_37	733	13	758	15	682	16	2.1	1.1	14.2	1.4	43.7	2.6	7.12	0.7	43.9	3	17.8	1.4	4.02	0.27	15.15	0.94	6.86	0.32	65.6	2.3	21.36	0.64	88.8	2.3	15.23	0.47	99.8	2.8	14.01	0.42			2.37	0.43	1.088	0.084
Tarn10ap_38	747	20	2122	48	572	17	LOD	LOD	18.2	2.7	131.7	7.4	47.5	3.2	510	22	456	12	123.6	3.1	176.9	4.9	49.8	1.4	188	4.8	24.91	0.69	62.1	2.1	6.62	0.26	45	1.5	5.32	0.29			8.79	0.52	0.319	0.06
Tarn10ap_39	1205	21	144	6	1610	42	1.76	0.6	362	12	1387	42	222	6.1	1181	30	353.7	8.6	5.23	0.36	256.7	6.4	61.8	1.7	296.1	6.7	53.6	1.3	169.8	4.1	21.78	0.63	133.9	3.6	17.9	0.64			16.96	0.65	10.44	0.29
Tarn10ap_40	1233	23	385	12	867	25	0.32	0.25	328	9.3	1095	25	165.2	4.9	863	23	238	6.9	5.87	0.37	187	4.2	38.8	0.94	166.4	4.7	29.81	0.79	93.9	2.5	10.92	0.36	66.5	1.8	9.03	0.44			7.67	0.36	10.49	0.24
Tarn10ap_41	1005	21	308	10	1092	27	7.3	1.8	502	17	1626	39	250.6	6.6	1281	37	341.6	9.1	9.46	0.51	268.7	6.5	55	1.6	213.2	5.8	36.1	1.2	119.2	3.7	12.79	0.45	78.5	2.6	9.54	0.47			26.53	0.87	9.75	0.3
Tarn10ap_42	1105	30	703	26	261	13	LOD	LOD	7	1.6	22.8	2.4	4.24	0.84	26.7	4.2	11.3	1.4	1.8	0.24	9.37	0.93	4.24	0.26	34.6	1.8	8.29	0.46	30.3	1.8	4.75	0.34	34.7	1.5	5.61	0.38			0.108	0.042	0.09	0.018
Tarn10ap_43	356	14	1113	23	369	12	4.3	1.5	33.6	3.3	156.8	7.1	32.7	1.7	244	12	117.4	4.7	33.1	1.3	78.8	3.1	26.89	0.98	123.9	4.2	17.37	0.6	37.5	1.3	3.28	0.18	19.3	1.1	2.34	0.16			0.94	0.15	1.16	0.15
Tarn10ap_44	928	18	826	15	926	21	0.41	0.31	25.6	2.4	72	3.4	12.83	0.84	84.2	4.4	45.2	2.4	14.73	0.59	51.8	1.7	27.85	0.85	215.8	4.8	39.2	1.1	93.9	2.5	11.85	0.41	69.6	2.1	8.93	0.36			1.75	0.29	0.417	0.033
Tarn10ap_45	1373	24	1103	21	214	27	2.5	1.1	26.5	2.3	107.3	4.1	19.4	1	122.9	5.7	71.1	2.7	19.68	0.68	62.4	2	21.51	0.77	81.3	4.7	7.46	0.67	12.9	1.9	1.01	0.22	7	1.2	0.79	0.15			0.64	0.11	1.38	0.23
Tarn10ap_46	280	10	2165	36	1324	27	LOD	LOD	125.4	7.7	493	29	87.8	5.1	535	27	305	12	93.6	2.6	213.4	6.7	75.2	1.7	386.6	7.2	58.8	1.3	138.1	3	15.37	0.45	84.2	2.1	9.25	0.31			1.05	0.11	0.465	0.029
Tarn10ap_47	1323	24	418	12	831	22	5.6	1.3	553	17	1741	94	256	6.8	1212	30	313.6	8.5	11.26	0.53	272.1	6	48.5	1.2	183.4	4.4	30.44	0.7	97.2	2.5	9.61	0.32	54.3	1.9	6.53	0.28			33.8	0.74	8.53	0.22
Tarn10ap_48	791	15	619	15	372.8	8.7	LOD	LOD	19.8	1.8	76.1	3.5	13.98	0.91	85.2	5	47.7	2	16.93	0.64	41	1.4	15.91	0.56	93.5	2.5	15.21	0.37	36	1.4	4.09	0.2	21.9	0.94	2.63	0.17			0.813	0.09	0.774	0.033
Tarn10ap_49	669	13	811	18	369	11	1.78	0.52	2.85	0.69	19.5	1.4	6.71	0.57	84.3	4.9	154.6	5.2	38.1	1.2	79.1	2.7	24.9	0.75	108.7	2.9	15.47	0.41	37.2	1.2	4.59	0.2	28.5	1.3	3.56	0.19			3.16	0.25	0.135	0.014
Tarn10ap_50	1335	42	165	14	1278	47	LOD	LOD	802	83	1990	190	253	17	1113	78	312	17	7.47	0.72	291	18	59.3	1.9	283.8	6.4	43.7	1.7	127.3	5.1	14.39	0.75	83.1	3.1	9.53	0.45			349	56	105.5	6.1
Tarn10ap_51	1112	27	280	15	590	33	LOD	LOD	218.1	9.5	710	26	108.1	5.9	551	30	159.1	8.3	4.24	0.51	121.9	4.9	25.46	0.96	109	3.8	19.8	1.3	59.5	2.5	6.88	0.35	42.2	2	5.49	0.4			4.45	0.43	7.69	0.26
Tarn10ap_52	1696	27	931	19	325.3	9.5	6.3	1.1	2588	51	3992	83	311	6.6	928	25	114.7	3.5	25.14	0.74	257.5	4.8	22.68	0.53	58.6	1.8	11.08	0.33	45.9	1.4	4.02	0.19	26.33	0.87	3.75	0.2			86.4	1.7	11.22	0.23
Tarn10ap_53	864	31	414	20	617	25	0.74	0.5	321	13	1057	36	151.4	5	715	31	228.4	7.6	7.88	0.61	187.7	6.1	39.8	1.6	161.1	4.9	23.7	1.1	68.9	3	6.51	0.38	36.6	2.2	4.52	0.34			LOD	LOD	45.5	1.4
Tarn10ap_54	857	15	825	17	459	13	LOD	LOD	20.8	1.7	93.5	4.1	20.7	1.1	152.8	7.1	182.9	6.7	15.05	0.55	104.9	2.6	30.93	0.79	138.7	3.2	20.46	0.55	48.7	1.5	6.04	0.27	37.9	1.2	4.75	0.18			1.157	0.09	1.438	0.05
Tarn10ap_55	1320	22	535	13	937	19	10.6	1.5	542	12	1663	36	248.1	5.9	1206	25	304.5	5.6	15.15	0.47	255.1	4.9	46.99	0.86	183.7	3.4	31.55	0.61	99.7	1.9	10.61	0.29	63.6	1.4	7.9	0.25			24.91	0.5	5.38	0.12
Tarn10ap_56	1258	18	446	11	888	18	2.98	0.7	696	17	2149	41	304.6	6.9	1466	28	346.1	7.7	11.02	0.49	308.4	6.5	53.4	1.1	198.9	5.1	32.7	0.72	102.5	2.4	9.65	0.31	53.9	1.6	6.46	0.23			26.24	0.56	13.53	0.27
Tarn10ap_57	1606	31	559	13	569	14	LOD	LOD	340.2	9.7	1024	27	143	3.9	684	20	165.4	4.6	8.42	0.41	152.6	4.1	26.71	0.65	109.1	2.6	19.68	0.52	60.4	1.6	6.56	0.31	40.9	1.3	5.16	0.24			5.05	0.21	7.46	0.18
Tarn10ap_58	320	10	447.8	9.6	86.1	3.8	LOD	LOD	0.52	0.23	3.04	0.59	0.7	0.19	3.86	0.9	1.56	0.32	0.62	0.1	1.99	0.33	1.04	0.1	9.89	0.62	2.98	0.15	11.27	0.54	1.66	0.1	8.68	0.53	1.14	0.11			0.008	0.007	0.011	0.004
Tarn10ap_59	1355	30	185.5	8	2155	43	0.38	0.35	496	11	1752	41	292.9	8.6	1555	42	496	10	8.83	0.5	367.7	9.2	82	2	390	7.7	69.6	1.5	215.6	5	28.52	0.76	184.2	4.3	23.52	0.82			32.96	0.95	32.43	0.61
Tarn10ap_60	1819	33	301	7.9	1316	27	0.18	0.18	540	14	1756	37	276.9	6.5	1354	39	367.2	8.8	9.13	0.5	315.2	6.1	61.1	1.2	271.4	6	47.11	0.94	148.2	2.7	17.55	0.41	113.6	2.8	14.74	0.38			18.76	0.47	23.11	0.4
Tarn10ap_61	15410	240	151.8	5.1	962	18	2.05	0.56	1097	21	3205	59	432.7	8.6	1883	37	397.9	7.8	8.38	0.37	417.3	7.6	61.3	1.2	204.3	3.3	33.89	0.68	118.4	2.4	11.96	0.33	76.6	1.5	10.04	0.33			23.9	2.5	10.26	0.19
Tarn10ap_62	532	14	424	11	516	13	5.5	2.9	138	21	294	47	33.9	5.8	128	22	29.1	4	6.64	0.75	37.7	4.9	8.59	0.49	67.1	2.1	19.28	0.68	69.7	2.4	10.83	0.36	65.1	2	8.88	0.39			5.44	0.34	1.534	0.089
Tarn10ap_63	526	12	419	10	84.9	3.6	LOD	LOD	16.6	1.5	35.3	2.6	4.21	0.48	18.4	2.1	4.69	0.61	1.09	0.15	4.9	0.53	1.39	0.14	9.57	0.68	2.71	0.17	10.59	0.53	1.94	0.1	13.3	0.67	2.14	0.11			3.45	0.3	1.296	0.067
Tarn10ap_64	1518	50	422	20	562	24	LOD	LOD	458	20	1357	55	191.7	7.9	904	41	247	15	7.4	0.61	217.6	6	38.9	1.8	134.8	5.3	19.75	0.7	59.8	2.4	6.03	0.45	37.5	1.9	5.28	0.5			6.19	0.99	17.5	1.1
Tarn10ap_65	499	16	1216	22	1149	30	0.3	0.22	114	27	400	85	73	14	433	77	194	23	56.3	4.8	158	17	52.8	2.6	299.6	9.9	47.66	0.93	116.7	3.2	12.91	0.38	71	1.7	7.85	0.24			0.414	0.046	1.83	0.17
Tarn10ap_66	1323	23	325.5	7.6	963	23	1.81	0.58	395	11	1280	30	202.5	4.9	1013	28	281.3	7	12.04	0.55	223.3	4.7	44.13	0.84	191.1	4.5	33.86	0.79	99.9	2.6	11.39	0.29	66.7	1.6	8.26	0.26			25.78	0.63	11.82	0.28
Tarn10ap_67	1723	24	393.2	9.8	631	14	LOD	LOD	366	10	1091	20	163.8	3.9	755	19	193.4	5.8	5.63	0.27	168.8	3.3	29.35	0.79	119.3	3.1	21.62	0.57	67.4	1.6	7.84	0.24	51.6	1.4	6.92	0.26			2.6	0.12	8.41	0.17
Tarn10ap_68	151.9	7.2	2229	41	157.8	5.2	LOD	LOD	7.9	1	51.6	2.6	12.24	0.77	89.1	4.4	64.1	2.6	16.91	0.6	39.7	1.5	13.15	0.39	60.7	6.2	7.09	0.27	14.38	0.61	1.338	0.097	7.37	0.41	0.74	0.078			0.022	0.011	0.065	0.009
Tarn10ap_69	1519	27	756	13	850	19	6.9	1	558	12	1702	32	243.5	5.6	1106	22	259.9	5.7	18.65	0.67	234.9	5.1	39.66	0.91	165.1	3.1	28.56	0.65	89	2.2	9.3	0.31	53.2	1.4	6.59	0.26			19.51	0.48	4.19	0.11
Tarn10ap_70	573	14	200.5	6.2	473	14	LOD	LOD	4.17	0.82	12	1.3	2.24	0.36	13.7	1.5	8.07	0.85	2.7	0.25	11.87	0.96	4.93	0.26	53.4	1.6	15.71	0.43	55.9	1.3	8.59	0.3	52.2	1.4	7.24	0.27			0.509	0.071	0.954	0.042
Tarn10ap_71	510	12	616	14	398.4	9.1	0.38	0.27	3.53	0.7	8.76	0.91	1.75	0.27	13.8	1.8	6.97	0.82	2.3	0.27	10.99	0.71	4.09	0.2	38.9	1.3	12.51	0.37	49.5	1.1	7.34	0.31	37.5	1.1	4.45	0.21			0.098	0.028	0.102	0.017
Tarn10ap_72	983	20	425	10	463	14	LOD	LOD	20.4	1.6	88.5	3.3	18.5	1.2	129.6	5	93.1	3.4	13.88	0.53	72.1	2.2	26.44	0.66	137.5	3.2	20.34	0.5	46.8	1.4	5.29	0.21	29.56	0.92	3.38	0.2			0.122	0.026	1.208	0.044
Tarn10ap_73	1033	21	1627	24	842	15	LOD	LOD	34.6	2.1	184.8	6.3	40.3	1.5	260.9	8	154.8	4.2	44	1.2	122.6	3.4	44.2	1	234.3	4.5	36.12	0.9	80.9	1.9	8.37	0.28	43.7	1.4	4.69	0.18			0.192	0.031	0.368	0.023
Tarn10ap_74	296	11	1530	30	544	17	LOD	LOD	30.7	2.3	104.5	4.8	19.04	0.97	111	5.6	62.5	2.5	18.98	0.67	59.2	1.8	23	0.77	139.2	3.8	22.82	0.67	57.8	1.6	7.34	0.23	43.5	1.3	5.64	0.23			0.588	0.076	1.043	0.043
Tarn10ap_75	428	14	892	23	716	22	LOD	LOD	17.4	1.8	72.2	4.4	14.77	0.92	91.5	6.3	57.8	3.2	20.13	0.81	62.3	2.9	24.8	0.83	167.4	5	30.29	0.96	75.1	2.4	9.05	0.36	47.5	2	5.36	0.33			0.114	0.032	1.114	0.053
Tarn10ap_76	15040	240	106.9	4.2	1865	40	1.8	0.59	197.6	6.4	735	19	122.6	3.6	596	16	248.2	6.2	7.91	0.37	189.7	4	58.7	1.3	349.2	6.2	63.4	1.3	183.6	3.6	25.9	0.7	169.2	3.2	21.99	0.6			1.64	0.78	47.39	0.91
Tarn10ap_77	1238	23	391	10	1012	29	6	1.4	490	17	1552	43	250.4	6.9	1186	30	327.7	8.6	10.79	0.57	267.1	5.8	48	1.3	203.6	5.1	35.34	0.92	108.8	2.6	12.21	0.37	73.8	2	8.92	0.39			19.97	0.52	9.8	0.22
Tarn10ap_78	1306	22	404	11	994	23	2.52	0.68	620	16	1972	42	300.8	7.5	1379	31	351.1	8.7	11.96	0.48	307.4	4.9	53	1.2	209.1	5.1	35.6	0.9	110.3	2.7	11.17	0.4	64.3	2	7.89	0.33			25.37	0.65	8.66	0.19
Tarn10ap_79	549	14	1456	26	1399	36	LOD	LOD	6.5	1.1	27.9	2.1	5.24	0.62	35.3	3.3	30.1	2.1	8.25	0.46	45.4	1.9	25.65	0.86	240.1	6.2	53.5	1.3	130.5	3.3	13.76	0.54	59.9	2.1	6.25	0.27			0.137	0.032	0.448	0.027
Tarn10ap_80	11310	370	120	12	2455	99	3.8	2.2	2180	270	5520	600	644	61	2470	250	596	42	11.71	0.64	634	56	105.1	5.7	472	15	79.7	2.5	248.9	6.1	30.6	1.1	188	5.9	20.86	0.9			1440	210	160	15

Supporting Information Tables S3.5: Apatite trace-element data (continued)

	55Mn	±	86Sr	±	89Y	±	90Zr	±	139La	±	140Ce	±	141Pr	±	146Nd	±	147Sm	±	153Eu	±	157Gd	±	159Tb	±	163Dy	±	165Ho	±	166Er	±	169Tm	±	172Yb	±	175Lu	±	182W	±	232Th	±	238U	±
Tan10ap_01	11620	290	106.7	7.6	2365	93	2.4	1.1	301	47	1070	98	169	13	764	44	322.2	9.1	7.36	0.52	265	12	73.4	2.3	400	13	76.5	2.6	221.6	6.9	28.5	1.3	186.0	6.5	22.00	0.9					65	21	59.5	2
Tan10ap_02	530	13	964	21	910	23	LOD	LOD	19	1.4	76.8	3.2	14.46	0.98	103.5	5	71.5	2.8	27.12	0.88	91	2.5	39.98	0.93	240.2	5.5	40.1	1	88.6	2.2	9.29	0.31	46.2	1.4	5.05	0.24					0.078	0.02	0.71	0.033
Tan10ap_03	1141	21	917	18	712	17	6.9	1.4	910	27	342.1	8.1	1477	42	388.7	7.3	16.65	0.63	312.1	7.2	43.4	1.1	146.9	3.8	25.39	0.61	84.9	2.1	7.74	0.29	44.6	1.2	5.21	0.29					26.17	0.67	9.79	0.22
Tan10ap_04	1164	22	383	11	1002	29	1.26	0.45	591	18	1877	42	290.4	5.4	1368	31	343.6	8.7	11.85	0.52	295.2	6.4	50.5	1.1	205.4	5.4	35.40	0.86	107	2.6	11.19	0.44	63.8	2	7.79	0.29					25.64	0.68	15.19	0.37
Tan10ap_05	1160	20	785	20	1003	26	4.04	0.76	600	21	1967	56	280.5	5.9	1233	35	370.7	8	19.57	0.72	260.2	7.4	39.93	0.87	156.9	4.6	27.04	0.74	83.2	2.1	8.71	0.24	49.8	1.7	5.67	0.23					27.63	0.86	9.85	0.27
Tan10ap_06	1185	20	3649	9.2	1003	26	3.17	0.67	540	15	1748	43	274.1	6.7	1265	29	339	8.4	9.62	0.43	290.9	5.5	51.2	1.1	215.3	4	37.53	0.91	116.6	2.3	13.07	0.35	80.1	1.9	9.68	0.36					25.39	0.58	14.7	0.34
Tan10ap_07	960	15	3957	8.9	900	18	1.52	0.51	615	14	1936	44	300.9	6.3	1370	33	337.8	7.3	10.96	0.49	3014	5.6	48.6	1.1	191.8	4.9	33.36	0.7	100.6	2.1	9.92	0.29	57.7	1.7	6.68	0.27					24	0.46	17.18	0.3
Tan10ap_08	675	12	1735	33	3161.9	39	444	13	LOD	LOD	42.3	1.4	170.9	3.8	1187	31	387	7.5	75.6	1.9	975.6	20.6	194.5	4.1	31.24	0.7	71.6	2	7.02	0.29	41.6	1.2	4.46	0.21					3.97	0.23	0.107	0.014
Tan10ap_09	993	17	1560	36	723	17	LOD	LOD	42.3	2.4	199	5.8	299.9	7.1	1157	33	387.6	9.4	34.2	0.93	967	19	141.7	3.7	31.24	0.7	71.6	2	7.02	0.29	41.6	1.2	4.46	0.21					1.63	0.11	0.06	0.009
Tan10ap_10	971	12	1734	34	1172	28	1.73	0.63	431	12	1516	36	305.2	7.4	1164	33	305.7	7.6	25.11	0.6	811	17	127.4	3.1	141.7	3.7	33.74	0.95	100	2.5	12.06	0.44	69.9	1.7	7.12	0.28					3.22	0.08	0.064	0.021
Tan10ap_11	2961	96	120.7	2.3	2684	40	1.21	0.11	407.6	7.1	1205	26	84.3	1.9	1421	24	423.5	8.8	10.97	0.43	338.8	7.2	43.79	0.93	242.1	5.6	41.63	0.91	106.3	2.2	12.06	0.36	69.7	1.8	6.93	0.24					29.46	0.97	17.01	0.41
Tan10ap_12	4602	9.4	1219	34	746	25	0.106	0.046	15.46	0.73	48.5	2.4	8.36	0.46	66.1	2.8	84.7	2.1	5.39	0.23	52.1	2	12.67	0.4	114.7	2.3	27.77	0.48	80	1.6	11.21	0.28	72.3	1.8	10.13	0.27	0.172	0.047	0.516	0.053
Tan10ap_13	3426	7.7	2852	69	1001	27	0.241	0.054	265	7.1	1035	27	268	7.1	1113	30	423.5	9.4	21.16	0.77	407.2	8.6	69.4	1.5	340.5	8.4	48	1.1	96.8	2.2	9.92	0.27	46.6	1.3	4.76	0.21	0.16	0.076	0.026	4.21	0.9
Tan10ap_14	2892	64	1276	37	1276	37	0.043	0.022	113.9	3.7	672	19	124.3	3.5	705	19	423.5	9.4	30.1	1.1	2220	43	353.6	7.8	355.4	8.6	81.1	1.8	19.47	0.53	99.7	2.5	14.03	0.4	7.51	0.23	0.049	0.022	2.03	0.65	0.46	0.027
Tan10ap_15	1187	22	1057	34	1057	34	1.57	0.53	513.9	15	1513	41	242.1	6.1	1054	33	423.5	8.5	9.89	0.43	339.3	6.7	48.97	0.73	288.7	6.5	52.4	1.3	129.4	3.1	15.39	0.45	89.4	2.4	9.61	0.34	0.124	0.04	30.63	0.83	1.94	0.24
Tan10ap_16	1734	47	100.9	3.5	2577	82	1.02	0.16	375	13	1248	39	253.2	8.2	1426	41	530	16	5.53	0.23	517	14	83.8	2.2	539	13	100.7	2.1	292.6	6.6	42.03	0.91	282.1	6.6	44	0.9	0.169	0.039	31.69	0.56	25.37	0.52
Tan10ap_17	356	10	961	27	1730	53	0.51	0.19	183	5.1	1030	27	136.4	3.6	1030	28	423.5	9.4	19.63	0.69	1106	23	190.5	4.6	1114	27	25.64	0.61	144.4	3.4	8.76	0.26	51.6	1.4	6.23	0.26	0.211	0.057	0.596	0.026
Tan10ap_18	157.4	3.4	1720	53	1401	43	3.4	1.1	446	13	1676	44	423.5	9.4	1676	43	423.5	9.4	3.23	0.13	265.6	6.5	45.4	1.4	273.3	6.4	65.3	1.5	146	3.4	16.5	1.8	67	1.1	9.4	1.2	0.106	0.035	0.19	0.021	0.478	0.032
Tan10ap_19	565	7.7	1592	31	1202	28	0.34	0.11	66.6	1.8	233.7	5.1	44.6	1	321	7.2	172.5	3.5	53.9	1.1	316.8	5.3	52.31	0.78	318.7	4.1	51.79	0.67	112.5	1.5	11.92	0.23	59.7	1.2	6.3	0.17	0.059	0.023	0.81	0.044	0.551	0.019
Tan10ap_20	885	20	451	12	1150	28	2.34	0.23	755	19	1931	46	423.5	9.4	1676	43	423.5	9.4	13.73	0.43	338.8	7.2	43.79	0.93	242.1	5.6	41.63	0.91	106.3	2.2	12.06	0.36	69.7	1.8	6.93	0.24	0.182	0.058	37.68	0.89	22.43	0.61
Tan10ap_21	1019	14	2351	6.4	1436	34	2.74	0.19	597	16	1593	42	297.6	7.5	1675	43	475	10	9.6	0.29	405.1	7.6	66.47	0.97	323.5	4	66.67	0.82	147.7	2.3	19.72	0.35	119.9	2.3	8.48	0.26	0.182	0.059	31.7	0.79	23.42	0.57
Tan10ap_22	965	11	189.9	3.3	1305	28	4.38	0.34	648	16	1404	34	384.5	8.5	1429	36	423.5	9.4	10.59	0.36	319.9	4.1	45.78	0.57	270.3	3.3	48.03	0.71	127.5	1.8	16.67	0.3	96.1	1.8	11.98	0.23	0.231	0.045	42.6	1.9	19.49	0.47
Tan10ap_23	442	11	505	18	512	20	74	22	9.5	1.1	27.7	2	4.83	0.27	31.1	2	16.83	0.92	4.97	0.31	44.7	2	9.5	0.32	79.7	2.4	17.88	0.41	56.1	1.4	8.25	0.27	52	1.7	6.47	0.23	1.32	0.16	3.35	0.49	4.52	0.32
Tan10ap_24	362.1	7.6	1755	53	2630.6	74	1.62	0.56	1134	24	1444	40	423.5	9.4	1676	43	423.5	9.4	6.24	0.25	2595	0.086	25.92	0.58	304	4.9	40.38	0.6	107.6	1.5	11.96	0.27	59.7	1.1	4.41	0.15	1.73	0.13	0.067	0.010	2.511	0.073
Tan10ap_25	392.7	6.9	1046	20	1134	24	0.016	0.011	70.7	1.6	240	6.2	48.5	1.3	335.6	7.8	184.5	4.5	56.3	1.3	307.1	6.3	49.64	0.92	304	4.9	40.38	0.6	107.6	1.5	11.96	0.27	59.7	1.1	6.3	0.17	0.046	0.017	0.144	0.03	0.483	0.017
Tan10ap_26	706	28	439	13	1126	33	6.36	0.35	683	22	1685	55	299	11	1470	56	377	15	12.26	0.64	302	17	38.8	1.1	213.7	7.1	36.96	0.71	92.7	2.5	10.88	0.34	57.5	1.8	7.28	0.38	0.174	0.11	33.9	1.3	20.01	0.61
Tan10ap_27	1243	28	183.3	5.2	1601	39	3.79	0.25	467	11	1272	33	241.5	7.1	1280	35	390	11	9.19	0.27	341	7.4	51.1	1.1	326.1	5.2	59.18	0.86	164.4	3	24.02	0.54	156.7	3.8	20.79	0.61	0.331	0.069	32.33	0.91	15.2	0.32
Tan10ap_28	637	10	4124	66	739	16	0.042	0.016	59.4	1.4	267.7	5.8	56.8	1.2	380.3	9.3	268	5.5	72.8	1.5	339.2	6	49.2	0.83	249	3.9	33.69	0.53	67	1.1	6.77	0.13	31.66	0.75	3.179	0.095	0.183	0.043	0.228	0.022
Tan10ap_29	379	10	1426	45	1126	33	3.4	2.3	3.03	0.27	10.6	0.72	2.14	0.14	14.6	1.2	9.4	1	3.23	0.24	30.2	1.7	8.74	0.34	111.7	3.1	36.52	0.91	125.4	3.3	15.88	0.55	84.8	2.6	9.58	0.49	0.169	0.032	0.092	0.01	0.111	0.175
Tan10ap_30	3779	80	2304	69	1801	48	0.218	0.046	268.1	5.8	775	22	104.3	2.4	1429	36	423.5	9.4	20.18	0.88	147.3	7.5	22.8	1.4	136	10	23.4	2.5	46.2	4.8	4.03	0.26	35.2	2.5	1.65	0.26	0.069	0.025	0.35	0.066	0.114	0.011
Tan10ap_31	1268	36	2045	9.9	1911	81	2.94	0.29	713	32	1891	84	339	15	1712	74	406	20	7.76	0.37	431	15	64.9	2.2	405	12	74.3	2.2	205.7	6.7	28.7	1.1	178.5	7	22.88	0.84	0.143	0.037	27	1.5	38.5	3.1
Tan10ap_32	1044	26	1902	54	1702	45	1.19	0.21	5.64	0.35	19.8	1.1	4.36	0.26	33.7	2	23.4	1.3	8.84	0.36	79.4	3	19.44	0.46	170.4	4	37.03	0.78	96.9	1.9	11.79	0.33	69.2	1.5	7.63	0.22	38	1.2	4.07	0.16	30.63	0.83
Tan10ap_33	923.6	9.6	1467	41	970	30	3.4	1.1	440	13	1602	44	423.5	9.4	1676	43	423.5	9.4	3.23	0.13	265.6	6.5	45.4	1.4	273.3	6.4	65.3	1.5	146	3.4	16.5	1.8	67	1.1	9.4	1.2	0.106	0.035	0.19	0.021	0.478	0.032
Tan10ap_34	492.1	9.4	1771	54	2577	82	1.02	0.16	375	13	1248	39	253.2	8.2	1426	41	530	16	5.53	0.23	517	14	83.8	2.2	539	13	100.7	2.1	292.6	6.6	42.03	0.91	282.1	6.6	44	0.9	0.169	0.039	31.69	0.56	25.37	0.52
Tan10ap_35	289.7	9.5	1773	51	1951	61	0.094	0.037	30.7	2.1	150.9	5.1	32.6	1.7	197.2	7.4	64	2.2	1.42	0.12	331	9.5	55.8	1.3	362.9	9.5	85.6	2.1	197.2	4.9	26.24	0.58	166.2	4.1	21.81	0.58	0.467	0.049	0.304	0.03
Tan10ap_36	322.7	8.5	339	12	440	17	0.81	0.18	11.28	0.49	26.3	1.2	3.81	0.23	19.2	1	7.92	0.48	7.37	0.32	13.79	0.63	2.973	0.095	32.06	0.81	15.12	0.4	107.2	2.3	30.91	0.76	362	12	80.9	2.6	0.283	0.054	5.24	0.27	0.057	0.009
Tan10ap_37	954	16	2285.7	6.1	915	27	0.218	0.046	268.1	5.8	775	22	104.3	2.4	1429	36	423.5	9.4	20.18	0.88	147.3	7.5	22.8	1.4	136	10	23.4	2.5	46.2	4.8	4.03	0.26	35.2	2.5	1.65	0.26	0.069	0.025	0.35	0.066	0.114	0.011
Tan10ap_38	1456	51	119.9	6.9	1397	66	5.4	1.6	169.5	8.9	590	27	92.5	4.9	490	25	187.6	8.9	13.28	0.64	227	8.7	45.2	1.4	314	6.2	57.71	0.77	153.9	2.5	19.94	0.64	110	4	12.22	0.52	4.68	0.31	0.038	0.051	13.65	0.69
Tan10ap_39	954	16	2285.7	6.1	915	27	0.218	0.046	268.1	5.8	775	22	104.3	2.4	1429	36	423.5	9.4	20.18	0.88	147.3	7.5	22.8	1.4	136	10	23.4	2.5	46.2	4.8	4.03	0.26	35.2	2.5	1.65	0.26	0.069	0.025	0.35	0.066	0.114	0.011
Tan10ap_40	1456	51	119.9	6.9	1397	66	5.4	1.6	169.5	8.9	590	27	92.5	4.9	490	25	187.6	8.9	13.28	0.64	227	8.7	45.2	1.4	314	6.2	57.71	0.77	153.9	2.5	19.94	0.64	110	4	12.22	0.52	4.68	0.31	0.038	0.051	13.65	0.69
Tan10ap_41	576	17	1380	60	757	32	LOD	LOD	10.56	0.93	79	3.6	17.06	0.69	138.2	5.5	89.7	4.1	24.56	0.9	177.4	5.3	26.13	0.7	180.5	3.6	30.29	0.52	70	1.5	7.94	0.23	41.6	1.4	4.81	0.17	0.154	0.035	0.066	0.015	0.424	0.021
Tan10ap_42	190.4	3.7	1711	35	956	25	0.102	0.026	11.96	0.47	47.1	1.3	10.09	0.37	76.5	2.3	52.7	1.5	17.66	0.49	166.1	3.8	33.78	0.7	240.5	4.7	42.51	0.78	89.6	1.8	8.72	0.25	35.2	1.3	2.81	0.12	0.048	0.018	0.581	0.064	0.223	0.012
Tan10ap_43	103.8	3.1	1630	75	768	37	LOD	LOD	62.8	3.1	292	14	57.7	2.7	345	15	172.5	7.3	51.4	2.1	241.7	7.7	41	1.1	225.7	5.1	32.98	0.66	69.2	1.5	7.63	0.22	38	1.2	4.07	0.16	0.061	0.026	0.408	0.028	0.238	0.017
Tan10ap_44	538	17	1693	78	1420	160	0.119	0.034	68	11	263	34	53.2	5.9	474	30	217	15	57.6	3.9	369	32	59.3	4.8	378	37	62.4	6.3	159	20	19	2.6	99	14	10.5	1.7	0.091	0.025	1.09	0.17	1.13	0.19
Tan10ap_45	1066	53	3542	99	1085	27	3.28	0.77	358	8.7	1736	43	474.2	11	1736	43	474.2	11	4.1	0.59	107.7	5	18.72	0.74	130	3.1	27.57	0.53	87.6	2.2	12.06	0.34	73.2	2.1	9.4	1.2	0.106	0.035	0.19	0.02	0.317	0.024
Tan10ap_46	1054	16	199.5	5.5	1743	40	0.78	0.36	494	15	1444	36	205.2	6.7	1531	42	48.1	2.4	13.23	0.41	104.6	3.4	15.85	0.48	100	2.3	19.78	0.37	64	1.1	6.76	0.22	39.8	1.3	4.97	0.21	0.115	0.036	38.1	2.4	1.032	0.096
Tan10ap_47	147.5	4.8	3780	200	986	53	0.065	0.028	38.2	2.5	187	11	39.5	2.2	280	12	155.4	6.6	52.5	2	251	8.3	46.2	1.3	260.5	6	40.32	0.72	125.4	3.3	15.88	0.55	84.8	2.6	9.58	0.49	0.169	0.032	0.092	0.01	0.111	0.175
Tan10ap_48	470	20	1021	59	896	50	0.032	0.022	46.5	2.8	203	11	37.2	2	232	12	131.8	6.3	40.6	1.8	222.4	8.4	41	1.3	243.2	5.5	37.88	0.7	85	1.6	9.66	0.31	47.4	2.2	4.69	0.22	0.143	0.037	27	1.5	38.5	3.1
Tan10ap_49	544	16	656	35	368	14	0.047	0.016	14.11	0.48	44.5	1.5	7.72	0.26	52.6	1.9	28.6	1.1	8.29	0.29	63	1.8	15.48	0.33	151.9	2.8	18.72	0.74	130	3.1	27.57	0.53	87.6	2.2	12.06	0.34	73.2	2.1	9.4	1.2	0.106	0.035
Tan10ap_50	569	18	1342	56	722	32	0.63	0.12	80.9	5.4	163.1	8.7	30.1	1.2	206.8	8.9	93.5	3.6	22.89	0.8	165.9	5	23.95	0.66	145	3.5	26.72	0.46	71.6	1.7	11.14	0.4	84.5	3.8	13.22	0.69	4.4	0.41	0.561	0.063
Tan10ap_51	978	18	412	12	1160	34	0.027	0.016	14.11	0.48	44.5	1.5	7.72	0.26	52.6	1.9	28.6	1.1	8.29	0.29	63	1.8	15.48	0.33	151.9	2.8	19.48	0.33	105	2.7	14.27	0.71	137.1	2.4	12.15	0.33	0.298	0.049	0.065	0.015	0.566	0.023
Tan10ap_52	446	12	1372	58	571	22	0.32	0.11	41.9	2.6	128.2	6.5	22.1	1.4	128.6	5.9	61.5	3.3	13.06	0.7	98.6	3.7	19.86	0.65	129	3.3	23.71	0.51	55.9	1.4	7.28	0.29	43.3	1.7	5.29	0.21	0.113	0.031	1.02	0.24	4.15	0.35
Tan10ap_53	1066	53	3542	99	1085	27	3.28	0.77	358	8.7	1736	43	474.2	11	1736	43	474.2	11	4.1	0.59	107.7	5	18.72	0.74	130	3.1	27.57	0.53	87.6	2.2	12.06	0.34	73.2	2.1	9.4	1.2	0.106	0.035	0.19	0.02	0.317	0.024
Tan10ap_54	3917	9.4	429	20	1901	59	0.81	0.15	17.6	1.6	44	2.9	7.15	0.37	48.1	2.4	44.3	2.9	13.23	0.41	104.6	3.4	15.85	0.48	100	2.3	19.78	0.37	64	1.1	6.76	0.22	39.8	1.3	4.97	0.21	0.115	0.036	38.1	2.4	1.032	0.096
Tan10ap_55	1913	47	3780	200	986	53	0.065	0.028	38.2	2.5	187	11	39.5	2.2	280	12	155.4	6.6	52.5	2	251	8.3	46.2	1.3	260.5	6	40.32	0.72	125.4	3.3	15.88	0.55	84.8	2.6	9.58	0.49	0.169	0.032	0.092	0.01	0.111	0.175
Tan10ap_56	1401	49	2460	110	820	31	LOD	LOD	37	2.4	170	10	35.6	1.8	241	12	142.2	6.6	46	2.1	282.1	7.9	45.4	1.4	310	6.2	34.7	0.91	62.7	1.9	6.35	0.24	29	1.3	2.99	0.17	0.116	0.032	7.2	1.4	0.72	0.11
Tan10ap_57	1426	45	656	35	368	14	0.047	0.016	14.11	0.48	44.5	1.5	7.72	0.26	52.6	1.9	28.6	1.1	8.29	0.29	63	1.8	15.48	0.33	151.9	2.8	19.48	0.33	105	2.7	14.27	0.71	137.1	2.4	12.15	0.33	0.298	0.049	0.065	0.015	0.566	0.023
Tan10ap_58	1085	27	412	12	1160	34	0.027	0.016	14.11	0.48	44.5	1.5	7.72	0.26	52.6	1.9	28.6	1.1	8.29	0.29	63	1.8	15.48	0.33	151.9	2.8	19.48	0.33	105	2.7	14.27	0.71	137.1	2.4	12.15	0.33	0.298	0.049	0.065	0.015	0.566	0.023
Tan10ap_59	338.7	9.3	309	14	434	19	0.067	0.021	20.6	1	53.4	2.4	10.02	0.52	64.8	3.1	62	3.2	3.12	0.14	82	3.6	11.12	0.43	111.2	2.2	27.39	0.46	80.1	1.5	13.63	0.35	73.6	1.9	10.07	0.37	0.197	0.047	2.93	0.36	1.031	0.054
Tan10ap_60	824	25	439	13	710	23	0.035	0.024	24.4	1.8	66.8	3.5	10.61	0.61	62	3.2	31.2	1.3	11.14	0.46	69.6	2.6	13.07	0.42	111.2	2.2	27.39	0.46	80.1	1.5	13.63	0.35	73.6	1.9	10.07	0.37	0.197	0.047	2.93	0.36	1.031	0.054
Tan10ap_61	805	25	403.3	54	723	19	0.28	0.07	160	35	560	100	107	17	622	86	242	21	68.1	4	310	15	45.4	1.3	233.4	5.7	34.7	0.91	62.7	1.9	6.35	0.24	29	1.3	2.99	0.17	0.116	0.032	7.2	1.4	0.72	0.11
Tan10ap_62	847	25	252.6	7.6	1664	65	2.74	0.21	615	19	1696	56	321	13	1736	70	518	26	11.16	0.37	465	20	63	2	368.3	8	71.2	1.5	173.8	5.8	23.68	0.83	140.8	4.7	19.46	0.64	0.134	0.043	58.6	2.2	36.3	1.5
Tan10ap_63	510.4	8.7	2670	65	967	22	LOD	LOD	45.4	1.2	209.7	4.6	44.7	1	286.8	7.4	168.9	3.8	51.5	1.1	276.2	5.3	48.14	0.9	275.4	3.2	44.47	0.56	90.2	1.4	9.88	0.2	50.7	1.1	5.58	0.16	0.062	0.02	0.322	0.024
Tan10ap_64	644	23	2673	38	1483	43	0.81	0.12	946	32	2070	46	417.2	6.6	1798	36	484.9	9.4	57.69	0.94	334.1	4.9	61.83	0.96	146.8	2.2	9.21	0.34	61.83	0.96	146.8	2.2	9.21	0.34	0.151	0.033	14.41	0.24	0.151	0.033
Tan10ap_65	622	17	669	30	885	43	0.238	0.053	15.93	0.86	60.6	2.6	14.58	0.64	120.4	5.1	76	3	19.38	0.66	162.1	4.9	28.48	0.95	182.3	3.6	35.41	0.64	88	1.7	11.75	0.31	71.3	2.2	9.21	0.34	0.299	0.046	0.628	0.04	1.127	0.056

Supporting Information Tables S3.5: Apatite trace-element data (continued)

	55Mn	±	86Sr	±	89Y	±	90Zr	±	139La	±	140Ce	±	141Pr	±	146Nd	±	147Sm	±	153Eu	±	157Gd	±	159Tb	±	163Dy	±	165Ho	±	166Er	±	169Tm	±	172Yb	±	175Lu	±	182W	±	232Th	±	238U	±
Tarn11ap_66	936	14	290.2	7	977	24	0.361	0.051	442	11	1193	26	205.9	5.1	1046	26	282.8	6.2	6.29	0.21	234.1	5	31.61	0.59	181.1	2.9	33.29	0.51	85.8	1.2	11.62	0.21	70.6	1.3	9.05	0.21	0.087	0.028	16.07	0.34	26.97	0.56
Tarn11ap_67	992	23	242.8	9.6	1361	53	5.74	0.32	568	20	1514	57	264.8	9.8	1330	43	367	13	9.56	0.36	311.1	7.4	45.69	0.97	275.8	4.7	51.32	0.79	135	2.2	19.06	0.42	119.2	2.8	15.68	0.53	0.058	0.022	28.1	0.97	16.2	0.6
Tarn11ap_68	389.2	8.2	1259	41	782	27	LOD	LOD	40.5	2.5	163.4	7.3	33.7	1.3	249.8	8.7	144.4	4.5	46	1.4	247.7	6.4	39.41	0.78	223	3.4	34.06	0.52	69.9	1.2	7.37	0.18	34.9	1	3.67	0.14	0.138	0.034	0.092	0.011	0.364	0.018
Tarn11ap_69	288.4	8.5	267	12	409	18	LOD	LOD	12.58	0.65	43.2	1.8	7.69	0.35	50.2	2.5	35.5	1.4	3.86	0.2	84.9	3	13.8	0.4	85	1.8	14.83	0.26	43.03	0.89	6.22	0.19	41.1	1.5	5.78	0.27	0.087	0.024	2.35	0.17	0.64	0.032
Tarn11ap_70	261.4	8.4	234.9	8.8	122.9	4.7	0.019	0.013	1.31	0.11	3.11	0.18	0.502	0.053	2.79	0.28	1.39	0.17	0.621	0.057	3.71	0.29	1.014	0.049	10.9	0.44	3.52	0.11	16.53	0.45	3.38	0.12	31.1	1.1	6.16	0.27	0.53	0.072	0.048	0.009	0.112	0.009
Tarn11ap_71	852	14	1243	31	584	16	0.242	0.069	25.62	0.89	91.7	2.7	17.64	0.53	123.7	3.7	79.4	1.8	16.97	0.43	119.6	2.6	19.23	0.38	122.3	2.4	22.02	0.39	61.3	1.1	8.65	0.17	59	1.1	8.39	0.21	0.387	0.069	0.151	0.013	0.529	0.023
Tarn11ap_72	1763	45	592	21	822	33	0.221	0.044	66.2	3.3	201.7	8.8	31.7	1.4	168.6	7.8	62.4	2.5	5.82	0.21	81.6	2.8	14.89	0.43	113.5	2.4	25.1	0.4	92.4	1.7	15.69	0.39	118.8	3.6	17.95	0.69	1.17	0.1	3.11	0.29	8.1	0.33
Tarn11ap_73	2147	44	180.6	6.1	2925	99	2.05	0.14	230.5	8.7	966	36	181.5	6.6	1024	34	500	16	16.35	0.52	579	15	105.6	2.5	702	11	124.5	1.9	356.2	6.3	49.1	1.2	305.3	8.4	38.6	1	0.119	0.035	47.1	1.4	278	10
Tarn11ap_74	945	21	522	17	983	30	0.565	0.067	756	23	1820	60	307	10	1480	47	369	11	10.84	0.35	310.7	7.6	39.33	0.82	216.2	3.7	35.9	0.49	90.3	1.6	10.57	0.26	55.6	1.4	6.75	0.22	0.083	0.026	29.87	0.93	25.93	0.77
Tarn11ap_75	915	15	204	5.4	1996	58	0.464	0.065	474	12	1404	40	271.6	7.4	1503	38	485	12	7.03	0.24	438.3	7.8	65.2	1.3	396.8	6.4	71	1.1	204.6	3.4	29.19	0.62	191.7	3.9	25.21	0.57	0.146	0.032	25.56	0.55	28.89	0.68
Tarn11ap_76	954	16	152.9	5.3	2438	77	9.04	0.4	299.2	9.8	1084	29	203.2	6.7	1188	35	462	13	6.23	0.22	469.5	9.9	75.7	1.4	489.3	7.4	87.8	1.2	256.2	3.6	36.49	0.61	232.3	5.1	30.46	0.77	0.122	0.036	27.09	0.63	9.57	0.27
Tarn11ap_77	378.6	6.4	727	20	783	22	0.052	0.02	8	0.33	29.2	1.9	5.03	0.19	36	1.1	29	1	10.85	0.35	104.8	2.3	22.24	0.45	160.9	3.4	28.6	0.5	73.4	1.3	9.3	0.23	52.6	1.4	6.24	0.18	0.149	0.032	0.884	0.061	2.621	0.085
Tarn11ap_78	891	16	332	10	1098	30	0.609	0.073	551	15	1453	45	261.1	7.7	1337	38	369	11	10.1	0.33	307.7	8.3	40.46	0.87	231	4.5	39.46	0.68	100.4	1.6	12.41	0.31	67.7	1.6	8.41	0.23	0.244	0.049	26.63	0.71	25.52	0.78
Tarn11ap_79	1838	56	265	12	1338	61	0.596	0.08	381	15	1134	35	196.2	7.5	1039	39	316	13	8.05	0.38	276.8	9.9	42.9	1.5	260.8	7.8	46.7	1.2	132.3	3.2	19.3	0.65	125	5.3	16.44	0.65	0.095	0.032	23.14	0.87	33.2	1.3
Tarn11ap_80	677	11	193.2	4.1	1600	38	2.04	0.17	368.5	9.1	1190	31	206.3	4.7	1133	26	360.6	8.2	10.33	0.33	341	6.6	50.8	0.8	315	4.7	57.2	1.1	163.2	3	23.34	0.42	146.8	2.6	19.74	0.42	0.128	0.034	29.99	0.59	31.11	0.6
Tarn11ap_81	898	14	315.7	9.2	1386	33	0.735	0.077	671	17	1781	50	317.6	7.7	1640	38	452	10	11.76	0.38	375.1	7.7	51.34	0.99	302.2	4.7	53.58	0.93	147.8	2.6	21.31	0.4	140.2	3	19.21	0.52	0.248	0.05	39.8	1	33.22	0.75
Tarn11ap_82	122.6	3.7	2080	64	642	28	0.025	0.013	1.81	0.14	7.13	0.34	1.64	0.11	17.3	1	35	1.1	25.88	0.82	194.5	6.3	38.68	0.99	208.9	5.8	29.22	0.94	56.5	1.9	6.03	0.27	34.3	1.5	4.65	0.22	0.079	0.026	1.11	0.048	1.998	0.062
Tarn11ap_83	829	13	298.8	5.4	859	21	0.119	0.04	382.7	8	1068	21	170.9	3.7	850	19	256.1	5.2	8.04	0.25	250.9	4.7	36.78	0.68	214.5	3.9	36.14	0.67	84	1.6	9.23	0.21	48.1	1.2	5.61	0.16	0.101	0.034	3.513	0.095	83.3	1.2
Tarn11ap_84	126.5	3.7	765	11	120.8	2.4	0.71	0.15	74.6	1.5	235.3	4.9	38.79	0.77	217.6	4.9	59.2	1.7	29.06	0.67	60.6	1.2	6.94	0.2	31.79	0.85	4.68	0.16	10.17	0.36	1.075	0.071	5.06	0.31	0.531	0.055	0.102	0.034	0.948	0.073	0.072	0.011
Tarn11ap_85	318	16	319	15	21.5	1.5	0.143	0.062	0.074	0.036	0.41	0.14	0.098	0.042	0.46	0.17	0.24	0.11	0.09	0.037	0.48	0.2	0.13	0.032	1.86	0.23	0.729	0.081	3.17	0.29	0.636	0.074	5.45	0.49	0.781	0.058	5.56	0.64	0.23	0.12	0.033	0.018
Tarn11ap_86	90.7	1.7	2080	26	1049	22	0.078	0.039	85.1	1.5	364.6	6.6	74.8	1.3	478.8	9	255.7	4	88.6	1.3	373	4.9	56.95	0.73	319.3	5.1	48.45	0.68	94.8	1.6	9.73	0.21	42.04	0.99	4.01	0.11	0.081	0.026	1.507	0.057	0.152	0.01
Tarn11ap_87	1430	20	226.7	3.9	1945	36	0.443	0.088	378.9	7.2	1212	22	204.1	3.7	1067	19	350.5	6.5	4.73	0.18	322.3	6	52.3	1	345.1	5.7	70.8	1.3	207.7	3.5	35.36	0.65	239	4.2	34.09	0.69	0.095	0.033	10.25	0.28	12.86	0.28
Tarn11ap_88	875.2	9.2	468	5.6	702	12	0.026	0.015	776	11	1865	31	303	4.3	1456	22	375.6	5.4	11.07	0.26	314.5	3.8	37.42	0.52	177	2.7	26.65	0.41	54.99	0.91	6.54	0.15	33.89	0.75	4.25	0.1	0.173	0.044	6.54	0.12	20.2	0.29
Tarn11ap_89	471	11	790	29	648	26	0.577	0.084	103.3	4.1	448	17	96	4	650	24	235.1	9.1	63.6	2.5	237.5	7.9	26.48	0.79	136.2	3.8	23.76	0.64	51.6	1.5	6.23	0.22	33.7	1.2	4.77	0.18	2.75	0.21	7.87	0.36	23.46	0.96
Tarn11ap_90	1174	9.5	312.7	4.8	1295	22	1.25	0.11	532.8	6.8	1374	17	244.2	3.2	1239	18	343.6	4.9	12.22	0.28	291.6	3.9	42.12	0.61	250.9	3.7	48.52	0.62	120.3	1.9	16.95	0.3	97	1.6	12.21	0.27	0.098	0.024	33.55	0.4	27.47	0.31
Tarn11ap_91	270	11	573	36	477	35	0.053	0.031	6.4	1.4	22.1	5.5	4.2	1.1	24	5.7	12.2	2.7	4.04	0.76	21.1	2.7	4.5	0.37	46.6	2.4	15.85	0.44	60.3	1.7	11.59	0.41	80.7	3.7	11.72	0.69	0.128	0.037	2.23	0.92	0.111	0.01
Tarn11ap_92	544	13	2191	54	822	20	0.348	0.093	7.15	0.35	26.4	1	5.19	0.24	35.2	1.9	18.85	0.78	8.21	0.3	40.7	1.2	9.17	0.23	86.9	1.5	28.08	0.42	94.1	1.5	15.12	0.36	86.9	1.9	11.3	0.23	0.132	0.03	0.782	0.096	0.371	0.024
Tarn11ap_93	213.6	2.7	1334	23	776	15	0.013	0.01	3.3	0.16	13.54	0.45	2.72	0.13	21.1	1.1	13.35	0.53	5.26	0.18	38.66	0.92	9.53	0.14	96.4	1.6	28.86	0.37	77.3	1.2	9.8	0.19	44.9	1.2	4.68	0.13	0.076	0.025	0.074	0.018	0.294	0.012
Tarn11ap_94	980	28	202.4	7	1134	37	0.2	0.045	626	23	1502	50	257.3	9.5	1195	34	317	11	6.79	0.32	266.9	8.5	37.2	1	224	4.6	44.2	0.76	103.9	1.9	14.91	0.38	86	2.8	11.17	0.35	0.84	0.1	12.3	0.55	24.95	0.91
Tarn11ap_95	87.5	2.8	14110	540	1181	45	LOD	LOD	112.4	4.6	471	19	92.1	4	573	25	312	13	109.8	4.4	463	17	73.6	2.2	386.4	9.3	62.3	1.1	117.6	3.1	13.38	0.52	60.2	2.2	6.28	0.27	0.071	0.025	2.23	0.12	0.481	0.025
Tarn11ap_96	997	25	1538	43	474	13	9.56	0.4	1681	51	3143	84	383	11	1440	44	223.7	6.8	53	1.7	160.1	5	18.84	0.5	101.5	1.8	19.86	0.31	43.34	0.71	5.52	0.17	29.23	0.98	3.79	0.14	0.052	0.019	88.2	2.5	12.53	0.37
Tarn13ap_0	201.2	3	4863	76	784	14	0.023	0.017	18.36	0.57	65	1.3	13.18	0.34	121.3	3.1	68.7	1.4	22.01	0.48	157.4	2.8	29.72	0.42	186.2	3.2	30.95	0.45	65.9	1	7.09	0.14	32.62	0.74	3.333	0.093	0.03	0.014	0.28	0.15	0.072	0.013
Tarn13ap_1	1232	94	1022	22	478.5	8.5	1.01	0.16	15.77	0.54	49.7	1.4	8.54	0.31	63	2.1	25.51	0.84	4.1	0.18	46.8	1.1	10.32	0.25	78	1.6	17.43	0.32	52.6	1.1	7.88	0.17	51.6	1	7.2	0.16	0.302	0.052	LOD	LOD	0.747	0.043
Tarn13ap_2	567	11	753	15	479	11	0.68	0.13	28.87	0.81	73.3	2.1	10.35	0.42	61.9	2.6	30.2	1.2	16.01	0.4	75.2	1.5	14.29	0.3	90.5	1.6	17.38	0.25	48.21	0.84	7.29	0.19	47.75	0.99	6.96	0.2	0.39	0.087	2.89	0.14	6.41	0.15
Tarn13ap_3	728	14	1620	140	856	20	3.24	0.42	98.6	8.4	229	16	37.9	2.1	289	11	143.8	4.3	46.1	1.7	277.4	5	45.13	0.93	242.3	5.7	36.92	0.81	79.9	2	8.83	0.25	44.6	1.3	5	0.2	0.139	0.051	1.05	0.16	0.951	0.094
Tarn13ap_4	997	14	1229	19	335.7	5.9	6.48	0.24	2479	48	3304	61	293	5.8	1113	23	112.8	2.3	26.73	0.64	83.6	1.6	10.08	0.2	55.3	1.2	10.7	0.19	29.59	0.59	4.13	0.077	25.68	0.55	4.02	0.1	0.052	0.018	96.3	1.4	14.12	0.23
Tarn13ap_5	3374	74	233.4	4.4	1453	35	0.128	0.032	94.7	2.2	364.4	7.3	66.2	1.5	474	9.6	182.5	3.3	9.75	0.21	253.9	3.6	49.28	0.8	329	4.8	63.62	0.92	167.1	2.3	22.02	0.39	129.6	1.6	16.92	0.29	1.49	0.11	0.601	0.048	33.68	0.58
Tarn13ap_6	213.2	5.2	319.4	7.4	916	19	2.75	0.3	302	8.9	922	26	157.2	5.1	1061	26	244.2	4.8	10.27	0.3	253.1	4.8	34.26	0.78	187.3	4.5	33.61	0.93	80.5	1.8	9.33	0.26	47.9	1.4	6.4	0.22	0.017	0.016	28.82	0.65	9.58	0.17
Tarn13ap_7	106.8	1.6	15700	150	344.2	4	2.55	0.13	2001	23	2583	32	266.4	3.5	1123	15	143.5	2	40.5	0.6	116	1.6	13.92	0.21	71.4	1.2	11.91	0.23	26.29	0.43	2.727	0.076	12.58	0.3	1.429	0.054	0.161	0.034	27.29	0.31	3.329	0.06
Tarn13ap_8	287.3	3.7	1354	18	754	44	0.47	0.11	15.73	0.39	74.3	1.2	18.05	0.4	188.2	4	103.8	2.4	26.53	0.65	181.2	5.1	28	1.1	169.4	8.5	30.4	1.8	68	4.3	7.92	0.67	38.9	3.3	4.76	0.57	0.201	0.043	0.191	0.032	0.284	0.041
Tarn13ap_9	372	4.8	469.2	7.9	322	5.4	0.34	0.13	50.5	1	175.4	3.2	34.05	0.75	274.2	5.4	77.4	1.5	16	0.33	80.8	1.2	10.1	0.18	56.2	1	11.15	0.18	28.86	0.51	3.69	0.1	22.2	0.52	3.444	0.095	0.458	0.057	1.41	0.13	21.33	0.4
Tarn13ap_10	326.3	5	95.8	2	971	21	0.294	0.048	266.6	6.7	790	17	118.7	2.3	741	15	159.4	2.9	6.63	0.22	168.8	2.8	24.28	0.4	153.4	3	33.51	0.61	103.4	2	15.77	0.33	111.1	2.4	19.63	0.48	10.73	0.34	11.47	0.3	9.25	0.22
Tarn13ap_11	306.4	4.6	2520	46	1399	29	0.037	0.017	11.33	0.33	38.9	1	7.81	0.24	70.4	2	38.48	0.87	12.42	0.27	127.4	2.4	32.37	0.57	286.5	4.4	61.18	0.94	141.1	2.1	15	0.24	69.1	1.2	7.57	0.19	0.058	0.022	0.877	0.094	0.31	0.015
Tarn13ap_12	4.11	0.86	304.9	3.8	170.4	2.6	0.2	0.11	63.2	1.1	142.1	2.5	27.34	0.58	169.7	3.7	36.02	0.88	8.87	0.22	37.2	0.74	4.85	0.13	27.16	0.69	4.6	0.11	9.16	0.23	0.812	0.041	2.45	0.18	0.191	0.018	0.051	0.019	2.25	0.074	0.447	0.048
Tarn13ap_13	275.8	4.1	141.8	3	511	12	0.64	0.1	416	11	1018	22	142.8	3.5	737	20	127.2	3	4.16	0.16	114.8	2.4	14.21	0.26	84	1.7	17.92	0.39	52.79	0.9	8.34	0.2	60.6	1.2	10.32	0.24	3.79	0.23	12.1	1	7.83	0.43
Tarn13ap_14	4310	66	203.6	3.6	1789	30	0.65	0.15	205	4.5	709	14	118.6	2.4	605	12	268.5	5	9.2	0.24	309.2	5.4	56.48	0.97	366.8	5.1	70.3	1.2	188	2.8	25.65	0.43	148.7	2.3	17.91	0.34	0.184	0.038	32.9	1.5	67.2	1.5
Tarn13ap_15	127.5	2.5	922	16	1002	21	0.055	0.036	30.08	0.8	112.7	2.8	22.46	0.64	152.2	4.1	101.3	2.5	36.22	0.83	261.6	4.2	46.26	0.76	274	4.7	44.92	0.82	98.1	1.8	10.98	0.24	53.63	0.99	5.77	0.14	0.052	0.021	0.81	0.45	1.193	0.057
Tarn13ap_16	1027	12	1487	17	421.3	6.3	12.22	0.33	1296	22	2582	44	314.6	5.1	1146	19	191.4	3.4	44.25	0.75	141.8	2.5	16.55	0.27	85.8	1.4	15.17	0.27	36.35	0.54	4.45	0.12	24.43	0.46	3.074	0.082	0.044	0.018	65.5	1.9	30.8	2.7
Tarn13ap_17	1663	24	596.9	9.5	794	16	0.072	0.031	42.71	0.99	145.7	2.9	22.79	0.49	106.2	2.1	42.9	1.2	8.34	0.2	59.6	1.2	13.02	0.22	105.7	1.5	26.77	0.41	81.7	1.4	9.81	0.17	43.7	0.94	4.03	0.13	0.19	0.043	1.19	0.34	4.63	0.1
Tarn13ap_18	3359	45	148.7	3.4	1825	43	0.71	0.11	161.2	3.9	651	17	113.6	2.9	570	15	277.4	6	6.7	0.19	324.7	6.9	62.3	1.2	415.2	7.8	80.3	1.2	217.5	3	31.38	0.65	197.2	3.7	25.31	0.64	0.069	0.031	5.14	0.2	117.3	3.1
Tarn13ap_19	207.6	3.2	184.2	4	1216	26	1.482	0.089	1630	37	3961	92	575	11	2361	50	475.6	9	68.2	1.3	394	6.5	49.67	0.89	273.9	4.3	49.59	0.72	123.4	1.6	15.1	0.22	83.3	1.2	10.53	0.22	0.065	0.021	73.8	1.3	20.7	0.44
Tarn13ap_20	358	4.9	1506	21	54.7	2.2	2.86	0.39	20	1.4	67.1	4.6	10.15	0.62	51.7	2.9	14.73	0.73	3.76	0.16	14.33	0.73	1.792	0.089	9.61	0.49	1.88	0.093	4.57	0.21	0.543	0.041	3.23	0.2	0.51	0.029	0.429	0.057	5.93	0.73	0.609	0.028
Tarn13ap_21	178.2	3.1	476.6	9.7	434.1	9.1	2.54	0.17	278.1	6.1	802	16	126.1	2.9	655	14	162.9	3.3	32.74	0.66	157.9	2.5	18.32	0.3	93.8	1.5	15.98	0.26	34.73	0.59	3.77	0.1	18.4	0.5	2.241	0.083	0.028	0.014	12.64	0.3	5.25	0.13
Tarn13ap_22	809	12	261.3	5.2	1044	19	0.58	0.21	247.9	5.9	820	18	138.1	2.9	736	18	236.4	4.2	4.34	0.18	215.3	4	30.75	0.54	177.7	3.2	33.87	0.61	91.8	1.7	13.46	0.3	85.6	1.6	11.85	0.25	0.09	0.033	6.18	0.13	10.63	0.18
Tarn13ap_23	650.1	9.5	123.7	2.6	1095	27	0.018	0.012	9.6	0.37	36.6	0.92	7.32	0.23	47.6	1.5	31.5	1.2	4.61	0.18	67.5	1.5	15.73	0.31	141.1	2.3	40.16	0.56	150	1.9	25.38	0.36	169.2	2.6	25.08	0.48	0.894	0.094	0.14	0.016	3.962	0.087
Tarn13ap_24	254.1	3.4	436	6.9	249	4.7	4.3	0.21	261.5	5.9	963	21	160.5	3.9	775	18	134.2	2.6	38.06	0.72	97	2	10.52	0.22	53.6	1.1	9.54	0.2	23.08	0.51	3.002	0.095	17.81	0.51	2.748	0.082	0.891	0.081	59	1.4	36.68	0.8
Tarn13ap_25	1312	19	1139	42	2054	55	0.531	0.087	146.9	5.8	595	20	106.3	3	606	14	293.8	4.9	13.97	0.62	384.2	5.9	71.8	1.5	447	11	82	2.2	206.8	6.3	26.41	0.87	144.2	6.1	16.69	0.82	0.203	0.04	7.54	0.47	41.94	0.81
Tarn13ap_26	221.5	4.1	7380	140	813	17	0.023	0.012	48	1.4	198.4	4.9	37.3	1.1	244.1	6.2	142.1	3.5	44.11	0.85	243.4	4.4	40.36	0.73	217.5	3.9	34.72	0.68	76.3	1.3	9.45	0.19	52	1.2	6.29	0.15	0.059	0.023	1.962	0.086	0.815	0.029
Tarn13ap_27	222.2	3.3	3001	41	1459	87	0.64	0.16	9.94	0.64	35.9	2.3	7.96	0.66	51.7	2.5	31.6	2.4	7.41	0.39	81.2	6.1	19.8	1.6	188	13	51.7	3.5	155	12	20.1	1.9	100	11	11.3	1.5	0.567	0.08	0.637	0.087	1.42	0.21
Tarn13ap_28	610.4	6.8	747.3	8.4	668	8.1	0.042	0.028	17.04	0.45	62.93	0.96	13.19	0.33	105.8	2.5	70.5	1.4	22.4	0.43	156.4	2.6	26.05	0.35	155.4	2.1	27	0.4	60.53	0.93	7.1	0.13	38.44	0.71	4.24	0.11	0.088	0.025	0.36	0.25	0.284	0.02
Tarn13ap_29	986	13	1350	17	294.8	4.5	6.64	0.25	2060	37	2874	55	265	4	838	11	102.1	1.9	23.33	0.37	75	1.5	8.95	0.16	49.02	0.78	9.69	0.22	26.53	0.47	3.638	0.085	22.75	0.5	3.208	0.086	0.05	0.022	79.4	1.1	12.32	0.2
Tarn13ap_30	1040	13	393.7	5.1	1011	20	0.2	0.037	610.3	9.5	1470	21	251.1	3.8	1292	17	339.4	3.9	11	0.23	282.6	3.8	37.56	0.52	203.2	3.2	36.54	0.55	92.2	1.6	12.56	0.24	77.3	1.4	9.61	0.23	0.934	0.082	20.77	0.85	23.04	0.31
Tarn13ap_31	216.5	2.7	189.4	2.8	157.4	2	0.135	0.03	5.23	0.23	19.1	0.47	3.65	0.13	24.56	0.89	10.69	0.48	2.63	0.12	18.14	0.56	3.319	0.096	23.85	0.56	5.38	0.14	15.45	0.37	2.063	0.074	11.78	0.38	1.729	0.073	1.45	0.15	1.815	0.072	2.756	0.059
Tarn13ap_32	964	13	1280	23	541	11	0.086	0.04	28.9	3.3	77.1	6.4	12.35	0.78	86	3.8	35.6	1.3	9.91	0.33	66.3	1.7	10.77	0.26	74.3	1.2	18.32	0.29	67.1	1.1	12.77	0.25	104	2	17.39	0.36	0.46	0.089	8.3	1.3	0.263	0.019
Tarn13ap_33	290.9	5	156.1	3.2	576	13	0.307	0.044	280.4	7.5	804	20	113.9	2.8	569	12	120.4	2.6	2.92	0.13	114.6	1.7	15.73	0.27	92.9	1.7	20.03	0.39	58.6	1.2	8.64	0.22	60.2	1.5	10.03	0.27	1.56	0.11	7.44	0.28	6.79	0.14
Tarn13ap_34	13.03	0.99	624.7	9.8	678	19	0.65	0.15	0.92	0.17	3.62	0.46	0.83	0.095	7.08	0.55	11.2	0.65	13.91	0.44	98.1	4.3	23.6	0.86	125.6	4.5	19.32	0.66	41.4	1.3	4.42	0.12	22.07	0.68	2.41	0.1	0.483	0.057	0.73	0.21	8.4	0.36
Tarn13ap_35	687	9.5	134.7	2.6	349.8	5.3	0.866	0.087	11.2	1.2	35.6	4.4	5.46	0.69	31	3.7	10.9	1	2.21	0.18	16.1	0.84	3.72	0.12	35.21	0.83	10.79	0.19	46.37	0.77	8.84	0.17	67.2	1.1	10.52	0.2	0.171	0.036	9.4	1.9	1.449	0.053
Tarn13ap_36	4.66	0.88	475.7	7.9	4.62	0.21	LOD	LOD	18.01	0.51	35.72	0.95	4.41	0.18	20.2	0.67	3.22	0.2	0.466	0.038	2.39	0.18	0.278	0.021	1.19	0.1	0.175	0.018	0.377	0.032	0.03	0.007	0.113	0.025	0.008	0.003	2.47	0.16	1.244	0.06	0.149	0.008
Tarn13ap_37	774	10	929	16	771	15	8.19	0.32	734	14	1648	33	290.6	6	1544	30	338.5	5.6	40.42	0.74	252.3	3.9	31.6	0.5	156.4	2.3	26.86	0.37	64.56	0.85	7.8	0.15	42.52	0.73	5.47	0.12	0.114	0.032	48.83	0.97	11.94	0.3
Tarn13ap_38	185.9	2.3	1992	19	1150	29	0.309	0.096	6.38	0.22	22.14	0.43	4.65	0.16	38.8	1.1	23.44	0.67	8.14	0.18	71.2	1.3	19.63	0.38	183.2	3.4	45.42	0.68	123	2.5	14.89	0.43	74.2	2.1	7.88	0.26	0.089	0.03	0.154	0.093	0.164	0.013
Tarn13ap_39	1013	8.5	361.2	3.2	1070	15	0.34	0.05	948	14	2082	27	349.2	3.6	1753	19	384.9	3.6	25.5	0.37	307.7	2.9	44.53	0.47	233.7	2.4	41.23	0.48	100.6	1.3	12.28	0.21	64.68	0.99	7.79	0.13	0.08	0.024	30.31	0.31	15.38	0.15
Tarn13ap_40	1031	16	1523	24	368.1	6.5	12.97	0.32	1211	21	2064	40	268.9	5.4	1163	19	167.9	3.3	38.06	0.68	122.3	2.2	15.58	0.32	75.1	1.4	13.03	0.26	31.24	0.58	3.692	0.097	19.95	0.55	2.691	0.081	0.047	0.02	27.07	0.41	5.565	0.08
Tarn13ap_41	1857	29	133.6	2.8	1722	44	0.063	0.022	170.6	4.3	539	13	98.4	2.3	626	14	254.1	5.6	9.85	0.27	353	7.1	70.8	1.2	416.5	7.5	73	1.2	174.5	2.7	21.71	0.33	121.9	1.8	15.61	0.3	0.21	0.04	1.36	0.1	34.56	0.77
Tarn13ap_42	873	13	304.3	4.8	1200	21	4.72	0.2	595	12	1347	28	251.7	4.7	1463	29	360	6.9	9.4	0.27	307	5.2	45.62	0.75	243	3.5	44.08	0.68	114.4	1.3	15.95	0.24	98.3	1.8	12.98	0.29	0.07	0.02	26.02	0.53	15.75	0.25
Tarn13ap_43	1478	21	175.6	3.8	1755	34	0.665	0.079	742	15	1706	35	311.9	5.6	1768	34	434.8	7.9	6.57	0.19	385.4	6.2	62.44	0.95	344.1	4.8	64.98	0.9	176	2.3	25.89	0.4	171.2	2.7	23.97	0.46	0.068	0.024	22.89	0.56	31.86	0.68
Tarn13ap_44	830	10	453.8	9	956	21	12.03	0.73	762	19	1623	39	294.8	6.2	1670	35	347	6.7	14.18	0.32	269.6	4.4	37.99	0.66	190	3	33.33	0.5	83.3	1.3	10.44	0.21	58.4	1.1	7.67	0.16	0.149	0.035	28.46	0.5	8.24	0.16
Tarn13ap_45	512	5.7	165.8	2.7	127.9	2.1	0.099	0.035	7.27	0.31	16.63	0.49	3.03	0.17	21.9	1.1	7.89	0.39	3.25	0.14	12.77	0.43	2.542	0.067	17.09	0.43	4.02	0.11	12.02	0.3	1.61	0.062	9.93	0.34	1.663	0.063	0.182	0.034	0.231	0.045	1.297	0.032

Chapter 4

The trace element composition of apatite and its application to detrital provenance studies

Formatted for submission to a scientific journal for publication

Co-authors David M. Chew, Gavin Kenny, Isadora A. Henrichs

ABSTRACT

Apatite is an effective mineral tracer as its heterogeneous geochemistry enables several fingerprinting approaches with which to determine its source, and these methods can be combined to provide specific source interpretations. In particular, apatite's ubiquity in crystalline rocks, its variability with regards to its trace element contents (particularly with regard to the REE, actinides and Sr), and its amenability to various dating techniques based on the decay of the radioisotopes U and Th, permit these highly specific provenance determinations. In this study, we first present a comprehensive description of the trace element behaviour of apatite in various kinds of bedrocks (igneous rocks from felsic through to ultrabasic compositions, metamorphic rocks from low to high grades and of diverse protolith composition, and authigenic apatite) in which we explain why apatite is so highly diverse in terms of its trace element composition. Next, we present a synthesis of bedrock apatite trace-element compositional data from previous work, assembling a library of apatite compositions that includes all the abundant apatite-bearing lithologies in the Earth's crust, and many lithologies of lesser abundance. Principal component analysis is then undertaken on this library in order to create an apatite-composition discriminant diagram, which is then applied to three provenance case studies to demonstrate its utility. The first study investigates Mesoproterozoic sediments in northwest Scotland where apatite trace element composition shows that different apatite U-Pb age-peaks can be convincingly linked to different lithology types. A second study investigates modern river detritus in the Massif-Central of France where apatite trace

element composition can be used to match detritus to specific source rocks; the final study investigates modern river detritus from the Southern Appalachians in the USA where combined apatite trace-element and U-Pb data can determine the terranes from which individual apatite are derived in a complicated, polyphase orogenic belt. In all of these previously published detrital studies, the original provenance interpretations were largely based on apatite U-Pb age data. We show that the addition of apatite trace-element information enables the determination of the source lithology, making the extraction of novel information and more specific provenance determinations possible, and opens possibilities in source-to-sink modelling.

4.1. INTRODUCTION

Apatite, $Ca_5(PO_4)_3(OH, F, Cl)$, is amongst the most ubiquitous mineral groups in the Earth's lithosphere, primarily due to the inability of the major rock-forming minerals to accommodate significant amounts of phosphorous within their crystal structures (Piccoli and Candela, 2002). Apatite is also *by far* the most abundant phosphate mineral; monazite ($(La, Ce, Th)PO_4$) and xenotime (YPO_4) are the only other phosphate minerals in non-trivial abundance in rocks of the Earth's lithosphere. The apatite mineral group has three natural end-member compositions, the F-endmember fluorapatite, the Cl-endmember chlorapatite and the OH-group endmember hydroxyapatite, with these varieties comprising a solid solution series.

Though ubiquitous, apatite nearly always occurs as an accessory phase in crystalline rocks. It is present in most igneous and metamorphic rocks, the clastic sediments derived from them (Piccoli and Candela, 2002), as diagenetic overgrowths in sediments (Bouch et al., 2002), and as biologically precipitated apatite, particularly in the mineralised body parts of vertebrates. Apatite is present as a rock-forming mineral only in certain pegmatites, cumulates (e.g. nelsonites), and carbonatites. The name apatite, from the Greek απατείν, means to deceive, owing to the diverse optical appearance of natural apatite, which in turn is a consequence of trace element substitutions in the apatite lattice. Amongst the most common substituting elements are the rare earth elements (REEs) and yttrium (REYs), Mn and Sr and the actinides U and Th, all of which substitute for Ca; the halogens Cl, F and Br (and OH); and small, highly charged ions that substitute for P such as Si, S, As and V. Differences in the abundances of these elements are host-rock specific and can be used to trace the chemical environment in which individual apatite grains formed (Abdullin et al., 2016; Morton and Yaxley, 2007). Also, the incorporation of U into the apatite lattice enables the routine dating of individual apatite grains by the fission track method, and the U-Pb method once a common-Pb correction has been applied (Chew and Donelick, 2012).

Due to the wide spectrum of elements incorporated into its lattice, apatite is being increasingly used as a geological tracer. Tracing applications include palaeodrainage and palaeotectonic reconstructions in basin analysis (e.g. Carrapa et al., 2009; Mark et al., 2016; Morton, 2007; Zattin et al., 2012), to the correlation and chronology study of tephra layers (e.g. Sell et al., 2015) and the vectoring of ore-deposits (e.g. Belousova et al., 2002; Mao et al., 2015). Additionally, the halogen and noble gas geochemistry of

apatite is being increasingly used to study lunar formation (e.g. Boyce et al., 2014; McCubbin et al., 2011) and magma geochemistry and mantle geochemistry (Belousova et al., 2001; Matsumoto et al., 1997; O'Reilly and Griffin, 2000). As a detrital tracer, apatite is able to record both the age (e.g. Carrapa et al., 2009) and lithology of its source (e.g. Abdullin et al., 2016); by combining age and lithological information in detrital apatite it is therefore possible to make highly specific provenance determinations (e.g. O'Sullivan et al., 2018).

4.1.1 Physical and chemical weathering properties of apatite

Among the non-opaque heavy mineral species apatite is of lesser chemical stability, being more prone to dissolution in acidic chemical environments than some other detrital heavy minerals, particularly the ZTR (zircon, tourmaline, and rutile) assemblage (Hubert, 1962) that is ultra-resistant to chemical dissolution in nearly all Earth-surface environments and during diagenesis. Apatite is prone to dissolution by acidic meteoric waters (e.g. Morton and Hallsworth, 1999 and references therein), however, once buried in a sedimentary sequence apatite is remarkably persistent during diagenesis, even often acquiring overgrowths due to the liberation of organic and adsorbed P (Bouch et al., 2002), and can sometimes even be the main cementing phase in detrital rocks (Joosu *et al.*, 2016).

Physical weathering is often incorrectly identified as an important cause for the abrasion and ultimate destruction of mineral phases in detritus, the so-called "maturity myth" described by Garzanti (2017). Instead, detrital assemblages typically do not evolve to more "mature" assemblages with increasing transport distance or time, with the existence of placer deposits of very soft minerals such as monazite supporting this assertion (e.g. Dill et al., 2012). Therefore, by discounting abrasion as a means of destroying mineral species in clastic sediments, the presence or absence of apatite in a given sediment can mostly be attributed to two factors. These are: 1) the abundance of apatite in the source material, which will only be very low if the source rocks are phosphorous-poor (such as chemically-precipitated sediments, quartzites, or depleted mantle rocks), and 2) the degree to which acidic chemical weathering has altered the detrital assemblage - whether in transport-limited (i.e. soil/humus forming) settings at the apatite source, during prolonged alluvial storage such as humid flood plain environments, or if the early diagenetic fluids are particularly acidic (Morton and Hallsworth, 1999 and references therein).

Apatite is hence often abundant in sediments, with abundances of 20-40% apatite not uncommon in modern fluvial heavy mineral assemblages (e.g. Bernoulli and Winkler, 1990; O'Sullivan et al., 2018), while apatite is very rarely absent in Quaternary sedimentary deposits worldwide (e.g. Nechaev and Isphording, 1993)

4.1.2 Geochemistry of apatite

The purpose of the sections below is to provide a grounding in apatite geochemistry, focussing on the REEs. In order to use apatite as a tracer it is crucial that its trace-element chemistry in all of the diverse environments that apatite can occur (magmatic systems, low-grade metamorphic systems, diagenetic environments etc.) is well characterised. This section provides a framework to explain why apatite from different bedrock lithologies is so readily separated on a PCA biplot, and to understand the nature and geometry of that separation, as shown in section 4.3.

The apatite unit cell can be simplified to the formula $A_5(XO_4)_3Z$ and typically exhibits a hexagonal crystallographic structure. The A-site hosts Ca in two structural sites, the IX-fold coordinated Ca1 site, and the VII-fold coordinated Ca2 site. The IV-fold X site hosts P^{5+}, and lastly, the monovalent Z-site hosts a halogen (Cl or F, with trace quantities of Br and I), an OH^- group, or a vacancy. Substituting elements in the A-site may include significant quantities of Sr^{2+}, Mn^{2+}, Pb^{2+}, U^{4+} and Th^{4+}. In the X-site, PO_4^{3-} can be replaced by small, highly charged cations such as S^{6+}, As^{5+}, V^{5+}, and Si^{4+} (Henrichs et al., 2018). Triply charged $REYs^{3+}$ also substitute into apatite via coupled substitution processes, with the main substitution mechanisms being (e.g. Rønsbo, 1989):

$$REE^{3+} + Na^{+} = 2Ca^{2+}$$

$$REE^{3+} + SiO_4^{4-} = Ca^{2+} + PO_4^{3-}.$$

REYs and Sr strongly partition into apatite in igneous melts, thus in magmatic systems apatite can control a significant portion of the whole-rock REE- and Sr-budget, and can be a useful tracer in igneous petrogenesis studies (Prowatke and Klemme, 2006). While some high-field-strength elements (HFSEs) such as U and Th are partitioned into apatite (to the extent that apatite can control the whole-rock U- and Th-budgets in lithologies where other actinide-hosts are absent (e.g. O'Reilly and Griffin, 2000), most

other HFSEs (e.g. Zr, Hf, Nb, Ta, Ti etc.) and the large-ion lithophile elements (LILEs; particularly the very largest such as Rb, Cs etc.) are not partitioned into apatite in significant quantities (Figure 1).

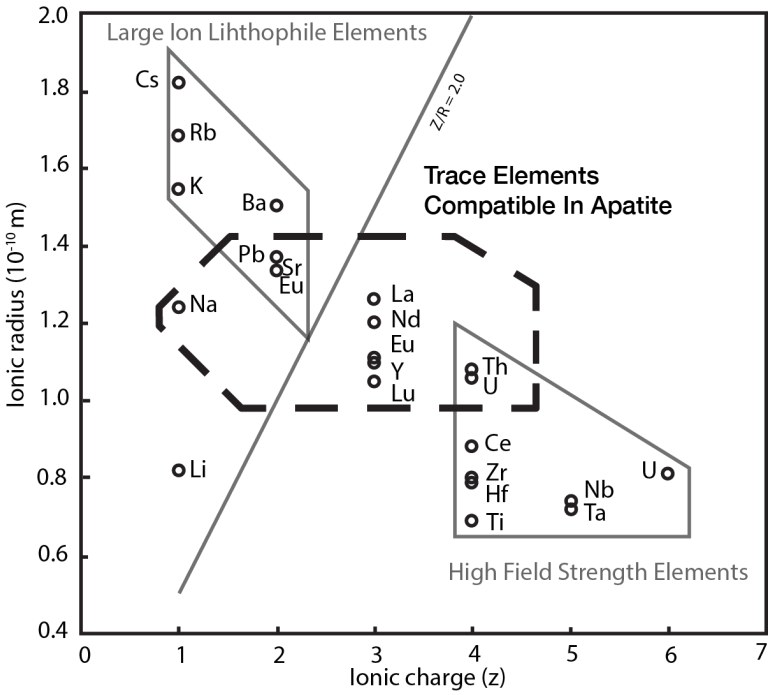

Figure 1, commonly incorporated trace-elements in apatite. Of the displayed elements, those with ionic radii between 0.9 and 1.4 10^{-10} m are commonly compatible as trace elements, or in some cases major elements, in apatite. Modified from Whittaker and Muntus (1970)

4.1.2.1 Igneous Apatite Geochemistry

In magmatic rocks apatite is a minor yet ubiquitous accessory phase, with the exception of some cumulates, rare igneous rock types such as nelsonites and certain pegmatites in which apatite is a major rock-forming phase (Piccoli and Candela, 2002). Apatite from igneous rocks is typically more actinide-rich and common-Pb (Pb_c) poor than metamorphic apatite and will be overrepresented in detrital apatite datasets acquired using only U-Pb dating techniques (e.g. O'Sullivan et al., 2018). The dominant factors controlling apatite solubility and crystallization in igneous rocks are SiO_2 and P_2O_5 concentrations in the melt, melt temperature (Piccoli and Candela, 2002), and also the aluminium saturation index (ASI) of the melt. Apatite solubility is thus strongly correlated to the degree of crustal contamination in the melt, with apatite in high-ASI anatectic melts (which are typically crustal melts) having much greater solubility in melt than apatite in low-ASI (usually more basic) igneous rocks (Hsieh *et al.*, 2008). Water content, pressure and the concentration of Ca in the melt are not important factors governing apatite solubility (Piccoli and Candela, 2002 and references therein).

Igneous apatite has been used successfully as a petrogenetic tool in many studies. Sha and Chappell (1999) demonstrated that apatite from crustally-derived "S-type" granites and felsic "I-type" granites is depleted in the light rare earth elements (LREEs) and Th, whereas apatite from less crust-contaminated I-type granites generally contain similar (or even enriched) chondrite-normalised abundances of these elements compared to the middle rare earths (MREEs) and U respectively. Belousova et al. (2001) and Hsieh et al. (2008) recognised that the difference in *trace element contents* of felsic *vs* basic granites is largely determined by the aluminium saturation index (ASI) of the magma rather than its SiO_2 content or the degree of fractionation of the host melt. As monazite crystallises as a primary phase in high ASI (i.e. ASI > 1.1) rocks, the topology of chondrite-normalised apatite REE-plots in felsic melts is therefore explained by the coeval or later crystallization of apatite with respect to monazite, which reduces the Th and LREE budget available to apatite (see the comparatively LREE-depleted REE patterns of S-type granite apatite vs for example I-type granitoids on figure 2) as these are major elements within the monazite lattice. La/Sm ratios may thus be used to recognise such magmas as there is strong partitioning between La and Sm in monazite, and this fingerprint may be recorded in cogenetic apatite (Belousova et al., 2001). Biplots of Sr vs Mn can also be used to determine the host-magma composition and to determine both the degree of magma fractionation and the oxygen fugacity of the melt (e.g. Sha and

Chappell, 1999; Hsieh *et al.*, 2008). The apatite Sr/Mn ratio is usually i) very low in apatite from highly fractionated melts due to the elevated apatite Mn-contents in such systems (up to 1 wt% or more), ii) close to unity in I-type granitoids (abundances of tens or several hundred ppm for each element), and iii) very high in basic melts (due to elevated Sr-contents of up to several thousand ppm) (Belousova et al., 2001; Tang et al., 2012). Features common to nearly all granitic apatites include pronounced negative Eu-anomalies (due to crystallization after feldspar), and generally high ΣREE abundances.

Mafic igneous apatite systematically differs from felsic granitoid apatite in trace-element composition (Figure 2). The La/Lu ratios are higher as a result of the melt composition of the mafic source and also the absence of cogenetic monazite crystallization (e.g. Belousova et al., 2002), resulting in strongly LREE-enriched REE-profiles. Th/U and Sr/Mn ratios are also typically higher that in granitoids, while Eu-anomalies vary depending on whether apatite crystallises before or after feldspar (e.g. Tang et al., 2012), and may even be mildly positive in feldspar-absent rocks such as lherzolites or carbonatites (e.g. O'Reilly and Griffin, 2000). Apatite from those ultramafic lithologies may also be readily discriminated from mafic apatite as ultrabasic apatite is much more enriched in Sr, and extremely depleted in the HREEs (O'Reilly and Griffin, 2000; Tang *et al.*, 2012).

Lastly, apatite from alkaline igneous rocks typically has very elevated REE contents. In particular, LREE contents are usually very enriched, with wt % contents of LREEs reported in studies of apatite from syenitic, agpaitic and phonolitic rocks (e.g. Rønsbo, 1989; Zirner et al., 2015). This behaviour of alkaline igneous apatite permits its discrimination from other igneous apatite (Figure 2).

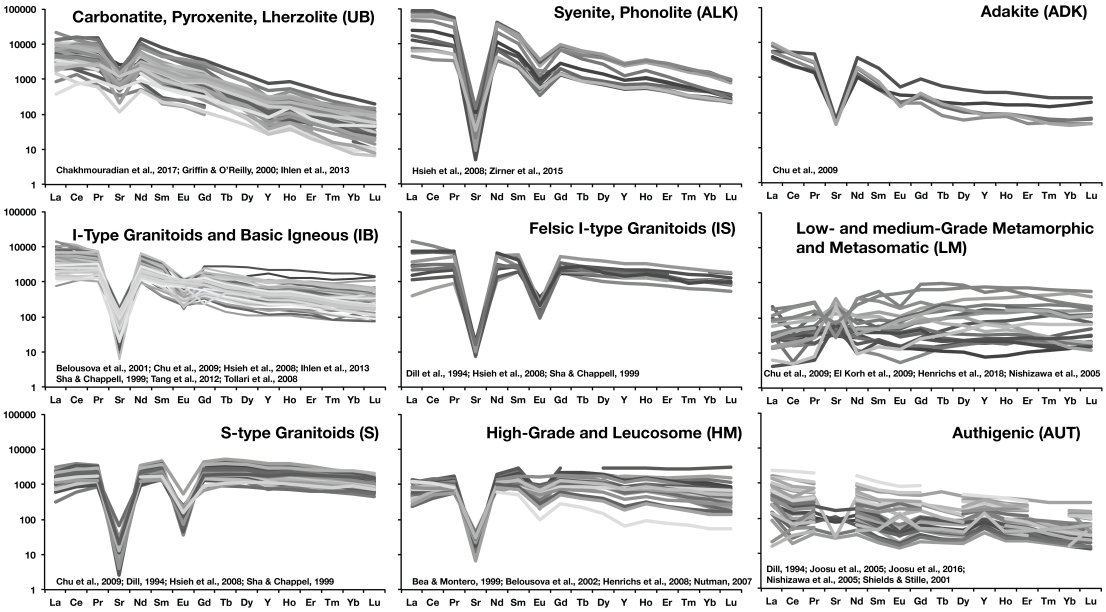

Figure 2, chondrite-normalised (McDonough and Sun, 1995) REY+Sr multi-element plots ('spidergrams') of apatite from different categories of igneous rocks, low- and high-grade metamorphic apatite, and authigenic and fossil apatite. See sections 4.1.2.2 and 4.1.2.4 for the definitions of low- and high-grade apatite. Gaps in data represent non-analysed elements. All data were acquired by LA-ICP-MS. The lithologies were classified by the authors of the individual studies. The same data suite, groups and abbreviations are used as the basis of the PCA in figure 3.

4.1.2.2 Low- and medium-grade metamorphic apatite geochemistry

The abundances and elemental ratios of trace elements of neocrystalline and reprecipitated apatite in low- and medium-grade metamorphic systems are highly distinct compared to those of magmatic apatite. Apatite in such rocks often present very variable and complex chondrite-normalised REE spectra, but with typically extremely low ΣREE abundances (Figure 2). Eu-anomalies vary from mildly negative to positive with typically low actinide contents, especially Th (e.g. Bea and Montero, 1999; El Korh et al., 2009; Henrichs et al., 2018; Nutman, 2007). Low- to medium-grade metamorphic rocks rarely preserve equilibrium assemblages even on a thin-section scale, as the reaction rates are slow compared with rates of change in the physical conditions the rock has experienced (P, T or changes in fluid composition). Low reaction rates result in incomplete reactions and chemical disequilibrium, and apatite grains from the same metamorphic rock samples can exhibit orders of magnitude variation in trace-element abundances (e.g. Henrichs et al., 2018; Gaweda et al., 2018).

Though the trace element signature of low- to medium-grade metamorphic apatite is highly distinct to that of igneous apatite, definitive discrimination of metamorphic apatite from different protolith types is not yet possible, with apatite from basic and pelitic lithologies often overlapping on multi-element plots (e.g. Henrichs et al., 2018). Similarly neither does apatite from high-pressure lithologies (e.g. blueschists and eclogites) exhibit distinguishing characteristics that consistently mark them apart from apatite from other metamorphic grades (e.g. El Korh et al., 2009; Henrichs et al, 2018).

The halogen/hydroxyl content of the Z-site in the apatite lattice can be an important control on whether apatite re-crystallises during metamorphism, as changes in fluid-composition in the metamorphic environment can be responsible for dissolution and reprecipitation of apatite with a halogen/hydroxyl composition in equilibrium with fluid (Kusebauch *et al.*, 2015). In metamorphic rocks recrystallized or reprecipitated apatite is generally dominated by the fluorapatite component (Spear and Pyle, 2002), with fluorine content increasing with increasing metamorphic grade due to the relative instability of chlorapatite *vs* fluorapatite in fluid-rich metamorphic systems which are typically F-rich (Kusebauch et al., 2015). Apatite in metamorphic lithologies also typically exhibits relative Sr, Eu and Pb_c enrichment, and relative depletion in the other REYs and Th compared to igneous apatite (e.g. Henrichs et al., 2018).

That metamorphic apatite from substantially different protolith types (pelites *vs* basic igneous rocks) is chemically indistinguishable (e.g. El Korh et al., 2009; Henrichs

et al., 2018) is surprising, but can be attributed to ubiquitous processes which most low- to medium-grade metamorphic rock types experience, and that in each case will ultimately render the resulting apatite REY- and Th-poor. Firstly, in most low- to medium-grade metamorphic rocks, apatite dissolution-reprecipitation or neocrystallization occurs as epidote is forming, with epidote capable of incorporating significant proportions of the actinides and REYs in its crystal structure (e.g. Henrichs et al., 2018). In such cases reprecipitated apatite may have its REY and actinide budgets scavenged by cogenetic epidote growth, while neocrystalline apatite will consequently precipitate in a REY- and actinide-depleted chemical environment. Secondly, metamorphic apatite may form as a product of P-bearing K-feldspar dissolution during greenschist-facies albitization reactions according to the 'berlinite' reaction as proposed by London (1992):

$$KAl_2PSiO_8\,(\text{K-feldspar, P end-member}) + Na^+ + 2Si^{4+} = NaAlSi_3O_8 + K^+ + Al^{3+} + P^{5+}$$

Liberated P^{5+} can be used to crystallise apatite, especially as metasomatic fluids are often Cl^- and F^- rich. Accordingly, neocrystalline apatite formed during this reaction inherits P, Sr and Eu from the precursor feldspar (e.g. Broska et al., 2004), but will be devoid of the actinides and the REYs (apart from Eu) as they are not commonly substituted into K-feldspar in appreciable amounts. Thirdly, dissolution-reprecipitation processes in apatite may provide sufficient REY, Th and P necessary to precipitate monazite and xenotime (which incorporate REYs and Th as major elements) along fractures or around the apatite grain boundary, leaving the resulting apatite devoid of those elements (Harlov, 2011; Zirner *et al.*, 2015). The dissolution-reprecipitation process causes the total dissolution of the mineral lattice (i.e. including Ca and PO_4 groups) and the reprecipitation of apatite on the surface of the grain as epitaxial overgrowths (e.g. Kusebauch et al., 2015), providing Th, P and REE for the growth of monazite and xenotime.

4.1.2.3 Metasomatic apatite geochemistry

Apatite formed during metasomatic processes often has trace-element compositions that are indistinguishable from low- to medium-grade metamorphic apatite, i.e. low REE contents, high Ca, F and Sr contents, and minor Eu-anomalies. Dissolution-reprecipitation reactions can occur during the cooling of igneous rocks for example, especially in fluid-rich systems such as pegmatites, where late-stage fluids may catalyse

the precipitation of REY-poor apatite, monazite and xenotime from REY-rich primary igneous apatite (e.g. Harlov, 2011), especially locally along fluid-pathways in the rocks. Altered portions of granites should therefore be avoided if trying to obtain U-Pb ages from igneous rocks, as REY-poor apatite is more likely to contain lower U and radiogenic Pb (Pb*) and higher Pb^c than primary igneous apatite (e.g. Henrichs et al., 2018). Conversely, REY-poor apatite thus may be a useful indicator mineral of ore-mineralisation in igneous terranes (Mao *et al.*, 2016), as in detritus the chemical signature may be useful as vector for the presence of metasomatised rocks in the hinterland.

4.1.2.4 Refractory Apatite in Metamorphic Rocks

In metamorphic rocks, it is important to be able to distinguish between pre-existing apatite assemblages inherited from the protolith (e.g. detrital apatite in a metasedimentary rock, or igneous apatite phenocrysts in a meta-igneous rock), from neocrystalline apatite that has grown in the metamorphic rock. In low-grade metamorphic rocks, both inherited apatite and metamorphic apatite can co-exist, as seen for example in lower-greenschist facies metasediments in the Haast schist of the New Zealand Alps where apatites with igneous compositions are preserved (Henrichs et al., 2018). Both Henrichs et al. (2018) and Nutman (2007) have shown that in metasedimentary rocks, detrital apatite will be consumed by the upper-greenschist facies, with new growth of apatite likely due to a coupled dissolution-reprecipitation process (e.g. Harlov, 2015). In situations where apatite is hosted in 'unreactive' lithologies (such as anhydrous coarse-grained plutonic lithologies, or mono-mineralic metasedmentary lithologies (such as marbles or quartzites), it is possible that detrital apatite will persist to higher metamorphic grades, similar to the behaviour of rutile hosted in unreactive assemblages (Luvizotto *et al.*, 2009).

Such behaviour has been observed by Schneider et al. (2015), who analysed apatite U-Pb ages in Variscan orthogneisses which have experienced Alpine 450-575°C overprinting in the Tauern window in Eastern Austria. The apatite U-Pb ages in these meta-granitoid orthogneisses were dispersed, with two peaks in the U-Pb age spectrum corresponding to the age of igneous emplacement and Alpine MT-LP orogenesis (although a continuous U-Pb age-distribution between these events was present). This implies that these Tauern apatite retain refractory U-Pb age information to temperatures much higher than suggested by Pb-diffusion models in apatite (c. 350-475°C, Cherniak, 2010).

4.1.2.5 High-grade metamorphic and leucosome apatite

At high-metamorphic grades, mineral assemblage equilibration rates are typically sufficiently fast that samples are often in chemical equilibrium on the scale of a thin section or hand sample; dispersed apatite trace element spectra are typically not encountered in such rocks (Bingen et al., 1996; Bea and Montero, 1999; Nutman, 2007; Henrichs *et al.*, 2018). This also indicates that all apatite present in the protolith before metamorphism occurred has long since been consumed. Apatite in higher-grade metamorphic rocks is almost always close to the fluorapatite end-member composition (Spear and Pyle, 2002), and also typically contains higher REE- and actinide-abundances than apatite from lower-grade metamorphic lithologies (Figure 2). In anatectic rocks alkali-rich fluids or partial-melts both promote the dissolution of other phosphate phases and increase the REE uptake of fluorapatite, especially in peralkaline melts (Krenn *et al.*, 2012).

Bingen et al. (1996) studied an amphibolite to upper granulite-facies transect in high-K calc-alkaline gneisses of the Agder region of southern Norway. The REE, Th and U contents of apatite increase progressively with increasing grade, firstly following dissolution of allanite, hornblende and titanite at the Cpx-in isograd where the MREE and HREE contents of apatite increase, and again upon the dissolution of monazite at the Opx-in isograd where the LREE- and Th-contents of apatite increase significantly. The decrease in monazite abundance is contemporary with biotite-breakdown at the Opx-in isograd and the consequent release of apatite-stabilising F, which also promotes the movement of REE into the apatite lattice in the form of NaF complexes (Krenn et al., 2012). Bingen et al. (1996) concluded that high-grade orthogneiss apatite can accommodate solid-state exchange of trace elements and thus the chemical composition of these apatites does not reflect the initial igneous apatite composition. However, when compared to analyses of granitoids from the literature (e.g. Chu et al., 2009; Hsieh et al., 2008; Sha and Chappell, 1999), the ultra-high-temperature apatite from the OPX-in isograd analysed by Bingen et al. (1996) yield REY + actinide spider-plot spectra that are essentially indistinguishable from those of granitoids. It may not therefore be possible to distinguish apatite from granulite-facies igneous rocks from non-metamorphosed igneous apatite by REY contents.

As apatite is unstable in igneous melts (Piccoli and Candela, 2002), in rocks that undergo anatexis apatite is consumed into the melt or fluid, from which apatite will then

crystallise upon cooling. For this reason P strongly partitions into the leucosome in high-grade or anatectic rocks, meaning that leucosomal apatite is both larger and more abundant than restitic apatite (e.g. Bea and Montero, 1999), and therefore detritus derived from a rock segregated into leucosome and melanosome, the apatite signal will be dominated by apatite that grew in the leucosome component. Leucosome apatite typically presents geochemical signatures similar to that of S-type granitoid apatite (Figure 2), with low Th/U, low La/Ce and flat chondrite-normalised REE-profiles (e.g. Bea and Montero, 1999; Nutman, 2007; Henrichs *et al.*, 2018a). In contrast, apatite in more mafic or restitic compositions, especially those that crystallise garnet, exhibits elemental abundances and REE-profiles similar to those of apatite from I-type granitoids; the depletion in HREE and Y is due to the incorporation of these elements into cogenetic garnet, yielding the high La/Lu ratios characteristic of restitic apatite (e.g. Bea and Montero, 1999). In the Cooma migmatite dome in the Lachlan Fold Belt of SE Australia, Th is strongly depleted relative to U in leucosome apatite in anatectic pelites, while LREE contents are depleted relative to lower-grade (biotite-isograd) rocks. Nutman (2007) ascribes the Th and LREE depletion to the cogenetic growth of monazite, this is similar to the paragenesis and composition of apatite from S-type granitoids documented in other studies (e.g. Hsieh et al., 2008). Similar Th and LREE depletion is also seen in high-grade paragneisses from the Peruvian Andes and the Cycladic metamorphic core complex in Paros (e.g. Henrichs et al., 2018), but from samples where anatexis was minor to absent. This implies that the distinctive trace element composition of high-grade apatite does not critically depend on its crystallisation from leucosome *per se*, but rather on the growth of a cogenetic Th- and LREE-bearing phase such as monazite.

4.1.2.6 Authigenic and chemical-precipitate apatite

Apatite is found as a chemical precipitate in some P-bearing chemical sediments, such as banded iron formations (e.g. Joosu et al., 2016 and references therein), and phosphorites where it may instead occur as the cryptocrystalline apatite phase collophane, or francolite. Additionally, apatite may grow during diagenesis (e.g. Bouch et al., 2002; Vermeesch et al., 2009), and may even occasionally occur as the major cement phase in detrital sediments (e.g. Gall et al., 2017; Joosu et al., 2016). Apatite grows in sediments due to the liberation of P from organic decay, and from the liberation of P adsorbed onto clay-mineral surfaces. While the process of liberation of organic-P can begin within the first five metres of burial as seen in modern sediment samples from the Mississippi delta

and Long Island Sound in the USA (e.g. Ruttenberg and Berner, 1993), adsorbed and early authigenic P is likely only to be mobilised under deep burial diagenesis with large apatite rims typically reported at depths below c. 3km in the North Sea (e.g. Bouch et al., 2002).

In studies of ancient authigenic apatite, ΣREE contents vary substantially (e.g. Bouch et a., 2002; Joosu et al., 2015; 2016), but the topology of the chondrite-normalised REE patterns are distinct compared to other categories of apatite (Figure 2). While in some well-preserved sections marine authigenic apatite may preserve REE-abundances, negative Ce-anomalies and distinct Y/Ho ratios (e.g. Y/Ho < 35) (Lawrence and Kamber, 2006) characteristic of the seawater REE-signal (e.g. basal Cambrian phosphorites from the Meischucun formation in southern China; Shields and Stille, 2001), diagenetic processes in many cases overprint this signal (Shields and Stille, 2001). Consequently, negative Ce-anomalies are less pronounced and ΣREE contents increase (especially the MREE) with increasing alteration. Apatite with pronounced negative Ce-anomalies is thus characteristic of an authigenic origin, but as this signal may often be obscured or destroyed during diagenesis, the absence of a seawater-like Ce-anomaly does not preclude an authigenic origin.

In altered authigenic apatite that no longer preserves seawater-like REY signatures, the sources for REY- and actinide-rich (e.g. Bouch et al., 2002; Vermeesch et al., 2009) overgrowths on apatite is probably the dissolution of other REY- and actinide-bearing phases in detritus (Bouch et al., 2002), most probably phases such as garnet, titanite, allanite and epidote which are unstable during burial diagenesis (Morton and Hallsworth, 1999 and references therein). In some cases apatite cementation may even be dated by the apatite fission-track (AFT) or U-Pb methods to provide timing constraints on the diagenetic history (e.g. Gall *et al.*, 2017).

4.1.3 Geochronology/thermochronology of apatite

Apatite often contains significant concentrations of the radionuclides U and Th and thus can be employed as a geochronological or thermochronological tool. Apatite fission track dating was first explored in the 1960s (e.g. Naeser 1967; Wagner, 1968), with the first publications on the apatite U-Th-He method appearing two decades later (Zeitler *et al.*, 1987). U-Pb dating of apatite was first undertaken in the 1970s by thermal ionisation mass spectrometry (TIMS) by Oosthuyzen and Burger (1973). Although that study yielded near-concordant apatite U-Pb age data, it should be noted they were Archean

samples with significant in-growth of radiogenic Pb (Pb*); subsequent studies have shown that apatite often yields strongly discordant U-Pb data due to high Pb_c / Pb*ratios. Apatite single-grain U-Pb geochronology only became possible with the advent of rapid *in situ* micro-beam dating techniques (e.g. secondary ionisation mass spectrometry, SIMS; laser-ablation inductively coupled plasma mass spectrometry, ICP-MS), along with the concomitant development of apatite U-Pb age-standards and data reduction schemes employing ^{207}Pb- or ^{204}Pb-based Pb_c corrections to age standards and unknowns (Thomson *et al.*, 2012; Chew *et al.,* 2014).

U-Pb dating of minerals (including apatite) by LA-ICP-MS is now a cheap, rapid and effective dating tool (e.g. Spencer et al., 2016). A precision better than 1% (2σ) is possible for Phanerozoic apatite samples (e.g. typically 20-30 cogenetic analyses from a magmatic or metamorphic rock), with a precision better than 2% possible even with Palaeogene apatites (e.g. Chew et al., 2014). The factors that govern whether a given unknown detrital apatite grain may be accurately and precisely dated by the U-Pb method are threefold. Firstly, the grain must have abundant U and Th to produce sufficient Pb* to yield favourable Pb* / Pb_c ratios; secondly, the age of the grain itself - as older grains are clearly more amenable to dating due to the longer duration of Pb* in-growth; and thirdly the grain must contain low initial Pb_c concentrations, or else in-grown Pb* in growth will never become a significant proportion of the total Pb in the grain, even with high initial U abundances.

4.2 METHODOLOGY

4.2.1 Data Synthesis for Principal Component Analysis

A central pillar of this paper is the synthesis of apatite trace element data published over the past three decades from nineteen papers (Dill, 1994; Bea and Montero, 1999; Sha and Chappell, 1999; O'Reilly and Griffin, 2000; Belousova *et al.*, 2001a; Shields and Stille, 2001; E. Belousova *et al.*, 2002; Nishizawa *et al.*, 2005; Nutman, 2007; Tollari *et al.*, 2008; Hsieh *et al.*, 2008; Chu *et al.*, 2009; El Korh *et al.*, 2009; Tang *et al.*, 2012; Ihlen *et al.*, 2014; Zirner *et al.*, 2015; Joosu *et al.*, 2015; Chakhmouradian *et al.*, 2017; Henrichs *et al.*, 2018b). This dataset incorporates apatite from 251 separate bedrock samples to provide an empirical record of apatite compositions. The bedrock samples span a diverse range of lithologies, ranging from S-type granites to I-type granitoids, alkaline igneous rocks, basic igneous rocks, ultrabasic igneous rocks, high-grade and low-grade metamorphic rocks of diverse protolith type, and authigenic apatite. In large datasets efficient data visualisation is paramount, as the volume of data points is too large to be conveniently assessed on a table or on a multi-element spidergram (Figure 2), particularly when hundreds or thousands of data points corresponding to unknown detritus are also added. Additionally, in order to adequately separate the data, typically several variables (elemental abundances or elemental ratios) need to be employed. Consequently, principal component analysis (PCA) is used here to separate and visualise the bedrock dataset. Median values for apatite in each individual sample are used. This comprehensive bedrock PCA biplot is then used to interpret apatite trace-element data from three previously published detrital case studies, where existing provenance information (e.g. U-Pb apatite age data) has resulted in non-unique provenance interpretations.

In order to visualise the data on PCA biplot, the studies must also have analysed the full suite of elements selected for the PCA used in the study (Sr, and the REEs except Tb and Tm). The exclusion of some potentially useful apatite datasets characterising lithologies not included in the PCA dataset (e.g. the high grade lower-crustal orthogneisses analysed by Bingen et al., 1996) stems from the absence of key elements in those published datasets. Likewise, the exclusion of elements of potential interest such as U, Th, Mn, Tb and Tm is also necessary, as too few published datasets include these elements. The apatite data from the bedrock dataset are derived from samples that cover the entire range of common igneous rocks (and many uncommon ones, including carbonatites, cumulates and lherzolites), authigenic and fossil apatite, and metamorphic rocks of diverse protolith, grade, age, and geographic location. Quality screening was

applied to the bedrock database; igneous and authigenic bedrock samples that authors described as altered were excluded, as were igneous bedrock samples that had experienced subsequent medium- to high-grade metamorphism (e.g. apatite from the Sybella and Kalkadoon plutons in the study of Belousova et al., 2001). Additionally, any samples that exhibited significant trace-element dispersion between grains were omitted as plotting a median value would therefore be misleading or meaningless (e.g. sample LT2 of Henrichs et al., 2018 which contains both a low-grade metamorphic apatite population and a detrital igneous population).

All element abundances and elemental ratio vectors chosen for the literature-based PCA have a sound geological basis for their inclusion. Each selected elemental abundance or ratio acts to increase the separation of the data on the PCA biplot, and is compatible with the detailed geochemical parageneses for the different lithology types described in section 4.1.2. The PCA biplots employed in this study are not intended to definitively identify highly specific source lithologies (e.g. to distinguish syenites from phonolites). For example, using particular element ratios and abundances it may be possible to more successfully discriminate certain rock types that overlap on the literature-based PCA discriminant diagram used in this study (cf. Belousova et al., 2002). However, this PCA discriminant diagram is intended as a provenance tool with broad applicability, which emphasises generalised lithological affinities (e.g. whether a detrital apatite is derived from chemical-sediments, metamorphic/metasomatised rocks, partial melts, basic rocks etc.) than the discrimination of highly specific rock types.

4.2.2 A recipe for an apatite PCA discriminant diagram

PCA biplots were made using the "R" software environment for statistical computing, particularly relying on the R library 'FactoMineR' (Lê et al., 2008). The software code used to make the diagrams used in this paper, representing a combination of code from that library (and other libraries referenced in the supplementary file) and code written by the authors, is provided in a supplementary file. The bedrock apatite data (the 251 bedrock samples taken from 19 papers) are used as the train dataset and plotted on PCA biplots that are hereafter treated as discriminant diagrams. Apatite unknowns, or 'test data', from each of the three detrital apatite case studies presented subsequently are plotted using the transformation derived from the bedrock apatite training dataset so as not to influence the transformation of the data. This allows direct comparison of the test data from different datasets. Where apatite groupings chosen for the bedrock PCA

discriminant diagrams almost completely overlapped, the lithologies were combined into broader lithological groupings. For example, as apatite from carbonatites, pyroxenites and lherzolites plot in the same space in the PCA, they are grouped as “UB” for ultrabasic apatite; likewise, mafic I-type granites, granodiorites and basic apatite significantly overlap and are therefore plotted together as a group called “IB” (for mafic ***I***-type and ***b***asic apatite).

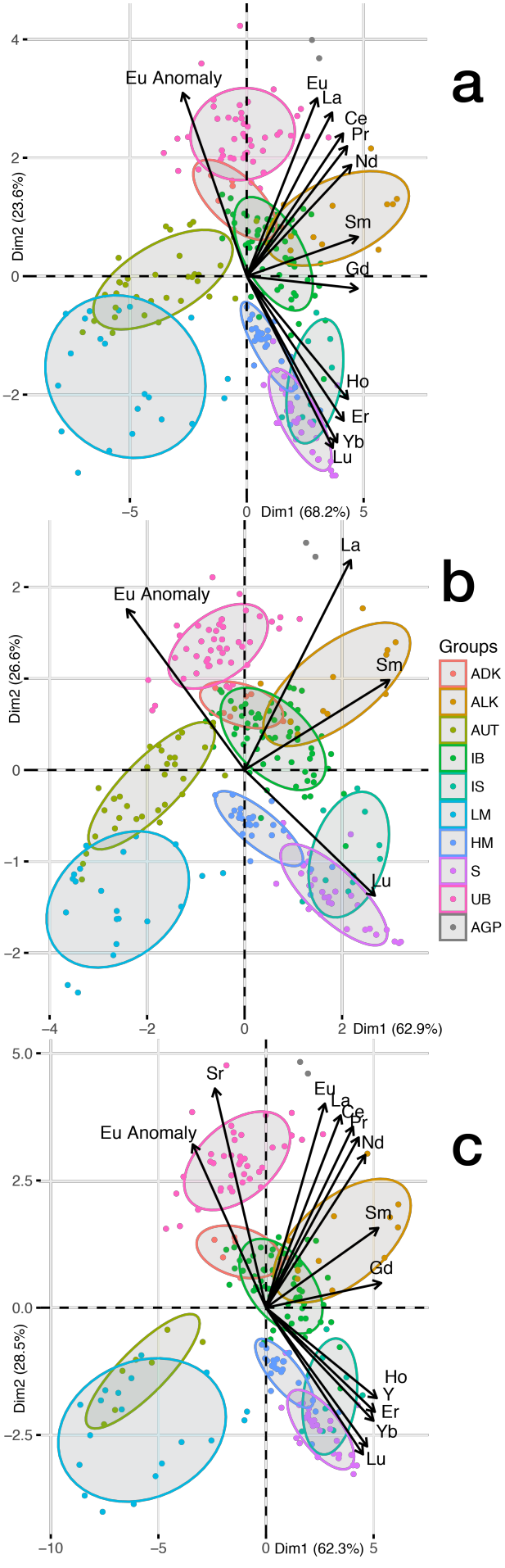
a
Eu Anomaly
Eu
La
Ce
Pr
Nd
Sm
Gd
Ho
Er
Yb
Lu
Dim2 (23.6%)
Dim1 (68.2%)
b
La
Eu Anomaly
Sm
Lu
Dim2 (26.6%)
Dim1 (62.9%)
Groups
ADK
ALK
AUT
IB
IS
LM
HM
S
UB
AGP
c
Sr
Eu
La
Ce
Pr
Eu Anomaly
Nd
Sm
Gd
Ho
Y
Er
Yb
Lu
Dim2 (28.5%)
Dim1 (62.3%)

Figure 3; Three iterations of an apatite bedrock PCA biplot. Ellipses are 1 S.D. Diagrams (a) and (b) contained the maximum number of bedrock data points, with eleven and four elements used as input variables respectively. Sr and Y are added in diagram (c), resulting in fewer bedrock data points as some studies do not analyse these elements (notice the much reduced number of samples in the AUT group for example). Each point represents the median value for a single sample, either as published in each respective paper or as calculated by the authors.

Abbreviations for categories: ADK = adakites; ALK = alkaline igneous rocks; AUT = authigenic, fossil, and chemically-precipitated apatite; IB = mafic I-type granitoids and basic rocks; IS = felsic I-type granitoids; LM = low-grade metamorphic (low- to medium-grade metabasites and metapelites, and metasomatised granitoids, i.e. sub-anatectic and sub-granulitic metamorphic rocks); HM = partial-melts/leucosomes/high-grade metamorphic; S = S-type granitoids; UB = ultrabasic rocks including carbonatites, lherzolites and pyroxenites; AGP = two datapoints of agpaitic composition (no ellipse) in the top of the NE quadrant of each diagram.

4.3. RESULTS

4.3.1 Discrimination of bedrock samples on the PCA biplot

Three different iterations of a PCA discrimination diagram are presented in Figure 3. The first includes the largest number of bedrock samples, and employs the REEs (La, Ce, Pr, Nd, Sm, Eu, Gd, Ho, Er, Yb and Lu) and the Eu-anomaly as input variables (Figure 3a). The second PCA biplot (Figure 3b) comprises the same set of bedrock samples from the literature as in Figure 3a, but with fewer variables (La, Sm, Lu, and the Eu-anomaly). The third PCA biplot comprises the same suite of elements in Figure 3a but with the addition of Y and Sr (Figure 3c). However, some bedrock data points had to be excluded as Y and Sr were not acquired in all of the literature studies, meaning some fields (particularly authigenic apatite) are less well constrained in Figure 3c.

Though all three versions of the bedrock PCA-diagram are effective for discriminating between the selected bedrock lithologies, the PCA and diagram in Figure 3b (fewest elements with most literature reference points) is chosen as the transformation with which to display the unknown samples in the detrital case studies in this paper. The metadata for Figure 3c is provided here (Figure 4) as it includes all elements and ratios and hence shows the behaviour of the complete suite of potential input values, even if only a subset (i.e. those employed in Figure 3b) are subsequently used. In figure 4 the scree plot shows that PC1 and PC2 account for the majority of the variance (>90%) in the data, and thus minimal information is lost by not displaying the other principal components. In Figure 4 the contribution of the elements employed is very similar, with all elements contributing to separate the data, while neither do any elements dominate. The screeplot and element contributions for the PCA used in Figure 3b (not shown) are similarly distributed to those of the PCA in Figure 3c, with no dominant elements as each of the four elements contribute between 24% and 26% of the variation. The two largest principal components account for 89% of the explained variance in the data and it is thus valid to plot as a biplot.

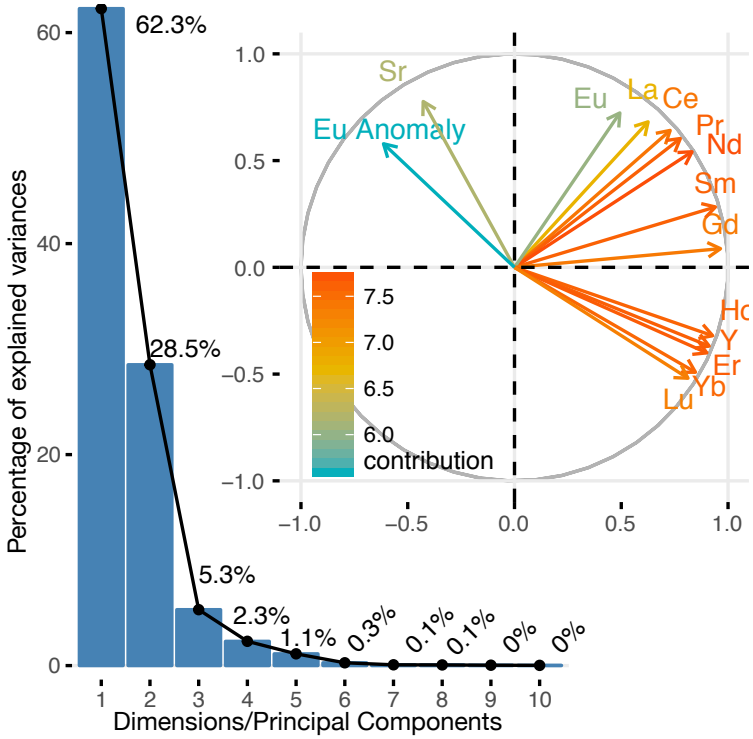

Figure 4, Scree plot, metadata for the PCA transformation displayed in Figure 3c showing the behaviour of the complete suite of potential input values.

On each of the PCA-diagrams, the LM (low-grade metamorphic), HM (high-grade metamorphic and leucosome), and AUT (authigenic) apatite groupings are separated from igneous apatite (UB, IB, IS, S, ALK, AGP), chiefly due to their lower ΣREE abundances, with these groupings additionally exhibiting positive to weakly negative Eu anomalies compared to the large negative anomalies characteristic of apatite from non-ultrabasic igneous rocks. LM apatite is the most REE-deficient, so it plots away from the REE-vectors; in comparison, AUT and HM apatite contain more LREE and HREE respectively, separating them from each other and from LM apatite. Igneous apatite is separated along a trend from the most felsic (S, figure 3) to the most ultrabasic rocks (UB, figure 3), chiefly governed by differences in the La/Lu ratio which is low in felsic igneous rocks (S and IS, figure 2) and high in mafic lithologies (IB, ADK, and UB, figure 2). Apatite from alkaline igneous rocks is distinct from this trend (ALK, Figure 3), plotting on the far-right side of the graph towards extremely enriched REE-abundances. The gap between S-type and felsic I-type (S and IS, figure 3) and mafic-I-type and basic apatite ("IB" apatite) is probably due to the crystallization of monazite in granitoids with high aluminium saturation indices (ASI) producing a step-change to much lower La/Lu ratio in felsic granitoids compared to granitoids which do not crystallise monazite. Lastly, ultrabasic apatite (UB, figure 2) is most effectively separated from other apatite categories with the addition of Sr, as seen in Figure 3c.

4.3.2 PCA applied to case study 1 – Mesoproterozoic sediments from NW Scotland

4.3.2.1. Short Background

Detrital apatite U-Pb age and trace-element data from the study of Kenny et al. (in prep) are re-investigated here to assess whether more specific provenance interpretations can be made using the new bedrock PCA discriminant diagram. The analysed apatite comes from the Stoer Group, a 2km-thick continental and lacustrine Mesoproterozoic sedimentary sequence in NW Scotland that was deposited unconformably on TTG-dominated Archaean crystalline basement of the Lewisian Complex (Stewart, 2002). The Stoer Group is a pre-Grenvillian sequence deposited near the margin of the Laurentian supercontinent that avoided Grenvillian deformation, and has yielded impact-related authigenic feldspar $^{40}Ar/^{39}Ar$ dates of 1177 ± 5 Ma near the top of the sequence (Parnell *et al.*, 2011), in an ejecta layer known as the Stac Fada member (Simms, 2015). The section was sampled below, within and above the Stac Fada Member at both Gruinard Bay and Stoer Bay for U-Pb detrital zircon and apatite analyses.

Based on these U-Pb data, Kenny et al. (in review. Appendix B) found no change in apatite or zircon provenance below, within or above the Stac Fada Member, indicating that either: i) there was no large-scale drainage reorganisation after the Stac Fada impact event; ii) there was consistent widely-sourced aeolian input to the Stoer Group, as documented by Ielpi and Ghinassi (2015) which has diluted any potential change in sedimentary provenance signal related to the impact event; or iii) drainage-network reorganisation did take place following the bolide impact, but the configuration of the sediment source areas was such that it could not be detected using the detrital provenance methods employed.

4.3.2.2 Stac Fada PCA results

The trace-element compositions of the dated apatite detritus in the Stoer Group sedimentary rocks are dominated by apatite of low-grade metamorphic (LM, 322 grains) affinity (e.g. El Korh *et al.*, 2009; Henrichs *et al.*, 2018), with a subsidiary population of apatite with I-type granitoid to basic igneous compositions (84 grains), shown by grains plotting in the "IB" field on the PCA biplot (Figure 5). 34 grains have high-grade metamorphic compositions (HM), while there are very few apatite grains with compositions matching those of apatite from alkaline igneous rocks (ALK, 3 grains), felsic I-type granitoids (IS, 4 grains), adakites (9 grains), or ultrabasic rocks (5 grains) (figure 5). No grains plot convincingly within the S-type granitoid field (S).

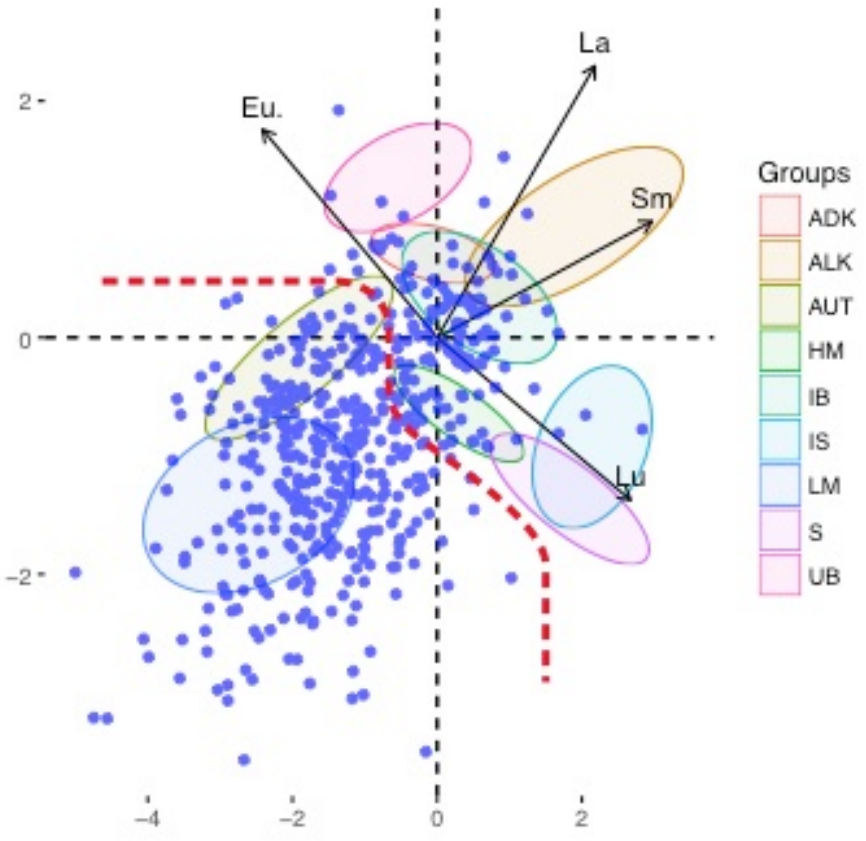

Figure 5. Composition of apatite detritus from all samples taken from Stoer Group sediments in Gruinard Bay, compared to the literature apatite database. Almost all apatite detritus is low-grade metamorphic (LM) or basic-igneous / mafic I-type granitoids (IB). The red curve is an arbitrary dividing line between apatite detritus of low to medium metamorphic grades, and igneous and high-grade metamorphic (HM) (right of line) used as the two categories to display U-Pb data on KDP in figure 6. Abbreviations are the same as used in Figure 3.

When only apatite grains that were considered 'dateable' by Kenny et al. (in prep) are considered (dateable in this case meaning apatite grains with ^{207}Pb-corrected U-Pb age uncertainties of less than 10%), a greater proportion of low-grade metamorphic apatites than igneous apatite grains are excluded (with these two broad fields as defined in Figure 5). This is in agreement with the findings of studies of apatite from low- to medium-grade metamorphic bedrock which is commonly extremely depleted in U and has low Pb^*/Pb_c ratios (e.g. Henrichs et al., 2018). U-Pb grains ages are displayed on a kernel density plot (KDP) in Figure 6 from these two broad categories, igneous and high-grade metamorphic, and low- to medium-grade metamorphic, as well as the U-Pb ages of detrital zircon from the same samples from the Stoer Group. The boundary between igneous and high-grade metamorphic *vs* low- to medium-grade metamorphic grains is taken as the red line on Figure 5. Apatite with igneous (and high-grade metamorphic) compositions (e.g. S, IS, IB, ALK, ADK, UB and HM) have U-Pb ages correlating more closely with those of the major post 2.8 Ga zircon U-Pb age peaks, and those of low- to medium-grade metamorphic apatite characterising different events, particularly a 1.65 Ga event that corresponds to a known amphibolite-facies metamorphic event (the Somerledian phase of the Laxfordian event; Kinny et al.,2005) in the Archaean-Proterozoic Lewisian basement of NW Scotland. These results demonstrate a strong correlation between lithology and age in detrital apatite, with specific lithologies obviously dominating particular time-intervals and events.

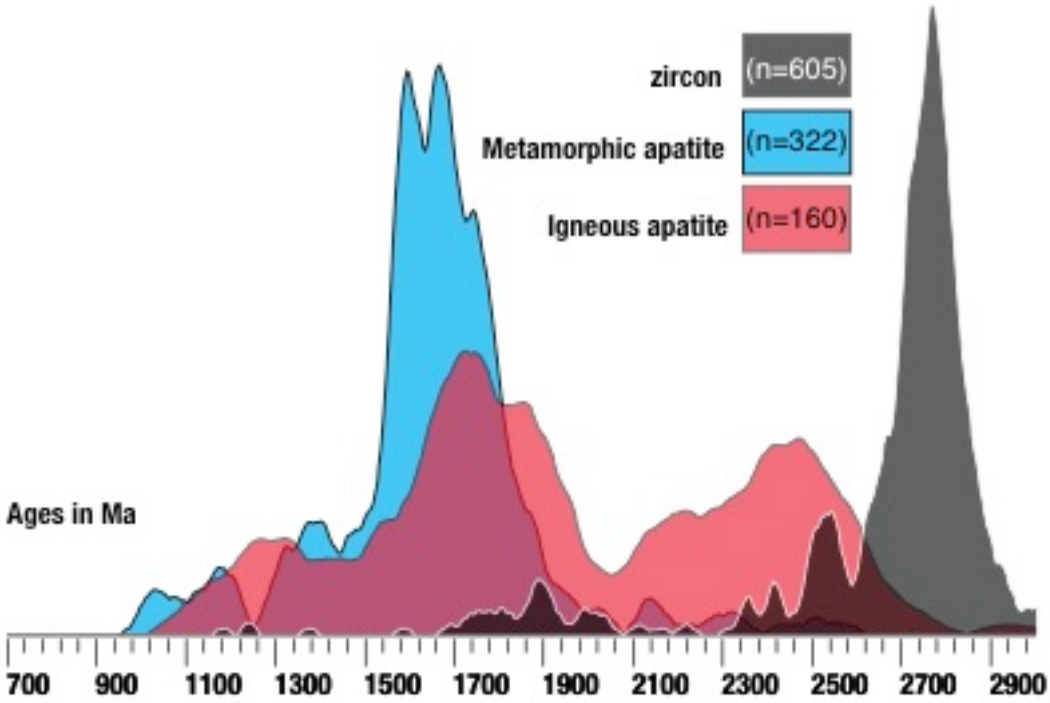

Figure 6. KDE plot of detrital zircon U-Pb ages, and igneous (and high-grade metamorphic) and metamorphic (low- to medium-grade) apatite U-Pb ages from the Stoer Group sedimentary rocks as identified using the discriminant diagram in Figure 5. Igneous apatite exhibits major U-Pb age peaks at 2.45 Ga, 1.85 Ga, and 1.75 Ga, whereas metamorphic apatite mostly records U-Pb ages of 1.75-1.6 Ga.

4.3.3 PCA applied to case study 2 – modern sediments, River Tarn, Central France

Case study 2 considers apatite from modern river sediment from the river Tarn in the southern Massif Central of France. These data are taken from O'Sullivan *et al.* (2018), where they were displayed on a PCA discriminant diagram based on a smaller literature bedrock apatite dataset compared to this paper, but employed a similar suite of trace elements. The Tarn and its tributaries drain the Cévennes sub-range of the Massif Central, which is composed of metasediments which experienced greenschist- to lower-amphibolite facies peak-Variscan metamorphism, and post-Variscan granitoids of broadly monzogranitic composition. A concise geological history of the southern Massif Central can be found in O'Sullivan et al., (2018), and in more detail in Faure et al. (2009).

When plotted on the PCA discriminant diagram (Figure 7), detrital apatite from the Tarn and its tributaries show different lithological affinities according to the sampled portion of the drainage system. A sample draining the Variscan metamorphic rocks primarily yields apatite detritus that overlaps with low- to medium-grade metamorphic apatite from the literature (e.g. El Korh et al., 2009; Henrichs et al., 2018), a sample draining the post-Variscan Cévennes granitoids is composed primarily of apatite with a strong geochemical affinity to granitoid apatite from the literature (e.g. Hsieh et al., 2008), while a sample draining an area containing a Miocene basanite pipe contains a very minor sub-population of apatite of basic trace-element affinity (e.g. Tang et al., 2012) and yielding Miocene U-Pb ages. Samples downstream of the mixing point of these streams show all three integrated trace-element and U-Pb age populations, with clear separation on the PCA discriminant diagram in Figure 7. These results demonstrate a clear link between trace element composition and both age and amenability to U-Pb dating. With most igneous apatite (S,IS,IB etc.) providing ages, and LM apatite almost entirely non-dateable.

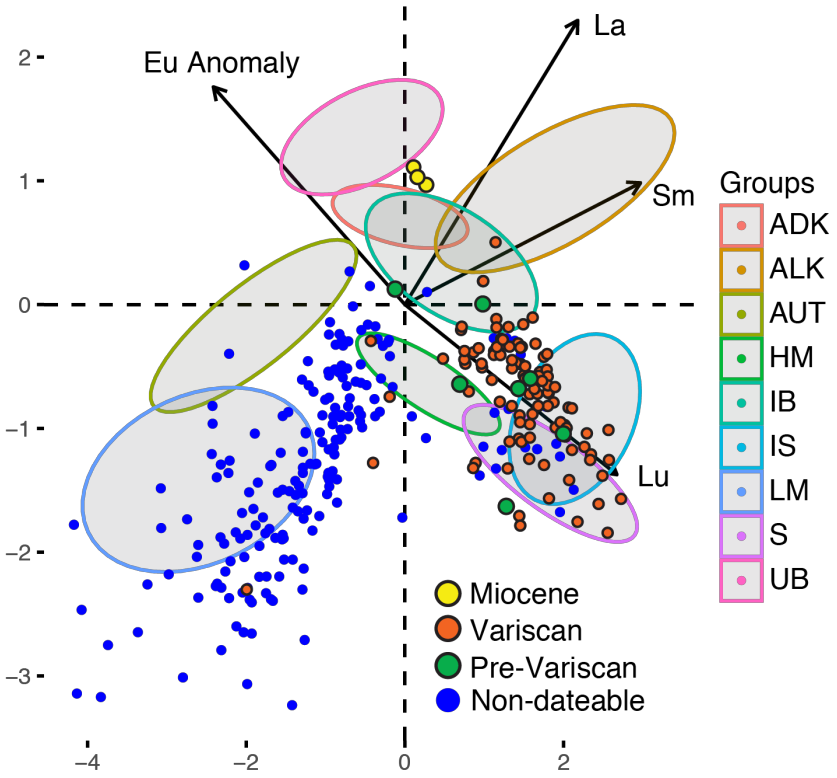

Figure 7. Detrital apatite from the river Tarn plotted on a PCA discriminant biplot from samples GOS11/14- 06, 07, and 08 (O'Sullivan et al., 2018) wherein all three major sediment sources – Variscan granitoids, metapelites, and Miocene basanite pipes have mixed. In that paper non-dateable grains were defined by errors larger than 20% of the ^{207}Pb corrected U-Pb age. Abbreviations the same as used in Figure 3.

4.3.4 PCA applied to case study 3 – Modern Sediments, French Broad River

4.3.4.1 Background information

Case study 3 considers apatite in modern fluvial detritus from the French Broad River (FBR). Apatite trace-element data from the study of O'Sullivan et al. (2016) have been plotted on a PCA discriminant diagram to investigate whether new provenance information can be obtained, as the original study relied solely on the U-Pb ages of the detritus.

The FBR is an orogen-bisecting river in the southern Appalachians of North Carolina and Tennessee in the United States (Figure 8). The drainage basin of the FBR has been affected by three major phases of post-Grenville (c. 1 Ga) Appalachian orogenesis - the Taconic orogeny at c. 470-440 Ma, the Neoacadian orogeny at c. 420-380 Ma, and the Alleghanian orogeny at c. 320-290 Ma (Hatcher, 2010). U-Pb zircon and monazite (Hietpas *et al.*, 2010) and U-Pb apatite and rutile (O'Sullivan et al., 2016) ages have all been published for the FBR detrital samples and all employ the original Hietpas et al. (2010) sample suite. The zircon U-Pb dataset fails to record the magma-poor Alleghanian (c. 320 Ma) orogeny, whereas monazite, rutile and apatite do. This is because these phases, unlike zircon, can grow during metamorphism, or if they are pre-metamorphic phases their U-Pb ages can be reset at medium- to high-metamorphic grades.

4.3.4.2 PCA results

Two suites of samples from the French Broad River are presented on separate PCA discriminant diagrams in Figure 9. The upstream samples FB2, FB3 and FB4 are located within the outcrop of the Henderson gneiss within the Western Inner Piedmont (WIP) and adjacent to the Brevard Fault Zone. The downstream samples FB13 and FB14 were collected from the lower reaches of the FBR as it exits the Appalachians after draining the Western and Eastern Blue Ridge terranes (WBR and EBR), Grenvillian basement windows, and non-metamorphosed Upper Palaeozoic sediments of the Valley and Ridge province (Figure 8).

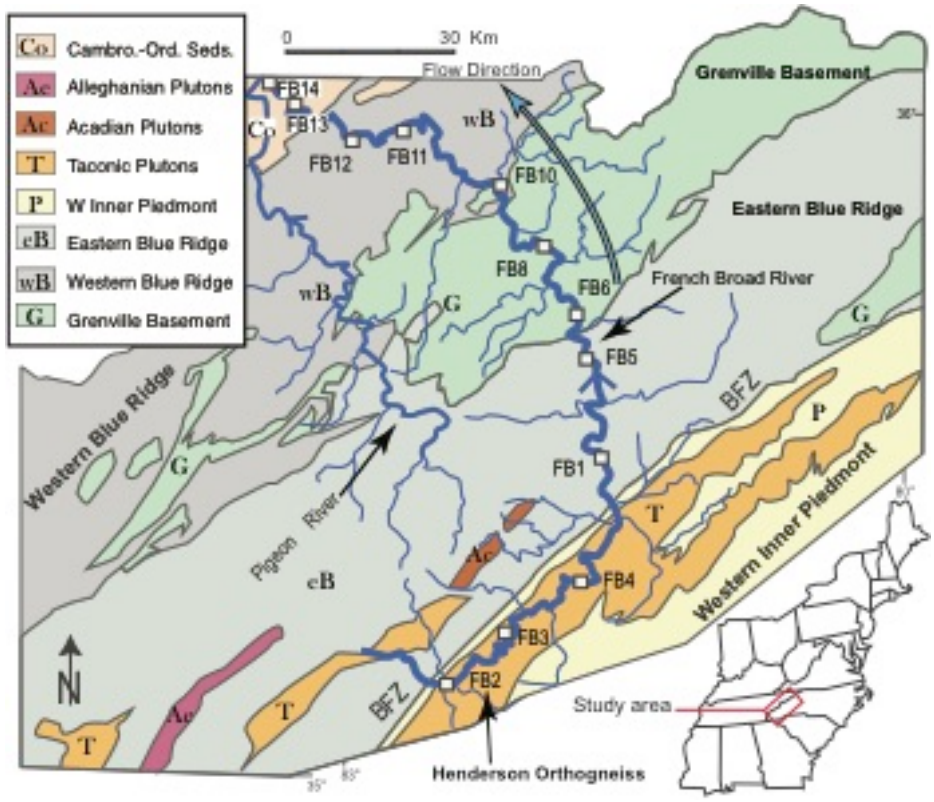

Figure 8. A map of sample locations and terranes within the FBR catchment, modified from O'Sullivan et al. (2016). Samples FB2, FB3 and FB4 are taken from the FBR within the Henderson orthogneiss of the Western Inner Piedmont Terrane and sample a limited range of lithologies; the downstream samples FB13 and FB14 source detritus from a much wider range of lithologies. The Blue Ridge terranes are predominantly composed of metasedimentary rocks.

In the upstream samples (FB2, FB3 and FB4, Figure 9a) the apatite detritus is largely characterised by a simple assemblage of low- to medium-grade metamorphic apatite (LM), and high-grade metamorphic apatite (HM). There are a handful of igneous grains with compositions mostly intermediate to the IB and IS groups, alkaline-igneous (ALK) and S-type granitoid (S) grains are not present (Figure 9a). On a U-Pb age KDP the modal peak for these samples defines an Alleghanian age (Figure 10a), but the age-distribution is dispersed with a spread of detrital apatite U-Pb ages between c. 290-400 Ma, within error of the Alleghanian (~ 320 Ma) and Neoacadian (~ 370 Ma) orogens.

In the downstream samples (FB13 and FB14, Figure 8), the age and trace-element signal is more dispersed as sediment has been sourced from a much larger catchment area (Figure 9b). In these samples Grenvillian-age apatite detritus with IB, IS, S and ALK compositions is all present (Figure 9b, Figure 10b). Probably due to sediment mixing, the proportion of apatite with high-grade metamorphic compositions and Alleghanian ages ("HM Alleghanian grains" Figure 9), a common sediment component in the upstream segment, has now been substantially diluted downstream (to just 3 of 64 downstream grains vs. 43 of 134 grains upstream).

Apatite with LM trace-element compositions exhibits very similar age-distributions in the upstream and downstream samples of the FBR (Figure 10c), the only difference being that the modal age-peak is shifted to the Neoacadian from the Alleghanian downstream. In comparison, apatite with igneous trace element-compositions (IB, IS, S, ALK) have mostly Neoacadian-Alleghanian U-Pb ages in the upstream samples (Figure 10d) and are only represented by compositions intermediate to the IB and IS groups in the upstream FBR samples (plotting in the same location as igneous detritus derived from monzogranites in the river Tarn case study, Figure 7), whilst in the downstream samples there is a much broader array of older ages (including Grenville detritus) of more diverse IB, IS, ALK and S compositions (figure 10d). No grains of UB composition are encountered in any sample, upstream or downstream.

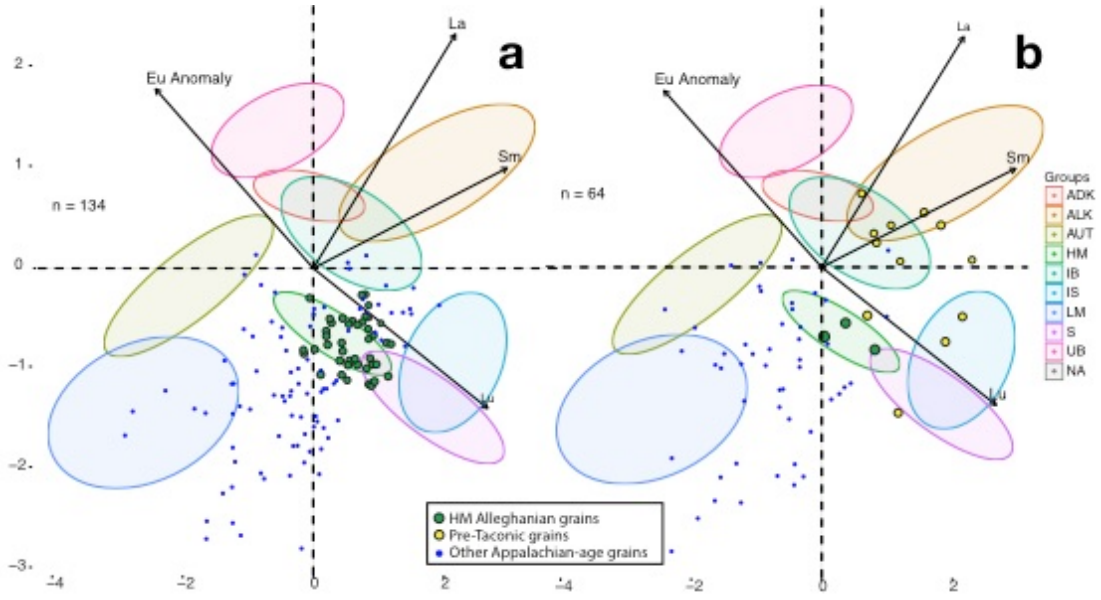

Figure 9. Comparison of detrital apatite compositions in (a) upstream samples (FB2, FB3 and FB4), and (b) downstream samples (FB13 and FB14). Abbreviations the same as used in Figure 3.

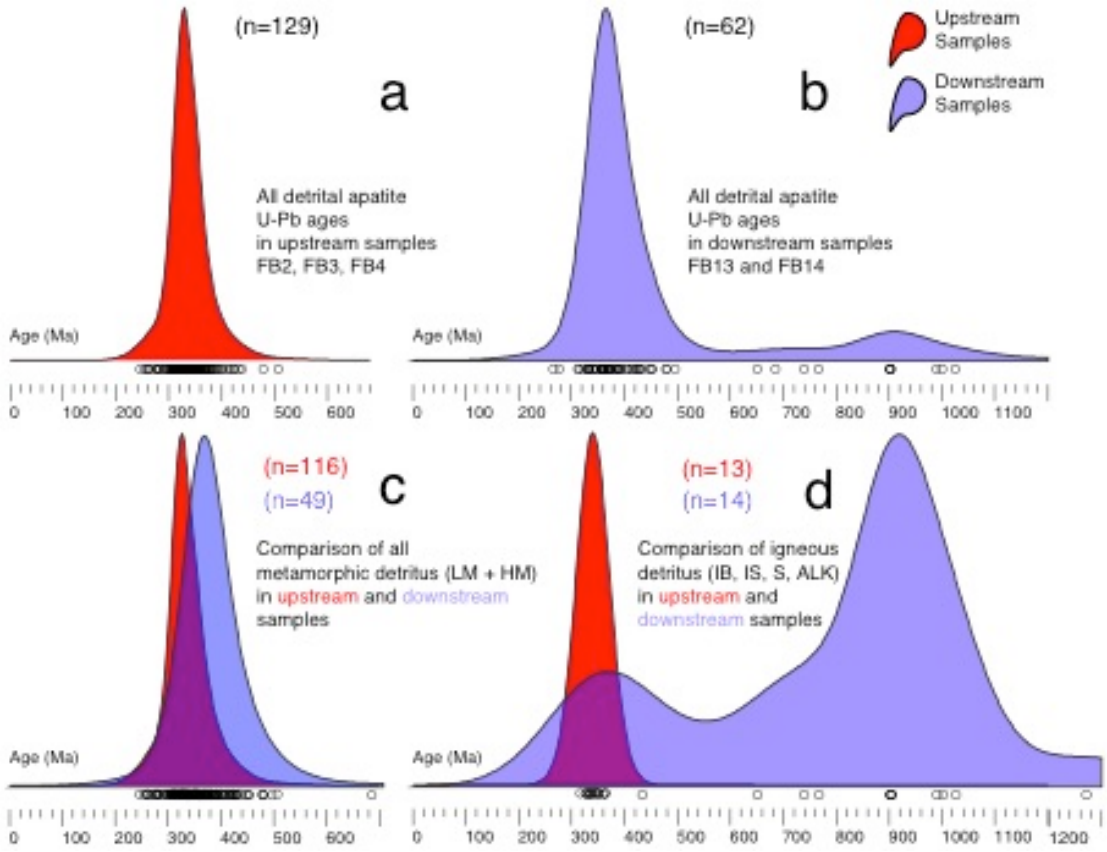

Figure 10, KDPs of apatite U-Pb ages in the FBR. The difference in age distribution between the upstream samples (a) and downstream samples (b) can mostly be explained by differences in the ages of grains with igneous compositions (d), as in comparison the ages of metamorphic apatite (c) are broadly similar in both groups of samples. In figure (d) very few grains define the age distribution so the KDP has a large uncertainty

4.4. DISCUSSION

4.4.1 Implication of the apatite discriminatory PCA, what information or insight does it provide, and how should it be used

On the bedrock PCA discriminant diagram (Figure 1), the apatite trace-element data can be separated into seven broad lithological classes: 1) high-grade metamorphic, leucosome and anatectic rocks (HM); 2) S-type granitoids (S); 3) I-type granitoids-to-basic igneous rocks (IB); 4) syenites and other alkaline igneous rocks (ALK); 5) ultrabasic igneous rocks (UB); 6) authigenic, fossil and chemical-precipitate apatite (AUT); and 7) low-grade metamorphic and metasomatised rocks (LM) – with "felsic I-type" granitoid apatite (IS) and adakitic apatite (ADK) representing distinct additional fields with fewer bedrock samples. These data show that apatite trace-element compositions can be convincingly related to their source-rock lithology, and additionally that apatite trace-element data from multiple studies are consistent with each other in terms of their trace-element systematics, and hence apatite can be used to determine the source protolith in detritus. While apatite trace-element compositions have been previously used as a provenance indicator (e.g. Abdullin et al., 2016; Dill, 1994; Morton and Yaxley, 2007), the data synthesis in this paper provides a simple, repeatable recipe for apatite species discrimination that characterises more lithologies than has been attempted before, with potentially as few as five elements (La, Sm, Eu, Gd, Lu) required to determine the source rock composition.

4.4.2 Stac Fada Discussion

The Stac Fada grain populations in the Mesoproterozoic Stoer group clastic sediments from northwest Scotland are separated into very broad 'metamorphic' (LM (+AUT, see last paragraph of this section)) and 'igneous' (HM, S, IS, IB, ALK, ADK, UB) apatite fields (dotted red line, Figure 5). When integrated with the existing U-Pb age data from these grains, it is apparent that these two geochemical groups of apatite record very different events (Figure 6), with the 'metamorphic' apatite KDP dominated by a c. 1675 Ma age peak corresponding to regional metamorphic events – the Laxfordian and Somerledian, Kinny et al., 2005 and references therein), and igneous and high-grade apatite recording several older events (as far back as the c. 2.5 Ga 'Badcallian' event) that are also detected by the detrital zircon U-Pb ages data from the same samples (Kenny et al., in prep).

When plotted on our new PCA discriminant diagram (Figure 5), the majority of apatite grains from the Stoer Group sediments match the composition of LM apatite (lower-grade metamorphic bedrock, Figure 1b; e.g. El Korh et al., 2009; Henrichs et al., 2018), and there are comparatively fewer grains that exhibit igneous and high-grade bedrock compositions. However, when only grains that passed the age-inclusion criteria (10% 2 S.E. of the 207Pb corrected age) in Kenny et al., (in review, Appendix B) are included, more LM-metamorphic than igneous and high-grade grains are excluded due to their lower average U and Pb^*/Pb_c values (e.g. O'Sullivan et al., 2018). Even still, 322 grains pass the acceptance criteria and have LM (+ AUT) compositions, while only 160 have igneous and HM compositions. Hence detrital apatite with LM compositions are far more frequent than any other grouping. Of the igneous and HM apatite grains, the majority (84) overlap with literature bedrock samples characterising melts in the "IB" (mafic I-type and basic igneous) field, most likely sourcing rocks most likely of TTG composition, which is the protolith composition of the majority of the Lewisian Gneisses of NW Scotland (Kinny et al., 2005 and references therein). Comparatively, in decreasing order there are much fewer grains with high-grade metamorphic (HM, 39 grains), adakitic (ADK, 9 grains), ultrabasic (UB, 5 grains), 'felsic-I-type' (IS, 4 grains) and alkaline igneous compositions (ALK, 3 grains), and no grains with compositions unequivocally matching S-type granitoids from the literature database (S, e.g. Sha and Chappell, 1999). Moreover, the U-Pb ages of apatite grains from these lower abundance igneous categories match events of known age and geochemical composition from NW Scotland, with three of the four felsic I-type igneous grains (IS) yielding ages between 1780-1605 Ma which corresponds to the known ages of granitoid emplacement in the nearby Rhinconich and Tarbert terranes (e.g. Kinny et al., 2005), while all of the five ultrabasic grains have ages between 1800-1900 Ma, corresponding to zircon U-Pb ages of apatite-bearing norite and diorite bodies in the South Harris Complex (Mason et al., 2004). The oldest apatite grain in the Stoer group sediments is a 2,950 ± 111 Ma grain of alkaline igneous composition.

On the discriminant PCA biplot (Figure 5) the grains with LM compositions appear to lie on a trend towards the compositions of IB igneous rocks, which could indicate that these grains are sourced from IB rocks that have experienced a later metamorphic event, with variable overprinting. Mixing of trace-element domains during LA-ICP-MS analysis may be partly responsible for the lack of a clear division between LM and IB compositions, as grains were not imaged before analysis. There is no

comparable trend in the LM detritus towards the S-type granitoid group for example (of which there is no apatite detritus in the Stoer Group sediments). Thus, the vast majority of apatite grains in the Stoer Group may be derived from similar TTG-type rocks that have been variably metamorphosed, with a much more minor contribution from felsic, ultramafic and alkaline magmas. This assemblage of compositions and ages can be explained by entirely local sources (e.g. Kinny and Love, 2005 and references therein), meaning that an extensive drainage system draining portions of present-day Greenland or Canada need not be invoked to explain the apatite provenance in the Stoer Group sediments. This explanation may also explain why drainage reorganisation caused by a possible large meteorite impact event, as shown by palaeocurrent indicators in the Stoer Group (e.g. Simms, 2015), does not result in a change in zircon or apatite provenance (e.g. Kenny et al., in prep). The sediment sources may not have changed from pre- to post-impact times due to small catchment sizes resulting in the sampling of similar detritus.

Lastly, it is clear from the PCA discriminant diagram that many of the Stac Fada data points plot within the authigenic apatite field (AUT, figure 5). However, we do not consider that a large proportion of the detrital apatite analysed is authigenic in origin. Instead, it is felt that this represents overlap from the partial resetting of the REE-compositions of the I-type and basic igneous ("IB") rock group along a mixing trend towards LM metamorphic compositions. Consequently, this does question the viability of our authigenic apatite field for discriminating detrital samples on this PCA. However, when Y/Ho ratios and Ce-anomalies are calculated for Stac Fada detritus plotting in this field, no analyses exhibit seawater-like ratios (Y/Ho < 35, negative CeN/Ce*; e.g. Joosu et al., 2016), supporting the assertion that these are not in fact authigenic grains but rather metamorphic apatite grains lying on a mixing line towards their "original" IB protolith apatite compositions.

4.4.3 River Tarn Discussion

Due to the limited variety and simple arrangement of lithologies in the upper river Tarn catchment, the river Tarn study provides some of the clearest separation of detrital apatite in the case studies discussed in this paper. The simple distribution of non-deformed granitoids and older metamorphic rocks (e.g. Brichau et al., 2008; Faure et al., 2009) leads to a bimodal distribution of apatite compositions on the PCA biplot (figure 7).

The link between lithology and amenability to U-Pb dating is also most evident in this case study. While a greater proportion of grains with igneous trace-element compositions are dateable than those with LM (low- to medium-grade metamorphic) compositions in every case study presented in this paper, this relationship is clearest in the river Tarn detrital samples as almost no grains with LM compositions were dateable. This may be due to the specific grade or protoliths of the metamorphic rocks in the river Tarn catchment, which are mostly greenschist-facies graphitic metapelites (Faure et al., 2009). Detrital rutiles derived from the metapelites in the Tarn catchment are also generally U-poor and Pb_c-rich (O'Sullivan et al., 2018).

4.4.4 French Broad River (FBR) Discussion

In the upstream FBR samples (FB2, FB3, FB4, Figure 8) almost all grains are Neoacadian or Alleghanian in age (Figure 10a). Grains with Neoacadian ages are almost certainly derived from pelites and gneisses in the Eastern Blue Ridge (EBR) and Western Inner Piedmont (WIP) that probably contain apatite that was not age-reset during the Alleghanian orogeny as peak metamorphism in the EBR and WIP is Neoacadian in age (Merchat, 2009). For example, white mica Ar-Ar ages from pelites in the EBR yield Neoacadian ages (Goldberg and Dallmeyer, 1997); the white mica Ar-Ar system has a very similar temperature sensitivity to that of the apatite U-Pb system (375-450 °C for apatite U-Pb (Cherniak, 2010) vs ca. 360 °C for Ar-Ar white mica (Hodges, 2005)). Grains with Alleghanian ages are instead more likely derived from near the Brevard shear zone (Figure 8), which was the locus of pervasive greenschist-facies metamorphism during the Alleghanian (Merchat, 2009), including the rocks of the Henderson orthogneiss. Samples FB2, FB3 and FB4 were collected where the FBR traverses the Henderson orthogneiss in close proximity to the Brevard Fault Zone and yield HM compositions and Alleghanian ages (green circles, Figure 9) therefore probably represent high-grade Neoacadian gneisses that were age-reset in the vicinity of the Brevard Fault Zone during greenschist-facies peak Alleghanian orogenesis (e.g. Merchat, 2009), but which retained HM REE-compositions as the diffusion of REEs in apatite only occurs above c 600 °C (Cherniak, 2010). A handful of HM-Alleghanian grains are still present in the downstream samples (FB13, FB14; Figure 9b), indicating that apatite from this source is still present in the FBR as it exits the Appalachians towards the Mississippi. The ability to assign a high likelihood of provenance from specific individual source

lithologies in a river catchment where no bedrock characterisation has been carried out is very promising for this provenance method.

Downstream, the FBR samples terranes that were not heated sufficiently during Appalachian orogenesis to reset Grenvillian U-Pb apatite ages or their igneous trace-element compositions (Figure 9b, Figure 10b). Grenvillian apatite detritus is highly distinct to Appalachian apatite detritus in terms of its trace-element composition (yellow circles, Figure 9). While there are only a limited number of Grenville-age grains in the studied samples, 11/12 have igneous compositions. This contrasts with 16/191 (8%) igneous grains in the Appalachian-age detritus (aggregated from all samples). This highlights the stark differences in the dominant lithologies in the Grenville and Appalachian orogens in this region. It can also help to explain the paucity of detrital Neoacadian and Alleghanian zircon U-Pb ages in the FBR as detrital zircon U-Pb is a poor recorder of sub-anatectic metamorphism (e.g. Hietpas et al., 2010; O'Sullivan et al., 2016). In comparison the trace-element composition of detrital apatite from the Appalachian orogen is almost entirely metamorphic-derived.

Interestingly, in common with the Stac Fada Scottish case study, apatites with LM trace-element compositions are commonly dateable in the FBR, indeed they comprise a majority of dated grains in both studies. This is in stark contrast with the river Tarn French case study wherein LM detritus is non-dateable. This begs the question what are the differences between the apatite detritus from the Southern Appalachians and the Lewisian of Scotland on one hand, and the southern Massif Central apatite detritus on the other that could explain this disparity in the amenability of LM apatite detritus to U-Pb dating? The river Tarn mainly sources pelitic that experienced single-phase peak-Variscan metamorphism, whereas the FBR and Stoer Group sediments are at least partly derived from polymetamorphic basement with diverse protolith types including igneous protoliths. This indicates that both metamorphic grade and protolith type determine whether metamorphic apatite is amenable to U-Pb dating. Additionally, perhaps poly-metamorphism makes metamorphic apatite more amenable to U-Pb dating, as apatite in high-grade metamorphic rocks might not necessarily recrystallize (and therefore lose U to other phases) upon reheating due to being located within dehydrated lithologies with negligible porosity, similar to the behaviour documented for rutile from such lithologies (e.g. Luvizotto et al., 2009).

4.5. CONCLUSIONS

The literature synthesis presented in this paper demonstrates that apatite-trace element geochemistry is highly diverse, with igneous, authigenic, metamorphic and leucosome apatite all easily discriminated on a PCA-diagram. Additionally, apatite composition varies greatly in igneous rocks, along a trend from S-type through I-type to ultrabasic rocks, which permits the identification of several sub-categories of igneous rocks, principally due to differences in LREE/HREE ratios, Sr-contents, and Eu-anomalies. The natural heterogeneity of apatite is compounded by its abundance in most bedrock samples due to the incompatibility of P in rock-forming minerals, making apatite trace-element chemistry an excellent tracer of lithology. Coupled with its usefulness as a chronometer, detrital apatite can thus provide specific provenance information to fingerprint its likely source rock, including mafic igneous lithologies that typically contribute little zircon to detritus.

As at a minimum only five elements are required as discriminant elements in this study, the required analytical protocol to reproduce the provenance methodology in this paper is extremely simple. The immobility of the REEs in apatite in the absence of recrystallization means that this protocol will also be useful for identifying apatite that has experienced metasomatism and can thus be very useful for tracking ore genesis.

4.5.1 Acknowledgements

This material is based upon works supported by Science Foundation Ireland under grant 12/IP/1663. We would also like to thank Cora McKenna for her assistance during LA-ICP-MS data acquisition. This publication has also emanated from research supported in part by a research grant from Science Foundation Ireland (SFI) under Grant Number 13/RC/2092 and co-funded under the European Regional Development Fund and by PIPCO RSG and its member companies.

4.7 REFERENCES

Abdullin, F., Solé, J., Solari, L., Shchepetilnikova, V., Meneses-Rocha, J. J., Pavlinova, N. and Rodríguez-Trejo, A. (2016) 'Single-grain apatite geochemistry of Permian-Triassic granitoids and Mesozoic and Eocene sandstones from Chiapas, southeast Mexico: Implications for sediment provenance', *International Geology Review*, 58(9), pp. 1132–1157. doi: 10.1080/00206814.2016.1150212.

Bea, F. and Montero, P. (1999) ‘Behavior of accessory phases and redistribution of Zr, REE, Y, Th, and U during metamorphism and partial melting of metapelites in the lower crust: An example from the Kinzigite Formation of Ivrea-Verbano, NW Italy’, *Geochimica et Cosmochimica Acta*, 63(7), pp. 1133–1153. doi: 10.1016/S0016-7037(98)00292-0.

Belousova, E. A., Walters, S., Griffin, W. L. and O'Reilly, S. Y. (2001) ‘Trace-element signatures of apatites in granitoids from the Mt Isa Inlier, Northwestern Queensland’, *Australian Journal of Earth Sciences*, 48(AUGUST), pp. 603–619. doi: 10.1046/j.1440-0952.2001.00879.x.

Belousova, E. A., Griffin, W. L., O’Reilly, S. Y. and Fisher, N. I. (2002) ‘Apatite as an indicator mineral for mineral exploration: Trace-element compositions and their relationship to host rock type’, *Journal of Geochemical Exploration*, 76(1), pp. 45–69. doi: 10.1016/S0375-6742(02)00204-2.

Belousova, E. A, Griffin, W. L., O’Reilly, S. Y. and Fisher, N. I. (2002) ‘Igneous zircon: trace element composition as an indicator of source rock type’, *Contributions to Mineralogy and Petrology*, 143(2002), pp. 602–622. doi: 10.1007/s00410-002-0364-7.

Bernoulli, D. and Winkler, W. (1990) ‘Heavy mineral assemblages from Upper Cretaceous South- and Austroalpine flysch sequences (Northern Italy and Southern Switzerland) : source terrances and palaeotectonic implications’, *Eclogae Geologicae Helvetiae*, 83(2), pp. 287–310. doi: 10.5169/seals-166588.

Bingen, B., Demaiffe, D. and Hertogen, J. (1996) ‘Redistribution of rare earth elements, thorium, and uranium over accessory minerals in the course of amphibolite to granulite facies metamorphism: The role of apatite and monazite in orthogneisses from southwestern Norway’, *Geochimica et Cosmochimica Acta*, 60(8), pp. 1341–1354. doi: 10.1016/0016-7037(96)00006-3.

Bouch, J. E., Hole, M. J., Trewin, N. H., Chenery, S. and Morton, A. C. (2002) ‘Authigenic Apatite in a Fluvial Sandstone Sequence: Evidence for Rare-Earth Element Mobility During Diagenesis and a Tool for Diagenetic Correlation’, *Journal of Sedimentary Research*, 72(1), pp. 59–67. doi: 10.1306/040301720059.

Boyce, J. W., Tomlinson, S. M., Mccubbin, F. M., Greenwood, J. P. and Treiman, A. H. (2014) 'The Lunar Apatite Paradox', *Science*, 344(6182), pp. 400–402. doi: 10.1126/science.1250398.

Brichau, S., Respaut, J. P. and Monié, P. (2008) 'New age constraints on emplacement of the Cévenol granitoids, South French Massif Central', *International Journal of Earth Sciences*, 97(4), pp. 725–738. doi: 10.1007/s00531-007-0187-x.

Broska, I., Williams, C. T., Uher, P., Konečný, P. and Leichmann, J. (2004) 'The geochemistry of phosphorus in different granite suites of the Western Carpathians, Slovakia: The role of apatite and P-bearing feldspar', *Chemical Geology*, 205(1–2), pp. 1–15. doi: 10.1016/j.chemgeo.2003.09.004.

Carrapa, B., DeCelles, P. G., Reiners, P. W., Gehrels, G. E. and Sudo, M. (2009) 'Apatite triple dating and white mica40Ar/39Ar thermochronology of syntectonic detritus in the Central Andes: A multiphase tectonothermal history', *Geology*, 37(5), pp. 407–410. doi: 10.1130/G25698A.1.

Chakhmouradian, A. R., Reguir, E. P., Zaitsev, A. N., Couëslan, C., Xu, C., Kynický, J., Mumin, A. H. and Yang, P. (2017) 'Apatite in carbonatitic rocks: Compositional variation, zoning, element partitioning and petrogenetic significance', *Lithos*, 274–275, pp. 188–213. doi: 10.1016/j.lithos.2016.12.037.

Cherniak, D. J. (2010) 'Diffusion in Accessory Minerals: Zircon, Titanite, Apatite, Monazite and Xenotime', *Reviews in Mineralogy and Geochemistry*, 72(1), pp. 827–869. doi: 10.2138/rmg.2010.72.18.

Chew, D.M. and Donelick, R.A. (2012) 'Combined apatite fission track and U-Pb dating by LA-ICP-MS and its application in apatite provenance analysis'. *Quantitative mineralogy and microanalysis of sediments and sedimentary rocks: Mineralogical Association of Canada Short Course*, *42*, pp.219-247.

Chew, D. M., Petrus, J. A. and Kamber, B. S. (2014) 'U-Pb LA-ICPMS dating using accessory mineral standards with variable common Pb', *Chemical Geology*. Elsevier B.V., 363, pp. 185–199. doi: 10.1016/j.chemgeo.2013.11.006.

Chu, M.-F., Wang, K.-L., Griffin, W. L., Chung, S.-L., O'Reilly, S. Y., Pearson, N. J. and Iizuka, Y. (2009) 'Apatite Composition: Tracing Petrogenetic Processes in Transhimalayan Granitoids', *Journal of Petrology*, 50(10), pp. 1829–1855. doi: 10.1093/petrology/egp054.

Chu, M. F., Wang, K. L., Griffin, W. L., Chung, S. L., O'Reilly, S. Y., Pearson, N. J. and Iizuka, Y. (2009) 'Apatite composition: Tracing petrogenetic processes in Transhimalayan granitoids', *Journal of Petrology*, 50(10), pp. 1829–1855. doi: 10.1093/petrology/egp054.

Dill, H. G. (1994) 'Can REE patterns and U-Th variations be used as a tool to determine the origin of apatite in clastic rocks?', *Sedimentary Geology*, 92(3–4), pp. 175–196. doi: 10.1016/0037-0738(94)90105-8.

Dill, H. G., Weber, B. and Klosa, D. (2012) 'Morphology and mineral chemistry of monazite-zircon-bearing stream sediments of continental placer deposits (SE Germany): Ore guide and provenance marker', *Journal of Geochemical Exploration*, 112, pp. 322–346. doi: 10.1016/j.gexplo.2011.10.006.

El Korh, A., Schmidt, S. T., Ulianov, A. and Potel, S. (2009) 'Trace Element Partitioning in HP-LT Metamorphic Assemblages during Subduction-related Metamorphism, Ile de Groix, France: a Detailed LA-ICPMS Study', *Journal of Petrology*, 50(6), pp. 1107–1148. doi: 10.1093/petrology/egp034.

Faure, M., Lardeaux, J. M. and Ledru, P. (2009) 'A review of the pre-Permian geology of the Variscan French Massif Central', *Comptes Rendus - Geoscience*, 341, pp. 202–213. doi: 10.1016/j.crte.2008.12.001.

Gall, Q., Davis, W. J., Lowe, D. G. and Dabros, Q. (2017) 'Diagenetic apatite character and in situ ion microprobe U – Pb age , Keeseville Formation , Potsdam Group , New York State', 797(March), pp. 785–797. doi: 10.1139/cjes-2016-0195.

Garzanti, E. (2017) 'The Maturity Myth In Sedimentology and Provenance Analysis', *Journal of Sedimentary Research*, 87(4), pp. 353–365. doi: 10.2110/jsr.2017.17.

Goldberg, S.A. and Dallmeyer, R.D., (1997) 'Chronology of Paleozoic metamorphism and deformation in the Blue Ridge thrust complex, North Carolina and Tennessee' *American Journal of Science*, *297*(5), pp.488-526. doi: 10.2475/ajs.297.5.488

Harlov, D. E. (2011) 'Formation of monazite and xenotime inclusions in fluorapatite megacrysts, Gloserheia Granite Pegmatite, Froland, Bamble Sector, southern Norway', *Mineralogy and Petrology*, 102(1–4), pp. 77–86. doi: 10.1007/s00710-011-0166-6.

Harlov, D. E. (2015) 'Apatite: A fingerprint for metasomatic processes', *Elements*, 11(3), pp. 171–176. doi: 10.2113/gselements.11.3.171.

Hatcher Robert D., J., (2010). The Appalachian orogen: A brief summary, in: Tollo, R.P., Bartholomew, M.J., Hibbard, J.P., Karabinos, P.M. (Eds.), From Rodinia to Pangea: The Lithotectonic Record of the Appalachian Region. Geological Society of America.

Henrichs, I. A., O'Sullivan, G. J., Chew, D. M., Mark, C., Babechuk, M. G., McKenna, C. and Emo, R. (2018) 'The trace element and U-Pb systematics of metamorphic apatite', *Chemical Geology*. Elsevier B.V, 483, pp. 218–238. doi: 10.1016/j.chemgeo.2017.12.031.

Hietpas, J., Samson, S., Moecher, D. and Schmitt, A. K. (2010) 'Recovering tectonic events from the sedimentary record: Detrital monazite plays in high fidelity', *Geology*, 38(2), pp. 167–170. doi: 10.1130/G30265.1.

Hodges, K. V. (2005) '40Ar/39Ar Thermochronology of Detrital Minerals', *Reviews in Mineralogy and Geochemistry*, 58(1), pp. 239–257. doi: 10.2138/rmg.2005.58.9.

Hsieh, P. S., Chen, C. H., Yang, H. J. and Lee, C. Y. (2008) 'Petrogenesis of the Nanling Mountains granites from South China: Constraints from systematic apatite geochemistry and whole-rock geochemical and Sr-Nd isotope compositions', *Journal of Asian Earth Sciences*, 33, pp. 428–451. doi: 10.1016/j.jseaes.2008.02.002.

Hubert, J. F. (1962) ‘A zircon-tourmaline-rutile maturity index and the interdependence of the composition of heavy mineral assemblages with the gross composition and texture of sandstones’, *Journal of Sedimentary Research*, 32(3), pp. 440–450. doi: 10.1306/74D70CE5-2B21-11D7-8648000102C1865D.

Ielpi, A. and Ghinassi, M. (2015) ‘Planview style and palaeodrainage of Torridonian channel belts: Applecross Formation, Stoer Peninsula, Scotland’, *Sedimentary Geology*, 325, pp. 1–16. doi: 10.1016/j.sedgeo.2015.05.002.

Ihlen, P. M., Schiellerup, H., Gautneb, H. and Skår, Ø. (2014) ‘Characterization of apatite resources in Norway and their REE potential - A review’, *Ore Geology Reviews*, 58(C), pp. 126–147. doi: 10.1016/j.oregeorev.2013.11.003.

Joosu, L., Lepland, A., Kirsimäe, K., Romashkin, A. E., Roberts, N. M. W., Martin, A. P. and Črne, A. E. (2015) ‘The REE-composition and petrography of apatite in 2Ga Zaonega Formation, Russia: The environmental setting for phosphogenesis’, *Chemical Geology*, 395, pp. 88–107. doi: 10.1016/j.chemgeo.2014.11.013.

Joosu, L., Lepland, A., Kreitsmann, T., Üpraus, K., Roberts, N. M. W., Paiste, P., Martin, A. P. and Kirsimäe, K. (2016) ‘Petrography and the REE-composition of apatite in the Paleoproterozoic Pilgujärvi Sedimentary Formation, Pechenga Greenstone Belt, Russia’, *Geochimica et Cosmochimica Acta*, 186, pp. 135–153. doi: 10.1016/j.gca.2016.04.043.

Kinny, P. D., Friend, C. R. L. and Love, G. J. (2005) ‘Proposal for a terrane-based nomenclature for the Lewisian Gneiss Complex of NW Scotland’, *Journal of the Geological Society*, 162(1), pp. 175–186. doi: 10.1144/0016-764903-149.

Krenn, E., Harlov, D. E., Finger, F. and Wunder, B. (2012) ‘LREE-redistribution among fluorapatite, monazite, and allanite at high pressures and temperatures’, *American Mineralogist*, 97, pp. 1881–1890. doi: 10.2138/am.2012.4005.

Kusebauch, C., John, T., Whitehouse, M. J., Klemme, S. and Putnis, A. (2015) 'Distribution of halogens between fluid and apatite during fluid-mediated replacement processes', *Geochimica et Cosmochimica Acta*. Elsevier Ltd, 170, pp. 225–246. doi: 10.1016/j.gca.2015.08.023.

Lawrence, M. G., Jupiter, S. D. and Kamber, B. S. (2006) 'Aquatic geochemistry of the rare earth elements and yttrium in the Pioneer River catchment, Australia', *Marine and Freshwater Research*, 57(7), pp. 725–736. doi: 10.1071/MF05229.

Lawrence, M. G. and Kamber, B. S. (2006) 'The behaviour of the rare earth elements during estuarine mixing-revisited', *Marine Chemistry*, 100, pp. 147–161. doi: 10.1016/j.marchem.2005.11.007.

Lê, S., Josse, J. and Husson, F. (2008) 'FactoMineR: An R Package for Multivariate Analysis', *J. of Statistical Software*, 25(1), pp. 1–18. doi: 10.1016/j.envint.2008.06.007.

London, D. (1992) 'Phosphorus in S-type magmas: the P2O5content of feldspars from peraluminous granites, pegmatites, and rhyolites', *American Mineralogist*, 77(1–2), pp. 126–145.

Luvizotto, G. L., Zack, T., Triebold, S. and Von Eynatten, H. (2009) 'Rutile occurrence and trace element behavior in medium-grade metasedimentary rocks: Example from the Erzgebirge, Germany', *Mineralogy and Petrology*, 97(3–4), pp. 233–249. doi: 10.1007/s00710-009-0092-z.

Mao, M., Rukhlov, A. S., Rowins, S. M., Spence, J. and Coogan, L. A. (2015) 'Detrital Apatite Trace-Element Compositions : a Robust New Tool for Mineral Exploration', *Economic Geology*, 111 (5), pp. 1187-1122. doi: 10.2113/econgeo.111.5.1187.

Mark, C., Cogné, N. and Chew, D. (2016) 'Tracking exhumation and drainage divide migration of the western Alps: a test of the apatite U-Pb thermochronometer as a detrital provenance tool', *GSA Bulletin*, 128 (9-10), pp. 1439-1460. doi: 10.1130/B31351.1.

Matsumoto, T., Honda, M., McDougall, I., Yatsevich, I. and O'Reilly, S. Y. (1997) 'Plume-like neon in a metasomatic apatite from the Australian lithospheric mantle', *Nature*, 388(6638), pp. 162–164. doi: 10.1038/40606.

McCubbin, F. M., Jolliff, B. L., Nekvasil, H., Carpenter, P. K., Zeigler, R. A., Steele, A., Elardo, S. M. and Lindsley, D. H. (2011) 'Fluorine and chlorine abundances in lunar apatite: Implications for heterogeneous distributions of magmatic volatiles in the lunar interior', *Geochimica et Cosmochimica Acta*, 75(17), pp. 5073–5093. doi: 10.1016/j.gca.2011.06.017.

McDonough, W. F., Sun, S. (1995) 'The composition of the Earth' *Chemical Geology*, 120(3–4), pp. 223–253. doi: 10.1016/0009-2541(94)00140-4.

Merschat, A.J., (2009). 'Assembling the Blue Ridge and Inner Piedmont: Insights into the nature and timing of terrane accretion in the southern Appalachian orogen from geologic mapping, stratigraphy, kinematic analysis, petrology, geochemistry, and modern geochronology' *PhD dissertation, University of Tennessee*

Morton, A., Yaxley, G. (2007) 'Detrital apatite geochemistry and its application in provenance studies', *Geological Society of America Special Paper,* 420, pp. 319–344. doi: 10.1130/2006.2420(19).

Morton, A. C. and Hallsworth, C. R. (1999) 'Processes controlling the composition of heavy mineral assemblages in sandstones', *Sedimentary Geology*, 124, pp. 3–29. doi: 10.1016/S0037-0738(98)00118-3.

Naeser, C. W. (1967) 'The use of apatite and sphene for fission track age determinations', *Geological Society of America Bulletin*, v. 78, p. 1523-1526

Nechaev, V. P. and Isphording, W. C. (1993) 'Heavy-Mineral Assemblages of Continental Margins as Indicators of Plate-Tectonic Environments', *Journal of Sedimentary Petrology*, 63(6), pp. 1110–1117. doi: 10.1306/D4267CB7-2B26-11D7-8648000102C1865D.

Nishizawa, M., Takahata, N., Terada, K., Komiya, T., Ueno, Y. and Sano, Y. (2005) 'Rare-earth element, lead, carbon, and nitrogen geochemistry of apatite-bearing metasediments from the similar to 3.8 Ga Isua supracrustal belt, West Greenland', *International Geology Review*, 47(9), pp. 952–970. doi: 10.2747/0020-6814.47.9.952.

Nutman, A. P. (2007) 'Apatite recrystallisation during prograde metamorphism, Cooma, southeast Australia: implications for using an apatite – graphite association as a biotracer in ancient metasedimentary rocks', *Australian Journal of Earth Sciences*, 54, pp. 1023–1032. doi: 10.1080/08120090701488321.

O'Reilly, S. Y. and Griffin, W. L. (2000) 'Apatite in the mantle: Implications for metasomatic processes and high heat production in Phanerozoic mantle', *Lithos*, 53(3–4), pp. 217–232. doi: 10.1016/S0024-4937(00)00026-8.

O'Sullivan, G. J., Chew, D. M., Samson, S. D. (2016) 'Detecting magma poor orogens in the detrital record', *Geology* 19, 44(10), pp. 871–874. doi: 10.1130/G38245.1.

O'Sullivan, G. J., Chew, D. M., Morton, A. C., Mark, C. and Henrichs, I. A. (2018) 'An Integrated Apatite Geochronology and Geochemistry Tool for Sedimentary Provenance Analysis', *Geochemistry, Geophysics, Geosystems*, pp. 1309–1326. doi: 10.1002/2017GC007343.

Oosthuyzen, E. J. and Burger, A. J. (1973) 'The suitability of apatite as an age indicator by the uranium-lead isotope method', *Earth and Planetary Science Letters*, 18(1), pp. 29–36. doi: 10.1016/0012-821X(73)90030-7.

Parnell, J., Mark, D., Fallick, A. E., Boyce, A. and Thackrey, S. (2011) 'The age of the Mesoproterozoic Stoer Group sedimentary and impact deposits, NW Scotland', *Journal of the Geological Society*, 168(2), pp. 349–358. doi: 10.1144/0016-76492010-099.

Piccoli, P. M. and Candela, P. A. (2002) 'Apatite in Igneous Systems', *Reviews in Mineralogy and Geochemistry*, 48, pp. 255–292. doi: 10.2138/rmg.2002.48.6.

Prowatke, S. and Klemme, S. (2006) 'Trace element partitioning between apatite and silicate melts', *Geochimica et Cosmochimica Acta*, 70(17), pp. 4513–4527. doi: 10.1016/j.gca.2006.06.162.

Ronsbo, J. G. (1989) 'Coupled substitutions involving REEs and Na and Si in apatites in alkaline rocks from the Ilimaussaq intrusion, South Greenland, and the petrological implications', *American Mineralogist*, 74(7–8), pp. 896–901.

Ruttenberg, K. C. and Berner, R. A. (1993) 'Authigenic apatite formation and burial in sediments from non-upwelling, continental margin environments', *Geochimica et Cosmochimica Acta*, 57(5), pp. 991–1007. doi: 10.1016/0016-7037(93)90035-U.

Schneider, S., Hammerschmidt, K., Rosenberg, C. L., Gerdes, A., Frei, D. and Bertrand, A. (2015) 'U-Pb ages of apatite in the western Tauern Window (Eastern Alps): Tracing the onset of collision-related exhumation in the European plate', *Earth and Planetary Science Letters*. Elsevier B.V., 418, pp. 53–65. doi: 10.1016/j.epsl.2015.02.020.

Sell, B. K., Samson, S. D., Mitchell, C. E., Mclaughlin, P. I., Koenig, A. E. and Leslie, S. A. (2015) 'Stratigraphic correlations using trace elements in apatite from Late Ordovician (Sandbian-Katian) K-bentonites of eastern North America The early Late Ordovician sedimentary', *Geological Society of America Bulletin*, (9), pp. 1–16. doi: 10.1130/B31194.1.

Sha, L.-K. and Chappell, B. W. (1999) 'Apatite chemical composition, determined by electron microprobe and laser-ablation inductively coupled plasma mass spectrometry, as a probe into granite petrogenesis', *Geochimica et Cosmochimica Acta*, 63(22), pp. 3861–3881. doi: 10.1016/S0016-7037(99)00210-0.

Shields, G. and Stille, P. (2001) 'Diagenetic constraints on the use of cerium anomalies as palaeoseawater redox proxies: An isotopic and REE study of Cambrian phosphorites', *Chemical Geology*, 175(1–2), pp. 29–48. doi: 10.1016/S0009-2541(00)00362-4.

Simms, M. J. (2015) 'The Stac Fada impact ejecta deposit and the Lairg Gravity Low: Evidence for a buried Precambrian impact crater in Scotland?', *Proceedings of the Geologists' Association*. The Geologists' Association, 126(6), pp. 742–761. doi: 10.1016/j.pgeola.2015.08.010.

Spear, F. S. and Pyle, J. M. (2002) 'Apatite, Monazite, and Xenotime in Metamorphic Rocks', *Reviews in Mineralogy and Geochemistry*, 48, pp. 293–335. doi: 10.2138/rmg.2002.48.7.

Spencer, C. J., Kirkland, C. L. and Taylor, R. J. M. (2016) 'Strategies towards statistically robust interpretations of in situ U-Pb zircon geochronology', *Geoscience Frontiers*. Elsevier Ltd, 7(4), pp. 581–589. doi: 10.1016/j.gsf.2015.11.006.

Stewart, A.D., (2002). 'The later Proterozoic Torridonian rocks of Scotland: their sedimentology, geochemistry and origin' Published by *The Geological Society of London,* Memoir no. 24

Tang, M., Wang, X. L., Xu, X. S., Zhu, C., Cheng, T. and Yu, Y. (2012) 'Neoproterozoic subducted materials in the generation of Mesozoic Luzong volcanic rocks: Evidence from apatite geochemistry and Hf-Nd isotopic decoupling', *Gondwana Research*. International Association for Gondwana Research, 21(1), pp. 266–280. doi: 10.1016/j.gr.2011.05.009.

Thomson, S. N., Gehrels, G. E., Ruiz, J. and Buchwaldt, R. (2012) 'Routine low-damage apatite U-Pb dating using laser ablation-multicollector- ICPMS', *Geochemistry, Geophysics, Geosystems*, 13(1), pp. 1–23. doi: 10.1029/2011GC003928.

Tollari, N., Barnes, S. J., Cox, R. A. and Nabil, H. (2008) 'Trace element concentrations in apatites from the Sept-Îles Intrusive Suite, Canada - Implications for the genesis of nelsonites', *Chemical Geology*, 252(3–4), pp. 180–190. doi: 10.1016/j.chemgeo.2008.02.016.

Vermeesch, P., Avigad, D. and McWilliams, M. O. (2009) '500 m.y. of thermal history elucidated by multi-method detrital thermochronology of North Gondwana Cambrian sandstone (Eilat area, Israel)', *Bulletin of the Geological Society of America*, 121(7–8), pp. 1204–1216. doi: 10.1130/B26473.1.

Wagner, G. A. (1968) ‘Fission track dating of apatites’, *Earth and Planetary Science Letters*, 4(5), pp. 411–415. doi: 10.1016/0012-821X(68)90072-1.

Whittaker, E. J.W. and Muntus, R., (1970) ‘Ionic radii for use in geochemistry’ *Geochimica et Cosmochimica Acta*, *34*(9), pp.945-956.

Zattin, M., Andreucci, B., Thomson, S. N., Reiners, P. W. and Talarico, F. M. (2012) ‘New constraints on the provenance of the ANDRILL AND-2A succession (western Ross Sea, Antarctica) from apatite triple dating’, *Geochemistry, Geophysics, Geosystems*, 13(10). doi: 10.1029/2012GC004357.

Zeitler, P. K., Herczeg, A. L., McDougall, I. and Honda, M. (1987) ‘U-Th-He dating of apatite: A potential thermochronometer’, *Geochimica et Cosmochimica Acta*, 51(10), pp. 2865–2868. doi: 10.1016/0016-7037(87)90164-5.

Zirner, A. L. K., Marks, M. A. W., Wenzel, T., Jacob, D. E. and Markl, G. (2015) ‘Rare earth elements in apatite as a monitor of magmatic and metasomatic processes: The Ilímaussaq complex, South Greenland’, *Lithos*. Elsevier B.V., 228–229, pp. 12–22. doi: 10.1016/j.lithos.2015.04.013.

4.8 SUPPORTING INFORMATION

Code S4.1: 'R' code for creating PCA biplots as used in this chapter

```
library(FactoMineR)
library(factoextra)
library(corrplot)
setwd("~/INSERT_TEXT.txt") #here is your working directory where your table is
read.table("INSERT_TABLE", header=TRUE, sep="", dec=".")->data #("data" is simply a new name given to your table)
data_transform<-data[1:X, 2:X] #data transform is your data with the first collumn removed so the PCA function can read the file
combined_pca_output<-PCA(data_transform, ind.sup=1+X:Y, graph=TRUE) #combined PCA output is the PCA. ind.sup is the test data
fviz_pca_ind(combined_pca_output, col.ind="red", col.ind.sup="blue", label="ind.sup") #a PCA without groupings
fviz_pca_biplot(combined_pca_output,pch=20,ellipse.level = 0.68,col.var="black",addEllipse=TRUE,label="var",habillage=data$Lithology[1:250],mean.point=FALSE)
#"habillage=data$Lithology" is used to color the different type of rock, rename it according to the name of your column hosting the rock type
#pch 15=square, 19=circle, 17=triangle if you want different shapes
eig.val<-get_eigenvalue(combined_pca_output) #from here on, these are just useful for displaying metadata concerning the PCA
eig.val
fviz_eig(combined_pca_output,addlabels=TRUE)#histogram
var<-get_pca_var(combined_pca_output)
var$coord
fviz_pca_var(combined_pca_output,col.var = "contrib",gradient.cols = c("#00AFBB", "#E7B800", "#FC4E07"))
fviz_pca_var(combined_pca_output)
corrplot(var$cos2, is.corr=FALSE)
```

Table S4.1 library of previously published apatite trace-element data

In column "averaging" C = median *calculated* by author of this thesis, M = *median* provided by author of the paper cited.

Sample Name	Code	Exact Lithology	Averaging	Source Paper	La	Ce	Pr	Sr	Nd	Sm	Eu	Gd	Tb	Dy	Y	Ho	Er	Tm	Yb	Lu	Eu/Eu*
Granite Squirrel	IB	I-type granite	M	Belousova et al. 2001.	2363.0	3988	393.0	134.0	1347	194.0	23.0	177.0		148.0	958	29.0	85.0	12.0	79.00	13.00	0.37
Granite Squirrel	IB	I-type granite	M	Belousova et al. 2001.	1976.0	3790	372.0	108.0	1210	166.0	24.0	147.0		116.0	868	25.0	78.0	11.0	80.00	15.00	0.46
Granite Squirrel	IB	I-type granite	M	Belousova et al. 2001.	1790.0	4036	446.0	88.0	1492	212.0	27.0	177.0		140.0	1054	32.0	90.0	14.0	95.00	16.00	0.41
Granite Squirrel	IB	I-type granite	M	Belousova et al. 2001.	1389.0	3972	554.0	50.0	2335	477.0	25.0	480.0		358.0	2649	72.0	201.0	29.0	198.00	33.00	0.16
Granite Squirrel	IB	I-type granite	M	Belousova et al. 2001.	3329.0	4938	477.0	218.0	1615	219.0	40.0	195.0		135.0	829	28.0	73.0	9.0	57.00	10.00	0.58
Granite Wirrabura	IB	I-type granite	M	Belousova et al. 2001.	2562.0	6259	696.0	46.0	2261	335.0	26.0	306.0		247.0	1795	54.0	159.0	23.0	163.00	27.00	0.24
Granite Wirrabura	IB	I-type granite	M	Belousova et al. 2001.	2230.0	3959	394.0	145.0	1274	161.0	31.0	146.0		109.0	828	25.0	73.0	10.0	73.00	14.00	0.60
Granite Wirrabura	IB	I-type granite	M	Belousova et al. 2001.	1639.0	3282	354.0	170.0	1210	171.0	29.0	159.0		127.0	939	28.0	84.0	12.0	89.00	18.00	0.53
Diorite Wirrabura	IB	I-type granite	M	Belousova et al. 2001.	1478.0	1857	154.0	342.0	447	56.0	12.0	52.0		41.0	267	8.0	21.0	2.0	19.00	2.00	0.67
Granite Mt Angelay	IB	I-type granite	M	Belousova et al. 2001.	1628.0	3641	481.0	218.0	1589	241.0	24.0	207.0		147.0	896	31.0	83.0	10.0	66.00	11.00	0.32
Granite Mt Angelay	IB	I-type granite	M	Belousova et al. 2001.	1814.0	2703	235.0	229.0	728	93.0	16.0	102.0		89.0	516	19.0	53.0	6.0	37.00	6.00	0.50
Granite Mt Angelay	IB	I-type granite	M	Belousova et al. 2001.	3161.0	6732	598.0	160.0	1844	169.0	28.0	125.0		86.0	704	19.0	58.0	9.0	75.00	14.00	0.56
Jiuzhou	S	S-type granite	C	Hsieh et al. 2008.	420.0	1426	229.0	65.3	1123	472.0	2.9	605.0	121.0	732.0	3698	137.0	323.0	41.1	244.00	29.70	0.02
Taima	S	S-type granite	C	Hsieh et al. 2008.	749.0	2338	328.0	48.7	1395	529.0	2.0	647.0	137.0	898.0	4391	175.0	438.0	57.7	347.00	40.70	0.01
Pubai	S	S-type granite	C	Hsieh et al. 2008.	391.0	1328	210.0	49.9	987	420.0	3.9	503.0	108.0	694.0	3372	139.0	365.0	50.6	324.00	40.90	0.03
Pubai	S	S-type granite	C	Hsieh et al. 2008.	369.0	1179	195.0	60.7	995	454.0	6.2	583.0	131.0	792.0	3722	142.0	336.0	43.0	266.00	31.00	0.04
Nadong	S	S-type granite	C	Hsieh et al. 2008.	597.0	1990	312.0	47.8	1582	622.0	2.5	827.0	167.0	1030.0	5384	202.0	500.0	58.6	326.00	35.90	0.01
Nadong	S	S-type granite	C	Hsieh et al. 2008.	606.0	1881	301.0	27.9	1554	675.0	30.5	876.0	184.0	1121.0	5974	217.0	524.0	63.6	365.00	41.20	0.12
Nadong	S	S-type granite	C	Hsieh et al. 2008.	548.0	2075	307.0	18.6	1361	592.0	2.6	692.0	151.0	911.0	4243	166.0	404.0	54.7	355.00	37.50	0.01
Zudi	IB	I-type granite	C	Hsieh et al. 2008.	1141.0	3012	387.0	359.0	1645	316.0	12.8	303.0	36.0	189.0	979	35.5	85.9	10.9	62.60	8.18	0.12
Changtai	IB	I-type granite	C	Hsieh et al. 2008.	1623.0	3581	435.0	249.0	1906	357.0	16.3	309.0	35.1	179.0	841	31.4	73.8	8.4	50.00	6.37	0.15
Danyang	IB	I-type granite	C	Hsieh et al. 2008.	1489.0	2912	304.0	97.0	1156	224.0	9.3	225.0	26.1	139.0	707	26.2	64.5	7.5	45.80	6.22	0.12
Fuzhou	IB	I-type granite	C	Hsieh et al. 2008.	567.0	2038	313.0	81.3	1519	510.0	17.6	554.0	100.0	621.0	3482	119.0	306.0	41.8	281.00	35.10	0.10
Yangjan	IB	I-type granite	C	Hsieh et al. 2008.	3312.0	5887	514.0	260.0	1634	196.0	29.4	254.0	19.5	107.0	726	28.7	67.3	10.0	68.10	11.60	0.40
Lianjiang	IB	I-type granite	C	Hsieh et al. 2008.	1460.0	3462	482.0	46.3	1850	375.0	30.9	360.0	49.5	286.0	1634	55.3	142.0	17.0	99.00	11.90	0.25
Guidong	IB	Granodiorite	C	Hsieh et al. 2008.	517.3	1582	246.3	131.9	1140	320.7	23.1	325.0	50.4	267.0	1523	47.2	120.2	14.7	89.23	12.17	0.26
Fogang	IS	Intermediate granite	C	Hsieh et al. 2008.	369.0	1221	199.9	55.7	1087	412.0	8.0	513.5	96.7	606.0	3474	118.0	308.3	40.3	249.50	31.10	0.05
Qitianling	IS	Intermediate granite	C	Hsieh et al. 2008.	3429.0	6442	668.0	117.0	2472	408.0	7.2	387.0	45.1	244.0	1405	47.5	121.0	15.7	96.80	12.80	0.05
Lianyang	IS	Intermediate granite	C	Hsieh et al. 2008.	1555.0	4243	598.0	57.1	2788	696.0	6.6	681.0	98.1	522.0	2524	95.8	225.0	26.4	152.00	19.30	0.03
Jiufeng	IS	Intermediate granite	C	Hsieh et al. 2008.	700.5	1918	290.5	135.5	1388	364.0	20.5	350.0	57.6	346.5	2334	70.5	185.8	26.5	185.70	25.10	0.18
Dadongshan	IS	Intermediate granite	C	Hsieh et al. 2008.	651.0	1891	284.0	54.1	1330	383.0	5.3	381.0	62.5	360.0	2017	68.9	179.0	25.0	182.00	28.90	0.04
Chebu	IB	Gabbro	C	Hsieh et al. 2008.	1439.0	2883	301.0	239.0	1127	188.0	22.6	86.0	20.6	111.0	549	21.6	54.9	6.9	44.10	5.93	0.42
Quanman	ALK	Syenite	C	Hsieh et al. 2008.	2989.0	6141	763.0	35.8	3323	613.0	40.4	557.0	65.6	332.0	1438	59.3	129.0	14.1	74.40	8.51	0.21
Paitan	ALK	Syenite	C	Hsieh et al. 2008.	1014.0	2174	303.0	518.0	1516	307.0	94.6	280.0	33.5	166.0	810	29.6	67.2	7.2	41.00	5.52	0.97
Ejinao	ALK	Syenite	C	Hsieh et al. 2008.	4006.0	7692	814.0	268.0	2972	416.0	27.2	384.0	39.9	208.0	1051	40.0	96.3	11.4	66.50	8.29	0.20
LZ1	IB	Basalt	C	Tang et al. 2012.	1356.8	2962	350.8	1321.2	1476	252.0	35.4	176.2	22.1	108.9	587	20.1	47.6	5.7	34.12	4.51	0.49
LZ2	IB	Basalt	C	Tang et al. 2012.	1161.3	2594	313.1	1185.5	1360	289.2	31.3	169.1	21.3	102.6	558	19.1	45.4	5.5	32.11	4.26	0.45
LZ3	IB	Basalt	C	Tang et al. 2012.	859.1	1852	229.0	1079.6	981	177.9	28.1	134.7	16.6	80.8	373	15.0	36.5	4.2	28.61	3.24	0.53
LZ6	IB	Basalt	C	Tang et al. 2012.	2090.9	5202	710.1	385.7	3062	537.1	70.0	395.9	49.6	244.4	1133	48.6	98.2	11.4	64.29	7.42	0.45
LZ7	IB	Basalt	C	Tang et al. 2012.	1996.3	5268	599.8	354.2	2535	448.1	64.8	327.4	41.7	205.4	898	35.9	81.9	9.5	53.65	6.62	0.49
Eclogite Core	LM	Eclogite	M	El Korh et al. 2009.	28.3	28	5.0	344.0	16	3.0	0.7	2.7	0.6	4.7	30	1.1	3.4	0.4	3.20	0.44	0.78
Eclogite Rim	LM	Eclogite	M	El Korh et al. 2009.	8.2	10	1.7	342.0	6	1.3	0.3	1.7	0.5	4.2	32	1.1	3.5	0.5	3.10	0.52	0.62
B'schist	LM	Blueschist	M	El Korh et al. 2009.	50.0	23	11.3	407.0	42	7.8	1.6	7.3	1.0	5.7	38	1.1	4.0	0.7	6.30	1.20	0.64
B'schist	LM	Blueschist	M	El Korh et al. 2009.	8.7	14	3.5	217.0	12	3.2	0.8	2.5	0.4	2.6	12	0.5	1.7	0.3	2.20	0.43	0.84
B'schist	LM	Blueschist	M	El Korh et al. 2009.	7.7	3	2.8	324.0	12	3.2	0.9	3.2	0.5	4.3	32	1.0	3.9	0.6	3.00	0.43	0.84
Micaschist Core	LM	Greenschist facies	M	El Korh et al. 2009.	18.0	60	9.6	937.0	54	22.0	6.3	37.0	8.9	81.0	545	21.0	68.0	11.0	79.00	10.00	0.67
Micaschist Rim	LM	Greenschist facies	M	El Korh et al. 2009.	5.7	14	1.8	268.0	8	3.5	0.9	5.5	1.6	16.0	119	4.6	16.0	2.8	19.00	3.00	0.59
T006C	S	S-type granite	C	Chu et al. 2009.	168.0	608	111.4	184.6	590	256.7	12.3	355.9	68.1	429.7	1920	76.3	185.8	23.5	137.89	17.40	0.12
T048C	S	S-type granite	C	Chu et al. 2009.	238.4	717	116.1	87.6	528	241.8	10.7	352.9	77.8	508.7	2715	87.9	216.5	28.9	172.37	21.17	0.11
T125A	S	S-type granite	C	Chu et al. 2009.	292.8	733	122.3	89.9	577	262.0	9.5	378.1	79.1	504.9	2630	86.4	211.7	28.1	168.68	20.67	0.09
T138A	S	S-type granite	C	Chu et al. 2009.	250.9	1008	169.1	74.1	882	375.5	10.8	489.0	98.4	666.1	3513	127.1	340.3	45.1	277.55	33.91	0.08
T170A	S	S-type granite	C	Chu et al. 2009.	506.1	1624	272.2	52.9	1358	558.2	4.2	716.7	140.9	896.0	4569	163.1	416.3	59.4	392.56	50.05	0.02
T172A	S	S-type granite	C	Chu et al. 2009.	352.4	1269	205.4	55.4	1007	425.4	3.2	545.5	107.7	682.5	3413	120.5	288.9	36.6	220.88	25.65	0.02
T036C	IB	I-type granite	C	Chu et al. 2009.	499.2	1421	187.2	524.5	809	169.2	21.7	143.0	17.1	95.5	568	19.0	51.9	7.3	47.37	6.98	0.41
T044	IB	I-type granite	C	Chu et al. 2009.	1542.0	2211	212.2	373.6	717	87.6	17.5	67.6	7.4	43.9	255	8.9	24.7	3.6	25.31	4.53	0.67
ET021E	IB	I-type granite	C	Chu et al. 2009.	1124.3	2237	243.7	321.7	832	119.6	14.8	94.8	12.3	72.6	429	15.0	41.3	5.6	36.01	5.69	0.41
ET026I	IB	I-type granite	C	Chu et al. 2009.	1340.9	1692	149.3	512.3	478	58.2	14.4	46.0	5.0	27.1	168	5.9	15.0	2.1	13.29	2.38	0.82
T148	IB	I-type granite	C	Chu et al. 2009.	770.6	1990	280.3	442.0	1244	288.0	18.5	298.9	42.2	276.6	1581	57.7	147.8	19.3	120.79	16.20	0.19

Table S4.1 library of previously published apatite trace-element data (continued)

Sample Name	Code	Exact Lithology	Averaging	Source Paper	La	Ce	Pr	Sr	Nd	Sm	Eu	Gd	Tb	Dy	Y	Ho	Er	Tm	Yb	Lu	Eu/Eu*
T150	S	S-type granite	C	Chu et al. 2009.	168.9	554	102.0	50.7	550	264.1	4.3	318.0	52.2	307.6	1698	58.9	184.7	18.4	113.76	14.82	0.04
T153	IB	I-type granite	C	Chu et al. 2009.	1565.7	3924	491.7	648.2	1914	314.2	13.0	235.3	26.9	141.7	725	25.9	62.4	7.8	46.07	6.25	0.14
ST104	IB	I-type granite	C	Chu et al. 2009.	1172.6	2645	345.7	249.7	1225	191.7	14.7	155.8	20.8	123.3	747	24.5	66.3	9.5	59.62	9.33	0.25
ST129	IB	I-type granite	C	Chu et al. 2009.	1172.2	2479	296.8	447.7	1156	183.3	16.6	144.0	16.5	89.1	458	17.0	42.3	5.3	32.30	4.86	0.30
ST141	IB	I-type granite	C	Chu et al. 2009.	1133.5	1840	186.1	577.6	652	88.3	13.8	65.9	7.3	37.4	187	6.9	17.2	2.0	12.13	1.83	0.53
ST144	IB	I-type granite	C	Chu et al. 2009.	958.9	2268	282.7	347.9	938	137.2	21.3	107.4	13.3	71.7	390	14.7	38.2	5.0	31.24	4.86	0.52
ST146	IB	I-type granite	C	Chu et al. 2009.	486.0	834	96.6	138.5	408	84.6	19.4	103.0	13.7	89.5	674	21.0	63.2	8.8	59.57	11.75	0.63
ST147	IB	I-type granite	C	Chu et al. 2009.	185.2	656	124.1	404.9	671	165.9	16.2	167.5	22.6	134.8	722	26.9	69.6	8.8	52.46	7.85	0.29
ST150	IB	I-type granite	C	Chu et al. 2009.	1071.6	2532	329.6	276.4	1364	259.2	14.7	238.6	31.5	186.5	1047	37.0	97.6	12.8	78.82	11.35	0.18
ST152	IB	Gabbro	C	Chu et al. 2009.	295.6	692	96.4	533.8	484	79.9	17.0	71.0	8.3	46.7	280	8.8	21.9	2.8	15.80	2.44	0.67
ST134	IB	I-type granite	C	Chu et al. 2009.	835.0	1485	192.4	295.1	736	170.0	25.0	196.0	33.4	200.5	911	34.9	97.8	13.2	74.54	11.06	0.42
T027	ADK	Adakite	C	Chu et al. 2009.	1346.3	3308	434.7	449.4	1711	265.9	29.9	180.6	20.1	107.4	587	20.0	50.9	6.7	41.73	6.44	0.39
T060B	ADK	Adakite	C	Chu et al. 2009.	1212.1	1869	161.7	407.7	487	64.7	10.3	36.6	2.9	14.8	114	4.2	7.8	1.2	7.66	1.18	0.59
ET023	ADK	Adakite	C	Chu et al. 2009.	844.0	1288	140.1	413.9	577	76.6	11.1	52.0	5.2	25.6	147	4.9	12.1	1.5	10.00	1.65	0.51
ET025	ADK	Adakite	C	Chu et al. 2009.	947.6	1357	128.5	419.4	454	66.3	17.9	59.6	7.1	42.4	286	9.1	25.9	3.7	25.94	4.81	0.85
ST107A	ADK	Adakite	C	Chu et al. 2009.	1897.8	2725	247.6	341.0	826	99.3	10.0	63.9	6.0	29.2	146	5.2	12.6	1.6	9.90	1.68	0.36
ST107B	ADK	Adakite	C	Chu et al. 2009.	2219.8	2919	260.3	328.5	905	112.5	8.1	72.4	6.5	30.1	132	5.1	11.1	1.2	6.97	1.18	0.26
BM901	UB	Lherzolite	M	Griffin & O'Reilly, 2000.	995.0	1438	168.0	5831.0	668	88.0	30.0	66.0			160	6.1	12.8		7.60	1.30	1.15
BM650	UB	Lherzolite	M	Griffin & O'Reilly, 2000.	2416.0	5082	440.0	14115.0	1215	120.0	34.0	79.0			168	5.8	12.5		9.10	1.12	1.00
BM655	UB	Lherzolite	M	Griffin & O'Reilly, 2000.	2730.0	5760	468.0	18290.0	1156	117.0	35.0	72.0			164	5.5	12.8		9.00	1.10	1.08
BM632	UB	Lherzolite	M	Griffin & O'Reilly, 2000.	2466.0	5752	510.0	19030.0	1210	128.0	36.0	73.0			146	5.1	10.8		7.40	0.98	1.04
LE15B	UB	Lherzolite	M	Griffin & O'Reilly, 2000.	1542.0	3120	361.0	12510.0	1093	146.0	43.0	104.0			238	8.5	17.6		9.70	1.16	1.01
ASK10	UB	Lherzolite	M	Griffin & O'Reilly, 2000.	1172.0	2430	160.0	9500.0	339	30.0	9.4	19.0			62	2.1	5.5		4.50	0.63	1.12
66AHR	UB	Lherzolite	M	Griffin & O'Reilly, 2000.	747.0	1115	109.0	4812.0	397	48.0	13.0	36.0			109	3.7	8.9		6.40	0.78	0.98
LhzB1	UB	Lherzolite	M	Griffin & O'Reilly, 2000.	835.0	2540	245.0	4125.0	800	105.0	32.0	74.0			200	7.3	17.0		12.30	1.20	1.05
LhzB3	UB	Lherzolite	M	Griffin & O'Reilly, 2000.	1136.0	2584	295.0	8262.0	1060	155.0	47.0	112.0			274	10.1	22.5		11.70	1.40	1.04
LhzB4	UB	Lherzolite	M	Griffin & O'Reilly, 2000.	862.0	1925	228.0	7100.0	738	108.0	31.0	80.0			282	7.2	14.4		9.80	1.10	0.97
LhzB5	UB	Lherzolite	M	Griffin & O'Reilly, 2000.	207.0	858	61.0	2409.0	237	39.0	13.8	31.0			75	2.0	7.6		4.40	0.50	1.17
LhzB6	UB	Lherzolite	M	Griffin & O'Reilly, 2000.	1196.0	3121	343.0	4272.0	1064	169.0	34.7	89.0			216	7.7	18.0		12.00	1.40	0.78
LhzB7	UB	Lherzolite	M	Griffin & O'Reilly, 2000.	540.0	1711	216.0	5608.0	771	133.0	38.9	88.5			139	5.1	8.5		2.67	0.24	1.08
AGC1	LM	Gneiss	C	Henrichs et al., 2018.	3.2	10	2.4	555.9	16	7.9	3.6	14.9	3.4	27.9	225	7.5	25.6	3.8	24.90	4.19	1.08
AGC2	LM	Amphibolite	C	Henrichs et al., 2018.	6.3	16	3.5	514.6	22	7.9	2.1	10.2	1.3	8.6	52	1.8	5.1	0.7	4.28	0.77	0.74
DC811a	LM	Schist	C	Henrichs et al., 2018.	6.9	20	2.9	452.2	18	5.6	2.1	9.0	0.8	5.4	34	1.2	2.9	0.4	2.33	0.37	0.84
DC811b	LM	Schist	C	Henrichs et al., 2018.	40.6	129	25.9	208.8	162	85.1	11.8	179.0	35.4	214.1	827	33.9	72.6	7.8	40.80	5.05	0.29
LT2	LM	Schist	C	Henrichs et al., 2018.	13.8	44	7.9	1749.0	46	16.4	3.1	20.1	2.5	15.4	64	2.6	6.2	0.7	3.74	0.48	0.52
TCH001	HM	Leucosome	C	Henrichs et al., 2018.	107.1	478	84.0	134.4	490	195.5	17.6	237.2	40.8	251.4	973	38.7	84.2	8.6	40.25	4.15	0.25
TCD003	HM	Leucosome	C	Henrichs et al., 2018.	175.8	684	118.7	147.0	678	276.1	13.0	326.6	54.0	318.8	1136	44.9	96.6	8.2	36.18	3.66	0.14
TCD007	HM	Leucosome	C	Henrichs et al., 2018.	57.0	247	51.3	296.0	367	175.8	50.8	230.7	43.3	252.3	983	40.0	89.9	9.1	40.71	4.26	0.83
RM13	HM	Leucosome	C	Henrichs et al., 2018.	165.4	666	128.7	118.9	776	335.2	18.9	429.8	74.2	479.4	2307	89.5	234.3	30.3	172.75	20.63	0.15
RM15	HM	Leucosome	C	Henrichs et al., 2018.	166.7	639	117.4	86.6	687	360.2	19.2	431.7	76.8	487.4	2366	91.1	248.1	34.1	217.45	28.00	0.16
IH1	LM	Schist	C	Henrichs et al., 2018.	5.7	20	4.2	301.1	21	8.6	2.8	16.2	3.6	32.8	275	8.7	26.9	3.1	15.39	1.75	0.67
IH2	LM	Schist	C	Henrichs et al., 2018.	3.6	12	2.5	2595.0	15	7.7	3.1	16.2	3.6	25.5	107	3.6	6.5	0.5	2.27	0.29	0.78
IH3	LM	Schist	C	Henrichs et al., 2018.	8.4	29	5.5	1532.5	32	13.0	4.3	25.5	5.8	48.8	375	12.3	36.4	6.0	35.58	4.35	0.67
AB6 AP3	IB	I-type granite	M	Sha & Chappell, 1999.	1310.0	3200	418.0	188.0	1620	299.0	13.0	235.0	34.0	177.0	1094	38.0	108.0	14.0	80.00	10.00	0.15
AB46 AP-A1	IB	I-type granite	M	Sha & Chappell, 1999.	602.0	1478	176.0	273.0	634	100.0	19.0	80.0	11.0	51.0	356	12.0	33.0	5.0	32.00	6.00	0.63
AB149 APD1	IB	I-type granite	M	Sha & Chappell, 1999.	1079.0	2350	290.0	399.0	1080	147.0	16.0	107.0	15.0	69.0	385	13.0	33.0	5.0	27.00	4.00	0.36
AB149 APG1	IB	I-type granite	M	Sha & Chappell, 1999.	815.0	1898	229.0	312.0	838	119.0	11.0	89.0	13.0	68.0	373	12.0	31.0	4.0	27.00	4.00	0.33
AB190 APG	IB	I-type granite	M	Sha & Chappell, 1999.	1540.0	3980	540.0	362.0	2180	427.0	24.0	369.0	55.0	302.0	1710	58.0	153.0	21.0	126.00	17.00	0.18
AB195GR AP1	IB	I-type granite	M	Sha & Chappell, 1999.	1094.0	2330	273.0	236.0	1018	152.0	20.0	125.0	17.0	84.0	525	18.0	46.0	7.0	43.00	8.00	0.44
AB195ME MAP2	IB	I-type granite	M	Sha & Chappell, 1999.	1668.0	4290	635.0	362.0	2830	558.0	51.0	477.0	67.0	336.0	1690	61.0	156.0	20.0	112.00	15.00	0.29
KB22 APB1	IB	I-type granite	M	Sha & Chappell, 1999.	411.0	1203	183.0	176.0	806	147.0	14.0	130.0	19.0	104.0	622	22.0	60.0	9.0	53.00	8.00	0.31
MG42 APB1	IB	I-type granite	M	Sha & Chappell, 1999.	1051.0	1916	206.0	329.0	717	102.0	16.0	90.0	12.0	58.0	332	12.0	32.0	4.0	25.00	4.00	0.51
MG42 APA1	IB	I-type granite	M	Sha & Chappell, 1999.	739.0	1584	182.0	314.0	668	106.0	18.0	98.0	13.0	65.0	379	13.0	34.0	5.0	30.00	5.00	0.54
MG44 AP1	IS	Intermediate granite	M	Sha & Chappell, 1999.	96.0	381	84.0	94.0	493	284.0	11.0	388.0	69.0	472.0	2000	72.0	169.0	69.0	171.00	21.00	0.11
MG44 AP2	IS	Intermediate granite	M	Sha & Chappell, 1999.	268.0	790	134.0	58.0	623	288.0	13.0	403.0	79.0	588.0	3020	101.0	272.0	79.0	319.00	43.00	0.12
VB230 APA1	IS	Intermediate granite	M	Sha & Chappell, 1999.	855.0	2650	489.0	74.0	2600	882.0	14.0	1016.0	163.0	979.0	5240	180.0	452.0	163.0	332.00	44.00	0.05
VB230 APB1	IS	Intermediate granite	M	Sha & Chappell, 1999.	502.0	1387	247.0	118.0	1294	443.0	6.0	510.0	80.0	472.0	2750	89.0	222.0	80.0	165.00	22.00	0.04
BB11 AP1	S	S-type granite	M	Sha & Chappell, 1999.	76.0	375	78.0	122.0	424	215.0	11.0	258.0	44.0	283.0	1130	46.0	105.0	15.0	85.00	11.00	0.15

Table S4.1 library of previously published apatite trace-element data (continued)

Sample Name	Code	Exact Lithology	Averaging	Source Paper	La	Ce	Pr	Sr	Nd	Sm	Eu	Gd	Tb	Dy	Y	Ho	Er	Tm	Yb	Lu	Eu/Eu*
CB84 AP1	S	S-type granite	M	Sha & Chappell, 1999.	143.0	526	90.0	81.0	439	207.0	6.0	263.0	48.0	337.0	1550	57.0	143.0	23.0	161.00	22.00	0.08
CB144 AP1	S	S-type granite	M	Sha & Chappell, 1999.	181.0	638	114.0	152.0	565	245.0	9.0	300.0	56.0	401.0	1980	76.0	195.0	30.0	191.00	24.00	0.11
KB32 AP4	S	S-type granite	M	Sha & Chappell, 1999.	221.0	655	115.0	116.0	570	248.0	10.0	289.0	50.0	335.0	1550	61.0	149.0	22.0	138.00	17.00	0.12
SV51 AP2	S	S-type granite	M	Sha & Chappell, 1999.	419.0	1327	216.0	138.0	1044	384.0	6.0	486.0	87.0	596.0	3200	124.0	311.0	40.0	208.00	26.00	0.04
VB1 AP5	S	S-type granite	M	Sha & Chappell, 1999.	207.0	757	141.0	99.0	712	346.0	9.0	413.0	74.0	507.0	2960	91.0	230.0	33.0	208.00	26.00	0.07
VB15 AP5	S	S-type granite	M	Sha & Chappell, 1999.	235.0	946	156.0	125.0	716	295.0	5.0	376.0	64.0	417.0	2340	80.0	206.0	28.0	165.00	19.00	0.05
VB17 AP6	S	S-type granite	M	Sha & Chappell, 1999.	223.0	797	142.0	175.0	735	303.0	6.0	396.0	65.0	400.0	2010	76.0	181.0	23.0	120.00	15.00	0.05
VB26 AP2	S	S-type granite	M	Sha & Chappell, 1999.	233.0	836	148.0	29.0	665	348.0	4.0	412.0	72.0	474.0	2300	72.0	183.0	27.0	173.00	24.00	0.03
VB30 AP3	S	S-type granite	M	Sha & Chappell, 1999.	174.0	630	119.0	142.0	629	276.0	10.0	373.0	66.0	448.0	2080	85.0	211.0	29.0	165.00	21.00	0.10
VB94 AP1	S	S-type granite	M	Sha & Chappell, 1999.	304.0	926	141.0	483.0	618	186.0	14.0	185.0	32.0	205.0	1190	38.0	103.0	16.0	102.00	13.00	0.23
VB140 AP6	S	S-type granite	M	Sha & Chappell, 1999.	265.0	792	126.0	93.0	582	252.0	12.0	365.0	65.0	446.0	2470	76.0	185.0	26.0	156.00	19.00	0.12
VB220 AP3	S	S-type granite	M	Sha & Chappell, 1999.	246.0	821	140.0	211.0	709	250.0	7.0	338.0	65.0	476.0	2600	98.0	271.0	37.0	210.00	27.00	0.08
VB221 AP9	S	S-type granite	M	Sha & Chappell, 1999.	242.0	861	149.0	145.0	735	277.0	7.0	370.0	68.0	472.0	2750	104.0	291.0	42.0	258.00	35.00	0.07
Carbo1	UB	Carbonatite	M	Chakhmouradian et al. 2017.	1199.6	3818	576.7	9591.0	2611	453.9	107.9	279.1	28.6	112.6	420	16.2	30.9	3.1	14.89	1.54	0.86
Carbo2	UB	Carbonatite	M	Chakhmouradian et al. 2017.	2137.5	6378	977.4	9275.0	4457	794.2	189.4	480.6	50.6	208.7	757	29.6	56.5	5.7	29.00	2.98	0.86
Carbo3	UB	Carbonatite	M	Chakhmouradian et al. 2017.	3236.3	9378	1431.4	9172.0	6488	1165.5	278.4	704.3	75.3	312.5	1176	45.3	88.2	9.1	46.03	4.78	0.87
Carbo4	UB	Carbonatite	M	Chakhmouradian et al. 2017.	4984.7	8393	886.1	6917.0	2596	285.7	85.0	288.1	19.3	90.9	414	16.0	36.8	4.7	27.11	3.64	0.89
Carbo5	UB	Carbonatite	M	Chakhmouradian et al. 2017.	1325.1	3530	466.8	3118.0	1750	280.1	75.4	202.8	19.9	89.4	309	13.1	25.2	2.6	12.84	1.41	0.92
Carbo6	UB	Carbonatite	M	Chakhmouradian et al. 2017.	465.4	1235	177.0	3369.0	688	119.5	37.1	98.9	9.7	43.2	142	6.8	11.9	1.2	5.44	0.74	1.01
Carbo7	UB	Carbonatite	M	Chakhmouradian et al. 2017.	645.2	1836	245.8	3822.0	962	163.3	46.6	126.1	12.2	53.3	159	7.8	14.3	1.4	6.08	0.75	0.95
Carbo8	UB	Carbonatite	M	Chakhmouradian et al. 2017.	908.6	2477	323.1	3615.0	1282	204.7	60.9	158.5	15.5	64.9	194	9.5	15.7	1.5	6.11	0.70	0.99
Carbo9	UB	Carbonatite	M	Chakhmouradian et al. 2017.	1302.1	3690	462.2	5779.0	1577	224.4	64.9	180.5	13.9	55.0	151	7.8	13.1	1.2	5.26	0.64	0.95
Carbo10	UB	Carbonatite	M	Chakhmouradian et al. 2017.	561.9	1766	227.6	4131.0	812	120.8	34.9	98.4	8.1	34.2	99	4.9	8.9	1.0	3.78	0.34	0.95
Carbo11	UB	Carbonatite	M	Chakhmouradian et al. 2017.	2472.8	6502	709.0	6714.0	2473	398.7	120.0	336.9	25.9	97.5	243	12.2	22.8	1.9	8.09	0.74	0.98
Carbo12	UB	Carbonatite	M	Chakhmouradian et al. 2017.	845.1	2246	298.1	5491.0	1085	225.3	78.4	217.4	22.4	95.3	251	12.3	21.0	1.7	6.86	0.54	1.07
Carbo14	UB	Carbonatite	M	Chakhmouradian et al. 2017.	2081.8	4555	439.3	5131.0	1365	174.3	51.5	163.1	14.3	66.4	286	11.7	26.3	3.1	16.65	2.16	0.92
Carbo15	UB	Carbonatite	M	Chakhmouradian et al. 2017.	1810.6	3895	415.9	6005.0	1315	165.3	41.4	128.3	13.2	71.1	333	12.8	31.4	4.0	22.89	2.95	0.83
Carbo16	UB	Carbonatite	M	Chakhmouradian et al. 2017.	727.1	2442	320.3	5157.0	1257	192.7	48.4	129.8	11.2	43.5	151	6.0	11.2	1.0	5.22	0.62	0.88
Carbo17	UB	Carbonatite	M	Chakhmouradian et al. 2017.	1550.6	2809	291.2	1525.0	915	93.4	23.3	48.9	5.0	21.5	82	3.2	6.5	0.7	3.21	0.45	0.94
Carbo18	UB	Carbonatite	M	Chakhmouradian et al. 2017.	333.7	484	56.7	827.0	212	33.0	9.9	22.9	2.8	12.3	43	2.0	4.0	0.4	2.15	0.26	1.04
Carbo19	UB	Carbonatite	M	Chakhmouradian et al. 2017.	3178.3	9695	1260.8	13245.0	4935	677.1	156.6	376.1	26.9	102.6	427	15.5	32.7	3.7	21.34	2.92	0.86
Carbo20	UB	Carbonatite	M	Chakhmouradian et al. 2017.	416.6	1712	309.0	7396.0	1453	280.3	74.9	164.3	15.1	60.8	255	9.6	21.5	2.5	13.93	1.90	0.98
Carbo21	UB	Carbonatite	M	Chakhmouradian et al. 2017.	1801.8	6150	845.7	4247.0	3586	654.0	204.0	595.2	53.7	196.5	476	25.1	44.4	3.7	15.72	1.61	0.98
Carbo22	UB	Carbonatite	M	Chakhmouradian et al. 2017.	1047.5	2653	319.6	5235.0	1166	174.6	49.2	130.9	13.0	55.9	180	8.2	15.7	1.6	7.71	0.98	0.95
Carbo23	UB	Carbonatite	M	Chakhmouradian et al. 2017.	819.9	2212	272.1	5225.0	992	148.2	42.4	108.9	10.4	42.6	127	6.1	10.9	1.0	4.33	0.51	0.97
Carbo24	UB	Carbonatite	M	Chakhmouradian et al. 2017.	89.7	429	81.7	3778.0	403	86.0	23.7	61.2	5.5	19.6	55	2.5	3.7	0.4	1.48	0.24	0.95
Carbo25	UB	Carbonatite	M	Chakhmouradian et al. 2017.	1121.5	2565	307.4	8377.0	1213	200.9	57.0	152.6	16.0	72.7	243	11.1	21.6	2.2	10.55	1.22	0.95
Carbo26	UB	Carbonatite	M	Chakhmouradian et al. 2017.	584.6	1997	255.2	8911.0	960	141.5	36.4	87.3	5.4	18.0	43	2.1	3.2	0.3	1.21	0.16	0.93
Carbo27	UB	Carbonatite	M	Chakhmouradian et al. 2017.	1694.7	5399	697.5	10664.0	2722	375.3	88.0	207.1	10.2	29.2	59	3.1	4.8	0.4	2.00	0.19	0.87
Ihlen_Nor_Carb	UB	Carbonatite	M	Ihlen et al. 2013.	1052.7	2501	295.3		1196	194.9	57.8	158.1	18.0	78.0	288	11.1	23.2	2.4	11.40	1.30	1.56
Ihlen_Nor_Carb	UB	Carbonatite	M	Ihlen et al. 2013.	2258.3	5046	578.6		2255	330.9	96.0	258.3	29.2	128.3	486	18.6	38.1	4.0	20.80	2.30	1.53
Ihlen_Nor_Pyrox	UB	Pyroxenite	M	Ihlen et al. 2013.	842.5	1649	166.7		677	82.4	21.5	62.3	6.7	32.5	132	8.7	11.8	1.2	7.70	1.10	1.37
Ihlen_Nor_Pyrox	UB	Pyroxenite	M	Ihlen et al. 2013.	486.5	1506	248.5		1277	269.6	59.8	214.9	28.7	105.9	426	15.9	32.6	4.0	22.60	2.70	1.17
Ihlen_Nor_Pyrox	UB	Pyroxenite	M	Ihlen et al. 2013.	658.6	1568	238.4		1075	208.7	45.8	160.7	16.1	67.6	253	8.7	16.9	2.1	12.00	1.40	1.15
Ihlen_Nor_Pyrox	UB	Pyroxenite	M	Ihlen et al. 2013.	456.3	1458	226.6		1113	231.0	50.2	183.1	20.0	85.0	335	12.1	26.1	3.1	16.70	2.30	1.14
Ihlen_Nor_Nelson	IB	Nelsonite	M	Ihlen et al. 2013.	651.6	1249	236.9		1225	286.5	10.4	304.7	45.4	279.2	1394	52.9	138.8	18.9	108.30	13.20	0.19
Ix y2	AUT	Phosphorite	M	Shields & Stille, 2001.	59.8	45	10.3		47	8.9	2.2	11.9	1.7	10.5	128	2.4	6.5	0.7	3.14	0.38	0.64
Ix y2.5	AUT	Phosphorite	M	Shields & Stille, 2001.	59.9	88	12.9		53	10.0	1.7	12.4	1.8	9.8	99	2.1	5.5	0.6	2.67	0.34	0.47
Ix y3.75	AUT	Phosphorite	M	Shields & Stille, 2001.	54.5	45	9.5		43	8.0	1.9	10.7	1.5	9.3	105	2.1	5.6	0.6	2.73	0.33	0.64
Ix 4	AUT	Phosphorite	M	Shields & Stille, 2001.	59.7	55	9.5	570.0	40	7.1	1.8	10.0	1.4	8.6	107	2.0	5.5	0.6	2.81	0.35	0.64
Ix 18	AUT	Phosphorite	M	Shields & Stille, 2001.	80.0	124	18.5		75	15.7	1.8	17.9	2.8	16.0	140	3.3	8.6	1.0	5.08	0.71	0.33
Ix 21	AUT	Phosphorite	M	Shields & Stille, 2001.	55.7	59	9.9		39	6.7	1.1	9.1	1.3	7.6	104	1.8	5.0	0.5	2.58	0.33	0.44
Ix 23	AUT	Phosphorite	M	Shields & Stille, 2001.	58.9	42	7.2	820.0	28	4.3	1.1	6.6	0.9	5.9	100	1.5	4.5	0.5	2.55	0.33	0.60
Ix 25	AUT	Phosphorite	M	Shields & Stille, 2001.	20.8	12	3.4	197.0	15	3.0	0.8	4.4	0.7	4.8	59	1.2	3.6	0.5	2.61	0.39	0.66
Ix 28	AUT	Phosphorite	M	Shields & Stille, 2001.	30.5	17	4.6	243.0	20	3.7	1.0	5.7	0.9	5.8	81	1.5	4.4	0.5	2.83	0.38	0.64
Ix 34	AUT	Phosphorite	M	Shields & Stille, 2001.	57.6	85	13.8	620.0	55	10.4	1.9	12.6	1.9	11.1	119	2.5	7.3	0.9	4.68	0.63	0.51
Ix 35	AUT	Phosphorite	M	Shields & Stille, 2001.	102.3	142	22.8		94	17.9	3.5	22.3	3.3	20.2	215	4.6	13.5	1.7	9.04	1.24	0.53
Ix 40	AUT	Phosphorite	M	Shields & Stille, 2001.	93.7	209	40.2	211.0	186	45.4	6.3	48.4	7.6	40.0	243	7.2	16.6	1.6	7.39	0.91	0.41

Table S4.1 library of previously published apatite trace-element data (continued)

Sample Name	Code	Exact Lithology	Averaging	Source Paper	La	Ce	Pr	Sr	Nd	Sm	Eu	Gd	Tb	Dy	Y	Ho	Er	Tm	Yb	Lu	Eu/Eu*
M 11	AUT	Phosphorite	M	Shields & Stille, 2001.	35.4	30	7.5		34	6.8	1.8	9.1	1.4	8.6	82	1.9	5.4	0.7	3.85	0.59	0.69
M 13	AUT	Phosphorite	M	Shields & Stille, 2001.	60.0	38	12.1		55	11.3	3.1	15.7	2.5	15.9	154	3.7	10.8	1.4	7.89	1.16	0.72
M 20	AUT	Phosphorite	M	Shields & Stille, 2001.	91.2	40	15.4		69	13.6	3.7	19.9	3.2	21.0	244	5.1	15.1	2.0	11.51	1.67	0.68
Z 26	AUT	Phosphorite	M	Shields & Stille, 2001.	202.3	128	20.8	1210.0	86	17.7	2.2	20.5	3.1	17.7	145	3.5	8.8	0.9	3.96	0.49	0.36
SSF 1	AUT	Fossil	M	Shields & Stille, 2001.	209.4	358	50.7		221	47.3	11.0	49.1	5.9	28.9		5.1	12.0	1.3	6.11	0.78	0.69
SSF 2	AUT	Fossil	M	Shields & Stille, 2001.	242.3	387	52.7		237	50.7	11.6	54.9	6.3	30.8		5.4	12.5	1.2	6.01	0.79	0.67
SSF 3 1st	AUT	Fossil	M	Shields & Stille, 2001.	152.9	169	33.3		146	30.8	7.0	32.3	3.7	17.8		3.2	7.3	0.6	3.70	0.49	0.67
SSF 3 2nd	AUT	Fossil	M	Shields & Stille, 2001.	150.4	252	33.3		147	30.9	7.1	33.6	3.8	19.5		3.3	8.1	0.9	4.43	0.58	0.67
JoosuP3	AUT	Phosphorite	C	Joosu et al. 2015.	136.9	192	31.9		139	31.0	16.3	39.6	365.7	41.0	366	9.6	27.1		19.29	2.43	1.42
JoosuP4	AUT	Phosphorite	C	Joosu et al. 2015.	136.2	188	33.0		147	33.1	15.1	48.8	404.6	45.1	405	10.5	29.7		19.90	2.48	1.21
JoosuP5	AUT	Phosphorite	C	Joosu et al. 2015.	114.5	168	29.4		134	30.4	15.9	39.9	340.9	41.1	341	9.1	26.2		18.47	2.33	1.40
JoosuP6	AUT	Phosphorite	C	Joosu et al. 2015.	143.3	194	34.0		153	35.2	17.3	46.2	420.2	46.3	420	10.2	29.1		19.91	2.45	1.31
JoosuP8	AUT	Phosphorite	C	Joosu et al. 2015.	105.3	154	25.5		115	28.3	14.5	36.8	281.3	32.5	281	7.0	19.0		10.50	1.00	1.37
JoosuP10	AUT	Phosphorite	C	Joosu et al. 2015.	33.0	43	7.3		30	6.9	7.8	9.6	218.6	9.4	219	2.1	5.3		2.63	1.38	2.90
JoosuP11	AUT	Phosphorite	C	Joosu et al. 2015.	85.7	107	18.8		86	22.3	10.3	34.8	269.7	39.0	270	10.0	30.8		24.83	1.00	1.13
JoosuP13	AUT	Phosphorite	C	Joosu et al. 2015.	79.3	157	37.6		217	75.8	13.0	101.9	123.0	85.7	123	16.2	38.5		21.69	0.69	0.45
HN-99-01	IB	Nelsonitic- trodolite	M	Tollari et al. 2008.	660.0	1692	268.0	856.0	1142	225.0	51.5	226.0	27.0	147.0	733	25.8	61.3	7.1	39.20	5.16	0.69
HN-99-04	IB	Nelsonitic- trodolite	M	Tollari et al. 2008.	747.0	2036	290.0	777.0	1215	225.0	30.8	213.0	25.9	149.0	785	26.7	66.7	7.8	42.50	5.56	0.42
HN-99-13	IB	Nelsonitic- trodolite	M	Tollari et al. 2008.	697.0	1934	299.0	857.0	1258	248.0	59.1	258.0	31.1	166.0	824	28.9	68.9	7.8	40.50	5.35	0.71
HN-99-45	IB	Troctolitic- nelsonite	M	Tollari et al. 2008.	370.0	896	139.0	526.0	685	152.0	38.6	162.0	19.5	110.0	631	19.1	45.6	5.3	28.20	3.82	0.74
HN-99-44	IB	Troctolitic- nelsonite	M	Tollari et al. 2008.	564.0	1470	228.0	982.0	974	201.0	64.2	217.0	26.3	139.0	647	23.8	58.4	6.3	33.20	4.23	0.93
HN-99-47	IB	Troctolitic- nelsonite	M	Tollari et al. 2008.	496.0	1101	185.0	865.0	902	192.0	48.0	203.0	24.8	141.0	738	25.0	60.1	7.0	37.60	5.06	0.74
HN-99-21	IB	Troctolitic- nelsonite	M	Tollari et al. 2008.	400.0	1102	170.0	704.0	772	163.0	46.2	171.0	20.5	117.0	585	20.4	49.7	5.8	32.00	4.29	0.84
HN-99-52	IB	Troctolitic- nelsonite	M	Tollari et al. 2008.	479.0	1208	197.0	1087.0	940	200.0	62.5	209.0	24.9	137.0	671	23.6	56.4	6.4	35.00	4.74	0.92
HN-99-25	IB	Nelsonite	M	Tollari et al. 2008.	248.0	781	116.0	758.0	530	114.0	41.3	116.0	13.4	72.0	352	12.1	27.6	3.1	16.50	2.15	1.08
HN-99-53	IB	Nelsonite	M	Tollari et al. 2008.	320.0	769	154.0	855.0	718	155.0	54.3	156.0	18.8	98.0	463	16.6	38.0	4.0	20.80	2.68	1.05
HN-99-29	IB	Nelsonite	M	Tollari et al. 2008.	282.0	695	117.0	621.0	595	135.0	42.7	47.0	17.3	96.0	459	16.3	37.7	4.2	21.90	2.93	1.32
HN-99-46	IB	Nelsonite	M	Tollari et al. 2008.	282.0	695	117.0	621.0	595	135.0	42.7	47.0	17.3	96.0	459	16.3	37.7	4.2	21.90	2.93	1.32
PegBel2002_1st	HM	Granite Pegmatite	M	Belousova et al. 2002.	159.0	548	99.0	48.0	542	230.0	11.0	281.0		385.0	2671	88.0	251.0	39.0	273.00	37.00	0.13
PegBel2002_3rd	HM	Granite Pegmatite	M	Belousova et al. 2002.	260.0	856	163.0	120.0	861	420.0	32.0	577.0		713.0	4616	156.0	453.0	66.0	474.00	77.00	0.20
Silurian Phos	AUT	Phosphorite	M	Dill, 1994.	192.0	251	67.0		303	94.0	26.2	88.0	20.7	102.0	618	21.1	52.0	6.9	46.00	7.00	0.86
Dacites	IS	Dacite	M	Dill, 1994.	1777.0	4530	673.0		2986	622.0	11.9	486.0	101.0	458.0	2287	89.0	216.0	22.7	162.00	23.00	0.06
Fichtelgebirge Granites	S	S-type granite	M	Dill, 1994.	267.0	790	122.0		539	199.0	12.6	133.0	34.0	276.0	1755	61.0	170.0	22.0	139.00	18.00	0.22
Oberpfalz Granites	S	S-type granite	M	Dill, 1994.	324.0	1007	162.0		733	253.0	8.7	178.0	40.0	282.0	1766	56.0	141.0	20.0	143.00	18.00	0.12
IH 11/13/04	LM	Schist	C	Henrichs et al., 2018.	1.0	3	0.6	487.7	4	3.2	0.8	5.0	0.8	5.5	40	1.4	4.3	0.6	4.24	0.73	0.55
IH 11/13/05	LM	Schist	C	Henrichs et al., 2018.	27.0	124	24.7	198.1	163	43.9	10.5	55.3	7.0	40.3	233	8.1	26.6	2.9	17.11	2.67	0.67
op1	LM	Schist	C	Henrichs et al., 2018.	1.5	3	0.7	1560.7	4	2.3	0.7	5.2	1.1	10.6	100	3.1	11.0	1.6	10.43	1.59	0.59
Augite Syenite Autolith	ALK	Syenite	C	Zimer et al., 2015.	5332.9	14211	1486.3	795.5	5175	777.9	53.2	536.8	64.2	338.9	1396	55.7	124.4	14.2	69.85	7.10	0.24
Augite Syenite Autolith	ALK	Syenite	C	Zimer et al., 2015.	18594.6	41332	4517.3	1026.3	15906	2118.0	158.7	1297.9	136.4	649.0	1913	94.6	184.3	18.0	75.81	6.70	0.27
Phonolite	ALK	Phonolite	C	Zimer et al., 2015.	1523.1	40873	4430.5	158.1	15234	2259.2	130.2	1594.0	186.0	987.8	3544	163.7	350.8	38.5	192.73	18.31	0.20
Phonolite	ALK	Phonolite	C	Zimer et al., 2015.	20488.4	53005	5121.0	241.5	18436	2781.0	167.4	1803.7	221.6	1167.8	4129	192.3	414.1	44.5	240.84	22.09	0.21
Pulaskite	ALK	Pulaskite	C	Zimer et al., 2015.	14069.2	36305	4237.6	66.0	16346	2637.0	194.6	1911.4	230.6	1184.7	4379	195.1	426.2	46.7	228.16	23.16	0.25
Agpaitic vein	AGP	Agpaite	C	Zimer et al., 2015.	25698.6	46012	4064.3	6298.2	11838	1037.6	64.3	468.5	33.1	119.8	353	13.8	22.7	1.7	5.79	0.44	0.24
Agpaitic vein	AGP	Agpaite	C	Zimer et al., 2015.	29727.4	43996	3749.6	6757.9	11487	1117.4	73.0	529.8	37.4	145.0	442	17.6	28.5	2.0	8.39	0.75	0.25
Marginal augite syenite	ALK	Syenite	C	Zimer et al., 2015.	1719.6	4094	466.7	289.1	1787	291.7	18.9	250.5	30.5	170.7	827	30.6	75.5	8.4	44.59	5.20	0.21
Middle augite syenite	ALK	Syenite	C	Zimer et al., 2015.	1461.9	3854	451.7	237.1	1811	317.2	31.0	262.2	31.1	169.7	814	29.9	71.2	8.2	46.72	5.88	0.32
Middle augite syenite	ALK	Syenite	C	Zimer et al., 2015.	11001.8	25930	2719.6	149.1	9502	1504.2	69.1	1295.9	171.2	966.0	4138	182.6	438.1	48.2	219.05	28.62	0.15
Inner augite syenite	ALK	Syenite	C	Zimer et al., 2015.	1501.7	3830	457.5	248.8	1854	317.6	29.7	266.2	31.6	172.2	818	30.1	72.0	8.2	44.48	5.45	0.30
Type A	AUT	Phosphorite	C	Joosu et al. 2016.	557.4	1331	176.5		737	162.1	45.5	174.8		119.9	667	20.7	47.0		24.21	3.16	0.88
Type B	AUT	Phosphorite	C	Joosu et al. 2016.	390.4	800	90.6		382	85.6	30.5	97.9		80.5	524	14.8	37.0		21.63	3.25	1.06
Type C	AUT	Phosphorite	C	Joosu et al. 2016.	340.5	791	102.1		430	93.2	30.0	104.4		75.3	452	13.4	31.3		19.06	2.81	0.96
Type D	AUT	Phosphorite	C	Joosu et al. 2016.	319.7	494	66.4		258	50.2	17.5	59.8		52.8	538	12.1	34.8		26.54	3.85	0.99
43-44A.420.y	AUT	BIF	M	Nishizawa et al. 2005.	5	31	5		21	7.2	6.5	9.2	1.6	8.90		2.1	7.1	1	8.5	1.5	2.43
43-44A.421.a	AUT	BIF	M	Nishizawa et al. 2005.	3.7	19.7	3.9		20	7.1	6.3	10.1	1.7	10.00		2.4	7.1	1	8.7	1.6	2.27
K485.l	LM	Psammite	M	Nishizawa et al. 2005.	5.1	27.6	5.5		23	8.0	5.6	27.6	8.6	48.80		11.2	28.4	4	18.4	3.1	1.03
K485.m	LM	Psammite	M	Nishizawa et al. 2005.	6.5	26.6	4.7		22	7.3	4.9	24.1	7.2	43.10		9.1	26.8	4	16.6	2.9	1.02
MtgG1	HM	Leucosome	M	Nutman, 2007.	126.5	514	94.4	154.6	532	231.8	33.7	341.1	63.3	416.1	1947	75.6	193.0	24.4	141.80	16.70	0.36
MtgG2	HM	Leucosome	M	Nutman, 2007.	273.7	877	130.7	138.2	635	213.9	24.1	273.1	45.4	276.6	1187	46.6	112.4	13.3	73.60	8.80	0.30

Table S4.1 library of previously published apatite trace-element data (continued)

Sample Name	Code	Exact Lithology	Averaging	Source Paper	La	Ce	Pr	Sr	Nd	Sm	Eu	Gd	Tb	Dy	Y	Ho	Er	Tm	Yb	Lu	Eu/Eu*
MigG3	HM	Leucosome	M	Nutman, 2007.	157.7	648	119.6	138.9	673	297.6	38.7	425.0	76.7	487.9	2077	88.9	208.3	26.8	158.00	18.90	0.33
MigG4	HM	Leucosome	M	Nutman, 2007.	107.7	406	72.3	156.1	410	178.9	35.8	274.3	49.4	310.3	1328	54.1	130.0	15.3	84.30	9.80	0.49
MigG5	HM	Leucosome	M	Nutman, 2007.	77.7	346	66.3	175.3	381	159.0	25.2	222.8	38.2	236.0	1007	39.5	95.4	11.5	64.60	7.70	0.41
MigG6	HM	Leucosome	M	Nutman, 2007.	104.5	397	72.1	192.0	405	169.9	29.5	242.6	42.5	265.3	1162	45.7	111.5	13.5	77.50	9.30	0.44
MigG7	HM	Leucosome	M	Nutman, 2007.	95.1	361	66.4	167.2	380	153.1	28.1	206.1	34.2	205.1	829	34.2	79.1	9.1	48.40	5.40	0.48
MigSed1	HM	Mig enclave	M	Nutman, 2007.	61.9	287	58.3	193.4	360	159.6	18.1	216.8	36.0	228.7	1011	40.0	102.0	12.8	74.50	9.30	0.30
MigSed2	HM	Mig enclave	M	Nutman, 2007.	93.6	355	65.1	251.8	383	165.0	33.5	242.7	41.6	260.3	1140	45.3	109.7	13.1	71.20	8.30	0.51
MigSed3	HM	Mig enclave	M	Nutman, 2007.	118.9	435	76.9	230.1	440	183.6	29.4	271.8	47.3	301.7	1340	58.0	131.5	15.9	87.40	10.30	0.40
MigSed4	HM	Mig enclave	M	Nutman, 2007.	91.8	360	67.7	222.1	391	172.0	29.8	247.7	48.1	266.7	1147	45.4	108.1	12.8	70.00	8.20	0.44
MigSed5	HM	Mig enclave	M	Nutman, 2007.	95.2	359	65.0	268.9	371	160.9	36.7	231.9	40.7	257.2	1114	44.9	111.4	13.3	73.50	8.70	0.58
MigSed6	HM	Mig enclave	M	Nutman, 2007.	76.4	305	57.6	267.1	336	148.7	35.9	213.0	37.2	232.1	1004	40.0	97.0	11.5	63.10	7.30	0.61
MigSed7	HM	Mig enclave	M	Nutman, 2007.	116.5	452	82.6	258.9	469	192.5	36.9	270.0	47.9	303.4	1361	54.4	135.4	16.5	91.90	10.90	0.49
MigSed8	HM	Mig enclave	M	Nutman, 2007.	109.3	436	81.4	262.4	467	194.1	37.3	273.6	47.4	300.5	1356	53.8	131.3	15.9	88.60	10.60	0.49
MigSed9	HM	Mig enclave	M	Nutman, 2007.	109.7	388	66.1	310.8	362	148.4	43.3	230.1	41.1	269.4	1262	50.7	127.9	16.3	93.30	11.60	0.71
MigSed10	HM	Mig enclave	M	Nutman, 2007.	93.5	347	60.4	245.7	339	147.8	34.4	228.2	40.7	263.3	1128	46.1	110.4	13.7	74.10	9.00	0.57
MigSed11	HM	Mig enclave	M	Nutman, 2007.	121.0	375	61.7	278.9	342	141.5	37.7	202.9	34.6	217.2	911	37.2	88.6	10.6	58.80	6.90	0.68
MigSed12	HM	Mig enclave	M	Nutman, 2007.	80.1	386	77.1	220.0	461	196.8	30.8	274.0	47.4	300.4	1294	52.0	126.4	15.3	84.90	9.80	0.40
T024	LM	Metasom. Granite	C	Chu et al. 2009.	20.4	63	14.3	485.6	106	63.9	27.9	125.5	23.4	174.5	1162	39.7	113.1	15.4	96.16	13.93	0.93

For collumn 'averaging' codes respond to whether only a median value was supplied by the author(s) of the paper <M>, or whether the median was calculated from individual grain values by the authors of this paper <C>

Note, values are logged before plotting on PCA

Chapter 5

Conclusions, synthesis & future work

5.1 CONCLUSIONS

The primary contributions of this thesis concern improvements to the understanding of apatite geochemistry in a holistic sense. The goals of this PhD were to develop and improve a tool that can be used to interpret the history of Earth surface denudation. This thesis also has other potential applications such as in ore-genesis studies as discussed in the 'future work' section.

The contribution of this thesis can be summarised as three primary findings that correspond to: 1) a greater understanding of what geological information the detrital apatite U-Pb system records, especially when compared to other more established U-Pb detrital chronometers; 2) improvements to methods of visualising and analysing detrital apatite trace-element compositional data for determining provenance; and 3) insights into the generation of lithological bias as detected by detrital apatite U-Pb age-spectra (a result that was a direct outcome of findings 1 and 2).

Finding 1: Detrital apatite U-Pb ages provide information from sub-anatectic metamorphic events, permitting the detection of orogens in the detrital record that may be undetectable using other mineral-isotope systems such as detrital zircon U-Pb (e.g. Hietpas *et al.*, 2010).

This finding is demonstrated in chapter 2, where detrital apatite and rutile U-Pb are sensitive to Alleghanian orogenesis (c. 320 Ma) in modern river detritus from the French Broad River (NC, USA), whereas the detrital zircon U-Pb system is insensitive to it, providing only a single Alleghanian age (a zircon rim) out of several hundred zircon analyses (Hietpas *et al.*, 2010) and instead mostly recording Proterozoic ages. A similar disparity in age distributions between zircon and apatite is also shown in chapter 4, where the distribution of detrital apatite and zircon U-Pb age peaks is again highly distinct in a Mesoproterozoic basin in NW Scotland (the Stoer Group). Here apatite characterises entire age-peaks on kernel density plots (KDP) that are only represented by one or two zircon grains, most notably the largest apatite U-Pb age peak corresponds to Somerledian

deformation (c. 1.6 Ga; Kinny et al., 2005) while there is only a single Somerledian detrital zircon U-Pb age out of 605 analyses from the same sediment fraction.

The mechanism causing these differences in the relative sensitivities of the detrital apatite and zircon U-Pb methods to tectonomagmatic events in the geological record is at least partly the amount of melting and igneous emplacement that occurs during an orogen. In chapter 4 for example the U-Pb record of detrital apatite with metamorphic trace-element compositions mostly records events that the zircon U-Pb record does not record, while the U-Pb record of detrital apatite with igneous trace-element compositions is much more similar to the zircon U-Pb record than that of the metamorphic apatite U-Pb record (Figure 6, chapter 4). Likewise, in chapter 2 it is demonstrated that the absence of Alleghanian zircon U-Pb ages from French Broad River detritus can be linked to the absence of igneous emplacement in the catchment area of the French Broad River during that event. Thus, apatite U-Pb can be employed as a detrital fingerprint of magma-poor orogens that are undetectable using the detrital zircon U-Pb method. It provides U-Pb information that is complementary to that of detrital zircon U-Pb age data, which records different U-Pb provenance information that is often more refractory and biased towards the emplacement of felsic igneous rocks (e.g. Moecher and Samson, 2006).

Finding 2: Based on the assembly of literature data on apatite trace-element compositions from bedrocks, apatite trace-element compositions (specifically the REYs, actinides and Sr+Mn) can now be used to reliably and quickly determine the source lithology of detrital apatite from all common lithologies on the Earth's surface.

Though apatite compositions have previously been used as a tracer of lithology in a handful of detrital studies (Morton and Yaxley, 2007; Abdullin *et al.*, 2016), there are issues with the methodology employed by those papers that left significant room for improvement. Firstly REE "spidergrams" as used in those papers are confusing when dealing with very large detrital datasets, where the number of apatite unknowns may number several thousand. Secondly two-element or two-ratio scatterplots also fail to incorporate all the trace-element information in the sample to fully characterise detrital apatite, leading to poor data separation (Figure 1). Instead, several element abundances and ratios are required to be used simultaneously to definitively assign a lithology to a detrital apatite. Lastly, the lack of a large and detailed database of apatite compositions up until this point has led to the development of discrimination tools and diagrams that

cope poorly with discriminating metamorphic apatite (e.g. Sr/Y diagrams such as those proposed by Belousova *et al.*, 2002; and the widely used La/Nd vs (La+Ce+Pr/EREE % apatite discrimination diagram of Fleischer and Altschuler, 1986). The Fleischer and Altschuler (1986) discriminant plot fails to distinguish metamorphic apatite as the defining characteristic of metamorphic apatite *vs* igneous apatite is not REE ratios, but rather that the overall trace element contents of metamorphic apatite are extremely low (particularly the REY and actinides) as shown in studies of bedrock metamorphic apatite (Spandler *et al.*, 2003; Nutman, 2007; El Korh *et al.*, 2009; Henrichs *et al.*, 2018) that are included in the literature database in chapter 4. Use of the aforementioned diagrams results in unsatisfactory and unclear separation of detrital metamorphic apatite from igneous apatite, as discussed for example by Abdullin et al. (2016). As metamorphic apatite can often comprise the bulk of apatite in detrital samples, as is the case in *every case study* in this thesis, this issue had to be addressed in order to convincingly categorise *individual* detrital grains.

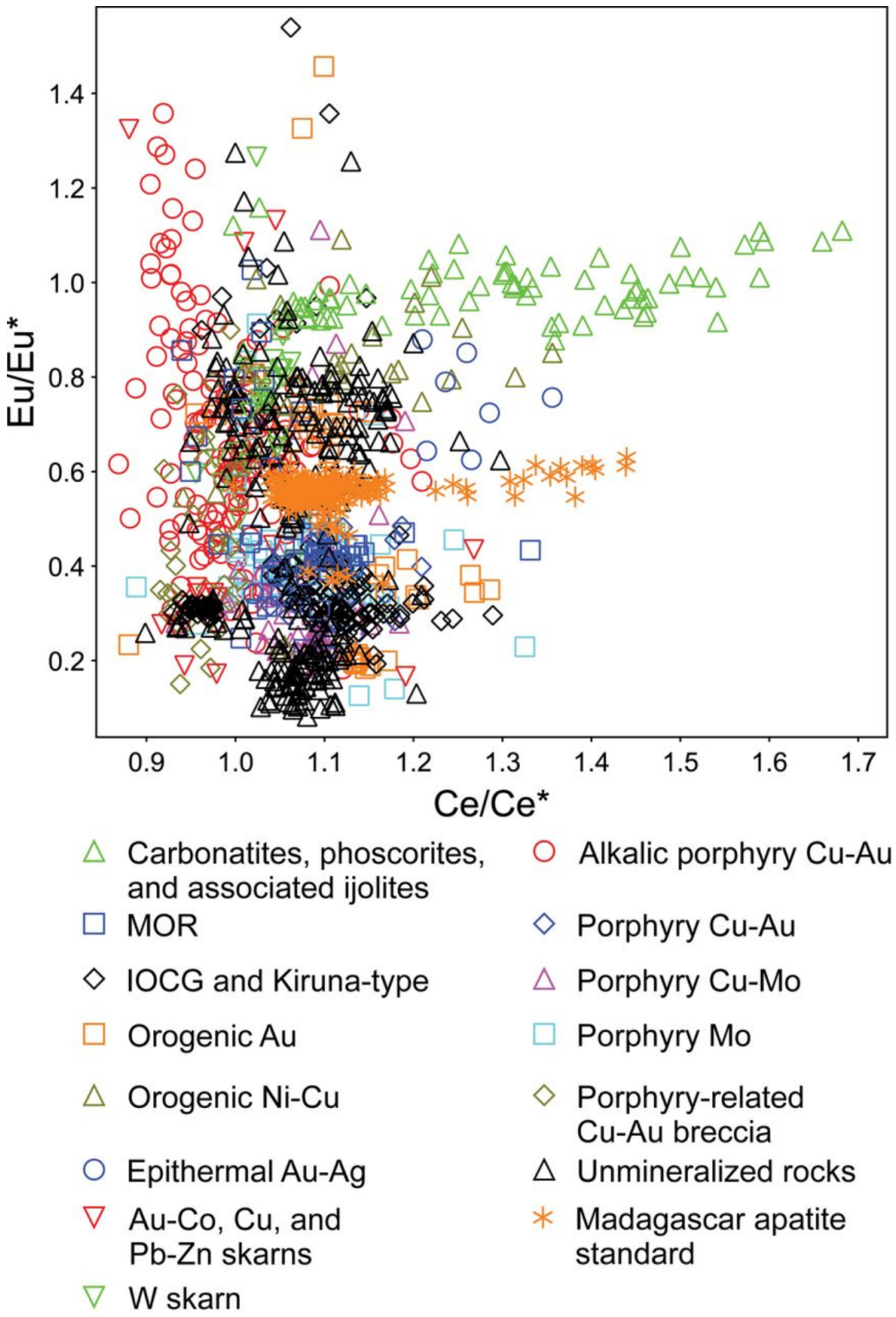

Figure 1. Two-element scatterplot apatite discriminant diagram from Mao et al. (2016), showing unclear separation and overlapping distribution of apatite from mostly ore-bearing rocks

Solving these visualisation and data separation issues became an important cornerstone of this PhD. Principal component analysis (PCA), an increasingly adopted data transformation and visualisation method in provenance analysis (e.g. Vermeesch, 2013), provided a technique with which to solve data visualisation issues in apatite compositional discrimination. It allows the simultaneous plotting of multiple elements and ratios, which is imperative to fully separating apatite compositions, and when plotted in log space it circumvents the 'zero-problem' where grains with low element abundances all cluster near the origin on a graph. The assembly of a large literature database was also a keystone to improving the range of detrital apatite compositional provenance. By assembling a database that accounts for the full range of common lithologies on the Earth's surface (and also several uncommon ones), this database can be used as an empirical record of apatite compositions that encompasses almost every rock type that geologists analysing detritus will commonly encounter.

The database ranges from metamorphic rocks of low- to high-grades and of pelitic and basic composition, metasomatised rocks, igneous rocks from the felsic (S-type granites) to ultrabasic (lherzolites, carbonatites, pyroxenites), and also including alkaline igneous rocks (syenites, phonolites, agpaitic melts etc.). Apatite trace element compositions from all these lithologies are highly distinct, meaning that detritus can be definitively linked to specific lithological groups.

Finding 3: As shown in chapters 3 and 4, the amenability of detrital apatite grains to U-Pb dating is linked to the trace element composition, and therefore the source lithology chemistry. Apatite from metasomatised rocks and metamorphic rocks, especially of low- to medium-grades, is much less likely to be 'dateable' than apatite from all igneous lithologies, due to low U contents and high common-Pb contents. Though this finding has been reported previously from individual bedrock samples (e.g. Henrichs et al., 2018), apatite from widely sourced detrital samples integrates detritus over a much wider area and erases any doubt that this finding is due to potential sample bias. In practice this effect will produce a bias in the detrital apatite *U-Pb record* to preferentially recording useable age-information from igneous lithologies over metamorphic lithologies (O'Sullivan *et al.*, 2018). This finding also has implications for apatite fission-track and U/Th-He dating methods in low- to medium-grade metamorphic terranes. Obviously this bias does not arise when provenance determinations are undertaken using apatite trace-element compositional data alone.

5.2 FUTURE WORK

As chapter 4 represents the most recently completed work presented in this thesis, the focus of this section on 'future work' largely follows on from that chapter, principally the application of the apatite-discrimination PCA biplot to further research.

Firstly, though the synthesis of published data on apatite trace element chemistry presented in this thesis is comprehensive (chapter 4), there are still additions and refinements that can be made to this database to broaden its applicability to new detrital provenance research. The addition of bedrock compositional data from granitic orthogneisses (from low- to high-metamorphic grades) would be highly valuable, as these are essentially the only common lithology that has little to no published compositional data for apatite and thus have not been included in the literature database presented in chapter 4. It would also be useful to further extend the database to incorporate metasomatic and ore-bearing rocks, and to undertake a detailed analysis of metasomatic apatite on a PCA biplot to see if specific metasomatic processes can be detected by apatite compositional data, and whether the pre-metasomatic composition of metasomatically-reprecipitated apatite can be reconstructed. Using the PCA method it may also prove possible to improve understanding of the link between apatite composition and its proximity to ore-bodies (*cf* Mao *et al.*, 2016), and thus apply apatite as a tool for vectoring ore bodies.

Incorporating more aspects of apatite chemistry *might* also improve the discriminatory power of the PCA biplots used in chapters 3 and 4. Elements occupying the halogen-hydroxyl site (the Z-site) in the apatite lattice (F, Cl, OH) were not used, nor were elements such as C, Na, Si and S that can substitute for P in apatite. Many of these elements were excluded due to the use of the LA-Q-ICP-MS method, which is for example unable to measure *trace quantities* of the halogens apart from Cl (e.g. Chew *et al.*, 2014). Cl, Si and S are difficult to analyse by LA-ICP-MS as their first ionization potential is similar (but still lower) than that of the Ar plasma gas: Si and S also suffer from high backgrounds due to N_2 and O_2-based polyatomic interferences. OH and F cannot be measured by LA-ICP-MS (the first ionization potential of F is higher than that of Ar). However, while discrimination of individual rocks with unusual apatite halogen compositions may be possible using halogen contents (e.g. Bamble apatite, Chew et al., 2014), the use of halogen-compositions in apatite as a discriminator of lithology is doubtful as halogen contents of apatite from felsic and mafic magmas significantly

overlap (e.g. Belousova *et al.*, 2001). Additionally the inability to measure F by LA-ICP-MS means that costly and time-consuming additional analysis using a different technique would have to be undertaken, that would undermine the attractiveness of the relatively streamlined combined U-Pb age and trace-element LA-ICP-MS method employed in this thesis. Reactions involving Na^{+} and Si^{4+} substitution into apatite may be coupled with REY^{3+} (e.g. $Si^{4+} + (Y+REE)^{3+} \Leftrightarrow P^{5+} + Ca^{2+}$ and $Na^{+} + (Y+REE)^{3+} \Leftrightarrow 2\ Ca^{2+}$; Harlov *et al.,* 2003), or with S^{6+} (e.g. $2\ P^{5+} \Leftrightarrow Si^{4+} + S^{6+}$ and $2\ P^{5+} + LREE^{3+} \Leftrightarrow 2\ S^{6+} + Na^{+}$; Harlov *et al.,* 2003), meaning that the incorporation of Na, Si and S into apatite lattice is independent of REY incorporation and may thus provide novel geochemical insights, particularly with regard to paleo-environmental signals. This warrants future investigation for use in provenance and mineralisation studies.

As already reported in several papers included in the apatite composition database in chapter 4 (e.g. Dill, 1994; Shields and Stille, 2001; Nishizawa *et al.*, 2005; Joosu *et al.*, 2015, 2016), authigenic apatite from non-metamorphosed sediments may characterise ancient seawater chemistry. All of these authigenic apatites have flat REE topologies, Sr-isotope ratios, negative Ce-anomalies and high Y/Ho ratios that are indicative of crystallization in the presence of marine waters (Y/Ho > 35 e.g. Lawrence *et al.,* 2006). This combination of features is not seen in non-authigenic apatite in the literature database (chapter 4 data tables; e.g. Hsieh *et al.*, 2008). With further study authigenic apatite could be developed as a tool to study the chemistry of the water column during the deposition of ancient sediments, especially with regard to its oxygen fugacity. Coupled with the ability to directly date authigenic apatite by the U-Pb method (e.g. Gall *et al.*, 2017) it could be possible to assign a date to the seawater chemistry recorded by authigenic apatite. Of the potential sources of authigenic apatite, phosphorites are a particularly intriguing potential target for combined U-Pb dating and seawater-chemistry analysis, as crucially phosphorites are typically U-rich, which could result in their precise U-Pb dating. They are composed primarily of apatite or amorphous apatite (collophane) and are formed at regions of ocean bottom-water upwelling and high biological production on continental slopes at the present day (Veeh et al., 1973). Phosphorites are typically precipitated in clastic-detritus starved waters, and typically occur as compressed-intervals in sedimentary successions that are typically shale-dominated and that are not possible to date using U-Pb geochronology. Importantly, phosphorites may be able to provide age information for poorly-constrained sedimentary sections, especially in

successions with poorly constrained fossil-records such as in pre-Ediacaran successions (e.g. Xiao et al., 1998).

Lastly, the methodology employed in this thesis of using a large database to make an empirical discriminant PCA-diagram for grain compositions could be undertaken for other mineral phases. There is plentiful published trace element composition data available from rutile (e.g. Meinhold *et al.*, 2008; G. L. Luvizotto *et al.*, 2009a; 2009b), and zircon (e.g. Hoskin *et al.*, 2000; Belousova *et al.*, 2002; Rubatto, 2002) that could benefit from modern 'big data' analysis methods such as PCA.

5.3 REFERENCES

Abdullin, F., Solé, J., Solari, L., Shchepetilnikova, V., Meneses-Rocha, J. J., Pavlinova, N. and Rodríguez-Trejo, A. (2016) 'Single-grain apatite geochemistry of Permian–Triassic granitoids and Mesozoic and Eocene sandstones from Chiapas, southeast Mexico: implications for sediment provenance', International Geology Review, 58(9), pp. 1132–1157. doi: 10.1080/00206814.2016.1150212.

Belousova, E. A., Griffin, W. L., O'Reilly, S. Y. and Fisher, N. I. (2002) 'Apatite as an indicator mineral for mineral exploration: Trace-element compositions and their relationship to host rock type', Journal of Geochemical Exploration, 76, pp. 45–69. doi: 10.1016/S0375-6742(02)00204-2.

Belousova, E. A., Walters, S., Griffin, W. L. and O'Reilly, S. Y. (2001) 'Trace-element signatures of apatites in granitoids from the Mt Isa Inlier, Northwestern Queensland', Australian Journal of Earth Sciences, 48, pp. 603–619. doi: 10.1046/j.1440-0952.2001.00879.x.

Belousova, E., Griffin, W., O'Reilly, S. Y. and Fisher, N. (2002) 'Igneous zircon: trace element composition as an indicator of source rock type', Contributions to Mineralogy and Petrology, 143(2002), pp. 602–622. doi: 10.1007/s00410-002-0364-7.

Chew, D. M., Donelick, R. A., Donelick, M. B., Kamber, B. S. and Stock, M. J. (2014) 'Apatite Chlorine Concentration Measurements by LA-ICP-MS', Geostandards and Geoanalytical Research, 38, pp. 23–35. doi: 10.1111/j.1751-908X.2013.00246.x.

Dill, H. G. (1994) ‘Can REE patterns and U-Th variations be used as a tool to determine the origin of apatite in clastic rocks?’, Sedimentary Geology, 92(3–4), pp. 175–196. doi: 10.1016/0037-0738(94)90105-8.

El Korh, A., Schmidt, S. T., Ulianov, A. and Potel, S. (2009) ‘Trace Element Partitioning in HP-LT Metamorphic Assemblages during Subduction-related Metamorphism, Ile de Groix, France: a Detailed LA-ICPMS Study’, Journal of Petrology, 50(6), pp. 1107–1148. doi: 10.1093/petrology/egp034.

Fleischer, M., and Altschuler, Z.S. (1986). The lanthanides and yttrium in minerals of the apatite group - an analysis of the available data. Neues Jahrbuch fuer Mineralogie, Monatshefte, (10), 467-480.

Gall, Q., Davis, W. J., Lowe, D. G. and Dabros, Q. (2017) ‘Diagenetic apatite character and in situ ion microprobe U – Pb age , Keeseville Formation, Potsdam Group , New York State’, Canadian Journal of Earth Science, 797, pp. 785–797.

Harlov, D. E., Förster, H.-J. and Schmidt, C. (2003) ‘High P-T experimental metasomatism of a fluorapatite with significant britholite and fluorellestadite components: implications for LREE mobility during granulite-facies metamorphism’, Mineralogical Magazine, 67(1), pp. 61–72. doi: 10.1180/0026461036710084.

Henrichs, I. A., O’Sullivan, G. J., Chew, D. M., Mark, C., Babechuk, M. G., McKenna, C. and Emo, R. (2018) ‘The trace element and U-Pb systematics of metamorphic apatite’, Chemical Geology, 483, 218-238. doi: 10.1016/j.chemgeo.2017.12.031.

Hietpas, J., Samson, S., Moecher, D. and Schmitt, A. K. (2010) ‘Recovering tectonic events from the sedimentary record: Detrital monazite plays in high fidelity’, Geology, 38(2), pp. 167–170. doi: 10.1130/G30265.1.

Hoskin, P. W. O., Kinny, P. D., Wyborn, D. and Chappell, B. W. (2000) 'Identifying Accessory Mineral Saturation during Differentiation in Granitoid Magmas: an Integrated Approach', Journal of Petrology, 41(9), pp. 1365–1396. doi: 10.1093/petrology/41.9.1365.

Hsieh, P. S., Chen, C. H., Yang, H. J. and Lee, C. Y. (2008) 'Petrogenesis of the Nanling Mountains granites from South China: Constraints from systematic apatite geochemistry and whole-rock geochemical and Sr-Nd isotope compositions', Journal of Asian Earth Sciences, 33, pp. 428–451. doi: 10.1016/j.jseaes.2008.02.002.

Joosu, L., Lepland, A., Kirsimäe, K., Romashkin, A. E., Roberts, N. M. W., Martin, A. P. and Črne, A. E. (2015) 'The REE-composition and petrography of apatite in 2Ga Zaonega Formation, Russia: The environmental setting for phosphogenesis', Chemical Geology, 395, pp. 88–107. doi: 10.1016/j.chemgeo.2014.11.013.

Joosu, L., Lepland, A., Kreitsmann, T., Üpraus, K., Roberts, N. M. W., Paiste, P., Martin, A. P. and Kirsimäe, K. (2016) 'Petrography and the REE-composition of apatite in the Paleoproterozoic Pilgujärvi Sedimentary Formation, Pechenga Greenstone Belt, Russia', Geochimica et Cosmochimica Acta, 186, pp. 135–153. doi: 10.1016/j.gca.2016.04.043.

Kinny, P. D., Friend, C. R. L. and Love, G. J. (2005) 'Proposal for a terrane-based nomenclature for the Lewisian Gneiss Complex of NW Scotland', Journal of the Geological Society, 162(1), pp. 175–186. doi: 10.1144/0016-764903-149.

Lawrence, M. G., Jupiter, S. D. and Kamber, B. S. (2006) 'Aquatic geochemistry of the rare earth elements and yttrium in the Pioneer River catchment, Australia', Marine and Freshwater Research, 57(7), pp. 725–736. doi: 10.1071/MF05229.

Luvizotto, G. L., Zack, T., Meyer, H. P., Ludwig, T., Triebold, S., Kronz, a., Münker, C., Stockli, D. F., Prowatke, S., Klemme, S., Jacob, D. E. and von Eynatten, H. (2009) 'Rutile crystals as potential trace element and isotope mineral standards for microanalysis', Chemical Geology, 261(3–4), pp. 346–369. doi: 10.1016/j.chemgeo.2008.04.012.

Luvizotto, G. L., Zack, T., Triebold, S. and Von Eynatten, H. (2009) 'Rutile occurrence and trace element behavior in medium-grade metasedimentary rocks: Example from the Erzgebirge, Germany', Mineralogy and Petrology, 97(3–4), pp. 233–249. doi: 10.1007/s00710-009-0092-z.

Mao, M., Rukhlov, A. S., Rowins, S. M., Spence, J. and Coogan, L. A (2015) 'Detrital Apatite Trace-Element Compositions : a Robust New Tool for Mineral Exploration', Economic Geology, 111 (5), 1187-1222. doi: 10.2113/econgeo.111.5.1187.

May, T. W. and Wiedmeyer, R. H. (1998) 'A Table of Polyatomic Interferences in ICP-MS', Atomic Spectroscopy, 19(5), pp. 150–155. doi: 10.1039/C7JA00051K.

Meinhold, G., Anders, B., Kostopoulos, D. and Reischmann, T. (2008) 'Rutile chemistry and thermometry as provenance indicator: An example from Chios Island, Greece', Sedimentary Geology, 203, pp. 98–111. doi: 10.1016/j.sedgeo.2007.11.004.

Moecher, D. P. and Samson, S. D. (2006) 'Differential zircon fertility of source terranes and natural bias in the detrital zircon record: Implications for sedimentary provenance analysis', Earth and Planetary Science Letters, 247(3–4), pp. 252–266. doi: 10.1016/j.epsl.2006.04.035.

Morton, A. and Yaxley, G. (2007) 'Detrital apatite geochemistry and its application in Provenance Studies', in Arribas, J., Critelli, S., and Johnsson, M. J., eds., Sedimentary Provenance and Petrogenesis: Perspectives from Petrography and Geochemistry: Geological Society of America Special Paper 420, pp. 319–344. doi: 10.1130/2006.2420(19).

Nishizawa, M., Takahata, N., Terada, K., Komiya, T., Ueno, Y. and Sano, Y. (2005) 'Rare-earth element, lead, carbon, and nitrogen geochemistry of apatite-bearing metasediments from the similar to 3.8 Ga Isua supracrustal belt, West Greenland', International Geology Review, 47(9), pp. 952–970. doi: 10.2747/0020-6814.47.9.952.

Nutman, A. P. (2007) ‘Apatite recrystallisation during prograde metamorphism, Cooma, southeast Australia: implications for using an apatite – graphite association as a biotracer in ancient metasedimentary rocks’, Australian Journal of Earth Sciences, 54, pp. 1023–1032. doi: 10.1080/08120090701488321.

O’Sullivan, G. J., Chew, D. M., Morton, A. C., Mark, C. and Henrichs, I. A. (2018) ‘An Integrated Apatite Geochronology and Geochemistry Tool for Sedimentary Provenance Analysis’, Geochemistry, Geophysics, Geosystems, pp. 1309–1326. doi: 10.1002/2017GC007343.

Rubatto, D. (2002) ‘Zircon trace element geochemistry: Partitioning with garnet and the link between U-Pb ages and metamorphism’, Chemical Geology, 184, pp. 123–138. doi: 10.1016/S0009-2541(01)00355-2.

Shields, G. and Stille, P. (2001) ‘Diagenetic constraints on the use of cerium anomalies as palaeoseawater redox proxies: An isotopic and REE study of Cambrian phosphorites’, Chemical Geology, 175(1–2), pp. 29–48. doi: 10.1016/S0009-2541(00)00362-4.

Spandler, C., Hermann, J., Arculus, R. and Mavrogenes, J. (2003) ‘Redistribution of trace elements during prograde metamorphism from lawsonite blueschist to eclogite facies; implications for deep subduction-zone processes’, Contributions to Mineralogy and Petrology, 146(2), pp. 205–222. doi: 10.1007/s00410-003-0495-5.

Veeh, H.H., Burnett, W.C. and Soutar, A., 1973. Contemporary phosphorites on the continental margin of Peru. Science, 181(4102), pp.844-845. doi: 10.1126/science.181.4102.844

Vermeesch, P. (2013) ‘Multi-sample comparison of detrital age distributions’, Chemical Geology. Elsevier B.V., 341, pp. 140–146. doi: 10.1016/j.chemgeo.2013.01.010.

Xiao, S., Zhang, Y. and Knoll, A. H. (1998) ‘Three-dimensional preservation of algae and animal embryos in a neoproterozoic phosphorite’, Nature, 391(6667), pp. 553–558. doi: 10.1038/35318.

Appendix A

The trace element and U-Pb systematics of metamorphic apatite

Published in 'Chemical Geology', 2018 (483) p. 218-238

Authors: Isadora A. Henrichs, Gary J. O'Sullivan, David M. Chew, Chris Mark, Michael G. Babechuk, Cora McKenna, Robert Emo

ABSTRACT

Apatite is a common accessory mineral in igneous, sedimentary and metamorphic rocks. It has potential as a provenance indicator in sedimentary systems, as it can host a wide variety of trace elements in its crystal structure and can yield thermochronological age information. However, the processes controlling the trace element and U-Pb systematics of metamorphic apatite remain poorly understood, and metamorphic apatite remains significantly under-represented in compositional provenance databases linking apatite trace-element chemistry to its corresponding parent rock type. We investigate the trace-element and U-Pb systematics of metamorphic apatite from a suite of 22 bedrock samples of diverse metamorphic grade and protolith type, sampled from a variety of metamorphic terranes. Metamorphic apatite from low- to medium-grade metapelites and metabasites can be easily distinguished from granitic apatite as it is significantly depleted in Th, REE, and Y. Depletion in Th and REE+Y is attributed to growth of co-genetic epidote, which is the dominant carrier phase of the REE+Y, Th, and U in all the low- to medium-grade samples mapped by laser ablation quadrupole inductively coupled plasma mass spectrometry (LA-Q-ICP-MS) and energy dispersive X-ray spectroscopy (EDS). Apatite U contents in low- to medium-grade metapelites and metabasites are more variable than the Th and REE+Y contents, but are typically low. Consequently, grains from these rock types are often undateable by the U-Pb LA-ICP-MS method and thus are underrepresented in apatite U-Pb detrital datasets, but can still be identified as low- to medium-grade metamorphic apatite by their trace-element characteristics. Low-grade metapelite apatite is difficult to distinguish from low-grade metabasite apatite, which is likely due to the growth of U-, Th-, and REE-rich epidote in both lithologies. Detrital

(granitic) apatite is stable in very low-grade (e.g. pumpellyite-actinolite facies) metasedimentary samples, while neo- or re-crystallised metamorphic apatite is widespread by the upper-greenschist facies. LA-Q-ICP-MS imaging demonstrates that low REE+Y, Th, and U metamorphic apatite rims can nucleate on detrital igneous apatite precursors with high REE+Y, Th, and U. With increasing metamorphic grade, 1) relict detrital apatite is consumed, 2) the coherence of the U-Pb concordia systematics dating metamorphism improve, and 3) the degree of dispersion on metamorphic apatite multi-element plots decreases. The highest-grade metamorphic apatite samples investigated are paragneisses, some of which have locally undergone anatexis. Apatites from these samples yield well constrained TW concordia intercept ages and minor dispersion on multi-element plots (which is attributed to the absence of epidote) and closely resemble apatite from S-type granites in their trace element characteristics.

A.1. INTRODUCTION

Apatite is a common accessory mineral in igneous, sedimentary and metamorphic rocks (Hughes and Rakovan, 2015). It has strong potential in sedimentary provenance studies as it hosts a wide variety of trace elements in its crystal structure. It can yield reliable low-temperature thermochronological age information from the apatite fission-track and U/Th-He dating methods, and also provides medium-temperature age information using the U-Pb chronometer once a common Pb correction is applied (Chew et al. 2011; Chew and Spikings, 2015). Additionally, it is more likely to represent first-cycle detritus than more refractory detrital phases such as zircon due to its instability during chemical weathering (Morton and Hallsworth, 1999). This study first evaluates the potential of apatite as a provenance indicator in sedimentary systems by reviewing both its trace element and U-Pb systematics in common source lithologies (i.e. igneous and metamorphic rocks) based on existing data from the literature. We then investigate the trace-element and U-Pb systematics of metamorphic apatite on a suite of 22 bedrock samples collected from Barrovian terranes, as metamorphic apatite remains significantly under-represented in the existing compositional database linking apatite trace-element chemistry to its corresponding parent rock type.

A.1.1 Igneous apatite trace-element chemistry

The formula of apatite can be simplified as $A_5(XO_4)_3Z$. The A-site usually accommodates Ca in two structural sites, Ca1 (IX-fold coordination) and Ca2 (VII-fold coordination), but they can be substituted by a variety of trace elements including Mn^{2+}, Sr^{2+}, U^{4+}, Pb^{2+}, Th^{4+}, Y^{3+} and $REE^{2+,3+}$. The tetrahedral X-site is occupied mainly by P^{5+} (as PO_4^{3-}) and can be replaced by other small, highly-charged cations (e.g. Si^{4+}, S^{6+}, As^{5+}, V^{5+}). The monovalent anion Z-site is occupied by OH- or the halogens F-, Cl- (Piccoli and Candela, 2002). Fluorapatite is by far the most common species in the apatite group, and especially so in metamorphic rocks. Hence when discussing the data from this study, references to apatite can be considered as synonymous with fluorapatite unless otherwise stated. Due to its ability to substitute multiple elements, apatite retains a large amount of the whole-rock budget of REE+Y and Sr, and is thus a very useful mineral in igneous petrogenesis studies (Prowatke and Klemme, 2006). Apatite has also proven to be a useful indicator mineral in mineral exploration studies due to its trace element variability and the ability to fingerprint these elements back to its igneous or ore deposit source (Belousova *et al.,* 2002; Mao *et al.,* 2016).

Sha and Chappell (1999) recognized that apatites from S-type and felsic I-type granites are depleted in LREE and Th, whereas apatites from more mafic I-type granites are enriched in these elements and exhibit higher Eu/Eu* ratios, where Eu* = $(Sm_N+Gd_N)/2$ on a chondrite-normalised plot. Belousova et al. (2002) used apatite Ce/Yb ratios to differentiate carbonatites and mantle-derived lherzolites (with chondrite-normalised Ce/Yb ratios of 100 and 200 respectively) from pegmatites (that typically have very low Ce/Yb ratios of less than unity). Other studies have determined that the REE ratios in apatite correlates with the Al saturation index (ASI) of its host granite (Belousova et al. 2001), while apatite Sr and Mn contents can be correlated with the degree of fractionation and magma oxygen fugacity respectively (e.g. Sha and Chappell et al., 1999; Hsieh et al., 2008; Broska et al., 2004; Cao et al., 2012; Miles et al., 2014). The trace element chemistry of apatite from basic igneous rocks is also highly distinct from that of crustally-contaminated igneous lithologies. Basic apatite has very high La/Lu giving steep rightward-declining REE-profiles; Th/U and Sr/Mn ratios are typically much higher than that encountered in felsic rocks; while Eu-anomalies are non-existent or very moderate and depend on whether apatite crystallises from melt before or after feldspar respectively (Tang et al., 2012).

A.1.2 Metamorphic apatite trace-element chemistry

While the behaviour of trace elements in igneous apatite is well established, the behaviour of trace elements in metamorphic apatite is less well understood. However, the available data implies that the trace-element composition of metamorphic apatite is significantly different to that of igneous apatite.

The redistribution of REE, Th, and U in metamorphic apatite in progressive (amphibolite- to granulite-facies) high-temperature metamorphism of a calc-alkaline orthogneiss series was studied by Bingen et al. (1996), who demonstrated that the MREE and HREE content of apatite increased with increasing metamorphic grade due to the breakdown of hornblende, allanite, and titanite around the clinopyroxene-in isograd. With increasing metamorphic grade, apatite LREE and Th contents increased at the orthopyroxene-in isograd as monazite was progressively consumed. The apatite U content in this amphibolite- to granulite-facies orthogneiss suite is similar (3-25 ppm) to granitic apatite, but is clearly substantially higher than that of the low- to medium-grade metapelite and metabasite apatites investigated in this study.

Bea and Montero (1999) studied the redistribution of REE, Y, Zr, Th, and U during middle amphibolite- to granulite-facies metamorphism and partial melting of metapelites intercalated with gabbros, diorites and mantle tectonites from the Ivrea-Verbano Zone, NW Italy, an exhumed section of the lower to middle crust. During progressive metamorphism of the granulite-facies pelites to lower-crustal restitic pelite, biotite was consumed, the modal abundance of garnet increased, and correspondingly the Y, HREE, and MREE content of the apatite progressively decreased. Whole rock increases in Th/U ratios and loss of U from the metamorphic system due to melt/fluid extraction resulted in a steep drop in apatite U contents in the lower-crustal restitic pelite during progressive metamorphism, ultimately producing apatite with trace element characteristics indistinguishable from those of basic igneous rocks.

Nutman et al. (2007) analysed apatite from Cooma, Australia from a flysch-type sequence that has undergone progressive metamorphism from greenschist- through to granulite-facies, and observed that the apatite chondrite-normalized REE patterns are very similar for almost all samples, with a negative depletion in Eu and a relative LREE depletion probably due to the growth of co-existing monazite. With increasing metamorphic grade, the apatite Th abundances and Th/U ratios decrease, while the REE patterns from individual apatites converge, suggesting increasing chemical equilibrium.

These studies have indicated that the evolving prograde assemblage during progressive metamorphism can exert a strong influence on the trace element abundances in metamorphic apatite. However, many of these studies were restricted in terms of protolith type and variation in metamorphic grade. In comparison, this study examines apatite from terranes characterised by regional metamorphism for several different protolith types including (meta-)pelites, basalts, and granites, with a range in metamorphic grade that ranges from the pumpellyite-actinolite facies through to paragneisses that have locally undergone anatexis. These lithologies are extensive on the Earth's surface and thus likely to be well-represented in the detrital record.

A.1.3 U-Pb dating of apatite by LA-ICP-MS

U-Pb zircon dating by laser ablation inductively coupled plasma mass spectrometry (LA-ICP-MS) is now a rapid and routine tool (Spencer et al., 2016). However, apatite U-Pb dating by LA-ICP-MS is more challenging due to the typically low U abundances and elevated common Pb contents in both age-reference and unknown apatites, although common Pb in apatite age standards can now be corrected for (e.g. Chew et al. 2014;

Thomson et al., 2012; Chew et al., 2011). Recent studies employing the LA-ICP-MS U-Pb apatite technique include dating of granites (Gaweda et al., 2014), carbonatites (Chen et al. 2013), dolerites (Pochon et al., 2016) and iron oxide-apatite deposits (Neymark et al. 2016). Inverse modelling of apatite U–Pb dates can also produce temperature-time histories assuming Pb has been lost by volume diffusion (Cochrane et al., 2014). Chew et al. (2014) have demonstrated the accuracy of U-Pb apatite secondary standards using the latest generation of quadrupole (Q) ICP-MS instruments, showing that a precision of < 1% (2σ) for Phanerozoic apatite standards and 2σ uncertainties of < 2% for Paleogene apatite standards can be obtained.

A.1.4 Apatite as a provenance tool

Apatite has strong potential as a provenance tool in sedimentary and mineral exploration. It is a common accessory component in clastic sedimentary rocks as it is very common in metamorphic and igneous sources (Morton and Yaxley, 2007). It is a nearly ubiquitous accessory phase in igneous rocks, due in part to the low solubility of P_2O_5 in silicate melts and the limited amount of P incorporated into the crystal lattices of the major rock-forming minerals (Piccoli & Candela, 2002). For the same reason, it is near-ubiquitous in metamorphic rocks of most common protolith compositions (pelitic, carbonate, basaltic, and ultramafic protoliths) and from temperatures and pressures ranging from the zeolite-facies through to the granulite- and eclogite-facies (Spear and Pyle, 2002).

Apatite can also be used as a detrital chronometer in provenance studies, and can be employed as a triple-dating proxy by combining the apatite U-Pb, fission track (AFT) and U-Th/He methods (e.g. Carrapa, 2009, Zattin et al., 2012). Due to the medium-temperature sensitivity (~375-550°C) of the apatite U-Pb system, a temperature range typically encountered in medium-grade metamorphic belts, U-Pb dating of detrital apatite has been applied as a provenance tool in magma-poor orogenic belts, which are often poorly recorded by the zircon U-Pb technique (e.g. Mark et al., 2016, O'Sullivan et al., 2016).

In comparison with detrital apatite chronometry, the utility of apatite trace-element compositions in provenance studies has received less attention in the literature. Recent provenance studies utilizing (igneous) apatite trace-element chemistry include Abdullin et al. (2016) who analysed apatite Sr, Y, Th, U, and REE contents to determine the source area of Mesozoic and Eocene sandstones from Chiapas, Mexico, and Jafarzadeh et al. (2014) who utilized apatite REE chemistry to demonstrate that Tethyan Oligocene–

Miocene sandstones in NW Iran were derived from mafic/intermediate volcanic rocks of both alkaline and calc-alkaline composition. Nevertheless, a lack of a comprehensive database on apatite compositions in potential source rocks has to date been a barrier to routine provenance studies using apatite geochemistry, particularly for metamorphic apatite (cf. Morton and Yaxley, 2007; Abdullin et al., 2016).

For apatite to be employed successfully as a sedimentary provenance tool, a comprehensive database on apatite compositions that can be linked to the composition of their corresponding parent rock type is key. Hence, this study aims to fill in the gaps in the metamorphic apatite database, by determining apatite trace-element abundances in samples from Barrovian terranes (i.e. orogenic belts characterised by regional metamorphism). Twenty-two samples of differing metamorphic grade and protolith composition are investigated, and compared with the trace-element composition of magmatic apatite from the literature. Three samples (particularly greenschist-facies pelites and greywackes) yield two discrete apatite populations based on their trace-element chemistry. These represent populations of neocrystalline metamorphic apatite and detrital magmatic apatite; *in situ* LA-Q-ICP-MS trace element mapping was undertaken on selected samples to investigate the relationship between neocrystalline metamorphic apatite growth and detrital magmatic apatite grains.

A.2. SAMPLES – REGIONAL GEOLOGICAL SETTING

A.2.1 Ireland and Scotland

Nine samples were collected from the Dalradian Supergroup of the Grampian terrane of Scotland and NW Ireland (LT1, LT2, DC8/11/1a, DC 8/11/1b, and IH11/13/01 through to IH11/13/05, Table 1, Supplementary Figure 1), while two samples (AGC1 and AGC2, Supplementary Figure 1, Table 1) were collected from the structurally-underlying basement in NW Ireland, the Paleoproterozoic Annagh Gneiss Complex. The Grampian terrane in NE Scotland is the type locality for Barrovian (regional) metamorphism, and resulted from the collision of eastern Laurentia with an infant oceanic arc and supra-subduction ophiolite during the Early to Middle Ordovician (Dewey, 2005). This tectonic event is termed the Grampian orogeny, and is equivalent to the Taconic orogeny of the Appalachians and eastern maritime Canada. The Neoproterozoic to early Paleozoic Dalradian Supergroup represents a basin deposited during the breakup of the Rodinia supercontinent, with the younger parts of the Dalradian sequence recording the transition to sedimentation on the Laurentian passive continental margin. It records a wide range of sedimentary environments (alluvial, tidal, deltaic, shallow marine, turbiditic, debris flow), a phase of rift-related ca. 600 Ma basaltic magmatism (basic sills and volcanics) associated with Rodinia breakup, and experienced a subsequent complex (polyphase) structural and metamorphic history. Abundant geochronological data demonstrate that Barrovian metamorphism of the Dalradian Supergroup occurred over a short time period (10 Myr) between ca. 475 and 465 Ma during the Grampian orogeny (Dewey, 2005).

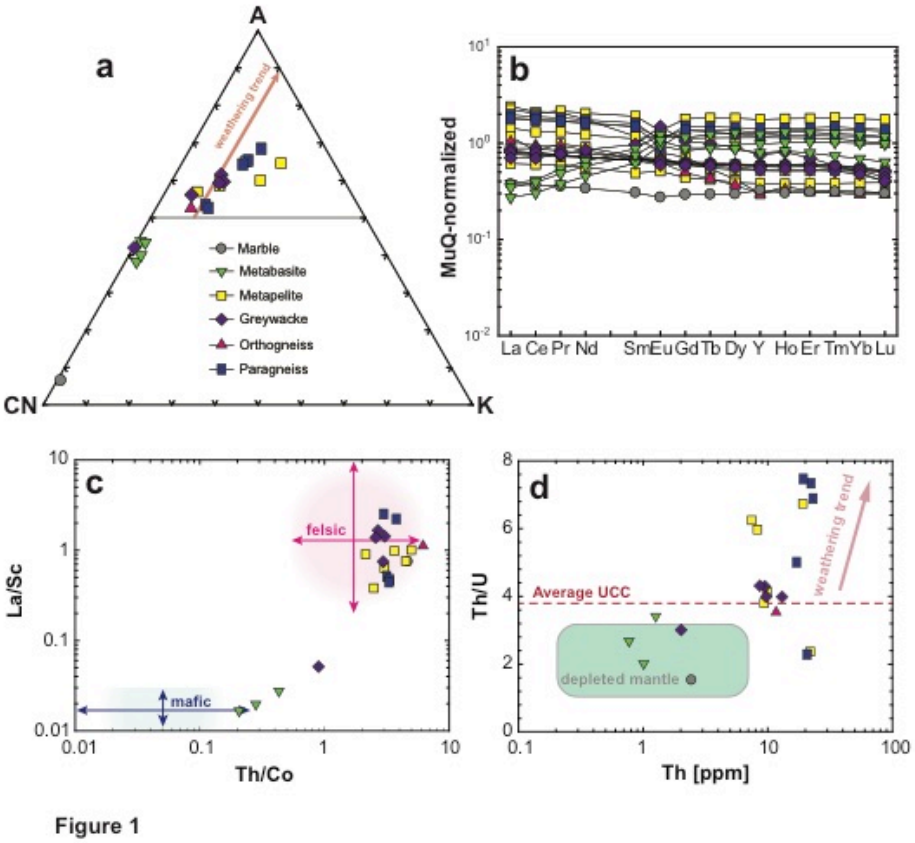

Figure 1

Figure 1. Whole rock major and trace element figures illustrating broad compositional differences (mafic vs felsic) and probable pre-metamorphic chemical weathering history (for sedimentary protoliths) to establish the context for apatite chemistry in each rock. (a) Chemical index of alteration (CIA) molar Al_2O_3 (A)–CaO*+Na_2O (CN)–K_2O (K) plot with the predicted chemical weathering trend (arrow) of a granodiorite that represents average upper continental crust (UCC), where CaO* is the amount of CaO incorporated in the silicate fraction of the rock. (b) REE+Y shale-normalized plot (mud of Queensland or MUQ, a sediment composite, which is an approximate weathered UCC). (c) La/Sc vs. Th/Co plot with division into felsic and mafic rocks after Cullers (2002). (d) Th/U vs. Th plot (McLennan et al., 1993) showing compositional difference (range of depleted mantle and average UCC) and the influence of U loss during chemical weathering or U addition (e.g., authigenic enrichment). In all plots, the marble, basite/dolerite, pelite, greywacke, orthogneiss, and paragneiss samples are represented by filled circles, inverted triangles, squares, diamonds, triangles, and hexagons, respectively.

2.1.1 Grampian (ca. 470 Ma) regional metamorphism of Dalradian Supergroup samples

Samples IH11/13/01 (pelite), IH11/13/02 (semi-pelite), and IH11/13/03 (metabasite) were collected from the Central Ox Mountains inlier, NW Ireland (Supplementary Figure 1, Table 1). Peak Grampian staurolite-kyanite zone metamorphism is estimated at 8 ± 2 kbar and 620 ± 30 °C (Yardley et al., 1987). Samples IH11/13/04 (metabasite) and IH11/13/05 (pelite) were collected from the southern limit of the NW Mayo Inlier, NW Ireland. Here blueschist-facies assemblages (10.5 ± 1.5 kbar, 460 ± 45 °C) are developed in Dalradian rocks contemporaneous with amphibolite-facies Barrovian metamorphic assemblages close to the contact with the structurally-underlying Palaeoproterozoic Annagh Gneiss Complex basement farther to the north (Chew et al., 2003). Samples DC8/11/1a (metabasite) and DC8/11/1b (metapelite) were collected from Dalradian rocks (Appin Group) in the Tummel Steep belt in the central Grampian Highlands of Scotland, where peak metamorphic conditions (locally staurolite-kyanite zone) are estimated at 9 kbar and 550 °C (Dempster and Harte, 1986). Samples LT1 (impure calcite marble) and LT2 (graphitic pelite) were collected from the Loch Tay Limestone (Upper Argyll Group) 30 km to the SSW. Pelites in the adjacent schists contain abundant garnet, and the metamorphic grade is upper greenschist- to epidote-amphibolite facies.

A.2.1.2 Grampian (ca. 470 Ma) regional metamorphism of Annagh Gneiss Complex samples

The Palaeoproterozoic Annagh Gneiss Complex (AGC) in NW Mayo, Ireland originated as juvenile Palaeoproterozoic crust represented by the 1753 ± 3 Ma calc-alkaline Mullet gneisses (Daly, 1996). Sample AGC1 was collected from the Mullet orthogneisses. Subsequent intrusive phases in the AGC include Late Mesoproterozoic granitoids. This was followed by two phases of Grenville deformation between 1177–1015 Ma and 995–960 Ma separated by a phase of migmatization and pegmatite emplacement between 995 and 980 Ma (Daly, 1996). U-Pb titanite analyses from the AGC gneisses yield a weighted mean $^{207}Pb/^{206}Pb$ age of 963 ± 8 Ma, which records cooling following Grenville metamorphism (Daly and Flowerdew, 2005). Sample AGC2 is a metamorphosed basic dyke within the AGC, which cuts all AGC Grenville fabrics and has only experienced Grampian orogenesis. Local P-T estimates for this Grampian metamorphism is derived from the structurally overlying Dalradian Supergroup, with P-T estimates for staurolite-kyanite zone metamorphism of 8 ± 2 kbar and 620 ± 30 °C (Yardley et al. 1987).

A.2.2 New Zealand Alps

Six meta-greywacke samples were collected from the low-grade pumpellyite-actinolite (samples Hunt4, Hunt6, and Hunt9) to greenschist-facies (samples CP1, CP2, and Pisa1) portions of the Haast Schist, New Zealand (Supplementary Figure 2, Table 1). The Haast Schist is a polyphase pumpellyite-actinolite to amphibolite-facies metamorphic belt that has overprinted the accretionary complex rocks of the Caples, Bay of Islands and Rakaia Terranes (Mortimer, 2004). Geographic subdivisions of the Haast Schist into the Otago, Alpine, and Marlborough Schist are also used (Turnbull et al., 2010). The Rakaia Terrane protoliths comprised Permian to Late Triassic turbiditic quartzofeldspathic sandstone-mudstone units (Mortimer, 2004), that were likely derived from an active continental arc (MacKinnon, 1983; Roser and Korsh, 1999). The Caples Terrane comprises a weakly metamorphosed marine volcaniclastic sequence composed of Permian-Triassic greywackes and argillites (Mortimer, 2004) that formed in an offshore island-arc with minor continental sediment input (Adams et al., 2009). The lowest-grade parts of the Haast Schist were exhumed around 110 Ma, while the higher-grade portions have been exhumed from 20 Ma up to the present day along the Alpine Fault (Mortimer, 2004; Warren-Smith et al., 2016).

A.2.3 Eastern Cordillera of Peru

The Eastern Cordillera of Peru consists of a series of Paleozoic metasedimentary rocks termed the Marañón Complex north of 11°S and the Huaytapallana Complex south of 11°S (Mégard, 1978), which are intruded by several Paleozoic syn- and post-tectonic granitoid suites (Chew et al., 2007). Some of the highest-grade rocks in the Huaytapallana Complex occur in the Huaytapallana Massif south of Glaciar Huaytapallana (Supplementary Figure 3), where high-grade garnet-sillimanite-biotite bearing paragneisses have yielded U-Pb and Th-Pb monazite ages of ca. 267 to 261 Ma and U-Pb ages of 260.4 ± 2.5 Ma from low Th/U metamorphic zircon rims (Chew et al., 2016a). The zircon and monazite data are interpreted as recording crystallization at ca. 262 Ma during peak high-grade metamorphism. Three samples (TCH001, TCH003, and TCH007) collected from the high-grade portion of the Huaytapallana Complex (Chew et al., 2016a; Supplementary Figure 3) yield apatite U-Pb ages (c. 230 – 250 Ma) consistent with post-orogenic cooling from the ca. 262 Ma orogenic peak and are investigated

further in this study. Only sample TCH003 exhibits macroscopic evidence of anatexis, with foliation-parallel quartz-plagioclase-biotite leucosomes up to 1 cm thick.

A.2.4 Paros, Greek Cyclades

The Attic-Cycladic Belt in the south-central Aegean region of Greece is characterised by crustal-scale extensional detachment systems that accommodated the southward-retreating Hellenic subduction zone (Lister et al., 1984). On the islands of Naxos and Paros in the central Cyclades, the Naxos-Paros ductile low-angle fault (Jolivet et al., 2010) separates unmetamorphosed upper crustal rocks from a polyphase higher-grade metamorphic core, and represents a classic Cordilleran-style metamorphic core complex (e.g. Lister et al., 1984). The deepest portions of the core on Naxos are comprised of tightly-folded migmatitic gneiss associated with a gently-plunging stretching lineation, attributed to contemporaneous upper crustal N-S extension and deeper E-W compression (Kruckenburg et al., 2011). The regional metamorphic history of the Attic-Cycladic Belt comprises an early (ca. 50 Ma) high-pressure event (M1) (Wijbrans and McDougall, 1988) followed by Barrovian-type metamorphism (M2) at around 20-12 Ma on Naxos (e.g. Cao et al., 2016; Bolhar et al., 2017), which locally formed migmatites in the dome core (PT estimates of 6.0 ± 2.5 to 8.0 ± 2.5 kbar at ca. 670 °C (Buick and Holland, 1989). While most work to date has focused on Naxos, the Miocene tectonothermal evolution of the neighbouring island of Paros is very similar (*cf* Bargnesi et al., 2013). Two samples (a weakly foliated leucocratitc quartz-feldspar-biotite gneiss, sample RM13; and a foliated paragneiss with no prograde muscovite, sample RM15) were collected from the core of the migmatite dome on Paros (Supplementary Figure 4).

A.3. ANALYTICAL METHODS

Detailed analytical methods are presented in the supplementary material. All apatite U-Pb and trace element spot analyses were undertaken exclusively on apatite mineral separates, using a Teledyne Photon Machines Analyte Excite 193nm ArF Excimer laser-ablation system coupled to a Thermo Scientific iCAP-Q ICP-MS at Trinity College Dublin (TCD), Ireland. For U-Pb geochronology, the ca. 473 Ma U-Pb Madagascar apatite standard (Thomson et al., 2012) was used as the primary reference material in this study, and McClure Mountain apatite ($^{207}Pb/^{235}U$ TIMS age of 523.51 ± 1.47 Ma; Schoene and Bowring, 2006) and Durango apatite (31.44 ± 0.18 Ma; McDowell et al., 2005) were employed as secondary standards. For trace-element analyses, NIST612 standard glass

was used as the primary reference material and a crushed aliquot of Durango apatite, which has been characterised by solution (S) Q-ICP-MS (Chew et al., 2016b), was employed as a secondary standard. The U-Pb data were reduced using VisualAge_UcomPbine, a modified version of the VizualAge data reduction scheme of Petrus and Kamber (2012) for the Iolite software package (Paton et al., 2011) that accounts for the presence of common Pb in the primary age standard materials (Chew et al., 2014). Small inclusions (e.g. of metamorphic matrix phases such as monazite) can be common in metamorphic apatite (cf. Harlov and Förster, 2003), and can be difficult to detect during hand picking and may not even be visible on scanning electron microscope (SEM) images as they may occur a few microns below the crystal surface. Apatite can incorporate a wide variety of trace elements in its lattice, but the high-field strength elements (HFSE) such as Zr^{4+} are typically present at the ppb level. Appreciable yet transient Zr signals (several to hundreds ppm), which are often also rich in Th and LREE, are sometimes detected in time-resolved data of apatite unknowns yet never in the apatite U-Pb standards. The transient Zr-rich portions of the signal are likely zircon inclusions, while the Zr-, Th-, and LREE-enriched inclusions are either epidote/allanite or monazite (in pelites) or epidote/allanite (in metabasites). These transient portions of the signal attributed to inclusions were avoided during data reduction.

LA-Q-ICP-MS trace-element imaging was undertaken exclusively on thin sections, using two different LA-ICP-MS instrumental setups in TCD (see supplementary material). Over 100 apatite grains in three metapelite samples (Pisa1, CP1, and CP2) were first identified *in situ* by EDS (energy-dispersive X-ray spectroscopy) SEM mapping of thin sections using a Tescan TIGER SEM at TCD, and 18 grains on these thin sections were then selected for LA-ICP-MS mapping (Figures 7, 8, Supplementary Figure 5). Back-scattered electron (BSE) maps and the spatial positions of these apatite grains were recorded, which were then used to aid the LA-ICP-MS element mapping. Large rectangular areas of 1 and 1.5 mm^2 on two metabasite samples (Supplementary Figures 6 and 7) were also imaged by LA-Q-ICP-MS. The LA-Q-ICP-MS trace-element mapping procedure and data reduction is similar to that adopted by Ubide et al. (2015) and Chew et al. (2016), and is described in detail in the supplementary material.

Trace element abundances on 22 samples were determined at TCD by solution Q-ICP-MS measurements using a Thermo Scientific iCAP-Qc ICP-MS. The ICP-MS analyses follow the experimental design of Eggins et al. (1997) with modifications described in Kamber et al. (2003) and Babechuk et al. (2010). Whole rock powders were

made by crushing a representative aliquot of each sample and milling it in an agate planetary ball mill, and the subsequent sample digestion protocol is described in the supplementary material (available online at the following address: https://www.sciencedirect.com/science/article/pii/S000925411730712X#ec0005). Following sample digestion, gravimetric dilutions in 2 mL centrifuge tubes were prepared using an aliquot of the sample and an internal standard bearing ^{6}Li, Rh, Re, Bi, and ^{235}U, which cover the full mass range of analysed elements and ionization potentials. The addition of the internal standard mix facilitates correction of matrix-related signal suppression and instrumental drift during the measurement session. Oxide interferences are corrected according to Ulrich et al. (2010), while a range of dilutions of the USGS standard reference material W-2a was used for calibration. The United States Geological Survey (USGS) rock standards SCO-1, GSP-2, and BHVO-2 were interspersed with sample unknowns to check the external accuracy of the trace element data, which is monitored through the long-term compilation of different USGS and Geological Survey of Japan (GSJ) rock standards. Previous publications have documented the accuracy and precision of the method, the latter of which is typically less than 3% for most trace elements (e.g. Babechuk et al., 2015). The whole rock trace-element ICP-MS data are combined with X-Ray Fluorescence (XRF) major element data in Table 3. The XRF data were obtained from ca. 2g aliquots of the milled whole-rock powders fused with lithium borate. Fourteen elements (Al_2O_3, BaO, CaO, Cr_2O_3, Fe_2O_3, K_2O, MgO, MnO, Na_2O, P_2O_5, SO_3, SiO_2, SrO, TiO_2) were determined by wavelength dispersive-XRF analysis on the fused beads at OMAC Laboratories, Co. Galway, Ireland. Loss-on-ignition (LOI) was determined by a thermogravimetric analyser at a maximum temperature of 1000°C.

A.4. RESULTS

A.4.1 Whole rock geochemistry

A selection of geochemical plots in Figure 1 demonstrate the broad compositional variations present in the metamorphic rock suite, and are used to develop a contextual framework to accompany the variations observed in the apatite chemistry. The position of the samples on these plots is due to a combination of effects acting on the protolith (e.g. sedimentary sorting, chemical weathering), diagenesis and metamorphism, but the first-order controls are interpreted as magmatic (for igneous protoliths), or authigenic element enrichment and chemical weathering (for sedimentary protoliths). Despite not observing highly refractory mineral phases in metabasite sample IH11/13/03 or its digestion residue, incomplete digestion was suspected based on its very LREE-depleted whole rock chemistry. A more evolved composition than its initial classification as a metabasite is also suggested by its high SiO_2 concentration and its apatite chemistry that implies it likely contains detrital phases (Section A.4.2.2). Thus, the bulk rock trace element chemistry of this sample was not considered in the bulk geochemical plots or in its associated whole rock-normalised apatite trace element plot (Fig. 3D).

Rocks are grouped based on their metamorphic rock classification into (meta)basite/dolerite, (meta)pelite, (meta)greywacke, orthogneiss, paragneiss, and marble. The chemical index of alteration (CIA) molar Al_2O_3 (A)–CaO*+Na_2O (CN)–K_2O (K) plot (Fig. 1A) illustrates: (1) the difference between rocks with a mafic protolith (along the A-CN join below a value of 50); (2) felsic (near or above the CN-K tie line at 50 for the feldspars); and (3) rocks with a higher degree of inferred chemical weathering prior to metamorphism, i.e., the pelites and paragneisses plotting higher than orthogneisses and greywackes, and close to the predicted weathering trend for average upper continental crust as represented by granodiorite (Nesbitt & Young, 1984). A REE+Y plot (normalized to an upper continental crust proxy) shows that the basite/dolerite samples typically exhibit LREE depletion (e.g. low La_n/Sm_n). The remaining rocks have flatter REE patterns similar to the concentrations of the upper continental crust, with the exception of the marble (lowest total REE concentration), with some variation in the magnitude of their Eu anomalies. A La/Sc vs. Th/Co plot (e.g. Cullers, 2002) exploits the enrichment of Th and La relative to Sc and Co in felsic rocks over mafic rocks to illustrate the broad division in bulk composition of the selected samples (Fig. 1C). Finally, a plot of Th vs. Th/U (Fig. 1D; McLennan et al., 1993) shows the difference between mafic (lower Th and Th/U) and felsic (higher Th and Th/U) rocks,

and those that were likely subjected to the loss of U during chemical weathering (pelites, paragneisses) or authigenic U enrichment (pelite sample LT2; Th/U = 2.37, U = 9.25 ppm), based on deviation from an average upper continental crust Th/U value of ~3.8. The paragneiss sample (RM15) also exhibits low Th/U (2.28) at high Th concentration (20.64 ppm), which suggests either authigenic U enrichment in the protolith sedimentary rock or a later metamorphic event to enrich U. Notably, with the exception of the U-enriched samples, the increase in Th/U correlates with increasing CIA values, providing some support that the rocks inherit these features from their pre-metamorphic chemical weathering history. Finally, the combination of low Th (2.02 ppm), Th/Co (0.05), La/Sc (0.90), and low CIA (42) of the greywacke sample CP2 suggests a plagioclase-rich mineralogy and a mafic-dominated provenance.

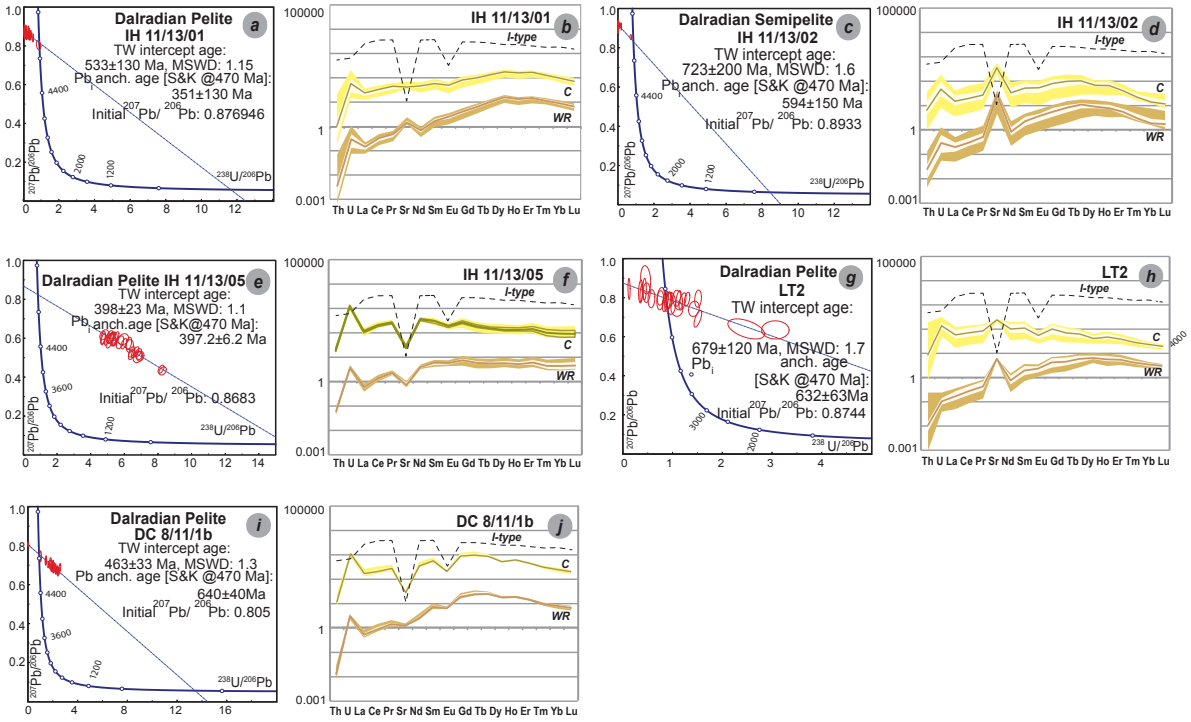

Figure 2

Figure 2. (A-J). Left column: Tera-Wasserburg Concordia diagrams for metapelite samples: a) IH 11/13/01, c) IH 11/13/02, e) IH 11/13/05, g) LT2, and i) DC 8/11/1b. Right column: Chondrite-normalized trace element and whole-rock normalized trace element plots of metapelite samples b) IH 11/13/01, d) IH 11/13/02, f) IH 11/13/05, h) LT2, and j) DC 8/11/1b. Dashed black reference line is I-type granite sample AB190 from Sha and Chappell (1999). Chondrite values are from McDonough and Sun (1995). In all the normalized trace element plots, the median and the 10^{th}-90^{th} and 30^{th}-70^{th} percentile limits of all analyses are illustrated.

A.4.2 Apatite U-Pb ages and trace element chemistry

U-Pb apatite Tera-Wasserburg (TW) concordias for all samples are presented in Figures 2 to 6, and are based exclusively on LA-ICP-MS spot analyses of mineral separates. Apatites in the three pumpellyite-actinolite facies metagreywackes (Hunt4, Hunt6, and Hunt9) are rounded and 70-90 μm in diameter, while in all other samples the apatites are more prismatic (aspect ratios between 3:1 and 4:1) and with long axes ranging from 100-300 μm. Lower intercept ages are presented for all samples which yield a coherent linear array (i.e. one apatite age population is present). Lower intercept ages are calculated for all samples without imposing constraints on the initial $^{207}Pb/^{206}Pb$ ratio, i.e. the lower intercept age is constrained by the analyses alone. Lower intercept ages were also calculated for all Dalradian Supergroup and Annagh Gneiss Complex samples which have undergone Grampian (ca. 470 Ma) metamorphism (with the exception of sample LT1) by anchoring the discordia at an $^{207}Pb/^{206}Pb$ initial ratio of 0.8675, which is the calculated value at 470 Ma using the Stacey and Kramers (1975) terrestrial Pb isotope evolution model (Figures 2-4). The common-Pb composition can alternatively be calculated from the Pb isotopic composition of co-genetic phases (e.g. K-feldspar), but this was not done as U-Pb dating was not *sensu stricto* the main focus of this study.

Chondrite-normalised (CI-chondrite; McDonough and Sun, 1995) multi-element (Th, U, Sr, Y, and the REE) plots are presented next to the corresponding TW concordia for each sample (Figures 2-6). The trace elements are presented on these plots in order of increasing compatibility for small fraction melts of the mantle (i.e. Th and U before the REE; Sr interspersed between Pr and Nd; Y between Dy and Ho). Although such plots are primarily designed for igneous systems, they are employed here to facilitate direct comparison of the metamorphic apatite trace element spectra with those of igneous apatite. Accordingly, a representative I-type granitic apatite composition from the study of Hsieh et al. (2008) is also presented on all the multi-element diagrams for reference. In the metamorphic apatite samples that exhibit unimodal trace-element compositions, the median and the 10^{th}-90^{th} and 30^{th}-70^{th} percentile limits of all (typically 25-35) spot analyses are presented in Figs 2-6. In the three samples (LT1, CP2 and Pisa1) that contain both metamorphic apatite and detrital igneous apatite, all individual analyses are plotted and are colour-coded according to likely grain type (metamorphic *vs* detrital igneous). For comparison with the CI-chondrite normalisation, the apatite data (Th, U, Sr, Y, and the REE) are also normalised to the corresponding whole rock composition (with the exception of sample IH11/13/03) and presented on the same diagrams.

A.4.2.1 Dalradian Supergroup metapelites

Samples LT2 and IH11/13/05 are upper greenschist-facies pelites, while samples DC 8/11/1b, IH11/13/01, and IH11/13/02 are amphibolite-facies pelites (Table 1). Two amphibolite-facies samples yield unanchored U-Pb apatite Tera-Wasserburg (TW) lower intercept ages consistent with crystallization (or U-Pb age resetting associated with volume diffusion of Pb) during the ca. 470 Ma Grampian orogeny: samples IH11/13/01 (533±130 Ma, Fig. 2A) and DC 8/11/1b (463±33 Ma, Fig. 2I). One amphibolite-facies sample (IH11/13/02) and both upper greenschist-facies pelites (LT2, IH11/13/05) yield TW lower intercept ages which do not overlap with the Grampian ca. 470 Ma metamorphic peak: IH11/13/02 (723 ± 200 Ma, Fig. 2C), IH11/13/05 (398 ± 23 Ma, Fig. 2E), and LT2 (679 ± 120 Ma, Fig. 2G). The variable precision on the TW lower intercept age is a result of the low and variable U contents of these grains (0.01 to 10 ppm, Supplementary Table 1), which typically results in high common Pb to radiogenic Pb ratios.

All these samples exhibit very low Th/U ratios relative to both their corresponding whole rock values and the representative I-type granitic apatite composition from Hsieh et al. (2008). Samples IH11/13/05 (Fig. 2F) and DC8/11/1b (Fig. 2J) yield only minor dispersion in their chondrite-normalized trace element spectra, with low Sr-contents, weak to moderately negative Eu-anomalies (Eu/Eu* ranges from 0.218 - 0.355 in DC 8/11/1b and 0.439 - 0.908 in IH11/13/05), and the highest U and LREE contents of the Dalradian Supergroup metapelites. Sample IH11/13/01 (Fig. 2B) similarly yields minimal dispersion in the trace element plot but with lower Th, U, and LREE contents, no Eu anomaly, and a slight enrichment in the HREE. Samples IH11/13/02 (Fig. 2D) and LT2 (Fig. 2H) yield significantly more dispersed trace element spectra (particularly in Th, U, and the LREE), minor enrichment of the LREE / MREE over the HREE, higher Sr contents, and a small negative Eu anomaly (sample LT2 only – Eu/Eu* = 0.333 - 0.709). It is noted that the samples with the most dispersed trace-element spectra (LT2 and IH11/13/02) yield TW lower intercept ages which are older (and importantly not within analytical uncertainty) of a ca. 470 Ma Grampian age (see discussion). Sample LT2 (a graphitic pelite) also has a low Th/U whole rock value, which may reflect variable authigenic U enrichment in the pelitic protolith and may explain the variability in apatite chemistry and U-Pb systematics. Mean sample apatite Mn values are 23.5 ppm ± 27% (1 relative standard deviation or RSD) for sample LT2, 142 ppm ± 25%

(DC 8/11/1b), 343 ppm ± 36% (IH11/13/01), 460 ppm ± 11% (IH11/13/05), and 489 ppm ± 32% (IH11/13/01).

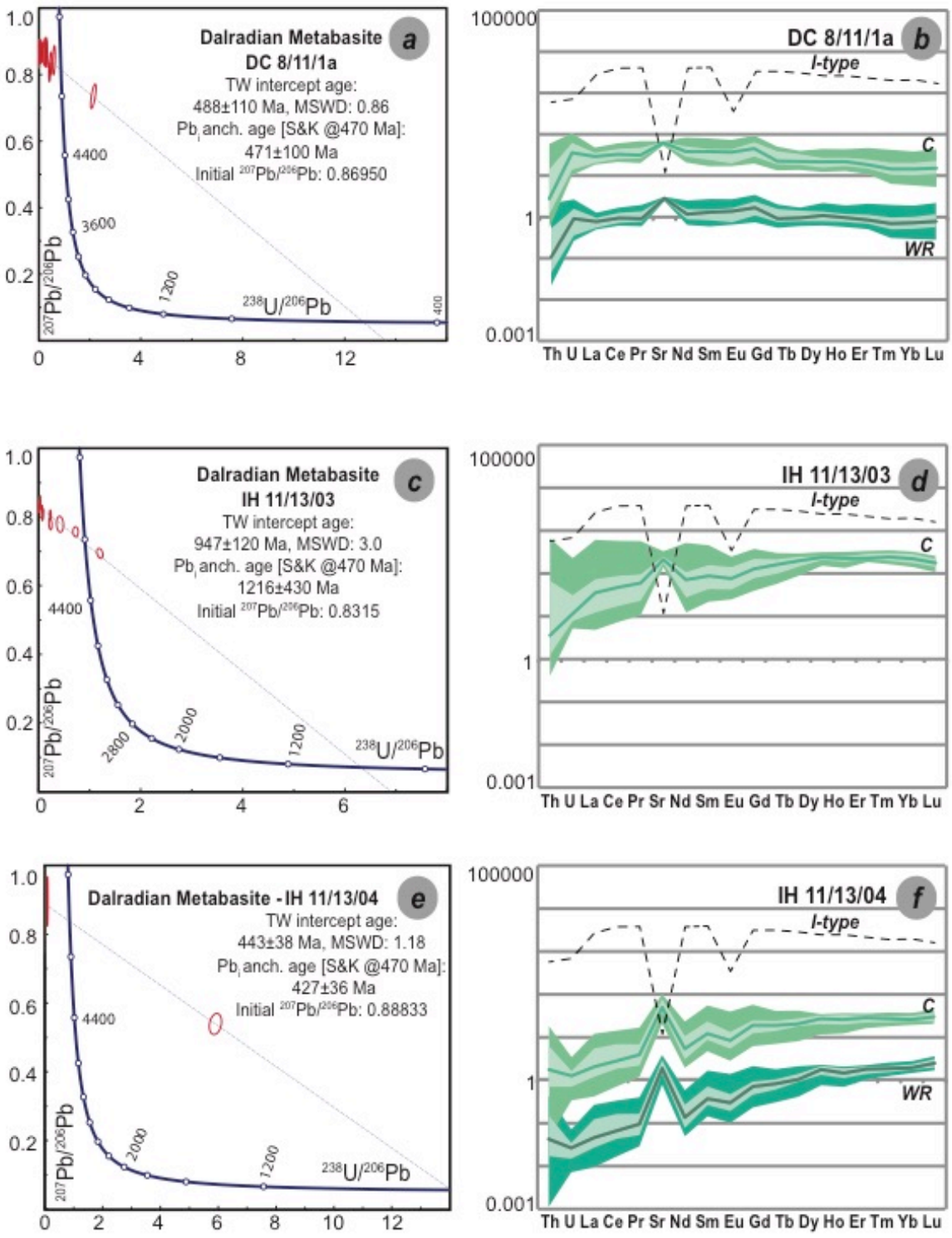
Dalradian Metabasite
DC 8/11/1a
a
TW intercept age:
488±110 Ma, MSWD: 0.86
Pb$_i$ anch. age [S&K @470 Ma]:
471±100 Ma
Initial $^{207}Pb/^{206}Pb$: 0.86950
4400
3600
1200
400
$^{207}Pb/^{206}Pb$
$^{238}U/^{206}Pb$
DC 8/11/1a
b
I-type
C
WR
Th U La Ce Pr Sr Nd Sm Eu Gd Tb Dy Ho Er Tm Yb Lu
Dalradian Metabasite
IH 11/13/03
c
TW intercept age:
947±120 Ma, MSWD: 3.0
Pb$_i$ anch. age [S&K @470 Ma]:
1216±430 Ma
Initial $^{207}Pb/^{206}Pb$: 0.8315
4400
2800
2000
1200
IH 11/13/03
d
Dalradian Metabasite - IH 11/13/04
e
TW intercept age:
443±38 Ma, MSWD: 1.18
Pb$_i$ anch. age [S&K @470 Ma]:
427±36 Ma
Initial $^{207}Pb/^{206}Pb$: 0.88833
IH 11/13/04
f

Figure 3

Figure 3. (A-F) Left column: Tera-Wasserburg Concordia diagrams of metabasite samples a) DC 8/11/1a, c) IH 11/13/03, and e) IH 11/13/04. Right column: Chondrite-normalized (labelled "C") trace element and whole-rock normalized (labelled "WR") trace element plots of metabasite samples b) DC 8/11/1a, d) IH 11/13/03, and f) IH 11/13/04. Dashed black reference line is I-type granite sample AB190 from Sha and Chappell (1999). Chondrite values are from McDonough and Sun (1995).

A.4.2.2 Dalradian Supergroup and Annagh Gneiss Complex metabasites

Samples DC8/11/1a, IH11/13/03 and AGC2 are amphibolite-facies metabasites, while sample IH11/13/4 is a metabasite that straddles the blueschist/greenschist facies transition (Table 1). The apatite U contents in these metabasite samples are very low, ranging from 0.02 to 2.75 ppm, resulting in very high common Pb to radiogenic Pb ratios (Supplementary Table 1). Despite the low U contents, samples DC8/11/1a (488 ± 110 Ma, Fig. 3A), IH11/13/04 (443 ± 38 Ma, Fig. 3E), and AGC2 (440 ± 63 Ma, Fig. 4E), yielded U-Pb apatite TW lower intercept ages consistent with a ca. 470 Ma Grampian orogenic event. However, sample IH 11/13/03 yields a much older TW lower intercept age of 947 ± 120 Ma. The chondrite-normalized patterns of the metabasite samples are variable. They are in general characterised by lower Th, U, and REE contents than the Dalradian metapelites, but have similar Sr contents and minor Eu anomalies (mean Eu/Eu* = 0.737). Samples IH11/13/03 (Fig. 3D) and IH11/13/04 (Fig. 3F) exhibit HREE enrichment relative to the LREE, whereas samples DC8/11/1a (Fig. 3B) and AGC2 (Fig. 4F) exhibit relatively flat REE patterns with very minor enrichment of the MREE. Only sample DC8/11/1a contains garnet. Compared to the other three metabasite samples, IH11/13/03 exhibits substantially more dispersion in the apatite trace-element spectra, has significantly higher apatite REE contents, and has higher SiO_2 whole rock contents (55.7 wt% SiO_2 vs < 50% for all other metabasite samples). This sample likely represents a reworked basaltic tuff, and the anomalously old apatite age of 947 ± 120 Ma is attributed to detrital input of ca. 1 Ga Grenville apatite which was not reset during ca. 470 Ma Grampian orogenesis. Mean sample apatite Mn values for the three Dalradian metabasites are relatively consistent at 197 ppm ± 31% 1RSD (IH11/13/04), 229 ppm ± 25% (DC 8/11/1a), and 231 ppm ± 19% (11/13/3), with the Annagh Gneiss Complex (AGC2) metabasite sill higher at 637 ppm ± 27%.

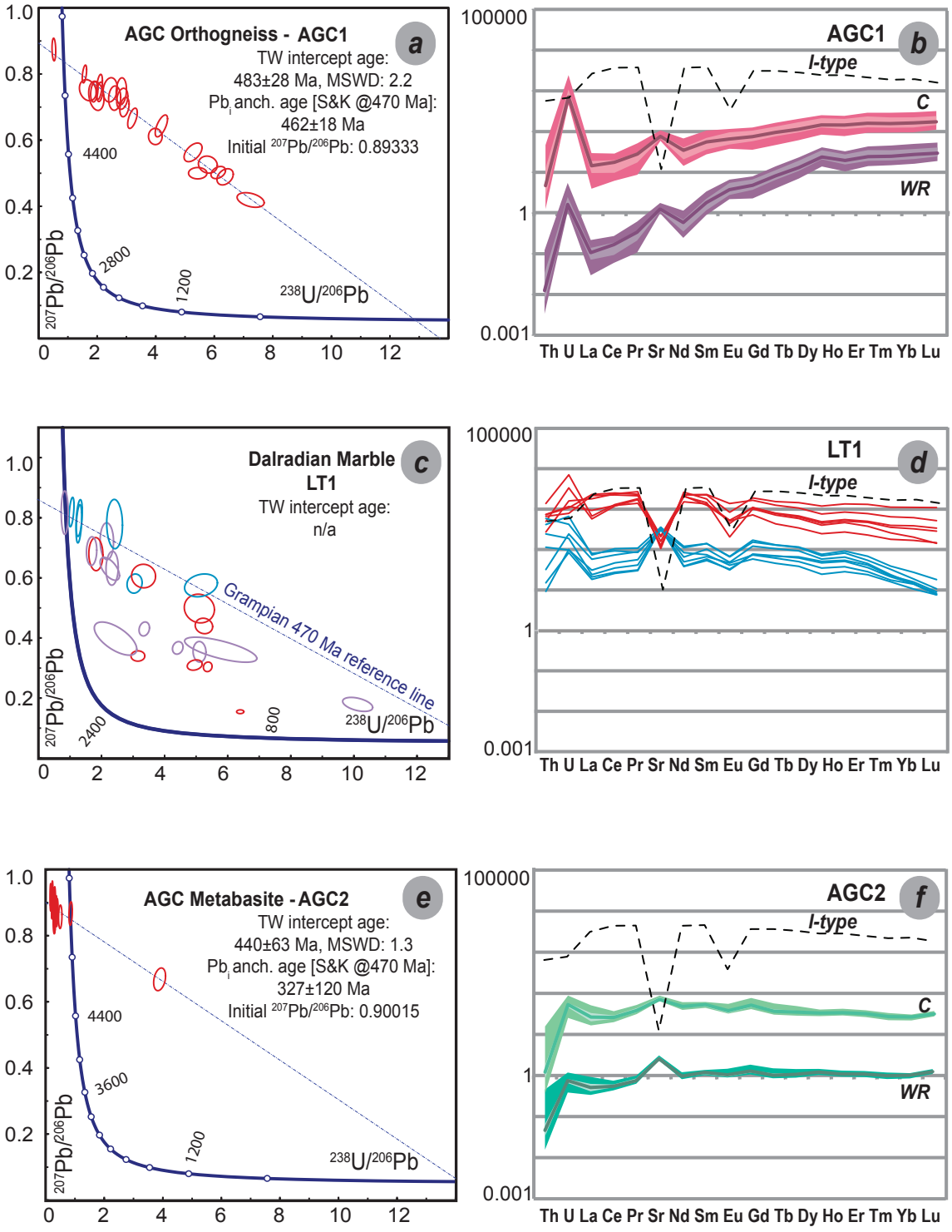
AGC Orthogneiss - AGC1
a
TW intercept age:
483±28 Ma, MSWD: 2.2
Pb$_i$ anch. age [S&K @470 Ma]:
462±18 Ma
Initial $^{207}Pb/^{206}Pb$: 0.89333
4400
2800
1200
$^{207}Pb/^{206}Pb$
$^{238}U/^{206}Pb$
AGC1
b
I-type
C
WR
Th U La Ce Pr Sr Nd Sm Eu Gd Tb Dy Ho Er Tm Yb Lu
Dalradian Marble
LT1
c
TW intercept age:
n/a
Grampian 470 Ma reference line
2400
800
LT1
d
AGC Metabasite - AGC2
e
TW intercept age:
440±63 Ma, MSWD: 1.3
Pb$_i$ anch. age [S&K @470 Ma]:
327±120 Ma
Initial $^{207}Pb/^{206}Pb$: 0.90015
4400
3600
1200
AGC2
f

Figure 4

Figure 4. (A-F) Left column: Tera-Wasserburg Concordia diagrams of samples a) AGC1 (orthogneiss), c) LT1 (marble), and e) AGC2 (metabasite). Right column: Chondrite-normalized (labelled "C") trace element and whole-rock normalized (labelled "WR") trace element plots of samples b) AGC1 (orthogneiss), d) LT1 (marble), and f) AGC2 (metabasite). Dashed black reference line is I-type granite sample AB190 from Sha and Chappell (1999). Chondrite values are from McDonough and Sun (1995). Sample LT1 contains both metamorphic apatite (pale blue analyses) and detrital igneous apatite (dark blue analyses); purple analyses represent either detrital igneous apatite - metamorphic apatite mixtures, or grains of uncertain affinity.

A.4.2.3 Other Caledonian samples: AGC orthogneiss and Dalradian Supergroup marble

Sample AGC1 is a Paleoproterozoic orthogneiss (the Mullet gneiss, section A.2.1.2, Supplementary Figure 1 and Table 1), which has undergone both ca. 1 Ga Grenville and ca. 470 Ma Grampian orogenesis. The U-Pb apatite data yield a TW lower intercept age of 483 ± 28 Ma (Fig. 4A), indicating that these apatite grains are either neo-crystalline or were age reset due to Pb volume diffusion during the ca. 470 Ma Grampian orogeny. The trace element plot exhibits only minor dispersion (Fig. 4B), strong depletion in Th and the LREE (but not U) relative to both the representative I-type composition of Hsieh et al. (2008) and its corresponding whole rock values, and a mean Mn value of 123 ppm (± 17% 1RSD). The paragenesis of the AGC1 apatite grains is discussed later in section A.5.

Sample LT1 is an impure greenschist-facies marble (the Loch Tay marble) from the Dalradian Supergroup in Scotland. The apatite chondrite-normalized trace element pattern is strikingly bimodal in this sample (Fig. 4D). Th contents range from 0.28 to 120 ppm, while the U content varies from 0.41 to 56.4 ppm. The first population (blue analyses on figures 4C and 4D) has low U contents and hence high common Pb to radiogenic Pb ratios, and lies on a 470 Ma Grampian TW discordia (initial Pb calculated at 470 Ma using the Stacey and Kramers (1975) terrestrial Pb isotope evolution model, combined with a 470 Ma concordia lower intercept). These grains also exhibit low Th and REE contents, high Sr contents (around 2450 ppm), very low Mn values (19.4 ppm ± 22% 1RSD), and similar moderate negative Eu anomalies (mean Eu/Eu* = 0.482). These grains are interpreted as neocrystalline metamorphic apatite (section A.5). The second population (red analyses on figures 4C and 4D) is composed of grains with older (pre-Grampian) U-Pb ages that plot below the 470 Ma reference line, and exhibit significantly higher Th, U, and REE contents, lower Sr contents (ca. 1130 ppm on average), moderate Mn values (126 ppm ± 45%). Eu-anomalies are more negative (mean Eu/Eu* = 0.400) and exhibit significantly more variation than the metamorphic apatite population (Fig. 4D). These grains are interpreted as detrital igneous apatite grains (section A.5).

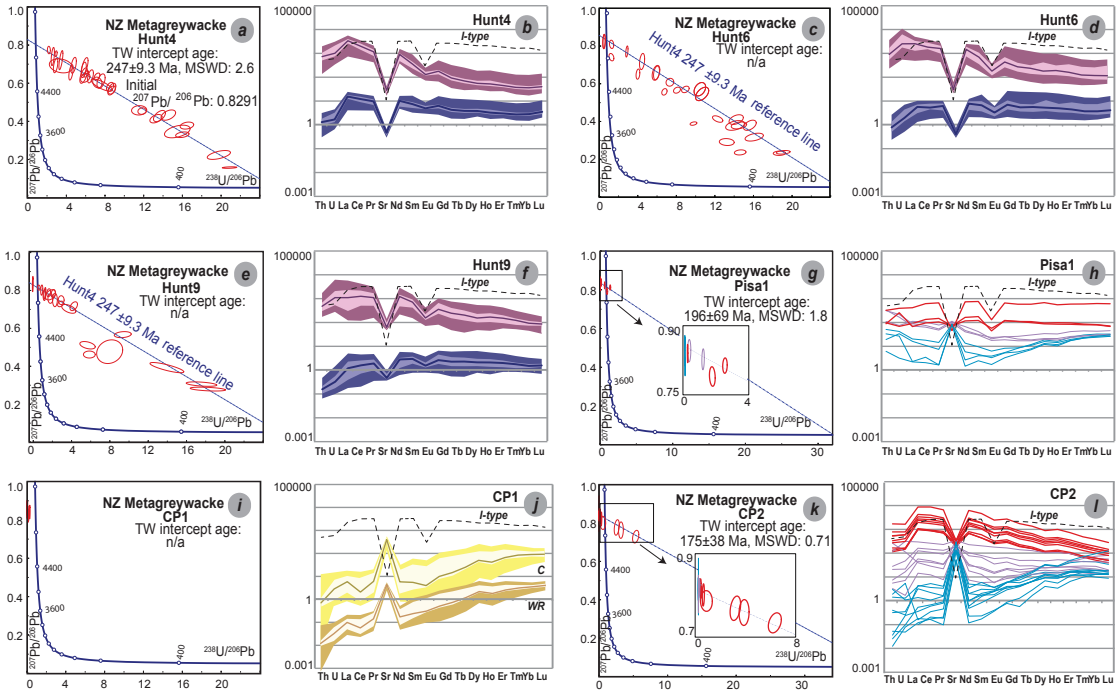

Figure 5

Figure 5. (A-L) Left column: Tera-Wasserburg Concordia diagrams of low-grade NZ samples a) Hunt4, c) Hunt6, e) Hunt9, g) Pisa1, i) CP1, and k) CP2. Right column: Chondrite-normalized (labelled "C") trace element and whole-rock normalized (labelled "WR") trace element plots of low-grade NZ samples b) Hunt4, d) Hunt6, f) Hunt9, h) Pisa1, j) CP1, and l) CP2. Dashed black reference line is I-type granite sample AB190 from Sha and Chappell (1999). Chondrite values are from McDonough and Sun (1995). Samples Pisa1 and CP2 contain both metamorphic apatite (pale blue analyses) and detrital igneous apatite (dark blue analyses); purple analyses represent either detrital igneous apatite - metamorphic apatite mixtures, or grains of uncertain affinity.

A.4.2.4 Low-grade New Zealand meta-greywackes

Samples Hunt4, Hunt6, and Hunt9 are pumpellyite-actinolite facies meta-greywackes, and samples CP1, CP2, and Pisa1 are greenschist-facies meta-greywackes (section A.2.2). The apatite U content in these samples varies by nearly five orders of magnitude, from a minimum value of 0.008 ppm in sample CP2 to a maximum of 161 ppm in sample Hunt4. Samples Hunt4, Hunt6, and Hunt9 exhibit negative Eu anomalies (mean Eu/Eu* = 0.45), and high Th, U, and LREE contents (Figs 5B, 5D, 5F). These trace element systematics closely resemble I-type granitoid apatite (Hsieh et al., 2008) although these three samples are slightly more LREE-enriched and HREE-depleted, and contain significantly more Sr and less Mn (Hunt4: 566 ppm Sr, 748 ppm Mn; Hunt6: 418 ppm Sr, 969 ppm Mn; Hunt9: 1082 ppm Sr, 527 ppm Mn; representative I-type apatite: 81.3 ppm Sr; 2908 ppm Mn). Sample Hunt4 exhibits the lowest dispersion in the trace element plots of the three pumpellyite-actinolite facies meta-greywackes, and yields a TW lower intercept age of 247±9.3 Ma (Fig. 5A). Samples Hunt6 and Hunt9 exhibit more dispersion in their trace element plots, and clearly do not yield unimodal apatite age populations on TW Concordia (Figs. 5C and 5E; the Hunt4 247 Ma discordia is added to the Hunt6 and Hunt9 TW concordias for reference).

The greenschist-facies meta-greywacke sample CP1 exhibits enrichment in the HREE over LREE in most grains. The dispersion in REE concentrations is approximately one order of magnitude for the LREE and HREE, and two orders of magnitude for the MREE (Fig. 5J). The mean apatite Mn content is 189 ppm (± 15% 1RSD) while the sample also shows significant depletion in Th (0.004 to 1.5 ppm, Supplementary Table 1) and U (0.03 to 0.47ppm, Supplementary Table 1), which results in high common Pb to radiogenic Pb ratios. Consequently, the grains in sample CP1 are not dateable by the U-Pb method and likely represent metamorphic apatite.

Sample CP2 shows even larger dispersion in trace element composition, spanning three orders of magnitude for Th, U, and LREE (Fig. 5L), and one order of magnitude for the HREE. Two “end-member” populations can be determined (similar to the Dalradian Supergroup marble LT1, Fig. 4D). One group (red analyses) on figures 5K and 5L exhibits high Th, U, and REE contents with LREE enrichment relative to the HREE, and likely represents detrital igneous apatite (Section A.4.3, Section A.5). The second population (blue analyses) exhibits very low U, Th, and REE contents, with a positive REE-slope towards the HREE and likely represents metamorphic apatite. The mean Eu/Eu* values of both populations are similar (0.691 for the igneous grains and 0.746 for

the metamorphic population, Fig. 5L). Spot analyses that are intermediate between these two end-member populations (purple analyses in Figures 5K and 5L) likely represent mixtures of these two discrete components, based on the evidence from the LA-Q-ICP-MS trace element imaging which shows high U, Th, and REE detrital igneous apatite grains are overgrown by metamorphic apatite rims (Section A.4.3, Section A.5). These core-rim textures were not detected by either BSE or cathodoluminescence (CL) imaging prior to LA-ICP-MS spot analysis, as these SEM-based imaging approaches typically do yield sufficient contrast to clearly highlight core-rim textures.

Sample Pisa1 also exhibits two populations of grains. These include one minor population (red analyses) with a relatively flat REE pattern, high ΣREE, very negative Eu anomalies (mean Eu/Eu* = 0.263), and another more abundant group (blue analyses) with low ΣREE and HREE enrichment and less pronounced negative Eu anomalies (mean Eu/Eu* = 0.628, Fig. 5H). The U content of the apatite in CP2 and Pisa1 varies from 0.0005 to 7.2 ppm (Supplementary Table 1). Both samples Pisa1 and CP2 (Fig. 5G and 5K) yield TW lower intercept ages, but the ages are poorly constrained. The TW discordias are controlled by only a few high U (and high Th + REE) apatite grains of likely detrital igneous affinity.

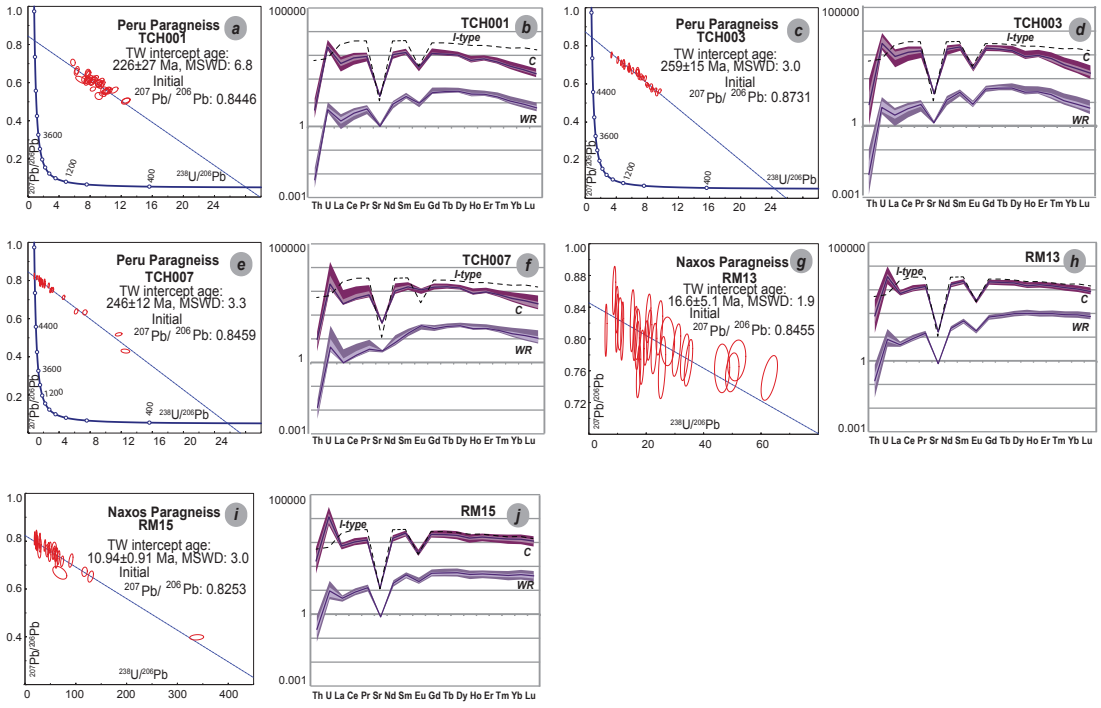

Figure 6

Figure 6. (A-J) Left column: Tera-Wasserburg Concordia diagrams of high grade samples from the Eastern Cordillera of Peru and the Greek Cyclades a) TCH001, c) TCH003, e) TCH007, g) RM13, and i) RM15. Right column: Chondrite-normalized (labelled "C") trace element and whole-rock normalized (labelled "WR") trace element plots of high grade samples from the Eastern Cordillera of Peru and the Greek Cyclades b) TCH001, d) TCH003, f) TCH007, h) RM13, and j) RM15. Dashed black reference line is I-type granite sample AB190 from Sha and Chappell (1999). Chondrite values from McDonough and Sun (1995).

A.4.2.5 Paragneisses from the Eastern Cordillera of Peru and Paros, Greek Cyclades

Apatite from all five paragneiss samples from Peru and Paros exhibits low Th/U ratios. They typically have the lowest Sr contents of all the analysed samples (ca. 190 ppm for the Peru samples and ca. 100 ppm for the Paros samples), and minor enrichment of the MREE over the LREE and HREE, resulting in a slightly convex REE-pattern. Samples TCH001 (Fig. 6B), TCH003 (Fig. 6D), RM13 (Fig. 6H), and RM15 (Fig. 6J), display very negative Eu anomalies (mean Eu/Eu* = 0.178), while the Eu anomaly in sample TCH007 (Fig. 6F) is less significant (mean Eu/Eu* = 0.725). These samples have trace element compositions that are very similar, both to each other and to S-type granitoids (e.g. Sha and Chappell, 1999; Belousova, 2001; Hsieh et al., 2008), implying similar geochemical and paragenetic conditions of growth (section A.5.1). They also yield well-defined U-Pb TW concordia lower intercept ages, particularly the Paros samples (Figs 6G and 6I). This is a function of the very high apatite U contents in these paragneisses, which average 34 and 147 ppm in samples RM13 and samples RM15 respectively (Supplementary Table 1). Mean sample apatite Mn values are very high at 1823 ppm ± 44% 1RSD (TCH001), 2428 ppm ± 51% (TCH003), and 2985 ppm ± 14% (TCH007) for the Peru samples and 1761 ppm ± 6% (RM13) and 3393 ppm ± 11% (RM15) for the samples from Paros; similar to S-type granitoids in the literature (e.g. Darongshan granites, Hsieh et al., 2008).

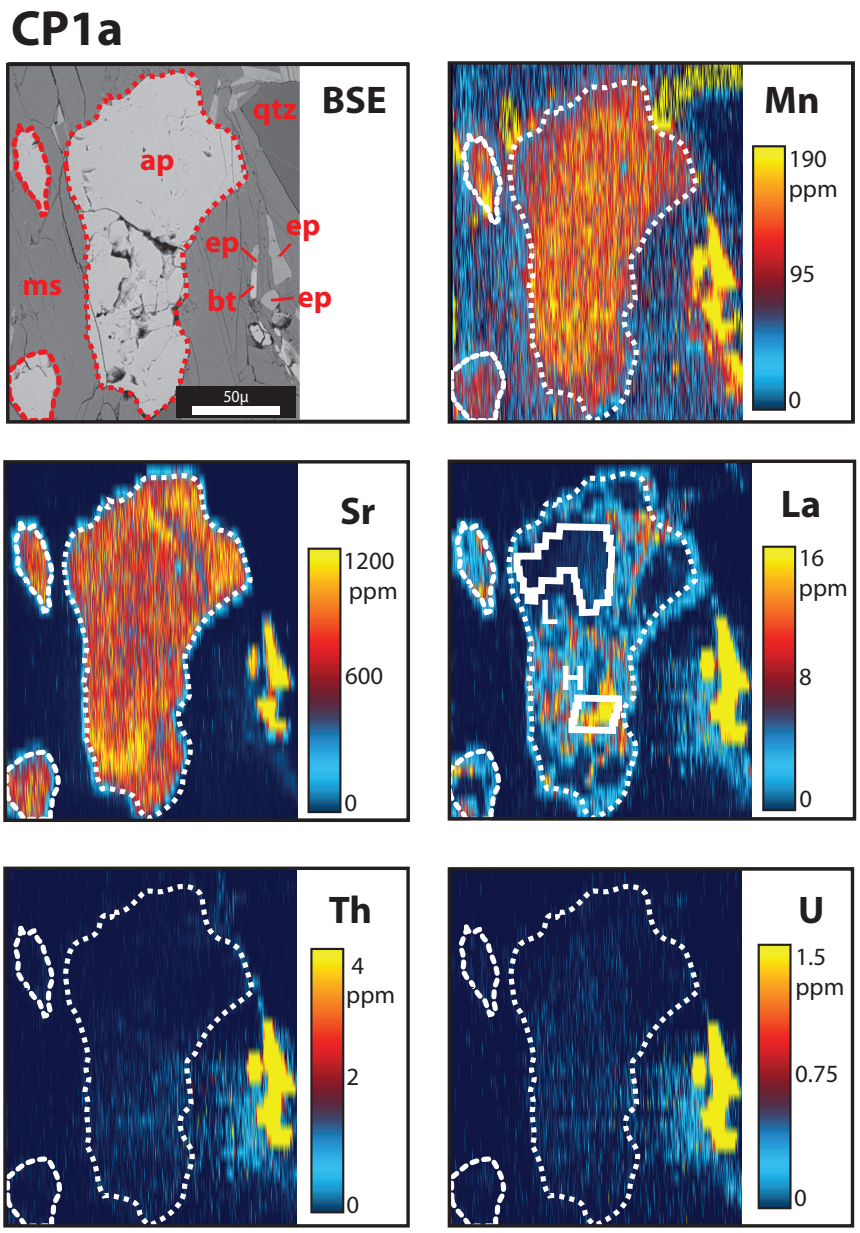

Figure 7

Figure 7. LA-ICPMS trace-element mapping of apatite CP1a (ms=muscovite, ep=epidote, ap=apatite, bt=biotite, qtz=quartz).

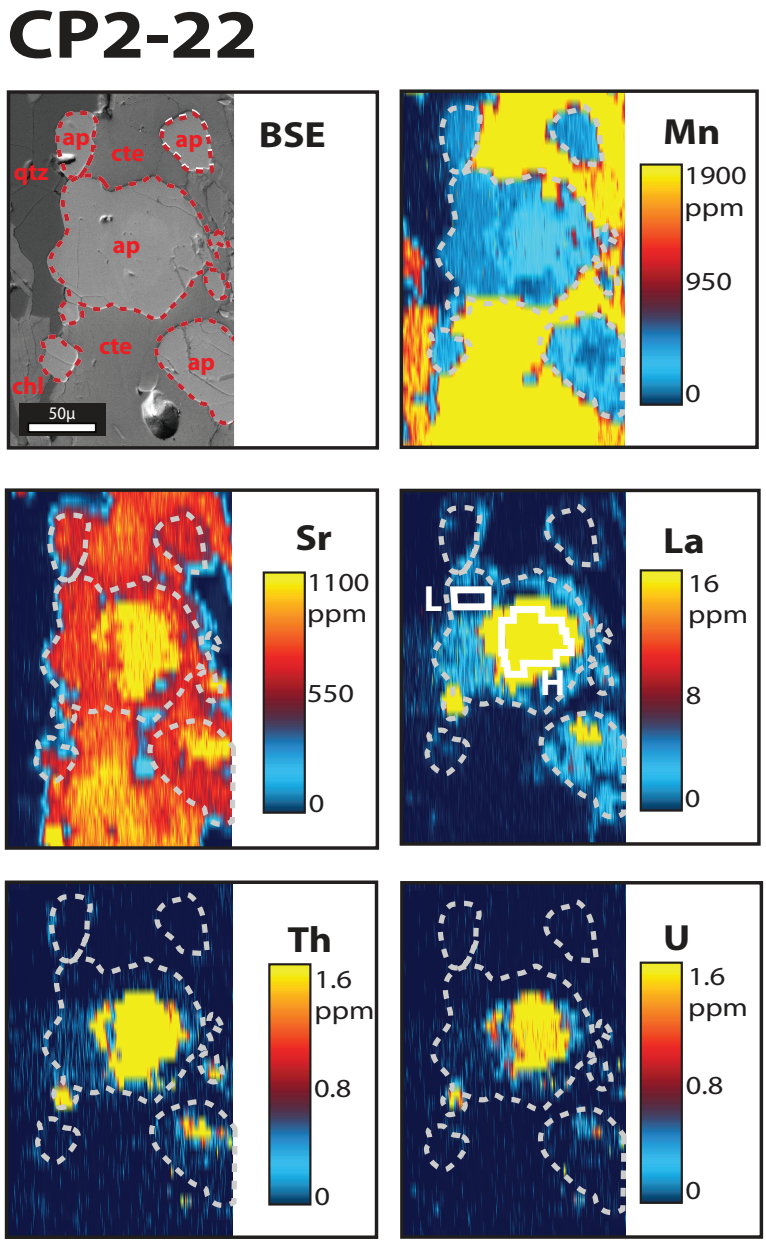

Figure 8

Figure 8. LA-ICPMS trace-element mapping of apatite CP2-22 (ap=apatite, qtz=quartz, cte=carbonate, chl=chlorite).

A.4.3 LA-Q-ICP-MS imaging of New Zealand metagreywackes and Caledonian metabasites

The low-grade meta-greywacke samples CP2 and Pisa1 from New Zealand and the Dalradian Supergroup marble LT1 yield two discrete apatite populations based on their trace element chemistry. In each case, these are interpreted as populations of neocrystalline metamorphic apatite (very low U, Th, and REE) and detrital granitoid apatite (high U, Th, and REE) respectively (section A.5). LA-Q-ICP-MS *in situ* trace-element mapping was undertaken on two samples (CP2 and Pisa1) to investigate the relationship between neocrystalline apatite growth and detrital magmatic apatite grains, and also on a meta-greywacke sample (CP1) from the southern New Zealand Alps which exhibits only a metamorphic apatite population.

Spot analyses from CP1 yielded low REE, Th (0.004 to 1.5 ppm), and U (0.03 to 0.47 ppm) contents characteristic of low- to medium-grade metamorphic apatite (section A.5). The eight mapped CP1 grains display some regions (typically fractures or zones with micro-inclusions) enriched in La. These zones, marked as high La areas ("H") on the apatite maps (e.g. Cp1a on Figure 7 and the CP1 maps in Supplementary Figure 5), have La values ranging from 15 ppm to 131 ppm, which is significantly lower than the I-type average of Hsieh et al. (2008) of 1600 ppm La. Thorium and U concentrations on the high La ROIs (regions of interest) range from 0.11 to 5.2 ppm and 0.03 to 0.58 ppm respectively. The low La areas ("L") on the CP1 maps are significantly depleted by between two to three orders of magnitude relative to the representative I-type composition of Hsieh et al. (2008), ranging from 0.11 to 3.4 ppm. The highest Th and U concentrations in these low La ROIs are 0.022 and 0.011 ppm. The dominant carrier phase of REE, Th, and U in the adjacent rock matrix was identified by subsequent EDS mapping as small (5 to 25 μm) grains of epidote. The mean trace element composition of 16 epidote crystals determined using the Monocle tool on sample CP1 is 2480 ppm Mn, 10381 ppm Sr, 970 ppm La, 593 ppm Th, and 121 ppm U (Table 4), and mean epidote Eu/Eu* = 0.66 (apatite mean Eu/Eu* = 0.562). While the epidote La, Th, and U contents are highly variable on the thin section scale, these data are often less dispersed on the scale of an individual LA-ICP-MS map (e.g. the CP1-o epidote data in Table 4). Titanite is less abundant than epidote and is also significantly depleted in La, Th, and U (mean contents of 51, 15, and 3 ppm respectively, Table 4).

The five mapped grains in sample CP2 show pronounced intra-grain variation in Sr, La, Th, and U. In each grain, there is at least one well-defined core with Sr, La, Th,

and U enrichment and also abrupt depletion of these elements in the surrounding rim (e.g. grain CP2-22 in Fig. 8 and the CP2 maps in Supplementary Figure 5). Two ROIs were defined on each grain using the variation in La as a guide. The high La cores range from 342 to 659 ppm La, with Th and U contents ranging from 9.02 to 16.92 ppm and 2.47 to 3.57 ppm, respectively. The low La rims range from 0.06 to 0.67 ppm La, and the highest Th and U concentrations in these ROIs are 0.043 and 0.025 ppm, respectively. The high Sr, La, Th, and U internal areas are interpreted as detrital igneous cores, whereas the low Sr, La, Th, and U overgrowths are interpreted as metamorphic apatite rims (section A.5). The dominant carrier phase of the REE, Th, and U in the adjacent rock matrix again is epidote, with the mean trace element composition of four epidote crystals determined using the Monocle tool of 3143 ppm Mn, 4377 ppm Sr, 530 ppm La, 86 ppm Th, and 10 ppm U (Table 4), and a mean epidote Eu/Eu* = 1.07 (for reference, the mean apatite Eu/Eu* = 0.691 for the detrital igneous population and 0.746 for the metamorphic population from this sample, section A.4.2.4).

Similar to the spot analyses data for sample Pisa1 (Fig. 5H), most of the grains in the Pisa1 laser maps are depleted in La, Th, and U. However, small patchy zones a few microns across, with enrichment in these elements, can be found in most maps (see Supplementary Figure 5). In particular the grain Pisa1-17 has prominent small patches enriched in Th, U, and La. Two ROIs were defined on the La map in this grain, with a high La zone of 993 ppm La, and Th and U contents of 35.7 and 20.4 ppm, respectively. The low La zone in the same sample (0.78 ppm La) yields Th and U contents of 0.35 and 0.008 ppm, respectively. These small (5 to 10 μm) high La patches in this sample have been identified by EDS mapping as epidote. It is likely that the volumetrically minor, high La, Th, and U population in the spot analyses dataset of Pisa1 (Fig. 5H) are ablations which hit a higher proportion of small inclusions. Unlike in sample CP2, the five mapped grains in sample Pisa1 do not exhibit well-defined cores with Sr, La, Th, and U enrichment. The mean trace element composition of 12 epidote crystals (matrix porphyroblasts) determined using the Monocle tool in Pisa1 is 2049 ppm Mn, 10270 ppm Sr, 1245 ppm La, 387 ppm Th, and 70 ppm U (Table 4) with a mean epidote Eu/Eu* = 0.700 (for reference, the mean apatite Eu/Eu* = 0.263 and 0.628 for the detrital igneous and metamorphic populations respectively, section A.4.2.4).

Rectangular areas between 1 and 1.5 mm^2 on two metabasite samples (AGC2, Supplementary Figure 6 and IH11/13/04, Supplementary Figure 7) were imaged to determine the dominant carriers of the REE, Th, and U. All EDS and LA-Q-ICP-MS

maps are supplied in the supplementary material. In sample AGC2, there is a strong spatial association between the occurrence of titanite (red colours on the EDS map) and the Y (ca. 500 ppm, Table 5) and the HREE (Lu, ca. 5ppm in Table 5) distribution. Importantly, small epidote crystals on the EDS maps are spatially associated with zones enriched in the LREE (La = ca. 6,000 ppm and Ce = ca. 13,000 ppm, Table 5), and Th and U (ca. 500 ppm and 50 ppm respectively, Table 5). The AGC2 apatite grain separates yield average concentrations of La = ca. 11 ppm, Ce = 26.5 ppm, Sm = 8.5 ppm, Lu = 0.5 ppm, Th = 0.5 ppm, and U = 0.7 ppm (Supplementary Table 1) and are thus substantially depleted in the REE, Th, and Lu relative to epidote. Titanite clearly controls the Y and HREE budget in AGC2, while epidote is the dominant carrier for the LREE, Th, and U despite being less abundant than titanite. The dominant REE, Th, and U carrier in sample IH11/13/04 is again epidote. However, relative to AGC2, the epidote is significantly depleted in the REE, Th, and U with only small zones of REE, Th, and U enrichment in the cores of some epidote crystals (La = ca. 38 / 719 ppm, Ce = 107 / 2283 ppm, Sm = 50 / 266 ppm, Lu = 1.1 / 1.2 ppm, Th = 4.7 / 125.1 ppm, and U = 4.4 / 10.0 ppm; values listed are the averages of the low- and high-REE epidotes respectively in Table 5).

A.5. DISCUSSION

The chondrite-normalised trace-element spectra in Figures 2 to 5 demonstrate that metamorphic apatite from low- to medium-grade metapelites and metabasites is significantly depleted in Th and the LREE relative to the representative I-type composition of Hsieh et al. (2008), and also relative to its corresponding whole rock chemistry. The U content of metamorphic apatite from low- to medium-grade metapelites (0.01 to 10 ppm) and metabasites (0.02 to 2.75 ppm) is more variable, and some low- to medium-grade metapelitic apatites even exceed the U contents (ca. 4.6 ppm) of the representative I-type granite composition (Fig. 2F, 2J, samples IH11/13/05 and DC8/11/1b). The Th, U and REE whole rock contents of the low- to medium-grade metapelites are similar to those of the paragneisses (Table 3, Figure 1), and hence the elevated REE and U contents in paragneiss apatite relative to lower grade metapelite apatite cannot simply be related to protolith composition.

Although distinguishing apatite from low- to medium-grade metapelites and metabasites from igneous apatite from the literature is easily achieved by a cursory inspection of the trace element spectra, distinguishing between metapelitic and metabasic apatite is significantly more difficult. A variety of bivariate, ternary and PCA (principal

component analysis) plots were constructed to attempt discriminate between these lithologies. Figure 9 is a plot of Mn/Sr *vs* Th, which successfully separates detrital granitic apatite from paragneiss apatite. Both these fields in turn can also be distinguished low- to medium-grade metamorphic apatite (metapelites and metabasites), but the metapelite and metabasite fields show considerable overlap in their compositions. The reason for this similarity is likely due to the crystallization of actinide- and REE-rich epidote in both cases (see section A.5.1 below), which leaves both apatite suites similarly depleted in these elements and hence difficult to discriminate.

Similar to the limitations encountered in applying binary or ternary diagrams to discriminate between the tectonic settings of basalts (e.g. Li et al., 2015), more diagnostic discriminant information can be obtained from utilizing normalized multi-element plots. Strontium was interspersed between Pr and Nd in the chondrite-normalised trace element plots. In all four metabasite samples Sr is elevated relative to Pr and Nd (Figs. 3B, 3D, 3F, 4F). In the chondrite-normalised multi-element plots for metapelitic apatites, Sr can be either elevated (Fig. 2D, 2H) or lower (Fig. 2F or 2J) than Pr and Nd. Interestingly, these metasedimentary apatite samples, which show depletion of Sr relative to Pr and Nd, also i) exhibit U contents similar to the representative I-type composition of Hsieh et al. (2008) and ii) show significantly less dispersion on the normalized multi-element plots.

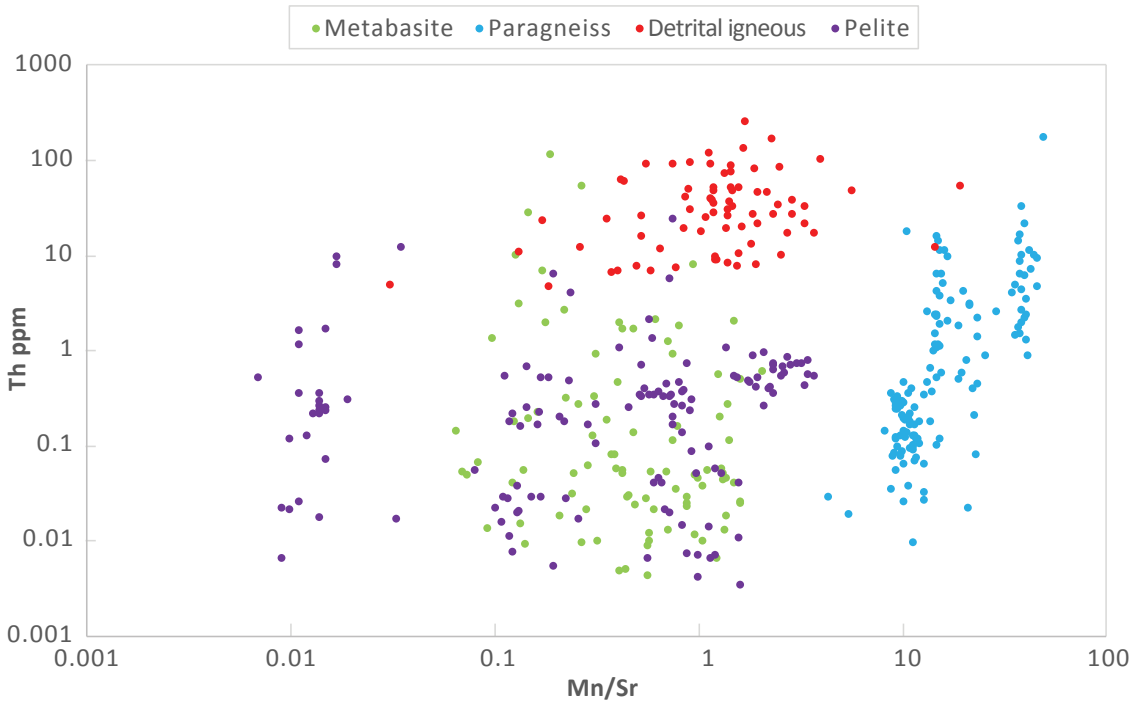

Figure 9. Plot of apatite Th ppm *vs* Mn/Sr from metabasites (IH11/13/03, IH11/13/04, AGC2 and DC8/11/1a), paragneisses (TCH001, TCH003, TCH007, RM13, RM15), pelites (CP1, LT2, DC 8/11/1b, CP1, IH 11/13/01, -02, and -05) and detrital igneous samples (Hunt4, -6 and -9).

A.5.1 Paragenesis of metamorphic apatite

The bimodal apatite compositions best seen in samples LT1 (Figure 4D), and CP2 (Figure 5L) are explained by the populations representing a mixture of i) old detrital grains of granitic origin (high Th, U, and REE that broadly overlaps with the composition of granitic apatite from the literature) and ii) neocrystalline metamorphic apatite with low Th, U and REE contents. The LA-Q-ICP-MS maps of the five grains from sample CP2 show well-defined cores with La, Th, and U enrichment interpreted as relict detrital granitic apatites and abrupt depletion of these elements in a surrounding rim of inferred metamorphic origin (Fig. 8). These metamorphic rims are clearly undateable by the LA-ICP-MS U-Pb method given their extremely low U contents (10s of ppb). The cause of the substantial depletion in U, Th and the LREE in the metamorphic rims is attributed to growth of co-genetic epidote. Epidote is the dominant carrier phase of the REE, Th, and U in the adjacent rock matrix in the five metasedimentary and metabasite samples characterised by LA-Q-ICP-MS and EDS mapping.

There is complete miscibility among the epidote-group minerals clinozoisite-epidote and allanite (*cf* Gieré and Sorensen, 2004), and the REE content in epidote can vary from the hundreds of ppb to the wt% level (Frei et al., 2004; Budzyn et al. 2011, 2017). The U and Th contents of REE-rich epidote from metapelites and metabasites usually reflects that of the protolith, with metabasite epidote U and Th contents typically an order of magnitude lower than metapelite epidote (Frei et al., 2004). Growth of co-genetic epidote can also explain the negative Eu anomalies seen in many of the apatite trace element spectra in this study. Pelitic epidote typically yields positive Eu-anomalies (*cf* Yang and Rivers, 2002), although in this study the epidote Eu anomalies are usually negative but still more positive than the corresponding metamorphic apatite Eu anomaly in the same sample (samples CP1, CP2 and Pisa1, section A.4.3). In samples where both detrital igneous and metamorphic populations are present, negative Eu anomalies in the detrital igneous apatite population are either similar in magnitude (samples LT1, CP2) or more negative (sample Pisa1) than the corresponding metamorphic apatite population from the same rock.

Although based on a limited dataset from samples Hunt4, Hunt6, and Hunt9, detrital granitoid-sourced apatite appears stable and records reliable U-Pb information in the pumpellyite-actinolite facies (<300°C), which is consistent with the medium-temperature sensitivity (~375-550°C) of the apatite U-Pb system. The formation of new metamorphic apatite is widespread by the upper-greenschist facies. The one exception is

the impure calcite marble sample (LT1), which is associated with garnet-zone schists and yet still yields a population of detrital igneous apatite in addition to a population of metamorphic apatite. This is likely due to the primary metamorphic assemblage (predominantly calcite) being relatively refractory, and thus the detrital igneous apatite precursor does not always undergo prograde metamorphic reactions.

Apatite from the five paragneiss samples from Peru and Greece (Figure 6) exhibits low Th/U ratios, typically the lowest Sr contents of all analysed samples, high total REE with a slightly convex pattern peaking in the MREE, and high U contents relative to the representative I-type composition of Hsieh et al. (2008). U is also significantly enriched relative to the corresponding whole rock composition, unlike the low- to medium-grade metapelites. Combined with the high Mn contents (averaging ca. 2,500 ppm), the apatite from these paragneisses very closely resembles apatite from S-type granites (Sha and Chappell, 1999; Belousova, 2001; Hsieh et al., 2008), especially those with high Al saturation indexes (ASi), which consequently crystallise monazite. The relative Th and LREE depletion in the paragneiss samples could thus be related to cogenetic growth of apatite and monazite at high temperatures or during anatexis. A pronounced depletion in Sr and a negative Eu anomaly is visible in chondrite-normalized and whole-rock normalized trace-element plots for the paragneisses. While some Eu and Sr depletion may be inherited from the paragneiss protolith due to depletion in these elements during chemical weathering, it is likely principally associated with simultaneous growth of feldspar during anatexis.

A.5.2 U-Pb systematics of metamorphic apatite

Typically, the U contents in apatite from low- to medium grade metapelites and metabasites are low. As a consequence, grains from these rock types are often undateable by the U-Pb LA-ICP-MS method and thus are underrepresented in detrital apatite U-Pb datasets (*cf* Mark et al., 2016). It is noted that the low-grade Grampian metapelitic samples (LT2 and IH11/13/02) and the metabasite sample (likely a basaltic tuff) with the most dispersed trace-element spectra (IH11/13/03) also yield TW lower intercept ages which are older than (and importantly not within analytical uncertainty of) a ca. 470 Ma Grampian age. This is likely related to the presence of relict portions of older detrital apatite in these apatites (*cf* sample CP2 from the New Zealand Alps). The Dalradian Supergroup metapelite samples (IH11/13/05 and DC8/11/1b) yield more precise ages consistent with Caledonian metamorphism. These samples yield only minor dispersion in

the trace element spectra, depletion of Sr relative to Pr and Nd, negative Eu-anomalies, and the highest U and LREE contents of the Dalradian Supergroup metapelites. The degree of dispersion on the multi-element plots is less in the paragneisses, and these samples exhibit more coherent concordia systematics. This is consistent with enhanced chemical equilibrium in these high-grade metamorphic rocks, some of which have locally undergone anatexis.

A.6. CONCLUSIONS

Metamorphic apatite from low- to medium-grade metapelites and metabasites can be easily distinguished from granitic apatite based on their significant depletion in Th, REE, and Y (particularly Th and the LREE). The cause of substantial depletion in Th and REE+Y in metamorphic apatite in these samples is attributed to growth of co-genetic epidote, since epidote is the dominant carrier phase of the REE, Th, and U in all samples characterised by LA-Q-ICP-MS and EDS mapping in this study.

The U content of metamorphic apatite from low- to medium-grade metapelites (0.01 to 10 ppm) and metabasites (0.02 to 2.75 ppm) is more variable, but is typically low (10s to 100s of ppb), even though some metapelitic apatites may exceed the average U content (ca. 4.6 ppm) of I-type granites. As a consequence, apatite from these rock types is often undateable by the U-Pb LA-ICP-MS method, and thus are underrepresented in detrital apatite U-Pb datasets, but can still be identified as low- to medium-grade metamorphic apatite by their trace-element characteristics. Trace element plots can successfully discriminate between granitic and paragneissic apatite, and both these fields can also be distinguished from low- to medium-grade metamorphic apatite (metapelites and metabasites). However, discriminating between metapelite and metabasite apatite is more problematic as their respective fields on bivariate and ternary discrimination diagrams usually overlap.

Detrital granitic apatite is abundant in very low-grade (e.g. pumpellyite-actinolite facies) metasedimentary samples with greywacke or sandstone protoliths, and detrital apatite may even survive to at least upper-greenschist facies conditions if hosted in an unreactive mineral assemblage (e.g. calc-silicates). Neocrystalline or recrystallised metamorphic apatite is widespread by the upper greenschist-facies, and LA-Q-ICP-MS imaging demonstrates that low Th, U, and REE+Y metamorphic apatite rims can nucleate on detrital igneous apatite precursors with high Th, U and REE+Y.

The degree of dispersion on multi-element plots from metamorphic apatite often correlates with the coherence of the U-Pb concordia systematics, with spot ablation datasets with small amounts of dispersion typically yielding better constrained TW concordia intercept ages. This is particularly true of the paragneisses, which exhibit minor dispersion on multi-element plots and well constrained TW concordia intercept ages. These paragneiss apatite samples yield the lowest Sr and highest Mn and U contents of all analysed samples, and closely resemble apatite from S-type granites.

A.6.1. Acknowledgements

The authors thank Diane Seward and Emily Warren-Smith for providing the New Zealand Alps samples, Giovanni Pedemonte for the samples from the Eastern Cordillera of Peru, Ken Chew for field assistance in Scotland and Paul Guyett for the EDS mapping. This study was funded by the Brazilian Science Without Borders Programme (CAPES grant no. BEX- 1127-13-6) and Science Foundation Ireland (grant no. 12/IP/1663).

A.8. REFERENCES

Abdullin, F., Solé, J., Solari, L., Shchepetilnikova, V., Meneses-Rocha, J.J., Pavlinova, N., Rodríguez-Trejo, A., 2016. Single-grain apatite geochemistry of Permian–Triassic granitoids and Mesozoic and Eocene sandstones from Chiapas, southeast Mexico: implications for sediment provenance. International Geology Review 58, 1132–1157.

Adams, C.J., Campbell, H.J., Griffin, W.L., 2009. Tracing the Caples Terrane through New Zealand using detrital zircon age patterns and radiogenic isotope signatures. New Zealand Journal of Geology and Geophysics 52, 223–245.

Babechuk, M.G., Kamber, B.S., Greig, A., Canil, D., Kodolányi, J., 2010. The behaviour of tungsten during mantle melting revisited with implications for planetary differentiation time scales. Geochimica et Cosmochimica Acta 74, 1448–1470.

Babechuk, M.G., Widdowson, M., Murphy, M, Kamber, B.S. 2015. A combined Y/Ho, high field strength element (HFSE) and Nd isotope perspective on basalt weathering, Deccan Traps, India. Chemical Geology 396, 25-41.

Bargnesi, E.A., Stockli, D.F., Mancktelow, N., Soukis, K., 2013. Miocene core complex development and coeval supradetachment basin evolution of Paros, Greece, insights from (U–Th)/He thermochronometry. Tectonophysics 595, 165–182.

Bea, F., Montero, P., 1999. Behavior of accessory phases and redistribution of Zr, REE, Y, Th, and U during metamorphism and partial melting of metapelites in the lower crust: an example from the Kinzigite Formation of Ivrea-Verbano, NW Italy. Geochimica et Cosmochimica Acta 63, 1133–1153.

Belousova, E.A., Griffin, W.L., O'Reilly, S.Y., Fisher, N.I., 2002. Apatite as an indicator mineral for mineral exploration: trace-element compositions and their relationship to host rock type. Journal of Geochemical Exploration 76, 45–69.

Belousova, E.A., Walters, S., Griffin, W.L., O'Reilly, S.Y., 2001. Trace-element signatures of apatites in granitoids from the Mt Isa Inlier, Northwestern Queensland. Australian Journal of Earth Sciences 48, 603–619.

Bingen, B., Demaiffe, D., Hertogen, J., 1996. Redistribution of rare earth elements, thorium, and uranium over accessory minerals in the course of amphibolite to granulite facies metamorphism: The role of apatite and monazite in orthogneisses from southwestern Norway. Geochimica et Cosmochimica Acta 60, 1341–1354.

Bolhar, R., Ring, U., Ireland, T.R., 2017. Zircon in amphibolites from Naxos, Aegean Sea, Greece: origin, significance and tectonic setting. Journal of Metamorphic Geology 35, 413–434.

Broska, I., Williams, C.T., Uher, P., Konečný, P., Leichmann, J., 2004. The geochemistry of phosphorus in different granite suites of the Western Carpathians, Slovakia: the role of apatite and P-bearing feldspar. Chemical Geology 205, 1–15.

Buick, I.S., Holland, T.J.B., 1989. The P-T-t path associated with crustal extension, Naxos, Cyclades, Greece. Geological Society, London, Special Publications 43, 365–369.

Budzyn, B., Harlov, D.E., Williams, M.L., Jercinovic, M.J., 2011. Experimental determination of stability relations between monazite, apatite, allanite, and REE-epidote as a function of pressure, temperature, and fluid composition. American Mineralogist 96, 1547–1567.

Budzyn, B., Harlov D.E., Kozub-Budzyn, G.A., Majka, J., 2017. Experimental constraints on the relative stabilities of the two systems monazite-(Ce) – allanite-(Ce) – apatite and xenotime-(Y) – (Y,HREE)-rich epidote – (Y,HREE)-rich apatite, in high Ca and Na-Ca environments under P-T conditions of 200–1000 MPa and 450–750 °C. Mineralogy and Petrology 111, 183–217.

Cao, M., Li, G., Qin, K., Seitmuratova, E.Y., Liu, Y., 2012. Major and Trace Element Characteristics of Apatites in Granitoids from Central Kazakhstan: Implications for Petrogenesis and Mineralization. Resource Geology 62, 63–83.

Cao, S., Neubauer, F., Bernroider, M., Genser, J., Liu, J., Friedl, G., 2016. Low-grade retrogression of a high-temperature metamorphic core complex: Naxos, Cyclades, Greece. Geological Society of America Bulletin 129, 93-117.

Carrapa, B., 2009. Tracing exhumation and orogenic wedge dynamics in the European Alps with detrital thermochronology. Geology 37, 1127–1130.

Chen, W., Simonetti, A., 2013. In-situ determination of major and trace elements in calcite and apatite, and U–Pb ages of apatite from the Oka carbonatite complex: Insights into a complex crystallization history. Chemical Geology 353, 151–172.

Chew, D.M., Pedemonte, G., Corbett, E., 2016a. Proto-Andean evolution of the Eastern Cordillera of Peru. Gondwana Research 35, 59–78.

Chew, D.M., Babechuk, M.G., Cogné, N., Mark, C., O'Sullivan, G.J., Henrichs, I.A., Doepke, D., McKenna, C.A., 2016b. (LA,Q)-ICPMS trace-element analyses of Durango and McClure Mountain apatite and implications for making natural LA-ICPMS mineral standards. Chemical Geology 435, 35–48.

Chew, D.M., Petrus, J.A., Kamber, B.S., 2014. U–Pb LA–ICPMS dating using accessory mineral standards with variable common Pb. Chemical Geology 363, 185–199.

Chew, D.M., Strachan, R. A., 2014. The Laurentian Caledonides of Scotland and Ireland. Geological Society, London, Special Publications 390, 45–91.

Chew, D.M., Sylvester, P.J., Tubrett, M.N., 2011. U–Pb and Th–Pb dating of apatite by LA-ICPMS. Chemical Geology 280, 200–216.

Chew, D.M., Schaltegger, U., Košler, J., Whitehouse, M.J., Gutjahr, M., Spikings, R.A., Miškovíc, A., 2007. U-Pb geochronologic evidence for the evolution of the Gondwanan margin of the north-central Andes. Geological Society of America Bulletin 119, 697–711.

Chew, D.M., Daly, J.S., Page, L.M., Kennedy, M.J., 2003. Grampian orogenesis and the development of blueschist-facies metamorphism in western Ireland. Journal of the Geological Society 160, 911–924.

Cochrane, R., Spikings, R.A., Chew, D., Wotzlaw, J.-F., Chiaradia, M., Tyrrell, S., Schaltegger, U., der Lelij, R. Van, 2014. High temperature (>350°C) thermochronology and mechanisms of Pb loss in apatite. Geochimica et Cosmochimica Acta 127, 39–56.

Cullers, R.L., 2002. Implications of elemental concentrations for provenance, redox conditions, and metamorphic studies of shales and limestones near Pueblo, CO, USA. Chemical Geology 191, 305–327.

Daly, J.S., 1996. Pre-Caledonian History of the Annagh Gneiss Complex North-Western Ireland, and Correlation with Laurentia-Baltica. Irish Journal of Earth Sciences 15, 5–18.

Daly, J.S., Flowerdew, M.J., 2005. Grampian and late Grenville events recorded by mineral geochronology near a basement–cover contact in north Mayo, Ireland. Journal of the Geological Society 162, 163–174.

Dempster, T.J., Harte, B., 1986. Polymetamorphism in the Dalradian of the central Scottish Highlands. Geological Magazine 123, 95–104.

Dewey, J.F., 2005. Orogeny can be very short. Proceedings of the National Academy of Sciences 102, 15286–15293.

Eggins, S.M., Woodhead, J.D., Kinsley, L.P.J., Mortimer, G.E., Sylvester, P., Mcculloch, M.T., Hergt, J.M., Handler, M.R., 1997. A simple method for the precise determination of > 40 trace elements in geological samples by ICPMS using enriched isotope internal standardisation. Chemical Geology 134, 311-326.

Frei, D., Liebscher, A., Franz, G., Dulski, P., 2004. Trace Element Geochemistry of Epidote Minerals. Reviews in Mineralogy and Geochemistry 56, 553–605.

Gaweda, A., Szopa, K., Chew, D., 2014. LA-ICP-MS U-Pb dating and REE patterns of apatite from the Tatra Mountains, Poland as a monitor of the regional tectonomagmatic activity. Geochronometria 41, 306–314.

Giere, R., Sorensen, S.S., 2004. Allanite and Other REE-Rich Epidote-Group Minerals. Reviews in Mineralogy and Geochemistry 56, 431–493.

Harlov, D.E., Förster, H.-J., 2003. Fluid-induced nucleation of (Y+REE)-phosphate minerals within apatite: Nature and experiment. Part II. Apatite. American Mineralogist 88, 1209–1229.

Hsieh, P.-S., Chen, C.-H., Yang, H.-J., Lee, C.-Y., 2008. Petrogenesis of the Nanling Mountains granites from South China: Constraints from systematic apatite geochemistry and whole-rock geochemical and Sr–Nd isotope compositions. Journal of Asian Earth Sciences 33, 428–451.

Hughes, J.M., Rakovan, J.F., 2015. Structurally Robust, Chemically Diverse: Apatite and Apatite Supergroup Minerals. Elements 11, 165–170.

Jafarzadeh, M., Harami, R.M., Friis, H., Amini, A., Mahboubi, A., Lenaz, D., 2014. Provenance of the Oligocene–Miocene Zivah Formation, NW Iran, assessed using heavy mineral assemblage and detrital clinopyroxene and detrital apatite analyses. Journal of African Earth Sciences 89, 56–71.

Jolivet, L., Lecomte, E., Huet, B., Denèle, Y., Lacombe, O., Labrousse, L., Pourhiet, L. Le, Mehl, C., 2010. The North Cycladic Detachment System. Earth and Planetary Science Letters 289, 87–104.

Kamber, B.S., Greig, A., Schoenberg, R., Collerson, K.D., 2003. A refined solution to Earth's hidden niobium: implications for evolution of continental crust and mode of core formation. Precambrian Research 126, 289–308.

Kruckenberg, S.C., Vanderhaeghe, O., Ferré, E.C., Teyssier, C., Whitney, D.L., 2011. Flow of partially molten crust and the internal dynamics of a migmatite dome, Naxos, Greece. Tectonics 30, TC3001.

Li, C., Arndt, T., Tang, Q., Ripley, E.M., 2011. Trace element indiscrimination diagrams. Lithos 232, 76–83.

Lister, G.S., Banga, G., Feenstra, A., 1984. Metamorphic core complexes of Cordilleran type in the Cyclades, Aegean Sea, Greece. Geology 12, 221–225.

MacKinnon, T.C., 1983. Origin of the Torlesse terrane and coeval rocks, South Island, New Zealand. Geological Society of America Bulletin 94, 967–985.

Mao, M., Rukhlov, A.S., Rowins, S.M., Spence, J., Coogan, L.A., 2016. Apatite trace elements compositions: A robust new tool for mineral exploration. Economic Geology 111, 1187–1222.

Mark, C., Cogné, N., Chew, D., 2016. Tracking exhumation and drainage divide migration of the western Alps: a test of the apatite U-Pb thermochronometer as a detrital provenance tool. Geological Society of America Bulletin 128, 1439–1460.

McDonough, W.F., Sun, S., 1995. The composition of the Earth. Chemical Geology 120, 223–253.

McDowell, F.W., McIntosh, W.C., Farley, K.A., 2005. A precise 40Ar–39Ar reference age for the Durango apatite (U–Th)/He and fission-track dating standard. Chemical Geology 214, 249–263.

McLennan, S.M., Hemming, S., McDaniel, D.K., Hanson, G.N., 1993. Geochemical approaches to sedimentation, provenance, and tectonics . In: Johnnson, M.J., Basu, A. (Eds.), Processes Controlling the Composition of Clastic Sediments, Geological Society of America, pp. 21-40. Special Paper 285.

Miles, A.J., Graham, C.M., Hawkesworth, C.J., Gillespie, M.R., Hinton, R.W., Bromiley, 2014. Apatite: A new redox proxy for silicic magmas? Geochimica et Cosmochimica Acta 132, 101–119.

Mortimer, N., 2004. New Zealand's Geological Foundations. Gondwana Research 7, 261–272.

Morton, A., Yaxley, G., 2007. Detrital apatite geochemistry and its application in provenance studies. Geological Society of America Special Papers 420, 319-344.

Morton, A.C., Hallsworth, C.R., 1999. Processes controlling the composition of heavy mineral assemblages in sandstones. Sedimentary Geology 124, 3–29.

Nesbitt, H.W., Young, G.M., 1984. Prediction of some weathering trends of plutonic and volcanic rocks based on thermodynamic and kinetic considerations. Geochimica et Cosmochimica Acta 48, 1523–1534.

Neymark, L.A., Holm-Denoma, C.S., Pietruszka, A.J., Aleinikoff, J.N., Fanning, C.M., Pillers, R.M., Moscati, R.J., 2016. High spatial resolution U-Pb geochronology and Pb isotope geochemistry of magnetite-apatite ore from the pea ridge iron oxide-apatite deposit, St. Francois Mountains, Southeast Missouri, USA. Economic Geology 111, 1915–1933.

Nutman, A. P., 2007. Apatite recrystallisation during prograde metamorphism, Cooma, southeast Australia: implications for using an apatite – graphite association as a biotracer in ancient metasedimentary rocks. Australian Journal of Earth Sciences 54, 1023–1032.

O'Sullivan, G.J., Chew, D.M., Samson, S.D., 2016. Detecting magma-poor orogens in the detrital record. Geology 44, 871-874.

Paton, C., Hellstrom, J., Paul, B., Woodhead, J., Hergt, J., 2011. Iolite: Freeware for the visualisation and processing of mass spectrometric data. Journal of Analytical Atomic Spectrometry 26, 2508–2518.

Petrus, J.A., Chew, D.M., Leybourne, M.I., Kamber, B.S., 2017. A new approach to laser-ablation inductively-coupled-plasma mass-spectrometry (LA-ICP-MS) using the flexible map interrogation tool "Monocle." Chemical Geology 463, 76–93.

Petrus, J.A., Kamber, B.S., 2012. VizualAge: A Novel Approach to Laser Ablation ICP-MS U-Pb Geochronology Data Reduction. Geostandards and Geoanalytical Research 36, 247–270.

Piccoli, P.M., Candela, P. a., 2002. Apatite in Igneous Systems. Reviews in Mineralogy and Geochemistry 48, 255–292.

Pochon, A., Poujol, M., Gloaguen, E., Branquet, Y., Cagnard, F., Gumiaux, C., Gapais, D., 2016. U-Pb LA-ICP-MS dating of apatite in mafic rocks: Evidence for a major magmatic event at the Devonian-Carboniferous boundary in the Armorican Massif (France). American Mineralogist 101, 2430–2442.

Prowatke, S., Klemme, S., 2006. Rare earth element partitioning between titanite and silicate melts: Henry's law revisited. Geochimica et Cosmochimica Acta 70, 4997–5012.

Roser, B.P., Korsch, R.J., 1999. Geochemical characterization, evolution and source of a Mesozoic accretionary wedge: the Torlesse terrane, New Zealand. Geological Magazine 136, 493–512.

Schoene, B., Bowring, S.A., 2006. U–Pb systematics of the McClure Mountain syenite: thermochronological constraints on the age of the Ar-40/Ar-39 standard MMhb. Contributions to Mineralogy and Petrology 151, 615–630.

Sha, L.-K., Chappell, B.W., 1999. Apatite chemical composition, determined by electron microprobe and laser-ablation inductively coupled plasma mass spectrometry, as a probe into granite petrogenesis. Geochimica et Cosmochimica Acta 63, 3861–3881.

Spear, F.S., Pyle, J.M., 2002. Apatite, Monazite, and Xenotime in Metamorphic Rocks. Reviews in Mineralogy and Geochemistry 48, 293–335.

Spencer, C.J., Kirkland, C.L., Taylor, R.J.M., 2016. Strategies towards statistically robust interpretations of in situ U–Pb zircon geochronology. Geoscience Frontiers 7, 581–589.

Stacey, J.S., Kramers, J.D., 1975. Approximation of terrestrial lead isotope evolution by a two-stage model. Earth and Planetary Science Letters 26, 207–221.

Tang, M., Wang, X-L., Xu, X-S., Zhu, C., Cheng, Z., Yu, Y., 2012. Neoproterozoic subducted material in the generation of Mesozoic rocks: Evidence from apatite geochemistry and Hf-Nd isotopic decoupling. Gondwana Research 21, 266-280.

Thomson, S.N., Gehrels, G.E., Ruiz, J., Buchwaldt, R., 2012. Routine low-damage apatite U-Pb dating using laser ablation–multicollector–ICPMS. Geochemistry, Geophysics, Geosystems 13, Q0AA21.

Ubide, T., McKenna, C.A., Chew, D.M., Kamber, B.S., 2015. High-resolution LA-ICP-MS trace element mapping of igneous minerals: In search of magma histories. Chemical Geology 409, 157–168.

Ulrich, T., Kamber, B.S., Woodhead, J.D., Spencer, L.A., 2010. Long-Term Observations of Isotope Ratio Accuracy and Reproducibility Using Quadrupole ICP-MS. Geostandards and Geoanalytical Research 34, 161–174.

Warren-Smith, E, Lamb, S., Seward, D., Smith, E., Herman, F. Stern T., 2016. Thermochronological evidence of a low-angle, mid-crustal detachment plane beneath the central South Island, New Zealand, Geochemistry, Geophysics, Geosystems, 17, 4212–4235. doi:10.1002/2016GC006402.

Wijbrans, J.R., McDougall, I., 1988. Metamorphic evolution of the Attic Cycladic Metamorphic Belt on Naxos (Cyclades, Greece) utilizing 40Ar/39Ar age spectrum measurements. Journal of Metamorphic Geology 6, 571–594.

Yang P., Rivers T. 2002 The origin of Mn and Y annuli in garnet and the thermal dependence of P in garnet and Y in apatite in calc-pelite and pelite, Gagnon Terrane, Western Labrador. Geological Materials Research 4, 1, 1-35.

Zattin, M., Andreucci, B., Thomson, S.N., Reiners, P.W., Talarico, F.M., 2012. New constraints on the provenance of the ANDRILL AND-2A succession (western Ross Sea, Antarctica) from apatite triple dating. Geochemistry, Geophysics, Geosystems 13, Q10016.

Appendix B

On the track of a Scottish impact structure: a detrital zircon and apatite provenance study of the Stac Fada Member and wider Stoer Group, northwest Scotland

Under review in a scientific journal for publication
Authors: Gavin G. Kenny, Gary J. O'Sullivan, Stephen Alexander, Michael J. Simms, David M. Chew and Balz S. Kamber

ABSTRACT

No impact structures have yet been unequivocally identified on the mainland of the British Isles. The Stac Fada Member of the Stoer Group, northwest Scotland, is widely regarded as a melt-rich, impact ejecta horizon, but no agreement has yet been reached on the whereabouts of the impact structure or even its distance from, or direction relative to, the 50 km-long north-south-trending section of Stac Fada Member outcrops. The most recent sedimentological analysis suggests a source to the east and it has been proposed that a distinct geophysical anomaly more than 50 km east of the Stac Fada Member outcrops, near the village of Lairg, may represent a buried impact structure. Here we aim to shed further light on the possible location of the impact structure through provenance studies of detrital zircon and apatite in samples from the Stoer Group.

Our new zircon U-Pb data for the Stoer Group are consistent with earlier interpretations that the detritus was derived largely from local Lewisian Gneiss Complex basement, but the larger number of analyses for this study has yielded ages previously undocumented in the Stoer Group; these include grains at *ca.* 3.5 Ga and *ca.* 3.2-3.1 Ga, as well as others of Mesoproterozoic provenance. U-Pb age distributions for detrital apatite contrast starkly with those for zircon. The zircon record is dominated by Archaean grains (>2.5 Ga), but the apatite data for the Stoer Group display a single major peak at *ca.* 1.7 Ga, consistent with regional Laxfordian metamorphism. The almost complete absence of apatite of Archaean age is best explained by heating the >2.5 Ga Lewisian basement (the likely source region) significantly above the closure temperature of the apatite U-Pb system (*ca.* 375-450°C).

The only potential evidence for impact-induced shock metamorphism encountered in this study was a single zircon grain that displayed planar fractures (PFs) on its exterior. Although a number of zircon and apatite grains in the Stoer Group yield U-Pb ages within uncertainty of the 1177 ± 5 Ma $^{40}Ar/^{39}Ar$ age for the Stac Fada Member, neither of the two such zircon grains displayed textures indicative of shock metamorphism and there is no clear evidence for impact-induced Pb loss in the dataset.

Despite well-documented changes in sedimentary environment and possible change in flow direction coincident with the deposition of the Stac Fada Member, the U-Pb age distributions for both zircon and apatite showed no significant variation with stratigraphic level in the Stoer Group. This may be interpreted as evidence that there was no major change in provenance during the course of the deposition of the Stoer Group or that, if there was any significant change, the different source regions were characterised by similar apatite and zircon U-Pb age populations. Regardless, the new data do not provide independent constraints on the location of the structure associated with the Stac Fada Member impact event.

B.1. INTRODUCTION

The geological record of the British Isles records a rich history of events spanning almost 3 Gyr, but no impact structures have yet been identified. Indirect evidence of impact events has been proposed at three stratigraphic levels: the Mesoproterozoic Stac Fada Member impact ejecta horizon in the Stoer Group, northwestern Scotland (Amor et al. 2008) with well-documented shock features such as shocked quartz (Amor et al. 2008; Osinski et al. 2011) and the high-pressure polymorph of zircon, reidite (Reddy et al. 2015); a horizon of reworked microtektites in the late Triassic Mercia Mudstone Group of southwestern England, in which shocked quartz has also been well documented (Walkden et al. 2002; Kirkham 2003); and a purported Paleogene impact ejecta layer on the Isle of Skye, Scotland (Drake et al. 2017) that awaits confirmation with unequivocal documentation of shock features. Only the microtektite-bearing Triassic deposit has been linked to a known impact structure – the *ca.* 100 km-in-diameter Manicouagan impact structure, Quebec, Canada (Thackrey et al. 2009). The impact structure associated with the Stac Fada Member has yet to be identified, but various lines of evidence (including sedimentary features, thickness variations and an anisotropy of magnetic susceptibility study) have been used to suggest possible source locations (Lawson 1972; Stewart 2002; Young 2002; Amor et al. 2011; Simms 2015). Most recently, Simms (2015) proposed that a *ca.* 40 km-in-diameter geophysical anomaly known as the Lairg Gravity Low, centred more than 50 km east of the Stac Fada Member outcrops, may indicate the location of the now-buried structure. Despite a lack of consensus on the likely location or size of the impact structure associated with the Stac Fada Member, it presently represents the best prospect for the first identification of an impact structure in the British Isles. In this context, we here report the results of a detrital zircon and apatite U-Pb provenance study of sedimentary rocks of the Stac Fada Member and wider Stoer Group with the ultimate aim of shedding light on the possible location of the impact structure associated with this event, via potential changes in sediment source area.

B.1.1The Stac Fada Member

The Stac Fada Member is a unique horizon within the *ca.* 2 km-thick, predominantly alluvial and lacustrine sedimentary succession of the Mesoproterozoic Stoer Group, northwest Scotland, which overlies Archaean crystalline basement rocks referred to as the Lewisian Gneiss Complex (Stewart 2002).

The unit, which is usually ~10 m thick and can be traced along strike for more than 50 km (Fig. 1), has a distinctive appearance with fragments of dark green, vesicular, devitrified glass accompanying mudstone, sandstone and gneiss clasts up to 0.5 m across in a poorly sorted sand matrix (Stewart 2002). Sandstone rafts reach 15 m in length at the unit's type locality at Stoer (Stewart 2002). The Stac Fada Member was previously interpreted as a mudflow, or series of mudflows, related to endogenic volcanic processes (e.g., (Lawson 1972; Sanders & Johnston 1989; Stewart 1990; Young 2002) but the identification of unequivocal shock features in quartz (planar deformation features – PDFs) led to its reinterpretation as an ejecta deposit associated with a bolide impact (Amor et al. 2008). Other evidence supporting an impact-related origin for the unit include elevated abundances of platinum group elements (PGEs) and an excess of ^{53}Cr (Amor et al. 2008), as well as the presence of shock metamorphosed zircon with lamellae of the high-pressure $ZrSiO_4$ polymorph reidite (Reddy et al. 2015).

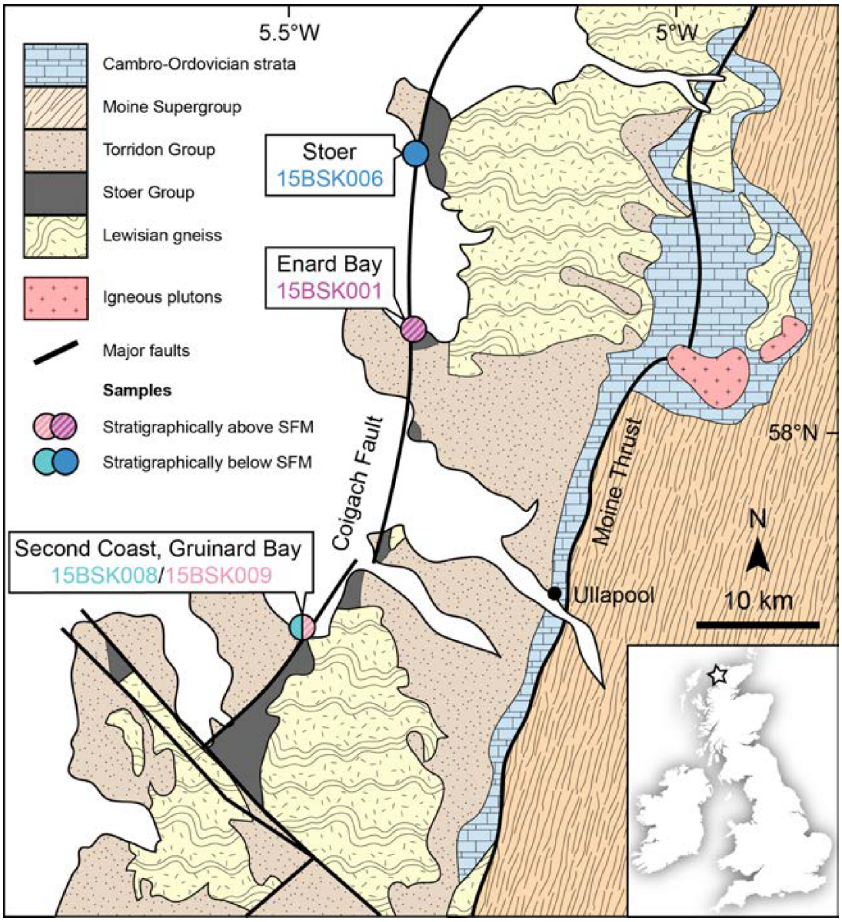

Figure 1. Regional geology of northwest Scotland with sample locations for this study. Sample 15BSK_X_SFM is a combination of rocks from the Stac Fada Member (SFM) at all three localities. Map modified from Simms (2015). The Minch basin, proposed as a possible location of the Stac Fada Member-related impact structure by Amor et al. (2008), lies offshore (i.e., where the legend is situated on the map) whereas the centre of the Lairg gravity low, suggested as a possible impact site by Simms (2015), lies *ca.* 30 km east of the Moine Thrust.

Following its reinterpretation as an impact-related deposit, the Stac Fada Member has been divided into three distinct units at the Enard Bay section (Branney & Brown 2011). The lowermost stratigraphy, which varies from 4 to 10 m thick, comprises a massive suevite with matrix-supported devitrified melt fragments as well as gneiss and mudstone clasts. This grades into a similar unit, distinguished by its abundant matrix-supported whole and broken accretionary lapilli and the onset of stratification near its top. The uppermost portion of the Stac Fada Member comprises a thin (≤3 cm) layer of clast-supported dust pellets. The two lower units together are interpreted to have formed from a decelerating granular density current that rapidly waxed and then waned, whereas the thin layer of pellets is interpreted to represent direct fallout from a residual atmospheric dust plume (Branney & Brown 2011).

B.1.2. Locating the impact site

Various lines of evidence have been put forward in attempts to constrain the location and proximity of the source material for the Stac Fada Member but there is not currently any consensus. The most pertinent points are noted below.

Upon interpreting the Stac Fada Member as an impact-related unit, Amor et al. (2008) suggested that the relatively thick and distinctively continuous nature of the unit over tens of kilometres is indicative of quite a proximal source location, although no distance was specified. However, the lack of seismites or any significant soft-sediment deformation in the underlying succession has been interpreted as suggesting that the impact structure was still a significant distance away – "perhaps tens of kilometres" (Simms 2015; p. 755).

Variations in thickness and lithology along the effectively linear outcrop trace of the Stac Fada member (Fig. 1) have been cited as indicative of proximal-distal changes. The greater thickness of the deposit in the more northerly outcrops (*ca.* 10-15 m thick at Stoer and Enard Bay compared to 4-6 m thick further south; Simms 2015) has been interpreted as tentative evidence that the southern sites may be more distal to the impact (Amor et al. 2008; Simms 2015). The abundance of accretionary lapilli in the Stac Fada Member at Enard Bay, and their absence further south, has been proposed as evidence that Enard Bay is the most proximal (presently exposed) outcrop to the source (Lawson 1972; Young 2002; Amor et al. 2008; Branney & Brown 2011). Smaller and less abundant accretionary lapilli to the north (for example, at Stoer) might also indicate that these sites were more distal to the source than was Enard Bay (Simms 2015).

There is a paucity of sedimentary structures that might indicate the emplacement direction in the largely non-erosively emplaced and massive Stac Fada Member. Wedge-shaped intrusions of melt-bearing breccia into the strata beneath the Stac Fada Member have been regarded as among the few potential indicators but different authors have interpreted them as indicating different directions of movement. Lawson (1972) and Amor et al. (2008) proposed that material was moving from west to east, leading Amor et al. (2008) to suggest that the impact structure may be offshore beneath the Minch Basin. Conversely, Stewart (2002) interpreted the same folds and upturned beds as indicating movement from east to west. Sanders & Johnston (1989) described the wedge-shaped geometry of the base of the Stac Fada Member at Stoer and documented thinning to the north and west (their Figs 2 and 3). Young (2002) interpreted small-scale asymmetrical folds and flame structures in sandstones within the Stac Fada Member as evidence for movement of material from two opposing directions, one from the south-south-west and the other from the north-north-east.

With the recognition that the Stac Fada member was impact-derived (Amor et al. 2008), it follows that the deposit must originate from a single location. Simms (2015) suggested that the directional variability reported by Young (2002) may be due to rotation of the sandstone rafts during transportation, an interpretation supported by the rafts' apparently random palaeomagnetic orientations (Irving & Runcorn 1957; Stewart 2002). Most recently, Simms (2015) has interpreted the Stoer intrusions as evidence for emplacement from a source to the east (his Fig. 5) and argued that because the oversteepened sandstone beds above the intrusive wedges are anchored into the pre-impact stratigraphy they preserve a more robust record of the emplacement direction of the ejecta.

Other sedimentary features that may indicate transport directions have been documented at Enard Bay. These include planar cross beds and lapilli long axes in the upper part of the Stac Fada Member, as well as gently plunging troughs subsequently incised into the lapilli beds. Simms (2015) interpreted all of these features to indicate that material was broadly moving from east to west during deposition. Further south, Simms (2015) documented curved fractures on the upper surface of the Stac Fada Member, and suggested that these may be ogives related to the transport direction, with their convex-westwards configuration indicating the direction of flow. Similarly, if the concave-up surfaces documented by Simms (2015) within the Stac Fada Member can be interpreted as thrust planes within a viscous flow, they would also be consistent with movement from the east.

Amor et al. (2011) reported, in a non-peer reviewed abstract, the results of an anisotropy of magnetic susceptibility study of the Stac Fada Member and that supports an impact structure lying to the west of the present Stac Fada Member outcrops.

In light of the varying interpretations of the evidence for a source location within the Stac Fada Member itself, the overlying succession has also been studied with the aim of elucidating a possible source location for the impact ejecta material. The Stac Fada Member is succeeded by up to 100 m of lacustrine, planar-bedded sedimentary rocks (the Poll à Mhuilt Member; Fig. 2) at all but the most southerly sites (Stewart 2002; Simms 2015) before fluvial deposition resumes in the Meall Dearg Formation. These two lithostratigraphic units evidence a dramatic reconfiguration of the regional drainage pattern following deposition of the Stac Fada Member (Stewart 2002). The Poll à Mhuilt Member was interpreted as a post-impact lake by Amor et al. (2008). Ripple cross-lamination (Stewart 2002) and cross bedding (Simms 2015) indicate that flow into the lakes was broadly from the west, suggesting that eastward flowing rivers were dammed by debris located east of the present outcrops (Simms 2015).

In contrast to the variable palaeocurrent azimuths of the pre-Stac Fada Member succession, the fluvial sediments of the Meall Dearg Formation consistently record flow to the west (Stewart 2002; Simms 2015; Lebeau & Ielpi 2017) but with evidence for a broadly radial drainage configuration centred on a focal point to the east (Simms 2015; his Fig. 6). Stewart (2002) had interpreted this palaeoflow configuration as related to tectonic uplift on the eastern flank of the basin but, in light of the impact evidence, Simms (2015) reinterpreted the apparently radial drainage system of the Meall Dearg Formation as a consequence of post-impact regional doming.

Geophysical data can play a key role in the study of impact structures once unambiguous evidence for an impact has already been documented (such as the identification of shock metamorphism-induced microstructures, e.g. PDFs in quartz). This is particularly relevant to structures that are not, or are only partially, exposed at the Earth's surface (e.g., the Chicxulub structure buried on the Yucatán Peninsula, Mexico (Hildebrand et al. 1998). A common geophysical anomaly associated with impact structures is a broadly concentric gravity low which in larger structures (D >30 km) is likely to contain a central gravity high (Grieve & Pilkington 1996; Morgan & Rebolledo-Vieyra 2013). Simms (2015) proposed that a significant gravity low centred near the village of Lairg in northern Scotland, *ca.* 50 km east of the Stac Fada Member outcrops, may represent the impact structure from which the Stac Fada Member material was

derived, which is consistent with his interpretation of directional data from the Stac Fada Member and the overlying succession. Previous interpretations have ascribed this gravity low to a Caledonian granite pluton, an Archaean granite in the basement, a buried wedge of Torridonian Supergroup sedimentary rocks, or a region of thickened Moine Supergroup rocks (e.g., Butler & Coward 1984, and see discussion in Leslie et al. 2010). Although a conspicuous gravity low exists to the west of the Stac Fada Member outcrops, in the Minch Basin proposed as the impact site by Amor et al. (2008, 2011), the thick post-Palaeozoic sediment fill there (Binns et al. 1975) provides the most plausible explanation of this feature.

Despite the numerous lines of investigation there is no consensus on the location of the impact structure associated with the Stac Fada Member relative to the currently exposed outcrops.

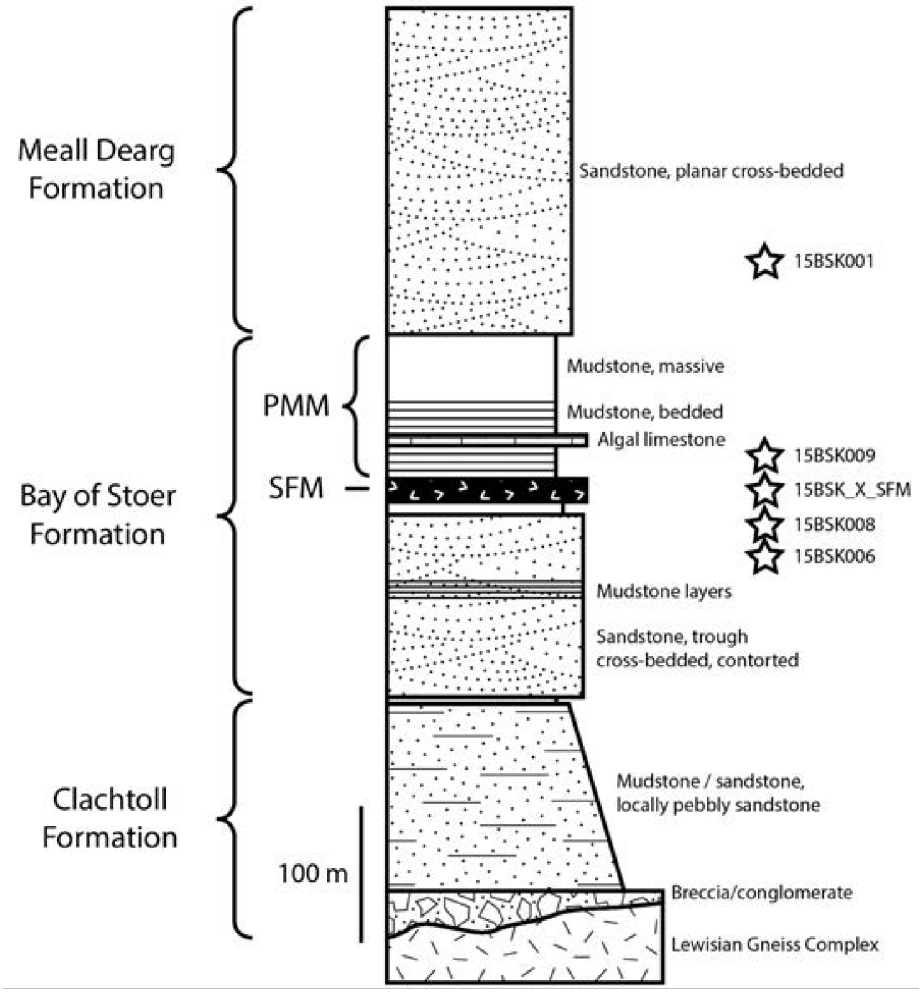

Figure 2. Generalised stratigraphic column for the Stoer Group at Stoer. Modified from Goodenough & Krabbendam (2011; their Fig. 32). Note that only sample 15BSK006 was taken at this locality and the stratigraphic location of the other samples are indicative on a relative time basis. There is significant lateral lithology variation within the Stoer Group (Stewart 2002). SFM – Stac Fada Member. PMM – Poll à Mhuilt Member.

B.1.3. A new approach

In this study we aimed to shed light on the possible location of the impact structure through a detrital zircon and apatite U-Pb provenance investigation of five samples stratigraphically within, above and below the impact-related unit (Fig. 2). Zircon is a physically and chemically robust mineral that is readily dateable by the U-Pb method and is ubiquitous in clastic sediments, and is a well-established and powerful tool in provenance studies (e.g., Thomas 2011). Recent advances in U-Pb dating of common Pb-bearing minerals (e.g., Chew et al. 2011; Thomson et al. 2012; Chew et al. 2014) mean that it is now possible to potentially complement detrital zircon analyses with data from other U-bearing heavy minerals (e.g., Mark et al. 2016; O'Sullivan et al. 2016). Advantages of including apatite in detrital studies (O'Sullivan et al. 2016) stem from the fact that it crystallises in significant volumes in a much wider range of igneous rock types, particularly basic rocks than zircon (as a result of the limited ability of rock-forming minerals to accept the amount of phosphorus that occurs in most rocks into their structure; Piccoli & Candela 2002) and, unlike zircon, it crystallises in significant volumes in metamorphic rocks of all grades and most protolith types (Spear & Pyle 2002). Secondly, apatite is more likely than zircon to represent first-cycle detritus due to its chemical instability during prolonged periods of alluvial storage in humid climates or extensive weathering at source (Morton & Hallsworth 1999, and references therein), despite this apatite is found in essentially all Quaternary sediment deposits (Nechaev & Isphording 1993) and is usually very stable during diagenesis due to the liberation of organic-P and P adsorbed onto the surfaces of clay minerals (e.g., (Bouch et al. 2002). These factors result in detrital apatite U-Pb (i) being able to record events such as magma-poor orogenesis that are not well represented in the detrital zircon record (O'Sullivan et al. 2016), and (ii) having a greater likelihood of recording more recent tectonic events than the detrital zircon U-Pb system, which is more likely to include plentiful polycyclic detritus.

Although the Stoer Group has previously been studied in terms of detrital zircon U-Pb analysis (Rainbird et al. 2001; Kinnaird et al. 2007), we build on this work with a high-analysis-number, coupled zircon and apatite U-Pb study. Our specific aims were to understand:

whether there are new U-Pb age populations in the succession overlying the impact-related horizon that might reflect the presence of previously unexposed rocks brought to the Earth's surface by the impact event;

whether the absence of any specific U-Pb age populations in the lacustrine sediments (Poll à Mhuilt Member) above the Stac Fada Member reflects specific source terrain(s) being cut-off as a consequence of impact-related drainage reconfiguration;

whether there is any discernable difference between the heavy mineral assemblage of the fluvial sediments underlying the Stac Fada Member, which were sourced from multiple directions, and those of the fluvial sediments above the Stac Fada Member, which were sourced solely from the east, and whether this might indicate a possible location of the impact structure;

whether detrital apatite in the Stoer Group records different ages and events to detrital zircon, and if the former might have additional utility for recording stratigraphic changes through its ability to highlight a wide range of events and/or its increased likelihood of representing first-cycle detritus.

B.2. MATERIALS AND METHODS

B.2.1. Samples

Five samples were processed for zircon and apatite U-Pb analysis. Two were collected from stratigraphically beneath the Stac Fada Member, one from the Stac Fada Member itself, and two from stratigraphically above the impact-related layer (Fig. 2). The samples are listed below in stratigraphic order from lowest to highest, relative to the Stac Fada Member.

Sample 15BSK006 (Stoer; 58.20134ºN, 5.34757ºW; Fig. 1) is a flat-bedded sandstone from the pre-impact fluvial succession. It was sampled approximately 10 m stratigraphically below the base of the Stac Fada Member at the Bay of Stoer in what is mapped as undivided Bay of Stoer Formation (British Geological Survey 2002).

Sample 15BSK008 (Second Coast, Gruinard Bay; 57.86136ºN, 5.49697ºW) is a sandstone similar to sample 15BSK006 and was collected immediately below the Stac Fada Member, where the sediment was disturbed by ballistically emplaced boulders of country rocks.

Sample 15BSK_X_SFM is composed of a number of hand samples of green, devitrified glass-bearing Stac Fada Member material from all three sample sites (Fig. 1).

Sample 15BSK009 (Second Coast, Gruinard Bay; 57.86107ºN, 5.49795ºW) is a well-sorted, fine-grained sandstone of the Poll à Mhuilt Member lacustrine sequence immediately overlying the Stac Fada Member.

Sample 15BSK001 (Enard Bay; 58.07096ºN, 5.35579ºW) is a trough cross-bedded sandstone and is the stratigraphically highest sample. It was collected from the Meall Dearg Formation which represents a return to fluvial sedimentation above the Poll à Mhuilt Member of the Bay of Stoer Formation.

B.2.2. Analytical Methods

Zircon and apatite grains were separated from whole rock samples using standard crushing, milling, heavy liquid and magnetic separation techniques at Trinity College Dublin. A selection of zircon grains from each sample were placed on conducting carbon tabs and their exteriors were imaged in backscatter electron (BSE) mode on a Tescan Mira XMU Field Emission Scanning Electron Microscope (SEM) at the Irish Centre for Research in Applied Geosciences (iCRAG) lab at Trinity College Dublin. A larger number of zircon and apatite grains were picked and were mounted in 2.5 cm-diameter epoxy mounts. The mounts were polished with 6 and 1 μm diamond polishing paste to

reveal the grain midsections. After application of a *ca.* 10 nm-thick carbon coat to the mounts, all zircon grains were imaged in cathodoluminescence (CL) mode using a KE Developments Centaurus system attached to the SEM. An accelerating voltage of 10 kV and working distance of *ca.* 10 mm were used. Following removal of the carbon coat with a very brief (*ca.* 30 seconds) polish using 1 μm diamond polishing paste, the zircon and apatite grains underwent laser ablation inductively coupled plasma mass spectrometry (LA-ICPMS) U-Th-Pb analysis.

All zircon analyses were conducted on a Photon Machines Analyte Excite 193 nm ArF Excimer laser coupled to a Thermo Scientific iCAP-Qc ICP-MS at the Department of Geology, Trinity College Dublin, in a single analytical period (December 2015). The methodology closely followed that of Rodrigues et al. (2015). The laser produced a circular spot 30 μm in diameter and operated with a nominal fluence of 2.5 Jcm^{-2} for 180 shots at a 4 Hz laser repetition rate. Nine isotopes were measured during the analyses (^{88}Sr [3], ^{91}Zr [3], ^{202}Hg [2.5], ^{204}Pb [50], ^{206}Pb [50], ^{207}Pb [70], ^{208}Pb [50], ^{232}Th [20], ^{238}U [40]; the dwell time for each isotope is give in milliseconds in square brackets; total cycle time of 288.5 ms). 91500 standard zircon ($^{206}Pb/^{238}U$ age isotope dilution thermal ionization mass spectrometry [ID-TIMS] age of 1062.4 ± 0.8 Ma [all uncertainties are quoted at the 2σ level unless otherwise stated]; Wiedenbeck et al. 1995) was used as the calibration reference material (RM) and Temora 2 ($^{206}Pb/^{238}U$ TIMS age of 416.78 ± 0.33 Ma; Black et al. 2004) was analysed as a quality control material (QCM). The raw isotope data were reduced using the 'VizualAge' data reduction scheme (DRS; Paton et al. 2010; Petrus & Kamber 2012) in the IOLITE package (v. 2.5) of Paton et al. (2011). Processed data were plotted in the Isoplot 4.15 add-in (Ludwig 2012) for Microsoft Excel.

Apatite U-Pb analyses were conducted over two separate analytical periods (December 2015 and September 2016). The analyses performed during the first analytical period (on samples 15BSK001 and 15BSK009) were conducted on the same LA-ICPMS system as described above, following the procedure of Chew et al. (2014). A circular spot of 60 μm diameter was ablated for 225 shots at 5 Hz. The analyses performed during the second analytical period (on samples 15BSK006, 15BSK008 and 15BSK_X_SFM) were conducted on the same laser ablation system, which was on this occasion coupled to an Agilent 7900 ICP-MS. For these analyses, a circular spot 60 μm in diameter and operated with a fluence of 3.25 Jcm^{-2} for 280 shots at a 10 Hz laser repetition rate. During the first analytical period thirty-four isotopes were measured during the analyses (^{24}Mg [10], ^{31}P

[5], ^{35}Cl [30], ^{43}Ca [25], ^{51}V [10], ^{55}Mn [10], ^{71}Ga [10], ^{73}Ge [10], ^{75}As [10], ^{88}Sr [20], ^{89}Y [5], ^{90}Zr [10], ^{139}La [5], ^{140}Ce [5], ^{141}Pr [5], ^{146}Nd [5], ^{147}Sm [10], ^{153}Eu [10], ^{157}Gd [10], ^{159}Tb [10], ^{163}Dy [10], ^{165}Ho [10], ^{166}Er [10], ^{169}Tm [10], ^{172}Yb [10], ^{175}Lu [10], ^{182}W [10], ^{202}Hg [10], ^{204}Pb [25], ^{206}Pb [60], ^{207}Pb [65], ^{208}Pb [10], ^{232}Th [20] and ^{238}U [40]; dwell time for each isotope in milliseconds in square brackets; total dwell time of 515 ms). During the second analytical period twenty-nine isotopes were measured (as above but excluding ^{24}Mg, ^{31}P, ^{71}Ga, ^{73}Ge and ^{182}W). For all apatite analyses, a *ca.* 1 cm-sized crystal of Madagascar apatite (Thomson et al., 2012; an in-house aliquot of fragments of this crystal has yielded a weighted average ID-TIMS concordia age of 473.5 ± 0.7 Ma) was used as the RM and McClure Mountain apatite (^{207}Pb/^{235}U TIMS age of 523.51 ± 1.47 Ma; Schoene & Bowring 2006) was analysed as the QCM. The raw isotope data were reduced using the 'VizualAge_UcomPbine' DRS (Chew et al. 2014) in Iolite (Paton et al. 2011).

Unlike zircon, which excludes common (i.e. initial or non-radiogenic) Pb (Pb_c) during crystallisation, apatite often has considerable Pb_c contents that can result in significant discordance in the U-Pb system. This is coupled with generally low U-contents resulting in apparent lesser accumulation of radiogenic Pb (Pb*), hence resulting in high Pb_c/Pb* ratios that might hinder the dating of certain grains. Pb_c in the Madagascar apatite RM was corrected for using a ^{207}Pb-based method employing the known ^{207}Pb/^{206}Pb ratio (Chew et al. 2014). However, detrital apatite has by definition been isolated from co-genetic low-U phases that might have been used to estimate the grain's initial Pb isotopic composition; hence the initial Pb isotopic composition must be estimated from Pb evolution models. In this study variable Pb_c in individual detrital apatite grains was corrected for by (i) using a starting estimate for the age of the grain, (ii) calculating its corresponding initial Pb isotopic composition in the model of Stacey & Kramers (1975), and then (iii) adopting an iterative approach utilising on a ^{207}Pb correction, based on the procedure of Chew et al. (2011).

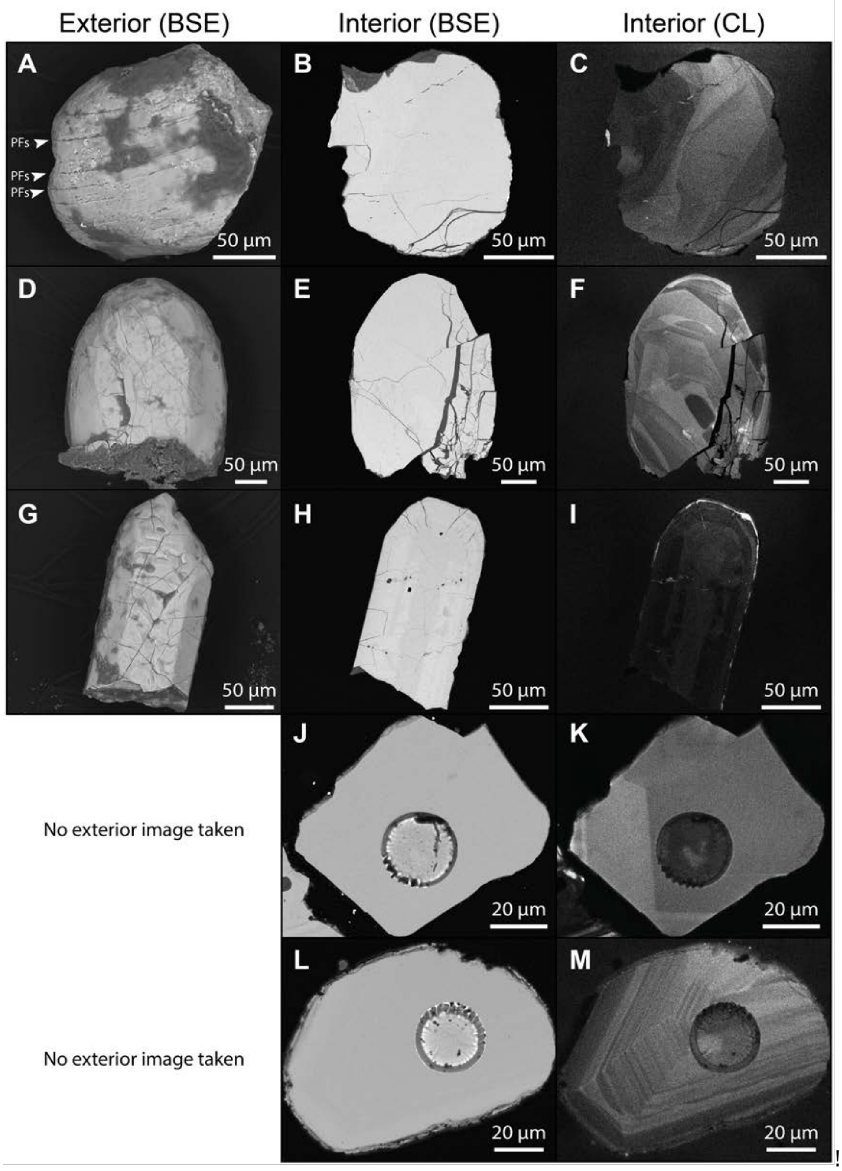

Figure 3. Zircon imaging. A-C) Zircon grain from sample 15BSK001 (taken from stratigraphically above the Stac Fada Member) which shows potentially impact-related planar microstructures on its exterior. **D-I)** Two zircon grains that not did not display any potentially impact-related textures – typical of most grains in this study. Both are from the Stac Fada Member itself. **J-M)** The two youngest detrital zircon grains in the Stoer Group – grain 15BSK009/Z/41 (J-K) and grain 15BSK_X_SFM/Z/82 (L-M). Circular features are laser ablation U-Pb analysis pits. BSE – backscattered electron; CL – cathodoluminescence; PFs – planar fractures.

B.3. RESULTS

B.3.1. Shocked features in zircon

External and internal imaging of zircon grains from all samples showed little evidence of potential shock features. A single grain in sample 15BSK001, stratigraphically above the Stac Fada Member, displayed planar microstructures that may be impact-related (Fig. 3A-C). In zircon, no neoblasts or granular textures, potentially related to impact-induced recrystallisation, were observed. Such features have been shown to record the impact age at a number of impact structures (e.g., Vredefort, South Africa – Moser 1997; Moser et al. 2011; Cavosie et al. 2015; Sudbury, Canada – Kenny et al. 2017) and would provide an opportunity to obtain the first direct U-Pb age for the impact event related to the Stac Fada Member deposits if they could be identified. The apparent rarity of shock features in zircon in the samples studied here is consistent with the observation of Osinski et al. (2011) that some samples of the Stac Fada Member contain no shocked quartz and, in general, the unit appears to contain an order of magnitude less shocked material than proximal impact melt-bearing ejecta layers (such as suevite from the Ries impact structure, Germany; e.g. Engelhardt 1997).

B.3.2. Zircon U-Pb age data

Studies of detrital zircon generally exclude from consideration analyses with discordance greater than an arbitrary cut-off value (e.g., Fedo et al. 2003); here, analyses that were >10 % discordant (grey ellipses in Fig. 4) were not considered further.

The five analysed samples of the Stoer Group display very similar zircon age distributions (Figs 4-6). Their age populations are all dominated by a major peak at 2.9-2.7 Ga with minor populations at *ca.* 3.2-3.1 Ga, *ca.* 2.5 Ga, *ca.* 2.4 Ga, *ca.* 1.9 Ga and *ca.* 1.75 Ga (Figs 4-5). The youngest concordant analyses are from two grains in sample 15BSK009, which have $^{206}Pb/^{238}U$ ages of 1.43 ± 0.02 Ga and 1.23 ± 0.02 Ga, and a grain in sample 15BSK_X_SFM, which has a $^{206}Pb/^{238}U$ age of 1.24 ± 0.01 Ga. Overall, the detrital zircon U-Pb distributions for the Stoer Group reported here are very similar to those reported by Rainbird et al. (2001) and Kinnaird et al. (2007) but the higher number of analyses here (a total of 553 analyses that were <10 % discordant, compared to 127 and 16 respectively in the previous studies) has allowed additional insights. For example, the youngest detrital zircon ages encountered here are significantly younger than the invariably >1.7 Ga ages reported previously. However, we note that caution should be

applied when interpreting single detrital zircon analyses, particularly in the interpretation of youngest ages (Nelson 2001). Additionally, this study confirms the presence of a distinct *ca.* 3.2-3.1 Ga population (which was previously represented by only a single <10 % discordant analysis) and reports the first Paleoarchaean age for a zircon grain from the Stoer Group – the oldest concordant analysis in this study has a $^{207}Pb/^{206}Pb$ age of 3529 ± 30 Ma (Fig. 4D inset). With a total of 696 <10 % discordant zircon U-Pb analyses for the Stoer Group from this and previous studies (Rainbird et al. 2001; Kinnaird et al. 2007); Fig. 7), there is now 95 % confidence that no fractions of the zircon population composing ≥1.2 % of the total have been missed (*cf* Vermeesch 2004).

Figure 4 (next page). Concordia diagrams for detrital zircon (left panels) and apatite U-Pb data (right panels). For zircon data, grey ellipses represent analyses that are more than 10 % discordant. For apatite data, grey ellipses represent analyses for which the 2σ uncertainty on the ^{207}Pb-corrected age was greater than 5 %. Number of concordant (for zircon) or low uncertainty (for apatite) analyses vs. total number of grains analysed given for each sample.

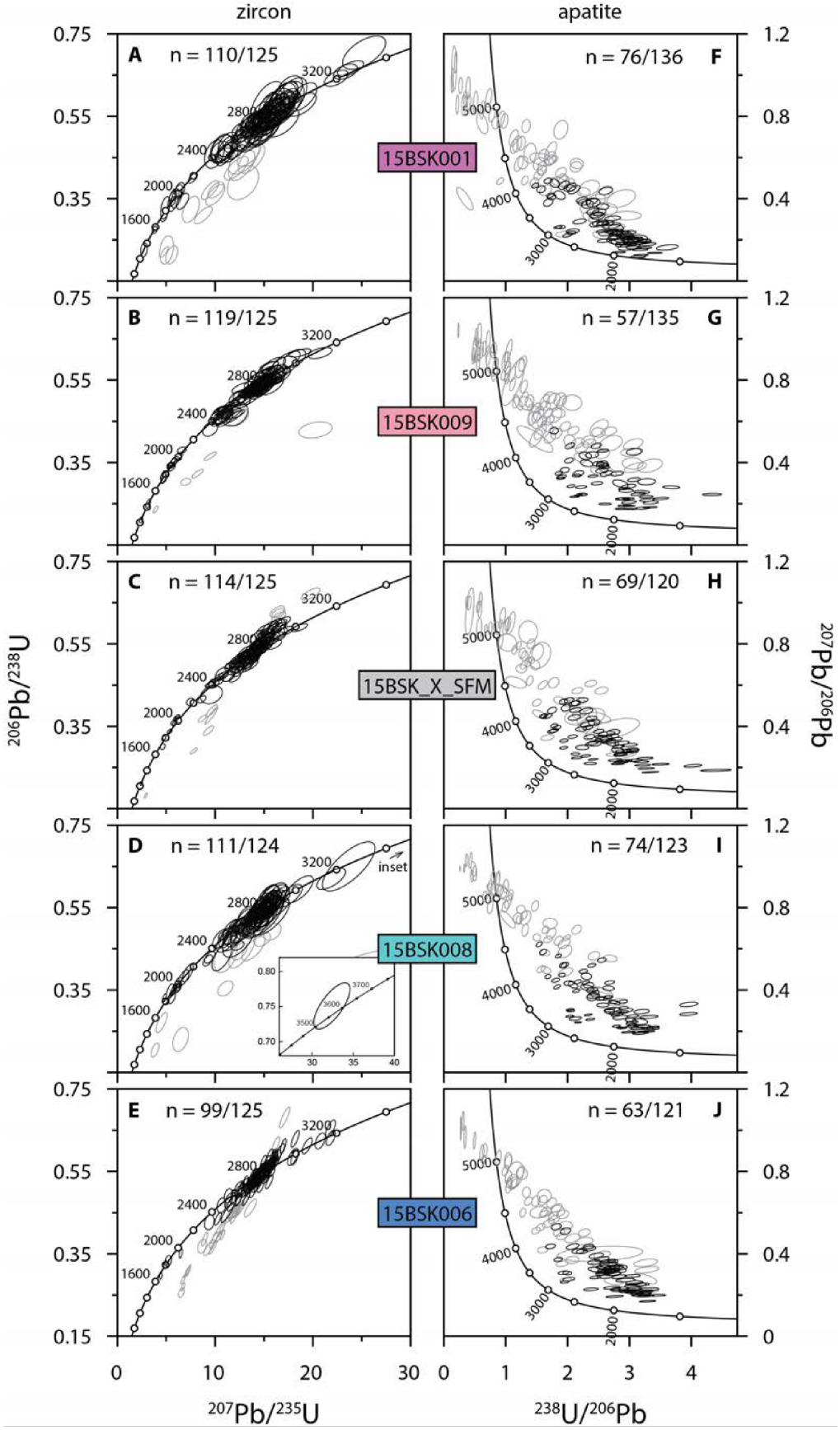
zircon
apatite
A n = 110/125
B n = 119/125
C n = 114/125
D n = 111/124
E n = 99/125
F n = 76/136
G n = 57/135
H n = 69/120
I n = 74/123
J n = 63/121
15BSK001
15BSK009
15BSK_X_SFM
15BSK008
15BSK006
inset
206Pb/238U
207Pb/206Pb
207Pb/235U
238U/206Pb

Visual comparison of the samples on histograms and kernel density estimates (Fig. 5), as well as cumulative distribution function (CDF) and quantile-quantile (QQ) plots (Fig. 6), shows that 15BSK006 (the stratigraphically lowest and geographically most northern sample) is the single sample with a noticeable, although still only slight, difference in zircon age distribution. This observation is supported by the results of a Kolmogorov-Smirnoff (K-S) statistical test which demonstrates that only sample 15BSK006 is statistically likely (at a 95 % confidence level) to have been sourced from a different population to any of the other samples (Table 1A). We note that in this study the K-S test results support observations that were first made by visual inspection but that, in general, the p-value of the K-S test may be considered a poor measure of dissimilarity between samples due to the strong dependence of results on sample size (Vermeesch 2013). The reason that sample 15BSK006 appears to be distinct is largely as a result of it lacking the *ca.* 1.9 Ga age population observed in all other samples.

B.3.3. Apatite U-Pb age data

Due to the nature of the ^{207}Pb-based correction for common Pb, no apatite U-Pb age data can be excluded on the basis of discordance. Instead, grains with ^{207}Pb-corrected 2σ age uncertainties above a certain threshold value (which may be absolute and/or a percentage) are not considered further (e.g., Zattin et al. 2012; Mark et al. 2016; O'Sullivan et al. 2016). Here, this value was set at 5 %. This corresponds to an absolute age threshold similar to that employed in studies of mostly Phanerozoic-aged apatite grains which is typically screened at 20 % (e.g., O'Sullivan et al. 2018).

Similar to the zircon data, the five samples all display quite similar apatite age distributions (Figs 4-6). Visual inspection of the data on histograms and kernel density plots (Fig. 5), as well as CDF and QQ plots (Fig. 6), is again supported by K-S test results indicating no statistically significant difference in age distributions between samples (Table 2). However, the age peaks are different to those in the zircon record; all samples display a range of ages between *ca.* 2.6 and *ca.* 2.15 Ga and a broad and dominant peak between *ca.* 1.8 and *ca.* 1.55 Ga, and most samples also have minor peaks centred at *ca.* 1.4 and *ca.* 1.15 Ga (Fig. 5). Sample 15BSK006, which appeared to be the most distinctive in terms of zircon U-Pb age distribution, is the only sample that lacks apatite grains younger than 1500 Ma.

Two apatite grains in the filtered dataset (339 grains in five samples) have ^{207}Pb-corrected U-Pb ages (1101 ± 38 Ma and 1109 ± 40 Ma) that are younger than the current

estimate for the deposition of the Stac Fada Member – a 1177 ± 5 Ma $^{40}Ar/^{39}Ar$ age for authigenic K-feldspar (adularia) which precipitated in degassing structures in the Stac Fada Member itself (Parnell et al. 2011). Both of these grains are from sample 15BSK008, which was taken from stratigraphically above the Stac Fada Member (Fig. 2). The two grains which gave ages younger than the currently accepted age of deposition for the unit may be explained by, for example, a) subtle Pb loss from these two crystals, or b) inaccuracy in the $^{40}Ar/^{39}Ar$ age. The latter appears unlikely given the robust nature of the $^{40}Ar/^{39}Ar$ results from samples from a number of localities. Regardless, the presence of shock metamorphosed zircon in the unit (Reddy et al. 2015) suggests that there may also be the possibility for future studies to obtain a direct U-Pb age for the impact event through analysis of shocked accessory phases such as zircon (e.g., Bohor et al. 1993; Krogh et al. 1993a; Krogh et al. 1993b; Kamo et al. 1996; Moser 1997; Moser et al. 2011; Cavosie et al. 2015; Kenny et al. 2017), monazite (e.g., Erickson et al. 2017) or baddeleyite (e.g., White et al. 2017).

Figure 5 (next page). Detrital zircon and apatite U-Pb age distributions.
Zircon data are $^{207}Pb/^{206}Pb$ ages for analyses which were less than 10 % discordant whereas apatite data are ^{207}Pb-corrected apatite U-Pb ages which had 2σ age uncertainties less than 5 % (black ellipses in Fig. 4). Kernel density estimates were plotted in the 'DensityPlotter' program of Vermeesch (2012) in which the optimal bandwidth is calculated according to the method of Botev et al. (2010). SFM – Stac Fada Member.

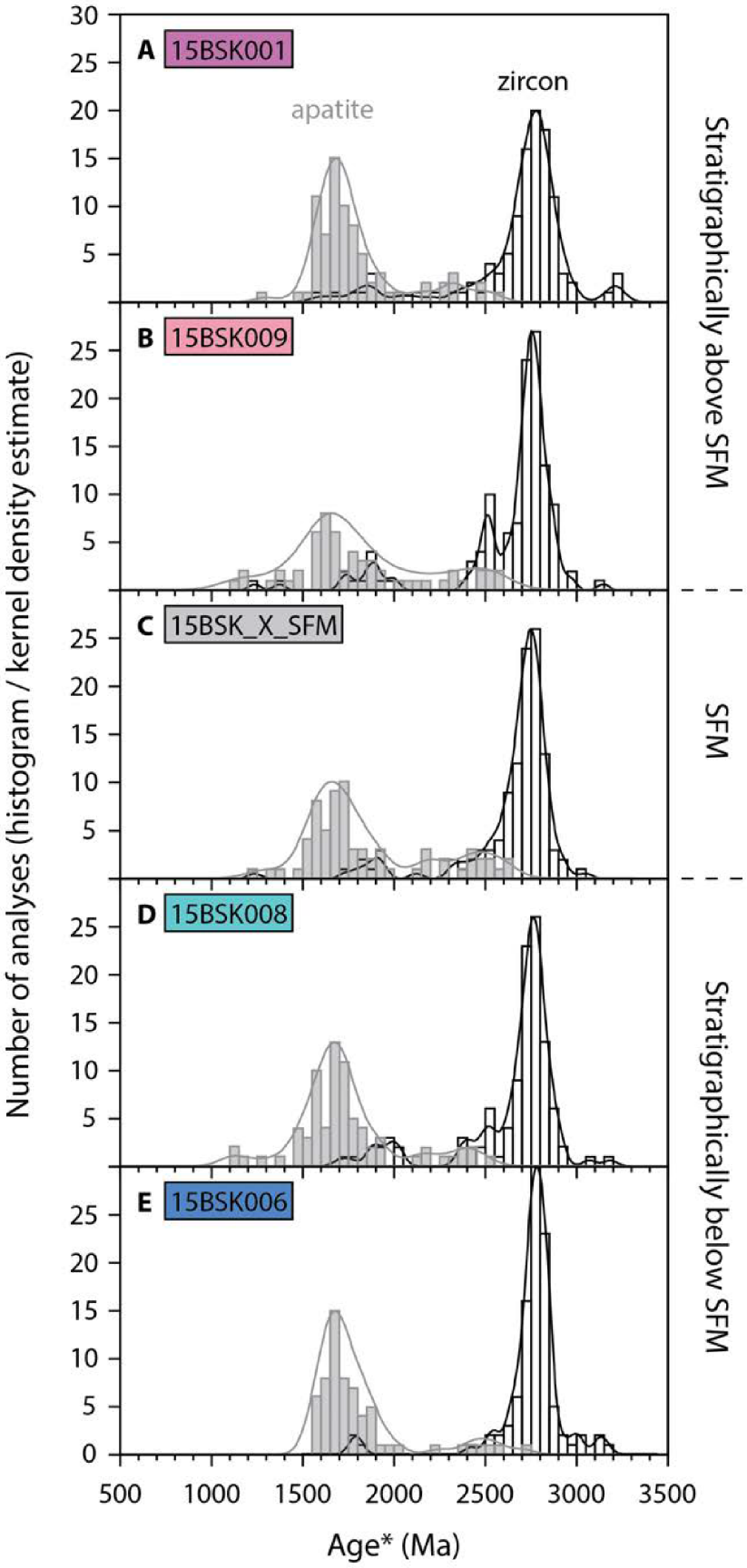
A 15BSK001
zircon
apatite
B 15BSK009
C 15BSK_X_SFM
D 15BSK008
E 15BSK006
Stratigraphically above SFM
SFM
Stratigraphically below SFM
Number of analyses (histogram / kernel density estimate)
Age* (Ma)
0
5
10
15
20
25
30
500
1000
1500
2000
2500
3000
3500

B.4. DISCUSSION

B.4.1. Stratigraphic variation

The lack of significant stratigraphic variations in zircon or apatite U-Pb age distributions through the Stoer Group, northwest Scotland, may be interpreted as evidence that there was no major change in the source of detritus during the Stoer Group deposition. Alternatively, there may have been a significant change in sediment source but it could not be detected as the different source regions shared similar apatite and zircon U-Pb age populations.

The polycyclic nature of zircon and the ability of intermediate repositories to overwhelm local provenance (e.g., Sircombe & Freeman 1999) mean that changes in sedimentary provenance throughout a succession may not necessarily result in any major change in the detrital zircon age distribution. Apatite, by contrast, is more likely to represent first-cycle detritus (Morton & Hallsworth 1999 and references therein) and may therefore be more likely than zircon to record major shifts in provenance throughout a succession. The relatively constant nature of detrital apatite U-Pb age distributions across the Stac Fada Member may therefore lend support to the first hypothesis – i.e. that there was not a major shift in drainage pattern.

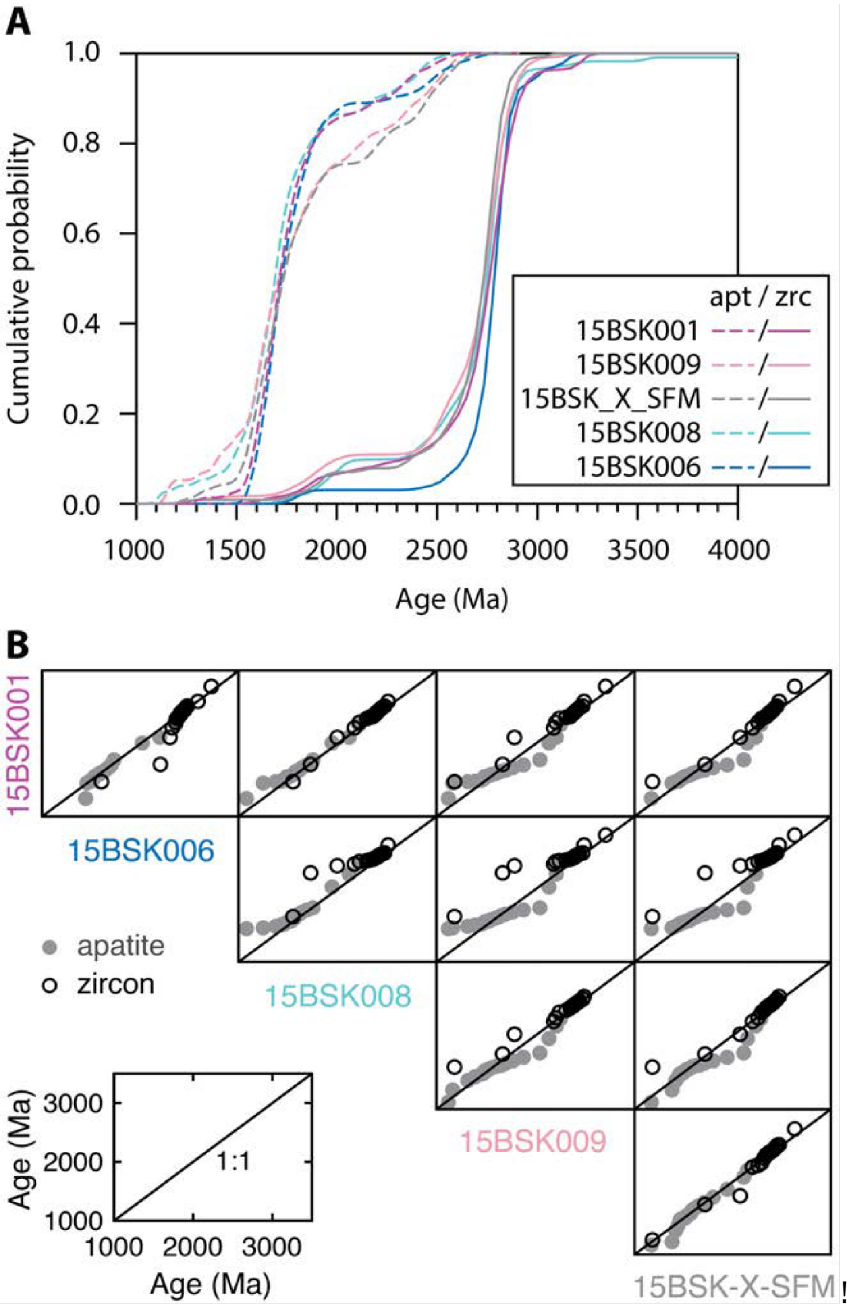

Figure 6. Cumulative distribution function (CDF) and quantile-quantile (QQ) plots for detrital zircon $^{207}Pb/^{206}Pb$ ages and detrital apatite ^{207}Pb-corrected ages. **A)** apt – apatite; zrc – zircon. **B)** Dots represent the 0, 5, 10, ..., 95 and 100 percentiles (or 'quantiles') of the samples whose names are shown on the X- and Y-axis, respectively. A pair of samples have identical distributions if their percentiles fall on the 1:1-line (Vermeesch 2013).

Consistency in detrital zircon and apatite U-Pb age distributions throughout a stratigraphic section could conceivably be related to extensive reworking of underlying sediments. The lower part of the Stoer Group appears to have been deposited in a series of narrow, high-gradient bedrock and alluvial valleys that were only partially connected, whereas the younger parts of the Stoer Group appear to have been deposited in broader, low-gradient alluvial settings, with aeolian processes on-going in areas far from basement highs (Ielpi et al. 2016). It has been suggested that this transition in the Stoer Group led to more mature and hydrologically open drainage which was capable of remobilizing fine-grained detritus, with "mobilization and reworking of sandy detritus in extra-channel areas also enhanced by the absence of plant rooting" (Ielpi et al. 2016, p. 309; Went 2005).

The zircon and apatite U-Pb age results need to be considered in the context of palaeocurrent data for the Stoer Group. The well-documented changes in flow direction throughout the unit – from variable palaeocurrent directions below the Stac Fada Member, to broadly eastward movement in the up to 100 m thick lacustrine sedimentary rocks of the Poll à Mhuilt Member immediately overlying the Stac Fada Member, to broadly westward flow directions in the post-Poll à Mhuilt Member (Stewart 2002; Simms 2015), indicate that there was at least some change in the regional drainage network coincident with the deposition of the Stac Fada Member.

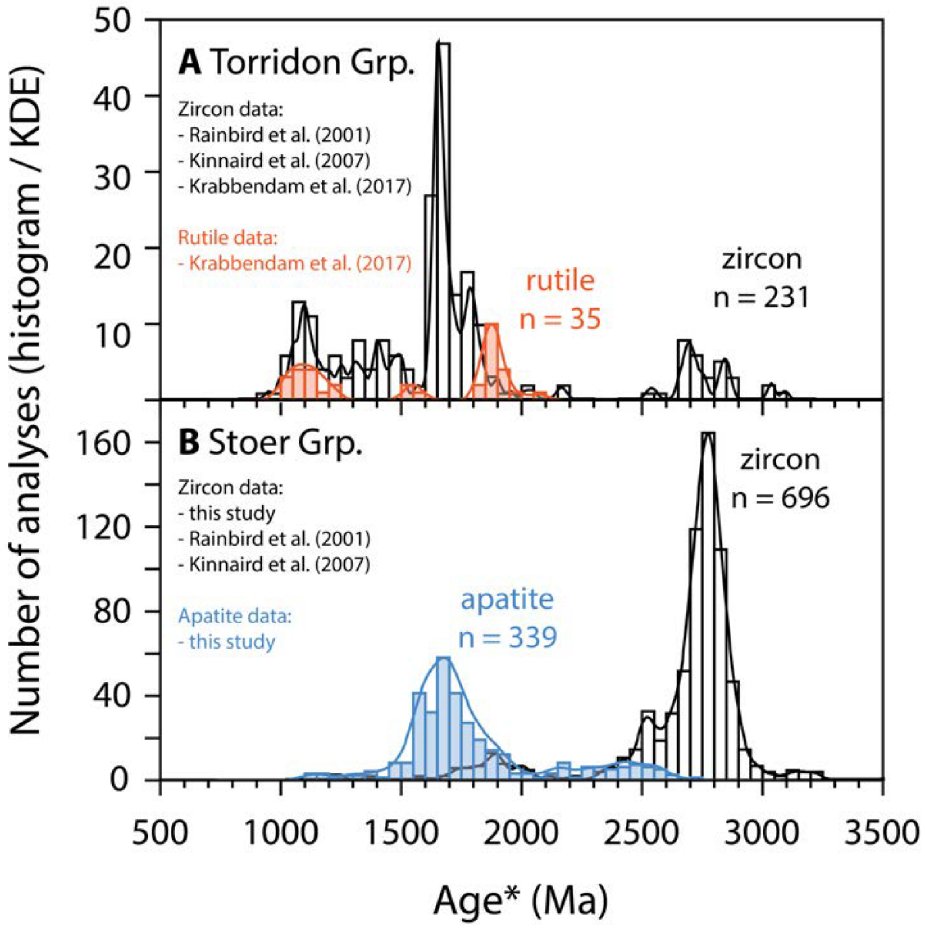

Figure 7. Compiled detrital zircon, apatite and rutile U-Pb age distributions for the Stoer and Torridon Groups. Note that zircon and rutile data for the Torridon Group from Krabbendam et al. (2017) are only from sample ZY320 (which was taken at Gruinard Bay, near Rainbird et al.'s [2001] sample GY96-56; Krabbendam et al. 2017; p. 76), and therefore does not include data for Krabbendam et al.'s sample ZY327, which was taken *ca.* 60 km further south. Zircon and rutile data are $^{207}Pb/^{206}Pb$ ages for analyses that were less than 10 % discordant whereas apatite data are ^{207}Pb-corrected apatite U-Pb ages that had 2σ age uncertainties less than 5 %. KDE – kernel density estimate.

Regardless of whether the relatively constant age distributions of heavy minerals in the Stoer Group can be interpreted as indicative of a lack of major shift in sediment source, they do not provide independent evidence that the impact associated with the Stac Fada Member: (i) brought previously unexposed rocks to the Earth's surface, (ii) cut off specific source terrain(s), or (iii) resulted in any major change in the regional Stoer Group sedimentary system that might indicate a location of the impact structure.

The very minor differences between the U-Pb age spectra may be related to geographic or stratigraphic factors. For example, if the lack of a *ca.* 1.9 Ga zircon population and apatite grains younger than 1.3 Ga in sample 15BSK006 are genuine features of the sample population, these differences may be related to its northernmost location (Fig. 1) or its lowermost stratigraphic position of the five studied samples (Fig. 2). The identification of two *ca.* 1.9 Ga zircon grains ($^{207}Pb/^{206}Pb$ ages of 1866 ± 62 and 1912 ± 30 Ma) in samples from even lower in the Stoer Group stratigraphy at the relatively southern location of Gruinard Bay (Rainbird et al., 2001) suggests that if the absence of *ca.* 1.9 Ga zircon grains in sample 15BSK006 is a real feature, it is unlikely related to the sample's stratigraphic position and rather more likely related to its northernmost location.

B.4.2. Provenance

The new zircon U-Pb data for the Stoer Group are consistent with the U-Pb data of Rainbird et al. (2001) and Kinnaird et al. (2007) and earlier interpretations that the detritus was largely derived from local Lewisian Gneiss Complex basement (e.g., Stewart 1982, 1990; Van de Kamp & Leake 1997; Stewart 2002). For example, as outlined by Rainbird et al. (2001), the major detrital zircon age peak at 2.9-2.7 Ga corresponds to protolith ages for rocks of the Lewisian Gneiss Complex in the Gruinard Bay area (Whitehouse et al. 1997b; Corfu et al. 1998) as well as high-grade metamorphic events in the north-central part of the Lewisian. The zircon peak at *ca.* 2.5 Ga corresponds to the 2490-2480 Ma Inverian event of the Lewisian central region (Humphries & Cliff 1982; Corfu et al. 1994), while the <2.0 Ga ages may be related to the Loch Maree Group in the southern region of the Lewisian Gneiss Complex (Whitehouse et al. 1997a), granulite facies metamorphism in South Harris at *ca.* 1.83 Ga (Cliff et al. 1998) and Laxfordian metamorphism at *ca.* 1.70 Ga (e.g., Heaman & Tarney 1989; Waters et al. 1990; Corfu et al. 1994; Kinny & Friend 1997; Zhu et al. 1997). The detrital populations in the Stoer Group that had not previously been identified (including grains at *ca.* 3.5 Ga and *ca.* 3.2-3.1 Ga, as well as Mesoproterozoic ages) can also be attributed to sources in the Lewisian Gneiss Complex. The Paleo-archaean ages reported from the Stoer Group (3529 ± 30

Ma) may be related to the *ca.* 3550 Ma inherited core found in a grain from the northern part of the Lewisian Gneiss Complex (Kinny & Friend 1997). Similarly, the few *ca.* 3.2-3.1 Ga analyses may be related to the 3115 ± 18 Ma analysis on a zircon core from the central region of the Lewisian Gneiss Complex (Kinny & Friend 1997).

The detrital apatite U-Pb data for the Stoer Group contrast greatly with those from zircon. Whereas some apatite ages are likely related to rocks and events already known from the detrital zircon record of the Stoer Group (with the former potentially offset to younger ages due to the lower closure temperature of its U-Pb system) others are likely related to events unrepresented by zircon. For example, the main apatite age peak centred at *ca.* 1.7 Ga, probably reflects amphibolite-facies metamorphism of the *ca.* 1.7 Ga Laxfordian event which is recorded in titanite and rutile ages (Heaman & Tarney 1989; Corfu et al. 1994; Kinny & Friend 1997), as well as in rare zircon rims (Kinny & Friend 1997) in the Lewisian Gneiss Complex. This event might also be represented by a very minor number of *ca.* 1.75 Ga zircon analyses in this study.

Considering the broad bell-shape of apatite ages between 2.6 and 2.1 Ga, it is noteworthy that zircon, by contrast, is relatively scarce between 2.4 and 2.1 Ga but represented by a clear peak in zircon $^{207}Pb/^{206}Pb$ ages at *ca.* 2.5 Ga (Fig. 7B). Some of the younger apatite ages may be related to discrete events simply not recorded by zircon (e.g., at *ca.* 2.15 Ga) but others may conceivably date prolonged cooling and exhumation after the 2490-2480 Ma high-grade Inverian metamorphism of in the central region of the Lewisian Gneiss Complex (Humphries & Cliff 1982; Corfu et al. 1994), to which the *ca.* 2.5 Ga detrital zircon age peak in the Stoer Group has been attributed (Rainbird et al. 2001).

Considering the youngest detrital mineral ages measured in the Stoer Group, the two zircon grains which gave *ca.* 1.25 Ga ages (and are within 2σ analytical uncertainty of the 1177 ± 5 Ma $^{40}Ar/^{39}Ar$ age for authigenic K-feldspar in the Stac Fada Member; Parnell et al. 2011) are likely to represent the same source as the small number of apatite grains with *ca.* 1.2 Ga ages (Fig. 7B). The two youngest zircon grains lack any evidence of impact shock features typical of age resetting (Fig. 3J-M), such as granular textures (e.g., (Bohor et al. 1993; Krogh et al. 1993a; Krogh et al. 1993b; Kamo et al. 1996; Moser 1997; Moser et al. 2011; Cavosie et al. 2015; Kenny et al. 2017). This suggests that these youngest ages are not related to Pb loss or recrystallisation associated with the Stac Fada Member impact event itself and is also supported by the lack of evidence for impact-related U-Pb discordance in the dataset in general (Fig. 4). We note that no features diagnostic of shock metamorphism in apatite have yet been documented in the literature

but planar microstructures in apatite, which strongly resemble planar fractures in zircon, have been reported at the Sante Fe impact structure (Cavosie & Lugo Centeno 2014) and apatite with apparent "spongy recrystallisation" along its margin has been noted at the Carswell impact structure in Canada (Alwmark et al. 2017). In addition to inducing shock deformation and age resetting in zircon, medium to large impact events can also crystallise new igneous zircon in slowly cooled impact melts. These grains, which post-date the impact and therefore lack shock features, appear to be indistinguishable from igneous zircon related to endogenic melting of Earth's crust (e.g., in terms of CL-visible zoning or trace-element abundances; e.g., Kenny et al. 2016). Zircon newly crystallised from impact melts seems to generally be restricted to the largest terrestrial impact structures (Vredefort, South Africa – Kamo et al. 1996; Sudbury, Canada – Davis 2008; Manicouagan, Canada – Hodych & Dunning 1992; and Morokweng, South Africa – Hart et al. 1997; Koeberl et al. 1997) but has also been reported at the 28 km-diameter Mistastin Lake crater, Canada (Sylvester et al. 2013). Given the time required for zircon to crystallise from an impact melt, it appears unlikely that the youngest detrital zircon grain in the Stac Fada Member reworked ejecta horizon (Fig. 5C) has a melt sheet origin. Although it cannot be ruled out entirely, an impact origin appears similarly unlikely for the single *ca.* 1.25 Ga zircon grain in the overlying Poll à Mhuilt Member (Fig. 5D).

We note that the Stoer Group is generally considered to have been deposited prior to the Grenville Orogeny in Scotland (Stewart 2002), which is dated to *ca.* 1.1 to 1.0 Ga (e.g., Sanders et al. 1984; Brewer et al. 2003), and the youngest detrital grains are therefore unlikely to be related to even very early Grenvillian orogenesis. However, ages of between 1.1 and 1.3 Ga have previously been reported from the Lewisian Gneiss Complex. Early Rb-Sr and K-Ar biotite ages fall in the range of *ca.* 1148-1169 Ma (Giletti et al. 1961; Moorbath & Park 1972). More recently, Sherlock et al. (2008), reported $^{40}Ar/^{39}Ar$ ages for pseudotachylite in the Lewisian at *ca.* 1.0 Ga (i.e., temporally overlapping with the Grenville Orogeny), and ages for the hosting amphibole at *ca.* 1.6 Ga and for hosting biotite at *ca.* 1.1-1.3 Ga. The authors interpreted the host rock ages as being related to a thermal event prior to 1.6 Ga (namely, the *ca.* 1.7 Ga Laxfordian event) and a later, somewhat enigmatic, event in which temperatures reached at least the 300°C required to reset biotite but not *ca.* 500-550°C required to reset amphibole, respectively. Given the relatively low temperature of the apparent later event recognised by Sherlock et al. (2008), it is unlikely to have been a source of the two *ca.* 1.25 Ga zircon grains in the Stoer Group.

B.4.3. Comparison of apatite and zircon age distributions

There are a number of possible reasons for the contrasting detrital age distributions of apatite and zircon in the Stoer Group (Figs 5, 7B). The first is that certain geological events are more likely to be recorded by one mineral than the other. For example, the occurrence of zircon is known to be biased towards felsic igneous sources and this mineral's ability to record low- to medium-grade metamorphic lithologies is very limited. By contrast, apatite crystallises across a larger spectrum of rock types and may provide a more complete record of orogenesis (e.g., O'Sullivan et al. 2016 and references therein). Our study of apatite U-Pb age distributions in the Stoer Group may therefore highlight lithologies in the source terrain(s) that were previously little known or undocumented. A second contributing factor to the contrasting age distributions is that apatite is more likely to represent first-cycle detritus than chemically-resistant minerals such as zircon, rutile and tourmaline due to its instability under weathering at source and during alluvial storage (e.g., Morton & Hallsworth 1999 and references therein). A third cause of contrasting age populations may be that the relatively lower closure temperature of the U-Pb system in apatite relative to that in zircon means that the former may be recording prolonged cooling and exhumation after the higher-T granulite-facies Archaean events. Zircon cools much faster through its partial retention window for Pb (>900°C) and records thermal events much more sharply. Finally, rocks with Archaean zircon U-Pb ages may yield Proterozoic apatite U-Pb ages due to resetting of the U-Pb system in apatite during subsequent lower-grade events. Given the complex thermal history of the Lewisian Gneiss Complex source region, the almost complete absence of >2.5 Ga apatite ages in the Stoer Group, despite the abundance of zircon of this age, appears to be most easily explained by the last hypothesis listed – i.e., that the source rocks were heated well above the partial retention window for Pb in apatite (*ca.* 375-450°C) while not reaching temperatures necessary to reset the zircon U-Pb systematics.

B.5. CONCLUSIONS

1) Minimal evidence for shock metamorphism or associated Pb loss in zircon or apatite was encountered in this study. Despite extensive efforts at SEM imaging, potentially impact-related planar fractures (PFs) were only identified on the exterior of a single zircon grain. Although a number of zircon and apatite grains in the Stoer Group yielded U-Pb ages within uncertainty of the 1177 ± 5 Ma $^{40}Ar/^{39}Ar$ depositional age constraint for

the Stac Fada Member, neither of the two such zircon grains displayed textures indicative of shock metamorphism and overall there was no clear evidence for impact-induced Pb loss in the dataset.

2) The new zircon U-Pb data for the Stoer Group reported here are consistent with earlier interpretations that the detritus was derived largely from local Lewisian Gneiss Complex basement but the larger number of analyses in this study resulted in the identification of ages previously undocumented in the Stoer Group; these include grains at *ca.* 3.5 Ga (the first PaleoArchaean ages reported from the Stoer Group) and *ca.* 3.2-3.1 Ga, as well as Mesoproterozoic ages.

3) Detrital zircon and apatite in the Stoer Group display contrasting age distributions. The first apatite age data for the Stoer Group highlights events either under-represented or absent in the zircon record, with the apatite record dominated by the *ca.* 1.7 Ga Laxfordian event. Conversely, detrital apatite U-Pb fails to record events older than *ca.* 2.5 Ga, indicating that all rocks in the sediment source regions older than 2.5 Ga have been heated above the closure temperature of the apatite U-Pb system (*ca.* 375-450°C).

4) Neither zircon nor apatite recorded significant changes in U-Pb age distribution across the impact-related Stac Fada Member of the Stoer Group, northwest Scotland. The U-Pb systems in detrital apatite and zircon assemblages do not provide independent support for a major shift in regional drainage patterns associated with the Stac Fada Member impact event and, as such, do not shed light on the likely location of the impact structure.

B.5.1 Acknowledgements

This research was supported by an Irish Research Council EMBARK Initiative scholarship to Kenny and Science Foundation Ireland (SFI) grant SFI/12/ERC/E2499 to Kamber. The U-Pb data in this publication have been obtained on infrastructure supported in part by a research grant from SFI under Grant Number 13/RC/2092 and is co-funded under the European Regional Development Fund and industry partners of the Irish Centre for Research in Applied Geosciences (iCRAG). The SEM data in this publication have been obtained on infrastructure supported in part by a research grant from SFI under Grant Number SFI/RI/3227.

B.7. REFERENCES CITED

Alwmark, C., Bleeker, W., LeCheminant, A., Page, L. & Scherstén, A. 2017. An Early Ordovician ^{40}Ar-^{39}Ar age for the ~50 km Carswell impact structure, Canada. *GSA Bulletin*, **129**, 1442-1449.

Amor, K., Hesselbo, S.P., Porcelli, D., Thackrey, S. & Parnell, J. 2008. A Precambrian proximal ejecta blanket from Scotland. *Geology*, **36**, 303-306.

Amor, K., Taylor, J., Hesselbo, S.P. & MacNiocaill, C. 2011. An anisotropy of magnetic susceptibility study of the Stac Fada Member suevite: constraints on the impact crater location. *Meteoritics & Planetary Science*, **46**, A10.

Binns, P.E., McQuillin, R., Fannin, N.G.T., Kenolty, N. & Ardus, D.A. 1975. Structure and stratigraphy of sedimentary basins in the Sea of the Hebrides and the Minches. *In*: Woodland, A.W. (ed) *Petroleum and the Continental Shelf of North-West Europe*. Applied Science Publishers, Barking, 93-102.

Black, L.P., Kamo, S.L., Allen, C.M., Davis, D.W., Aleinikoff, J.N., Valley, J.W., Mundil, R., Campbell, I.H., *et al.* 2004. Improved $^{206}Pb/^{238}U$ microprobe geochronology by the monitoring of a trace-element-related matrix effect; SHRIMP, ID–TIMS, ELA–ICP–MS and oxygen isotope documentation for a series of zircon standards. *Chemical Geology*, **205**, 115-140.

Bohor, B., Betterton, W. & Krogh, T. 1993. Impact-shocked zircons: discovery of shock-induced textures reflecting increasing degrees of shock metamorphism. *Earth and Planetary Science Letters*, **119**, 419-424.

Botev, Z.I., Grotowski, J.F. & Kroese, D.P. 2010. Kernel density estimation via diffusion. *The Annals of Statistics*, **38**, 2916-2957.

Bouch, J.E., Hole, M.J., Trewin, N.H., Chenery, S.P. & Morton, A.C. 2002. Authigenic apatite in a fluvial sandstone sequence: evidence for rare-earth element mobility during diagenesis and a tool for diagenetic correlation. *Journal of Sedimentary Research*, **72**, 59-67.

Branney, M.J. & Brown, R.J. 2011. Impactoclastic density current emplacement of terrestrial meteorite-impact ejecta and the formation of dust pellets and accretionary lapilli: evidence from Stac Fada, Scotland. *The Journal of Geology*, **119**, 275-292.

Brewer, T.S., Storey, C.D., Parrish, R.R., Temperley, S. & Windley, B.F. 2003. Grenvillian age decompression of eclogites in the Glenelg–Attadale Inlier, NW Scotland. *Journal of the Geological Society*, **160**, 565-574.

British Geological Survey. 2002. *Point of Stoer. Scotland Sheet 107W. Solid and Drift Geology.* Keyworth, Nottingham: British Geological Survey.

Butler, R.W.H. & Coward, M.P. 1984. Geological constraints, structural evolution, and deep geology of the northwest Scottish Caledonides. *Tectonics*, **3**, 347-365.

Cavosie, A.J. & Lugo Centeno, C. 2014. Shocked apatite from the Sante Fe impact structure (USA): a new accessory mineral for studies of shock metamorphism. *Lunar and Planetary Science Conference* abstract #1691.

Cavosie, A.J., Erickson, T.M., Timms, N.E., Reddy, S.M., Talavera, C., Montalvo, S.D., Pincus, M.R., Gibbon, R.J.*, et al.* 2015. A terrestrial perspective on using ex situ shocked zircons to date lunar impacts. *Geology*, **43**, 999-1002.

Chew, D.M., Sylvester, P.J. & Tubrett, M.N. 2011. U–Pb and Th–Pb dating of apatite by LA-ICPMS. *Chemical Geology*, **280**, 200-216.

Chew, D.M., Petrus, J.A. & Kamber, B.S. 2014. U–Pb LA–ICPMS dating using accessory mineral standards with variable common Pb. *Chemical Geology*, **363**, 185-199.

Cliff, R.A., Rex, D.C. & Guise, P.G. 1998. Geochronological studies of Proterozoic crustal evolution in the northern Outer Hebrides. *Precambrian Research*, **91**, 401-418.

Corfu, F., Heaman, L.M. & Rogers, G. 1994. Polymetamorphic evolution of the Lewisian Complex, NW Scotland, as recorded by U-Pb isotopic compositions of zircon, titanite and rutile. *Contributions to Mineralogy and Petrology*, **117**, 215-228.

Corfu, F., Crane, A., Moser, D. & Rogers, G. 1998. U-Pb zircon systematics at Gruinard Bay, northwest Scotland: implications for the early orogenic evolution of the Lewisian complex. *Contributions to Mineralogy and Petrology*, **133**, 329-345.

Davis, D.W. 2008. Sub-million-year age resolution of Precambrian igneous events by thermal extraction-thermal ionization mass spectrometer Pb dating of zircon: Application to crystallization of the Sudbury impact melt sheet. *Geology*, **36**, 383-386.

Drake, S.M., Beard, A.D., Jones, A.P., Brown, D.J., Fortes, A.D., Millar, I.L., Carter, A., Baca, J.*, et al.* 2017. Discovery of a meteoritic ejecta layer containing unmelted impactor fragments at the base of Paleocene lavas, Isle of Skye, Scotland. *Geology*, **46**, 171-174.

Engelhardt, W. 1997. Suevite breccia of the Ries impact crater, Germany: Petrography, chemistry and shock metamorphism of crystalline rock clasts. *Meteoritics & Planetary Science*, **32**, 545-554.

Erickson, T.M., Timms, N.E., Kirkland, C.L., Tohver, E., Cavosie, A.J., Pearce, M.A. & Reddy, S.M. 2017. Shocked monazite chronometry: integrating microstructural and in situ isotopic age data for determining precise impact ages. *Contributions to Mineralogy and Petrology*, **172**, 11.

Fedo, C.M., Sircombe, K.N. & Rainbird, R.H. 2003. Detrital zircon analysis of the sedimentary record. *Reviews in Mineralogy and Geochemistry*, **53**, 277-303.

Giletti, B.J., Moorbath, S. & Lambert, R. 1961. A geochronological study of the metamorphic complexes of the Scottish Highlands. *Quarterly Journal of the Geological Society*, **117**, 233-264.

Goodenough, K.M. & Krabbendam, M. 2011. *A geological excursion guide to the North-west Highlands of Scotland*. Edinburgh Geological Society and NMS Enterprises.

Grieve, R.A. & Pilkington, M. 1996. The signature of terrestrial impacts. *AGSO Journal of Australian Geology and Geophysics*, **16**, 399-420.

Hart, R.J., Andreoli, M.A.G., Tredoux, M., Moser, D., Ashwal, L.D., Eide, E.A., Webb, S.J. & Brandt, D. 1997. Late Jurassic age for the Morokweng impact structure, southern Africa. *Earth and Planetary Science Letters*, **147**, 25-35.

Heaman, L.M. & Tarney, J. 1989. U–Pb baddeleyite ages for the Scourie dyke swarm, Scotland: evidence for two distinct intrusion events. *Nature*, **340**, 705.

Hildebrand, A.R., Pilkington, M., Ortiz-Aleman, C., Chavez, R.E., Urrutia-Fucugauchi, J., Connors, M., Graniel-Castro, E., Camara-Zi, A.*, et al.* 1998. Mapping Chicxulub crater structure with gravity and seismic reflection data. *Geological Society, London, Special Publications*, **140**, 155-176.

Hodych, J.P. & Dunning, G.R. 1992. Did the Manicouagan impact trigger end-of-Triassic mass extinction? *Geology*, **20**, 51-54.

Humphries, F.J. & Cliff, R.A. 1982. Sm–Nd dating and cooling history of Scourian granulites, Sutherland. *Nature*, **295**, 515.

Ielpi, A., Ventra, D. & Ghinassi, M. 2016. Deeply channelled Precambrian rivers: Remote sensing and outcrop evidence from the 1.2 Ga Stoer Group of NW Scotland. *Precambrian Research*, **281**, 291-311.

Irving, E. & Runcorn, K. 1957. II. Analysis of the paleomagnetism of the Torridonian sandstone series of North-West Scotland. I. *Philosophical Transactions of the Royal Society of London. Series A, Mathematical and Physical Sciences*, **250**, 83-99.

Kamo, S.L., Reimold, W.U., Krogh, T.E. & Colliston, W.P. 1996. A 2.023 Ga age for the Vredefort impact event and a first report of shock metamorphosed zircons in pseudotachylitic breccias and Granophyre. *Earth and Planetary Science Letters*, **144**, 369-387.

Kenny, G.G., Whitehouse, M.J. & Kamber, B.S. 2016. Differentiated impact melt sheets may be a potential source of Hadean detrital zircon. *Geology*, **44**, 435-438.

Kenny, G.G., Morales, L.F., Whitehouse, M.J., Petrus, J.A. & Kamber, B.S. 2017. The formation of large neoblasts in shocked zircon and their utility in dating impacts. *Geology*, **45**, 1003-1006.

Kinnaird, T.C., Prave, A.R., Kirkland, C.L., Horstwood, M., Parrish, R. & Batchelor, R.A. 2007. The late Mesoproterozoic–early Neoproterozoic tectonostratigraphic evolution of NW Scotland: the Torridonian revisited. *Journal of the Geological Society*, **164**, 541-551.

Kinny, P.D. & Friend, C.R.L. 1997. U-Pb isotopic evidence for the accretion of different crustal blocks to form the Lewisian Complex of northwest Scotland. *Contributions to Mineralogy and Petrology*, **129**.

Kirkham, A. 2003. Glauconitic spherules from the Triassic of the Bristol area, SW England: probable microtektite pseudomorphs. *Proceedings of the Geologists' Association*, **114**, 11-21.

Koeberl, C., Armstrong, R.A. & Uwe Reimold, W. 1997. Morokweng, South Africa: A large impact structure of Jurassic-Cretaceous boundary age. *Geology*, **25**, 731-734.

Krabbendam, M., Bonsor, H., Horstwood, M.S.A. & Rivers, T. 2017. Tracking the evolution of the Grenvillian foreland basin: Constraints from sedimentology and detrital zircon and rutile in the Sleat and Torridon groups, Scotland. *Precambrian Research*, **295**, 67-89.

Krogh, T.E., Kamo, S.L. & Bohor, B.F. 1993a. Fingerprinting the K/T impact site and determining the time of impact by U-Pb dating of single shocked zircons from distal ejecta. *Earth and Planetary Science Letters*, **119**, 425-429.

Krogh, T.E., Kamo, S.L., Sharpton, V.L., Marin, L.E. & Hildebrands, A.R. 1993b. U-Pb ages of single shocked zircons linking distal K/T ejecta to the Chicxulub crater. *Nature*, **366**, 731-734.

Lawson, D.E. 1972. Torridonian volcanic sediments. *Scottish Journal of Geology*, **8**, 345-362.

Lebeau, L.E. & Ielpi, A. 2017. Fluvial channel-belts, floodbasins, and aeolian ergs in the Precambrian Meall Dearg Formation (Torridonian of Scotland): Inferring climate regimes from pre-vegetation clastic rock records. *Sedimentary Geology*, **357**, 53-71.

Leslie, A.G., Krabbendam, M., Kimbell, G.S. & Strachan, R.A. 2010. Regional-scale lateral variation and linkage in ductile thrust architecture: the Oykel Transverse Zone, and mullions, in the Moine Nappe, NW Scotland. *Geological Society, London, Special Publications*, **335**, 359-381.

Ludwig, K.R. 2012. User's Manual for Isoplot 3.75: A geochronological toolkit for Microsoft Excel. *Berkeley Geochronological Center Special Publication No. 5*.

Mark, C., Cogné, N. & Chew, D.M. 2016. Tracking exhumation and drainage divide migration of the Western Alps: A test of the apatite U-Pb thermochronometer as a detrital provenance tool. *Geological Society of America Bulletin*, **128**, 1439-1460.

Moorbath, S. & Park, R.G. 1972. The Lewisian chronology of the southern region of the Scottish mainland. *Scottish Journal of Geology*, **8**, 51-74.

Morgan, J. & Rebolledo-Vieyra, M. 2013. Geophysical studies of impact craters. *In*: Osinski, G.R. & Pierazzo, E. (eds) *Impact cratering processes and products*. Wiley-Blackwell, 211-222.

Morton, A.C. & Hallsworth, C.R. 1999. Processes controlling the composition of heavy mineral assemblages in sandstones. *Sedimentary Geology*, **124**, 3-29.

Moser, D.E. 1997. Dating the shock wave and thermal imprint of the giant Vredefort impact, South Africa. *Geology*, **25**, 7-10.

Moser, D.E., Cupelli, C.L., Barker, I.R., Flowers, R.M., Bowman, J.R., Wooden, J. & Hart, J.R. 2011. New zircon shock phenomena and their use for dating and reconstruction of large impact structures revealed by electron nanobeam (EBSD, CL, EDS) and isotopic U–Pb and (U–Th)/He analysis of the Vredefort dome. *Canadian Journal of Earth Sciences*, **48**, 117-139.

Nechaev, V.P. & Isphording, W.C. 1993. Heavy-mineral assemblages of continental margins as indicators of plate-tectonic environments. *Journal of Sedimentary Research*, **63**, 1110-1117.

Nelson, D.R. 2001. An assessment of the determination of depositional ages for Precambrian clastic sedimentary rocks by U-Pb dating of detrital zircons. *Sedimentary Geology*, **141-142**, 37-60.

O'Sullivan, G.J., Chew, D.M. & Samson, S.D. 2016. Detecting magma-poor orogens in the detrital record. *Geology*, **44**, 871-874.

O'Sullivan, G.J., Chew, D.M., Morton, A.C., Mark, C. & Henrichs, I.A. 2018. An integrated apatite geochronology and geochemistry tool for sedimentary provenance analysis. *Geochemistry, Geophysics, Geosystems*, **19**.

Osinski, G.R., Preston, L., Ferriere, L., Prave, T., Parnell, J., Singleton, A. & Pickersgill, A.E. 2011. The Stac Fada "impact ejecta" layer: not what it seems. *Meteoritics & Planetary Science*, **46**, A181.

Parnell, J., Mark, D., Fallick, A.E., Boyce, A. & Thackrey, S. 2011. The age of the Mesoproterozoic Stoer Group sedimentary and impact deposits, NW Scotland. *Journal of the Geological Society*, **168**, 349-358.

Paton, C., Hellstrom, J.C., Paul, B., Woodhead, J.D. & Hergt, J.M. 2011. Iolite: Freeware for the visualisation and processing of mass spectrometric data. *Journal of Analytical Atomic Spectrometry*, **26**, 2508-2518.

Paton, C., Woodhead, J.D., Hellstrom, J.C., Hergt, J.M., Greig, A. & Maas, R. 2010. Improved laser ablation U-Pb zircon geochronology through robust downhole fractionation correction. *Geochemistry, Geophysics, Geosystems*, **11**.

Petrus, J.A. & Kamber, B.S. 2012. VizualAge: A novel approach to laser ablation ICP-MS U-Pb geochronology data reduction. *Geostandards and Geoanalytical Research*, **36**, 247-270.

Piccoli, P.M. & Candela, P.A. 2002. Apatite in Igneous Systems. *Reviews in Mineralogy and Geochemistry*, **48**, 255-292.

Rainbird, R.H., Hamilton, M.A. & Young, G.M. 2001. Detrital zircon geochronology and provenance of the Torridonian, NW Scotland. *Journal of the Geological Society*, **158**, 15-27.

Reddy, S.M., Johnson, T.E., Fischer, S., Rickard, W.D.A. & Taylor, R.J.M. 2015. Precambrian reidite discovered in shocked zircon from the Stac Fada impactite, Scotland. *Geology*, **43**, 899-902.

Rodrigues, B., Chew, D.M., Jorge, R.C.G.S., Fernandes, P., Veiga-Pires, C. & Oliveira, J.T. 2015. Detrital zircon geochronology of the Carboniferous Baixo Alentejo Flysch Group (South Portugal); constraints on the provenance and geodynamic evolution of the South Portuguese Zone. *Journal of the Geological Society*, **172**, 294-308.

Sanders, I.S. & Johnston, J.D. 1989. The Torridonian Stac Fada Member: an extrusion of fluidised peperite? *Transactions of the Royal Society of Edinburgh: Earth Sciences*, **80**, 1-4.

Sanders, I.S., Van Calsteren, P.W.C. & Hawkesworth, C.J. 1984. A Grenville Sm–Nd age for the Glenelg eclogite in north-west Scotland. *Nature*, **312**, 439.

Schoene, B. & Bowring, S. 2006. U–Pb systematics of the McClure Mountain syenite: thermochronological constraints on the age of the 40Ar/39Ar standard MMhb. *Contributions to Mineralogy and Petrology*, **151**, 615-630.

Sherlock, S.C., Jones, K.A. & Park, R.G. 2008. Grenville-age pseudotachylite in the Lewisian: laserprobe $^{40}Ar/^{39}Ar$ ages from the Gairloch region of Scotland (UK). *Journal of the Geological Society*, **165**, 73-83.

Simms, M.J. 2015. The Stac Fada impact ejecta deposit and the Lairg Gravity Low: evidence for a buried Precambrian impact crater in Scotland? *Proceedings of the Geologists' Association*, **126**, 742-761.

Sircombe, K.N. & Freeman, M.J. 1999. Provenance of detrital zircons on the Western Australia coastline—Implications for the geologic history of the Perth basin and denudation of the Yilgarn craton. *Geology*, **27**, 879-882.

Spear, F.S. & Pyle, J.M. 2002. Apatite, monazite, and xenotime in metamorphic rocks. *Reviews in Mineralogy and Geochemistry*, **48**, 293-335.

Stacey, J.S. & Kramers, J.D. 1975. Approximation of terrestrial lead isotope evolution by a two-stage model. *Earth and Planetary Science Letters*, **26**, 207-221.

Stewart, A.D. 1982. Late Proterozoic rifting in NW Scotland: the genesis of the 'Torridonian'. *Journal of the Geological Society*, **139**, 413-420.

Stewart, A.D. 1990. Geochemistry, provenance and climate of the Upper Proterozoic Stoer Group in Scotland. *Scottish Journal of Geology*, **26**, 89-97.

Stewart, A.D. 2002. The later Proterozoic Torridonian rocks of Scotland: their sedimentology, geochemistry and origin. *Geological Society of London, Memoir*, **24**, 130.

Sylvester, P.J., Crowley, J.L. & Schmitz, M.D. 2013. U/Pb zircon age of Mistastin Lake crater, Labrador, Canada - implications for high-precision dating of small impact melt sheets and the end Eocene extinction. *Mineralogical Magazine*, 2295.

Thackrey, S., Walkden, G., Indares, A., Horstwood, M., Kelley, S. & Parrish, R. 2009. The use of heavy mineral correlation for determining the source of impact ejecta: A Manicouagan distal ejecta case study. *Earth and Planetary Science Letters*, **285**, 163-172.

Thomas, W.A. 2011. Detrital-zircon geochronology and sedimentary provenance. *Lithosphere*, **3**, 304-308.

Thomson, S.N., Gehrels, G.E., Ruiz, J. & Buchwaldt, R. 2012. Routine low-damage apatite U-Pb dating using laser ablation–multicollector–ICPMS. *Geochemistry, Geophysics, Geosystems*, **13**.

Van de Kamp, P.C. & Leake, B.E. 1997. Mineralogy, geochemistry, provenance and sodium metasomatism of Torridonian rift basin clastic rocks, NW Scotland. *Scottish Journal of Geology*, **33**, 105-124.

Vermeesch, P. 2004. How many grains are needed for a provenance study? *Earth and Planetary Science Letters*, **224**, 441-451.

Vermeesch, P. 2012. On the visualisation of detrital age distributions. *Chemical Geology*, **312–313**, 190-194.

Vermeesch, P. 2013. Multi-sample comparison of detrital age distributions. *Chemical Geology*, **341**, 140-146.

Walkden, G., Parker, J. & Kelley, S. 2002. A Late Triassic Impact Ejecta Layer in Southwestern Britain. *Science*, **298**, 2185-2188.

Waters, F.G., Cohen, A.S., O'Nions, R.K. & O'Hara, M.J. 1990. Development of Archaean lithosphere deduced from chronology and isotope chemistry of Scourie Dykes. *Earth and Planetary Science Letters*, **97**, 241-255.

Went, D.J. 2005. Pre-vegetation alluvial fan facies and processes: an example from the Cambro-Ordovician Rozel Conglomerate Formation, Jersey, Channel Islands. **52**, 693-713.

White, L.F., Darling, J.R., Moser, D.E., Reinhard, D.A., Prosa, T.J., Bullen, D., Olson, D., Larson, D.J.*, et al.* 2017. Atomic-scale age resolution of planetary events. *Nature Communications*, **8**, 15597.

Whitehouse, M.J., Bridgwater, D. & Park, R.G. 1997a. Detrital zircon ages from the Loch Maree Group, Lewisian Complex, NW Scotland: confirmation of a Palaeoproterozoic Laurentia—Fennoscandia connection. *Terra Nova*, **9**, 260-263.

Whitehouse, M.J., Claesson, S., Sunde, T. & Vestin, J. 1997b. Ion microprobe U-Pb zircon geochronology and correlation of Archaean gneisses from the Lewisian Complex of Gruinard Bay, northwestern Scotland. *Geochimica et Cosmochimica Acta*, **61**, 4429-4438.

Wiedenbeck, M., Allé, P., Corfu, F., Griffin, W.L., Meier, M., Oberli, F., Quadt, A.V., Roddick, J.C.*, et al.* 1995. Three natural zircon standards for U-Th-Pb, Lu-Hf, trace element and REE analyses. *Geostandards Newsletter*, **19**, 1-23.

Young, G.M. 2002. Stratigraphy and geochemistry of volcanic mass flows in the Stac Fada Member of the Stoer Group, Torridonian, NW Scotland. *Earth and Environmental Science Transactions of The Royal Society of Edinburgh*, **93**, 1-16.

Zattin, M., Andreucci, B., Thomson, S.N., Reiners, P.W. & Talarico, F.M. 2012. New constraints on the provenance of the ANDRILL AND-2A succession (western Ross Sea, Antarctica) from apatite triple dating. *Geochemistry, Geophysics, Geosystems*, **13**.

Zhu, Z.K., O'Nions, R.K., Belshaw, N.S. & Gibb, A.J. 1997. Lewisian crustal history from in situ SIMS mineral chronometry and related metamorphic textures. *Chemical Geology*, **136**, 205-218.

Appendix C

Titles pages of other co-authored works

From the following papers:

1) (LA,Q)-ICPMS trace-element analyses of Durango and McClure Mountain apatite and implications for making natural LA-ICPMS mineral standards.

Chew, D.M., Babechuk, M.G., Cogné, N., Mark, C., **O'Sullivan, G.J.**, Henrichs, I.A., Doepke, D., McKenna, C.A., 2016. (LA,Q)-ICPMS trace-element analyses of Durango and McClure Mountain apatite and implications for making natural LA-ICPMS mineral standards. Chem. Geol. 435, 35–48. doi:10.1016/j.chemgeo.2016.03.028

2) Variscan post-collisional cooling and uplift of the Tatra Mountains crystalline block constrained by integrated zircon, apatite and titanite LA-(MC)-ICP-MS U-Pb dating and rare earth element analyses.

Gawęda, A., Szopa, K., Chew, D., **O'Sullivan, G.J.**, Burda, J., Klötzli, U., Golonka, J., 2018. Variscan post-collisional cooling and uplift of the Tatra Mountains crystalline block constrained by integrated zircon, apatite and titanite LA-(MC)-ICP-MS U-Pb dating and rare earth element analyses. Chem. Geol. 484, 191–209. doi:10.1016/j.chemgeo.2018.03.012

(LA,Q)-ICPMS trace-element analyses of Durango and McClure Mountain apatite and implications for making natural LA-ICPMS mineral standards.

Chemical Geology 435 (2016) 35–48

Contents lists available at ScienceDirect

Chemical Geology

journal homepage: www.elsevier.com/locate/chemgeo

(LA,Q)-ICPMS trace-element analyses of Durango and McClure Mountain apatite and implications for making natural LA-ICPMS mineral standards

David M. Chew [a,*], Michael G. Babechuk [a,b], Nathan Cogné [a], Chris Mark [a], Gary J. O'Sullivan [a], Isadora A. Henrichs [a], Daniel Doepke [a], Cora A. McKenna [a]

[a] Department of Geology, School of Natural Sciences, Trinity College Dublin, Dublin 2, Ireland
[b] University of Tuebingen, Department of Geosciences, Wilhelmstraße 56, 72074 Tuebingen, Germany

ARTICLE INFO

Article history:
Received 6 November 2015
Received in revised form 26 March 2016
Accepted 29 March 2016
Available online 12 April 2016

Keywords:
Apatite
Trace elements
Reference materials
ICPMS
Laser ablation
Durango apatite

ABSTRACT

Apatite, the most abundant phosphate mineral in the Earth's crust and uppermost mantle, is able to accept a wide variety of trace elements into its crystal structure. Many of these trace element substitutions are below the detection limit of Electron Microprobe Analysis, but can be determined by laser-ablation inductively coupled plasma mass spectrometry (LA-ICPMS). LA-ICPMS elemental abundance determinations typically employ sample-standard bracketing using either standard glasses or an appropriate matrix-matched reference material. In this study we have undertaken laser ablation (>3000 analyses) and low-blank solution Q(quadrupole)-ICPMS trace-element analyses on crushed 150–300 μm aliquots of Durango and McClure Mountain apatite to assess the accuracy of apatite elemental abundance determinations when using NIST 612 standard glass as the primary LA-ICPMS trace element standard. An accuracy (relative to the solution data) and precision of <5% can be obtained for most trace elements (Y, the REE, Sr, Mn, V, Th and U) in LA-ICPMS analyses of crushed Durango separates; the McClure Mountain data are similarly accurate for most trace elements but yield larger intra-crystal variability. Durango raster and image mapping experiments demonstrate some Durango crystals are more homogenous than others; the raster experiments also show that Durango typically exhibits less zoning parallel to the C-axis compared to perpendicular to the C-axis. A protocol for developing a homogenous Durango apatite trace-element reference material is suggested, and involves slicing the interior portions of several Durango crystals parallel to the C-axis, undertaking rapid LA-ICPMS raster experiments to characterize trace-element zoning, crushing the most homogenous crystal to 150–300 μm and determining its trace-element contents by low-blank solution ICPMS. This generic approach can easily be modified and applied to characterize other natural LA-ICPMS mineral standards.

© 2016 Elsevier B.V. All rights reserved.

1. Introduction

Apatite, $Ca_5(PO_4)_3(F,Cl,OH)$, is a very common accessory mineral in igneous rocks, as apatite typically has a low solubility in silicate melts and phosphorous is not easily incorporated in the crystal lattices of the major rock-forming minerals (Piccoli and Candela, 2002). Apatite also occurs in metamorphic rocks of pelitic, carbonate, basaltic, and ultramafic composition at all metamorphic grades, and is virtually ubiquitous in clastic sedimentary rocks. Apatite can incorporate more than half of the periodic table into its crystal structure due to the variety of cation sites — a regular tetrahedron and two distinct M (M1 and M2) polyhedra (Hughes and Rakovan, 2015 and references therein). Divalent cations such as Sr, Ba, Pb, Cd, Mg, Fe, Mn, Co, Ni, Cu, and Zn typically substitute into the M1 and M2 sites, while trivalent cations such as the REE are envisaged to undergo more complex charge-coupled substitutions within the disparate M polyhedra, such as $Na^{+} + REE^{3+} \leftrightarrow 2Ca^{2+}$ and $Si^{4+} + REE^{3+} \leftrightarrow P^{5+} + Ca^{2+}$ (Hughes et al., 1991). The variable chemical composition of apatite has resulted in a variety of applications in a large variety of fields including mineralogy and crystal chemistry, petrology, biomineralization, geochronology, biomedical applications and materials science (Kohn et al., 2002).

While apatite has been routinely characterized for decades (e.g. Roeder et al., 1987) by Electron Microprobe Analysis (EPMA), many of the trace element substitutions in apatite are below the detection limit of EPMA (~100 μg/g). The high sensitivity of laser-ablation inductively coupled plasma mass spectrometry (LA-ICPMS) is ideally suited for measuring trace-element contents in geological materials, and in particular the very low counting mode background noise for all REE elements ensures detection at the sub-μg/g level. Elemental abundance determinations by LA-ICPMS in minerals (such as apatite) typically employ sample-standard bracketing using standard glasses, as natural mineral standards are often insufficiently homogeneous, especially in terms of their trace-element abundances. LA-ICPMS is typically a

* Corresponding author.
E-mail addresses: chewd@tcd.ie (D.M. Chew), babechmg@tcd.ie (M.G. Babechuk).

http://dx.doi.org/10.1016/j.chemgeo.2016.03.028
0009-2541/© 2016 Elsevier B.V. All rights reserved.

Variscan post-collisional cooling and uplift of the Tatra Mountains crystalline block constrained by integrated zircon, apatite and titanite LA-(MC)-ICP-MS U-Pb dating and rare earth element analyses.

Chemical Geology 484 (2018) 191–209

Contents lists available at ScienceDirect

Chemical Geology

journal homepage: www.elsevier.com/locate/chemgeo

Invited research article

Variscan post-collisional cooling and uplift of the Tatra Mountains crystalline block constrained by integrated zircon, apatite and titanite LA-(MC)-ICP-MS U-Pb dating and rare earth element analyses

Aleksandra Gawęda[a,*], Krzysztof Szopa[a], David Chew[b], Gary J. O'Sullivan[b], Jolanta Burda[a], Urs Klötzli[c], Jan Golonka[d]

[a] Faculty of Earth Sciences, University of Silesia in Katowice, Będzińska st. 60, 41-200 Sosnowiec, Poland
[b] Department of Geology, School of Natural Sciences, Trinity College Dublin, Dublin 2, Ireland
[c] Department of Lithospheric Research, University of Vienna, Althanstrasse 14, 1090 Vienna, Austria
[d] Faculty of Geology, Geophysics and Environmental Protection, AGH University of Science and Technology, Al. Mickiewicza 30, 30-059 Kraków, Poland

ARTICLE INFO

Keywords:
Tatra Mountains
Amphibolite
Apatite
Titanite
U-Pb dating
REE patterns

ABSTRACT

LA-ICP-MS U-Pb dating of apatite, titanite and zircon from the metamorphic cover of the Western Tatra granite was undertaken to constrain the timing of metamorphic events related to the final stages of Variscan orogenesis and subsequent post-orogenic exhumation. Zircon was found only in one sample from the northern metamorphic envelope. U-Pb ages from the outermost rims of zircons define a concordia age of 346 ± 6 Ma, while the inner rims yield a concordia age of 385 ± 8 Ma. Apatite from three samples from the northern metamorphic envelope yield U-Pb ages of 351.8 ± 4.4 Ma, 346.7 ± 5.9 Ma and 342.6 ± 7.1 Ma. Titanite from an amphibolite from the southern metamorphic envelope yields a U-Pb age of 345.3 ± 4.5 Ma. The age of c. 345 Ma is interpreted to represent the climax of metamorphism and the onset of simultaneous exhumation of the entire Tatra Mountains massif, and is recorded mainly in the northern part of the metamorphic cover.

In the southern metamorphic envelope, distinct populations of apatite can be recognized within individual samples based on their rare earth element (REE) and actinide contents. One population of apatite (Ap1) yields a relatively imprecise U-Pb age of 340 ± 31 Ma. This population comprises apatite grains with very similar trace element compositions to apatite in the northern amphibolite samples, which suggests they crystallized under similar metamorphic conditions to their northern counterparts. A second apatite population (Ap2) yields an age of c. 328 ± 22 Ma, which is interpreted as neocrystalline apatite that formed during a late-Variscan (hydrothermal?) process involving (P, F, Ca, REE)-rich fluid migration. The youngest generation of apatite (Ap3) yields a U-Pb age of 260 ± 8 Ma and may have resulted from thermal resetting associated with the regional emplacement of Permian A-type granites. The proposed tectonic model assumes that rapid uplift (and cooling) of the Tatra block initiated at ca. 345 Ma, contemporaneous with anatexis. Subsequent fluid migration, possibly facilitated by extension related to the opening of Paleo-Tethys, affected only the southern part of the Tatra block.

1. Introduction

Understanding the timescales of cooling and exhumation of basement terranes is one of the key problems in geology, and in particular the exhumation rates of the deep crust are the subject of active debate (e.g. Corsini et al., 2010 and references therein). Equally, recognizing exhumed deep crust is important in geodynamics because it yields constraints on the magnitudes and rates involved in the transfer of mass and heat during orogeny (e.g. Teyssier, 2011 and references therein). Accessory minerals such as zircon, titanite and apatite can preserve U-Pb isotopic age information and are commonly used as probes for the evolution of the Earth's crust in exhumation studies. Because of its low diffusivity for Pb, the U-Pb zircon system is a robust and widely-used geochronometer (Lee et al., 1997) which can be used to date high-temperature metamorphic events (e.g. Roberts and Finger, 1997; Rubatto, 2002, 2017), with a closure temperature of at least 900 °C (Lee et al., 1997). Titanite typically exhibits relatively high U, Th and Pb contents and is commonly used to date magmatic crystallization in igneous rocks, while in metamorphic rocks the U-Pb titanite system can be used to date moderate- to high- temperature thermal events (Möller

* Corresponding author.
E-mail address: aleksandra.gaweda@us.edu.pl (A. Gawęda).

https://doi.org/10.1016/j.chemgeo.2018.03.012
Received 27 April 2017; Received in revised form 25 January 2018; Accepted 7 March 2018
Available online 10 March 2018
0009-2541/ © 2018 Elsevier B.V. All rights reserved.